

Faculty  
of Engineering

**Czech University of Life Sciences Prague**

**Conference Proceeding**

**4<sup>th</sup> International Conference TAE 2010**

**Trends in Agricultural Engineering 2010**

**7 - 10 September, 2010**

**Prague, Czech Republic**

© 2010 Czech University of Life Sciences Prague; Faculty of Engineering



ČESKÁ  
ZEMĚLSKÁ  
UNIVERZITA V PRAZE

**2010**





Faculty  
of Engineering

**Czech University of Life Sciences Prague**

**Conference Proceeding**

**4<sup>th</sup> International Conference TAE 2010**

**Trends in Agricultural Engineering 2010**

**7 - 10 September, 2010**

**Prague, Czech Republic**

© 2010 Czech University of Life Sciences Prague; Faculty of Engineering



**2010**

Title: Trends in Agricultural Engineering 2010  
Editor: © 2010 Czech University of Life Sciences Prague; Faculty of Engineering  
([www.tf.czu.cz](http://www.tf.czu.cz))  
The conference is organised in cooperation with CIGR ([www.cigr.org](http://www.cigr.org))  
Type publication: Conference Proceedings  
Approved: Deanship of Faculty of Engineering; Czech University of Life Sciences  
Prague  
Edition: First  
Circulation: 150  
Imprint date: 2010

The articles in the publication are reviewed

The Conference Proceedings designed by Jan Malat'ák and Martin Libra

**ISBN: 978-80-213-2088-8**

Note: Objective correctness and language guaranteed by authors



## DEAR COLLEAGUES AND FRIENDS

---

It is my privilege and great pleasure to invite you to participate in the 4th International Conference on Trends in Agricultural Engineering 2010 to be held 7 – 10 September 2010 in Prague.

I would like to remember the successful past conferences held in 1994, 1999 and 2007. The organizers of this year conference hope that the fourth conference will be the successful continuation of the previous conferences. Its participants will have an excellent opportunity to exchange new experience, ideas and scientific results in the wide range of scientific disciplines.

Sixteen years of the conferences on trends in agricultural engineering also illustrate changes in this discipline. While at the beginning of this period the main domain of the discipline consisted mainly of improving the technology of the agricultural machinery and development of automation and robotics, now the main role is to detect the product quality and to precise agricultural technologies to become more friendly to environment.

Our conference offers an interesting scientific programme followed by an attractive social events in the beautiful city of Prague. On behalf of my colleagues in the organizing committee I would like to point out that we are ready to prepare the most pleasant conditions for all of you - our conference participants.

I look forward to meeting you in September in Prague.

---

Martin Libra  
Chairman of the Scientific Board

## SCIENTIFIC BOARD

---

Martin Libra (chairman, Czech Republic)  
Vladimír Jurča (Dean, Czech Rep.)  
Jiří Blahovec (Czech Republic)  
Josse DeBaerdemaeker (Belgium)  
Jozef Horabik (Poland)  
Stavros Yanniotis (Greece)  
Richard Godwin (United Kingdom)  
Osman Yaldiz (Turkey)  
Dmitry Strebkov (Russia)

---

## BOARD OF REVIEWERS

---

Radomír Adamovský (FE, CULS Prague)  
Jiří Blahovec (FE, CULS Prague)  
Milan Brožek (FE, CULS Prague)  
Boleslav Kadleček (FE, CULS Prague)  
Miroslav Kavka (FE, CULS Prague)  
František Kumhála (FE, CULS Prague)  
Martin Libra (FE, CULS Prague)  
Jan Malaťák (FE, CULS Prague)  
Jiří Mašek (FE, CULS Prague)  
Josef Pošta (FE, CULS Prague)  
Miroslav Přikryl (FE, CULS Prague)  
Adolf Rybka (FE, CULS Prague)  
Václav Slavík (FE, CULS Prague)  
Jaromír Volf (FE, CULS Prague)

---

## LOCAL ORGANIZING COMMITTEE

---

Martin Libra (chairman)  
Jan Malaťák (secretary)  
Pavel Kic  
Miroslav Müller  
Jan Sedláček  
Jarmila Jiříčková  
Jiří Zeman

---

## CONTENTS

### Invited Lectures

<b>JOSSE DE BAERDEMAEKER</b> AGRICULTURAL ENGINEERING AND THE COMPLEXITY OF MULTI-SCALE PROCESSES	1 – 6
<b>RICHARD J. GODWIN</b> THE USE OF PRECISION AGRICULTURE IN SOIL MANAGEMENT	7 – 13
<b>J. HORABIK, J. WIĄCEK, M. MOLEND</b> SIMULATION OF THE PACKING STRUCTURE, LOAD DISTRIBUTION AND FLOW PATTERN IN A 2-DIMENSIONAL MODEL SILO USING DISCRETE ELEMENT METHOD	14 – 17
<b>MIROSLAV KAVKA, LADISLAV NOZDROVICKÝ, FRANTIŠEK KADLEC, MIROSLAV MIMRA</b> ANALYSIS OF THE EFFECTS OF THE MACHINE LIFE-TIME ON THE DIRECT UNIT COST AND MINIMAL ANNUAL USE OF THE FIELD MACHINES IN TRACTOR-MACHINE SETS	18 – 24
<b>STREBKOV D.S.</b> RENEWABLE ENERGY SOURCES AND RURAL DEVELOPMENT	25 – 34
<b>OSMAN YALDIZ, DURMUŞ KAYA, H. İBRAHİM SARAÇ, KAMIL EKİNCİ, GÜNNUR KOÇAR, BERK KÜÇÜKKARA</b> POWER PRODUCTION FROM AGRICULTURAL WASTES AND IMPLEMENTATIONS	35 – 41
<b>STAVROS YANNIOTIS</b> ANALYSIS OF FOOD PROCESSING OPERATIONS USING CFD	42 – 47

### Papers

<b>ADAMOVSÝ RADOMÍR, NEUBERGER PAVEL, ŠEĐOVÁ MICHAELA</b> INFLUENCE OF DRAWING ENERGY FROM THE SOIL MASS TO ITS TEMPERATURE	48 – 52
<b>ZDENEK ALES</b> TRIBOLOGICAL PROPERTIES OF TRANSMISSION OILS	53 – 58
<b>AILTON DE ALMEIDA, LUIS FERNANDO BARBOSA XAVIER, DANIEL SEBASTIÃO DA SILVA, CELINA DE ALMEIDA, INÁCIO MARIA DAL FABBRO</b> PARTICULATE MATERIAL EMISSION AT THE CALCIUM CARBONATE INDUSTRY IN PRUDENTE DE MORAIS, MG, BRAZIL	59 – 63
<b>CELINA DE ALMEIDA, SANDRA CRISTINA DOS SANTOS ROCHA, INACIO MARIA DAL FABBRO</b> WATER VAPOR ABSORPTION BY HYDROXY-ETHYL CELLULOSE COATED SEEDS	64 – 68
<b>G.A.BARANI, V.KALANTARI, M.B.RAHNAMA</b> LAB INVESTIGATION OF FLOW COEFFICIENT ON TRIANGULAR SHAPE SIDE WEIRS	69 – 72
<b>GENADI PARTSKHALADZE, TAMAR DUDAURI, MALKHAZ BEREZHIANI, ANA BEREJIANI, BESARION METREVELI, TAMAR SVANIDZE</b> CO <sub>2</sub> BASED FREEZE-EXPLOSION METHOD FOR INCREASING HYDROLYSIS OF CELLULOSE	73 – 77
<b>DAINIS BERJOZA, VILNIS PIRS</b> MATHEMATICAL MODEL OF MOTOR VEHICLE EXPLOITATION PARAMETER CALCULATION USING BIO ETHANOL FUELS	78 – 83
<b>S.R. HASSAN-BEYGI, H. VALE GHOZHDI AND M.H. KIANMEHR</b> DETERMINING SHEAR STRENGTH AND ENERGY OF SAFFRON STALK AS AFFECTED BY BEVEL ANGLES AND CUTTING RATES	84 – 89
<b>S.R. HASSAN-BEYGI, M.H. KIANMEHR AND H. VALE GHOZHDI</b> MOISTURE DEPENDENT COEFFICIENT OF FRICTION OF SAFFRON FLOWER AND ITS COMPONENTS	90 – 95
<b>S.R. HASSAN-BEYGI, H. VALE GHOZHDI AND A. SEIFPOUR ABOLHASSANI</b> MOISTURE DEPENDENT TERMINAL VELOCITY OF SAFFRON FLOWER AND ITS COMPONENTS	96 – 100
<b>JIRÍ BLAHOVEC</b> THERMAL ANALYSIS OF SOFT CELLULAR PRODUCTS CONTAINING STARCH	101 – 105
<b>DAVID BLAŽEJ, JIRÍ SOUČEK</b> EXPLOITATION PARAMETERS OF A PELLET PRODUCTION LINE MONITORING	106 – 109
<b>ZDENEK BOHUSLAVEK</b> DEVELOPMENT OF DATA LOGGER FOR DATA ACQUISITION FROM FOUR CUP ANEMOMETERS	110 – 114
<b>MILAN BROŽEK, ALEXANDRA NOVÁKOVÁ, RASTISLAV MIKUŠ</b> STUDY OF WEAR RESISTANCE OF HARD FACINGS USING WELDING POWDERS ON THE NiCrBSi BASIS	115 – 118

<b>PAVEL CYRUS, BOHUSLAV ZAJÍC</b> TENSILE MECHANISM HOOK TMB PS 600 - THE TENSILE ANALYSIS	119 – 121
<b>OLDRICH DAJBÝCH</b> LOADING CAPACITY OF THE WOODEN BONDED SCARF JOINT SIMPLIFIED DETERMINATION	122 – 125
<b>EDMOND DEMOLLARI, ALTIN DORRI, ARTAN HOXHA</b> REAL BEHAVIOUR INJECTION GROUP AND INFLUENCE OF HOLE GEOMETRY IN THE CAVITATION PHENOMENA OF DIESEL INJECTORS	126 – 131
<b>TOMASZ K. DOBEK, PATRYCJA SALAGAN, PETR ŠAŘEC</b> ESTIMATING THE ECONOMIC AND ENERGY EFFICIENCY OF WINTER WHEAT (TRITICUM AESTIVUM) AND WINTER RAPE (BRASSICA NAPUS) CULTIVATION FOR BIOFUELS PRODUCTION	132 – 136
<b>FRANTIŠEK DVOŘÁK, FRANTIŠEK LACHNIT</b> THE ANALYSIS OF THE DEVELOPMENT OF TRANSPORT IN AGRICULTURE	137 – 141
<b>ŠÁRKA DVOŘÁKOVÁ, JOSEF ZEMAN</b> DIFFERENTIAL MODEL OF SUMMER CIRCULATION	142 – 145
<b>RAHIM EBRAHIMI, DAVOUD GHANBARIAN</b> PERFORMANCE ANALYSIS OF AN OTTO ENGINE WITH ETHANOL AND GASOLINE FUELS	146 – 150
<b>JAN FICHTNER, MIROSLAV ANDRT</b> COLLECTION OF BEVERAGE CANS IN CZECH REPUBLIC - IMPLEMENTATION AND PRACTICE	151 – 157
<b>JANA GALAMBOŠOVÁ, VLADIMÍR RATAJ, MICHAL VAŠEK</b> EFFECTS OF CONTROLLED TRAFFIC FARMING	158 – 162
<b>JONATHAN GAZZOLA, CLODOALDO CALLOGERO, INACIO MARIA DAL FABBRO, LUIZ GUSTAVO REIS TEIXEIRA, KELEN CRISTIANE CARDOSO</b> DETERMINATION OF ISOTHERMS SUPPORTED BY A MOIRÉ TECHNIQUE	163 – 167
<b>JONATHAN GAZZOLA, INÁCIO MARIA DAL FABBRO, JULIO SORIANO, RENATO LAURENTI</b> COMPARISON BETWEEN MOIRÉ AND HOLOGRAPHY AS PHOTOELASTIC METHODS IN STRESS DISTRIBUTION DETERMINATION	168 – 172
<b>JONATHAN GAZZOLA, INÁCIO MARIA DAL FABBRO, JULIO SORIANO, SILVESTRE RODRIGUES</b> SHADOW MOIRÉ TECHNIQUES APPLIED TO STRESS DETERMINATION ON METALLIC BEAMS UNDER FLEXURAL LOADS	173 – 177
<b>DAVOUD GHANBARIAN AND ROOHOLLAH FARHADI</b> COMPARISON OF CONVENTIONAL REGRESSION METHODS AND ARTIFICIAL NEURAL NETWORKS FOR POTATO MASS MODELING WITH DIMENSIONAL ATTRIBUTES	178 – 183
<b>DAVOUD GHANBARIAN AND AFSANEH KARAMI</b> COMPACTION BEHAVIOR OF ALFALFA GRINDS	184 – 190
<b>SHAHAM KARIMI-GOOGHARI</b> DAILY PAN EVAPORATION ESTIMATION USING A NEURO-FUZZY-BASED MODEL	191 – 195
<b>IOANNIS GRAVALOS, SPYROS LOUTRIDIS, DIMITRIOS MOSHOU, THEODOROS GIALAMAS, DIMITRIOS KATERIS, PANAGIOTIS XYRADAKIS, ZISIS TSIROPOULOS, ANASTASIOS GEORGIADIS</b> EFFECTS OF THE ROTOR SYSTEM ON BALL BEARING DYNAMIC CHARACTERISTICS	196 – 201
<b>TARAHOM MESRI GUNDOSHMIAN, ASGHAR MAHMOUDI, M. OMID, ADEL HOSAINPOUR</b> SCREENING PISTACHIO NUTS USING A NEURAL NETWORK BASED INTELLIGENT SYSTEM	202 – 206
<b>DAVID HERÁK, ALEŠ SEDLÁČEK, ABRAHAM KABUTEY</b> DETERMINATION OF THE COMPLETE GEOMETRY OF THE WORM EXTRUDER SCREWLINE FOR COMPRESSIVE PRESSING OF THE OIL BEARING CROPS	207 – 210
<b>PETR HERMÁNEK, ADOLF RYBKA, IVO HONZÍK, BOHUSLAV JOŠT</b> ANALYSIS OF CUTTING MECHANISM ON THE CUTTER USED FOR HOPS GROWN ON LOW TRELLIS	211 – 215
<b>PETER HLAVÁČ</b> TEMPERATURE DEPENDENCIES OF MILK DYNAMIC VISCOSITY DURING STORAGE	216 – 221
<b>ADEL HOSAINPOUR, MOHAMMAD H. KOMARIZADE, ASGHAR MAHMOUDI, TARAHOM MESRI GUNDOSHMIAN, MAHROKH G. SHAYESTEHI</b> HIGH SPEED DETECTION OF POTATO AND CLOD USING AN ACOUSTIC BASED INTELLIGENT SYSTEM	222 – 227
<b>PETR HRABĚ, ROSTISLAV CHOTĚBORSKÝ, JURAJ RUŽBARSKÝ, JOZEF ŽARNOVSKÝ</b> COMPARISON OF HIGH CHROMIUM AND BORIDE HARDFACING	228 – 231
<b>JOSEF HULA, PAVEL KOVARICEK</b> WATER INFILTRATION INTO SOIL AND SURFACE WATER RUNOFF IN MAIZE GROWING BY THREE CULTIVATION TECHNOLOGIES	232 – 235

<b>LADISLAV CHLÁDEK, MIROSLAV PŘIKRYL, PETR VACULÍK, JAN MALAŤÁK, ONDŘEJ SUCHÝ</b> POSSIBILITIES OF THE VERIFICATION OF THE EFFICIENCY OF SANITATION PROCESS IN AGRICULTURAL AND FOOD INDUSTRY	236 – 240
<b>JERZY CHOJNACKI</b> THE RESISTANCE OF BENEFICIAL NEMATODES TO LIQUID STATIC PRESSURE	241 – 243
<b>ROSTISLAV CHOTĚBORSKÝ, ABDUL HAMID RUSUL, MONIKA NAVRÁTILOVÁ, PETR HRABĚ</b> EFFECTS OF WELDING PROCESS PARAMETERS ON THE GEOMETRY AND DILUTION OF THE BEAD IN THE AUTOMATIC SURFACING	244 – 247
<b>KOJI INOOKU, TOMOHIKO OTA, SUMIHIKO MIYAHARA</b> REDUCTION OF CHEMICALS DRIFT IN FRUIT ORCHARD IN JAPAN	248 – 253
<b>PETR JEVIČ, ZDEŇKA ŠEDIVÁ, JAN MALAŤÁK</b> SPECIFICATION AND CLASSES OF SOLID BIOFUELS IN EUROPEAN STANDARDS	254 – 262
<b>VLADIMÍR JURCA, VERONIKA VITKOVA, ZDENEK ALES</b> COMPUTERIZED MAINTENANCE MANAGEMENT SYSTEMS IN AGRICULTURE	263 – 268
<b>BOLESLAV KADLEČEK, MIROSLAV RŮŽIČKA, LADISLAV PEJŠA</b> THE METHOD OF FUEL CONSUMPTION INDIRECT QUANTIFICATION	269 – 273
<b>BOLESLAV KADLEČEK, MIROSLAV RŮŽIČKA, LADISLAV PEJŠA</b> THE MEASUREMENT OF VEHICLES' DRIVE DYNAMICS	273 – 277
<b>BOLESLAV KADLEČEK, MIROSLAV RŮŽIČKA, LADISLAV PEJŠA</b> THE CALCULATION OF FUEL CONSUMPTION IN RELATION WITH VEHICLES' DYNAMICS	279 – 284
<b>AIVARS KAKITIS, IMANTS NULLE, DAINIS ANCANS</b> STALK MATERIAL ORIENTATION IN BIOMASS COMPOSITE BRIQUETTES	285 – 290
<b>KÁRA JAROSLAV, ADAMOVSKEJ RADOMÍR, RUTKOWSKI KAZIMIERZ</b> CURRENT STATUS AND PROSPECTS OF BIOGAS TECHNOLOGY IN THE CZECH REPUBLIC	291 – 295
<b>HASSAN KARIMI, HOSSEIN NAVID, ALI ROSTAMI, ADEL TAHERI-HAJIVAND</b> DESIGN AND FABRICATION OF "GRAIN LOSS MONITORING SYSTEM" IN COMBINE	296 – 301
<b>AKOS KERTESZ, ESZTER VOZARY, ZUZANA HLAVACOVA, LENKA PRIATKOVA</b> CHANGES IN MOISTURE CONTENT AND ELECTRICAL IMPEDANCE OF CARROT SLICES DURING DRYING	302 – 306
<b>V.V. KHARCHENKO, B.A. NIKITIN, P.V. TIKHONOV</b> ESTIMATION AND FORECASTING OF PV CELLS AND MODULES PARAMETERS ON THE BASIS OF THE ANALYSIS OF INTERACTION OF A SUNLIGHT WITH A SOLAR CELL MATERIAL	307 – 310
<b>PAVEL KIC, LADISLAV CHLADEK</b> MICROCLIMATE IN TUTORIAL AND RESEARCH BREWERY DURING WINTER SEASON	311 – 315
<b>LIBOR KOPECKÝ</b> RELIABILITY IN THE PRODUCTION LINES	316 – 321
<b>GEORGI KOSTADINOV, MILENA MOTEVA</b> OPTIMUM USE OF THE IRRIGATIONAL WATER IN A MAIZE (GRAIN) FIELD	322 – 328
<b>PAVEL KOVAŘÍČEK, KAROLÍNA MAREŠOVÁ, JOSEF HŮLA, MILAN KROULÍK, MARCELA VLÁŠKOVÁ</b> EFFECT OF SOIL LOOSENING INTENSITY ON WATER RUNOFF RATE UNDER SIMULATED RAIN CONDITIONS	329 – 333
<b>ANNA KRAKOWIAK-BAL</b> SPATIAL DIFFERENTIATION OF THE INFRASTRUCTURAL EQUIPMENT OF RURAL AREAS IN POLAND	334 – 337
<b>ANDRIS KRONBERGS, ERIKS KRONBERGS, MAREKS SMITS AND ELGARS SIRAKS</b> INVESTIGATION OF COMMON REED CUTTING METHODS	338 – 342
<b>MILAN KROULÍK, VÁCLAV BRANT, JIŘÍ MAŠEK, PAVEL KOVAŘÍČEK</b> INFLUENCE OF SOIL TILLAGE TREATMENT AND COMPOST APPLICATION ON SOIL PROPERTIES AND WATER INFILTRATION	343 – 349
<b>JOSEF KRUPÍČKA, BLAHOŠLAV HANOUSEK</b> GRANULOMETRIC STUDY FERTILIZERS SUPERPHOSPHATE	350 – 352
<b>KAREL KUBÍN, MARTIN PEXA</b> EVALUATION OF TRANSPORT PROCESSES IN AGRICULTURE	353 – 358
<b>FRANTIŠEK KUMHÁLA, VÁCLAV PROŠEK</b> THE SENSITIVITY OF CAPACITIVE THROUGHPUT SENSOR ON MEASURED MATERIAL MOISTURE CONTENT CHANGES	359 – 362
<b>FERNANDO KUNINARI, CELINA DE ALMEIDA, INACIO MARIA DAL FABBRO, ENRICO DI RAIMO, ADILSON MACHADO ENES</b> SHAPE DETERMINATION OF TOMATO FRUITS ( <i>Lycopersicon esculentum</i> Mill) BASED ON MOIRÉ METHODS	363 – 367

<b>MARTIN KÜNZEL, BŘETISLAV BENDA, GUNNAR KÜNZEL</b> MEASURING OF CONDUCTING POLYMER PROPERTIES	368 – 372
<b>KVESITADZE G., SADUNISHVILI T., DUDAURI T., METREVELI B., PARTSKHALADZE G., UGREKHELIDZE V.</b> FERMENTATION OF CELLULOSE AND HEMICELLULOSE CARBOHYDRATES TO ETHANOL AND HYDROGEN BY ANAEROBIC SACCHAROLYTIC BACTERIA	373 – 377
<b>ZDENĚK KVÍZ, ADOLF RYBKA, MARTIN TACHECÍ</b> POSSIBILITIES OF POTATO TUBERS YIELD MONITORING IN POTATO HARVESTING TECHNOLOGIES	378 – 3832
<b>JANIS LACEKLIS-BERTMANIS, ERIKS KRONBERGS, EDGARS REPSA</b> IMPLEMENT TRANSPORT IMPACT ON HITCH-SYSTEM PRESSURE OSCILLATION	383 – 388
<b>JANA LENDELOVÁ, ŠTEFAN MIHINA, ŠTEFAN POGRAN</b> ANALYSE OF UTILISED BEDDING MATERIALS IN CUBICLES	389 – 393
<b>MARTIN LIBRA, PETR SEDLÁČEK, JAN MAREŠ, VLADISLAV POULEK</b> COMPARISON OF PV SYSTEMS WITH FIXED AND ADJUSTABLE INCLINATION OF PV PANELS	394 – 397
<b>RADEK LISKA, PAVEL KIC</b> DRYING PROCESS OF POULTRY MANURE AT VARIOUS TEMPERATURES	398 – 400
<b>ALEKSANDER LISOWSKI, MAGDALENA DĄBROWSKA, MICHAŁ SYPUŁA</b> CHARACTERISTICS OF PARTICLES OF MILLED ENERGETIC PLANT MATERIAL	401 – 405
<b>S. LOUTRIDIS, I. GRAVALOS, D. MOSHOU, TH. GIALAMAS, D. KATERIS, P. XYRADAKIS, Z. TSIROPOULOS</b> DIAGNOSIS OF GEARBOX FAULTS IN AGRICULTURAL MACHINERY USING ENERGY OF TRANSIENT FEATURES	406 – 409
<b>MARIAN LUKEŠ, MICHAŁ KOSTELECKÝ</b> TRANSPORT LINKS IN THE EDUCATIONAL CENTRES	410 – 414
<b>MIROSLAV MACAK, LADISLAV NOZDROVICKÝ</b> PHOTO-OPTICAL IMAGE ANALYSIS AS AN ALTERNATIVE METHOD FOR DETECTION OF THE FERTILIZER PARTICLE SIZE DISTRIBUTION	415 – 420
<b>MALÁŤÁK JAN, PETR JEVIČ, PETR VACULÍK</b> EVALUATION OF SMALL COMBUSTION EQUIPMENTS FOR SOLID BIOMASS	421 – 428
<b>JIRÍ MAŠEK, MILAN KROULÍK, ZDENĚK KVÍZ, PAVEL PROCHÁZKA</b> CONSERVATION SOIL TILLAGE TECHNOLOGIES	429 – 433
<b>PETR MILER, JAN HROMÁDKO</b> ECOLOGICAL BENEFIT OF FUEL E50	434 – 437
<b>MIROSLAV MIMRA, VLASTIMIL ALTMANN</b> THE EFFECT OF COMPOSTS APPLICATION ON SUGAR BEET	438 – 441
<b>TOTKA MITOVA, MILENA MOTEVA, VALENTIN KAZANDJIEV, VESKA GEORGIEVA, GALIN GANCHEV</b> CLIMATIC RISKS FOR RAPESEED (BRASSICA NAPUS, L.) PRODUCTION IN BULGARIA	442 – 447
<b>DIMITRIOS MOSHOU, DIMITRIOS KATERIS, IOANNIS GRAVALOS, SPYROS LOUTRIDIS, NADER SAWALHI, THEODOROS GIALAMAS, PANAGIOTIS XYRADAKIS, ZISIS TSIROPOULOS</b> DETERMINATION OF FAULT TOPOLOGY IN MECHANICAL SUBSYSTEMS OF AGRICULTURAL MACHINERY BASED ON FEATURE FUSION AND NEURAL NETWORKS	448 – 453
<b>MIROSLAV MÜLLER, PETR VALÁŠEK, LUKÁŠ TOMEK</b> MECHANICAL PROPERTIES OF POLYMERIC PARTICLE COMPOSITES	454 – 458
<b>MIROSLAV MÜLLER, JURAJ RUŽBARSKÝ, JÁN PAŠKO, JOZEF ŽARNOVSKÝ, PETR HRABĚ</b> THE QUALITY OF CUT SURFACE WITHOUT COOLING	459 – 462
<b>STANISLAVA PAPEZOVÁ, VACLAV PAPEZ</b> PHOTOVOLTAIC POWER SUPPLY FOR A DISTANT STANDPOINT	463 – 467
<b>ILZE PELECE</b> CALCULATIONS AND MEASUREMENTS OF ENERGY GAIN FROM SEMI-SPHERICAL SOLAR COLLECTOR	468 – 472
<b>BOHUSLAV PETERKA</b> DEVICE FOR LONG-TERM DURABILITY TESTING OF TRANSMISSION OILS	473 – 475
<b>MARTIN PEXA</b> MOMENT OF INERTIA OF ENGINE	476 – 481
<b>MARTIN POLÁK, VÁCLAV POLÁK</b> INTRODUCING A PRACTICAL MODEL FOR TURBINES' DESIGNING IN SMALL HYDROPOWER PLANTS	482 – 487
<b>JOSEF POŠTA</b> EXTERNAL PURIFICATION OF HYDRAULIC AND MACHINE OILS	498 – 492



<b>RADEK PRAŽAN, VÁCLAV PODPĚRA</b> THE SIMULATION OF THE ENERGY INTENSITY BY USING THE TWO SECTIONAL SELF-PROPELLED MIXER FEEDER	493 – 498
<b>PATRIK PRIKNER, ZDENĚK ALEŠ</b> ASSESSMENT OF SOIL COMPACTION RISK BY AGRICULTURAL TYRES	499 – 504
<b>MIROSLAV PRIKRYL, JOSEF MALOUN, JIRI KLIMA†</b> THE POSSIBILITIES OF REDUCTION OF MILKING ENERGY COMSUMPTION	505 – 509
<b>PAVEL PROCHAZKA, KROULIK MILAN, JIRI MASEK, HULA JOSEF, PROSEK VACLAV</b> FIELD AERIAL PHOTOGRAPHS TAKING FROM AN AIRCRAFT MODEL	510 – 512
<b>DENIS PRONITSYN, FRANTISEK KUMHALA</b> THE MASS FLOW SENSORS - CURRENT STATE	513 – 516
<b>RAHNAMA MOHAMMAD BAGHER, ZAMZAM ABBAS</b> QUANTITATIVE AND QUALITATIVE SIMULATION OF GROUNDWATER BY MATHEMATICAL MODELS IN AN ARID REGION USING MODFLOW & MT3DMS	517 – 523
<b>JAVAD ROBATI, MEHDI REZAEI, HOSSEIN NAVID</b> ELECTRO HYDRAULIC CONTROL OF AN AGRICULTURAL TRACTOR STEERING SYSTEM ALONG WITH THE SIDE SHIFT CONTROL OF THE ATTACHED ROW CROP CULTIVATOR	524 – 529
<b>MIROSLAV RŮŽIČKA, MARTIN KOTEK</b> TRANSPORT ENERGY USED IN THE SUBURBAN SPACE	530 – 534
<b>ADOLF RYBKA, PETR HERMÁNEK, IVO HONZÍK, KAREL BERNÁŠEK</b> ANALYSIS OF TENSILE STRENGTH OF HOP STRINGS AND THEIR ATTACHMENTS TO HOPFIELD SUPPORTING STRUCTURE	535 – 539
<b>KAMIL SACILIK, Y. BENAL YURTLU, H. GURAN UNAL</b> THIN LAYER CONVECTIVE DRYING AND MATHEMATICAL MODELING OF EINKORN	540 – 548
<b>PETR ŠAŘEC, ONDŘEJ ŠAŘEC</b> YIELDS AND HARVEST LOSSES OF SUGAR-BEET VARIETIES IN THE YEARS 2008 AND 2009	549 – 554
<b>PETR ŠAŘEC, ONDŘEJ ŠAŘEC, MAREK RYNKIEWICZ</b> VARIETY TRIALS OF MAIZE FOR GRAIN IN THE YEARS 2008 AND 2009	555 – 560
<b>PETR ŠAŘEC, ONDŘEJ ŠAŘEC, MILOŠ MALÝ</b> TECHNOLOGICAL AND ECONOMIC PARAMETERS OF WINTER WHEAT PRODUCTION USING DIFFERENT SOIL CULTIVATION METHODS	561 – 566
<b>PETR ŠAŘEC, ONDŘEJ ŠAŘEC, MARTIN KLAIN</b> TECHNOLOGICAL AND ECONOMIC PARAMETERS OF GRAIN MAIZE PRODUCTION USING DIFFERENT SOIL CULTIVATION METHODS	567 – 572
<b>PETR ŠAŘEC, VÁCLAV VOLTR, ONDŘEJ ŠAŘEC</b> TECHNOLOGICAL PROCESSES OF PRODUCTION OF MAJOR FARM CROPS RELATED TO SOIL CONDITIONS IN INDIVIDUAL PRODUCTION AREAS OF CR	573 – 577
<b>JAN SEDLACEK, JIRI DOLEJSI</b> PHYSICAL DESCRIPTION OF COFFEE COOLING IN A POT – PRINCIPLE OF DRINKS COOLING	578 – 583
<b>LIBOR SEVERA, JAN TRNKA, ŠÁRKA NEDOMOVÁ, PAVLA STOKLASOVÁ, JAROSLAV BUCHAR</b> DESTRUCTIVE AND NON-DESTRUCTIVE EVALUATION OF PEACH FIRMNESS	584 – 587
<b>HIROSHI SHIMADA, EIKICHI SHIMA, KATSUYUKI TANAKA, TAKESHI NAGAYOSHI, MITSUHIKO KATAHIRA</b> PERSONAL REMOTE SENSING SYSTEM FOR PRECISION FARMING	588 – 593
<b>VLADIMÍR ŠLEGER, PAVEL NEUBERGER, MARTIN POLÁK</b> CLIMATIC CONDITIONS FOR DESIGNING HEATING/COOLING SYSTEM	594 – 597
<b>STREBKOV D.S., SVENTICKIY I.I., ZHMAKIN I.K., KOROLEV V.A., MUDRIK V.A.</b> THE OPTIMUM MANAGEMENT IN THE AGRARIAN PRODUCTION AND NATURE-USE ON THE SELF-ORGANIZATIONAL BASE	598 – 602
<b>DARIUSZ TOMKIEWICZ</b> APPLICATION OF THE METHOD OF DYNAMIC MODEL IDENTIFICATION FOR GRAIN WATER CONTENT ESTIMATION	603 – 607
<b>TRNKA JAN, STOKLASOVÁ PAVLA</b> OPTICAL COHERENT METHODS FOR ANALYSING TRANSIENT RESPONSES IN AGRICULTURE PRODUCTS	608 – 613
<b>SIGITA TUNKELE, JĀNIS MĀRCIŅŠ</b> VALUE ADDED CHAIN ASSESSMENT OF FOREST INDUSTRY IN LATVIA	614 – 618
<b>PETR VACULÍK, JAN MALAŤÁK, LADISLAV CHLÁDEK</b> RECENT TRENDS IN THE PROCESSING OF CONSTRUCTION AND DEMOLITION WASTE	619 – 622

<b>PETR VALASEK, MIROSLAV MÜLLER</b> STATISTICAL COMPARISON OF THE HARDNESS OF POLYMERIC PARTICLE COMPOSITES WITH A FILLER ON THE BASIS OF WASTE FROM MECHANICAL SURFACE TREATMENT, CAUSED BY GRAVITATION INDUCED SEDIMENTATION	623 – 626
<b>VERONIKA VITKOVA, VLADIMIR JURCA, PETR TULACH</b> LEAN REVERSE LOGISTICS IN BEVERAGES	627 – 632
<b>JAROMIR VOLF, MIROSLAV DVORAK, JOSEF VLCEK</b> PROCESSING OF TACTILE INFORMATION BY USING OF HELMHOLTZ EQUATION	633 – 637
<b>V.VOLTR, Z. HOFMAN, P. ŠAŘEC</b> SOIL RESISTANCE IN THE RELATION TO THE USED TECHNOLOGY OF THE SOIL CULTIVATION	638 – 642
<b>JIRI VONDRICKA, ZDENEK ALES, MARTIN PEXA, VLADIMIR JURCA</b> USING OF INVESTMENT SIMULATIONS FOR PLANNING OF MAINTENANCE	643 – 647
<b>VIKTORIJA ZAGORSKA, ULDIS ILJINS, IMANTS ZIEMELIS</b> CALCULATIONS OF A HEATED FLOOR PANEL FOR PIGLETS RESTING PLACES	648 – 653
<b>JESKO ZANIS, ILJINS ULDIS, ZIEMELIS IMANTS</b> MATHEMATICAL MODEL OF FLAT-PLATE SOLAR COLLECTOR	654 – 659

## Letters

<b>ALTMANN VLASTIMIL, MIMRA MIROSLAV, SALCMAN MILOŠ</b> EVALUATION OF PACKAGING BIODEGRADATION BY COMPOSTING TECHNOLOGY	661 – 663
<b>ALTMANN VLASTIMIL, MIMRA MIROSLAV, KULHÁNKOVÁ ANNA</b> ASSESSMENT OF ECONOMIC IMPACT OF THE SIZE AREA ON PRODUCED COMPOST PRICE	664 – 667
<b>VÁCLAV BERÁNEK, MARTIN LIBRA</b> MONITORING SYSTEM FOR PHOTOVOLTAIC POWER PLANTS	668 – 675
<b>MARTIN CINDR, MARTIN PEXA, KAREL KUBÍN</b> MEASUREMENT OF AGRICULTURAL ENERGY DEVICE POWER PARAMETERS USING GPS	676 – 679
<b>JULIANA APARECIDA FRACAROLLI, ADILSON MACHADO ENES, INACIO MARIA DAL FABBRO, SILVESTRE RODRIGUES</b> MONITORING PAPAYA (CARICA PAPAYA) RIPENING THROUGH BIOSPECKLE TECHNIQUES	680 – 684
<b>VACLAV LEGAT, ZDENEK ALES</b> EXPECTED TRENDS IN DEPENDABILITY MANAGEMENT WITHIN AGRICULTURAL ENGINEERING AND MANUFACTURING	685 – 690
<b>LARISA MAJINOVSKA, ANETE MEŽOTE</b> COMMUNICATION SKILLS OF ENGINEERING STUDENTS	691 – 695
<b>Y. BENAL YURTLU, KERIM EKMEKCI, ELCIN YESILOGLU, BAHADIR DEMIREL, HUSEYIN SAUK</b> SAFER AGRICULTURE FOR EMPLOYEES IN RURAL	696 – 698







## AGRICULTURAL ENGINEERING AND THE COMPLEXITY OF MULTI-SCALE PROCESSES

JOSSE DE BAERDEMAEKER

Professor

Katholieke Universiteit Leuven,

Department of Biosystems, division MeBioS- Mechatronics, Biostatistics and Sensors

Kasteelpark Arenberg 30 , B3001 LEUVEN (Heverlee), Belgium

[Josse.debaerdemaeker@biw.kuleuven.be](mailto:Josse.debaerdemaeker@biw.kuleuven.be)

### INTRODUCTION

Agricultural production is also part of a long chain of activities that starts from the seeding (or even earlier) and stretches all the way to the consumer. There are also needs for technology development because of the need to reduce land degradation or to optimize water use. The (bio)technological revolution, genetically modified crops or crops for green chemicals need different planting, tending, harvesting and handling equipment. Society has high expectations from these activities, but at the same time they are more and more subjected to international agreements on trade. This makes that competition between producers or regions of production becomes an important item in decision making. Nevertheless this competition should not impair food safety to consumers or long term food security for society. They should meet consumer expectations in terms of quality, safety and also value or price. Many intermediate steps are involved and these often involve handling, storage and transportation across national borders or continents. Information should be transferred across this chain.

The automation that will be a major part of the future agricultural and biological production systems also faces some challenges posed by the systems characteristics that will have to be dealt with.

When we look at the processes in agricultural production systems then we can say that they are *complex in nature*. Indeed, as we gain a better understanding of biological processes we also find that they have a great complexity and that in many cases this complexity remains difficult to formulate in exact terms.

The complexity also arises from the fact that *processes occur on different scales*, from molecular or sub-cellular processes to organs, fruits or seeds, and to fields or regions. Besides these spatial scales, there are also different time scales involved.

The *dynamic systems* models that we intend to use must take these different scales into account. Furthermore, these processes have a *time variable behavior* which adds to the difficulty to model or control them or to design suitable equipment.

The processes are *very variable* (natural variability of biological processes) and they are also subjected to *many disturbances*, most of which are unpredictable. Again this complicates the design and control of equipment.

### MULTI-SCALE PROCESSES IN PLANTS

When looking at crops then processes are taken place on a nanometer scale (for example the transfer properties across cell walls) up to a scale of several meters and beyond when looking at plants or even fields. In these scales there are processes at the cell wall level, the cells and the intercellular space, the gas exchange at the plant level or nutrient exchange at the field level. The time scales to study the transport phenomena are also very different. Aquaporins are proteins embedded in the cell membrane that regulate the flow of water. Up to one billion water molecules can pass through a single aquaporins channel each second. The opening or closing of stomata, the evapo-transpiration or the gas exchange of a plant or a field can be observed over seconds or over days. These processes certainly affect growth of single plants and thus also crop production in a

field or part of a field. Understanding these processes at a very small scale will contribute to better control processes at a macro scale. Also, the knowledge about processes at lower scales can be assembled to a higher scale and this in space as well as in time. On the other hand, processes that are or can be observed at a higher scale may give information about underlying important physical and physiological process at a small scale. For example, an increase in leaf temperature is an indication that evapo-transpiration is reduced, that stomata are closed most of the time, that gas exchange is reduced. This reduces photosynthesis. Of course, the reduction of water loss also indicates that water supply by the roots is insufficient. The water stress will limit the crop growth. Observations of the leaf temperature tell something about what is happening in a number of processes in and outside the plant. In this way one can introduce the concept of 'speaking plants' as a tool in precision crop production (Morimoto and Hashimoto, 2009). Different locations in a field may in this case have different signals implying that 'speaking plants' provide spatial variability information. Even when the same signals are observed in different locations, the underlying processes that lead to the signals may be different and one probably needs additional observations or sensors to detect the processes that cause the variability and to set up a strategy for process control.

### **MULTI-SCALE PROCESSES IN SOILS**

Heterogeneity of soils within fields is generally accepted as one of the driving factors for site specific farming as is expressed by the concept of 'farming by soil type'. Good mathematical or statistical models have been developed to describe the spatial soil variability over the area of a field. In most cases this mathematical description is only done in two dimensions, while incorporating the soil profile as a third dimension is a bit more complicated. There are a large number of soil properties that can vary across a field. They can relate to water, to fertility (NPK, secondary nutrients and micronutrients), the soil chemistry (salinity, cation exchange capacity, organic

matter), physical properties (texture, compaction) or topography.

Looking at some of the processes, one can start with the spatial soil texture variability that can be noticed across fields. This texture variability leads to variability on moisture-holding capacity and in drainage rates for water. Coarse-textured sandy soils have a lower moisture-holding capacity due to high porosity and drain excess water quicker than fine-textured soils. Fine-textured soils, loam or clay soils, have a higher moisture-holding. Soil texture and soil drainage class variability leads to variability in available water for crop growth. In addition, the water drainage also affects the movement of nutrients, the soil temperature and the biological processes related to soil organic matter conversions. Indeed, here again we find spatial variability (texture) that is combined with variability in time (conversion rate) and ultimately affects crop growth. Looking at a smaller scale (square meters or smaller, rather than hectares) then the soil structure and structure stability can vary. For example we find a large variation in pores from macro pores to micro pores. These are related to texture, soil organic matter and also earthworm activity. This description of all processes that are ongoing in the soil is very incomplete and is only intended as a simple example of processes in the soil that happen at different spatial and temporal scales. Also here it will not be possible to involve all these processes to come to a useful precision management system. However, knowledge of these scale effects can contribute to setting up good monitoring schemes (for example soil sampling or soil sensors) and to interpretation and control of crop growth and yield

### **MODELLING VARIABILITY FOR CONTROL OF FIELD MACHINERY**

During field operations with machinery there are often various processes ongoing at the same time and all require attention or control actions. It is necessary to measure the actual inputs and outputs of these processes and preferably also the different states. Based on these measurements and on other (theoretical) knowledge a process model

can be build. This maybe very useful for process simulations but it also can be the basis for model based (predictive) control.

An interesting example here can be the optimal control processes in a combine harvester.

As expected, it has been observed in field trials that a relation exists between the feedrate of crop into the harvester and the losses from the straw walkers. This relationship is very variable, not only during the harvesting season but also in the course of one day or over the different positions in a field. They are due to above described spatial variability of underlying processes. They show up as variable crop conditions such as ripeness, grain/straw ratio, moisture content, threshability, etc. Using the advanced measurement systems that are currently under development for field machinery, one can come to on-line modelling of the crop or field condition, for example during harvest. The current threshability or crop density entering the machine is the basis for estimating or modelling the crop conditions in nearby areas such that for the next strip to be harvested the machine has early information on what is coming and automatic adjustment can be started. This model is then one of the ingredients in the optimization of some harvesting processes. This approach has the psychological advantage that the machine seems to be responding to crop conditions in a way similar to an operator who has the same information based on his visual perception..

## **DEALING WITH UNCERTAINTY IN PROCESS CONTROL**

Biologically inspired modeling and control algorithms like neural networks, genetic algorithms or photosynthesis based algorithms have been used for some time now and it appears that more applications of such biological phenomena will evolve for processes that are very complex for rigorous mathematical modeling. They may also be very suitable for applications in stochastic processes or where there are many uncertainties. In the latter case Model-based Predictive Control is another approach.

Indeed, as shown above, one of the main challenges of controlling agricultural equipment is the close interaction between the system and the biological variation of the crop in the field which influences the process input. We will again discuss this using a combine grain harvester as a test case, but it can easily be extended to most equipment used in agriculture. In combine grain harvesting there is the interaction of crop characteristics with the cutting, threshing and separation processes in the machine. Moreover, a machine such as a combine harvester contains nonlinearities which cause any linear model to depend on the current working point. Due to this spatio-temporal variability of the system (and of the crop), the model uncertainty is just as important as the model itself. Time-varying, uncertain systems form a very important model class. A lot of work has been done to make control systems robust to model uncertainties, but most of these approaches started from a deterministic point of view. In view of the importance of constraints and disturbance prediction, Model-based Predictive Control (MPC) is a well-suited control methodology for this application.

An extension to MPC to deal with stochastic information (information about uncertainties) is derived as a form of so-called Stochastic MPC. Stochastic MPC is implemented and extensively tested on several real-life control problems of uncertain systems in the area of agricultural automation. Stochastic MPC can greatly simplify one of the major challenges of control theory in practice, namely tuning. The methodology enables an automatic correction of the trade-off between control error and input effort depending on the actual plant condition. This allows swift, aggressive control if the model uncertainty is small, without compromising on stability in situations where the model is less accurate.

## **SYNERGISTIC CONTROL FOR PRODUCTION AGRICULTURE**

The data that are available can also be used in mathematical system models that lead to decision and control models. The models help to interpret variable and uncertain data as an input to the

decision making and they are a vital element to get strong solutions based for example on the use of soft sensors.

It is not clear at this moment that for each spot or homogeneous zone in a field sufficient information is available on potential production levels and therefore on required inputs. To have precise information in space and time on potential production is one of the main challenges of precision agriculture. Indeed, up to now the decisions are mostly based on experience and on data averaged over conditions involving many fields and many years. Bouma (1997) regards the “reactive” options for precision crop treatments as attractive if the required sensors are available. However a major limitation is the fact that stress phenomena have to be present and observed. For example, the information provided by the optical sensors for crops is biased by factors other than N. To overcome this obstacle to detect N deficiency, normalization procedures such as the well-fertilized reference plot, the no-N reference plot, and relative yield are often used (Samborski et al., 2009). For the “proactive” approach computer simulations can be used to estimate crop growth and solute fluxes. Of course good weather predictors are needed. In that case a risk assessment for example for nitrate leaching can be carried out. It is clear that in the future a combination of “reactive” and “pro-active” decision making will be implemented.

Given the multitude of processes and of sensors, the optimization of the crop production can be considered as multivariate process control where different production parameters can be studied and monitored simultaneously and combined in a single control chart (Mason and John Young, 2002). In this approach the mentioned simulation models can be used to estimate the crop growth and to handle the time-variable characteristic of the crop. The model can be pure mechanistic but can also be constructed on the basis of data from a process that is clearly ‘in control’. These data can be from historic records or from the current process. The control chart is used to test, on the basis of further measurements, if the process remains in control. If so, then these

data points can be used for model updating. The main application of such control charts appears to be for process changes over time, but perhaps it can also be used for spatial variability analysis and decision making. For example sensors on a fertilizer spreader detect chlorophyll content of leaves and the measured data are online analyzed to for real out-of control situations arise where the application rate has to change. This can be done on-line, but in a similar way the data can be used for off-line process control decisions.

## BIOLOGICAL AND TECHNOLOGICAL PROCESS ENGINEERING

Technological developments have sometimes evolved based on solid knowledge of the physics of the processes, while in other cases their development was hindered by long established cultivation methods. A few examples are given here.

Robotic harvesting of fruit, for example tomatoes, cucumbers, apples has been under development for some time. It turns out that a real breakthrough was only possible when new growing systems were adapted such that fruit becomes more accessible to vision sensors and to gripping systems. This may seem obvious to engineers, but it requires a new approach to crop maintenance like leaf and shoot pruning and shaping of the plant which is not obvious at first glance. We can expect that similar new cropping systems will be required to make progress in automation of the harvest of fruits like apples, pears, oranges, grapes and others.

Fruit damage has for a long time being treated using engineering mechanics on the basis of Hertz contact theory and failure stresses. The discoloring of the bruised area is the most visible indication of the mechanical damage. Recent research on tomato damage however indicates that shocks or other mechanical loads can also trigger enzymatic activity with no obvious visible damage. This enzymatic activity goes on at a different scale, but it weakens the tissue, causing what may be called a delayed effect of the mechanical action.

The two examples show that automation of processes requires also the modeling or control of

underlying physiological or biochemical processes at different spatio-temporal scales.

## BIOMIMETICS

Living organisms have themselves very elaborate sensing and control systems. It is then no surprise that engineering looks at these organisms to learn or to borrow from these living organisms. This is the area of biomimetics, which can be seen either as biology inspired design or as biology inspired modeling and control. The biology inspired design can be novel materials like for example spider web materials or nanoparticle surface coating that is inspired by the self-cleaning water repellent behaviour of the leaf surface of the lotus flower (Bartloth and Neinhuis, 1997 ).

Sensing systems of insects or animals or even plants are also a source of inspiration because of their uniqueness in type or sensitivity or also in the amount of information that is acquired and processed. Insects are able to detect volatiles released by damaged plants in order to find food sources or mating partners. The "biological nose" of insects can be combined with a bioelectronic interface to yield a "bioelectronic nose" (Schütz et al., 2000). Such a bioelectronic sensor system is also very sensitive to detect volatiles at the onset of fungal infection. For precise detection and location of onset of fungal diseases in crops this can lead to interesting applications.

The housefly impresses by its rapid flight feats, which make it so difficult for humans to catch it (Bos et al., 1999). Even from the rear is not to be approached. It has a compound eye. The two half-spherical eyes consist of a multiplicity (approximately 3,000) tiny single eyes. These single eyes are fine-mechanical masterpieces that collect up to two one hundred pictures per second separately allowing for the rapid response and the agile motion of the fly. A biologically inspired artificial compound eyes was already described (Ki-Hun Jeong, 2006). It can serve as inspiration for novel sensing applications in agriculture and food equipment.

## CONCLUSIONS

Automation of agricultural and biological production processes has to consider the phenomena that happen at the different spatio-temporal scales. If these are better understood and can be modeled in an efficient way then new perspectives appear for process design and process control. This is however a formidable challenge for experimentation as well as for modeling. It also requires a close cooperation across engineering and biological disciplines.

The engineering community has already recognized that observing and imitating biological systems can lead to considerable improvements in design of physical systems. Given sufficient support, this may lead to exciting developments that will contribute to the food and fiber supply as well as to a number of other needs of the society.

## REFERENCES

- ASABE Focus on automation technology, Resource, Published by ASABE, The American Society for Agricultural and Biological Engineers, September 2005 and October 2005
- Barthlott W. and C. Neinhuis. Purity of the sacred lotus, or escape from contamination in biological surfaces, *PLANTA* 202 (1): 1-8 MAY 1997
- Bos, F., A. Huber und Y. Lüthi, A work about the connection of biology and technique for Thinkquest 1999, <http://library.thinkquest.org/27468/>
- Bouma J. 1997. Precision agriculture: introduction to the spatial and temporal variability of environmental quality. Ciba Foundation Symposium 210 - Precision Agriculture: Spatial and Temporal Variability of Environmental Quality. © Ciba Foundation 1997.
- Ki-Hun Jeong, Jaeyoun Kim, Luke P. Lee, Biologically Inspired Artificial Compound Eyes. *Science* 312, 557 -561 (2006)
- Lewinger, W.A., C.M. Harley, R.E. Ritzmann, M.S. Branicky, and R.D. Quinn. Insect-like Antennal Sensing for Climbing and Tunneling Behavior in a Biologically-inspired Mobile Robot, IEEE International Conference on Robotics and

Automation (ICRA'05) Video Proceedings, Barcelona, Spain, April 18-22, 2005.

Morimoto T. and Y. Hashimoto. 2009. Speaking plant/fruit approach for greenhouses and plant factories. *Environ. Control Biol.*,47(2):55-72.

Schütz, S., M. J. Schöning, P. Schroth, Ü. Malkoc, B. Weißbecker, P. Kordos, H. Lüth and

H. E. Hummel, An insect-based BioFET as a bioelectronic nose, *Sensors and Actuators B: Chemical*, Volume 65, Issues 1-3, , 30 June 2000, Pages 291-295.

Wang CX, Wang L, Thomas CR, Modelling the mechanical properties of single suspension-cultured tomato cells. *ANNALS OF BOTANY* 93 (4): 443-453 APR 2004



# THE USE OF PRECISION AGRICULTURE IN SOIL MANAGEMENT

RICHARD J. GODWIN\*

Dick Godwin Associates Ltd., 9 Holly Walk, Silsoe, Bedford. MK454DT, UK.

Phone: +44-1525-861053, E-mail: r.godwin@iagre.biz

## Abstract

Soil compaction is a significant problem affecting crop growth, the infiltration of rainfall and tillage energy requirements. It can be exacerbated by the weight of modern farm equipment if sufficient care is not taken. Where possible, preventing compaction – both severity and depth – is preferable to the techniques for remediation. Recommendations are given concerning the general approach to the problem by correct selection of tyre size and inflation pressure and on the benefits of using rubber tracks and operating in controlled pathways. Advice is given on soil remediation methods and techniques for determining the extent of compaction prior to minimising the work, time and costs involved in remediation by targeting the compacted zones.

## Introduction

Soil compaction can be a significant factor in restricting root growth and hence in limiting crop yields (Soane *et al.*, 1981). The degree of soil compaction is generally governed by the strength of soil when subjected to surface loads and pressures from agricultural operations. Soehne (1958) concluded that contact pressure has the greatest influence on the degree of compaction and load and the depth to which it occurs. He also postulated that the greater the speed of the operation the lower the compacting effect. Hence, it is imperative that we do all that is economically feasible to reduce both load and contact pressure. Whilst machine forward speed has increased modern farming operations are still relatively slow.

The contact pressure for pneumatic tyres consists of two components: firstly and most obvious is the tyre inflation pressure recommended by the manufacturer for a given load and speed rating (typical range is 0.5bar to 7bar); secondly is the effect of the carcass stiffness, which was shown by an indirect method to be of the order of 0.5bar for the front tyres of combine harvesters (Plackett, 1984). This has now been replaced using a direct pressure measurement technique at 25mm below the soil surface (Misiewicz *et al.*, 2008). The most recent data indicate carcass stiffness between 0.5 and 0.7bars for rear combine harvester tyres inflated at between 1.0 and 2.5bar, carrying loads of 4.5t.

The critical times for the creation of compaction effects are during establishment of

the crop on previously loosened soil. Problems during harvests, when both harvesting machines and their crop load, can be in the range 30t to 44t. This is especially crucial for late crops such as maize and sugar beet which are harvested in the autumn and winter, when soil moisture contents are high and soil strength is low, but can also be problematic for cereal crops in wet harvest periods such as those that have been experienced recently. Not only are the combine, pea and beet harvesters causes of problems but also the trailers and trucks can be inappropriately equipped with tyres for road and not field use.

Modern equipment can cause compaction problems at depths of 0.4 to 0.6m (Ansorge and Godwin, 2007), which are both difficult and expensive to remediate. They can also reduce infiltration of rainfall and increase the energy for both primary and secondary tillage by factors of 2.5 and 3.25 respectively (Chamen *et al.*, 1992 a & b).

While we should endeavour to manage soil without causing compaction, studies concluded in 1985 by Silsoe College and ADAS showed that in the field centres crop yields only benefited from deep loosening/subsoiling in sandy soils, with spring-sown crops in years of moderate to severe drought (Marks and Soane, 1987). This suggests that subsoiling the headlands, the gateway apron (with care) and significant wheel tracks following harvesters and trailers might have been beneficial. Fortunately, in many sandy loam soils which upon loading tend to form the densest subsoil and do not have the capacity for self rejuvenation in the way of

the cracking clays, former root paths and worm channels can be sufficient for some roots to penetrate to depths beyond the compacted zone.

### Prevention is better than cure

The best strategy for managing compaction is to try to avoid the creation of compact zones in the field by operating with smaller loads, ultra-low contact pressures and well defined traffic lanes. These can be either positively managed as with controlled traffic (Chamen, 2006) or targeted for remediation. Figure 1 shows the range of options available to farmers and growers, all of which are feasible alternatives given the range of operational constraints and many have been tried over the past 30 years. Gentries, whilst technically feasible, have not proven to be commercially viable, probably because they cannot be easily

moved. However, controlled traffic, following the work of Tullberg *et al.* (2003) and others in Australia, is now showing promise in Europe with innovative methods that can accommodate the restrictions caused by narrower roads and high traffic densities (Chamen, 2009).

Linking operations can be beneficial as it can reduce the number of wheel passes. However, there are two constraints: the combination of operations is limited by the speed of the slowest operation; and most soil damage is caused by the first pass of the tractor. The suggested restriction on equipment in excess of 20t in the uncontrolled traffic option has not happened and currently this weight has been significantly exceeded. Wider wheels/tyres, lower inflation pressure and new wheel track systems are left as options to accommodate higher machine weights.

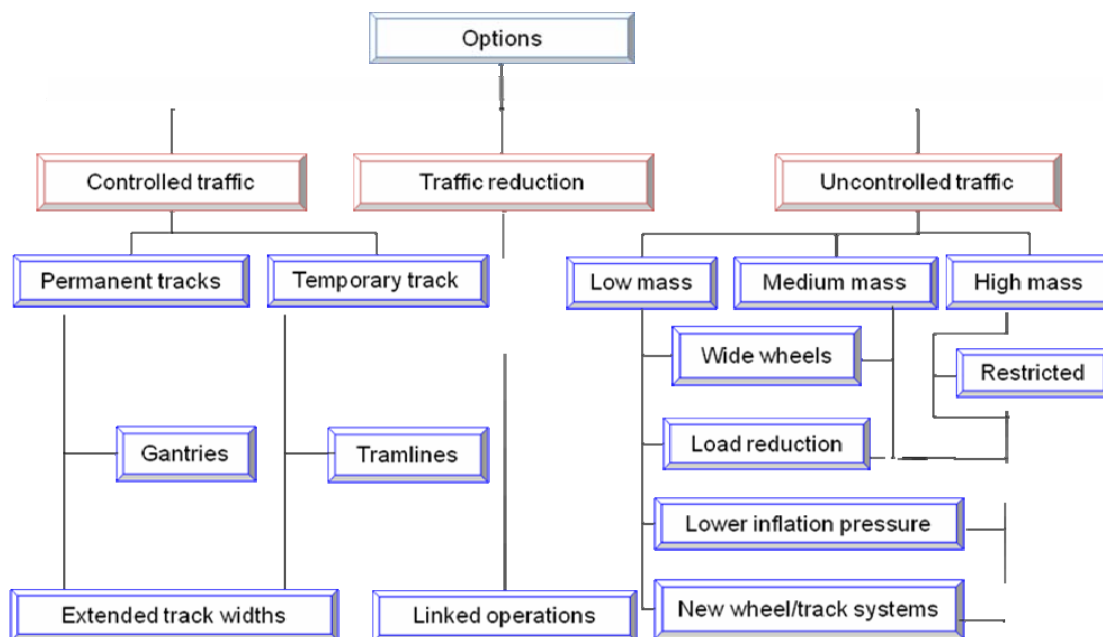


**Figure 1.** Options for controlling compaction (Redrawn by the author from Soane, 1979)

The simplest strategy for the farmer/contractor is to purchase equipment with the largest tyre footprint and lowest safe operating pressure. Recent tyre developments from a number of manufacturers have seen safe inflation pressures at less than 1bar for a number of applications; however there is some evidence that not all equipment manufacturers offer these as original specification options.

Laboratory studies by Dresser *et al.* (2006a) with pea harvester tyres have shown significant reductions in rut depth, depth of deformation and penetrometer resistance when tyre inflation pressure is reduced from the road speed recommendation of 2.25bar to the field speed recommendation of 1bar. The pea harvester case is a good example of where two distinct tyre pressures are required. Operators have been

faced with selecting the road safe option for relatively high transport speeds over the lower slower field operating pressure. The advent of central tyre inflation pressure control systems means that changing tyre pressures on entering and exiting the field is now an option. Parallel field studies showed that the drivers of pea harvesters found the “ride” somewhat uncomfortable at 1bar but increasing the inflation pressure to *c* 1.2bar cured the nausea sensation. The reduction in inflation pressure was also critical in providing additional mobility for the harvesters in the wet summer of 2007 (Wright, C. Personal communication).

As machine sizes have increased it becomes more difficult in parts of Europe to equip tractors and harvesters with dual (or, in North America, triple) tyres because of the constraints of narrow roads and gateways. However, this problem has been overcome by the developments in the rubber belted track. The rubber track enables machines to operate on the road without the special precautions required for steel tracks; it has larger footprint than the equivalent tyre and is narrower which also increases mobility in transport mode. These factors probably explain its success in the UK, where the combine harvester manufacturer Claas reports that the majority of all combines sold where rubber tracks are an option are equipped with them (Tyrell, T. Personal communication). The Claas marketing department would say this is at a cost of Euro1.25 for every hectare harvested over the life of the machine.

Recently reported laboratory work by Ansoorge and Godwin (2007 and 2008), compared a range of combine harvester front tyres sizes and rubber tracks, both independently and followed by rear tyres of different sizes. Their results showed the near vertical displacement of the soil below both the track and the tyre, with the amount and the depth of displacement for the track significantly less than that of the tyre where the front 900mm wide tyre followed by both the 500mm and 700mm wide rear tyre cause significantly greater disturbance than the track followed by the same two rear tyres. The data clearly show that the depth of compaction is significantly less, resulting in a *c*63% reduction in loosening draught force/energy and cost (Ansoorge, 2007). The results from tyres that were fitted to the

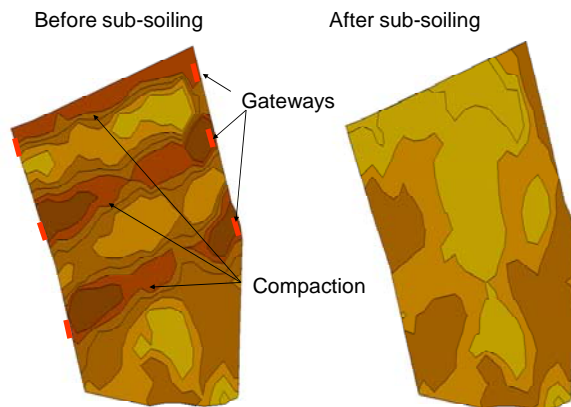
Dominator combine harvester used extensively in the 1970's and 1980's at a gross machine weight of 11t indicate that the current 33t machines on tracks cause similar soil compaction effects to the 11t wheeled combines of some 30 years past. Reducing the load on the rubber track from 12t to 5t significantly reduces soil pressure at 250mm below the soil surface. Hence we should continue to request machine designers to improve their designs by using lighter high strength materials and improved stress analysis techniques to reduce machine weight whilst maintaining ruggedness and reliability.

Studies by Dresser et al (2006b) show that the soil pressure at depths of 250mm resulting from the passage of a loaded road tyre at 7bar inflation pressure that are frequently fitted to trucks and sometimes trailers are significantly higher than the effects of load and pressure for a range of agricultural machines.

The benefits of these preventative measures can be seen in data collected by Cranfield University and The Arable Group at Morley in Norfolk where “normal” operational traffic resulted in a winter wheat yield of 10.84t/ha, zero traffic 12.52t/ha and zero traffic plus a tracked combine 12.14t/ha.

### **Targeting compaction and remediation**

The best indicator of the effects of compaction is the crop and observation of relative crop performance during the growing season is very valuable especially if it is followed by profile pit examination of root growth and development. Typically the poorer areas for crop growth will be gateway margins, headlands (especially those used for turning) and redundant tramlines and temporary roadways as illustrated by the electro-magnetic induction data (EM38) given in Figure 2. As farmers are not excessively keen to dig holes this approach can be used to give an indication of soil variability using selective sampling to determine the cause of variability i.e. whether soil texture or soil structure is causing the variation (Godwin and Miller, 2003).



30 hectare field, scanned 14<sup>th</sup> September 1998 and re-scanned August 25<sup>th</sup> 1999 following sub-soiling in the previous autumn

**Figure 2.** Electro-magnetic induction data from a sandy loam field in Bedfordshire before and after subsoiling, illustrating the effects of compaction in gateways and field traffic between them (Data courtesy of Justin Smith, in Godwin and Miller, 2003).

Vertical penetrometers, whether recording or not, are a useful technique to determine the extent of compaction beyond the profile pits but because of their intermittent nature are very time-consuming. A number of studies (e.g. Chung *et al.*, 2004 and Verschoore *et al.*, 2003) investigated the value of pulling with a tractor a series of horizontal penetrometers through the soil mounted at different depths on a tine leg. Sharifi *et al.* (2007) further developed the ideas of Verschoore *et al.* (2003) by measuring the forces on eight pairs of 50mm high flaps with an included angle of 34° from the soil surface to a depth of 0.40m. The results of an experiment with pea harvesters given in Figure 3 show the effect of depth on the relative forces, where

forces significantly increase with depth and the lower three flaps clearly demonstrate the passage of the pairs of pea harvester wheels/tyres. Very importantly the data clearly show the benefit of operating the pea harvesters with 16psi (1.1bar) over 32 psi (2.2bar) inflation pressures on soil strength and hence remedial tillage forces.

Whilst the work of Sharifi *et al.* (2007) demonstrated the value of this technique as a research method it is some way off being a practical field tool. The authors recommended, using a single pair of flaps mounted on a very narrow subsoiler leg at depths between 0.30 to 0.40m deep. This could, if drawn perpendicular to the prevailing field traffic pattern, with the force data synchronised with that from a global positioning system (GPS), locate the effects of previous wheels passes that are not obvious from the surface. This, however, could become a redundant exercise, as with time, many tractors and harvesters will be equipped with GPS systems with sufficient resolution to locate previous traffic patterns such that navigating subsoiling operations to address the previous compaction zones could be relatively easy. A typical GPS derived traffic pattern, as shown in Figure 4, results from the movement of one of a pair of tractor and trailers supporting two pea harvesters, where the transport truck is located in the top right of the field. The challenge here relates to relative precision of the GPS over a period time in comparison with the width of the subsoiler disturbance. Whilst real time kinematic (RTK) GPS can provide high accuracies, not all operations justify the cost at the current time.

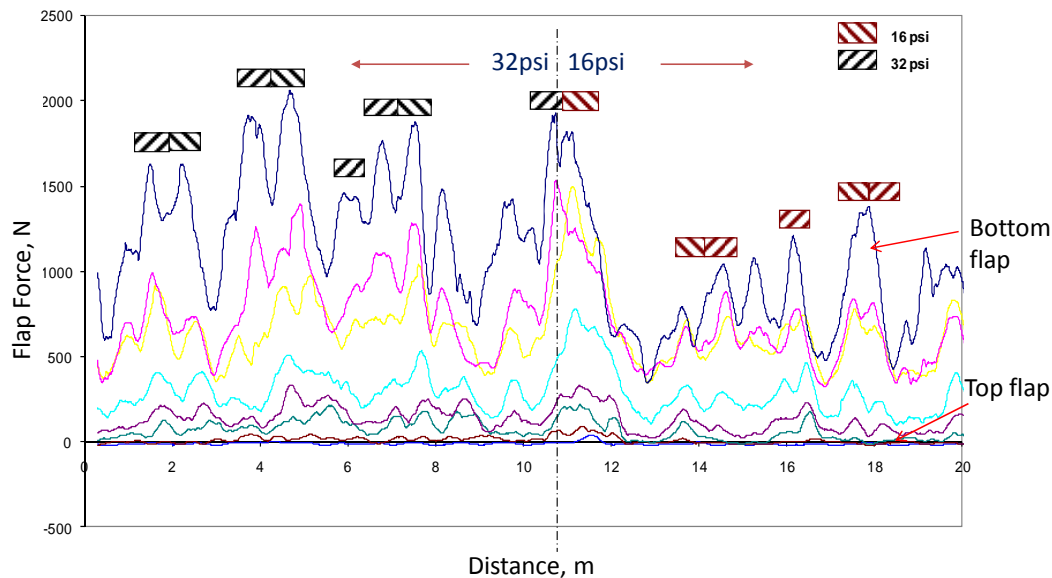
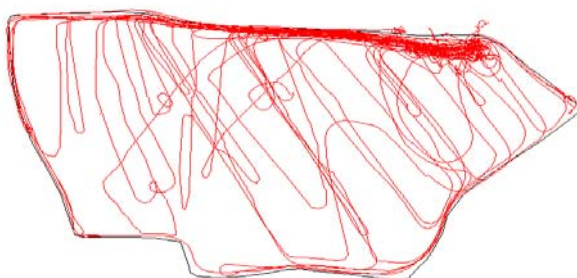


**Figure 3.** Compaction sensor force at a range (50 to 400mm) of depths crossing the wheel tracks of a 30t pea harvester at 32 (2.2bar) and 16 psi (1.1bar) inflation pressures (Sharifi *et al.*, 2007).

This is for only 1 tractor and trailer of a pair:

Field area is 14.8 ha



Tractor wheel marks total 20km (1 tractor)

**Figure 4.** GPS record of a tractor and trailer collecting peas from a harvester and transporting them to a truck in the top right (Data courtesy of Masstock Dalgety/Birds Eye).

As remediation is a relatively expensive operation (c £47/ha: Nix, 2008) it should be carefully targeted and worked into a sensible overall strategy (Spoor, 2006). Loosened soils are weak and hence vulnerable to re-compaction. For effective overall soil loosening the recommendations for the use of subsoilers equipped with wings and leading shallow tines given by Spoor and Godwin (1978) should be followed providing that the soil is not immediately re-compacted by heavy equipment. This technique would be very suitable for the

removal of compaction in the inter-wheel mark zones when controlled traffic systems are being established. A pair of winged subsoiler tines spaced at tractor wheel centres, to match the previous traffic patterns is the most efficient method of removing previous wheel mark effects. Each of these might best be preceded by a pair of very shallow leading tines operating to approximately 150mm within the width of each wheel mark to reduce the size of the resulting soil aggregates. The use of non-winged subsoiler tines should also be investigated where heavy loads are expected soon after loosening; the tines if operated below their critical depth will produce 45° herringbone cracks like those produced by mole ploughs (Godwin *et al.*, 1982) which may be more stable. The same technique linked to GPS guidance would be beneficial for loosening before the establishment of widely spaced row crops. This practice has been recommended in the United States for cotton production.

### Conclusions and recommendations

The following simple guidelines should help to reduce the effects of compaction and assist in the development of good soil management. These follow the strategy that prevention is better than cure and then target the most compact zones, should they require remediation.



1. Do all you can to reduce load and pressure; do not work with under inflated tyres.
2. Spread load where possible; fit the largest sensible tyres or rubber tracks.
3. Keep compaction as shallow as possible as its long-term effects are easier and cheaper to remove: do not operate subsoilers deeper than necessary as this costs energy, time and money.
4. Target problems in gateways and headlands where significant turning has occurred.
5. Minimise random traffic and conduct field work in sensible patterns; consider the use of controlled traffic as suggested by Chamen (2006, 2009).
6. Repair damage, if it occurs, as soon as is practicable.
7. Follow the soil loosening principles given by Spoor and Godwin (1978) and Spoor (2006), but use them carefully. Do not compact freshly loosened and vulnerable soils with subsequent operations.
8. Use the most appropriate technique linked to crop performance and the results of profile pit examination for determining the extent of the compaction problem.
9. Target the compaction problem.
10. Consider the use of GPS guidance systems to remove earlier wheel mark zones and for the establishment of loosened strips for row crops.

### Acknowledgements

This paper is abstracted from a presentation made by the author to the Home Grown Cereals Authority entitled "Precision management of soil compaction and alternative approaches" on the 29<sup>th</sup> October 2009.

### References

1. Ansoorge, D. (2007). Soil reaction to heavily loaded rubber tracks and tyres. Unpublished PhD Thesis, Cranfield University, Silsoe, Bedford, UK.
2. Ansoorge, D., Godwin, R. J. (2007). The effect of tyres and a rubber track at high axle loads on soil compaction, Part 1: Single axle studies. *Biosystems Engineering* 98, 115 -126.
3. Ansoorge, D., Godwin, R. J. (2008). The effect of tyres and a rubber track at high axle loads on soil compaction, Part 2: Multi axle studies. *Biosystems Engineering* 99, 338-347.
4. Chamen, W. C. T. (2006) Controlled traffic on a field scale in the UK. Proceedings of the 17th Triennial Conference of the International Soil Tillage Research Organisation, Kiel, Germany. 845-852.
5. Chamen, W. C. T. (2009) Controlled traffic farming as a tool for reducing in field variation. Precision in arable farming – current practice and future potential. HGCA, Belton Woods, Lincolnshire.
6. Chamen, W.C.T., Vermeulen, G.D., Campbell, D.J. & Sommer, C. (1992a). Reduction of traffic-induced soil compaction: a synthesis. *Soil & Tillage Research*, 24: 303–318.
7. Chamen, W.C.T., Watts, C.W., Leede, P.R. & Longstaff, D.J. (1992b). Assessment of a wide span vehicle (gantry), and soil and crop responses to its use in a zero traffic regime. *Soil & Tillage Research*, 24: 359–380.
8. Chung, S. O., Sudduth, K. A., Plouffle, C., Kitchen, N. R. (2004) Evaluation of an on-the-go soil strength profile sensor using soil bin and field data. ASABE, Paper No. 04-1039, St. Joseph, Michigan, USA.
9. Dresser, M. L., Stranks, S. N., Sharifi, A. & Godwin, R. J. (2006a) Improved Soil Management For Pea Crop Production. Proceedings 17th Triennial Conference International Soil Tillage Research Organization. Kiel, Germany.
10. Dresser, M. L., Blackburn, D. W. K., Stranks, S.N., Dain-Owens, A. P., Godwin R. J. (2006b). Effect of tillage implements and vehicle loads on buried archaeology. Proceedings 17<sup>th</sup> Triennial Conference of the International Soil Tillage Research Organization. Kiel, Germany.
11. Godwin, R. J., Spoor, G., Leeds-Harrison P. B. (1981). An experimental. investigation into the force mechanics and resulting soil disturbance of mole ploughs. *Journal of Agricultural Engineering Research* 26, 477 – 497.
12. Godwin, R. J., Miller P. C. H. (2003). A review of the technologies for mapping within-field variability. *Biosystems Engineering* 84, 393–407.

13. Marks, M. J., Soane, G. C. (1987). Crop and soil response to subsoil loosening, deep incorporation of phosphorous and potassium fertiliser and subsequent soil management on a range of soil types. Part 1. Responses of arable crops. *Soil Use and Management* 3, 115-123.
14. Misiewicz, P.A., Richards, T.E., Blackburn, K., Brighton, J.L., Hann, M.J., and Godwin, R.J. (2008). Techniques for estimating contact pressure resulting from loaded agricultural tyres, ASABE, Paper No. 08-3511, St. Joseph, Michigan, USA.
15. Nix, J. (2008). 38<sup>th</sup> Edition, Farm Management Pocket Book. Wye College.
16. Plackett, C. W. (1984). The ground pressure of some agricultural tyres at low load and with zero sinkage. *Journal of Agricultural Engineering Research*, 29, 159–166.
17. Sharifi, A., Godwin, R. J., O'Dogherty, M. J., Dresser, M. L. (2007). Evaluating the performance of a soil compaction sensor. *Soil Use and Management* 23, 171-177.
18. Soane, D. B. (1979). SAWMA Conference, NCAE, Silsoe, Bedford.
19. Soane, D. B., Dickson, J. W. and Blackwell, P. S. (1979). Some options for reducing compaction under wheels on loose soil, Proceedings 8<sup>th</sup> Triennial Conference International Soil Tillage Research Organization, Stuttgart, 2, 347–352.
20. Soane, B. D, Blackwell, P. S., Dickson, J. W. and Painter, D. J. (1981). Compaction by agricultural vehicles: A review II. Compaction under tyres and other running gear, *Soil Tillage Res.*, 1, 373 – 400.
21. Soehne, W. (1958). Fundamentals of pressure distribution and soil compaction under tractor tyres. *Agricultural Engineering*. 39, 276 -281, 290.
22. Spoor, G., Godwin, R. J. (1978). An experimental investigation into the deep loosening of soil by rigid tines. *Journal of Agricultural Engineering Research* 23, 243–258.
23. Spoor, G. (2006). Alleviation of soil compaction: requirements, equipment and techniques. *Soil Use and Management*, 22, 113-122.
24. Tullberg, J., Yule, D. F., McGarry, D. (2003). 'On track' to sustainable farming systems in Australia. Keynote paper, 16th, Triennial Conference International Soil Tillage Research Organization, Brisbane, Australia.
25. Verschoore, R., Pietrers, J. G., Seps, T., Spriet, Y., Vangeyet, J. (2003). Development of a sensor for continuous soil resistance measurement. Proceedings of European Conference of Precision Agriculture, Berlin, Germany.

## **SIMULATION OF THE PACKING STRUCTURE, LOAD DISTRIBUTION AND FLOW PATTERN IN A 2-DIMENSIONAL MODEL SILO USING DISCRETE ELEMENT METHOD**

J. HORABIK\*, J. WIĄCEK, M. MOLENDĄ

Institute of Agrophysics Polish Academy of Sciences, Lublin, Poland

Phone: +48 81 7445061, Fax: +48 81 7445067, E-mail: j.horabik@ipan.lublin.pl

### **Abstract**

The filling and discharge of a two-dimensional wedged-bottom silo holding circular objects was modeled using Discrete Element Method to determine the influence of the method of silo filling, friction coefficient, viscous dumping and distance to the wall on distribution of orientations of unit vectors normal to contact points and normal contact forces. It was found that packing structure formed through method of generation of grain bedding significantly influenced distribution of contact normal directions. The influence of frictional conditions and number of particles in system on distribution of contact normal directions was analyzed. Increase in number of objects reduced disturbance from boundaries on behavior of assembly. Distribution of loads on silo bottom obtained in simulation for different wall roughness was found in qualitative agreement with experimental data.

### **Introduction**

Storage, handling and processing of granular materials are employed in numerous industries and are of interest to various branches of science and technology such as physics, chemistry, mechanics, agriculture and engineering. Agriculture and the food industry are, next to chemical and pharmaceutical industries largest producers and users of granular materials. Two basic conditions have to be fulfilled by equipment for storage and processing of granular materials: predictable and safe operations and obtaining high quality of final products.

Increasing number of processes and operations involving granular materials have resulted in a growing need for new theory and technology. This was accompanied with growing interest in investigations of physical properties of granular materials. Elaboration of effective design methods of technological processes requires detailed knowledge of physical properties of the processed material as well as proper understanding of their interaction with construction materials. Some macroscopic effects taking place in particulate systems still cannot be properly explained due to the lack of possibility of analyzing inter-particle interactions which are easier to be modeled than measured.

Very powerful tool of modeling behavior of granular solids in micro scale is Discrete Element Method (DEM) proposed by Cundall and Strack (1979) that provides very deep insight

into mechanisms of stress transition and strain formation at the scale of individual particles. The method is based on calculation of forces acting between granules in the system according to Newton's second law of dynamics and determination of velocity and position of each particle through motion integration.

Masson et al. (2000) investigated the geometric properties of assemblies in dependence on mechanical properties of single grains using the DEM. These authors reported an increase in isotropy of contact orientations with an increase in roughness of grains. The influence of vertical silo walls on granular structure in their vicinity was also observed.

In the reported project the 2D simulations of filling and discharge of a silo were performed and analyzed to illustrate effects of bedding structure and different mechanical properties of particles on load distribution. The influence of the method of generation of bedding on the distribution of contact normal directions was examined. The distribution of contact forces acting between grains, as dependent on friction (particle-to-particle and particle-to-wall) and packing structure of the assembly, was examined at the onset of silo discharge.

### **DEM simulations**

The computer simulations were conducted using the 2D DEM code adopted from Wassgren (1997). Discharge process of silos filled with



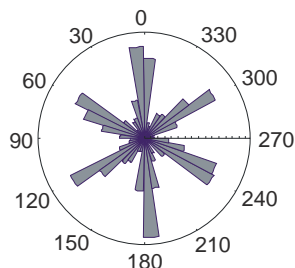
circular elements with diameter uniformly distributed between 1.8 and 2.2 mm was modeled. The linear contact model with the normal and tangential spring constants of  $36.9 \cdot 10^3$  N/m and normal dashpot coefficient of  $1.54 \cdot 10^{-2}$  Ns/m were applied. Simulations were performed for particle-particle  $\mu_p$  and particle-wall  $\mu_w$  friction coefficients of 0.1 and 0.7 respectively with a simulation time step of  $5 \cdot 10^{-6}$  s. The simulations were performed with 2000 particles contained in a 70 mm wide and 120 mm high silo and with 6000 particles in a 120 mm wide and 210 mm high silo (Sykut et al., 2007, 2008). During generation of an assembly particles free to rotate and move were dropped down onto the bottom of the silo under gravitational force. Discharge of the silo into the lower silo of identical geometry was performed through four distributed orifices placed in the flat bottom of silo (sprinkle filling) or one central orifice placed in the bottom of wedge-shaped hopper (central filling) to generate beddings with different packing structure. Central discharge of the lower silo was conducted in the next phase of simulation. During generation of an assembly particles settled with or without global damping in the case of the 2000-particles system. 6000-particles assembly was generated using global damping only. Coefficient of global damping, understood as proposed by Cundall et al. (1979), equal to 0.5, was applied.

## Results

Numerical experiments have shown that simulations with the relatively low number of two-dimensional particles (2000 and 6000) can reflect adequately some effects of behavior of granular assembly observed in physical experiments. The method of filling the silo markedly influenced the geometric structure of

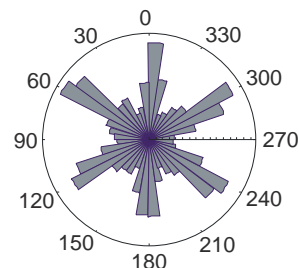
the assembly observed as distribution of vectors normal to contact points. Distribution of directions of vectors normal to contact points was found to be more uniform for 6000 particles than in the case of 2000 particles. This effect may be attributed to the disturbance introduced into the geometrical structure of the assembly by the silo wall that is vanishing with the distance increase. That effect was caused by decreasing influence of walls with an increase in number of particles in the assembly. Orientations of contact normal directions concentrated along three directions forming a nearly hexagonal network in the bedding generated by central filling. The distribution of normal directions was almost hexagonal for smooth particles (Fig. 1a). Increase in the friction coefficient creates the more diffused distribution (Fig. 1b). In the case of the 2000 particles system a slight diffusion of the distribution of contact normal directions was observed when global damping was applied (Fig. 1c). Vertical direction of ordered chains of grains was enforced by the walls in their nearest neighborhood. The particles of the next layer filled spaces created between grains resulting in regular geometric structure of assembly. In the case of sprinkle filling (Fig. 1e) a higher anisotropy of contact normal directions was observed. The most uniform distribution of normal directions at contact points was observed in the case of assemble of 6000 rough particles ( $\mu_p = 0.7$ ) with the global dumping applied during filling procedure (Fig. 1d). All considered factors: the method of silo filling, frictional and viscous dumping and distance to the wall influence the distribution of normal directions in contact points.

a)



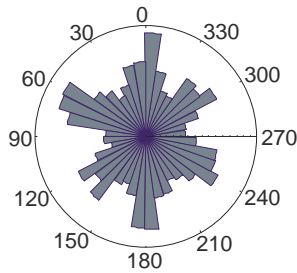
Central filling, 2000 particles,  $\mu_p = 0.1$

b)



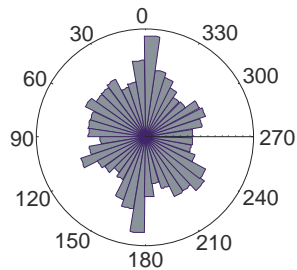
Central filling, 2000 particles,  $\mu_p = 0.7$

c)



Central filling, 2000 particles,  $\mu_p = 0.7$ , global dumping  $\alpha_{gl} = 0.5$

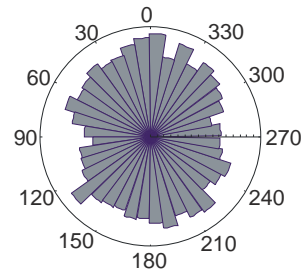
e)



Sprinkle filling, 2000 particles,  $\mu_p = 0.7$

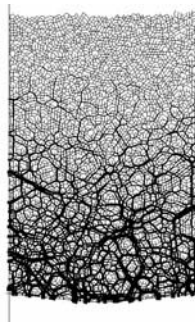
Fig. 1. Distribution of normal directions in contact points (Sykut et al., 2007)

d)



Central filling, 6000 particles,  $\mu_p = 0.7$ , global dumping  $\alpha_{gl} = 0.5$

a)



b)

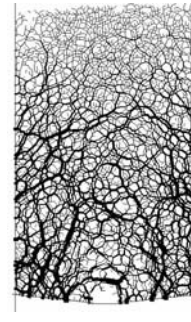


Fig. 2. Contact force transmission after filling the silo ( $N=6000$ ) for: a) smooth ( $\mu_p = \mu_w = 0.1$ ) and b) rough particles and walls ( $\mu_p = \mu_w = 0.7$ ) (Sykut et al., 2008)

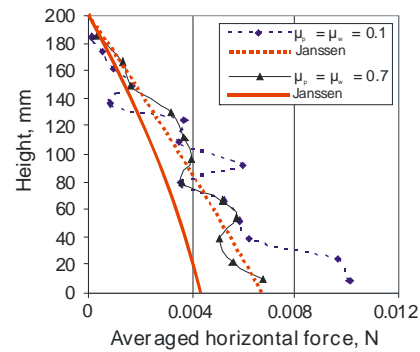
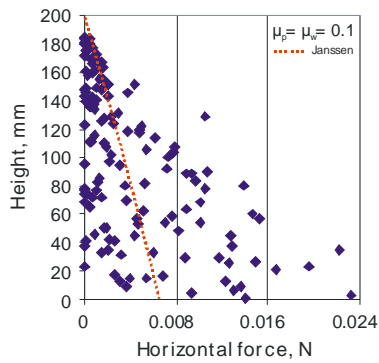


Fig. 3. Wall pressure distribution for smooth and rough particles and walls: DEM simulations and Janssen approach

Frictional conditions were found to modify distinctly the distribution of intergranular forces at the onset of discharge. In the case of  $\mu_p = \mu_w = 0.7$  the extent of region of high contact normal forces was larger than in the case of  $\mu_p = \mu_w = 0.1$  where high intergranular forces concentrated in a region close to the floor (Fig. 2a, b). The high scatter in horizontal forces acting on vertical walls in assembly consisted of 6000 particles with interparticle and particle-wall friction coefficients of 0.1 compared to analytical solution according to Janssen (1895) approach is presented in Fig. 3a. Averaged horizontal forces (Fig. 3b) are in good agreement Janssen approach in upper part of the silo while in the lower part are considerably higher in both cases of friction coefficient. Experimentally determined decrease in the pressure on silo floor with an increase in wall roughness (Molenda et al., 1996) was not observed in numerical simulations.

### Conclusions

1. DEM simulations with a number of 2D elements larger than  $10^3$  can be effectively used for adequate modeling some typical effects of behavior of granular assembly observed in laboratory testing.
2. The method of silo filling, friction coefficient, viscous dumping and distance to the wall influence the distribution of normal directions in contact points. The method of filling markedly influenced the geometric structure of the assembly observed as distribution of vectors normal to contact points.
3. Frictional conditions, i.e. coefficient of friction between particles  $\mu_p$  and wall friction coefficient  $\mu_w$ , were also found to influence markedly the distribution of contact normal directions. In the case of centric filling with  $\mu_p = \mu_w = 0.1$  the directions of contact normal directions formed a nearly regular hexagonal structure. In the case of centric filling with  $\mu_p = \mu_w = 0.7$  the distribution of contact normal directions was more diffuse, with a larger number of the vectors pointing to directions other than the three mentioned above.

### References

1. Cundall P.A., Strack O.D.: A discrete element model for granular assemblies. *Géotechnique*, 1979, 29, 47-65.
2. Janssen H.A.: Versuche über Getreidedruck in Silozellen. *Verein Deutscher Ingenieure, Zeitschrift* (Dusseldorf), 39, 1045-1049, 1895.
3. Masson, S., Martinez, J.: Effect of particle mechanical properties on silo flow and stress from distinct element simulations. *Powder Technology*, 2000, 109, 164-178.
4. Molenda M., Horabik J., Ross I.J.: Effect of filling method on load distribution in model grain bins, *Transactions of the ASAE*, 1996, 39, 219-224.
5. Sykut J., Molenda M., Horabik J.: Discrete Element Method (DEM) as a tool for investigation of granular materials' properties. *Polish Journal of Food and Nutrition Sciences*, 2007, 57(2A), 169-173.
6. Sykut J., Molenda M., Horabik J.: Influence of filling method on packing structure in model silo and DEM simulations. *Granular Matter*, 2008, 10, 273-278.
7. Wassgren C.R.: Vibration of granular materials. Unpublished PhD Thesis, Pasadena, California, USA: California Institute of Technology, 1997.

## ANALYSIS OF THE EFFECTS OF THE MACHINE LIFE-TIME ON THE DIRECT UNIT COST AND MINIMAL ANNUAL USE OF THE FIELD MACHINES IN TRACTOR-MACHINE SETS

MIROSLAV KAVKA<sup>1\*</sup>, LADISLAV NOZDROVICKÝ<sup>2</sup>, FRANTIŠEK KADLEC<sup>3</sup>,  
MIROSLAV MIMRA<sup>1</sup>

<sup>1</sup>Czech University of Life Sciences in Prague, Faculty of Engineering, Prague – Suchbát

<sup>2</sup>Slovak University of Agriculture in Nitra, Faculty of Engineering, Nitra

<sup>3</sup>Czech University of Life Sciences in Prague, University Farm in Lány

### Abstract

Minimal annual use of the field machine can be generally considered as point where profit brought by machine operation in the set with tractor is equal to zero. That point determines the usefulness of the machine acquirement in comparison with the using of the contract to provide the field operation. The value of minimal annual use is effected by operational costs and estimated life-time of the machine. In a paper there is presented the analysis of the effects of life-time of field machines and power unit on the direct unit costs and minimal annual use of machine-tractor sets. The analysis is related to the tractor John Deere 8320 used with the machines for soil tillage operations in conditions of University farm in Lány.

**Key words:** machine-tractor sets, costs, machine annual use

### 1. Introduction

The control of machinery costs is a key factor in improving the profitability of a farm (LANDERS, A., 2000). Minimal annual use of the field machine can be generally considered as point where profit brought by machine operation in the set with tractor is equal to zero (KAVKA, M., 1997). That point determines the usefulness of the machine acquirement in comparison with the using of the contract to provide the field operation. The value of minimal annual use is effected by operational costs and expected life-time of the machine. In a paper there is presented the analysis of the effects of life-time of field machines and power unit on the direct unit costs and minimal annual use of machine-tractor sets. The analysis is related to the tractor John Deere 8320 used with the machines for soil tillage operations in conditions of University farm in Lány.

### 2. Material and methodology

Analysis of the effects of machine life-time on the direct unit costs and minimal annual machinery use in tractor-machine set can be considered as a more complex approach to evaluation of the field machinery exploitation. Within this analysis there must be combined the operational parameters having effect on the

process of profit generation, i.e. first of all:

- benefits obtained when machine is used in tractor-machine set,
- costs related to the operation of the given machine characterized by acquisition price and method of financing. There must be taken into account also the effects of machine life-time and changes of costs and other operational parameters in relation to the annual machine use.

In general we are speaking about the combination of the price of custom work on the market with the machine life-time, machine acquisition price and machine annual use (ABRHAM, Z. 2007). Other parameters, such as technical level of machine, technological suitability, theoretical machine capacity, are considered as an initial and conditional criterions for machine acquisition and subsequent its effective exploitation during field works on the farm.

#### *Calculation of the revenues from the using of machine in machine-tractor set*

Annual revenue  $rV_{supr}$  from the using of machine in machine-tractor set can be calculated as a conjunction of the price of market machine custom work  $C_p(t)$  and machine annual use  $rW_s$  (equation 1):

$$rV_{\text{supr}} = C_p \cdot rW_s \text{ [CZK.year}^{-1}] \quad (1)$$

The machine custom work is determined by the unit costs related to the machine operation and is effected at a time by inflation (increasing of the machine prices, labour prices, fuel prices, etc.). It is effected also by the market demand and offer of the machine custom work. In our calculations we have neglected these effects due to ambiguity of their determination.

#### **Calculation of the costs of operation of the machine or tractor**

Machine operation costs, analogous to tractor operation costs, can be considered as an important indicator of the machine exploitation, and also as a criterion when buying a new machine.

Costs of operation (RATAJ, V. 2005) consist of two basic components: 1. Fixed costs and 2. Variable costs. Study of the fixed costs is based on the level of annual use of machine. Variable costs are related to the unit of the worked area, unit of the processed products or 1 working hour. When analysing the costs in

relation to the machine life-time  $t$  it is necessary to take into account also the annual use of machine (annual capacity -  $rW_s$ ) as it is the basis for the conversion of annual fixed costs  $rN_f(t)$  on the unit costs  $jN_f(t)$  and unit variable costs  $jN_v(t)$  on the annual variable costs  $rN_v(t)$ . Equation 2 expresses the method of the calculation of the total machine costs  $rN_s(t)$  and Fig. 1 can be considered as a graphic representation of the Equation 2. Likewise the Equation 3 expresses the method of the calculation of the total unit costs  $jN_s(t)$  and Fig. 2 is a graphic representation of the Equation 3.

$$rN_s(t) = rN_f(t) + jN_v(t) \cdot rW_s(t) \text{ [CZK.year}^{-1}] \quad (2)$$

$$jN_s(t) = \frac{rN_f(t)}{rW_s(t)} + jN_v \text{ [CZK.ha}^{-1}] \quad (3)$$

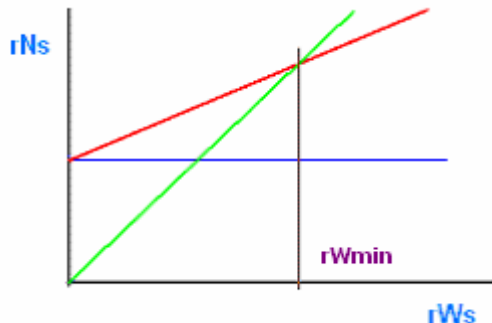


Fig. 1

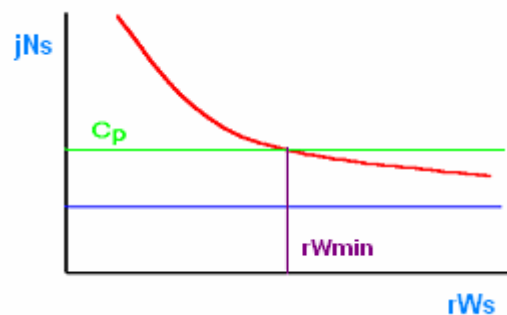


Fig. 2

During standard machine life-time (for example, 6 years) the unit costs can be used as initial information for the calculation of the machine custom work (Equation 4).

$$C_p = jN_c(6) + jZ + DPH \text{ [CZK.ha}^{-1}] \quad (4)$$

$jZ$  - profit charge (up to 15 % from the total unit costs),  
DPH - value added tax.

#### **Structure of the annual fixed costs**

Fixed costs consists of depreciation, remuneration of own capital in combination with

the bank loan interest or margin of finance leases, machine storage costs, insurance and taxes. These fixed costs do not depend how much the machine is used during a year.

For determination of the machine exploitation strategy the depreciation is most important and therefore this type of costs is studied in details. For other components of fixed costs there are presented only equations which can be used for the calculation.

#### **Costs related to depreciation $rN_a(t)$**

Annual depreciation costs can be considered as a basic source for the machine renewal. For the calculation of this financial source we can



use either tax depreciation or accounting depreciation. In case of accounting depreciation we have to know the loss of machine value due to the age. For both methods the costs related to depreciation can be determined by using of equation 5, where  $C_m$  means purchase price of the machine in CZK and  $a(t)$  means annual depreciation rate in  $\% \cdot \text{year}^{-1}$ .

$$rN_a(t) = C_m \cdot \frac{a(t)}{100} \quad (5)$$

[CZK. $\text{year}^{-1}$ ]

From the point of contractor, who provides the costs calculations with the aim to select the right business strategy, i.e. first of all custom work costs, time use of the machine and machine annual use, it is necessary to prefer in calculations the higher values of annual depreciation rate. As it can be seen from Fig. 3 and Fig. 4 the higher value of the annual depreciation rate can be observed in the case of **degressive loss of the machine value**, which represents the accounting depreciation method (JEHLIČKA, T. 1997, SAILER, J. 2008) up to the machine age 4 - 6 years.

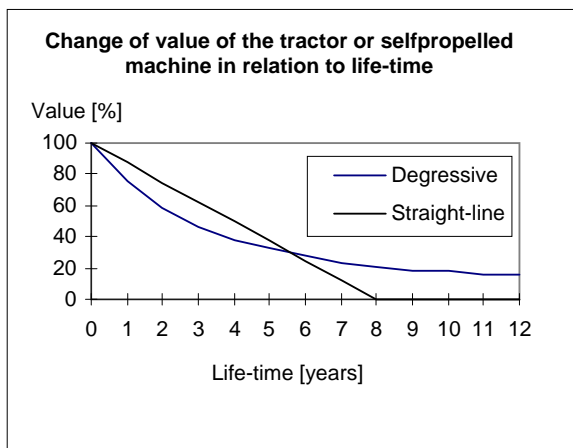


Fig. 3

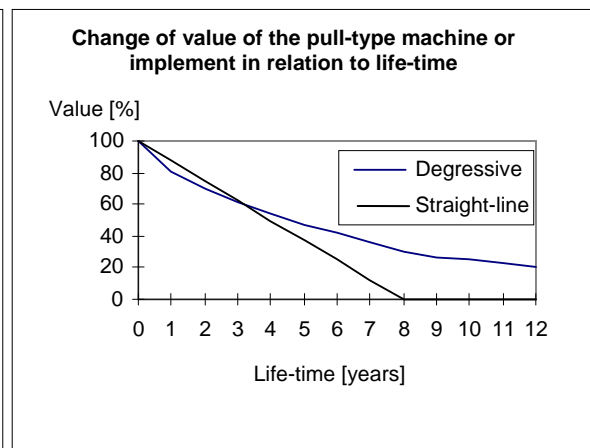


Fig. 4

On the contrary, when the machine is used for longer time (more than 6 years), it is better to use the straight-line depreciation, which represents tax depreciation method. Strategy based on shorter time of machine use is suitable for contractors, who are able to ensure the high annual machine use. They have sufficient financial resources for regular machine fleet renewal by sooner old machine sale and purchase of a new one. This is especially true for more expensive and more complicated self-propelled machines (Fig. 3). For the pulled machines and tractor-mounted machines (Fig. 4) it is possible to recommend the straight-line depreciation rate even in the case that machine has amortized value.

### Structure of the unit variable costs

Variable costs consist of fuel (energy) and lubricants costs, costs of maintenance and

repairs, and costs of labour. All these costs depend upon the annual use of machine working in tractor-machine set.

### Minimal annual exploitation of the machine $rW_{\min}(t)$ in the tractor-machine set

From the point of economical theory the minimal annual exploitation of the machine in the tractor-machine set can be considered as Break-Even-Point, which determines the convenience of the sole ownership in comparison with other form of acquiring farm machinery (contracting or hiring). Initial equation for the calculation of the minimal annual exploitation (annual machine capacity) in relation to the machine-life time is based on the balance of the costs, revenues and partial financial benefit of the machine in the tractor-machine set – equation 6. If the equation 6 is equal to zero, it is possible to formulate the equation 7 for the determination of the minimal annual exploitation of the

machine:

$$rZ_{sopr}(t) = rV_{sopr} \cdot rN_{sopr}(t) = 0$$

[CZK.year<sup>-1</sup>] (6)

where

$rZ_{sopr}(t)$  - annual profit from the machine operation [CZK. year<sup>-1</sup>]  
 $rV_{sopr}$  - annual revenue from the machine operation [CZK. year<sup>-1</sup>]

$rN_{sopr}(t)$  - annual machine operational costs [CZK. year<sup>-1</sup>]

$$rW_{min}(t) = \frac{rN_f(t)}{C_p - jN_v(t)}$$

[unit.year<sup>-1</sup>] (7)

$C_p$  - price of machine custom work

[CZK.ha;t;h<sup>-1</sup>]

Because the annual fixed costs and unit variable costs depend upon the selected value of the annual machine use therefore the value of minimal annual machine capacity will also depend upon the annual machine use.

Consequently, if  
 $jN_f(4) > jN_f(6) > jN_f(8)$  than  
 $rW_{min}(4) > rW_{min}(6) > rW_{min}(8)$ . **Above facts should be taken into account already in the process of acquiring the machine.**

### 3. Results of calculations and discussion

At the University farm of the Czech university of Life Sciences in Prague there is used the tractor John Deere 8320 with the annual use of 1600 hours.year<sup>-1</sup>. Tractor is used with machines their parameters are given in Table 1. There was used also following data:

- gross salary of the tractor operator  
110 CZK.h<sup>-1</sup>
- price of fuel without VAT  
22,90 CZK.l<sup>-1</sup>
- rate of remuneration of own capital  
1 %

By using of computer advisory system TechConsult for each tractor-machine set (combination of tractor with machine) there were calculated costs related to tractor-machine set operation and minimal annual use for different life time (4, 6 and 8 years both tractor and machine). Graphic display of the costs and

minimal annual use for the life time 4, 6 and 8 years is given on the Fig. 5 (an example for plough Kverneland PW used with tractor John Deere 8320).

From the Table 2 and Fig. 5 the following conclusions can be formulated:

A. Generally, in determining of the right strategy of the exploitation of the machine in the tractor-machine set it is necessary to combine 5 basic operational parameters or marketing variables:

- a) machine acquiring price,
- b) real (expected) machine annual use,
- c) requested minimal machine annual capacity,
- d) machine life-time,
- e) price of machine custom work.

B. For combination of the operational parameters ad A. with information ad C. and D. it is valid that:

- a) annual fixed costs and unit variable costs depend upon the chosen machine annual use and therefore also the minimal annual capacity depends upon the machine annual use with the machine custom rate which is valid for the given site and time;
- b) requested minimal machine capacity when compared with the real machine annual use has effect on the maximal acquiring machine price of which are determined total unit operational costs.

C. Results of research confirmed that decrease of the value of the mobile farm machinery and tractors in relation to the machine life-time has digressive character (Fig. 3 and Fig 4). This fact implies knowledge (Fig. 5), that first of all the fixed costs are bigger for the shorter machine life-time than for longer machine life-time. It also follows that requested minimal annual use (Table 2) must be bigger for the shorter machine life-time than for the longer machine life-time, respectively

if  $jN_f(4) > jN_f(6) > jN_f(8)$ , then  
 $rW_{min}(4) > rW_{min}(6) > rW_{min}(8)$ .

D. Above statement is valid also for the application of maintenance costs coefficient (see Table 1) in relation to the requested machine life-time, which acts in opposite direction than digressive decrease of the value of machine or tractor.

- E. The facts related to the ad C. and D. (see Table 2) must be taken into account already in the stage of decision making related to the acquiring of machine. Contractors having sufficient financial resources can select shorter machine life-time and vice-versa. If there are not enough jobs for the machine in the tractor-machine set (potential machine annual use), it is better to carry out the field operation under contract for other farmers not having available machinery or to select less expensive farm machine.
- F. Due to the fact that majority of the high-capacity machines are acquired on the bank loan the same strategy can be used also by contractors planning to use the machine within long machine-life during which the bank loan will be reimbursed (if there are not available other financial resources).

#### 4. Conclusion

The evaluation of the use of tractor-machine sets, based on John Deere 8320 tractor, confirms that for the acquisition of new investment, particularly the cost of expensive machinery and tractors, it is possible to recommend the using of appropriate strategies for calculations. In practice this means that when buying the machine, the user should consider what will be the life-time of the machine and customize it according to its annual use.

*(This paper was supported by grants from research project MSM 6046070905)*

#### References

- ABRHAM, Z. et al. 2007. Technické a technologické normativy pro zemědělskou výrobu (Technical and technological standards for the agricultural production). Praha: VÚZT v.v.i., 29 s. ISBN 978-80-86884-26-4
- JEHLÍČKA, T. et al. 1997. Experimentální stanovení funkčních závislostí činitelů celkových nákladů na provoz souprav a jejich využití při optimalizaci technických systémů. Disertační práce. (Experimental verification of the functional relations of the total costs of the tractor-machine sets and their implementation for optimization of the technical systems. PhD. Thesis) Praha: ČZU v Praze, Technická fakulta, 145 s.
- KAVKA, M. 1997. Využití zemědělské techniky v podmínkách tržního hospodářství (Exploitation of the agricultural machinery in conditions of market economy). Praha: ÚZPI Praha, 32 s. ISBN 1211-9199
- LANDERS, A. 2000. Farm machinery: Selection, Investment and Management. Resource Management. Farming Press, Tonbridge, Kent, 2000, 152 p. ISBN 0-85236-540-3
- RATAJ, V. 2005. Projektovanie výrobných systémov – Výpočty a analýzy (Designing of the production systems - Calculations and analysis). Nitra: SPU v Nitre, 121 s. ISBN 80-8069-609-8.
- SAILER, J. et al. 2008. Vliv doby používání zemědělských strojů na jejich provozní parametry (Effect of the annual use of the agricultural machines on their operational parameters). Mechanizace zemědělství, 62, 10, s. 52-55. ISSN 0373-6776



**Table 1 – Parameters of the machines used in set with the tractor John Deere 8320**

	Tractor John Deere 8320	Machine			
		Plough Kverneland PW 100	Harrows 12 m (own production)	Disk cultivator Dowlands 6000	Chisel plough Ecolands EVO
Acquisition price without VAT $C_m$ [CZK]	4611500	1600000	26000	693964	745760
Share of own resources [%]	1	100	100	0	0
Bank loan interest [%]	1	-	-	-	-
The repayment period of bank credit [year]	5	-	-	-	-
Number of payments per year [1]	4	-	-	-	-
Lease coefficient [1]	-	-	-	1,1611	1,1611
Insurance rate [%]	1,25	0,95	0	during lease payment 1,03 %, otherwise 0	during lease payment 1,03 %, otherwise 0
Expected life time $t$ [year]	4, 6, 8				
Annual decrease of the tractor/machine value in relation to the age [%]	4	15,5	15,5	12,3	12,3
	6	13,0	13,0	10,7	10,7
	8	11,0	11,0	9,0	9,0
Width $S$ [mm]	2545	3000	2870	3020	3000
Length $D$ [mm]	6300	13500	7000	8000	8500
Working width $B_p$ [m]	-	4	12	6	6
Number of operators $n$ [1]	1	0	0	0	0
Fuel consumption [l.ha <sup>-1</sup> ]	According to the machine	22,6	5,5	13,0	14,5
Machine capacity $hWs$ [ha.h <sup>-1</sup> ]	-	1,5	7,3	3,5	3,5
Annual machine use $rW(t)$ [ha.year <sup>-1</sup> ] (for tractor [h.year <sup>-1</sup> ])	1600	1200	2500	300	500
Maintenance unit costs $jNu(t)$ in relation to the age [CZK.ha <sup>-1</sup> ] for machines or [CZK.h <sup>-1</sup> ] for tractors	4	70	420	270	260
	6	90	435	280	280
	8	100	450	290	300
Price of machine custom work $C_p$ [CZK.ha <sup>-1</sup> ]	-	1700	280	1200	1200

Source: Farm accounting records from the University farm Láňy

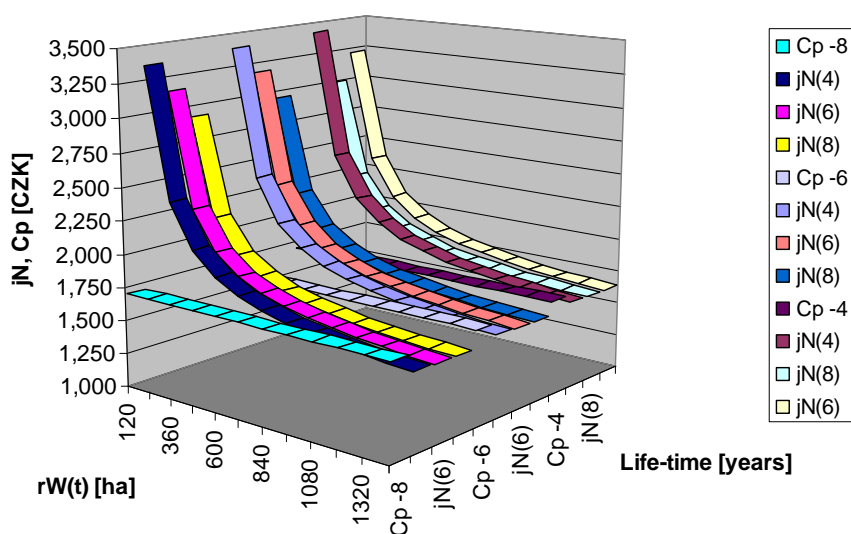


Fig. 5 Effect of annual use and machine life-time on the direct unit costs - plough Kverneland PW used with tractor John Deere 8320

Tab. 2 Effect of estimated time of tractor and machine use on the requested minimal annual use [ha.rok<sup>-1</sup>]

Machine	Requested minimal annual use of the machine working in machine-tractor set [ha.year <sup>-1</sup> ]								
	<i>Estimated John Deere 8320 tractor-life in years</i>								
	4			6			8		
	Estimated machine life-time in years								
	4	6	8	4	6	8	4	6	8
Plough Kverneland PW 100	1086	1032	961	923	867	797	811	757	690
Harrows 12 m (own production)	1965	1786	1610	1413	1275	1137	1124	1011	896
Disc harrow Dowlands 6000	306	278	246	293	266	236	283	257	227
Chisel plough Ecolands EVO	327	305	275	312	290	261	300	278	250

## RENEWABLE ENERGY SOURCES AND RURAL DEVELOPMENT

STREBKOV D.S.

All-Russian Research Institute for Electrification of Agriculture,  
2, 1st Veshnyakovsky pr., 109456. Moscow, Russia

Phone: +7-499-171-19-20, Fax: +7-499-170-51-01, E-mail: [viesh@dol.ru](mailto:viesh@dol.ru)

According to UN terminology, all types of sources based on the solar energy, are termed renewable energy sources (RES). The following energy types fall into the category of unconventional renewable energy sources: hydraulic, solar, geothermal, wind and tidal energy; the energy of waves; thermal gradient of the sea; the energy of biomass conversion; energy obtained by burning wood, charcoal, peat, shale oil or bituminous sand; energy of draught animals.

Renewable energy resources are tremendous and available to each country. The amount of the solar energy incident on the territory of Russia within a week, exceeds the total Russian energy reserves in petroleum, gas, coal and uranium.

The share of the renewable energy in the form of biomass and hydraulic power within the total energy production makes 6 % in Russia and 80 % in developing countries [1]. The share of RES in the power consumption for EU countries shall increase from 6 % in 2000 to 12 % by 2010; The total power consumption in EU countries was equal to 2 880 TW-hr.

In 2030, the forecasted worldwide installed capacity of solar power plants(SPP) using the photoelectric conversion method, shall make 300 GW, the price being equal to 1000 Euro per 1 kW; the electric energy price shall make 0.05 to 0.12 euro per 1 kW-hr [2]. The renewable energy sources shall substitute coal, oil, gas and uranium in producing electric power, heat and hydrogen.

At the Summit in Okinawa (Japan) in July, 2000, the leaders of the "Group of Eight Countries" created a specialized international group and a consulting group aimed at elaborating the strategy for the development of world-wide renewable energy systems. In the report [3], prepared by the specialized group and authorized by the leaders of the "Group of Eight Countries" at the Summit in Genoa in July, 2001, the problem for providing 1.8 billion people in the world with electric energy, using RES, has been set. According to the World Energy

Conference, 1.8 billion people in the world had no access to electric energy systems in 1993.. The concept for agriculture electrification in developing countries has been also proposed [4]. The leaders of the Eight Countries have declared at the Genoa Summit: "We shall include RES development into our national plans and support research works and investments into new technologies".

The purpose of this paper is to define essential factors and technologies which determine the ways and prospects for developing global sources of renewable energy and their role in the power engineering of the future. This role is determined by the opportunities of developing and using new physical principles, technologies, materials and structures for competitive SPP [5].

In order to compete with fuel-consuming power systems, the RES shall meet the following requirements:

- SPP efficiency shall be at least 25 %.
- Annual usage period for the solar power system shall be equal to 8 760 hours. It means, that this system shall produce electric power 24 hours a day, 12 months per year.
- SPP service life shall be 50 years.
- The cost of an installed SPP shall not exceed 1000 euro per 1 kW of peak power.
- SPP annual installed capacity should be 100 GW.
- Annual production of the solar grade silicon feedstock for solar cells (SC) shall reach 1 million tons, its price shall not exceed 15 euro per 1 kg.
- Materials and technologies for solar cells and modules shall be ecologically clean and safe.

Let us analyze the present-day goals and RES development trends in the view of the above-stated criteria.

### **Increase of Solar Energy Conversion Efficiency**

Maximum laboratory efficiency of SC based on cascade heterostructures makes 42%; the efficiency of silicon SC reaches 24 %. In practice, all Russian and foreign factories produce solar cells with an efficiency of 14 to 17 %. In 2003, the Sun Power Corporation (USA) started to manufacture silicon SC, having an efficiency of 20 %.

30 years ago, SC models, using new physical principles, materials and structures, were proposed in Russia [6]; their theoretical efficiency reached 93 %. Main efforts are aimed at maximum use of the whole sunlight spectrum and the total photon energy in accordance with the following principle: each photon shall be absorbed in a graded-gap or cascade semiconductor whose band-gap corresponds to the energy of this photon. As the result, the SC loss may be reduced by 47 %. The following devices are being developed for this purpose:

- cascade SC based on semiconductors with different band-gap widths;
- SC with graded band-gap;
- SC with impurity levels inside the band-gap, which shift the long-wave photoeffect threshold due to multi-photon absorption.

Other ways for increasing SC efficiency are related to the use of concentrated sunlight, polymeric and matrix SC and nanostructures based on silicon and fullerenes [2]. We developed matrix solar cells of third generation having efficiency 20-24% and power density 1-10 W/cm<sup>2</sup> under concentrated solar radiation.

Within several years, new technologies and materials will help to increase the efficiency of SC based on cascade heterostructures up to 44 % in the laboratory and up to 35 % in mass production; the efficiency of silicon SC will be increased up to 30 % and 25 % respectively.

### **Increasing Annual Usage Period for the Installed SPP**

The average annual usage period makes 5 200 hr for installed thermal power plants, 1000 to 4 800 hr for hydroelectric power plants, 2 000 to 3 000 hr for wind power plants, and 1000 to 2 500 hr for the SPP [7].

A stationary solar power plant characterized by an efficiency of 25 % and a peak power of 1 kW, produces annually 1 000 kW-hr in Central

Russia or in Germany and up to 1750 kW-hr in the Sahara Desert. In case of tracking the Sun, the energy production under the same conditions increases up to 1400 kW-hr in Russia and up to 2500 kW-hr in the Sahara. The produced energy variation with day time and its dependence on the weather are key SPP drawbacks (as compared to power plants using mineral fuel). Therefore, large-scale projects for the development of solar power systems were provided till now with energy accumulation systems, based on the electrolysis of water and accumulation of hydrogen.

The opportunities of 24-hour and year-round energy production by means of a global system including several solar power plants are considered.

In connection with the development of power grid systems in Europe, in North America and in South America, and with the proposals for global electric power system over the Earth, the problems for developing systems capable to transmit terawatt transcontinental streams of electric power have appeared. A third method can interfere in the competition between the alternating and direct current power transmission systems: the high-frequency resonant single-conductor method for electric power transmission, proposed by N. Tesla in 1897 [8].

### **Increasing SPP Service Life**

The service life of thermal and nuclear power plants ranges from 30 to 40 years. The service life of semiconductor SC exceeds 50 years, because the interaction of photons with atoms and electrons does not degrade the crystalline structure or change the velocity of surface and volume recombination for minority carriers. However, the service life of solar modules is about 20 years in tropical climate and 25 years in temperate climate due to aging of polymeric materials: ethylene vinyl acetate and tedlar which are used in the modules for SC hermetic capsulation. In order to enhance the service life of modules, it is necessary to exclude polymeric materials from the module structure. In a new solar module structure, designed at the VIESH, the solar cells are located in a hermetic double glass packet. The glass sheets are joined together along the borders by soldering or welding. (see Figs. 1 and 2) [9]. The technique for border capsulation guarantees module

hermiticity within 50 years. In order to improve SC thermal regime and reduce the optical loss, the module is filled with an organic-silicon fluid.



Fig. 1. Photoelectric solar module with organic-silicon polymeric materials (manufactured at the VIESH). Dimensions: 450 × 970 mm; electric power: 50 W; voltage: 12 V



Fig. 2. Double-sided photovoltaic receiver, intended for a stationary concentrator (designed at the VIESH).

Dimensions: 2 m × 0.12 m; expected service life: 40 years; electric power: 20 W; voltage: 6 V

The new technique for assembling solar modules, with new organic-silicon polymeric materials, was used to manufacture highly-efficient evacuated transparent thermal insulation. The insulation block consists of two glass plates, welded along the borders, with a 50- $\mu$ m vacuum space between them. [10]. The insulation parameters are specified in table 1. If the internal glass surface is covered with a coating, reflecting infrared radiation, the thermal resistivity (per 1 m<sup>2</sup> of the surface) may be enhanced by factor of 10 compared to a single glass sheet. Solar collectors, equipped with the evacuated thermal insulation, will heat water up to 90°C (instead of 60°C); they are transformed from installations for hot water supply to a new type of installations, suitable for heating buildings. The thermal loss in greenhouses and winter gardens may be reduced by 50 %. If the southern facade of a building is covered with the blocks of evacuated transparent thermal insulation, 12 mm in thickness, it will represent a huge solar collector; it is equivalent to increasing the brick wall thickness by 1 m.

Table 1 Thermal resistivity of evacuated transparent thermal insulation (per 1 m<sup>2</sup>)

Name	Thickness, mm	Thermal resistivity, m <sup>2</sup> °C/W
Single glass sheet	6	0.17
Two glass sheets, spaced by 16 mm	30	0.37
Evacuated thermal insulation	6	0.44
The same, with IR-coating over 1 sheet	6	0.85
The same, with IR-coating over 2 sheets	6	1.2
Double insulation with IR-coating over 2 sheets	12	2.0
Brick wall	600	1.2

The use of the evacuated thermal insulation is particularly efficient for southern RF regions, as well as in the republics of Buryatia and Yakutia during anticyclones. In this condition, the temperature of the selectively reflecting coating reaches +90°C, if the air temperature is – 30°C, and the insulation block width is 10 mm. The use of the evacuated thermal insulation in summer months will reduce the cost of building conditioning by 50 %.

### Reducing SPP Cost

The average cost of an installed power capacity for different power plant types (in USD per 1 kW) is the following:

- 1000 to 2 500 for a hydroelectric power plant;
- 800 to 1400 for a thermal power plant;
- 800 to 3 000 for a wind power plant;
- 2 000 to 3 000 for a nuclear power plant [8].



The most expensive component of modern SPP is the solar module, containing the silicon SC. The module cost ranges from 3 000 to 4 000 USD per 1 kW, in case of annual module output, corresponding to 1 GW. The SPP cost ranges from 6 000 to 8 000 USD / kW; its predicted cost will be reduced to 1000 euro / kW by 2020 [2].

Main ways for reducing the SPP cost are the following:

- enhancement of SPP efficiency;
- enhancement of module dimension and annual output;
- reduction of solar-grade silicon cost;
- reduction of silicon consumption (per 1 kW of SPP power)
- combined production of electric energy and heat by the SPP;
- use of the stationary concentrator PV module.

Maximum dimension of the solar module is limited by the glass sheet dimension; it has reached now  $2.5 \times 3$  m with the produced electric

power of 1 kW. The output of solar modules grows annually by 30 %; their cost has decreased by factor of 10 since 1976.

A new chlorine-free technology has been developed in Russia (see table 2); the produced solar-grade polysilicon costs 15 euro/kW, which is twice lower than the cost of polysilicon in the European market [10]. In this case, metallurgical silicon and ethanol (instead of hydrochloric acid) are used as primary components; the intermediate components of the process are 3-ethoxysilane and monosilane. The cost reduction is reached due to lowering the process temperature and energy consumption. The ecological characteristics of the manufacture process are also considerably improved, and the material quality is upgraded, so that it reaches the semiconductor-grade level. The predicted term for reaching annual polysilicon output of 1000 to 5 000 tons (using the new technology) is 2004 to 2016.

Table 2 Chlorine-free technology for producing polysilicon

Primary components: ethanol and metallurgical silicon	
$\text{Si} + 3 \text{C}_2\text{H}_5\text{OH} \Rightarrow \text{SiH}(\text{OC}_2\text{H}_5)_3$	
$4\text{SiH}(\text{OC}_2\text{H}_5)_3 \Rightarrow \text{SiH}_4 + 3 \text{Si}(\text{OC}_2\text{H}_5)_4$	
$\text{SiH}_4 \Rightarrow \text{Si} + 2\text{H}_2$	
Results of realizing the technology:	
■	2-fold reduction of polysilicon cost (to 15 USD / kg)
■	10-fold increase of polysilicon purity (up to 99.999 %), quality improvement
■	The manufacture process becomes ecologically safe

Silicon and other materials take 75% of the solar cell cost (see table 3).

Table 3 Structure of SC price

• Silicon	60 %
• Other materials	15 %
• Wages	10 %
• Other expenses	15 %
Total	100 %

The ways for reducing silicon consumption include increasing the ingots volume and reducing the SC thickness. In 2010, the mass of the silicon ingot, grown by the method of directional crystallization, will reach 1000 kg (which corresponds to a volume of  $0.4 \text{ m}^3$ ). The SC thickness will be reduced from 400  $\mu\text{m}$  in

2000 to 200  $\mu\text{m}$  in 2010 and to 100  $\mu\text{m}$  in 2015; it will reach 20  $\mu\text{m}$  or less in 2020.

The most efficient way for reducing SPP cost and reaching gigawatt output level lies in using solar concentrators. The cost of a glass mirror concentrator (per  $1 \text{ m}^2$ ) is 10 times lower, than the cost of the solar module. Stationary

concentrators having a concentration factor of 3.5 to 10 and an aperture angle of  $48^\circ$ , have been developed at the VIESH. They enable concentrating both direct and diffused components of the solar radiation within the

limits of the aperture angle (see Figs. 3 and 4) [11]. The use of low-cost solar-grade polysilicon and stationary concentrators ensures to shorten the term for reaching the module cost of 1000 euro / kW from 2020 to 2015 (see Fig. 3).

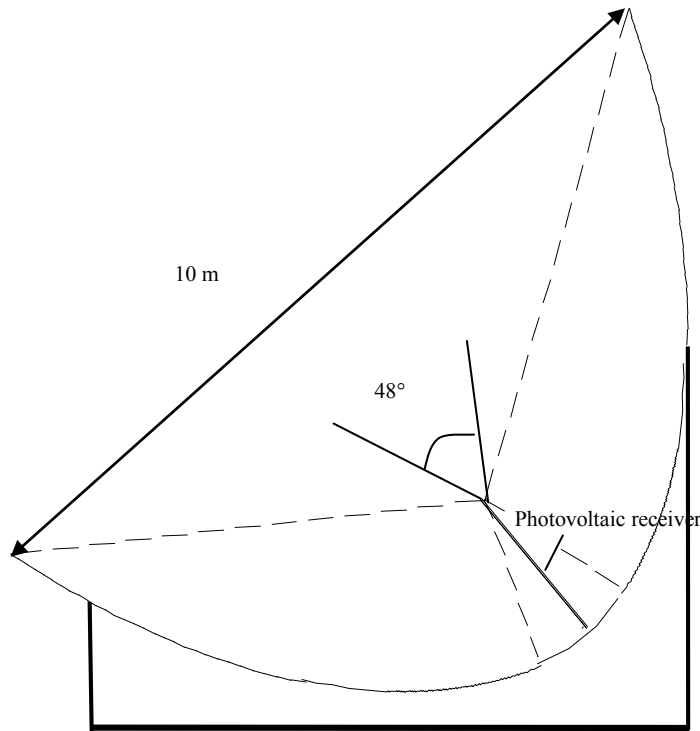


Fig. 3. Optical scheme for a symmetric stationary solar concentrator with a concentration factor of 3,5

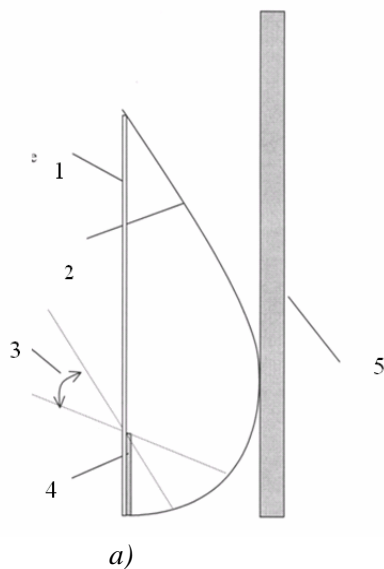


Fig. 4. *a* – Solar facade with an asymmetric vertical solar module, having an aperture angle of  $48^\circ$ : 1 – glass cover; 2 – reflector; 3 – aperture angle; 4 – double-sided photovoltaic receiver; 5 – southern facade of the building *b* – Photo of an experimental module with a solar concentrator



Cogeneration solar power plants are intended to supply industrial and dwelling buildings with electric energy, hot water and heat. The efficiency of using solar energy makes 50 to 60 %; the electric efficiency ranges from 15 to 20 %. The use of stationary concentrators enables to increase the heat carrier temperature up to 90°C and to reduce the SPP cost to 1000 euro/kW. VIESH researchers develop small cogeneration power plants for multi-family apartments, single-family houses and industrial buildings, as well as stationary SPP for cities, villages, agricultural and industrial enterprises, based on concentrator modules. The plants are connected to the power supply mains. Autonomous cogeneration power plants equipped with backup diesel electric generators utilizing the heat of the cooling system and exhaust gas, are also developed.

Enhancement of SPP efficiency results in reducing the material consumption (per 1 kW of power), as well as the dimensions and cost of the SPP territory. The cost of installed solar modules with stationary concentrators versus SC efficiency is plotted in Fig. 5. If the efficiency is 20 %, the module cost becomes much lower, than 1000 euro/kW.

### Increasing the Output of the Semiconductor Material for the SPP

Silicon solar modules make more than 85 % of the SPP production volume (whose present-day annual level exceeds 12 GW). According to our forecast, silicon will dominate in the future solar module industry. This forecast is based on an established principle which says that the structure of material consumption approaches (in a long-term perspective) to the structure of their available resources in the world [12]. It is known that the earth's crust consists of silicon to the extent of 29.5 % (which is the second after oxygen).

Assuming the annual SPP output of 100 GW and the consumption of solar-grade silicon equal to 10 000 tons per 1 GW, the annual world consumption of silicon will reach  $10^6$  tons. New techniques for manufacturing solar-grade silicon are being developed, in addition to the chlorine-free technology, considered above. They are based on electrophysical methods for deoxidating ultra-pure quartzites by means of plasmatrone. New technologies for manufacturing silicon SC in the form of thin sheets, ribbons or films, using automatic cutting procedures by means of a laser, are also under development.

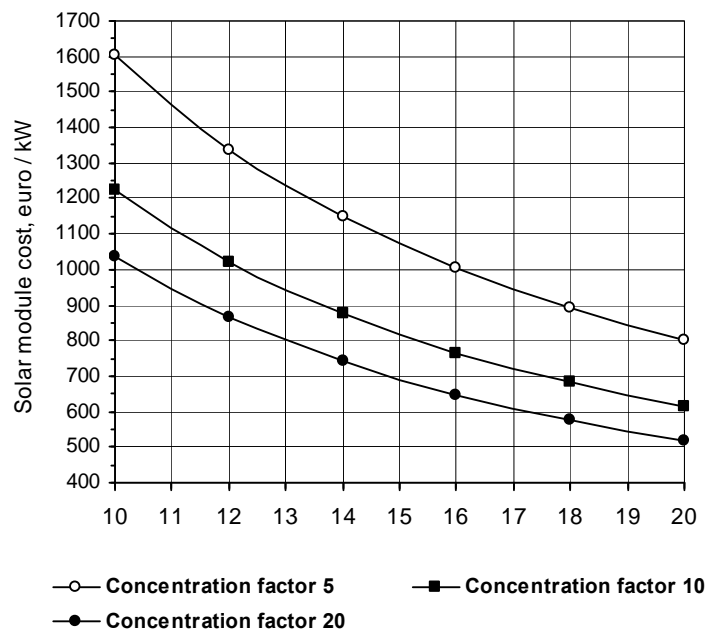


Fig. 5. Cost of an 1-kW stationary module (intended for northern territories) with a cylinder parabolic concentrator having an aperture angle of 36°

### Ensuring Ecological Parameters of the Energy Generating Process

The mankind will not be threatened with an energy crisis due to exhaustion of oil, gas and coal resources, if the technique for using renewable energy is developed. In this case, many other problems will be solved, including cleaning the environment of power plant and transport exhaust, providing with high-quality food, obtaining education and medical aid, enhancement of life duration and quality. SPP development ensures new workplaces, improves life quality, energy security and independence of SPP owners due to fuel-free and distributed energy generation.

In newly developed SPP technologies, ecologically unacceptable chemical procedures of etching and treatment are replaced with vacuum, plasma-chemical, electron-beam and laser processes. Special attention is given to waste recovery and recycling SPP components after use [13].

When using SPP, natural landscape and habitation objects may be easily combined with power systems. The SPP form architectural compositions, including solar facades or solar roofs of apartment houses, farms buildings, shops, warehouses or covered parkings.

Other large-scale renewable energy projects are under development at the VIESH and other enterprises of Russia. They include producing liquid and gaseous fuel from biomass using fast-pyrolysis techniques with fuel yield exceeding 50 % of the raw material mass, designing ecologically pure wind power plants, using rotor without blades (see Fig. 6), combined solar-wind-diesel power plants, vehicles operated by solar energy (see Fig 7)

A method for pyrolysis-aided conversion of humid organic substance into gaseous and liquid

fuel has been developed. At the first stage, the moisture is removed from the substance by heating it to the critical temperature, at which the water specific heat of vaporization is close to zero. As a result, the energy consumption is reduced; the water content in the liquid fraction is decreased, and the combustion heat of the obtained liquid fuel is enhanced. At the second stage, the dried substance is treated in a hermetic chamber at a high temperature [14].

The installation realizing the pyrolysis process is illustrated in Fig. 8. The raw material, intended for treating, is loaded into the reception bunker 1 and delivered into the moisture-removing chamber 3 through the dosing unit 2. The chamber 3 is used to heat the substance rapidly to a temperature of 250 to 375°C by means of the unit 17. The generated steam is directed to the steam-engine 6, or to the heat exchanger 7 (for the purpose of obtaining heat) through the bypass contour 10 with the faucets 11. The cold water enters the heat exchanger 7 through the pipe 8, the hot water goes out through the pipe 9.

The dried substance enters the hermetic conversion chamber 4 where it is exposed to a rapid heating to a temperature of 650 to 750°C by means of the unit 18. The gaseous fuel, obtained as a result of pyrolysis, is directed through the pipe 22 to the heat engine 12, intended for generating electric power and heat. It may be also fed into the heat exchanger 14 (through the bypass contour with the faucets 11) for obtaining heat and liquid fuel. The liquid fraction is condensed in the unit 15 and stored in the tank 16. The solid remainder formed in the chamber 4, is delivered to the tank 5 through the dosing unit 2.

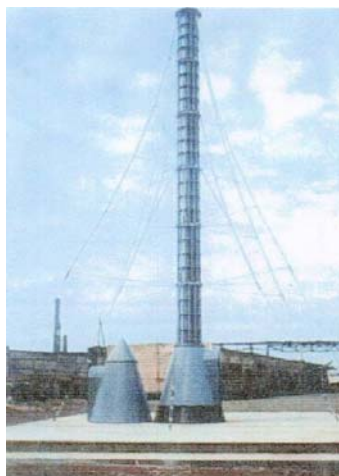


Fig. 6. Wind generator without blades



Fig.7. Solar vehicle

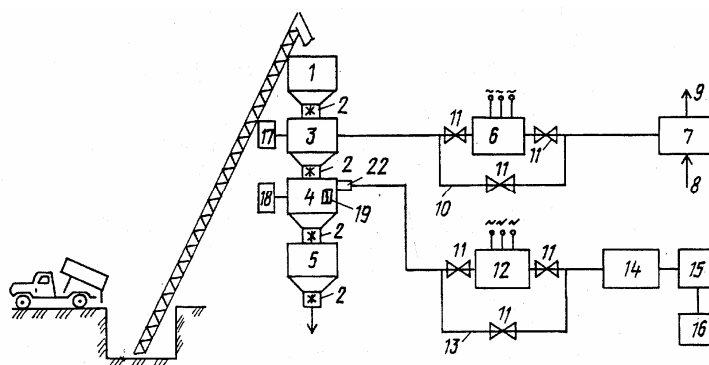


Fig. 8. Block diagram of an installation for conversion of humid organic substance into gaseous and liquid fuel

The conversion chamber 4 for treating the substance by means of a high-frequency cold-plasma discharge is shown in Fig.9. The discharge electrode 19 is connected to the high-voltage power supply 21 through the insulator 20. The operating voltage ranges from 1 to 500 kV at a frequency of 1 to 300 kHz. The treated organic substance is heated rapidly to a temperature of 650 to 750°C, which accelerates its destruction and increases the liquid fuel output; its quality is improved due to enhancement of the share of light fractions. The proposed method ensures the increase of fuel output by 50 to 70 % in mass, depending on the type of the used organic substance.

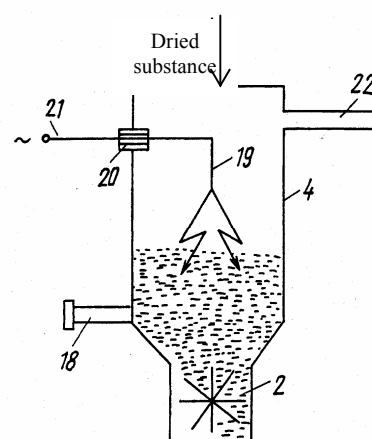


Fig. 9. Chamber for treating the substance by means of a high-frequency cold-plasma discharge

If 30 million hectares of deserted lands in Russia are converted to energy plantations, they may be used to grow annually 450 million tons of dry biomass and to obtain 200 million tons of biofuel (see Figs. 10 to 12).



Fig. 10. Energy plantations of sorghum, cultivated by Corresponding Member of the Russian Academy of Agricultural Sciences B.N Malinnovskii (on the right) in the Rostov region, ensuring a productivity of 130 tons per hectare and biofuel output of 15 tons per hectare

#### Economic parameters of biofuel production by means of rapid pyrolysis of the vegetative mass

##### A. Sorghum

Cultivation expenditures: 100 US \$ per hectare;  
Productivity in dry biomass : 30 tons per hectare;  
Biofuel production: 15 tons per hectare;  
Biofuel cost: 250 US \$ per ton;  
Biofuel sale price: 500 US \$ per ton;  
Annual sale volume: 7500 US \$ per hectare.

##### B. Wheat

Average productivity: 2 tons per hectare;  
Sale price: 150 US \$ per ton;  
Annual sale volume: 300 US \$ per hectare.



Fig. 11. General view of the installation for obtaining fluid and gaseous biofuel with a productivity of 0.5 tons per day, developed in VIESH by M.V. Yerkhov, and a diesel generator, 30 kW in power (on the right), fed with the biofuel.

The share of renewable energy in the global energy production is illustrated in Figure 12 . Up to the beginning of the 18-th century, the solar energy and the energy of wood burning (using

the solar energy accumulated due to photosynthesis) were sole power sources for the mankind. At present, 20 % of world-wide energy production is based on wood burning, energy of rivers and wind (which originate from the solar energy).

New principles for producing renewable energy, new techniques for manufacturing solar-grade silicon and solar cells, capsulation of solar modules, use of stationary solar concentrators and new methods for power transmission (useful for the global solar power system) will ensure the share of renewable energy in the global production up to 60 or 90 % by the end of the century.

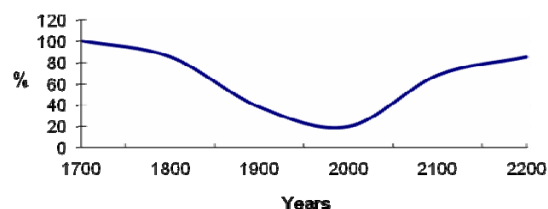


Fig. 12. Share of renewable energy in the global energy production

In 1975, R. Bukminster Fuller proposed to combine regional electric power systems into a united power system of the Earth. This problem is intensively developed explicates and popularized by the Global Energy Network Institute (GENI), registered in California (USA).

The GENI president Peter Meisen participated in the International Solar Congress (Moscow) in 1997; he has also given a scientific report at the VIESH. Works on electric power transmission over long distance are also carried out by the Siberian Power Institute, St.-Petersburg State Technical University, VEI, as well as by the ABB, Siemens and other corporations. The following united power system are under development: united systems for 10 countries in South America and for several Arabian countries; Baltic and Black-Sea power ring grids; power transmission line Siberia – China. Power grid systems are used, connecting the following countries: Russia and CIS countries, USA and Canada, Scandinavian and European countries.

The existing techniques enable transmitting energy streams, 10 GW in power, over a distance of several thousand kilometers. The voltage in dc



and ac transmission lines reach 0.6 to 1.2 million volts. The line cost exceeds 1 million USD per 1 km; taking into account matching, control and converting devices, it exceeds 5 million USD per 1 km. The electric energy loss in transmission lines makes 8 to 10 %. Maximum transmitted electric power is limited by the following three factors: current density of 1.0 to 1.5 A/mm<sup>2</sup> (related to the loss in the wire resistance), leakage through the air at a level of  $1.5 \cdot 10^6$  V and electromagnetic stability of the line.

Resonant methods for power transmission are used to realize single-conductor cables, matching and converting devices, which will unite power sources and consumers of all countries into the global power system [15]. The resonant technique enables transmitting energy streams of several terawatts over distances in the order of 20 000 km [16].

## References:

1. Strebkov D.S. Renewable Energetics in the Third Millennium // *Energy Policy*, 2001, No. 2, pp. 23–27 (in Russian).
2. Novak S. Photovoltaic in the World. Status and Future Trends // *Seminar in PV Research & Technological Development in European Union New Member and Candidate States*. Warsaw, Poland, November 15, 2004.
3. Bezrukikh P.P., Strebkov D.S., et al. 2001 G8 Renewable Energy Task Force Chairmen's Report, 61 p., Chairmen Report Annexes, 75 p. Printed by the Italian Ministry of Environment, 2001.
4. Strebkov D.S. Renewable Energetics: For Developing Countries or for Russia? // *Energy: Economy, Techniques, Ecology*. Moscow: Published by the Russian Academy of Sciences, 2002, No. 9, pp. 11–14.
5. Bezrukikh P.P., Strebkov D.S. Renewable Energetics: Strategy, Resources, Technologies. Moscow: VIESH, 2005. – 264 p.
6. Lidorenko N.S., Evdokimov V.M., Zaitsev A.K., Koltun M.M., Ryabikov S.V., Strebkov D.S. New models of solar cells and prospects for optimizing them // *Solar Engineering*. 1978. No. 3.p.p. 3-7
7. Strebkov D.S. Role of the Solar Energy in the Power of the Future // *Proceedings of the 4-th Research and Development Conference of Central and Eastern European Institutes of Agricultural Engineering (CEE Ag Eng)*. Moscow, VIESH, May, 12–13, 2005, pp. 3–19.
8. Bezrukikh P.P., Strebkov D.S., Tyukhov I.I. Renewable energy for Russian Economy // *Advances in Solar Energy*, American Solar Energy Society, Boulder, Colorado 2005. Vol. 16, pp. 423–463.
9. Strebkov D.S., Zadde V.V., Pinov A.B., Touyryan K., Murphy L. Crystalline Silicon Technology in CIS Countries // *11-th Workshop on Crystalline Silicon Solar Cell Materials and Process*. Colorado, August 19–22, 2001, Extended Abstracts and Papers. NREL, 2001, pp. 199–207.
10. Strebkov D.S., Litvinov P.P., Tverianovich E.V. Research of Functioning of a Class of V-Shaped Stationary Concentrators // *Eurosun – 2004*. Freiburg, Germany. 14 Intern. Sonnenforum, Vol. 2, pp. 3-072–3-078.
11. Strebkov D.S., Koshkin N.L. On Development of Photovoltaic Power Engineering in Russia // *Thermal Engineering*, 1996, Vol. 43, No. 5, pp. 381–384.
12. Tsuo Y.S., Touyryan K., Gee J.M., Strebkov D.S., Pinov A.B., Zadde V.V. Environmentally Benign Silicon Solar Cell Manufacturing // *2-nd World Conference and Exhibition on Photovoltaic Solar Energy Conversion*. July 6–10, 1998, Hofburg Kongresszentrum, Vienna, Austria, pp. 1199–1204.
13. Meisen P. Global Energy Network Institute GENI. San Diego, California, USA, 2004. – 12 p.
14. RF Patent No. 2203922. Method and Apparatus for Converting Humid Organic Substance into Liquid and Gaseous Fuel / Strebkov D.S., Vaynshteyn E.F., Chirkov V.G. // *Inventor's Bulletin*, 2003, No. 13
15. Dmitry Strebkov. A Global Round-the clock Solar Power System. *Energy Bulletin*, Moscow 2009, № 4(7) p.45-51
16. Dmitry Strebkov, Aleksey Nekrasov. Resonant methods of electric Power transmission and application. Published by VIESH, Moscow 2008, 350 pp.

## POWER PRODUCTION FROM AGRICULTURAL WASTES AND IMPLEMENTATIONS

OSMAN YALDIZ<sup>1</sup>, DURMUŞ KAYA<sup>2</sup>, H. İBRAHİM SARAÇ<sup>3</sup>, KAMIL EKİNCİ<sup>4</sup>,  
GÜNNUR KOÇAR<sup>5</sup>, BERK KÜÇÜKKARA<sup>1</sup>

<sup>1</sup>Akdeniz University Faculty of Agriculture Department of Agricultural Machinery  
07058 Antalya – TURKEY

Phone: +90 242 310 2436, Fax: +90 242 227 4564, E-mail: yaldiz@akdeniz.edu.tr

<sup>2</sup>TÜBİTAK Marmara Research Center, Energy Institute,  
Gebze / Kocaeli / TURKEY

<sup>3</sup>Kocaeli University Faculty of Engineering,  
Kocaeli / TURKEY

<sup>4</sup>Suleyman Demirel University Faculty of Agriculture Department of Agricultural Machinery,  
Isparta / TURKEY

<sup>5</sup>Ege University, Solar Energy Institut, İzmir/TURKEY

### Abstract

The management of agricultural wastes in distribution of scarce resources is an important factor in the economics. The task of the management of material flow becomes relevant for agriculture with the beginnings of the industrial production. Utilization of agricultural wastes for energy production means an income for agricultural sector. Agricultural sector is the largest business sector since the past in Turkey. Depending on the country's development reduces the share of this sector but maintains of total production and employment. In Turkey, the agricultural sector constitutes 90% of field crops and livestock (Kaya vd,2006) [1].

This study was constructed by considering the environmental, economical and social benefits and focus of this study is the production biogas from agricultural and animal wastes and utilization of obtained gases in integrated energy conversion technologies. The tasks in these study includes: review biogas and energy production technologies, system simulations and DSS modeling, design and development of two lab-scale (one for animal waste and other for agricultural waste) and one pilot scale (250 kW capacity) integrated biogas plant, integration of the pilot plant with energy conversion systems, experimental study, feasibility study including techno-economical analysis of the whole system, life cycle analysis and dissemination of the project results.

**Keywords:** Power production, agricultural waste, animal wastes, biogas

### Introduction

Energy consumption per capita increases due to population growth in the world and widespread usage of products resulted from technological improvements which ease the human being's life. This causes the energy consumption increase in the world. Primary energy requirement in the world in 2003 was approximately 10.6 million ton oil equivalent (toe). It is estimated that with a 2.3 percent increase in a year, projected primary energy requirement is 12.4 in 2010 and 15.4 toe in 2020, respectively.

Based on the data in 2007, 83% of the primary energy requirement of the world was maintained from fossil based resources

(Anonymous, 2010,b) [7]. It is expected that if no measures are taken, oil, natural gas and coal reserves will run out of after 41, 62 and 230 years later, respectively. The fact of energy sources being depleted causes not only to use fossil based energy sources efficiently but also to utilize renewable energy sources more effectively and widely.

Biogas is one of the renewable energy sources. Electrical energy production through combustion of biogas employing gas turbines makes this technology more attractive among the other renewable energy sources. While electrical energy production from biogas in the world was approximately 5000 GWh in 1990's, it reached to 28669 GWh in 2007's. It has been recorded



that electrical energy production from biogas was 7469 GWh in USA, 5194 GWh in England, 8520 GWh in Germany, 1448 GWh in Italy, 638 GWh in France in 2007 (Anonymous, 2010,b) [7]. Biogas plants and biogas productions are getting widespread in the world due to purchasing electrical energy generated from biogas plants in countries where biogas plants usage is very intensive with the price which is close to retail price and necessitating the processing of the

organic wastes. Organic wastes is processed in countries where biogas plants usage is very intensive to obtain energy, to conserve the nature (prevention of pollution of soil and water) by sterilizing the wastes which harm the environment and utilize the wastes generated from biogas plants as fertilizer in plant production. An example of circular agricultural waste management is shown Fig. 1 (Çetinkaya H. 2006) [2].

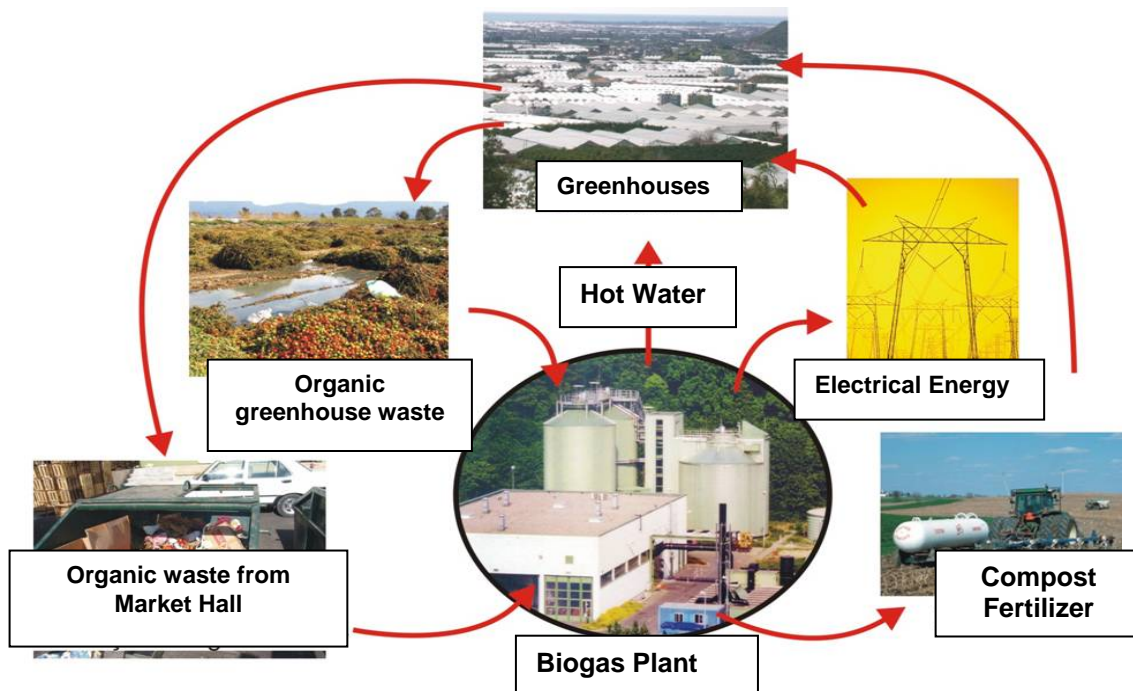


**Figure 1:** Circular Agricultural Waste Management (Çetinkaya,2006)

The classical refuse economy already represents a simple form of material flow systems in agriculture. While the input materials in agricultural production are soil, fertilizer, seed, plant protection agents and fuel, the output materials are yield product and residual substances. The yield product can be sold or used but agricultural wastes can not be sold. It actually contains disposal and never used in production and is not valuable product for agricultural enterprises. Therefore the classical waste management is not sustainable. Regional, ecological, social aspects are not evaluated in this perspective.

Sixty five million tons of residues from field crops ( wheat, barley, tobacco, cotton, rice, etc.) having fundamental importance in Turkey agricultural sector and 160 million tons of animal manure from animal production exist in each

year (Anonymous, 2007,a) [3]. Wastes which is not used for feeding is burned in the field or abandoned to degrade naturally. In addition, animal manure is usually accumulated in pile outside. Manure from livestock building, when not stored properly, causes environmental problems including odor and visual pollution.

The environmental, economical and social benefits were constructed and the expectations from this study;

- Development of a pilot biogas plant utilizing various wastes for energy conversion,
- Energy production from a renewable energy source and contribution to the economy,

- Contribute to widespread manufacturing of biogas production technologies in the nation,
- Achievement and gaining of experiences on development of biogas production systems,
- Gaining of experience on integration of biogas with internal combustion engines and micro turbines,
- Rational use of resources and reduce the environmental damage caused by wastes,
- Contribution to the economy by utilizing fertilizers which are rich in nutritional values and is obtained as by-products from the biogas plant,
- Determining techno-economic criteria needed for enlargement of the systems for industrial use.

Modeling of biogas production systems and to determine the optimum working conditions, Computational Fluid Dynamics (CFD) method was used for the decomposition of animal and vegetable wastes in the anaerobic conditions of the fermentors. In the pilot plant, continually loaded and completely mixed tank reactor was used for the decomposition of vegetable and animal wastes. In this reactor, gas production and at the same time result of the burning of gas will be produced to maximize the energy of the operating parameters were optimized. There are many factors which affects the integrated biogas and energy production [4]. There are;

- Characteristics of the waste material,
- Design parameters of fermenters,
- Operational parameters of fermentors,

- Parameters of energy conversion systems,
- Location features of the facilities.

All these variables will be obtained to the amount of energy production and amount of wastes which is output of the plant. Optimization study, five different dry matter ratio (9.0, 10.1, 11.2, 12.4, 13.6) and different volumetric flow rates (5, 10, 12.5, 15, 20, 25 and 35 m<sup>3</sup>/day) were performed. Each simulation was performed for 100 days. Different hydraulic loading has occurred depending on volumetric flow and dry matter rate. Biogas, CH<sub>4</sub>, CO<sub>2</sub> and H<sub>2</sub> quantities, volatile fatty acids and biomass concentration was investigated in each simulation. Gaussian function was used in the evaluation of simulations. Two different laboratory-scale biogas plant was manufactured for all these parameters to be implemented in pilot plant [5]. While agricultural wastes were used in one of this laboratory-scale biogas plant, animal wastes (different characters) were used in the other. Also animal and agricultural wastes were used together for the experimental work. One of these laboratory-scale biogas plant has 1,2 m<sup>3</sup> gross volume but the net volume of fermentation is 1m<sup>3</sup>. It was geometrically designed as the same way with the pilot plant consideration. This mechanism was placed on a platform with wheels. This mechanism consists fermenter, water channel which will be using for heating system, two mechanic mixer, material preparation tank and control console. Also there is trolley for the carry out output material. This laboratory-scale biogas plant is shown in Figure 2.

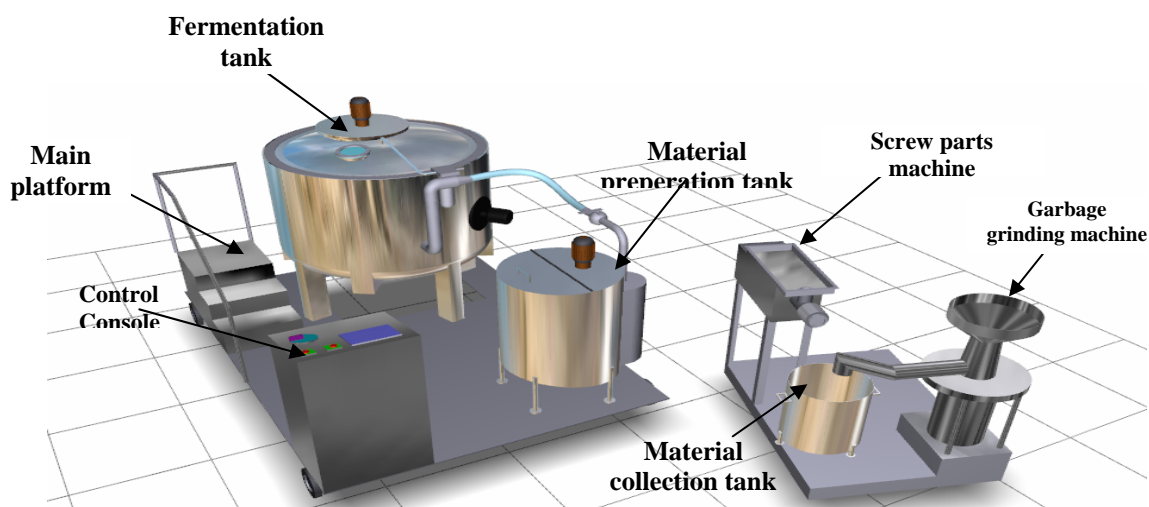


**Figure 2.** Laboratory-scale kit for agricultural waste

Second laboratory-scale biogas plant has 1,2 m<sup>3</sup> gross volume and 1 m<sup>3</sup> net volume. This system consists of mixer, akuple, material preparation tank, biogas reactor, biogas storage tank and fermented manure discharging tank. Maximum working pressure was selected as 700 mbar and the test pressure was selected as 1200 mbar. Mechanic mixing system of reactor has 1.5 kW electric motor with frequency converter. Reactor was isolated with 6 cm rock wool and outside of the isolated material was covered with AISI 304 stainless steel. Gas storage volume is 1m<sup>3</sup>. Mixing system was chosen as the binary system. Hydraulic and mechanical mixing was observed to effects on biogas production. Various stages of biogas production was considerate when automation system was

creating. An advanced control unit which was used in this system is providing reliable data transmission. Also this system helped to solve problems in pilot scale system.

Design of pilot scale biogas plant was made by using knowledge of literature studies, simulation exercises, laboratory-scale experimental studies and overseas technical visits. Pilot scale of biogas plant consists of 2 reactors (Fig 2) and they have 2400 m<sup>3</sup> gross volume and 2089 m<sup>3</sup> of net volume each. They are connected to each other both in series and in parallel (Fig.4). The volume of the final manure storage is 1000 m<sup>3</sup> (Fig. 3). Technical specifications of the fermenters and final manure storage are shown in Table 1.

**Table 1.** Technical specifications of the fermenters and final manure storage

Definition	Explanation	Value
<b>Fermenters</b>	Diameter (m)	19,5
	Height (m)	8
	Wall thickness (m)	0,3
	Diameter (m)	16
<b>Final manure storage</b>	Height (m)	5
	Wall thickness (m)	0,3

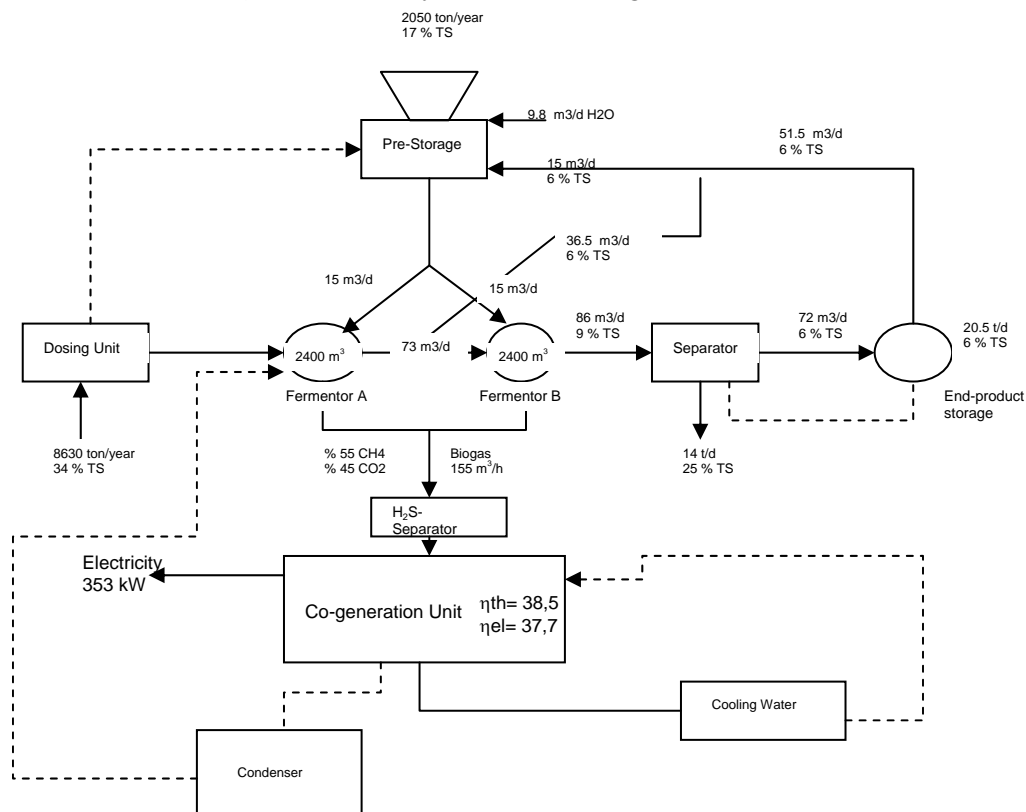


**Figure 2.** Inside of fermenter



**Figure 3.** Final Manure Storage

**Figure 4.** Plant layout and flow diagram



Feedback technique is used in the system in order to be able to regulate the solid matter ratio in the reactor and use the maximum potential within the feed material. The feedback technique consists of feeding back 51.5 m<sup>3</sup> of material taken from the final storage, which is at 6% solidity and in the form of thin slurry, in to fermenter I and II. The residence time at the plant is 47 days; ratio of organic dry matter is 9% and the fermentation temperature is 37-38°C under mesophilic conditions. The plant has

biological sulfur removal system for removal of H<sub>2</sub>S. The system can be considered as biological treatment of hydrogen sulfide (H<sub>2</sub>S), where a special wooden system is mounted on the reactor ceiling (Fig 2) and certain amount of oxygen (O<sub>2</sub>) is supplied in the region (Kaya vd. 2009) [6]. Store and wholesale food waste (i.e. green vegetable and fruit wastes), inner tripe from slaughterhouses, cattle waste from regional farms, grass wastes and chicken manure wastes will be used in the pilot plant (Table1).

**Table 1.** Daily and annual amount of waste used in the plant and average values of DM, ODM and N analysis results for five samples taken at different times

Material	Amount (ton/day)	Amount (ton/year)	DM (%)	ODM (%)	N (kg/t)
Grass	16	5 900	26.01	89.91	6
Agr. Wastes <sup>1</sup>	5.6	2 050	8.97	91.65	4
Inner tripe	1.17	430	16.81	89.11	6
Chicken manure	5.34	1 950	71.92	37.10	40
Cattle manure	0.96	350	16.44	75.39	6
<b>Total</b>	<b>29.07</b>	<b>10 680</b>	<b>140.15</b>	<b>383.16</b>	<b>62</b>

DM= Dry Matter, ODM=Organic Dry Matter, N=Nitrogen, <sup>1</sup> Wastes of vegetable and fruits

Produced gas continuously delivered to the motor generator group. The gas storage units

were mounted separately on the generator in the form of single layer membran and each volume



membran is 700 m<sup>3</sup>. This volume is enough to store produced gas during 16 hours.

Biogas obtained from the plant can be used to produce heat and/or power by means of a combined heat and power (cogeneration) system (Fig 5). In that case, heat released during burning can be recovered using an appropriate heat exchanger. Some of the recovered heat can be

used to heat the fermenter, and the rest for general heating. In that case, cogeneration enables the utilization of the total energy 81,5%. When we consider of energy consumed (60kW) of the biogas plant, net energy efficiencies 72,2%, 37,7% in the form of power and 38,5% in the form of heat (Kaya D. vd. 2009) [6].



**Figure 5.** Combined heat and power (cogeneration) system

**Table 5.** Data used for technical evaluation of the plant and determination of energy efficiency

Variable	Value
Electrical energy production (kW <sub>el</sub> )	353
Thermal energy (kW <sub>th</sub> )	361
Raw material equivalent of total energy production (kW)	876 (660 TOE/year)
Energy consumption of plant (kW)	60

Data used for technical evaluation of the plant and determination of energy efficiency is given in Table 5.

### Conclusion

The purpose of this study, create a suitable model for Turkish conditions and contribute to widespread of biogas in Turkey. This study consist biogas production and energy technology research, system simulation and decision support system (DSS) modeling, manufacture of two laboratory-scale biogas plant and experimental studies. The waste used in the pilot scale plant; grass waste, wholesale food waste, chicken manure, cattle manure, inner tripe from slaughterhouses. The residence time at the plant is 47 days; ratio of organic dry matter is 9 % and the fermentation temperature is 37-38°C under

mesophilic conditions. Approximately %31 rates of solids (DM), 31.6 t/d raw material and 9.8 m<sup>3</sup>/d water have entered to fermenters. A total of 876 kW/h of power would be consumed for producing the design amounts of 353 kW of electric power and 361 kW of heat. The total and net energy efficiencies for biogas-fired CHP plant were 81,5% and 76,2%, respectively. The organic dry fertilizer of 5.100t/y at the dry matter rate of %25 and liquid fertilizer of 8.330 t/y at dry matter rate of %6 at the end of the process were planned. Plant configuration was completed. Moreover, Decision Support Systems, simulation and modeling study was also completed. After the installation of cogeneration unit, the biogas plant will start production. Layout of pilot scale biogas plant is shown in Figure 6.



**Figure 6.** Pilot Scale Biogas Plant

### Acknowledgement

The financial support of The Scientific and Technological Research Council of Turkey (TUBITAK), Kavaklıdere/Ankara, TURKEY is greatly noted.

### Reference Example:

- [1] Kaya D., Çanka Kılıç F., A Guide on Exploitation Of Agricultural Waste in Turkey, Project No: Life 03 Tey/ Tr/ 000061, Prepared by TUBITAK MRC, Contributed by: Cukurova University Agricultural Engineering, Exergia, CRE Under Life Third Countries Programme, Gebze, KOCAELİ-TURKEY December 2005.
- [2] Çetinkaya, H., Deutsche-Türkische Konferenz in Stoffstrommanagement, Klimaschutz und Nachhaltige Entwicklung, 6-7 October 2006, Antalya.
- Kuhn, E. 1995. Kofermantaion, Arbeitspapier, 219; Hrsg. KTBL, Darmstadt
- Heck, P., Bemann, U., 2002. Praxishandbuch. Stoffstrommanagement. 2002/2003. Fachverlag Deutscher Wirtschaftsdienst GmbH & CO. ISBN 3-87156-481-8.

- [3] Anonymous, 2007, a. <http://www.agrowaste-tr.org/>
- [4] Simulation of the energy Conversion Systems (boiler, gas engines and micro turbines) and the integration, Biogas Project Technical Report-4 No. 112 106 G, TÜBİTAK MAM, October 2008, Gebze-Kocaeli.
- [5] Laboratory-Scale Biogas System Works, Biogas Project Technical Report-5 No. 112 106 G, TÜBİTAK MAM, October 2008, Gebze-Kocaeli.
- [6] Kaya D., Tırıs M., Ozturk H. H., Ekinci K., Ertekin C., Bascetincelik A., Yaldız O., “**Energy and Exergy Efficiencies for Biogas-Fired Combined Heat and Power Plant**”, IWES - 2. Atıktan Enerji Sempozyumu ve Sergisi, Wow Convention Center, İstanbul, 04-05/11/2009
- [7] Anonymous, 2010, b. <http://www.iea.org/stats/prodresult.asp?PRODUCT=Renewables>



## ANALYSIS OF FOOD PROCESSING OPERATIONS USING CFD

STAVROS YANNIOTIS

Agricultural University of Athens, Department of Food Science and Technology

Iera odos 75, 118 55 Athens, Greece

Phone: +30 210 529 4703, Fax: +30 210 529 4731, e-mail: yanniotis@aua.gr

### Abstract

Computer simulation is a powerful tool for prediction and optimal design in food and agricultural engineering operations. Partial differential equations describing momentum, heat and mass transfer coupled with equilibrium and kinetic equations, which usually form a model for a processing operation, can be solved easily with today's computing capabilities. In this paper, a brief description of the principles of Computational Fluid Dynamics (CFD) for the solution of fluid flows with heat and mass transfer is given. Selected examples from the food and agricultural engineering literature including applications in ventilation systems for greenhouses, animal housing, orchard spraying, airflow in refrigerated trucks, air flow through vented packages, drying of fruits, spray drying of liquid foods, chilling of meat, baking ovens design, heat exchanger design, canning and more are presented.

### Introduction

The aim of the food industry today is to provide safe, nutritious and of high sensory quality food to the consumers. This aim is achieved by applying basic concepts of chemistry, microbiology and engineering to food processing. There are many unit operations in the food industry where steady or unsteady state transport phenomena are taking place e.g. pasteurization, sterilization, blanching, dehydration, evaporation, cooling, freezing etc. Very often in these operations heat transfer is combined with mass transfer and/or momentum transfer. Heat, mass and momentum transfer in these operations is of primary importance and affect the hygienic, nutritional and sensory quality of the product.

In applying transport phenomena in food processing, one must take into account that food industry usually deals with difficult raw materials. As biological materials, in many cases they are non-uniform and of variable consistency. The shape of the products is often irregular and some times changes during processing. Many food products undergo physical property changes during heating and some even composition changes. Some, are shear-dependant, others are time-dependant. In some cases, the materials are anisotropic. The effect of heat treatment on the food product depends on the combination time-

temperature because, in addition to temperature changes during processing, biochemical and microbiological changes take place. Heat transfer and reaction kinetics considerations must be taken into account in designing thermal processes of foods. Over processing, by applying high heat treatment has a negative effect on the product quality and its nutritional value. Under processing may result in spoilage of the product [43].

Because of these complexities, the unsteady state momentum, heat and mass transfer partial differential equations can be solved analytically only with several simplifying assumptions. Recently, Computational Fluid Dynamics (CFD) codes have been applied to food and agricultural engineering problems. This approach is rapidly penetrating the field of food and agricultural engineering so that techniques, methods and models currently widely available in other scientific and practical areas of engineering and science are expected to find application in the agro-food industry in the coming years [36]. The present paper attempts to give a short review of the recent scientific activity on the applications of CFD in the agro-food sector.

CFD involves the solution of integrated Navier-Stokes conservation equations in the general form of :

$$\frac{\partial}{\partial t}(\rho\phi) + \frac{\partial}{\partial x_j}(\rho u_j \phi) = \frac{\partial}{\partial x_j} \left( \Gamma \frac{\partial \phi}{\partial x_j} \right) + S_\phi \quad (1)$$

where  $\rho$  is the fluid density,  $u_j$  the air velocity component,  $\phi$  any variant (velocity components, enthalpy),  $\Gamma$  a diffusion coefficient and  $S_\phi$  a source term. For  $\phi$  equal to unity, the above equation reduces to the continuity equation. On the left hand side of the equation, the first term on denotes the rate of change and the second the convection flux. On the right hand side, the first term stands for the diffusion flux and the second for any generation and/or destruction of variable  $\phi$ .

## APPLICATIONS

Selected examples of the use of CFD in food and agricultural engineering are provided below.

CFD has been applied by several researchers in cooling and freezing operations, as for example by Hu and Sun [19] in the analysis of the turbulent flow field and the heat and moisture transfer in a 3-D air-blast chiller containing cooked meats of cylindrical and elliptical shapes, by Trujillo and Pham [41] in the study of simultaneous heat and mass transfer in beef chilling. The air temperature fluctuation that is observed in a freezer due to the ON/OFF action of the compressor and the automatic defrost cycle affects the temperature of frozen products. A CFD model was used to predict the product temperature variation caused by the air temperature fluctuation in a domestic freezer [2]. Foster [12] studied the optimization of air movement through doorways in refrigerated rooms.

Moureh et al. [32] studied the effectiveness of insulating devices in reducing the rate of temperature changes during product transportation on vehicles in the absence of refrigeration, Moureh [32] studied the case of optimization of airflow in refrigerated truck configuration loaded with pallets, Ferrua and Singh [11] presented a model for airflow through vented packages containing horticultural products.

Heat transfer in heat exchangers is another area of CFD applications with emphasis on the hydrodynamics thermal and fouling analysis of

plate heat exchangers aiming at the prediction of flow and temperature profiles in the channel in order to optimized the design of the plate shape and corrugation profile [15], [22].

CFD has also been used in studying spray dryers for the drying of dairy and other liquid food products. Focus is mostly placed on understanding the flow patterns, the particle trajectories, the temperature and humidity profiles inside the dryer, the wall deposition and the droplet/particle collisions [38], [24], [20], [14], [20], [21], [16], [23].

Oven design and analysis is another area of application of CFD with the aim to maintain the baking temperature profile at the optimum condition and optimize the oven design and control system. Zhou and Therdthai [45] studied a 3-D continuous industrial baking process, Therdthai *et al.* [40] simulated a 2-D cross section of a bread baking oven, Mondal and Datta [31] simulated a crustless bread baking process and Verboven et al. [42] presented a model of an oven with convection heating with hot air and microwave heating.

Sterilization is one of the areas where CFD has been applied in recent years. Thus, several researchers have predicted numerically, transient temperature and velocity profiles during natural convection heating in still cans or pouches containing liquid foods as for example in [7], [8], [13]. CFD analysis has helped to envision the flow field inside the can. Liquid inside the can is moving due to the natural convection currents that are developed. During the heating phase, liquid is moving upwards to the top of the can due to buoyancy in the near-metal wall region of the can and then is moving downwards through the centre. During the cooling phase, the movement is to the opposite direction i.e. liquid adjacent to the metal wall of the can starts moving towards the bottom of the can, while liquid in the centre is moving upwards to the top of the can. The thickness of the ascending or descending liquid layer adjacent to the metal wall is about 3-5 mm. Vortices are observed in the near-metal wall region of the can in the heating as well as in the cooling phase. Liquid is moving with high velocity at the

beginning of the heating and cooling phases where the temperature difference between the heating/cooling medium and the liquid is large. A sharp increase in velocity at the beginning of the cooling phase is also observed. It is known that the slowest heating zone (SHZ) for a can containing only a solid food or a very viscous food lies in the geometric centre of the can. The SHZ of a can containing liquid foods or solids immersed in a liquid has been calculated using CFD to be at a point close to the geometric centre at the beginning but moves fast towards the bottom as the liquid is heated. It moves to the point that lies about 10-15% of the can height from the bottom. The slowest cooling zone (SCZ) during the cooling phase of the can is located on the central axis of the can at a point that lies about 10-15% of the can height from the top of the can. The number of solid items in the can and the concentration of the brine/syrup affects slightly the temperature in the SHZ, as calculated using CFD.

Other researchers used CFD in various applications as for example Mirade [28] in calculating the air velocity field in modern meat dryers, Denys et al. [6] in the analysis of intact egg pasteurization processes, Mirade [29] in assessing the operation and indoor atmosphere of industrial cheese ripening rooms, Yanniotis and Xerodemas [44] in the simulation of the operation of a pad humidifier, Chanteloup and Mirade [4] in assessing the ventilation efficiency inside forced-ventilation food plants, Le Page et al [25] in simulating the effect of airflow on heat and mass transfer of unwrapped food products, Amanlou and Zomorodian [1] in designing a fruit cabinet dryer.

The design of ventilation systems for agricultural production systems such as greenhouses and animal housing is another area of application of CFD. Lee et al.[26] studied the internal airflow patterns in a piglet house, Sun et al. [39] also developed a three-dimensional CFD model to predict the airflow pattern and ammonia distribution for summer conditions within an experimental hog building, Maïzi et al. [27] modelled prediction of odorous compound dispersion, Bjerg et al. [3] investigated different methods to model wall inlets with CFD

simulations of airflow in livestock rooms, Norton et al. [34] modelled air mixing in a naturally ventilated livestock building. Factors such as ventilation rates, airflow patterns, ventilation efficiencies distribution of humidity, fan and pad evaporative cooling system have been analyzed in greenhouses using CFD, considering structural types, natural climate factors such as wind direction and vent configurations as for example in [18] and [35].

CFD has been used to simulate airflow and droplets movement in sprayers with the aim of reducing losses of pesticides and providing good distribution uniformity of the spray [5], [9], [10], [30].

## CONCLUSION

The short review presented here shows that CFD has been used in a broad range of applications in the agro-food processes in recent years. It is a mature, useful, reliable and comparable simple tool which can be used to extend knowledge and understanding of various processes especially with the increased computing power that is available today.

## References

1. Amanlou, Y.-Zomorodian, A.: Applying CFD for Designing a New Fruit Cabinet Dryer. *J. of Food Eng.*, In Press, 2010
2. Antoniou, J.-Yanniotis, S.: CFD modeling of air temperature fluctuation in a domestic freezer, Paper in preparation, 2010.
3. Bjerg, B.-Svidt, K.-Zhang, G.-Morsing, S.-Johnsen, J.O.: Modeling of air inlets in CFD prediction of airflow in ventilated animal houses. *Computers and Electronics in Agriculture* 34, 2002, p.223–235.
4. Chanteloup, V.-Mirade, P.S.: Computational fluid dynamics (CFD) modelling of local mean age of air distribution in forced-ventilation food plants. *J. of Food Eng.* 90 (1), 2009, p. 90-103.
5. Delele, M. A.-Jaeken, P.-Debaer, C.-Baetens, K.-Melese, A.-Ramon, E.H.-Nicolai, B.M.-Verboven, P.: CFD prototyping of an air-assisted orchard sprayer aimed at drift

- reduction. *Computers and Electronics in Agriculture* 55 (1), 2007, p. 16-27.
6. Denys, S.-Pieters, J.-Dewettinck, K.: CFD Analysis of Thermal Processing of Eggs. In *Computational Fluid Dynamics in Food Processing*, Edited by Da-Wen Sun, CRC Press, Boca Raton London New York, p.347-380.
  7. Dimou, A.-Yanniotis, S.: CFD Modelling of asparagus canning. Paper in preparation, 2010.
  8. Dimou, A.-Yanniotis, S.: CFD analysis of thermal processing of olives in a can. Paper in preparation, 2010.
  9. Endalew, M.-Debaer, C.-Rutten, N.-Vercammen, J.-Delele, M.A.-Ramon, H.-Nicolai, B.M. – Verboven, P.: A new integrated CFD modelling approach towards air-assisted orchard spraying. Part I. Model development and effect of wind speed and direction on sprayer airflow. *Computers and Electronics in Agriculture* 71 (2), 2010, p.128-136.
  10. Endalew, M.-Debaer, C.-Rutten, N.-Vercammen, J.-Delele, M. A.-Ramon, H.-Nicolai, B. M.-Verboven, P.: A new integrated CFD modelling approach towards air-assisted orchard spraying-Part II: Validation for different sprayer types. *Computers and Electronics in Agriculture* 71 (2), 2010, p. 137-147.
  11. Ferrua, M.J.-Singh, R.P.: Modeling Airflow through Vented Packages Containing Horticultural Products. In *Computational Fluid Dynamics in Food Processing* Edited by Da-Wen Sun, CRC Press, Boca Raton London New York, 2007, p.649-696.
  12. Foster, A.M.: CFD Optimization of Air Movement through Doorways in Refrigerated Rooms. In *Computational Fluid Dynamics in Food Processing* Edited by Da-Wen Sun, CRC Press, Boca Raton London New York, 2007, p.167-194.
  13. Ghani, A.G.A.-Farid, M.M.: Thermal Sterilization of Food Using CFD. In *Computational Fluid Dynamics in Food Processing* Edited by Da-Wen Sun, CRC Press, Boca Raton London New York, 2007, p.331-346.
  14. Goula, A.M.-Adamopoulos, K.G.: Influence of spray drying conditions on residue accumulation – Simulation using CFD. *Drying Technology* 22(6), 2004, p.1107-1128.
  15. Grijseerd, K.-Hazarika, B.-Vucinic, D.: Application of computational fluid dynamics to model the hydrodynamics of plate heat exchangers for milk processing. *J. Food Eng.*, 57, 2003, p.237-242.
  16. Guo, B.Y.-Fletcher, D.F.-Langrish, T.A.G.: Simulation of the agglomeration in a spray using Lagrangian particle tracking. *Appl. Math. Model.*, 28 (3), 2004, p. 273-290.
  17. Hamdami, N.-Monteau, J.Y.-Le Bail, A.: Heat and mass transfer in par-baked bread. *Food Research International* 37, 2004, p. 477-488.
  18. Hong, S.W.-Lee, I.B.-Hwang, H.S.-Seo, I.H.-Bitog, J.P.-Yoo, J.I.-Kim, K.S.-Lee, S.H.-Kim, K.W.-Yoon, N.K.: Numerical simulation of ventilation efficiencies of naturally ventilated multi-span greenhouses in Korea. *Trans. ASAE* 51, (4), 2008, p. 1416-1432.
  19. Hu, Z.-Sun, D.W.: Predicting local surface heat transfer coefficients by different turbulent k- $\epsilon$  models to simulate heat and moisture transfer during air-blast chilling. *J. Refrigeration* 24, 2001, p. 702-717.
  20. Huang, L.-Kumar, K.-Mujumdar, A.S.: A parametric study of the gas flow patterns and drying performance of co-current spray dryer: results of a computational fluid dynamics study. *Drying Technology*, 21(6), 2003, p. 957-978.
  21. Huang, L.-Kumar, K.-Mujumdar, A.S.: Use of computational fluid dynamics to evaluate alternative spray dryer chamber configurations. *Drying Technology*, 21(3), 2003, p.385-412.
  22. Jun, S. – Puri, V.M.: Plate Heat Exchanger: Thermal and Fouling Analysis. In *Computational Fluid Dynamics in Food Processing* Edited by Da-Wen Sun, CRC Press, Boca Raton London New York, 2007, p.417-432.

23. Kuriakose, R.-Anandharamakrishnan, C.: Computational fluid dynamics (CFD) applications in spray drying of food products. Trends in Food Science & Technology, In Press, 2010.
24. LeBarbier, C.-Kockel, T.K.-Fletcher, D.F.-Langrish, T.A.G.: Experimental measurement and numerical simulation of the effect of swirl on flow stability in spray dryers. Chem. Eng. Res. Des., 79 (A3), 2001, p. 260-268.
25. Le Page, J.F.-Chevarin, C.-Kondjoyan, A.-Daudin, J.D.-Mirade, P.S.: Development of an approximate empirical-CFD model estimating coupled heat and water transfers of stacked food products placed in airflow. J. of Food Eng. 92 (2), 2009, p. 208-216.
26. Lee, I.B.-You, B.K.-Kang, C.H.-Jeun, J.G.-Kim, G.W.-Sung, S.H.-Sase, S.: Study on forced ventilation system of a piglet house. JARQ 38 (2), 2004, p. 81-90.
27. Maïzi, A.-Dhaouadi, H.-Bournot, P.-Mhiri, H.: CFD prediction of odorous compound dispersion: Case study examining a full scale waste water treatment plant. Biosystems Engineering, 106,(1), 2010, 68-78.
28. Mirade, P.S.: CFD Prediction of the Air Velocity Field in Modern Meat Dryers. In Computational Fluid Dynamics in Food Processing Edited by Da-Wen Sun, CRC Press, Boca Raton London New York, 2007, p.223-248.
29. Mirade, P.S.: CFD Modeling of Indoor Atmosphere and Water Exchanges during the Cheese Ripening Process. In Computational Fluid Dynamics in Food Processing Edited by Da-Wen Sun, CRC Press, Boca Raton London New York, 2007, p.697-726.
30. Molari, G.-Benini, L.-Ade, G.: Design of a recycling tunnel sprayer using CFD simulations. Trans. of the ASABE. 48(2), 2005, p.463-468.
31. Mondal, A.-Datta, A.K.: Two-dimensional CFD modeling and simulation of crustless bread baking process. J. of Food Eng. 99 (2), 2010, p.166-174.
32. Moureh, J.: CFD Optimization of airflow in refrigerated truck configuration loaded with pallets. In Computational Fluid Dynamics in Food Processing Edited by Da-Wen Sun, CRC Press, Boca Raton London New York, 2007, p.43-82.
33. Moureh, J.-Laguerre, O.-Flick, D.-Commere, B.: Analysis of use of insulating pallet covers for shipping heat-sensitive foodstuffs in ambient conditions. Computers and Electronics in Agriculture, 34, 2002, p.89-109.
34. Norton, T.-Grant, J.-Fallon, R.-Sun, D.W.:A computational fluid dynamics study of air mixing in a naturally ventilated livestock building with different porous eave opening conditions Biosystems Engineering 106 (2), 2010, p.125-137.
35. Sapounas, A.-Bartzanas, T.-Nikita/Martzopoulou, C.-Kittas, C.: Aspects of CFD modelling of a fan and pad evaporative cooling system in greenhouse. International Journal of Ventilation 6 (4), 2008, p. 379-388.
36. Sardi, A.-Yanniotis, S.: Numerical modelling of heat transfer in the food industry-recent developments and applications. In Heat Transfer in Food Processing, Edited by S. Yanniotis and B. Sunden, WIT Press, Southampton, Boston, 2007, p.1-26.
37. Sase, S.K.M.-Okushima, L.: Optimization of vent configuration by evaluating greenhouse and plant canopy ventilation rates under wind-induced ventilation. Transactions of the ASAE 47 (6), 2004, p. 2059-2067.
38. Straatsma, H.-Verschuere, M.-Gunsing, M.-Jong, P.-Verdurmen, R.E.M.: CFD Simulation of Spray Drying of Food Products. In Computational Fluid Dynamics in Food Processing Edited by Da-Wen Sun, CRC Press, Boca Raton London New York, 2007, p.249-286.
39. Sun, H.-Keener, H.-Michel, F.: Comparison of predicted and measured ammonia distribution in a high-rise hog building (HRHB) for summer conditions. ASAE Paper No. 024117. St. Joseph, Mich., USA (2002) (cited by Lee et al 2004).
40. Therdthai, N.-Zhou, W.-Adamczak, T.: Two-dimensional CFD modelling and simulation of



- an industrial continuous bread baking oven. *J. of Food Eng.* 60, 2003, p.211-217.
41. Trujillo, F. J.-Pham, Q.T: CFD Modeling of Simultaneous heat and mass transfer in beef chilling. In *Computational Fluid Dynamics in Food Processing* Edited by Da-Wen Sun, CRC Press, Boca Raton London New York, 2007, p.195-222.
42. Verboven, P.-Nicola, B.M.-Datta, A.K.: Computation of airflow effects in microwave and combination heating. In *Computational Fluid Dynamics in Food Processing* Edited by Da-Wen Sun, CRC Press, Boca Raton London New York, 2007, p.313-330.
43. Yanniotis, S.: Computational methods in food processing: Applications in heat transfer. *Advanced Computational Methods in Heat Transfer VI*, WIT press, 2000, p. 595-604
44. Yanniotis, S.-Xerodemas, K.: Air humidification for seawater desalination. *Desalination*, 158, 2003, p.313-319.
45. Zhou, W.-Therdthai, N.: Three-Dimensional CFD modeling of a continuous industrial baking process. In *Computational Fluid Dynamics in Food Processing* Edited by Da-Wen Sun, CRC Press, Boca Raton London New York, 2007, p.287-312.



## INFLUENCE OF DRAWING ENERGY FROM THE SOIL MASS TO ITS TEMPERATURE

ADAMOVSKEÝ RADOMÍR, NEUBERGER PAVEL, ŠEĐOVÁ MICHAELA

Czech University of Life Sciences Prague, 165 21 Czech Republic,

Phone: +4202224484176, E-mail: adamovsky@tf.czu.cz

### Abstract

The article is devoted to temperature changes in the ground massif with the horizontal heat exchanger as an energy source for a heat pump. The article was aimed at analyzing temperature changes in the ground massif with the horizontal heat exchanger at the beginning, in the course of and at the end of the heating season. Another aim was to analyze temperature differences in the area of the horizontal exchanger and the reference lot. The heat flow utilized in the evaporator of heat pump was extracted from the ground exchanger (nominal output at the condenser was 10.5 kW). Temperatures of the ground massif with the horizontal heat exchanger were measured in its plane in depths of 0.75 m, 0.5 m and 0.25 m. The temperature inside the ground massif on the reference lot and ambient parameters were measured as well. It is obvious that the difference of energetic potentials inside the ground massif with the heat exchanger and on the reference lot is insignificant at the beginning of the heating season. During the heating season, the difference of ground massif energetic potentials increases; at the end it is constant. The difference of temperatures in horizontal planes was not significant at the beginning of the heating season; however, it gradually increased. Maximum differences were detected in the area of the heat exchanger. In higher strata, the difference between temperatures decreases. During a major part of the heating season, temperatures at pipes of the ground exchanger were negative. This fact affected amounts of heat extracted from the ground massif.

**Key words:** Heat pump; Horizontal ground heat exchanger; Ground source heat pump; Heat transfer; Energy potential; Heat season; Ground temperature; Temperature distribution.

### Introduction

During the heating season, the horizontal heat exchanger - as a source of energy - carries off the heat accumulated inside the ground massif in the summer. The ground massif temperature, together with the thermal characteristics of the massif, are dominant factors determining the availability of the entire energy system. The following thermal characteristics of the ground massif may be defined:

- conductivity  $\lambda$  [ $\text{W}\cdot\text{m}^{-1}\cdot\text{K}^{-1}$ ], expressing the ability to share thermal energy among directly adjoining rock particles;
- specific thermal capacity  $c$  [ $\text{J}\cdot\text{kg}^{-1}\cdot\text{K}^{-1}$ ], expressing the quantitative ability to absorb and release the heat energy;
- temperature conductivity  $a$  [ $\text{m}\cdot\text{s}^{-2}$ ], characterizing the speed of propagation of temperature changes in the ground massif during its heating and cooling.

The effect of ground massif conductivity and the material of exchanger piping on the function the horizontal exchanger should perform was studied by Song, Yao and No [9]. They developed the horizontal ground heat exchanger as a source for the heat pump. They simulated the effect of ground/piping conductivity on the thermal field and the exchanger's thermal capacity.

In their paper, Mihalakakou, Santamouris, Lewis and Asimakopoulos [6] present a model for predicting the daily and yearly variations of the ground massif temperature. This model is based on the differential equation which describes convection, using the boundary condition of the formula for energy balance on the ground massif's surface.

A new approach to simulating the horizontal type of ground exchanger is presented by Piechowski [7]. His mathematic model and measurements are concentrated on the boundary between the ground and the piping. The model

considers the heat and humidity transfer inside the ground massif; it enables prediction of the heat field and heat flows inside the massif (due to heat off-take by the horizontal ground exchanger) more precisely

Regarding the system's energy efficiency it is important that the ground massif temperature should not decrease at the beginning of subsequent heating seasons; i.e. the energy accumulated in summer should always cover the deficiency of energy (due to its removal) at the end of the heating season.

This article links up to the results of testing published last year [1]. It confirms and amends many results. The aim of this article is to analyze the differences of ground temperatures in the area of the horizontal heat exchanger and on the reference lot. Another aim is to analyze the temperature changes in the ground massif at the beginning, in the course and at the end of the heating season.

## Methods

### 1. Theoretical analysis

Inside the ground massif and at its boundary with the atmosphere, complex processes of heat transfer take place, comprising conduction, convection and radiation. Other thermal processes of heat transfer are represented by changes in state - evaporation, condensation, melting, freezing.

The equation for total specific heat flow in the ground massif may be written as (adapted according to [3]; [8])

$$q_{\tau,t} = q_{\tau,\lambda} + q_{\tau,\alpha,w} + q_{\tau,\alpha,v} + q_{\tau,r} + q_{\tau,lat} \quad (1)$$

[W.m<sup>-2</sup>]

Where:  
 $q_{\tau,t}$  - total specific heat flow in the ground massif [W.m<sup>-2</sup>];

$q_{\tau,\lambda}$  - specific heat flow transferred via conduction [W.m<sup>-2</sup>];

$q_{\tau,\alpha,w}$  - specific heat flow transferred via convection between water and ground [W.m<sup>-2</sup>];

$q_{\tau,\alpha,v}$  - specific heat flow transferred via convection between vapour and ground [W.m<sup>-2</sup>];

$q_{\tau,r}$  - specific heat flow transferred via radiation [W.m<sup>-2</sup>];

$q_{\tau,l}$  - specific heat flow transferred during the change in the state of water [W.m<sup>-2</sup>].

Individual specific heat flows are analyzed in the article [2]

A major heat ratio transferred via conduction inside the ground massif enables us (especially in cases where the dimensions of the ground particles and pores are negligible if compared to the volume of the ground itself) to ignore other kinds of heat transfer. For instance, Firlag and Rucińska (2007) introduce the formula for calculating the ground massif heat resistance  $R_G$ :

$$R_G = \frac{I(X_{dz}) - I(X_{2H})}{2\pi \cdot \lambda_{gr}} \quad [\text{m.K.W}^{-1}] \quad (2)$$

Where:  $\lambda_{gr}$  - coefficient of the ground massif heat conductivity [W . m<sup>-1</sup>. K<sup>-1</sup>];

$I(X_{dz})$  - function for  $X = dz$ ;

$I(X_{2H})$  - function for  $X = 2H$ ;

$d_z$  - piping diameter (horizontal ground exchanger) [m];

$H$  - depth of the ground exchanger placement [m].

The values of functions  $I(X)$  are calculated according to formulae (14) and (15):

For  $0 < X < 1$  it is valid:

$$I(X) = \frac{1}{2} (-\ln X^2 - 0.57721566 + 0.99999193 X^2 - 0.24991055 X^4 + 0.05519968 X^6 - 0.00976004 X^8 + 0.00107857 X^{10}) \quad [-] \quad (3)$$

For  $1 \leq X < \infty$  this is valid:

$$I(X) = \left[ \frac{1}{2X^2 \cdot e^{X^2}} \right] \cdot \left( \frac{A}{B} \right) \quad [-] \quad (4)$$

Coefficients  $A$  and  $B$  are described by following equations:

$$A = X^8 + 8.5733287X^6 + 18.059017X^4 + 8.637609X^2 + 0.2677737 \quad [-] \quad (5)$$

$$B = X^8 + 9.5733223X^6 + 25.6329561X^4 + 21.0996531X^2 + 3.9684969 \quad [-] \quad (6)$$

### 2. Measuring methods

The site of our testing is situated in Southern Bohemia (Hlinice village, Tábor District) at an altitude of 480 m. In this area, the outdoor calculated temperature is -15°C; the average temperature during the heating season is 3°C.

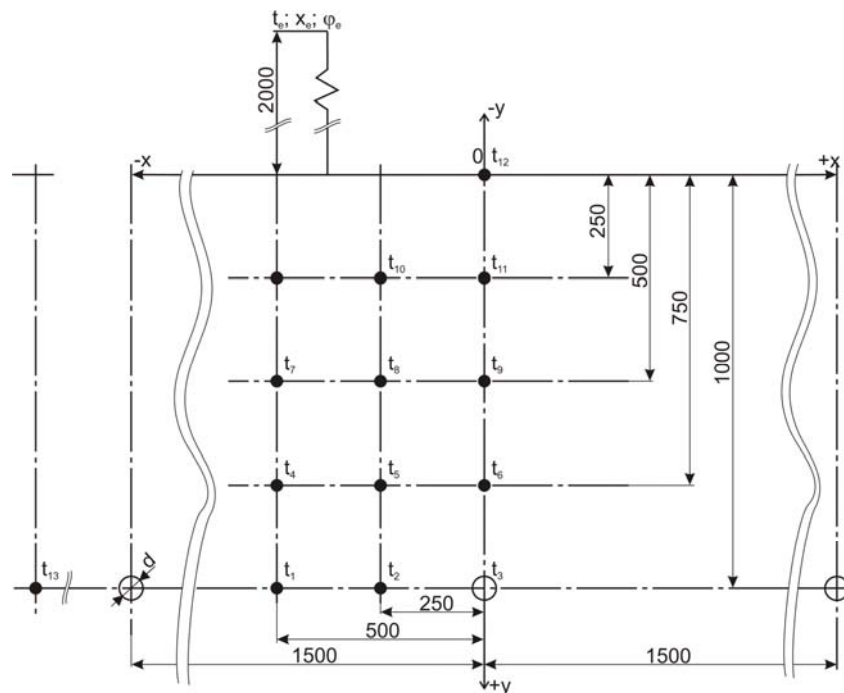


**Figure 1.** Scheme of measuring temperatures in the profile of the horizontal exchanger

The horizontal heat exchanger in the ground massif was made of polyethylene pipes ( $D = 40$  mm, pipe wall thickness = 2.5 mm, length = 400 m). The lot's ground plan was 27 x 25 m. Before the realized measurements, the ground exchanger had been operated for 4 years. The exchanger was working as a heat source for a heat pump evaporator; its nominal output at the condenser was 10.5 kW.

The temperatures of the ground massif were measured by special NiCr-Ni sensors with a spike, intended for measuring ground temperatures. The points of measuring are specified in Fig. 1. The  $t_{13}$  sensor measured the ground massif temperature on the reference lot. The air temperature and relative humidity ( $t_e, \varphi_e$ ) were measured beyond the reference lots by a combined sensor modified for meteorological measurements (2 metres above the ground surface). The measured parameters were detected once an hour in the course of one year.

### Results and discussion

The results of testing have proved the fact that before the beginning of the heating season, the average temperature of the ground massif with a heat exchanger in the depth of 1.0 m ( $t_1$ ,

$t_2$ ,  $t_3$  according to Fig.1) was 0.2 K lower than on the reference lot. This result demonstrates the fact that even in the depth of the exchanger placement, the heat energy dissipated during the heating season was compensated due to the accumulated solar irradiation and the heat from precipitation. The behaviour of the temperatures in the ground massif with a heat exchanger (Fig. 2) shows that the differences of the temperatures measured at particular depths are 0.1 – 0.2 K. They may be considered insignificant.

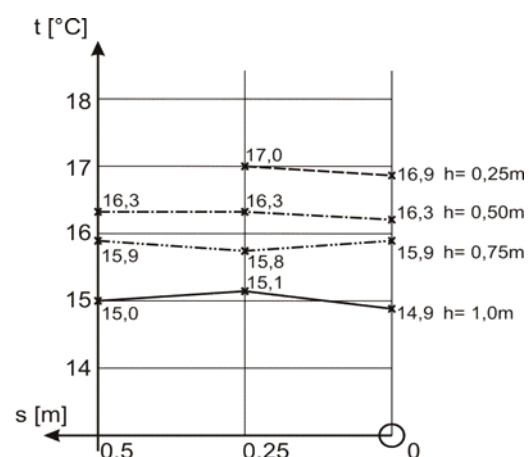


**Figure 2.** Behaviour of temperatures in the ground massif with a horizontal heat exchanger before the heating season.

(10/9/2008, 17:15)  $t_{12} = 22.2$  °C;  $t_{13} = 15.2$  °C;  $\varphi_e = 0.561$ ;  $t_e = 19.7$  °C.

The temperatures in the ground massif (Day 96 of heating season) are given in Fig. 3. The temperature difference near the heat exchanger and on the reference lot increased markedly to 3.3 K. The average temperature of the heat exchanger transferring medium at the inlet to/outlet from the heat pump evaporator was  $-3.4^{\circ}\text{C}$ . The temperature behaviour in particular ground layers demonstrates the fact that the maximum difference at particular depths was 0.1 K; the temperatures in 0.75 and 1.0 m were identical. The temperature differences may be considered non-significant, too. In the middle of the heating season, the temperatures of the ground massif in the zone of the exchanger are negative.

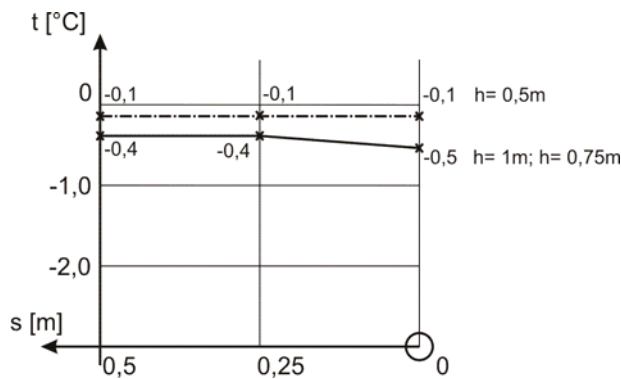


**Figure 3.** Temperature behaviour in the ground massif with a horizontal heat exchanger during the heating season.

(31/12/2008, 7:37)  $t_{12} = -4.9^{\circ}\text{C}$ ;  $t_{13} = 2.8^{\circ}\text{C}$ ;  $\varphi_e = 0.988$ ;  $t_e = -12.05^{\circ}\text{C}$ ;

The temperatures of the ground massif at the end of the heating season (Day 155 of the heating system operation) are shown in Fig. 4. The temperature differences in the zone of the ground heat exchanger and on the reference lot achieved 2.6 K; they are thus less than in the middle of the heating season. The medium temperature of the heat transferring medium in the ground exchanger was  $-3.5^{\circ}\text{C}$ . The temperature behaviour in particular ground massif layers shows the fact that at the depth of the exchanger placement, the difference of the average temperatures ( $t_1, t_2, t_3$ ) was 1.2 K; in 0.75 m ( $t_4, t_5, t_6$ ) it was 0.4 K and at depths of 0.5 m and 0.25 m ( $t_7, t_8, t_9, t_{10}, t_{11}$ ) it was 0.2 K. The temperature difference cannot be considered

important. The temperatures of the ground massif in the exchanger zone are negative.

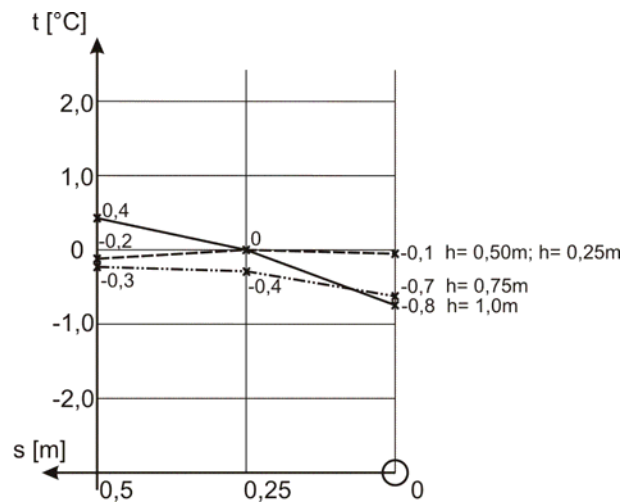


**Figure 4.** Temperature behaviour in the ground massif with a horizontal heat exchanger at the end of the heating season.

(28/2/2008, 14:50)  $t_{12} = 0.2^{\circ}\text{C}$ ;  $t_{13} = 1.8^{\circ}\text{C}$ ;  $\varphi_e = 0.968$ ;  $t_e = 5.31^{\circ}\text{C}$ ;

## Conclusion

The results of monitoring temperatures in particular layers in the plane perpendicular to the pipes of the ground exchanger have demonstrated that the temperature differences ( $t_1, t_2, t_3$  and others) were in the range of 0.1 – 1.2 K within the entire heating season. With regards to the given spacing of the pipes in the ground exchanger and their depth of placement, the temperature differences may be considered unimportant. From the middle of the heating season, the temperatures in the ground massif were negative in the zone of the exchanger piping. According to expert literature [4], if the temperature of the ground massif decreases, water diffuses into the zone of the piping placement. At negative massif temperatures near pipes, diffused water changes its state. Considering the high value of the latent heat of water freezing ( $334 \text{ kJ} \cdot \text{kg}^{-1}$ ), this change affects the heat flow distributed to the heat pump evaporator. A certain effect on the heat flow dissipated from the ground massif also results from the fact that the coefficient of ice heat conductivity ( $2.21 \text{ W} \cdot \text{m}^{-1} \cdot \text{K}^{-1}$ ) is almost four times higher than for water. The caloric capacity of ice ( $2.06 \text{ kJ} \cdot \text{kg}^{-1} \cdot \text{K}^{-1}$ ) is also half that of water.

The difference of the energy potentials inside the ground massif in the zone of the heat exchanger and on the reference lot (at the beginning of the heating season; expressed by temperature difference  $t_3 - t_{13}$ ) was 0.3 K. At the end of the first half of the heating season, the temperature difference increased to 3.3 K. In the second half of the heating season, the difference did not increase. From the results of the first tests it implies that the energy potential of the ground massif regenerated during summer.

Within further routine tests of horizontal ground heat exchangers we want to focus on specifying the caloric characteristics of the ground massif and the effect of its humidity on their values. We also want to create a mathematical model of heat flows and heat fields in the ground massif and to verify the possibility to increase the massif's energy potential via the heat pump's reverse operation in summer.

## References

- [1] Adamovský, R., Neuberger, P. Šed'ová, M. Temperature changes in heat pump horizontal ground source. *Infrastructure and Ekology of Rural Areas*, (7), 2009, p. 17-24.
- [2] Adamovský, R., Neuberger, P. Šed'ová, M. Analyzing temperature changes in the ground massif with a horizontal heat exchanger in the course of the heating season. *Infrastructure and Ekology of Rural Areas*, (6), 2010, p. 27-35.
- [3] Brandl, H. Energy fundations and other thermo – active ground structures. *Geotechnique*, 56, (2), 2006, p. 81-122.
- [4] Dvořák, Z., Klazar, L., Petrák, J. *Tepelná čerpadla*. Praha, SNTL Nakladatelství technické literatury. 1987, 340 p.
- [5] Firlag, S., Rucińska, J. Simplified Metod of designing on air-ground heat exchanger. CESB 07 PRAGUE Conference, 2007, Session M3B: Building Design 1.
- [6] Mihalakakou, G., Santamouris, M., Lewis, J., Asimakopoulos, D. N. On the application of the energy balance equation to predict ground temperature profiles. *Solar Energy*, Vol. 60, Nos.3/4, 1997, p. 181 – 190.
- [7] Piechowski, M. Heat and mass transfer model of ground heat exchanger. 1997 , ([https://intraweb.stockton.edu/eyos/energy\\_studies/content/docs/proceedin/PIECH.PDF](https://intraweb.stockton.edu/eyos/energy_studies/content/docs/proceedin/PIECH.PDF))
- [8] Rees, S.W., Adjali, M. H., Zhou, Z., Davies, M. (2000). Ground heat transfer effects on the thermal performance of earth – contact structures. *Renewable and SustainableEnergy*, 4, (2) 2000, p. 213-265.
- [9] Song, Y., Yao, Y., Na, W. Impacts of soil and pipe thermal conductivity on performance of horizontal pipe in a ground – source heat pump. *Proceedings of Sixth International for Enhanced Building Operations* Shenzhen, China, November 6 – 9, 2006.



## TRIBOLOGICAL PROPERTIES OF TRANSMISSION OILS

ZDENEK ALES

Czech University of Life Sciences Prague, Faculty of Engineering  
Department for Quality and Dependability of Machines  
Kamycka 129, 165 21 Prague 6 – Suchbát  
Phone: +420 224 383 254, E-mail: ales@tf.czu.cz

### Abstract

Biodegradable oils represent one of the ways how to achieve sustainable operation of machines and devices with regard to ecology. Transmission oils are facing higher ecological and performance requirements at present. Especially customer's demand and tighten up legislation on operation of machinery and devices are main factors of mentioned requirements. Beyond all doubt, lubricants have negative influence on environment, especially in context of soil, water and food chain contamination. Biodegradability is a property of particular product which is affecting environmental balance during its life cycle.

Currently constructed and produced machines work with mineral oils which are considered as harmful in relation to the environment. Transition to biodegradable oils involves several technical issues. It is necessary to carry out laboratory experiments to describe influence of biodegradable oils incidence on an operation and machinery life cycle.

The main objective of this article is to describe process of verification of the suitability of biodegradable transmission oils. This objective was achieved by several sub-experiments which are described in this paper.

### Introduction

Machinery operated in agriculture and forestry is required to use less harmful vital fluids in last few years. These requirements are highly urged especially for machines which are operated close to natural ecosystems (aquatic resources, water flows, fields, forests, etc.). Biodegradable vital fluids from environmental viewpoint seem as suitable solution. On the other hand from the technical viewpoint their usage seems sort of problematic. [1]

Transition to biodegradable oils involves several technical issues. It is necessary to carry out laboratory experiments to describe influence of biodegradable oils incidence on an operation and machinery life cycle. [3]

To assess the lubrication anti-wear capabilities of lubricants there were developed many mechanical dynamic tests simulating different conditions under which a lubricant performs in practice. Based on the test results it is possible to suggest if the lubricant is able to perform under the given conditions in a satisfactory way and reduce wear and friction.

Paper describes experiment which was conducted under laboratory conditions. The main objective of this experiment was to design laboratory tribometric device that will compare two different oils under identical conditions.

After laboratory testing of specific transmission oil it is suitable to carry out operational test. During operational testing of biodegradable transmission oils it is appropriate to collect information about operational time. It is also essential to keep track of other indicators which are affected by biodegradable oil. For the period of the experiment it is necessary to keep track of mechanical part wear (surface of gear teeth) as well as changes of biodegradable oil properties. [2]

### Materials and methods

The idea of laboratory test device was based on the concept of two transmissions, which were exposed to approximately the same operational load. Two identical gearboxes (integrated with electromotor) were connected through a flexible coupling.



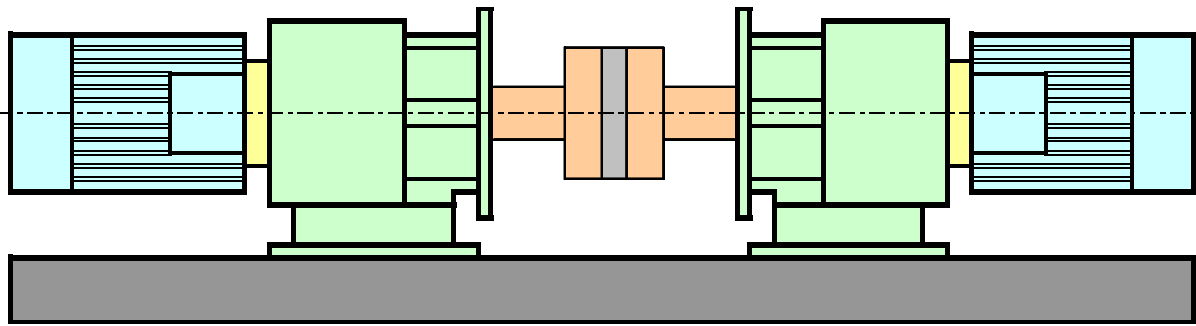


Figure 1 Designed laboratory test device

One of the motors was controlled by a frequency converter so that its frequency was maintained at over-synchronous speed. Such a setting allowed second electromotor run as a

generator of an electric power. The whole constructed device is shown at Figure 1. Table 1 describes technical parameters of electromotor.

Table 1 Technical parameters of electromotor

Variable	Symbol	Value / Units
Frequency	$f$	50 Hz
Nominal Output	$P$	0,75 kW
Rotation Speed	$n$	1375 min <sup>-1</sup>

Table 2 shows the values that were set to a frequency converter during entire experiment. Gearboxes were filled with gear oil (transmission

01 - Mineral Gear Oil ISO VG 220, Transmission 02 - Biodegradable Gear Oil ISO VG 220).

Table 2 Parameter setting of electromotor

Variable	Symbol	Value / Units
Frequency	$f$	55 Hz
Voltage	$U$	398 V
Electric Current	$I$	1,7 A

Operational experiment was focused on comparison of biodegradable and mineral transmission oil in operational conditions. Rear gearboxes of wheel tractor were used for experiment. During operating time measuring was used MPH II measuring device for exact

monitoring and counting of operating time of machine. Right hand side end rear gearbox was disassembled and mechanically cleaned at the beginning of the experiment. Each part of gearbox was degreased. Left hand side end rear gearbox was only rinsed out with clean oil.

Table 3 Technical specification of used transmission oils

Property	Gyrogate PP 90	EP Gear Synth 150
Density at 20°C	0,88 – 0,95 g.cm <sup>-3</sup>	0,921 g.cm <sup>-3</sup>
Viscosity at 40°C	145 – 150 mm <sup>2</sup> .s <sup>-1</sup>	150 mm <sup>2</sup> .s <sup>-1</sup>
Viscosity at 100°C	14,5 mm <sup>2</sup> .s <sup>-1</sup>	18,8 mm <sup>2</sup> .s <sup>-1</sup>
Pour Point	-28°C	-43°C
Viscosity Index	95	142
API Service	GL – 4	GL – 4

Both end rear gearboxes were filled with tested transmission oils. Mineral transmission oil Gyrogate PP 90 was filled to the left hand side

end rear gear box. Biodegradable fully synthetic transmission oil EP Gear Synth 150 - Panolin was filled to the right hand side end rear gear

box. Technical specifications of both transmission oils are shown at Table 3. It is obvious that transmission oil EP Gear Synth 150 has higher parameters compared to transmission oil Gyrogate PP 90, especially in case of viscosity, viscosity index, flash point and pour point.

Measuring device MPH II was used for exact monitoring of operating time of end gear boxes. This measuring device keeps tracking several data specifications in time related with traveling wheel of farming tractor.

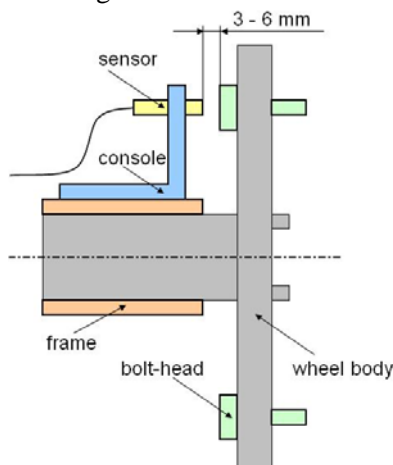


Figure 2 Scheme of sensor installation

Used measuring device consists of axle speed sensor, console for sensor position fixing, board computer and electrical installation connection to the electrical system of the tractor. Measuring device MPH II was installed on the tractor. It was necessary to ensure the proper position of the axle speed sensor of end rear wheel, as it is shown on the Figure 2.

Collected data are saved in detachable memory. This memory is designed to connect through USB cable with personal computer. It is possible to transfer saved data to personal computer through the interface of program Center Point. It is possible to transfer collected data from program Center Point straight to MS Excel. It is appropriate to process data into summaries pivot tables and charts for better visualization of data with MS Excel tools. Processed data provides information about operating time of end gear boxes.



Figure 3 Particle counter and shape classifier LaserNet Fines

Operation of machines causes deterioration of individual parts of machines. In order to determine technical state of machinery, it is possible to analyze oil sample taken from gear box of particular machinery. There are several analytic methods for determination of wear during operational time. LaserNet Fines is a suitable technique for machine condition monitoring. In terms of condition monitoring it is necessary to find out extension and type of concrete wear. Particle counter and particle shape classifier LaserNet Fines (Figure 3) provides a highly accurate particle count in major dimension and is able to classify them into six categories: cutting, severe sliding, fatigue, oxides, fibers, and water droplets.

Oil samples were continuously collected during both experiments. Taken samples were analyzed with LaserNet Fines.

## Results and discussion

Realization of first experiment conducted in laboratory conditions. At the beginning of the experiment sampling interval of the oil samples was set at 168-hour. There was a power outage for eight hours in the fourth week of the experiment. The twelfth week of the experiment started simulation of variable operation conditions for 28 days when the entire device was running only 160 hours of operation. From the fourteenth week the interval of transmission oil sampling was extended up to 34 days because of consistent creating of wear particles. After fifteenth sampler the sampling interval was extended to 70 days. During last period, the static fracture occurred in the gearbox with gearbox 01, where mineral transmission oil was used for lubrication.

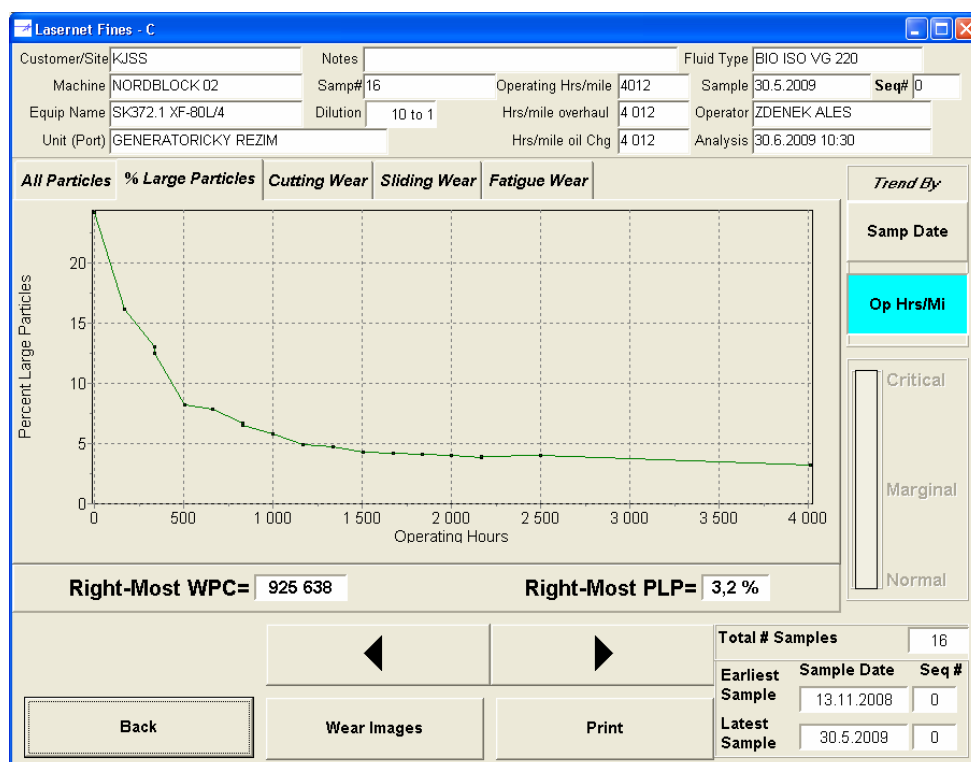


Figure 4 Percentage representation of large particles in transmission oil sample

The initial period of both gearboxes is characterized by intensive wear (run-in period). It is evident from the declining share of percentage representation of large particles for both investigated gearboxes. Figure 4 describes the percentage representation of large particles during the experiment in taken samples. Figure 4 shows the run-in period when the first three weeks of operation (504 hours) occurred to generate a greater number of large particles. After run-in period proportion of large particles stabilized at share of 5% and this ratio during the experiment decreased slightly to 3.2% of final value.

In case of second experiment the operating time was monitored and kept tracked almost year and half and wheel tractor drove nearly 7.000 km. Measuring device MPH II for farming machinery was during this period sufficiently accurate and besides that it provided complete information about machine performance. Suitable processing of collected data helped to obtain lucid summaries about machine

performance in given period. Seven oil samples were taken from the gear boxes during this period. Realized analyses with particle counter LaserNet Fines are very complex. Figure 5 shows total particles in each transmission oil sample. It is obvious that mineral transmission oil Gyrogate PP 90 contained more particles in comparison with biodegradable transmission oil EP Gear Synth 150.

Deeper analytical view in Figure 5 shows that mineral transmission oil Gyrogate PP 90 has lower ability to form proper boundary oil layer compare to other transmission oil. That is apparent due to higher increase of percentage representation of fatigue particles during the experiment. It is necessary to mention that transmission oil Gyrogate PP 90 was filled into gear box which was only rinsed out with clean oil. Nevertheless, the experience from agricultural companies shows that there is not time to proper disassembling and cleaning before each oil change. These conditions simulate rather conditions similar to real operation.

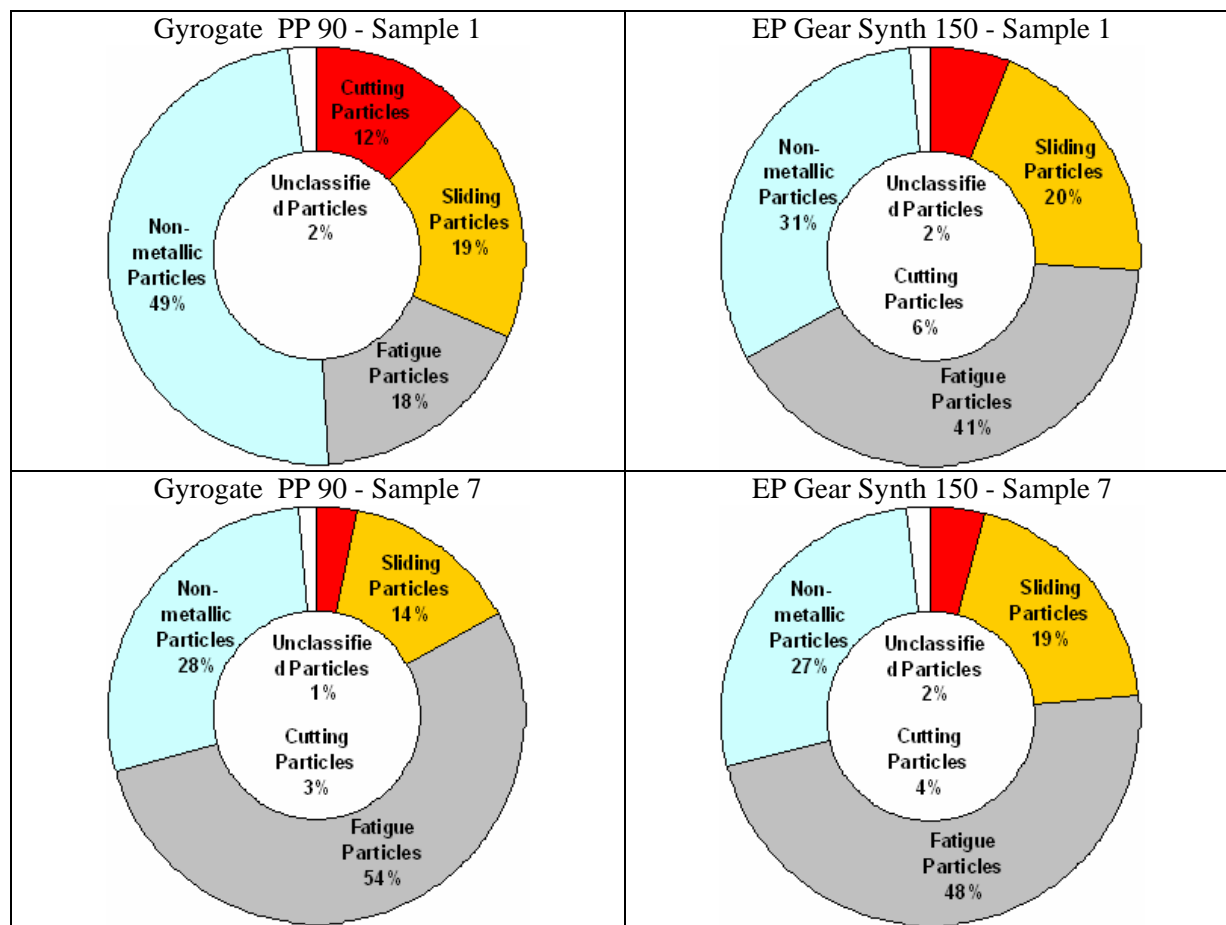


Figure 5 Percentage representation of different particles in transmission oil samples

## Conclusions

The main objective of first experiment was to design a laboratory experiment tribometric device that will compare two different transmission oils in identical operational conditions. The proposed device was constructed and measurements verified its suitability for laboratory conditions. In terms of the cleanliness code according to ISO 4406:1999, mineral transmission oil for one to two cleanliness codes better values compare to biodegradable transmission oil. Analysis using LaserNet Fines indicated the suitability of biodegradable gear oils. Even though it was not possible to monitor gearboxes over a longer period, it can be concluded that the designed device for laboratory tribological measurements is suitable for comparison of two different transmission oils. At the same time, this experiment confirmed the suitability of biodegradable transmission oil for this particular application.

Second experiment was focused on comparison of two different transmission oils during operational time. Results of experiment showed suitability of usage of biodegradable transmission oil. In spite of the fact that mineral transmission oil Gyrogate PP 90 has lower ability to form proper boundary oil layer, this lubricant is more than seven times cheaper compare to transmission biodegradable oil EP Gear Synth 150. This is the main issue why most companies prefer to purchase mineral oil. The question is if it is wise to give priority to only economic factors.

Current trend indicates that the entrepreneurs in agriculture sector are compelled by legislation and they are forced in most cases to use biodegradable fillings in their machinery. Thus, such a trend is commonsensible in order to achieve sustainable growth.

**References:**

- [1] Ales, Z.: *Field experience with transmission oil EP Gear Synth 150*, Research in Agricultural Engineering, Volume 55, ISSN 1212-9151. 2009, p. 18 – 23.
- [2] Jurca, V. – Hladik, T. – Ales, Z.: *Possibilities of data assimilation from maintenance management systems*, Monography, CSJ, Prague, ISBN 80-02-01595-9, 2004, p. 74. (in Czech)
- [3] Krzan, B. – Vizitin, J.: *Tribological properties of an environmentally adopted universal tractor transmission oil based on vegetable oil*, In: Centre for Tribology and Technical Diagnostics, University of Ljubljana, Slovenia, ISSN 1221-4590, 2003, p. 827 – 833.

*Presented results were obtained within solving IGA TF project “Keeping track of operating time of biodegradable transmission oils”, nr.: CZU: 31190/1312/313115 and “Tribomeric laboratory experiments of biodegradable transmission oils”, nr.: CZU: 31190/1312/313114.*

## PARTICULATE MATERIAL EMISSION AT THE CALCIUM CARBONATE INDUSTRY IN PRUDENTE DE MORAIS, MG, BRAZIL

AILTON DE ALMEIDA <sup>(1)</sup>, LUIS FERNANDO BARBOSA XAVIER <sup>(2)</sup>, DANIEL SEBASTIÃO DA SILVA <sup>(2)</sup>, CELINA DE ALMEIDA <sup>(3)</sup>, INÁCIO MARIA DAL FABBRO <sup>(3)</sup>

<sup>(1)</sup> Teacher, State University of Minas Gerais, FaEng, João Monlevade, MG, Brazil.

<sup>(1)</sup> Teacher, FEAMIG, Belo Horizonte, MG, Brazil, [aailton2003@ig.com.br](mailto:aailton2003@ig.com.br)

<sup>(2)</sup> Undergraduate Student, State University of Minas Gerais, Belo Horizonte, MG, Brazil.

<sup>(3)</sup> Teacher, Faculty of Agricultural Engineering, State University of Campinas, Campinas, SP, Brazil, Phone: 55-19-35211059, Fax: 55-19-352110, E-mail: [inacio@agr.unicamp.br](mailto:inacio@agr.unicamp.br)

### Abstract

Particulate material is considered the most important pollutant generated in the calcium carbonate production. Buildings, vegetation and structures near by the industrial facilities are permanently covered by a typical dust released to the atmosphere during the production activities. The above described situation has motivated this research work, in presenting the pollutant types, damages caused to the human population, to the livestock, to crops, as well as to the wild animals, associated to the calcium carbonate industry located at Prudente de Moraes, MG, Brazil. The paper presents the final conclusions, including recommendations to the manufacturing process to minimize particle emission and to improve air quality.

**Keywords:** calcium carbonate production, particulate emission, air pollution.

### Introduction

Industrial processing plants as well as automotive engines release significant amount of pollutants in the atmosphere. These pollutants are composed of gases as well as of solid particles which are harmful to the human health. As reported by Derisio (2000) these gases are generally composed of sulfur (SO<sub>x</sub>), nitrogen (NO<sub>x</sub>), carbonic organic radicals, carbon monoxide, carbon dioxide, halogenic compounds, as well as particulate solids. The first thematic world conference on biodiversity and environment, named "United Nations Conference on Human Development" took place in Stocolm in 1972 which released the document entitled "Declaration of the Human Environment". Since last decades, the reduction of non sustainable practices associated to the use of natural resources as well as to the environmental degradation, has been worldwide discussed and negotiated. The growth of already overpopulated urban areas has pushed the demand for industrialized products, generating an uncontrolled environmental detriment. The pertinent literature discloses relevant reports on air quality, but only few mentions on actions toward particle emission minimization. This

research work presents a monitoring system for gaseous emissions released by the chimney and ducts at stationary sources by means of an Isocinetic Atmospheric Pollutants Collector (IAPC) with the main objective of quantifying at the particulate material in suspension at a calcium carbonate industry in Prudente de Moraes, MG, Brazil.

### Methodology

The city of Prudente de Moraes was founded in 1969 and it is located near by Belo Horizonte, in the state of Minas Gerais, Brazil, at 19°28'55" south latitude and 44°09'18" west longitude, at 748 m above sea level, exhibiting a population of 8 874 habitants, covering an area of 125,783 Km<sup>2</sup>. The industry under consideration in this study is located at 3 km from the city and started commercial activities in 1968, exploiting, processing and selling limestone. In 1989 the enterprise started to commercialise hydrated lime supported by a 300 t/day capacity horizontal rotative oven. A new oven of 500 t/day was set in the production line in 2005. Sampling was based on isocinetic point to point collection at the filter inside the chimney with simultaneous sampled gas volume readings



The filter holds a retention ability of 99,95% of particles with a limiting diameter of 0,3  $\mu\text{m}$ . Particle concentration is referred to mass/volume and minimum detection supported by that method is 1  $\text{mg}/\text{Nm}^3$ . Three samples have been collected in each semester, during a time interval of 1 hour each, observing the sampling as recommended by the Brazilian Association of Technical Norms (ABNT) and EPA (Environmental Protection Agency/USA). The sampling period was of two and half years including 2005 to 2008. The data collection procedure included (1) sampling planning, determination of sampling points, gas velocity and flow rate, molecular mass to a dry basis, moisture content, particulate material, equipment calibration,  $\text{SO}_2$ ,  $\text{SO}_3$ , fog and determination particulate filter in the chimney. Lime production starts at the limestone mining area where the rocks are broken by means of explosives. The limestone is composed of calcium carbonate as well as of magnesium carbonate and others, constituting the raw material for lime production. Rocks are then perforated to fit the explosives, according to previous geological studies, desired stone quantities and grain size. It should be noted that at the explosive detonation, a major dust quantity is released to the atmosphere. Obtained stones are then transported on trucks to the milling facilities for further breaking and particle size classification by means of vibrating sieves and transported to the deposits to feed the ovens by means of transporting belts. Inside the oven the rocks are pre-heated to eliminate moisture before the calcination process. In the calcination process, the carbonates are transformed into calcium oxide and magnesium oxide, respectively, in which process mineral coal and natural gas burning takes part. The final product, named hydrated lime, is continuously released from the oven and forwarded to a cooling process by means of forced ventilation and then transported through belts to the silos. At that step

the material can undergo to a grinding process to adequate the product to costumers needs. The silos are protected against environmental factors.

## Results and Discussions

Beyond the collected data information, a close observation at the overall scenery reveals surrounding the industrial facilities reveals important information. Particulate material released at the factory, covers the vegetation, equipment, roofs, the ground, etc, resulting in significant harm to the industry. The foliage is noted to be covered by a thick layer of calcium carbonate, modifying also the general vegetation appearance. Covered roofs are noted to experience serious corrosion due to the contact with the carbonates. Structures also are submitted to serious overloading with possible collapse. Retention walls were also noted to undergo through a miss function process due to overload and esthetic modifications. Powder material quite frequently flows out at equipment joints and connections, as at the auger transporter, at the hammer mill, mainly at non enclosed equipments. During breaking time, in the weekends, footprints are noted on all over the interior factory ground, being possible to observe a significant amount of carbonate deposition. The release of particulate material via chimney takes place during gases discharge, including rejected substances generated at the combustion process. The dust cloud takes a feather shape which expands as chimney temperature increases generating a volumetric expansion of the gases composed of  $\text{CO}$ ,  $\text{O}_2$  and  $\text{CO}_2$ , i.e., the distance between the molecules increases, turning the substances lighter, reducing particle humidity which increase the gases velocity as well as the real flow rate in the duct and so its dispersion. As consequence, PM concentration is minimized and PM emission increases, since the material dispersion is homogeneous through the atmosphere and not deposited at the factory surroundings.

Table 06. Monitoring Results of the First Semester of 2005

Parameters	unit	date/ sampling		
		22/02/05		
		1 <sup>st</sup> sampling	2 <sup>nd</sup> sampling	3 <sup>rd</sup> sampling
Temperature	° C	119,5	123,3	123,0
Humidity	% Vol.	6,43	6,52	6,01
Velocity	m/s	14,20	14,64	14,32
Flow Rate (duct conditions)	m <sup>3</sup> /h	67.838,58	69.953,85	68.413,35
Flow Rate (CNTP- 0° C / 1 atm)	Nm <sup>3</sup> /h	37.973,62	38.747,15	38.119,78
<b>Concentration PM</b>	mg/Nm <sup>3</sup>	10.706,25	9.760,42	10.995,97
PM emission Rate	Kg/h	406,56	378,19	419,16
Isocinetics	%	100,89	99,15	100,32

From Table 06 it can be noted that in the first semester of 2005, sampling during February shows extremely high temperature, because both ovens were using the same Sleeve Filtering System. It is also noted that at high temperatures gases expansion makes the gas velocity as well

as the flow rate to increase inside the chimney. However, emitted flow rate is very high when compared with the in the first semester and PM concentrations exhibited double values as shown on Table 07, which is of major concern to air pollution.

Table 07. Monitoring Results of the Second Semester of 2005

Parameters	unit	date / sampling		
		06/10/05		
		1 <sup>st</sup> Sampling	2 <sup>nd</sup> Sampling	3 <sup>rd</sup> Sampling
Temperature	° C	130,5	130,6	130,5
Humidity	% Vol.	8,23	8,85	8,16
Velocity	m/s	17,98	17,89	19,93
Flow Rate (duct conditions)	m <sup>3</sup> /h	85.900,64	85.484,62	85.661,38
Flow Rate (CNTP- 0° C / 1 atm)	Nm <sup>3</sup> /h	46.104,61	45.346,03	45.785,89
<b>Concentration PM</b>	mg/Nm <sup>3</sup>	20.310,01	20.604,65	19.904,29
PM emission Rate	Kg/h	936,38	934,34	911,34
Isocinetics	%	98,58	100,30	99,12

A serious concern is associated to the collected data which exceeds the allowed value of 100 mg/Nm<sup>3</sup>. Table 06 represents the variability between sampling emphasizing divergences where the factors involved are the main variables associated to the results. In the second semester of 2005 the monitoring presented on Table 07 indicates that the equipment is still working under overloading

conditions. The temperature makes the gas velocity and volumetric expansion to increase inside the chimney. However, since particles moisture content increased in relation to the preceding semester and despite the real flow rate increased, PM concentration reaches twice as the former value. That observation is probably related to rainfall during the period under consideration.

Table 08. Monitoring Results of the First Semester of 2007.

Parameters	unit	date/ sampling		
		13/02/07		
		1 <sup>st</sup> Sampling	2 <sup>nd</sup> Sampling	3 <sup>rd</sup> Sampling
Temperature	° C	42,7	42,7	43,1
Humidity	% Vol.	0,05	0,03	0,04
Velocity	m/s	4,91	4,91	5,05
Flow Rate (duct conditions)	m <sup>3</sup> /h	20.669,26	20.670,10	21.265,11
Flow Rate(CNTP - 0° C / 1atm)	Nm <sup>3</sup> /h	16.247,26	16.248,62	16.692,87
<b>Concentration PM</b>	mg/Nm <sup>3</sup>	51,16	41,00	32,05
PM emission Rate	Kg/h	0,83	0,67	0,54
Isocinetics	%	104,14	105,38	103,74

As shown on Table 07 the graph demonstrates the divergences noticed before allowing a better understanding of the final results. The adoption of the new sleeve filter in 2007 which is a more powerful equipment to assist only one oven, as it can be noticed on Table 08 the resulting monitoring exhibited a significant change. Since the temperature decreased, gases experienced low expansion, generating lower gas velocity as well as elevation of PM concentration, reducing PM emission, exhibiting non critical results due to low moisture of the PM in the chimney. Table 08a demonstrates monitoring analysis as stated

before, emphasizing the significant improvement on the monitoring procedure when a sleeve filter is associated to an unique oven. Table 09 referring to the second semester of 2007 for the month of July, presents a significant temperature increase resulting gas expansion which causing gas expansion and decreasing PM concentration, reducing PM emission, since the particles moisture content are higher, turning heavier the PM reducing gas dispersion in the atmosphere. Results shown on Table 09a clearly demonstrate the system improvement, mainly between the particulate material emission rate and concentration.

Table 09. Monitoring Results of the Second Semester of 2007.

Parameters	unit	date/ sampling		
		05/07/07		
		1 <sup>st</sup> Sampling	2 <sup>nd</sup> Sampling	3 <sup>rd</sup> Sampling
Temperature	° C	69,50	70,40	70,50
Humidity	% Vol.	9,58	13,29	9,66
Velocity	m/s	8,95	9,07	9,04
Flow Rate(duct conditions)	m <sup>3</sup> /h	36.422,85	36.919,14	36.787,00
Flow Rate(CNTP- 0° C / 1atm)	Nm <sup>3</sup> /h	23.881,45	23.150,38	24.029,99
<b>Concentration PM</b>	mg/Nm <sup>3</sup>	26,15	40,93	22,79
PM emission Rate	Kg/h	0,62	0,95	0,55
Isocinetics	%	97,92	101,12	98,22

Table 10, referring to the 1st semester of 2008, it is noted that even at low gas temperatures, decreasing gas velocity, since the

volumetric expansion is low, but in the other side, chimney flow rate did not decrease because the PM did not reach low values, generating PM

concentration as well as PM reduction. Low air streams incidence and equipment working at full power contributed to the situation described above. During the first semester of 2008 it can be observed on the graph of Table 10 that despite the increasing gas flow rate and decreasing PM moisture content, the concentration of PM did not decrease which confirms the observation that

low rainfall and airstreams did not generate increments on the PM concentration rate. Factory location is an important issue, since the occurrence of some inconvenient as the collision of the cloud expelled by the chimney with natural barriers and further return to the factory yard or to urban areas.

Table 10. Monitoring Results of the First Semester of 2008.

Parameters	unit	date/sampling		
		25/07/08		
		1 <sup>st</sup> Sampling	2 <sup>nd</sup> Sampling	3 <sup>rd</sup> Sampling
Temperature	° C	67,6	67,2	65,8
Humidity	% Vol.	4,94	1,44	4,90
Velocity	m/s	4,89	5,36	5,44
Flow Rate (duct conditions)	m <sup>3</sup> /h	93.177,23	102.077,94	103.653,89
Flow Rate(CNTP- 0° C / 1 atm)	Nm <sup>3</sup> /h	64.907,27	73.802,67	72.618,99
Concentration PM	mg/Nm <sup>3</sup>	31,33	11,01	30,63
PM emission Rate	Kg/h	2,03	0,81	2,22
Isocinetics	%	103,27	102,22	103,74

## Conclusions

Based on what it has been exposed before it can be concluded that the production of calcium carbonate generates significant impacts on the physical environment. At all processing steps since mining up to storage, particulate material is released to the atmosphere, generating critical occurrences to the vegetation, to the fauna as well as to the over all neighboring environment. It is also concluded that despite the (to use) application of the Isocinetic Atmospheric Pollutant Collector (IAPC), the visual observation indicates serious negatives impact to the overall environment concentrated at the factory surroundings generate by PM deposition. Such deposition concentration is so significant that even the flora, fauna and factory facilities are seriously affected. Since the factory is placed in a rural area, the risk to human population is limited to the employees. Governmental fiscalization inspection is quite conniving to present situation, impeding drastic as well as necessary changes.

## References

- [1] ALMEIDA, Ivo Torres. Poluição Atmosférica por Material Particulado na Mineração a Céu Aberto. Tese Mestrado. São Paulo, 1999.
- [2] AQUA RPS Ltda. Relatório Técnico de Monitoramento Atmosférico ano 2005. Tabelas de Avaliação.
- [3] Relatório Técnico de Monitoramento Atmosférico ano 2007. Tabelas de Avaliação.
- [4] Relatório Técnico de Monitoramento Atmosférico ano 2008. Tabelas de Avaliação.
- [5] FRANÇA, Júnia Lessa. Manual para normalização de publicações técnico-científicas. 8ed. Belo Horizonte: UFMG, 2008.
- [6] GIL, Antonio Carlos. Métodos e Técnicas de Pesquisa Social. 5° ed. São Paulo, 2006.

## WATER VAPOR ABSORPTION BY HYDROXY-ETHYL CELLULOSE COATED SEEDS

CELINA DE ALMEIDA<sup>1\*</sup>, SANDRA CRISTINA DOS SANTOS ROCHA<sup>2</sup>, INACIO MARIA DAL FABBRO<sup>1</sup>

<sup>1</sup>Faculty of Agricultural Engineering, State University of Campinas, Campinas, SP, Brazil,  
Phone: 55-19-35211059, Fax: 55-19-352110, E-mail: celina.almeida@agr.unicamp.br

<sup>2</sup>Faculty of Chemical Engineering - State University of Campinas, Campinas, SP

### Abstract

The objective of this research work was to study broccoli seeds coating in spouted bed employing a suspension of hidroxy-ethyl-celluloses, with the purpose of protecting the seeds from water vapor saturated environment at room temperature. Seed moisture content variation determination was carried by keeping the samples at  $25 \pm 1^\circ\text{C}$  in a water vapor saturated environment during the first 24 hours after coating, following by weight determination at pre-established time intervals. The broccoli seeds of average diameter  $1,6 \times 10^{-3}$  m, were coated with an aqueous suspension of hydroxy-ethyl-cellulose in a spouted bed, at the following values: spout air temperatures of 50 and  $70^\circ\text{C}$ , atomizing air pressure of 15 and 25 psi and coating suspension mass flow rate of 6 and 8 ml/min. At the end of the water vapor absorption test, coated seeds in spouted bed had 2 to 10% less moisture content than the uncoated seeds, evidencing a discreet protective behavior provided by the hydroxy-ethyl-cellulose in the container with saturated water vapor pressure at temperatures of  $25^\circ\text{C}$ .

### Introduction

*Brassicaceae* family includes countless *oleracea* members, as cabbage, cauliflower, radish, arugula, watercress and broccolis. Broccolis occupies relevant economical importance among the other family members, which is confirmed by the growing sale volume carried at Supplying Centers (FILGUEIRA, 2000). According to the National Research Center (CNPq/Embrapa), it was introduced the cultivar "Ramoso de Brasília" in 1993 in Brasilia as well as in São Paulo. That type of broccolis has 31 to 32 cm stem length, allowing the first harvest in 80 days after seeding which extends to 55 days, yielding 18 metric ton/ha, being of high quality and exhibiting good acceptance by the domestic market. In the center-western Brazilian region, broccolis seeding takes place during fall and winter seasons. Broccolis seed sensitivity to temperature and relative humidity variations highly influences harvesting period and yielding (WURR *et al.* 1991; 1992). Commercial seed coating objectives are to guarantee germination during adverse weather periods, combining coarse sand to control water exchange between soil and seed. Solution of hydrophobic substances as polypropylene provided porosity close to 15-25% in lettuce seeds (SCOTT, 1989). However other coating substances, as

magnesium carbonate, which is a hygroscopic material and combined with insoluble particles holding an average diameter less than  $3 \mu\text{m}$ , will improve available water to the seed during germination (SCOTT, 1989). WEST *et al.* (1985) reported test results of polyvinilidene chloride coating on soybean seeds under high water vapor saturated atmosphere, verifying that after 24 hours seeds showed only 9% moisture increase meanwhile non coated ones exhibited 17% moisture increase. The authors also observed no alteration of free water on field conditions. The authors finally concluded that the thin polyvinilidene chloride coating layer of  $8 \mu\text{m}$  reduced water vapor absorption by the seeds. DREW (1987) reported fluidization tests carried on *Brassica napus L.* seeds, holding temperature at 25, 30, 35 and  $40^\circ\text{C}$  and processing time of 30, 40, 60 and 180 minutes. Treated seeds processed at  $25^\circ\text{C}$  experienced decreased from 5,32 to 4,83% in 60 minutes and from 4,83 to 4,51% after 180 minutes. Seeds processed at  $40^\circ\text{C}$  had water content decreased from 5.2 to 3.88% in 60 minutes and from 5.2 to 3.3% in 180 minutes. Considering what it has been exposed before, the objectives of this research work can be stated as to test thin hydroxy ethyl cellulose film in coating to protect broccolis seeds against



saturated water vapor pressure at temperatures of 25°C.

### Experimental arrangement

In this research work, *Brassica oleracea* var. *italica* cultivar “Ramoso de Brasília” seeds, which is a very common broccoli type growing in Brazil, were obtained from the National

Research Center (EMBRAPA) and forwarded to tests. Seeds were analyzed for germination test, vigor, purity and mass of 1000 individuals, as soon they reach the lab facilities which results are expressed on Table 01. Seeds were stored during the whole testing period at 4°C in a refrigerator in sealed containers to prevent moisture exchange with environment.

Table 1. Broccoli seeds characterization.

Analysis	Methods	Reference
Mass of 1000 individuals	Weight\ Coefficient of variation	Brasil (1992)
Vigor	Accelerated Aging Test	Vieira and Carvalho (1994)
Germination	Warm (Standard) Germination	ISTA (1985)
Moisture content	Seed drying shall be 24 hr at 105 ± 1°C	Brasil (1992)
Analysis of Purity	Inert Substances	Brasil (1992)
	Other Seeds	
	Pure Seeds	

Table 2. Spouted Bed Test Operational Conditions.

Operational Conditions		Trial 1	Trial 2
Spouted Bed	Air Temperature	70°C	50°C
Atomization	Air pressure	25 psi	25 psi
Coating	Suspension Flux	6 ml/min	8 ml/min
Coating	Process Timing	120 min	90 min

Table 3. Hydroxy-ethyl-cellulose Suspension Formulation.

Components	Suspension(g)
Hydroxy-ethyl-cellulose	3,5
PEG 6000	0,75
Magnesium Stearate	1,0
Titanium Dioxide	2,25
Gypsum	3,5
Water	89

Seeds were coated in an experimental spouted bed, setting the following experimental conditions: spouted bed air temperature, atomization manometric air pressure, coating suspension flux and coating process timing, as shown on Table 2. Suspension atomization was carried by means of an atomizing nuzzle set at the bed top keeping the jet directed toward the seeds, without interruption.

Employed coating formulation was identified as a hydroxy ethyl cellulose water solution with 11% of solids, which provided a uniform coating surface, water soluble, permitting air moisture absorption. Table 3

displays the formulation referred above, as recommended by Ataíde (1996).

Moisture content was determined through the oven method at 105 ± 3°C, during 24 hours, selecting three samples from each group, following the Rules of Seed Analysis (Brasil, 1992), expressing the results in percentage of humid basis ( $U_{bu}$ ). Water vapor absorption test was based on the research work of WEST *et. al.* (1985) in which seed surfaces are exposed during fixed time interval to a constant temperature of 25 ± 1°C together with a high water vapor concentration. Three replications of 10g each were placed on a sieve, above the water level in a



*Petri* dish. Each dish was filled with 30 ml of water and kept under pre established conditions. Seed moisture content was obtained at 2, 4, 6, 8, 10 and 24 hours permanence in the chamber. After weighing, seeds humid base moisture content was calculated  $U_{bu}$  (%). A second period of 24 hours at  $105 \pm 2^\circ\text{C}$  was set for seed dry weigh calculation. Equation 1 was used to obtain the values mentioned above.

$$U_{bu} = \frac{P_a}{P_a + P_s} \times 100 \quad (1)$$

### Results and discussion

Broccolis seeds were analyzed according to the methodology described above. The results are presented on Table 4 and on Table 5.

Table 4. Broccoli seeds characterization.

Analysis		Values
Mass of 1000 individuals		$4,2 \times 10^{-3} \text{ kg}$ 2,37 %
Vigour		73,75%
Germination		93,71%
Moisture content		6,02%
Analyses of Purity	Inert Substances	0,439 %
	Other Seeds	0 %
	Pure Seeds	99,56 %

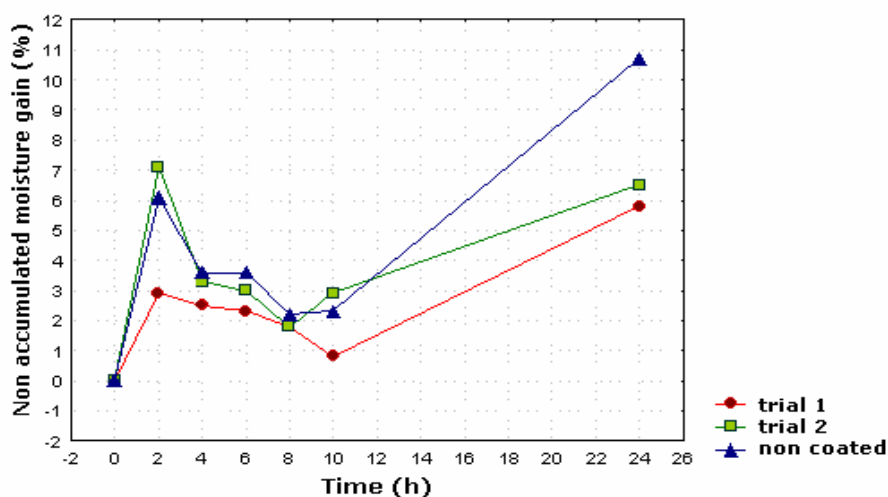


Figure 1. Non accumulated moisture gain (%) as function of time (h), for coated broccoli seeds, trial (1) and for non coated seeds, trial (2).

Seed moisture content variation data during the tests generated non accumulated moisture gain curves for coated and non coated seeds, as shown on Figure 1.

Coated and non coated seed non accumulated moisture gain was obtained at each 2 hours interval. It is observed in the first two hours the water vapor absorption of coated seeds was less intense when compared with uncoated

ones. The largest difference in seed moisture was noted during the last 14 hours of test, in which coated seed absorbed about 5% of moisture meanwhile non coated ones absorbed about 9% of moisture. Figure 2 illustrates the moisture content curve for trial (1), showing that initial seed moisture content was of 7.3%  $U_{bu}$  which was lower of those from the witness individuals.

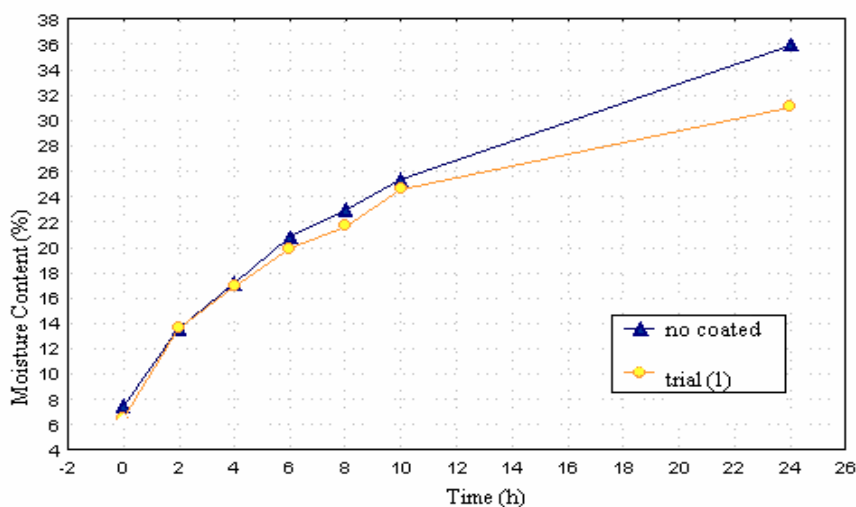


Figure 2. Moisture content curve for test (1) and witness individuals.

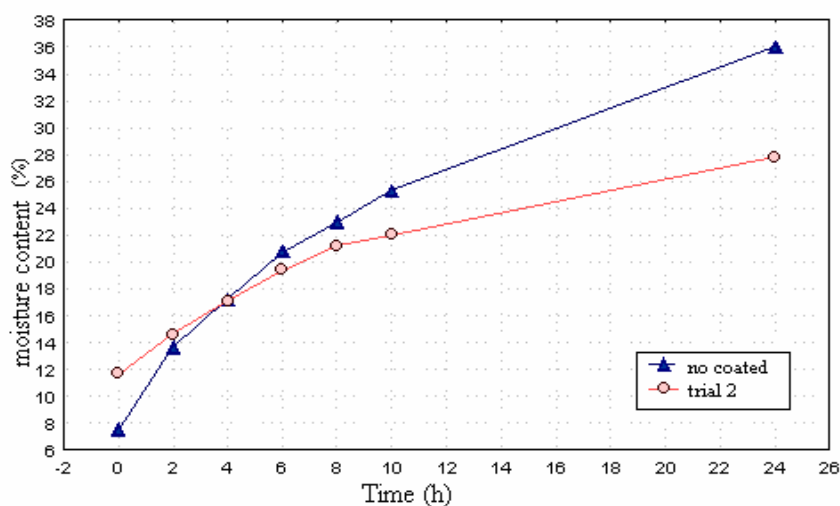


Figure 3. Seed Moisture Curves for Test (2) and for witness.

Curves reveal an outstanding moisture gain for coated and non coated seeds during the two first test hours, which bared the values of about 6 to 14%  $U_{bu}$  followed by a gradually gain decrease, up to 24 hours of observation period. Coated seeds in the test (1) reached 31%  $U_{bu}$  moisture content, meanwhile witness seeds kept higher moisture content values when compared with coated seeds, reaching the value of 36%  $U_{bu}$  at test end, i.e., at 24 hours of observation.

Seed moisture curve for trial (2) as shown on Figure 3, indicates that witness seed initial moisture content was higher than 7.3%  $U_{bu}$  which is lower than the value of 12%  $U_{bu}$  exhibited by the coated seeds at the beginning of

the test. At the end of trial (2), coated seeds reached 28%  $U_{bu}$  meanwhile non coated seeds experienced higher moisture increase, i.e., 36%  $U_{bu}$  during the 24 test hours. It is also observed that non coated seeds experienced exceeding moisture when compared with coated ones in a time interval of 4 hours of exposure at the test conditions. The lowest moisture content increment was observed during trial (2), meanwhile a difference of 8% in moisture content between the coated seeds and non-coated ones was observed.

## Conclusion

Based on what it has been exposed before, it can be concluded that hydroxy ethyl cellulose suspension modified broccoli coated seeds moisture content under saturation water vapor pressure at temperatures of 25°C in container.

## References

- [1] ASSOCIATION OF OFFICIAL SEED ANALYSIS. Seed Vigor Testing Handbook. Washington: AOSA, 93p. 1983.
- [2] Ataíde, C. H. Estudo do Recobrimento de Comprimidos em Leito de Jorro e Jorro Fluidizado. Campinas: Faculdade de Engenharia Química. UNICAMP, 1996, 188p. Tese (Doutorado).
- [3] Brasil, Ministério da Agricultura, Laboratório Nacional de Referência Vegetal, Regras para Análise de Sementes, Brasília, 1992, 365p.
- [4] Drew, R.L.K. The effects of duration and temperature of treatment in a prototype fluidized-bed seed treatment on the subsequent germination of seed of oilseed rape *Brassica napus* L. *Seed Science and Technology*, v.17, p.7-13, 1987.
- [5] FILGUEIRA, F. A. Cultura e Comercialização de Hortaliças. Manual de Oleicultura, 1972, 451p.
- [6] INTERNATIONAL SEED TESTING ASSOCIATION (ISTA). International rules for seed testing. *Seed Science and Technology*, v.13, p.322-326, 1985.
- [7] Mohsenim, N. N. Physical Properties of Plant and Animal Materials. 2ed. New York: Gordon and Breach Science. Cap. 2-3, 1986, 734p.
- [8] Peçanha, R.P.; Massarani, G. Dimensão característica e forma de partícula. In: Encontro sobre Meios Porosos, 14., Campinas, 1986. Anais. p.302-312.
- [9] Scott, J. M. Seed Coatings and Treatments and Their Effects on Plant Establishment *Advances in Agronomy*, v. 42, p. 43-83, 1989.
- [10] Vieira, R. D.; Carvalho, N. M. Teste de Vigor em Sementes. Jaboticabal, FUNEP-UNESP, 1994, 163p.
- [11] West, S. H. Polymers as Moisture Barriers to Maintain Seed Quality *Crop Science*, v. 25, p. 941-944, 1985.

## LAB INVESTIGATION OF FLOW COEFFICIENT ON TRIANGULAR SHAPE SIDE WEIRS

G.A.BARANI<sup>1\*</sup>, V.KALANTARI<sup>2</sup>, M.B.RAHNAMA<sup>3</sup>

<sup>1</sup>Professor of Civil Engineering Dept. Shahid Bahonar University, Kerman Iran, Email: [gab@mail.uk.ac.ir](mailto:gab@mail.uk.ac.ir), phone: +989131404433,

<sup>2</sup>Graduate student of C.E. Dept. Shahid Bahonar University, Kerman Iran, Email: [vahid.1060@gmail.com](mailto:vahid.1060@gmail.com)

<sup>3</sup>Assistant Professor of Water Eng. Dept. Shahid Bahonar University of Kerman Iran, Email: [mbr@mail.uk.ac.ir](mailto:mbr@mail.uk.ac.ir), phone: +989131404423

### Abstract:

Flow over side weirs is a spatially varied type with decreasing discharge. Among several types of side weirs, the triangular shape has been less investigated compare to the other types. It is necessary to introduce a suitable and correct method to calculate the flow coefficient over this type of weirs.

In this study, a physical model include a flume with a triangular side weir has been used. Different flow rates were applied to this model and the hydraulic parameters of flow were measured. Using measured data, the flow coefficient has been calculated. Also using dimensional analysis and least square method, equation of flow coefficient has been obtained. Comparison of these two equations show a good agreement.

**Key words:** triangular side weirs, dimensional analysis, flow coefficient, spatially varied flow

### Introduction

Flow over side weirs is a spatially varied type flow which can be used to discharge a specified flow rate from rivers, irrigation canals and reservoirs, Ayumaz, 2005. Flow over side weirs has been investigated by many researches. For the first time demarche (1934) introduced equation of side weirs based on assumption of constant specific energy along the rectangular side weirs. Also, Subramanya and Awasthy (1972) have been investigated flow over side weirs based on assumption of constant specific energy along the weir, the flow coefficient for sub critical and supercritical flows have been suggested. They stated that for sub critical flow, the flow coefficient depends on Froude number of flow upstream of weir, while for supercritical flow this coefficient does not strongly depends on Froude number. Flow over triangular side weirs sharp and broad crested types installed at a rectangular canal have been investigated by Kumar and Pathk (1987) and equation of flow coefficient presented. Oliveto(2001) had studied flow over circular side

weirs and presented the equation of flow coefficient for this type of weirs. Muslu(2002) used regression and introduced the rectangular side weir models to obtain the hydraulic parameters of flow. Many equations which have been introduced by different researchers, results different flow coefficients for a fixed Froude number. In the present study using experimental data and dimensional analysis equation of flow coefficient for triangular side weirs of 60 and 90 degrees have been developed.

### Flow equations on triangular side weirs

The spatially varied flow with decreasing discharge can be described by the following equation:

$$\frac{dy}{dx} = \frac{S_0 - S_f - \frac{\alpha Q}{gA^2} \cdot \frac{dQ}{dx}}{1 - \frac{\alpha Q^2 B}{gA^3}} \quad (1)$$

Which  $S_0$  and  $S_f$  represent bed and friction slopes,  $A$  is the flow cross section area,  $\frac{dQ}{dx}$  is the flow rate at unit length of side weir and  $\alpha$  is energy coefficient.

For uniform distribution of velocity at rectangular canal equation (1) becomes:

$$\frac{dy}{dx} = \frac{Qy(-\frac{dQ}{dx})}{gB^2y^3 - Q^2} \quad (2)$$

Also, equation of flow over unit length of triangular side weir is (kumar and pathak , 1987):

$$-\frac{dQ}{dx} = \frac{\frac{8}{15}C_m\sqrt{2g}\tan\frac{\theta}{2}(y-s)^{\frac{5}{2}}}{2(y-s)\tan\frac{\theta}{2}} = \frac{4}{15}C_m\sqrt{2g}(y-s)^{\frac{3}{2}} \quad (3)$$

For constant specific energy, the channel flow equation can be:

$$Q = BY\sqrt{2g(E-Y)} \quad (4)$$

Combination of equation (2), (3) and (4) results:

$$\frac{dy}{dx} = \frac{8C_m}{15B} = \frac{\sqrt{(E-Y)(Y-S)^3}}{3y-2E} \quad (5)$$

Assuming independent  $C_m$ , integration of equation (5) between section 1 and 2 of Fig (1) result:

$$Q = \frac{2E-3S}{E-S} \sqrt{\frac{E-Y}{Y-S}} - 3\sin^{-1} \sqrt{\frac{E-Y}{E-S}} \quad (6)$$

$$X = x_2 - x_1 = \frac{15B}{4C_m}(Q_2 - Q_1) \quad (7)$$

Using measured flow rate at the beginning of side weir ( $Q_1$ ) and at the end of side weir ( $Q_2$ ) in equation (7), the side weir flow coefficient  $C_m$  can be calculated.

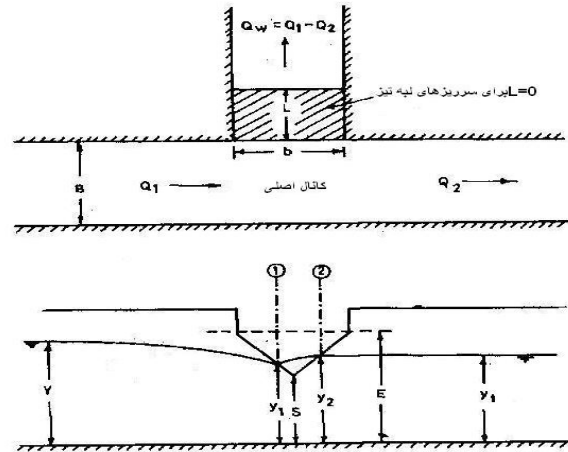


Fig. 1 Plan and longitudinal section of triangular side weir at rectangular canal.

### Model Description

Model includes a rectangular glassed canal of 11 meters length and 0.128 meters width. A triangular weir installed at the beginning of this canal to measure the inflow rate. A 60 degree triangular side weir has been installed at 7-m downstream of the beginning of the canal. To measure the water surface profile along the side weir, a series of piezometers have been installed along this side weir. A digital velocity meter located at the end of canal to determine the outflow rate.

### Experiments

To perform experiments, the maximum available discharge was  $0.0061 \frac{m^3}{sec}$ , so, experiments have been done for inflow rate of 0.002, 0.003, 0.004, 0.005 and  $0.006 \frac{m^3}{sec}$ . Two triangular side weirs of 90 and 60 degrees with sill elevations of 10, 11 and 12 cm from the canal bed have been used. Experiments have been performed for three canal bed slopes of 0.0005, 0.0001, and 0.0015. For fixed inflow rate and variable position of end canal gate different flowrate over the side weir as a result, different Froude numbers were performed. Over all 720 experiments were performed and the hydraulic

parameters of flow such as discharge rate, water surface profile. Along the side weir was measured.

### Side weir flow coefficient ( $C_m$ )

To use the triangular sideweirs, the following constraints should be considered.

$$1- \frac{H_d}{S} \leq 1.2$$

$$2- 0.049_m \leq H_d \leq 0.61_m$$

$$3- S \geq 0.09$$

4-the water surface elevation downstream of side weir should be lower than weir crest,  $H_d$  is the water depth above the side weir crest.

Using the measured data and dimensional analysis, the following equation resulted:

$$C_m = C_{de} (1 - k_1 f_r^{k_2})^{k_3} \quad (8)$$

Where  $C_{de}$  is a function of side weir angle ( $\theta$ ), and can be obtained from Fig (1),  $k_1, k_2$  and  $k_3$  are the constant coefficients. For very small Froude numbers  $C_m$  will become equal to  $C_{de}$  and the side weir operates as a normal weir.

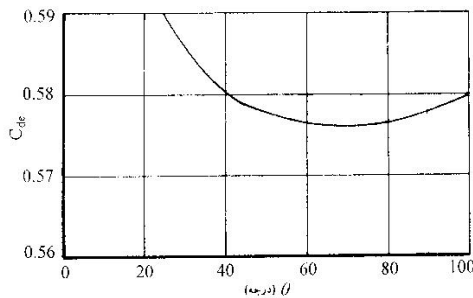


Fig 2  $C_{de}$  as a function of ( $\theta$ ) [2]

To obtain the values of  $K_1$ ,  $K_2$  and  $K_3$ , the measured data have been applied to the least-square method. The following equation can be written for flow coefficients:

$$\begin{aligned} C_{m1} &= C_{de1} (1 - K_1 f_{r1}^{K_2})^{K_3} \\ C_{m2} &= C_{de2} (1 - K_1 f_{r2}^{K_2})^{K_3} \end{aligned} \quad (9)$$

$$C_{mn} = C_{den} (1 - K_1 f_{rn}^{K_2})^{K_3}$$

So, using the least-square method, the following matrices can be obtained:

$$\begin{aligned} b &= \begin{bmatrix} C_{m1} - C_{de1} (1 - K_1 f_{r1}^{K_2})^{K_3} \\ C_{m2} - C_{de2} (1 - K_1 f_{r2}^{K_2})^{K_3} \\ \vdots \\ C_{mn} - C_{den} (1 - K_1 f_{rn}^{K_2})^{K_3} \end{bmatrix} \quad X = \begin{bmatrix} K_1 \\ K_2 \\ K_3 \end{bmatrix} \\ A &= \begin{bmatrix} \frac{\partial C_{m1}}{\partial K_1} & \frac{\partial C_{m1}}{\partial K_2} & \frac{\partial C_{m1}}{\partial K_3} \\ \frac{\partial C_{m2}}{\partial K_1} & & \dots \\ \vdots & & \\ \frac{\partial C_{mn}}{\partial K_1} & \frac{\partial C_{mn}}{\partial K_2} & \frac{\partial C_{mn}}{\partial K_3} \end{bmatrix} \end{aligned} \quad (10)$$

Assuming initial values for  $k_1$ ,  $K_2$  and  $k_3$  in the  $A$  and  $b$  matrices, the matrix  $X$  can be calculated as:

$$A * X = b \Rightarrow X = [A^T A]^{-1} A^T b \quad (11)$$

The calculated  $X$ -matrix is compared to the previous  $X$ -matrix, when no changes have been observed in the  $X$ -matrix, the values of  $X$ -matrix is the real values of  $k_1$ ,  $K_2$  and  $k_3$ .

Applying the calculated  $k_1$ ,  $K_2$ , and  $k_3$  in the equation of side weir coefficient (equation-8), the following equations resulted for 90 and 60 degrees triangular side weirs.

$$C_M = C_{de} (1 - 0.382 f_r^{2.445}) \quad (12)$$

$$C_M = C_{de} (1 - 0.3197 f_r^{0.8503}) \quad (13)$$

The calculated and measured  $C_m$  were plotted for different froude numbers on Fig (3) and Fig (4).



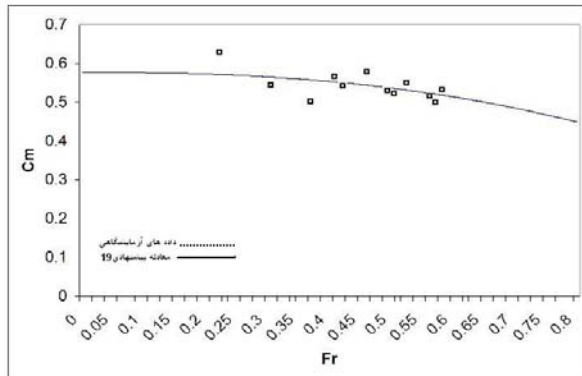


**Fig 3** The values of  $C_m$  as a function of Froude numbers for  $\theta = 90^\circ$

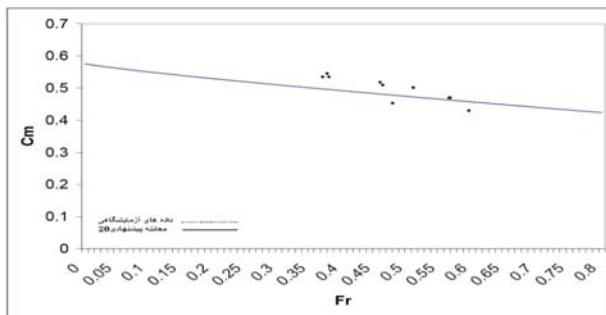


**Fig 4** The values of  $C_m$  as a function of Froude numbers for  $\theta = 60^\circ$

### Conclusion:

Using two triangular side weirs of 60 and 90 degrees in a hydraulic model, the flow parameters were measured. Based on the measured data, dimensional analysis and least-square method, equation of flow coefficient over triangular side weir ( $C_m$ ) were suggested. (Equ.12 and 13)

Using these equations, the flow coefficients for 60 and 90 degrees triangular side weirs were calculated.

Comparison of the calculated  $C_m$  and the measured ones, show a good agreement Figs (3) and (4). These equations ((12),(13)) show that for very small Froude numbers the side weirs operate as a normal weir and the flow coefficients of these

triangular side weirs are 0.576 for  $\theta = 60^\circ$  And 0.577 for  $\theta = 90^\circ$ .

### References:

- [1] Ayumaz, A." Discharge control by a side weir in a triangular main channel."10<sup>th</sup> International conference on urban Drainage, Copenhagen, Danmark, 2005.
- [2] Hossein, S.M., and Abrishami, J." Open – channel Hydraulics, 2<sup>nd</sup> Ed., astane ghods razavi, Mashhad2006.
- [3] Subramanya, D., and Awasthy, SC. "Spatially varied flow over side weirs". J. Hydr, Engrg. ASCE,98(1) 1972, p1-10.
- [4] Kumar, C.P., and pathak, S.L."Triangular side weirs", J. Irrig and Drain. Engrg, ASCE 113(1), 1987, P98-106.
- [5] Oliveto, G., Biggiero, V., and Fiorentino, M. "Hydraulic features of supercritical flow Along Prismatic side weirs", ASCE, J. Hydraulic Research, vol. 39, 2001, No.1, 73-82.
- [6] Muslu, Y. () " Technical Note of Lateral weir flow Model using a curve fitting Analysis", ASCE J. Hydraulic Engineering, Vol. 128, 2002, No.7.

## CO<sub>2</sub> BASED FREEZE-EXPLOSION METHOD FOR INCREASING HYDROLYSIS OF CELLULOSE

GENADI PARTSKHALADZE<sup>1</sup>, TAMAR DUDAURI<sup>1</sup>, MALKHAZ BEREZHIANI<sup>1</sup>, ANA BEREJIANI<sup>2\*</sup>, BESARION METREVELI<sup>2</sup>, TAMAR SVANIDZE<sup>3</sup>

<sup>1</sup>National High Technology Center of Georgia Tbilisi, Georgia

<sup>2</sup>Durmishidze Institute of Biochemistry and Biotechnology. David Agmashenebeli avenue 10<sup>th</sup> km, 0159, Tbilisi, Georgia, Phone: +995 32 697 360, e-mail: a.berezhiani@soon.com

<sup>3</sup>Georgian Parliament National Library, Tbilisi, Georgia

### Abstract

Production of fuels and chemicals by fermentation of renewable, low cost and plentiful cellulosic materials has received increasing attention due to several reasons including dwindling of fossil fuels. One of the key problems in the fermentation of lignocellulosic wastes to liquid fuel like ethanol or chemicals is the relatively low reactivity nature of cellulose. A number of factors are believed to influence cellulose reactivity, including particle size and surface area, lignin content, and cellulose crystallinity. Significant increase of cellulose hydrolysis by some economical and environmentally sound method is considered one of the important points to make cellulosics based fuel ethanol production cost competitive with gasoline. Cellulosic materials pretreatment method reported here has been developed to increase cellulose reactivity, in particular to increase the rate and extent of cellulose hydrolysis. Proposed method is based on the treatment of cellulosic material with a liquefied carbon dioxide under pressure followed by pressure release. It involves combination of the following processes: (i) saturation of cellulosic materials with water; (ii) contact of cellulosic materials with liquefied CO<sub>2</sub> under pressure at temperature less than those which degrade sugars; (iii) pressure release that causes the evaporation of liquid CO<sub>2</sub>. Temperature decrease associated with evaporation of the volatile liquid tends embrittle the fiber and enhances the effect of the pressure release on overall fiber disruption. Changes in cellulose polymerization degree and specific surface area have been determined when cellulosic wastes like wheat straw and corn stalks were frozen at -5°C, -10°C, -21°C and -31°C. Studies showed that cellulose polymerization degree was decreased about 2 times and cellulose specific reactionary surface area was increased around 10 times when above cellulosic wastes were frozen at -31°C and milled in 3-5 mm particles in the frozen state.

**Key words:** lignocellulosics, lignin, cellulose reactivity, polymerization degree, specific reactionary surface area

### Introduction

Plant biomass, mostly referred to a lignocellulose, is predominantly composed of three major polymers: cellulose (an insoluble linear unbranched homopolysaccharide consisting of glucose subunits linked via  $\beta$ -(1,4) glycosidic linkages), hemicellulose (polysaccharide mainly composed of xylan, mannans and glucans) and lignin (an intricate polyphenolic structure). It is built up as cellulose fibers that are partially arranged in a crystalline structure, integrated with hemicellulose and embedded in a matrix of lignin [1]. Both the cellulose and hemicellulose are the sources of fermentable sugars. Compared to starch and sugar crops, effective release of sugars from recalcitrant lignocellulosics is complex and

therefore requires suitable pretreatment and hydrolysis steps.

Many techniques have been used over the years to increase cellulose digestibility. These techniques can be characterized as chemical, physical or their combination.

Chemical pretreatments with strong acids or bases such as sulphuric acid or sodium hydroxide or with other cellulose swelling/dissolving agents also effectively increase hydrolysis of cellulose. These chemicals are generally corrosive, costly and must be recovered for reuse. Furthermore, they are often toxic or inhibitory to biological systems so that their removal from the treated cellulosic material must be very complete. The most problems with these chemical treatments is that recovery of the chemicals generally requires

a wash steam which itself must be purified. All these factors increase the expenses and difficulty of such chemical treatment methods.

An interesting approach for hemicellulose hydrolysis and pretreatment for cellulose hydrolysis is the «carbonic acid» process which employs hot compressed water saturated with carbon dioxide as a reagent for promoting hemicellulose hydrolysis and breaking up of lignocellulose structures to enhance subsequent cellulose enzymatic hydrolysis. This method prevents the use of mineral acids and associated waste production [2].

Another treatment which involves both physical and chemical aspects is the steam explosion process. Cellulosic materials are saturated with water under pressure at elevated temperature. When the pressure is released, water evaporates rapidly and cellulose fibers tend to separate, increasing surface area for hydrolysis. In addition the moisture and high temperature liberate plant acids which further improve digestibility of cellulose. This process requires considerable expensive thermal energy in the form of steam. It has additional disadvantage, in particular some of the sugars degrade by the high temperatures involved even at small reaction times.

The physical treatments include ball milling to very small mesh sizes, two-roll milling, and attrition milling. These physical treatments are effective in producing more reactive cellulose; however power requirements for such grinding/milling are too large and make these methods quite costly. Ammonia freeze-explosion techniques that also can be attributed to physical pretreatment method showed obviously increase the yield of fermentable sugars from alfalfa. Here anhydrous ammonia is used to swell and decrystallize cellulose [3]. However, conditions of above pretreatment promote production of fermentation inhibitors [4]. To overcome this drawback chemically inert CO<sub>2</sub> was introduced here as a heat agent for cellulose pretreatment by freeze-explosion.

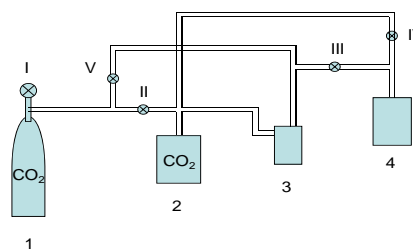
## Materials and methods

Corn stalks and wheat straw harvested in post physiological maturity in different regions of Georgia were dried naturally and studied for chemical composition, polymerization degree and specific surface area. Percentage of cellulose, xylan, lignin, crude protein, soluble

solids and ash was determined using the standard methods. Cellulose polymerization degree was determined by the viscosimetry method. Samples of cellulosic wastes were dissolved by copper-ammonia complex and the viscosities of obtained solutions were measured by using Oswald viscosimeter. For cellulose specific surface area determination the method based on chemotripsin absorption was used. Samples of corn stalks and wheat straw were kept in the solution of chemotripsin and the amount of absorbed enzyme was measured by decrease in enzymatic activity. Computation of specific surface area was done on the assumption that on the analytical sample monomolecular layer of enzyme was formed.

CO<sub>2</sub> based freeze explosion method introduced for cellulose pretreatment involved combination of the following processes: 1) saturation of cellulosic materials (corn stalks and wheat straw) with water; 2) contact of cellulose with liquid CO<sub>2</sub> at temperature less than those which degrade sugars; 3) pressure release that causes the evaporation of liquid CO<sub>2</sub>. During the evaporation of liquid CO<sub>2</sub> temperature drops to negative value and water contained in cellulose freezes. Due to anomalous characteristic of water on phase transfer: water – ice, specific volume of water increases by 10%. So, when freezing, water contained in cellulose expands and causes mechanical stress followed by partial destruction of cellulose structure. 4) Mechanical milling of frozen cellulosic materials enhances subsequent breaking of cellulose that results in the further increase of cellulose specific surface area accessible for enzymes.

Schematic lay-out of laboratory arrangement for biomass pretreatment via CO<sub>2</sub> based freeze explosion method is given in fig 1.



1. CO<sub>2</sub> container; 2. Receiver; 3. High pressure compressor; 4. Chamber for biomass freezing. I, II, III, IV and V – valves.

Fig. 1

In the course of experiments cellulosic materials saturated with water was placed in the

high pressure vessel (4). From container (1) gaseous carbon dioxide first goes to receiver (2) whence it is delivered to high pressure compressor (3). Using machine (3), CO<sub>2</sub> can be compressed achieving different pressure values. After delivery of compressed carbon dioxide to vessel (4) valve (III) is closed and valves (IV) and (V) are opened. Due to this, carbon dioxide's pressure sharply decreases and liquefied CO<sub>2</sub> rapidly evaporates that result in the drop of temperature followed by freezing of water contained in saturated cellulosic materials (4). After the freezing process is finished, gaseous CO<sub>2</sub> goes to compressor (3). By that moment valves (II), (III) and (IV) are closed and valves (I) and (V) are opened. In this way CO<sub>2</sub> is compressed back in container (1).

Contact time of liquid CO<sub>2</sub> and cellulosic material saturated with water was 30 min. Frozen biomass was milled in 2-3 mm size particles. To estimate amount (kg) of CO<sub>2</sub> needed for freezing of 1 kg cellulosic materials saturated with 1 kg water theoretical calculations have been done using the formula given below:

$$m_{CO_2} = \frac{c_1 m_1 \Delta T_1 + c_2 m_1 \Delta T_2 + c_3 m_3 \Delta T_3}{h'' - h'}$$

Where  $m_{CO_2}$  is the amount (kg) of carbon dioxide that is to be compressed in the high pressure vessel where cellulosic materials saturated with water are placed.  $h'$  and  $h''$  are the initial and final values of CO<sub>2</sub> enthalpy. Water

specific heat –  $c_1 = 4,19$  kJ/kg;  $m_1$  = amount of water  $\Delta T_1$  change in water temperature, ice specific heat –  $c_2 = 2,04$  kJ/kg;  $\Delta T_2$  – ice temperature change interval;  $c_3 = 2,39$  kJ/kg – specific heat of cellulosic materials,  $m_2$  – mass of cellulosic sample;  $\Delta T_3$  – temperature change interval for cellulosic materials.

Thermal and mechanical work needed for transforming of certain amount of carbon dioxide from gaseous state at given temperature and pressure into saturated liquid was calculated using the following formula:

$$q_2 = m_{CO_2} x(h - h')$$

Where  $h$  is the enthalpy of carbon dioxide in the gaseous state. Data given in standard thermodynamic tables were used for such calculations.

Efficiency of pretreatment was assessed according to the changes in cellulose specific reactionary surface area, cellulose polymerization degree and the yield of fermentable sugars during the enzymatic hydrolysis. *Trichoderma reesi* enzyme level of 40 IU/g dry fiber was used for cellulose hydrolysis.

## Results and discussions

Wheat straw and corn stalks analysis were performed prior to the pretreatment. These results are summarized in table I.

Table I. Chemical composition and structural characteristics of corn stalks and wheat straw

Sample	Cellulose (%)	Xylan (%)	Lignin (%)	Crude protein (%)	Soluble solids (%)	Ash (%)	Cellulose specific surface area (m <sup>2</sup> /g)	Cellulose polymerization degree
Corn stalks								
sample 1	35.5	27.1	19.4	4.6	8.3	5.1	0.016	733
sample 1	31.3	29.6	16.2	5.5	9.5	7.9	0.021	687
Wheat straw								
sample 1	42.7	19.7	19.0	3.8	13.4	4.4	0.027	461
sample 1	36.8	15.9	16.8	2.1	20.7	7.7	0.032	544

On a dry basis wheat straw and corn stalks in post physiological maturity in different regions of Georgia contain 35 – 42 % cellulose and 16 – 29% xylan (hemicellulose), values not too much less than that of many tree species.

The variables in the pretreatment were as follows; weight of water used for saturation of 1 kg wheat straw and corn stalks, CO<sub>2</sub> pressure, time and temperature of the treatment. Frozen cellulotics were milled in 3-5 mm particles.

Table II shows changes in cellulose specific reactionary surface area and polymerization degree when freezing 1 kg cellulosic material

saturated with 1 kg tap water at temperatures -5<sup>0</sup>C; -10<sup>0</sup>C, -21<sup>0</sup>C and -31<sup>0</sup>C.

Table II. Changes in cellulose polymerization degree and specific surface area when freezing cellulosic materials at different temperatures

Sample	Initial value		Freezing temperature							
	CSSA* (m <sup>2</sup> /g)	CPD**	-5 <sup>0</sup> C		-10 <sup>0</sup> C		-21 <sup>0</sup> C		-31 <sup>0</sup> C	
			CSSA (m <sup>2</sup> /g)	CPD	CSSA (m <sup>2</sup> /g)	CPD	CSSA (m <sup>2</sup> /g)	CPD	CSSA (m <sup>2</sup> /g)	CPD
Corn stalks										
sample 1	0.016	733	0.04	531	0.07	497	0.09	386	0.16	365
sample 1	0.021	687	0.08	502	0.09	480	0.11	375	0.21	360
Wheat straw										
sample 1	0.027	461	0.032	392	0.046	347	0.050	295	0.061	220
sample 1	0.032	544	0.047	408	0.051	380	0.058	305	0.070	254

CSSA\* - cellulose specific surface area (m<sup>2</sup>/g)

CPD\*\* - cellulose polymerization degree

Freezing temperature effect on hydrolysis rate of pretreated corn stalks and wheat straw was estimated by the glucose yield (mg) per g dry mass of pretreated cellulose. For these purposes *Trichoderma reesi* enzyme complex was used. Results are given in table III.

Table III. 36 hour hydrolysis of non treated and treated corn stalks and wheat straw

Sample	No treatment Sugar yield (mg glucose/g dry fiber)	% of theoretical conversion	Freezing temperature	Sugar yield (mg glucose/g dry fiber)	% of theoretical conversion	Freezing temperature	Sugar yield (mg glucose/g dry fiber)	% of theoretical conversion
Corn stalks								
sample 1	187	46.7	-5 <sup>0</sup> C	207	51.7	-21 <sup>0</sup> C	360	78.3
sample 1	192	48.0	-10 <sup>0</sup> C	312	67.8	-31 <sup>0</sup> C	400	86.9
Wheat straw								
sample 1	185	46.2	-5 <sup>0</sup> C	200	43.5	-21 <sup>0</sup> C	369	80.2
sample 1	178	44.5	-10 <sup>0</sup> C	305	66.3	-31 <sup>0</sup> C	404	87.8

## Conclusions

CO<sub>2</sub> based freeze explosion method enables to significantly improve cellulose digestibility. No fermentation inhibitors are produced in the course of treatment process. Practically no carbon dioxide remains with the treated fiber at room temperature. CO<sub>2</sub> recovery is a simple and relatively inexpensive. Thus, cellulosic materials pretreatment method reported here can be

considered environmentally friendly and economically sound process.

**Acknowledgement**

This work was supported financially by the International Science and Technology Center (ISTC), Moscow. Project # G – 1624. Financing parties: EU and Korea.

**References**

[1]. Coombs J. Bioconversion assessment study. 1996; EC, DG XII, Science, Research and Development; Brussels

[2]. Zheng Y et al. 1998. Pretreatment for cellulose hydrolysis by carbon dioxide explosion. *Biotechnology Progress*, Issue 14:890-896

[3]. Bruce E. Dale and Maria J. Moreira. "A freeze-explosion technique for increasing cellulose hydrolysis." 1982 Proceedings of the fourth symposium on Biotechnology in Energy Production and Conservation. Gatlinburg, Tennessee, May 11-14

[4]. N. I. Nikitin., *The chemistry of cellulose and wood*. Moscow 1966. Nauka



## MATHEMATICAL MODEL OF MOTOR VEHICLE EXPLOITATION PARAMETER CALCULATION USING BIO ETHANOL FUELS

DAINIS BERJOZA, VILNIS PIRS

Motor Vehicle Institute, Faculty of Engineering, Latvia University of Agriculture,  
5 J. Cakstes boulv., Jelgava, LV-3001, Latvia, e-mail: [dainis.berjoza@llu.lv](mailto:dainis.berjoza@llu.lv);  
[vilnis.pirs@llu.lv](mailto:vilnis.pirs@llu.lv).

### Abstract

Automobile exploitation parameters can be determined in two basic ways – performing experimental research or analytical calculations. Analytical calculations are cheaper but not always as exact as experimental data. Within the frame of the research a mathematical model has been developed for determination of such automobile exploitation parameters as the speed of movement, characteristics of traction, distribution of power in the kinds of resistance, dynamic factor, run-up acceleration and run-up time. Original methods have been developed for determination of the run-up time if the acceleration is known at which graphic integration is not applied. The capacity for work of the model is approbated with data of actual automobiles and they are compared to the theoretically obtained data.

**Key words:** exploitation parameters, run-up time, acceleration, characteristic curves, speed

### Introduction

Fuel is used for any internal combustion engine as the main source of energy. There are different kinds of fuel – gasoline, diesel fuel, different biofuels, natural gas, liquefied gas etc. that differ with their physical and chemical properties, due to this also the specificity of their application is different. The fuel properties influence the specificity of motor operation as well as the efficiency of motor operation that is closely related to the characteristic values of the motor power and torque, fuel consumption and composition of exhaust gases.

The automobile exploitation parameters can be influenced by such automobile characteristic values as the motor power, torque as well as weight. In turn, the motor power and the torque are influenced by the kind of the used fuel as for different fuels, for instance, biofuel can have lower heat capacity. The mathematical algorithm for determination of the motor vehicle exploitation parameters offered in the research can be used if either the motor power  $N_e$  or the torque  $M_e$  at different revolutions, or the outer characteristic curves of the motor power or the torque are known. The construction principles of the outer characteristic curves according to the nominal motor power are discussed in our previous publications (Aboltins, A et al 2010). The developed mathematical algorithm being inserted in a modeling software can be used for

determination of the exploitation parameters operating automobiles with pure biofuel as well as with fossil fuel and biofuel mechanical blends. With the mathematical algorithm it is possible to determine: theoretical driving speed in all gears, power balance, traction balance, dynamic factor, run-up acceleration at different gears and run-up time in the whole range of the driving speed.

It is possible to obtain more precise calculations of the above mentioned exploitation parameters if the experimentally obtained outer characteristic curve of power is used. The power curves that are obtained on the rolling stand or on the motor dynamometric power stand can be used. Application of the algorithm is especially useful performing wide research in the usage of a definite fuel in a large number of motor vehicles or for blends of wide range fossil fuel and biofuel, for instance, in the case of usage of bioethanol from E5 to E100 (the figure at the letter “E” shows the percentual admixture of bioethanol to fossil fuel). The developed algorithm does not identify whether the motor is able to operate with the corresponding kind of biofuel in definite conditions, but development of such algorithm is planned in separate investigations.

## 1. Algorithm for calculation of motor vehicle exploitation parameters

### 1.1. Theoretical speed of motor vehicle movement

The theoretical speed of motor vehicle movement can be calculated for all gears in the gearbox in case if the mechanic gearbox is used. The theoretical speed of motor vehicle movement m/s can be calculated:

$$v_{teor} = 0,10472 \frac{n_e r_k}{i_t} (ms^{-1}), \quad (1)$$

where  $r_k$  – kinematic or rolling radius of the wheel, m;

$n_e$  – frequency of motor crankshaft rotation,  $min^{-1}$ ;

$i_t$  – motor vehicle transmission gear ratio.

The gear ratio, if the clutch and universal joint gear ratio are not considered, for motor vehicles can be calculated:

$$i_t = i_k i_p i_0, \quad (2)$$

where  $i_k$  – gearbox gear ratio;

$i_p$  – secondary regulator gear ratio;

$i_0$  – final drive gear ratio.

The kinematic radius of the wheel can be calculated:

$$r_k = 0.0127 d_r + 0.91 b_r k_r, \quad (3)$$

where  $d_r$  – wheel disc diameter, in inches;

$b_r$  – width of the tyre, m;

$k_r$  – coefficient of the tyre height.

### 1.2. Motor vehicle power and traction balance

The motor vehicle power balance in every gear is calculated considering all kinds of resistance acting on the power vehicles. The most often used full power balance can be calculated:

$$N_e = N_f + N_\alpha + N_w + N_j + N_p, \quad (4)$$

where  $N_f$  – power to clear the rolling resistance, kW;

$N_\alpha$  – power to clear the upgrade resistance, kW;

$N_w$  – power to clear the air resistance, kW;

$N_j$  – power to clear the inertia resistance, kW;

$N_p$  – power to clear the trailer resistance, kW.

Traction power to the driving wheels if the automobile does not pull a trailer:

$$N_k = N_e \eta_T = N_\psi + N_w + N_j, \quad (5)$$

where  $\eta_T$  – transmission efficiency coefficient.

It is useful to calculate the free power if also the dynamic factor is calculated:

$$N_b = N_k - N_w. \quad (6)$$

The power for overcoming the road resistance can be calculated according to the expression:

$$N_\psi = \psi G_a v, \quad (7)$$

where  $\psi$  – road resistance coefficient,

$G_a$  – weight of the automobile.

Road resistance coefficient:

$$\psi = f \cos \alpha + \sin \alpha, \quad (8)$$

where  $f$  – road resistance coefficient of the corresponding road surface;

$\alpha$  – upgrade angle, in degrees.

Power to clear the air resistance:

$$N_w = k F v^3, \quad (9)$$

where  $k$  – air resistance coefficient;

$F$  – automobile front area,  $m^2$ .

Power to clear the inertia resistance:

$$N_j = m_a \delta j v, \quad (10)$$

where  $m_a$  – automobile mass, kg;

$\delta$  – rotation mass coefficient;

$j$  – automobile acceleration,  $m \cdot s^{-2}$ .

The motor vehicle balance is calculated using the power balance and considering that:

$$P = \frac{N}{v}. \quad (11)$$

Traction balance according to the correlation (4):

$$P_k = P_f + P_\alpha + P_w + P_j + P_p, \quad (12)$$

where  $P_f$  – force to clear the rolling resistance, kN;

$P_\alpha$  – force to clear the upgrade resistance, kN;

$P_w$  – force to clear the air resistance, kN;

$P_j$  – force to clear the inertia resistance, kN;

$P_p$  – force to clear the trailer resistance, kN.

Free force can be calculated analogous to the free power:

$$P_b = P_k - P_w. \quad (13)$$

In the traction balance the driving wheel road adherence force  $P_\phi$  for definite road conditions

can be calculated. The road adherence force curves characterize the possibility to use the traction force in the corresponding gear in definite road adherence conditions. For calculation of the road adherence force the load on the driving wheels  $Q_k$ , kN for completely loaded automobile and the road adherence coefficient  $\varphi$  are used:

$$P_\varphi = Q_k \varphi. \quad (14)$$

If there is no trailer ( $P_p=0$ ), calculating every balance value and considering that  $P_\psi = P_f + P_a$  the most often used traction balance formula is obtained:

$$P_k = P_\psi + P_w + P_j. \quad (15)$$

Deciphering every balance value we get:

$$\frac{M_e i_T \eta_T}{r_k} = \psi G_a + kFv^2 + m_a \delta \ddot{j} = f G_a \cos \alpha + G_a \sin \alpha + kFv^2 + m_a \delta \ddot{j}. \quad (16)$$

The inertia force  $P_j$  is found as the differences between  $P_k$  and other resistance forces. It gives an insight on the potential inertia resistance and so on the possibilities to accelerate the pace of the motor vehicles. Increasing the speed,  $P_j$  usually decreases. If  $P_j=0$ , it is not possible to accelerate the pace and the maximal driving speed is achieved  $v_{max}$ , when  $P_k = P_\psi + P_w$ .

### 1.3. Motor vehicle dynamic factor and acceleration

The motor vehicle dynamism is characterized by the dynamic factor the calculation of which is most often used for automobiles. The dynamic factor for every gear can be calculated according to the correlation:

$$D = \frac{P_k - P_w}{G_a} = \psi + \frac{\delta \times j}{g}. \quad (17)$$

Dynamic factor according to the road adherence for the corresponding road conditions:

$$D_\varphi = \frac{P_\varphi - P_w}{G_a} = \frac{\varphi Q_k - kFv^2}{G_a}, \quad (18)$$

The motor vehicle acceleration for all gears can be calculated according to the dynamic factor:

$$j = \frac{g}{\delta} (D - \psi), \quad (19)$$

where  $g$  – free fall acceleration,  $m \cdot s^{-2}$ .

The mass coefficient for every gear can be calculated according to the empiric formula:

$$\delta = 1,04 + 0,0025 i_k^2 i_0^2. \quad (20)$$

Acceleration according to the road adherence can be determined according to the correlation:

$$j_\varphi = \frac{g}{\delta} \left( D_\varphi - \frac{\varphi Q_k}{G_a} \right). \quad (21)$$

### 1.4. Acceleration inverse value and run-up time

The acceleration inverse value and acceleration are most often calculated for fast speed motor vehicles, for example, automobiles. The acceleration inverse value is calculated in order to graphically precisely determine the gear shift moment running up with the maximal intensity:

$$\frac{1}{j} = \frac{\delta}{g(D - \psi)}. \quad (22)$$

The speed of movement at which the gear is to be shifted in order to ensure the fastest run-up can be determined analytically taking two proximal gears  $n$  and  $n+1$ :

$$\frac{1}{j_n} = \frac{1}{j_{n+1}} = \frac{\delta_n}{g(D_n - \psi)} = \frac{\delta_{n+1}}{g(D_{n+1} - \psi)} \quad (23)$$

Accepting that in the moment of gear shift the traction force on the wheels will be stable and considering the correlation 17 the optimal driving speed is obtained for shifting from the gear  $n$  to  $n+1$ :

$$v_{n \rightarrow n+1} = \sqrt{\frac{P_{k,n} - \psi G_a}{kF}}, \quad (24)$$

where  $P_{k,n}$  – traction force in the moment of gear shift from  $n$  to  $n+1$ .

The run-up time can be calculated up to reaching any potential driving time of the automobile, nevertheless it is useful to calculate up to the characteristic driving regimes:

- 50 kmh<sup>-1</sup> – driving speed determined in the city traffic in a great part of countries;
- 90 kmh<sup>-1</sup> – driving speed determined in the traffic on highways outside cities;
- 100 kmh<sup>-1</sup> – the value of the driving speed determined by the producers characterizing the automobile run-up dynamics.

The run-up time is found transforming the expression  $j = dv/dt$ :

$$dt = \frac{dv}{j} \quad (25)$$

Integrating this expression the run-up time is obtained:

$$t_{ie} = \int_{v_1}^{v_2} \frac{dv}{j} \quad (26)$$

Integration is done in the range of every gear from the moment of gearing in to shifting but in the highest gear – to the margin speed, for example,  $v_{rob} = (0, 90 \dots 0, 95) v_{max}$ . The run-up starting speed  $v_I = 0$ , bet  $v_2 = v_k$ . In this case  $v_k$  characterizes the driving speed at the first gear in

$$\begin{aligned} t_{ie} &= \int_{v_1}^{v_{rob}} \frac{dv}{j} = \int_{v_0}^{v_1} \frac{dv_0}{j_0} + \int_{v_1}^{v_2} \frac{dv_I}{j_I} + \int_{v_2}^{v_3} \frac{dv_{II}}{j_{II}} + \dots + \int_{v_n}^{v_{n+1}} \frac{dv_n}{j_n} = \\ &= \int_{v_0}^{v_1} \frac{\delta \cdot m_a \cdot dv_0}{P_{k0} - G_a \psi - kFv_0^2} + \int_{v_1}^{v_2} \frac{\delta \cdot m_a \cdot dv_I}{P_{kI} - G_a \psi - kFv_I^2} + \int_{v_2}^{v_3} \frac{\delta \cdot m_a \cdot dv_{II}}{P_{kII} - G_a \psi - kFv_{II}^2} + \dots + \int_{v_n}^{v_{n+1}} \frac{\delta \cdot m_a \cdot dv_n}{P_{kn} - G_a \psi - kFv_n^2} \end{aligned} \quad (27)$$

The first value of the expression 27 characterizes the run-up starting time till the moment when the clutch is released, the second value – movement in gear 1, the third in gear 3 and so up to the highest gear  $n$ .

Function (27) usually cannot be integrated in a wide range as there is not the description of the correlation  $j=f(v)$  that is different in different gears. Precise integration can be done only in the range of one gear. Due to this reason integration is done in a narrow range, for example, assuming the driving speed change by  $1 \text{ m} \cdot \text{s}^{-1}$  as a step. In this interval it can be assumed that the speed and acceleration change linearly. Calculating the run-up time in a small speed change interval:

$$t_{ie}' = \frac{v_2 - v_1}{j'} \quad (28)$$

where  $v_I$  – driving speed at the beginning of the calculated interval;

$v_2$  – driving speed at the end of the calculated interval;

$j'$  – average run-up acceleration in the calculated stage.

The average run-up acceleration in the calculated stage is determined according to the correlation:

$$j' = \frac{j_1 + j_2}{2} \quad (29)$$

the gearbox and in the motor crankshaft rotation frequency moment when the clutch is completely engaged. Depending on the driving style and the necessity to run up more or less intensively the motor revolutions in the moment of clutch engagement can be in the range from  $1000 - 3000 \text{ min}^{-1}$ . The possibly highest acceleration is usually achieved in the first gear but due to the limited wheel road adherence this acceleration has only theoretical character.

Run up till the margin speed using all automobile gears and considering the correlations 1, 17, 21, 19 and 26, we obtain:

where  $j_I$  – momentary acceleration corresponding to  $v_I$ ;

$j_2$  – momentary acceleration corresponding to  $v_2$ .

If  $1 \text{ m} \cdot \text{s}^{-1}$  is accepted as the speed interval, inserting the correlation  $j'$  (28) in the expression 27, we obtain:

$$t_{ie}' = \frac{2}{j_1 + j_2} \quad (30)$$

Taking the speed change of another value when  $v_2 - v_1 \neq 1 \text{ m} \cdot \text{s}^{-1}$ :

$$t_{ie}' = \frac{2(v_2 - v_1)}{j_1 + j_2} \quad (31)$$

At the beginning of run-up the fastest increase of acceleration can be observed from 0 to the acceleration value that is close to the maximal run-up acceleration in the corresponding road adherence conditions. In practical calculations in the correlation 28 it is useful to use  $j_I = 0$  and  $j_2 = j_\phi$ , in cases when  $j_2 \leq j_\phi$  and to assume that the character of acceleration changes is linear. If  $j_2 \geq j_\phi$ ,  $j_2$  values should be taken.

This way the partial run-up time is obtained running up by  $1 \text{ m} \cdot \text{s}^{-1}$  or any other interval. In order to obtain the run-up time till a definite movement speed, for example, to  $50 \text{ km} \cdot \text{h}^{-1}$ , or

$13.89 \text{ m}\cdot\text{s}^{-1}$  all the partial run-up times in the corresponding interval should be added up:

$$t_{ie50} = t_{ie1} + t_{ie2} + t_{ie3} + \dots + t_{ie,n} \quad (32)$$

The input parameters of the algorithm developed by us will be the motor power at different rotation frequencies (external motor characteristics) but output – graphic characteristics of the theoretical driving speed,

traction balance, power balance, dynamic factor, run-up acceleration and run-up time as well as the optimal driving speed for optimal gear shift.

## 2. Research results

Applying the developed algorithm the following motor vehicle characteristic curves have been obtained (See Fig. 1).

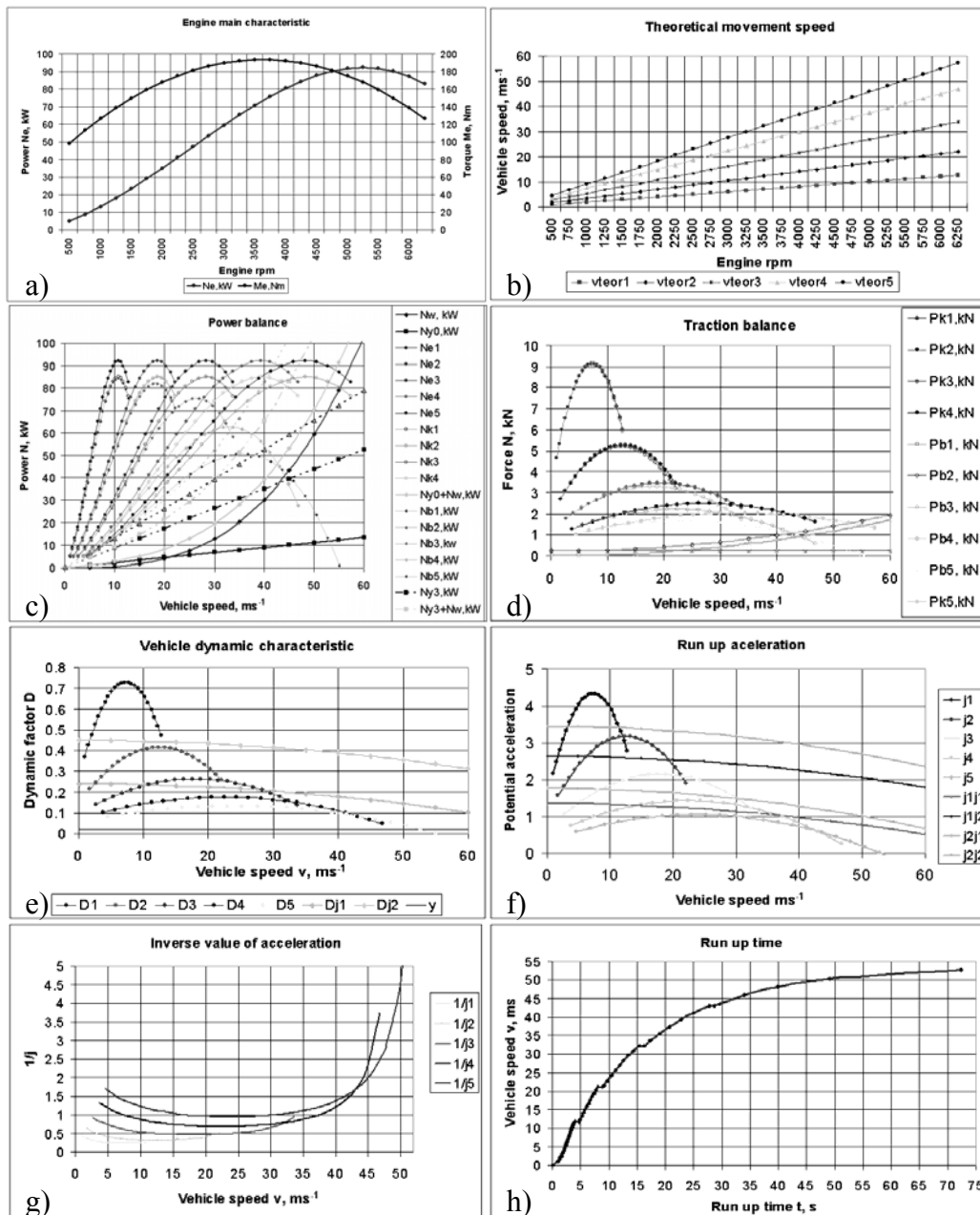


**Fig. 1.** Motor vehicle exploitation parameter characteristic curves: a – engine main characteristic; b – theoretical movement speed; c – power balance; d – traction balance; e – dynamic factor; f – run-up acceleration; g – inverse value of acceleration; h – run-up time.

The model can be easily used in the research in biofuels of different composition obtaining comprehensive characteristics of automobile exploitation properties that can afterwards be used for detailed analysis.

### Conclusions

1. Experimental determination of exploitation parameters of several motor vehicles can be very work consuming and expensive, therefore it is useful to develop an up-dated algorithm for determination of these parameters.
2. A modified algorithm for determination of motor vehicle exploitation parameters has been developed and adopted for its application in different computer modeling tools.
3. The main input parameters of the algorithm are the characteristic curves of power that are advisable to be taken from the experimental results, for instance, measuring power on the rolling power stand
4. The developed algorithm has been tested using the modeling tool AnyLogic and accepted as able to work.
5. It is advisable to apply the developed algorithm and model for wide comparative research in investigations with the motor operating with blends of different composition biofuel and fossil fuel.

6. The output parameters of the algorithm allow to judge about the advantages of usage of the corresponding fuel in comparison to other kinds of fuel, the choice of the optimal movement regime and power vehicle dynamics.

### Reference

1. Aboltins A., Berjoza D., Pirs V. Theoretical model of exploitation of automobiles operated with bioethanol-gasoline mixture fuels. 2010. *Proceedings of the 9th International Scientific Conference „Engineering for Rural Development”*. Jelgava : LUA, pp. 133. – 138.
2. Automotive Handbook 7th Edition. Robert Bosch GmbH, July 2007. 1196 p. ISBN 978-0-470-51936-3.
3. Pommers J., Liberts G. Theory of automobile. Riga: Zvaigzne, 1985. 248 p.
4. Blivis J. Gulbis V., Kazoks J. a.o. Constructions, theory and calculation of motors of tractors and ground motor vehicles. Riga: Zvaigzne, 1980. 375 p.
5. Berjoza D. Theory of automobile. Methodic guidelines for development course paper, objectives and lecture notes. Jelgava: LLU, 2007. – 54 p.
6. Berjoza D. Theory of automobile. Jelgava: LLU, 2008. – 200 p.



## DETERMINING SHEAR STRENGTH AND ENERGY OF SAFFRON STALK AS AFFECTED BY BEVEL ANGLES AND CUTTING RATES

S.R. HASSAN-BEYGI\*, H. VALE GHOZHDI AND M.H. KIANMEHR

Department of Agro-technology, College of Abouraihan, University of Tehran, Pakdasht, Iran

\*Corresponding author: Phone and Fax: +98-292-3040614 and e-mail address: [rhbeigi@ut.ac.ir](mailto:rhbeigi@ut.ac.ir)

### Abstract

The shear strength and shear energy per unit area of flowers are important parameters to design and develop harvesting mechanisms. In this study shear strength and shear energy per unit area of saffron (*Crocus sativus* L.) stalk were determined as a function of bevel angle and shear velocity. The experiments were conducted on samples selected from fields of Kashmar. The effect of cutting rate at three levels of 20, 200 and 500 mm/min and bevel angle of cutting blade at three levels of 17, 20 and 24° were investigated on the shear force and energy by using two factors completely randomized design. The results showed that with an increase in bevel angle of cutting blade from 17 to 20°, the shear strength and shear energy per stalk area were not increased significantly ( $P>0.01$ ). However, with further increasing in the bevel angle from 20 to 24° the shear strength and energy per unit area of the stalk increased significantly ( $p<0.01$ ) in the ranges of 0.156 to 0.190 MPa and 0.388 to 0.443 mJ/mm<sup>2</sup>, respectively. With increasing cutting rate from 20 to 200 mm/min the average values of shear strength and shear energy per stalk area decreased significantly ( $P<0.01$ ) in the ranges of 0.179 to 0.158 MPa and 0.467 to 0.340 mJ/mm<sup>2</sup>, respectively. Further increase in cutting velocity in the range of 200 to 500 mm/min was not decreased shear strength and shear energy significantly. The obtained data was useful in designing and development of saffron harvesting mechanisms.

**Key words:** Saffron, harvesting, tensile strength, shear strength

### Introduction

Saffron (*Crocus sativus* L.) is a perennial spice species of Iridaceae family. This plant is the most precious spice in the world. At present, saffron plant cultivates in Greece, Central Asia, India, Iran, Italy, Morocco, Spain, Switzerland and Turkey. However, Iran and Spain are known as the main saffron producers in the world (9). The saffron flower has three stigmas, which are the most important economic part of the plant and known as saffron. Saffron has general ingredients such as carbohydrates, proteins, minerals and vitamins. The world's total production of dried saffron is estimated around 300 tons per year (7). Iran produces more than 90 percent world's total production of saffron. More than 92 percent of Iranian saffron cultivates in Khorasan province with about 210 tons annual production. Unique agrological and eco-physiological characteristics of saffron along with aroma, flavor and yellow dye attributes were reserved a special place for this

plant in pharmaceutical, food and textile industries (3, 9). The novel use of saffron in recent years has been associated with cancer cure (2). Saffron's processing is included harvesting of flower from field, separating stigma from flower, drying of stigma, packaging and exposition. The flower harvesting is one of the main stages of saffron's processing, which is performed by hand at present. Harvesting of flower by hand cause lack of local labors in saffron cultivation areas at harvesting time. Furthermore, increases production costs as well as infection of stigma.

Shear strength and shear energy per unit stalk area of plants are important in designing and developing cutting mechanisms. Many studies have been conducted to determine the shear properties of plants. Prasad and Gupta studies showed that with increasing cutting rate from 200 to 1000 mm/min the shear strength of maize stalk decreased from 3.63 to 2.10 MPa (14). The average values of shear strength and shear energy

of grasses were reported 16 MPa and 12 mJ/mm<sup>2</sup>, respectively by McRandal and McNulty (12). Kushwaha *et al.* investigations revealed that the average value of shear strength of wheat straw was in the range of 8.6 to 13.0 MPa (11). Persson believes that the bevel angle of blade to be effective on force and energy of cutting process of agricultural materials. When there was not problem of stalk holding versus cutting blade, Persson recommends using smooth blade for cutting of grasses due to the lower force and energy requirement (15). Khazaei *et al.* reported that with increasing cutting rate from 20 to 200 mm/min the shear strength of pyrethrum stalk decreased (10). The maximum values of shear force and energy for cutting of hemp were 243 N and 2.1 J, respectively (6). Ince *et al.* reported that the maximum shear stress and specific shear energy of sunflower stalk were 1.07 MPa and 10.08 mJ/mm<sup>2</sup>, respectively (8). Chattopadhyay and pandy reported that the shear strength of sorghum stalk decreased from 3.74 to 1.94 MPa at the forage stage and decreased from 4.68 to 2.20 MPa at the seed stage when the cutting rate was increased from 10 to 100 mm/min at knife bevel angle of 30° (4).

Literature survey showed that there was no detailed study concerning the shear strength and shear energy of saffron stalk. So in this study the shear strength and shear energy per unit stalk area of saffron were determined as function of cutting rate and bevel angles of blade. The obtained data would be useful in designing and developing harvesting equipments of saffron.

### Materials and Methods

The samples were considered for this study selected from different fields of Kashmar city in Khorasan province, east of Iran, on Nov., 2008. The initial moisture content of the sample was determined by using air oven method. The oven temperature was set at 105±3 °C for 24 hours (1). The shear force of stalk was measured by using a texture analyzer machine (Farnel QTS25 model), which equipped with 250 N load cell with an accuracy of ±0.001 N.

To measure shear force of the stalk a special device (Fig. 1) was made. The device was fixed at

stationary jaw of the texture analyzer. Steel cutting blade of reciprocating mower was used as cutting blade in this device. The cutting blade was connected to moving jaw of the texture analyzer. A distance between the cutting blade and ledger plate was fixed at 1 mm. The saffron stem was laid on the device so that the cutting of stalk was performed 15 mm lower than receptacle of flower. The stalk was cut due to downward motion of the moving jaw of the test machine. The shear force-displacement curve was recorded in a computer during the cutting process. The maximum value of force in the force-displacement curve was considered as shear force of the saffron stalk. The shear energy of the stalk was calculated from area under force-displacement curve. Diameter of the stalk at cutting point was measured by a caliper with accuracy of ±0.01 mm to calculate cutting cross section area. The shear stress (MPa) and specific shear energy (mJ/mm<sup>2</sup>) of stalk were calculated, respectively based on the shear force and energy divided by the cutting cross section area (13, 4, 6). The effect of cutting rate at three levels of 20, 200 and 500 mm/min and bevel angle of cutting blade at three levels of 17, 20 and 24° were investigated on the shear force and energy by using two factors completely randomized design. Each experiment was replicated 5 times.

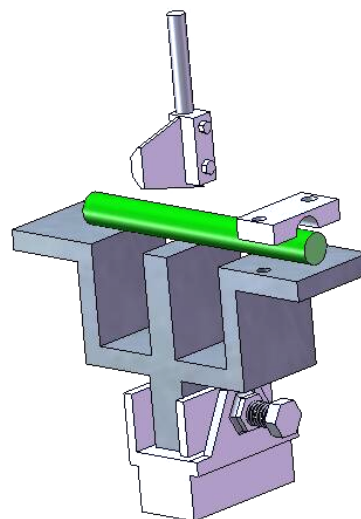


Fig. 1. The developed special device used in cutting test of saffron stalk.

## Results and Discussion

The initial moisture content of the samples was 89.8% (w.b.). The effects of cutting rate on the shear strength and shear energy per unit area of saffron stalk for 17, 20 and 24° bevel angle of cutting blade are shown in Figs. 2 and 3, respectively. As depicted from these figures, with increasing cutting rate the shear strength and specific shear energy were decreased for all of the bevel angle levels. The results of analysis of variance (ANOVA) also showed that the effect of the cutting rate on both the shear strength and energy were significant. The results of Duncan's multiple range tests to compare mean values of cutting rate effect on the shear strength and specific shear energy are given in Table 1. As shown in this table, with increasing cutting velocity from 20 to 200 mm/min the shear strength and the specific shear energy decreased significantly ( $P < 0.01$ ) in the ranges of 0.179 to 0.158 MPa and 0.467 to 0.340 mJ/mm<sup>2</sup>, respectively. Further increase in cutting velocity in the range of 200 to 500 mm/min was not increased significantly the shear strength and energy. The reason for decreasing shear strength and shear energy with an increase in cutting rate could be contributed to this phenomenon that at low cutting rate the stalk was compressed against the blade. However, at higher cutting rate elastic wall of cells was not enough time to transmit the shear force to viscous fluid within the cells so the stalk cut with lower force. Similar results were reported by previous researchers for example Prasad and Gupta reported that the shear strength of maize stalk was decreased with increasing rate of loading from 200 to 1000 mm/min (14). The investigations of Chattopadhyay and Pandey showed that with increasing cutting rate from 10 to 100 mm/min the shear strength of sorghum stalk decreased from 3.74 to 1.94 MPa (4). Khazaei *et al.* research work showed that with increasing cutting velocity from 20 to 200 mm/min the shear strength of pyrethrum stalk decreased from 2.4 to 2.1 MPa. They also

reported that the shear energy of the pyrethrum stalk decreased from 3.23 to 2.76 mJ/mm<sup>2</sup> with increasing cutting velocity from 200 to 500 mm/min (10). Chegini *et al.* reported that the shear energy of chrysanthemum flower decreased from 1.977 to 1.433 MPa when cutting velocity increased in the range of 10 to 500 mm/min (5).

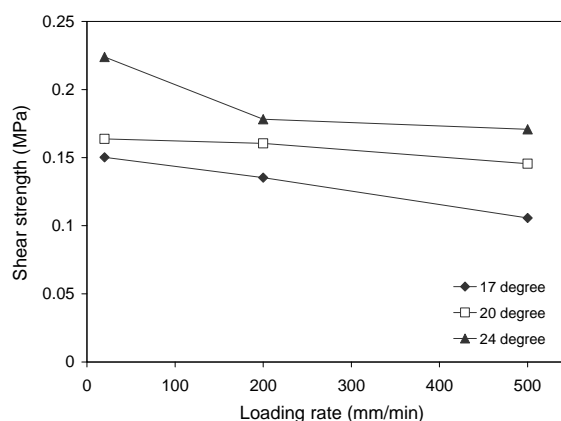


Fig. 2. Effect of cutting rate on saffron stalk shear strength for different bevel angles of blade

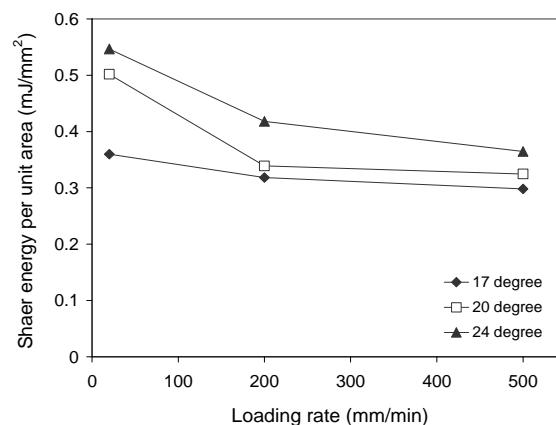


Fig. 3. Effect of cutting rate on saffron stalk specific shear energy for different bevel angles of blade

Table 1. Effect of cutting rate on the shear strength and energy of saffron stalk

Cutting rate (mm/min)	Shear strength (MPa)	Shear energy per unit area (mJ/mm <sup>2</sup> )
20	0.179 <sup>a</sup>	0.467 <sup>a</sup>
200	0.158 <sup>b</sup>	0.340 <sup>b</sup>
500	0.140 <sup>b</sup>	0.329 <sup>b</sup>

Common letter means that there was non- significant at 1% probability level by Duncan's test.

The effects of bevel angle of blade on the shear strength and shear energy per unit area of saffron stalk at different cutting rate are shown in Figs. 4 and 5, respectively. As depicted from these figures, with increasing bevel angle of blade the shear strength and specific shear energy were increased for all of the loading rates. The results of analysis of variance (ANOVA) also showed that the bevel angle of cutting blade were significant on the shear strength and specific shear energy. The results of Duncan's multiple range tests to compare mean values of bevel angle effect on the shear strength and specific energy are given in Table 2. As shown in this table, with increasing the bevel angle of blade from 17 to 20° the shear strength and the specific shear energy were not increased significantly ( $P>0.01$ ). However, with further increasing of the bevel angle from 20 to 24° the shear strength and energy per unit area of the stalk increased in the ranges of 0.156 to 0.190 Mpa and 0.388 to 0.443 mJ/mm<sup>2</sup>, respectively. The reason for increasing the shear strength and energy with an increase in bevel angle could be contributed to this phenomenon that with increasing the bevel angle, the blade more willing to compress and squash the stalk instead of cutting it, so the shear resistance and energy will be increased. In this connection Persson believes that the required energy to compress and squash the stalk may be in amount of 40 to 60 percent of total energy (15). Similar results were found by other researchers for example Chattopadhyay and Pandey studies revealed that with increasing bevel angle of blade from 30 to 70° the shear strength of sorghum stalk in the stages of grass and seed increased in the ranges of 3.74 to 8.18 Mpa and 4.68 to 9.02 Mpa, respectively (4). Khazaei *et al.* investigations also showed that with increasing bevel angle in the

range of 15 to 19° the shear strength and energy of pyrethrum flower stalk were not increased significantly, while further rising of bevel angle in the range of 19 to 27° the shear strength and energy per unit area increased in the ranges of 1.86 to 3.14 Mpa and 2.30 to 4.21 mJ/mm<sup>2</sup>, respectively (10).

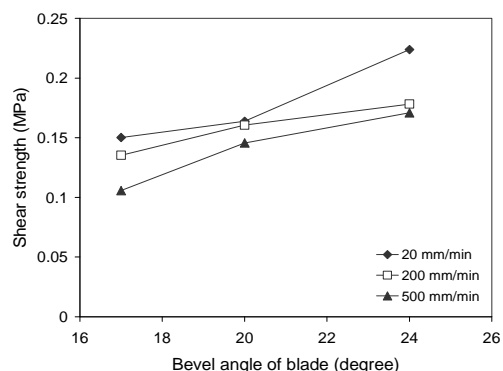


Fig. 4. Effect of bevel angle of cutting blade on saffron stalk shear energy for different loading rate

## Conclusions

1. Increasing the cutting velocity in the range of 20 to 200 mm/min reduce the shear energy consumption and shear strength of the stalk while further rising rate of cutting were not decreased the shear strength and energy.
2. Increasing the bevel angle of cutting blade increased the shear strength and energy per unit area so the bevel angle of 17° was recommended. The average values of the shear strength and required energy were 0.159 Mpa and 0.379 mJ/mm<sup>2</sup>, respectively.
3. The obtained data of the shear strength and shear energy per unit area is useful in developing cutting mechanisms of saffron. As well, the force and required energy for picking flower from stem

and tensile strength are necessary to develop picking mechanisms for saffron flower harvesting.

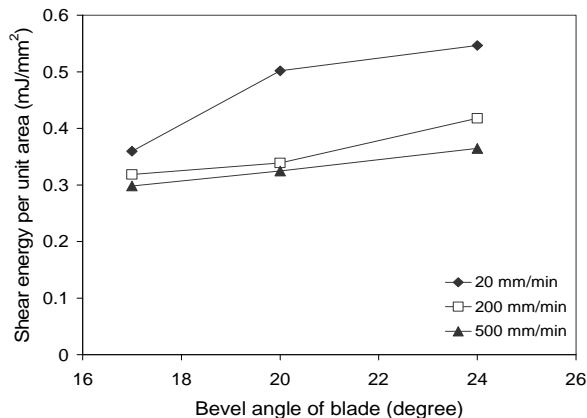


Fig. 5. Effect of bevel angle of cutting blade on saffron stalk specific shear energy for different loading rate.

Table 2. Effect of bevel angle on the shear strength and energy of saffron stem

Bevel angle (degree)	Shear strength (Mpa)	Shear energy per unit area (mJ/mm <sup>2</sup> )
17	0.130 <sup>b</sup>	0.305 <sup>b</sup>
20	0.156 <sup>b</sup>	0.388 <sup>b</sup>
24	0.190 <sup>a</sup>	0.443 <sup>a</sup>

Common letter means that there was non-significant at 1% probability level by Duncan's test.

### Acknowledgements

The authors would like to express their appreciation to University of Tehran for full support of the project. As well, the authors express special thanks to Dr. Saeedirad for cooperation in this study.

### References

- [1] Abbasi K. 2009. Determination of thermal properties and drying kinetics of saffron. MSc. Thesis, University of Tehran, Tehran, Iran. (in Persian).
- [2] Abdullaev F.I. 2004. Biomedical properties of saffron and its potential use in cancer therapy and chemoprevention trials. *Cancer Det. Preven.* 28 (6):426-432.
- [3] Basker D. and Negbi M. 1983. Uses of saffron. *Econ. Bot.* 37: 228-236.
- [4] Chattopadhyay P.S. and Pandey K.P. 1998. Mechanical properties of sorghum stalk in relation to quasi-static deformation. *Journal of Agricultural Engineering Research*. Vol. 73: 199-206.
- [5] Chegini Gh.R.; Hashemi-Fard S.H.; Kianmehr, M.H. and Khostagaza M.H. 2008. Study of mechanical properties of chrysanthemum flower stem. *Proceedings of 5th National Congress on Agricultural Machinery Engineering and Mechanization*, Mashhad, Iran. (in Persian).
- [6] Chen, Y., Gratton, J.L. and Liu, J. 2004. Power requirements of hemp cutting and conditioning. *Biosystems Eng.* 87(4): 417-424.
- [7] FAO. 2008. [www.faostat.org](http://www.faostat.org)

- [8] Ince A., Ugurluay S., Guzel E. and Ozcan M.T. 2005. Bending and shearing characteristics of sunflower stalk residue. *Biosystems Engineering*. 92 (2): 175–181.
- [9] Kafi M., Rashed M.H., Koocheki A. and Mollafilabi A. 2002. Saffron: Production Technology and Processing. Center of Excellence for Agronomy (Special Crops). Faculty of Agriculture, Ferdowsi University of Mashhad, Iran.
- [10] Khazaei J., Rabani H. and Golbabaie F. 2002. Determining the shear strength and picking force of pyrethrum flower (in Persian). *Iranian Journal of Agricultural Sciences*, Vol. 33 (3): 433-444.
- [11] Kushwaha R.L., Vashnav A.S. and Zoerb G.C. 1983. Shear strength of wheat straw. *Canadian Agricultural Engineering*. 25(2): 133-142.
- [12] McRandal D.M. and McNulty P.B. 1980. Mechanical and physical properties of grasses. *Transactions of the ASAE*. 23(4): 816-821.
- [13] Mohsenin N.N. 1986. *Physical Properties of Plant and Animal Material*. Gordon and Breach. New York, USA.
- [14] Prasad J. and Gupta C.B. 1975. Mechanical properties of maize stalks as related to harvesting. *Journal of Agricultural Engineering Research*. 20(1): 79-87.
- [15] Persson S., 1987. *Mechanics of Cutting Plant Material*. Published by ASAE. 287. PP. USA.



## MOISTURE DEPENDENT COEFFICIENT OF FRICTION OF SAFFRON FLOWER AND ITS COMPONENTS

S.R. HASSAN-BEYGI\*, M.H. KIANMEHR AND H. VALE GHOZHDI

Department of Agro-technology, College of Abouraihan, University of Tehran, Pakdasht, Iran

\*Corresponding author Phone and Fax: +98-292-3040614 and e-mail address: [rhbeigi@ut.ac.ir](mailto:rhbeigi@ut.ac.ir)

### Abstract

The coefficient of friction of saffron (*Crocus sativus* L.) flower and its components (stigma, stamina, petal and stem) are prerequisite to design and development of handling and separating equipments. Therefore, the coefficient of static friction of saffron flower, stigma, stamina, petal and stem were determined by using inclined plane method on steel, galvanized steel and polyethylene sheet surfaces at three levels of moisture content in the range of initial moisture content at harvesting to 3 days after picking from field (91% to 40% w.b.). The experiments were conducted on samples selected from fields of Kashmar, east of Iran. The data was statistically analyzed using the three factors completely randomized design to study the effects of moisture content, type of the saffron components and frictional surface types on coefficient of friction. The results showed that the simple effect of friction surface types, moisture content and saffron components parameters were significant ( $P < 0.01$ ) on coefficient of static friction. As well, the interaction of friction surface types by saffron components and interaction of saffron component types by moisture content were significant ( $P < 0.01$ ) on coefficient of static friction. The average values of friction coefficient of saffron flower and its components on the friction surfaces were in the range of 0.52 to 1.1. The coefficient of friction of the petal, stigma and stamina were the maximum values on polyethylene surface. As well, the coefficient of friction of the stem and flower were the maximum values on steel surface. However, the coefficient of friction for all of the components was the minimum values on galvanized iron surface. With decreasing moisture content from harvesting level to 40% (w.b.) the average values of coefficient of friction increased significantly for all of the components. The coefficient of friction of the stigma and flower were the maximum and minimum values, respectively at different levels of moisture content.

**Key words:** Saffron; Flower, *Crocus sativus*, Coefficient of friction, Moisture content

### Introduction

Saffron (*Crocus sativus* L.) is a perennial spice species of Iridaceae family and has been grown for a long time in Mediterranean, central and west of Asia (7). This plant is the most precious spice in the world. Unique agrological and eco-physiological characteristics of saffron along with aroma, flavor and yellow dye attributes were reserved a special place for this plant in pharmaceutical, food and textile industries (4, 7). The novel use of saffron in recent years has been associated with cancer cure (2). At present, saffron plant cultivates in Central Asia, Greece, India, Iran, Italy, Morocco, Pakistan, Spain, Swiss and Turkey. However, Iran and Spain are known as the main saffron producers in the world (7). The

saffron flower has three stigmas, which are the most important economic part of the plant and known as saffron. The world's total production of dried saffron is estimated around 300 tons per year (5). Iran produces more than 90 percent world's total production of saffron. More than 92 percent of Iranian saffron cultivates in Khorasan province with about 210 tons annual production.

The coefficient of friction data are necessary for designing and development of handling and separating equipments. Tunde-Akintunde *et al.* studied the effect of moisture content on coefficient of friction of two varieties of melon seeds on friction surfaces of glass, galvanized steel and plywood. They reported that the coefficient of friction decreased with increasing in moisture

content (10). Sessiz *et al.* investigated the physical properties of caper fruit as affected by moisture content. They reported that the coefficient of friction of caper fruit decreased with increase in moisture content in the range of 71.85 to 82.93%, w.b. (9). Razavi *et al.* reported that the coefficient of friction of both nuts and kernels of pistachio on surfaces of rubber, fiberglass, glass, galvanized iron and plywood decreased linearly with decreasing moisture content in the range of 45 to 5%, w.b. (8). Yalcin *et al.* reported that the coefficient of friction of pea seed on surfaces of rubber, aluminum, stainless steel and galvanized steel increased linearly with increasing moisture content from 10.06 to 35.08%, d.b. (11).

Literature survey showed that there was limited data concerning the coefficient of friction of saffron flower and its components including stigma, petal, stamina and stem. So the main objective of present work was to measure the coefficient of friction of saffron flower and its components as a function of moisture content. The obtained data would be useful in designing and development of handling equipment of saffron as well as in separating different components of saffron from each other.

### Materials and Methods

The samples were considered for this study selected from different fields of Kashmar city in Khorasan province, east of Iran, on Nov., 2008. The coefficient of friction of saffron flower, stamina, petal, stigma and stem were measured at three contents levels in the range of initial moisture content at harvesting to 3 days after picking from field (91% to 40%, w.b.). Each experiment was replicated 10 times. The moisture contents of the saffron flower and its components were determined by using air oven method. The oven temperature was set at  $105 \pm 3$  °C for 24 hours (1).

The coefficient of static friction of the samples was determined by using inclined plane method on steel, galvanized steel and polyethylene sheet surfaces. The apparatus used for measuring coefficient of friction is shown in Fig. 1. A box or cylinders were placed on the surfaces. The samples of flower arranged in a box without cap and floor

with dimensions of  $150 \times 100 \times 40$  mm<sup>3</sup> (8), the samples of stigma and stamina arranged in a cylinder without cap and floor with diameter of 50 mm and height of 50 mm (11, 3) and the samples of stem and petal arranged in a cylinder without cap and floor with diameter of 80 mm and height of 50 mm (6). The box or cylinders were slowly lifted up to avoid friction between the box or cylinders and the friction surfaces. The friction surfaces were gradually raised by an electric motor and transmission system when the samples started sliding over the surfaces. The angle of friction surfaces with horizontal was measured by a protractor and the coefficient of static friction was calculated by equation (1). The experiments were replicated 10 times for each treatment.

$$\mu_s = \tan \alpha \quad (1)$$

where:  $\mu_s$  is coefficient of static friction,

$\alpha$  is angle that the incline makes with the horizontal when sliding begins.

The data was statistically analyzed using the three factors completely randomized design to study the effects of the three moisture content levels, type of the saffron components and frictional surface types on the coefficient of friction. Further, Duncan's multiple range tests was used to compare the means.

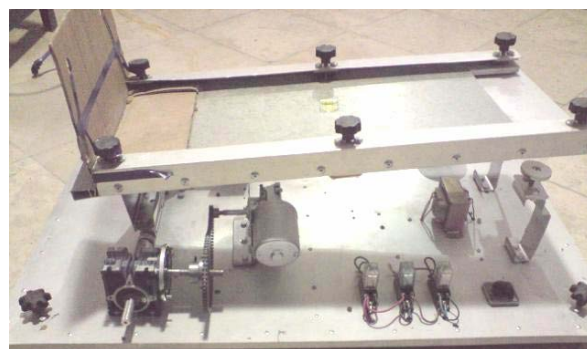


Fig. 1. The coefficient of friction apparatus.

### Results and Discussion

The initial moisture contents at harvesting were 88% (w.b.) for flower, 91% (w.b.) for stem, 75% (w.b.) for stigma, 89% (w.b.) for petal and 86% (w.b.) for stamina. The results of analysis of

variance (ANOVA) of the moisture content, the friction surface types and the type of components parameters on the coefficient of friction were given in Table 1. As depicted from this table, the simple effects of the moisture content, surface types and type of components parameters were significant ( $P < 0.01$ ) on the coefficient of friction. Furthermore, interaction of the surface types by type of components and the moisture content by type of components as well as the triple effect of the surface types  $\times$  type of components  $\times$  moisture content were significant ( $P < 0.01$ ) on the coefficient of friction.

The interaction of the surface types by type of components on the coefficient of friction is given in Table 2. As shown in this table, there was significant difference among the mean values of coefficient of friction of stem and petal on all of the friction surfaces. There was not significant difference ( $P > 0.01$ ) among the mean values of coefficient of friction of stamina and stigma on steel and galvanized steel surfaces. However, the coefficient of friction on these surfaces was significantly lower than that of polyethylene surface. In the case of flower, the coefficient of friction on galvanized steel significantly lower than the other surfaces. The friction coefficient of flower on galvanized steel was lower than that of steel and polyethylene. As the results on steel surface the coefficient of friction of the stem and flower were maximum and minimum, respectively.

Of course on this surface there was not significant among the mean values of the coefficient of friction of petal, stamina and stigma. On galvanized steel surface the coefficient of friction of the stamina and stigma were the greatest and those of flower and stem were the lowest values. On polyethylene surface the differences among the coefficient of friction of the stem, petal, stamina and stigma were significant ( $P < 0.01$ ). However, there were not significant differences between the mean values of the stem and flower. Generally, it could be stated that the coefficient of friction of petal, stamina, flower and stigma were the maximum on polyethylene surface. The friction coefficient for all of the components was the minimum on galvanized steel. The higher values of coefficient of friction on polyethylene surface could be contributed to more roughness of polyethylene than the other surfaces.

There is separation possibility for the components from each other due to existence of significant difference among the friction coefficient of components on the different surfaces. For example, if the inclination of a polyethylene sheet increased gradually at first the flower and stem separate from the other components due to less coefficient of friction. With further increase in the inclination of sheet the petal, stamina and stigma would be separate, respectively.

Table 1. Analysis of variance of effective parameters on the coefficient of friction

Source of variations	Degree of freedom	Mean square
Surface types	2	0.439 <sup>**</sup>
Moisture content	2	0.322 <sup>**</sup>
Type of components	4	0.297 <sup>**</sup>
Surface types $\times$ Moisture content	4	0.0016 <sup>ns</sup>
Surface types $\times$ Type of components	8	0.1022 <sup>**</sup>
Moisture content $\times$ Type of components	8	0.0061 <sup>**</sup>
Surface types $\times$ Type of components $\times$ Moisture content	16	0.005 <sup>**</sup>
Error	88	0.0009
C.V.	-	4.362

<sup>\*\*</sup>stand for significant at 1% probability level and ns means non-significant.

Table 2. Interaction of type of components by surface types parameters on the coefficient of friction

Type of components	Surface types		
	Steel	Galvanized steel	Polyethylene
Stem	$0.81 \pm 0.11^c$	$0.55 \pm 0.06^{gh}$	$0.64 \pm 0.09^f$
Petal	$0.69 \pm 0.06^e$	$0.58 \pm 0.11^g$	$0.77 \pm 0.08^d$
Stamina	$0.72 \pm 0.06^e$	$0.72 \pm 0.04^e$	$0.94 \pm 0.07^b$
Stigma	$0.73 \pm 0.08^e$	$0.73 \pm 0.09^{de}$	$1.10 \pm 0.13^a$
Flower	$0.63 \pm 0.07^f$	$0.52 \pm 0.08^h$	$0.64 \pm 0.02^f$

Common letter means that there was non- significant at 1% probability level by Duncan's test.

Table 3. Interaction of type of components by moisture content parameters on the coefficient of friction

Type of components	Moisture content (% w.b)		
	Harvesting	70	40
Stem	$0.56 \pm 0.07^g$	$0.67 \pm 0.15^d$	$0.76 \pm 0.11^c$
Petal	$0.59 \pm 0.11^{fg}$	$0.67 \pm 0.07^d$	$0.78 \pm 0.08^c$
Stamina	$0.75 \pm 0.09^c$	$0.78 \pm 0.12^c$	$0.86 \pm 0.12^b$
Stigma	$0.75 \pm 0.15^c$	$0.85 \pm 0.19^b$	$0.97 \pm 0.21^a$
Flower	$0.52 \pm 0.08^h$	$0.61 \pm 0.06^{ef}$	$0.65 \pm 0.04^{de}$

Common letter means that there was non- significant at 1% probability level by Duncan's test.

The interaction of the moisture content by type of components on the coefficient of friction is given in Table 3. As shown in this table, with decreasing moisture content from harvesting level to 40% (w.b.) the coefficient of friction for all of the components was increased significantly ( $P < 0.01$ ). This increase was significant for stem, petal and stigma at all of the moisture content levels. In the case of stamina with decreasing moisture from harvesting to 70% (w.b.) the coefficient of friction was not increased significantly; but further decreasing of moisture content increased the coefficient of friction significantly. In the case of saffron flower decreasing of moisture content from harvesting level to 70% was increased the coefficient of friction significantly from 0.52 to 0.61, but further decreasing of moisture content from 70 to 40% (w.b.) was not increased the coefficient of friction. The reason for reducing the coefficient of friction with increasing of moisture content could be contributed to adhesion reducing between the samples and friction surfaces. As the results (Table 3), the maximum values of the coefficient of friction at harvesting moisture content level were related to stamina and stigma and that of flower

was the lowest one. However, there was not significant difference between the mean values of the coefficient of friction of stem and petal at this moisture level. At 70% and 40% (w.b.) moisture content levels there were not significant differences ( $P > 0.01$ ) between mean values of the coefficient of friction of stem and petal, but the other components had significant differences so that the maximum and minimum values of the coefficient of friction were related to stigma and flower, respectively. Generally, it could be stated that at all of the moisture content levels there was not separation possibility for the stem and petal from each other by using coefficient of friction. As well, at all of the moisture content levels the flower could be separated from the other components due to the lowest coefficient of friction of this component.

The greatest mean value of the coefficient of friction (1.10) was related to stigma on polyethylene surface at 40% (w.b.) moisture content, which might be contributed to the adhesion between stigma and polyethylene surface. The lowest mean value of the coefficient of friction (0.52) was related to flower on galvanized steel surface at harvesting (88% w.b.) moisture

level, which might be contributed to the smoothness of galvanized steel and less content area of flower with the friction surface. The maximum values of the friction coefficient for all of the components were on polyethylene surface at 40% (w.b.) moisture content with the exception of stem.

Similar results was observed by previous researchers for example Sessiz *et al.* were reported that with increasing moisture content from 71.85% to 82.93% (w.b.) the coefficient of friction of the caper fruit decreased in all of the frictional surfaces. As well, they reported that the maximum and minimum coefficient of friction were on wood and rubber, respectively (9). Tunde-Akintunde *et al.* also reported that with increasing moisture content from 4.06% to 16.81% (d.b.) the coefficient of friction of the two varieties of melon seeds decreased significantly from 0.271 to 0.212. They obtained the maximum coefficient of friction (0.361) on plywood surface at 4.06% moisture content and the minimum coefficient of friction (0.191) on glass surface at 16.81% moisture content (10).

### Conclusions

1. The coefficient of friction of stigma and flower were the maximum and minimum at all of the moisture content, respectively.
2. The average values of friction coefficient of the saffron flower and its components were significantly different ( $P < 0.01$ ) on different frictional surfaces. The greatest and lowest values of the friction coefficient were on polyethylene and galvanized steel, respectively.
3. With decreasing moisture content from harvesting level to 40% (two days after harvesting) the average values of friction coefficient of saffron flower and its components were significantly ( $P < 0.01$ ) decreased.
4. The greatest coefficient of friction (1.10) was related to stigma on polyethylene surface at 40% (w.b.) moisture content as well as the lowest coefficient of friction (0.52) was related to flower on galvanized steel surface at harvesting (88% w.b.) moisture level.

5. The obtained data are useful for designing and development of saffron flower and its components handling equipments. As well, it may be developed a mechanism for separating the saffron flower and its components from each other by using significant difference among the coefficient of friction of them.

### Acknowledgements

The authors would like to express their appreciation to University of Tehran for full support of the project. As well, the authors express special thanks to Dr. Khazaei for cooperation in this study.

### References

- [1] Abbasi, K. 2009. Determination of thermal properties and drying kinetics of saffron. MSc. Thesis, University of Tehran, Tehran, Iran.
- [2] Abdullaev, F.I. 2004. Biomedical properties of saffron and its potential use in cancer therapy and chemoprevention trials. *Cancer Det. Preven*, 28 (6):426-432.
- [3] Al-Mahasneh, M. A., and T. M. Rababah. 2007. Effective moisture content on some physical properties of green wheat. *Journal of Food Engineering*. Vol 79, 1467-1473.
- [4] Basker, D., Negbi, M., 1983. Uses of saffron. *Econ. Bot*, 37: 228-236.
- [5] FAO. 2008. [www.faostat.org](http://www.faostat.org)
- [6] Haciseferogulları, H., Gezer, I., Ozcan, M, M., and B. M. Asma. 2007. Post harvest chemical and physical-mechanical properties of some apricot varieties cultivated in Turkey. *Journal of Food Engineering*. Vol. 79: 364-373.
- [7] Kafi, M., Rashed, M.H., Koocheki, A. and Mollafilabi, A. 2002. Saffron: Production Technology and Processing. Center of Excellence for Agronomy (Special Crops). Faculty of Agriculture, Ferdowsi University of Mashhad, Iran.
- [8] Razavi, S. M. A., Mohammad Amini, A., Rafe, A. and B. Emadzadeh. 2007. The physical properties of pistachio nut and its kernel as a function of moisture content and variety. Part III: Frictional properties. *Journal of Food Engineering*. Vol. 81: 226-235.

- [9] Sessiz, A., Esgici, R., and S. Kizil. 2007. Moisture- dependent physical properties of caper (*Capparis ssp.*) fruit. *Journal of Food Engineering*. Vol. 79: 1426-1431.
- [10] Tunde-Akintunde, T. Y., Akintunde, B. O., and O. J. Oyelade. 2007. Effect of moisture content on terminal velocity, compressive force and frictional properties of melon seeds. *Agricultural Engineering International: the CIGR Ejournal*. Vol. IX.
- [11] Yalcin, I., ozarslan, C., and T. Akbas. 2007. physical properties of pea (*Pisum sativum*) seed. *Journal of Food Engineering*. Vol. 79: 731- 735.



## MOISTURE DEPENDENT TERMINAL VELOCITY OF SAFFRON FLOWER AND ITS COMPONENTS

S.R. HASSAN-BEYGI<sup>1\*</sup>, H. VALE GHOZHDI<sup>1</sup> AND A. SEIFPOUR ABOLHASSANI<sup>2</sup>

<sup>1</sup>Department of Agro-technology, College of Abouraihan, University of Tehran, Pakdasht, Iran  
GeoParsian Company, Tehran, Iran

\*Corresponding author: Phone and Fax: +98-292-3040614 and e-mail address: [rhbeigi@ut.ac.ir](mailto:rhbeigi@ut.ac.ir)

### Abstract

The terminal velocity data are necessary for designing and development of pneumatic conveying, fluidized bed dryer, separating and cleaning equipments. In this paper, the terminal velocity of flower, stigma, stamina, petal and stem of saffron (*Crocus sativus* L.) were determined as a function of moisture content at three moisture content levels in the range of initial moisture content at harvesting to 3 days after picking from field (91% to 40% w.b.) by using a vertical wind column device. The experiments were conducted on samples selected from fields of Kashmar, east of Iran. The data was statistically analyzed using the two factors completely randomized design to study the effects of the three moisture content levels and type of the saffron components on the terminal velocity. The results showed that the simple effect of component types and moisture content parameters as well as interaction of component types by moisture content were significant ( $P < 0.01$ ) on terminal velocity. The terminal velocity of the saffron flower, stigma, stamina, petal and stem at different levels of moisture content were in the range of 1.03 to 5.3 m/s. With decreasing moisture content from harvesting level to 40% (w.b.) the terminal velocity of the flower and stem decreased significantly but the differences between average values of terminal velocity were not significant for the stigma, petal and stamina. At moisture content of harvesting the terminal velocity of the stem and petal were the maximum and minimum values, respectively. The terminal velocity of the petal was also the minimum value at moisture contents of 70% and 40% (w.b.). Generally, at moisture content of harvesting it is possible to separate the flower, petal, stamina, stigma and stem from each other with changing air stream velocity. As well, it is possible to separate the petal from the other components at moisture levels of 70% and 40% (w.b.) using wind column device.

**Keywords:** Saffron, Terminal Velocity, Moisture Content

### Introduction

Saffron crocus (*Crocus sativus* L.) is a perennial spice species of Iridaceae family and the most valuable crop species in the world, which has been cultivated for more than 3000 years. This plant has been grown for a long time in many parts of the world including Spain, Italy, Greece, Austria, Morocco, France, Turkey, India and Iran. However, Iran and Spain are known as the main saffron producers in the world (10). The saffron flower has three stigmas, which are the most important economic part of the plant and known as saffron. Saffron is often dried and the world's total production is estimated around 300 tons per year (8). The dried saffron has been used as food additive, culinary purpose, medicinal, colouring

agents, odour, taste and pigment (5, 10). The novel use of saffron in recent years has been associated with cancer cure (2). Separation of stigma from the other parts of saffron flower is one of the most important stages in saffron processing, which is performing by hand at present. Limited time for separating of stigma caused for lack of local labors in saffron cultivation areas at harvesting time of flower. Furthermore, separation of stigma by hand increases production costs as well as infection of stigma.

The terminal velocity data are necessary for designing and development of pneumatic conveying, fluidized bed dryer, separating and cleaning equipments. Bilanski and Ial studied aerodynamics characteristics of seed and straw of

wheat. They reported that the terminal velocity of straws with lengths of 10 to 100 mm were in the range of 2.50 to 4.75 m/s (6). Rabbani and Khazaei research work revealed that the average values of the terminal velocity of pyrethrum flower at small, medium and large diameters were in the range of 8.5 to 11.5 m/s (13). Aydin and Akar reported that with increasing moisture content from 11.3 to 50.0 percent (d.b.) the terminal velocity for Soltani and Amasya varieties of gumbo fruit increased in the range of 7.30 to 9.29 m/s and 5.76 to 5.83 m/s, respectively (3). Aydin also reported that the terminal velocity of kernel of peanut increased from 7.25 to 7.93 m/s with increasing in moisture content from 4.8 to 32.0 percent (d.b) (4). Hemmat *et al.* were determined the terminal velocity of chopped corn silage and their parts including leaf, stalk and corncob. They reported that at moisture content levels of 40-50, 50-60 and 60-70% (w.b.) the average of terminal velocity of chopped corn were 7.1, 7.3 and 7.8 m/s, respectively. As well the average values of terminal velocity of leaf, stalk and corncob were 3.8, 6.8 and 8.8 m/s, respectively (9).

Literature survey showed that there was limited data concerning the terminal velocity of saffron flower and its components including stigma, petal, stamina and stem. So the main objective of present work was to measure the terminal velocity of saffron flower and its components as a function of moisture content. The obtained data would be useful in designing and development of pneumatic conveyer and fluidized bed dryer of saffron as well as in separating stigma from the other components of saffron flower.

### Materials and Methods

The samples were considered for this study selected from different fields of Kashmar city in Khorasan province, east of Iran, on Nov., 2008. The terminal velocity of saffron flower and its parts i.e. stamina, petal, stigma and stem were measured at three moisture contents levels in the range of initial moisture content at harvesting to 3 days after picking from field (91% to 40% w.b.). Each experiment was replicated 10 times. The moisture contents of the saffron flower and its

components were determined by using air oven method. The oven temperature was set at  $105 \pm 3$  °C for 24 hours (1).

In this study, the terminal velocity of the samples was measured by using a vertical wind tunnel device shown in Fig. 1. The device had an electrical motor for driving a centrifugal fan (backward flow), an inverter for electrical motor speed control, a diffuser with high angle, a honey comb test area and a test channel. Outlet cross sectional area of test channel was  $20 \times 20$  cm<sup>2</sup>. A sample of about 20 g of saffron flower or the each other components (petal, stamina, stigma and stem) was placed on the screen and the fan speed was gradually increased by inverter until the particle was floated in a level. The air velocity at the moment of the samples floating was measured by a hot wire anemometer (Q116497 Taiwan) at center of outlet cross section about 50 cm above the screen. (14, 12, 11).

The data was statistically analyzed using the two factors completely randomized design to study the effects of the three moisture content levels and type of the saffron components on the terminal velocity. Further, Duncan's multiple range tests was used to compare the means.



Fig. 1. Vertical wind column device.

## Results and Discussion

The initial moisture contents at harvesting were 88% (w.b.) for flower, 91% (w.b.) for stem, 75% (w.b.) for stigma, 89% (w.b.) for petal and 86% (w.b.) for stamina. The effect of moisture content on the terminal velocity of saffron flower and its components is shown in Fig. 2. As depicted from this figure, with decreasing moisture content from harvesting time to two days after harvesting the terminal velocity of petal, stamina and stigma were not considerably changed. However, the terminal velocity of flower and stem were decreased with decreasing moisture content from harvesting time to two days after harvesting. It is clear from this figure that the differences of terminal velocity at harvesting moisture content were considerably more than those of the other moisture contents. The results of analysis of variance (ANOVA) also showed that the effect of the moisture content and the type of component parameters as well as interaction of the moisture content by the type of components were significant ( $P < 0.01$ ) on the terminal velocity (Table 1).

Table 1. Analysis of variance of effective parameters on the terminal velocity

Source of variations	Degree of freedom	Mean square
Type of components	4	7.611**
Moisture content	2	4.273**
Type of components × Moisture content	8	1.075**
Error	28	0.0005
C.V.	-	0.814

\*\*stand for significant at 1% probability level and ns means non-significant.

The interaction of moisture content by type of components on the terminal velocity is given in Table 2. As shown in this table, there was not significant difference among the mean values of terminal velocity of stigma, petal and stamina with decrease in moisture content from harvesting level to 40% (w.b.). With decrease in moisture content from harvesting level to 40% (w.b.) only terminal velocity of stem decreased significantly ( $P < 0.01$ ). The terminal velocity of complete flower was not

decreased significantly with decreasing moisture content from harvesting level (88%) to 70% (w.b.). However, the terminal velocity of flower decreased significantly with further moisture decreasing (from 70% to 40%). As shown in Table 2, the maximum and minimum values of the terminal velocity were related to stem and petal, respectively at harvesting moisture content. There was not significant difference between the terminal velocity of flower and stigma at harvesting moisture content. Of course, the terminal velocity of flower and stigma was higher than that of petal and stamina. At moisture content level of 70% (w.b.), there was not significant difference ( $P > 0.01$ ) among the terminal velocity of flower, stem and stigma. However, the terminal velocity of the mentioned components was higher than those of petal and stamina. The terminal velocity of petal was the minimum value at this moisture content. At moisture content level of 40% (w.b.), the terminal velocities of stigma and complete flower were the greatest and the terminal velocity of petal was at least. The maximum terminal velocity (5.30 m/s) was related to stem at harvesting moisture content level (91% w.b.) which could be contributed to the high moisture content and low surface area of this component. The minimum value of the terminal velocity (1.03 m/s) was related to petal at all of the moisture content levels, which could be contributed to the low weight and high surface area of this component.

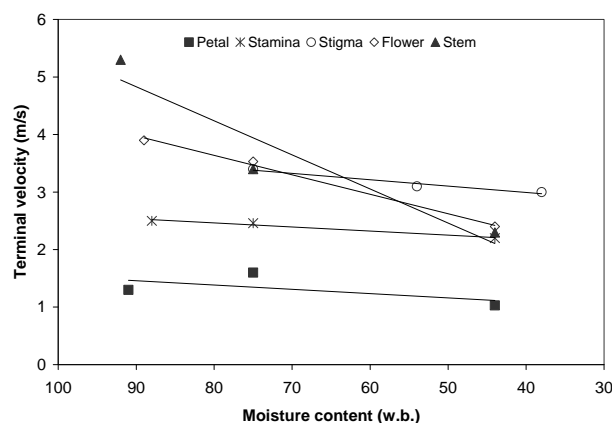


Fig. 2. Effect of moisture content on terminal velocity of saffron and its components

Generally, it could be inferred that at harvesting moisture content level there is a possibility to separate the entire components from each other by changing in air stream velocity except the flower and stigma. With decreasing moisture content to one day after harvesting level (70% w.b.) the flower, stem and stigma could not be separated from each other using air stream. However, there is a possibility to separate the petal and stamina from the other components by changing in air stream velocity. With further decrease in moisture content to 40% (w.b.) there was not possibility to separate the flower, stem and stamina from each other, of course in this case petal could be separated from the other components. The reason for separating the most of components from each other at harvesting moisture content by changing in air stream could be contributed to different levels of

moisture exist in saffron flower and its components. Furthermore, the reason for separating of petal in all of the moisture content levels could be contributed to low weight and large surface area of this component.

Figure 2 shows that with decreasing in moisture content, the mean values of terminal velocity of flower and its component decreased significantly ( $P < 0.01$ ) from 3.3 to 2.4 m/s, which could be contributed to become lighter flower and its component due to lost some of moisture. Yalcin *et al.* reported that with decreasing moisture content of pea seed from 38.9% to 12.01% (d.b.) the mean values of terminal velocity decreased from 9.61 to 9.31 m/s (15). Dursun *et al.* also reported that with decreasing moisture content of sugar beet seed from 14.0% to 8.4% (d.b.) the mean values of terminal velocity decreased linearly from 6.6 to 5.6 m/s (7).

Table 2. Interaction of type of components by moisture content parameters on the terminal velocity

Type of component	Moisture content (% w.b.)		
	Harvesting	70	40
Flower	$3.90 \pm 0.40^b$	$3.53 \pm 0.35^{bc}$	$2.40 \pm 0.50^{ef}$
Petal	$1.30 \pm 0.20^h$	$1.60 \pm 0.20^{gh}$	$1.03 \pm 0.25^h$
Stem	$5.30 \pm 0.30^a$	$3.40 \pm 0.30^{bc}$	$2.30 \pm 0.10^f$
Stigma	$3.40 \pm 0.20^{bc}$	$3.10 \pm 0.20^{cd}$	$3.00 \pm 0.30^{cde}$
Stamina	$2.50 \pm 0.10^{def}$	$2.46 \pm 0.15^{def}$	$2.20 \pm 0.30^{fg}$

Common letter means that there was non- significant at 1% probability level by Duncan's test.

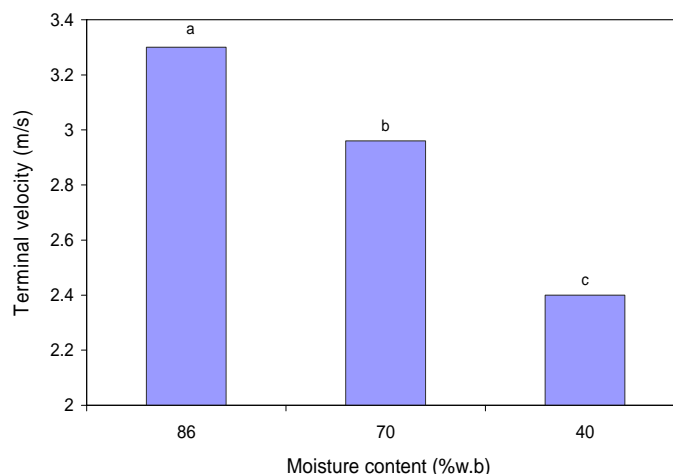


Figure 2. Mean values of the terminal velocity of saffron flower and its components

## Conclusions

1. The terminal velocity of saffron flower, stamina, stem, stigma and petal were all moisture dependent.
2. With decreasing moisture content from harvesting level to 40% (two days after harvesting) the average values of terminal velocity of saffron flower and its components were significantly ( $P < 0.01$ ) decreased.
3. The greatest terminal velocity (5.30 m/s) was related to stem at harvesting moisture content level (91% w.b.) as well as the lowest terminal velocity (1.03) was related to petal at 40% (w.b.) moisture level.
4. The obtained data are useful for designing and development of saffron flower and its components pneumatic conveying, fluidized bed drying and separating equipments.
5. It is possible to separate petal at all of the moisture content levels by changing in air velocity stream.
6. At harvesting moisture content level, it is possible to separate all of the components from each other by changing in air velocity stream.

## Acknowledgements

The authors would like to express their appreciation to University of Tehran for full support of the project. As well, the authors express special thanks to Dr. Saeedirad for cooperation in this study.

## References

- [1] Abbasi, K. 2009. Determination of thermal properties and drying kinetics of saffron. MSc. Thesis, University of Tehran, Tehran, Iran.
- [2] Abdullaev, F.I. 2004. Biomedical properties of saffron and its potential use in cancer therapy and chemoprevention trials. *Cancer Det. Preven.* 28 (6):426-432.
- [3] Aydin, C. and Akar, R. 2005. Some physical properties of gumbo fruit varieties. *Journal of Food Engineering*. Vol. 66: 387-393.
- [4] Aydin, C. 2007. Some engineering properties of peanut and kernel. *Journal of Food Engineering*. Vol. 79:810-816.
- [5] Basker, D. Negbi, M. 1983. Uses of saffron. *Econ. Bot.* 37: 228-236.
- [6] Bilanski, W.K., and Lal, R. 1965. The behavior of threshed materials in a vertical wind tunnel. *Trans. ASAE*, 8(3): 411-413.
- [7] Dursun, I., Tugrrul, K. M., and E. Dursun. 2007. Some physical properties of sugar beet seed. *Journal of Stored Products research*. Vol. 149-155.
- [8] FAO. 2008. [www.faostat.org](http://www.faostat.org)
- [9] Hemmat, A., Emamy, M., Razavi, S.J. and Masoumi, A.A. 2007. Terminal Velocity of Chopped Corn Silage and Its Separate Fractions as Affected by Moisture Content. *Journal of Agricultural Science and Technology*. Vol. 9: 15-23
- [10] Kafi, M., Rashed, M.H., Koochehi, A. and Mollafilabi, A. 2002. Saffron: Production Technology and Processing. Center of Excellence for Agronomy (Special Crops). Faculty of Agriculture, Ferdowsi University of Mashhad, Iran.
- [11] Khoshtaghaza, M.H. and Mehdizadeh, R. 2006. Aerodynamic Properties of Wheat Kernel and Straw Materials. *Agricultural Engineering International: the CIGR Ejournal Manuscript* FP 05 007. Vol. VIII.
- [12] Masoumi, A.A., Rajabipour, A., Tabil, L. and Akram, A.A. 2003. Terminal velocity and frictional properties of garlic (*Allium sativum* L.). Paper No. 03-330. CSAE/SCGR 2003 Meeting Montréal, Québec July 6 - 9, 2003
- [13] Rabbani, H. and Khazaei, J. 2005. Aerodynamic characteristics determination of pyrethrum flower. *International Congress on Information Technology in Agriculture, Food and Environment (ITAFE' 05)*. 12-14 Oct., Cukurvrova University, Adana, Turkey.
- [14] Singh, K.K. and Goswami, T.K. 1996. Physical properties of cumin seed. *Journal of Agricultural Engineering Research*. Vol. 64: 93-98.
- [15] Yalcin, I., ozarslan, C., and Akbas, T. 2007. physical properties of pea (*Pisum sativum*) seed. *Journal of Food Engineering*. Vol. 79: 731- 735.



## THERMAL ANALYSIS OF SOFT CELLULAR PRODUCTS CONTAINING STARCH

JIŘÍ BLAHOVEC

Czech University of Life Sciences in Prague, 16521 Prague 6 – Suchbátka, Czech Republic,  
Phone: +4202, Fax: +4202-20921361, E-mail: [blahovec@tf.czu.cz](mailto:blahovec@tf.czu.cz)

### Abstract

The basic information on thermal analysis of raw soft vegetable tissue is given. The information on energy changes of the heated cell product is obtained by differential scanning calorimetry (DSC) whereas the textural changes in the heated products are given by other means used in thermal analysis, especially by dynamical mechanical analysis (DMA). The experience with DMA analysis of potato tubers at temperatures 30-90 °C is reviewed. The main observed change was connected with internal starch gelatinization followed by the starch swelling and expansion. Whereas the energy changes accompany mainly starch gelatinization at temperatures just above 50 °C, the texture changes accompany the some interaction of the swollen starch with the cell walls at higher temperatures.

### Introduction

Potato tuber is strongly asymmetric product with gradients of composition and properties in axial direction (stem to bud) and in radial direction from the central pith to the outer skin. These gradients are mentioned mainly for tuber density (starch content) and cell dimension (van Es and Hartmans, 1981). Most tuber cells form parenchyma tissue (cortex) with big cells and very thin cell walls. With increasing temperature the potato tissue generally softens and is more permeable either for different molecules or electric charges (Personius and Sharp, 1938). This trend can be modified by some temperature dependent characteristic processes, like melting of the cellular membranes (Heimburg, 2007), loss of the cell wall function (fall down of potato electric resistivity at approx. 60 °C - Personius and Sharp, 1938), protein denaturation (in range 50-80 °C) and starch gelatinization at temperatures above 50 °C (Lelievre and Liu, 1994).

Starches from different plant sources were studied with attention to structural and physicochemical properties (Singh et al. 2003). The physical and functional properties depend on the biological source, the temperature and the relation to water including the history of these relations. Among others the sorption properties play an important role (van den Berg, 1981, Blahovec and Yanniotis, 2008). During thermal processing of starches of different origin, the most important changes are connected with its gelatinization and retrogradation (Donald, 2004, Bao and Bergmann, 2004, Zoebel and Stephen,

2006, Ratnayake and Jackson, 2007, 2009). These structural changes are easily detected by means of thermal analysis (Lelievre and Liu, 1994) and also by changes in starch rheological properties (Bao and Bergmann, 2004, Kaur et al. 2002). The whole process of the starch changes during its heating is sensitively connected either with the structural properties of the starch grains, or their dimensions and composition (Singh et al. 2003, Kaur et al. 2002). Detailed analysis of the gelatinization process shows the importance of starch composition, starch structure, water availability and the time scale factor of the process (Ratnayake and Jackson, 2009). Karlsson and Eliasson (2003 a,b) and Liu et al. (2005) found that starch gelatinization in potato dry matter is observed at higher temperatures than in extracted starch.

Dynamic mechanical analysis (DMA) belongs among the methods applied to thermal analysis of materials (Haines, 2002). The DMA is based on analysis of the specimen toughness instead of heat-temperature relation as is done in DSC. This method is ready for relatively quick dynamic scans of the mechanical properties of a specimen with aim to determine physical states at which mechanical properties are changed. There is not necessary to compare the analyzed specimen with some etalon like in the DSC. Then the method can be easily applied to specimens like the whole product; in our case potato parenchyma. This method has not been used to thermal analysis of vegetable flesh, may



be due to problems with the flesh drying during the scan.

The aim of this paper is to show the basic applications of the DMA analysis to study thermal stimulated changes in the potato tuber tissue in area of the starch gelatinization.

### Materials and Methods

The potatoes of different cultivars were bought on the local market and/or cultivated in standard conditions by Potato Research Institute (PRI) in Havlickuv Brod. The cultivated tubers were stored in cold and wet conditions (4 °C, 85 % relative humidity) and then transported to the laboratory. The other potatoes were transported directly to laboratory. After a few days storage in a refrigerator at (7±1) °C, they were washed in cold water. The selected defect-free tubers of mediate size (5 to 8 cm in diameter) were then left at room temperature for testing the next day.

Rectangular specimens 8 mm (width) × 3 mm (thickness) × 22 mm (length) with the long axis parallel to the tuber axis (connection of stem and bud sides of tuber) were cut from the tuber cortex tissue on the border between stem and bud part of tuber using the special jigs. From one tuber there was prepared one specimen. The density of the individual specimen was determined by two weightings, in air and in water. Moisture content was determined gravimetrically by drying of the special specimens at 104 °C.

The DMA experiment was performed with a special DMA instrument, constructed by RMI company (Pardubice, Czech Republic), model DX04TC with single cantilever fixing of specimens. The specimen was carefully mechanically fixed in two points so that the longitudinal axis was perpendicular to the fixing jaws. The free length of the specimen between the jaws was 4.4 mm. The height of the fixed specimen was appr. 3 mm. One of the jaws was fixed and the other moved up and down with a constant amplitude of 1 mm and a frequency of 1 Hz. The force connected with the oscillation was recorded, being the basis for the complex modulus determination. Every experiment started at a temperature of 30 °C and air humidity in the test chamber of 90 % which was kept constant during the whole experiment. The control of air humidity in the test chamber was based on direct humidity measurement by special hygrometer as

basis for water vapour ejection into the chamber. The humidity control system was supplied as a part of the DMA model DX04TC. The temperature scan proceeded up to 90 °C with a rate of 1 °C/min. In case of cv. 'Saturna', the regular change of temperature (30-90 °C) was followed by cooling with the same (cooling) rate of 1 °C/min to 30 °C and then temperature increased again up to the final value of 90 °C with heating rate of 1 °C/min.

The obtained results were analysed using the standard laboratory software Origin<sup>®</sup>, OriginPro Ver. 7 (OriginLab, Northampton, MA, USA). The module derivatives versus temperature were smoothed by adjacent averaging of three neighbour points. ANOVA one-way test in combination of Tukey test at 95% confidence level were used for determination of significant differences among the data sets.

### Results and Discussion

Typical temperature scans of the modulus of elasticity are given in Fig. 1. The basic plot represents the development of the 'relative storage modulus (SM)' in the whole temperature as was obtained at cv. 'Saturna'. The SM was obtained as a ratio of the storage modulus and its initial value at 30 °C multiplied by 100, so that the initial value of SM is 100 %. The SM decreases with increasing temperature up to a temperature  $T_0$  of ~72 °C (peak onset temperature), where a peak starts to develop. This peak was observed as the most important change of the scan. The tuber tissue behaves at temperatures higher than 50 °C similarly to the gelatinizing starch although the deformation of the tissue is more complicated than the deformation of the extracted starch. The SM peaks were observed at temperatures ( $T_p$ ) higher than those given for starch gelatinization either by DSC ( $T_{pDSC}$ , e.g. Perry and Donald, 2002, Donald, 2004) or rheology (Kaur et al. 2002) analysis in the extracted starch, even in presence of limited water content (Donovan, 1979) or where instead of water the sucrose water solutions were used for wetting the starch (Perry and Donald, 2002, Donald, 2004). The obtained SM peak data were also higher than the endothermic peaks of DSC data (Liu et al. 2005) obtained for dried and rewetted potato tissue (close to 74 °C). This difference can be caused

either by *in situ* potato tissue used in our experiments or by more complex loading of the potato tissue in DMA test where the gelatinization effects in the closed cells are combined with the internal cell starch swelling. The similar behaviour was observed for sweet potato (Li et al. 2010). The process responsible for the observed SM peak consists in cell wall interaction with the gelatinizing starch inside the cells.

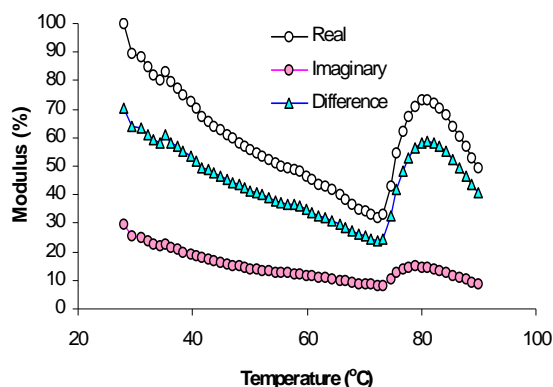


**Fig. 1** Temperature scan of the component module: real (storage) and imaginary (loss) and their difference. The values are plotted as percentage of the initial storage modulus (at temperature 30 °C).

The ‘relative loss modulus’ (LS) is represented by the regular loss modulus divided by the initial value of storage modulus (at 30 °C) multiplied by 100. Its temperature development is very similar to the development of SM, but the initial value is about 1/3 of SM. The temperature plot for LS is similar to the SM plot. It means that mechanism controlling the DMA peak formation leads to both components SM and LM. Figure 1 shows that the peak is more pronounced at SM than LM; the difference between the plots expresses also marked peak.

Evaluation of the obtained data is presented in Tables 2, 3, and 4. Table 2 contains information on the peak part of SM: the onset of peak (temperature and SM-value) and the peak maximum by the same parameters as the peak onset. Table 3 contains similar information on LM. Slope analysis of the modulus-temperature plots (see Fig. 1c) gave the points of the maximal modulus-temperature derivatives. The data obtained for them are given in Table 4.

The coefficients of variation for the characteristic SM- and LM- values, as well as the coefficient of variations of characteristic slope-values were in order of tens percent. There is not surprising that cultivar differences in these values were difficult to prove (Tables 1, 2). The better results were obtained for the characteristic temperatures for which coefficient of variation moves in range of percent. The cultivar differences were denoted by superscripts: in onset temperature  $T_o$ , peak temperature  $T_p$  and the temperature corresponding to maximum slope of peak ( $T_d$ ). The marks were selected in the following manner: the medium temperature values were denoted by superscript *a*, for the significantly lower temperatures the superscript *b* was used, and for the significantly higher temperatures the mark *c* was used as the superscript. The lower temperature values ( $T_o$ ,  $T_p$ , or  $T_d$  - denoted by *b*) were observed for 3 cultivars: ‘Amandine’, ‘Liseta’ and ‘Sibu’. Similarly, the higher characteristic temperatures (*c*) were observed at cv. ‘Secura’ and partly also at cvs. ‘Marabel’ (onset temperature at SM) and ‘Saturna’ (peak temperature).

Table 1 DMA peak characteristics for SM; the onset of peak (temperature and modulus value as a percentage of the initial value), the top of peak by the same parameters as the peak onset.

Cultivar	Onset of peak				Peak			
	Temperature		Value		Temperature		Value	
	MV [°C]	CV [%]	MV [%]	CV [%]	MV [°C]	CV [%]	MV [%]	CV [%]
‘Agata’	72.9 <sup>a</sup>	1.1	25.1 <sup>a</sup>	25.0	80.0 <sup>a</sup>	3.7	61.4 <sup>a</sup>	48.0
‘Amandine’	72.1 <sup>a</sup>	2.8	39.7 <sup>c</sup>	35.3	78.3 <sup>a</sup>	3.2	42.8 <sup>b</sup>	39.0
‘Liseta’	72.0 <sup>a</sup>	1.1	32.9 <sup>a</sup>	48.5	78.1 <sup>a</sup>	3.4	58.2 <sup>a</sup>	55.9
‘Marabel I’	73.5 <sup>c</sup>	2.4	31.7 <sup>a</sup>	28.2	80.4 <sup>a</sup>	0.4	45.5 <sup>b</sup>	25.1
‘Marabel II’	73.8 <sup>c</sup>	2.1	26.5 <sup>a</sup>	23.6	80.5 <sup>a</sup>	1.8	61.9 <sup>a</sup>	4.4
‘Saturna’	72.3 <sup>a</sup>	1.9	41.1 <sup>c</sup>	23.0	82.0 <sup>a</sup>	2.8	106.7 <sup>c</sup>	40.6
‘Secura’	73.6 <sup>c</sup>	1.9	27.1 <sup>a</sup>	25.6	81.6 <sup>a</sup>	4.3	55.8 <sup>a</sup>	35.0
‘Sibu’	70.5 <sup>b</sup>	1.5	18.6 <sup>b</sup>	49.4	78.8 <sup>a</sup>	2.3	66.9 <sup>a</sup>	56.0

The same superscripts at MV (mean value) mean the same values at 0.05 level, CV (coefficient of variation)

Table 2 DMA peak characteristics for LM

Cultivar	Onset of peak				Peak			
	Temperature		Value		Temperature		Value	
	MV [°C]	CV [%]	MV [%]	CV [%]	MV [°C]	CV [%]	MV [%]	CV [%]
‘Agata’	72.6 <sup>a</sup>	3.7	9.6 <sup>a</sup>	53.4	77.6 <sup>a</sup>	1.4	18.0 <sup>a</sup>	40.8
‘Amandine’	73.1 <sup>a</sup>	2.4	12.1 <sup>a</sup>	58.1	75.4 <sup>b</sup>	3.3	13.0 <sup>a</sup>	26.2
‘Liseta’	72.2 <sup>b</sup>	1.5	13.6 <sup>a</sup>	33.3	76.8 <sup>a</sup>	1.3	17.6 <sup>a</sup>	30.2
‘Marabel I’	73.5 <sup>a</sup>	2.0	9.5 <sup>a</sup>	24.1	79.2 <sup>a</sup>	2.9	11.7 <sup>a</sup>	25.3
‘Marabel II’	74.2 <sup>a</sup>	0.5	11.9 <sup>a</sup>	42.6	79.2 <sup>a</sup>	1.5	20.0 <sup>a</sup>	1.5
‘Saturna’	73.3 <sup>ab</sup>	1.1	13.1 <sup>a</sup>	30.9	81.0 <sup>c</sup>	3.5	24.0 <sup>c</sup>	42.2
‘Secura’	75.8 <sup>c</sup>	5.2	9.3 <sup>a</sup>	49.1	80.1 <sup>c</sup>	5.0	14.7 <sup>a</sup>	42.0
‘Sibu’	70.8 <sup>b</sup>	0.7	6.0 <sup>a</sup>	41.9	78.3 <sup>a</sup>	2.1	15.2 <sup>a</sup>	47.1

The same symbols as in Table 2, the modulus data are given in percents of the SM initial value

The SM and LM give nearly the same information about the gelatinization process. No significant differences between characteristic temperatures given by SM and LM were statistically proved.

## Conclusions

The heating of potato tissue to temperatures above starch gelatinization (~70 °C) leads to toughening of the tissue previously softened by the precedent heating at lower temperatures. The toughened tissue behaves as tougher and more viscose matter than previously at lower temperatures. This effect is detected by DMA in temperature scan as peaks of both storage and loss module. The basic peak characteristics (onset and peak temperatures) are cultivar dependent.

## Acknowledgements

The authors thank Dr. J. Vacek for experimental material and Dr. S. Yanniotis for stimulating discussion. The paper was supported by the Research Intention MSM 6046070905 (Czech Republic).

## References

- Bao, J., Bergmann C.J. (2004). The functionality of rice starch. In: *Starch in Food. Structure, Functions and Applications*. (edt. A-C. Eliasson). Woodhead Publishing Limited and CRC Oxford: Press LLC, pp. 258-294.
- Blahovec, J., Yanniotis, S. (2008). GAB Generalized Equation for Sorption Phenomena. *Food Bioprocess Technol.* 1, 82-90.
- Donald, A.M. (2004). Understanding starch structure and functionality. In: *Starch in Food. Structure, Functions and Applications*. (edt. A-C. Eliasson). Oxford: Woodhead Publishing Limited and CRC Press LLC, pp. 156-184.

- Haines, P.J. (2002). Principles of thermal analysis and calorimetry. The Royal Society of Chemistry, Cambridge.
- Heimburg, T. (2007). *Thermal Biophysics of membranes*. Weinheim: Wiley-VCH Verlag GmbH & Co. KGaA.
- Karlsson, M.E., Eliasson, A.-C. (2003a). Effects of time/temperature treatments on potato (*Solanum tuberosum*) starch: a comparison of isolated starch and starch *in situ*. *Journal of the Science of Food and Agriculture* 83, 1587-1592.
- Karlsson, M.E., Eliasson, A.-C. (2003b). Gelatinization and retrogradation of potato (*Solanum tuberosum*) starch *in situ* as assessed by differential scanning calorimetry (DSC). *Lebensmittel-Wissenschaft und-Technologie* 36, 735-741.
- Kaur, L., Singh, N., Sodhi, N.S. (2002). Some properties of potatoes and their starches. II Morphological, thermal and rheological properties of starches. *Food Chemistry*, 79, 183-192.
- Lelievre, J., Liu H., (1994) A review of thermal analysis studies of starch gelatinization, *Thermochimica Acta*, 246, 309-315.
- Li, Q., Li, D., Wang, L., Özkan, N., Mao, Z. (2010). Dynamic viscoelastic properties of sweet potato studied by dynamic mechanical analyzer. *Carbohydrate Polymers* 79, 520-525.
- Liu, Q., Lu, X., Yada, R. (2005). The effect of various potato cultivars at different times during growth on starch content determined by DSC. *Journal Thermal Analysis and Calorimetry* 79, 13-18.
- Perry, P.A., Donald, A.M. (2002). The effect of sugars on gelatinisation of starch. *Carbohydrates Polymers* 49, 155-165.
- Personius, C., Sharp, P.F. (1938) Permeability of potato-tuber tissue as influenced by heat, *Food Research* 3, 525-541.
- Ratnayake, W., Jackson, D.S. (2007). A new insight into the gelatinization process of native starches. *Carbohydrate Polymers*, 67, 511-529.
- Ratnayake, W., Jackson, D.S. (2009). Starch gelatinization. *Advances in Food and Nutrition Research*, 55, 221-268.
- Singh, N., Singh, J., Kaur, L., Sodhi, N.S., Gill, B.S. (2003). Morphological, thermal and rheological properties of starches from different botanic sources. *Food Chemistry*, 81, 219-231.
- van den Berg, C. (1981). Vapour sorption equilibria and other water-starch interactions: A physico-chemical approach. PhD thesis, Wageningen: Agricultural University.
- Van Es, A., Hartmans, K.J. (1981). Structure and chemical composition of the potato. In: *Storage of Potatoes. Postharvest behaviour, store design, store practice, handling*. (eds. A. Rastovski, A. van Es et al.). Wageningen: Centre for Agricultural Publishing and Documentation.
- Zaidul, I.S.M., Nik Norolaini, N.A., Nohd. Omar, A.K., Yamauchi, H., Noda, T. (2007a). RVA analysis of mixtures of wheat flour and potato, sweet potato, yam, and cassava starches. *Carbohydrate Polymers*, 69, 784-791.
- Zobel, H.F., Stephen, A.M. 2006. Starch: Structure, analysis and application In: *Food Polysaccharides and their Application*. (ed. A.M. Stephen, G.O. Phillips, P.A. Williams). Boca Raton: CRC, pp. 25-85.

## EXPLOITATION PARAMETERS OF A PELLET PRODUCTION LINE MONITORING

DAVID BLAŽEJ<sup>1\*</sup>, JIŘÍ SOUČEK<sup>2</sup>

<sup>1</sup>Czech University of Life Sciences Prague, 16521 Prague 6 – Suchbátka, Czech Republic,  
Phone: +420224383140, E-mail: blazej@tf.czu.cz

<sup>2</sup> Research Institute of Agricultural Engineering, Prague, Czech Republic

### Abstract

The following article describes a research in cooperation between Czech University of Life Sciences in Prague and the Research Institute of Agricultural Engineering. The project is primarily focused on monitoring and measuring the exploitation parameters of the semi-industrial experimental pellet production line located at Research Institute of Agricultural Engineering in Prague. Materials commonly available in Czech Republic were used during required pellet samples production.

**Keywords:** pellets, biomass, flax awn, exploitation parameters, energetic parameters

### Introduction

Suitable biomass utilization can significantly support economy of agriculture companies and can also represent an environmentally friendly source of energy. Many research results showed that the industrial and energy use of biomass is reasonable. (Abrahám, Jevič, Kovářová, 2008) One of the widely used products of high-pressure biomass compression are pellets – factory-pressed granules with a cylinder shape.

Flax awn taken from the flax-mill Lenka Kácov was used for pellets production in this research. These are woody remains of stems removed during the processing in the flax mill. Awn is commonly used for construction and isolation materials, as a biofuel or in the chemical industry. (Malat'ák – Vaculík, 2008)

Main goal of this research was to monitor and evaluate the basic parameters of flax awn pellets production and to determine the properties of the produced pellets. Based on these parameters the potential of the flax awn as a material for pellets production, as well as problems occurred during this production were discussed.

### Experimental arrangement

The Kovo Novák MGL 200 granulation line was used for making pellet samples. The line is designed for granulation of wooden sawdust, hay, other biomass, paper or feeding mixtures. Produced pellets can be 6 or 8 mm in diameter.

MGL 200 has modular construction welded mostly by steel sections and plates (Image 1). Main parts are:

- Dosing worm conveyor with a receiving hopper
- Material compounder
- Granulation press
- Pellet sorting apparatus with a cooler

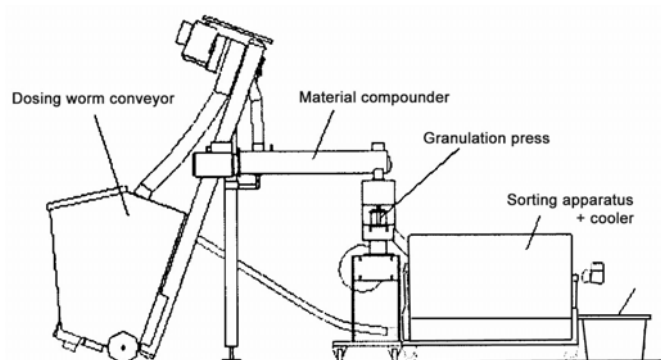


Image 1 – MGL 200 scheme (Novák, 2007)

#### Technical/Catalog Information:

Power input:	up to 8.85 kW
Weight:	310 kg
Area used (approx.):	4m <sup>2</sup>
Voltage/Current:	400V/25A safety limit switch C or D cat. and 230V/16A

Receiving hopper can be filled manually or by using a filling auger. For disruption of material clamber, rotating steel rods are installed inside. Dosing worm conveyor transports the material to the filling piping, surplus material falls back to the hopper. Material is adjusted for further processing in the compounder, where the chosen additional substances (water in our case)



are dosed and added by an adjustable dosing pump.

Granulation press consists of matrix, rollers and its own drive with a gearbox. Pressed pellets are falling to the bottom part of the press and then they are transported to the sorting apparatus with the cooler. Cooling is effected on the principle of flowing air during the rotation of a sifting drum. Small particles and pellet fragments are falling through the sifting drum and are transported back to the receiving hopper. The pellet temperature after cooling can reach up to 50 °C. Theoretical one-hour capacity of the line is 50 – 100 kg per hour for wooden pellets and 50 – 150 kg per hour for other biomass – hay etc. (Novák, 2007)

Monitored and calculated were: Total weight of produced pellets, power consumption, one-hour capacity of the line, power consumption per kg, water consumption per kg, combustion heat and heating value of pellets, solids and water content of pellets.

Solids and water contents were measured by calorimetric method according to the ČSN 44 1377:1978 on MEMMERT laboratory drier and Kern 572 balance. Combustion heat and heating value were determined and calculated according to the ČSN: ISO 1928 1999 on HAAKE fisons HC 10 calorimeter and METTLER AE 160 balance.

## Results and discussions

Attempts to use non-separated material for pellets production were unsuccessful. Clumps of material created mostly by long fibers were blocking the dosing worm and/or the material compounder. Therefore a sieving to separate of the longer fibers and constant disruption of material inside the hopper was necessary.

Solids content (Table 2, Graph 1) was 91.84% in case of raw (non-separated) and 91.38% in case of separated flax awn. Power consumption was 6.83 kWh for producing 63.50 kg of pellets during the time of 75 minutes, which means slightly less than 0.11 kWh.kg<sup>-1</sup>. One-hour capacity of the line was approx. 50.80 kg.h<sup>-1</sup>. According to the high dryness of the material, additional moistening by using a dosing pump was needed. Water consumption was about 0,07 l.kg<sup>-1</sup> (Table 1).

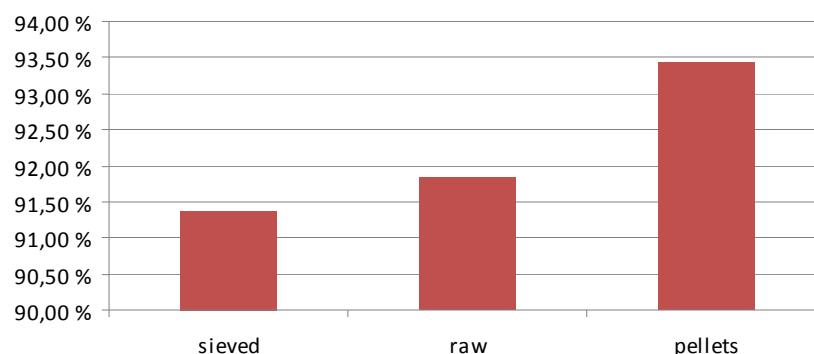
Weight of pellets	63,50 kg
Power consumption	6,83 kWh
One-hour capacity	50,80 kg.h <sup>-1</sup>
Water consumption	0,07 l.kg <sup>-1</sup>
Pellets diameter	6,00 mm

Table 1 – measured line parameters

Solids content of pellets was 93.43% (Table 2, Graph 1). This means 2.05% of water content reduction against sieved and 1.59% against raw flax awn (Table 2, Graph 2). The combustion heat of pellets was 19,70 MJ.kg<sup>-1</sup>, heating value is 18,33 MJ.kg<sup>-1</sup> (Table 2, Graph 3).

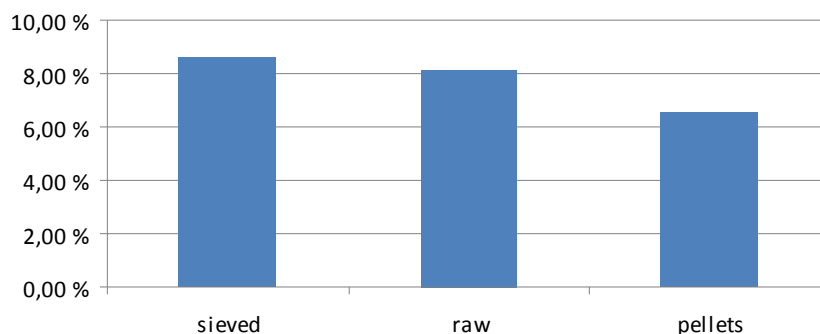
	solids cont.	water cont.	heating value	combustion heat
Raw flax awn	91,84 %	8,16 %	17,71 MJ.kg <sup>-1</sup>	19,13 MJ.kg <sup>-1</sup>
Sieved flax awn	91,38 %	8,62 %	17,93 MJ.kg <sup>-1</sup>	19,36 MJ.kg <sup>-1</sup>
Pellets	93,43 %	6,57 %	18,33 MJ.kg <sup>-1</sup>	19,70 MJ.kg <sup>-1</sup>

Table 2 – flax awn and pellets parameters

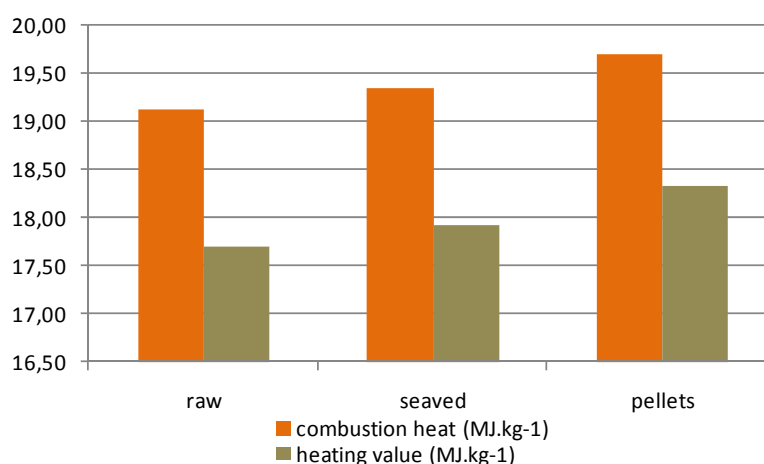


Graph 1 – Solids content





Graph 2 – Water content



Graph 3 – combustion heat and heating value

### Conclusions

According to the serious problems with blocking the patency of the line by long fibers, there is a need to additional sieving the flax awn and use of the longer fibers for another purpose. One-hour capacity of the line is close to lower threshold provided by the manufacturer, power and water consumptions are corresponding to the material parameters. Dryness of used material was very high, which resulted to production of pellets with low water content with suitable combustion parameters. But the increase of heating value against raw material is relatively small. Heating value of pellets is higher than usual hay pellets values and corresponds with the usually reported value of wood pellets.

### Acknowledgement

This proceeding originated within the project IGA TF – 31180/1312/3137.

### References

- [1] Abrahám Z., Jevič P., Kovářová M.: Energetické využití slámy a stébelnaté biomasy [Energetic utilization of Hay and Stalky Fytomass] [online]. 2008-02-11 [cit. 2010-06-13]. Available from URL: <[http://www.ceskaenergetika.cz/nezarazene\\_clanky/energeticke\\_vyuziti\\_slamy\\_a\\_stebel\\_nate\\_fytomasy.html](http://www.ceskaenergetika.cz/nezarazene_clanky/energeticke_vyuziti_slamy_a_stebel_nate_fytomasy.html)>.
- [2] CSN: ISO 1928 1999. Solid fuels – Determination of combustion heat by calorimetric method in pressure vessel and calculation of heating value. Czech Institute of Standards. Prague.
- [3] CSN 44 1377 (441377). Solid fuels – Determination of water content. Czech Institute of Standards. Prague.
- [4] Maláček, J. - Vaculík, P.: Biomasa pro výrobu energie [Biomass for Energy Production]. CULS, Faculty of Engineering, Prague, 2008. ISBN: 978-80-213-1810-6

[5] Novák, Jan. Granulation line MGL 200 – Operating and installation manual. Kovo Novák Citonice. 2007.

[6] Verner, Vladimír: Alternativní pelety [Alternative Pellets]. Biom.cz [online]. 2007-12-31 [cit. 2010-06-13]. Available from URL: <[http://biom.cz/cz-obnovitelne-zdroje-energie/odborne-clanky/alternativni-pelety?apc=/cz-obnovitelne-zdroje-energie/odborne-clanky/alternativni-pelety&nocache=invalidate&sh\\_itm=ed675c739749ec8265632886b07df6c1&add\\_disc=1](http://biom.cz/cz-obnovitelne-zdroje-energie/odborne-clanky/alternativni-pelety?apc=/cz-obnovitelne-zdroje-energie/odborne-clanky/alternativni-pelety&nocache=invalidate&sh_itm=ed675c739749ec8265632886b07df6c1&add_disc=1)>. ISSN: 1801-2655.

## DEVELOPMENT OF DATA LOGGER FOR DATA ACQUISITION FROM FOUR CUP ANEMOMETERS

ZDENEK BOHUSLAVEK

Czech University of Life Sciences Prague,  
Kamycka str. 129, 165 21 Prague 6 – Suchbát, Czech Republic  
Phone: +420-224383300, bohuslavec@tf.czu.cz

### Abstract

This paper describes a development of a synchronized data recording from cup anemometers. Data logger was developed for application in research and optimizing of windbreaks. Measuring equipment consist of 4 masts placed one data logger which records data from four analog anemometers. The anemometers measure wind speed and direction in different levels above the ground. Data logger controlled by microprocessor allows a data recording in a sample interval from 2 to 60 second during 12 hours. Retiming of clock generator, starting and stop time, and also data archiving is executed by computer program, which was developed for this purpose. The program makes possible also calibration of sensors (anemometers), and on-line measuring with the anemometers. PC and data loggers are connected by USB interface.

**Keywords:** Data logger, wind speed, windbreaks, anemometers

### Introduction

It was necessary to measure the influence of windbreaks on airflow changes in the landscape during research on the effectiveness of the proposed exact windbreaks, so as to obtain a reduction in wind erosion of soil. For this purpose it was necessary to measure wind speed and direction at four levels above the soil surface at least four sites. Previously developed measuring devices with wireless data transmission allows only one measurement in one sensor at one level. No data logger of the known devices from other companies meet the requirements for measuring and archiving data. They are known as data loggers from companies Dickson [1], Pelago [2], Fourier Systems Company [3], EMBRO [4]). Data loggers from quoted companies are prepared for the purpose of processing universal signals (standardized voltages and currents, the inputs and outputs) or to connect common temperature sensors, humidity sensors, etc. Only expensive types allow you to connect a wind sensor with pulse output, and only after modification of hardware (HW) and software (SW). For these reasons it was elected its own development path data loggers.

### Materials and methods

#### a) Requirements for measuring and recording data in one data loggers

- Measuring and recording the signals from four sensors wind speed and direction
- When using sensors Davis evaluating data on the wind direction by position of the runners 500 Ohm potentiometer and an indication of the speed of closing the contact (switch) once per revolution
- Assessing the speed to a maximum of 30 m/s with an accuracy of 0.1 m/s and wind direction in the range 0 to 360° accurate to 5 degrees
- Recording data in a predefined interval from 2s to 120s with a period of up to 24 hours
- Synchronizing start and end of the record's internal clock (accuracy better than 0.2s in the 48 hours)
- Linking during setup and data archiving to a PC via USB
- Power supply built-in battery capacity allowing operation for 48 hours after
- Extension HW data logger of RF module for wireless data transmission at distances up to 300 m

#### b) The requirements for a computer utility software

- Applications for Windows XP and later versions
- The start and end of the registration record of

the year, month, day, hour, minute and seconds to the current real-time clock synchronization according to PC

- Logging the measured and stored data from all sensors in the table
- Export loaded in TXT and XLS
- On line measurement of the selected sensor
- Calibrating of sensors with calibration table storage and with an option to export.

### c) The hardware design solutions - design method

- Development of hardware-based eight bit microcontroller with integrated A / D converter and sixteen bit counters - on the basis of experience with AVR orientating selection in this direction
- Writing data to Flash EEPROM memory
- Using circuit FTDI for USB interface
- Implementing an automatic system for charging NiMH battery pack also to HW

### d) The method and design environment for software (SW) of data logger and software for PC

- The SW recorder will design by using the design studio AVR and will minimize the size of the program-level by assembler programming
- Conversion of the final drive speed and direction will not be made by using SW data logger, but the measured values of the binary will be left to the conversion SW on the PC (the reason is to save memory space)
- For proposal of SW PC will use environment TEST POINT or LAB VIEW, both using an efficient method of graphical programming of measuring systems.
- For controlling communication via USB will be used own proposed DLL

## Results and discussion

### a) A description of the basic solution concept

Data logger is designed on base of microprocessor the Atmel AVR ATmega 64L type, possessing the requisite number of peripherals, especially 8 AD converters. They are used for measuring the voltage of potentiometers pursuing the wind direction. Pulses from the sensors of wind speed are detected an interrupt inputs, which control pulse counters of the internal generator. Figure 1 captures specific circuit solution, describes the

circuitry of the microprocessor and Figure 2, where is the circuit diagram with connector for the sensor (anemometer No. 2.). The figure shows that the wind direction determined voltage (A. DIR 0-3) in sliding contact (Wiper) of potentiometer is evaluated on the analog inputs of microprocessor (AD4 - 7). The wind speed determined by frequency switching contacts (A. SPEED 0-3) activates inputs (INT 2-5).

Ridici mikroprocesor:

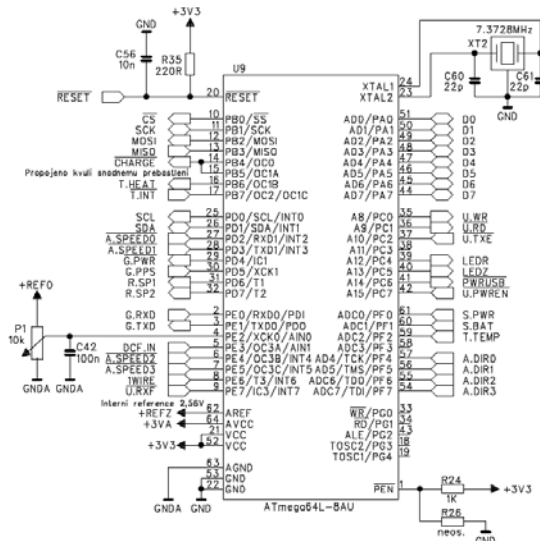


Fig. 1 Electrical scheme of CPU datalogger

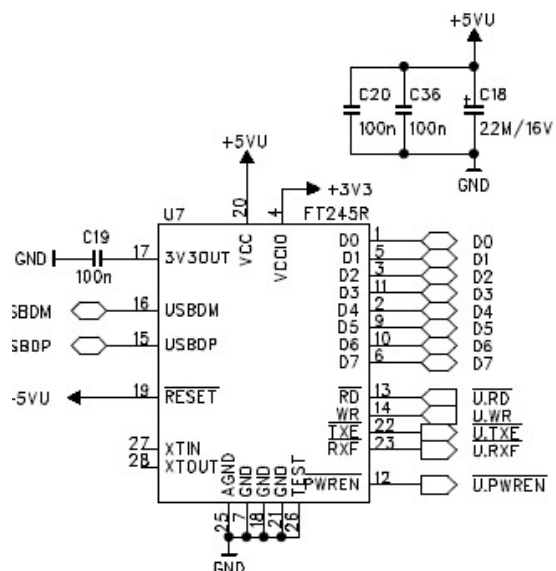


Fig. 2 Electrical scheme of input for the anemometer

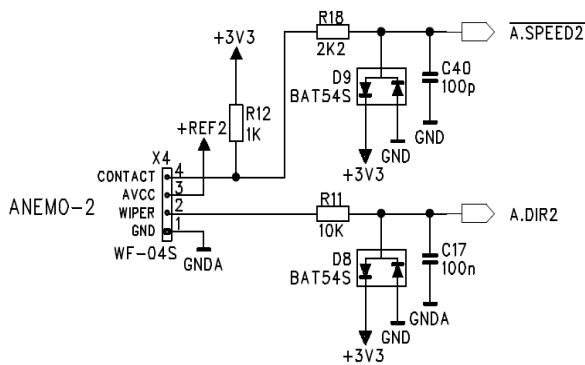


Fig. 3 Scheme of the circuitry of USB controllers

Controller type FT245R provides communication between the microprocessor of datalogger and personal computer (PC). Circuitry is showed by the scheme on Fig.3.

For easy battery charging of datalogger only by its connected to the USB, hardware is complemented by computer-controlled inverter with automatic disconnection when sufficient battery charge, processing governed by the microprocessor via pin CHARGE and G.PWR, see Fig.1.

#### b) Archiving data logger memory

Memory for storing the measured data must by one sample store data of wind speed and direction of the four anemometers. One sampling refers to measurements of two byte of wind speed (sampling resolution: 16 bit) and 1 byte of wind direction from each sensor. It is necessary to save data storage space with a capacity of 12 bytes in one sampling. When requiring a 12-hour measurements and record the maximum Sampling rate 2 seconds based on the requirement of memory capacity 12 hours x 1800

sample per hour x 12 = 259,200 Byte = 2 073 200 bits. The flash memory AT45DB161B with a capacity of 2,162,688 Byte is used in data loggers, which theoretically allows recording of up to 97 hours.

#### c) Synchronization and accuracy of internal clock

Circuit real-time RTC DS1339 is another element of the hardware, which communicates with the processor via 2-wire serial interface and its power supply is provided by battery of data logger and also 3V lithium cell. Integrated circuit RTC has sufficient accuracy for the 12-hour measurement. The circuit RTC reaches 0.1s deviation up to 24 hours and with that is guaranteed sufficient overlapping of the four data loggers over whole maximum period of measurement and recording.

#### d) Brief description of the program on a PC for configuration and archiving data of data loggers

The program DATALOGGER WIND was proposed in a development environment TEST POINT for creating applications for virtual instrumentation. After the program starts, the main user control panel with virtual buttons and other display elements (display tables, etc.) displays, cf. Fig. 4. By controlling virtual buttons it is possible to activate the starting RESCAN function which will check its connection datalogger and its serial number identification. At this time, you can perform other functions data logger (SETUP Dataloggers, READ DATA ON LINE MEASUREMENT, etc), which are described below.

Panel1 [App.#1 VITR7ENG.TST]

Rescan

Description

SerialNumber

Reading

4100

450

40

Read data

Table of measured values

	rel.time [s]	time	a1 [m]	cnt1 [n]	a2 [m]	cnt2[n]	a3 [m]	cnt3 [n]	a4 [m]	cnt4 [n]
0										
1										
2										
3										
4										
5										
6										
7										
8										
9										
10										
11										
12										
13										
14										
15										
16										
17										

SampleRate

StartYear

StartMonth

StartDay

StartHour

StartMin

StartSec

StopYear

StopMonth

StopDay

StopHour

StopMin

StopSec

Setup data logger

Table on-line measurement

	a1 [m]	count1 [n]	a2 [m]	count2[n]	a3 [m]	count3 [n]	a4 [m]	count4 [n]
0								

on line measurement

Archiving to TXT

TXT file - option

File

Save table to file: data.txt

Calibration

Archiving to XLS

Enter the index of A to D

Save table to file Excel: C:\merenadata(index).xls

State of storage

Fig. 4 Main panel of program DATALOGGER WIND

- The **SETUP Dataloggers** allows you to configure measurement interval and start time and end measurements on the attached datalogger.
- The **READ DATA** implements retrieval of measured data from data logger to table **MEASURED DATA TABLE**, where the values can be viewed.
- The function **Archiving of measured data to a TXT file** allows you to select an existing file with any name and click **FILE** button function performs the appropriate description.
- The function **Archiving of measured data to a XLS file** allows you to select an existing XLS file on the disk C: with title from dataA.xls to dataD.xls. In which four sets data will be stored you determine by inserting the index A up to the D into corresponding input.
- The **ON LINE MEASUREMENT** allows for testing of functionality of individual sensors, which is advantageous in the preparation of measurement.

The calibration function is included into the program, which opens its own control panel. Before performing the calibration values it

must complete white objects with the required information: the number of sensors on a mast, pole location, wind speed in the tunnel test, time (interval) of measurements in the test tunnel.

The findings of the calibration values is performed by button **MEASURE AND COUNT**. Then you can verify the correctness of the calculation immediately using the constant in the function of direct measurements in units of velocity (m/s) function **MEASURE SPEED**. Like a table of measured values is possible button **SAVES TABLE TO TXT FILE** archiving of 16 calibration values into the TXT file.

## Conclusion

The paper presents the development of a unique device that allows you to transfer and store data from four sensors fy Davis type 6410 for measuring wind speed and direction (Fig. 2). The shortest interval of recording (sampling) activates 2s, the maximum recording time of this mode is 48 hours (holding time of NiMH Akku). The data logger contains still working clock in real time, and therefore recorder data is archived simultaneously with the actual



timestamp. Given this important fact, it is possible the synchronous start of record number of records answering the same time, the variation in hours in records does not exceed 0.1s over with in 24 hours. Recorded (archived) data is stored in the memory recorder and after an arbitrarily long time it is possible that data (data on wind speed and direction from up to four sensors and an indication of the time) to pass through the serial USB and with help program DATALOGGER WIND into computer. These are archived in the txt file or excel. The file contains all the measured values, and therefore it is possible subsequently to perform any statistical analysis, and this is very important for research, dynamic analysis of changes in wind velocity and direction at different height levels above ground.

## References

- [1] Dickson. Temperature Data Logger. [Online] 2009. [Citace: 2. 3 2009] Dostupne z: [http://www.dicksondata.com/product/model\\_WT100.php](http://www.dicksondata.com/product/model_WT100.php)
- [2] Pelago Data Acquisition Systems. Products. [Online] 2003/2004. [Citace: 2. 3 2009] Dostupne z: <http://www.pelago.co.uk/html/temperature.html>
- [3] Fourier Systems' MicroLite USB data logger. [Online] 2009. [Citace: 2. 1 2009] Dostupne z: [http://www.fouriersystems.com/products/intelligent\\_network/data\\_logger/](http://www.fouriersystems.com/products/intelligent_network/data_logger/)
- [4] Ebro - Products - Data Loggers. [Online]. [Citace: 2. 3 2009] Dostupne z: [http://www.ebro.com/en/products/index\\_data\\_loggers.php](http://www.ebro.com/en/products/index_data_loggers.php)

## STUDY OF WEAR RESISTANCE OF HARD FACINGS USING WELDING POWDERS ON THE NiCrBSi BASIS

MILAN BROŽEK<sup>1</sup>, ALEXANDRA NOVÁKOVÁ<sup>2</sup>, RASTISLAV MIKUŠ<sup>3</sup>

<sup>1</sup>Czech University of Agriculture in Prague, 165 21 Prague 6 – Suchbát, Czech Republic,

Phone: +420 224 383 265, E-mail: [brozek@tf.czu.cz](mailto:brozek@tf.czu.cz),

<sup>2</sup>Czech University of Agriculture in Prague, Czech Republic

<sup>3</sup>Slovak University of Agriculture in Nitra, Slovak Republic

### Abstract

One of the most frequent reasons of machine parts premature outage is their excessive wear. It is possible to prevent this effect by the welding powder deposition on the most stressed surfaces. In the paper the wear resistance results of hard facings made using welding powders on the NiCrBSi basis are presented. Four powder types were tested, which differ by the different chromium content. Besides this one powder contained the tungsten carbide  $W_2C$  particles, too. The laboratory tests were carried out using the apparatus with abrasive cloth (bonded abrasive) and apparatus with grinding vessel (free abrasive). The wear rate was evaluated by the test specimens mass loss. It was proved that using the powder with tungsten carbide the best results were reached. Next it was proved that the wear resistance increases with increasing chromium content.

### Introduction

One of the most frequent reasons of the machine parts damage are the effects connected with friction and wear processes. Damage even of one machine part usually results in the necessity to put of operation the whole machine plant (in the worse case its breakdown). This produces minor or major economical losses to the owner. In last years it is the main reason why the task of stressed machine parts service life prolongation appears in foreground. They are several possibilities of solution. One of them is the use of the hard facing technology – special wear resistant layer deposition on the functional surface.

In practice the hard facing technology is used in two ways, namely as preventive deposits (new parts production) and as renovation deposits (repairs of worn out parts). Using the suitable application the hard facing can bring significant economical effects, namely saving in material and energy, labor consumption decrease and service life increase.

The hard facing using overlay materials of special properties is one of the most rapidly developing applications of welding technology. It is used not only in machine industry, but in agriculture, building industry, digging, mining, material handling and in many next fields of human activity, too. For the optimum hard facing

use the detailed knowledge of single overlays materials technical and technological properties and their behaviour under various working load is necessary. These and economical data are the most important criterions for the suitable hard facings use in practice.

### Materials and Methods

For the ferrous metals wear resistance determination against single wear types in principle field tests, pilot tests and laboratory tests are used. Each of mentioned tests is of advantages, but also of disadvantages. Therefore each of test types is most suitable for other field of application. The wear resistance test type is always necessary to be chosen with regard to the wear process dominant conditions and to the demanded test results.

In inland and foreign literature a sufficient number of abrasion wear testing machines for testing of machine parts material or assemblies is published. According to the conditions in the contact area between the working surface and the medium the apparatuses for the abrasive wear resistance testing are divided into:

- Apparatuses with bonded abrasive particles – Fig. 1 a,
- Apparatuses with free abrasive particles – Fig. 1 b.

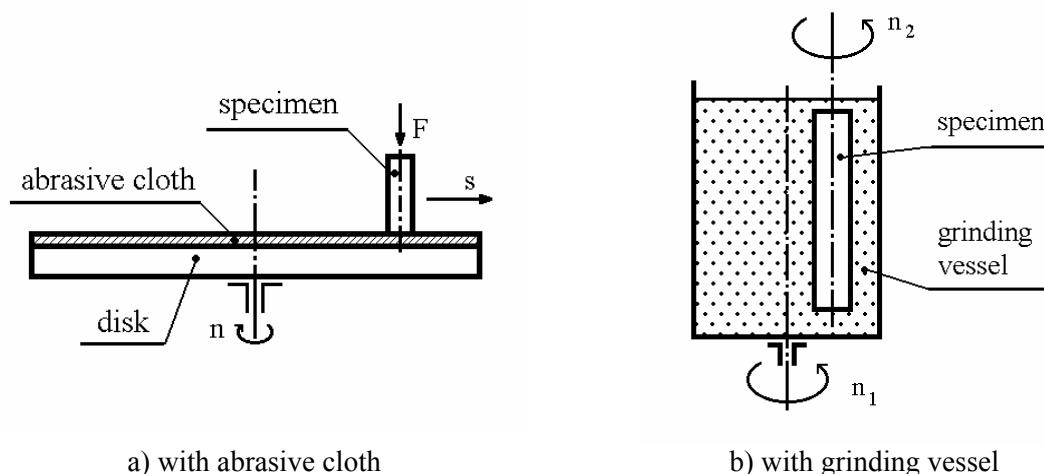


Fig. 1 Diagrammatic representations of apparatuses for the abrasive wear resistance testing

The subject matter of both tests is relatively simple and evident from the above mentioned figures. For the test with bonded abrasive the apparatus with abrasive cloth (Fig. 1 a) was used. The test was carried out according to the standard CSN 01 5084. The specimens were worn using the abrasive cloth (corundum twill) of 240, 120 and 60 grit. It corresponds to the abrasive grain average size of 44.5, 115.5 and 275  $\mu\text{m}$ . For the tests with free abrasive the apparatus with grinding vessel (Fig. 1 b) with the synthetic corundum of F 24 grit (grain size 0.71 – 0.85  $\mu\text{m}$ ) was used.

But between both tests one fundamental difference exists still. At the tests with bonded

abrasive the by standard determined friction path is 50 m. At used test parameters the specimen covers this distance in about 5 minutes. This test can be considered as the short term one. At the tests with free abrasive the covered distance is over 200 km. The corresponding test time is over 116 hours. Therefore it is the long term test.

In principle at both tests the mass loss is determined. Therefore all specimens were weighed before and after the test using the weight of  $10^{-5}$  g accuracy.

In the paper the test results of four welding powder types (manufacturer VUZ Bratislava) on the NiCrBSi basis, determined for hot coating (Tab. 1), are published.

Tab. 1 Chemical composition (% by weight) and hardness of tested materials

Powder type	C	Si	B	Fe	Cr	Cu	W	Mo	Ni	Hardness HRC
NP 52	max. 0.5	max. 5.0	max. 3.5	max. 5.0	8.0 – 14.0	xx	xx	xx	Rest	48 – 54
NP 58	max. 0.6	max. 4.5	max. 4.0	max. 10.0	max. 15.0	max. 2.5	max. 2.5	max. 2.5	Rest	54 – 59
NP 60	max. 0.6	max. 5.0	max. 3.9	max. 5.0	max. 16.0	xx	xx	xx	Rest	56 – 62
NP 60 WC 20	max. 0.6	max. 5.0	max. 3.9	max. 5.0	max. 20.0	xx	xx	xx	Rest	75 – 82 <sup>*)</sup>

Note: <sup>\*)</sup> Powder NP 60 WC 20 contains 20 %  $\text{W}_2\text{C}$ , the mentioned hardness relates to the carbide component part. The matrix hardness is of 56 – 62 HRC.

On the test specimens the powders were deposited by use of oxyacetylene flame. Using the apparatus with abrasive cloth the specimens were of 10 mm diameter and 60 mm length. Tested powders of NP 58, NP 60 and NP 60 WC 20 types were deposited on the circular face of

10 mm diameter. Using the apparatus with grinding vessel the specimens were of 10 mm diameter and 200 mm length. Powders were deposited on the cylindrical jacket in the length of 120 mm. At the powders application all

technological conditions specified by the powder manufacturer were kept.

### Tests results

The test results are graphically presented in Fig. 2 (for bonded abrasive) and in Fig. 3 (for free abrasive).

Using the apparatus with abrasive cloth the test results show that the mass loss increases with the grain size. It corresponds to the results published by other authors. Next it is ascertained that using smaller abrasive grains the mass loss difference is relatively higher. At the increasing abrasive grain size this difference is smaller.

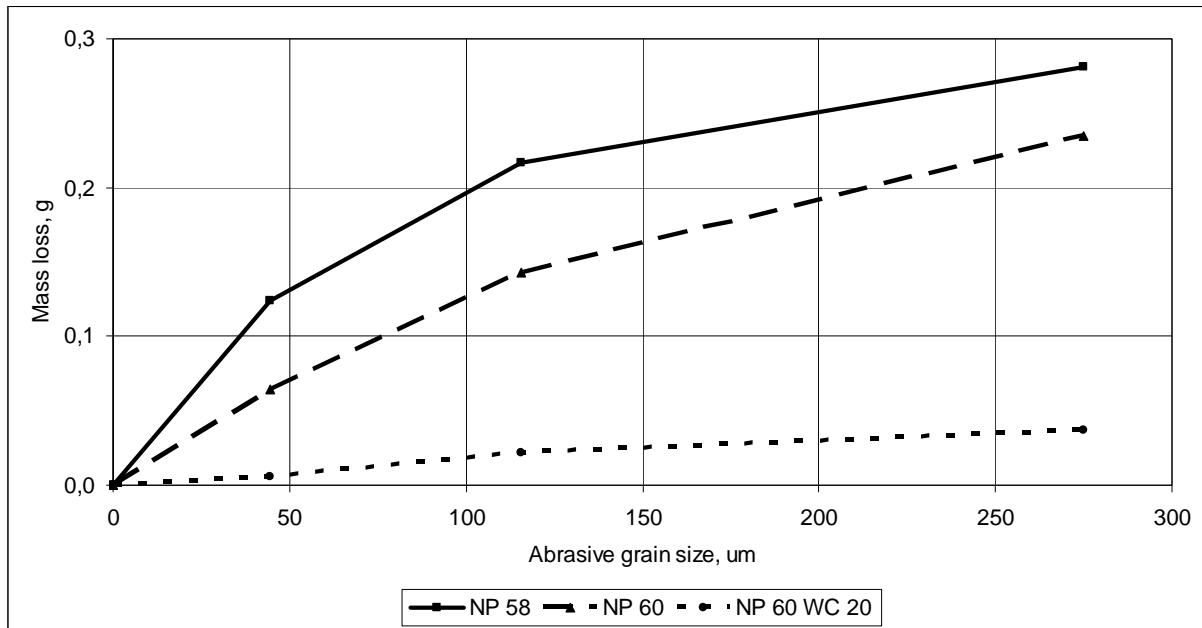


Fig. 2 Test results – bonded abrasive

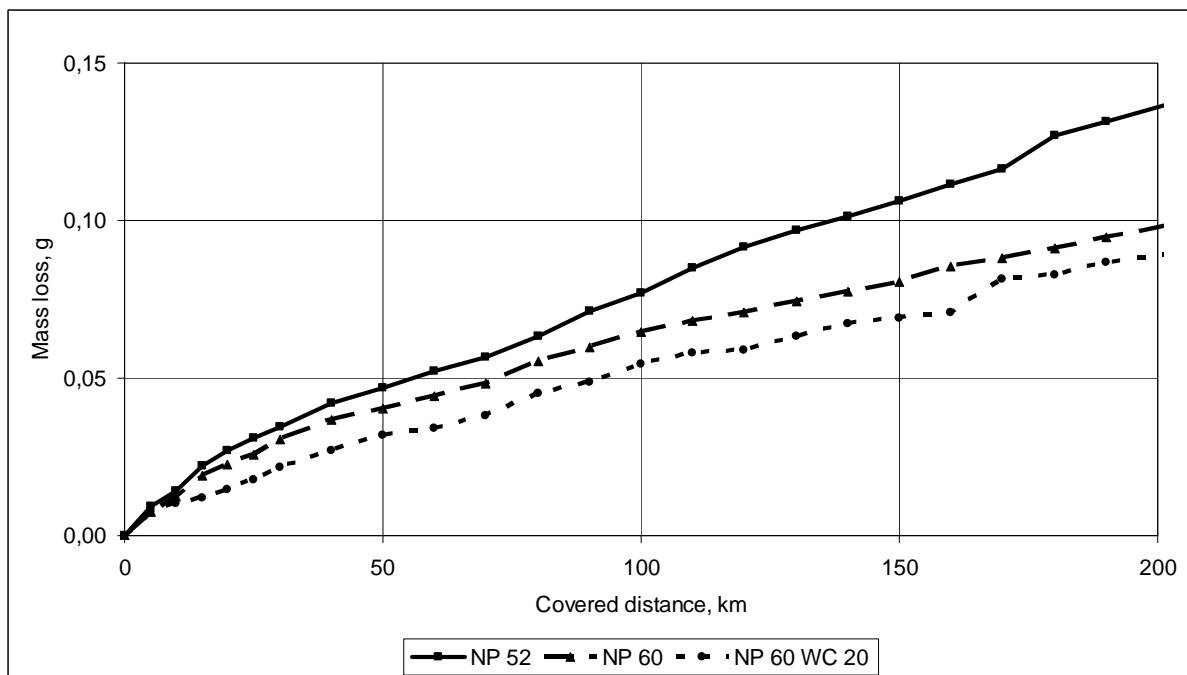


Fig. 3 Test results – free abrasive

From the test results carried out using the apparatus with grinding vessel it follows that after 5 – 20 km of the hard facing running in (according to the powder type) the mass loss over the whole friction path is practically linear.

The highest abrasive wear resistance showed, in correspondence with the assumption, the test specimens with the hard facing of NP 60 WC 20. On the contrary, the lowest abrasive wear resistance showed the powder NP 52, which contains minimum chromium of all tested powder types.

### Conclusion

In the paper the laboratory abrasion wear resistance test results of four metal powders determined for hot deposition are published, using the apparatus with bonded abrasive and the apparatus with free abrasive.

From the test results it is evident that the unambiguously best results were determined using the powder with 20 % tungsten carbide. But in this connection it is necessary to remind that in this way found out “technical quality” of the powder is only one (even very important) criterion. For the complex evaluation of the concrete powder for concrete use it is necessary to be busy with the total technical-economical evaluation (which was not the subject of this phase of tests).

### Reference:

Brožek, M.: Vybrané problémy navařování (Selected Problems of Sufracing). [Habilitační práce] (Inaugural Dissertation). Praha 1995. 148 p. - Česká zemědělská univerzita. Technická fakulta. (in Czech).

Friction and Wear Testing. American Society for Testing and Materials, West Conshohocken, PA, 1987. 186 p.

Chasuj, A. – Morigaki, O.: Naplavka i napylenije. Moskva, Mašinostrojenije 1985. 240 p. (in Russian).

Repair and Maintenance Welding Handbook. ESAB AB, 120 p.

Vocel, M.: Experimentální metody hodnocení tření a opotřebení (Experimental Methods of Friction and Wear Evaluation). Kovové materiály, 21, 1983, No. 6, p. 711 – 722. (in Czech).

Vocel, M. – Dufek, V. et al.: Tření a opotřebení strojních součástí (Friction and Wear of Machine Parts). Praha, SNTL 1976. 376 p.

ČSN 01 5050. Opotřebení materiálu (Wear of materials). Názvosloví (Terminology). 1969. (in Czech).

ČSN 01 5084. Stanovení odolnosti kovových materiálů proti abrazivnímu opotřebení na brusném plátně (Determination of metal material resistance against wear by abrasive cloth). 1974. (in Czech).

Kovové prášky na nanášanie za tepla (Metal powders for hot deposition). Product catalogue. [online] [viewed 22. 10. 2009]. Available: <http://www.vuz.sk/?cid=874> (in Slovak).

## TENSILE MECHANISM HOOK TMB PS 600 - THE TENSILE ANALYSIS

PAVEL CYRUS<sup>1\*</sup>, BOHUSLAV ZAJÍC<sup>2\*</sup>

<sup>1</sup>Czech University of Life Sciences Prague, 16521 Prague 6 Suchbát, Czech republic, Phone +420 224383180, Fax +420 220921361, E-mail [cyrus@tf.czu.cz](mailto:cyrus@tf.czu.cz)

<sup>2</sup>University of Hradec Králové, Hradec Králové, Czech republic

### Abstract

The paper describes the placing and construction of the tensile mechanism of the hook TMB PS 600 projected for the Škoda Felicia car. A 3D computer model of the hook was designed for setting how the intensity of selected sections of the body is spread; the model subsequently underwent the intensity and strength analysis. The computer analysis was made by the finite element method applying the IDA NEXIS programme. Some of the results received in the programme, e.g. spreading of normal and tangential intensity in single sections of the body and deformations under the selected load, are presented in the paper.

### 1 Introduction

Suspensory devices for cars are constructed in various ways. Each car producer provides recommendations on what type is the most suitable for a certain purpose, so that the utility features were used and safety rules kept. That is why a wide range of types have appeared on the roads. Each user - technician - is interested whether the given device is able to carry the load presented in the log book. The solidity of single parts of the tensile mechanism hanger can be proved by the software providing the finite element computer analysis

### 2 Materials and methods

So that the solidity of tensile mechanism elements of TMB PS 006 [1], constructed for a Škoda Felicia car, could be checked, the IDA NEXIS programme [2] was applied running on the principle of the finite element method. Figure 1 shows a hook on the rear part of the car. The hook is fixed to the rear frame of the car, according to figure 2. The hook was fixed to the

thill of the transportation dray. The calculation was made for the type SPORT JACHT [3] dray of total weight 350 kg.



Figure 1 The tensile mechanism hook, a Škoda-Felicia car



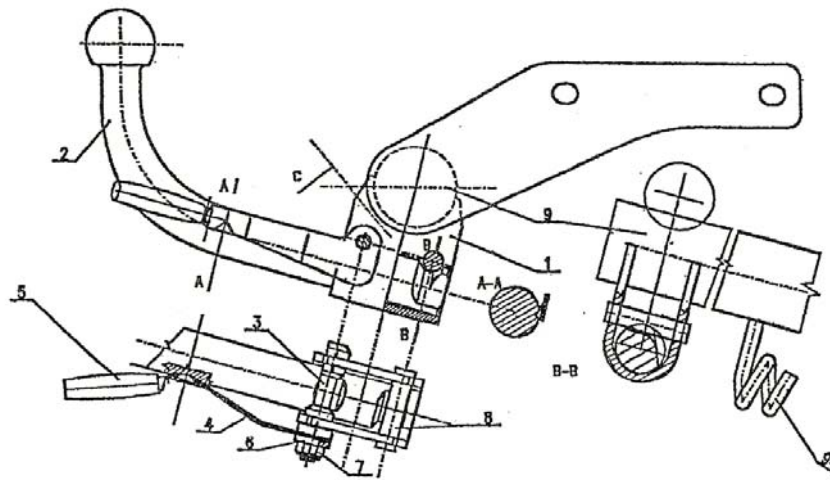


Figure 2 Design hook fixing

1-Hanger clamb, 2-Towing bar with coupling ball, 3-Eccentric, 4- Lever bar, 5-Handle, 6-Wascher, 7- Self-securing nut, 8- Transverse pin

Figure 3 displays the photograph of the hook.



Figure 3 Photograph of the tensile mechanism hook

The computational model presented in figure 4 was created by the IDA NEXIS programme. The model was loaded by single forces  $F_x$ ,  $F_y$  in point 1.

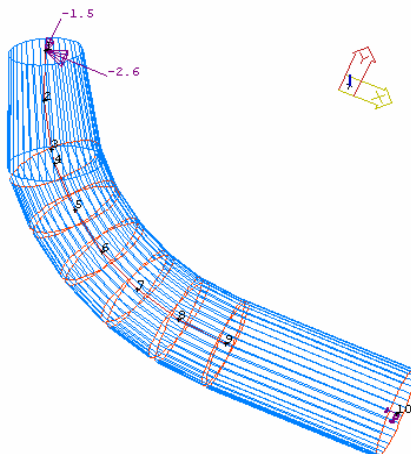


Figure 4 Computational model of the tensile mechanism hook

### 3 Results

Consequently, the computational model of the hook underwent the strength and stiffness analysis for the load of  $F_x = 2,6$  kN,  $F_y = 1,5$  kN by the IDA NEXIS programme. The results of the analysis are presented in figures 5, 6 and 7. Figure 5 displays distribution of normal tensity in the marked sections of the hook. Maximal calculated value of normal tension was 106 MPa.

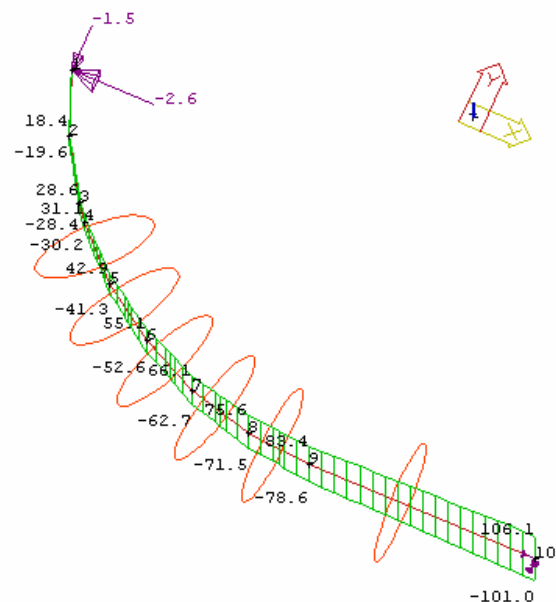


Figure 5 Distribution of normal tensity (MPa) in the marked sections of the hook

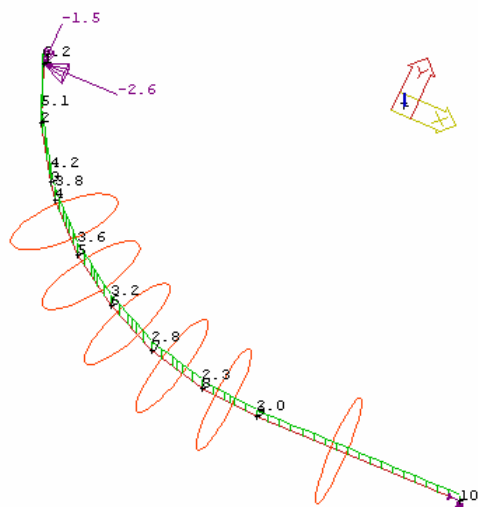


Figure 6 Distribution of shear tensile in the marked sections of the hook

Figure 6 presents distribution of shear tensile in the marked sections of the hook. The shear tensile in comparison to the normal tensile reaches insignificant values.

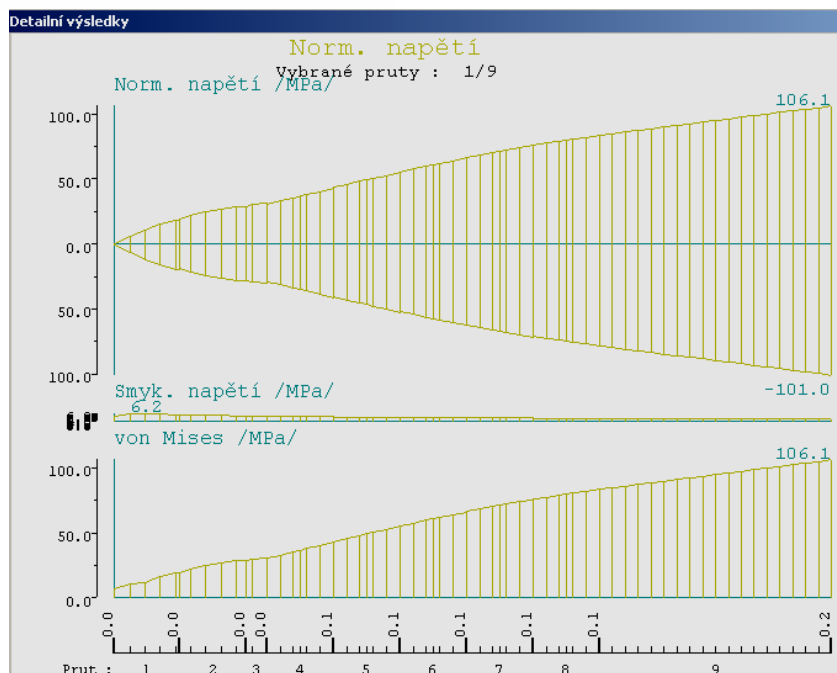


Figure 7 Total tensile of the hook in single sections

Figure 7 shows a diagram presenting distribution of total tensile in single sections of the hook calculated according to the Mises hypothesis.

#### 4 Discussions and conclusions

Currently, in the field of construction parts and machines we cannot do without computational computer programmes. They enable both 3D modelling of single parts and their strength and stiffness analysis. The paper presents an example of the strength analysis of

the tensile mechanism hook of the SPORT JACHT dray to a Škoda Felicia car. Results which were reached by the IDA NEXIS software prove the correct constructional design of the hook, which has been also verified by practical technical experience.

#### References:

- [1] Tensile mechanism of the ŠKODA FELICIA, TYPE TMB PS 006 - manual
- [2] IDA NEXIS – reference manual
- [3] SPORT JACHT – manual

## LOADING CAPACITY OF THE WOODEN BONDED SCARF JOINT SIMPLIFIED DETERMINATION

OLDRICH DAJBYCH\*

Czech University of Agriculture in Prague, 16521 Prague 6 – Suchbát, Czech Republic,

Phone: +4202-2438-3186, E-mail: [dajbych@tf.czu.cz](mailto:dajbych@tf.czu.cz)

### Abstract

Paper is focused on wooden bonded scarf joint loading capacity determination process simplification. Percentual force distribution on surface method was used for this purpose. The method is based on joint surface virtual division into 2 sections – normal stress is applied on first and shear stress on second. Loading capacity of selected joint was experimentally determined for several wooden materials and for several bevel angles from 0° to 90°. Then theoretical dependencies for accordant joints were calculated from values for 0° and 90° and results compared. Experiment showed that selected method can be used for joints from 0° to approx. 70° of bevel angle with acceptable accuracy.

### Introduction

Wooden bonded joint design is based on experience followed by experimental testing of product prototypes. This process increases time demand and development costs. On the other hand the methods based on intermolecular bond characteristics give very low accurate results (usually 50% and less) and they are absolutely unusable for practical exploitation [10],[11].

Previously published method [3] of wooden bonded scarf joint loading capacity determination requires measurement of whole stress on bevel angle dependency for given wood and adhesive combination. Another method [4] is yet simplified and requires only knowledge of ultimate force for clearly normal and clearly tangential strain. Given method is based on tangential on normal stress dependency substitution by ellipse. Method used in this paper brings another simplification as its result is not in contrast to previous method irrational function by maintaining the same input requirements.

### Materials and methods

Wood is organic material composed of cells. Typical wood materials, which are used in constructions and for instance in furniture industry, were taken as basic material for experiments. Concretely *Picea abies*, *Tilia cordata*, *Quercus robur* woods. Wood moisture was 8 - 12% depending on wood material type and experiment period, in view of the fact that experiments proceeded within several months when natural process of drying carried on. No

significant effect of wood moisture content variation in given range on glued joint parameters wasn't noticed.

Basic elements for samples were wooden blocks with following dimensions – 15 x 20 ± 1 mm, thus 300 mm<sup>2</sup> cross section, with length of 200 ± 10 mm. These blocks were cut with saw under bevel angle of 0, 15, 30, 45, 60, 75 and 90 degrees. Then the surfaces of cuts were modified on angle cutter to get exact angles, purified, degreased and prepared by adhesive producer instructions and according to Czech standard [2]. Special equipment for set of 21 samples was designed to keep necessary time and force for proper joints hardening. These 21 samples were prepared for each experiment period, thus 3 for each angel. The goal was to gain 10 valid values of force necessary for sample failure for each bevel angle. The experiment was considered as invalid when the value significantly missed the set of other values or the breach took place out of joint or in its small part [2].

Loctite Hysol 3425 glue was used, which is two-component adhesive based on epoxy resin. This type of adhesive is usually for joints with higher load. It can be used for bonding steel and other metals, masonry and of course wood.

Samples were brought to failure on shredder UTS 50 Testsysteme which is intended for wood testing. Experiments had been processed in laboratory of Department of Wood Processing – Faculty of Forestry, Wildlife and Wood Sciences – Czech University of Life Sciences.



Fig. 1 – Set of 21 samples prepared for bonding process

Principle of simplified formula derivation is based on virtual division of joint surface into 2 sections – normal stress is applied on first and shear stress on second.

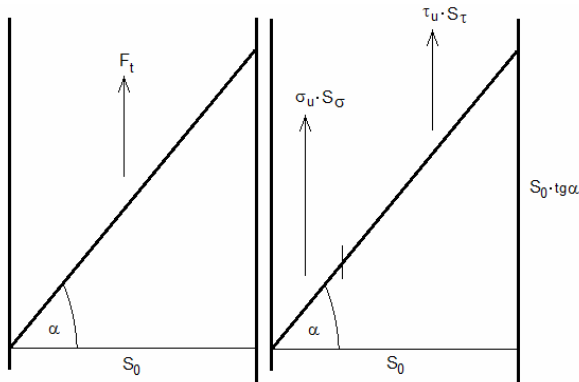


Fig. 2 – Simplification process principle

Joint surface is divided in ratio of perpendicular and parallel projection of given surface to axis of load application. Basic geometrical relations are obvious from fig. 2. We can write following formulae for particular surfaces:

$$S_{\sigma} = \frac{S_0}{\cos \alpha} \cdot \frac{S_0}{S_0 + S_0 \cdot \operatorname{tg} \alpha} = \frac{S_0}{\sin \alpha + \cos \alpha} \quad (1)$$

$$S_{\tau} = \frac{S_0}{\cos \alpha} \cdot \frac{S_0 \cdot \operatorname{tg} \alpha}{S_0 + S_0 \cdot \operatorname{tg} \alpha} = \frac{S_0 \cdot \operatorname{tg} \alpha}{\sin \alpha + \cos \alpha} \quad (2)$$

Where:

$S_0$  is sample cross section

$S_{\sigma}$  is virtual part of joint surface where only normal stress is applied

$S_{\tau}$  is virtual part of joint surface where only shear stress is applied

$\alpha$  bevel angle.

Ultimate force of joint in normal and tangential direction are gained from measurement for bevel angle 0 and 90 degrees. It is essential that joint surface for both straight and lap joint are equal for other operation to be valid.

$$\sigma_u = \frac{F_0}{S_0} \quad (3)$$

$$\tau_u = \frac{F_{90}}{S_0} \quad (4)$$

Where:

$\sigma_u$  a  $\tau_u$  are ultimate normal and shear stresses

$F_0$  a  $F_{90}$  are ultimate forces for bevel angle 0 and 90 degrees

$S_0$  je is sample cross section.

According to superposition theorem we can add normal and tangential part of load applied on accordant surface.

$$F_t = \sigma_u \cdot S_{\sigma} + \tau_u \cdot S_{\tau} \quad (5)$$

After substitution and simplification:

$$F_t = \frac{F_0 + F_{90} \cdot \operatorname{tg} \alpha}{\sin \alpha + \cos \alpha} \quad (6)$$

Where:

$F_t$  is total force necessary for failure of sample with bevel angle  $\alpha$

$F_0$  is force necessary for failure of straight joint (0 deg.)

$F_{90}$  is force necessary for failure of lap joint (90 deg.)

## Results and Discussion

Table 1. – Measured ultimate force [N]

	0°	15°	30°	45°	60°	75°	90°
<b>Picea</b>	3047	3325	4031	5202	6801	7664	2759
<b>Tilia</b>	4289	4386	5363	6009	7966	9694	3059
<b>Quercus</b>	3149	3368	4023	5021	6725	9195	2517

Measured values and derived function are displayed in following graphs. Real values are represented by line with highlighted points,

smooth line shows simplified function (6) calculated from measured values for 0 and 90 degrees.

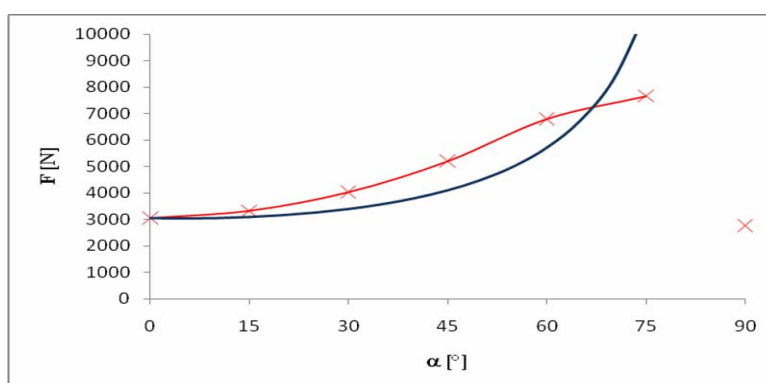


Fig. 3 – Results for Picea wood

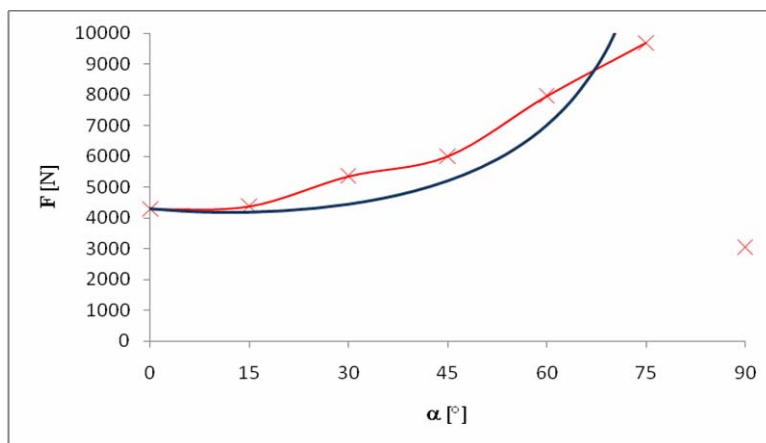


Fig. 4 – Results for Tilia wood

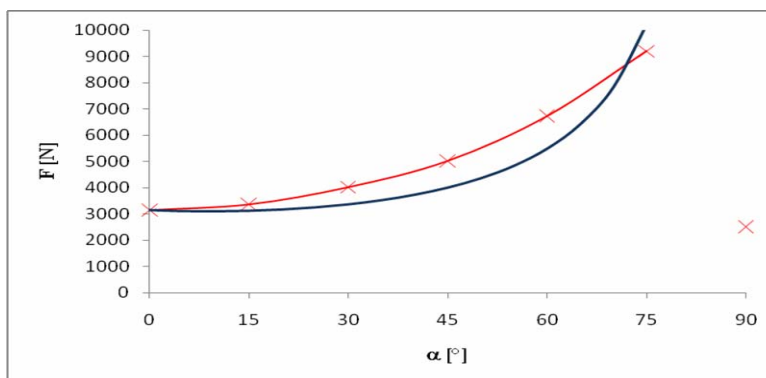


Fig. 5 – Results for Quercus wood

As shown in graphs, it is possible to use simplified formula safely for given wood and adhesive combinations for bonded joint bevel angle from 0 up to approx. 70 degrees.

Experiment also confirmed that absolute load capacity of joints with bevel angle greater than 70 degrees is lower, thus joint efficiency decreases above mentioned angle [4],[5]. When experimental results for bevel angle 60 and 75 degrees are compared, bevel surface is approximately double (double adhesive consumption, space demand for joint), but real ultimate force increase is much lower. The most probable reason is because of high angle of bevel the tips of bonded material are very sharp and thin. And also with regard to heterogeneity and anisotropy of wood is load capacity of basic material in direction perpendicular to fibers multiple times lower in contrast to parallel direction. This causes separation of thin tips of bonded parts, thus real active joint surface is smaller than theoretical.

### Conclusion

It had been confirmed that derived formula for determination of loading capacity depending on bevel angle of the wooden bonded scarf joint is usable for mentioned bevel angle range. Due to wood material properties (heterogeneity, anisotropy) and different technological conditions and procedures, it is necessary to make final experimental verification on designed product prototype. However this method could bring simplification and speedup in primary stadium of design process.

Experimental confirmation of simplification methods for other materials and adhesive combination will continue.

### Reference:

[1] ČSN EN 13183-2 (2002): Moisture content of a piece of sawn timber - Part 2:

Estimation by electrical resistance method. ÚNMZ, Praha. (in Czech)

[2] ČSN EN 205 (2003): Adhesives - Wood adhesives for non-structural applications – Determination of tensile shear strength of lap joints. ÚNMZ, Praha. (in Czech)

[3] Herák, D. – Müller, M. – Chotěborský, R. – Dajbych, O.: Loading capacity determination of the wooden scarf joint. Research in Agricultural Engineering. 2009, 55, p. 76–83, ISSN 1212-9151

[4] Dajbych, O. – Herák, D. – Sedláček, A. – Gúrdil, G.: Determination of loading capacity depending on bevel angle of the wooden bonded scarf joint. Research in Agricultural Engineering. 2010, (in print), ISSN 1212-9151

[5] Dajbych, O.: Stanovení únosnosti dřevěného lepeného spoje s úkosem. In: 50. Medzinárodná vedecká konferencia katedier častí a mechanizmov strojov, Žilina, Slovenská Republika, 2009, ISBN 978-80-554-0081-5

[6] Malyshev, B. M. – Salganik, R. L.: The strength of adhesive joints using the theory of cracks. International Journal of Fracture. 1984, 26, p. 261-275.

[7] Motohashi, K. - Tomita, B. - Mizumachi, H. - Sakaguchi H.: Temperature Dependency of Bond Strength of Polyvinyl Acetate Emulsion Adhesives for Wood. Wood and Fiber Science. 1984, 16, p. 72-85.

[8] Oberk, E. - Jone, F. D. - Horton, H. L. - Ryffel, H. H.: Machinery's handbook, 26th Edition, Industrial Press Inc. 2000, New York

[9] Özçifçi A.: Effects of scarf joints on bending strength and modulus of elasticity to laminated veneer lumber (LVL). Building and Environment. 2007, 42, p. 1510–1514.

[10] Peterka, J.: Lepení konstrukčních materiálů ve strojírenství, SNTL, 1980, Praha (in Czech)



## REAL BEHAVIOUR INJECTION GROUP AND INFLUENCE OF HOLE GEOMETRY IN THE CAVITATION PHENOMENA OF DIESEL INJECTORS

EDMOND DEMOLLARI<sup>1\*</sup>, ALTIN DORRI<sup>2</sup>, ARTAN HOXHA<sup>3</sup>

<sup>1</sup>Czech University of Agriculture in Prague, Kamycka Street 1070, 16521  
Prague 6 – Suchdol, Czech Republic

Phone: +420 608 243 678, E-mail: [demollari@yahoo.com](mailto:demollari@yahoo.com)

<sup>2</sup>Polytechnic University of Tirana, Sheshi: Nene Tereza Nr.4 Tirane, Albania

Phone: +355 686 014 993, E-mail: [altindorri@yahoo.it](mailto:altindorri@yahoo.it)

<sup>3</sup>Polytechnic University of Tirana, Sheshi: Nene Tereza Nr.4 Tirane, Albania

E-mail: [artanhoxha2003@yahoo.com](mailto:artanhoxha2003@yahoo.com)

### Abstract

In order to evidenciate the effects of the hole shape in the generation of the spray, in high pressure diesel nozzles, a numerical investigation has been carried out. In particular the effect of cylindrical and non-cylindrical hole geometry on spray characteristics has been investigated in order to understand the relationship between nozzles geometry and in-nozzle flow features. Flow is in function of viscosity, density. We know that the future of fuel is biodiesel. Biodiesel properties are shown here for showing how it affect at nozzles of the injectors. One phenomenon that is shown at nozzles is cavitation. It is a harmful phenomenon at injection system but at nozzles of injector, it affect for good. Cavitation is a physical phenomenon that generate whereas the pressure of the liquid phase goes down below the vapor pressure.

The formation of vapor's bubbles that follow the cavitation can be of heterogeneous or homogeneous type. If the nucleation of bubbles is favorited by the presence of micro-particles dispersed in the primary fluid or caused by the wall roughness of the duct that contains the fluid it is had heterogeneous cavitation, otherwise if it is entirely due to some conditions of nucleation it is had homogeneous cavitation. The ways with which the conditions of cavitation can be created inside the high pressure injectors are so many and not all known. In order to predict and control fuel sprays related to cavitation various experimental and theoretical research have been carried out.

### Introduction

Actual development of compression ignition engine is mainly related with the rising of injection pressure and the possibility of injecting several jets during a single injection cycle. Both modifications influence positively the engine characteristics and the emissions formation process. As a consequence the capillary diffusion in the injection systems of high pressure for Diesel Engine with direct injection has stimulated in the last decade the research in the field of complexes fluid dynamics phenomena located inside the injectors. Especially, phenomenon related to the cavitation inside the injectors have assumed particular importance as it regards the generation of the spray, a crucial phenomenon to get an efficient combustion and low emission of NO<sub>x</sub> and soot. Normally cavitation is well known as a harmful phenomenon, which favors the erosion of the

mechanical parts, as for example in narrow zones at the upper part of injector. But inside the nozzles (holes), it favors the pulverization of the fuel and as a consequence increases the performances regarding emissions, resulting therefore a phenomenon to be favored. The cavitation is strongly related to high injection pressures in the new injection systems (more than 100 MPa) and with the injector geometry. To get a spray constituted more and more by small bubbles goes toward geometry of multi-hole injector (also up to eleven holes) with diameters extremely reduced (order of 100 μm). The reduced sections of oil-fuel passage, elevated pressures of injection jointly with elevated angles of inclination of the holes are the causes for the formation of cavitation bubbles inside the holes of the injector. Cavitation is a physical phenomenon that generate whereas the pressure of the liquid phase goes down below the

vapor pressure. The formation of vapor's bubbles that follow the cavitation can be of heterogeneous or homogeneous type. If the nucleation of bubbles is favored by the presence of micro-particles dispersed in the primary fluid or caused by the wall roughness of the duct that contains the fluid it is had heterogeneous cavitation, otherwise if it is entirely due to some conditions of nucleation it is had homogeneous cavitation. The ways with which the conditions of cavitation can be created inside the high pressure injectors are so many and not all known

In order to predict and control fuel sprays related to cavitation various experimental and theoretical research have been carried out. Experimental observation evidenced that interesting differences in the permeability of nozzle geometries and a clear resistance of the conical nozzle to cavitation. Hountalas et al. setup an experimental investigation using three different nozzle hole types: *a standard*, *a convergent* and *a divergent* one to discern the effect of nozzle hole conical shape on engine performance and emissions. According to the experimental findings, an increase of soot and decrease of NO<sub>x</sub> was observed for the divergent nozzle hole compared to the other two.

On the other hand due to difficulty do set up experiments related this to small size of injector holes many numerical researches are conducted for this topic and many cavitation models have been developed. Numerical researches are mainly focused in the individualization of the appropriate physical models both as it regards the nucleation of bubbles, also as it regards their growth and collapse. Whatever, considering physics of two-phase phenomenon extremely complex and coupled to the phenomenon of mass transfer among the two phases as well as strongly correlated with the turbulence phenomenon inside the fluid, it results extremely arduous an unification of phenomenons and equations that govern this kind of phenomenona. Important factor in cavitation phenomena is the *cavitation number CN*, defined as:

$$CN = \frac{P_{inj} - P_{out}}{P_{out} - P_{vap}} \quad (1)$$

as well as the inside geometry of the injector that according to the fluid dynamics condition that produces inside the flow determines the conditions to increase the vapor bubbles generation. **In the present work we are mainly focused to the influence of holes geometry in the cavitation phenomena with some properties of biodiesel.**

### Some properties of biodiesel:

#### Viscosity

Viscosity is a measure of the internal friction or resistance of an oil to flow. As the temperature of oil is increased, its viscosity decreases, and it is, therefore, able to flow more readily. Viscosity is measured on several different scales, including Redwood No. 1 at 100 F, Engler Degrees, Saybolt Seconds, etc., the number of seconds required for 50 ml. of an oil to flow out of a standard Redwood viscosimeter at a definite temperature.

Viscosity is the most important property of biodiesel since it affects the operation of the fuel injection equipment, particularly at low temperatures when the increase in viscosity affects the fluidity of the fuel. Biodiesel has a viscosity close to that of Diesel fuels. High viscosity leads to poorer atomization of the fuel spray and less accurate operation of the fuel injectors. A novel process of BD fuel production has been developed by a noncatalytic supercritical methanol method. The viscosity of the distillate was 10.2 mm<sup>2</sup>/s at 311 K, which is higher than the ASTM specification for No. 2 Diesel fuel (1.9–4.1 mm<sup>2</sup>/s) but considerably below that of soybean oil (32.6 mm<sup>2</sup>/s). Used cottonseed oil from the cooking process was decomposed with Na<sub>2</sub>CO<sub>3</sub> as catalyst at 725 K to give a pyrolyzate containing mainly C8–20 alkanes (69.6%) besides alkenes and aromatics. The pyrolyzate had lower viscosity, pour point, and flash point than No. 2 Diesel fuel and equivalent heating values. The cetane number of the pyrolyzate was lower than that of No. 2 Diesel fuel (Bala BK, 2005). The vegetable oils were all extremely viscous, with viscosities ranging 10–20 times greater than that of No. 2 Diesel fuel. Castor oil is in a class by itself with a viscosity more than 100 times that of No. 2 Diesel fuel (Demirbas A 2003).

Table 1  
Fuel properties of methyl ester biodiesels

Source	Viscosity, cSt, at 313.2 K	Density, g/ml, at 288.7 K	Cetane number	Reference
Sunflower	4.6	0.880	49	[33]
Soybean	4.1	0.884	46	[34]
Palm	5.7	0.880	62	[33]
Peanut	4.9	0.876	54	[35]
Babassu	3.6	–	63	[35]
Tallow	4.1	0.877	58	[20]

Source: Demirbas. A / Energy Conversion and Management 47 (2006) 2271–2282

### Density

Density is another important property of biodiesel. It is the weight of a unit volume of fluid. Specific gravity is the ratio of the density of a liquid to the density of water. The specific gravity of biodiesels ranges between 0.87 and 0.89 (*Table 1*). Fuel injection equipment operates on a volume metering system, hence a higher density for biodiesel results in the delivery of a slightly greater mass of fuel. (*Demirbas.A 2006*)

The duty for improving an injection equipment need to know the real moving conditions and influence of special elements of this system. This result could achieve only if we take in consider a stationary typical behaviour of this group: pump-pipe-injector, without a simple analyze, which border only in special components and based on quasi-stationary hypothesis. Simulation of real behaviour of injection group is complex then must be done only through known calculation models. Also flux of a stationary of fuel could not be taken as incompressible models for reason of different high work pressures. (*Londo,2003*)

Through these models we can evaluate:

Phenomenon of cavitation at possibility point of its forming of diesel engine fuel system. Kinematic characteristic of main components of fuel system.

#### Injection characteristic

It is known that in a given section of hydraulic circuit, when the pressure goes down the sum value of the pressure of steam of liquid (in a given temperature) and the partial pressure of gases in liquid, form air bubbles or gases (*Londo,2003*). They became very dangerous when paste in the metallic wall of the part while cut off the contact with liquid mass.

So we have 2 phase situation: On one side is liquid and on other side air bubbles of this liquid

(air bubbles that begin to become free). When the pressure wave change the sign, the phenomenon turned to otherwise. The bubbles condensed in rapid way and start to explode by creating a rapid rise pressure situation, by letting free liquid column, for reactivating and for hitting the wall with high force. Their disposal is a rapid phenomenon (impulsive type), that hit and fatigue materials surface, by corroding bit by bit. The pin of injector is the most critical element of injector, looking from the damages that cavitation cause.

In the figure showed two different types of corrosion caused by cavitation that are verified in diesel engine injectors (*Ferrari,2001*). The first (figure a) have to be with upper part of arrived its support. The depression wave that accompanies, closed quickly, release steaming of fuel. The pasted bubbles in conic surface, near holding zone, explode as reason of rise up the pressure, by corroding the surface. The supporter in these conditions does not have long life so as consequence, we have leak of fuel. (*Ferrari,2001*)

The second type of corrosion from cavitation (fig. B) may happen near the recirculation of pin conic parts with that upper cylindrical, from detachment effect of the wall of fluid stream that moves in pump direction during the final step of pin close.

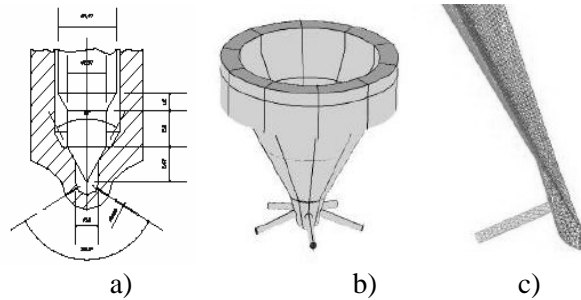
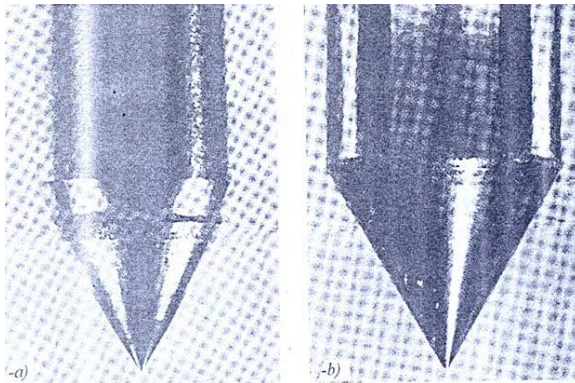


Figure 1: Injector under study: a) Cross section of injector, b) 3D view of nozzle domain, c) 3D mesh of nozzle sector object of simulation

Cavitation phenomenon could cause different kinds of problems, so this must elude. But, one positive effect from cavitation caused on nozzles. (Arcoumanis *et.al.*, 2000 ; Londo *et.al.* 2003). This affect on dividing on small particles the fuel amount for spray forming.

At the end we could say that simulation models of fuel system generally can be used for: Evaluation of different kinds of influence of valves with their expand volume and passing sections at transmeting of pressure impulses and the lost at the end of the cycle that may proved to reopen the pin and local forming of the steams inside the system, (cavitation).

### Injector under investigation

One of the main geometric characteristics of the injector holes is the variation of the cross-section along the length, which represents the orifice conicity. The injector object of simulations are mini-sac type with five holes, as in Figure 1, with nominal diameter of the holes  $D = 68 \mu\text{m}$ . The examined injectors differ only from holes conicity, expressed by:

$$C = \frac{D_{in} - D_{out}}{10} \quad (2)$$

where the dimensions of inlet diameter ( $D_{in}$ ) and outlet diameter ( $D_{out}$ ) are express in mm. The different values examined for the coefficient of conicity  $C$  have been:  $C = 0$  (cylindrical hole),  $C = +1.5$  (convergent conic hole),  $C = -1.5$  (divergent conic hole).

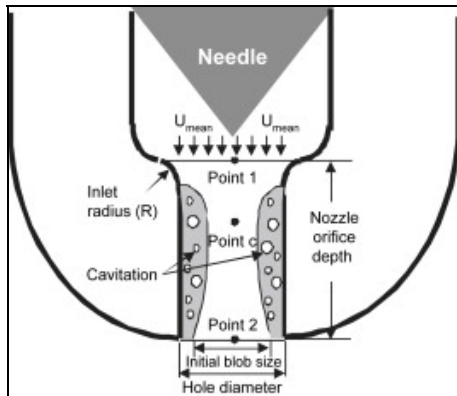
Based on the geometrical symmetry also on the similarity behaviors of five holes during the oil-fuel injection confirmed by De Risi A., Colangelo G., Laforgia D. was useful to limit the CFD study only for a fifth of nozzle so a 72 degree sector was simulated (Fig. 1.c). This has leded a decreasing of time consuming and less CPU used for the calculation. Another reason for this simplification was the limited capability of the computer used for the simulation.

### Cavitation model implemented in Fluent

CFD software used for the numerical simulations is *Fluent 5.5*, that it implements a model able to predict the beginning of fluids cavitation. Such cavitation model is able to model the behavior of the two phases, liquid and vapor, by solving a single set of momentum equations and the continuity equation for the secondary fluid (Fluent. Inc 2000). The model implemented can predict the inception of cavitation but not the collapsing of the bubbles. The cavitation model relies on the volume fraction concept (VOF) but differs from the VOF model in two substantial aspects: **i)** unlike of VOF (that model two unmixed fluids), does not assume that there is an interface between two immiscible fluids; it allows the fluids to be interpenetrating. The volume fractions of two phases ( $\alpha_v$  and  $\alpha_l$ ) for a control volume can therefore be equal to any value between 0 and 1, depending on the space occupied by each phases. **ii)** The cavitation model allows mass to be transferred from one phase to another. These allow us to model the formation of vapor from a liquid. The current implementation of the cavitation model assumes



a two-phase homogeneous model (no slip between the phases). Like the VOF model, it solves a single momentum equation for all phases and a volume fraction equation for the secondary phase. The volume fraction of the primary phase will be computed by subtracting the secondary-phase volume fraction from 1.



source: Nozzle flow and atomization characteristics of ethanol blended biodiesel fuel, Renewable Energy 35 (2010) 144–150

The continuity equation for the vapor phase is the basis of the volume fraction equation:

$$\frac{\partial}{\partial t}(\alpha_v) + \frac{\partial}{\partial x_i}(\alpha_v u_i) = \frac{1}{\rho_v}(\dot{m}_{vl} - \frac{d\rho}{dt}) \quad (3)$$

The liquid - phase volume fraction (VOF) will be computed based on the following expression:

$$\alpha_v + \alpha_l = 1 \quad (4)$$

Cavitation model implemented in Fluent hypothesizes that the phenomenon is isothermal, neglecting thermal exchanges and particularly the latent heat of vaporization, since cavitation bubbles will form in a liquid at low temperatures. Under this hypothesis the pressure within the bubble remains nearly constant at such conditions, and the change in bubble radius can be approximated by a simplified Rayleigh equation:

$$\frac{dR}{dt} = \sqrt{\frac{2(p_v - p)}{3\rho_l}} \quad (5)$$

Therefore total mass of vapor phase can be calculated as follow:

$$m_v = \rho_v \frac{4}{3} \pi R^3 n$$

(Arcoumanis et.al., 2000 ; Londo et.al. 2003).

## Conclusions

The aim of this paper has been to study the influence of hole geometry in cavitation phenomena and some influence properties of biodiesel. It is necessary to underline limits of cavitation model implemented by Fluent that it doesn't allow the evolution modeling of vapor bubbles forming, not succeeding in simulating the collapse. So the cavitation model is able to model the behavior of the two phases, liquid and vapor, by solving a single set of momentum equations and the continuity equation for the secondary fluid. By the side of properties, fuel injection equipment operates on a volume metering system, hence a higher density for biodiesel results in the delivery of a slightly greater mass of fuel. But the counter happen with viscosity, so temperature with viscosities are in disproportional.

## Nomenclature

$CN$	-	Cavitation number
$P_{inj}$	Pa	Pressure of injection
$P_{out}$	Pa	Outlet pressure
$P_{vap}$	Pa	Pressure of vapor
$C$	-	Conicity
$D_{in}$	mm	Inlet diameter of the hole
$D_{out}$	mm	Outlet diameter of the hole
$\alpha_v$	-	Volumetric fraction of the vapor phase
$\alpha_l$	-	Volumetric fraction of the liquid phase
$\rho_l$	kg/m <sup>3</sup>	Density of the liquid phase
$\rho_v$	kg/m <sup>3</sup>	Density of the vapor phase
$R$	mm	Radius of the vapor bubbles
$n$	-	Number of bubbles per unit volume
$\dot{m}_{vl}$	kg/s	Mass transferred between liquid phase and vapor phase

## References

**Demirbas. A** Biodiesel production via non-catalytic SCF method and biodiesel fuel characteristics. Energy Conversion and Management 47 (2006) 2271–2282.

**Bala BK.** Studies on biodiesels from transformation of vegetable oils for Diesel engines. *Energy Edu Sci Technol* 2005;15:1–43.

**Demirbas A.** Biodiesel fuels from vegetable oils via catalytic and non-catalytic supercritical alcohol transesterifications and other methods: a survey. *Energy Convers Mgmt* 2003;44:2093–109.

**De Risi A., Colangelo G., Laforgia D.,** “An Experimental Study of High Pressure Nozzles in Consideration of Hole-to-Hole Spray Abnormalities”, *SAE paper* 2000-01-1250, 2000.

**Arcoumanis C., Whitelaw J. H.,** “Is Cavitation Important in Diesel Engine Injectors?”, Proceeding of Thiesel ‘2000, *Conference on Thermofluiddynamic processes in Diesel Engines*, Valencia 13-14 September 2000.

**Arcoumanis C., Badami M., Flora H., Gavaises M.,** “Cavitation in Real-Size Multi-Hole Diesel Injector Nozzles”, *SAE paper* 2000-01-1249, 2000

**Ramadhas AS, Jayaraj S, Muraleedharan C.** Use of vegetable oils as IC engine fuels—A review. *Renew Energy* 2004;29:727–42.

**Mittelbach M, Gangl S.** Long storage stability of biodiesel made from rapeseed and used frying oil. *JAACS* 2001;78:573–7.

**Fluent. Inc.** Fluent 5.5 User's Guide, *Fluent Inc.*, Lebanon NH, 2000.



## ESTIMATING THE ECONOMIC AND ENERGY EFFICIENCY OF WINTER WHEAT (*TRITICUM AESTIVUM*) AND WINTER RAPE (*BRASSICA NAPUS*) CULTIVATION FOR BIOFUELS PRODUCTION

TOMASZ K. DOBEK<sup>1\*</sup>, PATRYCJA SAŁAGAN<sup>1</sup>, PETR ŠAŘEC<sup>2</sup>

<sup>1</sup>West Pomeranian University of Technology, Szczecin

ul. Papieža Pawła VI/3, 71-459 Szczecin, Poland, E-mail: tomasz.dobek@zut.edu.pl

<sup>2</sup>Czech University of Life Sciences Prague, Czech Republic

### Abstract

Economic and energy analysis and evaluation of winter wheat and winter rape production technology was carried out, as well as of processing of those crops into biofuels. Subsequently, economic and energy efficiency of biodiesel from winter rape and bioethanol from winter wheat production were estimated. Research shows that biofuels production can be profitable provided that not only biofuels, but also straw and, in the case of rape –post-extractive cake, will be sold. The same also applies to energy efficiency of biofuels production.

**Keywords:** biodiesel, bioethanol, costs of production, labor inputs, economic efficiency, energy efficiency

### Introduction

According to their definition, biofuels are completely flammable substances of non-fossil, but still biological origin [Mokrzycki 2005]. Processing biomass into energy has numerous advantages including reduction of toxic compounds emission, reduction of the greenhouse effect, biodegradability. However, the costs of biofuels production are high. First of all, the cost of manufacturing biofuels is determined the price of the raw material which depends on the technologies employed and subsidies systems for agriculture. Nowadays, fabricating the most known liquid fuels such as bioethanol or rape ester are, at current prices, approximately two times higher than the cost of manufacturing mineral fuels. An important element in evaluating biofuels production, apart from costs, is energy efficiency calculation. This calculation shows how high the the energy expenditures have to be to obtain an energy unit in biofuels. The advantage of energy calculation is its independence from the relationship of prices, what makes the comparison of the results possible. The research objective was to conduct economic and energy analysis and evaluation of production technology of winter wheat and winter rape, processing those crops into biofuels, as well as calculation of economic and energy efficiency of production of biodiesel from winter rape and bioethanol from winter wheat.

### Material and Methods

The studies were carried out in 2005/06 – 2007/08, at farms dealing with crop production in West-Pomeranian Voivodeship. In the production of winter rape the technology of a traditional tillage, meaning a mouldboard plough and a disc harrow, was used. In soil cultivation an aggregate for soil cultivation was used. Fertilization was performed four times with a trailed fertilizer spreader while sowing - with a universal seed drill. During the growing season spraying was performed four times with the use of trailed sprayer. Winter rape harvest was performed by one-stage method. A combine harvester with an adapter adapted to harvest the rape was used. The average yield of rape was 3.5 t·ha<sup>-1</sup>. In the production of wheat a mouldboard plough and a cultivator were used and the soil cultivator performed shaft tillage. Fertilization was performed three times with a trailed fertilizer spreader, and sowing - with a universal seed drill. During the growing season of winter wheat spraying was performed four times by a trailed sprayer. Winter wheat harvest was performed by one-stage method by means of a combine harvester. The average yield of winter wheat was 5.3 t·ha<sup>-1</sup>.

The costs of tested technologies consisted of the operating costs of machinery, tools and tractors, the costs of materials and raw materials, fuel costs and labour costs [Muzalewski 2005].

In the calculations only the direct costs are included.

Biofuels production costs are calculated on the basis of the relationship:

$$K_{pro} = K_{mat} + K_{agr} + K_{pal} + K_r + K_{prz}, \quad (1)$$

[PLN·ha<sup>-1</sup>]

where:

- $K_{pro}$  – the production costs of biofuels [PLN·ha<sup>-1</sup>],
- $K_{mat}$  – the costs of used materials and raw materials [PLN·ha<sup>-1</sup>],
- $K_{agr}$  – the costs of machinery and tools [PLN·ha<sup>-1</sup>],
- $K_{pal}$  – the costs of fuel consumed [PLN·ha<sup>-1</sup>],
- $K_r$  – human labour costs [PLN·ha<sup>-1</sup>].
- $K_{prz}$  – the costs of processing into biofuel [PLN·ha<sup>-1</sup>].

A method developed by IBMER [Anuszewski and others 1979, Wójcicki 2002] was used for analysis and evaluation of cumulative energy inputs in the production of winter rape and winter wheat. The calculations also included cumulative energy expenditure in plant production and processing into biofuel. Cumulative energy intensity included in the test procedures and processing into biofuel was calculated from the relationship:

$$E_{pro} = E_{mat} + E_{agr} + E_{pal} + E_r + E_{prz}, \quad (2)$$

[MJ·ha<sup>-1</sup>]

where:

- $E_{pro}$  – cumulative energy consumption in the production of biofuels [MJ·ha<sup>-1</sup>],
- $E_{mat}$  – cumulative energy contained in the materials and raw materials [MJ·ha<sup>-1</sup>],
- $E_{agr}$  – cumulative energy contained in the machines and tools [MJ·ha<sup>-1</sup>],
- $E_{pal}$  – cumulative energy contained in the fuel [MJ·ha<sup>-1</sup>],
- $E_r$  – the energy accumulated in the human labour [MJ·ha<sup>-1</sup>],
- $E_{prz}$  – the energy accumulated in the technology of processing yield into biofuel [MJ·ha<sup>-1</sup>].

The energy indicators used for technological processes in processing agricultural raw materials into biofuels, were taken from foreign and national literature [Mokrzycki 2005,

Richards 2000], and energy efficiency was calculated from the relationship:

$$W_{ee} = \frac{W_{prz}}{W_{pro}}, \quad (3)$$

where:

- $W_{ee}$  – energy efficiency of the tested technology,
- $W_{pro}$  – energy inputs accumulated in the production and processing the yield into biofuel [MJ·ha<sup>-1</sup>],
- $W_{prz}$  – cumulative energy contained in biofuel and the rest of biomass [MJ·ha<sup>-1</sup>].

## Results and Discussion

By analysing the total costs of production of winter wheat and winter rape (Table 1), it can be concluded that the costs of winter rape production are 3.8% lower than the cost of production of winter wheat. In the case of winter rape they amounted 2164.2 PLN·ha<sup>-1</sup>, and for winter wheat production 2246.5 PLN·ha<sup>-1</sup>. The cost of materials and raw materials and the maintenance costs of machinery and tools (together with the cost of harvesting straw) are the highest in the structure of the costs of production. In the case of rape production the costs of materials and raw materials amounted to 1180.9 PLN·ha<sup>-1</sup>, i.e. 54.57 %, while wheat production amounted to 1458.5 PLN·ha<sup>-1</sup>, constituting 64.92 % of the total cost of production.

The prominent position was also occupied by the operating costs of machinery and tools, which amounted to 726.5 PLN·ha<sup>-1</sup> (33.57 %) for winter rape and 522.5 PLN·ha<sup>-1</sup> (23.26 %) for wheat production. If we consider the operating costs of machinery and tools used in the particular procedures, it can be concluded that in the production of winter rape the highest costs were related to agriculture. They amounted to 255.2 PLN·ha<sup>-1</sup> (35.13 %), and with the harvest – 239.1 PLN·ha<sup>-1</sup> (32.91 %). It was different in case of winter wheat production. The highest costs concern harvesting wheat - 210.2 PLN·ha<sup>-1</sup> (40.23 %) - and tillage – 145.5 PLN·ha<sup>-1</sup> (27.85 %). The coefficient of economic efficiency of the analyzed technologies amounted to 1.60 for winter rape and 1.90 for winter wheat.

Table 1 – The costs of production of winter wheat and rape in the tested technologies

Description	Winter rape		Winter wheat	
	PLN·ha <sup>-1</sup>	%	PLN·ha <sup>-1</sup>	%
Cost of the operation of machinery and tools without fuel costs and human labour	726.5	33.57	522.5	23.26
Fuel costs	221.6	10.24	235.2	10.47
Cost of human labour	35.2	1.63	30.30	1.35
Cost of materials and raw materials	1180.9	54.57	1458.5	64.92
Total cost	2164.2		2246.5	
Economic efficiency in crop production	1.60		1.09	

Source: Author's calculations

Table 2 – The costs of production and processing yield of winter wheat and rape into bioethanol and biodiesel

LNo.	Description	Biodiesel	Bioethanol
		PLN·ha <sup>-1</sup>	PLN·ha <sup>-1</sup>
1	The costs of crop production	2164	2246
2	The costs of processing into biofuel	3255	4505
3	Total cost (item 1 + item 2)	5419	6751
4	The value of biofuels	5419	6751
5	The value of straw	465	466
6	The value of post-extractive residues	2150	–
7	Total income (item 4 + item 5 + item 6)	8034	7217
8	Economic efficiency of biofuel production (item 7/ item 3)	1.48	1.07

Source: Author's calculation

While processing the obtained crops into biofuels (biodiesel and bioethanol) additional costs, which very significantly decrease the efficiency of their production, are beared. The cost of processing rape into esters was 3255 PLN·ha<sup>-1</sup> and was 50.4 % higher than the cost of production of winter rape seeds (2164.2 PLN·ha<sup>-1</sup>). In case of bioethanol production the cost of processing was higher; it amounted to 4505 PLN·ha<sup>-1</sup> and was about 100.5 % higher than the production of wheat (2246.5 PLN·ha<sup>-1</sup>). Economic efficiency of biodiesel production amounted to 1.48, which indicates the profitability of production, and in case of bioethanol this value was 1.08. It means that the production of biodiesel was profitable, and the production of bioethanol is on the verge of viability (table 2). By analysing the percentage of the cost production of biodiesel and bioethanol (fig. 1) we can conclude that processing of raw material into biofuel (66.7% – bioethanol and 60.1% – biodiesel) is characterized by the highest costs, and human work (0.5% - bioethanol and 0.7% – biodiesel) by the lowest.

On the basis of the analysis of energy inputs accumulated in the evaluated crop production technologies we can conclude that the costs of production of winter wheat were higher – 41012 MJ·ha<sup>-1</sup>, which was 23.4% higher than the energy inputs accumulated in the production of winter rape – 33239 MJ·ha<sup>-1</sup>. In the structure of the energy inputs accumulated, materials and raw materials have the largest share, and the human labour the smallest (table 3). In winter wheat production energy inputs accumulated in materials and raw materials amounted to 30452 MJ·ha<sup>-1</sup>, which constitutes 41.4% of total expenditures, while in the winter rape production 22931 MJ·ha<sup>-1</sup>, i.e. 46.8%. While considering the cumulative energy expenditure on machinery and tools used in crop production we can conclude that tillage is characterized by the greatest energy intensity, which in the case of wheat is 2124 MJ·ha<sup>-1</sup>, which constitutes 145.3% of energy contained in machines and tools, and in case of rape 2282 MJ·ha<sup>-1</sup>, i.e. 149.2 %.

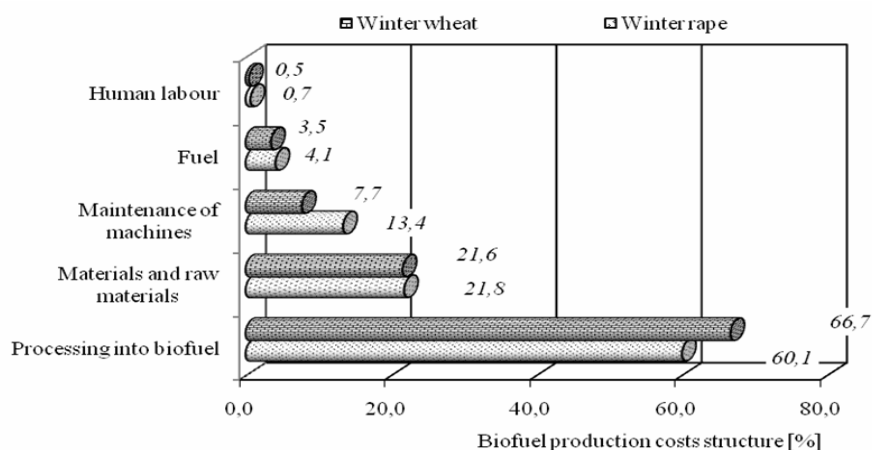


Fig. 1 – The cost structure of biodiesel and bioethanol

In terms of the energy inputs accumulated, the second position is occupied by the harvest. In case of winter wheat it is  $1723 \text{ MJ}\cdot\text{ha}^{-1}$  (33.06 %), and in case of rape –  $1645 \text{ MJ}\cdot\text{ha}^{-1}$  (28.92 %). The energy efficiency coefficient in winter wheat production technology was 1.22, while in winter rape production technology 1.43 (table 3). The structure of cost production of biofuels is shown in fig. 1.

To sum up, it can be concluded that the higher energy efficiency coefficient was obtained in the production of biodiesel from rape (2.41) rather than in the production of bioethanol from wheat (1.72). In analyzed technologies of winter

rape production and processing the crop into biodiesel the cumulative energy consumption amounted to  $46620 \text{ MJ}\cdot\text{ha}^{-1}$  (31.7% of the energy), i.e.  $14798 \text{ MJ}\cdot\text{ha}^{-1}$  is contained in the one processed into liquid biofuel.

On the other hand, in the production of bioethanol from winter wheat, in the considered technology in winter wheat production, the cumulative energy consumption was 56.9% higher than the energy intensity of production of biodiesel – it reached  $71063 \text{ MJ}\cdot\text{ha}^{-1}$ , of which  $41012 \text{ MJ}\cdot\text{ha}^{-1}$  (57.7 %) fell to wheat production, and  $32886 \text{ MJ}\cdot\text{ha}^{-1}$  (47 %) – to its processing into bioethanol.

Table 3 – The cumulative energy inputs of production of winter wheat and winter rape in crop production

The cumulative energy inputs	Winter rape	Winter wheat
	$\text{MJ}\cdot\text{ha}^{-1}$	$\text{MJ}\cdot\text{ha}^{-1}$
Machines and tools without fuel and human labour	5688	5211
Fuel	4169	5082
Human labour	451	267
Materials and raw materials	22931	30452
Total cumulative energy inputs	33239	41012
Energy efficiency in crop production	1.43	1.22

Source: Author's calculations

Table 4 – The energy balance of production and processing yield of winter wheat and rape for biofuels

Description	Rzepak ozimy	Pszenica ozima
	$\text{MJ}\cdot\text{ha}^{-1}$	$\text{MJ}\cdot\text{ha}^{-1}$
The energy content per production of biofuels	48037	71063
The energy content	46620	43884
The energy content of straw	68250	92400
The energy content of post- extractive residues	1117	–
Energy value obtained after processing	115987	136284
Energy efficiency ratio of biofuel production	2.41	1.92
Yield net energy	67950	65221

Source: Author's calculations

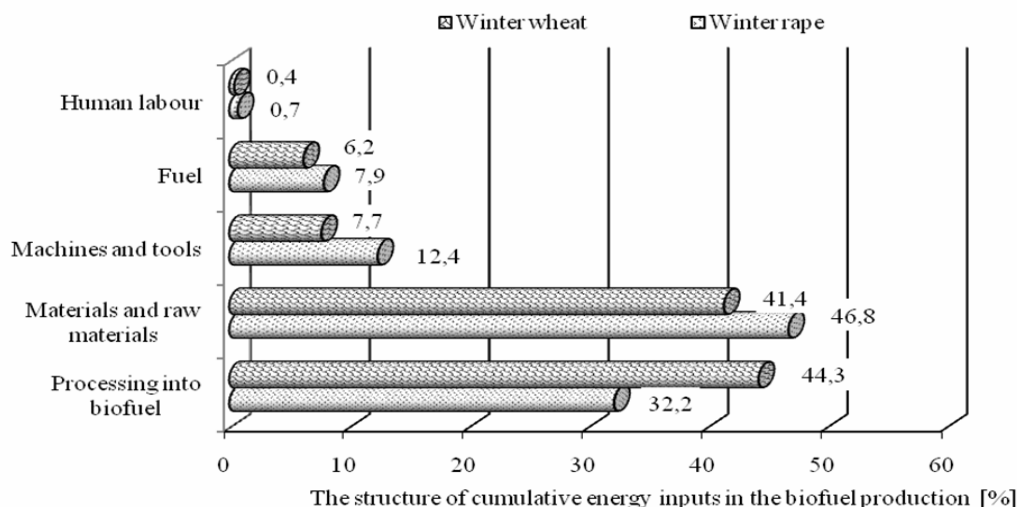


Fig. 2 – The structure of cumulative energy inputs in the production of biodiesel and bioethanol

By converting the products obtained per unit of energy, we can conclude that the yield net energy of biodiesel production amounted to  $67950 \text{ MJ}\cdot\text{ha}^{-1}$ , and the production of bioethanol  $65221 \text{ MJ}\cdot\text{ha}^{-1}$ , which means that less expenditure incurred in its production than it was recovered in the form of biofuels produced (table 4). The cumulative energy structure contained in biodiesel and bioethanol are presented in fig. 2.

By analysing the percentage of cumulative energy inputs in the production of biofuels in the structure (fig. 2) we can conclude that the process of biofuel processing has the largest share – 44.3% for bioethanol and 32.2% for biodiesel as well as materials and raw materials accordingly 41.4% and 46.8%. The lowest cumulative energy expenditures were included in human labour (0.4% bioethanol and 0.7% biodiesel).

### Conclusions

1. The study shows that biodiesel production can be profitable, provided that not only biofuels but also straw and post extractive residues are sold. This also applies to the energy efficiency of biodiesel production.
2. On the basis of the results, we can conclude that the production of biodiesel from winter rape (efficiency ratio 2.41) and bioethanol from winter wheat is profitable (efficiency ratio 1.92).
3. On the basis of the research, we can conclude that the yield net energy for biodiesel production amounted to  $67950$

$\text{MJ}\cdot\text{ha}^{-1}$ , while for the production of bioethanol  $65221 \text{ MJ}\cdot\text{ha}^{-1}$  – if we assume the use of straw and post extractive residues in case of rape.

*This work was supported by Research Project of the Ministry of Education of the CR no. MSM 6046070905.*

### References

- [1] Anuszewski R., Pawlak J., Wójcicki Z.: *Energochłonność produkcji rolniczej. Metodyka badań energochłonności produkcji surowców żywnościowych.* Wydaw. IBMER, Warszawa, 1979.
- [2] Mokrzycki E. i zespół.: *Podstawy gospodarki surowcami energetycznymi.* Wydawnictwo Naukowo-Dydaktyczne AGH Kraków, 2005.
- [3] Muzalewski A.: *Koszty eksploatacji maszyn.* Wydaw. IBMER, Warszawa, 2005.
- [4] Richards I.R.: *Energy balances in the growth of oilseed rape for biodiesel and of wheat for bioethanol.* Levington Agriculture Report, BABFO, 2000.
- [5] Wójcicki Z.: *Wposażenie i nakłady materiałowo energetyczne w rozwojowych gospodarstwach rolniczych.* Wydaw. IBMER, Warszawa, 2002.



## THE ANALYSIS OF THE DEVELOPMENT OF TRANSPORT IN AGRICULTURE

FRANTIŠEK DVOŘÁK, FRANTIŠEK LACHNIT

Czech University of Life Sciences Prague, Faculty of Engineering,

Department of Vehicles and Ground Transport,

165 21 Praha 6 –Suchbát, Czech Republic

Phone: +420 224 383 114, E-mail: [dvorak@tf.czu.cz](mailto:dvorak@tf.czu.cz)

Phone: +420 224 383 102, E-mail: [lachnit@tf.czu.cz](mailto:lachnit@tf.czu.cz)

### Abstract

Development of agriculture transport, specifics of agriculture transport, transported materials, properties and classification of materials, handling equipment, technical equipment of transportation and transport processes, loading operations, weights and weighing, towing vehicles, trailers and semitrailers, vehicle components, evaluation of vehicles and handling equipments, performance parameters for transport and handling equipments, new transport systems, monitoring and control of transport processes, environmental aspects of development of transport and traffic engineering, development prognosis of transport technologies and related techniques.

**Keywords:** transport, handling equipment, vehicle, agriculture

### 1. Introduction

Transport is the sum of activities by which the movement of means of transport on routes is executed, aimed at moving things by means of transport or facilities.

Transport logistics is a tool for optimization and cost reduction, organization, planning and management of material flows in order to meet all the requirements at minimum costs and expenses. Transport logistic co-ordinates, synchronizes and optimizes the material flow through the transport network. It is a spatial distribution, capacity and movements of all vehicles and equipment whose cooperation is necessary for the transportation. It is necessary for achieving a high-quality, reliable and fast transportation in the branch of material transportation.

### 2. The structure of agricultural transportation and transported materials

In agriculture, many kinds of materials are transported. These materials have different physical and mechanical properties that affect the transportation process. The main part of material is of biological origin and there are specific requirements for the transport of live animals. A significant part of materials consist of living organisms, these are sensitive to high or low temperatures, shocks, etc.

Generally it is possible to say that the agricultural materials have lower bulk density. The choice, respectively construction of transport and handling equipment must be adapted to this fact. Table 1 shows the bulk densities of some agricultural and non-agricultural materials.

Table 1: Bulk density of some materials [11]

Material	Bulk density [kg . m <sup>-3</sup> ]	Material	Bulk density [kg . m <sup>-3</sup> ]
Grains	400 – 850	Timber	300 - 600
Root-crops	560 -820	Coal/coke/ briquettes	380 - 1500
Straw, hay	20 – 90	Clay, soil	1000 - 1800
Straw, hay, pressed	110 - 250	Sand	1250 - 1700
Manure, compost	700 -1000	Gravel	1500 - 2000
Mineral fertilizers	700 - 1450	Stone	2200 - 2700



### 3. Selection and dimensioning of means, equipments and systems

The prerequisite for selecting the optimal mean, machinery or system is knowledge of relations, properties of transported and handled materials, the frequency of operations, performance, number of different kinds of materials and the total amount of materials, topology of roads, and various travel restrictions, frequency of warehouse operations, etc. Dimensioning can be understood as the assessment of the main technical parameters in order to meet the required performance parameters.

The total circulation time of a mean of transport is characterized by the full working cycle. This consists of the main time, when the vehicle performs work for which it is intended, and of the lateral time, which is characterized by regular and irregular activities, which may also be repeated, such as the loading operations, and enable the execution of the main time. Load weight in [t]. (Eq. 1, 2)

$$G = V \cdot \rho_v \cdot k_1 [t] \quad (1)$$

$$G = N \cdot k_2 [t] \quad (2)$$

$G$  – load weight, t

$N$  – load capacity, respectively effective load, t

$V$  – loading volume of the vehicle, m<sup>3</sup>

$k_1$  – coefficient of utilization of loading capacity,

$\rho_v$  – density of load, t . m<sup>-3</sup>

$k_2$  - coefficient of utilization of capacity.

### 4. Transport means, category and classification of vehicles

For agricultural transport there are used utility/freight trucks of different types, different load capacity, with various truck superstructures and various special equipment, wheeled tractors as towing vehicle of trailers and semi trailers and self-propelled road trains.

The categorization of transport means for freight transport can be classified according to the method of practising loading operations, by method of loading, unloading and reloading, into the transport means operated during loading operations by separate handling facilities and equipment, or loaded and unloaded manually, and self-service vehicles that are adjusted to autonomous implementation of the loading

operations i.e. they have additional devices for loading operations.

Utility vehicles can be divided by the total capacity into categories: up to 3.5 tonnes, from 3.5 to 7.5 tonnes, over 7.5 tonnes and special vehicles. Other classification is: single-function, multi-purpose, special and towing vehicle.

Special purpose vehicle means many variants of layout of a utility vehicle. Usually it is a specially modified truck with a specific superstructure, with a technological equipment e.g. tanker. Some special vehicles are not intended for use on public traffic roads.

Trailers and semi-trailers are one-axle and multi-axle. Multi-axle trailers and semi-trailers have some advantages such as increased capacity and more equally distributed load on the frame. If the spacing between the axles is larger, there is a requirement to steer the rear-wheel or whole rear-axles, steered rear-wheels or rear-axles are the furthest away from the towing vehicle. The tractor trailer use tandem axle which usually are not unsprung, contribute to a more uniform load of wheels, easily equalize small roughnesses of the track and provide a good lateral stability.

Container system is characterized among others by the fact that the servicing is realized out by one person, and container handling is quick and easy. The high variability in container design allows short-term storage too.

The swap body system is designed to transport by lorries resp. universal carrier with whose undercarriages are compatible. The advantage is the separation of loading and unloading of vehicle from the own loading and unloading of the swap body. It significantly increases the time-usage of vehicles. One vehicle can use a large number of swap bodies, both universal or special.

### 5. Transport of live animals and legislation

Legislation related to the protection of animals during transport and the related activities is very extensive. In recent years the monitoring and ensuring the conditions of animal welfare is considerable. For welfare is considered a balanced state where the animal is able to cope without problems by its own forces the exposure to the environment.

Transport of animals can be divided according to whether it is made in connection

with economic activity, then we talk about non-commercial transport, or if it is made without regard to economic activity, then we talk about commercial transport. For commercial transport of animals there are different conditions for the transport to 50 km, from 50 to 65 km and over 65 km, and for the duration of transport to 8 hours and over 8 hours.

Transport means, containers, cages, etc. must be constructed so as to ensure sufficient space for the animal standing in a natural position, and adequate ventilation must be maintained and operated so as to avoid injury and suffering of animals, and ensure the safety of the animals. It must also protect animals against unfriendly weather, high and low temperatures, etc. It must not allow the escape or falling out of animals, and must allow enduring the stress of the vehicle movement. Table 2 shows the minimum floor area for the transport of animals.

Table 2: Minimum floor area for the transport of animals [12]

Animal category	Animal weight, kg	Minimum floor area per one animal, m <sup>2</sup>
Adult cattle	325 – 700	0,95 – 1,60
Calves	50 – 200	0,30 – 0,95
Sheep	55	0,20 – 0,50
Goats	35 – 55	0,20 – 0,50

During transport of pigs the stocking density should not exceed 235 kg . m<sup>-2</sup>. During transport of poultry, the area is of 105-200 cm<sup>2</sup> on 1 kg, for one day old chicken the area is 21-25 cm<sup>2</sup>. During transport of horses the floor area is of 1.75 m<sup>2</sup> per horse, stall dimensions 0.7 x 2.5 m.

In the case of transport of horses for competitions, races, cultural events and for breeding, there may be different variations, which may be contrary to the normal provisions.

## 6. Loading operations and handling equipments and facilities

Works connected with loading, unloading and reloading of materials are collectively called the loading operations. These can be time-consuming, so it is important to pay attention to the implementation of these operations and the selection of equipment that carry them out. These devices can be divided into equipment operating cyclically and equipment operating continuously. Equipment operating continuously may be with

continuous stream of material or pulsating stream of material. Using various types of equipment depends on the nature of the manipulated material. Time duration of loading of the vehicle in [min.]. (Eq. 3)

$$T_n = t_{po} + (60 \cdot G / Q) + t_{zo} \text{ [min.]} \quad (3)$$

G – load weight, t

t<sub>po</sub> – time for preparatory operations, min.

t<sub>zo</sub> – time needed for finishing operations, min.

Q – performance of loading equipment, t . h<sup>-1</sup>, m<sup>3</sup>.h<sup>-1</sup>

The way of solving of loading operations, in particular loading, affects the efficiency of the transport process. In agriculture, it is influenced above all by the specifics of agricultural transport, especially including a large number of loading operations, which are executed at various places, various physical, chemical and biological properties of materials. Some of the loading operation which are executed in the ground space and in some cases under unfavourable conditions.

It is important to compliance of prescript for loading of vehicles and to know behaviour of load. There is a load of loading area, N. m<sup>-2</sup>, total weight, kg weight per axle, kg, uniform distribution of weight load on the whole surface of the vehicle centre of gravity of the load should be placed as low as possible and in the middle in the longitudinal direction of the vehicle.

## 7. Transport means, packing, weighing, and automatic identification

The implementation of transport means into the handling system requires creating of a comprehensive system of technical, organizational and other arrangements. Among the transport means we include storage boxes, crates, bulk bags, pallets, containers and swap bodies.

Packing helps to create handling or transport unit. Cover usually performs several functions simultaneously. Sizes of packing abide by standards, which guarantee the continuity of dimensions of different types of packaging.

Normalization of dimensions across the packaging sequence is very important. Technical standardization introduces the relationship of technical and technological systems. Its result is a unification, standardization and specialization

ensuring the desired state, i.e. finding the optimal dependency, their harmonization and enactment.

Weighing in business admits error specified by national standards. Weighing in technological processes follows the corporate resp. industry standards, which are a matter of users and operators.

Mobile weighing systems, respectively dynamic weighing of actual load of loaders or handling trucks speeds up working process, and prevents erroneous loading and downtimes, because there is no need to use the bridge weight. By weighing systems can be equipped utility vehicles, trailers, semi-trailers etc.

Electronic evaluation and control systems of weigh and software are still more extensive and more comfortable. This allows entry into the logistics business and technological processes, increases productivity, allows the creation of efficient logistic processes and better conditions for the organization and management.

Development in the identification of objects aims to automatic identification. Optical automatic identification systems include bar codes, EAN - European Article Number system has become the standards, the most commonly used are EAN 8, EAN 13, EAN 128. RFID - Radio Frequency Identification are based on radio transmission of information between the receiver / transmitter and the object resp. handling unit which is located on an identification tag. There is used either passive identification tag, which only transmits the recorded data, or an active identification tag that is capable of changing the data i.e. receive, transmit, store and modify. It is a rapidly evolving technology.

## 8. Monitoring and control of transport processes

Hardware and configuration for operational monitoring of vehicles are different depending on whether the transfer of information is required in real time, resp. on-line resp. active, or it is enough doses data collection and their transport after a certain off-line resp. passive period. Passive vehicle monitoring systems operate similarly as a "black box". Active vehicle monitoring systems monitor vehicles in real time. It is a direct continuous transmission of the obtained data to the control resp. dispatcher position.

In agricultural transport are likely to come to the application the systems for vehicle monitoring. These systems provide excellent and by operator unaffected information about utilization of traffic techniques and also checking of its using, resp. their utilization. Beside the perfect records of the activities of transport technology it provides monitoring of operating parameters, including data about cost of operation. In case of break down the records in the memory of the vehicle unit can be checked and the cause of failure can be diagnosed. In some cases, there is no need of the service engineer departure, because according to the instructions the driver can remove the problem.

## 9. Evaluation of vehicles, transport efficiency and transport costs

Beside the specific technical parameters and design there exist criteria for evaluation of the performance, the economic suitability or their combination, which have special significance.

Specific weight of the vehicle is the ratio of useful load of vehicle and the vehicle's own weight,  $t \cdot t^{-1}$ , the specific engine power is the ratio of engine power and vehicle gross vehicle weight,  $kW \cdot t^{-1}$ , resp. the ratio of the load on the driving axles which is the ratio of the load on the driving axles and the total load on all axles.

Performance reflects the amount of material transported per unit of time by the individual means of transportation in weight,  $t \cdot h^{-1}$ ,  $t \cdot d^{-1}$ , volume,  $m^3 \cdot h^{-1}$ ,  $m^3 \cdot d^{-1}$ , the number of units or pieces,  $pcs \cdot h^{-1}$ ,  $pcs \cdot d^{-1}$  etc.

Transport process can be evaluated by quantitative indicators such as the transportation output,  $t \cdot km \cdot h^{-1}$ ,  $t \cdot km \cdot d^{-1}$ , productivity of labour,  $h \cdot t^{-1}$ ,  $h \cdot m^{-3}$ ,  $h \cdot d^{-1}$ , or by qualitative indicators such as the coefficient of utilization of runs, coefficient of the use of load factor, coefficient of downtime, the coefficient of utilization of loading capacity, etc.

For economic proposal of transport there can be used unit transportation costs,

$CZK \cdot t^{-1}$ ,  $CZK \cdot m^{-3}$ ,  $CZK \cdot km^{-1}$ ,  $CZK \cdot t \cdot km^{-1}$ . In the agricultural company, where the transportation distance is usually the same, the comparison and evaluation is then easy.

## 10. Conclusion

Presuppositions for optimal organization of the transport process are important among others, knowledge of the structure of transport, of properties of transported materials and the timing of the transportation, transport distances, the requirements of suppliers and consumers resp. receivers.

On the transport process participate transport means resp. transport units, as well as equipment designed for operations as loading, unloading and reloading equipment and facilities. The loading operation should be solved in relation to the mode of transport, type and material properties, method of packaging and the local conditions of loading and unloading.

## References

- [1] Syrový, O., a kolektiv: Doprava v zemědělství. Profi Press s.r.o., Praha, 2008, ISBN 978-80- 86726-30-4.
- [2] Gerndtová, I., Syrový, O., Bartolomějev, A.: Analýza dopravy v zemědělství České republiky. Profi Press s.r.o., Praha, Mechanizace zemědělství, 6, 2007, s. 36 – 42, ISSN 0373-6776.
- [3] Jeřábek, K.: Stroje a zařízení pro manipulaci. ČVUT, Praha, 1989, ISBN N.
- [4] Bartolomějev, A.: Zemědělství a logistika. Profi Press s.r.o., Praha, Mechanizace zemědělství, 6, 2008, s. 46 – 50, ISSN 0373-6776.
- [5] Cempírek, V., Pivoňka, K., Široký, J.: Základy technologie a řízení dopravy. Univerzita Pardubice, Pardubice, 2002, ISBN 80-7194-471-8.
- [6] Svoboda, V., Latýn, P.: Logistika. ČVUT, Praha, 2003, ISBN 80-01-02735-X.
- [7] Pernis, P.: Traktorová doprava v teorii. Profi Press s.r.o., Praha, Mechanizace zemědělství, 11, 2008, s. 60 – 65, ISSN 0373-6776.
- [8] Stehno, L.: Traktorová doprava v praxi. Profi Press s.r.o., Praha, Mechanizace zemědělství, 6, 2005, s. 46 – 47, ISSN 0373-6776.
- [9] Vlk, F.: Stavba motorových vozidel. Nakl. Vlk, Brno, 2003, ISBN 80-238-8757-2.
- [10] Jílek, L., Pražan, R., Gerndtová, I.: Využití výkonu motoru a spotřeba paliva v dopravě. Profi Press s.r.o., Praha, Mechanizace zemědělství, 6, 2007, s. 56 – 59, ISSN 0373-6776.
- [11] Syrový, O., a kol.: Racionalizace manipulace s materiálem v zemědělství. SZN, Praha, 1983, ISSN N.
- [12] Ustanovení §4 vyhlášky č. 4/2009 Sb., o ochraně zvířat při přepravě.
- [13] Company publications and web pages of manufacturers and dealers of transport means, tractors, handling equipment and devices, information techniques and technology in ground transport, magazines and relating regulations of transport and archives of the authors.

## DIFFERENTIAL MODEL OF SUMMER CIRCULATION

ŠÁRKA DVOŘÁKOVÁ<sup>1\*</sup>, JOSEF ZEMAN<sup>2</sup>

<sup>1</sup>Czech University of Life Science Prague, Faculty of Engineering, Department of Mathematics, Kamýcká 129, 165 21 Prague 6 – Suchbát, Czech Republic,  
e-mail: dvorakovas@tf.czu.cz

<sup>2</sup>Czech University of Life Science Prague, Faculty of Engineering, Department of Physics

### Abstract

The aim of this article is an attempt to build a linear differential behavior model of Teplý potok during the dry season [2]. We present the first approach to description the dynamics of this flow, which is broadly consistent with reality. The main deviation is due to the assumption harmonically changing evaporation.

Experiments show that the behavior of water levels of unregulated sets of flow show in the summer period without rain some interesting similarities [1]. In a specific transitional period in a certain part of the day always occurs due to evaporation and respiration inhibition of one component of total flow. It is a component of nearsurface water. At night there is again an irrigation of surface layer and its contribution to the flow is evident [4]. Periods of total inhibition of this flow component is increasing day by day until it disappear completely [3].

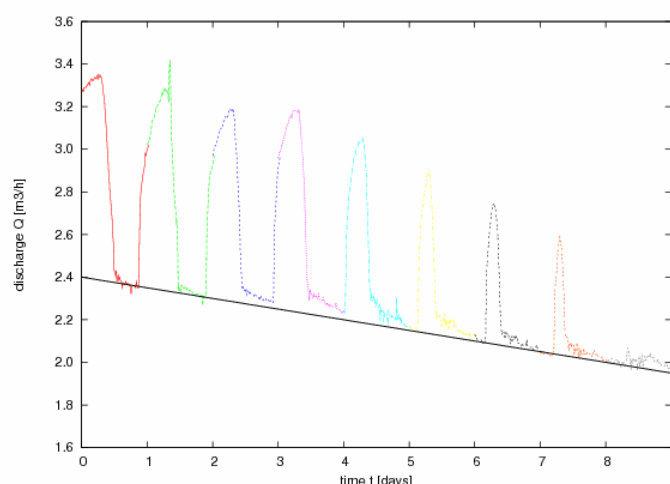


Fig. 1: Progression of water level in Teplý potok throughout the dry season 1.-9.8.2003, indicating an overall trend of decreasing levels.

We have compiled a set of linear differential equations of the 1<sup>st</sup> order to explore the dynamics of stream flow during the dry season. The structure of these equations corresponds to the idea of the overall stream flow is made up of contributions of groundwater, subsurface water and nearsurface water. During the summer drought is the only source of water reservoir of ground water. It supplies the watercourse directly and also part of the stream goes into the subsurface structure and from there by the capillary action to the nearsurface layer. From experiment implies, that we know the overall

time process of the sum of all layers contributions. The second water consumer forming the right side of third equation is the evaporation, which we try to estimate from the water vapour pressure and dew point, because during our experiments was measured both barometric pressure and humidity and temperature of the ground-level air. By fitting equations we conclude that it is necessary for satisfactory correlation to establish a respiratory parameter  $i_e$ , which indicates the water consumption of vegetation in the basin depending on the lighting.

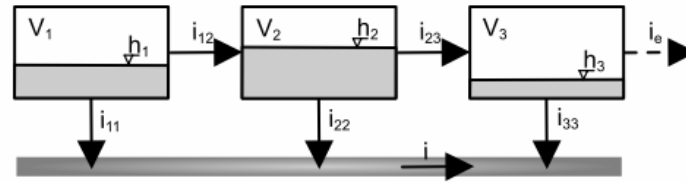


Fig. 2: Model scheme of small flow

$$i = i_{11} + i_{22} + i_{33}$$

$$i_{11} = h_1 \cdot a_{11} = 0$$

$$i_{22} = h_2 \cdot a_{22}$$

$$i_{33} = h_3 \cdot a_{33}$$

$$i_{12} = (h_1 - h_2) \cdot a_{12}$$

$$i_{23} = (h_2 - h_3) \cdot a_{23}$$

$$i_e = \beta \cdot (\sin(\omega t) + 1)$$

$\beta$  ... evaporating coefficient

$i_e$  ... evapotranspiration

Let A is a matrix with coefficients  $a_{11} \dots a_{33}$ , where:

$a_{11}$  .... groundwater runoff into the flow

$a_{22}$  .... runoff from the subsurface layer to the flow

$a_{33}$  .... runoff from the nearsurface layer to the flow

In the matrix we consider (except of diagonal)  $a_{ij} = a_{ji}$

$a_{12}$  ... runoff from the ground layer to the subsurface layer

$a_{13}$  ... equals 0, because the ground water doesn't flow directly to the nearsurface layer

$a_{23}$  ... runoff from the subsurface layer to the nearsurface layer

$V_1$  ... volume of the ground reservoir

$V_2$  ... volume of the subsurface reservoir

$V_3$  ... volume of the nearsurface reservoir

$h_1$  ... water saturation of the ground layer

$h_2$  ... water saturation of the subsurface layer

$h_3$  ... water saturation of the nearsurface layer

$$\frac{dh_1}{dt} = \frac{1}{V_1} (-a_{12} (h_1 - h_2))$$

$$\frac{dh_2}{dt} = \frac{1}{V_2} (a_{12} (h_1 - h_2) - a_{22} h_2 - a_{23} (h_2 - h_3))$$

$$\frac{dh_3}{dt} = \frac{1}{V_3} (a_{23} (h_2 - h_3) - a_{33} h_3)$$

After the breakdown of the coefficients for  $h_1$  to  $h_3$ :

$$\frac{dh_1}{dt} = \frac{1}{V_1} (-a_{12} h_1 + a_{12} h_2)$$

$$\frac{dh_2}{dt} = \frac{1}{V_2} (a_{12} h_1 - (a_{12} + a_{22} + a_{23}) h_2 + a_{23} h_3)$$

$$\frac{dh_3}{dt} = \frac{1}{V_3} (a_{23} h_2 - (a_{23} + a_{33}) h_3)$$

This system can be formally rewritten in the matrix form:

$$\frac{d\vec{h}}{dt} = B\vec{h} \quad (1)$$

Where the matrix B is



$$B = \begin{pmatrix} \frac{-a_{12}}{V_1} & \frac{a_{12}}{V_1} & 0 \\ \frac{a_{12}}{V_2} & \frac{-(a_{12} + a_{22} + a_{23})}{V_2} & \frac{a_{23}}{V_2} \\ 0 & \frac{a_{23}}{V_3} & \frac{-(a_{23} + a_{33})}{V_3} \end{pmatrix}$$

Equation (1) is a linear differential matrix equation with zero right side, for which we calculate eigenvalues  $\lambda_1$  to  $\lambda_3$ . General solution of this equation may be written assuming that the matrix B is nondegenerate matrix in shape

$$\vec{h}(t) = e^{\lambda_1 t} \vec{a} + e^{\lambda_2 t} \vec{b} + e^{\lambda_3 t} \vec{c}$$

where  $\vec{a}$ ,  $\vec{b}$ ,  $\vec{c}$  are eigenvectors of matrix B.

From the fact, that we know

- a) long-term trend decline of water in the creek,
- b) the total quantity of water flowed out, we can estimate the total capacity of the water reservoir of Teplý potok to  $V_1 = 1.5 \cdot 10^5 \text{ m}^3$ .

This reservoir is currently in drought obviously a source of all spillage and evaporated

water in the system. From the afternoon declines in water level, when the contribution of nearsurface water is already zero, we can estimate the size of the ground water reservoir to  $V_2 = 5000 \text{ m}^3$ .

In the night the surface layer will begin over certain time to deliver water into the stream. Delivery of water from this layer during the night continues to grow. This increase is more gradual. It is possible to estimate its limit value. From the integral of this increase in flow rate can be estimated the volume of nearsurface layer. This estimation is  $V_3 = 150 \text{ m}^3$ .

Similarly we obtain the other coefficients of matrix A, which is then shaped

$$A = \begin{pmatrix} 0 & 100 & 0 \\ 100 & 50 & 300 \\ 0 & 300 & 20 \end{pmatrix}$$

of which the matrix B has an approximate values

$$B = \begin{pmatrix} -6.7 \cdot 10^{-4} & 6.7 \cdot 10^{-4} & 0 \\ 0.02 & -0.63 & 0.06 \\ 0 & 2 & -2.4 \end{pmatrix}$$

Eigenvalues for these coefficients are 3 negative numbers

$$\lambda_1 = -2.46538, \lambda_2 = -0.564641, \lambda_3 = -0.00064687,$$

and the eigenvectors are

$$\vec{v}_1 = (8.88184 \times 10^{-6}, -0.0326734, 0.999466)$$

$$\vec{v}_2 = (-0.000803244, 0.67613, 0.736782)$$

$$\vec{v}_3 = (0.998992, 0.0344873, 0.0287471)$$

And therefore the general solution of homogeneous equation (1) for our concrete case is

$$\vec{h}_0(t) = C_1 e^{-2.465t} \begin{pmatrix} 0.0000088 \\ -0.0327 \\ 0.999 \end{pmatrix} + C_2 e^{-0.565t} \begin{pmatrix} -0.000803 \\ 0.676 \\ 0.737 \end{pmatrix} + C_3 e^{-0.00065t} \begin{pmatrix} 0.999 \\ 0.0345 \\ 0.0287 \end{pmatrix}$$

Now we can proceed to solve equation (1) with nonzero right side. The right side is formed by evaporation. For simplicity we assume that

evaporation is composed by the periodic function of the time independent on the layers hydration.

Evaporation  $O = \beta(\sin \omega t + 1)$ . Equation (1) can be then rewritten in the form

$$\frac{d\vec{h}}{dt} = B\vec{h} + \vec{v} \quad (2)$$

where  $\vec{v} = \begin{pmatrix} 0 \\ 0 \\ \beta(\sin \omega t + 1) \end{pmatrix}$ , because the

evaporation is only made from nearsurface layer not from the subsurface and ground layer. Coefficient  $\beta$  we estimated from the amplitude of daily fluctuation to 20 m<sup>3</sup>/day,  $\omega$  is daily period  $2\pi$ .

Solution of equation (2) we can find as sum of homogeneous solution  $\vec{h}_0(t)$  and solution  $\vec{h}_1(t)$  with right side equal to vector  $\vec{v}$ , tj.  $\vec{H} =$

$\vec{h}_0(t) + \vec{h}_1(t)$ . This solution equals  $\vec{h}_1(t) = U \cdot \int U^{-1} \vec{v}$  and it is possible to solve it analytically. We don't present it, because its written form is too long. Flow discharge we can calculate as dot product of final vector of solution  $\vec{H}$  and vector  $(a_{11}, a_{22}, a_{33})$ .

Sample solution for these fitted coefficients we can see in the fig. 3. By comparing the graphs in fig. 1 and 3 we coming to the view that we have gained a reasonable approximation to description of the Teplý potok arrangement. We assume that a better solution would be created especially by more realistic assumption, when evaporation is directly proportional to the saturation of nearsurface layer. However this assumption leads to a nonlinear equation which is not so easily solved.

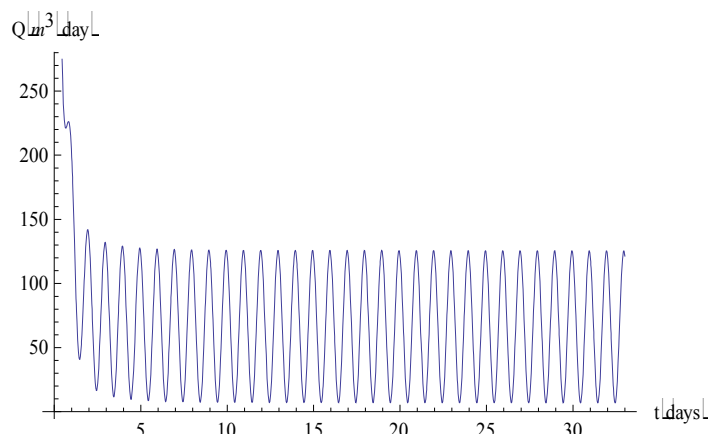


Fig. 3: Model discharge running in time

## CONCLUSION

We were able to build a linear model that describes the state of hydrological basin of Teplý potok during the dry season. This model generally captures the measured history and allows to determine several parameters that characterize the basin, such as throughput and volumes of three different watered layers.

## REFERENCE

- [1] BURT, T.P.: Diurnal variations in stream discharge and throughflow during a period of low flow, *Journal of Hydrology*, vol. 41, issue 3-4, 1979, pp. 291-301
- [2] DVOŘÁKOVÁ, Š: Možnosti využití hydrologických modelů v krajinném inženýrství (Possibilities to use hydrological models in

landscape engineering), (Ph.D. thesis) Fakulta lesnická a environmentální, Česká zemědělská univerzita v Praze, 2005, 162 pp.

- [3] DVOŘÁKOVÁ, Š.- ZEMAN, J.: Analysis of fluctuations in the stream water level during the dry season in forested areas, *Scientia Abriculae Bohemica*, will be printed

- [4] MUL, M.L.- SAVENIJE, H.H.G. – UHLENBROOK, S.: Base flow fluctuations from a forested and a cultivated hill slope in northern Tanzania. Conference proceedings (CD-Rom) of the 8th WATERNET / WARFSA / GWP-SA Symposium, Lusaka, Zambia, 31 Oct – 2 Nov 2007, 9pp

## PERFORMANCE ANALYSIS OF AN OTTO ENGINE WITH ETHANOL AND GASOLINE FUELS

RAHIM EBRAHIMI<sup>1\*</sup>, DAVOUD GHANBARIAN<sup>1</sup>

<sup>1</sup>Department of Agriculture Machine Mechanics, Shahrekord University, P.O. Box 115, Shahrekord, Iran

Fax: +983814424428, E-mail: Rahim.Ebrahimi@gmail.com

### Abstract

Energy conservation and its efficient use are nowadays a major issue. The evident reduction in oil reserves combined with the increase in its price, as well as the need for ‘cleaner’ fuels, have led in the past years to an increasing interest and research in the field of alternative fuels for spark ignition engines propulsion. Also, there are interesting to increase the technical focus on conventional cycles for making them more optimum in terms of performance. In this study, a comparative performance analysis and optimisation have been performed for irreversible Otto cycle with ethanol, methanol and gasoline fuels. The results show that the maximum power output, the working range of the cycle, the optimal power output corresponding to maximum thermal efficiency, the optimal thermal efficiency corresponding to maximum power output increase, the compression ratio at the maximum power output and the compression ratio at the maximum thermal efficiency when ethanol-engine operation is changed to gasoline-engine operation. The results obtained in this work can help us to understand how the power output and thermal efficiency are influenced by ethanol and gasoline fuels in an Otto engine.

**Keywords:** Otto cycle; Optimization; irreversible

### Introduction

Energy conservation and its efficient use are nowadays a major issue. The evident reduction in oil reserves combined with the increase in its price, as well as the need for ‘cleaner’ fuels, have led in the past years to an increasing interest and research in the field of alternative fuels for both compression and spark ignition engines propulsion. The combustion behavior of such alternative fuels is sometimes very interesting as regards either first- or second-law balances.

Since the finite time thermodynamics (FTT) or entropy generation minimization (EGM) was advanced [1–3], much work has been performed for the performance analysis and optimization of finite time processes and finite size devices [4–6]. The FTT performance of Otto cycle has been also analyzed for the power, specific power, efficiency, and ecological optimization objectives with the heat transfer irreversibility and/or internal irreversibilities [11–30].

In this paper we propose a simplified irreversible model for the air standard Otto cycle also in the FTT context. We obtain a maximization of power output and thermal efficiency, in terms of the compression ratio. Moreover, the effects of ethanol, methanol and

gasoline fuels on the irreversible cycle performance are analyzed.

### Performance Optimization for an Otto Cycle

$T$ - $S$  diagrams of a standard irreversible Otto cycle with air is shown in Fig. 1. In the  $T$ - $S$  diagram, the process 1–2 is an isentropic compression. The heat addition occurs in the constant volume process 2–3. Process 3–4 is an isentropic expansion. A constant volume heat rejection process, 4–1, completes the cycle. The heat added to the working fluid during the process 2 → 3 is

$$\dot{Q}_{in} = \dot{Q}_{23} = \dot{m}_t c_v (T_3 - T_2) \quad (1)$$

where  $m_t$  is the mass of air–fuel mixture inducted into the cylinder per cycle,  $c_v$  is specific heat at constant volume for the working fluid and  $T$  is the absolute temperature.

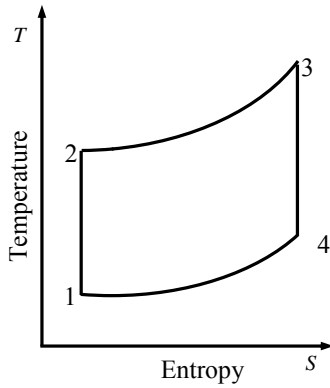


Fig. 1.  $T - S$  diagram for the air standard Otto cycle

The total energy of the fuel per second input into the engine can be given by [7]:

$$Q_{fuel} = \eta_{com} \dot{m}_f Q_{LHV} \quad (2)$$

where  $\dot{m}_f$  is the mass flow rate of the fuel,  $\eta_{com}$  is the combustion efficiency and  $Q_{LHV}$  is the lower calorific value of the fuel.

The heat loss through the cylinder wall is given in the following linear expression [8, 9]

$$Q_{ht} = \dot{m}_t B (T_2 + T_3) \quad (3)$$

where  $B$  is constant.

Since the total energy of the delivered fuel  $Q_{fuel}$  is assumed to be the sum of the heat added to the working fluid  $Q_{in}$  and the heat leakage

$Q_{ht}$ ,

$$Q_{in} = Q_{fuel} - Q_{ht} = \eta_{com} \dot{m}_f Q_{LHV} - \dot{m}_t B (T_2 + T_3) \quad (4)$$

The intake system -the air filter, carburetor, and throttle plate, intake manifold, intake port, intake valve- restricts the amount of air which an engine of given displacement can induct. The parameter used to measure the effectiveness of an engine's induction process is the volumetric efficiency. It is defined as the volume flow rate of air into the intake system divided by the rate at which volume is displaced by the piston [7]:

$$\eta_v = \frac{2\dot{m}_a}{\rho_{air} V_d N} \quad (5)$$

Where  $\eta_v$  is the volumetric efficiency,  $\rho_{air}$  is the inlet air density,  $V_d$  is the displacement volume,  $N$  is the engine speed.

The relations between  $\eta_v$  and  $\dot{m}_f$ , between  $\eta_v$  and  $\dot{m}_t$  are defined as [7]:

$$\dot{m}_f = \frac{\eta_v \rho_{air} V_d N \phi}{2(m_a/m_f)_s} \quad (6)$$

and

$$\dot{m}_t = \frac{\eta_v \rho_{air} V_d N}{2} \left( 1 + \frac{\phi}{(m_a/m_f)_s} \right) \quad (7)$$

Where  $\phi$  is the equivalence ratio and  $m_a/m_f$  is the air-fuel ratio and the subscript  $s$  denotes stoichiometric conditions.

The compression ratio,  $r_c$ , is defined as:

$$r_c = V_1/V_2 \quad (8)$$

For the processes  $1 \rightarrow 2$  and  $3 \rightarrow 4$ , one has

$$T_2 = T_1 r_c^{\gamma-1} \quad (9)$$

and

$$T_4 = T_3 r_c^{1-\gamma} \quad (10)$$

Combining equations (1), (4), (6) and (9) gives:

$$T_3 = \frac{\frac{\eta_{com} Q_{LHV} \phi}{(m_a/m_f)_s} + (c_v + B) T_1 r_c^{\gamma-1}}{c_v + B} \quad (11)$$

Substituting equation (11) into equation (10) yields:

$$T_4 = \frac{\frac{\eta_{com} Q_{LHV} \phi r_c^{1-\gamma}}{(m_a/m_f)_s} + (c_v + B) T_1}{c_v + B} \quad (12)$$

Every time the piston moves, friction acts to retard the motion. Considering the friction effects on the piston in all the processes of the cycle, we assume a dissipation term represented by a friction force ( $f_\mu$ ) that is linearly proportional to the velocity of the piston [9–10], which can be written as follows:

$$f_{\mu} = -\mu v = -\mu \frac{dx}{dt} \quad (13)$$

where  $\mu$  is the coefficient of friction, which takes into account the global losses on the power output,  $x$  is the piston's displacement and  $v$  is the piston's velocity. Therefore, the power lost due to friction is

$$P_{fri} = f_{\mu} v = -\mu \left( \frac{dx}{dt} \right)^2 = -\mu v^2 \quad (14)$$

For a four stroke cycle engine, the total distance the piston travels per cycle is

$$P_{otto} = Q_{in} - Q_{out} - P_{fri} = \frac{\eta_v \rho_{air} V_d N c_v}{2} \left( 1 + \frac{\phi}{(m_a/m_f)_s} \right) \left[ T_1 - T_1 r_c^{\gamma-1} + \left( \frac{\frac{\eta_{com} Q_{LHV} \phi}{(m_a/m_f)_s} + (c_v + B) T_1 r_c^{\gamma-1}}{c_v + B} \right) (1 - r_c^{1-\gamma}) - 16\mu [N x_2 (r_c - 1)]^2 \right] \quad (17)$$

The thermal efficiency of the Otto cycle engine is expressed by

$$\eta_{th} = P_{otto} / Q_{in} \quad (18)$$

where  $Q_{in}$  is:

$$Q_{in} = \dot{m}_t c_v (T_3 - T_2) = \frac{\eta_v \rho_{air} V_d N c_v}{2} \left( 1 + \frac{\phi}{(m_a/m_f)_s} \right) \left( \frac{\frac{\eta_{com} Q_{LHV} \phi}{(m_a/m_f)_s} + (c_v + B) T_1 r_c^{\gamma-1}}{c_v + B} - T_1 r_c^{\gamma-1} \right) \quad (19)$$

Notice that both power and efficiency are convex functions of the compression ratio.

### Numerical examples and discussions

As it can be clearly seen from Eqs. (18) and (19), the thermal efficiency and the power output of the Otto cycle are dependent on the volumetric efficiency. In order to illustrate the effect of this parameter, the relations between the power

$$4L = 4(x_1 - x_2) = 4x_2 (x_1/x_2 - 1) = 4x_2 (r_c - 1) \quad (15)$$

where  $x_1$  and  $x_2$  are the piston's position corresponding to the maximum and minimum volume, respectively, and  $L$  is the stroke of the piston. Running at  $N$  cycles per second, the mean velocity of the piston is

$$\bar{v} = 4LN \quad (16)$$

Assuming an ideal, non-reacting gas with specific heat, the net actual power output of the Otto cycle engine can be written as:

output and the compression ratio, and the optimal relation between power output and the efficiency of the cycles presented in figures 2–3. The values of the constants and the parameters used in this example are summarized in Table 1.

**Table 1**

Constants and parameters used in the numerical example [[11-14]

lower heating value of the gasoline	44000 $\text{kJ kg}^{-1}$
lower heating value of the ethanol	26900 $\text{kJ kg}^{-1}$
volume displacement	6360 $\text{mm}^3$
constant related to heat transfer	0.65 $\text{kJ kg}^{-1}\text{K}^{-1}$
air–gasoline ratio at stoichiometric conditions	14.6
air–ethanol ratio at stoichiometric conditions	9
engine speed	3000 $\text{rpm}$
compression ratio	1 → 27
intake temperature	350 $\text{K}$
combustion efficiency	100%
volumetric efficiency	100%
specific heat ratio	1.4
equivalence ratio	1

Figures 2-3 show the effect of the fuel on the cycle performance with heat resistance and friction losses. From these figures, it can be found that the fuel property plays important roles on the performance of the Otto engine. It is clearly seen that the effects of fuel property on the performance of the cycle is related to compression ratio. They reflect the performance characteristics of a real irreversible Otto cycle engine. The power output versus compression ratio characteristic and the thermal efficiency versus compression ratio characteristic are approximately parabolic like curves. It shows that the maximum power output point and the maximum efficiency point are very adjacent. It should be noted that the heat added and the heat rejected by the working fluid increase as ethanol-engine operation is changed to gasoline-engine operation. heat rejected by the working fluid increase as ethanol-engine operation is changed to gasoline-engine operation. It can also be seen that the curves of power output versus thermal efficiency are loop shaped.

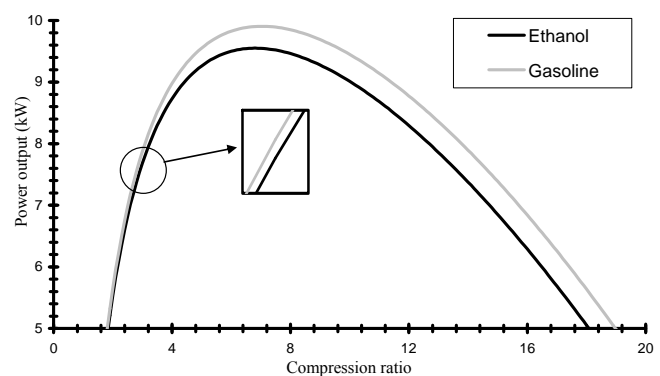


Fig. 2. Effects of ethanol and gasoline fuels on the variation of the power output with compression ratio

Referring to Figs. 2 and 3, it can be concluded that, throughout the compression ratio range, the power output and thermal efficiency for ethanol-engine operation is less than that for gasoline-engine operation. The results show that the maximum power output, the working range of the cycle, the optimal power output corresponding to maximum thermal efficiency, the optimal thermal efficiency corresponding to maximum power output, the compression ratio at the maximum power output and the compression ratio at the maximum thermal efficiency increase about 4.2%, 3.3%, 4.4%, 1.2%, 3.4% and 2.3%, respectively, when ethanol-engine operation is changed to gasoline-engine operation.



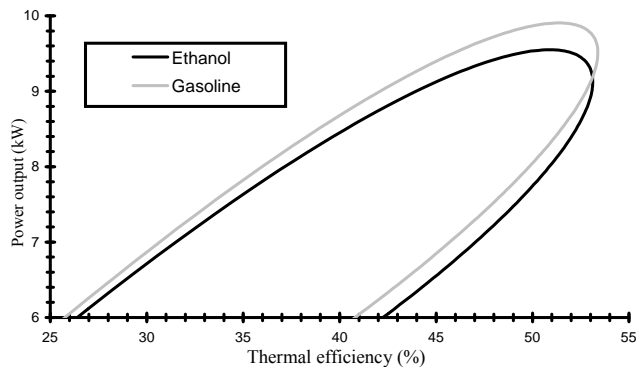


Fig. 3. Effects of ethanol and gasoline fuels on the variation of the power output with thermal efficiency

### Conclusion

In this paper, the effects of ethanol, methanol and gasoline fuels on the performance of an Otto cycle during the finite time are investigated. The general conclusions drawn from the results of this work are as follows:

- Throughout the compression ratio range, the power output and thermal efficiency increase when ethanol-engine operation is changed to gasoline-engine operation.
- The maximum power output, the working range of the cycle, the optimal power output corresponding to maximum thermal efficiency, the optimal thermal efficiency corresponding to maximum power output, the compression ratio at the maximum power output and the compression ratio at the maximum thermal efficiency increase when ethanol-engine operation is changed to gasoline-engine operation.

The results of this investigation are of importance when considering the designs of actual Otto engines with ethanol and gasoline fuels.

### References

[1] Chen L, Ge Y, Sun F. Unified thermodynamic description and optimization for a class of irreversible reciprocating heat engine cycles. *Proc IMechE Part D: J Automobile Engineering* 2008;222:1489-1500.  
[2] Chen L, Sun F, Wu C. The optimal performance of an irreversible Dual-cycle. *Applied Energy* 2004;79(1):3-14.

[3] Ebrahimi R. Effects of cut-off ratio on performance of an irreversible Dual cycle. *Journal of American Science* 2009a;5(3):83-90.  
[4] Ebrahimi R. Thermodynamic simulation of performance of an endoreversible Dual cycle with variable specific heat ratio of working fluid. *Journal of American Science* 2009b;5(5):175-180.  
[5] Mozurkewich M, Berry R. Optimal paths for thermodynamic systems: the ideal Otto cycle. *J Appl Phys* 1982;53(1):34-42.  
[6] Ebrahimi R. Effects of gasoline-air equivalence ratio on performance of an Otto engine, *Journal of American Science* 2010a;6(2):131-135.  
[7] J.B. Heywood, *Internal Combustion Engine Fundamentals*, Mc-Graw Hill Book Company, New York, 1988.  
[8] Chen, L., F. Zeng, Sun, F., Wu, C., 1996. Heat-transfer effects on net work and/or power as functions of efficiency for air-standard diesel cycles. *Energy*, 21(12): 1201-1205.  
[9] Angulo-Brown, F., Fernandez-Betanzos, J., Diaz-Pico, C.A., 1994. Compression Ratio of an Optimized Air Standard Otto Cycle Model. *Eur. J. Phys.*, 15:38-42.  
[10] Ge, Y., Chen, L., Sun, F., Wu, C., 2005. Thermodynamic simulation of performance of an Otto cycle with heat transfer and variable specific heats for the working fluid. *Int. J. Therm. Sci.*, 44(5):506-11.  
[11] Ge, Y., Chen, L., Sun, F., Wu, C., 2005. The effects of variable specific-heats of the working fluid on the performance of an irreversible Otto cycle. *Int. J. Exergy*, 2(3):274-83.  
[12] Y. Ge, L. Chen, F. Sun, Finite time thermodynamic modeling and analysis of an irreversible Otto cycle, *Applied Energy*, 85 (2008) 618-624.  
[13] Y. Ge, L. Chen, F. Sun, Finite time thermodynamic modeling and analysis for an irreversible Dual cycle, *Mathematical and Computer Modeling*, 50(2009) 101-108.  
[14] Parlak A, Sahin B. Performance optimization of reciprocating heat engine cycles with internal irreversibility. *J. Energy Inst.*, 2006;79(4):241-245.

## COLLECTION OF BEVERAGE CANS IN CZECH REPUBLIC - IMPLEMENTATION AND PRACTICE

JAN FICHTNER, MIROSLAV ANDRT

Czech University of Life Sciences, 16521 Prague 6 – Suchbát, Czech Republic

Phone: +420777108742, E-mail: fichtner@email.cz

### Abstract

Collection and recycling of aluminum packaging cans isn't solved today in Czech Republic. Last few decenniums the beverage consumption of this type of packaging had been dynamically increased. While in neighbours countries is that types very popular and its consumption is very high, in Czech Republic consumers are still "introducing" with the type of packages. But beverage cans hide huge potential in CZ. Low packaging weight and its "storage property" are more and more popular and consumption is rising every year. Implementation of beverage cans collection system into communal collection system has to be set up for easy recycling. The article reflects the current situation and answer to real future possibilities of improvement. For oncoming time is clear that recycling of beverage aluminum cans has to be solved that will be on the other hand economically acceptably.

### 1. Introduction

#### Beverages cans – undervalued waste commodity

Consumption of beverage packaging cans had been dynamically increased during last few decenniums. While in countries like Great Britain and Sweden is that beverage packages type very popular and its consumption is very high, in Czech Republic consumers are still "introducing" with this. It is by virtue of tradition of Czech market which was strongly oriented to backup glass packages. In this market a different type of packaging is looking forward itself consumers very slowly. But beverage cans hide huge potential in CZ. Low packaging weight and its "storage property" are more and more popular and consumption is rising every year. Increase of consumption of these packages is given in addition to this packaging replaced glass and PET bottles as well as how they are preferred especially by young consumers.

If we are engaged in packaging beverage cans, it is certain that it is an aluminum material. Therefore, in this article we will indicate the short name "ALU cans". This metal is a commodity in terms of recycling and purchase price very interesting. Just as the consumption of drinks in ALU cans is important for the food industry, this consumption is also important for waste management. ALU cans for waste management are an important feature. It is not a returnable cover. For this reason, each tin drinking drinks ends up in waste containers. The

question is whether the container is used for its collection, or for mixed municipal wastes.

Currently, the CR collection of beverage cans is not solved. The separate collection is secured by an authorized company EKO-KOM, which is part of the international systems of packaging, and which holds the license for granting the brand of "green dot", recommends on its official website [www.jaktridit.cz](http://www.jaktridit.cz) only that ALU cans should be in larger number handle to collection points for discarded scrapyard or household waste. The only collective system EKO-KOM, which ensures the management of packaging waste in the CR and is paid by manufacturers and distributors, in essence encourages waste ALU cans throw into the communal waste. Ordinary citizens and households are governed by instructions and throw aluminum cans into the communal waste. This is because there is not other choice, because the separate collection is not organized in the Czech.

### 2. Methods

#### Experimental collection of aluminum cans

In order to determine the potential of the waste collection it was needed an experimental collection. The test collection should provide basic information about the commodity beverage cans and the experience could be subsequently developed a plan for a mass gathering in the entire country.

The test collection was carried out in an industrial manufacturing company. The choice of

collection sites - a factory was given that the conditions for testing such a collection are ideal. Key benefits for the trial collection of aluminum cans in the factory are three:

1. within an industrial enterprise, which already runs a separate collection of recyclable classic ingredients - such as paper, plastics (PET bottles), glass is possible with the introduction of separate collection of waste other commodities watch how it changes the composition of mixed communal waste,
2. specific for this collection of that waste producers (employees) can not use any alternative disposal and all the produced waste, which is thrown into a limited number of waste containers can be uniquely identified,
3. the possibility of ensuring full awareness of waste producers (employees) how to separate waste – for example racing radio campaign supported training of established type of waste sorting and waste management.

Collection was made at the factory located in Ústí region, which is certified to system ISO 14001 and is an integrated IPPC permit holder. Manufacturing plant has 1,200 employees globally, equivalent to a population of larger village.

Collection containers for beverage ALU cans were in factory placed in a total of 12 major collection points, where it can be assumed the greatest occurrence of this waste (1 piece on each of five changing rooms for workers, 2 pieces at

the offices for technician staff, 1 piece in the smoking rooms, 1pc in the dining room, while the remaining 3 pieces in stock).

Employees had been informed of the change in the system of waste sorting and trained on the need to sort the cans separately.

Experimental collection covered the period from March 1st until June 30th 2009. It was divided into two stages. In the first phase of collection was assessed for the period from March 1st to March 31st. During this period, was introducing a collection and selected spring month in terms of annual average consumption of beverages periods (e.g. over the summer months). By that was eliminated the statistical measurement distortion of output. The second stage was evaluated over a period of 4 months.

Result of collection, together with the volume size of packaged beverages and consider the average weight of the package is shown in T 01.

In the segregated waste containers were found cans of various drinks. It was therefore carried out additional allocation of cans, depending on what type of beverage come. Additional division was introduced, inter alia, because in the factory can be purchased non-alcoholic beer and it is assumed that the normal municipal waste will occur of an alcoholic beer, which will be represented in the same volume. Distribution of origin of packaging waste is given in T 02.

### 3. Results and discussion

#### *Weight of packages*

*T - 01*

Type of packages	Measured tare weight [g]	Average weight [g]
0,25l	11,7 – 13,6	13
0,33l	15,6 – 16,4	16
0,50l	17,0 – 19,2	17,5

#### *Distribution of origin of the collected packaging waste*

*T - 02*

Type of packages 0,25l, 0,33l		Type of packages 0,5l	
The total number of cans	740 pcs.	The total number of cans	194 pcs.
<i>from that kind of drinks</i>		<i>from that kind of drinks</i>	
Customary lemonade drink	488 pcs.	Customary lemonade drink	30 pcs.
Energy drink	208 pcs.	Energy drink	132 pcs.
Non-alcoholic beer	16 pcs.	Non-alcoholic beer	31 pcs.
Instant Iced Coffee	27 pcs.	Instant Iced Coffee	0 pcs.
Other drinks	1 pcs.	Other drinks	1 pcs.

### Results of experimental collection of ALU cans

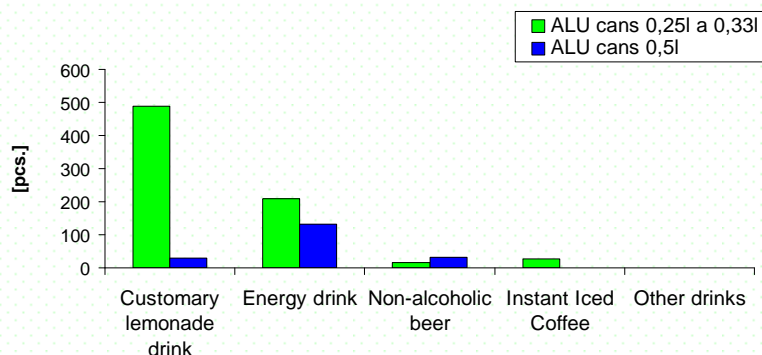


**Chart 1 Results of experimental collection of ALU cans**

The results of the experimental collection of waste collected ALU cans in the factory according to the origin beverages is shown in Chart 1.

From the results we see that the most significant part of the waste is from packaging lemonade drinks. Surprisingly it was found that the second most represented group is the packing energy drinks. Beverage packages of beer are represented only in third place.

Based on the measurement results we can conclude that the popular energy drinks are the consumers preferred the modern consumer packaging cans. On the contrary - the classic product of beer consumption is operated through the far glass bottles. And this consumption of beer in cans is estimated by European association

of manufacturers of cans BCME just will grow in the CZ.

During evaluated period of 4 months was generally collected 68 kilograms ALU cans (see T 03). Average monthly amount is graded 17 kg. It is obvious that the introduction of the collection over in March, when the collection reached the level of 13.2 kg, the collection points are more often used by factory staff and the collection is on very good organizational level.

According to measurement results is clearly that the collection has a good result. If we take into account that the consumption of beverage cans in the CR is low, then such a collection is successful. From the results we can estimate that each employee per month consumed an average of 1 drink packaged in a can 0,25 l.

#### Total volume of collected waste

#### T - 03

Period	1.3.2009 – 31.3.2009 (1 <sup>st</sup> month)	1.3.2009 – 30.6.2009 (4 months)
Number of employees	1200	1200
Total weight of waste	13,2kg	68kg
Performance of collection	0,011kg.person <sup>-1</sup> .month <sup>-1</sup>	0,014kg. person <sup>-1</sup> .month <sup>-1</sup>

#### Pressing or treading on? Cost savings of recovery system

One of the major cost components of ensuring the collection of sorted municipal waste is transport. Transport is not only in waste management, today big troubles. Transportation cost is one of the most challenging processes of each production and currently on this factor has not influence only the price of fuel, which was compared with those of recent years bear the higher excise taxes, but it is also necessary to

consider the additional burden of supporting legal fees carriers must pay, and which is obviously reflected in the price of transportation (tolls, road taxes, etc.)

In the area of waste management and recycling material is then understandable that it is necessary to find ways to minimize transportation costs. So it is the case of ALU collecting cans.

The experimental collection have been cans before putting into the collection bin pressed,

then were placed in plastic bags and PE taken to the terminal for further processing. Pressing waste is minimizing the amount of savings on transport.

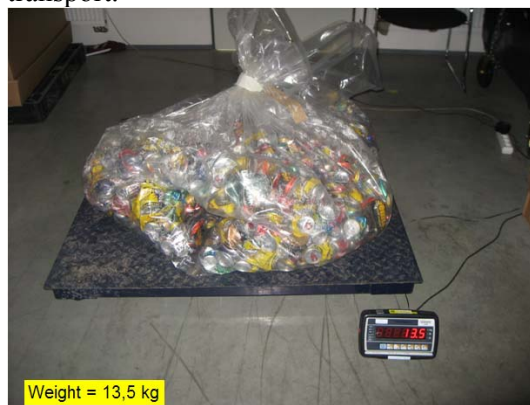


**Figure 1** Weighing of compressed ALU cans

Manual machine was used for pressing which reduce the volume of waste. For the collection of aluminum cans can not be assumed that these manual press commonly used by citizens and that the press was equipped with every household. It was therefore necessary to measure the reduction of waste crushing embrace of the manual press, and pressing the so-called normal form of the street - for the purposes of article entitled "tread on". Measurements were performed for two types of cans - volume of 0.25 liters and 0.5 liters Cans those volumes were measured and found that their dimensions are

standardized. Photo documentation, including size cans is shown in Figure 2.

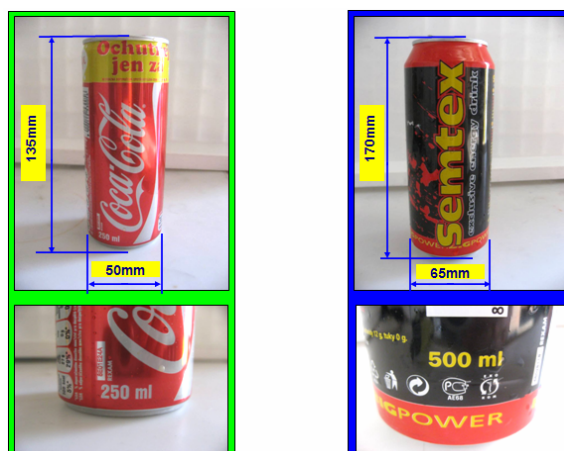


**Figure 2** Dimensions can of 0.25 liters and 0.5

The first of all cans were subjected to mechanical pressing with hand tool. Minimum height of compressed cans is 30mm. While aluminum cans volume 0.25 l was compressed into a compact symmetrical shape, canister volume of 0.5 l was pressed into the press shape letter "Z". The height of the two cans was extruded 30mm. Photo documentation pressing cans on hand tool press is shown in Figure 2.



**Figure 3** Hand tool manual pressing of ALU cans 0.25 liters and 0.5 liters



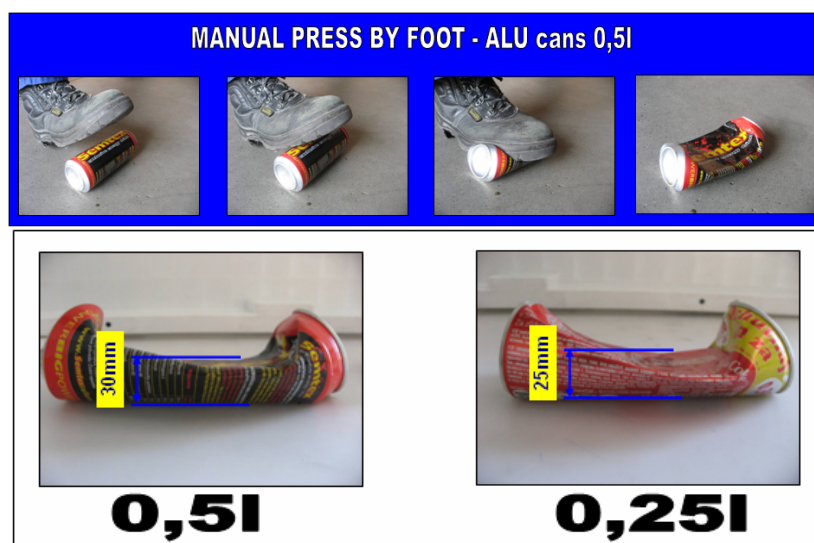


Figure 4 "Treading on" pressing of ALU cans 0,25l a 0,5l

#### Volume savings by pressing

T - 04

Volume of drink [l]	The original volume of cans [l]	Hand tool manual press		Treading on press	
		Volume [l]	Reduction [%]	Volume [l]	Reduction [%]
0,5	0,57	0,1	20	0,15	30
0,25	0,27	0,06	24	0,1	40

The next step was measured by treading on pressing. This pressing will be the most practical and therefore will be interesting to see how much the resulting compressed can and whether and how much this can save a collection volume of waste containers, respectively the cost of transportation. Photo documentation "treading on" pressing cans are presented in Figure 3, including the typical shape of compressed cans.

Volume savings by pressing is given in T 04.

Conclusions from measurements suggest that the use of hand press, the final value of compression is 20-24%. When pressing 's method "treading on" is possible when a common practice to achieve 30% compression of the volume of beverage cans 0.5 l and 40% for beverage cans in the volume of 0,25 l. Treading on pressing method can be considered efficient, because the volume of waste savings far exceeds 50%. By using this method - ie if householders will tread on pressing the ALU cans, we can save the collection operation up to 60% of the cost of transport. I think it is sufficient. Therefore, I suggest "tread on press method" as an effective tool for saving transport costs

#### Approximations of the growth of packaging waste cans

According to statistics from beverage manufacturers who use ALU cans as packaging, consumption of beverages sold in packages ALU cans grows. According to the Czech Beer and Malt Association in the first half of 2009, the proportion of beer sold in cans filled to the domestic market increased from last year's 1.7 percent to 2.3 percent (Source: [www.financninoviny.cz](http://www.financninoviny.cz)). The proportion of beer sold in cans is yet to Slovak Republic compared to fourfold. In neighboring countries, then the cans are sold a significant share of beer packaging - already mentioned in the UK are selling the cans 69 percent, in Poland and Hungary 47 percent.

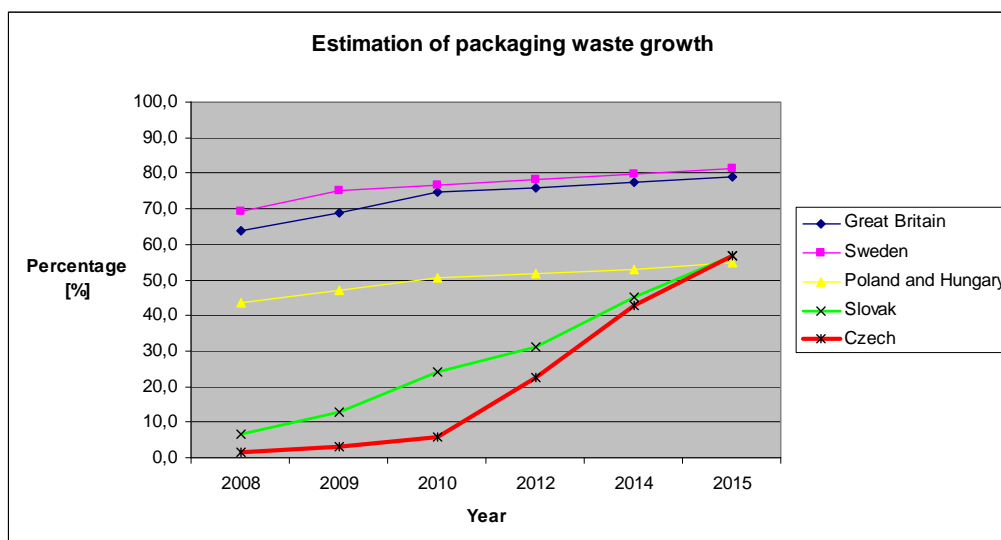
Overall, while market cans in Europe recorded an increase. As stated in the European Association of manufacturers of beverage cans (BCME = Beverage Can Makers Europe) Europe-wide increase is compared with last year at 8%, in the Czech and the Slovak Republic is 28%. Hence, the separate collection system of the ALU cans has the high future potential.

Estimate growth in consumption of drinks in cans was approximated by a trial within the



meaning of expected consumption, which was estimated at 75% level reported in the neighboring eastern European countries - Poland

and Hungary. Theoretical increasing trend is shown in the chart.



According to our estimation of packaging waste growth is evident that in 2015 the consumption of packaging ALU cans, we mean the production of waste, about 20 times current levels by 2009. Just in terms of beer packaged in cans, its consumption in 2015 is comparable with the countries Slovakia, Poland and Hungary, and will exceed 50% of the total sales of beer in the country.

### Estimate and calculate the volume of the collection in the CZ

To design a system of separate collection of cans in the CZ in the collection of sorted municipal waste components will need to know at least approximate the flow of waste, especially after the mass volume. Therefore, estimates the mass flow of waste.

Mass flow in 2015 was estimated based on the results of the experimental collection. The basic parameter of the distribution by type of beverage containers, were obtained from measurements. These data were estimated increase in the volume of packaging for different types of beverage containers in particular. This method was chosen because the increase will be different for each drink. For example, it is not expected that an increased consumption of energy drinks (growth factor 1), beer cans on the other hand, expects a steady increase up to twenty times the current state (growth rate 20). The total estimated increase in weight of waste, including an increase rates is given in T 05. For small packages of beer and instant iced coffee drinks was the anticipated volume of 0.33 l.

### Estimation of the increase beverage cans - by type of drink

**T - 05**

Year	2009		Growth factor	2015	
Type of packages	0,25l, 0,33l	0,5l		0,25l, 0,33l	0,5l
Total weight of cans	9,749kg	3,395kg		41,730kg	15,820kg
from that kind of drinks					
Customary lemonade drink	6,344kg	0,525kg	5	31,720kg	2,625kg
Energy drink	2,704kg	2,310kg	1	2,704kg	2,310kg
Non-alcoholic beer	0,256kg	0,542kg	20	5,120kg	10,850kg
Instant Iced Coffee	0,432kg	0kg	5	2,160kg	0kg
Other drinks	0,013kg	0,017kg	2	0,026kg	0,035kg

**The total mass flow of waste in the CR in 2015**

**T - 06**

Period	2009 1 month	2015 1 month	2015 1 month	2015 yearly
Numbers of inhabitant	1200	1200	all ČR <sup>1)</sup>	all CZ <sup>1)</sup>
Total weight of waste	13,2kg	57,5kg	503t	6036t

1) number of inhabitants (population) in Czech Republic is considered 10489183 person (source: ČSÚ, accessed on June 30, 2009)

From the Table 5 is clearly that the total mass of beverage cans waste, produced by the number of 1200 people, is 57.5 kg. Absolute growth rate of the waste can then be expressed as the percentage of waste 57.5 kg/13, 2 kg. Absolute growth rate is 4.35.

The total mass flow of waste is given in T 06. For purposes of summarizing the designation "employees" of T 03, who participated in the pilot project, changed the designation of "inhabitants".

#### 4. Conclusion

Collecting aluminum cans is worthwhile. Although today is the consumption of drinks in cans only in size, we need to start collecting now. Consumers must "learn" that the ALU can be one of the components collected, sorted municipal waste and must be sorted. Aluminium as a metal, it is certainly interesting for waste management commodity, and therefore will be no problem for subsequent application in the recycling loop. On a large scale we can talk about a certain return and weight of waste to be produced in 2015 (about 6000 tons of aluminum) is an emphatic argument for the initiation of a national collection.

#### Reference:

- [1] Market Reports 2008 – Europe, BCME (Beverage Can Makers Europe), 2009, Bruxelles, Belgium
- [2] ČTK, Spotřeba alkoholu v ČR roste, [online] Available from: <http://www.financninoviny.cz> Access: 31.12.2008,
- [3] Český statistický úřad, Bilance počtu obyvatel ke dni 30.9.2009. Praha, 2009.
- [4] Firemní literatura PEPSI, 2009. [online] Available from: <http://www.pepsico.com/index.html> Access: 14.9.2009
- [5] Článek „Zvyšuje se podíl piva prodaného v plechovkách“, časopis Podnikatel.cz, Praha, 2008. [online] Available from: <http://www.podnikatel.cz/aktuality/zvysuje-se-podil-piva-prodaneho-v-plechovkach/>. Access: 8.9.2008.

## EFFECTS OF CONTROLLED TRAFFIC FARMING

JANA GALAMBOŠOVÁ\*, VLADIMÍR RATAJ, MICHAL VAŠEK

Slovak University of Agriculture in Nitra, 949 76 Nitra, Slovak Republic,

Phone: +421 37 6414344, Fax: +421 37 7417003, E-mail: jana.galambosova@uniag.sk

Slovak University of Agriculture in Nitra

### Abstract

Controlled traffic farming (CTF) confines soil compaction to wheel tracks and maximize the remaining undamaged soil area for cropping. In practice it means matching machinery tracks so they take up the least possible area. The main reasons of applying this technology is improvement of soil quality and better crop growth and so improve the economic efficiency of crop production.

Experiments were conducted at University farm in Koliňany in fields growing spring barley followed by oil seed rape. To compare effects of controlled and random traffic farming the penetration resistance of soil was measured. Trafficked area and non trafficked area was assessed at two monitoring points representing controlled trafficked system and random trafficked system respectively. After the first year of CTF implementation the increase of soil compaction at non trafficked areas was lower for controlled traffic farming field compared with random traffic. However, it has to be considered that these are one year results.

In order to estimate the possible economic effects, the cost-benefit analysis was conducted for the area of approximately 715 hectares. Obtained results showed that calculated machinery operating costs would increase of 28.65 €·ha<sup>-1</sup>. However, the saving on used material (chemical, fertilizers etc.) would be 14.09 €·ha<sup>-1</sup>. These are results of small overlaps when using the autopilots compared to overlaps when using the mechanical markers. With the assumption of yield increase, which can be assessed based on published results between 10 – 15%, the returns from crop production increase. The cost-benefit analysis pointed out that the investments connected to this technology causes the negative effect on economics, however, in subsequent years the investment comes to return and later to profit.

**Key words:** controlled traffic farming, soil compaction, economic evaluation, cost-benefit analysis

### Introduction

Soil properties effect the overall crop husbandry efficiency. Soil compaction became one of the most important issues. Its negative effect has been described by many authors. Based on Kobza et al. (2005), it causes lower soil porosity, what means little space for air and water in the soil, which are essential for root growth; also it increases runoff and erosion. One of the possibilities to eliminate soil compaction is technology based on controlled traffic. Controlled traffic farming (CTF) confines soil compaction to narrow strips across the land and maximize the remaining undamaged soil area for cropping. In practice it means matching machinery tracks so they take up the least possible area (Chamen, 2010). This technology has been used mainly in Australia, US, but there is potential of its implementation also in European conditions.

### Materials and methods

To compare effects of controlled and random traffic farming, long term experiment was established in spring 2009. Detailed description is given in Galambošová et al. (2010). Controlled trafficked field and random trafficked field, both with loamy soil, were selected. The “Out track” CTF system was introduced when drilling the spring barley; the crop rotation followed with oil seed rape. In the first year of the system implementation, the penetration resistance (PR) of soil was measured. The measured values were corrected according to soil moisture (Law number 220/2004 of Slovak Collection of Laws). The measurements were conducted in upright way of machine movement along 12 meters (the half of track width) with the spacing of 50 cm in spring and 20 cm in autumn.

Two monitoring points were selected for the detailed measurement, where following areas were evaluated at each monitoring point:

- trafficked area (area of permanent wheel tracks – used for all field operations, area “harvest” used by combine harvester during the spring barley harvest),
- non trafficked area.

In order to assess the perspective of the CTF effect, the cost - benefit analysis was calculated. The methodology of the calculation was based on Nozdrovický et al. (1999) and Rataj (2005). Model of cost and benefit changes was calculated for 6 years and for the area of approximately 715 hectares. These include areas of cereals and oil crops at the University farm. Original (random traffic) and the alternative (controlled traffic) technology was compared. Machinery used for both technologies is given in Table 1.

In terms of costs, CTF technology requires purchase of GPS guidance for the John Deere

8230 and purchase of a new 104 kW tractor with RTK satellite guidance system.

All machinery operations were analysed and the operation costs were calculated. Benefits were calculated with the assumption of 10 % yield increase, what is based on published results (Chamen, 2009). Yield average and average selling prices were used based on the Report on agriculture and food industry of the Ministry of Agriculture SR (2009). The discount factor of 4% was used for the analysis.

### Results and discussion

Results of measurements conducted at the CTF field are given in Figure 1. The PR at trafficked areas was higher than the PR measured at non trafficked areas. The values are similar for both permanent wheel tracks and tracks of harvester. The combine harvester caused higher soil compaction in the lower soil depths.

Table 1 Machinery used for original and alternative technology

<b>Random traffic (Original technology)</b>	<b>Controlled traffic (Alternative technology)</b>
John Deere 8230 + Lemken Rubin 9	John Deere 8230 ( <b>autopilot</b> ) + Lemken Rubin 9
John Deere 8230 + Lemken Sy-kompaktor	John Deere 8230 ( <b>autopilot</b> ) + Lemken Sy-kompaktor
John Deere 8100 + Lemken Solitair 9	<b>Tractor 104 kW (RTK autopilot)</b> + Lemken Solitair 9
New Holland T 6070 + AGRIO NAPA	New Holland T6070 + AGRIO NAPA
John Deere 118	<b>contractor</b>
New Holland T6070 + Amazone ZA-M 1500	New Holland T6070 + Amazone ZA-M 1500
New Holland T6070 + CLAAS Quadrant lis	<b>Tractor 104 kW (RTK autopilot)</b> + CLAAS Quadrant

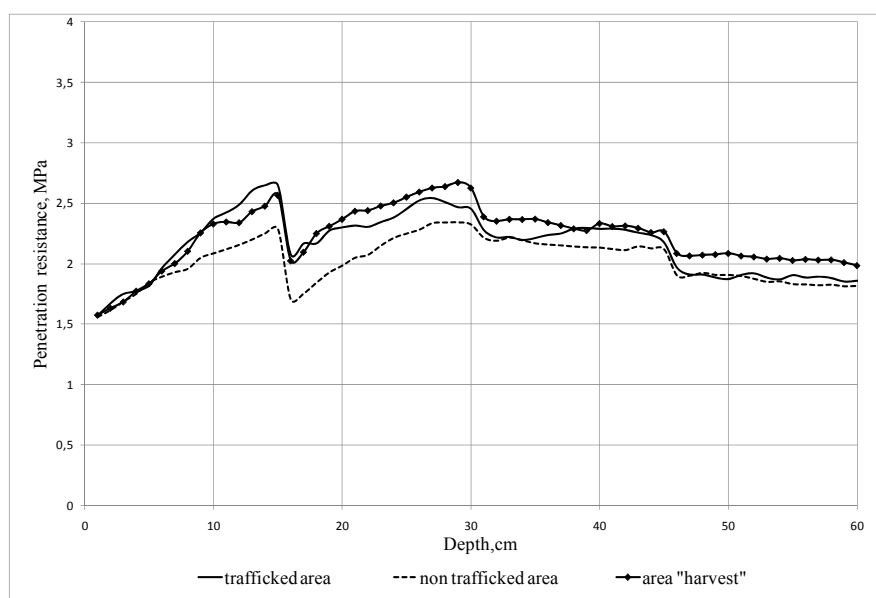


Fig. 1 The average values of the PR in trafficked and non trafficked areas of the CTF field (autumn, 2009)

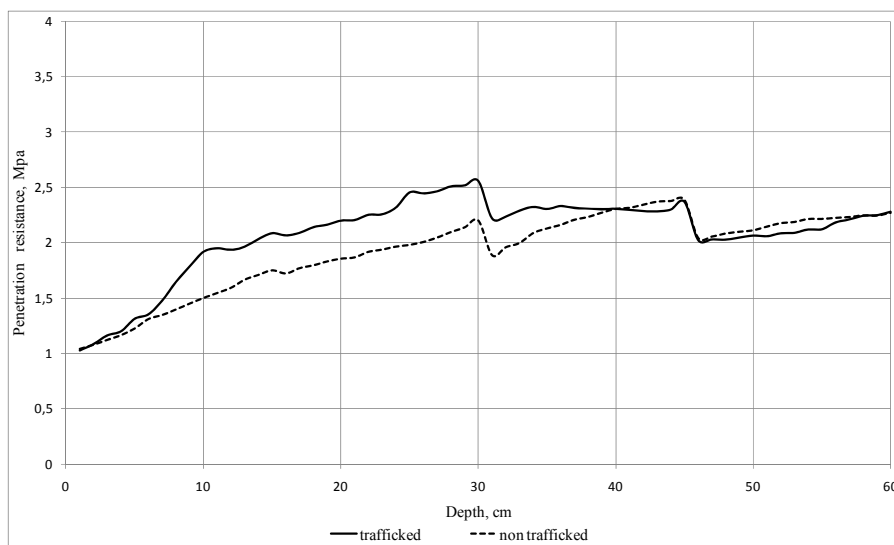


Fig. 2 The average values of the PR in trafficked and non trafficked areas of the random trafficked field (autumn, 2009)

At the random traffic field, the measurements were carried out on the basis of same methodology. Due to the random traffic it was not possible to identify the area “harvest” at this field. Two areas were distinguished – tramlines of oil seed rape crop and non trafficked area. The PR at trafficked area was higher than the PR measured at non trafficked area (Figure 2), as it was expected. The increase of PR in two upper soil depths at both fields demonstrates the effect of machines traffic on soil compaction.

Difference of PR absolute values between fields was not significant.

The effect of the controlled traffic farming system was assessed through the magnitude of soil compaction increase as well. Measurements taken after drilling the spring barley were compared with those from autumn, when oil seed rape was grown. Basic statistics of obtained values is given in Table 2, trafficked and non trafficked areas are not considered in this table.

Table 2 Basic statistic of the PR at both fields and the difference in PR from spring to autumn

Field traffic	Depth, cm	Spring					Autumn					Difference in average, MPa
		Average value, MPa	Standard deviation, MPa	Minimum, MPa	Maximum, MPa	Number of measurements	Average value, MPa	Standard deviation, MPa	Minimum, MPa	Maximum, MPa	Number of measurements	
controlled	1 – 15	1,49	0,20	1,12	1,86	50,00	1,89	0,30	1,35	2,77	129,00	0,40
	16 – 30	1,59	0,36	0,87	2,56	50,00	2,12	0,41	0,93	3,25	129,00	0,53
	31 – 45	1,72	0,26	1,28	2,38	50,00	2,18	0,26	1,57	3,13	129,00	0,46
	46 – 60	2,00	0,23	1,65	2,80	50,00	1,89	0,24	1,09	2,64	129,00	-0,11
random	1 – 15	1,45	0,26	1,05	2,30	40,00	1,46	0,23	1,05	2,17	120,00	0,01
	16 – 30	1,20	0,34	0,57	1,96	40,00	2,02	0,39	1,15	3,23	120,00	0,82
	31 – 45	1,78	0,22	1,17	2,51	40,00	2,28	0,28	1,62	3,24	120,00	0,50
	46 – 60	1,94	0,29	1,27	2,68	40,00	2,25	0,26	1,60	3,35	120,00	0,31

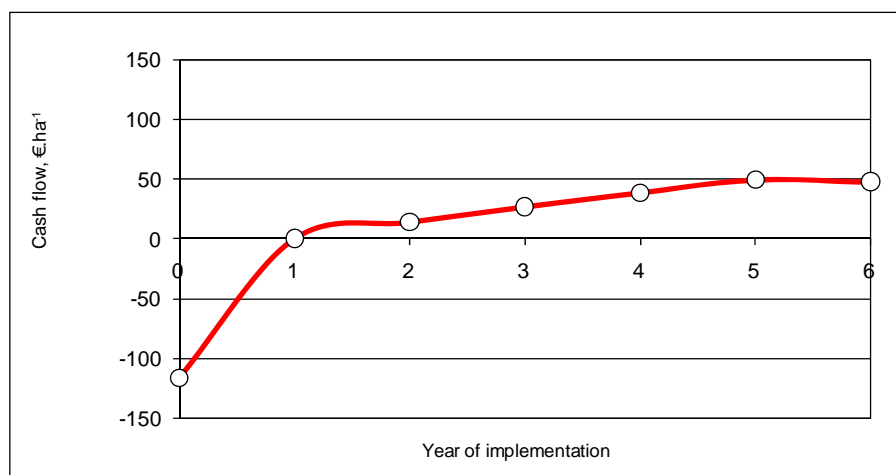
Obtained results showed, that the soil compaction up to 45 cm increased at both fields after one growing season. At the controlled trafficked field, there was determined increase of average PR of 0.4 MPa in the first depth horizon and 0.53 MPa in the second depth horizon. The increase in first depth horizon at the random

trafficked field was negligible. However, the increase in second depth horizon reached the value of 0.82 MPa. After the first year of introducing the CTF system, it can be concluded that the increase of soil compaction in second soil depth was lower compared to random trafficked field.

In order to assess the perspective of this system in terms of economic efficiency the cost-benefit analysis was used. Effects of CTF implementation were determined as follows:

- increase in machinery operation costs of 28,65 €/ha, due to the purchase of new equipment,
- savings of 14,09 €/ha on used material (fertilisers, herbicides, etc.) due to elimination of overlaps,
- increase of 10% in 5 years (based on published results), what increases the benefit of approximately 75 €/ha in the 5<sup>th</sup> year.

The cost-benefit analysis pointed out that the investments connected to this technology cause the negative effect on economics in the first year. The investment comes to return and later to profit in subsequent years (Figure 3). The effect of yield increase and material saving starts to influence the overall efficiency after first year, when it overcomes costs. As proposed by Rataj (2005), the temporal variability of yield together with discount factor of 4% was considered during this analysis.



However, there are many other benefits which were not included in this analysis. Based on published literature (Chamen, 2009; Kroulik, 2009), these may be summarized as following:

- fuel savings due to the lower rolling resistance at permanent wheel tracks,
- fuel savings due to the lower soil compaction and lower power requirements,
- environmental effects.

### Conclusions

Controlled traffic farming appears to be an efficient tool for eliminating soil compaction. CTF was introduced at University farm in Koliňany field growing spring barley and oil seed rape in 2009. Experimental measurements at two selected monitoring points showed that after the first year of CTF implementation the increase of soil compaction at non trafficked areas was lower for controlled traffic farming field compared with random traffic. However, it

has to be considered that these are one year results.

The economic analysis was conducted for the area of approximately 715 hectares. The cost-benefit analysis showed that there are high investments connected with introducing this technology. However, effects from yield increase and material saving overcome the increase of machinery operation costs in the second year.

### Reference

- [1] CHAMEN, T. 2009. Controlled Traffic Farming – an essential part of reducing in-field variability. In: GPS autopiloty v zemědělství. [CD ROM]. Praha: ČZU v Praze, 2009, p. 9-17, ISBN 978-80-213-1993-6
- [2] CHAMEN, T. 2010. What is CTF? [online] [Accessed: 2010-01-20]. Available at: <<http://www.controlledtrafficfarming.com/content/whatisctf.aspx>>
- [3] GALAMBOŠOVÁ, J. 2010. Controlled traffic farming and minimum tillage: results



- of initial experiments and a layout of a long term experiment. In: XVIIth World Congress of CIGR held in Québec City, Canada on June 13-17, 2010, in press, available at: [www.cigr2010.ca](http://www.cigr2010.ca)
- [4] KROULÍK, M. et al., 2009. Hodnocení intenzity zatížení půdy pneumatikami zemědělských strojů. In: GPS autopiloty v zemědělství. [CD ROM]. Praha: ČZU v Praze, 2009, p. 28-33, ISBN 978-80-213-1993-6.
- [5] NOZDROVICKÝ, L. - HALAJ, P. - RATAJ, V. 1999. A complex approach for evaluation of soil tillage practices. In Trends in Agricultural Engineering : Proceedings of the International Conference : Praha 15.-17.9.1999. - Praha : Zemědělská univerzita, 1999. ISBN 80-213-0517-7, s. 221-227.
- [6] RATAJ, V. 2005. Projektovanie výrobných systémov – Výpočty a analýzy. Nitra : SPU, 2005, 120 p. ISBN 80-8069-609-8.
- [7] Zákon č. 220/2004 Zb. z. o ochrane a využívaní poľnohospodárskej pôdy a o zmene zákona č. 245/2003 Z.z. o integrovanej prevencii a kontrole znečisťovania životného prostredia a o zmene a doplnení niektorých zákonov. 2004. Available at: <http://www.zbierka.sk/zz/predpisy/default.aspx?PredpisID=17855&FileName=04-z220&Rocnik=2004>.
- [8] Ministry of Agriculture SR. 2009. Report on agriculture and food industry in Slovak republic. Available at: <http://www.land.gov.sk/sk/index.php?navID=122&id=1964>

## DETERMINATION OF ISOTHERMS SUPPORTED BY A MOIRÉ TECHNIQUE

JONATHAN GAZZOLA<sup>1\*</sup>, CLODOALDO CALLOGERO<sup>2</sup>, INACIO MARIA DAL FABBRO<sup>1</sup>, LUIZ GUSTAVO REIS TEIXEIRA<sup>3</sup>, KELEN CRISTIANE CARDOSO<sup>4</sup>

(1) FEAGRI, State University of Campinas, Campinas, SP, Brazil.

Phone (55)(19) 3521-1059, E-mail: jonathan\_gazzola@yahoo.com.br

(2) SENAI, Rio Claro, SP, Brazil.

(3) CASP Industry, Amparo, SP, Brazil

(4) Schaeffler Industry, Sorocaba, SP, Brazil

### Abstract

This research work reports a study of the thermal stress associated to temperature distribution on a flat metal plate. A steel rod was welded at the center of a steel flat plate and thermocouples were positioned in a radial distribution around the surface center. The surface was then painted with white opaque color to improve optical contrast, following by an optical grid projection during the experimental trials. The free rod end was heated up to generate heat conduction to the plate center, as well as a radial temperature distribution. Temperature data obtained by the thermocouples were correlated with the radial plate deformation obtained from the moiré tests. The paper conclusions pointed to the application of the proposed method in obtaining temperature distributions on more complex cases.

**Keywords:** heat transfer, isotherms, moire methods.

### Introduction

The determination of temperature propagation through testing specimens can be carried by means of analytical solutions, experimental tests and numerical models (Martins, 2007). Heat transfer theory states that two points at different temperatures,  $T_1$  and  $T_2$ , where  $T_1 > T_2$  heat will flow to the lower temperature point until equilibrium is reached. (Incropera et al., 2005). Figure 01 shows

association of the expected heat conduction in an isotropic specimen in ideal conditions. It is well known that numerical and experimental methods can provide solutions for temperature distribution on anisotropic and discontinuous bodies. Thermal loading is frequently associated to body deformation with direct relation with stress distribution, in that case named *thermal stress*.

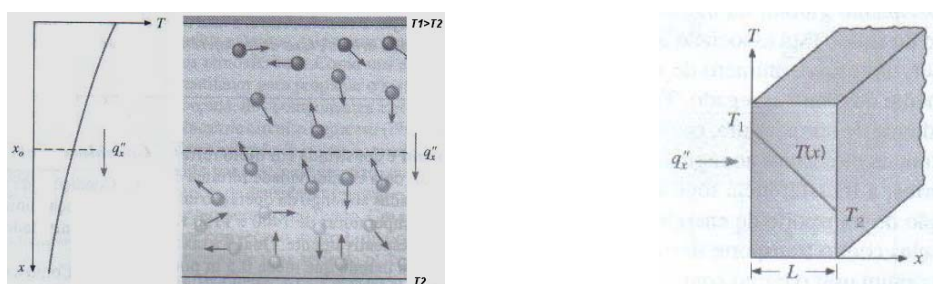


Figure 01. heat transference for conduction to isotropic specimen in ideal conditions. Source: Incropera, 2.005.

Photoelastic methods exhibit important characteristics in the identification and evaluation of stress and strain distribution at specific points of a testing specimen or structural member (MYIAKE, 2004). The photoelasticity is based on the analyses of isocline and

isochromatic fringes generated on loaded specimens. There are several kinds of photoelastic methods, as the classical photoelasticity, interferometric speckle, holography and more recently, the *moiré* techniques. The name *moiré* in French refers to

wave like pattern, generated when screens of certain mesh density are superposed, moving when its relative positions are displaced (Schiammarella, 1982). The technique consists in generating interference patterns between a grid and its own shade projected onto a body surface. These patterns are known as *moiré* fringes which can be processed to obtain the contour lines, describing, in that way, the object surface topography. These phenomena are well understood and describe the light propagation as waves (Saleh, 1991). When two waves of same frequency and amplitude exist simultaneously in the same spatial region, the total wave function is the summation of these waves and their phase relationship will generate fringe patterns of different light intensities (Saleh, 1991). Different methods to generate fringes derive different kind of *moiré* techniques. *Moiré* methods include a large number of techniques as shadow *moiré*, projection *moiré* and others as reported by Takasaki (Degrieck, 2001). Shadow *moiré* method employs one physical grid, made of usual transparency projected onto the object surface by means of an overhead projector (Gazzola et al., 2009). GAZZOLA et al. (2009) has qualified successfully stress distribution in specimens through thermal loading. Based what has been exposed, this research work objectives to determine heat propagation on metal plaque by means of a *moiré* technique. Temperature in real time will be recorded through data logger and results of heat propagation will be correlated to stress distribution generated by a *moiré* technique.

### Materials and methods

The experimental setup selected to carry the shadow *moiré* tests in this research work included a SONY MAVICA digital camera 7.1 mega pixels with remote control to avoid any undesired movement, a white light source, a set of Ronchi Grids of 0.2 mm period, as recommended by DAL FABBRO et al. (2005) and also a heat source, a metal plaque, a set of 7 J wire thermocouples, a datalogger and FieldChart Novus software for temperature recording. Metal plaque made of steel 1020 dimensioned with 150 x 150 mm of sectional area was painted with opaque color to improve optical contrast. The Ronchi grid was positioned in front of the specimen meanwhile the light

source and digital camera were positioned in front of the Ronchi grid as shown on Figure 02.

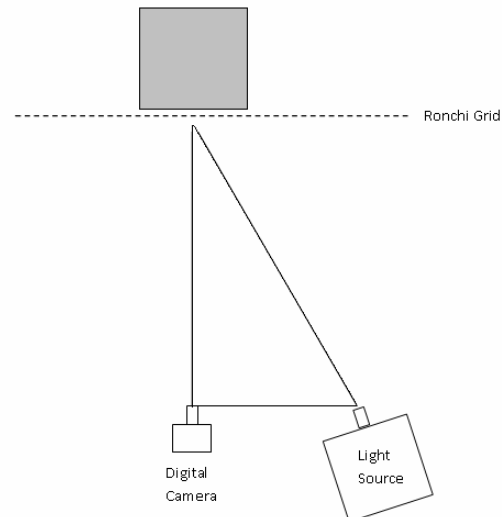


Figure 02. Shadow *moiré* setup applied to carry heat propagation and thermal stress test.

Thermocouples were radially distributed around the plate center meanwhile the rod end was heated by the heat source for 40 minutes, as shown on Figure 03 and the images were recorded at each minute.

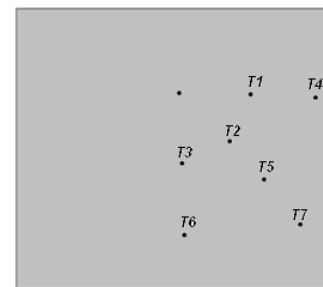


Figure 03. Thermocouples positions.

Thermal loaded and non thermal loaded specimen images were captured through the following procedure. (1) The Ronchi grid was projected onto the specimen surface with no thermal load and photographed to generate the image  $I_1(x,y)$ . (2) The grid was projected onto the specimen under thermal loading transmitted to the metal plate center, producing the image  $I_2(x,y)$ . Image processing was then initialized. The procedure to obtain stress distribution map was carried as follows. (3) The set of images were transferred to ImageJ software and converted to 8-bit scale. (4) An outline related to the specimen on  $I_1(x,y)$  was selected and through

**Creat Mask** command, a vectorial image composed by two areas containing black color (vector modulus = 225) and white color (vector modulus = 0) with outlined specimen and background, respectively, was obtained and named as  $I_3(x,y)$ . (5) the mask was created by converting  $I_3(x,y)$  into an image containing a vector modulus with 0 and 1 through **Math**

Command. This step requires use of **Divide** operation dividing all pixels of image by 225. The mask was created by converting  $I_3(x,y)$  in an image containing the vector modulus with 0 and 1 through **Math** command. This step requires the use of **Divide** operation dividing all pixels of image by 225. Figure 03 shows algorithm used to create the mask.

$$\begin{bmatrix} I_3(x,y) & \text{Mask} \\ \text{Vector Modulus} = 225 \rightarrow \text{Vector Modulus 1} \\ \text{Vector Modulus} = 0 \rightarrow \text{Vector Modulus 0} \end{bmatrix}$$

Figure 03. Algorithm to create Mask image.

(6) Specimen and background was separated in another image through **Image Calculator** command using Equation 01 and named as  $I_4(x,y)$ .

$$I_4(x,y) = I_3(x,y) \times \text{Mask} \quad (01)$$

(7) Image  $I_4(x,y)$  was filtered by the ImageJ software by applying the **Gaussian Blur** filter with 2.0 intensity, generating  $I_5(x,y)$  related to non loaded image and saved as bitmap file. (8) The same procedures described on 03 to 07 steps were applied to  $I_2(x,y)$  loaded image taking the same outline points. The final loaded image is named as  $I_8(x,y)$ . (9)  $I_5(x,y)$  and  $I_8(x,y)$  were transferred to Idrisi Kilimanjaro software to obtain a colored stress mapping distribution through **Image Calculator** command using Equation 02. The final image was named as  $\Delta(x,y)$ .

$$\Delta(x,y) = I_8(x,y) - I_5(x,y) \quad (02)$$

(10)  $\Delta(x,y)$  image was transferred to Paint Brush software and selecting only stress mapping

distribution. This image was saved in bitmap file and named as  $\Delta_L(x,y)$ . (11)  $\Delta_L(x,y)$  was transferred to ImageJ software and split in red, blue and green channels, through **Split Channels** command. (12) Green channel image was selected to obtain the map of isocline lines. Through the **Interactive 3D Surface Plot** command it was obtained the isoclines line mapping. This image was saved as bitmap files and named as  $\Delta_I(x,y)$ . That procedure was repeated for each thermal loading to be analyzed.

## Results and Discussons.

Figure 04 shows the temperature distribution for each thermocouple obtained through the datalogger. It is noted a starting temperature decrease, but after some minutes temperature increases all time with some peaks. Difference among temperatures was stable, showing that heat distribution was equal along specimen surface. Images were recorded at the thermal peak occurrence, i.e. at 00:07, 00:13, 00:33 and 00:57 minutes of specimen heating.

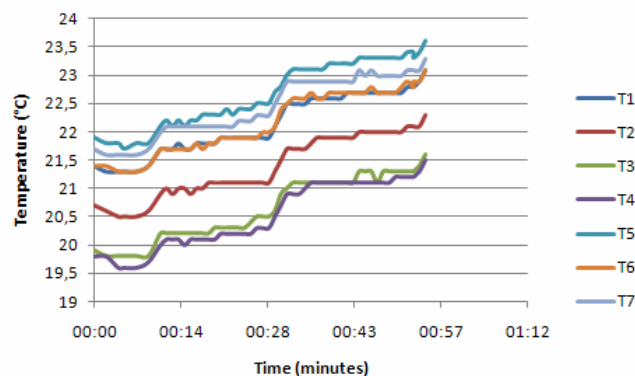


Figure 04. Thermal loading data obtained through datalogger.

Figure 05 shows resulting image as processed by the ImageJ software according to steps (03) to (08). Fringes are noted on specimens under different thermal loading. These differences are due to heat propagation which generates deformation as well as stress loading and consequently the generation of optical fringes. The discontinued white point on the images are positioned at plate center from where heat is propagated.

Figures 06 displays the resulting image from the Idrisi Kilimanjaro software processing, showing the heat propagation mapping according to the isochromatics.

According Figure 05, the temperature data indicates cooling occurrence on the metal plate, i.e., when temperature decreases, then the metal

plate is retracted, otherwise, when temperature increases along specimen, dilatation can be observed. By analyzing these figures it is noted that for Figure 06 (a) heat propagation is different when compared to images 02 (b), 02 (c) and 02 (d). When the temperature increases, the color intensity followed the same behavior, exhibiting higher color intensities. The most intense the colors appears next to the central point from where heat was propagated, showing close agreement to the temperature data readings from the thermocouples. Figure 07 shows isoclines lines obtained through ImageJ software according to steps (10) to (12). Black points were inserted on the final image to indicate the selected points of temperature readings, as well as punctual heat source as showed on Figure 06.

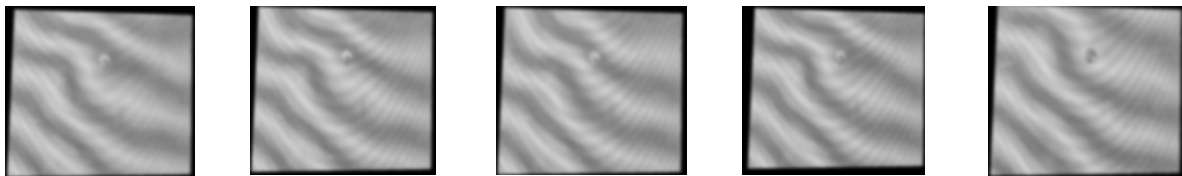


Figure 05. Fringes formed on metal plate to time 00:00, 00:07, 00:13, 00:33 and 00:57 minutes, respectively.

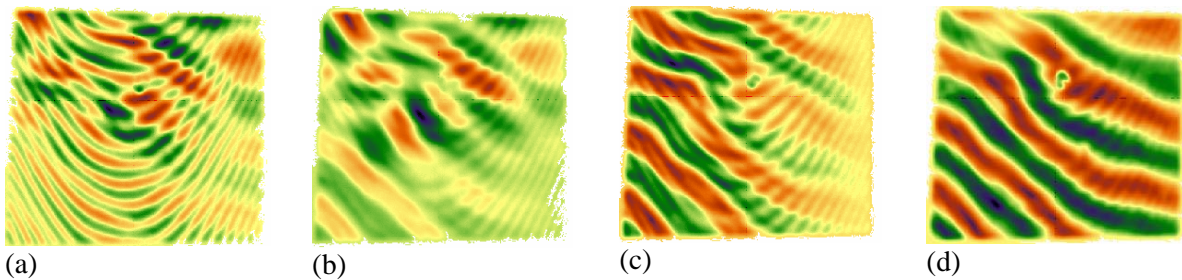
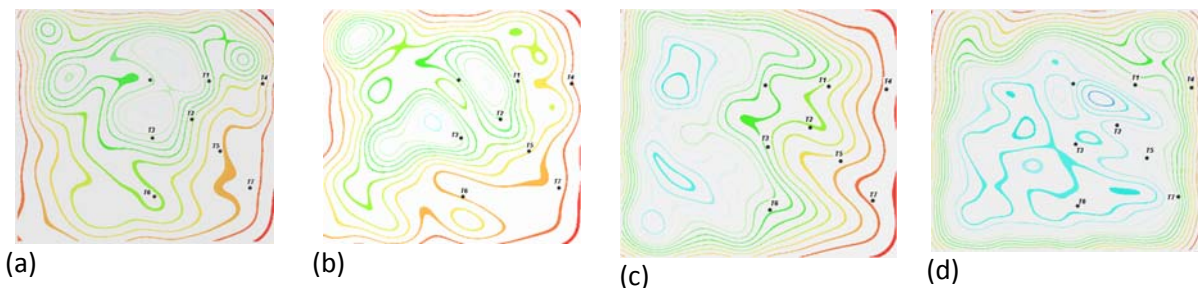


Figure 06. Heat propagation mapping to 00:07, 00:13, 00:33 and 00:57 minutes, respectively.



Figures 07. Isocline lines to metal plate for 00:07, 00:13, 00:33 and 00:57 minutes, respectively

Finally, these figures allow analyzing heat propagation along specimen. Thermocouples T1 and T4 represents horizontal direction, thermocouples T2, T5 and T7 represents inclined

direction meanwhile thermocouples T3 and T6 represents vertical direction. Temperature data indicated that horizontal line exhibited the highest temperature variation during the test with



1.6 °C and the vertical direction obtained the second highest temperature variation of 1.5°C and inclined direction obtained the lowest variation of 1.1°C. Horizontal line showed negative modulus, which it can be retracted. Vertical and inclined lines obtained positive variations which represents dilatation. Every treated image indicated that isoclines are more concentrated at the horizontal direction. Vertical direction showed more concentrated isoclines, as well as inclined direction showed the lowest isoclines concentration. Besides Figure 07 (c) have showed that inclined direction indicated more heat propagation than vertical line, however an overall comparison it is noted that moiré technique is in close agreement with temperature distribution obtained through the thermocouples. By analyzing the metal plate it is observed on Figure 07 (a) that central point concentrated more isoclines than plate the boundaries. According to heat propagation increase, isoclines concentration was displaced to the boundary. By comparing isoclines behavior with heat propagation it is observed that the initial temperature is higher at the central point than the boundary and as temperature increases, the highest temperatures were read at thermocouples placed at the boundary. Moiré technique gives a good picture of heat propagation behavior on metal the plaque.

### Conclusion

Based in what has been exposed, it is concluded that shadow moiré technique determined temperature distribution on metal plaque. Data of temperature variation were in close agreement with results obtained by the moiré technique. Results are in close agreement with the pertinent literature. As low cost equipments were required to carry the tests the proposed technique can be considered feasible. It is recommended as future research works the application of moiré technique in objects of complex geometry.

### Bibliographic References

- [1] DAL FABBRO, I.M.; GAZZOLA, J.; RODRIGUES, S.; RABELO, G.F.; FUJII, A. K. Moiré assisted mechanical behavior of sugarcane stalks under axial compression. In: Proceedings of the International Congress on Information Technology in Agriculture, Food and Environment, ITAFE05. (CD ROM) Vol. I, pp.242-245, (ISBN 975-487-125-6). Balcali Campus, Çukurova University, Adana, Turkey, October 12-14, 2005.
- [2] DEGRIECK, J.; VAN PAEPEGEM, W.; BOONE, P., (2001). Application of Digital Phase-shift shadow *moiré* to micro deformation measurements of curved surfaces. Optics and Lasers in Engineering, 36, pp. 29-40.
- [3] GAZZOLA, J.; DAL FABBRO, I.M.; OLIVEIRA, R. A. *Moiré* optical methods applied to the analysis of bodies under thermal loads. In: Proceedings of the Bulgarian Agrojournal Research. Research work has already accepted to publication, Sophia, 2.009.
- [4] INCROPERA, Frank P. e DEWITT, David P., Fundamentos de Transferência de Calor e de Massa. Editora: LCT. Rio de Janeiro, 2.005.
- [5] MARTINS, M.M.; BRISAN, J.D.; JUNIOR, M.V. Simulação numérica da distribuição de temperatura transiente em placa tridimensional no choque térmico. In: Proceedings of Congresso Brasileiro de Engenharia de Fabricação, COBEF(2009). Vol. 1, Belo Horizonte, Brazil, April, 2.009.
- [6] MYIAKE, Eloisa T.; SOLLERO, Paulo ; PAIVA, William Portilho de. . Análise Experimental de Tensões Usando Processamento Digital de Imagens Fotoelásticas de Reflexão. Anais... Ilha Solteira: Sociedade Brasileira de Matemática Aplicada e Computacional, v.1, p. 1427-1431, 2004.
- [7] SALEH. B. E. A.; TEICH, M. C. 1991. Fundamentals of Photonics. John Wiley & Sons, New York.
- [6] SCHIAMMARELLA, C. A. The *moiré* method – A review. Experimental Mechanics. v.44, n.8, p. 418-433, nov., 1982.
- [7] TAKASAKI, H. 1970. Moiré topography. Applied Optics. .9 (6), pp. 1457-52, Washington.



## COMPARISON BETWEEN *MOIRÉ* AND HOLOGRAPHY AS PHOTOELASTIC METHODS IN STRESS DISTRIBUTION DETERMINATION

JONATHAN GAZZOLA<sup>\*1</sup>, INÁCIO MARIA DAL FABBRO<sup>2</sup>, JULIO SORIANO<sup>2</sup>,  
RENATO LAURENTI<sup>3</sup>

(1) FEAGRI, State University of Campinas, Campinas, SP, Brazil.

Phone (55)(19) 3521-1059, E-mail: jonathan\_gazzola@yahoo.com.br

(2) State University of Campinas, Campinas, SP, Brazil.

(3) Federal Rural University of Pernambuco, Recife, PE, Brazil.

### Abstract

Photoelastic methods exhibit important characteristics in identification and evaluation of stress distribution at specific points of a testing specimen or structural components. The literature reveals many photoelastic methods, as the classical photoelasticity, interferometric speckle and holography. Shadow moiré methods can also give support to photoelastic techniques, offering many technical advantages as low cost equipment requirement. This research work compares stress distribution results obtained from a shadow moiré technique with those obtained by the classical holographic photoelasticity showed by the pertinent literature. A cylindrical specimen painted with white opaque color was diametrically compressed by means of a rubber band, meanwhile an optical grid was projected onto the specimen surface. The shadow moiré experimental setup included a 7.2 Mega Pixels digital camera, a Ronchi grid of 0.2 mm of period and as well as a conventional white light source. The results obtained with the shadow moiré technique was compared with holographic method results previously analyzed by CRESPO (2.006) using similar specimen. It was concluded that the results generated by the shadow moiré were in close agreement with the holographic method results.

**Keyword:** photoelastic methods, shadow moiré, stress determination

### Introduction

The pertinent literature presents several methods based on experimental tests, numerical analysis, as well as analytical procedures to determine stress and strain distributions on bodies under load. Photoelastic methods exhibit important characteristics in identifying and in evaluating stress and strain distribution in any specific point of testing specimen or structural member (Myiake et al., 2004) requiring no destructive procedures, being applicable to loaded bodies of any geometric configuration (Cohen, E.A. 2.001). Photoelastic concepts are based on studies of optical fringes generated on loaded specimens named isoclines and isochromatics. Isocline fringes offer information about stress direction, meanwhile the isochromatic lines provide information on punctual stress intensity (Spinelli et al, 2003). In other words, isocline lines approximation indicates stress concentration, while isochromatic line color intensity indicates stress intensity on the specimen surface (Brodsky &

Caputo, APUD Siqueira 2009). The photoelasticity is a family of methods of experimental stress and strain analysis applied in evaluating, validating and developing of structural elements which is subjected to mechanical loadings (Gazzola et al., 2009). Photoelastic techniques include classical photoelasticity, interferometrical speckle, holography and interferometrical *moiré*.

Holography is an optical technique based on an interferometric phenomenon characterized by high efficiency in registering three dimensional object image (Maschio, 2008). MONTEIRO et al. (1997) affirms that interferometrical holography allied to photoelastic concepts allow a complete mapping of the stressed area. The subtraction of two interferograms associated to two expositions, exhibits standardized fringes which describe the relative displacement of points on the object surface. The advantage of holography is based on its accuracy and high precision on measurements (Oliveira et al., 2008). WICKERT (1978)

comments about some disadvantage of holography as position and illumination of the testing object which must be tied to avoid any movement during the test. This technique is highly sensible to any vibration, besides high equipments cost requirement to carry the test. CRESPO (2006) has applied interferometrical holography to determine stress distribution in cans under diametrical compression as shown on Figure 01. Results indicates stress concentration under the rubber band which surroundings the specimen.



Figure 02. Stress distribution in cans with diametrical compression loading. (Crespo, 2006)

*Moiré* interferometry gives support to similar photoelastic techniques, allowing similar applications as the conventional methods, presenting high precision and confidence as well (Gazzola et al., 2009). *Moiré* methods are of low cost experimental setup requirements and generate reliable results (DAL FABBRO et al. 2005). Besides, this technique is not so sensible to vibrations as holographic methods are. These patterns are known as *moiré* fringes which can be processed to obtain the contour lines, describing, in that way, the object surface topography. These phenomena are well understood and describe the light propagation as waves (Saleh, 1991, APUD Gazzola et al. 2009). GAZZOLA et al., (2009) obtained successful results by applying shadow *moiré* technique to determine uniaxial loading in rubber specimens comparing the results with finite element methods. Shadow *moiré* technique consists in illuminating the object in study after a grid by a white light source, generating, that way, an optical interference between the grid and its shade.

This research work objectives the comparison between stress mapping obtained by a shadow *moiré* technique with those generated by an interferometric hologram photoelastic method as reported by CRESPO (2006).

### Materials and methods

The selected experimental setup to carry the shadow *moiré* tests in this research work included a SONY MAVICA digital camera 7.1 Mega pixels with remote control to avoid any undesired movement, a white light source, a set of Ronchi Grids of 0.2 mm period, as recommended by Dal Fabbro et al. (2005). Testing sample constituted of a can dimensioned as 66.00 mm of diameter and 122.00 mm of height diametrically compressed by means of an rubber band. Specimen was painted in white opaque color to improve optical contrast. The Ronchi grid was positioned in front of the specimen meanwhile the light source and digital camera were positioned in front of the Ronchi grid as shown on Figure 02.

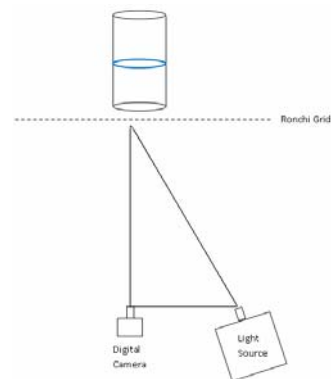


Figure 02. Shadow *moiré* setup applied to carry compression testing on cylindrical specimen

Loaded and non loaded specimen images were captured through the following procedure. (1) The Ronchi grid was projected onto the specimen surface with no load and photographed to generate the image  $I_1(x,y)$ . (2) The grid was projected onto the specimen under a compressive loading applied at the middle height of the cylindrical specimen, producing the image  $I_2(x,y)$ . Image processing was then initialized. The procedure to obtain stress distribution map was carried as follows. (3) The set of images were transferred to ImageJ software and

converted to 8-bit scale. (4) An outline related to the specimen on  $I_1(x,y)$  was selected and through **Creat Mask** command, a vectorial image composed by two areas containing black color (vector modulus = 225) and white color (vector modulus = 0) with outlined specimen and background, respectively, was obtained and named as  $I_3(x,y)$ . (5) The mask was created by converting  $I_3(x,y)$  into an image containing a vector modulus with 0 and 1 through the **Math Command**. This step requires the use of **Divide** operation dividing all pixels of image  $I_3(x,y)$  by 225. Figure 03 shows the algorithm used to create the mask.

$$\left[ \begin{array}{l} I_3(x,y) \\ \text{Vector Modulus} = 225 \rightarrow \text{Vector Modulus 1} \\ \text{Vector Modulus} = 0 \rightarrow \text{Vector Modulus 0} \end{array} \right] \text{Mask}$$

Figure 03. Algorithm employed to create Mask image

(6) Specimen and background were separated into another image through **Image Calculator** command using Equation 01 and named as  $I_4(x,y)$ .

$$I_4(x,y) = I_1(x,y) \times \text{Mask} \quad (01)$$

(7) Image  $I_4(x,y)$  was filtered by the ImageJ software by applying the **Gaussian Blur filter** with 2.0 intensity, generating  $I_5(x,y)$  related to non loaded image and saved as bitmap file. (8) The same procedures described on 03 to 07 steps were applied to  $I_2(x,y)$  loaded image taking the same outline points. The final loaded image was named as  $I_8(x,y)$ . (9)  $I_5(x,y)$  and  $I_8(x,y)$  were transferred to Idrisi Kilimanjaro software to obtain a colored stress mapping distribution



Figure 03. Non loaded specimen image

through the **Image Calculator** command using Equation 02. The final image was named as  $\Delta(x,y)$ .

$$\Delta(x,y) = I_8(x,y) - I_5(x,y) \quad (02)$$

(10)  $\Delta(x,y)$  image was transferred to the Paint Brush software and selecting only stress mapping distribution. This image was saved in bitmap file and named as  $\Delta_L(x,y)$ . (11)  $\Delta_L(x,y)$  and transferred to the ImageJ software and split into red, blue and green channels, through **Split Channels** command. (12) Green channel image was selected to obtain the map of isocline lines. Through **Interactive 3D Surface Plot** command the isoclines line mapping was obtained. That image was saved as bitmap files and named as  $\Delta_I(x,y)$ . (13) Final image containing specimen and isoclines line mapping was obtained through the **Image Calculator** command and **Difference** operational command of the ImageJ software, using Equation 03. The final image was named as  $I_9(x,y)$ .

$$I_9(x,y) = \Delta_I(x,y) - \Delta_L(x,y) \quad (03)$$

### Result and discussions

Figure 03 and Figure 04 show images obtained of the non loaded and loaded specimen and correspondent to the steps (01) and (02).

In this experimental test, the angle was set between the object, the camera and the light source was selected to avoid noises on image as flashes produced by light source, blocking fringes visualization. Figure 05 and Figure 06 show images treated in the ImageJ software of non loaded and loaded images. These images are correspondent to the steps (03) up to step (08).



Figure 04. Loaded specimen image

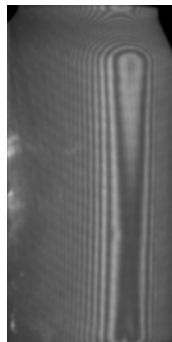


Figure 05. Non loaded specimen image processed on the ImageJ software.

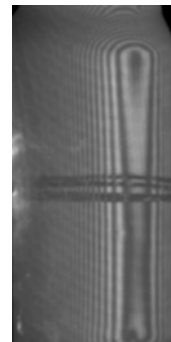


Figure 06. Loaded specimen image processed on the ImageJ software.

These steps generated separated images, i.e., specimen image and background image and by the application of the Gaussian Blur filter some noises produced by grid reflection had been eliminated. A clear differentiation between fringes generated on non loaded and loaded specimen can be observed. These differentiations allow obtaining stress mapping distribution. Figure 07 shows the result of stress mapping distribution obtained from the Idrisi Kilimanjaro which correspond to step (09).

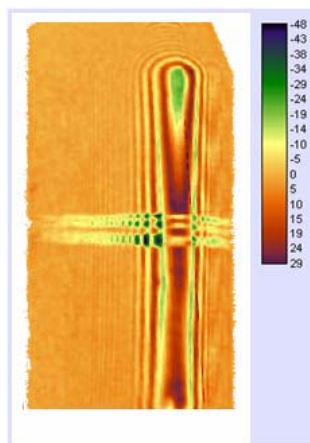


Figure 07. Stress mapping distribution ( $\Delta(x,y)$ )

The software Idrisi Kilimanjaro generated the isochromatic fringes, i.e., through the color distribution on the specimen turning possible the determination of stress intensity for each point along the specimen. The highest concentration is observed at the object frontal side and the stress inversion from compression to traction is noted at the rubber band position represented by green color. This inversion on image color indicates that the rubber band applies the stress meanwhile

the specimen reacts which explains this phenomenon. Figure 08 shows isoclines lines obtained through  $\Delta(x,y)$  image treatment in the ImageJ. A shadow image of specimen outline was placed behind the isocline lines to improve comprehension of stress concentration along specimen surface. These images are related to the steps (10), (11) and (12).



Figure 08. Isocline mapping ( $\Delta(x,y)$ )

Analyses of isoclines indicated the occurrence of stress concentration at the object middle height as well as along the diameter. However the stress concentration observed at the specimen frontal side and at specimen boundaries, were not so intense. Remaining areas showed no isoclines and consequently no stress concentration. By comparing these results with those reported by CRESPO (2006) it can be affirmed that both are in close agreement, i.e., photoelastic moiré and photoelastic holography techniques can generate equivalent results.

## Conclusions

Based on what has been exposed before, it can be concluded that moiré technique is reliable as photoelastic hologram in determining stress distribution. The experimental setup required by moiré methods are of low cost if compared with those of holographic photoelasticity. Future research works should include precision analyzes of moiré methods.

## References

- [1] CRESPO, D.; QUIROGA, J.A.; GOMEZ-PEDRERO, J.A. Fringe extreme: State of the art software for automatic processing of fringe patterns, Proc. SPIE 6616 66163-1-66163 (2006).
- [2] COHEN, E. A. **Investigação da Concentração de Tensões em Furos de Chapas Ortotrópicas Usando o Método da Fotoelasticidade de Reflexão**. 103 p. Dissertação de Mestrado em Engenharia Civil – Escola Politécnica, Universidade de São Paulo, 2.001.
- [3] DAL FABBRO, I.M.; GAZZOLA, J.; RODRIGUES, S.; RABELO, G.F.; FUJII, A. K. Moiré assisted mechanical behavior of sugarcane stalks under axial compression. In: Proceedings of the International Congress on Information Technology in Agriculture, Food and Environment, ITAFE05. (CD ROM) Vol. I, pp.242-245, (ISBN 975-487-125-6). Balcali Campus, Çukurova University, Adana, Turkey, October 12-14, 2005.
- [4] GAZZOLA, J.; DAL FABBRO, I.M.; OLIVEIRA, R. A. *Moiré* optical methods applied to the analysis of bodies under thermal loads. In: Proceedings of the Bulgarian Agrojournal Research. Research work has already accepted to publication, Sophia, 2.009.
- [5] MASCHIO, A.V. A Estereoscopia: investigação de processos de aquisição, edição e exibição de imagens estereoscópicas em movimento. 231 p. Dissertação de Mestrado em Comunicação e Artes – Faculdade de Arquitetura, Artes e Comunicação, Universidade Estadual Paulista, 2.008.
- [6] MONTEIRO, J. M; CHOUZAL, J. A.; VAZ, M. A. Vibration analysis by laser interferometry techniques. International workshop on Aerospace and Powered Lift Technologies, Universidade da Beira Interior, Covilhã, 7-9 Julho 1997.
- [7] MYIAKE, Eloisa T.; SOLLERO, Paulo ; PAIVA, William Portilho de. . *Análise Experimental de Tensões Usando Processamento Digital de Imagens Fotoelásticas de Reflexão*. **Anais...** Ilha Solteira: Sociedade Brasileira de Matemática Aplicada e Computacional, v.1, p. 1427-1431, 2004.
- [8] OLIVEIRA, G.N.; dos SANTOS, P.A.M.; NUNES, L.C.S.; Controlled phase mismatch in sectioned dynamic holographic moiré - like patterns. Optics and Lasers in Engineering. Vol. 46, 2008, pp. 721– 725
- [9] SIQUEIRA, Dayana Pousa Paiva de et al. *Análise fotoelástica de um modelo de vértebra humana com parafuso perpendicular*. **Acta Ortopédica Brasileira**, Ribeirão Preto, v. 17, n.3, p. 149-151, 2009.
- [10] SPINELLI, Hione de Aquino. ; SILVA, Fernando de Azevedo. *Aplicação da Fotoelasticidade na Análise Estrutural de uma Junta Rebitada de Uso Aeronáutico*. In: **Anais...** Guaratinguetá, 2003.
- [11] WICKERT, L. *Uso de holografia interferométrica no estudo de sementes*. 70 p. Dissertação de Mestrado em Ciências – Instituto de Física Gleb Wataghin, Universidade Estadual de Campinas, 1978.



## SHADOW MOIRÉ TECHNIQUES APPLIED TO STRESS DETERMINATION ON METALLIC BEAMS UNDER FLEXURAL LOADING

JONATHAN GAZZOLA<sup>\*1</sup>, INÁCIO MARIA DAL FABBRO<sup>2</sup>, JULIO SORIANO<sup>2</sup>,  
SILVESTRE RODRIGUES<sup>3</sup>

(1) FEAGRI, State University of Campinas, Campinas, SP, Brazil.

Phone (55)(19) 3521-1059, E-mail: jonathan\_gazzola@yahoo.com.br

(2) State University of Campinas, Campinas, SP, Brazil.

(3) Federal University of Sergipe, Aracaju, SE, Brazil.

### Abstract

The pertinent literature discloses several stress determination methods including analytical solutions, experimental loading tests, destructive and non destructive tests. Photoelastic methods are based on non destructive tests and exhibit important characteristics in mapping stress and strain distributions over the testing body or structure. Shadow *Moiré* technique is a simple photoelastic method which does not require expensive equipments, gathering the attention of researchers toward further developments. The objective of this research work was to analyze stress distribution on a metal beam under flexural loading by means of a Shadow *Moiré* technique. A metallic beam painted with opaque white color was supported by a rigid steel structure during loading tests, meanwhile concentrated flexural loading was applied at the middle width of the testing specimen. A Ronchi grid of 0.2 mm of period was projected onto the specimen surface by a multimedia projector connected to PC. Images were captured by a 7.2 MegaPixels digital camera. Image processing was carried by means of the Idrisi Kilimanjaro, Paint Brush and ImageJ softwares. Obtained results were compared to expected results according to literature. The conclusions include consideration on the feasibility and reliability of the Shadow *Moiré* method in determining stress and strain distributions on isotropic specimens.

**Keyword:** photoelasticity, shadow moiré, flexural loading, beams, structure members.

### Introduction

The literature reveals several methods aiming stress distribution determination on regular or on irregular bodies under static as well as under dynamic loadings. A didactic classification would include *analytical methods*, *numerical methods* and *optical methods*. Analytical solutions are close associated to structural elements of regular geometry, meanwhile numerical and optical methods can handle symmetric as well as asymmetric bodies under a variety of loading situations. The rules of strength material science state that a beam of any material has the same mechanical behavior. BEER & JOHNSTON (1996) affirm that a beam submitted only to a flexural load, will exhibit three different loading zones. A compression loading zone is set at the force application point, a traction loading zone takes place at the beam base, meanwhile a neutral zone is set between the two others which it is also named *neutral*

*line*, where traction and compression loads are null. Figure 01 shows the mechanical behavior of a beam under flexural loading.

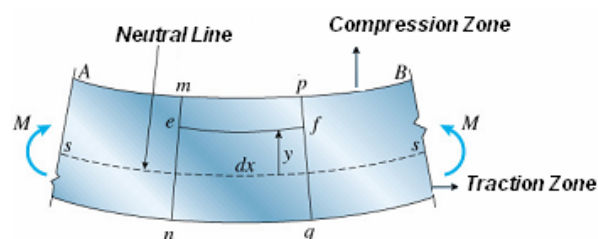


Figure 01. Mechanical behavior of beams under flexural loading according literature. Source: Beer & Johnston, 1996

The literature also discloses several photoelastic methods, as the classical photoelasticity, interferometric speckle, holography and *moiré* techniques. Photoelastic methods are based on optical interference which produces fringes on the loaded specimen,



defining isocline and isochromatic lines. Conventional photoelastic methods exhibit important characteristics in the identification and evaluation of stress and strain distribution at specific points of on a loaded specimen (MYIAKE, 2004). Among the optical methods the moiré techniques are gaining popularity due to simplicity, reliability, requiring low cost experimental setups. However, the moiré phenomenon also gives support to photoelastic methods beyond its shape determination capabilities Lino (2008). When two waves of same frequency and amplitude exist simultaneously in the same space, the total wave function is the summation of these waves and their phase relationship will generate fringe patterns of different light intensities (Saleh, 1991). The name *moiré* in French refers to wave like pattern, generated when screens of close mesh density are superposed producing fringes which move when its relative positions are displaced (Sciammarella, 1982). That phenomenon is named *moiré effect* which has generated a family of methods named *moiré methods*, as shadow moiré, projection moiré and others as reported by Takasaki (APUD Degrieck, 2001). GAZZOLA et al., 2010 reported successful tests to determine stress concentration on wooden beam applying shadow moiré technique. Based in what has been exposed above, the objective of this research work was based in obtaining the stress and strain distributions on metallic beam under flexural loading supported by the Shadow Moiré technique. A metallic beam painted with opaque white color was supported by a rigid steel structure during loading tests; meanwhile concentrated flexural load was applied at the middle width of the beam.

### Materials and methods

The experimental setup selected to carry the shadow *moiré* tests in this research work included a SONY MAVICA digital camera with 7.1 mega pixels with remote control to avoid any undesired displacement, a conventional white light source, a set of Ronchi grids of 0.2 mm period, a testing press, as recommended by Gazzola et al. (2010). Testing sample constituted of a steel beam dimensioned as 20.00 mm of width, 20.00 mm height and 1,200.0 mm length,

painted in white opaque color to improve optical contrast, having their extremities leaned on the testing press, meanwhile a flexural force was applied at its middle width. The grid was positioned in front of the specimen, before the light source and the digital camera as shown on Figure 02.

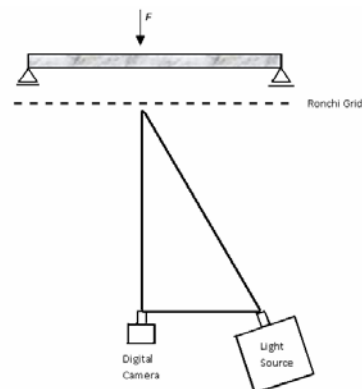


Figure 02. Shadow *moiré* setup applied in association with flexural loading of a steel beam

Loaded and non loaded specimen images were captured through the following procedure. (1) The grid was projected onto the specimen surface with no load and photographed to generate the image  $I_1(x,y)$ . (2) The grid was projected onto the specimen under a flexural force applied at the middle point of the metallic beam length, producing the image  $I_2(x,y)$ . Image processing was then initialized. The procedure to obtain stress distribution map was carried as follows. (3) The set of images was transferred to the **ImageJ** software and converted to 8-bit scale. (4) An outline of the specimen area was selected using image  $I_1(x,y)$  and through the **Create Mask** command, a vectorial image composed of two areas containing black color (vector modulus = 225) corresponding to specimen, meanwhile white color (vector modulus = 0) corresponding background area. That image was named as  $I_3(x,y)$ . (5) Then, the mask was created by converting  $I_3(x,y)$  into an image containing a vector modulus with 0 and 1 through the **Math** Command. That step requires the use of **Divide** operation to divide all pixels of the image by 225. Figure 03 shows algorithm used to create the mask.

$$\begin{bmatrix} I_2(x,y) & Mask \\ \text{Vector Modulus} = 225 \rightarrow \text{Vector Modulus 1} \\ \text{Vector Modulus} = 0 \rightarrow \text{Vector Modulus 0} \end{bmatrix}$$

Figure 03. Algorithm to create Mask image

(6) Specimen and background were separated into another image through the **Image Calculator** command by using Equation 01 and named as  $I_4(x,y)$ .

$$I_4(x,y) = I_1(x,y) \times Mask \quad (01)$$

(7) Image  $I_4(x,y)$  was filtered by the ImageJ software by applying the **Gaussian Blur** filter with 2.0 intensity, generating  $I_5(x,y)$  related to non loaded specimen image and saved as bitmap file. (8) The same procedures described on 03 to 07 steps were applied to  $I_2(x,y)$  loaded image, taking the same outline points. The final loaded image was then named as  $I_8(x,y)$ . (9)  $I_5(x,y)$  and  $I_8(x,y)$  were transferred to the **Idrisi Kilimanjaro** software to obtain a colored stress mapping distribution through the **Image Calculator** command by using Equation 02. The final image was named as  $\Delta(x,y)$ .

$$\Delta(x,y) = I_8(x,y) - I_5(x,y) \quad (02)$$

(10)  $\Delta(x,y)$  image was transferred to the **Paint Brush** software and selecting only stress mapping distribution. That image was saved in bitmap file and named as  $\Delta_L(x,y)$ . (11)  $\Delta_L(x,y)$  was transferred to **ImageJ** software and split in red, blue and green channels, through the **Split Channels** command. (12) Green channel image was selected to obtain the map of isocline lines. Through the **Interactive 3D Surface Plot** command it was obtained the isoclines lines mapping. That image was saved as bitmap files and named as  $\Delta_I(x,y)$ . (13) Final image containing specimen and isoclines line mapping was obtained through the **Image Calculator** command and through the **Difference operational** command of the **ImageJ** software by using Equation 03. The final image was then named as  $I_9(x,y)$ .

$$I_9(x,y) = \Delta_I(x,y) - \Delta_L(x,y) \quad (03)$$

These steps were repeated for each loading case. In this research work, three different flexural forces were applied on specimen, as 150 N, 300 N and 450 N.

## Results and discussions

Figure 04, Figure 05 and Figure 06 show stress mapping distribution obtained through the Idrisi Kilimanjaro software, respectively for 150N, 300 N and 50 N.

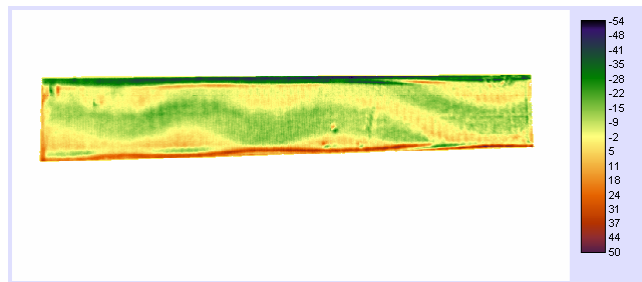


Figure 04. Stress mapping distribution to flexural force (150 N)

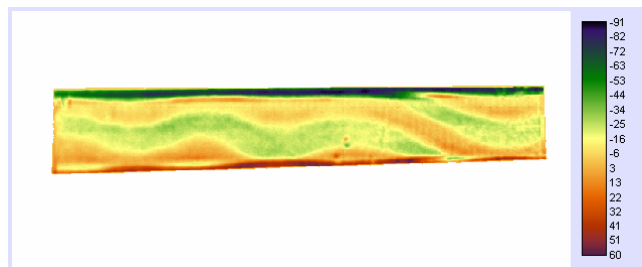


Figure 05. Stress mapping distribution to flexural force (300 N)

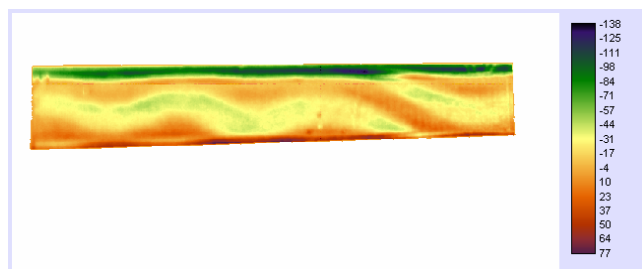


Figure 06. Stress mapping distribution to flexural force (450 N)

Informations obtained through these maps has been carried by isochromatic lines analyzes generated on the specimen, which indicates stress intensity. It is noted the border region to exhibit green color which is associated to compression meanwhile the red color is related to traction, emphasizing that the color intensities

are balanced, according to the presented color scale. Figure 05 and Figure 06 present differences between compression and traction loading, indicating increasing unbalancing as the applied flexural loading increases. It is also observed that color intensity is stronger as loading increases and the waves are closer, indicating stress concentration on the specimen surface.

Figure 7, Figure 9 and Figure 9 show the final stress mapping distribution containing isoclines with red color indicating neutral line position. Isocline lines provide informations related to stress concentration as well as their directions. These images were obtained through Image J processing which correspondent to the step (10) up to the step (13).

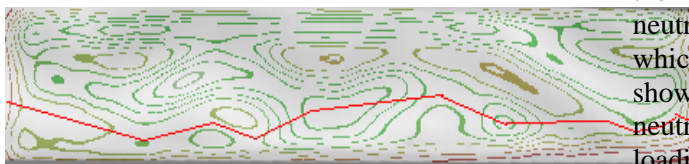


Figure 7. Isocline lines mapping for flexural force (150 N)

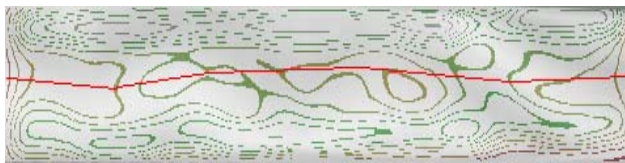


Figure 8. Isocline lines mapping for flexural force (300 N)



Figure 9. Isocline lines mapping for flexural force (450 N)

By analyzing the isoclines on Figure 14 it is noted stress concentration for low flexural force positioned at the top of the specimen meanwhile low stress concentration appeared at the base, i.e., more compressive loading took place than traction loading. In Figure 14 and Figure 15 the isoclines are more concentrated on the compression region, however isoclines are closer together for 300 N load than for 150 N load. Also, the relation between the region over the

neutral line to the region under that line, i.e., compression to traction is higher for 150 N load. Figure 16 shows higher stress concentration for traction and compression loadings which is indicated by the higher isoclines concentration when compared with the previous flexural loading. An overall analyzes of the figures presented above shows the stress concentration to be higher at the top of the specimen as indicated by the isoclines distribution, where compressive loads take place. As load increases, isoclines get closer, i.e., it indicates stress concentration along the specimen. By analyzing the horizontal isoclines, it is possible to observe the stress concentrations to be similar at right and left sides, indicating material isotropy. Neutral line was defined in regions where isoclines show the lowest concentration. Figure 7 indicated the neutral line position at the base of specimen which it was expected since traction loading showed lower concentration. Figure 7 indicates a neutral line displacement to the middle height as loading increases, meanwhile Figure 9 indicates a neutral line discontinuity. Such occurrence can be explained by the specimen characteristic as the hollowed sectional area as well as a possible torsional loading occurrence, despite their extremities were pretty tied up. That situation is important to structural elements employed in engineering projects, because flexural loadings generates shear stress.

## Conclusions

Based on what has been exposed above, *moiré* technique demonstrated the behavior of steel beam under flexural loading according as it was expected and supported by the strength materials theories, exhibiting compressive as well as traction loads effects, and the neutral line evidence. *Moiré* technique can be considered as a reliable photoelastic method, showing results is in close agreement with the theory, exhibiting simplicity and low cost of experimental setup.

## References

- [1] BEER, Ferdinand P.; JOHNSTON Jr. E. Russel. **Resistência dos materiais**. São Paulo: Ed. Makron Books, 1.996.
- [2] DEGRIECK, J.; VAN PAEPEGEM, W.; BOONE, P., (2001). Application of Digital Phase-shift shadow *moiré* to micro deformation

- measurements of curved surfaces. *Optics and Lasers in Engineering*, 36, pp. 29-40.
- [3] GAZZOLA, Jonathan; DAL FABBRO, Inácio Maria; RODRIGUES, S. **Moiré supported flexural tests on wooden beams. Proceedings...** Sansum: ITAFFE, v. 1, p. 859-863, 2010.
- [4] LINO, Antonio Carlos Loureiro. **Aplicação de moiré de projeção com deslocamentos de fase na construção de modelos digitais topográficos de órgãos vegetais.** 92 p. Tese de Doutorado em Engenharia Agrícola – Faculdade de Engenharia Agrícola, Universidade Estadual de Campinas, 2008.
- [5] MYIAKE, Eloisa T.; SOLLERO, Paulo ; PAIVA, William Portilho de. . **Análise Experimental de Tensões Usando Processamento Digital de Imagens Fotoelásticas de Reflexão. Anais...** Ilha Solteira: Sociedade Brasileira de Matemática Aplicada e Computacional, v.1, p. 1427-1431, 2004.
- [6] SALEH, B.E.A.; TEICH, M.C. (1991). **Fundamentals of phtononics.** John Wiley & Sons, New York.
- [7] SCIAMMARELLA, C. A. The moiré method – A review. **Experimental Mechanics.** v.44, n.8, p. 418-433, nov., 1982.

## COMPARISON OF CONVENTIONAL REGRESSION METHODS AND ARTIFICIAL NEURAL NETWORKS FOR POTATO MASS MODELING WITH DIMENSIONAL ATTRIBUTES

DAVOUD GHANBARIAN\* AND ROOHOLLAH FARHADI

Department of Agricultural Machinery Engineering, Shahrekord University, Shahrekord, Iran,  
Tel: +98-381-4424546, Fax: +98-381-4424428, E-mail: Ghanbarian51@yahoo.com

### Abstract

Finding the best relation that could predict mass of product versus its dimensional attributes is one of essential cases in the design and development of sorting machines. In this research, ordinary regressions methods and artificial neural network (ANN) were applied for finding relations between potato tubers dimensions (length, width and thickness) as input data and mass of tuber as output data. After application of various regression methods, smoothing spline technique had best results concerning comparison of coefficients of  $R^2$ , SSE and RSE for mass prediction, while the GRNN model in view of MAE and SDAE conducted best results between ANNs methods. The comparison of best regression and ANN methods showed that in the most cases ANNs methods have less errors and better precision. As a result, the GRNN method having three inputs and MAE=9.14 gram recommends as the best method for predicting mass of potato tubers.

### Introduction

Potato is one of the most important agricultural products in Iran and other countries of the world. Grading seed tubers is a basic post harvest operation of this product. The best method of potato sorting is gradation based on mass according to researches of Goryachkin (1968), Shaym (1982), and Butler et al. (2005). Although weight of tubers is the best criterion for separating seed tubers but, weight sizing mechanisms because of slowness and costliness are not customary and it usually is performed by the dimensional attributes (length, width and thickness of tubers). Therefore, determining the best relationship between mass and dimensions is one of the researchers' activities. Recently, artificial neural networks as powerful implements for modeling complex relation between inputs and outputs are attended to agriculture researchers (Ghaboussi et al. (1991), Hall (1992), Altendorf (1993), Drummond et al. (1995), Zhang and Kushwaha (1999)). Examinations of done researches in the potato

gradation field show most researchers have used ordinary regression methods for finding relation of potato and its dimensions. Then the objective of this research is investigation of ANN efficiency and performance comparison of conventional regression methods and artificial neural networks for potato mass modeling with dimensional attributes.

### Material and methods

**Data selection and measurement:** 475 numbers potatoes of Morfana variety randomly picked from farm in Hamedan province. Morfana variety is one of most conventional important potato varieties in Iran (Author, 2005). After cleaning them, dimensions and mass were measured by caliper and digital balance respectively with precision of 0.1 mm and 0.1 gram. Data characteristics after transfer to spreadsheet Excel software has presented in table 1.



Table1. Statistical characteristics of measured data

	Mass	Height	Width	length
	gr	mm	mm	mm
Mean	155.8	51.4	60.5	73.3
Standard deviation	128.8	25.6	16.3	22.7
Min	11.1	21.1	26.3	30.1
Max	833.4	112.0	109.0	170.0
Coefficient of variation (%)	82.7	49.8	26.9	31.0

Table2. Data distribution at three sorts of small, mean and large

		Mass	Height	Width	length
		gr	mm	mm	mm
Difference of min and max		822.3	90.9	82.7	139.9
Sorts distances		274.1	30.3	27.6	46.6
distribution status	Small	numbers	405	16	3
		%	85.26	3.37	0.63
	Mean	numbers	63	354	198
		%	13.26	74.53	41.68
	large	numbers	7	105	274
		%	1.48	22.1	57.68

**Study of data distribution status:** Difference between minimum and maximum was measured and divided by three for each characteristic (length, width, height and mass) until three sorts of: small, mean and large appear. Circumstance of data dispensation was shown in table 2.

**Division and data random selection:** 2/3 of data was used for relation calculation (317 data) and 1/3 for examination and evaluation (158 data). Whereas mass criterion contains more importance at gradation and 158 selective data for test should have same dispensation of original data until all input range is tested and examined at relation, distribution percentage of table 2 part mass was exerted for data. Hence 158 test data should choose from total input data according table 3. A special program with FORTRAN language was written for selection of random data without repeats according to table 3 pattern.

Table3. Test data distributions circumstance

	Small	Mean	Large	Sum
Percentage	85.26	13.26	1.48	100
Numbers	135	21	2	158

**Conventional regression methods:** The following three methods generally are used for mass prediction according tuber dimensions:

1. One variable regression consisting in relation between mass and each dimension separately:  $M=f(L)$ ,  $M=f(W)$ ,  $M=f(H)$ .
2. Two variable regression consisting in relation among mass and dual components of dimensions:  $M=f(L, W)$ ,  $M=f(L, H)$ ,  $M=f(H, W)$ .
3. Three variable regression consisting in relation among mass and all dimensions:  $M=f(L, W, H)$ .

MATLAB software was used for regression calculations. This software contains complete and comprehensive collection of regression methods and graphical capabilities perfects its operation. Ten methods of curve fitting toolbox were applied for one variable and Quadratic response surface model for others. The best choice criterion was based on maximum of determination coefficient ( $R^2$ ) and minimum of SSE (Sum of squares due to error) and RSE (Regression standard error) in one variable state. Quadratic response surface model utilizes following equation for fitting and software presents related coefficients ( $b_i$ ,  $b_{ij}$ ):

$$y = b_0 + b_1x_1 + b_2x_2 + b_3x_3 + b_{12}x_1x_2 + b_{13}x_1x_3 + b_{23}x_2x_3 + b_{11}x_1^2 + b_{22}x_2^2 + b_{33}x_3^2$$

**Artificial neural network method:** ANN is formed by some neurons that position beside to



one another with special order. Each net contains minimum two layers: input and output. Also several hidden layers can be between input and output layers (figure 1).

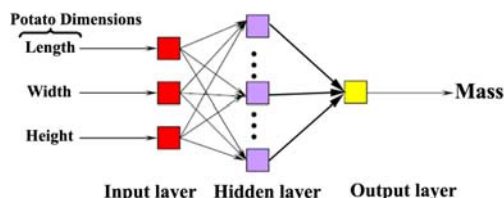


Figure 1. The ANN different layers

More ANN architectures and algorithms change by alteration of neuron model, relation among neurons and weight function. Two ANN types of Generalized Regression Neural Networks (GRNN) and BP were selected at MATLAB neural network toolbox. These two models have been applied in most researches for function approximation and relation creation between inputs and outputs. The BP model contains different training methods that Levenberg-Marquardt (trainlm) and quasi-Newton (trainbfg) had the best results concerning various tests. Thus, for computation at next stages these methods were used. Other points that should determine in the BP model are layers numbers and neurons of each layer with applied functions. This part plentifully depends on experience and demands examination of different phases. Chosen model after abundant efforts has three layers of 1-500-1 (first layer may be 2 or 3 based on input condition) with transfer functions of Logsig and Purelin presented better results than other states (figure 2).

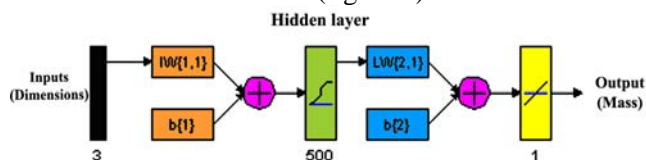


Figure 2. Applied BP model with three inputs

In the GRNN model neuron numbers equals input layers. Figure 3 shows its architecture. Its input condition is similar to the BP model. The best result was selected with examination of

various spread values. Then model was prepared for use. Spread exhibits band width that neurons respond at input distance. Spread should be large enough to cover input distance strongly and presents proper respond. If spread value becomes very large each neuron effectively responds at wide zone and suitable result is not obtained.

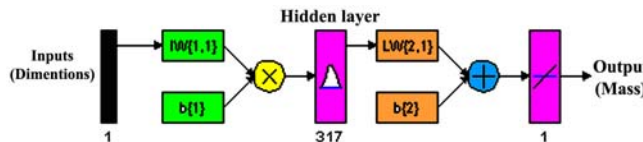


Figure 3. The GRNN model exhibition

**Test and comparison fashion:** 158 test data were used for evaluation and comparison of regression methods. Results of regression calculation and actual data were compared then mean and standard deviation of absolute value of error were computed as following formulas:

$$MAE = (1/n) \sum_{i=1}^n |m_{a_i} - m_{e_i}|$$

$$SDAE = \sqrt{[1/(n-1)] \sum_{i=1}^n [m_{a_i} - m_{e_i} - MAE]^2}$$

Where MAE: mean of absolute value of error;  $M_a$ : actual mass;  $M_e$ : estimated mass; N: numbers of inputs; ADSE: standard deviation of absolute value of error.

In the ANN after definition and training of model results were calculated. Similar to regression methods mean and standard deviation of absolute value of error were computed. Finally outcomes of the ANN and regression methods based on mean of absolute value of error were compared with test of two mean comparisons (t-test).

## Results and discussion

**Regression:** Among conventional regression methods (one variable) smoothing spline has the best results for mass prediction with regard to  $R^2$ , SSE and RSE values comparison. Table 4 show calculation results of w-m state for instance.

Table 4. Results of ten regression methods for w-m state

Methods	Equations	Regression results		
		RSE	SSE	R <sup>2</sup>
Exponential	$ae^{bx} + ce^{dx}$	34.894	381103.08	0.926
Logarithmic	$a \ln x + b$	61.335	1185038.3	0.770
Fourier	$a_0 + (a_1 \cos x + b_1 \sin x) + \dots + (a_8 \cos 8x + b_8 \sin 8x)$	123.768	4580227.6	0.110
Gaussian	$a_1 e^{\frac{x-b_1}{c_1}} + \dots + a_8 e^{\frac{x-b_8}{c_8}}$	29.178	249444.4	0.952
Polynomial	$a_0 + a_1 x + \dots + a_9 x^9$	34.810	372004.41	0.928
Power	$ax^b + c$	34.713	378364.69	0.926
Rational	$\frac{a_0 + a_1 x + \dots + a_5 x^5}{a_0 + a_1 x + \dots + a_4 x^4}$	33.060	335544.6	0.935
Smoothing spline	Variable polynomial oscillating 1 to 3 degrees (Linear, Quadratic and cubic equations)	23.195	90158.643	0.982
Sum of Sin functions	$a_1 \sin(b_1 x + c_1) + \dots + a_8 \sin(b_8 x + c_8)$	208.659	1.28 E7	-1.479
Weibull	$abx^{(b-1)} e^{(-ax^b)}$	202.232	1.29 E7	-1.503

**Artificial neural network:** Calculation summary concerning ANNs is presented in table5. This point is indicated as mention that intention of mean and standard deviation (SD) respectively is error absolute value mediocre and standard deviation between actual test data mass (158 data) and computed value by ANNs. The GRNN model

has better conditions and lower error than BP model as it is seen in table5.

**Results comparison:** The best values of regression methods (smoothing spline and multiple quadratic regressions) and artificial neural network (GRNN) are presented in table 7 in addition to comparative test results for differences significance discernment.

Table5. Comparison calculation results of the GRNN and BP model

	Models							
	GRNN				BP			
	GRNN results		Spread value		trainlm		trainbfg	
	Mean	SD			Mean	SD	Mean	SD
M=f(L)	26.636	28.152	5		31.550	33.980	28.920	34.916
M=f(W)	21.076	29.582	2		23.449	30.702	23.100	31.817
M=f(H)	27.848	37.434	5		31.585	44.826	33.471	48.251
M=f(L,W)	12.820	14.643	3		16.382	18.690	15.695	20.867
M=f(L,H)	14.646	20.502	5		18.206	21.580	16.832	23.794
M=f(W,H)	19.992	28.641	6		34.464	56.607	23.557	31.195
M=f(L,W,H)	9.144	16.247	3		16.484	28.340	20.993	28.382

Table 7. Absolute values of error for comparison of best regression methods and ANNs

	Regression		Neural network		Comparison		
	Smoothing spline / multiple quadratic regression		GRNN		t	t <sub>5%</sub>	Differences condition
	Mean	SD	Mean	SD			
M=f(L)	35.37	43.65	24.64	28.15	2.11	1.969	*
M=f(W)	27.02	35.56	21.08	29.58	1.62	1.968	-
M=f(H)	35.5	54.41	27.85	37.43	1.64	1.969	-
M=f(L,W)	12.19	16.09	12.82	14.64	0.36	1.968	-
M=f(L,H)	12.58	16.41	14.65	20.5	0.99	1.968	-
M=f(W,H)	20.35	22.87	19.99	28.64	0.12	1.968	-
M=f(L,W,H)	8.86	15.67	9.14	16.25	0.16	1.968	-

\* Significant at 95% confidence level.

- Non significant

Artificial neural network fashion contains lower absolute value of error in many cases than regression methods. Although artificial neural network primacies do not have significant difference apart one item but this itself declares that ANN has competition ability and equality with the best conventional regression methods. Figure 4 shows an instance of the GRNN predicted mass versus test data.

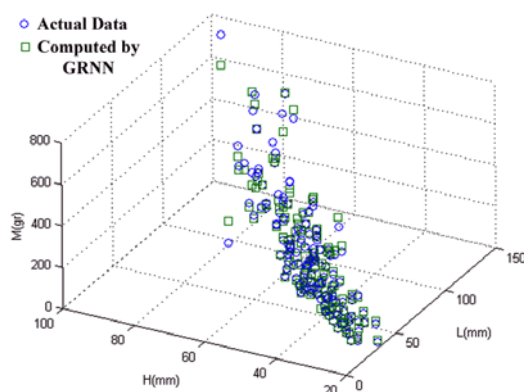


Figure 4. The GRNN predicted mass vs. actual data

## Conclusion

- The best regression method was smoothing spline with comparison of results at whole cases (singly order state).
- Minimum error values obtained at perfect state then two variables and finally at singly order.

- Between two neural networks models of GRNN and BP the first possessed better operation and had lower error at total cases.
- Regression method only at two cases contains less error as those differences with neural network was not significant too.
- The GRNN model function as proper, competitive and coequal method to the best regression techniques and are very powerful based outcome results.

## References

- [1] Altendorf, C. A. 1993. Estimating Soil Water Content using Soil Temperatures and Neural Network. Unpublished Ph.D. Dissertation. Department of Biosystems and Agricultural Engineering. Oklahoma State University, Stillwater Oklahoma.
- [2] Butler, G.P., T. Bernet and K. Manrique. 2005. Mechanization of potato grading on small- scale farms: A case study from Peru. Expl. Agric. 41:81-92.
- [3] Drummond, S. T., K. A. Suddeth and S.J. Birrell. 1995. Analysis and Correlation Methods for Spatial Data. ASAE Paper 95-1335. ASAE, 2950 Niles Rd., St. Joseph, MI 49085-9659.
- [4] Ghaboussi, J., J.H. Garrett and X. Wu. 1991. Knowledgebase modeling of material behavior with neural networks. Journal of engineering mechanics 117(1): 132-153.

- [5] Goryachkin, V.P. 1968. About potato grading. Collected works, Kolos, Moscow, Pp. 190-202 (In Russian).
- [6] Hall, J. W. 1992. Emulating Human Process Control Functions with Neural Networks. Unpublished Ph.D. Dissertation. Department of Mechanical Engineering. University of Illinois, Urbana Illinois.
- [7] Peleg, K. 1985. Produce handling, packaging, and distribution. The AVI Publishing Company. Inc. Westport, Connecticut, 55–95.
- [8] Shaym, M. 1982. Criteria for separating potato tubers in to different size- grades. J. Agric. Eng. 19 (4): 77-83.
- [9] Zhang, Z.X. and R.L. Kushwaha. 1999. Application of neural networks to simulate soil-tool interaction and soil behavior. Canadian agricultural engineering 41(2):119-125.

## COMPACTION BEHAVIOR OF ALFALFA GRINDS

DAVOUD GHANBARIAN\* AND AFSANEH KARAMI

\* Department of Agricultural Machinery Engineering, Shahrekord University, Shahrekord, Iran,  
Tel: +98-381-4424546, Fax: +98-381-4424428, E-mail: Ghanbarian51@yahoo.com

### Abstract

Densification of biomass is one of the important processes for effective handling and storage of bulky hay materials. To design and development of pellet mill equipments, it is required to understand compaction behavior of alfalfa grind. In this research, to simulate the pelleting process, alfalfa grind compressed in a plunger and die assembly. The experiments were done on alfalfa grinds at 10, 15 and 20 % moisture content (w.b.) and 3.26 and 4.75 mm grind size. The results showed that at any particular pressure the density of pellets was highest for 10% moisture content and 3.26 mm grind size. Seven compression models namely: Jones, Butler-Mc Colly, Perezhagin, Garyachkin, Kawakita, Mewes, and Panelli-Filho were fitting on the test results to predict the compaction behavior of alfalfa grinds. The results showed that compressibility of alfalfa grind changes during compaction test. There was a rapid increase in density of pellets at lower compression pressures, but at higher compaction pressures, density values continued to increase at a lower rate. Among the seven studied models, Jones's model had higher coefficient of determination ( $R^2$ ) and lower standard error of regression (RSE).

**Keywords:** Alfalfa pellet, Compaction behavior of grind, Compression models

### Introduction

Study of compaction behavior of alfalfa grinds is required to design of pellet mill. Jones (1960) expressed the density-pressure data of compacted metal powder in the form of following equation:  
$$Ln\rho = mLnP + b.$$

Where,  $\rho$  is bulk density of compact powder mixture, kg/m<sup>3</sup>;  $m$  and  $b$  are constants. Butler and Mc Coly (1962) described the density-pressure data of alfalfa particles at moisture content 12% in the form of equation:  $P = Ae^{n\gamma}$ .

Where,  $\gamma$  is compacted alfalfa density at  $P$  pressure;  $A$  and  $n$  are constants. Perezhagin (1963) proposed an equation that expressed density-pressure data of hay materials:  
$$\gamma = (\gamma_0 + AP^n) \times [1 + 0.03(w - 12)].$$

Where,  $P$ -pressure;  $\gamma_0$  -initial density;  $W$ -moisture content;  $A$  and  $n$ - constants. Gariachkin (1965) considered the pressure-piston displacement of hay in the form of equation:

$$P = aP_{\max} \left(1 - \frac{S^2}{L^2}\right) + b.$$

Where,  $P$ -pressure;  $S$ -piston displacement;  $L$ -Cylinder length;  $P_{\max}$ -final pressure;  $a$  and  $b$ -constants. Kawakita and Ludde (1971) performed compression experiments and proposed an equation for compaction of powder materials based on observed relationship between pressure and

$$\text{volume: } \frac{P}{C} = \frac{1}{ab} + \frac{p}{a}.$$

Where,  $P$  is pressure;  $C$  is degree of volume reduction or engineering strain;  $a$  and  $b$  are constants. Kawakita-Ludde' model constants related to characteristic of the powder materials.

The linear relationship between  $\frac{P}{C}$  and  $P$  allows

the constants to be evaluated graphically. This compression equation holds true for soft and fluffy powders, but particular attention must be paid on the measurement of the initial volume of the value of  $V_0$ . The constant  $a$  is equal to the values of  $C = C_{\infty}$  at infinitely large pressure  $P$ :

$$a = C_{\infty} = \frac{V_0 - V_{\infty}}{V_0}.$$

Where,  $V_{\infty}$  = net volume of the powder,  $m^3$ .

It has been reported that the constant  $a$  is equal to the initial porosity of the sample, while constant  $1/b$  is related to the failure stress in the case of piston compression (Mani *et al.*, 2004). Mewes (1974) considered compression behavior of hay material and described density-pressure data as follow:  $P = A(\gamma^n - \gamma_0^n)$ .

Where,  $\gamma$  is density at P pressure;  $\gamma_0$  is initial density;  $n$  is constant. A new compression equation was proposed by Panelli-Filho (2001), given as:

$$\ln\left(\frac{1}{1 - \rho_r}\right) = A\sqrt{P} + B$$

where,  $\rho_r$  is the relative density of the compact; A is a parameter related to densification of the compact by particle deformation and B is a parameter related to powder density at the start of compression. Therefore, the objectives of the current study were to: 1) review of various compression models to choose the best model for predicting the relation of pressure, volume and density of alfalfa grinds; and 2) study compression behavior of alfalfa particle at different level of moisture content and particle size.

### Materials and methods

The alfalfa was obtained from Isfahan province in center of Iran. A hammer mill (CH model) with power of 1.5 Kw and 3450 rpm was used to grind alfalfa hay. The experiments were down on alfalfa grinds at 10, 15 and 20 % moisture content (wb). Moisture contents were determined according ASAE S358.2 standard. In order to simulate the pelleting process, samples compressed in a plunger and die assembly using instron machine. Crosshead speed was set at 2.5 mm/s.

Seven compression models were fitting to the test results to analyze the compaction behavior of alfalfa grinds by Excel and Sigma plot soft wares, namely: Jones, Butler-Mc Colly, Perezhagin, Gariachkin, Kawakita, Mewes and Panelli-Filho models. The best model was chosen based on the coefficient of determination ( $R^2$ ) value and standard error of regression (RSE).

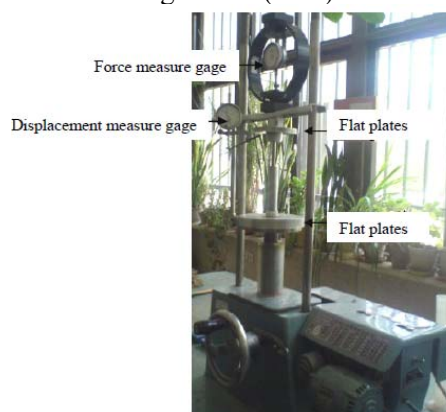


Figure1-CBR set compress alfalfa particle in plunger and die assembly

### Results and discussion

Tables 1 and 2 show the effect of applied pressure on changes of pellet density in different compaction stages at two particle sizes of 3.26 and 4.75 mm. In both particle sizes, density decrease as moisture increase. Therefore samples with higher moisture content require more compaction force to attain determined density. Also in comparison between tables 1 and 2, smaller particle size (3.26) compacted easily, so have more density in related to larger particle size (4.75mm). Therefore, maximum density happened at 10% moisture content and 3.26 mm particle size.



Table 1- Density change of alfalfa grinds during compression at 3.26mm particle size

Force (N)	Pressure (Mpa)	) $\frac{Kg}{m^3}$ Density (		
		10% moisture content	15% moisture content	20% moisture content
500	7.86	1000.27±13.7	974.37±30.2	970.47±6.01
1000	15.72	1.9 1068.15±	1066±32.84	1031.38±12.74
1500	23.58	1113.74±10.22	1110.1±30.68	1033.33±1.78
2000	31.44	1131.67±12.76	1130.34±21.5	1057.6±8.52
2500	39.3	1144.62±8.76	1142.73±0	1101.54±18.41

Table 2- Density change of alfalfa grinds during compression at 4.75mm particle size

Force (N)	Pressure (Mpa)	) $\frac{Kg}{m^3}$ Density (		
		10% moisture content	15% moisture content	20% moisture content
500	7.86	975.6±8.27	960.61±0	951.86±6.59
1000	15.72	5.62 1060.82±	1058.85±18.9	1015.13±3.43
1500	23.58	1086.76±26.27	1070.96±9.07	1031.27±1.77
2000	31.44	1108.79±25.4	1103.74±10.22	1045.83±3.64
2500	39.3	1132.73±0	1127.94±21.47	1055.44±8.12

Figures 2 and 3 show the pressure-density plot of individual pellets at each preset compressive load. In the beginning, most of the present air in voids was expelled out and particle rearrangement

occurred. As compressive force progressed, the slope increased indicating densification by elastic and plastic deformation of biomass grinds.

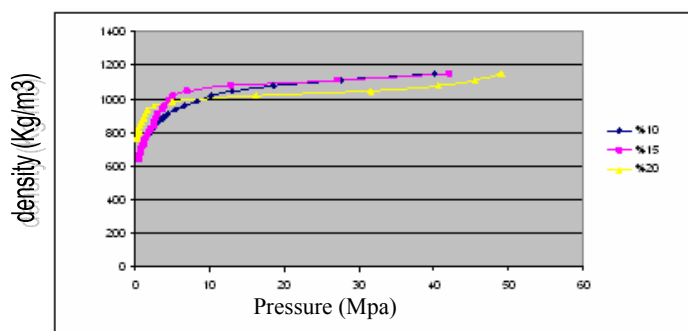


Figure2- pressure-density plot of alfalfa particles at 3.26 mm size

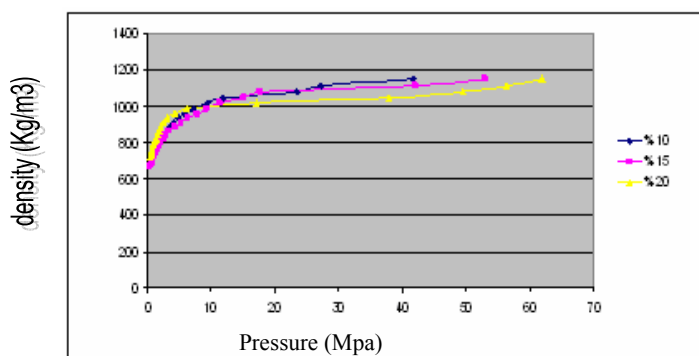


Figure3- pressure-density plot of alfalfa particles at 4.75 mm size

The pressure-density data samples were fitted to the Jones, Butler-Mc Colly, Perezhagin, Gariachkin, Kawakita, Mewes and Panelli-Filho models. One of the main purposes of fitting experimental data to an equation is usually to linearize the plots in order to make comparisons

easier between different sets of data. Table 3 shows the model parameters for all samples at tree different moisture content 10,15 and 20% and two particle sizes 3.26 and 4.75 mm that in table 3 introduce by a and b respectively.

Table 3- Fit of models to the compression data

$Ln\rho = mLnP + b$				Jones model	
Constants		RSE	R <sup>2</sup>	Particle size	moisture
$m = 0.127$	$b = 6.61$	0.01	0.99	a	10
$m = 0.116$	$b = 6.64$	0.02	0.98	b	
$m = 0.15$	$b = 6.6$	0.05	0.94	a	15
$m = 0.118$	$b = 6.61$	0.02	0.99	b	
$m = 0.067$	$b = 6.67$	0.03	0.95	a	20
$m = 0.084$	$b = 6.63$	0.03	0.95	b	
$\frac{P}{C} = \frac{1}{ab} + \frac{p}{a}$		Kawakita model			
$a = 0.45$	$b = 0.57$	2.21	0.99	a	10
$a = 0.45$	$b = 0.62$	1.87	0.99	b	
$a = 0.53$	$b = 1.76$	4.93	0.94	a	15
$a = 0.46$	$b = 0.38$	1.43	0.99	b	
$a = 0.42$	$b = 1.27$	2.65	0.99	a	20
$a = 0.43$	$b = 1$	2.7	0.99	b	
$P = aP_{\max}(1 - \frac{S^2}{L^2}) + b$		Gariachkin model			
$a = 0.63$	$b = 23.3$	4.9	0.86	a	10
$a = 0.74$	$b = 25.21$	5.77	0.73	b	
$a = 0.53$	$b = 19.9$	6.3	0.56	a	15

$a = 0.8 \quad b = 29.5$	7.54	0.68	b	20
$a = 1.43 \quad b = 40.96$	8.6	0.79	a	
$a = 1.47 \quad b = 46.7$	11.03	0.74	b	
$P = Ae^{n\gamma}$ Butler-Mac coly model				
$A = 0.002 \quad n = 0.009$	0.08	0.99	a	10
$A = 0.001 \quad n = 0.009$	0.17	0.98	b	
$A = 0.005 \quad n = 0.007$	0.26	0.95	a	15
$A = 0.001 \quad n = 0.01$	0.17	0.99	b	
$A = 1.87E - 006 \quad n = 0.01$	0.38	0.96	a	20
$A = 4.48E - 005 \quad n = 0.01$	0.32	0.97	b	
$\gamma = (\gamma_0 + AP^n) \times [1 + 0.03(w - 12)]$ Perezhagin model				
$A = 163.1 \quad n = 0.04$	0.097	0.96	a	10
$A = 172.5 \quad n = 0.38$	0.098	0.96	b	
$A = 123.2 \quad n = 0.6$	0.3	0.84	a	15
$A = 142.2 \quad n = 0.44$	0.143	0.95	b	
$A = 272.6 \quad n = 0.19$	0.11	0.92	a	20
$A = 211 \quad n = 0.26$	0.16	0.89	b	
$Ln(\frac{1}{1 - \rho_r}) = A\sqrt{P} + B$ Panelli-Filho model				
$A = 0.42 \quad B = 0.54$	0.02	0.99	a	10
$A = 0.39 \quad B = 0.61$	0.07	0.99	b	
$A = 0.44 \quad B = 0.55$	0.15	0.95	a	15
$A = 0.35 \quad B = 0.62$	0.08	0.99	b	
$A = 0.24 \quad B = 1.03$	0.21	0.92	a	20
$A = 0.24 \quad B = 0.91$	0.19	0.96	b	
$P = A(\gamma^n - \gamma_0^n)$ Mewes model				
$A = 6.98E - 27 \quad n = 9.05$	1.25	0.99	a	10
$A = 5.57E - 30 \quad n = 10.08$	1.39	0.98	b	
$A = 6.12E - 30 \quad n = 10.04$	2.7	0.92	a	15
$A = 1.84E - 28 \quad n = 9.61$	2.8	0.97	b	
$A = 2.42E - 24 \quad n = 8.29$	7.47	0.9	a	20
$A = 1.37E - 27 \quad n = 9.37$	5.87	0.93	b	

Among seven compression models, based on the coefficient of determination ( $R^2$ ) value and standard error of regression (RSE), the Jones and Panelli-Filho models fitted fairly well with the compression data at 10 and 15% (wb) moisture

content and 3.26 and 4.75 mm particle sizes. At 20% moisture content and 3.26 mm particle size Jones and Panelli-Filho models and at the same moisture content and 4.75 mm particle size Jones, Butler-Mc Colly provided an excellent fit to

pressure-density data. To consider all level of moisture content and particle size, the Jones model fitted fairly well to compaction datd. Figures 4 and 5 show Jones model plots for alfalfa grinds at 3.26 mm size respectively.

and 4.75 mm particle size respectively. In these figure moisture content 10,15 and 20% were introduce by  $m_1$ ,  $m_2$  and  $m_3$ .

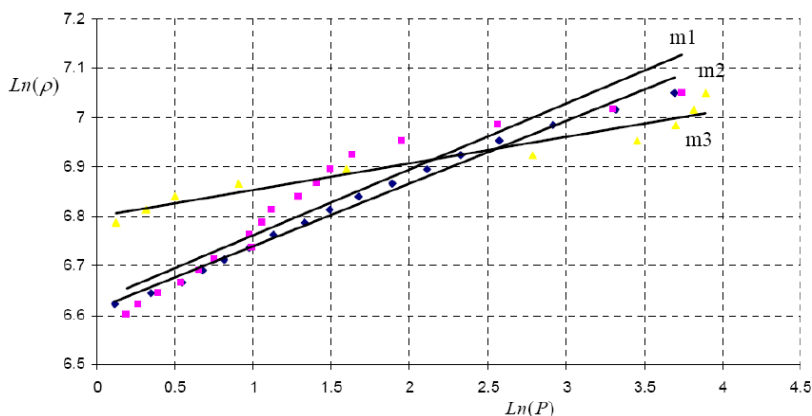


Figure 4- Jones plots of alfalfa particles at 3.26 mm size

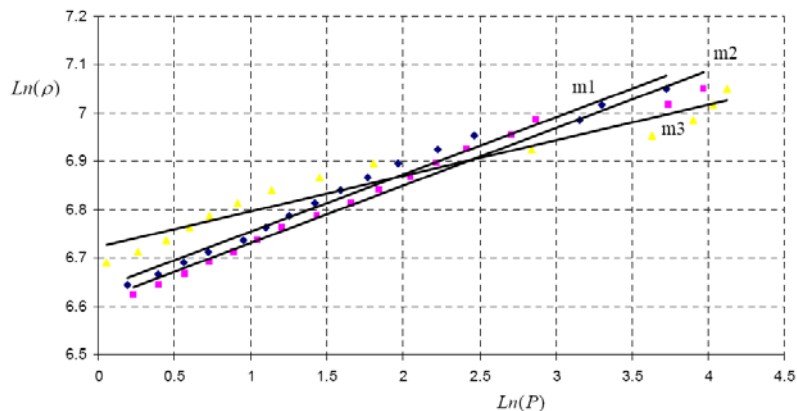


Figure 5- Jones plots of alfalfa particles at 4.75 mm size

## References

- [1] ASABE. 2006. ASAE S358.2 – Moisture measurement – forages. In ASABE Standards, 608. St. Joseph, MI.: American Society of Agricultural and Biological Engineers.
- [2] Asoboff, V.I, Vasilief, G.K and Galianovski, A.V. 1974. Mashines troienie. Moscow. (In Russian)
- [3] Butler, I.L and Mc Colly, H.F. 1962. Factors affecting the pelleting of hay. Agricultural Engineering. 40:442-446.
- [4] Gariachkin, V.P. 1965. Sobranie Sochinenie. TOM3 Kolos. (In Russian)
- [5] Jones, W.D. 1960. Fundamental Principles of Powder Metallurgy. Edward Arnold Publishers Ltd. London. 242-370.

- [6] Kawakita, K and Ludde, K.H. 1971. Some Considerations on Powder Compression Equations. Powder Technology. 4: 61-68.
- [7] Mani, S, Tabil, L.G and Sokhansanj, S. 2004. Evaluation of Compaction Equations Applied to Four Biomass Species. Canadian Biosystems Engineering. 46: 355-361
- [8] Panelli, R and Filho, F.A. 2001. A Study of a New Phenomenological Compacting Equation, Powder Technology. 114: 255-261.
- [9] Perezhagin, M.A and Sergeief, M.P. 1963. Davlenie V Kamere Pressa I energoiekomb briketorivania groubikh karmof. Masgiz. 157-162. (In Russian).

## DAILY PAN EVAPORATION ESTIMATION USING A NEURO-FUZZY-BASED MODEL

SHAHRAM KARIMI-GOOGHARI\*

Assistant Professor, Department of Water Engineering, Shahid-Bahonar University of Kerman, Kerman, Iran ([shkarimi1352@gmail.com](mailto:shkarimi1352@gmail.com))

### Abstract

Evaporation, as a water loss, is important in water resources development and management. In arid zones where water resources are scarce, the estimation of this loss becomes more interesting in the planning and management of irrigation practices. This paper investigates the abilities of Adaptive Neuro-Fuzzy Inference System (ANFIS) technique to improve the accuracy of daily evaporation estimation. Different ANFIS models comprising various combinations of daily climatic variables, that is, air temperature, daily sunshine hours, wind speed, and relative humidity are developed to evaluate degree of effect of each mentioned variables on evaporation for two stations located in central part of I.R. Iran. A comparison is made between the estimates provided by the ANFIS models and the multiple linear regressions. Various statistic measures are used to evaluate the performance of the models. Based on the comparisons, it was revealed that the ANFIS computing technique could be employed successfully in modeling of evaporation process from the available climatic data. The ANFIS also increased the accuracy of evaporation estimation compare to the multiple linear regression models.

**Keywords:** Evaporation Estimation, ANFIS, Climatic Variables.

### Introduction

Evaporation (E) is a complex and non-linear process since it depends on several interacting factors, such as sunshine hour, temperature, humidity and wind speed. Accurate estimation of E is importance for many studies, such as hydrologic water balance, irrigation system design and management, and water resources planning and management. For many years engineers and researchers have used loss from evaporation pans, multiplied by a coefficient applicable to the particular pan, as an estimate of the evaporation loss from reservoirs. The most widely used pan is the US Weather Bureau Class A pan which is 4 ft in diameter and 10 in. deep and is mounted on a timber grill about 6 in. above the soil surface. Pan evaporation has been widely used as an index of evapotranspiration and for estimating lake and reservoir evaporation [1].

It is impractical to place evaporation pans at every point where there is a planned or existing reservoir and irrigation project. It is also highly unlikely to have in inaccessible areas where accurate instruments can not be established or maintained. A practical means of estimating the amount of pan evaporation where no pans are available is of considerable significance to the

hydrologists, agriculturists, and meteorologists. A number of methods have developed to estimate the evaporation values from climatic variables [2-5] and most of these methods require data that are not easily available. Simple methods that are reported [e.g., 2] try to fit a linear relationship between the variables. However, the process of evaporation is highly non-linear in nature, as it is evidenced by many of the estimation procedures. Many researchers have emphasized the need for accurate estimates of evaporation in hydrologic modeling studies [6]. This requirement could be addressed through better models that will address the inherent non-linearities in the process.

Soft Computing (SC), an innovative approach to constructing computationally intelligent systems, has recently come into the limelight. It is realize that complex real-world problems require intelligent systems that combine knowledge, techniques, and methodologies from various sources. Artificial neural networks (ANN) and fuzzy inference systems (FIS) are the most popular and successful approaches resulting from advances in a branch of nonlinear system theoretic modeling. ANN models have been used successfully to model complex nonlinear input-output time series relationships in a wide variety

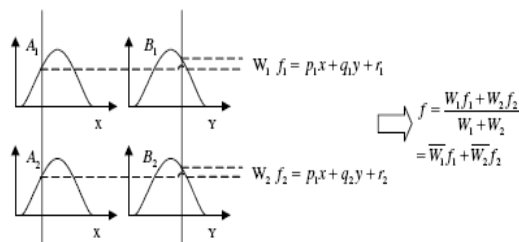


of water resources fields. FIS have been used in controller systems and model identification also. The synergism allows soft computing to incorporate human knowledge effectively to deal with imprecision and uncertainty, and learn to adapt to unknown or changing environment for better performance [7]. Fuzzy systems and neural networks share their ability to improve the intelligence of systems working in uncertain, imprecise, and noisy environments. Neuro-fuzzy networks combine the explicit knowledge representation of fuzzy logic with the learning power of neural networks [8]. For this reason, recently interest in using the adaptive neuro-fuzzy inference system (ANFIS) is increasingly raised. ANFIS is a typical Neuro-fuzzy [9] which uses the Takagi-Sugeno fuzzy inference engine model with a six layers feed-forward network. Neuro-fuzzy approach has been employed successfully in some fields of water resources engineering such as rainfall-runoff modeling [10] and reservoir water level prediction [11].

The potential of the ANFIS-based models for estimating of the evaporation using climatic variables is investigated and discussed in this study. The performance of the ANFIS models is compared with multiple regression method.

### Adaptive neuro-fuzzy inference system (ANFIS)

Adaptive neuro-fuzzy inference system (ANFIS), first was proposed by Jang [9], can



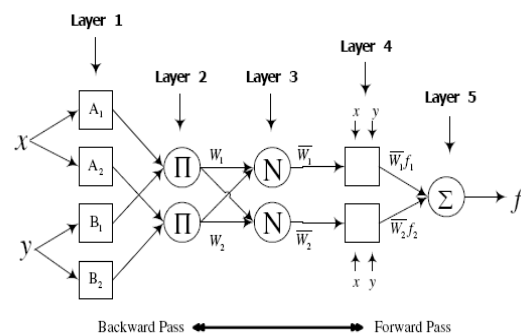
(a)

achieve a highly nonlinear mapping and it is superior to common linear methods in producing nonlinear time series [7]. Throughout this research, it was considered the ANFIS architecture for the first order Sugeno fuzzy model. The ANFIS is a multilayer feed forward network which uses neural network learning algorithms and fuzzy reasoning to map an input space to an output space [3]. Assuming the fuzzy inference system under consideration has two inputs,  $x$  and  $y$ , and one output,  $f$  for a first-order Sugeno fuzzy model, a common rule set with two fuzzy if-then rules can be expressed as:

Rule 1: If  $x$  is  $A_1$  and  $y$  is  $B_1$  then  $f_1 = p_1 x + q_1 y + r_1$  (1)

Rule 2: If  $x$  is  $A_2$  and  $y$  is  $B_2$  then  $f_2 = p_2 x + q_2 y + r_2$  (2)

Where  $A_1$ ,  $A_2$  and  $B_1$ ,  $B_2$  are the membership functions (mfs) for inputs  $x$  and  $y$ , respectively;  $p_i$ ,  $q_i$  and  $r_i$  ( $i = 1$  or  $2$ ) are linear parameters in the consequent part of the first-order Sugeno fuzzy model. Figure 1(a) illustrates the fuzzy reasoning mechanism for this Sugeno model to derive an output function ( $f$ ) from inputs  $x$  and  $y$ . The corresponding equivalent ANFIS architecture is showed in Figure 1(b), where nodes of the same layer have similar functions. ANFIS consists of five layers as illustrate in Figure 1(b). More details are explained in Jang paper [9].



(b)

Figure 1. (a) A two input first order Sugeno fuzzy model with two rules; (b) Equivalent ANFIS structure [7].

### Study Area and Data

The daily climatic data of two weather stations, Esfahan Station (latitude  $32^{\circ} 37' N$ ,

longitude  $51^{\circ} 40' E$ ) and Kashan station (latitude  $33^{\circ} 59' N$ , longitude  $51^{\circ} 27' E$ ) operated by Iranian meteorological organization are used in

the study. The elevations are 1550 and 982 m for the Esfehan and Kashan Stations, respectively. The data sample consisted of ten years (1995–2005) of daily records of air temperature (T), sunshine hour radiation (SH), wind speed (W), relative humidity (RH) and pan evaporation (E).

For each station, the 70 percent if data were used to train the models and the remaining data were used for validation and testing. The statistics properties of collected data are presented in Table 1.

Table 1. The statistics properties of the data

Parameter	Unit	Kashan Station					Esfehan Station				
		Ave.	Min.	Max	Std.	Skeness	Ave.	Min	Max	Std.	Skeness
<b>T</b>	°C	23.36	0.1	38.5	8.22	-0.441	20.1	0.1	38.4	7.15	-0.4
<b>H</b>	%	33.98	7	93	15.8	1.217	29.83	8	88	13.5	1.33
<b>SH</b>	hour	9.3	0.1	13.5	2.98	-1.39	10.16	0.1	13.9	2.64	-1.63
<b>W</b>	m/sec	0.348	0	4.59	0.6	2.45	1.16	0.1	9.95	1.2	1.56
<b>E</b>	mm	8.02	0.1	17.3	4.14	-0.092	8.007	0.1	18.2	3.84	-0.04

### Application and Results

The weather parameters considered in the study are the air temperature (T), solar radiation (SR), wind speed (W), pressure (P) and humidity (H). The study examined various combinations of these parameters as inputs to the ANFIS models so as to evaluate the degree of effect of each of these variables on evaporation. Building the ANFIS model several times with one different variable added into the input combination per time. Thus, the input combinations evaluated in the present study are: (i) T; (ii) T and SH; (iii) T, SH and W; (iv) T, SH, W and RH. The Gaussian membership function was considered. Subtractive clustering (SC) was used for determining number of membership functions and rules with different value of influence range and squash factor. The ANFIS model implementation was carried out using the Fuzzy Logic Toolbox of MATLAB software. The different fuzzy inference systems were trained by hybrid method and validation data was considered to avoid over-training. The performance of selected models which were developed in this study was evaluated by using a variety of standard statistical performance

evaluation measures. The performance of selected models which were developed in this study was evaluated by using a variety of standard statistical performance evaluation measures specifically, 4 different statistical performance indices have been employed: average absolute relative error (AARE), Pearson's correlation coefficient (R), Nash–Sutcliffe efficiency (CE), and normalized root mean square error (NRMSE). Tables 2 and 3 show the performance values for different ANFIS models in each station during training and testing process.

The higher values of performance indices, belonged to models with more variables (refer to Table 2 and 3). The selected models were KA4 and ES4 for Kashan and Esfehan station respectively. The minimum values of NRMSE and AARE indices and maximum values of R and CE show the superiority KA4 and ES4 clearly. In order to assess the ability of ANFIS modes relative to the multiple regression models, a linear model is developed using the KA4 and ES4 model inputs. The linear model for Kashan and Esfehan stations are:

Kashan Station	Esfehan Station
$E = -1.17 + 0.402(T) + 0.055(SH) + 0.353(W) + 0.022(RH)$ (R=0.903)	$E = 0.541 + 0.35(T) + 0.102(SH) + 0.508(W) + 0.046(RH)$ (R=0.847)

Table 2- The ANFIS models and their performance values for Kashan station.

During Training						
Model Inputs	No. of Rules	Name	R	CE	AARE	NRMSE
T	2	KA1	0.9	0.814	0.352	21.69
T, SH	2	KA2	0.905	0.82	0.341	21.34
T, SH, W	2	KA3	0.908	0.825	0.34	21.04
<b>T, SH, W, RH</b>	<b>2</b>	<b>KA4</b>	<b>0.911</b>	<b>0.83</b>	<b>0.307</b>	<b>20.8</b>
During Testing						
Model Inputs	No. of Rules	Name	R	CE	AARE	NRMSE
T	2	KA1	0.914	0.834	0.438	21.29
T, SH	2	KA2	0.915	0.837	0.424	21.12
T, SH, W	2	KA3	0.916	0.839	0.419	21.01
<b>T, SH, W, RH</b>	<b>2</b>	<b>KA4</b>	<b>0.92</b>	<b>0.84</b>	<b>0.381</b>	<b>20.94</b>

Table 3- The ANFIS models and their performance values for Esfahan station.

During Training						
Model Inputs	No. of Rules	Name	R	CE	AARE	NRMSE
T	2	ES1	0.822	0.676	0.42	26.97
T, SH	2	ES2	0.832	0.692	0.396	26.29
T, SH, W	2	ES3	0.847	0.717	0.378	25.19
<b>T, SH, W, RH</b>	<b>2</b>	<b>ES4</b>	<b>0.855</b>	<b>0.73</b>	<b>0.357</b>	<b>24.5</b>
During Testing						
Model Inputs	No. of Rules	Name	R	CE	AARE	NRMSE
T	2	ES1	0.818	0.667	0.427	26.46
T, SH	2	ES2	0.832	6.89	0.406	25.55
T, SH, W	2	ES3	0.842	0.707	0.396	24.8
<b>T, SH, W, RH</b>	<b>2</b>	<b>ES4</b>	<b>0.845</b>	<b>0.72</b>	<b>0.366</b>	<b>24.24</b>

The R in training period for linear model using all four input variables is equal to KA1 which uses only temperature variable. The results of estimating evaporation for testing period are illustrated in figure 2, 3, for ANFIS

and linear models for Kashan station. Results show that the KA1 model performs better than linear model. The similar results can be found in Esfahan station (Figure 4 and 5).

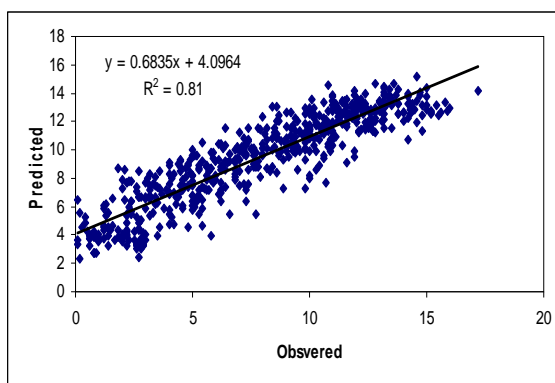


Figure 2- The observed and estimated evaporation of the Kashan Station in test period using linear model.

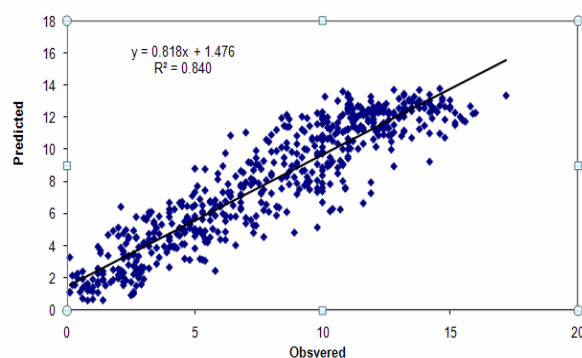


Figure 3- The observed and estimated evaporation of the Kashan Station in test period using KA4 model.

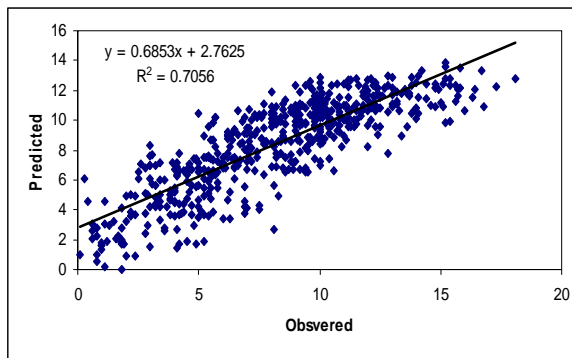


Figure 4- The observed and estimated evaporation of the Esfahan Station in test period using linear model.

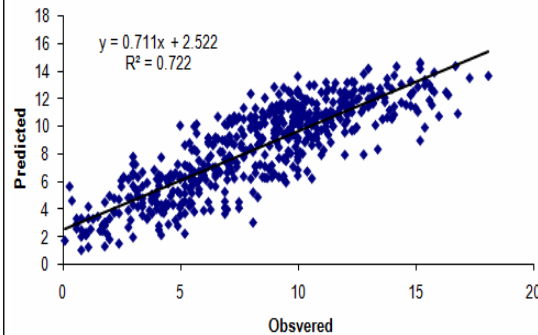


Figure 5- The observed and estimated evaporation of the Esfahan Station in test period using ES4 model.

## Conclusions

The potential of the ANFIS computation technique for estimation of evaporation using climatic variables has been illustrated in this paper. The study demonstrated that modeling of daily evaporation is possible through the use of ANFIS technique. The ANFIS model whose inputs are the air temperature, sunshine hour, wind speed, and relative humidity performed the best among the input combinations tried in the study. This indicates that all these variables are needed for more accurate evaporation estimating model constructing. In order to assess the ability of ANFIS model relative to that of the linear regression technique, the comparison was made. The developed ANFIS models for two stations located in central part of Iran perform better than the linear models.

## References:

- [1] Kisi, O.: Daily pan evaporation modelling using a neuro-fuzzy computing technique. *Journal of Hydrology* 329, 2006, 636– 646.
- [2] Stephens, J.C., Stewart, E.H.: A comparison of procedures for computing evaporation and evapotranspiration. Publication 62, International Association of Scientific Hydrology. International Union of Geodynamics and Geophysics, Berkeley, CA, 1963, pp. 123–133.
- [3] Reis, R.J., Dias, N.L.: Multi-season lake evaporation: energybudget estimates and CRLE

model assessment with limited meteorological observations. *J. Hydrol.* 208, 1998, 135–147.

- [4] Irmak, S., Haman, D., Jones, J.W.: Evaluation of class 'A' pan coefficients for estimating reference evapotranspiration in a humid location. *J. Irrig. Drain. Eng. ASCE* 128 (3), 2002, 153–159.
- [5] Gavin, H., Agnew, C.A.: Modelling actual, reference and equilibrium evaporation from a temperate wet grassland. *Hydrol. Process.* 18, 2004, 229–246.
- [6] Sudheer, K.P., Gosain, A.K., Rangan, D.M., Saheb, S.M.: Modelling evaporation using an artificial neural network algorithm. *Hydrol. Process.* 16, 2002, 3189–3202.
- [7] J.-S.R. Jang, C.-T. Sun, and E. Mizutani, *Neuro-Fuzzy and Soft Computing*, Prentice-Hall Inc. ISBN 0-13-2874679, 1997.
- [8] R. Babuska, and H. Verbruggen, Neuro-fuzzy method for nonlinear system identification. *Annual Reviews in Control.* 27, 2003, pp.73-85.
- [9] J.-S.R. Jang, ANFIS: adaptive-network-based fuzzy inference systems, *IEEE Trans. Systems Man Cybernet.* 23, 3, 1993, pp. 665–685.
- [10] F.-J. Chang, and Y.-C., Chen, A counterpropagation fuzzy-neural network modeling approach to real time stream-flow prediction, *J.of Hydrol.*, 245, 2001, pp. 153–164.
- [11] F.-J. Chang, and Y.-T. Chang, Adaptive neuro-fuzzy inference system for prediction of water level in reservoir. *Adv. in Water Resour.*, 29, 1, 2006, pp. 1-10.

## EFFECTS OF THE ROTOR SYSTEM ON BALL BEARING DYNAMIC CHARACTERISTICS

IOANNIS GRAVALOS<sup>1\*</sup>, SPYROS LOUTRIDIS<sup>2</sup>, DIMITRIOS MOSHOU<sup>3</sup>,  
THEODOROS GIALAMAS<sup>1</sup>, DIMITRIOS KATERIS<sup>3</sup>, PANAGIOTIS XYRADAKIS<sup>1</sup>,  
ZISIS TSIROPOULOS<sup>1</sup>, ANASTASIOS GEORGIADIS<sup>1</sup>

<sup>1</sup>Technological Educational Institute of Larissa, School of Agricultural Technology,  
Department of Biosystems Engineering, 41110 Larissa, Greece.

Phone: +320-4210684216, Fax: +320-2410282209, E-mail: gravalos@teilar.gr

<sup>2</sup>Technological Educational Institute of Larissa, School of Technological Applications,  
Department of Electrical Engineering, 41110 Larissa, Greece.

<sup>3</sup>Aristotle University, School of Agriculture, Department of Hydraulics, Soil Science and  
Agricultural Engineering, 54124 Thessaloniki, Greece.

### Abstract

The stiffness, rotational accuracy and vibration characteristics of a rotor system are partly controlled by the ball bearings that support it. A horizontal rotor system demonstrates interesting vibration behavior because of the unbalance force and the varying compliance effects. In this paper, the effects of the vibration of the rotor system on ball bearing dynamic characteristics are studied. The dynamic behavior of the rotor-bearing system is investigated experimentally under different operating conditions regarding speed, load and position. The vibration of the rotor-bearing system was recorded with single axis accelerometers in the frequency range from 1 Hz to 15 kHz. The sensors were mounted on the ball bearings body. A Vibrotest 60 (Brüel & Kjaer) portable data logger-analyser was used to monitor, record, and analyze the results in the frequency range of interest. The analysis of frequency spectra show the appearance of instability in the dynamic response as the speed, disk load and disk position of the rotor-bearing system is changed.

### Introduction

Vibration generated by rotating machinery has always been an interesting subject in automobiles, agricultural machinery and industrial machines. High speed rotating machine elements supported by ball bearings has been widely used in rotating machinery systems (electric motors, gearboxes, etc.), because of ease of maintenance and reduced rotor dynamic instability [1]. In the field of rotor dynamics (rotating machinery dynamics), many researchers have found that a large number of parameters, which include stiffness distribution of a rotating shaft, disk properties and bearing support stiffness can influence the dynamic behaviour of a rotor-bearing system [2], [3], [4] and [5]. Rotating element failures are one of the foremost causes of failures in rotating machinery systems. For this reason, many researchers have studied the rotor-bearing system on a fault diagnosis basis [6], [7] and [8].

Ball bearings are commonly used machine elements in rotating machinery systems. They have been employed as one of the essential parts in different mechanical equipments. Because of the requirement of acquiring higher performance in the design of rotor-bearing systems, the accurate prediction of vibration characteristics has become increasingly important [9]. An analysis of ball bearing dynamic behavior is essential in order to predict the whole system response. The rotor-bearing system displays nonlinear behavior due to nonlinear contact force, which exists between the various components of the bearings: rotating elements, races and shafts [10]. The effect of varying compliance on bearing static equilibrium was studied by many researchers: Gupta [11] developed a dynamic model for dynamic performance simulations of a ball bearing. Gad [12] simulated the axial and radial vibration phenomena of a rotor supported by ideal or non ideal ball

bearings. De Mul et al. [13] presented a five degree of freedom model for calculation of the equilibrium and associated load distribution in ball bearings. Harsha et al. [14] observed the effect of surface waviness and internal radial clearance of ball bearings on the vibration characteristics of a balanced rotor with two degrees of freedom. Purohit and Purohit [15] developed a theoretical model to observe the effect of varying the preload and number of balls on the vibration characteristics of a defect free system. A two-degree of freedom system is considered with the assumption that there is no friction between the balls and raceways and that both bearings are positioned symmetrically so that their moving parts are synchronized.

In this paper, the effects of the vibration of the rotor system on ball bearing dynamic characteristics are analysed. The dynamic behavior of rotor-bearing system is investigated experimentally under different operating conditions (varying speed, disk load and disk position).

### Method and Materials

The experimental set up of the rotor-bearing system is shown in Fig. 1. The rotor-bearing system was mounted on a cast-iron frame insulated from the surrounding environment with rubber dampers in order to remove possible external disturbances and was driven through belt transmissions by an electric 1.2 hp dc motor. A dc voltage controller was used to adjust the power supply so that the electric motor speed could be continuously increased or decreased in the range between 0 and 3800 rpm. Two dial gauge method is used to correct the shaft misalignment and base line signal has been measured at different speeds 800, 1800 and 3600 rpm to check the concentricity. The rotor shaft was supported by two identical ball bearings and had a length of 466 mm with a

diameter of 19 mm. The bearings were mounted on aluminium housings which were in turn fixed to the cast-iron frame. One or two identical massive disks of 160 mm in diameter and 19 mm in thickness were mounted separately or together on the rotor shaft at different positions (drive end bearing, shaft centre, and non drive end bearing). Each disk weighs around 3700 grams. The disks were clamped to the shaft by means of semi-circular plates and bolts.

To measure the vibration of the rotor system on ball bearings, the following instrumentation was used: a) a Vibrotest 60 (Brüel & Kjaer) portable data logger-analyser was used to monitor, record and distinguish the appropriate frequency ranges, and b) two single axis accelerometer sensors (type AS-065) with a frequency range from 1 Hz to 15 kHz. The vibration acceleration sensors were attached on the bearing housings. The bearing housings have threaded holes for the installation of the sensors. The vibrations were measured on the X-axis. Frequency spectra were analysed in one-third (1/3) octave bands, from 1 Hz to 4 kHz. The vibration magnitude was expressed in terms of Root Mean Square values (RMS).

Identification of dynamic behavior of rotor-bearing system is conducted under different operating conditions. Specifications for the three test cases are presented below:

- Test Case 1: Rotor-bearing system with one disk on centre of rotor at different dc motor speeds (800, 1800 and 3600 rpm).
- Test Case 2: Rotor-bearing system rotating at 1800 rpm with one disk assembled at different positions (drive end bearing, shaft centre, and non drive end bearing).
- Test Case 3: Rotor-bearing system rotating at 1800 rpm with different disk loads on centre of rotor (3700 and 7400 grams).



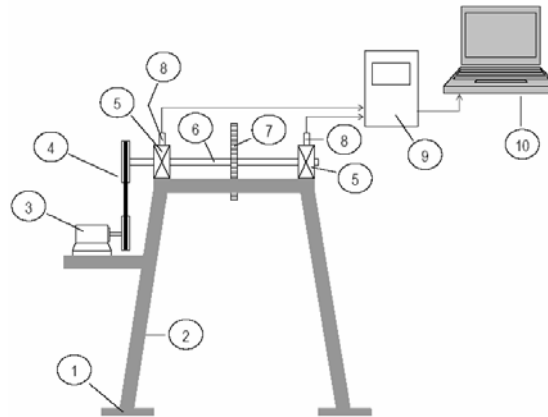


**Figure 1.** Experimental set up of rotor-bearing system

1- Vibration damper, 2- Frame, 3- dc Motor, 4- Belt transmissions, 5- Ball bearings, 6- Rotor shaft, 7- Disk, 8- Accelerometers, 9- Vibration analyser, 10- Computer

### Results and discussion

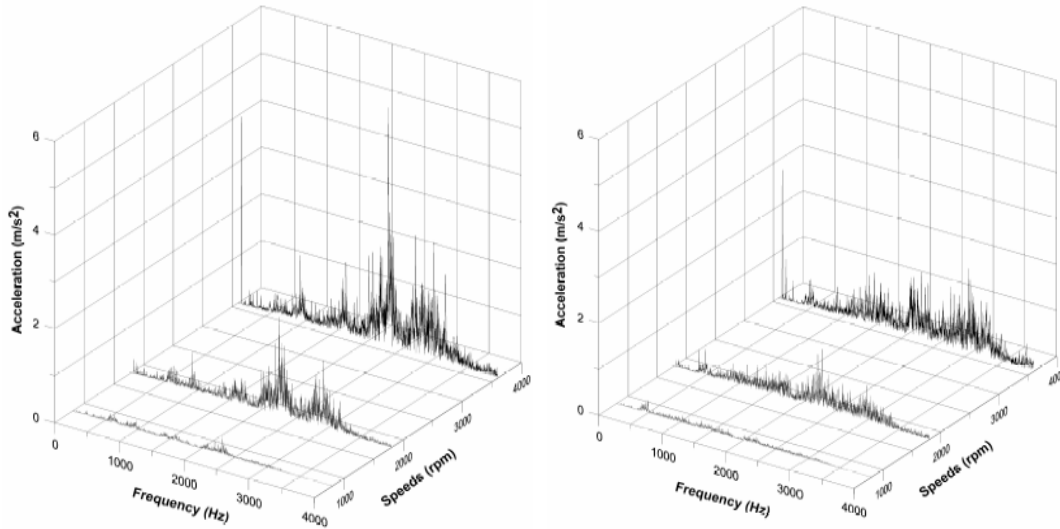
The rotor-bearing system has the outer race of the two ball bearings fixed to a rigid support and the inner race fixed rigidly to the shaft. A constant vertical radial force acts on each bearing. The excitation is due to the unbalance force which introduces the rotational frequency and the varying compliance vibrations of the bearing which arise because of the geometric and elastic characteristics of the bearing. The measured frequency spectra were obtained for the three test cases described

above. Frequency spectra that are measured experimentally using the dual channel vibration analyzer are shown in Figs. 2 - 4. Table 1, shows the peak acceleration values at the test cases under consideration.

Fig. 2 shows the response of rotor-bearing system with one disk on centre of rotor at different dc motor speeds (800, 1800 and 3600 rpm), the peak amplitude of vibration is appeared to higher dc motor speeds.

**Table 1. Peak acceleration values at different test cases**

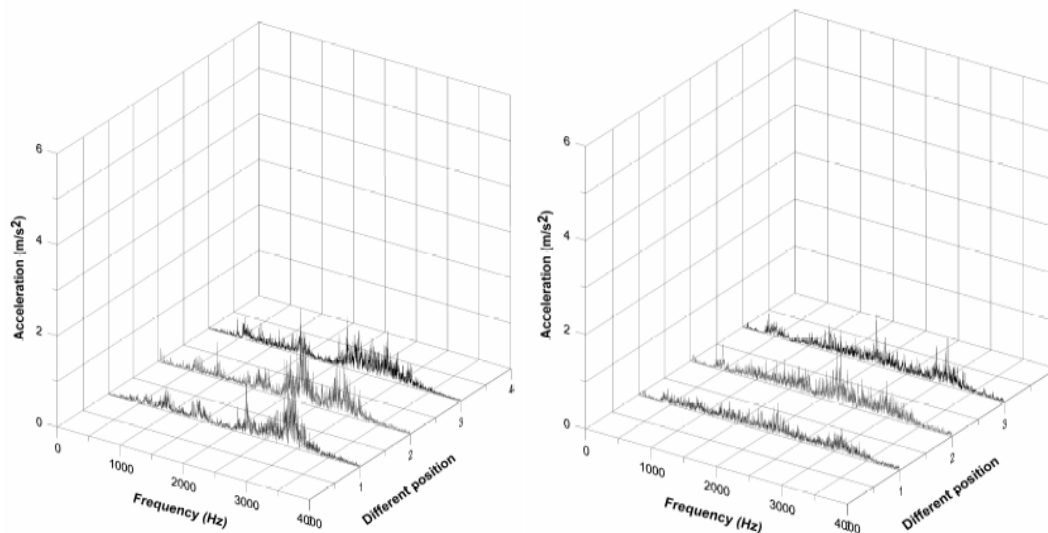
Test cases	Drive end bearing		Non drive end bearing	
	Frequency	Acceleration values	Frequency	Acceleration values
	[Hz]	[m/s <sup>2</sup> ]	[Hz]	[m/s <sup>2</sup> ]
<b>Test case 1:</b> Rotor-bearing system with one disk on centre of rotor at different dc motor speeds				
800 rpm	2312.50	0.3629	2212.5	0.1716
1800 rpm	2267.19	2.0879	2307.81	1.2872
3600 rpm	2309.38	5.0915	2975.00	1.8305
<b>Test case 2:</b> Rotor-bearing system rotating at 1800 rpm with one disk assembled at different positions				
At shaft centre	2926.56	2.0879	2307.81	1.2872
Near drive end bearing	2267.19	1.4976	2143.75	1.0889
Near non drive end bearing	2209.38	1.0971	2043.75	0.6705
<b>Test case 3:</b> Rotor-bearing system rotating at 1800 rpm with different disk loads on centre of rotor				
0 grams	2346.88	1.5149	3139.06	0.8275
3700 grams	2267.19	2.0879	2307.81	1.2872
7400 grams	2343.75	2.0455	3087.50	1.1122



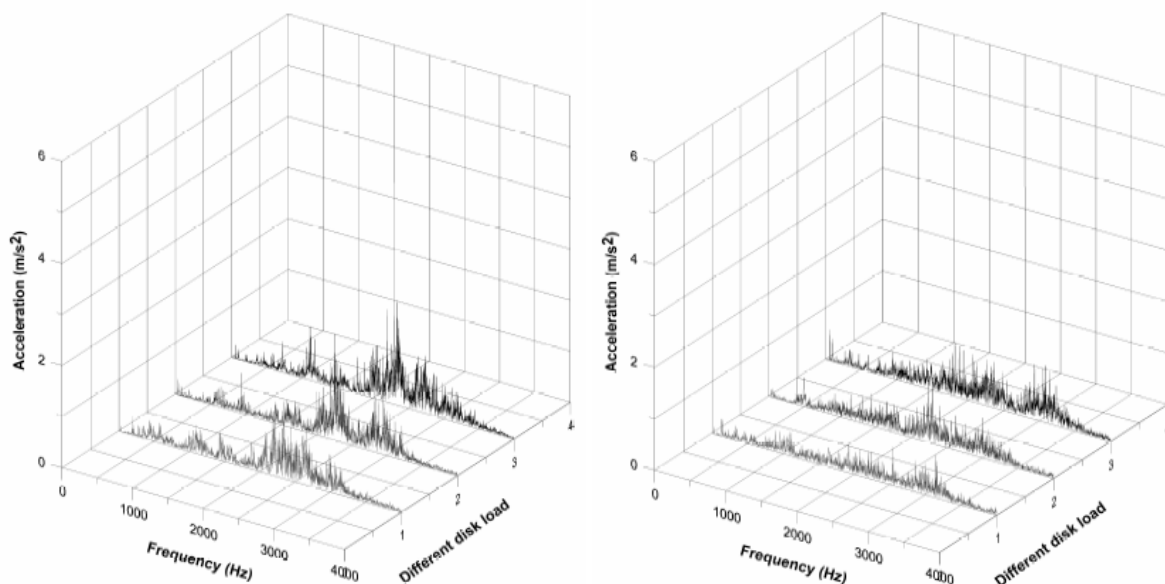
**Figure 2.** Frequency spectra of rotor-bearing system with one disk on centre of rotor at different dc motor speeds. a) Drive end bearing, b) Non drive end bearing

Fig. 3 shows the response of rotor-bearing system rotating at 1800 rpm with one disk assembled at different positions (drive end bearing, shaft centre, and non drive end bearing). The peak amplitude of vibration appears at drive end bearing when disk was assembled at shaft centre (at Hz

2926.56 - acceleration value =  $2.0879 \text{ m/s}^2$ ). Fig. 4 shows the vibration response of rotor-bearing system rotating at 1800 rpm, when disk load is increased from 3700 to 7400 grams there is slightly increase in the peak amplitude of vibration at the drive end and non drive end bearings.



**Figure 3.** Frequency spectra of rotor-bearing system rotating at 1800 rpm with one disk assembled at different positions. a) Drive end bearing, b) Non drive end bearing.



**Figure 4.** Frequency spectrum of rotor-bearing system rotating at 1800 rpm with different disk loads on centre of rotor. a) Drive end bearing, b) Non drive end bearing.

## Conclusions

In the present study, the nonlinear vibration response of a rotor-bearing system was examined due to variations in the dc motor speed, disk position and disk load. The nonlinear dynamic response of drive end bearing is found to be associated with the belt transmission frequency. The electric motor rotational speed is one of the most important parameters in the dynamic analysis of a rotor bearing-system and it is useful for controlling the system vibrational response. The disk position is also an important parameter for the vibration analysis of a rotor bearing-system and should be carefully considered during the design stage. It is also shown that the system response is not sensitive to variations of the disk load.

## References

- [1] Lee,D.S.-Choi,D.H.: A dynamic analysis of a flexible rotor in ball bearings with nonlinear stiffness characteristics. *International Journal of Rotating Machinery*, 3(2),1997, p.73-80.
- [2] Gargiulo,E.E.: A simple way to estimate bearing stiffness. *Machine Design*, 52,1980, p.107-110.
- [3] Lim,T.C.-Singh,R.: Vibration transmission through rolling element bearing, Part I: Bearing stiffness formulation. *Journal of Sound and Vibration* 139 (2), 1990, p.179-199.
- [4] Tiwari,M.-Gupta,K.: Dynamic response of an unbalanced rotor supported on ball bearings. *Journal of Sound and Vibration*, 238(5), 2000, p.757-779.
- [5] Sadeghi,M.H.-Zehsaz,M.-Jafari,S.: The effect of bearing stiffness on the frequency response function of a turbo-pump shaft-comparative study. *European Journal of Scientific Research*, 139(3), 2010, p.381-395.
- [6] Mechefske,C.K.-Mathew,J.: Fault detection and diagnosis in low speed rolling element bearings Part I: The use of parametric spectra. *Mechanical Systems and Signal Processing*, 6(4), 1992, p.297-307.
- [7] Bolaers,F.-Cousinard,O.-Marconnet,P.-Rasolofondraibe,L.: Advanced detection of rolling bearing spalling from de-noising vibratory signals. *Control Engineering Practice*, 12(2), 2004, p.181-190.

- [8] Lou,X.-Loparo,K.A.: Bearing fault diagnosis based on wavelet transform and fuzzy inference. *Mechanical Systems and Signal Processing*, 18, 2004, p.1077-1095.
- [9] Bai,C.-Zhang,H.-Xu,Q: Effects of axial preload of ball bearing on the nonlinear dynamic characteristics of a rotor-bearing system. *Nonlinear Dyn*, 53, 2008, p.173-190.
- [10] Harsha,S.P.: Nonlinear dynamic analysis of an unbalanced rotor supported by roller bearing. *Chaos, Solitons and Fractals*, 26, 2005, p.47-66.
- [11] Gupta,P.L.: Dynamics of rolling element bearings, parts I to IV. *ASME J. Lubr. Technol.*, 101, 1979, p.293-326.
- [12] Gad,E.H.-Fukata,S.-Tamura,H.: Computer simulation of rotor axial and radial vibrations due to ball bearings. *Mem. Fac. Eng. Kyushu Univ.*, 44(2), 1984, p.169-189.
- [13] Mul,J.M.-Vree,J.M.-Maas,D.A.: Equilibrium and associated load distribution in ball and roller bearings loaded in five degrees of freedom while neglecting friction. Part I: general theory and application to ball bearings. *ASME J. Tribol.*, 111,1989, p.142-148.
- [14] Harsha,S.P.-Sandeep,K.-Prakash,R.: The effect of speed of balanced rotor on nonlinear vibrations associated with ball bearings. *Int. J. Mech. Sci.*, 45, 2003, p.725-740.
- [15] Purohit,R.K.-Purohit,K.: Dynamic analysis of ball bearings with effect of preload and number of balls. *Int. J. of Applied Mechanics and Engineering*, 11(1), 2006, p.77-91.

## SCREENING PISTACHIO NUTS USING A NEURAL NETWORK BASED INTELLIGENT SYSTEM

TARAHOM MESRI GUNDOSHMIAN<sup>1\*</sup>, ASGHAR MAHMOUDI<sup>1</sup>, M. OMID<sup>2</sup>, ADEL HOSAINPOUR

<sup>1</sup> Department of Agricultural Machinery Engineering-Faculty of Agriculture University of Tabriz, Tabriz, Iran, Phone +98 914 305 7284, Email: [mesrigtm@gmail.com](mailto:mesrigtm@gmail.com) ; [mesrigtm@tabrizu.ac.ir](mailto:mesrigtm@tabrizu.ac.ir)

<sup>2</sup> Department of Agriculture Machinery Engineering, Faculty of BioSystem Engineering, University of Tehran, Karaj, Iran

### Abstract

In this paper, an artificial neural network based system, is presented to separate closed pistachio nuts from the open ones in the real-time. This intelligent system includes a feeding part, an acoustical recognition part, and a pneumatic air rejection mechanism. Features of pistachio nut types are extracted by analysis of sound signal in both time and frequency domains through fast Fourier transform, power spectral density, and principal component analysis methods. These features are used as input vector to LVQ models, and various LVQ learning algorithms, including LVQ1, OLVQ, LVQ4.a are evaluated. Further, the performance of the LVQ-based system is compared with those system using MLP.

The best performance is obtained through LVQ4.a algorithm; that is the correct separation rates for closed shell and open shell ones are 96.5% and 96.83%, respectively and overall 96.67%. The designed system due to its nondestructively, does not cause any damage to the kernels of open shell pistachios.

**Key words:** Pistachio Nuts, LVQ, Classification, Sorting, Acoustic, Principle component analysis.

### Introduction

Pistachio (*Pistacia vera* L.) is a dry-climate deciduous tree producing nuts in clusters. By producing approximately 300 million kg per year, Iran is the world's leading pistachio nut producer. Mixing of pistachio nuts of different varieties may occur as a result of mixed plantation, during harvesting, transportation, handling and storage. Separation of the mixed nuts is important for both economical as well as esthetical reasons, and to offer consumer a uniform product. Inspection and separation by hand is tedious and often does not bring the desired results. The task of classification could most efficiently be performed by a machine vision system. Sorting systems have to be flexible in use, due to the wide variety of products available in the market. On the other hand, the need to be able to test new products requires a high degree of processing adaptability. The test system should not require lengthy resetting times or complex (software) engineering. It is for this reason that one has to rely upon intelligence trainable systems. The

robustness, capability of approximating a posterior distribution, and high potential for parallel processing makes ANN a suitable choice for classification of agricultural products.

Recently, acoustical experiments have been increasingly employed in agriculture. Garsia et al applied this technique for classification of fruits by determining the ripeness or stiffness(Garsia *et al.*, 2003). Pearson used discriminate analysis on data obtained from sound signal sampling, in time domain, for separation of open and closed shell Kerman variety of pistachio nuts(Pearson 2001). In the ongoing study the results of application of non destructive acoustic technique incorporated with ANN for classification of open and closed shells. The aim of this study was to design and present a suitable algorithm for identification and separation of open and closed shells pistachio nuts with LVQ Neural Network Algorithms.

### Materials and methods

Processing systems need to be flexible especially their software. Diversity of processing

products and their necessity of compatibility with new products is essential parameter of processing machines. Automatic processing systems software needs to be accurate, quick and simple and able to cover this diversity of products (Mahmoudi *et al.*, 2005). Nondestructive methods for sorting agricultural materials is more important. To train the system on how to differentiate between these varieties, traditional procedures for system modeling become unmanageable or virtually insoluble if either the basic system can no longer be adequately linearly approximated or if a large number of measured variables (features) have to be considered simultaneously. One approach to avoid these drawbacks is using automatic trainable classifier, such as artificial neural networks (ANNs) in other hand We proposed system with LVQ neural network for this system.

We use 3200 pistachio nuts (1600 closed shells and 1600 open shells) from 2004 harvest season. A Panasonic Electret capsule microphone (VM-034CY) was employed for detecting sound signals in nuts. The microphone was installed inside an isolated acoustic chamber to eliminate environmental noise effects. The sensor picks up the impact of sound and sends the data, in real-time, to a PC based data acquisition system via a

sound card. Feature extraction is performed on the collected data. The input signal for the block "feature extraction" represents the digital sound signal in time domain with the output from this stage being the feature vector. Signal analysis procedures from the time domain (e.g. peak values), the frequency domain (e.g. FFT and PSD) and statistical methods (e.g. PCA) are then used for feature extraction. These features are fed to classification system. The classification was performed with ANNs. There are several types of ANNs, each with its own advantages and drawbacks. In a training process, the classifier is given specimen signals, then sets its weight coefficients in the training phase so that it is able to reproduce the classification results as adequately as possible. The individual system states are represented at the input of the stage for knowledge based interpretation by a class statement based on available expert knowledge. This expert knowledge was then fed to the system in the training phase (figure 1). The system was designed to feed pistachio nuts to an impact surface, catch the sound signal upon impact, process the data, and divert the product into two class: class1: Opened shells and class2: Closed shells.



Figure 1: Typical ANN based classification system for pistachio nuts

Sound signal data in time domain were saved for preprocessing analysis. Data acquisition Toolbox from MATLAB software was used for data collection. Since the maximum frequency (sampling rate) of used sound card was equal to 44/1 kHz, data acquisition continued for 5.67ms after triggering. This produced 250 data points for each nut. The Fast Fourier Transform (FFT) is an algorithm for calculating the Discrete Fourier Transform (DFT). FFT utilizes sharp algorithms does as DFT, but in much less time. Feature extraction from impact sound is the first step for designing a successful pistachio nut classification system. Useful features can be extracted, for input vector to ANN model, by considering signal amplitude in time domain and calculation of magnitude power spectral density (PSD) of FFT components in frequency domain.

For real time systems, once the dimension of the input vector is large, but the components of the vectors are highly correlated (redundant). It is useful in this situation to reduce the dimension of the input vectors. An effective procedure for performing this operation is using PCA. PCA analysis was performed with MATLAB software. PCA results as well as eliminated percentage of the total variation in the data set, in relation to selected principle components. According to time and frequency domains analysis of sound signals three sets of features were utilized for PCA purposes.

#### Artificial neural networks classifier

Learning Vector Quantization (LVQ), was adapted by Kohonen for pattern recognition (Kohonen 1986). Its main idea is to



divide the input space  $R_n$  into a number of distinct regions, called decision regions (Voronoi cells), and for each region one codebook (Voronoi) vector is assigned. Classification is performed based on the vicinity of the input vector  $x$  to the codebook vectors;  $x$  will be classified as the label of its nearest neighbor among codebook vectors. During the training, the codebook vectors and consequently the borders of decision regions are adjusted through an iterative process (Vakil-Baghmisheh *et al.*, 2002). Seven features( $x$ ) selected as input of network. The 3200 nut data were divided to two sets: 62.5% of data were used for training, 37.5% for testing.

### Early training algorithms for LVQ

#### LVQ1

Let  $x_q$  be an input vector (from training set):  $x_q \in R_n$ ;  $q = 1; \dots; 2000$  and  $w_m$  be the  $m$ th codebook vector:  $w_m \in R_n$ .  $w_c$  is the winner codebook vector, so adjust  $w_c$ :

$$w^c(t+1) = w^c(t) + \alpha(t)s(t)[x^q - w^c(t)]$$

in which:  $0 < \alpha(t) < 1$ ;  $s(t) = +1$  if classification is correct,  $s(t) = -1$  if classification is wrong and  $\alpha(t)$  is a monotonically decreasing function of time.

#### Preliminary LVQ4 algorithm

In this manner updated formula for winner neuron  $w^c$  is:

$$w^c(t+1) = w^c(t) + \alpha(n)s(n)[x^q - w^c(t)]$$

$0 < \alpha(n) < 1$ ;  $s(n) = d_c(n)$  if classification is correct;  $s(n) = -1$  if classification is wrong and  $\alpha(n)$  is a monotonically decreasing function of time and  $d_c(n)$  is the “equalizing factor”. In addition,  $\alpha(n)$  and  $d_c(n)$  must be kept constant during a training epoch.  $d_c(n)$  is defined as:

$$d_c(n) = \frac{E_c(n)}{P_c(n)}$$

where  $E_c(n)$  and  $P_c(n)$ , respectively, are the numbers of wrong and correctly classified patterns by codebook vector  $c$  in the current

epoch. For estimating  $d_c(n)$  four methods are offered:

$$d_c(n) = d_{total}(n-1)$$

$$d_c(n) = d_c(n-1)$$

$$d_c(n) = d_c(n-1) \frac{d_{total}(n-1)}{d_{total}(n-2)}$$

$$d_c(n) = d_c(n-1) \frac{d_c(n-1)}{d_c(n-2)}$$

Considering the irregularities as  $n = 1$  and  $2$  and the cases of zero terms in the denominator, more detailed formulas would be:

$$d_c(n) = \begin{cases} \varepsilon & n = 1, \\ d_{total}(n-1) & n \geq 2, \end{cases}$$

$$d_c(n) = \begin{cases} \varepsilon & \text{if } n = 1 \\ d_c(n-1) & \text{if } n \geq 2, P_c(n-1) \neq 0 \\ \lambda & \text{if } n \geq 2, P_c(n-1) = 0 \end{cases}$$

$$d_c(n) = \begin{cases} \varepsilon & \text{if } n = 1, 2 \\ d_c(n-1) \frac{d_{total}(n-1)}{d_{total}(n-2)} & \text{if } n \geq 3, P_c(n-1) \neq 0 \\ \lambda & \text{if } n \geq 3, P_c(n-1) = 0 \end{cases}$$

$$d_c(n) = \begin{cases} \varepsilon & \text{if } n = 1, 2 \\ d_c(n-1) & \text{if } n \geq 3, d_c(n-1) = 0 \\ d_c(n-1) \frac{d_c(n-1)}{d_c(n-2)} & \text{if } n \geq 3, d_c(n-1) \neq 0 \end{cases}$$

in the fourth method,  $d_c(n-1)$  is calculated as follows:

$$d_c(n) = \begin{cases} \frac{E_c(n-1)}{P_c(n-1)} & \text{if } P_c(n-1) \neq 0 \\ \lambda & \text{if } P_c(n-1) = 0 \end{cases}$$

After experiments the best learning rate functions were found to be:

For LVQ4  $a(n) = k(\exp(-(20 - epoch)/100))$ ,

We simulate all of above algorithms on training mode and results presented in figure 2, 3, 4, 5, 6, 7, 8. In table 1 and 2 we summarized results of early LVQ and LVQ4 algorithms on train and test respectively.

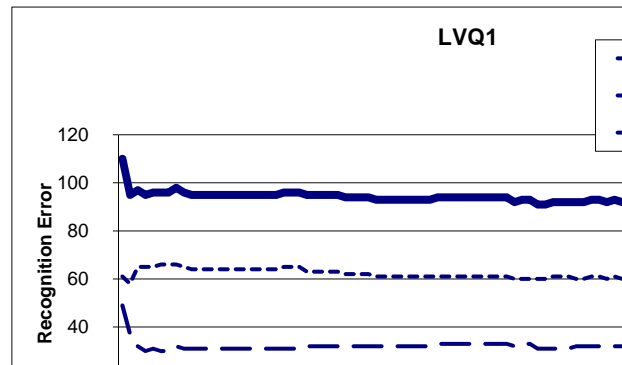


Figure 2. convergence diagrams of LVQ1 on training database

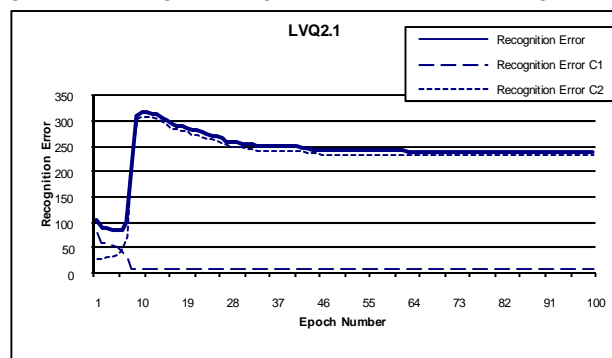


Figure 3. convergence diagrams of LVQ2.1 on training database

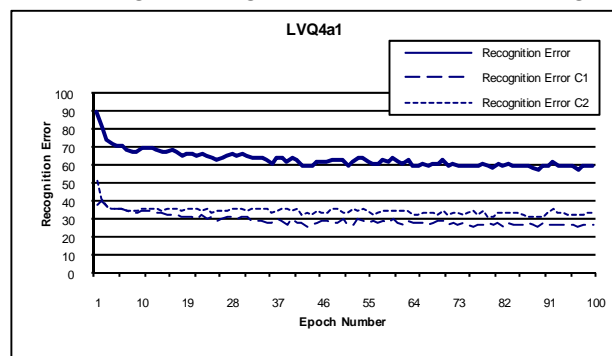


Figure 4. convergence diagrams of LVQ4a1 on training database

Table 1. Recognition errors of early LVQ algorithms on databases

Training algorithms	Initialazing factor			Recognition error Train Mode			Recognition error Test Mode		
	$\tau$	k	no	E c1	E c2	Overall	E c1	E c2	Overall
LVQ1	30	0.02	20	3.20	6.10	4.65	2	7.17	4.58
LVQ2.1	100	-	-	5.5	4.6	5.05	4.83	3	3.92

Table 2. Recognition errors of LVQ4 algorithms on databases

Training algorithms	Number of codebook vector	Recognition error (Train Mode)			Recognition error (Test Mode)		
		E c1	E c2	Overall	E c1	E c2	Overall
LVQ4a1	20	2.40	2.90	2.65	2.33	4.00	3.167
LVQ4a2	20	2.7	3.3	3.00	2.17	5	3.58

## Results and Discussions

The first evident point in Table 1 and 2 is the outstanding performance of new training algorithms and the weak performance of early algorithms i.e. LVQ1 and LVQ2.1 on training and test sets of all databases. In training mode it is obviously found that recognition errors of LVQ4 algorithms had less recognition errors in comparison with early LVQ learning algorithm. We test some number of codebook vector for this classification and the best result achieved when 20 codebook vector selected, 10 codebook vector for class 1 which indicate opened shells pistachio nut and remainder for closed shells pistachio nut.

## Conclusions

In this paper a separation system, based on combination of acoustic detection and artificial neural networks, was designed for classifying open shells and closed shells pistachio nut. LVQ network was employed for pistachio nut classification. Features of pistachio nut varieties were extracted from analysis of sound signals in both time and frequency domains by means of FFT, PSD and PCA methods. Altogether 7 features were selected for classifications: 4 amplitude features and 3 PSD features. A combination of these 7 features resulted in a minimum feature number highest classification accuracy in network training time. Selected optimal neural network for classification exhibited LVQ4a structure.

## REFERENCES

- [1] Garsia-Ramos, F. J., Ortiz-Canavate, J., Ruiz-Altisent, M., Diez, J., Flores, L., Homer, I. , and Chavez, J. M. 2003. Development and implementation of an onœline impact sensor for firmness sensing of fruits. *J. Food Eng.*, 58: 53-7.
- [2] Kohonen T. 1986. Learning Vector Quantization for Pattern Recognition, Technical Report TKKF-A601, Helsinki Uni. of Tech., Finland.
- [3] Mahmoudi, A., Omid, M., Aghagholzadeh, A., and Borghei, A.M. 2005. Development of a Pistachio sorting system based on acoustic technique. IV Int. Symp. Pistachios & Almonds, ISHS, Tehran: Iran, 22-25 May 2005, pp, 164.

- [4] Pearson, T. C. 2001. Detection of pistachio nuts with closed shells using impact acoustics. *Applied Engineering Agriculture*, 17: 249-53.
- [5] Vakil-Baghmisheh, M. T., Pavešić, N. 2002. Premature clustering phenomenon and new training algorithms for LVQ. *Journal of Pattern Recognition* 36: 1901 – 1912.

## DETERMINATION OF THE COMPLETE GEOMETRY OF THE WORM EXTRUDER SCREWLINE FOR COMPRESSIVE PRESSING OF THE OIL BEARINGS CROPS

DAVID HERÁK\*, ALEŠ SEDLÁČEK, ABRAHAM KABUTEY

Czech University of Life Sciences Prague, Kamýcká 19, Praha 6, Prague, 16521, Czech Republic, phone: +420 224 383 181, email: [herak@tf.czu.cz](mailto:herak@tf.czu.cz)

### Abstract

The development of a complete geometry of the worm extruder screwline is useful for describing and understanding the mechanical behavior of oilseeds during compression. Integral part of this study is derivation of mathematical model which attempts to describe the relationships between pitch angle of worm shaft, middle diameter of worm shaft, friction of pressed mixtures, shaft materials and compressive force. The influence of the worm shaft power and rotation of the press material during pressing were focused in this model. The study defines this model in real situations and endeavours to validate it on the real problems for industrial use. Also the change of oil temperature during pressing and its effect on the friction and compressive force were considered. Seeds of jatropha, flax and sunflower were used using screw extruder with seven pressing chambers. The results of the experiment showed that increase in temperatures of oil and shaft in pressing chambers are dependent on the compression ratio and fitted curve thus the dependency between temperature and pressing chamber positions would play an important role in the previous derived model.

### Introduction

One of the main factors affecting the energy demand of vegetable oil is the degree of the pressing force. By adjusting the size of the pressing force optimal amount of oil in proportion to the minimum input energy can be achieved. The size of the pressing force generates compressive stress in pressed mixture and this is an important factor which affects the ratio of input and output energy. In oil extrusion with usual extruders used in industrial practice, there is non linear compression of pressed mixture incurred during the processing. This means that the compression is combination of translate moving and rotary moving. For better understanding of mechanical behavior of the plant seeds under compression loading, it is necessary first to understand the mechanical behavior of one free placed seed and one layer seeds with limited deformation and also mechanical behavior of more layers of the seeds. In compression of more layers of materials, there is occurrence of cumulating deformation energy in the compressed material during the process of compression. In rupturing some of the cells, the stress of this cell is transmitted to other cells with only small losses of energy consumed to displace liquid from broken cells. There is stress gradient not only in the radial direction but also in the axial direction [1]. In some cases, the initial

temperature of the pressing mixture is higher than ambient temperature and it occurs when there is heat transfer between the mixture, the pressing tool and the environment.

### Mathematical model

From simple cross section of the screw shaft and scheme of the developed screwline (fig. 1) mathematical dependency between pitch angle of the screwline  $\alpha$  ( $^\circ$ ) and the pitch thread of the screw  $P$  (mm) and middle shaft diameter  $D$  (mm) can be described by equation (1).

$$\operatorname{tg} \alpha = \frac{P}{\pi \cdot D} \quad (1)$$

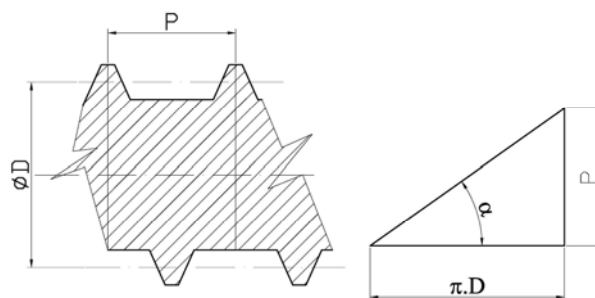


Fig. 1 The scheme of screw shaft

By equilibrium equation of the force (fig. 2) acting on the element of the seed in the thread of the screw shaft the relationships between pressing force  $F_p$  and circumferential force  $F_w$ , where  $N$  is normal force,  $T$  is friction force and  $\varphi$  is friction angle between seed and screw surface can be obtained. The weight force of the seed element  $G$  is neglected in this equation.

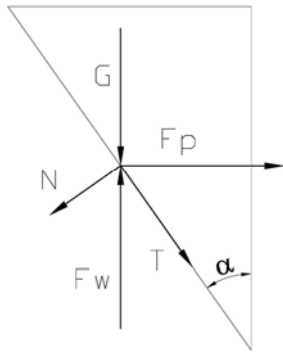


Fig. 2 The force scheme in the screw thread

$$F_w = F_p \cdot \operatorname{tg}(\alpha + \varphi) \quad (2)$$

Relationship between torsion moment  $M_w$  and pressing force can be described by equation (3), which is a product of circumferential force (2) and screw radius.

$$M_w = F_w \cdot \frac{D}{2} = F_p \cdot \operatorname{tg}(\alpha + \varphi) \cdot \frac{D}{2} \quad (3)$$

From the basic conditions of the strength of materials the relationship between torsion moment  $M_w$  (Nm), extruder power  $P_s$  (kW) and shaft revolutions  $n$  ( $\text{mm}^{-1}$ ) can be obtained equation (4)

$$M_w = 9550 \cdot \frac{P_s}{n} \quad (4)$$

Equation (5) shows the relationship between pressing force and operational and design parameters of the screw extruder by combining equations (3) and (4).

$$F_p = \frac{9550 \cdot P_s \cdot 2}{\operatorname{tg}(\alpha + \varphi) \cdot n \cdot D} \quad (5)$$

Mechanical behavior of pressed mixture under compression loading can be described by equations of mechanical behavior (6), [2], [3], [4] determined in previous experiments

$$F_{pe} = A \cdot \operatorname{tg}(B \cdot x) \quad (6)$$

Where  $F_{pe}$  (N) is deformation force,  $x$  (mm) is deformation,  $A$  (N) is force coefficient of mechanical behavior,  $B$  ( $\text{mm}^{-1}$ ) is deformation coefficient of mechanical behavior. From the above equation (6) it is clear that for ideal setting of the pressing force it is important to consider the relationship between the compressive force and deformation which are described by the equation (6). Figure (fig. 3) shows the ideal setting of the pressing force for maximum efficiency in different positions of the extruder.

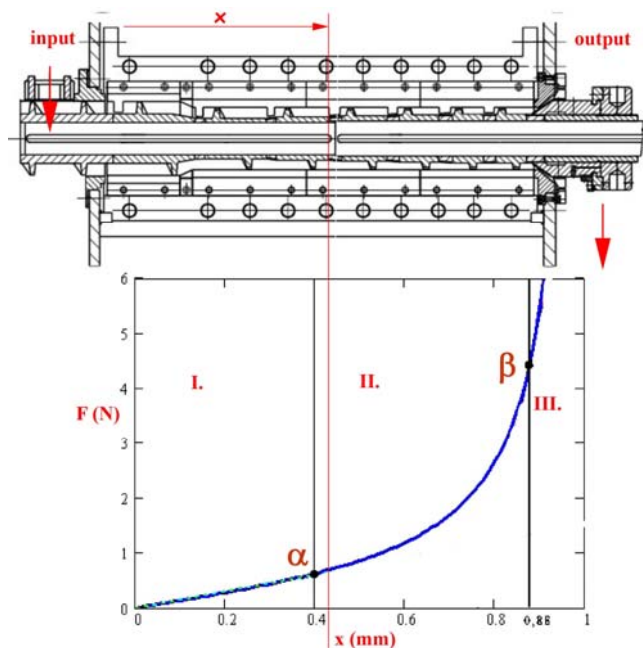


Fig. 3 Deformation characteristic of pressed mixture at different positions of screw extruder shaft

## Discussion

From the previous study describing the development of a mathematical model, it is clear that the size of the compression force depends on the mechanical behavior of molded mixtures and also on the operational and structural characteristics of the extruder. Operational parameters affecting the compression strength are revolutions  $n$  and power  $P_s$  and these parameters are variable in the operational process. Design parameters also affecting the compression force are pitch angle  $\alpha$ , medium screw diameter  $D$ , material properties of the screw surface and friction angle  $\varphi$  respectively and these parameters remains constant during

operational process. Currently, due to the use of extruders in different operating conditions (education service, climatic and geographic conditions of operation, etc.) such as the operating conditions of Asian and African equatorial developing countries or former Soviet Union countries, which are very different from those of developed countries in the world it is necessary to design a machine with the operating parameters which will be stable throughout the operational life of the machine, ie machine is designed for only one kind of speed and power. From a given model, it is clear that geometrical properties can be changed by the change of pitch angle and medium diameter of screw shaft; in its nature it affects the size of the pressing force. Changing the size of the pitch angle depending on the location of the pressing screw together with changing the medium diameter of screw depending on the location of the pressing screw, may affect the compressive force and this is identical to the ideal compression force required for pressing the mixture of seeds, for example

the tangential equation (6), (fig. 3), i.e. the optimal setting of design parameters for the output oil at maximum efficiency. Pressing force can also be affected by changing material properties of the surface of the screw shaft, but this change usually affects the compression strength consistently throughout the process of pressing and this cannot be just an insignificant change of the material properties during the pressing force relating to the needed compressive force of the pressed mixture (6), determined from the previous experiments [3] [4], but this change may positively affect the lifetime and in combination with the previous geometrical modifications as well as the output oil. From previous experiments [2], [3], [4] it is also clear that these factors described above, affect the efficiency of complex system, gain of oil, temperature of the oil or pressed mixture and their relationships are interrelated. These relationships are shown in figures (Fig. 4) (Fig. 5).

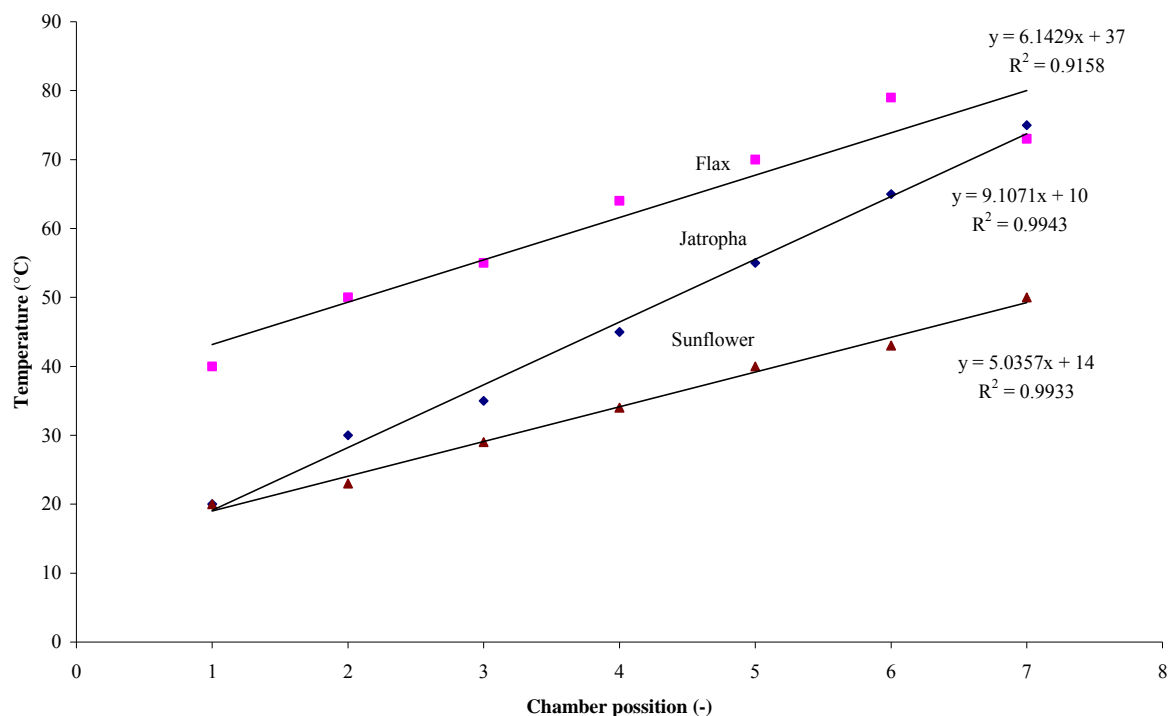


Fig. 4 Dependency between temperatures of obtained oil and chamber positions on the screw shaft



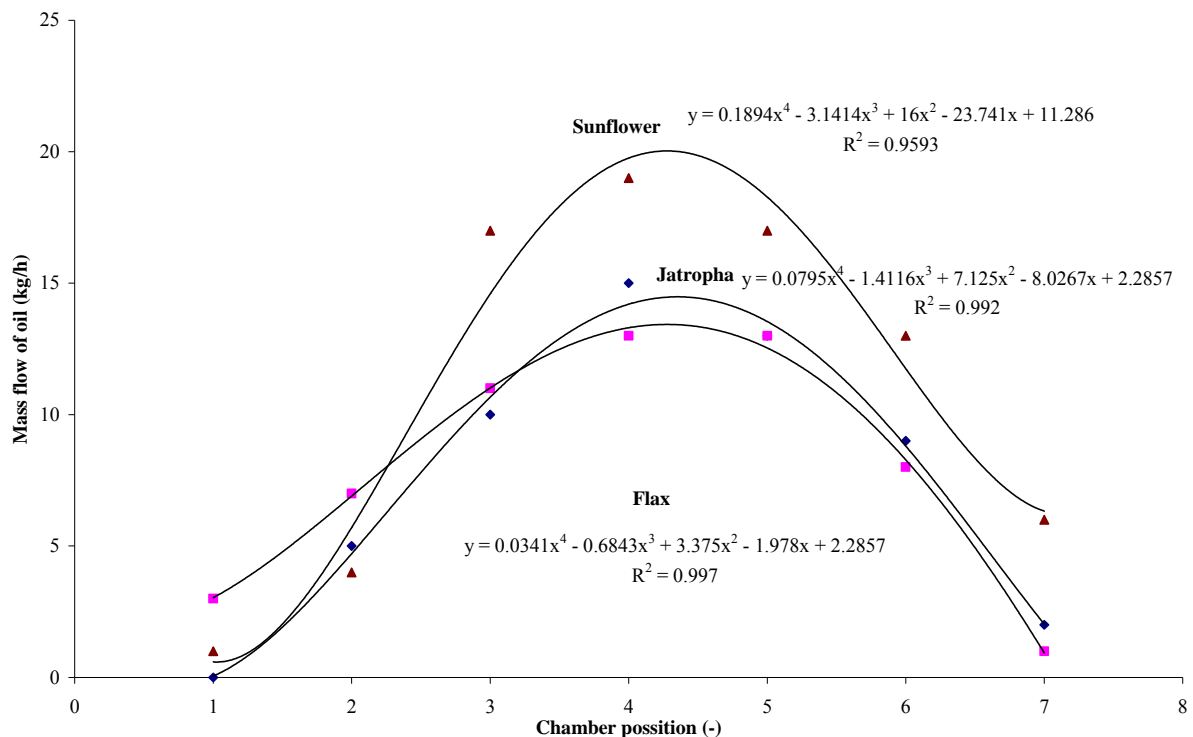


Fig. 5 Dependency between mass flow of obtained oil in each chamber and chamber positions on the screw shaft

## Conclusion

The development of mathematical model is useful for describing and understanding the mechanical behavior of pressed mixture under nonlinear compressive loading. In the technology line, screw extruders with maximum output but minimum loss of oil without any modification of the operational characteristics during functional life of the extruder can be designed. This mathematical model can be used as a fundamental element for establishing a model of transformation between the linear and non linear loading of pressed mixture.

## References

- [1] Blahovec, J., Reznicek, R.: Fractionation of forage, Frakcionace píce (in Czech), Praha, VSZ v Praze, 1980
- [2] Herák, D. et al.: Energy demands for pressing *Jatropha curcas* L. seeds, Biosystems Engineering, 2010, doi:10.1016/j.biosystemseng.2010.06.002
- [3] Herák, D. et al.: Tangent curve utilization for description of mechanical behavior of pressed mixture, Research in Agricultural Engineering, 2010, (in press)
- [4] Kabutey, A. et al.: Behavior of different moisture contents of *Jatropha curcas* L seeds under compression loading, Research in Agricultural Engineering, 2010, (in press)

## ANALYSIS OF CUTTING MECHANISM ON THE CUTTER USED FOR HOPS GROWN ON LOW TRELLIS

PETR HEŘMÁNEK, ADOLF RYBKA, IVO HONZÍK, BOHUSLAV JOŠT  
Czech University of Agriculture in Prague, 165 21 Prague 6 – Suchbátka, Czech Republic,  
Phone: +4202-24383126, Fax: +4202-24383122, E-mail: [hermanek@tf.czu.cz](mailto:hermanek@tf.czu.cz)

### Abstrakt:

Technology of low-trellis hop growing has been tested since the early 90s of the last century not only abroad (USA, England, Germany, Bulgaria) but also in the Czech Republic. So far, however, it has not been very widespread, mainly for reasons of missing suitable varieties and machinery (Rybáček et al., 1980).

One of the basic operations related to hop growing is the spring cutting which, if carried out at a proper time, slows down the hopvine growth (Štranc et al., 2007). Nevertheless, for the time being there is no company to make the hop cutter for low-trellis hopfields. It is not even possible to use the hop cutter designed for high-trellis hopfields, as in the low-trellis hopfields the machine must operate under a supporting net whose bottom edge is at a distance of only 0.25 to 0.3 m above the ground. It is due to these reasons that our author team has begun to participate in the development of a new hop cutter targeted for low-trellis hopfields.

This article deals with a design and functional tests of rotary drive for cutting disc used to cut hopvines. The rotary drive is provided by a hydraulic motor with external gear. The whole system is fed by an additional hydraulic aggregate. The article also presents the cutting mechanism kinematics. The designed drive system, including its control, was tested on the premises of Hop Research Institute Co., Ltd. seated in the town of Žatec. The testing procedures measured flow rate and pressure in hydraulic circuit for cutting disc drive. On the basis of these parameters an energy intensity of the cutting disc was assessed.

**Keywords:** cutting mechanisms, hop, low trellis

### Introduction

One of the basic operations related to hop growing is the spring cut which, if carried out at a proper time, slows down the hopvine growth. Nevertheless, for the time being there is no company to make the hop cutter for low-trellis hopfields. It is not even possible to use the hop cutter designed for high-trellis hopfields, as in the low-trellis hopfields the machine must operate under a supporting net whose bottom edge is at a distance of only 0.25 to 0.3 m above the ground.

### Material and methods

Low trellis hopfield is formed by rows of poles of 100 mm in diameter and a height of 3 m. The spacing of poles in a row is approximately 9 m. The distance of pole rows is 3 m. The trellis is strengthened lengthwise by means of steel ropes at the height of 0.25 up to 0.3 m above the ground, in the middle, and in the top part of the poles. Anchors at the end of the pole rows are fixed in the ground at a depth of about 2 m

(Figure 1). There is a drop irrigation system hung on the bottom anchoring rope. Instead of hop strings formed by guide wires a polypropylene net with meshes sized 150 x 150 mm is used which takes advantage of the self-twining ability of hopvines. After the harvest, hopvines stay on the net uncut off their root parts until next spring.

Our design of a cutting mechanism was based on the following requirements. As a tool carrier we used a tool carrier made by Wallner Landtechnik company. The frequency of the cutting disc rotation was designed to be within the range of 0 to 17 s<sup>-1</sup>. The cutting allowed for a maximum cut depth of 100 mm and working space under the bottom anchoring rope where cannot occur any damage of the net or drop irrigation system, which is approximately from 200 to 250 mm above the ground. During the cut the maximum work speed of tractor and cutter will be up to 5 km.h<sup>-1</sup>. Avoiding the hopfield trellis poles was solved by means of handling the carrier by tractor driver. When creating the design we respected dimensional parameters of

the hopfield trellis and dimensional parameters of the machines used for operation on ground communications.



Fig. 1 Anchorage of a low-trellis hopfield

On the basis of the aforementioned requirements it was decided to use Zetor tractor, type 7745. For low trellis it seemed to be the most advantageous solution the usage of single-disc hop cutter with a tool in the form of a toothed cutting disc with 600 mm in diameter and at a thickness of 3.5 mm. The disc was made of material 75Cr1 with 48 flat teeth with the rake angle of 15°.

Together with hop cut also the last year's hopvines are cut off, and either at the same time or at a short time in advance. This operation is carried out by fixing two blades, which cut the old hopvines, above the cutting disc.

Our effort was to design a hydraulic rotary drive. The hydraulic circuit was formed by means of Automation Studio software, version 5.3. (Figure 2). The circuit was tested by means of animation during which was simulated the load by changing the frequency of hydraulic-motor rotation, by loading due to a different rotational moment and a different pressure.

On the basis of a research for possible applications of different types of hydraulic motor we chose as the most advantageous solution the hydraulic motor with external gear (Danfoss, type CGM). This hydraulic motor is in Figure 3. Regulation of hydraulic-motor rotation frequency will be realized by means of throttle valve.

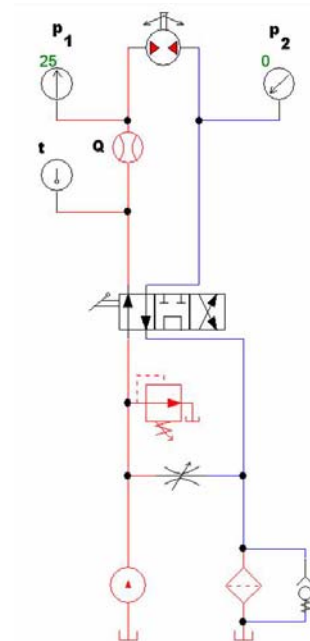


Fig. 2 Simulation of the hydraulic circuit by means of Automation Studio 5.3.

$p_1$ -pressure before the hydraulic motor;  $p_2$ -pressure after the hydraulic motor;  $Q$ -flow;  $t$ -temperature



Fig. 3 Gear hydraulic motor for the drive of the cutting disc

The cutting disc was placed on the tool carrier made by Wallner Landtechnik company. This carrier (Figure 4) is placed between the front and the rear tractor axle. It has three rectilinear hydraulic motors. Two hydraulic motors provide the movement on vertical and horizontal position, and the third hydraulic motor deflects the suspension desk for tools from the tractor by up to 18°. This deflection is unusable for work in low-trellis hopfields. The carrier construction makes a robust impression and exceeds the tractor outline considerably.

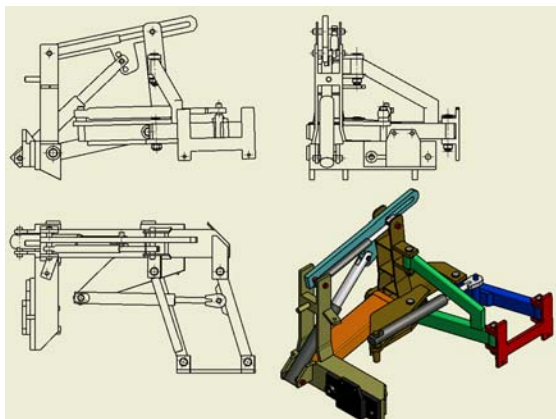


Fig. 4 Scheme of the tool carrier by Wallner Landtechnik company

The main precondition concerned the axis of the cutting disc which has to be identical in its operating position with the axis of a hop plant row. But it is also necessary to have the possibility to deflect the cutting disc outside the hopfield poles. A kinematic scheme of the carrier is shown in Figure 5. When the cutter is in operation (interrow travel) an increased caution of the operators was necessary, as the set of tractor-cutter did not drive in the interrow axis.

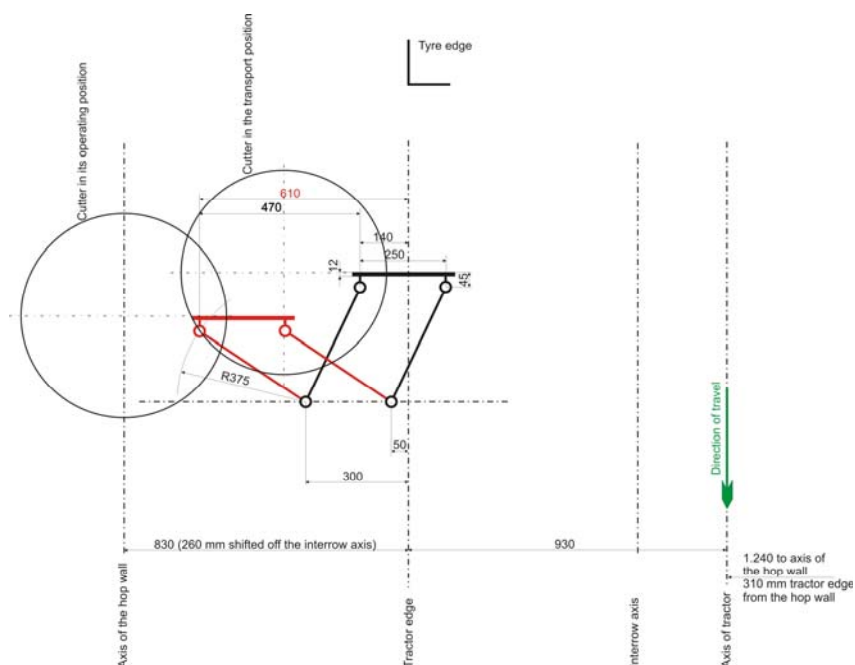


Fig. 5 Kinematic scheme of the tool carrier by Wallner Landtechnik company  
*red parallelogram – maximum diversion of the carrier, black parallelogram – transport position of the carrier*

During the measurements of power parameters (Figure 6) (pressure and flow) of the hop cutter hydraulic drive the hydraulic oil was held at a temperature of 40 °C. The measurements were provided by measuring equipment by Hydrotechnik Multi System company, type 5060. As there was no supporting wheel on the cutter, the recess was chosen in the tractor driver's estimation to be app. 50 mm.



Fig. 6 Hop cutter during measurement

The measuring time was set for 30 s with a measuring interval of 500 ms. The measured values were saved on the memory card of the measuring equipment. After the measurements were finished, the measured data were

downloaded into the computer by means of HydroCom program and converted into a form which is able to proceed in Microsoft Excel.

The measured values are shown in the following graph (Figure 7).

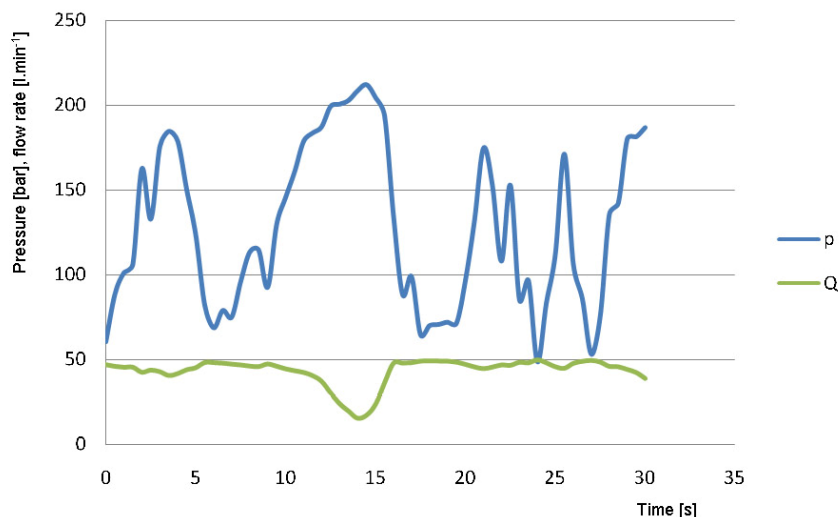


Fig. 7 Graph of the course of pressure, flow, and oil temperature of hop cutter in operation

### Discussion and conclusion

The designed drive system, including its control, was tested on the premises of Hop Research Institute Co., Ltd. seated in the town of Žatec.

Through the measurements the values of pressure and flow of the oil in hydraulic circuit of the cutter. These values show that the hydraulic aggregate has its safety pressure valve set up at a value of 20 MPa. That is why a deeper recess causes a rise in pressure and a decline in oil flowing into the hydraulic motor. At a partial recess of the disc occurs a decline in oil pressure and the oil flow rises. The interruption and the decline of oil flow are seen in the graph (Figure 7).

After this deficit is removed it will be necessary to substitute the gear hydraulic motor for a piston converter which has a higher rotational moment at a lower oil pressure. But a piston hydraulic motor is substantially higher (longer) than a gear one. Thus it will be necessary to insert a conical gearbox. Next precondition of a right function of the cutter will be a necessity to supply the equipment with a functional supporting wheel to ensure a precise set up and maintenance of the cut depth.

During the cut it is necessary to regulate the frequency of the disc rotation and to choose an optimal rotation frequency. This will be the subject of next research. For it will be necessary to find the optimal solution of the drive, not only from the point of view of the right set up of rotation frequency, but also from the point of view of the circuit energy intensity. Therefore there will be two ways of rotation regulation tested – by means of a throttle valve connected in parallel, or by means of a three-way flow regulator.

*This article was written with the contribution of the Ministry of Education, Youth and Sports of the Czech Republic as a part of the research project of MSM 6046070905 and the project of the Ministry of Industry and Trade of the Czech Republic FI-IM5/181.*

### References

- [1] Kolektiv: Projektování a konstrukce hydraulických zařízení. Příručka hydrauliky. Lohr am Main: Mannesmann Rexroth GmbH, 1988, 362 p., ISBN 3-8023-02664
- [2] Kučík, P.-Strážovec, I.-Křiššák, P.: Hydraulický přenos energie – mobilné



- pracovné stroje. Žilina: Žilinská univerzita, 2000, 384 p., ISBN 80-7100-725-0
- [3] Neuhauser, H.-Rödel, G.-Rossbauer, G.: Cutting equipment for hop growing in low trellis systems. Landtechnik, 2002, 57, 1, p. 20-21.
- [4] Rybáček, V. et al.: Chmelařství. SZN Praha, 1980, 426 p. ISBN 07-068-80
- [5] Štranc, P., et al.: Řez chmele. Praha: ČZU v Praze, 2007, 48 p. ISBN 978-80-87111-03-1



## TEMPERATURE DEPENDENCIES OF MILK DYNAMIC VISCOSITY DURING STORAGE

PETER HLAVÁČ

Slovak University of Agriculture in Nitra, Faculty of Engineering, Department of Physics,  
Tr. A. Hlinku 2, SK - 949 76 Nitra, Slovak Republic,  
p.n.:+04216414749, e-mail: peter.hlavac.mf@uniag.sk

### Abstract

At quality valuation of food material is important to know their physical properties particularly mechanical, rheologic and thermophysical. Automatically controlled processes at manufacturing, at handling and holding require exact knowledge about physical quantities of materials. Rheologic properties were measured by many authors. Results from measuring of rheologic properties of three types of milk are shown in this paper. Measuring was performed by digital rotational viscosimeter Anton Paar (DV-3P) and principle of measuring by this viscosimeter is based on dependency of sample resistance against the probe rotation. Samples of milk were stored in special cool box in temperature 5 °C and were measured in different days during one week. Measurements were done after the temperature stabilization from 8 °C to laboratory temperature. Dependencies of dynamic viscosity on temperature and on time of storing are described. Dynamic viscosity values for different types of milk are compared.

**Keywords:** milk, rheologic properties, dynamic viscosity, temperature, time of storing

### 1 Introduction

In this paper are shown results from measuring of rheologic properties of milk. We can include into rheologic properties these parameters: dynamic viscosity, kinematic viscosity, fluidity and tangential tension. Materials, where internal friction is generated, can be characterized by viscosity. Dynamic viscosity  $\eta$  is defined as a constant between tangential tension  $\tau$  and gradient of layer velocity  $\text{grad } v$ .

$$\tau = \eta \text{ grad } v$$

Physical unit of dynamic viscosity is Pa.s and unit of tangential tension is Pa. Kinematic viscosity  $\nu$  is defined as a ratio between dynamic viscosity  $\eta$  and density of used material  $\rho$ .

$$\nu = \frac{\eta}{\rho} \quad (1)$$

Physical unit of kinematic viscosity is  $\text{m}^2 \cdot \text{s}^{-1}$ . Reciprocal value of dynamic viscosity  $\eta$  is called fluidity  $\phi$  and physical unit of fluidity is  $\text{Pa}^{-1} \cdot \text{s}^{-1}$ .

$$\phi = \frac{1}{\eta} \quad (2)$$

Rheologic properties were measured by many authors. Buchar et al. (2005, 2003), investigated these properties of eggs yolk, milk products and ketchups. Hlaváč (2007) examined rheologic properties of plum jam. Severa et al. (2007, 2010b.) examined influences of storing and temperature on viscosity of egg fluids. Severa and Los (2008), Hlaváč (2008) were looking for influence of temperature on dynamic viscosity of dark beer. Kubík (2006) examined influence of long term storage on apple flesh. Marudova and Zsivánovits (2005) described rheologic properties of pectin films. Patočka et al. (2006) examined rheological behaviour of dairy products. Rheological profile of raw whey was investigated by Severa et al. (2010a.). Biczó et al. (2005) examined methods for determination of rheologic properties of chocolate mass. At quality valuation of food material is important to know their physical properties particularly mechanical, rheologic and thermophysical (Božiková, 2005). Automatically controlled processes at manufacturing, at handling and holding require exact knowledge about physical quantities of materials. Still are detected new methods that are utilizing new modern apparatuses and microscopic components. Very

fast development is possible to observe at utilization of microwave at measuring properties of soil and food (Hlaváčová, 2002).

## 2 Material and methods

Three types of milk were used during measurement. These milks had different value of fat content. First milk had 0.5 % of fat content; second sample had 1.5 % of fat content and third milk 3.5 % of fat content.

Measuring was performed by digital rotational viscosimeter Anton Paar (DV-3P). Principle of measuring by this viscosimeter is based on dependency of sample resistance against the probe rotation. Probe with signification R2 was used in our measurements. It is possible to choose frequency of probe rotation from  $0.3 \text{ min}^{-1}$  to  $200 \text{ min}^{-1}$ . Our measurements were performed only at one frequency  $200 \text{ min}^{-1}$  (example of measurement on Fig. 1).

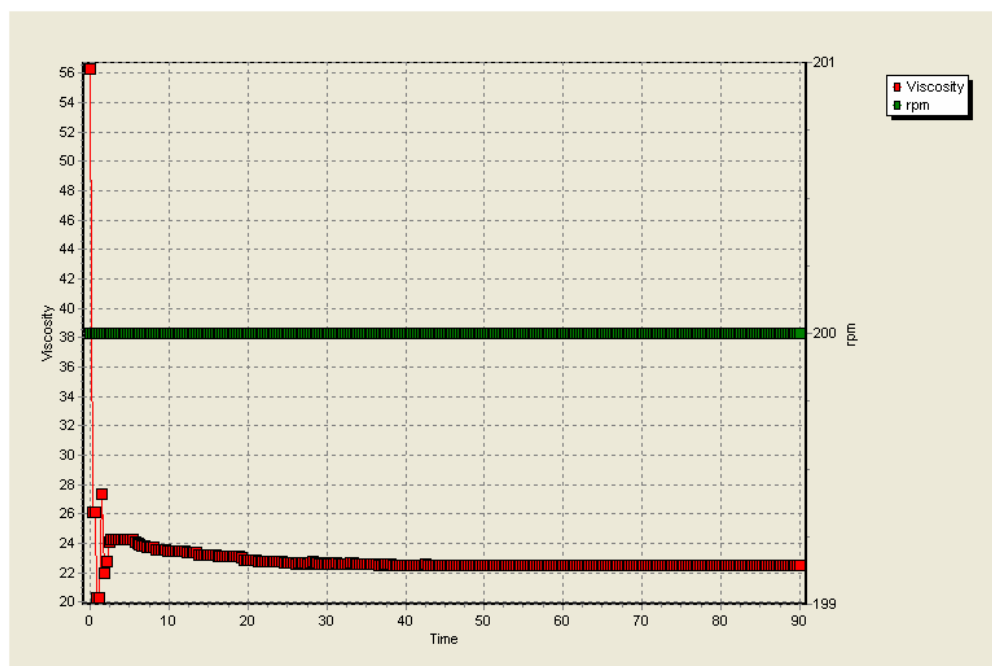


Fig. 1 Dependency of milk dynamic viscosity on rotational time (sample with 3.5 % of fat content; frequency of rotation  $200 \text{ min}^{-1}$ ; temperature  $24 \text{ }^{\circ}\text{C}$ , rotational time 90 s)

Samples of milk were stored in special cool box in temperature  $5 \text{ }^{\circ}\text{C}$  and were measured in different days during one week. Measurements were done after the temperature stabilization from  $8 \text{ }^{\circ}\text{C}$  to laboratory temperature. Dependencies of dynamic viscosity on temperature are constructed and dependencies of dynamic viscosity on time of storing are described. Dynamic viscosity values for different types of milk are compared. Dependency of dynamic viscosity on temperature can be described by Arrhenius equation

$$\eta = \eta_0 e^{-\frac{E_A}{RT}} \quad (3)$$

where  $\eta_0$  is reference value of dynamic viscosity,  $E_A$  is activation energy,  $R$  is gas constant and  $T$  is temperature. This equation has decreasing exponential shape.

## 3 Results

For illustration on Fig. 2 – 7 are shown dependencies of milk dynamic viscosity on temperature without storing and after one week of storing. Progress of graphic dependencies can be described by decreasing exponential function (4) and in this temperature range also by decreasing linear function (5)

$$\eta = A e^{-B\left(\frac{t}{t_o}\right)} \quad (4)$$

$$\eta = C - D \left( \frac{t}{t_0} \right) \quad (5)$$

where  $t$  is temperature,  $t_0 = 1$  °C; A, B, C, D are constants dependent on kind of material, and on ways of processing and storing .

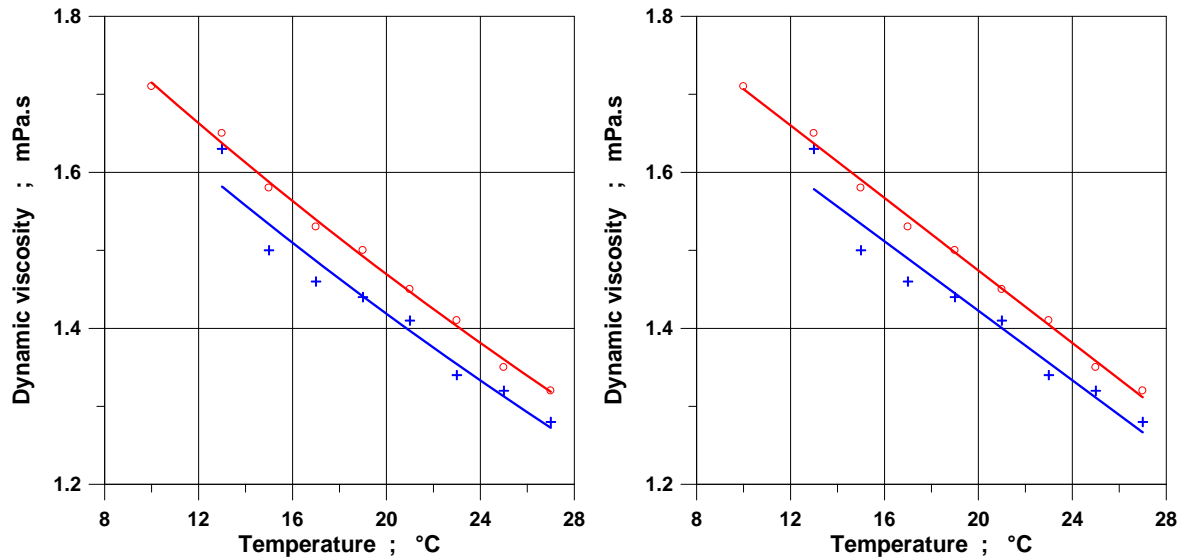


Fig. 2 – 3 Dependencies of milk (0.5 % of fat content) dynamic viscosity on temperature: first measurement without storing +, last measurement after one week of storing ○ (exponential function on the left, linear function on the right)

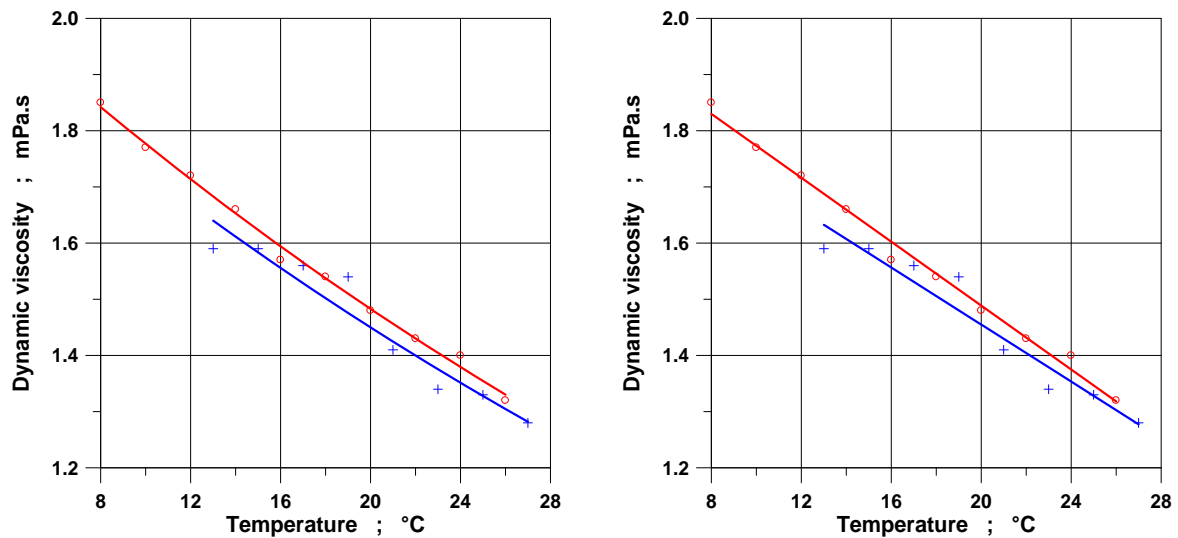


Fig. 4 – 5 Dependencies of milk (1.5 % of fat content) dynamic viscosity on temperature: first measurement without storing +, last measurement after one week of storing ○ (exponential function on the left, linear function on the right)

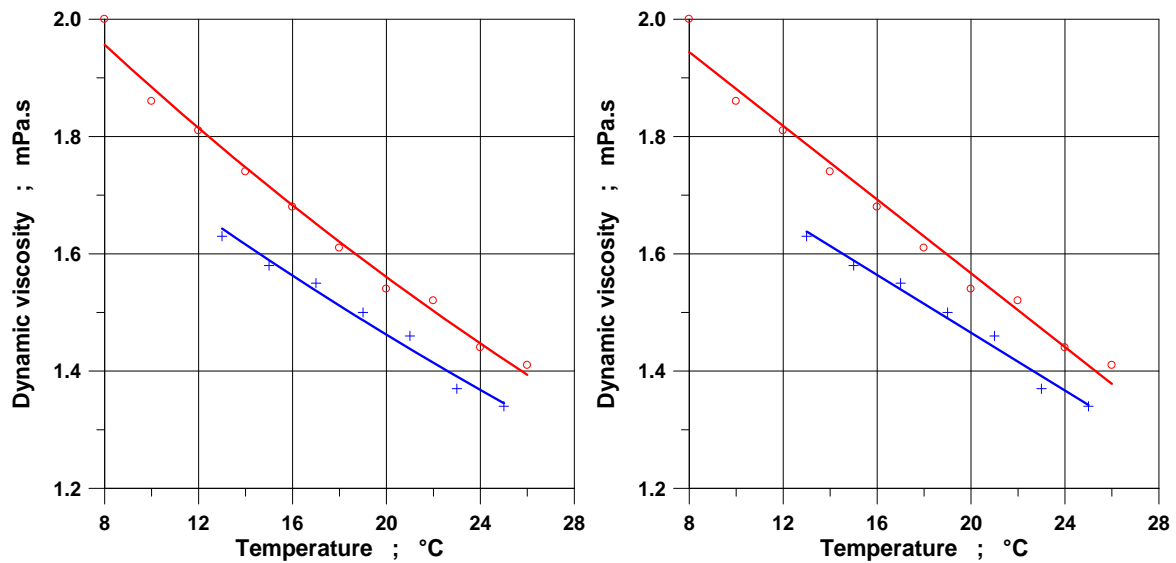


Fig. 6 – 7 Dependency of milk (3.5 % of fat content) dynamic viscosity on temperature:  
first measurement without storing +, last measurement after one week of storing o  
(exponential function on the left, linear function on the right)

Table 1 – Coefficients A, B, C, D of regression equations (4, 5), and coefficients of determination

	Exponential function (4)			Linear function (5)		
Measurement/ Sample	Coefficients					
	A	B	R <sup>2</sup>	C	D	R <sup>2</sup>
First m. / milk 0.5 % f. c.	1.935 56	0.015 533 1	0.953 616	1.867 74	0.022 261 9	0.940 254
Last m. / milk 0.5 % f. c.	2.001 91	0.015 462 4	0.996 109	1.938 97	0.023 239 6	0.995 269
First m. / milk 1.5 % f. c.	2.061 29	0.017 590 1	0.928 499	1.962 14	0.025 357 1	0.929 617
Last m. / milk 1.5 % f. c.	2.128 80	0.018 08	0.994609	2.057 21	0.028 424 2	0.991740
First m. / milk 3.5 % f. c.	2.040 10	0.016 656 7	0.977 339	1.958 21	0.024 642 9	0.982 865
Last m. / milk 3.5 % f. c.	2.274 74	0.018 847 0	0.990 008	2.195 21	0.031 424 2	0.980 678

In Tab. 1 can be seen coefficients A, B, C, D of regression equations (4, 5), and also that coefficient of determination had high values for all measurements. Coefficients of determination are bit higher at exponential function than at linear function almost in all cases, but the differences are very small. Arrhenius equation (3) has decreasing exponential shape and that is why it can be used also for describing temperature dependencies of milk dynamic viscosity.

Temperature dependencies of milk dynamic viscosity had decreasing exponential

and it is almost linear shape for all measurements (Fig. 2 – 7). It is also evident that dynamic viscosity had increased a bit with time of storing (Fig. 2 – 7) for all samples of milk.

Comparison of dynamic viscosity values for all samples of milk is on Fig. 8. It is evident that fat content has influence on dynamic viscosity values. Biggest values of dynamic viscosity were measured on milk sample with 3.5 % of fat content. Lowest dynamic viscosity values were found on sample with smallest fat content.

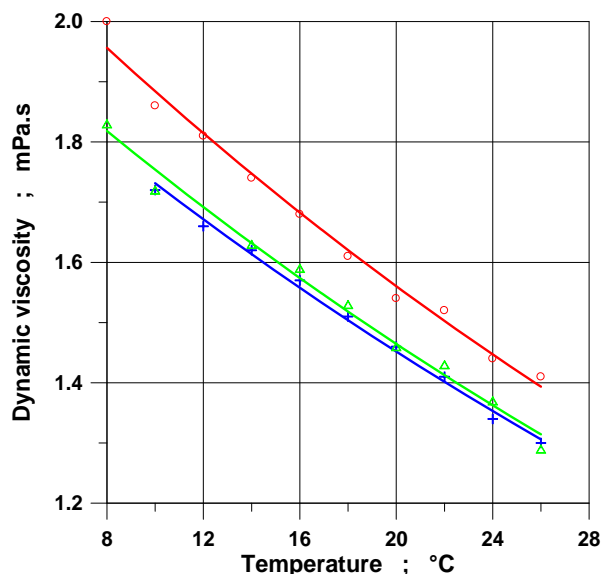


Fig. 8 Dependencies of milk dynamic viscosity on temperature: first sample milk (0.5 % of fat content) +, second sample milk (1.5 % of fat content)  $\Delta$ , third sample milk (3.5 % of fat content)  $\circ$  (exponential functions)

#### 4 Conclusions

At quality valuation of food material is important to know their physical properties particularly mechanical, rheologic and thermophysical. Automatically controlled processes at manufacturing, at handling and holding require exact knowledge about physical quantities of materials. Rheologic properties were measured by many authors.

Temperature dependencies of milk dynamic viscosity had decreasing exponential shape, and in this temperature range it is almost linear shape for all measurements. Coefficients of determination are bit higher at exponential function than at linear function almost in all cases, but the differences are very small. Arrhenius equation (3) has decreasing exponential shape and that is why it can be used also for describing temperature dependencies of milk dynamic viscosity.

It is also evident that milk dynamic viscosity had increased a bit with one week of storing. It is evident that fat content has influence on dynamic viscosity values. Biggest values of dynamic viscosity were measured on milk sample with 3.5 % of fat content. Lowest dynamic viscosity values were found on sample with smallest fat content.

Measured values of dynamic viscosity were obtained with good precision and all drawn

dependencies had very high coefficients of determination.

#### References

1. Biczó, V., Scherer, R., Fekete, A. 2005. Measurement Methods for the Viscosity of Chocolate Mass. In: Proceedings of International Conference: Research and Teaching of Physics in the Context of University Education, Nitra, June 8. Slovak University of Agriculture in Nitra, p.198 – 201, ISBN 80-8069-528-8
2. Božíková, M. 2005. Some chosen thermophysical parameters of apples and applesauce. In: Acta technologica agriculturae. Nitra: SPU Nitra, ročník 8, č. 4, 2005, ISSN 1335-2555, 89 – 92
3. Buchar, J., Simeonová, J., Křivánek, I. 2003. Squeezing Flow of Soft Semi – Liquid Food. 2003. Acta Univ. Agric. et Silv. Mendel. Brun., 2003, vol. LI, issue number 3, p. 75 – 88
4. Buchar, J., Křivánek, I., Severa, L. 2005. Thixotropic Properties of the Egg Yolks. In: Proceedings of International Conference: Research and Teaching of Physics in the Context of University Education, Nitra, June 8. Slovak University of Agriculture in Nitra, p. 10 – 13, ISBN 80-8069-528-8

5. Hlaváč, P. 2007. The rheologic properties of plum jam. In: *PTEP Journal on processing and energy in agriculture*, Novi Sad, Serbia, 2007, p. 106 – 108, ISSN 1450-5029
6. Hlaváč, P. 2008. Temperature and time of storing dependencies of dark beer rheologic properties. In: *PTEP Journal on processing and energy in agriculture*, 2008, vol. 12, no. 3, p. 114 – 117, ISSN 1450-5029
7. Hlaváčová, Z. 2002. Electrical Properties Utilization in Food Treatment. *PTEP Journal on processing and energy in agriculture*, 6, 2002(1-2), 5 – 8
8. Kubík, L. 2006. *Fractal Analysis of the Long – Term Storage Influence on the Apple Flesh*. In: *PTEP. Journal on Processing and Energy in Agriculture*. 2006, 10, 2006(3-4), ISSN 1450-5029, 63 -67
9. Marudova – Zsivánovits, M., Zsivánovits, G. 2005. Swelling Behaviour and Tensile Properties of Concentrated Cross-linked Pectin Networks. In: *International Conference: Research and Teaching of Physics in the Context of University Education*, Nitra, June 8. Slovak University of Agriculture in Nitra, p. 206 – 210, ISBN 80-8069-528-8
10. Patočka, G., Červenková, R., Narinea, S., Jelen, P. 2006. Rheological behaviour of dairy products as affected soluble whey protein isolate, In: *International dairy journal*, vol. 16, p. 399 – 405
11. Severa, L., Buchar, J., Křivánek, I., Nedomová, Š. 2007. On the influence of storing on viscosity of egg yolks In: *Multiauthor book of International Conference: Research and Teaching of Physics in the Context of University Education*, Nitra June 6. SUA in Nitra, 2007, p.57 – 62, ISBN 978-80-8069-898-0
12. Severa, L., Buchar, J., Nedomová, Š., Šustová, K. 2010a. Rheological profile of raw whey, In: *Acta univ. agric. et silvic. Mendel. Brun*, 2010, vol. LVIII, n. 2, ISSN 1211-8516
13. Severa, L., Los, J. 2008. On the influence of temperature on dynamic viscosity of dark beer. In: *Acta Univ. Agric. et silvic. Mendel. Brun.*, 2008. Vol. LVI, n. 2, p. 303 – 307, ISSN 1211-8516
14. Severa, L., Nedomová, Š., Buchar, J. 2010b. Influence of storing time and temperature on the viscosity of an egg yolk. In: *Journal of Food Engineering*, 2010, Vol. 96, n. 2, p. 266 – 269, ISSN 0260-8774

#### Acknowledgement

This work was supported by research project VEGA 1/0643/09 of Slovak Grant Agency for Science.



## HIGH SPEED DETECTION OF POTATO AND CLOD USING AN ACOUSTIC BASED INTELLIGENT SYSTEM

ADEL HOSAINPOUR<sup>1\*</sup>, MOHAMMAD H. KOMARIZADE<sup>2</sup>, ASGHAR MAHMOUDI<sup>3</sup>, TARAHOM MESRI GUNDOSHMIAN<sup>3</sup>, MAHROKH G. SHAYESTEH<sup>2</sup>

<sup>1</sup> Department of Agricultural Machinery, College of Agriculture, University of Urmia, Urmia, Iran, Phone +98 914 300 2974, Fax: +98 411 3356007

Email: a.hosainpour@urmia.ac.ir, a\_hoainpour12@yahoo.com

<sup>2</sup> University of Urmia, Urmia, Iran

<sup>3</sup> Department of Agricultural Machinery, College of Agriculture, University of Tabriz, Tabriz, Iran

### Abstract

In this study, an acoustic-based intelligent system was developed for high speed discriminating between potato tubers and soil clods. About 500kg mixture of potato tubers and clods were loaded on a belt conveyer and were impacted against a steel plate at four different velocities. The resulting acoustic signals were recorded, processed and potential features were extracted from the analysis of sound signals in both time and frequency domains. A multilayer perceptron neural network with a back propagation algorithm was used for pattern recognition. Optimal network was selected based on mean square error, correct detection rate and correlation coefficient. At the belt velocity of 1 m s<sup>-1</sup>, detection accuracy of the presented system was about 97.3% and 97.6% for potatoes and clods, respectively. By using this system, it is expected that a potato harvester may operate at a capacity of 20 ton hr<sup>-1</sup> with the accuracy of about 97%.

**Keywords:** Acoustics, Clod, Discriminating, Neural networks, Potato, Separation

### 1. Introduction

Potato is one of the most prominent crops in the world with an estimated annual production of approximately 325 million ton (FAO, 2008). This enormous amount of potato needs fully automated harvesters. The clods and stones must be removed before entry into the potato harvester container; because they occupy a large space of the container and with their abrasive nature may mechanically damage potato tubers. Accompanying mixture of potato also reduces the air circulation and prevents proper temperature and humidity control (Main, 1971). Discriminating between potato tubers and clods is the first step in developing an automatic separation system on potato harvesters. Developing an automated system for separating clods from potato tubers is more challenging, because potato tubers have a wide diversity in shape, size and color. Moreover, the shape, size, and moisture content of clods are not predictable in harvesting condition. Partially and completely muddy potatoes add another obstacle in developing automated separator systems.

Separating potatoes from its impurities has been investigated in many research studies. Most researchers have examined mechanical methods to solve the problem (Brantley et al., 1975; Feller et al., 1985; Gan-Mor et al., 1986; Shyam et al., 1990). Although some of these methods are being used in some potato harvesters, they cause surface damages and bruises on potato tubers (McGeachan, 1980). Moreover, large space occupancy and high energy consumption are other main drawbacks of these systems. Some machine vision based systems have been developed for discriminating between potato tubers and clods (Marchent et al., 1988; Morrow et al., 1990; Al-Mallahi et al., 2008). Operational problems are most likely to be faced, by using this system under field conditions (i.e. rain, moisture, dust, vibration). High price of the cameras and other auxiliary devices as well as inefficiency in detecting clod and muddy potatoes are other disadvantages of this method.

Recently, non destructive acoustical experiments have been increasingly implemented in detection and classification of agricultural products (Pearson, 2001; Mahmoudi, 2006;

Diezma-Iglesias et al., 2004; Pearson et al., 2007). A good correlation between fruit firmness and resonant frequency has been reported in some investigations (Younce & Davis, 1995; Sugiyama et al., 1998; Jivanuwong, 1998; Garsia-ramos et al., 2003). Quite recently, Elbatawi (2008) used an acoustic impact method to detect hollow heart of potato tubers. Artificial neural networks (ANN) offer much faster and more flexible approach in classification fields. Also, in noisy obscure pattern, ANN models are more efficient than statistical pattern classifiers (Kavdir & Guyer, 2008).

The main goal of this study is to investigate the feasibility of using impact sound signals for rapid detection of clods in potato harvesters. An artificial neural network was used as a decision making unit for this purpose. Experiment was performed in off-line and on-line stages. In off-line experiments, potential features were extracted from analysis of emitted sound signals, whereas in on-line stage, extracted features were used in real-time detection of clods and potato

tubers. Moreover, the effect of sample velocity on detection accuracy was investigated.

## 2. Materials and Methods

About 500 kg of a mixture of potato tubers, clods and stones were collected just from the entrance of a potato harvester container in the 2008 harvesting season. Four varieties of potato tubers namely *Marfona*, *Agria*, *Kosima* and *Granola*, commonly grown in Iran were used in this study. All samples of potatoes, clods and stones were weighed and pieces smaller than 40 g were neglected. Table 1 shows some physical characteristics of the used samples. During weighing, mixture was manually sorted into two discrete groups; potato and non-potato. Since the number of stones was much lower than the number of clods (Table 1), hereafter in this paper the non-potato category is simply called "clods". It is worth mentioning that hard enough clods were selected as samples and other flimsy clods were crumbled and removed before reaching the potato container.

Table1. Numbers and physical characteristic of used samples

samples	Variety	Number N	Mean weight g	Std g
Potato	Marfona	378	186	82
	Agria	443	158	73
	Kosima	446	150	88
	Granola	625	115	50
Clod		1483	123	72
Stone		38	108	40

### 2.1 Experimental Apparatus

A test rig was built to feed samples, drop them onto an impact plate, acquire sound signal upon impact, process the signal data and discriminate between potato tubers and clods. The schematic diagram of the experimental apparatus is shown in figure 1. The system consisted of a feeding platform, an impact plate, an acoustic unit and a PC based data acquisition system. A 5 m long and 0.35 m wide belt conveyor was designed and fabricated as feeding platform. The belt conveyor was driven by a 1 kW hp electric motor. The velocity of the conveyer belt could be changed by using a variable frequency drive (Inverter IG5). Some special cups were mounted on the belt for singulating and better control of the sample movement. The impact plate was a polished block of stainless steel approximately  $22.5 \times 30$

$\times 1.5$  cm. To study the effect of velocity on detection accuracy, four levels of belt conveyer velocity at 1, 1.5, 2 and  $2.5 \text{ m s}^{-1}$  were examined throughout the study.

A low cost Panasonic Electret capsule microphone (VM-034CY model), sensitive to frequencies up to 100 kHz, was used for capturing impact sound signals. For environmental noise elimination, the data acquisition system was triggered by a piezoelectric sensor mounted on the impact plate. By adding this electronic circuit, only impact emission sound signals from samples were recorded and the environmental noises did not interfere with the actual desired signals. Microphone output was send to a PC based data acquisition system, where it was digitized using a sound card (Intel® 82801 BA/BAM AC'97Audio controller) at a sampling frequency

of 44.1 kHz, with 16 bit resolution. A personal computer (Pentium IV) was used for acquiring, saving and processing of data as well as controlling the system.

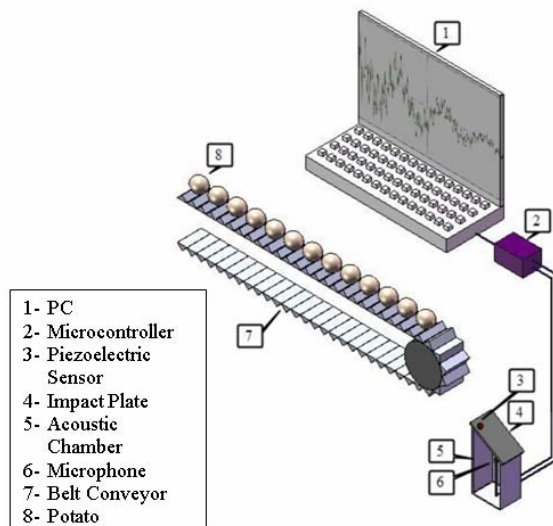


Figure1. Schematics of experimental apparatus

In each stage of off-line experiment, about 45 samples of potato or clod were manually loaded in the cups on the belt. By switching the belt conveyor power on, samples were made to fall onto the impact plate separately and one by one. The emitted sound signals were acquired by the microphone, digitized by the sound card and saved by using Matlab data acquisition toolbox (MathWorks, 2007). Similar procedures were repeated for all belt velocities. Since the maximum frequency of the sound card was 44.1 kHz and data acquisition continued for 11.61 ms after triggering, upon receiving a trigger signal the computer acquired 512 data points from every sample in the time-domain.

## 2.2 Signal Processing and Feature Extraction

For extracting potential features, recorded sound signals were processed and analyzed in both time and frequency-domains. Although the maximum peak values of clod sound signals were slightly larger than potato ones, the preliminary attempts to use only time-domain features were not successful. However, in order not to lose any useful transient feature, all 512

data point amplitude (Amp) values were considered as features. A 1024-point fast Fourier transform (FFT) was computed from each sound signal, using a Mathwork Windows.

The magnitude, power spectral density (PSD) and peak frequency (the frequency corresponding to the peak value of FFT in frequency spectrum) of each spectrum was computed and a low pass filter was applied to remove the jagged spikes in the spectrum. In addition, the 25 normalized FFT magnitudes before peak frequency and 25 points afterwards were saved as another frequency-domain feature. A total of 1075 features were obtained for each sample. For real time systems, this dimension of the input vector is large, but the components of the vectors are highly correlated. Principle Component Analysis (PCA) was used to reduce the dimension of the input vectors to a maximum of 30 features. After normalization of data, PCA analysis was performed on data using Matlab software. Table 2 shows the relation between number of principle components and percentage of eliminated component variance.

The Multilayer Perceptron (MLP) with the Back Propagation Algorithm (BPA) was used as ANN in this study. Gradient descent with momentum (GDM) learning rule was used to speed up learning and stabilizing convergence throughout this study. In order to minimize ANN training time, only one hidden layer was considered in the network. The number of neuron in hidden layer was determined using an exhaustive search from 1 to 40 nodes. The Neural Network with 29 nodes in hidden layer had the least standard deviation error as well as high stability. In developing ANN models, the linear function at the input layer and the non-linear hyperbolic tangent function at both hidden and output layer were used as transfer functions. Learning rate was 0.7 throughout the momentum learning rule. As an additional guard against over-fitting, the data sets were divided into three randomly selected data sets; 70% of data were used for training, 15% for testing and the remaining 15% were used for cross validation. NeuroSolutions 5.0 software was used for designing and testing of ANN models (NeuroSolutions 5.0 for Excel, 2005).

Table 2. Relation among eliminated components variance and number of selected principle components

Percentage of eliminated components variance	Number of selected features		
	Amp	PSD	NFFT
2%	9	1	1
0.5%	28	4	3
0.1%	98	34	11

### 3. Results and Discussion

To find the best combinations of potential features and optimal ANN configuration, 31 different combinations of principle component features were selected and tested by neural network. These features were fed to the ANN models and their performances were determined by evaluation of the mean square error (MSE), correct detection rate (CDR) and correlation coefficient ( $r$ ). Table 3 shows the summary of off-line experiment using the belt velocity of  $1\text{ m s}^{-1}$ . In summary, the best combination was 9 amplitudes, 4 PSD, 3 NFFT and one peak frequency feature. The final structure of network was 17 input nodes, 29 hidden nodes and 2 output nodes. Table 4 shows the performance of optimal ANN configuration.

After extracting potential features in off-line stage, on-line experiment was performed to evaluate real-time detection accuracy. In this stage, about 540 samples of potatoes and clods were randomly selected and off-line procedures were repeated for them. Table 5 shows the performance of on-line system at different belt conveyer velocities. Increasing the belt velocity resulted in the reduction of detection accuracy and increase in the number of miss classified samples. Low detection accuracy in high velocity was caused by high sound signal intensity. Although the distance between feeder and impact plate had been adjusted before, saturated and weak sound signals were likely at the high velocity of belt conveyor.

Table 3. Performance of off-line experiment for subsets of features

Features	Number of features	Correct detection rate (%)		Cross validation MSE
		potato	clod	
Amp	28	90.2	84.2	0.068
Amp	9	87.4	73.6	0.163
PSD	4	89.3	91.4	0.032
NFFT	3	91.8	80.1	0.070
PF	1	88.6	92.5	0.018
Amp+PSD	9+4	92.2	91.2	0.019
Amp+NFFT	9+3	92.7	86.8	0.067
PSD+NFFT	4+3	94.3	92.2	0.019
Amp+PSD+NFFT	9+4+3	95.4	93.3	0.016
Amp+PSD+PF	9+4+1	93.4	94.5	0.013
Amp+NFFT+PF	4+3+1	95.2	95.4	0.013
Amp+PSD+NFFT+PF	9+4+3+1	97.3	97.6	0.011

Table 4. Performance of optimal ANN model

Performance	Potato	Clod
MSE	0.0113	0.0105
CDR (%)	97.3%	97.6%
$r$	0.989	0.992

Table 5. Detection accuracy of on-line system at different belt velocity

Belt velocity (m s <sup>-1</sup> )	Correct detection				Cross validation MSE
	Potato		Clod		
	Ratio	%	Ratio	%	
1	176/181	97.2	79/81	97.5	0.011
1.5	174/182	95.6	81/84	96.4	0.018
2	162/178	91	77/82	93.9	0.045
2.5	157/184	85.2	71/81	87.6	0.165

The signal acquisition and computational procedures took about 25 ms for a sample at throughput rate of 40 samples per second. However there were some mechanical disturbances that limited the detection capacity under 15 samples per second. A potato harvester by using this system can perform at the field capacity of 7.2 ton hr<sup>-1</sup>. By devising four potato stream lines on the belt at the velocity of 1 ms<sup>-1</sup>, detection capacity of 20 ton hr<sup>-1</sup> with the accuracy of 97% is possible.

#### 4. Conclusions

In the present study, an acoustic-based intelligent system was used for discriminating between potato tubers and clods. Main advantages of this system are high accuracy, large capacity and practicality as well as requiring small space and low cost of equipment and computation.

#### References

- [1] Al-Mallahi, A., Kataoka, T. & Okamoto, H. (2008). Discrimination between potato tubers and clods by detecting the significant wavebands. *Biosystems Engineering*, 100, 329–337.
- [2] Brantley, S. A., Hamann, D. D. & Whitfield, J. K. (1975). A multiple belt adjustable Vee size grader for sweet potatoes and cucumbers. *Transactions of the ASAE*, 18, 350–362.
- [3] Diezma-Iglesias, B., Ruiz-Altisent, M. & Barreiro, P. (2004). Detection of internal quality in seedless watermelon by acoustic impulse response. *Biosystems Engineering*, 88, 221–230.
- [4] Elbatawi, I. E. (2008). An acoustic impact method to detect hollow heart of potato tubers. *Biosystems Engineering*, 100, 206–213.
- [5] Feller, R., Morgolin, E., Zacharin, A. & Pasternak, H. (1985). Development of a clod separator for potato packing houses. *Transactions of the ASAE*, 28, 1019–1023.
- [6] Food and agriculture Organization of the United Nations. (2008). <http://www.fao.org/corp/statistics/en>.
- [7] Gan-Mor, S., Zacharin, A., Galili, N., Feller, R. & Margolin, E. (1986). Absorbing stone impact to enable separation from potatoes. *Transactions of the ASAE*, 29, 1526–1529.
- [8] Garsia-Ramos, F. J., Ortiz-Canavate, J., Ruiz-Altisent, M., Diez, J. & Chavez, M. (2003). Development and implementation of an on-line impact sensor for firmness sensing of fruits. *Journal of Food Engineering*, 58, 53–57.
- [9] Jivanuwong, S. (1998). Nondestructive detection of hollow heart in potatoes using ultrasonics. Master of Science thesis. Submitted to the faculty of Virginia Polytechnic Institute and State University, Blacksburg, Virginia, pp. 76.
- [10] Kavdir, I. & Guyer, D. E. (2008). Evaluation of different pattern recognition techniques for apple sorting. *Biosystems Engineering*, 99, 211–219.
- [11] Mahmoudi, A. (2006). Development of a suitable algorithm using Artificial Neural Networks for sorting of pistachio nuts with closed shells using impact acoustics, PhD thesis, Department of Agricultural Machinery, University of Tehran, Karaj: Iran, p. 144.
- [12] Main, J. C. (1971). Potatoes in the UK, Developments in production and marketing. *Span*, 14, 87–90.
- [13] Marchant, J. A., Onyango, C. M. & Street, M. J. (1988). High speed sorting of potatoes using computer vision. *ASAE Paper No.* 88-3540.
- [14] MathWorks, MATLAB User's Guide, the Math Works, Inc., (2007).
- [15] McGeachan, M. B. (1980). An investigation into the damage sustained by different varieties of potatoes during riddling to

- remove soil. *Journal of Agricultural Engineering Research*, 25, 345–353.
- [15]Morrow, C. T., Sommer, J. H., Heinemann, P. H. & Tao, Y. (1990). Automated machine vision inspection of potatoes. *ASAE Paper No. 90-3531*.
- [16]NeuroSolutions for Excel, NeuroDimension, Inc., (2005).
- [17]Pearson, T. C. (2001). Detection of pistachio nuts with closed shells using impact acoustics. *Applied Engineering in Agriculture*, 17, 249-253.
- [18]Pearson, T. C., Cetin, A.E., Tewfik, A. H. & Haff, R. P. (2007). Feasibility of impact-acoustic emissions for detection of damaged wheat kernels. *Digital Signal Processing*, 17, 617–633.
- [19]Shyam, M., Singh, V. & Singh, R. (1990). Design and development of potato grader. *AMA*, 21, 40-49.
- [20]Sugiyama, J., Katsurai, T., Hong, J., Koyama, H. & Mikuriya, K. (1998). Melon ripeness monitoring by a portable firmness tester. *Transactions of the ASAE*, 41, 121-127.
- [21]Younce, F. L & Davis, F. D. C. (1995). A dynamic sensor for cherry firmness. *Transactions of the ASAE*, 38, 1467–1476.



## COMPARISON OF HIGH CHROMIUM AND BORIDE HARDFACING

PETR HRABĚ<sup>1</sup>, ROSTISLAV CHOTĚBORSKÝ<sup>1</sup>, JURAJ RUŽBARSKÝ<sup>2</sup>, JOZEF ŽARNOVSKÝ<sup>3</sup>

<sup>1</sup>Czech University of Agriculture in Prague, 16521 Prague 6 – Suchbátka, Czech Republic,  
Phone: +420224383263, Fax: +4202-20921361, E-mail: hrabe@tf.czu.cz

<sup>2</sup>Juraj Ružbarský, Technical University of Košice, 080 01 Prešov, Slovakia, Phone: +421 51 77 23 012, Fax: +421 51 773 3453, E-mail: juraj.ruzbarsky@tuke.sk

<sup>3</sup>Slovak University of Agriculture in Nitra (SUA), Nitra, Slovakia, Phone: +421 37 6414 305,  
fax: +421 37 7417 003, E-mail: Jozef.Zarnovsky@uniag.sk

### Abstract

Throughout history, mankind continually addresses the problems of unwanted friction and excessive wear in welding technology. The problems of wear on mechanical components thus improve the economic efficiency of fast wearing parts affecting most manufacturing processes. Durability and reliability of a series of machine parts are largely influenced by friction and wear. The concept of hard surfacing in welding technology extends into many areas of human activity, enabling the creation of sophisticated design, economical production of machinery and equipment and utility equipment, including art. This is used not only as part of the production technology but also for increasing technology durability of machinery, equipment and tools in production, maintenance and repair. Also surfacing in the past decades had widespread distribution through the development of welding technology and weld materials. Best use of this method of production is the use of this technology, which is suitable especially in terms of job requirements and long life. This paper compares selected high chromium and boride overlay materials against abrasive wear. Weld deposits and tube electrodes are also considered.

### Introduction

A great part of machine malfunctions has its origin in the wear of single parts. The seizing of functional surfaces, affected by impeded working conditions, causes machine defects, too. At some events these defects can be prevented by various design adaptations. From constructional reasons we cannot sometimes change the machine design. Then it is necessary to choose the suitable material or to accommodate the surfaces of functional planes and edges.

Above all the material suitability depends on the wear type. The machine part wears more quickly if it works at heightened or even at high temperature and in chemically active environment. Wear is a very complicated physical-chemical effect. Simply schematically we can imagine the wear as the scraping or the abrasion of the functional surface. Owing to wear the part stops to have the specified size and form, the set becomes minor effective and reliable and within the further operation the critical condition can be reached and the failure occurs.

One of the effective provisions in order to increase the wear resistance is the surfacing of

functional surfaces using the suitable overlay material. The used overlay materials have different properties. At their choice we must respect the stress mode and the composition of the basic metal. Other overlay materials are suitable for work with sand and gravel, other ones for tools for soil cultivation.

At high stressed parts, where we wish the most long service life, we must choose the better material than the basic metal is. To this purpose we have at disposal the various alloy steels, alloys containing high percentage of carbide generating elements, hard nonferrous alloys on the cobalt or nickel basis, overlays with tungsten carbides etc.

The surfacing is used not only for renovation but for new machine parts production, too. It may bring a significant effect in saving of material, costs and time. The advantage of the surfacing is the quick wear resistance increase. As a rule it is applied where we cannot reach the required surface quality using the usual methods of heat or chemic-heat treatment, e.g. face hardening, case hardening, nitriding, carbonitriding or hard chroming, by reason of

difficult working conditions. The signification of the surfacing becomes evident at big machine parts which are very hard worn out. Otherwise the whole part has to be made from a costly material. In many cases the surfacing is the sole solution how to keep the mentioned mechanism working without expensive reconstructions or without the performance decrease. The machine parts with overlays have often so long service life that the choice of this more expensive metallurgical surface treatment is multiple rewarding.

For surfacing of minor stressed surfaces it is possible to use the cheaper electrodes. On the functional surfaces, which must be more resistant, it is necessary to use the more resistive material.

### Tested overlay materials

In the repair practice many overlay alloys of different properties are used. It is possible to classify them into these classes:

1) Martensitic overlays: this class includes all overlays which can acquire the martensitic structure by hardening. The maximum hardness of the heat treated martensitic overlay depends above all on the carbon content. The hardening or the other heat treatment is exceptional, therefore for the classification the hardness reached by cooling by heat removal into the basic material, so called natural hardness, is decisive.

2) Austenitic overlays: they are very wear resistant after the strain hardening. These steels are very ductile, but they have relatively low hardness – about 200 HV. By hard strokes the surface formation hardens and the hardness increases till to 500 HV and is more wear resistant.

3) Ledeburitic overlays: in contrast to martensitic and austenitic overlays the overlay from the alloyed cast iron has the characteristic ledeburitic structure of very high abrasive wear resistance. Above all the hypereutectic cast irons, containing the long needles of free carbides in the basic more ductile eutectic, are very suitable for hard wear conditions caused by mineral abrasive. Partly the cheaper white cast irons are used, which differ only by the higher chromium content (2 to 5 %), partly the high alloyed cast irons, which contain 20 to 30 % of chromium.

4) Nonferrous materials on the cobalt and nickel basis: nonferrous materials on the cobalt basis are used with regard to their excellent properties to special purposes. Their merits are:

- high hardness till to about 700 ° C,
- maximum hardness can be reached without the heat treatment,
- high stability to chemical attack,
- high wear resistance.

5) Carbides: the tungsten carbides have the high hardness and the abrasive wear resistance by minerals. The overlay demands the ductile basement of the basic material to acquire besides the abrasive wear resistance the impact resistance, too.

Four overlay materials were chosen. The abrasive wear resistance of single layer was compared. The directive chemical composition of tested materials is presented in Tab. 1.

Use field:

ELEKTRODE 1 is the universal overlay material determined for the hardening of parts, which are exposed to the intense emery wear at low effort, e.g. conveyer screws, dipper teeth, sand pump mixers and for cover layers on the ductile weld metal or on the hard Mn steel.

ELEKTRODE 2 is determined for the hardening of parts, which are exposed to the intense mineral wear at increased temperatures to 500° C. The high wear resistance is reached thanks to Mo, V, W, Nb carbides. It is suitable for the use to tool hardening for the soil cultivation parts, parts in the building and stone industry as spiders and sintering grates.

ELEKTRODE 3 is determined for the universal hardening of parts from steels, alloy steels and Mn hard steels which are exposed to abrasion, pressure and impact. Preferred use field is the surfacing of parts for soil working, e.g. elevation dredger teeth, and parts for working of rock, e.g. breaker jaw, breaker cone, impact strip and hammer of the grinding mill bruiser, cutting edge and working surface of the cool work tool. Machining of the weld metal is possible only by grinding.

ELEKTRODE 4 is determined for the hardening of the parts which wear out at uniform impacts. The main use field is the surfacing of tools soil working machines and for rock breakers. Machining of the weld metal is possible only by grinding.

Tab. 1 Nominal chemical composition (%)

overlay material	C	Si	Cr	Mn	Mo	Nb	B	W	V	Ni
1	3,2	1,0	29	x	x	x	x	x	x	x
2	4,4	x	23,5	x	6,5	5,5	x	2,2	1,5	x
3	2,3	0,4	10	0,4	x	x	4	x	x	x
4	0,3	0,4	0,3	1,1	x	0,5	4,8	x	x	1,5

The test specimens of 25 x 25 x 17.5 mm size were made using the grinding apparatus for the metallographic samples preparation. The supply of a great quantity of the cooling liquid is its advantage. Then during the grinding any excessive heating does not occur. Using the above mentioned process 3 specimens were cut from each plate.

The etalons were made from the bar steel 12 014 of the square section of 25 x 25 mm. The hardness HV 30 of all specimens was measured using the hardness tester HPO 250. The measured results are presented in Fig. 2.

The relative wear value  $\psi_h$  [%] is calculated as a ratio of the mass lost of the test specimen to the mass lost of the reference specimen (etalon). The test results are presented in Fig. 2. As we do not know the density  $[\rho]$ , the relation presented in the standard ČSN 01 5084 was adapted and the relative wear value is calculated using the relation (1).

$$\psi_h = \frac{W_{hZ}}{W_{hPZ}} \cdot 100 \quad [\%] \quad (1)$$

Where  $W_{hZ}$  - mean mass of lost of the tested specimen [g]

$W_{hPZ}$  - mean mass of lost of reference specimen (etalon) [g]

The tests of the abrasive wear were carried out using the pin-on-disk machine with abrasive cloth according to ČSN 01 5084 (Fig. 1). The pin-on-disk machines with abrasive cloth are used most often. Their advantages are the simplicity and the reliability. The results variance is relative small. The disadvantage is the variable quality of the abrasive cloth, which must be continuous compensated by use of etalons. The machine consists of the uniform rotating disk whereon the abrasive cloth is fixed. The test specimen is fixed in the holder and pressed against the abrasive cloth by the weight of 2.35 kg. The screw makes possible the radial feed of the specimen. The limit switch stops the

test. During the test the specimen moves from the outer edge to the centre of the abrasive cloth and a part of the specimen surface comes in contact with the unused abrasive cloth.

The test machine according to the ČSN 01 5084 was accommodated. The holder is adapted for the specimens of 25 x 25 x 17.5 mm size.

The wear resistance tests were carried out as the comparison tests. The wear was determined by weighing. The test conditions, as load, speed, length of the path were equal. The specimens and etalons were tested alternately.

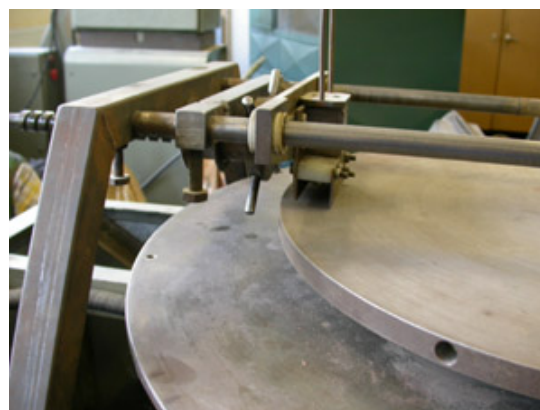


Fig. 1 The pin-on-disk machine for the wear resistance tests

## Results and discussion

The test results are presented in Fig. 2. The tested materials are arranged according to the increasing wear resistance under conditions of intensive abrasion by bonded particles. It is evident from the table of the chemical composition that the overlays marked 1 and 2 are high alloyed with chromium. The overlay material 2 does not contain Si, but it contains next alloying elements (Mo, Nb, W, V). All these elements create with C carbides. The overlay material 600 and 650 pertain to the class of lower chromium content. The overlay materials 3 and 4 alloyed with boride.

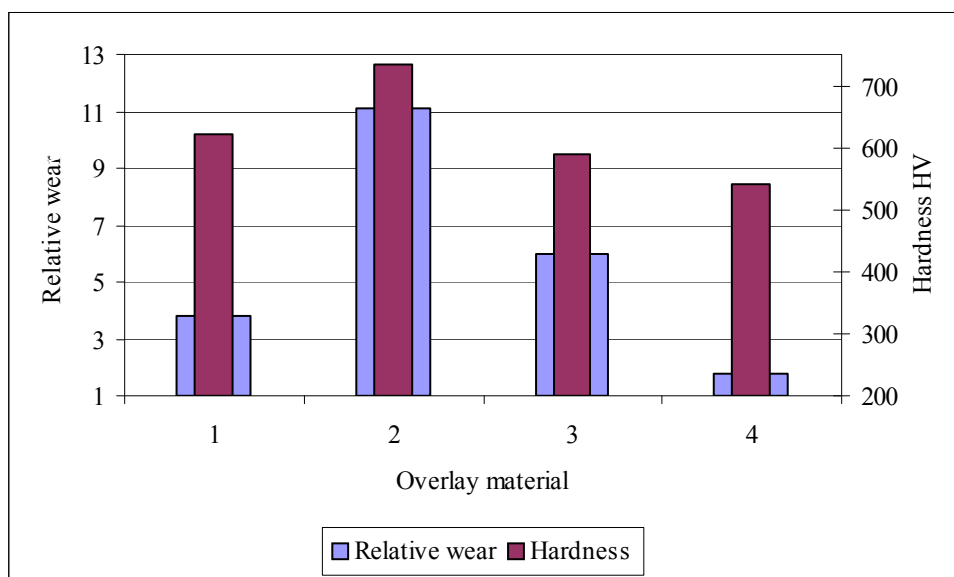


Fig. 2 The pin-on-disk machine for the wear resistance tests

## Conclusion

In the paper there are published the abrasive wear results of overlay materials. The wear resistance, using the pin-on-disk machine with abrasive sloth according to CSN 01 5084, was tested at single layer overlays.

It is evident from the table of the chemical composition that the overlays marked 60, 65, 1701, 1745, 1747 are high alloyed with chromium. Si alloying elements Mo, Nb, W, V, all these elements create with C carbides.

For every use the overlay material must be chosen according to the load mode. Commonly the hardest overlay material of high wear resistance (vide Fig. 2 – overlay material 2) is impossible to use when the impact, tensile and bend occur, because they are less failure resistant. The producer recommends this overlay material for the constructional parts hardening, when the intense emery wear at low load occurs and for the cover layer on the ductile weld material or Mn hard steel. Conversely the overlay material 1771 has got the lower wear resistance, but it can be used when impact occurs. Its matrix is more ductile and therefore the splitting does not occur. The producer recommends this overlay material for the constructional parts hardening where the wear and even impact occurs. Always we must look for the optimum choice with regard to wear resistance x toughness.

When solving a definite problem it is necessary to take into consideration the technical and economical problems. It means that the problem must be realizable with low costs of the whole surfacing process

## References

- [1] Brožek, M.: Posouzení odolnosti proti abrazivnímu opotřebení elektrod firmy INTERWELD, ČZU, Praha, 2001,
- [2] Budinski, K. G.: Surface Engineering for Wear Resistance, Prentice-Hall, Inc., New York, NY, 1988
- [3] Dogan ON, Hawk JA.: Effect of carbide orientation on abrasion of high Cr white cast iron, *Wear*, 1995, vol. 189, p. 136-142
- [4] Eroglu M., Ozdemir N.: Tungsten-inert gas surface alloying of a low-carbon steel, *Surf Coat Technol*, 2002, vol. 154, p. 209-217
- [5] Fernández, J. E., et al.: Abrasive wear analysis using factorial experiment design, *Wear*, 2003, vol. 255, s. 38-43
- [6] Sahin, Y.: Optimization of testing parameters on the wear behaviour of metal matrix composites based on the Taguchi method, *Materials Science and Engineering A*, 2005, vol. 408, s. 1-8
- [7] Vnouček, M., 2001. Surfaře effects by use of GDOES: disertační práce. ZČU, Plzeň.

## WATER INFILTRATION INTO SOIL AND SURFACE WATER RUNOFF IN MAIZE GROWING BY THREE CULTIVATION TECHNOLOGIES

JOSEF HULA<sup>1\*</sup>, PAVEL KOVARICEK<sup>2</sup>

<sup>1</sup>Czech University of Life Sciences Prague, 16521 Prague 6 – Suchbát, Czech Republic

Phone: +420 224383123, E-mail: hula@tf.czu.cz

<sup>2</sup>Research Institute of Agricultural Engineering, Prague, Czech Republic

### Abstract

A pilot field trial was conducted on light soil to evaluate the influence of three soil cultivation technologies and silage maize sowing on surface water runoff and soil washout under sprinkling with a rainfall simulator. The highest contribution to soil protection against erosion was observed in the treatment of maize sowing onto freezing catch crop without spring seedbed preparation. Lowered water infiltration into soil and increased soil washout during surface water runoff were found out in conventional technology – treatment with ploughing, without catch crop, with spring seedbed preparation for maize. The results of the field trial confirm the contribution of soil-conservation technologies of soil cultivation to a reduction in the hazard of water erosion of soil.

**Keywords:** soil erosion; soil-conservation measures; freezing catch crops

### Introduction

The harmfulness of water erosion for agricultural land is sufficiently known – it is an irreparable impairment of production and non-production functions of soil but damage is also incurred outside agricultural lands (urban areas, water resources, silting of water reservoirs). Of course, soils were also vulnerable to torrential, erosive rains in the past. Currently, there arise new combinations of risky factors – the concentration of crops insufficiently protecting the soil from erosion on large areas (it mainly applies to maize in the Czech Republic) and the use of conventional soil cultivation and sowing technologies, especially on light soils, are such examples.

The importance of leaving plant residues of a forecrop or catch crop biomass on the soil surface in order to increase the soil protection against water erosion was documented by Truman, Shav and Reeves (2005). These authors reported that the removal of plant residues from the soil surface led to an increase in surface water runoff by 18 to 25%, and the soil washout by water increased 1.5 to 7 times. Roth et al. (1988) documented that leaving all post-harvest residues on the soil surface allowed water infiltration at a rainfall amount up to 60 mm while conventional soil cultivation allowed the infiltration of only 20% of the same rainfall amount after a longer time since cultivation.

### Experimental arrangement

The influence of three soil cultivation technologies on soil resistance to water erosion was compared in a pilot field trial on the loam-sandy soil of small topsoil thickness in conditions of an increased risk of water erosion for arable land due to soil texture. A part of the plot where a pilot field trial was laid out is situated at an altitude of 450 m a.s.l.

After the application of nonselective herbicide Roundup Rapid to a perennial fodder crop (lucerne) in 2007 skimming and ploughing were carried out in the field after a lapse of time with a seven-furrow reversible hillside plough Kverneland PB 100. Considering the topsoil depth, the ploughing depth was 0.18 m. Following the seedbed preparation for catch crop – white mustard – was sown at the beginning of September 2007 (treatments B and C).

Glyphosate (Roundup Rapid) was applied to white mustard (treatments B and C) in spring 2008, two weeks before maize sowing. Two weeks after killing the catch crop maize was sown with a KINZE seed drill (8 rows) attached to a CASE 7220 tractor. After maize sowing the herbicides Guardian Safe Max and Click were applied to the field, along with the liquid fertilizer DAM at a rate 200 l.ha<sup>-1</sup>.

Treatments of a pilot field trial in 2008:

A - conventional technology: coarse furrow was left over winter, drag and harrows (working width 8 m, CASE 7220 tractor) were used in



spring, Kompaktomat field cultivator (Farmet, working width 6 m, CASE 7220 tractor) was used for seedbed preparation for maize, and maize was sown with Kverneland Optima seed drill (6 rows, Z-114 41 tractor),

- B - maize was sown onto a part of the field with the killed catch crop (white mustard) where spring soil cultivation with AMAZONE Catros 3501 disk cultivator with a roller was performed,
- C - maize was sown after killing the catch crop (white mustard) with glyphosate, without spring seedbed preparation.

Sprinkling was used to evaluate water infiltration into soil, surface water runoff and soil washout – a rainfall simulator was employed (Kovaricek et al. 2008) – fig. 1. To evaluate physical properties of soil standard methods based on the collection and subsequent laboratory analysis of undisturbed soil samples were applied (Valla, Kozak et al. 2000).

### Results and discussion

Tab. 1 shows the average values of soil surface coverage by dead biomass of white mustard at the time of measuring water infiltration into soil and surface water runoff during sprinkling. Even though the amount of dead plant residues on the soil surface is not large, based on previous experience

this biomass can be assumed to reduce the surface runoff of precipitation water and to diminish the soil washout in a sloping field. Figures 2, and 3 show the parameters illustrating surface water runoff and soil washout.



Fig. 1: Rainfall simulator

Tab. 1: Coverage of the soil surface by dead biomass (12.6.2008) and slope of parts of the field

Treatment	Coverage of soil surface [%]	Slope [°]
A - conventional technology – sowing after spring seedbed preparation, without catch crop	1.3	5.8
B - sowing after spring seedbed preparation, catch crop	2.6	5.8
C - sowing without spring seedbed preparation, catch crop	10.9	5.2

Fig. 2 represents the surface water runoff rate during sprinkling on 12<sup>th</sup> June 2008. The graph documents the latest beginning of surface water runoff in treatment C – maize sowing without spring seedbed preparation while dead

aboveground parts of white mustard plants are present on the soil surface. No greater difference in this parameter was observed between the other two treatments.



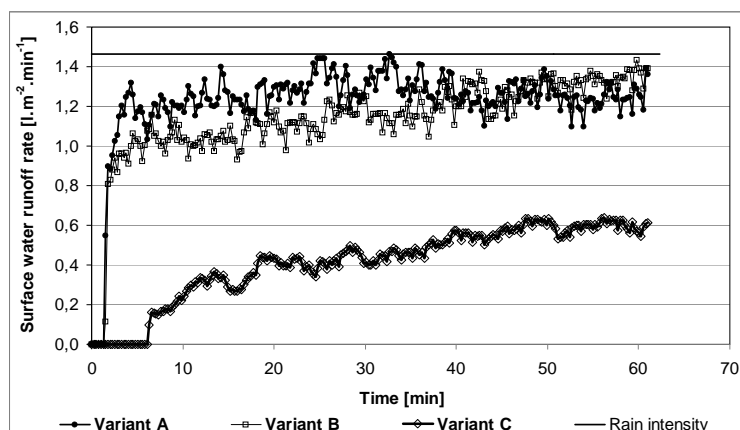


Fig. 2: The surface water runoff rate  
A, B, C – experimental treatments

Infiltration rate ( $\text{l.m}^{-2}.\text{min}^{-1}$ ) is related to the surface water runoff. The highest infiltration rate was recorded in treatment C.

Fig. 3 documents the soil washout by surface water runoff. The graph shows the percentage proportion of soil in water running off on the soil

surface. The highest values, many times exceeding the values in the other two treatments, were measured in treatment A – conventional technology with ploughing, sowing after spring seedbed preparation, without catch crop.

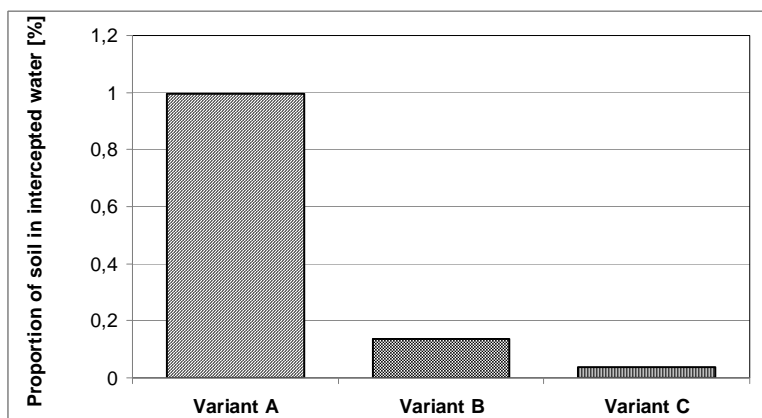


Fig. 3: The proportion of soil in intercepted water (in surface water runoff)  
A, B, C – experimental treatments

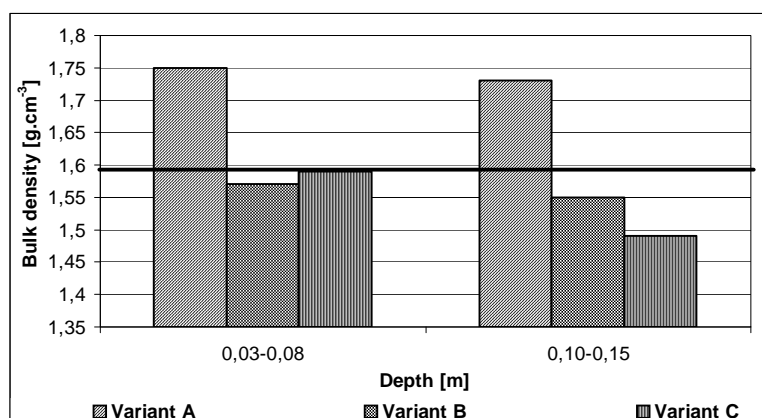


Fig. 4: Bulk density of soil in topsoil at the time of measurement

As to the physical properties of soil at the time of measurement, bulk density is shown (Fig. 4). The red line in the graph designates the limit value of reduced bulk density for loam-sandy soil while the values exceeding this limit indicate undesirable soil compaction. The figure documents that the limit value of reduced bulk density in topsoil was exceeded in June in treatment A (without catch crop, spring seedbed preparation). It can be deduced that the soil condition at this site can easily become adverse with regard to its physical properties. In conditions of a pilot field trial the use of a freezing catch crop appeared to contribute to the preservation of favourable physical properties of soil – which is closely related with the above-mentioned water infiltration into soil and with surface water runoff (high bulk density of topsoil – low porosity – decreased water infiltration into soil).

The above results obtained at a site with light soil demonstrate the importance of soil-conservation technology – in this case the technology based on maize sowing into freezing catch crop. When measuring water infiltration into soil, surface water runoff and soil washout the omission of shallow soil cultivation in spring in connection with the presence of catch crop dead biomass on the soil surface appeared to be a positive factor that contributed to a reduction in the intensity of erosion process under controlled sprinkling of the soil surface.

A comparison of the above-mentioned results with results obtained in previous years at a site with heavy-textured clay-loamy soil shows a marked difference. The results confirm a high vulnerability of light soils to water erosion, particularly when maize is included in crop rotations in these fields. Heavy-textured soils, even on steeper slopes, are considerably less vulnerable to soil erosion. These results are consistent with the findings of authors who studied the influence of different soil cultivation technologies in maize growing on water infiltration and soil loss (Bradford and Chi-Hua 1994). The importance of plant residue utilization to increase the erosion resistance of soil has been confirmed (Truman, Shaw and Reeves 2005). The above results document that

there may be marked differences in soil resistance to water erosion even though technologies with ploughing are used – it may be maize sowing onto dead catch crop, without spring seedbed preparation.

## Conclusion

The results presented in this paper confirm the efficiency of erosion-control technologies, especially in conditions of potential high vulnerability of soils (light soils, high representation of maize in crop rotations). It is advisable to combine several methods aimed at soil protection from erosion so that the required erosion-control efficiency will be ensured. They include first of all soil-conservation technologies (e.g. maize sowing into freezing catch crops while the timely sowing of a catch crop is important so that sufficient biomass will be produced), application of at least a minimum of the strip cropping principle - in this aspect maize is compatible with winter cereals and winter oilseed rape very well.

*This paper was supported by research project of Ministry of Agriculture: QH92105 and QH82191.*

## References

- Bradford, J.M. - Chi-Hua, H.: Interrill soil erosion as affected by tillage and residue cover. *Soil Tillage Res.* 31, 1994, p. 353-361.
- Kovaricek, P. - Sindelar, R. - Hula, J. - Honzik, I.: Measurement of water infiltration in soil using the rain simulation method. *Research in Agricultural Engineering.* 54, 2008, p. 123-129.
- Roth, C.H. - Meyer, B. - Frede, H.G. - Derpsch, R.: Effect of mulch rates and tillage systems on infiltrability and other soil physical properties of an Oxisol in Parana, Brazil. *Soil and Tillage Research*, 11, 1988, p. 81-91.
- Truman, C.C. - Shaw, J.N. - Reeves, D.W.: Tillage effects on rainfall partitioning and sediment yield from an ultisol in central Alabama. *Journal of Soil and Water conservation*, 60, 2005, p. 89-98.
- Valla, M. - Kozak, J. et al.: *Pedologicke praktikum.* Praha, ČZU, 2000, 148 p.

## POSSIBILITIES OF THE VERIFICATION OF THE EFFICIENCY OF SANITATION PROCESS IN AGRICULTURAL AND FOOD INDUSTRY

LADISLAV CHLÁDEK<sup>1\*</sup>, MIROSLAV PŘIKRYL<sup>1</sup>, PETR VACULÍK<sup>1</sup>, JAN MALAŤÁK<sup>1</sup>,  
ONDŘEJ SUCHÝ<sup>1</sup>

Czech University of Life Sciences in Prague, 16521 Prague 6 – Suchbát, Czech Republic,  
Phone: +42022357, Fax: +4202-20921361, E-mail: Chladekl@tf.czu.cz

### Abstract

Sanitation process in the in the agriculture and food industry is a very important activity term for hygienic disposal or recycling of waste materials. There are three main types of food contaminant: microbiological, biological, chemical and physical or radioactive (Lelieveld, H.L. at all 2005). There are some reliable methods used for quick test of efficiency of sanitation process, e.g. colony counting in microscope, flow cytometry, measurement of haze, change of pH value, change of conductivity value, gas chromatography, application of enzymes for determination of metabolites of microorganisms, measurement of activity of esterase, etc (Chladek, L. 2010). In the laboratory of Faculty of Engineering of Czech University of Life Sciences in Prague equipped with tutorial brewery and three vessels sanitation station (hot caustic soda tank heated by steam, acid tank, hot water tank,, was recently introduced a new apparatus Hy Lite 2 (developed by German company Merck) using a principles of measurement of detecting ATP (adenosine triphosphate), a substance found in all living cells and in most biological material. Unlike traditional microbiological methods, which detect the presence of bacteria and other micro-organisms, ATP detection also reveals the presence of residues, even on superficially sterilized surfaces, potentially capable of supporting microbial contamination. A sample taken from the test area is mixed with enzyme reagent in the specially developed HY-LiTE pen, used for swabbing of cleaned area. Any ATP present reacts with the enzymes and produces light. Hy Lite 2 is a pre-prepared, one-shot device delivered in two formats – for surface testing – and for rinse water control, both formats have been used for experimental activities. The principle of measurement is a quite simple, the more ATP present, the brighter the light and the higher measured value, shown on the display are registered by PC. The measured values of ATP are in close relationship to the amount of microbiological contamination, food residue or animal debris in a crevice, on a surface, or in a rinse water sample. The measured results obtained by apparatus Hy Lite 2 were compared with the results gained from other tests and results discussed.

**Key words:** sanitation, agriculture and food industry, contamination, Adenosine triphosphate,

### 1. Introduction

Sanitation process in the in the agriculture and food industry is a very important activity term for hygienic disposal or recycling of waste materials. For food production is very important to know the result of sanitation, carried out on food plant. The topic of this paper is compare two different ways of evaluation of the efficiency of sanitation process in agricultural and food industry using HY LITE 2 and traditional microbiologic way of colony counting.

### 2. Materials and methods

For the test of verification of the efficiency of sanitation process have been used both microscopic tests (these have been done in very well equipped microscopic laboratory of an

industrial brewery outside of Prague) and HY-Lite<sup>®</sup> 2 (chapter 2.4.2), further has been used following equipments of the tutorial and research brewery of the Czech university of life sciences in Prague:

2.1 Vessels and pipe – line. For the test have been used insulated fermentation and lager tanks made from stainless steel, volume 2 000 liters, equipped with temperature control, cleaning head, man whole, cooling jacket for glycol circulation and pipe-line for wort, yang beer, beer and CIP agents circulation DN 32.

#### 2.2 CIP Station

CIP station of the tutorial brewery (picture 1) consists of stainless steel 3 vessels, first insulated vessel heated by steam for hot alkaline or acid

agents (e.g. 2% NaOH at 85°C or hot acid) volume 300 liters, second vessel without heating for disinfection agents (e.g. PerSteril), volume 300 liters, third insulated vessel with steam heating for hot water, volume 2 000 liters The lay-out of the CIP station is shown in Fig. 2.

### 2.3 CIP pumps.

Force two-stage pump type CDXM 120/20 EBARA (manufactured by Ebara Italy) with frequency control was used with a flow range 2,9 – 8,7 m<sup>3</sup>.h<sup>-1</sup> which approximately corresponds to the flow velocity in the range of  $c = 1 - 3 \text{ m.s}^{-1}$ , at the pressure of 0.125 - 0.205 MPa, for cleaning agent circulation via cleaning heads and back-pump for clean agent transport from cleaning vessel back to CIP station, the pipeline circuit DN 32 (0,032 m),



Fig. 1 CIP station

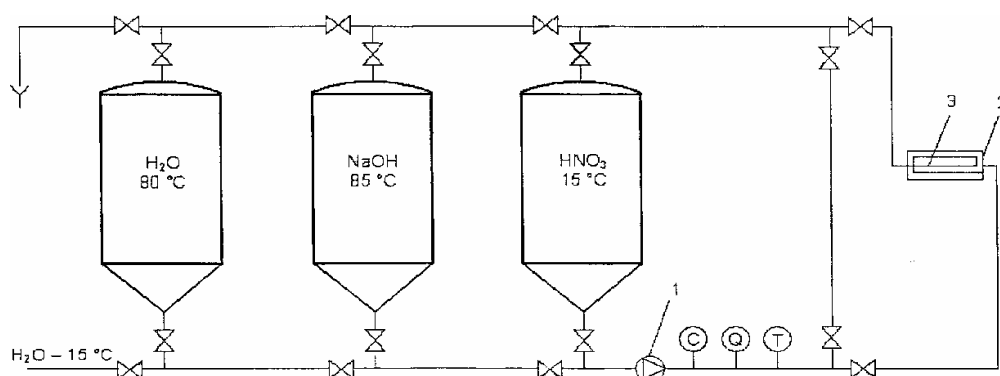


Fig. 2 Lay out of CIP station



Fig. 3 Conductivity probe LMIT 08 and flow meter Optiflux 6 300 (left to right)

## 2.4 Used measurement equipment:

### 2.4.1 Conductivity probe LMIT 08 Transmitter.

Transmitter for electrodeless conductivity and temperature measurement (LMIT 08, made by Lang Apparatenbau ECOLAB, Germany) measuring ranges: 5 conductivity measuring ranges: 0-200  $\mu\text{S}/\text{cm}$  to 0-2  $\text{S}/\text{cm}$ . The transmitter was installed in CIP force pipe line (Fig. 3).

### 2.4.2 Electromagnetic flow meter Optiflux 6300.

Optiflux 6300 DN 40 electromagnetic flowmeter (Krohne Messtechnik GmbH, Hamburg, Germany): separate flow sensor, process standard flange DN 40, ASME B.16.5, flow measurement range  $c_{\min} = 0 - 5,3 \text{ m}\cdot\text{s}^{-1}$ , accuracy  $\pm 0.1\%$ , operating pressure 0-1.6 MPa (0 - 232 psig), operating temperature  $-25^{\circ}\text{C} - 120^{\circ}\text{C}$  (Fig. 3).

### 2.4.3 Luminometer HY Lite 2.

Luminometer Hy Lite 2 (Merck, Germany), accessories for testing surface or in liquid:

The HY –Lite 2 Pen, ready prepared test cuvette designed for use

- “white” stick for accurate sampling of the liquid to be tested, filled by an extractant, which releases ATP from cellular material. The stick also transfers the sample into the cuvette and in later step opens the reagent chamber,
- a cuvette filled with test buffer for dilution, buffering and neutralization of the samples,
- a reagent chamber sealed with aluminium foil, containing freeze – dried and stabilized Luciferin/luciferase reagent.



Fig. 4 Luminometer HY- Lite 2 Merck Germany

## 2.5 Process of cleaning using CIP station:

Process of cleaning of vessels and of pipe – line using CIP station was following:

- rinsing by water for 5 minutes,
- cleaning by hot cleaning agent (2,5% NaOH at temperature  $85^{\circ}\text{C}$ ) for 20 minutes,
- rinsing by hot water for at least 5 minutes till pH reached the desired value,
- circulation by disinfection agent for 10 minutes,
- final rinsing with a tap water for 5 minutes.

## 2.6 Parts of tutorial brewery used for test to be sanitized by CIP station and foam cleaning:

In the tables 1,2,3,4 are shown both results, obtained both from ATP measurement device Hy-Lite 2 and from classical microscopic colony counting in a laboratory of an industrial brewery, the test have been taken from three different places before and after cleaning of internal surfaces of vessels or pipe – line. In the table 5 (Fig. 5, 6) are results form external surface of fermentation tank, cleaned by foam sanitation. The evaluation of these comparisons is in chapter 3.

- 2.6.1 hot wort pipe – line connecting brewhouse with a whirlpool (Table 1)
- 2.6.2 Internal surface of whirlpool (Table 2)
- 2.6.3 Cold wort pipe – line connecting heat exchanger with fermentation tank (Table 3)
- 2.6.4 External surface of fermentation tank before and after cleaning (Fig.5 + 6, Table 4)
- 2.6.5 Internal surface of fermentation tank (Table 5)



Fig. 5 External surface of fermentation tank before cleaning





Fig. 6 External surface of fermentation tank after cleaning

Table No. 1 hot wort pipe – line connecting brew house with a whirlpool tank before and after cleaning

Swab No.	Description	Microscopic tests - colony counting ( 1 )	Hy Lite 2 (RLU)
1	Before cleaning	126	82
2	Before clearing	135	71
3	Before cleaning	144	63
4	After Clearing	0	0
5	After Cleaning	0	0
6	After Cleaning	0	0

Table No. 2 Internal surface of whirlpool tank before and after cleaning

Swab No.	Description	Microscopic tests - colony counting ( 1 )	Hy Lite 2 (RLU)
1	Before cleaning	220	120
2	Before clearing	225	132
3	Before cleaning	222	125
4	After Clearing	0	0
5	After Cleaning	0	0
6	After Cleaning	0	0

Table No. 3 Cold wort pipe – line connecting heat exchanger with fermentation tank before and after cleaning

Swab No.	Description	Microscopic tests - colony counting ( 1 )	Hy Lite 2 (RLU)
1	Before cleaning	218	105
2	Before clearing	220	102
3	Before cleaning	221	103
4	After Clearing	0	0
5	After Cleaning	0	0
6	After Cleaning	0	0

Table No. 4 Internal surface of fermentation tank before and after cleaning

Swab No.	Description	Microscopic tests - colony counting ( 1 )	Hy Lite 2 (RLU)
1	Before cleaning	235	145
2	Before clearing	225	132
3	Before cleaning	222	125
4	After Clearing	0	0
5	After Cleaning	0	0
6	After Cleaning	0	0



Table No. 5 External surface of fermentation tank before and after cleaning

Swab No.	Description	Microscopic tests - colony counting (1)	Hy Lite 2 (RLU)
1	Before cleaning	25	145
2	Before clearing	23	132
3	Before cleaning	22	125
4	After Clearing	0	1
5	After Cleaning	0	0
6	After Cleaning	0	1

### 3. RESULTS AND DISCUSSION

All results, obtained from HY – LITE 2 apparatus are in good oneness with these from microscopic laboratory of an industrial brewery. The big advantage is a very short time for realisation all test taking a few minutes only to compare with several days necessary to get results from microscopic laboratory.

### ACKNOWLEDGEMENT

This paper was processed within the frameworks of the grant MŠM “Innovation of instrumkent equipment” Nr. 99800/1181/1802 and grant IGA TF “Optimation of sanitation in agricultural and food industry”, Nr. 31170/1312/3133.

### REFERENCES:

1. LELIEVELD,H.L.- Mostert,M.A. – Holah,J.: *Handbook of hygiene control in the food industry*, 2005, CRC Press Boca Raton Boston New York Washington DC, pp. 13-14)
2. CHLÁDEK,L.: *Pivovarnictví*, Grada, 2007, pp. 125-162, ISBN: 978-80-247-1616-9,
3. BASAŘOVÁ,G.- Šavel,J. – Basař, P. – Lejsek,T.: *Pivovarství*, Praha VŠCHT, 2010. p. 743 – 749, ISBN 978-80-7080-734-7,
4. CHLÁDEK,L. at all: „*Možnosti rychlého stanovení účinnosti provedeného sanitačního procesu v agropotravinářském komplexu*“, Sborník přednášek z Mezinárodní vědecké konference „Technika v agropotravinářském a odpadovém hospodářství, Praha 2010, ISBN 978-80-213-2079-6.
5. Manual for HY – LITE 2 Apparatus, MERCK Germany 2010.

## THE RESISTANCE OF BENEFICIAL NEMATODES TO LIQUID STATIC PRESSURE

JERZY CHOJNACKI

Koszalin University of Technology, 15-17 Raclawicka Str., 75-620 Koszalin, Poland  
Phone: +48602578142, Fax: +48943426753, E-mail: jerzy.chojnacki@tu.koszalin.pl

### Abstract

The Nematodes of the species of *Heterorhabditis bacteriophora*, *Heterorhabditis megidis*, *Pharmarhabditis hermaphrodita*, used as natural factors in the protection of plants, were subjected to the pressure of 50 MPa. The duration of pressure was 30 minutes. It was not noted that that pressure caused death of the nematodes.

### Introduction

Beneficial nematodes are used as means of combating plant vermin in organic agriculture [1]. The most frequent use of nematode application is spraying them mixed with water by the means of sprayers. During the application, the nematodes are pumped through a hydraulic installation of the sprayers, where they can be destroyed [2],[3]. The cause of nematode destruction can be liquid static and dynamic pressures inside the installation [4]. Static pressure of liquid in the sprayers is the result of liquid pushing on the walls of the sprayer. During the spraying of nematodes, pressure can reach up to 2000 kPa (Szapiro- Ilan 2006). The dynamic pressure is associated with kinetic energy in the flowing liquid. It's value depends on the speed of liquid passing through individual elements of the sprayer.

In order to avoid the damage to the nematodes generated in the sprayers, one has to find causes of its prevalence.

### Purpose

The goal of the carried out experiments, was to determine whether the static pressure in the installation of the sprayers can cause destruction of beneficial nematodes during the spraying process.

### Materials and Methods

The materials used in the experiments were biological agents of plant protection: B-green, *Heterorhabditis* System and *Phasmarhabditis* System, manufactured by Biobest b.v. Biopesticide B-green contains nematodes *Heterorhabditis bacteriophora*, used in the destruction of white grubs in the soil. Active ingredients of *Heterorhabditis* System are insect

parasitic nematodes *Heterorhabditis megidis*, which seek out and destroy vine weevil larvae in compost. *Phasmarhabditis* System is based on a selected strain of the mollusc parasitizing nematode *Pharmarhabditis hermaphrodita*, which searches the soil for slugs in order to subsequently destroy them. Before the commencing of the experiment, individual species of nematodes were mixed with water. Concentration of nematodes *Heterorhabditis bacteriophora* was 5000 elements in 1 ml of liquid, *Heterorhabditis megidis* – 4000 and *Pharmarhabditis hermaphrodita* 2000.

It has been concluded that the assessment of influence of static pressure in the sprayer on the nematodes is very difficult, because only a small amount of nematodes can undergo destruction. Too minor a number of damaged nematodes may be nearly impossible to count by traditional methods due to their inaccuracies. Such a method is, for example, counting of life and dead nematodes by an observer in samples of liquid taken from a sprayer. Additionally, in the sprayer there exist both static and dynamic pressures. Therefore, one had to design this testing equipment in order to eliminate the influence of dynamic pressure on nematodes and obtain a warning of possible nematode destruction. For this purpose, it was assumed that the influence of static pressure on the damage of nematodes has a linear correlation, and hence it was decided to multiply the static pressure in the testing equipment, as compared to the pressure in the sprayer.

The value of experimental static pressure was set to 50 MPa, while time of operation was 30 minutes.

The testing equipment, prepared for experiments, is shown on fig. 1. It consisted of a

pump, which was powered by an electrical motor, and generated high water pressures. The pressure was controlled by a pressure valve and its values were displayed on a manometer. Additionally, it was possible to compare them on a computer monitor, since there was an electronic pressure sensor built in as well.

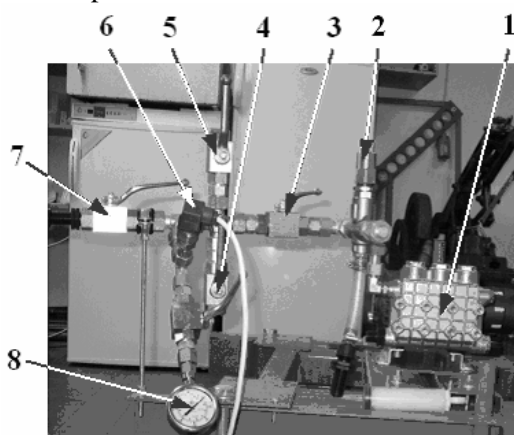


Fig. 1. View of experiment device: 1 – high pressure pump, 2 – pressure control valve, 3 – cut-off valve, 4 – lower ball valve, 5 – upper ball valve, 6 – pressure sensor, 7 – drain valve, 8 – manometer.

Samples with nematodes were introduced into the installation through the opening in the upper ball valve, while it stayed open, and were removed through the lower ball valve, also after opening it. After the placement of a sample in the installation and filling out free space with water, the upper valve was closed. Then the cut-off valve was opened to allow the pumped water to reach the sample and raise its pressure.

To prevent the damage to the nematodes due to other than static pressure factors, the testing equipment was constructed in such a way not to allow any contact between nematodes and any of its moving elements, which could possibly carry away the nematodes with the stream of moving liquid. 2,5 ml samples with nematodes consisted of pipes and removable corks. This prevented any damage to the nematodes during the filling out and emptying of samplers. A sampler was placed on the bottom of the conduit with valves. Its height was small enough to be placed below the crossing of the pipes feeding the installation with the liquid (Fig.2).

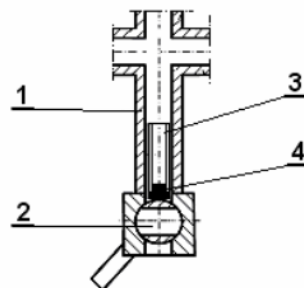


Fig. 2 . Probe placement scheme: 1 – pipe of device, 2 – lower ball valve, 3 – probe pipe, 4 – probe plug

The influence of liquid pressure on survivability of nematodes was assessed through their changes of relative nematode viability. The relative nematode viability was counted through the following formula:

$$V_r = \frac{N_l}{N_t} 100 \quad (1)$$

Where:

$N_l$  - number of living nematodes,

$N_t$  - number of total nematodes

The relative nematode viability was determined from liquid samples with nematodes taken before subjecting them to pressure and afterwards. The samples taken before experiment and after, were left in the thermostatic box (at 18 deg. C for 24 hours) . It was assumed that during that time, those nematodes which sustained damage from pressure would die. The experiment was repeated twice for each species of nematodes. In each experiment, six samples of liquid 0,050 ml were taken to asses viability. The assessment was made by observations of samples under a microscope and counting live and dead nematodes in each one.

## Results

Fig. 3 shows mean values of relative nematode viability for individual species of nematodes. Additionally, standard deviation was assessed based on the results.

For all species of nematodes, the differences between mean relative viability for pressures of 0 Mpa (nematodes not subjected to any pressures) and pressures of 50 MPa, are within the value of standard deviation. That means that the pressure of liquid of 50 MPa for 30 minutes, did not cause nematodes any damage.

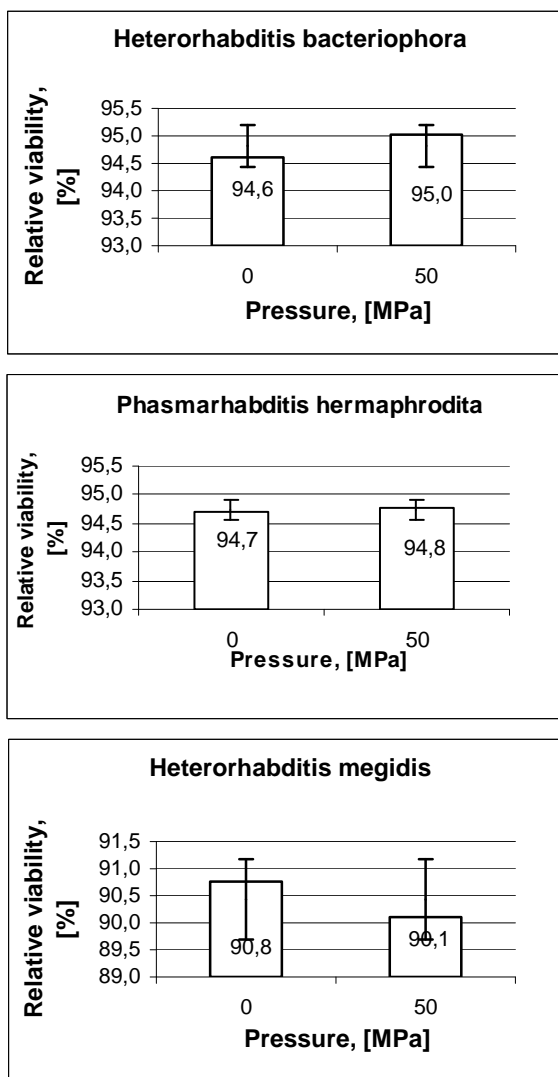


Fig. 3. Mean values of nematode relative viability before and after treatment

### Conclusion

The static pressure of liquid, which exists within the installation of industrial sprayers, should not

cause any damage to the beneficial nematodes, sprayed by the means of such devices.

### References

- [1] Grewal P.S., Ehlers R.U., Shapiro-Ilan D.I.: 2005. Nematodes as Biocontrol Agents. CAB International. ISBN 0851990177
- [2] Chojnacki J.: Using sprayers to the application of plant protective biological agents. Warsaw University of Technology. Bioagrotechnical Systems Engineering. Vol 1 – 2 (17-18) 2008, p. 9-11.
- [3] Nilsson U., Gripwall E.: Influence of Application Technique on the Viability of the Biological Control Agents *Verticillium lecanii* and *Steinernema feltiae*. Crop Protection 18(1), 1999, p. 53-59.
- [4] Fife J. P., Derksen R. C., Ozkan H. E., Grewal P. S.: Effects of pressure differentials on the viability and infectivity of entomopathogenic nematodes Biological Control 27. 2003, p. 65–72.
- [5] Shapiro-Ilan D. I. , Gouge D. H., Piggott S. J., Fife J. P.: Biological Application technology and environmental considerations for use of entomopathogenic nematodes in biological control . Biological Control 38, 2006, p. 124–133.

## EFFECTS OF WELDING PROCESS PARAMETERS ON THE GEOMETRY AND DILUTION OF THE BEAD IN THE AUTOMATIC SURFACING

ROSTISLAV CHOTĚBORSKÝ, ABDUL HAMID RUSUL, MONIKA NAVRÁTILOVÁ,  
PETR HRABĚ

<sup>1</sup>Czech University of Life Sciences Prague, 16521 Prague 6 – Suchbát, Czech Republic,  
Phone: +420224383274, Fax: +4202-20921361, E-mail: choteborsky@tf.czu.cz

### Abstract

Automatic weld surfacing is being employed increasingly in the process, mining and power industries. GMAW has become a natural choice for automatic surfacing due to its important properties. These include: high reliability, all positions capabilities, ease of use, low cost and high productivity. With increasing use of GMAW in its automatic mode, the use of mathematical models to predict the dimensions of the weld bead has become necessary. The development of such mathematical equations using a four factor central factorial technique to predict the geometry of the weld bead in the deposition of SK45-O electrode onto structural steel S235JR is discussed. The models developed have been checked for their adequacy and significance by using the *F* test and the *t* test, respectively.

### Introduction

Gas metal arc welding (GMAW) is one of the processes of manufacturing and repair that has been increasingly used in industrial assembly lines. This is due to its versatility and the levels of productivity that it offers. When, however, the process is automated there are certain difficulties associated with the use of the correct parameters and their values. This is due to the set of variables involved and their control. There are also the ever-present errors that are inherent to the equipment and methods that are used. These exist even in the case of robotic systems.

With the increase of mechanization and robotic applications, it is essential to have a high degree of precision in predicting weld bead shape and dimensions. Also, successful surfacing requires an optimization of the process parameters to secure low dilution and a crack-free overlay. This needs a thorough understanding of the process characteristics affecting the technological and metallurgical characteristics of the overlays. Thus, it is essential to develop mathematical models to predict not only the weld bead dimensions but also the effects of various process parameters influencing dilution. With a view to achieving the above-mentioned aim, statistically designed experiments based on the factorial technique were used to reduce the cost and time, as well as to obtain the required information about the main and the interaction effects on the response parameters. Automatic submerged arc surfacing

was carried out by depositing SK45-O onto structural steel S235JR plate of 20 mm thickness and the observed data was used to develop the mathematical model. The controllable process parameters were retained in an optimum region for achieving the acceptable quality. The quality of the surfaced layer depends upon the weld dimensions, especially on the dilution. The experiments were based on a central composite design matrix of five level full factorial technique. Regression analysis was used to develop the models and the variance method was used to test their adequacy.

The research work was planned to be carried out in the following steps:

- 1) identifying the important process control variables;
- 2) finding the upper and lower limits of the control variables, viz., open circuit voltage (V), wire feed-rate (F), welding speed (S) and nozzle to – plate distance (N);
- 3) developing the design matrix;
- 4) conducting the experiments as per the design matrix;
- 5) recording the responses, as penetration (P), weld width (W), reinforcement (R), and dilution (D);
- 6) development of mathematical models;
- 7) calculating the coefficients of the polynomials;
- 8) checking the adequacy of the models developed.



**Tab. 1** Control parameters and their levels

Parameter	Units	Notation	Factor levels				
			-2	-1	0	1	2
Open-circuit voltage	volt	U	24	26	28	30	32
Arc current	Ampere	I	140	180	220	260	300
Welding speed	cm.min <sup>-1</sup>	S	20	30	40	50	60
Nozzle-to-plate distance	mm	N	12	16	20	24	28

The independently controllable process parameters were identified to enable the carrying out of the experimented work and the development of the mathematical models: they were open-circuit voltage (V), wire feed-rate (F), welding speed (S), and nozzle-to-plate distance (N).

The selected design matrix is a central composite rotatable factorial design consisting of 31 sets of coded conditions. It comprises a full replication of 24 (= 16) factorial design plus 7 centre points and 8 star points. All welding variables at the intermediate (0) level constitute the centre points and the combinations of each of the welding variables at either its lowest (-2) or highest (+ 2) with the other three variables of the intermediate levels constitute the star points. Thus the 31 experimental runs allowed the estimation of the linear, quadratic and two-way interactive effects of the welding variables on the bead geometry.

The experiments were conducted as per the design matrix at random, to avoid systematic errors infiltrating the system. SK45-O wire of 1.6 mm diameter and was used to deposit onto structural steel plate S235JR of 20 mm thickness. Keeping the positive polarity, four beads each of 150 mm length.

The surfaced plates were cross-sectioned at their mid-points to obtain test. These specimens were prepared by the usual metallurgical polishing methods and etched with 2% nital. The weld-bead profiles were traced using picture analysis software and width, penetration, and reinforcement, were measured.

The response function representing any of the weld bead dimensions was expressed as  $Z = f(U, I, S)$  and the relationship selected, representing a second-degree response (1) was also expressed as follows:

$$Y = b_0 + b_1 \cdot U + b_2 \cdot I + b_3 \cdot S + b_{11} \cdot U^2 + b_{22} \cdot I^2 + b_{33} \cdot S^2 + b_{12} \cdot U \cdot I + b_{13} \cdot U \cdot S + b_{23} \cdot I \cdot S \quad (1)$$

The values of the coefficients were calculated by regression with the help of STATISTICA software. A computer programme was also used developed to calculate the value of these coefficients for different responses.

#### Checking the adequacy of the models developed

The adequacies of the models were tested using the analysis of variance technique. According to this technique, if the calculated value of the  $F$  ratio of the model developed does not exceed the standard tabulated value of  $F$  ratio for a desired level of confidence (95 %) and the calculated value of the  $R$  ratio of the model developed exceed the standard tabulated value of  $R$  ratio for desired level of confidence (95 %), then the model may be considered adequate within the confidence limit.

#### Testing the coefficients for significance

The value of the regression coefficients gives an idea as to what extent the control variables affect the responses quantitatively. The less significant coefficients can be eliminated along with the responses with which they are associated without estimating much accuracy which to avoid cumbersome mathematical labour. To achieve this, Student's  $t$  test is used. According to this test when the calculated value of  $t$  corresponding to a coefficient exceeds the standard tabulated value for the desired level of probability (95 %), the coefficient becomes significant. After determining the significant coefficients, the models were developed using only these coefficients.

#### Development of the final models

The final mathematical model ( $R^2 = 0.959$ ) for width as determined by the above analysis is shown below:



$$w = 7.76 - 0.2278 \cdot U - 0.0043 \cdot I - 0.000097 \cdot I^2 - 0.07986 \cdot N^2 + 0.002604 \cdot U \cdot I \quad (2)$$

The mathematical models given above can be employed to predict the geometry of the weld bead and the dilution for the range of parameters used in the investigation by substituting their respective values in the coded form. Based on these models, the main and the interaction effects of the process parameters on the bead geometry were computed and plotted. Also, by substituting the values of the desired bead geometry, the values of the control factors, can be obtained.

### Results and discussion

Typical dependency between measured values of the geometry weld bead and predicted values using mathematical model is shown in Fig. 1.

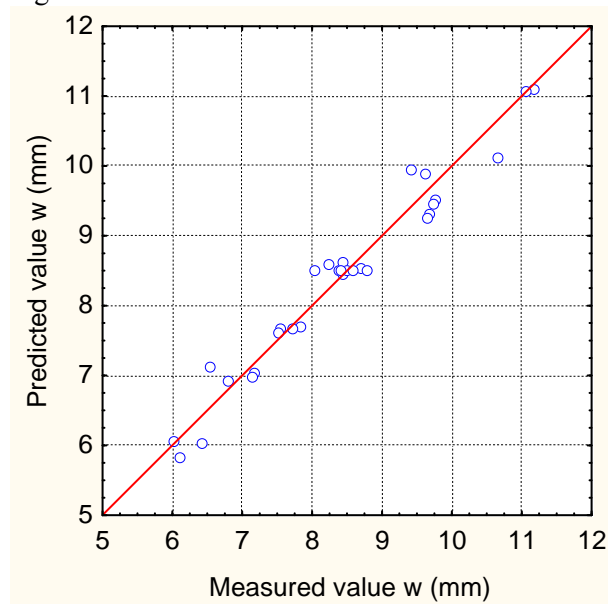


**Fig. 1** Typical dependence between measured and predicted values of bead geometry (plot for width of weld bead)

The main and interaction effects of the different process parameters on the dimensions of the weld bead predicted from mathematical models are shown in Fig. 2 – 3, showing the general trends between cause and effect.

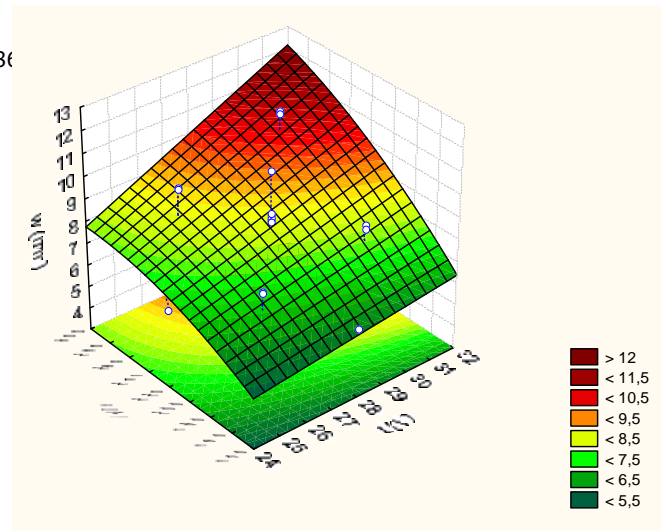


**Fig. 2** Response surface for predicted value width (mm) of weld bead ( $N = 20$  mm,  $S = 40$  cm.min<sup>-1</sup>)

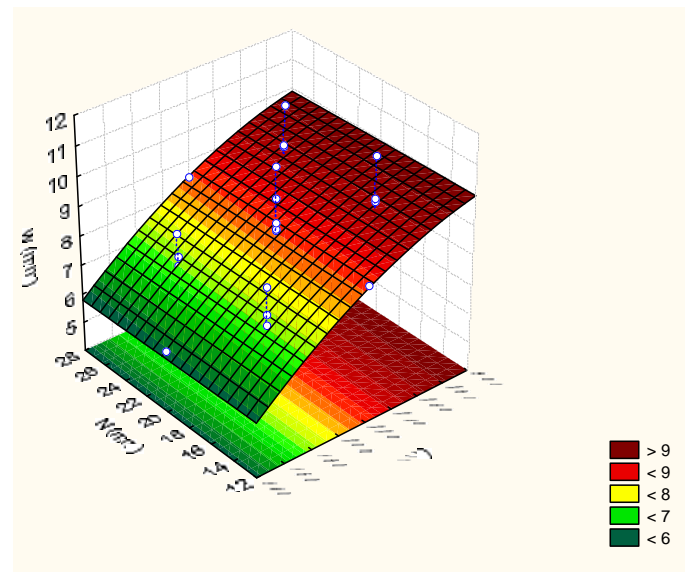


**Fig. 3** Response surface for predicted value width (mm) of weld bead ( $U = 28$  V,  $S = 40$  cm.min<sup>-1</sup>)

From Fig. 2 and Fig. 3, the width increased gradually with increase in voltage (U) and arc current (I). With increased speed of welding (S), the width of weld bead decreasing. The nozzle – to – distance (N) had a minimal effect for change width of weld bead. The mathematical models for other weld bead geometry and dilution or physical properties can be determined by using the same principles as width weld bead.

## Conclusion

The following conclusions were made from the study:

(1) A five level factorial technique can be employed easily for developing mathematical models for predicting weld bead geometry within the optimal region of control parameters or operating variables for hardfacing.

(2) The models developed can be employed easily in automated or robotic hardfacing in the form of a program for obtaining weld bead of the desired high quality.

(3) For high productivity these must be high width and reinforcement weld bead. Thus means arc current must be high and open circuit voltage must be low.

## Reference Example

- [1] Correia, D. S., et al.: Comparison between genetic algorithms and response surface methodology in GMAW welding optimization, *Journal of Materials Processing Technology*, 160, 2005: 70-76.
- [2] DuPont, J. N., Marder, A. R.: Dilution in single pass arc welds, *Metallurgical and materials transaction B*, 27B, 1996: 481-489.
- [3] Ellis, T., Garrett, G. G.: Influence of process variables in flux-cored arc welding of hardfacing deposits, *Surface Engineering*, 2, 1986: 55-66.
- [4] Chotěborský, R., et al.: Abrasive wear of high chromium Fe-Cr-C hardfacing alloys, *Research in Agriculture Engineering*, 54, 2008: 192-198.
- [5] Kim, I. S., et al.: Sensitivity analysis for process parameters in GMA welding processes using a factorial design method, *International Journal of Machine Tools and Manufacture*, 43, 2003: 763-769.
- [6] Kim, I. S.: A study on relationship between process variables and bead penetration for robotic CO<sub>2</sub> arc welding, *Journal of Materials Processing Technology*, 136, 2003: 139-145.

## REDUCTION OF CHEMICALS DRIFT IN FRUIT ORCHARD IN JAPAN

KOJI INOOKU\*, TOMOHIKO OTA, SUMIHIKO MIYAHARA

Institute of Agricultural Machinery, National Agriculture and Food Research Organization,

Nisshin 1-40-2, Kita-ku Saitama-City, Saitama, Japan,

Phone: +81-48-654-7084, Fax: +81-48-654-7133, E-mail: [inooku@affrc.go.jp](mailto:inooku@affrc.go.jp)

### Abstract

Chemical pest control has always used the self-propelled air blast sprayer in the fruit orchard in Japan. The air blast sprayer mainly consists of a fan, nozzles, a pump, a liquid tank and an engine. Apple is the most produced fruits in Japan and chemicals spray is easy to lead spray drift. Recently, growers are interest in the pesticide residue and wish to reduce the drift. Therefore, the authors investigated the relationship of the spray drift and the way of spray (nozzles, air volume and so on), in the apple dwarf tree field which is easy to work.

### 1. Introduction

Apple is the most produced fruits in Japan. The cultivation area of apple in Japan is 39,500ha, 0.8 % of the all cultivation area in the world. The yield of apple in Japan is 910,700t, 1.3 % of the yield in the world. Tolerance pesticide residue is set for all crops. Reducing of the spray drift is the big interest for growers which have neighbor field of other crops or other fruit tree. Apple dwarf growing system is expected increasing the production area in Japan. Because a work burden is lower and a higher benefit than traditional Japanese growing system under the situation of aging of Japanese fruit growers. The authors investigated the spraying technique for the reduction spray drift in apple dwarf tree field.

### 2. Field test

1) General of Japanese sprayer for fruit tree  
The self-propelled air blast sprayer (Fig. 1) is the most popular sprayer in Japanese fruit tree. 2000 - 3000 self-propelled air blast sprayers are sold every year in Japan. This type of sprayer is used in most of apple orchard. This type of sprayer consists of a fan, nozzles, a pump, a tank and an engine (Fig. 2). The

sprayer spread pesticides of 400-500 L/10a of thin density of the ratio 1000-2000 with the air blow of air volume 600-700m<sup>3</sup>/min and spray pressure 1.5 MPa. The pesticides with particle diameter 90µm are spread to the object tree. The sprayer is able to spray the pesticide to 3-4 m height at the tree with the exuberance foliage (Fig. 3).



Fig. 1 Air blast sprayer

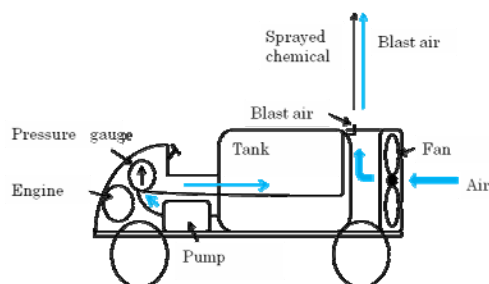


Fig.2 Component of sprayer

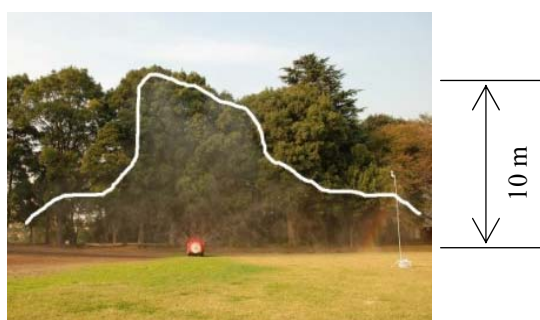


Fig. 3 Sprayed range by sprayer

## 2) Objectives of the field test




The authors investigated the influence of the nozzle types, the air volume and the natural wind to the spray drift. In addition to basic factors to the spray drift of orchard, the authors investigated the influence of the tree thickness and the spraying position in the orchard.

## 3) Nozzle and sprayer

Following three types of nozzles were tested (Table 1). Two types of sprayers were tested (Table 2).

- (1) Normal nozzles with the cone spraying pattern.
- (2) DL nozzles with the hollow-cone spraying pattern and double value of VMD compared to the hollow-cone spraying nozzles.
- (3) SV nozzles with the quarter sector shaped spraying pattern and VMD 170 $\mu$ m.

Table 1 Nozzles specification for field test

No.	Name	Spraying shape		VMD ( $\mu$ m)	Percentage of particle less than 100
1	Normal nozzle	Hollow cone	(80° ) 	90	50~70
2	SV nozzle	Quarter sector	(50° ) 	170	10~20
3	DL nozzle	Hollow cone	(80° ) 	185	10~20

Pressure :1.0~1.5MPa

Table 2 Sprayer specifications

Sprayer	Engine power (kW)	Tank volume (L)	Fan		Number of nozzles (pieces)	Discharge rate of pump (L/min)
			Air volume (m <sup>3</sup> /min)	Rotation speed (rpm)		
A	25	600	600~300	2300	18	90
B	25	1000	760,470	2200	29	114

#### 4) Spraying method and measurement method of spraying drift

Field test of spraying was conducted at the dwarf apple field in Iwate Agricultural Research Center (Table 3). The spraying experiments were conducted at the 3 path between tree rows from the edge of the tree row by both-sides spraying (Fig. 4). The spray drift were measured by using the petri dishes at the position of 10 m and 20 m distance from the edge tree. The petri dishes were collected after spraying at each path.

The tracer is magnesium sulfate heptahydrate salt. The ingredient amount of magnesium was set at 300 ppm. Collected tracer was analyzed by the atomic absorption

photometer (Shimazu Co. , Ltd.). Spraying performance to the tree was measured and evaluate by using the water sensitive paper (Spraying System Japan Co. , Ltd., 52 x 76 mm, Fig. 5).

The experiments were set at the following spraying condition.

- (1) Air volume: 400, 500, 600 m<sup>3</sup>/min.
- (2) Spraying path and method: Both-side spraying at the path of 1, 2 and 3 path apart from the edge path and one-side spraying at the edge path.

Drift rate was defined as following.

Drift rate (ppm) = Ingredient amount of magnesium collected by petri dishes (μg)/  
Ingredient amount of magnesium sprayed (g)

Table 3 Tree condition and meteorological condition

Variety	Mixed planting of Fuji, Jonagold, Ourin
Average tree height	4.0 m
Planting area	13.6 m <sup>2</sup>
Average area of tree canopy	36.0 m <sup>3</sup>
Planting density	71 trees/10a
Temperature	18-26 °C
Relative humidity	80-95 %
Natural wind speed	Almost calm

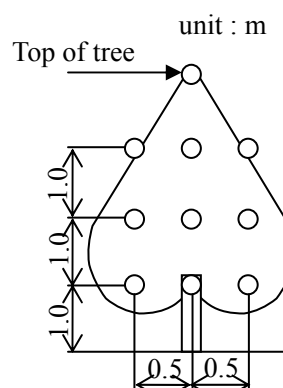


Fig.5 Spraying performance measurement position by water

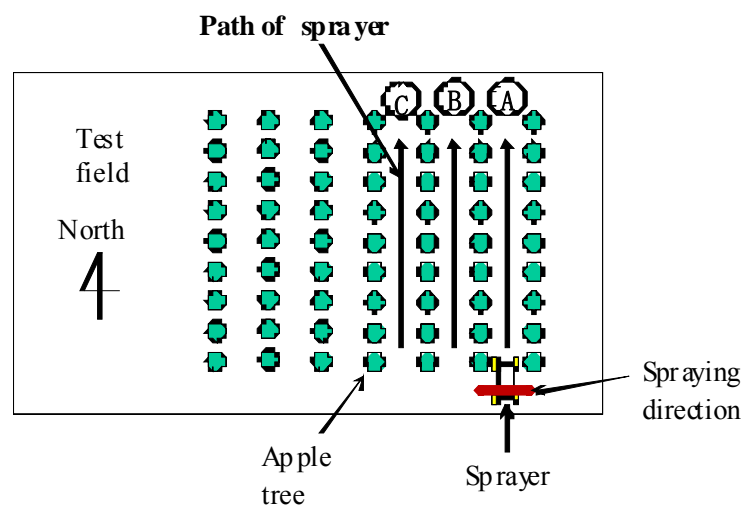


Fig.4 Path and direction of spraying in test field

#### 4. Result and discussion

##### 1) Drift of different nozzles

Fig. 6 shows the drift rate of the different nozzles. The drift rate of the hollow-corn nozzles (No.1) was higher than the drift rate of SV nozzles (No.2) and DL nozzles (No.3) regardless of air volume. The difference between the drift rate of SV nozzles and DL nozzles was not shown in the experiment.

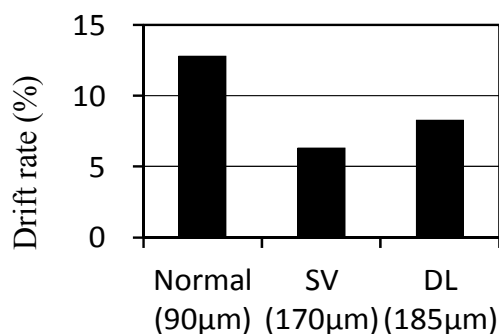


Fig.6 Drift rate at different

##### 2) Drift of different air volume

Fig. 7 shows the drift of different air volumes at spraying. Air volumes at spraying and natural wind are important factor. Drift rate of spraying at August was fewer amounts, because the thickness of the tree was highest at August. The drift rates increased, as the air

volumes. So it is necessary for the reduction of the drift to reduce the air volume at spraying.

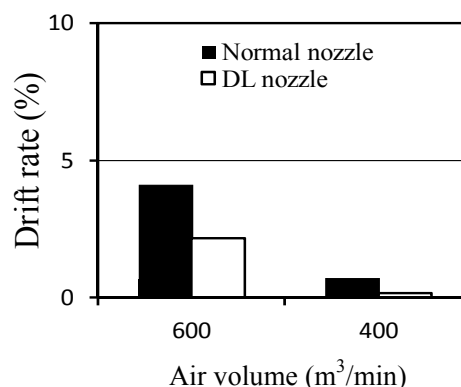


Fig.7 Relationship drift and air

##### 3) Influence of natural wind to drift rate

Fig. 8 shows the effect of the wind speed 0-2 m/s of the natural wind. The drift rate at 10 m from edge of the test apple field increased as the wind speed of the natural wind in spite of the air volume and the spraying position (path).



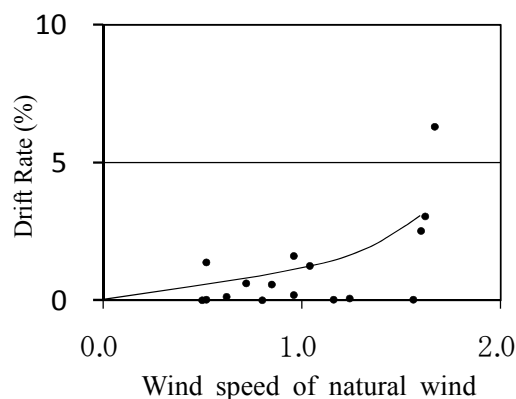


Fig.8 Influence of wind speed of natural wind to drift rate

#### 4) Relationship of thickness of tree and drift rate

Fig. 9 shows the relationships of the drift rate and the thickness of tree at May and August. The thickness of the apple tree at August is higher than that at May. It was seen that the number of the experiments of the lower drift rates at August than May was much more than the number of the experiments at May. It is thought the tree row were screen against spraying with the air blast. It is expected that no spraying to upper reduce the drift rate at the season of thin thickness of tree.

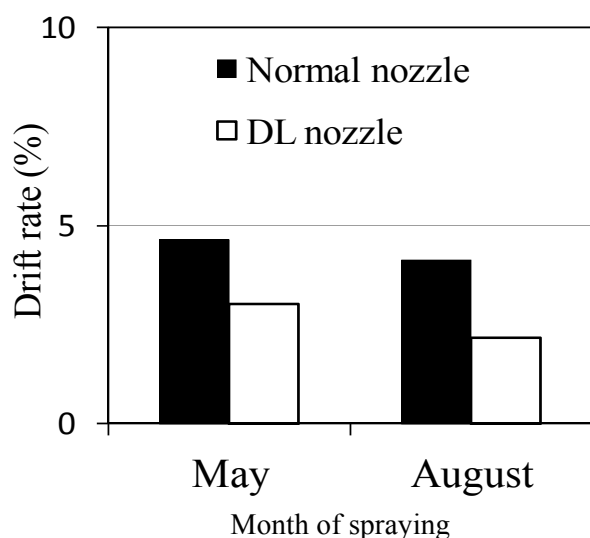


Fig.9 Relationship of thickness of tree and drift rate

#### 5) Spraying method of reducing drift rate

Fig. 10 shows the influence of natural wind to drift rate. The drift rates under the natural wind were the highest in other tracer positions. Generally the drift rate during spraying to the right angle of tree row at edge of tree row was considered the highest drift rate during spraying other directions in other tree rows. But spraying at the same wind direction as tree row caused the higher or almost same as drift rate than that of spraying to the right angle of tree row. The drift rate of the wind speed 1.5 and the right angle to the tree row was almost same as the drift rate of the wind speed less than 1.0 m/s and the parallel wind direction of the tree row. For the reduction of the drift rate, the natural wind direction of the right angle of the tree row is also as important as the natural wind direction of the parallel angle of the tree row.

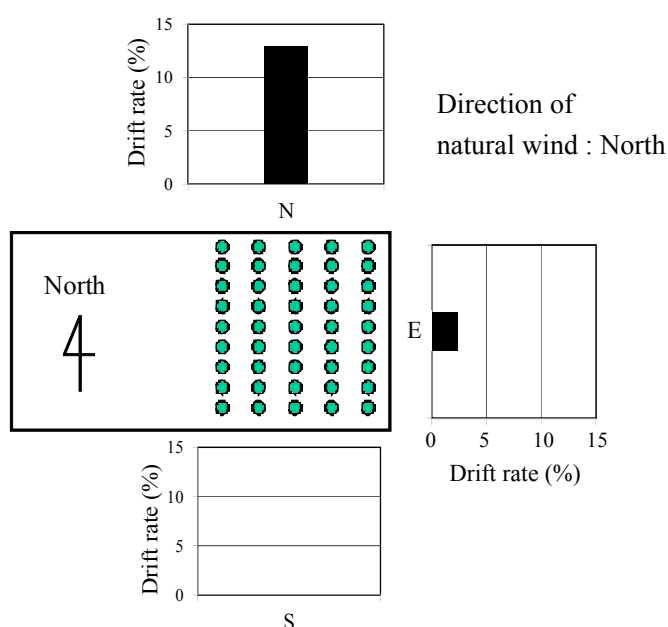


Fig.10 Influence of natural wind to drift rate

#### 5. Conclusions

The authors confirmed that the drift rate of the normal nozzles spraying small particle was

more than that of DL and SV nozzles spraying large particle. The drift rate increased as the air volume increased. So it is important for reduction of the drift to spray by the air volume corresponding to the thickness condition of the tree. In thin tree thickness condition on May or spring, air volume at spraying should be reduced to low value. In the condition of no branch at overhead of path of dwarf apple tree, upper part of nozzles should not be open for reduction of the spray drift. The natural wind with direction of tree rows caused spray drift. Because the field path became the wind path for the spray drift. Even natural wind speed of less than 1.0 m/s caused the spray drift of drift rate 5-10 %. So the growers should be careful of natural wind at spraying.

The authors suggest the method of reduction of spray drift in Japanese orchard. The growers

should use the DL nozzles and reduce the air volume a little. At the edge of tree row, the growers should spray with lower air volume at lower natural wind speed more carefully.

## 6. References

- [1] D. R. Miller, E.W. Huddleston, J.B. Ross, W.E. Steinke : Airblast spray partitioning in a mature pecan orchard. Trans. ASAE46(6) 1495-1501
- [2] G. A. Matthews : Pesticide application methods. Blackwell Science, 2000.
- [3] Koji Inooku et al : Reduction of chemicals drift by air blast sprayer (in Japanese).  
Abstracts and Data of Paper of Spring Meeting JSFWR 2007, p.71-72

## SPECIFICATION AND CLASSES OF SOLID BIOFUELS IN EUROPEAN STANDARDS

PETR JEVIČ<sup>1,2\*</sup>, ZDEŇKA ŠEDIVÁ<sup>1</sup>, JAN MALAŤÁK<sup>2</sup>

<sup>1</sup>Research Institute of Agricultural Engineering, p.r.i., 161 01 Prague 6, Czech Republic,  
Phone: +420-233022302, Fax: +420-233312507, E-mail: petr.jevic@vuzt.cz

<sup>2</sup>Czech University of Life Sciences Prague, Faculty of Engineering, Department of  
Technological Equipment of Buildings, 165 21 Prague 6, Czech Republic

### Abstract

Solid biofuels are specified according to origin, source, major traded forms and properties. In the hierarchical classification system the main origin - based solid biofuel groups are woody, herbaceous and fruit biomass, and blends and mixtures. The second level of classification describes fuels from different sources within the main groups, primarily stating whether the biomass is a virgin material, a by-product or a residue from the industry. Presented is in connection with the classification scheme solid biofuels, examples of specification properties for briquettes, pellets, straw bales and woody pellets high quality classes are recommended for smaller scale appliances.

### Introduction

The basic aim of specification of solid biofuels classification is to promote the trade of biofuels, so that the customer and the seller can unanimously define the quality [1, 2, 3]. Solid biofuels are fuel produced directly or indirectly from biomass. Among basic biomass resources which are defined as a material of biological origin excluding material embedded in geological formations and transformed to fossil belong:

- products from agriculture and forestry,
- vegetable waste from agriculture and forestry,
- vegetable waste from the food processing industry,
- wood waste, with the exception of wood waste which may contain halogenated organic compounds or heavy metals as a result of treatment with wood preservatives or coating, and which includes in particular such wood waste from construction and demolition waste,
- fibrous vegetable waste from virgin pulp production and from production of paper from pulp, if it is co-incinerated at the place of production and heat generated is recovered,
- cork waste.

### Classification of origin and sources of solid biofuels

The classification is based on the biofuel origin and source. In the hierarchical classification system (Table 1) the main origin-based solid biofuel groups are [3]:

- woody biomass;
- herbaceous biomass;
- fruit biomass;
- blends and mixtures.

Woody biomass is biomass from trees, bushes and shrubs. Herbaceous biomass is from plants that have a non-woody stem and which die back at the end of the growing season. It includes grains and their by-products such as cereals. Fruit biomass is the biomass from the parts of a plant which are from or hold seeds. If appropriate, also the actual species (e.g. spruce, wheat) of biomass should be stated. The term "Blends and mixtures" in Table 1 refers to material of various origin within the given box in the classification table and appears on four levels. Blends are intentionally mixed biofuels, whereas mixtures are unintentionally mixed biofuels. The origin of the blend and mixture shall be described using Table 1. If solid biofuel blend or mixture may contain chemically treated material it shall be stated.

The second level of classification in Table 1 describes fuels from different sources within the main groups, primarily stating whether the biomass is a virgin material, a by-product or a residue from the industry. Groups in Table 1 are further divided into third and fourth level sub-groups. The purpose of Table 1 is to allow the possibility to differentiate and specify biofuel material based on origin with as much detail as needed.

Table 1 Classification of origin and sources of solid biofuels [3]

1. Woody biomass	1.1 Forest,plantation and other virgin wood	1.1.1 Whole trees without roots	1.1.1.1 Broad-leaf
			1.1.1.2 Coniferous
			1.1.1.3 Short rotation coppice
			1.1.1.4 Bushes
			1.1.1.5 Blends and mixtures
		1.1.2 Whole trees with roots	1.1.2.1 Broad-leaf
			1.1.2.2 Coniferous
			1.1.2.3 Short rotation coppice
			1.1.2.4 Bushes
			1.1.2.5 Blends and mixtures
		1.1.3 Stemwood	1.1.3.1 Broad-leaf
			1.1.3.2 Coniferous
			1.1.3.3 Blends and mixtures
		1.1.4 Logging residues	1.1.4.1 Fresh/Green, Broad-leaf (including leaves)
			1.1.4.2 Fresh/Green, Coniferous (including needles)
			1.1.4.3 Stored, Broad-leaf
			1.1.4.4 Stored, Coniferous
			1.1.4.5 Blends and mixtures
	1.1.5 Stumps/roots	1.1.5.1 Broad-leaf	
		1.1.5.2 Coniferous	
		1.1.5.3 Short rotation coppice	
		1.1.5.4 Bushes	
		1.1.5.5 Blends and mixtures	
	1.1.6 Bark (from forestry operations)		
	1.1.7 Segregated wood from gardens, parks, roadside maintenance, vineyards and fruit orchards		
	1.1.8 Blends and mixtures		
	1.2 By-products and residues from wood processing industry	1.2.1 Chemically untreated wood residues	1.2.1.1 Without bark, Broad-leaf
			1.2.1.2 Without bark, Coniferous
			1.2.1.3 With bark, Broad-leaf
			1.2.1.4 With bark, Coniferous
			1.2.1.5 Bark (from industry operations)
		1.2.2 Chemically treated wood residues, fibres and wood constituents	1.2.2.1 Without bark
			1.2.2.2 With bark
			1.2.2.3 Bark (from industryoperations)
			1.2.2.4 Fibres and wood constituents
		1.2.3 Blends and mixtures	
	1.3 Used wood	1.3.1 Chemically untreated wood	1.3.1.1 Without bark
			1.3.1.2 With bark
			1.3.1.3 Bark
		1.3.2 Chemically treated wood	1.3.2.1 Without bark
			1.3.2.2 With bark
			1.3.2.3 Bark
		1.3.3 Blends and mixtures	
	1.4 Blends and mixtures		
2. Herbaceous biomass	2.1 Herbaceous biomass from agriculture and horticulture	2.1.1 Cereal crops	2.1.1.1 Whole plant
			2.1.1.2 Straw parts
			2.1.1.3 Grains or seeds
			2.1.1.4 Husks or shells
			2.1.1.5 Blends and mixtures
		2.1.2 Grasses	2.1.2.1 Whole plant
			2.1.2.2 Straw parts
			2.1.2.3 Seeds
			2.1.2.4 Shells
			2.1.2.5 Blends and mixtures
		2.1.3 Oil seed crops	2.1.3.1 Whole plant
			2.1.3.2 Stalks and leaves
			2.1.3.3 Seeds
			2.1.3.4 Husks or shells
			2.1.3.5 Blends and mixtures
		2.1.4 Root crops	2.1.4.1 Whole plant
			2.1.4.2 Stalks and leaves
	2.1.4.3 Root		

		2.1.5 Legume crops	2.1.4.4 Blends and mixtures	
			2.1.5.1 Whole plant	
			2.1.5.2 Stalks and leaves	
			2.1.5.3 Fruit	
			2.1.5.4 Pods	
			2.1.5.5 Blends and mixtures	
		2.1.6 Flowers	2.1.6.1 Whole plant	
			2.1.6.2 Stalks and leaves	
			2.1.6.3 Seeds	
			2.1.6.4 Blends and mixtures	
	2.1.7 Segregated herbaceous biomass from gardens, parks, roadside maintenance, vineyards, and fruit orchards			
	2.1.8 Blends and mixtures			
	2.2 By-products and residues from herbaceous processing industry	2.2.1 Chemically untreated herbaceous residues	2.2.1.1 Cereal crops and grasses	
			2.2.1.2 Oil seed crops	
			2.2.1.3 Root crops	
			2.2.1.4 Legume crops	
			2.2.1.5 Flowers	
			2.2.1.6 Blends and mixtures	
		2.2.2 Chemically treated herbaceous residues	2.2.2.1 Cereal crops and grasses	
			2.2.2.2 Oil seed crops	
			2.2.2.3 Root crops	
			2.2.2.4 Legume crops	
	2.2.2.5 Flowers			
	2.2.2.6 Blends and mixtures			
	2.2.3 Blends and mixtures			
	2.3 Blends and mixtures			
3. Fruit biomass	3.1 Orchard and horticulture fruit	3.1.1 Berries	3.1.1.1 Whole berries	
			3.1.1.2 Flesh	
			3.1.1.3 Seeds	
			3.1.1.4 Blends and mixtures	
		3.1.2 Stone/kernel fruits	3.1.2.1 Whole fruit	
			3.1.2.2 Flesh	
			3.1.2.3 Stone/kernel	
			3.1.2.4 Blends and mixtures	
		3.1.3 Nuts and acorns	3.1.3.1 Whole nuts	
			3.1.3.2 Shells/husks	
			3.1.3.3 Kernels	
			3.1.3.4 Blends and mixtures	
		3.1.4 Blends and mixtures		
	3.2 By-products and residues from fruit processing industry	3.2.1 Chemically untreated fruit residues	3.2.1.1 Berries	
			3.2.1.2 Stone/kernel fruits	
			3.2.1.3 Nuts and acorns	
			3.2.1.4 Crude olive cake	
			3.2.1.5 Blends and mixtures	
		3.2.2 Chemically treated fruit residues	3.2.2.1 Berries	
			3.2.2.2 Stone/kernel fruits	
			3.2.2.3 Nuts and acorns	
			3.2.2.4 Exhausted olive cake	
			3.2.2.5 Blends and mixtures	
	3.2.3 Blends and mixtures			
	3.3 Blends and mixtures			
	4 Blends and mixtures	4.1 Blends		
4.2 Mixtures				

## Specification of solid biofuels based on traded forms and properties

Solid biofuels are traded in many different sizes and shapes. The size and shape influence the handling of the fuel as well as its combustion properties. Biofuels may be delivered for example in the forms shown in Table 2.

At the standardized symbols:

<i>d</i>	dry (dry basis)
<i>daf</i>	dry, ash-free
<i>ar</i>	as received
w-%	weight-percentage
A	Designation for ash content [w-%, dry basis]
BD	Designation for bulk density as received [kg/m <sup>3</sup> ]
D	Designation for diameter as received [mm]
<i>D</i>	Diameter as received [mm]
DE	Designation for particle density as received [g/cm <sup>3</sup> ]
DT	Designation for deformation temperature [°C]
DU	Designation for mechanical durability as received [w-%]

<i>E<sub>ar</sub></i>	Energy density as received [GJ/m <sup>3</sup> or MWh/m <sup>3</sup> loose or stacked volume] (amount of energy/volume unit)
<i>E</i>	Designation for energy density [GJ/m <sup>3</sup> or MWh/m <sup>3</sup> loose or stacked volume]
<i>F</i>	Designation for amount of fines (w-%, as received)
<i>L</i>	Length as received [mm]
<i>L</i>	Designation for length as received [mm]
<i>M<sub>ar</sub></i>	Total moisture content as received [w-%] on wet basis
<i>M</i>	Designation for moisture content as received [w-%]
<i>P</i>	Designation for particle size distribution as received [mm]
<i>q<sub>V,gr,d</sub></i>	Gross calorific value at constant volume on dry basis [MJ/kg]
<i>q<sub>p,net,d</sub></i>	Net calorific value at constant pressure on dry basis [MJ/kg]
<i>Q</i>	Designation for net calorific value as received, <i>q<sub>p,net,ar</sub></i> [MJ/kg or kWh/kg or MWh/t] at constant pressure

Table 2 Major traded forms of solid biofuels [3]

Fuel name	Typical particle size	Common preparation method
Whole tree	> 500 mm	No preparation or delimbed
Wood chips	5 mm to 100 mm	Cutting with sharp tools
Hog fuel	Varying	Crushing with blunt tools
Log wood/firewood	100 mm to 1000 mm	Cutting with sharp tools
Bark	Varying	Debarking residue from trees Can be shredded or unshredded
Bundle	Varying	Lengthways oriented & bound
Fuel powder	< 1 mm	Milling
Sawdust	1 mm to 5 mm	Cutting with sharp tools
Shavings	1 mm to 30 mm	Planing with sharp tools
Briquettes	Ø ≥ 25 mm	Mechanical compression
Pellets	Ø < 25 mm	Mechanical compression
Bales		
Small square bales	0,1 m <sup>3</sup>	Compressed and bound to squares
Big square bales	3,7 m <sup>3</sup>	Compressed and bound to squares
Round bales	2,1 m <sup>3</sup>	Compressed and bound to cylinders
Chopped straw or energy grass	10 mm to 200 mm	Chopped during harvesting or before combustion
Grain or seed	Varying	No preparation or drying except for process operations necessary for storage for cereal grain
Fruit stones or kernel	5 mm to 15 mm	No preparation or pressing and extraction by chemicals
Fibre cake	Varying	Prepared from fibrous waste by dewatering

NOTE: Also other forms may be used.

Examples of various forms and differences of solid biofuels present Fig. 1 and 2.



Figure 1 Examples of various forms of solid biofuels

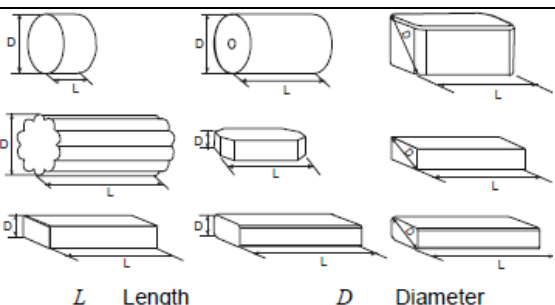




Figure 2 Difference between wood chips (left) and crushed wood fuel (right) [3]

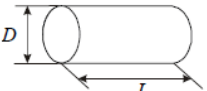
Presents on example of the specification of properties for briquettes Table 3, pellets Table 4, straw bales Table 5.

Table 3 Specification of properties for briquettes [3]

	Master table			
	Origin: According to Table 1		Woody biomass (1), Herbaceous biomass (2), Fruit biomass (3), Blends and mixtures (4)	
	Traded Form (see Table 2)		Briquette	
Normative	Dimensions (mm)			
	Diameter ( $D$ ) or equivalent (diagonal or cross cut), mm			
	D 40	$25 \leq D \leq 40$		
	D 50	$\leq 50$		
	D 60	$\leq 60$		
	D 80	$\leq 80$		
	D 100	$\leq 100$		
	D 125	$\leq 125$		
	D 125+	$> 125$ (maximum value to be stated)		
	Length ( $L$ ), mm			
L 50	$\leq 50$			
L 100	$\leq 100$			
L 200	$\leq 200$			
L 300	$\leq 300$			
L 400	$\leq 400$			
L 400+	$> 400$ (maximum value to be stated)			
Moisture, $M$ (w-% as received)				
M10	$\leq 10 \%$			
M15	$\leq 15 \%$			
	Ash, $A$ (w-% of dry basis)			
	A0.5	$\leq 0,5 \%$		
	A0.7	$\leq 0,7 \%$		
	A1.0	$\leq 1,0 \%$		
	A1.5	$\leq 1,5 \%$		
	A2.0	$\leq 2,0 \%$		
	A3.0	$\leq 3,0 \%$		
	A5.0	$\leq 5,0 \%$		
	A7.0	$\leq 7,0 \%$		
	A10.0	$\leq 10,0 \%$		
	A10.0+	$> 10,0 \%$ (maximum value to be stated)		
	Particle density, $DE$ (g/cm <sup>3</sup> )			
	DE0.8	$\geq 0,8$		
	DE0.9	$\geq 0,9$		
	DE1.0	$\geq 1,0$		
DE1.1	$\geq 1,1$			
DE1.2	$\geq 1,2$			
DE1.2+	$> 1,2$ (maximum value to be stated)			
Additives (w-% of pressing mass)		Type and content of pressing aids, slagging inhibitors or any other additives have to be stated		
Net calorific value as received, $Q$ (MJ/kg or kWh/kg)		Minimum value to be stated		

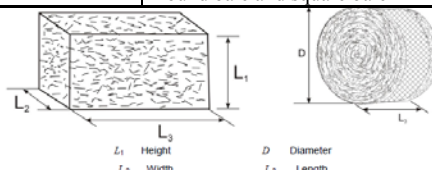
Normative / Informative	Mechanical durability, DU (w-% of briquettes after testing)		
	DU95.0	≥ 95,0 %	Informative: only if traded in bulk
	DU90.0	≥ 90.0 %	
	DU90.0-	< 90.0 % (minimum value to be stated)	
	Nitrogen, N (w-% of dry basis)		
	N0.3	≤ 0,3 %	Normative: Chemically treated biomass (1.2.2, 1.3.2, 2.2.2, 3.2.2)
	N0.5	≤ 0,5 %	
	N1.0	≤ 1,0 %	Informative: All fuels that are not chemically treated (see the exceptions above)
	N2.0	≤ 2,0 %	
	N3.0	≤ 3,0 %	
	N3.0+	> 3,0 % (maximum value to be stated)	
	Sulphur, S (w-% of dry basis)		
	S0.02	≤ 0,02 %	Normative: Chemically treated biomass (1.2.2, 1.3.2, 2.2.2, 3.2.2) if sulphur containing additives have been used.
	S0.05	≤ 0,05 %	
	S0.08	≤ 0,08 %	Informative: All fuels that are not chemically treated (see the exceptions above)
	S0.10	≤ 0,10 %	
	S0.20	≤ 0,20 %	
	S0.20+	> 0,20 % (maximum value to be stated)	
	Chlorine, Cl (w-% of dry basis, %)		
	Cl0.02	≤ 0.02 %	Normative: Chemically treated biomass (1.2.2, 1.3.2, 2.2.2, 3.2.2)
	Cl0.03	≤ 0.03 %	
	Cl0.07	≤ 0.07 %	Informative: All fuels that are not chemically treated (see the exceptions above)
	Cl0.10	≤ 0.10 %	
	Cl0.10+	> 0.10 % (maximum value to be stated)	
Informative: Ash melting behaviour (°C)		Deformation temperature, DT should be stated	

Table 4 Specification of properties for pellets [3]

Normative / Informative	Master table	
	Origin: According to Table 1	Woody biomass (1), Herbaceous biomass (2), Fruit biomass (3), Blends and mixtures (4)
	Traded Form (see Table 2)	Pellets
	<p style="text-align: center;"> <math>L</math> Length      <math>D</math> Diameter    Figure 4 Dimensions (mm) </p>	
	Diameter ( $D$ ) and Length ( $L$ )	
	D06	6 mm ± 1,0 mm, and 3,15 ≤ $L$ ≤ 40 mm
	D08	8 mm ± 1,0 mm, and 3,15 ≤ $L$ ≤ 40 mm
	D10	10 mm ± 1,0 mm, and 3,15 ≤ $L$ ≤ 40 mm
	D12	12 mm ± 1,0 mm, and 3,15 ≤ $L$ ≤ 50 mm
	D25	25 mm ± 1,0 mm, and 10 ≤ $L$ ≤ 50 mm
	Moisture, M (w-% as received)	
	M10	≤ 10 %
	M15	≤ 15 %
	Ash, A (w-% of dry basis)	
	A0.5	≤ 0,5 %
	A0.7	≤ 0,7 %
	A1.0	≤ 1,0 %
	A1.5	≤ 1,5 %
	A2.0	≤ 2,0 %
	A3.0	≤ 3,0 %
	A5.0	≤ 5,0 %
	A7.0	≤ 7,0 %
	A10.0	≤ 10,0 %
	A10.0+	> 10,0 %
	Mechanical durability, DU (w-% of pellets after testing)	
	DU97.5	≥ 97,5 %
	DU96.5	≥ 96,5 %
	DU95.0	≥ 95,0 %
	DU95.0-	< 95,0 % (minimum value to be stated)

Amount of fines, F (w-%, < 3,15 mm) after production when loaded or packed		
F1.0	≤ 1,0 %	
F2.0	≤ 2,0 %	
F3.0	≤ 3,0 %	
F5.0	≤ 5,0 %	
F5.0+	> 5,0 % (maximum value to be stated)	
Additives (w-% of pressing mass)		Type and content of pressing aids, slagging inhibitors or any other additives have to be stated
Bulk density (BD) as received (kg/m <sup>3</sup> )		
BD550	≥ 550 kg/m <sup>3</sup>	
BD600	≥ 600 kg/m <sup>3</sup>	
BD650	≥ 650 kg/m <sup>3</sup>	
BD700	≥ 700 kg/m <sup>3</sup>	
BD700+	> 700 kg/m <sup>3</sup> (minimum value to be stated)	
Net calorific value as received, Q (MJ/kg or kWh/kg)		Minimum value to be stated
Sulphur (w-% of dry basis)		
S0.02	≤ 0,02 %	Normative: Chemically treated biomass (1.2.2, 1.3.2, 2.2.2, 3.2.2) or if sulphur containing additives have been used.
S0.05	≤ 0,05 %	
S0.08	≤ 0,08 %	
S0.10	≤ 0,10 %	
S0.20	≤ 0,20 %	
S0.20+	> 0,20 % (maximum value to be stated)	
Nitrogen, N (w-% of dry basis)		
N0.3	≤ 0,3 %	Normative: Chemically treated biomass (1.2.2, 1.3.2, 2.2.2, 3.2.2)
N0.5	≤ 0,5 %	
N1.0	≤ 1,0 %	Informative: All fuels that are not chemically treated (see the exceptions above)
N2.0	≤ 2,0 %	
N3.0	≤ 3,0 %	
N3.0+	> 3,0 % (maximum value to be stated)	
Chlorine, Cl (w-% of dry basis)		
Cl0.02	≤ 0.02 %	Normative: Chemically treated biomass (1.2.2, 1.3.2, 2.2.2, 3.2.2)
Cl0.03	≤ 0.03 %	
Cl0.07	≤ 0.07 %	Informative: All fuels that are not chemically treated (see the exceptions above)
Cl0.10	≤ 0.10 %	
Cl0.10+	> 0.10 % (maximum value to be stated)	
Informative: Ash melting behaviour (°C)		Deformation temperature, DT should be stated

Table 5 Specification of properties for straw bales, reed canary grass bales and Miscanthus bales [3]

Table 5 Specification of properties for straw bales, Reed canary grass bales and Miscanthus bales [5]			
Normative	Master table		
	Origin: According to Table 1.		2.1.1.2 Cereal crop straw, 2.1.2.1 Whole plant (Reed canary grass and Miscanthus, 2.1.2.2 Grass straw, 2.1.3.2 Oil seed crops stalks and leaves
	Traded Form		Round bale and square bale
			
	Figure 5 Dimensions (m)		
Round bale	Diameter ( $D$ )	Length ( $L_3$ )	
D 1	1,2 - 1,5	1,2	
D 2	1,6 - 1,8	1,5	
Square bale	Height ( $L_1$ )	Width ( $L_2$ )	Length ( $L_3$ )
P1	$\leq 0,35$	$\leq 0,4$	$\leq 0,5$
P2	$\leq 0,9$	$\leq 1,2$	1,5 - 2,8
P3	$\leq 1,3$	$\leq 1,2$	1,0 - 3,0
P3+	Maximum values to be stated		
Bale density. (BD) ( $\text{kg/m}^3$ )			

	BD100	≥ 100
	BD120	≥ 120
	BD160	≥ 160
	BD180	≥ 180
	BD220	≥ 220
	BD220+	> 220 (minimum value to be stated)
	Moisture, M (w-% as received)	
	M10	≤ 10 %
	M15	≤ 15 %
	M20	≤ 20 %
	M25	≤ 25 %
	M30	≤ 30 %
	M30+	> 30 % (maximum value to be stated)
	Ash, A (w-% of dry basis)	
	A5.0	≤ 5 %
	A7.0	≤ 7 %
	A10.0	≤ 10 %
	A10.0+	> 10 % (maximum value to be stated)
	Species of biomass	Has to be stated (Example: spring harvested reed canary grass ( <i>Phalaris arundinacea</i> L.) or Miscanthus ( <i>Miscanthus Giganteus</i> ))
	Net calorific value, Q (MJ/kg as received) or energy density, E (kWh/m <sup>3</sup> loose or MWh/m <sup>3</sup> loose)	Minimum value to be stated
Informative	Production method	It is recommended to declare production methods that influence the size of the straw particles in the bale. That is for instance whether the crop has been trashed by rotation or oscillation or whether it has been chopped. Harvested as a whole plant for Reed canary grass and Miscanthus
	Chlorine, Cl (w-% of dry basis)	
	Cl0.01	≤ 0.01 %
	Cl0.03	≤ 0.03 %
	Cl0.07	≤ 0.07 %
	Cl0.10	≤ 0.10 %
	Cl0.10+	> 0.10 % (maximum value to be stated)
	Binding type of bales	Tying material recommended to be specified (net binding, plastic line)
	Ash melting behaviour (°C)	Deformation temperature, DT should be stated

The following examples are specifications for high quality classes of biofuels pellets recommended for household usage. Household usage needs special considerations for the following reasons:

- Small-scale equipment does not usually have advanced control and gas cleaning;
- Unprofessional management;

- Often located in living and populated districts.

**Sample:** Chemically untreated wood residues from wood processing industry, without bark - 1.2.1.1 and 1.2.1.2 pellets, diameter 6 mm, mass 4 kg  
D06 diameter 6 ± 1 mm, length: 3,15 ≤ L < 40 mm  
Fuel composition: Proximate and ultimate analysis, energy content

Composition	Unit	As received	Dry	prEN 14961-2:2009 [4]
Moisture M	w-% *	5,38	-	M10 ≤ 10
Flammable mat volatile	w-%	79,29	83,80	-
Flammable mat non-volatile	w-%	14,93	15,78	-
Ash A	w-%	0,40	0,42	A0.5 ≤ 0,5 dry
C, Carbon	w-%	47,99	50,72	-
H, Hydrogen	w-%	4,30	4,54	-
N, Nitrogen	w-%	<0,1	<0,11	N0.3 ≤ 0,3 dry
S, Sulphur	w-%	0,02	0,021	S0.05 ≤ 0,05 dry
O, Oxygen	w-%	41,91	44,29	-
Cl, Chlorine	w-%	0,015	0,016	Cl0.2 ≤ 0,2 dry
Cu, Copper	mg.kg <sup>-1</sup>	5,0	5,28	≤ 10 dry
Zn, Zinc	mg.kg <sup>-1</sup>	20,0	21,14	≤ 100 dry
Pb, Lead	mg.kg <sup>-1</sup>	<1	<1,06	≤ 10 dry
Hg, Mercury	mg.kg <sup>-1</sup>	0,038	0,040	≤ 0,1 dry
Cd, Cadmium	mg.kg <sup>-1</sup>	0,01	0,011	≤ 0,5 dry
Cr, Chromium	mg.kg <sup>-1</sup>	2,4	2,54	≤ 10 dry
Ni, Nickel	mg.kg <sup>-1</sup>	4,1	4,33	≤ 10 dry

Composition	Unit	As received	Dry	prEN 14961-2:2009 [4]
As, Arsenic	mg.kg <sup>-1</sup>	0,04	0,042	≤ 1 dry
Gross calorific value	MJ.kg <sup>-1</sup>	19,12	20,34	-
Net calorific value	MJ.kg <sup>-1</sup>	18,05	19,21	-

\* Mass per cent

#### Amount of fines F:

0,05 w-% sampling (a sieve with round screen holes of 3.15 mm diameter)

F1.0 ≤ 1,0 w-%

#### Density:

1,28 kg/dm<sup>3</sup> ≥ 1,12 kg/dm<sup>3</sup>

#### Mechanical durability DU:

prEN 14961-2:2009 (durability tester for pellets)

98,06 w-% - DU 97,5 ≤ 97,5 w-%

#### Fusibility of ash temperature:

Sphere temperature 1185 °C

Hemisphere temperature 1195 °C

Flow temperature 1240 °C

#### Conclusion

The purpose of quality classification and specification of solid biofuels is to determinate their quality within whole supply chain from origin until the certificated solid biofuel delivery and to assure corresponding confidence to the qualitative requirements. This is a basis for market preparation and development with solid biofuels. Requirements for production will be met through assurance of quality and its control. Principle of the solid fuel quality assurance is based on its clearly defined determination and limited demands for product.

*The work comprises partial results of the research project of the Ministry of Agriculture of*

*the Czech Republic 0002703102 – Part 5 “Technological processes of sustainable production and utilization of bio-raw materials and energy carrier of new generation with respect to food security and global market with relevant products”.*

#### References

- [1] JEVIČ, P., MALAŤÁK, J., DUBROVIN, V.O. Quality and specification of solid biofuels in Europe. Journal of Research and applications in agricultural engineering. Poznaň, 2007, vol. 52 (1), s. 13–20. ISSN 1642-686X
- [2] ALAKANGAS, E. Fuel specification and classes - introduction to task IV and feedback from industry and classification of used wood in fuel specification and classes (EN 14961) multipart standard. In. BioNorm II, pre-normative research on solid biofuels for improved European standards. German Biomass Research Centre non profit research company, 4<sup>th</sup> November 2009, Leipzig, s. 71 - 80
- [3] ČSN EN 14961-1: Solid biofuels – Fuel specifications and classes - Part 1: General requirements (Tuhá biopaliva - Specifikace a třídy paliv - Část 1: Obecné požadavky). January 2010 (červenec 2010), ÚNMZ, s. 52
- [4] prEN 14961-2: Solid biofuels – Fuel specifications and classes - Part 2: Wood pellets for non-industrial use. 2009, CEN/TC 335, s. 9

## COMPUTERIZED MAINTENANCE MANAGEMENT SYSTEMS IN AGRICULTURE

VLADIMIR JURCA, VERONIKA VITKOVA, ZDENEK ALES  
Czech University of Life Sciences Prague, Faculty of Engineering  
Department for Quality and Dependability of Machines  
Kamycka 129, 165 21 Prague 6 – Suchbátov  
Phone: +420 224 383 322, E-mail: jurca@tf.czu.cz

### Abstract

The purpose of this paper is to introduce the application of information systems for maintenance management being increasingly used by Czech companies (including within the agro-industrial complex) in recent years. The paper describes the use of CMMS and their implementation in enterprises. The use of CMMS helps to create a variety of scenarios with an emphasis on the need for analytical instruments processing data integration in order to improve the efficiency of the maintenance system and identify its weaknesses.

While the CMMS is widespread within the agro-industrial scope in the manufacturing industry, in primary agricultural production and agricultural machinery servicing, it has yet to be utilized. The paper also describes some possible applications of CMMS in the sphere of the agro-industrial complex, the differences between their applications and the potential use of CMMS in the case of fully or partially outsourced agricultural equipment maintenance.

### Introduction

The maintenance status of Czech companies has changed considerably in recent years in favor of maintenance, which previously was often seen by management as a kind of necessary evil, which only derives from corporate resources. In currently prosperous companies maintenance is becoming to be one integral process, where you need to apply similar principles of quality management, such as by manufacturing and all other areas of business management. One of the important principles of quality management is a "continual improvement", which must be a sustainable objective of any organization.

Successful quality management in general, including the maintenance management system is based on full documentation of all related activities. Anyone who deals with maintenance issues, it is clear that well-functioning efficient maintenance system must be planned and transparent documented. It must be clearly determined when, who and how was the maintenance carried out with. It must be back indictable how, by whom and when the maintenance was implemented, what costs were for the maintenance expended, and what quality and reliability performs the system and its elements. There is a large amount of factors which should be documented, frequently

analyzed and requires in most of business to use necessarily the information system. Maintenance Information System (CMMS) is designed to simplify and standardize a documentation process of data maintenance. Beside this a specialized information system promotes the process approach, a systematic approach of management and enables a continuous improvement of maintenance. The maintenance information system in particular allows decision making based on facts, which are accessible in the system and which are promptly to obtain in order to analyze and make a decision on the rational basis.

The CMMS use is already widespread in the Czech manufacturing industry. The CMMS was first introduced in the mid 90s in automotive and related sectors. At the turn of the century the CMMS began to be utilized also in agro-industrial complex (dairies, bake house, sugar-houses, breweries etc.), but in the enterprises with primary agricultural production the CMMS is being used only exceptionally although the agricultural machinery is getting to be more computerized and costlier in terms of their purchase and operation. A well-functioning maintenance system can significantly reduce operating costs, particularly in the following areas:



- Enhance the reliability of production equipment and thus improve its elementary properties (especially availability, safety and durability)
- Significantly alter the ratio between maintenances after failure and planned maintenances on behalf of planned system and thus reduce idle time and subsequently increase machine utilization
- Essentially minimize the number of failures and thus lower a number of maintenances after the failure, thereby the consumptions of expensive spare parts decrease, which tend to be unnecessarily drawn just for emergency breakdowns
- Cost cutting due to the lower overtime of maintenance workers and cost reduction for emergency maintenance outsourced services
- Reduction of overall maintenance cost in the longer time period
- Based on data registration related to failures and their analysis are significantly reduced repeated failures
- A number of non-conforming products will decrease and thus lower the cost of non-quality
- Within the Integrated quality management system that includes increasing effectiveness of maintenance is reasonable to expect a decrease in the environmental impact of its activities and improve the health and safety at work.

Currently, it is already common for the maintenance management system is supported by the information system. Without support CMMS is not possible to assess the effectiveness of maintenance (unreliable data), but can not competently manage maintenance (make decisions based on facts that are missing) and to plan is difficult and in the short time period. If we assume that maintenance is supported by the CMMS, it can get a number of indicators, which enable to quantify most of the above benefits CMMS - they are already certified in the industrial sector and there is no reason why the agriculture sector despite certain specifics should be an exception. Why, then, has not a certified system also expanded in the agro-industrial complex?

### Material and method

The general principle CMMS based on the principles of logistics management system, whose main objective is to plan, manage and control material and information flow so as to achieve the performance and economic goals. A substantial part of the logistics management system is an information system (IS), whose goal is to capture, store, process and transmit data planned and actual. It is beneficial not only in policy documents on the upkeep and maintenance activities associated with (it is a starting point, not an end), but also save time in preparing and implementing maintenances, saving human resources, materials and spare parts, rapid elimination of vulnerabilities, reducing the number of nonconforming products, increasing the reliability of production equipment, etc. All this, however, provided that the IS was correctly chosen (a user-friendly, open to change, but at the same time stable), successfully implemented (in the implementation phase is very important to the full support of senior management and effective participation of all interested workers) and appropriate use.

CMMS encourages electronically record documents a series of stages of operation – asset inventory, chronological record of object maintenance operations, work orders, a stock of spare parts, a chronological record parameters, production plans and schedules, chronological records of activities of workers and dozens of others. The basic prerequisite for using CMMS maintenance management is proper records maintained objects (based on the "asset inventory"), which is connected to the planning and registration maintenances carried out mostly with stock items utilization. Following additional sources of information (maintenance personnel availability, equipment and tools disposability, the cost of maintenance, failure codes, maintenance requirements, etc.) are recorded in long-planned and unplanned maintenance - their causes, labor, downtime, cost, etc. The maintenance data stored commonly used for planning and various operating system maintenances analysis - for example, to identify costs, labor intensity and duration of downtime of the selected object for a selected period, to determine the monthly maintenance costs for individual departments or production lines, to monitor the failure of machinery and the removal

of the frequent causes of failures, to summarize the maintainers labour worked each year, etc. The data can be recorded, however, the theoretical background knowledge to obtain the appropriate procedures as well as many other

indicators that can greatly assist in planning, evaluation, and thus the continuous improvement of maintenance. Simplified diagram CMMS preventive maintenance management in industries is shown in Figure 1.

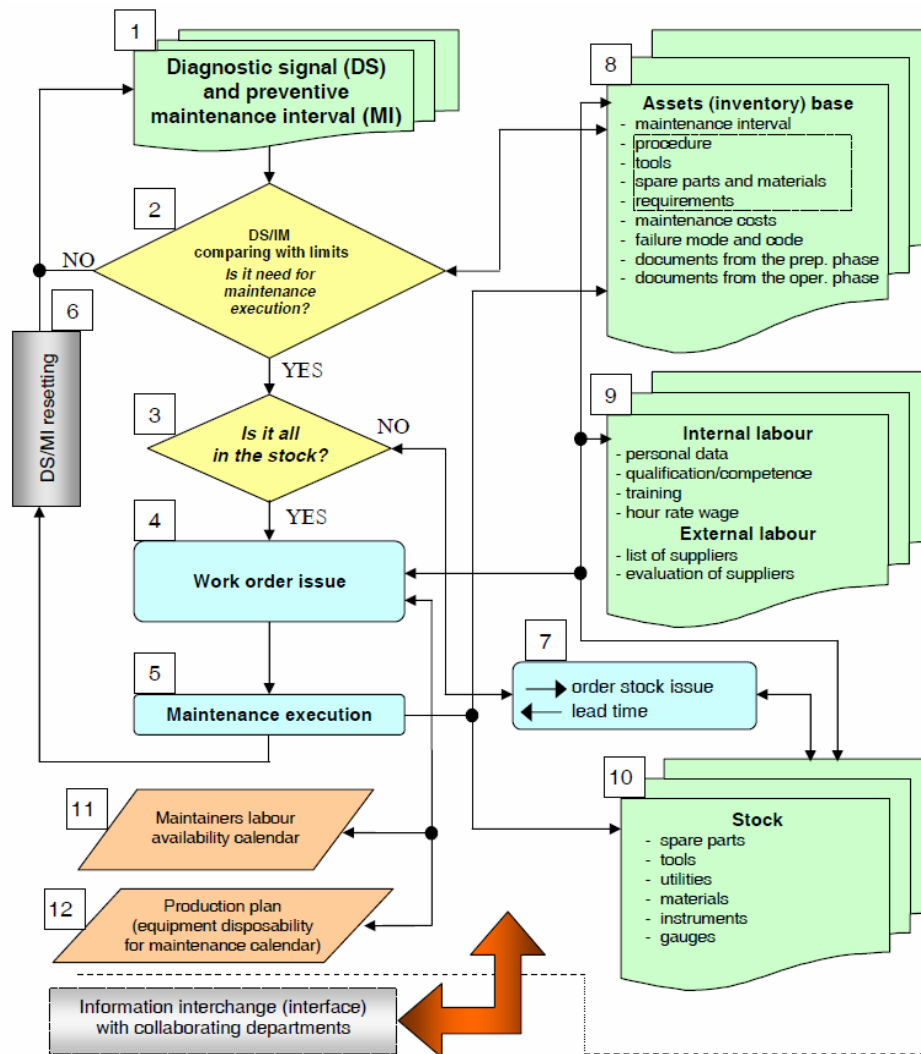


Fig. 1 Simplified CMMS flowchart for preventive maintenance

Even for agricultural business can use the same principle CMMS, if the selection and implementation of CMMS will be done with respect of agricultural specifics versus industrial.

### Results and discussion

Although it seems at first sight that maintenance systems in industrial and agricultural companies are very different, in fact they are not. Apparent obstacles using CMMS in agricultural companies exist in other sectors too, but these obstacles do not prevent using of CMMS - such as seasonal

work exists in the sugar-houses, where the CMMS is used, as well weather conditions apply to construction companies, etc. The main causes of lower extension of the maintenance management system in general and its computer support in agricultural companies are mainly these:

- in the Czech Republic are relatively few large agricultural companies which could effectively use CMMS

- affordable, yet high-quality applications CMMS on the market in the Republic appeared just recently
- agricultural companies still do not appreciate the positive aspects of well-functioned maintenance system – similar situation was apparent in an industrial companies 10 years ago
- lack of software and hardware facilities in agricultural companies causes poor data communication between the divisions of agricultural companies and between agricultural companies and companies engaged in the maintenance outsourcing
- for complex machineries the maintenance is outsourced through dealers of specific brand and maintenance system is entirely managed by the dealer; for simple machineries maintenance after the failure is usually applied by own workers, often unskilled
- lack of companies offering outsourced maintenance of agricultural machineries without a narrow link on a specific

manufacturer or supplier of agricultural machineries

However, it is possible to assume that in the up-coming years CMMS will be extended to larger agricultural companies. Some dealers of farm machinery have been working on applications that will ensure efficient flow of data within a communication channel dealer (repair service company) – agricultural company. These applications enclose evidence, planning and managing of maintenance activities, etc. Density of the service networks of suppliers of agricultural machinery is already sufficient, and it is still constantly growing – as an example at Figure 2 the allocation of „STROM“ dealers and services in the Czech Republic is shown. Each outlet covers approximately 1.600 km<sup>2</sup>. All these outlets are connected via the corporate Web applications on a central server with data store and access to knowledge bases, spare part inventories, etc.

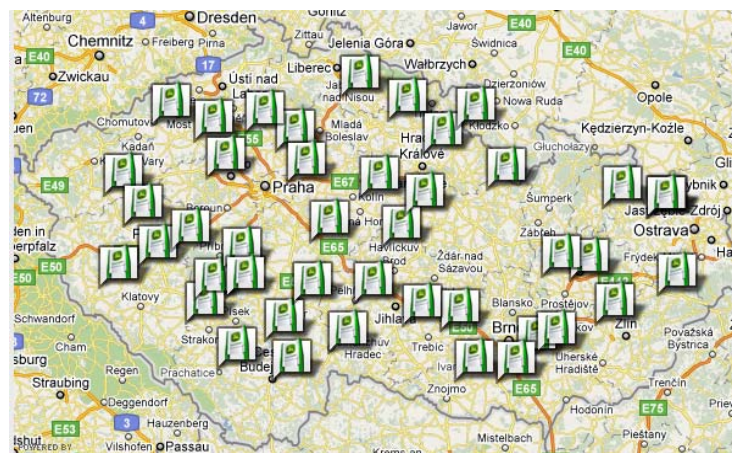


Figure 2 Allocation of „STROM“ dealers and repair services in the Czech Republic

Effective maintenance systems should be based on collaboration and data link at least the level of largest suppliers of agricultural machineries in the Czech Republic with individual agricultural companies. Consolidated information system should share necessary data for maintenance management of particular agricultural companies, evidence of maintenance history and plans of preventive maintenance etc.

However, this solution is not an option because of concerns about misuse of enterprise data shared by cooperating companies. These concerns are often completely unnecessary,

information technology allows access to data configuration for participating users, but in practice it is clear that sometimes claustrophobic fears about misuse of data will not be overcome in the near future.

#### A. Traditional in-house maintenance system

This model could be functional identically as in industry, where using the CMMS system of maintenance procedures is managed without relationship to the external environment and various maintenance subcontractors (outsourcing maintenance). Maintenance carried out by own

workers are registered and CMMS planned essentially in the same way as outsourced maintenance. Maintenance system setting, the continuous monitoring and optimization of efficiency is controlled by the maintenance manager of agricultural company. This model is already running in several agricultural companies in the Czech Republic, but its disadvantage is the need to duplicate records of major machineries, for which maintenance is provided by external companies (usually dealers of the brand that have delivered machinery) who are also interested to record maintenance activities. By recording maintenance data on the same machinery in two different information systems often leads to errors due to human error, and quite often, the dealer has different data than the agricultural company. Agricultural companies are not usually equipped with devices for collecting diagnostic signals (which have dealers). Such a fact results in situation that agricultural companies do not have relevant and valuable information about the technical state of machinery - particularly for predicting the evolution of the technical condition of the machine and thus the need of future preventive maintenance.

#### B. Shared maintenance system

This system has the advantage that it eliminates the major insufficiencies of traditional in-house maintenance system. Agricultural company and dealer work together with the data collected on a single server, the CMMS set rights for individual users for access to input and view data. Unlike the previous model, the maintenance manager of the agricultural company could analyze the output of diagnostic device from dealer. On the other hand, the dealer should have a detailed overview of the planned maintenance which provides for the agricultural company, failure of machines, the need for spare parts, etc. The great advantage of this model is that if the planned maintenance in the CMMS is approved, both interested partners can prepare in advance. Affordable CMMS also includes failure monitoring module, so if a requirement is entered into CMMS by agricultural company, it immediately informs the dealer and the failure may be quickly removed. Even it is useful for both sides, described model is not spread in agricultural sector (minor share of this model in industry). This model is facing the above-

mentioned reluctance to share data among partners.

#### C. Outsourcing of maintenance of agricultural machinery

Like in the industry, also in agriculture it is possible to expect the establishing of specialized companies for the maintenance of various agricultural machines. These companies could completely ensure the maintenance of machinery for agricultural companies by supply method. All data collected during maintenance of agricultural machinery would be owned and maintained by CMMS in outsourcing company. Using of CMMS would be in the interest of outsourcing company for easy planning of preventive maintenances and analysis capabilities of maintenances and also in order to increase its effectiveness. This model is typically used in the industry (chemical industry, heating plants, electric grids, etc.), but it has disadvantage, which is complicated communication in terms of dates of scheduled maintenance activities, and as well recovery of operational failures. There is a direct result of the absence of feedback dealers, and agricultural equipment manufacturers, for whom data of the maintenance of their machines during the life cycle is valuable informational basis for further development.

#### Conclusion

Effective maintenance management in any sector must necessarily be supported by an information system that provides the necessary data for decision making based on real facts. CMMS are increasingly used to manage maintenance systems in the companies. Ten years ago use of CMMS was rather exceptional. CMMS was used scarcely only in industrial enterprises, are now it is almost the rule. Managers of these companies understand that properly implemented maintenance system is another source for the company to reduce costs, and that without the computer aided support the whole company can not achieve effective outcomes. CMMS are increasingly being used in larger agricultural companies in the Czech Republic, where using of the traditional model of in-house maintenance system poses problems for outsourced maintenance of agricultural machinery dealers. In the following years, it is possible to assume that there will be closer

cooperation between dealers and agricultural companies and expansion of a shared maintenance system of CMMS.

### References

- [1] Jin, G.Y., et al. Semantic Integrated Condition Monitoring and Maintenance of Complex System. In: IEEE 16th International Conference on Industrial Engineering and Engineering Management. Beijing, PRC : 2009. p. 670-674.
- [2] Jurca, V.; Hladik, T.; Ales, Z. *Possibilities of data assimilation from maintenance management systems*. Prague: CSJ, 2004. ISBN 80-02-01595-9. p. 74. (in Czech Možnosti využití a zpracování dat z řízení údržby)
- [3] Kans, M. An approach for determining the requirements of computerised maintenance management systems. *COMPUTERS IN INDUSTRY* . 2008, 59, p. 32-40.
- [4] Westerkamp, T.A. Maintaining maintenance - How smart managers plan and execute successful CMMS implementations. *INDUSTRIAL ENGINEER* . 2006, 38, p. 37-42.



## THE METHOD OF FUEL CONSUMPTION INDIRECT QUANTIFICATION

BOLESLAV KADLEČEK<sup>1\*</sup> - MIROSLAV RŮŽIČKA<sup>2</sup> - LADISLAV PEJŠA<sup>3</sup>

<sup>123</sup>Czech University of Agriculture in Prague, 16521 Prague 6 – Suchbát, Czech Republic,  
Phone: +420 224381111, Fax: +4202-20921361, E-mail: kadlec@tf.czu.cz,  
ruzicka@tf.czu.cz, pejsa@tf.czu.cz

### Abstract

Costs significantly affect the usage of fuel consumption. The aim of beginning research task was to determine fuel consumption in dependency on real traffic conditions. The research was consequently carried out from analogical access with the use of contract carriers' data to the proposal of synthetic model enabling the prediction of fuel consumption according to a vehicle type and operational conditions.

### Introduction

The public transit belongs by its character into those public concerns as education, health services etc. Their assuring and accessibility for public is one of the elementary tasks for the state or municipal administration. These interests are ensured and subsidies from public budgets (taxes) and it is necessary to cover these expenditures according to the transport performance – to determine the price of transit performance (it is not the term legislative category, but used term that expresses the sum of entitled requirements and treated part of adequate profit).

Private companies (bus transit) influence the process of transit price fixing and they add an aspect to it i.e. profit necessity that is done by their entrepreneur activities. It means that the price of transit performance should content the amount of appropriate profit derived from carried out entrepreneur activities as well. The adjustment of calculation of the price could be seen as problem. Current conditions of calculation are derived from companies' level of costs. The fixing of the transit price then becomes a business opportunity for private companies - where order party (district authority) stands on one side to negotiate the lowest price and on the other side private companies stand with an opposite endeavour. The determination of transit performance price is conditioned by total assessment of sum of economically entitled costs. The process of price fixing initiates an increase of real costs declared by companies (e.g. fuel consumption).

This situation calls for the determination of realistic and objective indicators of machines' operation and their appraisal. Following step

should be the permanent check of transport quality development that is provided by transit companies and the check of transit performance price. The determination of transit performance price is complicating, mutual comparison of single companies even on the level of district (region) is significantly influenced by many objective factors i.e. demographic density, geographic, orographic, climatic conditions and structure of transport fleet (operational life, types etc.) used by contract carrier etc.

Nowadays standard values are not available to use them for realistic comparison of costs for specific types of techniques (mainly fuel consumption e.g. litres per 100 kilometres), maintenance and repair costs in dependency on machine's operational life, expected costs on pneumatic tyre per km etc. The contemporary valid directive (ordinance) is derived from contract carrier's real costs (i.e. it does not take into account optimal value of specific indicator in dependency on real operational conditions) and from selected operational indicators. The resulting reality can be seen as a generalization of mutual objective comparison of transit performance price. This fact consequently brings inadequate reimbursement of proven losses to contract carrier caused above mentioned objective factors (population density etc.).

According to carried out analysis of fuel consumption it is evident that influence of operational conditions should take into account:

- a) superelevation of a road on transit line;
- b) fluency of drive done by number, distance of bus stops, curves etc.;
- c) fluency of drive done by traffic congestions;
- d) differences of vehicle's occupancy;



e) atmospheric conditions – outside temperature;

f) meteorological conditions (rain, snow etc.);

Proposed methodology tries to eliminate driver's impact on fuel consumption. The final proposal of methodology should enable to calculate differences of fuel consumption directly but with the use of supporting and necessary data inputs. The methodology will take into accounts issues from above mentioned list a – d.

Ad. e) *atmospheric conditions* – outside temperature. This issue will be corrected by coefficient that will be determined by analogical way i.e. carriers' data analysis.

Ad. f) *meteorological conditions* – research team proposes to take these data as insignificant. This insignificance is based on research team's experience done by many years' work in this specific topic.

### Experimental arrangement

The **instantaneous and cumulative** of specific vehicles' **fuel consumption** on specific routes is possible to measure by these ways.

Direct measurement of fuel consumption

**1a. External fuel-meter** is mounted into the combustion engine's fuel system during the whole time of measurement.

This way of measurement is labour-intensive (mounting works) and contemporary vehicles' engine does not usually enable them. If it is possible then these mounting works are linked with complicating impacts on engines' fuel system. Even more high probability of fuel pressure change (usually decrease) exists here. This change could influence as an engine's power parameters as a fuel consumption. Emission production will be influenced consequently as well.

#### **1b. Onboard-meter of fuel consumption**

Onboard-meter of fuel consumption is usually based on the principle of instantaneous values' determination of fuel consumption linked with the time duration of injection and injection pressure. These data are processed by the onboard computer and output can be presented as instantaneous fuel consumption in litres per 100 km, average fuel consumption in litres per 100 km eventually hour consumption. These data can be obtained from a vehicle's producer (data

protocol of CAN-BUS) with the use of appropriate reading equipment (operating unit or directly CAN-BUS). The advantages of this data obtaining way are (if we neglect accessibility of protocols) lower labour-intensity and namely non-existence of possibilities to influence a vehicle's fuel system. From the point of research aims and following applications is necessary to remark that the use of onboard-meter has several problematic aspects i.e.:

- If the measurement is carried out in mode "directed by onboard computer", the measurement is not independent and its results can be modified by the computer on purpose;

- If the measurement is carried out every ride must be mapped by the specific vehicle type and it performs very expensive and laboured way of data collecting;

- Every new vehicle involved into the current fleet and lines requires new measurement of the whole system and its appraisal.

Indirect measurement of fuel consumption

**2a. Dynamics of drive is measured** on specific routes and for calculation of instantaneous and cumulative fuel consumption are used:

- Mechanical characterisation of vehicle's specific type;
- Fuel characteristic of vehicle's specific type.

This way of measurement is approximately as precise as the one carried out with fuel-meter according the column **1a.** or **1b.** and it is characterised by the following properties:

- The advantage of this way is that it not necessary to mount the fuel-meter into the measured vehicle neither mechanically on the fuel system (1a) nor electronically to the onboard computer (1b);
- The advantage is quite independent measurement, e.g. with a support of GPS, and without any link with operational data of vehicle;
- The disadvantage is that the knowledge of vehicle mechanical and fuel consumption characteristics of every measured vehicle is needed. It possible to obtain these characteristics from homologation protocols but it must be arranged on the basis of a conditional

- agreement with the vehicle's producer;
- But still it is necessary to drive by every bus line by specific type of vehicle and during this operation is measured fuel consumption in real time.

**2b. Dynamics of drive is modelled** on specific routes and instantaneous or cumulative fuel consumption is used for this calculation:

- Mechanical characteristics of specific vehicle type;
- Fuel system characteristics of specific vehicle type;
- Transport infrastructure (road) characteristics of specific route;
- Characterisation of traffic regulations and drive conditions specific route.

This way is radically different in quality in comparison with former procedures especially in the meaning that prevailing part of mechanical and organisational activities is shifted on computers' processing. This solution enables to determine operatively a fuel consumption of any new type of technically defined vehicle for any technically defined bus line within minimal time and minimal work difficulties.

Operating methodology of selected fuel consumption determination

From the point of above listed possibilities the fuel consumption measurement is solved above mentioned topic **2a** in this part of specified research. It is the determination way of fuel consumption based on measurement of driving vehicle dynamics on specific routes of chosen bus lines. The solution of the topic requires:

- theoretical analysis;
- proposal of realisation methodology;
- laboratory assessment of methodology;
- design of measuring assessing software;
- experimental vehicles' drives;
- sequent correction of software;
- determination of limits for practical use of obtained results.

### Basic properties of computing software

In the frame of research new software was wrote to use it for an indirect measurement of fuel consumption with a support of driving vehicle's dynamics data and their analysis. Input data of the software applied in line buses are:

Vehicle's mechanical characteristics that involves

- engine's parameters of torque and power in dependence on revolutions;
- gear ratio including mechanical losses;
- air resistance and rolling resistance during drive;
- vehicle's mass linked with axles;
- wheels' moment of inertia;
- gears' moment of inertia;
- moment of inertia of every vehicle's moving part.

**Fuel system characteristics** of engine, obtained from producer or by measurement, is three dimensional dependence of specific fuel consumption on power parameters and revolutions

**Vehicle's drive dynamics data**, measured on the specific route with back up of GPS receiver.

The basis of measurement is obtained from a row of positional points of driving vehicle that are determined by northern latitude and eastern longitude (in decimal fractions of angular degree) and by altitude (in meters above sea level). Parameters as vehicle's speed, acceleration, road upgrade or downgrade, road curve radius are derived from this basis.

Remark: practical usage of above described system including calculating algorithms was verified by experiments but with regards to limited range of this paper it is published in a different place of publication.

### Results and discussion

It is evident that it would be more purposeful in the future to be aimed at the task **2b**. i.e. determination of fuel consumption on the basis of dynamics modelling of the drive. It should be carried out for specific routes of bus lines with the use of every above mentioned practical advantage of these applications. Topic **2b**. is only possible to solve when the topic **2a**. would be practically tested and verified and that is the reason why such full attention is devoted to this issue.

It has been proved in former research studies of this paper's authors (Grant of Ministry of transport No. 1F44G/092/120) that it is possible to describe dynamics of driving vehicle by GPS signals with a similar preciseness as with the 3D

acceleration detector. But the use of GPS in comparison with acceleration detector provides more possibilities especially the determination of vehicle's position. It could be expected that the technical development of these satellite systems as GPS or European Galileo is a guarantee for a beneficial utilisation within this research task.

Unfortunately results of received and analysed GPS signals do not have adequate preciseness in shielding spaces. The used programme corrects these disproportions by adjustable level of filtration and missing signals are substituted by linear interpolation. The GPS receiver has one of outputs to evaluate credibility of concrete measured rows of data matrix. It is only necessary to use it and to adjust suitably the limiting condition of filtration. It has been carried out experimentally in the frame of the research task.

## Conclusion

The proposed method is only applied in the output form of instantaneous and cumulative fuel consumption. But it is possible to say that this computing system of fuel consumption is possible to use instead of this purpose for another ones. The system is possible to enrich by emission characteristics defined by similar way and it provides possibilities to obtain driving bus's instantaneous and cumulative emission mass production of single harmful fractions of exhaust gases without any enlarging measurement. This topic is not included with current subsidy system of operation of line buses and even not in this research task. But it is important to be interested in the problem of environmental aspects of fuel combustion. Results of the system like this could be used easily for emission monitoring and consequently for creating of instruments (economic, legislative etc.) that would minimise emission production.

## References

- [1] Project MD ČR č. 1F44G/092/120: Economical, ecological and safety solution of electronic toll system, research reports in years 2004, 2005, 2006, 2007 [in Czech].
- [2] Kadleček, B. Pejša, L.: "Measuring Method on the free rollers for lorries, tractors and special vehicles and its utilization at the emission, fuel consumption and technical

state test, MŠMT Project OC 346 Annual reports 2003, 2004, 2005, TF CUA Prague. in frame European project COST 346.10 : "Emissions and fuel consumption from Heavy duty vehicles.

- [3] Hickman, A. J.: Methodology for calculating transport emission and energy consumption, project report SE/491/98, Transport Research Laboratory 1999.
- [4] Joumard, R.- Sérié, E.: Modelling of cold start emissions for passenger cars INRETS report n° LTE 9931 December 1999, 86 pages.
- [5] Sturm P.J., Hausberger, S.: "Emissions and fuel consumption from Heavy duty vehicles", COST 346 – Final Report, 2005, Graz University of Technology , ISBN-10: 3-902465-48-4, ISBN-13: 978-3-902465-48-1
- [6] Kadleček, B., et al.: "Methods for evaluation and multidisciplinary assessment of transport impacts on sustainable environment" MŠMT Project OC 193 Annual reports 2007, 2008, TF CUA Prague, in frame European project COST 356, "EST - Towards the definition of a measurable environmentally sustainable transport"
- [7] Kadleček, B., Pexa, M., Pejša, L.: The Possibilities of Indirect Emission Measurement of Combustion Engines in: Advances In Automotive Engineering , Volume I, p. 121-131, First edition in Tribun EU 2008, 200 pages, ISBN 978-80-7399-496-9
- [8] Kadleček, B., Pexa, M., Pejša, L.: The Operational Emission Measurement of Combustion Engines in: Advances In Automotive Engineering , Volume I, p. 121-131, First edition in Tribun EU 2008, 200 pages, ISBN 978-80-7399-496-9

## Acknowledgment:

**This paper is supported by:**

- [1] Ministry of Education, Youth and Sports Czech Republic, Project OC193 "Metody hodnocení a multidisciplinární ocenění vlivů dopravy na trvale udržitelné životní prostředí." *Methods for evaluation and multidisciplinary assessment of transport impacts on sustainable environment*, in frame project EU COST 356: "EST -

- Towards the definition of a measurable environmentally sustainable transport“
- [2] Ministry of Transport Czech Republic (project No. CG912-058-520), “Metodika kvantifikace a vyhodnocení environmentálních a bezpečnostních vlivů dopravy”, “*Methodology of quantification and assessment of transport’s environmental and safety impacts*“

## THE MEASUREMENT OF VEHICLES' DRIVE DYNAMICS

BOLESLAV KADLEČEK\*, MIROSLAV RŮŽIČKA, LADISLAV PEJŠA  
Czech University of Agriculture in Prague, 16521 Prague 6 – Suchbátka, Czech Republic,  
Phone: +420 224381111, Fax: +4202-20921361, E-mail: kadlec@tf.czu.cz,  
ruzicka@tf.czu.cz, pejsa@tf.czu.cz

### Abstract

This paper is linked with the paper "THE METHOD OF FUEL CONSUMPTION INDIRECT QUANTIFICATION" that contains the analysis of possibilities in a creating of technical support for municipal authorities' decision making within a bus transit sphere. Specifically it is the partial technical support that deals with the determination of operational costs per fuel consumption. The costs will be used for a modelling and planning purposes. Contract carrier's proven losses should be determined by these activities. The content of this paper is a description of created software algorithm used for selected way of GPS data processing obtained from driving vehicle on specific routes. The basis of calculation is done by measured drive dynamics data of bus line in Prague's public transport.

### Introduction

As example was chosen No. 356 bus line (see Fig. 1. route is drawn by bold red colour line) and the concrete route ensured by Karosa B 951 E bus, tare weight 10,2 tonnes, engine Iveco Cursor F2 B with power 180 kW. The route of this bus line is located from terminal bus stops Dejvická to Statenice. The route has partially urban and suburban character.

### Experimental arrangement

*Remark: Following text in italics are comments*

Marking of quantities

$M^o$  is matrix of directly measured data

- Time increment is 1 second;

- Measured zero values in a tunnel, or by different way of shielded spaces are **definitely deleted** i.e. adequate rows of data matrix do not exist anymore;

- The condition for above mentioned deleting is determined by the instantaneous value of measuring preciseness that is provided by GPS receiver as the one of its outputs.

$t^o$  [s] is real time, measured in seconds from the midnight of specific day, every other measured quantity is dependant on real time.

$N^o$  [°] are directly measured values of northern latitude in degrees (6 decimal places).

$E^o$  [°] are directly measured values of eastern longitude in degrees (6 decimal places).

$H^o$  [m] are directly measured values of altitude in meters above sea level.

$M_a$  is matrix of processed measured data

- Linearly interpolated data in tunnel or other shielded space;

- Calculation of others derived quantities from data  $M^o$ ;

- Eventual "smoothing" of data anomalies is necessary in less precise measurement of altitude.

$t^o$  [s] is real time in seconds from the beginning of measured route.

$N$  [°] is northern latitude in degrees (6 decimal places).

- in a tunnel or shielded spaces missing signals are linearly interpolated (not smoothed).

$E$  [°] is eastern longitude in degrees (6 decimal places).

- in a tunnel or shielded spaces missing signals are linearly interpolated

$H$  [m] is altitude (m. s. l.)

- in a tunnel or shielded spaces missing signals are linearly interpolated and consequently statistically processed by the method of smallest squares in moving time window (follows term "smooth data" only)

$dH$  [m/s] is from quantities  $H$  and  $t^o$  derived increment of altitude per increment of time, caused by road upgrade in the direction of drive.

$v'$  [km/h] is the vertical projection of a vehicle's velocity, determined from  $N$  and  $E$ .

$v$  [km/h] is the velocity in a vehicle axis, determined from  $v'$  and  $dH$ .

$a$  [m/s<sup>2</sup>] is acceleration in a vehicle axis, determined as the increment of velocity per increment of time.



**Figure. 1** Map of measured line



**Table 1.** Measured values matrix sample

<b>M° = sample of directly measured data matrix</b>										
	Number of measurement	t° [s] time from mid-night	Date	Hour, minute, second	N° [°] Degrees northern latitude	E° [°] Deg- rees Eastern longitude	H° [m] altitude	Bus line number	Occupancy	
	0	1	2	3	4	5	6	7	8	9
103	105	27362	5112008	73602	50.101133	14.395233	221	356	20	0
104	106	27363	5112008	73603	50.101117	14.395233	221	356	20	0
105	107	27364	5112008	73604	50.1011	14.395233	222	356	20	0
106	108	27365	5112008	73605	50.1011	14.395233	221	356	20	0
107	109	27366	5112008	73606	50.101083	14.395233	222	356	20	0
108	110	27367	5112008	73607	50.101067	14.395217	221	356	20	0
109	111	27368	5112008	73608	50.10105	14.395217	221	356	20	0
110	112	27369	5112008	73609	50.101017	14.3952	221	356	20	0

Next there are data processed from matrix M° by linear interpolation of measured quantities, their eventual by-passes GPS signal's

missing spaces and saved into the data matrix Ma:

**Table 2.** Overview of measured data processing

Math. procedure	Saving into matrix Ma	Name of quantity
	$Ma_{i, 0} := t_i$	$t_i$ [s] is real time from the start of measurement of driven route with the substitution of missing GPS signal
$N_i := \text{interp}(t^\circ, N^\circ, t_i)$	$Ma_{i, 1} := N_i$	$N$ [°] are not smoothed and by linear interpolation by-passed values of northern latitude, determined from GPS.
$E_i := \text{interp}(t^\circ, E^\circ, t_i)$	$Ma_{i, 2} := E_i$	$E$ [°] are not smoothed and by linear interpolation by-passed values of eastern longitude, determined from GPS.



Math. procedure	Saving into matrix Ma	Name of quantity
$H_i := \text{linterp}(t^\circ, H^\circ, t_i)$	$Ma_{i,3} := H_i$	$H$ [m] are not smoothed and by linear interpolation by-passed values of altitude, determined from GPS.
	$Ma_{i,4} := M^\circ_{i,7}$	number of bus line
	$Ma_{i,5} := M^\circ_{i,8}$	Total number of persons on bus in real time.
	$Ma_{i,6} := M^\circ_{i,9}$	Number of children from the total persons on bus.

**Table 3.** Sample from matrix used for calculation of necessary data, processed by interpolation in case of missing GPS signals

t [s] time from the measurement start	N [°] Degrees northern latitude	E [°] Degrees Eastern longitude	H [m] altitude	bus line number	Occupancy	
					Total persons	children
0	1	2	3	4	5	6
105	50.1011	14.395233	222	356	20	0
106	50.1011	14.395233	221	356	20	0
107	50.101083	14.395233	222	356	20	0
108	50.101067	14.395217	221	356	20	0
109	50.10105	14.395217	221	356	20	0
110	50.101017	14.3952	221	356	20	0
111	50.101	14.395183	221	356	20	0
112	50.101	14.395183	222	356	20	0
113	50.1009	14.395033	221	356	20	0

### Calculation of vertical vehicle velocity

According to the fact that altitude data measured by GPS have a larger dispersion and it possible to expect small continuous changes in road upgrade, researchers take as sensible to smooth these altitude spots  $H$  and next the

vertical velocity should be determined with including interpolation in shielded spaces or tunnels. Road upgrade is contented in this vertical velocity and it not quantified independently.

$Hh := \text{ksmooth}(t, H, 5)$	"ksmooth(t,H,x)" use subroutine that statistically process values $H$ by the method of smallest squares in moving time window $x=5$ into „smoothes“ values $Hh$ .
---------------------------------	---

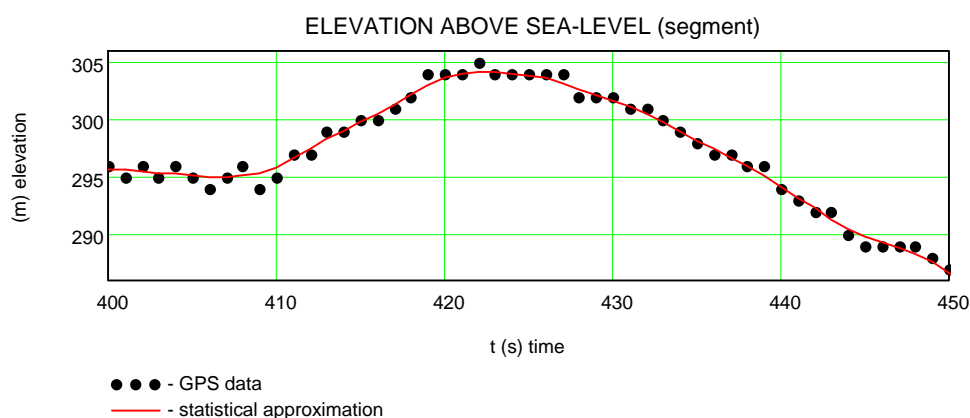


**Figure 2.** Sample from statistically processed data of vehicle's altitude

$dH_i := \frac{Hh_{i+1} - Hh_{i-1}}{2}$	$dH_i$ [m/s] is increment of altitude in meters per second i.e. vertical velocity during vehicle's drive in the $i$ -th step of measurement.
---	--

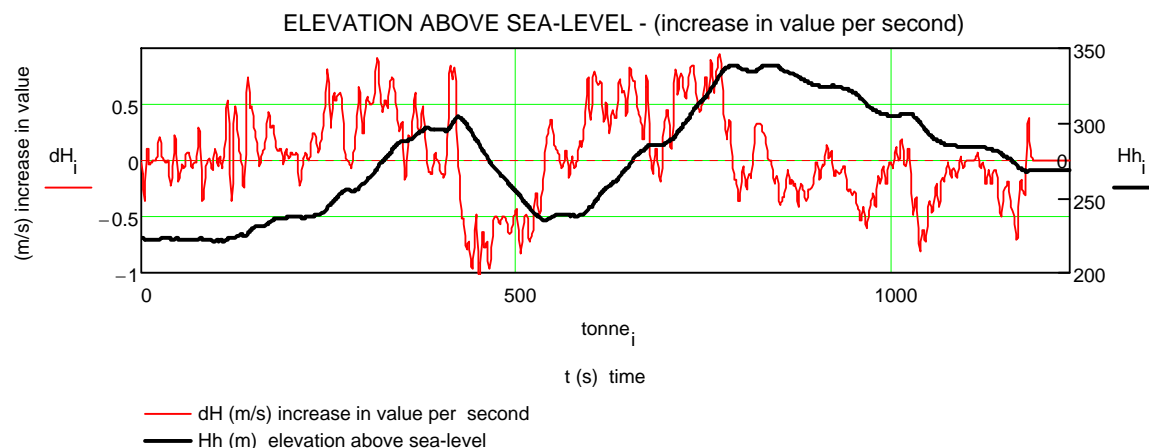


**Figure 3.** Increment of altitude in meters per second (vertical velocity) during vehicle's drive.

#### Calculation of vehicle's horizontal velocity

$cN := \frac{40000}{360}$	$cN = 111.111111$ [km/degree] is constant for recalculation in kilometres per degree in the direction <b>north –south</b> , valid on any meridian. This constant $cN$ is used in $i$ -th step of measurement to multiply difference of two parallels: $N_{i+1} - N_i$ in degrees and their distance is obtained: $dSN = (N_{i+1} - N_i) cN$ in kilometres.
$cE(N) := \cos\left(\frac{\pi}{180} \cdot N\right) \cdot \frac{40000}{360}$	$cE(N)$ [km/degree] is constant of recalculation in kilometres per degree, in dependence on parallel $N$ in degrees, in direction <b>east-west</b> . This constant $cE(N)$ is used in $i$ -th step of measurement to multiply difference of two meridians: $E_{i+1} - E_i$ in degrees and and their distance is obtained: $dSE_i = (E_{i+1} - E_i) \cdot cE(N_i)$ in kilometres.

Remark : On any meridian (in direction north-south), is:

- one millionth of degree = 0.111111 m (rounded 11 cm),
- one ten thousandth of degree = 1.11111 m (rounded 11 m)

The same is valid for 0-th parallel (equator), it means that with growing degrees of

parallels the presented distance decreases. Prague's parallel with 50,14 degrees is:

- one millionth of degree = 0.071420846 m (rounded 7 cm)
- one ten thousandth of degree = 0.71420846 m (rounded 7 m)

$ds'_i := 1000 \cdot \sqrt{[(N_{i+1} - N_i) \cdot cN]^2 + [(E_{i+1} - E_i) \cdot cE(N_i)]^2}$	$ds'_i$ [m/s] is vertical projection increment of drive in the $i$ -th increment of time.
$v'_i := 3.6 \cdot ds'_i$	$v'_i$ [km/h] is vertical projection of vehicles' velocity in $i$ -th increment of time, not directly measured but calculated from the consequences of geodetic coordinates $N$ a $E$ .
$ds_i := \sqrt{(ds'_i)^2 + (dH_i)^2}$	$ds_i$ [m/s] is increment of drive in vehicle's axis in $i$ -th increment of time.
$v_i := 3.6 \cdot ds_i$	$v_i$ [km/h] is velocity in vehicle's axis in $i$ -th increment of time.
$vh := ksmooth(t, v, 5)$	$"ksmooth(t, v, x)"$ is subroutine that process quantity $v$ statistically by method of smallest squares in moving time window $x=5$ „smoothed“ quantities $vh$ .

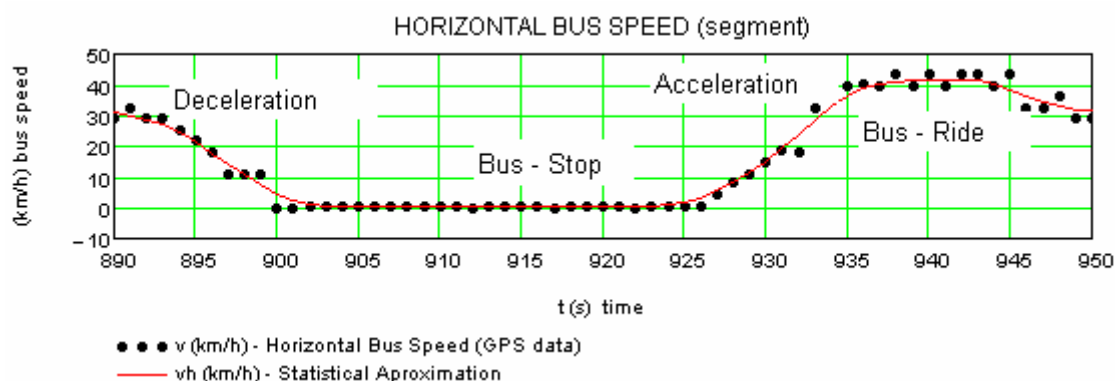


**Figure 4.** Sample from a file of calculated and statistically processed data of horizontal velocity of driving vehicle in detail of measured route fraction.

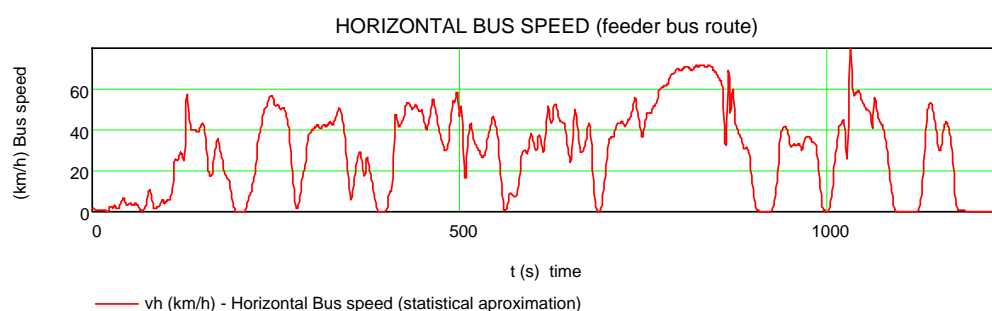


**Figure 5.** Calculated and statistically processed data of axis velocity of driving vehicle in detail of measured route.

## Results and discussion

In the case of missing GPS signals it would be possible to use obtained data from an acceleration sensor but this solution is not applied in this research. It is evident that the need of acceleration sensor is not expected for a use in the future and the former studies have submitted a proof of sensor's inutility. Calculation results of high quality GPS data (any shielding) were compared with the ones deleted in time window. Practically the vehicle really was driven on a selected route and in the same time virtually was driven on the same route in a tunnel. When the need of acceleration sensor in the future would be found out it does not cause any problem to apply it. The GPS signal processed in the vertical projection of vehicle's velocity brings problems. Interpolation used under shielded conditions produces results that do not provide quite true information. That is why the vehicle's velocity was calculated just from geodetic coordinates **N** and **E** that are linearly interpolated under shielded conditions. Operationally calibrating altimeter has not been used yet in the form of

independent equipment during this phase of a research. The main reason of it is that the operational application of the proposed method expects a use of inputs in the form of known altitude figures of driven roads. Received and analysed GPS signals do not have always required preciseness under shielded conditions. That the reason why these signals are filtrated on some adjustable level by proposed software and missing signals are substituted (by-passed) by an linear interpolation. GPS receiver already has as one of its outputs the evaluation of credibility of concrete measured rows of data matrix. It is necessary to use this property only and to determine the limiting level of filtration. These steps were done experimentally during this phase of the research.

## References

See paper "THE METHOD OF FUEL CONSUMPTION INDIRECT QUANTIFICATION"

## THE CALCULATION OF FUEL CONSUMPTION IN RELATION WITH VEHICLES' DYNAMICS

BOLESLAV KADLEČEK<sup>1\*</sup> - MIROSLAV RŮŽIČKA<sup>2</sup> - LADISLAV PEJŠA<sup>3</sup>

<sup>123</sup>Czech University of Agriculture in Prague, 16521 Prague 6 – Suchbát, Czech Republic,  
Phone: +420 224381111, Fax: +4202-20921361, E-mail: kadlec@tf.czu.cz,  
ruzicka@tf.czu.cz, pejsa@tf.czu.cz

### Abstract

This paper is linked with papers “THE METHOD OF FUEL CONSUMPTION INDIRECT QUANTIFICATION” and “THE MEASUREMENT OF VEHICLES' DRIVE DYNAMICS”. It deals with the partial technical support during the determination of fuel consumption costs for purposes of modelling and planning of contract carrier's proven financial losses. The content of this paper is focused on the sample derived from designed and used software i.e. chosen way of direct measurement of driving vehicle's dynamics on specific routes with the backup of GPS and followed the indirect measurement of fuel consumption.

### Introduction

Characteristics of specific type of vehicle's mechanic parameters were used for this calculation. Measured data of drive dynamics for

the bus Karosa B 951 E, tare weight 10,2 tonnes, engine Iveco Cursor F2 B with power 180 kW were used for the calculation.

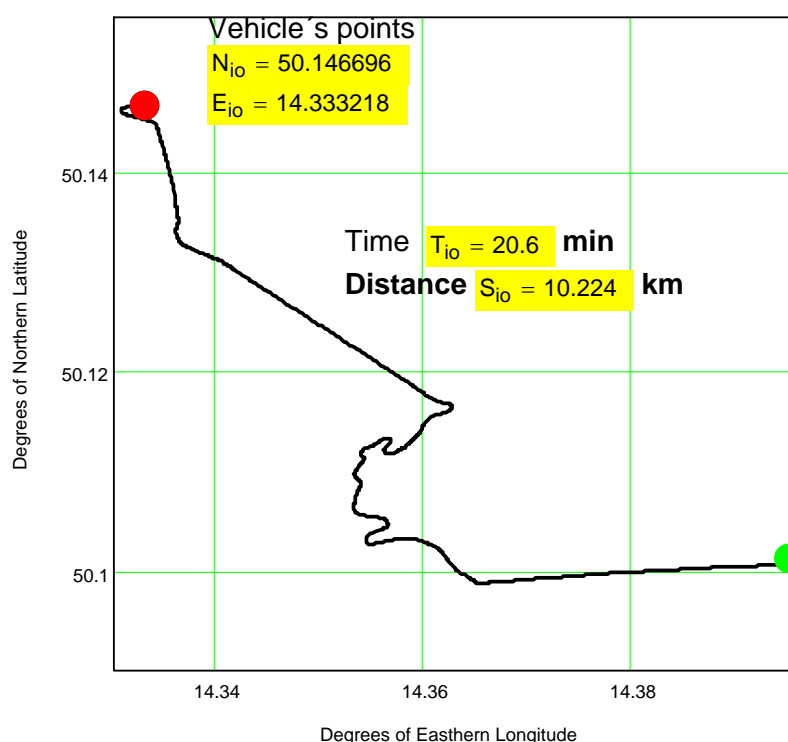


**Figure 1.** The route of analyzed drive passed by bus Karosa B 951 E, in coordinates GPS

The vehicle is positioned in the target bus stop (red point) with coordinates 50,146696 degrees of northern latitude and 14,333218

degrees of eastern longitude. The driven distance was 10,224 km per 20,6 minutes from the starting bus stop.

## Experimental arrangement

Calculation of a horizontal acceleration

Vehicle's horizontal velocity (without gravitational fraction) is determined from statistically processed GPS data.

$a_i := \frac{vh_{i+1} - vh_{i-1}}{7.2}$	$a$ [ $m/s^2$ ] is an acceleration in the vehicle's axis, without gravitational fraction, determined from GPS.
--	--

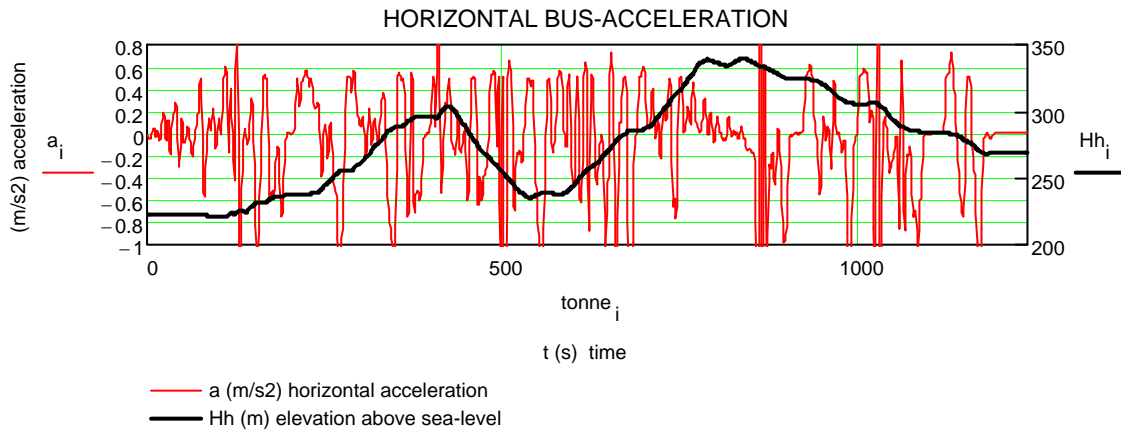


**Figure 2.** Horizontal acceleration of driving vehicle on the whole measured route

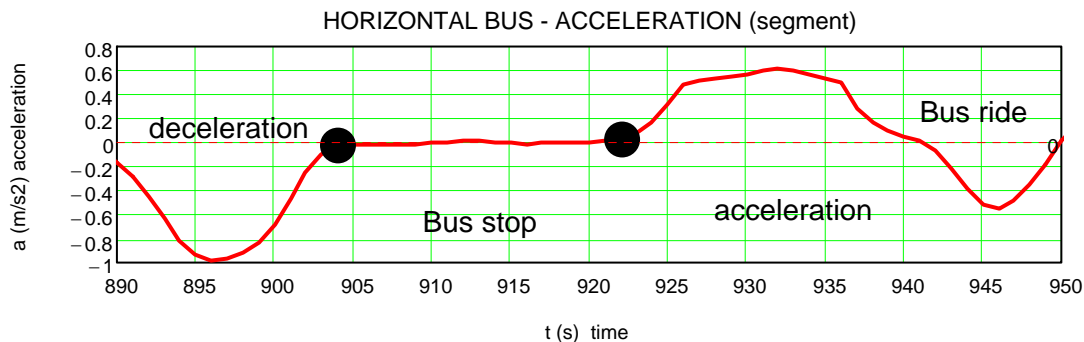


**Figure 3.** Horizontal acceleration of driving vehicle (chosen detail)

## 1.2 Calculation of the acceleration and gravitational power

The acceleration power is linked with a vehicle's horizontal acceleration. Gravitational power is in relation with the vehicle's change of

potential energy due to road up-grade. The total power on vehicle's wheels consists of aerodynamic resistance and rolling resistance fractions that would be determined independently.

$Pa_i := \frac{Ga}{1000} \cdot \left( a_i \cdot \frac{vh_i}{3.6} + 9.807 \cdot dH_i \right)$	$Pa$ (kW) is power dependant on vehicle's acceleration and change potential energy. Acceleration " $a$ " is measured and calculated nevertheless it does not include the gravitational part in itself. To determine the required power it necessary to add the gravitational part. The product of gravitational constant $9.807$ ( $m/s^2$ ), mass $G$ (kg) and velocity $dH$ (m/s) of vehicle's vertical up-grade, corrected by constant 1000 are summoned.
--	--

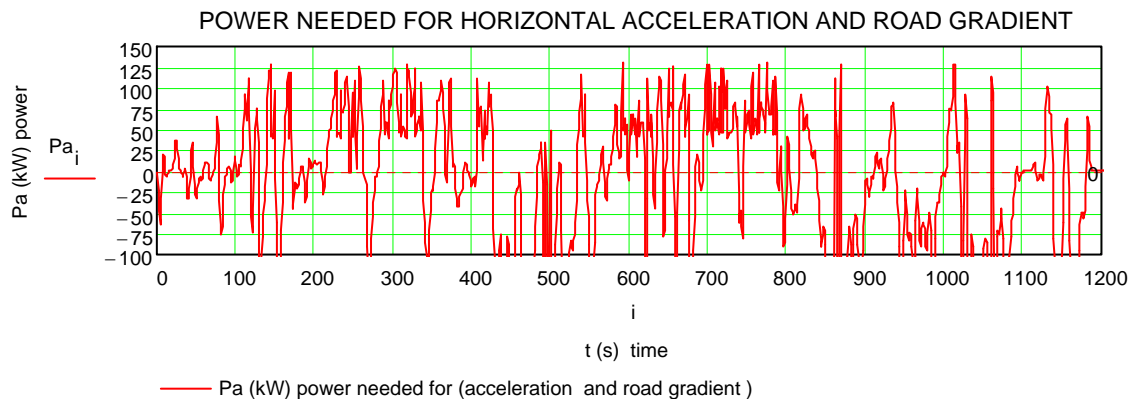


**Figure 4.** Acceleration and gravitational power of vehicle on the whole measured route.

$La := \sum_{i=0}^{\text{last}(Pa)}  Pa_i $	<p><b>La (kJ)</b> is from GPS determined summa of acceleration and potential energy that was absorbed (+), or returned (-) on a route of vehicle. It deals with energy balance i.e. absorbed and returned that is a part of vehicle's processes as acceleration and deceleration or up-grade and down-grade. This energy flow is taken into account without any influence of aerodynamic and rolling resistances.</p>
---	---

Presented energy balance performs just a smaller part, usually less then 20% of total energy that is necessary for the vehicle's drive in usual section of a road. From the point of a view

of driving vehicle's balanced energy the influence of preciseness to determine gravitational and acceleration energy can be seen as less important.

$S := \frac{\text{sumace}(ds')}{1000}$	<p><b>S<sub>i</sub> [km]</b> is vertical projection of driven route from the beginning of measurement in i-th time increment, where sum (ds') is done by the adequate subroutine.</p>
--	---

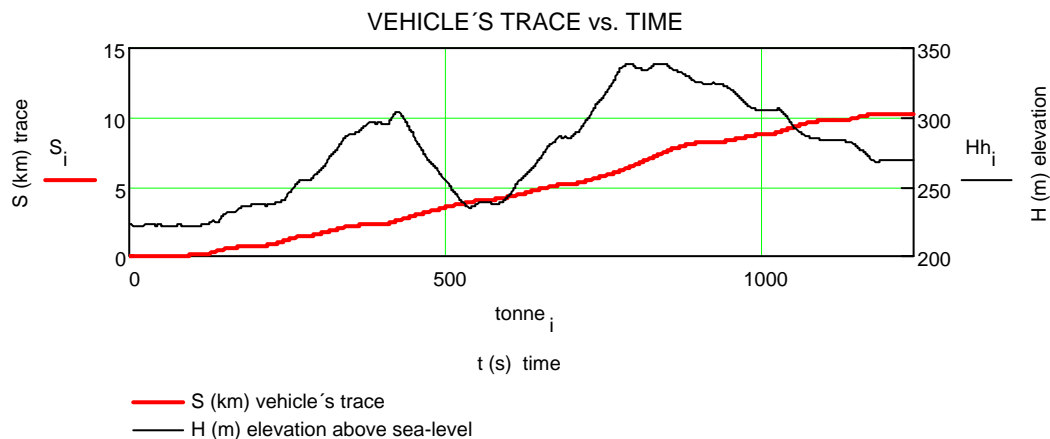


**Figure 5.** Distance and altitude on the whole measured route.

### 1.3 Calculation of aerodynamic and rolling resistances

Characteristics of aerodynamic and rolling resistance during vehicle's drive, bus Karosa B 951, that were determined from available

technical documents but their preciseness is not proven up to now. In the following research these characteristics will be refine on by the method of analysis of vehicle's coasting velocity in a dependence on time and distance.

$Fv(v, vo) := \rho \cdot cx \cdot SP \cdot \frac{(v + vo) \cdot  v + vo }{-2 \cdot 3.6^2}$	<p><b>Fv [N]</b> is force of aerodynamic resistance; <b>v [km/h]</b> is velocity of vehicle; <b>vo [km/h]</b> is velocity of head wind;</p>
--	---



	<p><b>SP</b> [m<sup>2</sup>] is square of vehicle's head;  <b>cx</b> is coefficient of aerodynamic resistance;  <b>ρ</b> = 1,2929 [kg/m<sup>3</sup>] is air density.</p>
$\mathbf{Fr}(v) := 9.81 \cdot \mathbf{Ga} \cdot \mathbf{fr}(v)$	<p><b>Fr(v)</b> [N] is force of rolling resistance during the velocity <b>v</b> [km/h];  <b>Ga</b> [kg] is actual mass of vehicle;  <b>fr(v)</b> is coefficient of rolling resistance during the velocity <b>v</b>.</p>
$\mathbf{Fvr}(v, vo) := \mathbf{Fv}(v, vo) + \mathbf{Fr}(v)$	<p><b>Fvr(v)</b> [N] is summa of aerodynamic and rolling resistance.</p>

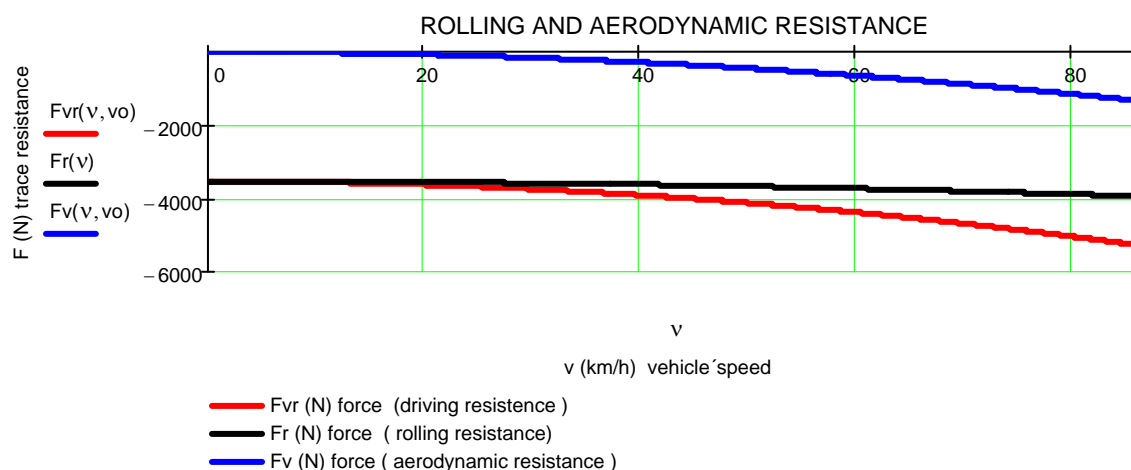


**Figure 6.** Characteristics of aerodynamic and rolling resistances bus Karosa B 951 E

Calculation of power on vehicle's wheels

$\mathbf{Pvr}_i := -\frac{\mathbf{Fvr}(\mathbf{vh}_i, \mathbf{vo}) \cdot \mathbf{vh}_i}{3600}$	<p><b>Pvr<sub>i</sub></b> [kW] power on vehicle's wheels; determined from aerodynamic and rolling resistance during the velocity <b>vh</b> [km/h] and head wind velocity <b>vo</b> [km/h] (positive value of head wind acts against the vehicle's velocity).</p>
$\mathbf{Ph}_i := \mathbf{Pvr}_i + \mathbf{Pa}_i$	<p><b>Ph<sub>i</sub></b> [kW] is total power on vehicle's wheels</p>

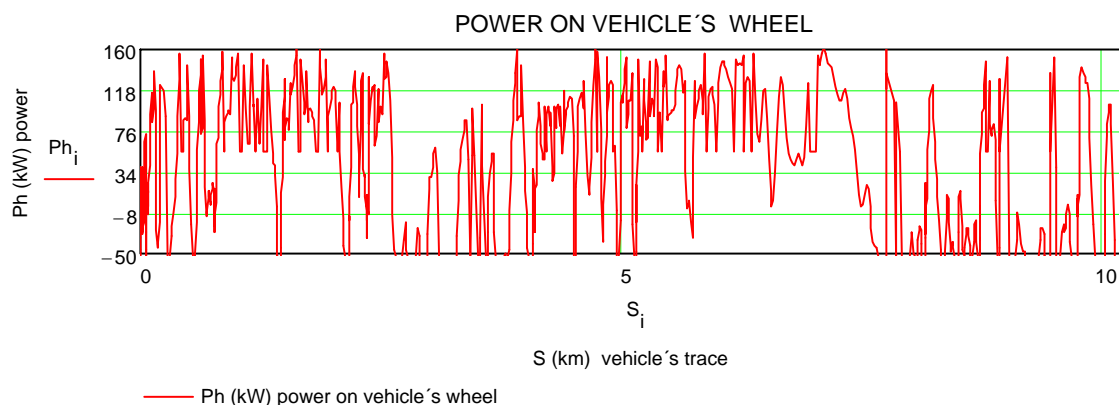


**Figure 7.** Power on bus' wheels on the measured route

## Results and discussion

Characteristics of fuel consumption informs about consumption per one hour of vehicle's drive during defined driving mode.

Defined driving mode:

- driving power  $P_h$  (kW) is developed to overcome all driving resistances on every vehicle's driving wheel;
- still wind conditions are expected;
- optimal selection of gears is expected.

**Remark 1:** In case of the above defined driving mode vehicle's technical conditions can influence the final calculation of an emission mass and fuel consumption nevertheless driver's activities do not influence it.

**Remark 2:** Really the shifted gear is usually different from the optimal one and the quantity of deviation can be included into the calculation as an experimental correction. In this case not only vehicle's technical conditions but even quality of driver's activities influences the final calculation of an emission mass. It supposes knowledge of instantaneous shifted gear but it is possible to solve with support of engines' revolutions sensor.

### Remark 3:

If a wind influence should be included the specific emission characteristics will be modified by wind direction and velocity just in at instantaneous time moment. But the correction like that would require the equipping of measured vehicle by wind velocity sensor. This solution is not recommended in the research project from these reasons:

\* When an emission mass production is determined during several days of vehicle's operation it can be supposed that changing influences of wind direction and velocities will be statistically balanced. Finally this balance causes that this natural phenomena (wind) will not affect financial expression of impacts. Different situation could be in regions with prevailing winds in one direction e.g. sea coast.

\* The permanent fixing of wind velocity detector on a vehicle should not cause any technical or economic problems. It can be seen as the easy and cheap action but the detector's use could cause problems in dependence on vehicle's onboard computer.

\* Just in a case when the GPS is used to measure the instantaneous vehicles' mass a knowledge of wind direction and velocities is needed.

These three quantities are: power on vehicle's driving wheels, vehicle's velocity (circumferential velocity of roller's surface) and a shifted gear. It is possible to say that the characteristic is relatively complicating nevertheless it is possible to obtain it by a realistic measurement. A mathematical approximation was used to substitute temporary these characteristics i.e. a basic four dimensional characteristics must be transformed in two dimensional one that performs hour fuel consumption (or emission production) in dependence on vehicle's power on wheels only. The used transformation unfortunately brings less preciseness app. 5% and it is possible to expect that this could happen in the case of bus or lorry.

The more detailed analysis, according to the above mentioned procedure, was carried out with Skoda – Octavia 2.0 TDI PD.

Therefore the above mentioned two dimensional fuel consumption characteristics, obtained by processing usually available technical data of Karosa B 951 E bus, was used. As soon as technically possible this type of bus or other ones will be tested on the currently built roller tester in the Faculty of engineering, Czech University of Life Sciences Prague and determination of characteristics will be more accurate.

It was found out that the fuel consumption in the target bus stop (blue point on Fig. 10) was: total 3,4 litres of fuel, average consumption 33,3 litres per 100 km and average unit consumption 311 grams of fuel per 1 kWh, absorbed on driving wheels.

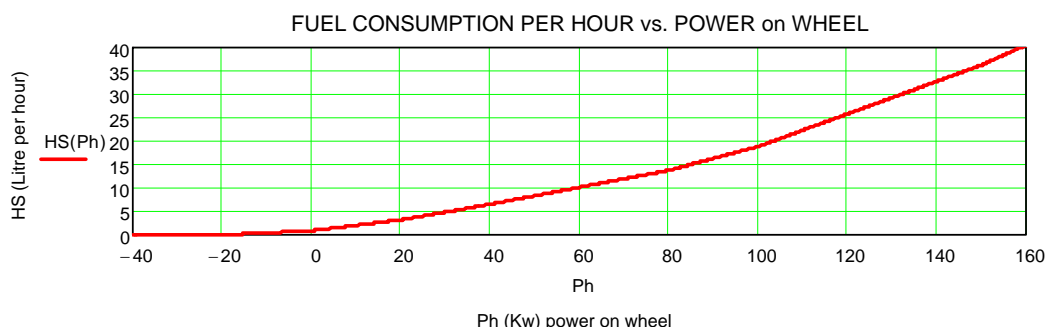


**Figure 9** Preliminary valid simplified fuel characteristics in the form of HS fuel consumption per hour of Karosa B 951 E bus, in dependence on Ph power on vehicle's wheels, carried out during optimal shifting of gears.

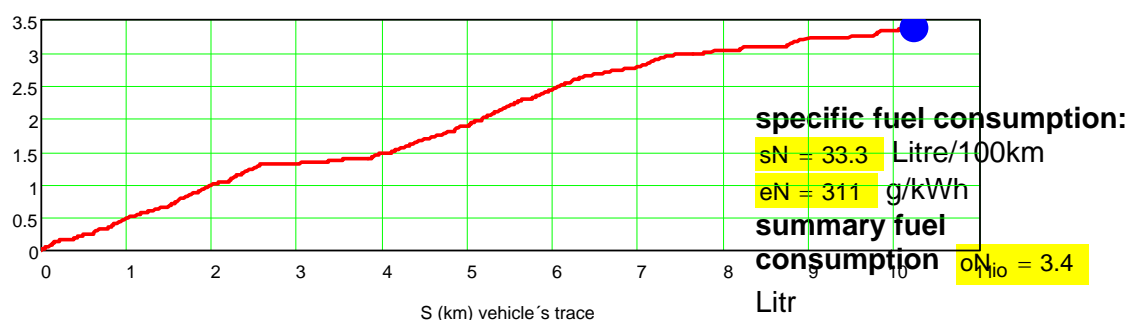


**Figure 10** The increase of fuel consumption during analysed drive of Karosa B 951 E bus.

## Conclusion

The proposed method of an indirect measurement of vehicles's fuel consumption, specifically buses, is based on the measurement of parameter sequences of drive dynamics i.e. vehicle's velocity, acceleration and road upgrade with constant vehicle's weight. From these parameters are derived instantaneous and cumulative values of fuel consumption with the use of known mechanical and fuel characteristics of the specific vehicle type. The fuel characteristics can be specified as 3D dependence of the instantaneous fuel consumption on vehicle's instantaneous realized power and on engine's revolutions with an adequate optimal gear grade at instantaneous drive dynamics. The principle of this method can be simplified in this way - if revolutions are not measured then it is not necessary to be linked with the onboard computer and it is supposed that a driver ever selects the optimal revolutions. It is evident that the presented method of fuel consumption is valid for the case if a drive is

carried out by a high quality driver (it is necessary to "gently control" a gas pedal to keep revolutions within optimal limits).

## References

See paper "THE METHOD OF FUEL CONSUMPTION INDIRECT QUANTIFICATION"

## STALK MATERIAL ORIENTATION IN BIOMASS COMPOSITE BRIQUETTES

AIVARS KAKITIS, IMANTS NULLE\*, DAINIS ANCANS

Latvia University of Agriculture in Jelgava, LV – 3001, Jelgava, J.Cakstes bulv. 5, Latvia,

Phone: +371 63080701, Fax: +371 63020762, E-mail: imants.nulle@llu.lv

### Abstract

To guarantee the quality of biomass (straw, reed) briquettes in the handling and usage processes, sufficient density and durability of briquettes should be provided. For the briquettes density standards determined the value  $\rho > 1.0 \text{ g}\cdot\text{cm}^{-3}$ . The mentioned value has been obtained in densification of straw and reed stalk material particle compositions with peat (particle size  $< 3 \text{ mm}$ ), if peat proportion exceeds 35%. Calculated energy consumption for common reed cutting to sizes less than 3 mm was  $> 7 \text{ kJ kg}^{-1}$  but for size 20 mm it was approximately  $1 \text{ kJ kg}^{-1}$ . The goal of the investigation was to obtain the necessary density and durability of briquettes of larger biomass particles by arranging them. The orientation of straw or reed stalks had to promote binding by the pressing operation. Crushing force dependence on particle size for arranged structure briquettes is stated in laboratory experiments. In comparison with unarranged structure briquetting crushing force for arranged structure briquettes increases on average from 3 to 5 times. Addition of 30% peat to coarse chopped straw or reed arranged structure briquettes increases density to recommended value  $1.0 \text{ g}\cdot\text{cm}^{-3}$ . Briquettes from flattened reed stalks showed even better results. The density of briquettes was  $> 1.0 \text{ g}\cdot\text{cm}^{-3}$  without peat additions, and specific splitting force was 1.3 times higher than for not flattened stalk briquettes.

**Keywords:** stalk materials, biomass conditioning, biomass briquettes, durability

### Introduction

The main mechanical properties of the standardized biofuels in form of briquettes are density and mechanical strength. These parameters depend on the used material, its structure, water content, compacting pressure and arrangement of particles in briquetting die. The basic standards for the briquettes are the Austrian ÖNORM M 7135 and German DIN 51731. These documents are valid for wood and bark extrusions. For the briquettes density standards determined the value  $\rho > 1.0 \text{ g cm}^{-3}$ . This value had been used for evaluation of herbaceous material densification results.

As investigation results it is stated, that density  $1.0 \text{ g cm}^{-3}$  has been obtained in compaction of wheat straw stalk material particle compositions with peat, if peat proportion exceeds 35%. Pressing energy consumption for briquetting of chopped common reed and straw stalk material particles (size 1 – 2 mm) with peat shows maximal value  $\sim 40 \text{ kJ kg}^{-1}$ .

To guarantee the quality of biomass briquettes in the handling and usage process, sufficient durability of briquettes will be provided. The mechanical strength of briquettes and its durability can be characterized by different parameters. For industrial durability

tests several standardized methods are recommended. Briquettes and pellets should be tested mechanically for abrasion test according to the standards: EN 15210-1:2010 Solid biofuels – Determination of mechanical durability of pellets and briquettes – Part 1: Pellets. EN 15210-2:2010 Solid biofuels – Determination of mechanical durability of pellets and briquettes – Part 2: Briquettes. International standard ISO 616:1995(E) specifies a method for determining durability of coke by shatter test.

For laboratory experimental testing of briquettes shear strength and crushing strength should be examined. Shear strength tests were performed for determining ultimate shear tests for briquettes with particles size less than 3mm. Ultimate shear stress was obtained in direction perpendicular of briquetting direction [1].

Maximal values of ultimate shear stress 1.5 MPa for pure peat (100%) briquettes had been obtained in durability investigations. Ultimate shear stress  $\sim 0.27 \text{ MPa}$  was obtained for coarse chopped (particles 2-3 mm) reed briquettes and for rape straw.

Wood chip briquettes with particle size less than 2 mm let obtain ultimate shear stress  $> 0.6 \text{ MPa}$ , but the same durability of reed briquettes can be obtained with particle size less

than 0.5 mm, ultimate shear stress 0.6 MPa for the straw briquettes can be obtained only by adding ~50% of peat.

To reduce cutting energy of stalk material it is advisable to use roughly shredded material. Experiments carried out in Laboratory of Mechanics at Latvia University of Agriculture showed decreasing of cutting specific energy from 20 to 40 times for increasing length of particles from 1 mm to 100 mm.

## Materials and methods

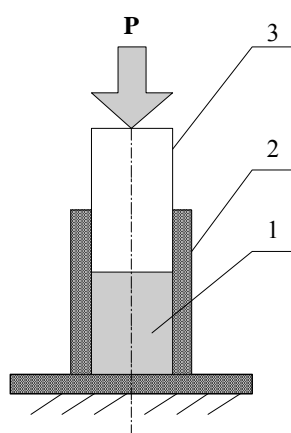


Fig. 1. Scheme of densification  
1 – stalk material composition,  
2 – closed die, 3 – piston

Length of straw and reed stalks was 30, 60 and 100 mm. Experiments was carried out with unarranged straw and reed stalks, arranged straw and reed stalks and with flattened and arranged reed stalks. Stalk flattening was performed with two rotating cylinders (Fig. 3).

Stalk material particles with certain length was arranged in closed die as it is presented in Fig. 2b. Arranged particles were located in direction of longitudinal axe of die. Displacement between ends of particles in different layers was approximately from 5 to 15 mm. Particles was slightly compacted in arranging process to obtain the same mass of material for every rerun. After arranging particles was compacted by hydraulic press with the maximum pressure 1580 bar. Length, diameter of briquette and weight was measured. Density of briquettes was calculated on the basis of dimension measurement and weighing.

For comparison 30 mm length straw and reed particles was placed in briquetting die without

Wheat straw, reed and reed composition with peat biomass densification experiments had been carried out by means of hydraulic press equipment in closed die (Fig. 1). Pressure and piston displacement measurement data were collected on the PC using Picolog software. Chopped to different length stalks with moisture content less than 10% was used for densification.

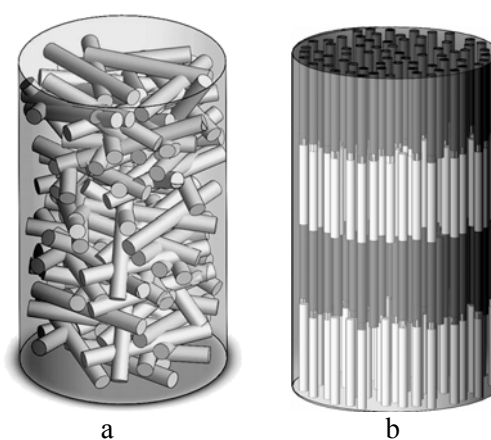


Fig. 2. Arrangement of stalk material in closed die before  
briquetting  
a – unarranged, b – arranged

arranging (Fig. 2a) and pressed with maximum pressure 1580 bar.

The briquette mechanical strength is characterized by the force necessary for its destruction [2, 3]. The briquette of circular cross section is exposed to the pressure force as shown in Fig. 4, i.e. its direction is perpendicular to its axis of symmetry. Briquette was placed on support plate of ZWICK testing machine and compression force  $F$  was applied to briquette in the direction perpendicular of briquetting direction. This force is gradually increased until the briquette disintegration and splitting. The destruction force intensity was investigated for 11 samples of each composition.

Briquettes diameter produced in experimental pressing device was 62 mm and length 60 mm.

For comparison industrially produced wood briquettes and pure peat briquettes was tested in the same way.

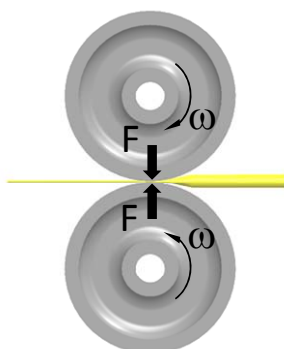


Fig. 3. Flattening of the reed stalk

### Results and discussion

In previous densification experiments of chopped straw, common reed stalk material particles and compositions with additives was stated that compacted with pressure 230 MPa compositions of straw particles from two fineness groups (2 – 3 mm and < 0.5 mm) have density  $> 1.0 \text{ g}\cdot\text{cm}^{-3}$ , if fineness proportion (amount of particles < 0.5) exceed 25%. Density  $1.0 \text{ g}\cdot\text{cm}^{-3}$  has been obtained in densification of straw and reed stalk material particle compositions with peat, if peat proportion exceeds 20%. Density of briquettes made from coarse chopped material (particle size more than 3mm) were significantly less than  $1.0 \text{ g}\cdot\text{cm}^{-3}$ .

Fine comminution of stalk material significantly increases energy of grinding. Increasing of particle length from 1 to 100 mm decreases specific cutting energy up to 40 times. Roughly shredded straw or reed material does not provide necessary density and durability of

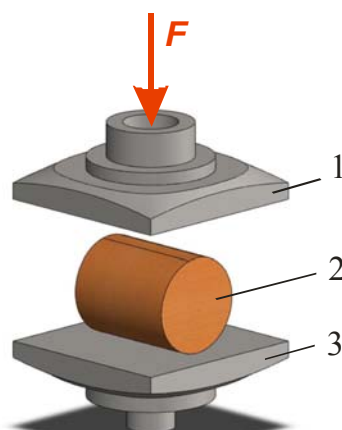


Fig. 4. Scheme of compression  
1 – compression plate, 2 – briquette,  
3 – support plate

briquettes, if material is unarranged in the closed die before cold briquetting.

The scope of investigation was to find method how to increase density and durability of coarse chopped material briquettes. Theoretical analysis of briquetting process was stated before experiments. If particles are inserted in briquetting die without arranging they lay down perpendicularly of pressing direction. Pressing force compact particles, but sharp adhesion between them does not occur because of hard stalk particle surface. The reason is flattening of stalk material particles and decreasing of bonding surface area. To increase density and strength of briquettes necessary maximize bonding surface area between particles.

Suitable arrangement of straw and reed particles in briquetting die allows changing deformation directions of particles. The stalk material curves and adhesion between particles increases (Fig. 5).



Fig. 5. Straw briquette in the ZWICK testing equipment.

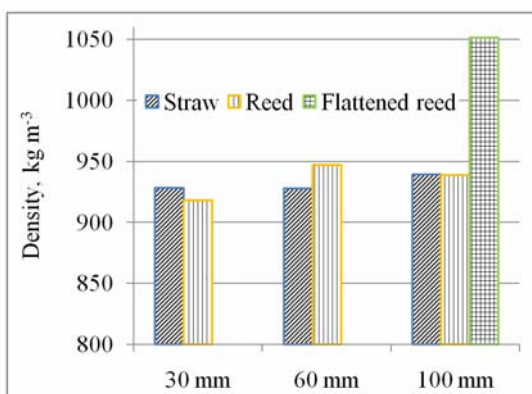


Fig. 6. Briquettes density dependence on the length of particles



Arranged particles were located in direction of longitudinal axis of die according Fig. 2b. Displacement between ends of particles in different layers was approximately from 5 to 15mm. Particles were slightly compacted in arranging process to obtain the same mass of material for every rerun.

Results of investigation of briquettes density dependence on arranged particle size is presented in Fig. 6. Increasing particle length from 30 to 100 mm does not affect significantly density of briquettes. Density of arranged straw briquettes varies between  $939 \text{ kg}\cdot\text{m}^{-3}$  (100mm) and  $928 \text{ kg}\cdot\text{m}^{-3}$  (30mm). It is less than recommended  $1.0 \text{ g}\cdot\text{cm}^{-3}$  and dependence on the length is less than 1.3%.

Density of arranged reed briquettes varies between  $927 \text{ kg}\cdot\text{m}^{-3}$  (30mm) and  $947 \text{ kg}\cdot\text{m}^{-3}$  (60mm). Density dependence on the particle length for reed briquettes does not exceed 3%.

The density of briquettes from flattened reed stalks is  $> 1.0 \text{ g}\cdot\text{cm}^{-3}$ . It shows that arranging and previously densification has good influence on briquettes density.

The addition of peat to wheat straw and reed particles increases density of briquettes. Fig. 7 presents the changes of briquettes density depending on peat content. The addition of 30% peat increases density of briquettes till  $\sim 1.0 \text{ g}\cdot\text{cm}^{-3}$ . Significant reed+peat briquettes density depending on material length was not stated (Fig. 7).

Durability test was carried out using ZWICK and GUNT material testing equipment. As a result of tests briquette splitting force dependence on briquette deformation was stated (Fig. 8). Evaluation of average splitting force for all reruns stated dependence of disintegration force on the particle length.

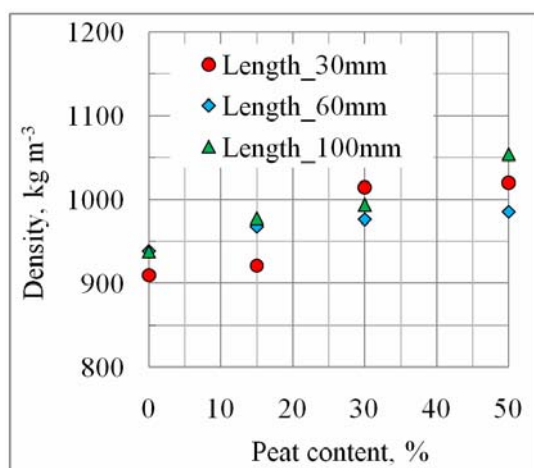


Fig. 7. Briquette density dependence on the peat content for reed+peat compositions

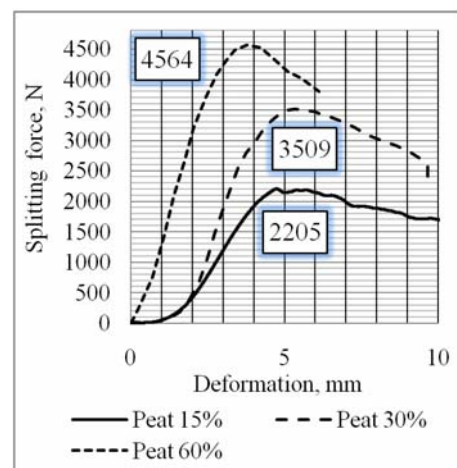


Fig. 8. Splitting force depending on deformation of briquettes

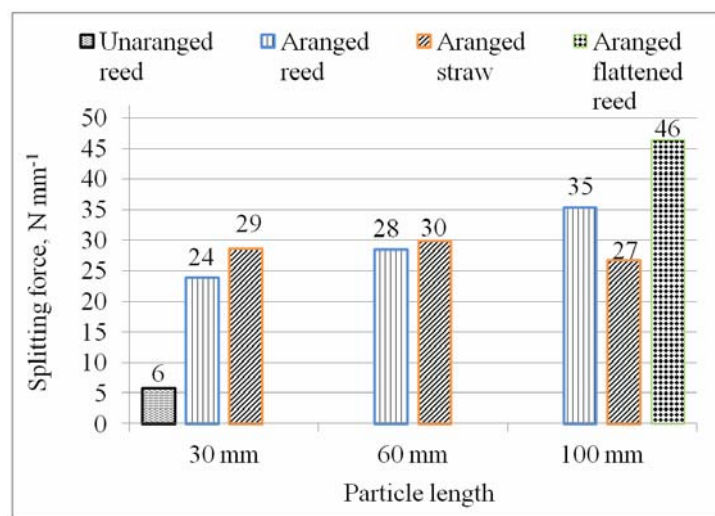


Fig. 9. Dependence of specific splitting force on particle length for straw and reed briquettes

Fig. 9 presents dependence of splitting force on the particle length for wheat straw and reed made from arranged structure briquettes. Increasing of durability by increasing of particle length was stated for reed briquettes, but for straw briquettes change of splitting force was not significant. Comparing unarranged reed stalks (30 mm) briquettes showed low specific destruction resistance – 6 N mm<sup>-1</sup>. Briquettes from flattened and arranged reed stalks showed good results. The splitting force of briquettes was 1.3 times higher than for not flattened stalk briquettes.

Peat additives let substantially increase splitting force of reed briquettes (Fig. 10). The addition of 15% peat increases durability of briquettes from 1.2 to 1.3 times for all lengths of particles. Increasing addition of peat till 30% and more, increases durability of briquettes, but

splitting force dependence on particles length is not significant (Fig. 10).

For comparison industrially produced wood, unarranged reed and wheat straw and pure peat briquettes were tested using the same method.

Unarranged reed particle (length 30 mm) briquettes shows specific splitting force approximately 6 N mm<sup>-1</sup> (Fig.11). The same value of splitting force was obtained for wheat straw (30 mm) unarranged briquettes destroying.

Specific splitting force for wood briquettes reaches 38 N mm<sup>-1</sup> and this value can be taken as a base for comparison of experimentally made briquettes. Pure peat briquettes showed splitting force 55 N mm<sup>-1</sup>.

The addition of 30% peat to arranged structure reed briquettes gives splitting force value equal to industrially produced wood briquettes.

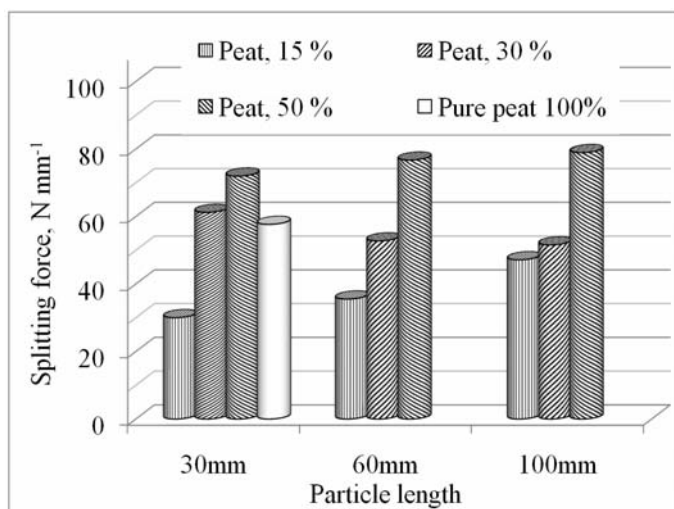


Fig. 10. Specific splitting force dependence on peat additive for reed+peat compositions

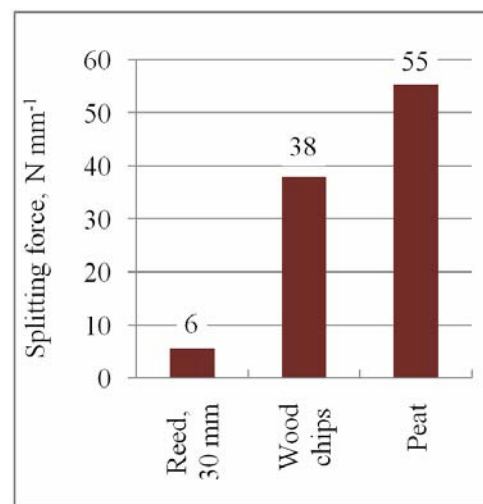


Fig. 11. Specific splitting force for unarranged reed, wood and pure peat briquettes

## Conclusions

1. Addition of 30% peat to coarse chopped straw or reed arranged structure briquettes increases density to recommended value  $1.0 \text{ g}\cdot\text{cm}^{-3}$ .
2. Increasing peat proportion in arranged structure straw and reed briquettes till 50% increases splitting force 2 – 3 times.
3. Destroying force of arranged structure coarse chopped wheat straw and reed briquettes reaches value  $35 \text{ N mm}^{-1}$ . It is approximately the same as industrially produced wood briquettes.
4. Arranged structure of biomass particles in briquetting die is recommended for significant increasing durability of stalk material briquettes.
5. Flattening of the herbaceous biomass stalks before briquetting arranged briquettes increases density of the briquettes to more than  $1.0 \text{ g}\cdot\text{cm}^{-3}$  and splitting force 1.3 times.
6. New briquetting equipment is necessary to design for biomass particle arranging before pressing.

## References

1. Kakitis A., Nulle I. Durability of stalk material briquettes, Proceedings of the International conference “Scientific achievements for wellbeing and development of society”, March 4-5, 2004. – Ržekne, pp. 26 – 31
2. Brožek M., 2001. Briketování nekovového odpadu. In: Sborník z mezinárodní konference XIV Diamatech.Krakow, Univerzita Radom: 84–87.
3. Plištil D., Brožek M., Malaták J., Hutla P. (2005): Mechanical characteristics of standard fuel briquettes on biomass basic. Research in Agricultural Engineering, 51: 66–72.

## Acknowledgements

The authors gratefully acknowledge the funding from ESF project Nr. 04.4-08/EF4/2010.02.35 “Mobilization of human resources for renewable energy research”

## CURRENT STATUS AND PROSPECTS OF BIOGAS TECHNOLOGY IN THE CZECH REPUBLIC

KÁRA JAROSLAV<sup>1</sup>, ADAMOVSKEÝ RADOMÍR<sup>2</sup>, RUTKOWSKI KAZIMIERZ<sup>3</sup>

<sup>1</sup>Research Institute of Agricultural Engineering, 161 01 Prague 6, Czech Republic

Phone: +4202233022334, E-mail: jaroslav.kara@vuzt.cz

<sup>2</sup>Czech university of Life Sciences Prague, 165 21 Prague 6 – Suchbátov, Czech Republic

Phone: +4202224484176, E-mail: adamovsky@tf.czu.cz

<sup>3</sup>Agricultural University in Krakow, 30-149 Krakow, Poland

Phone: +48126624629, E-mail: k.rutkowski@ar.krakow.pl

### Abstract

The present article specifies reasons for use of anaerobic fermentation, materials applicable for biogas production, types of biogas applications in the Czech Republic and possible future of the biogas technology. Furthermore, circumstances influencing capital costs of biogas plant development.

**Key words:** wastes; biogas; anaerobic fermentation; cogeneration.

### Introduction

Anaerobic digestion is a highly complex biochemical process consisting of a number of part and consequent physical, physical chemical and biological procedures. In general, this is a bioenergetical transformation of organic matter without reducing its fertilizing value. Final products comprise a biologically stable substrate with high fertilizing effects and biogas containing 50% - 70% of methane, with a calorific value of approx. 18-25 MJ.m<sup>-3</sup>. The process of anaerobic degrading the organic compounds is determined by a number of factors that are changing the microorganism environment and have essential impact on the process as such, which namely involves the following (Pastorek, Kára, Jevič, 2004):

- *Environmental moisture* – The methane bacteria are able to operate and reproduce only in humid conditions, with the minimum humidity of 50%;
- *Environmental temperature* – Methane can be produced within a wide range of temperatures (4° - 90°C). Current biogas plants in use mostly operate in the mesophilic temperature zone, i.e. 35 – 42 °C;
- *pH value* – Ideal pH for the growth of methanogenic microorganisms is 6.5 – 7.5;
- *Supply of nutrients* – The methane bacteria require soluble nitrogen compounds, minerals and trace elements for their cell structure;

- *Existence of toxic and inhibiting substances* – Toxic and inhibiting substances refer to compounds that negatively affect the biological process; mostly this may involve the inhibiting action of fatty acids and ammonia;
- *Digestion area load* – This is a number indicating the maximum quantity of organic dry matter per m<sup>3</sup> and day that can be supplied into a digestion area without overloading;
- *Steady substrate supplies* – In order to prevent overloading of the digestion area, the substrate must be provided in a steady manner.

### Methods

Applications that can be considered the main points of interest concerning the use of organic material anaerobic fermentation technology in the field of agriculture, municipal management and rural communities in the Czech Republic:

#### 1. Production of best-quality organic fertilizers

Quality of the fertilizers can be improved through anaerobic stabilization by homogenization and transformation of certain substances to a matter featuring enhanced fertilizing effects. A better quality fertilizer can be obtained if manure containing a higher quantity of potassium with a pig slurry featuring more phosphorus. In addition, reduced animal

pathogen contents as well as efficient inhibition of weed seed fertility is of importance.

## 2. Energy harvesting

Using biogas for person's or institution's own needs seems to be the most effective option. This may involve a direct use for water heating (social and technological purposes) or producing hot service water and electric power or cold by means of CHP units, which is even a better option. The Czech Energy Regulatory Office laid down minimum rates of purchase prices for electric energy from renewable resources, which for instance made CZK 4.12 per kWh for agricultural biogas in 2009.

## 3. Improved environment

The energetic use of biomass positively influences the air carbon dioxide concentration control. During the biomass development process, carbon dioxide is spent within photosynthesis and subsequently released into the atmosphere when biomass is used for energy production. This closes the short period of the CO<sub>2</sub> cycle. Replacing fossil fuels by biogas cuts the carbon dioxide production; in addition, methane emissions from dung-yards are reduced. The percentage of CO<sub>2</sub> released to the atmosphere within anaerobic processes can be up to 13% lower compared with normal aerobic composting.

## Results and discussion

### *Biomass for anaerobic fermentation*

#### 1. Biomass grown intentionally for energetic purposes:

##### a) Lignocellulose energy crops:

- Energy woods (willows, ashes, elders, black locusts and other tree and shrub species);
- Cereals (whole plant);
- Grass stands (Chinese silver grass, canary grass, permanent grass stands, etc.);
- Other plants (hemp, sorghum, knotweed, fodder sorrel and common hollyhock).

##### b) Oil energy crops:

- Rapeseed, sunflower, flax and pumpkins for seed.

##### c) Starch-sugar energy crops:

- Potatoes, sugar beet, cereals (grains), topinambur, sugar cane and corn.

#### 2. Waste biomass

- Plant remnants from primary agricultural production and maintenance of landscape (cereal, corn and rapeseed straw, remnants from shrub and natural forest seeding control, remnants from meadows and grazing lands, orchard and vineyard wastes, grass stands from fallow land and maintenance of parks);
- Animal production wastes (excrements from animal farms, remnants of feeds, dairy room wastes and wastes from accompanying processing capacities);
- Municipal organic wastes from rural settlement (wastewater sludges, organic part of solid municipal wastes, waste organic matter from maintenance of greenery and grass areas);
- Organic wastes from food and industrial production plants (processing and storage of plant production, slaughter-houses, dairy plants, distilleries and canned food industry, vine premises, wood processing plants, cuttings, chips and sawdust);
- Forest management wastes (wood mass from improvement cutting, bark, branches, tree stumps, roots left from logging, fuel wood, cuttings from handling, brushwood).

In general, every type of organic materials with high content of volatile substances and dry matter below 50% is applicable for anaerobic digestion; however, properties of any used material should be within a certain range (see below) for the processing to be effective: organic substances below 50%, dry matter 5-13%, carbon to nitrogen rate (C:N) 20-35 : 1, pH 6.6-7.5.

The properties listed above can be influenced through adequate treatment of the materials before entering the biogas plant or also through batch composition in case of co-fermentation of diverse types of organic matter: for instance, adding ensilage corn to pig slurry, where such pig slurry is high in nitrogen matter and low in dry matter, will optimize the carbon to nitrogen rate as well as dry matter content. Biological degradability and biogas yield is another important characteristic of the materials useful for anaerobic fermentation. Materials available in farms mostly present easily biologically



degradable substrates. The rate of organic matter biological degradability ranges from 60 to 80% in these substrates. Fermentor detention time of 25-30 days will be sufficient for most of these materials. After this period, biogas ceases to develop from these substrates, which approximates the cumulative biogas production to maximum. Even though the biogas production

continues following the 30-day period, any extension of the process is not effective in terms of economy and will have a minor impact on the biogas yield. The figure 1 shows an example of cumulative biogas production from varied corn hybrids co-fermented with pig slurry under laboratory conditions.

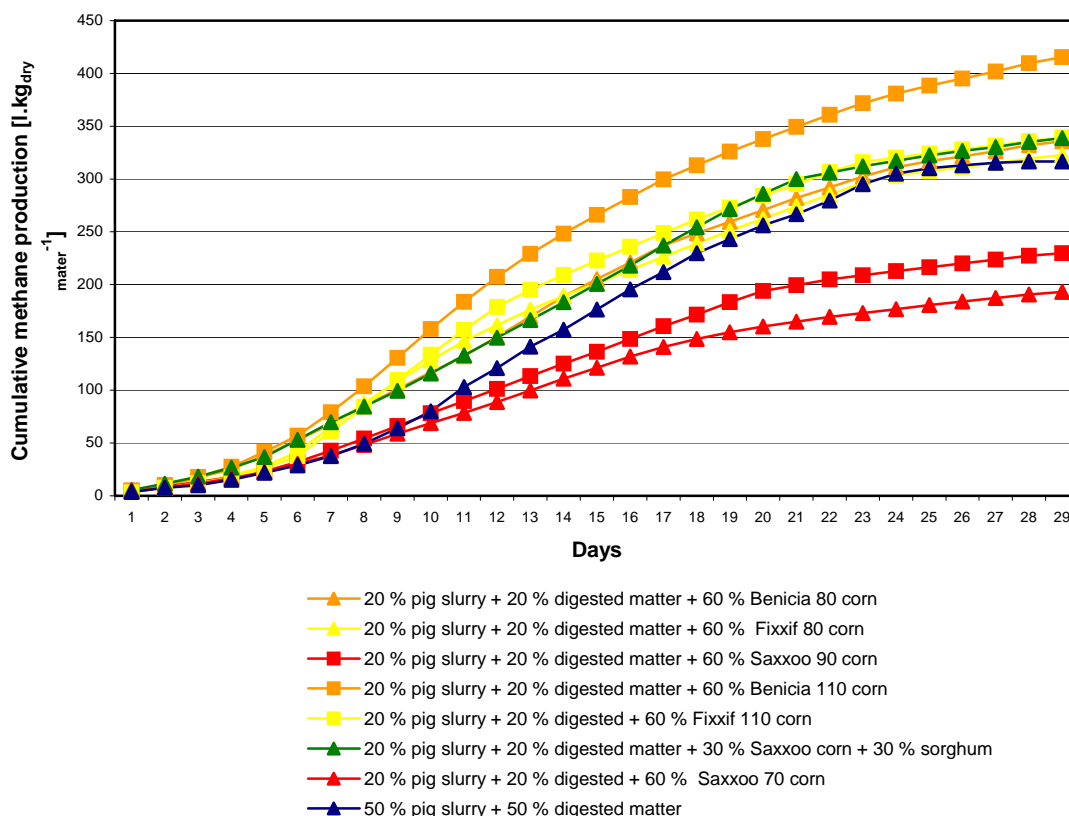


**Fig 1. Cumulative methane production based on co-fermentation of corn and pig slurry**

#### *Biogas using technologies*

The biogas calorific value is significantly influenced only by methane (CH<sub>4</sub>) content, which is namely determined by batch structure and biogas plant technological parameters. Sulphane (H<sub>2</sub>S) causing the development of sulphur acid (H<sub>2</sub>SO<sub>4</sub>) in biogas combustion presents a problematic compound of biogas, as sulphur acid that develops through condensation of flue gases causes corrosion. Therefore, sulphane must be eliminated from biogas if its concentration increases. This is mostly carried out by means of chemical adsorption of H<sub>2</sub>S into solid substances (FeO or Fe<sub>2</sub>O<sub>3</sub>) or biologically through the method using sulphur bacteria that

oxidise H<sub>2</sub>S to elementary sulphur and sulphates depending on temperature and pH under aerobic conditions.

Biogas can be used similarly as any other gas fuels. The most frequent biogas applications include:

- Direct firing (heating, drying, cooling, heating service water etc.);
- Electricity production and heat-transferring media heating (cogeneration);
- Electricity production, heat-transferring media heating and cooling (trigeneration);



- Fuelling combustion engines or turbines to gain mechanical power;
- Cleaning biogas to obtain natural gas quality and subsequent use;
- Use in fuel elements.

The most frequent real-life application using biogas is the CHP unit.

Cogeneration (also combined heat and power, CHP) is simultaneous generation of both electricity and heat energy. The major components of this energetic system include a gas engine or a turbine, and electric current generator. This biogas application method can achieve a high efficiency of energy conversion from biogas (80-90%) to both electric and heat energy. Using gross estimations, some 30% of biogas energy will convert to electricity, 60% to heat energy and the remainder involves heat loss.

To generate 1 kWh of electric energy, the CHP unit will need to burn approximately 0.6 - 0.7 m<sup>3</sup> of biogas containing about 60% of methane, meaning that generating 1 kWh of electric energy and 1.27 kWh of heat energy will require roughly 5 - 7 kg of waste biomass or 5 - 15 kg of municipal wastes or 4 - 7 kg of liquid municipal wastes. The table I lists biogas plants operated around the Czech Republic in December 2008.

*In Tables I means: A - Pig slurry, B - Cattle slurry, C - Ensilaged sunflower, D - Corn ensilage, E - Haylage, F - Straw-based manure, G - Slaughterhouse waste, H - Recyclate (the liquid after-separation component, I - Other biologically degradable wastes, J - Wastewater plant sludge, K - Poultry litter. L - Industrial biologically degradable wastes (meat and bone meal, paper mill sludges).*

## Conclusion

Currently, there are about 60 biogas plants around the Czech Republic, with additional 20-30 under varied stages of development. Thus, it may be stated that this period can see a significant interest in this technology as well as massive increase in numbers of biogas plants and their processing capacity. For comparison, there were only 15 biogas plants in the Czech Republic in 2007. On the other hand, available development potential of biogas plants is estimated to grow up fourfold compared with the end 2009 situation, with the municipal sphere being the greatest potential biogas plant

development area, in addition to agriculture. Treatment of biologically degradable municipal wastes at biogas plants can be seen as a promising form of disposal in many of the local governments. Cities with populations above 50,000 are estimated to operate their own plants with expected outputs including electricity, heat and composts, and also separated combustible residues, meaning that the number of the biogas plants around the Czech Republic might increase with at least 24 new biogas plants.

The relatively high capital costs as well as strict safety conditions (which presents considerable limitations namely to minor biogas plants) are still the biggest obstacles for further development of biogas technology in the Czech Republic. The capital costs are determined by a number of circumstances, such as construction site, potential use of existing facilities (collectors, ensiling pits, etc.), existing on-site infrastructure, properties of substrates to be processed, choice of technology, etc. Nevertheless, data from both abroad and Czech Republic imply that specific capital costs per kW decrease with increased rated electric power. Therefore, construction of biogas plants with rated electric power exceeding some 400 kW will be more cost-effective, as the specific costs decrease only slowly from this level.

The potential of use of the heat generated by the CHP unit is another important condition of cost-effective operation of biogas plants. The EU grant policy that is being implemented through the operational programs presents another factor that considerably assists the development of biogas technology in the Czech Republic. Recently, the level of funding support throughout the programs above has been agreed to be uniform and make 30%, which is a rate that seems to be sufficient for the majority of the submitted projects.

This article is based on the results of the research project titled QG 60083 *Competitiveness of bioenergetic products* implemented by the National Agency to the Ministry of Agriculture, Czech Republic.

## Reference

Pastorek, Z., Kára, J., Jevič, P. *Biomasa obnovitelný zdroj energie*. FCC PUBLIC s.r.o. Praha. 2004, 277 p.

**Tab. I. Biogas plants operated around the Czech Republic**

Biogas plant	Substrate processed $\text{m}^3 \cdot \text{day}^{-1}$	Fermentor capacity $\text{m}^3$	Number of fermentors pc	Detention time days	Annual biogas production $\text{m}^3$	Rated electric power kW	Annual electricity production kWh
Zákupy	A/G/I/J 15/10/15/10	3 700	2	60	1 616 771	220 + 120	6 369 904
Kladruhy, farma Vítání	A/G/I/J 15/10/15/10	2 040	2	28	1 076 579	150	2 120 996
Velký Karlov	A/B/J/G/I 120/60/9/35/6	10 400	8	30	6 407 600	2x 750 + 3x 180	12 622 917
Vladislav	I 18	2 000	1	18 (22)	1 279 583	2 x 360	1 600 000
Třeboň	A/J 85/15	6 000	2	40 - 60	1 140 625	220 + 430	700 000
Žihle	A/B/D/E 56/14/25/5	11 100	4	80	-	1000 + 500	-
Kněžice	A/L/G/I 40/10/5/15	2 500	1	35	-	330	-
Trhový Štěpánov	B/G 18/7	750	1	30	460 996	250	826
Plevnice	A/I 53/3	1 100	2	30 - 35	1 037 500	2 x 160	2 075 000
Velké Albrechtice I	A/L/I/H 32/5/53/30	5 000	2	42	2 436 548	6 x 150	4 800 000
Velké Albrechtice II	A/L/I/H 67/5/53/30	8 000	2	67	3 167 513	8 x 150	6 240 000
Čejč	A/D 30/32	9 000	3	72	2 559 167	2 x 500	6 225 000
Pustějov	A/B/D/E/L 40/40/10/3/8	4 000	2	40	1 843 274	2 x 700	3 631 250
Svojšín	A/F/G/D 36/14/8/5	1 800	2	50	-	2 x 526	-
Zavidov	A/K/D 7/5/3	500	1	30	152 167	2 x 21	299 838
Jindřichov	F 21,2	510	7	24	190 208	2 x 40	212 000
Šebetov	A 50	4 000	2	NZ	172 917	2 x 160	340 646
Dobřany u Plzně	A/G 93,4/0,7	3 400	1	36	753 299	2 x 190	1 484 000
Klokočov u Vítkova	A/L/I 30/25/24	5 000	2	42	2 131 980	3 x 150 + 500	4 200 000
Kroměříž	A/J 180/100	8 960	1	-	1 314 167	22	63
Skalice	K/A 10/170	2 160	1	-	933 750	-	-
Mimoň	A 120	3 600	1	-	1 210 417	-	-
Hustopeče	F 44	1 360	1	-	415 000	200	698
Vyšovice	F 11	1 440	1	-	121 042	-	-
Slavkov	-	-	1	-	41 500	-	-
Chotýčany	B/C/D/E	-	-	-	-	500	-
Krásná Hora	A/B/D/E	-	2	50	-	500	-

## DESIGN AND FABRICATION OF "GRAIN LOSS MONITORING SYSTEM" IN COMBINE

HASSAN KARIMI<sup>1</sup>, HOSSEIN NAVID<sup>2\*</sup>, ALI ROSTAMI<sup>3</sup>, ADEL TAHERI-HAJIVAND<sup>4</sup>

1. Department of Mechatronics, School of Engineering-Emerging Technologies, University of Tabriz, Tabriz, Iran

2. Agricultural Faculty, University of Tabriz, Tabriz, Iran. Tel.: +984113392782, E-mail: navid@tabrizu.ac.ir

3. School of Engineering-Emerging Technologies, University of Tabriz, Tabriz, Iran

4. Ph. D. Candidate, agricultural Faculty, University of Tabriz, Tabriz, Iran

### Abstract

In this paper, we try to present a grain loss monitoring system to indicate the amount of grain loss in the separating and cleaning units of a combine. One main advantage of this system is that it allows the combine operator to choose the maximum forward speed for a given amount of grain loss. For this aim, a load cell sensor is used. In order to prevent long straw from falling on the load cell a mesh plate has been used. For design of the proposed system, we are considering basic blocks including sensor, data-acquisition, central processing and power modules. The accuracy of the device is high and adjustable, and the device can recognize any grain loss up to 50mg. But, since a large amount of noise is produced at this level of accuracy and as the measurement of the losses done in product percent (i.e. there is no need for such accuracy), the initial accuracy of the device is set on 0.1g's. The output data of the load cell is demonstrated on a LCD monitor. After assembling the designed blocks, laboratory experiments were conducted to evaluate the proposed system. Results showed that the proposal system is so useful and effective.

**Keywords:** Separating unit, cleaning unit, grain loss, monitor, data acquisition.

### Introduction

Each combine harvester has an optimum operating speed for any particular crop condition. At one particular ground speed, the combine is capable of recovering the highest percentage of grain and minimum grain loss for that particular crop condition under which it is operating and this speed is normally determined by an operator who, depending upon his experience visually judges the crop conditions and knows the various adjustments and capabilities of his machine. Without a "Grain Loss Monitor", to ensure from combine operation, harvest must be stopped several times, to see the rate of grain loss and determine the origin of it. For this, we need considerable time and effort. Sometimes, the harvest conditions in the field vary strongly and it is not possible to use the combine with its complete efficiency. The combine may move very slowly which cannot cause desired complete capacity, or may move very fast which

can cause increasing the loss rate owing to the increase of combine load. Therefore, it is necessary to be aware of the loss rate in separator and cleaner units, regularly. Awaiting of grain loss helps the operator to select of optimum ground speed or changes the combine adjustments.

The "Grain Loss Monitor", (GLM), is an electronic measuring system which is used for measuring the combine losses in separator and cleaner units. Installing this device on a combine can make a lot of benefits, including: saving time, permanent display of loss rate, measuring losses without any need to stop combine, aware of real origin of losses, selecting the appropriate speed, controlling losses, and driver comfort and satisfaction. Various devices have been made for loss measurement till now.

Robert L. et al (1972), for measuring grain loss, designed a device which was formed from two augers and a flow meter. Grain and output

materials from the rear of combine, were conducted by augers in to the flow meter. Noticeable characteristics of this device are simplicity and cheapness. William P. et al (1977) used from the characteristics of sound for measuring grain loss. In this method, sensitive sensors to sound were installed at rear of combine. Sound of wheat seeds which hit the sensor, was received through a microphone and, then after amplification, filtering and calculating, the amount of grain loss was displayed. Sensors were installed at the end part of cleaner unit and under the separator unit. Kim W. et al (1985) used piezoelectric type of sensors for grain loss measuring. In this device, ceramic crystal was installed firmly to the combine cleaner unit. Grains fall on the sensor and an electric signal was produced. This signal after amplification awarded the user from loss rate.

Several researchers have used GLM for different proposes science previous years. Some of these researches will be mentioned at following. Hofman et al(1996) demonstrated with a research that if a combine is used for harvesting different crops, the grain loss measurement not only wouldn't limit the maximum advancing velocity, but also they could be used as correct feeding of combine for optimal capacity. Tayson et al (2001) as a consequence of a research reported that modern combine harvester which is equipped by grain loss measuring device can hold losses about 2-3 percent. Ferreria et al (2001) reported that grain loss measurement make combine harvesters to be able to operate with the best settings according to crop conditions. This means that once loss increasing occurs during the harvesting, new settings will take place and it will decrease loss again. Mostofi (2007), investigated device accuracy by installing it on a combine harvester, and compared its data with data obtained from conventional method. Results of combined analysis of data related to performing this method during two years showed that in 10-12 percent of grain moisture and drum speed of 750 rpm, the loss at the end of combine harvester is about 1 percent. Also, based on zero assumption, there wasn't any difference between measured loss by

conventional method and grain loss measuring device.

Considering the benefits which are mentioned for this device, preparation and installation of it on combine harvester seems reasonable and necessary. Therefore, in this research has been tried to design a GLM and ultimately be evaluated in laboratory.

### Materials and Methods

The main idea in this research is measure the output grains from the rear of combine harvester, for determination of grain loss in separator and cleaner units. For investigating this idea, a device was made which could be installed in the rear part of combine and scale grains before they fall on the ground. This is the GLM.

As we know, a large amount of straw with grain is removed from the rear part of combine harvester. In order to remove the effect of straw weight on the sensor, a mesh plate was installed at the rear part of combine and along the straw walker's path. The mesh plate was installed to control heavy straw and it didn't allow them to fall on the sensor. However, the holes of this mesh plate didn't refuse the light and small straw.

### Overall system Block diagram

Simple block diagram of the GLM data-acquisition and processing system is shown in the figure 1. Based on the grains falling on the sensor, a series of electrical signals were produced. These signals pre-amplified by a preamplifier and then transmitted to the next block which has a controllable amplifier. In this section, after removing offset and adjusting zero of the signal, it was strengthened to the desired amount and send to the A/D. There is a digital filter with controllable frequency in the A/D which eliminated noise of the signal and then these exiting signals from this filter, was quantized. The AVR will extract useful and related to wheat loss data. Then after processing incident data, the microcontroller will show desired information on LCD display.

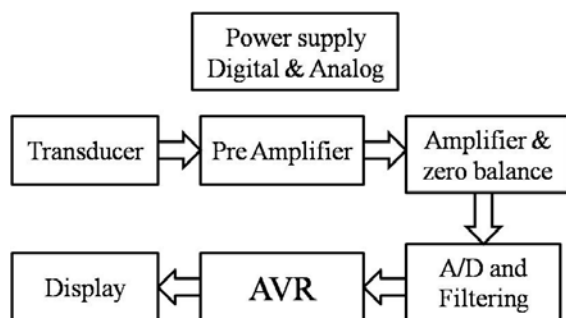


Fig 1. Block diagram of the GLM system

### System design

System design includes hardware and software parts.

### Hardware Design

The main circuit block diagram is shown in Fig 3. The main parts of the circuit are: gauge sensors for producing analog signals due to the weight losses, data-acquisition and processing system. The modular design method is used in the proposed system, including the sensor, data-acquisition, central processing and power units.

### Sensor module

The sensor used in this system is a load cell model 1004 of the Vishay Company. Its capacity was 1.5 kg with output rate of 0.9 mv/v and output impedance was 350 Ohms.

### Data-acquisition module

Sensor output signal was as a differential (bipolar) and very weak. So, at first an initial amplification was done on the signal by a differential amplifier. The second level amplifier has been considered an amplifier with variable gain; therefore it could adjust final gain according to operation condition. Op Amp OP200 and resistances with tolerance of 0.1 percent had been used for having a low offset in output, reducing noise effects, and eliminating fluctuations. An AD7710 (A/D) analog to digital converter (24 bits) with operation frequency of 8 MHZ has been used in order to convert analog signal to digital. It has a control register (24 bits) in order to programming the internal digital filter and sampling the number

of bit-rate and controlling it proportional to operating condition.

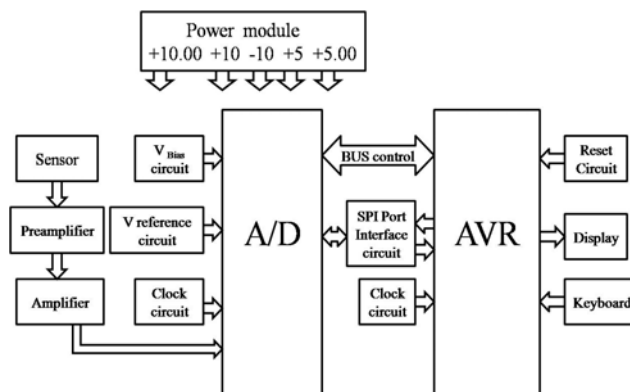


Fig.2 Block diagram of circuit major

### Central Processing Module

For understanding the signal functions of online data which obtained from the sensor system, an operating and processing system was required. ATMEGA32 has been used as the central processing unit, in which some of peripheral interface functions have been used, such as connecting with A/D control register, connecting SPI by a buffer circuit with A/D, a keyboard in order to receive command of operator, RESET circuit, 16MHZ clock circuit, and also a 2\*16 LCD display.

### Power module

Power module has been designed separately for analog and digital parts: in the analog section it was 10.00 V by the AD584 for A/D, 5.0 V by REF05 for A/D voltage reference and  $\pm 10$ V has been designed by LM317 and LM337 for sensors and amplifiers respectively. In the digital section, 5 V designed by the 7805 for the central system and other parts.



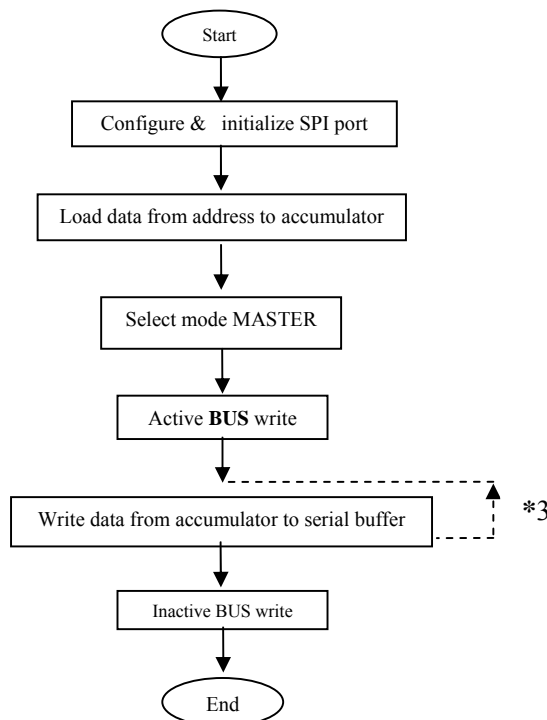


Fig 3. Flowchart for Write Operation

### Software Design

C programming language used and Code Vision choose as the programming environment. Firstly, A/D configuration adjusted proportional with operating conditions such as the length of sampling rate, the frequency of digital filter, the amount of internal gain and etc. Therefore, the 809000H wrote in A/D control register by the flowchart which demonstrated in figure3.

As you can see in this flowchart, at first we configured the SPI port from central system for writing the data. Then, we transferred the desired data from memory to accumulator and then by select the AVR Master mode and activating the write Bus. Finally, the data wrote in three stages as 8-bit from the accumulator to the control register A/D. Data acquisition and processing are the most important part of programming. In other words, how to read data from sensor, interval between data reading, and the method of loss calculation from the read data are very important. Consider Figure 4.

T1 is the time interval of changing data on display, N is the number of data sampling from sensor in this time interval, and T2 is the time interval between data sampling. N and T2 have a direct relationship. For starting and doing primary experiments, with the time interval between data sampling, i.e. T2, we choose N sample in time interval T1 and then we calculated the losses. This was very important that, these parameters be adjusted and optimized. This point has direct effect on accurate measurement of losses. These parameters should be set because the material losses on the sensor did not read twice and did not lost without reading. Data reading flowchart shows in figure5. We put a keyboard for our system to apply the setting. For this propose, an interrupt program considered in the original program. The system flexibility allowed that various experiments and the most appropriate operation state are selected.

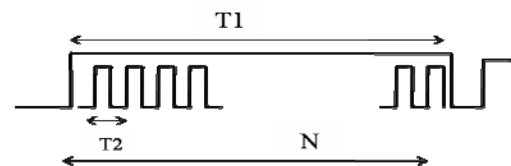


Fig.4 Reading timing data

### Results and Discussion

In field condition and real operation of combine harvester, the output of straw and grain from the rear part of combine is charging in time. Thus, the device must measure the weight of falling material on the sensor, during a certain time interval. This time interval must be in the range that materials weren't scaled twice or more on the sensor. To solve this problem the device was set so that the measured values by device stored in its memory and was displayed after 5 seconds. This time was changeable, and depends on conditions, could take different values. With this method, user could read these values and judge about them. The measuring operation was done 10 times during these 5 seconds. It means that in every half second, the weight on the sensor was scaled, and saved in memory and after 10 times scaling, sum of 10 values was displayed. A considerable point was that the required time for grain moving on the plate couldn't be more than 0.5s. Otherwise



measurement was been repeated. For evaluation of the device, we assumed that the crop yield and operation capacity are 4 (ton/ha) and 1.1, respectively different amounts of wheat proportion to 1, 2, and 3 percent of loss, were mixed with a given amounts of straw (in three stage of 500, 750, and 1000 (g)). For simulation of combine rear conditions, mixed materials spread on a conveyor belt. Its velocity was chosen so that all the materials were fallen on the sensor during 10 seconds. The numbers which displayed during the falling of materials were read and saved. Considering that the belt width was 40 cm, the width of sensor plate was selected 40 cm.

The slop of the sensor plate was selected 37°, because at this angle materials were falling perfectly after colliding with the sensor. Tests included 9 treatments and 4 repeat. Analysis of variance shows that the difference between values were significant with  $p < 0.01$ . It should be noted that a completely randomized design was used averages compare was performed with LSD test. The results of this experiment can be briefly stated such following:

1 – In the angle of 37°, with increasing of grain value, the measured value increased significantly. Then using proper calibration can measure the real values.

2 – with 500 g straw, system showed grain loss value, and difference between measured values for 1, 2.

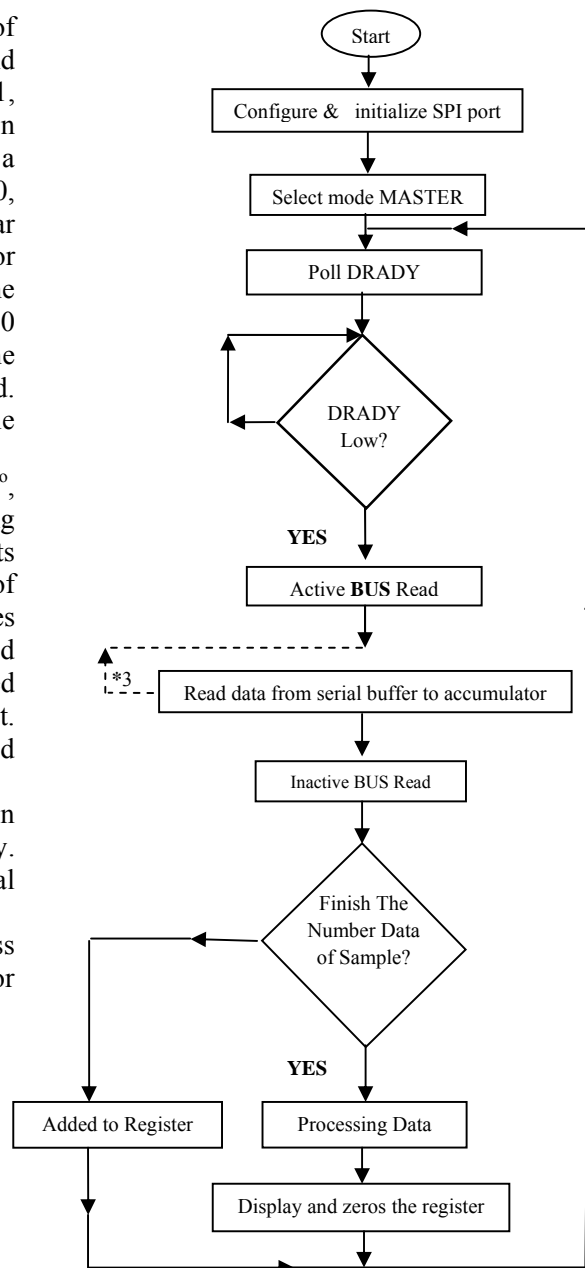


Figure.5 Flowchart for Read data Operations

**Reference**

Hofman,V.-Wiersma,J.-Allrich,T.: Grain Harvest Losses. University of Minnesota, North Dakota State. 1978, Accessed 8 August 2005. Available at: <http://www.smallgrains.org/Techfile/Sept78.htm>

Kim,W.-Blyth,R.-Clara.: Grain loss Indicator. United States Patent, 1985, Number 4,490,964.

Mostofi,M.R.: Field avaluation of grain loss monitor system in different harvested conditions on combine JD955. The fifth congress of agricultural engineering machinery and

mechanization, September 2007, Ferdowsi University of Mashhad.

Robert,I.D.-Rock,I.-Maurice,K.-Rockton.: Grain loss Monitoring Device. United States Patent, 1972, Number 3,638,659

Tyson,B-Hammond,W.C.: Harvesting, Drying & Storage. 2001. Available at: <http://www.ces.uga.edu/pubcd/B1190.htm>

William,P.S.-William,S,E.- and Dale,J.: Grain loss Monitor. United States Patent. 1977, Number 4,036,065.

## CHANGES IN MOISTURE CONTENT AND ELECTRICAL IMPEDANCE OF CARROT SLICES DURING DRYING

AKOS KERTESZ<sup>1\*</sup>, ESZTER VOZARY<sup>2</sup>, ZUZANA HLAVACOVA<sup>1</sup>,  
LENKA PRIATKOVA<sup>1</sup>

<sup>1</sup>Slovak University of Agriculture in Nitra, Tr. A Hlinku 2, SK-949 76 Nitra,  
Slovak Republic, [akos.kertesz0@gmail.com](mailto:akos.kertesz0@gmail.com)

<sup>2</sup>Corvinus University of Budapest, Somlói st. 14-16. H-1118 Budapest, Hungary

### Abstract

Electrical properties of food materials can give information about the inner structure, physiological state of biological tissues. Moisture content of foodstuffs frequently is determined by electrical measurements. Fruits, vegetables with low moisture content can be preserved long time. Generally the drying process of fruits and vegetables is followed by weight loss, but the weight loss in itself does not characterize the inner structural changes in tissue. The aim of this study was to measure the impedance spectra of carrot slices during drying and to correlate impedance parameters to moisture content in the different drying periods.

Cylindrical slices had been cut out from carrot root along the axis. Slices were dried in a Venticell 111 air oven at 50 °C. The mass of slices was measured with a Denver SI-603 electronic analytical and precision balance. Weighing of samples was performed every 30 minutes at the beginning of drying and after that every 60 minutes. The moisture content of samples was calculated on the wet basis. The magnitude and phase angle of electrical impedance of slices were measured with HP 4284A and 4285A precision LCR meters in frequency range from 30 Hz till 1 MHz, and from 75 kHz till 30 MHz, respectively, at voltage of 1 V. The impedance measurement was executed after the weighting. The change of impedance magnitude in drying time showed good correlation with change of moisture content.

**Keywords:** carrot slice, drying, moisture content, electrical impedance spectroscopy, LCR Meter

### 1. Introduction

Electrical properties of biological materials can give information about the inner structure, physiological state of biological tissues. The requirements of the user industry in terms of quality purchased vegetable are growing. In addition, vegetables must meet quality standards STN and of course the rules of the European Union. Therefore we need constantly monitoring and control its quality from producer to consumer. Alternatively, the keeping ability of carrot can be enhanced by drying and subsequent storage. Drying operations are important steps in food processing industry. Drying is one of the oldest methods of food preservation, and it represents a very important aspect of food processing. When studying the physical properties of tissue, it is necessary to consider its non-homogeneity from the macroscopic and microscopic points of view. When testing the electrical properties from the microscopic point of view, it is apparent that inside the cell is

conductive because there is conductivity of ion type in the content of the organic and inorganic matter solutions. The cell membranes are not conductors. From the macroscopic point of view, it is possible to regard the biological materials as non-homogeneous semi-conductors or dielectrics. The density and structural arrangement of the cells in them and the properties of each type of tissue influence the electrical properties of these materials. The characteristics of loose and porous materials are also influenced by the properties of air, which is trapped between the parts or in the pores, most especially its moisture content and temperature. The deployment of the parts in the pack, the size of parts, gappiness, contact surface and bulk density also influence the electrical properties of loose materials. Among the influential factors for porous materials the following can be involved: size and distribution of pores, porosity and bulk density. Further factors are temperature of the material, but the most significant is the influence

of the presence of water, its uneven deployment in the material, different binding energy in each water bond in the material and sorption properties (Hlaváčová, 2003).

The aim of this research was to determine the connection of impedance parameters and moisture content of carrot slices during drying.

### 3. Material and methods

The aim of this study was to measure the impedance spectra of carrot slices during drying and to correlate impedance parameters to moisture content in the different drying periods. Carrots (*Daucus carota* L.) procured from the local market were used in the studies. Samples in unclosed polyethylene bag were stored in a refrigerator at (5 – 7) °C in a room without ventilation. Samples were stored for a shorter period (about a day), or a longer period of time (about a week). At the start of each experiment, the carrots were washed and cut into cylindrical slices, which are consisted both orange exterior and yellow core, having the variable dimensions using a kitchen sheer.

Carrot slices were dried in cabinet dryer Venticell 111 air oven at 50 °C installed in the Physics and Control Department of Budapest Corvinus University. The air temperature was controlled by means of a proportional controller. Since biological materials can absorb moisture from the air, therefore after drying the samples were immediately wrapped in a thin film to stabilize its moisture content. Just before the measurement the thin film was removed and the samples were weighted. The initial moisture content of carrots was about 87.5 % (wet basis)

(AOAC, 1990). The mass of slices was measured with a Denver SI-603 electronic analytical and precision balance. Weighting of samples was performed every 30 minute at the beginning of drying and after that every 60 minutes. The moisture content of samples was calculated on the wet basis. The magnitude and phase angle of electrical impedance of slices were measured with HP 4284A and 4285A precision LCR meters in frequency range from 30 Hz till 1 MHz, and from 75 kHz till 30 MHz, respectively, at voltage of 1 V. As a sensor was used a special electrode with clips hp16451 B dielectric text fixture, intended for the said LCR meters hp4284A and hp4285A for measuring dielectric properties of materials. The dried slices of carrots were located between 2 plates of dielectric text fixture. The impedance measurement was executed after the weighing.

The change of impedance magnitude in drying time showed good correlation with change of moisture content.

### 4. Results and discussion

The effect of air temperature is reflected in drying rate. At higher than 70 °C, the dried product partially lost its fresh product characteristics (Mulet et al., 1987). From measured and calculated values are constructed graphical dependencies of electrical quantities on frequency. The moisture content versus time curves for thin layers number 1 (◆), 2 (■), 3 (▲), 4 (✕), 5 (\*), 6 (●), of carrots is shown in Fig. 1.

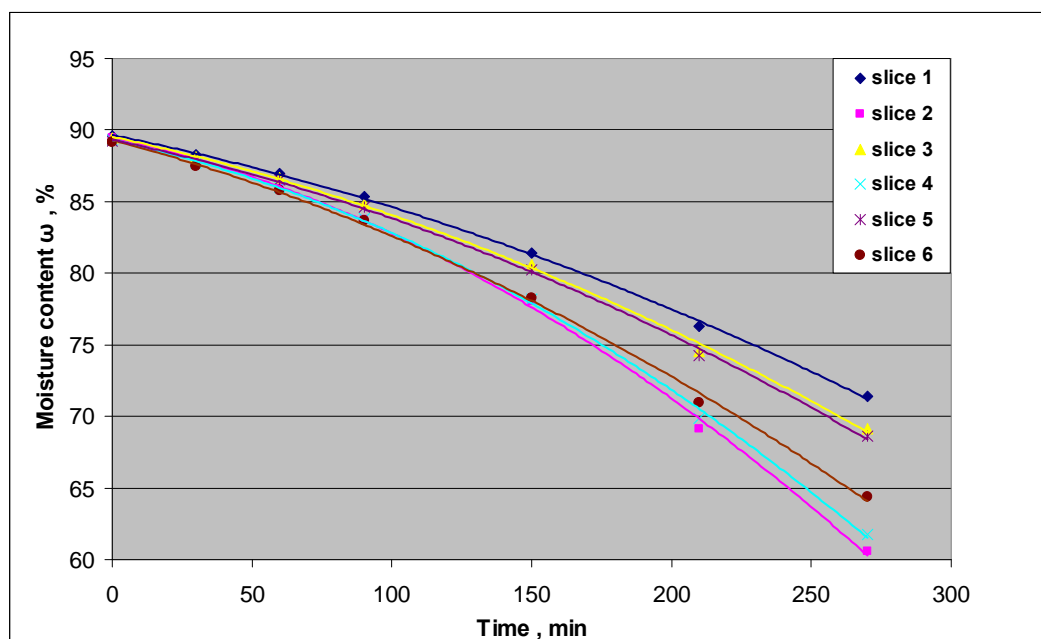


Fig 1. Time dependencies of the dried carrot slices moisture content

These illustrated curves we can approximate with polynomial function

$$\omega = at^2 + bt + c \quad (1)$$

where:  $\omega$  - moisture content,  $t$  - time,  $a$ ,  $b$ ,  $c$  - coefficients of regression equation (1).

Comparing the waveforms in Fig. 1 it can be seen, that the curves have a similar time course and during the drying time the moisture content of samples decreases.

In Table 2 are given the coefficients of determination for samples 1 (◆), 2 (■), 3 (▲), 4 (×), 5 (\*), 6 (●), which reached very high values.

Table 1 Drying conditions versus drying times observed

Drying time, min	Temperature, °C	Slice 1		Slice 2		Slice 3	
		Mass, g	$\omega$ , %	Mass, g	$\omega$ , %	Mass, g	$\omega$ , %
0	50	7,888	89,591	6,579	89,466	8,195	89,445
30	50	7,019	88,303	5,706	87,855	7,266	88,095
60	50	6,305	86,978	4,983	86,093	6,481	86,653
90	50	5,600	85,339	4,264	83,748	5,712	84,856
150	50	4,423	81,437	3,159	78,063	4,453	80,575
210	50	3,460	76,271	2,243	69,104	3,399	74,551
270	50	2,871	71,403	1,758	60,580	2,802	69,129
990	50	0,821	0,000	0,693	0,000	0,865	0,000
Drying time, min	Temperature, °C	Slice 4		Slice 5		Slice 6	
		Mass, g	$\omega$ , %	Mass, g	$\omega$ , %	Mass, g	$\omega$ , %
0	50	7,193	89,281	7,985	89,217	7,672	89,181
30	50	6,276	87,715	7,115	87,899	6,642	87,504
60	50	5,506	85,997	6,392	86,530	5,845	85,800
90	50	4,760	83,803	5,589	84,595	5,077	83,652
150	50	3,540	78,220	4,350	80,207	3,818	78,261
210	50	2,560	69,883	3,347	74,275	2,857	70,949
270	50	2,017	61,775	2,742	68,600	2,330	64,378
990	50	0,771	0,000	0,861	0,000	0,830	0,000

Table 2 Values of constants  $a$ ,  $b$ ,  $c$  and coefficients of determination  $R^2$

Sample	$a$	$b$	$c$	$R^2$
Slice 1 (◆)	-0,0001	- 0,0398	89,654	0,9992
Slice 2 (■)	-0,0002	- 0,0429	89,486	0,9988
Slice 3 (▲)	-0,0001	- 0,0419	89,53	0,9988
Slice 4 (✕)	-0,0002	- 0,0426	89,312	0,9990
Slice 5 (✱)	-0,0001	- 0,0416	89,325	0,9991
Slice 6 (●)	-0,0002	- 0,0516	89,300	0,9986

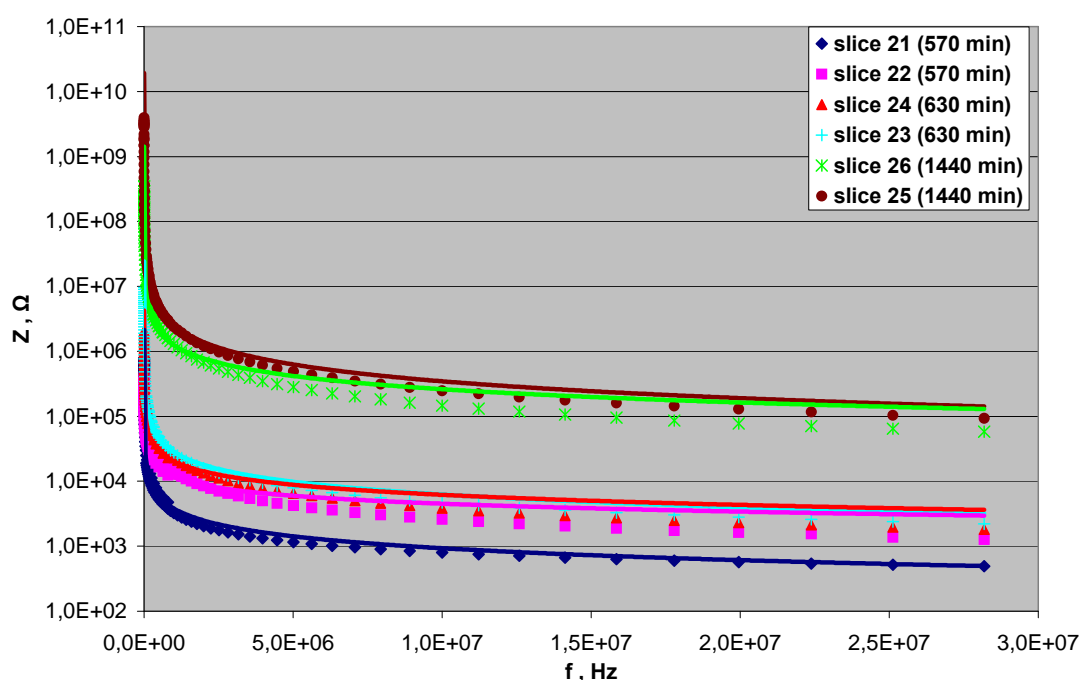


Fig. 2. Frequency dependencies of impedance for samples slice 21 (◆), 22 (■), 23 (+), 24 (▲), 25 (●), 26 (✕).

In Fig. 2 is frequency dependencies of impedance for samples of carrot slices No. 21 (◆), No. 22 (■), No. 23 (+), No. 24 (▲), No. 25 (●), No. 26 (✕), measured between the boards of special clamp HP 16451B Dielectric text fixture, intended for the said LCR meters hp4284A and hp4285A. The following charts are shown by the power function

$$Z = Z_o \left( \frac{f}{f_o} \right)^x \quad (2)$$

where:  $Z$  – impedance,  $Z_o$  – reference impedance,  $f$  – frequency,  $f_o = 1$  Hz,  $x$  – constant.

The constructed graph shows that the impedance depending on the frequency has downward tendency. The impedance of measured samples of the same dimensions is increases with the drying time, because the moisture content of the samples  $\omega$  decreases with drying time. In Table 3 are given the coefficients of determination for the aforementioned samples.



Table 3 Values of constants  $Z_0$ ,  $x$  and coefficients of determination  $R^2$ 

Sample	$Z_0, \Omega$	$x$	$R^2$
Slice 21 (♦) 570 min	2E+07	-0,6104	0,9820
Slice 22 (■) 570 min	3E+06	-0,4051	0,9239
Slice 23 (+) 630 min	2E+08	-0,6509	0,9834
Slice 24 (▲) 630 min	3E+07	-0,5154	0,9621
Slice 25 (●) 1440 min	4E+11	-0,8617	0,9706
Slice 26 (✱) 1440 min	1E+10	-0,6781	0,9561

## 5. Conclusion

The most important characteristics of carrot required for simulation and optimization of the drying were studied. The results of the measurements are specific impedance depending on frequency. We found that the impedance of the measured samples decreases with frequency according to functions described in this frequency range. The coefficients of determination of the regression equation reached high values for all measured quantities and materials. Based on the measured values and constructed graphics dependencies we can conclude that the impedance of the dried materials reaching higher values than for materials with higher moisture content. We conclude that the measured electrical properties are investigated to reveal the quality of food materials and even drying. The obtained results were published in the works Kertész and Vozáry (2009).

Measured values and designed graphics can be used to determinate the quality and moisture content of food materials.

## References

- [1] DOYMAZI, I. 2004. Convective air-drying characteristics of thin layer carrots. Journal of Food Engineering, 61, 359-364.
- [2] HLAVÁČOVÁ, Z. 2003. Low frequency electric properties utilization in agriculture and food treatment. RES. AGR. ENG., 49, 2003(4): 125-136, ISSN 1212-9151
- [3] KERTÉSZ, Á.-VOZÁRY, E. 2009. Connection between moisture content and electrical impedance of carrot slices during drying. In: Book of Abstracts of 15<sup>th</sup> Workshop: Energy and Environment 2009, Szent István University Gödöllő, p. 21
- [4] MULET, A.-BERNA, A.-BORRAS, M.-PINAGA, F. 1987. Effect of air flow rate on carrot drying. Drying Technology, 5(2), 245-258.

## Acknowledgement

This work was supported by research projects VEGA 1/0643/09 of Scientific Grant Agency of Slovak Republic

## ESTIMATION AND FORECASTING OF PV CELLS AND MODULES PARAMETERS ON THE BASIS OF THE ANALYSIS OF INTERACTION OF A SUNLIGHT WITH A SOLAR CELL MATERIAL

V.V. KHARCHENKO\*, B.A. NIKITIN, P.V. TIKHONOV

The All-Russia Institute of Electrification of Agriculture, Moscow, Russia,

Phone: +7(499)1719670, Fax: (499)1705101, E-mail: [kharval@mail.ru](mailto:kharval@mail.ru)

### Abstract

The approach based on the consideration of interaction of solar irradiation with solar cells material is suggested as a means of estimation and prediction of parameters of PV cells and modules at the different stages of its fabrication and use. The main point of the approach is analyzing of electron-hole pairs formation under influence of photons of given site at solar spectrum on the material of solar cell substrate. Some results of the approach applications are described.

### Introduction

PV solar power industry – the most quickly developing branch of world power with rates of growth more than 50 % a year and manufacture volume, for example, in 2008 6,1 GW for the sum of 43 billion US dollars. Development of PV technologies market in the field of an agricultural production and rural electrification is represented especially perspective.

Possibility to predict and evaluate parameters of PV solar cells and modules with high degree of accuracy on the all steps of their fabrication and use is the essential factor for development of works on perfection of characteristics of solar power systems.

It requires to develop a number of a fast, automated measurement systems which actually can't be available easy. In this case well proved approach based on theoretical calculations could be very usefull.

The big opportunities at the solution of this problem can provide the approach based on the analysis of interaction of an solar cells initial material with photons, amount and energy of which is determined by their position in the spectrum of solar radiation.

The amount of photons and their energies for each line of spectrum can be obtained on basis of the standard solar radiation of 1000 W/m<sup>2</sup> suggested and accepted by the International Electrotechnical Committee [1].

The sunlight spectrum is complicated enough and depends on a number of factors, such as removal from a core of the Sun, a thickness of a layer of air at sunlight passage to a surface of the Earth etc. In [2] in details a number of the factors influencing a spectrum of a sunlight in a context of the mechanism of its formation is consistently considered. These results are very useful when considering processes of sunlight and semiconductor interaction.

### Results of investigations

Estimation of any solar cell parameters in view of solar radiation spectral structure.

Studies in which purposefully processes in solar cells are considered in a context of the above mentioned factors especially concerning to the given photons position in the solar irradiation spectrum, acting in a working zone and the mechanism of their interaction with component of solar cells (especially directly in the p-n junction area, in the base, doped layer and on contacts) were described earlier [3]. In this work the standard table of the solar radiation spectral

structure was supplemented with obtained by calculations values connected to photons energy of respective wavelengths such as spectral photon density of a standard solar radiation as a derivative of energy spectral density and photons energy, and also the density of photon flows in each wavelengths sub-diapason of the considered table. Tables obtained looked to be very useful for subsequent investigation but they required a lot of space and were not included in the paper in original form and below represented as graphs. Fig.1 brought graph of the energy density distribution for the above-mentioned standard

solar radiation vs. wavelength. Fig. 2 illustrates the results of calculation for spectral photon density distribution of the solar radiation flow  $1000 \text{ W/m}^2$ .

On the basis of these data there were obtained a number of interesting results. Particularly the diagram of the spectral dependence of a silicon layer thickness in which the radiation flow of the given wavelength diminishes in  $e$  time was constructed. There was shown that the share of absorbed photons, for instance, in silicon layer are defined by the layer thickness and absorption coefficient corresponding to length of the waves of the standard spectrum of the solar radiation.

There was calculated solar irradiation absorption coefficient  $\alpha$  in silicon vs wavelength. It was shown that the absorption coefficient in silicon with wavelength increasing falls and becomes lower ( $\alpha=10 \text{ } \mu\text{m}^{-1}$ ). In the range of wave's lengths about  $1 \text{ } \mu\text{m}$  silicon becomes more transparent for long wave photon. However, for lengths of the waves about  $0,3 \text{ } \mu\text{m}$  coefficient of the absorption is enough high ( $\alpha=10^4 \text{ } \mu\text{m}^{-1}$ ), that practically explains high absorbing ability of heavy doped layer of the solar cell in this area of the spectrum.

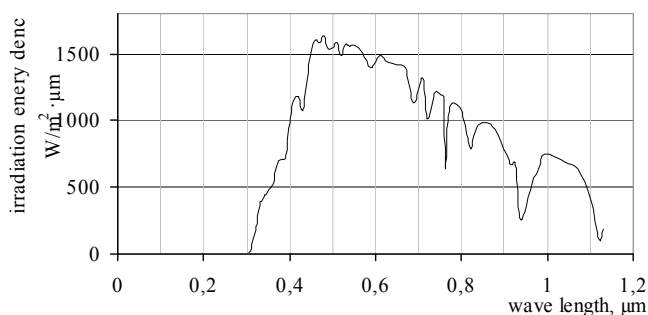


Fig.1. Energy density of solar irradiation vs wave lengths.

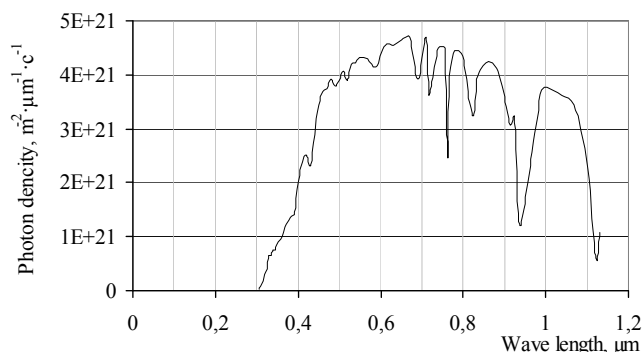


Fig. 2. Photon density for different wave length of standard solar radiation.

Estimation of limited solar cells efficiency coefficient vs forbidden gap of semiconductor.

Among the parameters representing the greatest interest could be emphasized the efficiency coefficient. However, at work on improvement of this parameter it is very important to imagine clearly and take into consideration those restrictions, which are caused by the nature of an initial semi-conductor material and the nature of the sunlight itself. The approach specified above has been used for a theoretical estimation of extremely possible effectiveness ratio of PV solar cells depending on width of the forbidden gap of an initial semiconductor material.

Expression for efficiency coefficient of a solar cell  $\eta$  looks like below [4]:

$$\eta = \frac{i_{sc} \cdot U_{oc} \cdot FF}{R}, \quad (1)$$

where

$i_{sc}$  - density of a short circuit current,

$U_{oc}$  - open circuit voltage of solar cell,

FF - fill-factor of I-U curve as factor of filling of area  $U_{os} \cdot i_{sc}$  by  $U_{opt} \cdot i_{opt}$ ,

R - level of light exposure of the photo converter, including standard level of solar radiation AM 1,5 ( $1000 \text{ W/m}^2$ ).

The parity  $i_{sc}$  and R is any constant k and thus expression (1) takes a form:

$$\eta = k \cdot U_{oc} \cdot FF, \quad (2)$$

The estimation of efficiency of solar cells is spent on the basis of theoretical (idealized) I-V curve under which it is stipulated such interrelation of a current and voltage at which consecutive resistance of a solar cell is equal

zero, and its shunting resistance is equal to infinity. The algorithm of an estimation of the efficiency coefficient of a solar cell with given value of forbidden gap width of the semiconductor is reduced to sequence of calculations in each range  $\Delta\lambda$  of the solar irradiation spectrum.

Fig.3. represent results of calculations of theoretical (utmost) efficiency of solar cell vs. width of the forbidden gap of an initial semiconductor [5].

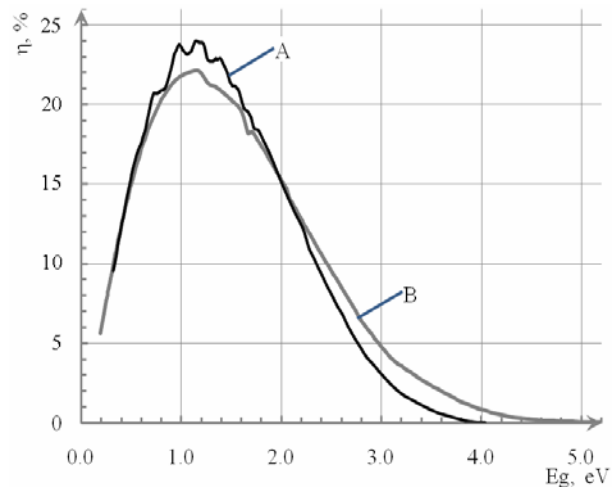


Fig.3. Theoretical (utmost) efficiency of solar cell vs. width of the forbidden gap of an initial semiconductor for standard terrestrial (A) and space (B) spectrum of solar radiation

In addition the similar curves were obtained for different temperatures of solar cells operation. These results submitted at fig.4.

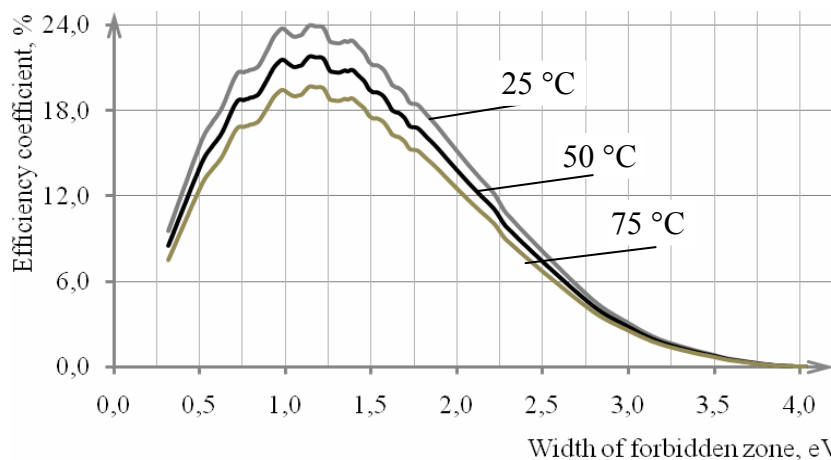


Fig.4. Solar cell efficiency coefficient vs width of forbidden zone of semiconductor for different temperature of operation.

These results show that temperature of operation is a very important parameter which should be taken under strong control to provide more efficient mode of operation of solar power plants.

Distribution of solar energy to heat and the electricity in PVThermal systems.

Last years a wide circulation have received so-called PVThermal systems.

PVT system is a device, reformative a solar energy in electricity by means of PV cells and in thermal by means of a thermal absorbing element (absorber).

It is important to realize what part of solar radiation could be used for heat and electricity production in such kind of devices. Suggested approach give an opportunity to identify these shares. Results of calculations represented at Fig.5.

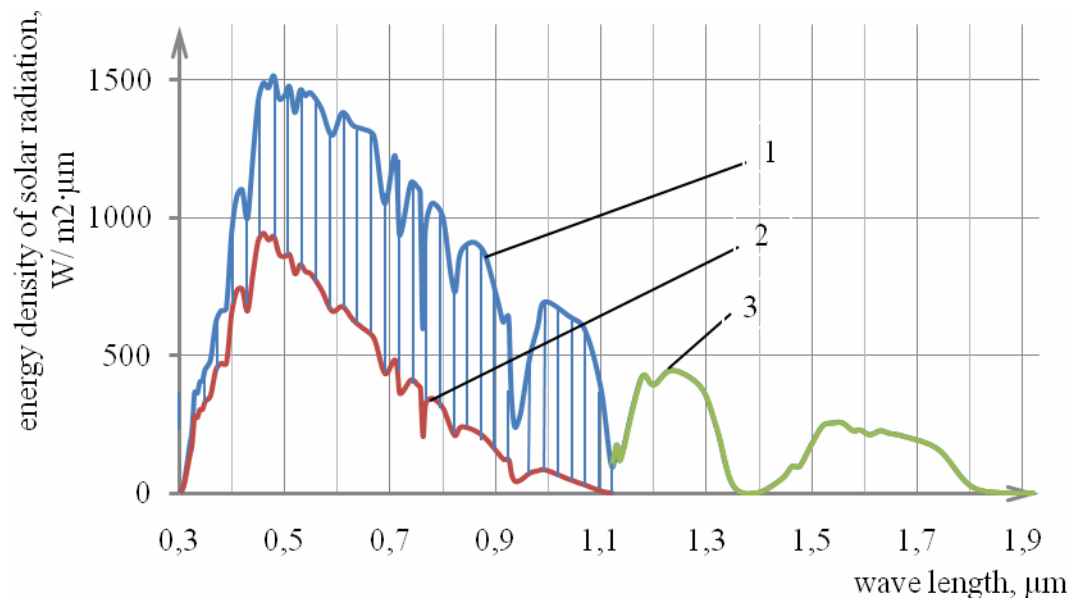


Fig. 5. Distributions of solar radiation energy in PVT system on heat and electricity.

1 – share of energy absorbed in PV cell 2 – share of absorbed energy transformed into heat in the solar cell volume; 3 – long wave part of spectrum passed through silicon and transformed into heat behind cell structure.

### Conclusion

Suggested approach looks to be useful for purposes declared, but for implementation in practice it needs to be approved and confirmed with experimental measurements.

### References:

- [1] R.E. BIRD, R.L. Hulstrom, L.J. LEWIS: Terrestrial Solar Spectral, data Sets. *Solar Energy*, v.30, №6, 1983. P. 563-573.
- [2] V.Poulek, M.Libra, Solar energy, CUA Prague, 2006, ISBN 80-213-1489-3, pp.25-31.
- [3] V.Kharchenko, B.Nikitin, D.Sherban, A.Simashkevich, L.Bruk, I. Usatiy, Estimation of solar cell parameters in view of solar radiation spectral structure. *Mold. Journal Phys. Sciences*, v.8, Nr. 3-4, 2009. P. 387-391.
- [4] Arbusov, Yu. D.; Evdokimov, V. M. *PVfundamentals*. UNESCO-BRESCE 2007, Moscow, VIESH, 2007. p.292.
- [5] V. Kharchenko, B. Nikitin, P.Tikhonov, V. Adomavicius, Utmost efficiency coefficient of solar cells versus forbidden gap of used semiconductor, *Proceedings of the 5<sup>th</sup> International Conference on Electrical and Control Technologies ECT-2010*, ISSN 1822-5934, Kaunas, Lithuania, 6-7 May 2010, pp.289-294.

## MICROCLIMATE IN TUTORIAL AND RESEARCH BREWERY DURING WINTER SEASON

PAVEL KIC, LADISLAV CHLADEK

Czech University of Life Sciences Prague, Faculty of Engineering, Department of Technological Equipment of Buildings, 165 21 Prague 6 – Suchbát, Czech Republic  
Phone: + 420 224 383 141, E-mail: [kic@tf.czu.cz](mailto:kic@tf.czu.cz), [chladekl@tf.czu.cz](mailto:chladekl@tf.czu.cz)

### Abstract

The temperature and humidity of ambient temperature in every brewery are very important factors for propagation of micro organisms, therefore is important to control those parameters within production process, that why the attention was paid to this phenomena. Beer production is rather complicated technological process, which consists of several departments equipped with different technological equipment and demand of particular microclimatic conditions (different temperature and humidity). In some departments of food plant can high humidity connected with low/high temperature support the propagation of different moulds and other micro organisms with spoiling impact on food. That was the reason for measuring the courses of humidity and temperature winter season (since 31/01 to 19/02/2010, and since 26/02 to 08/03/2010) in different departments of the Education and Research brewery of Czech University of Life Sciences in Prague. The obtained results confirmed the highest temperature in energetic department with cleaning plant and boiler and highest humidity in fermentation and lager cellar during cleaning process. The lager cellar due to highest concentration of moulds should be very often cleaned.

**Key words:** beer production, humidity, temperature, brewery, microclimatic conditions.

### Introduction

The temperature and humidity of ambient temperature in every brewery are very important factors for propagation of micro organisms, therefore is important to control those parameters within production process, that why the attention was paid to this phenomena. Beer production is rather complicated technological process, which needs several special rooms with different technological equipments and demands of particular microclimatic conditions according to the purpose of the room. The Education and research brewery of Faculty of Engineering of Czech University of Life Sciences in Prague, used for education and production of special traditional Czech beers according to the old traditional procedure consists from separated rooms used for specific purpose which needs very special equipment and also requires individual parameters of microclimatic conditions (Chládek, 2007; Kunze 2007). Especially winter conditions are quite complicated period of the year. Main indoor parameters were recorded by continues readings and also controlled by immediate measurement.

The indoor microclimate of the university brewery is due to production reasons divided in

five different departments, four production departments are located in first floor of the building and classroom is in second floor. The division of the education brewery is following:

- brew house (Fig. 1), consisting of two stainless steel (SS) vessels, each 10 hl capacity, heated by steam from boiler, two centrifugal pumps, two stirrers driven by electro motors, each motor has an input 3 kW,
- department of wort cooling, consisting of SS whirlpool (10 hl capacity), SS heat plate exchanger with a capacity 10 hl/h and SS hot water tank (20 hl).
- combined department of fermentation and maturation tanks (Fig. 2), equipped with two fermentation tank and (each 20 hl) and four maturation tanks (each 20 hl), cooled by glycol circulation from cooling unit,
- energetic centre, consists of boiler capacity 120 kg of steam 130°C, cooling unit 66 kW, lubrication / free air compressor, bottle/ and keg washer etc. The heat balance of energetic centre (boiler and cooling) during winter season was improved by thermo insulation of the big steel gate, which in winter season without insulation caused big heat losses,



- classroom for 32 students, with data beamer, over head projector etc.



Figure 1 Brewhouse of education and research brewery



Figure 2 Fermentation and lager tanks in education and research brewery

There was paid big attention to the microclimate, especially to temperature of fermentation in old literature about Czech beer production (Bělák, 1858). The process of fermentation is classified according to the temperature of solution, method of created yeast and process duration in two kinds: upper or bottom. The temperature of solution during upper fermentation should be about 12 to 15 °R (15 to 18,8 °C) and yeast raises to the top. Upper fermentation lasts about 48 h and it was used for beer production during summer but and also winter period. Generally, it was typical process production of Czech beer. The temperature of the wort during fermentation using bottom strain of yeast should be about 10°C to 12°C (6,3 °C to 10 °C), at the end of the fermentation process yeast is going to settle to the bottom. The fermentation process lasts 7 - 10 days, and before invention of

the machinery cooling plant had been used old traditional production of Czech beer only during the winter.

Next process is called maturation or lagering of beer, for this process is necessary to keep young beer at the temperature in the range 0 – 1°C.

For all main parts of production processes in brewery are defined optimum conditions for the best production and development of beer also in modern literature. Practical values (ČSN 060210) recommended for brew house are since 5 to 45 °C by relative humidity since 60 % to 90 % and lager cellar 2 °C by 80% to 90 %. According to Chyský 1993 there should be the optimum temperatures in fermentation cellar 8 to 15 °C, during artificial maturing 15 °C, and lager cellar before the consumption 5 °C.

Completely different microclimatic conditions are required for the people staying in those rooms. The main parameters are defined in the Czech hygienic regulations 361/2007. Working activity of in the brewery is according to the produced average metabolic energy in the Working Class IIa or IIb (since 81 to 105 or 106 to 130 W.m<sup>-2</sup>), which needs optimal operative temperature 20 ± 2 °C or 16 ± 2 °C and relative humidity of air 30 to 70 %. The activity of students in the classroom is in working class I (≤ 80 W.m<sup>-2</sup>), which requires operative temperature 22 ± 2 °C and the same humidity like the other rooms.

### Methods and Measuring Instruments

Measurement and control of winter microclimate was provided in Experimental Brewery in Department of Technological Equipment of Buildings in winter season. Indoor microclimate parameters were measured in these rooms by dataloggers Comet with registration of air temperature and humidity each fifteen minutes during two winter periods (since 31/01 to 19/02/2010, and since 26/02 to 08/03/2010). Measuring range is: temperature -30 to 70 °C (precision ± 0,4 °C), relative humidity 0 to 100 % (precision ± 3 %). The surface temperature of technological equipment and room walls were measured by thermovision camera IR Flexcam Pro (detector Focal Plane Array, 8 to 12 μm, range -40 to 600 °C, heat sensitivity < 0,1 °C by 30 °C).

## Results and Discussion

Temperature and relative humidity as main parameters are under particular interest of production conditions. The main statistical parameters of the recording measurement, air

temperature  $t$  (°C) and relative humidity  $rh$  (%) are observed in Tables 1, 2, 3 and 4. Tables contain average (aver), minimum (min), maximum (max) and standard deviation (sdev) of the measured variables.

Tab. 1 Statistical parameters of air temperature during the first period 31. 1. to 19.2. 2010

Room	External	Brew House	Cellar	Energetic Centre	Classroom
Value	$t_e$	$t_{i1}$	$t_{i2}$	$t_{i3}$	$t_{i4}$
-	°C	°C	°C	°C	°C
aver	-3,2	19,2	5,3	15,8	20,4
min	-10,8	16,2	3,7	9,6	17,4
max	2,8	22,1	8,6	30,4	23,6
sdev	2,3	1,0	0,7	2,8	1,0

Tab. 2 Statistical parameters of air temperature during the second period 26. 2. to 8.3. 2010

Room	External	Brew House	Cellar	Energetic Centre	Classroom
Value	$t_e$	$t_{i1}$	$t_{i2}$	$t_{i3}$	$t_{i4}$
-	°C	°C	°C	°C	°C
aver	0,4	19,3	6,5	15,4	20,9
min	-9,3	8,7	4,2	6,4	18,1
max	11,7	21,6	14,8	28,9	23,1
sdev	3,4	1,0	1,4	3,8	0,9

Tab. 3 Statistical parameters of relative humidity during the first period 31. 1. to 19.2. 2010

Room	External	Brew House	Cellar	Energetic Centre	Classroom
Value	$rh_e$	$rh_{i1}$	$rh_{i2}$	$rh_{i3}$	$rh_{i4}$
-	%	%	%	%	%
aver	81,1	29,0	95,6	41,5	26,5
min	55,7	21,9	69	8,6	20,3
max	95,6	42,2	100	100	40,6
sdev	6,6	2,8	4,6	7,9	2,4

Tab. 4 Statistical parameters of relative humidity during the second period 26. 2. to 8.3. 2010

Room	External	Brew House	Cellar	Energetic Centre	Classroom
Value	$rh_e$	$rh_{i1}$	$rh_{i2}$	$rh_{i3}$	$rh_{i4}$
-	%	%	%	%	%
aver	67,4	38,5	93,2	42,2	34,5
min	37,6	22,4	60,5	10,7	20,5
max	93,7	84,5	100	66,7	78,9
sdev	10,7	7,9	6,5	8,9	7,5

The average temperature was 19,2 °C in brew house, 5,3 °C in fermentation cellar and lager cellar, 15,8 °C in energetic centre (boiler and cooling) and 20,4 °C in classroom during the cold period since January 31<sup>st</sup> to February 19<sup>th</sup> 2010. Average relative humidity was about 29 % in brew house, 95,6 % in fermentation cellar and lager cellar, 41,5 % in energetic centre (boiler and cooling) and 26,5 % in classroom during the same period. Temperature and relative humidity

fluctuated extremely in energetic centre (boiler and cooling) according to the indoors activity and external temperatures.

Figure 3 shows the air temperatures in all departments of the brewery and outdoor air temperature during typical days of first measured period. Figure 4 shows the air relative humidity of the air in separated rooms of brewery and outdoor air temperature and relative humidity during the days of the same period.

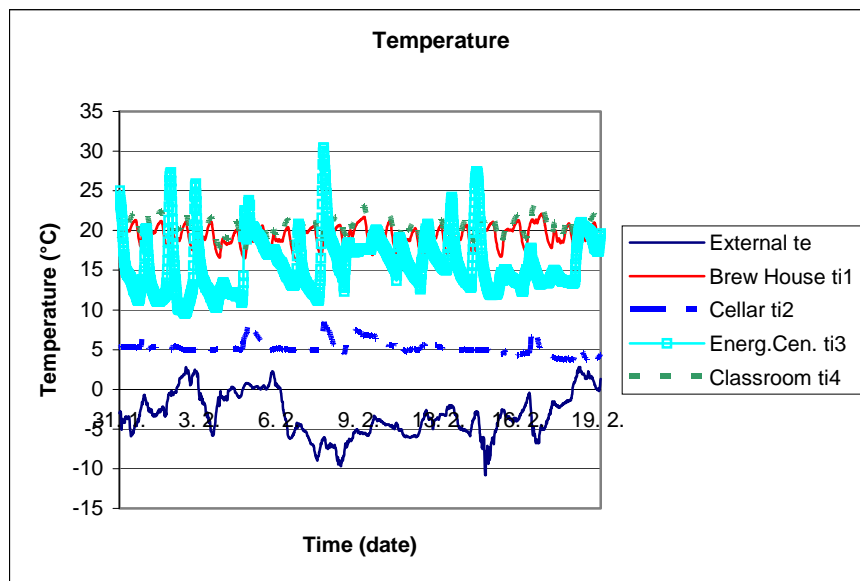


Fig. 3 Air temperatures in the separated rooms of brewery and outdoor air temperature

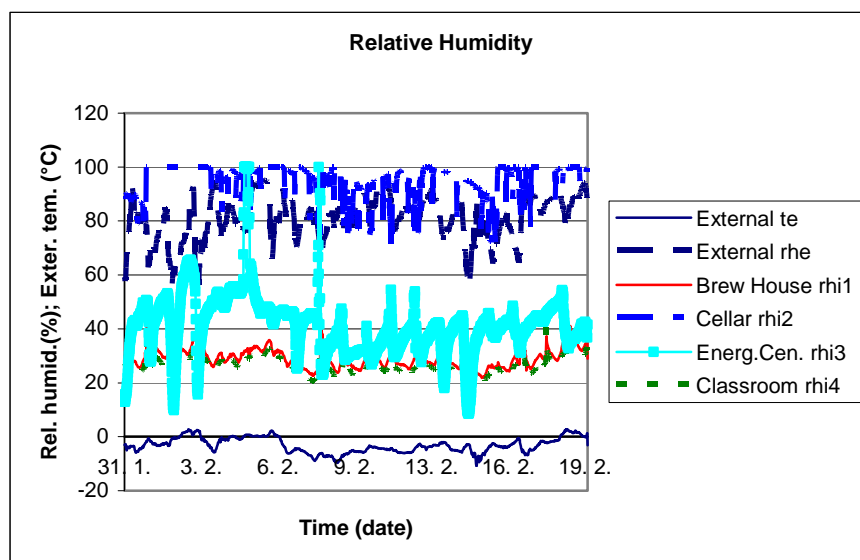


Fig. 4 Relative humidity of air in separated departments of brewery and outdoor air temperature and relative humidity

The average temperature during measuring period was 19,3 °C in brew house, 6,5 °C in fermentation cellar and lager cellar, 15,4 °C in energetic centre (boiler and cooling) and 20,9°C in classroom during the second measured period since February 26<sup>th</sup> to March 3<sup>rd</sup> 2010. Average relative humidity was about 38,5 % in brew house, 93,2 % in fermentation cellar and lager cellar, 42,2 % in energetic centre (boiler and cooling) and 34,5 % in classroom during the same period. Though the outside temperature was warmer then in the previous period, indoors conditions were regulated in similar limits.

From the obtained temperature records (Fig. 3) is possible to determine time of brewing, e.g. the highest temperatures in energetic centre (steam supply for brew house) were measured on Monday 8.2. 2010 and days of keg cleaning (3.02. 2010, 4.02. 2010, 14.2. 2010, 15.02. 2010 etc). Second highest temperature has been recorded in classroom, third one in brew house as presumed. Third highest temperature has been measured in brew house followed by energetic centre, the lowest temperature. Maximal, minimal and average air temperatures of all departments in first period from 31.01. 2010 to 19.2. 2010 and in second period from 26.2. 2010 to 8.03. 2010 are shown in Table 1 and 2.

The recorded humidity results (Fig. 4) showed highest humidity in fermentation/lager department (constantly 80 % - 100 %, reason of mould), second highest humidity has been recorded in energetic centre during brewing and keg washing, (3.02. 2010, 4.02. 2010, 14.2. 2010, 15.02. 2010 etc).

## Conclusions

The obtained results confirmed out presumptions of highest humidity and highest temperature in fermentation cellar with highest moulds attacks (humidity was in the range 80 % - 100 %), the humidity in energetic centre showed some peaks during steam supply (days of brewing). Second highest temperature was measured in classroom located above the brew house; this room has been obviously heated by warm air from brew house.

## Acknowledgement

This paper was prepared with a kind support of Grant: Optimalizace sanitačních procesů v agropotravinářském průmyslu z hlediska snižování zatěžování životního prostředí. Project Number: IGA TF 31170/1312/3133

## Reference:

1. Bělák, V.: *Listy o sladovnictví*. Posel z Prahy. Praha, 1858, p. 120-125, pp. 207-213, 303-309, 390-396,
2. Kunze, W.: *Technologie Brauer und Mälzer* 9.aktualizované vydání, VLB Berlin November 2007, p..639 ISBN 978-3-921690-56-7,
3. Chládek, L.: *Pivovarnictví*, Praha Grada 2007, 1. vydání, 218 pp.218, ISBN: 978-80-247-1616-9,
4. Chyský, J. et al: *Větrání a klimatizace*. Technický průvodce. Praha 1993, p. 490,
5. Nařízení vlády 361: *Podmínky ochrany zdraví při práci*. Sbírka zákonů ČR, částka 111, 2007.

## RELIABILITY IN THE PRODUCTION LINES

LIBOR KOPECKÝ

Czech University of Life Sciences Prague, Faculty of Engineering  
Department for Quality and Dependability of Machines  
Kamycka 129, 165 21 Praha 6 – Suchbát  
Phone: +420 22438 3304, E-mail: kopeckyl@tf.czu.cz

### Abstract

Operation reliability data collecting and processing is still an unsolved question in many companies. If companies collect some data about operation reliability in many cases these data are incomplete, untrustworthy and difficultly processible (because they are not in the uniform style). However, information about the operation reliability can be used as base for many important decisions. Operation reliability data collecting and processing is important for preventive and condition based maintenance planning, resource and spare parts planning, production planning, failure case determination, responsibility for repair determination etc.

“The availability of system will increase if the system reliability is increased or if the time to repair is reduced.” (Benbow and Broome, 2009) We need to know values of down time and up time. It is necessary to decide which data (data about times, items, failure cases, etc.), how many data (indenture level – a system, a subsystem, a component) and how to collect these data (automatically or manually). Very important is choose the best method for illustration reliability of items. The main objective of this article is to describe same parts of operation reliability data collecting and processing and point to some experience from practice.

### Introduction

Dependability according to ČSN EN 13306 is “collective term used to describe the availability and its influencing factors: reliability, maintainability and maintenance supportability”. It means operation reliability influences availability of items.

Information about operation reliability can be useful for:

- preventive and condition based maintenance planning,
- resource and spare parts planning,
- production planning,
- machines and systems improve,
- failure case determination, failure mode determination,
- weak items in the production links determination,
- responsibility for repair determination etc.

But operation reliability data collecting and processing is complex process especially in more complicated production lines and requires high accuracy of entered data. Production lines are often one component in higher systems and production material is supply from other systems. Another problem can be in data collecting because maintenance manager has to

decide which data (which type of data and how many?) will be collected.

Basic equation of availability calculate with uptime (operation time) and with downtime. Operation time is evident. Expression of downtime can be difficult because there are many possibilities of Failure Mode in a reliability data collecting system. These possibilities depend on purpose of expressed information. It is necessary to have written record of every downtime. Then we can divide downtime by Failure Mode.

Basic equation of availability (Ebeling, 2010)

$$\text{Availability} = \frac{\text{uptime}}{\text{uptime} + \text{downtime}}$$

### Operation Reliability Data Collecting Example of Production Line

Example from practice is from chemical company but these procedures can be useful for agricultural companies because some processes on the production lines are very similar.

There is an example of operation reliability data collecting and processing about production line in chemical company in this article. This production line produces caoutchouc from

butadiestyren latex. There is simplified diagram of production line in the figure 1 and 2. There are same three production lines in the figures. The production process begins with mixing, pressing

and graining of caoutchouc. Following operations are drying and again pressing to the blocks. These blocks are packed and put into the pallets.

Figure 1. Mixing, pressing, graining and drying process – profile.

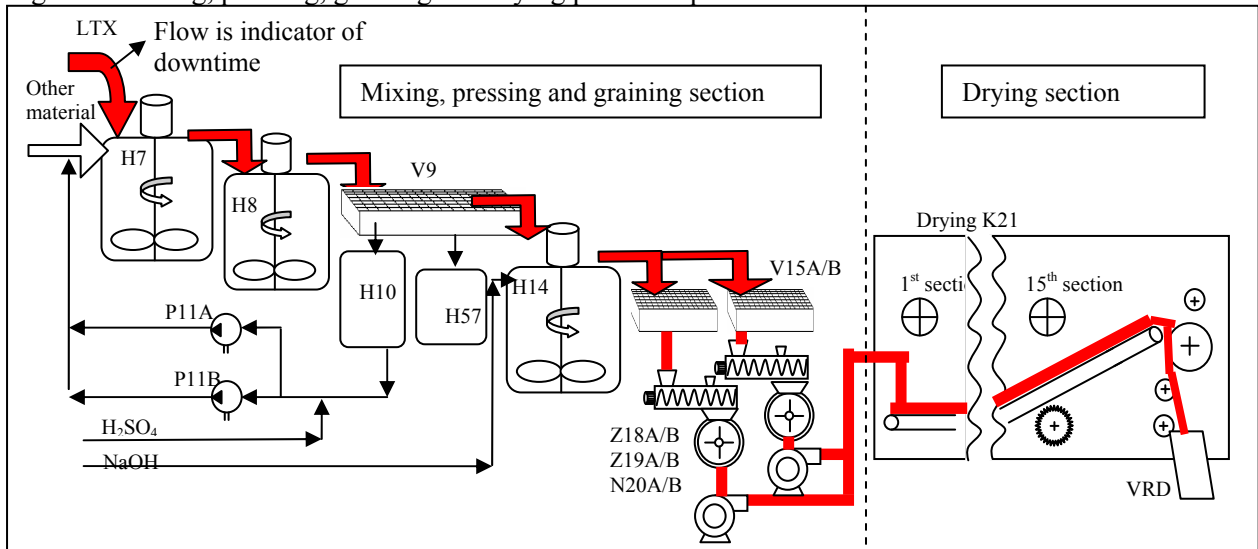
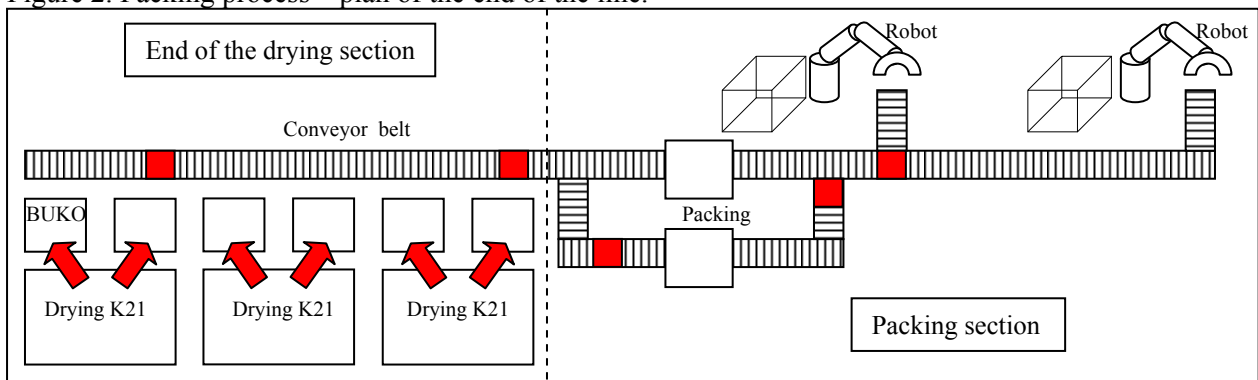


Figure 2. Packing process – plan of the end of the line.



### Operation Reliability Data System Introduction

It is necessary to do same steps before introduction operation reliability data collecting system. If some data about operation reliability exist in a company it is suitable these data process. Maintenance manager can get certain basis for a new data collecting system. There is an example of operation reliability data in the figure 3. Following step is determination of imperfections in the current system and preservation of good parts from the current data collecting system.



Figure 3: Operation reliability data – previous.

Line	Work Shift	Start of Downtime	End of Downtime	Failure Mode	Note
3	1	3.1.2008 6:50	3.1.2008 7:05	19 - other cause	failure of backer
3	1	3.1.2008 7:15	3.1.2008 13:15	11 - technical failure	K21 - link of the belt change
2	2	3.1.2008 8:25	3.1.2008 8:55	14 - purification, blockage	K21 - hard wiper
1	2	3.1.2008 9:00	3.1.2008 14:00	02 - purification, change of type	SBR 1712
2	2	3.1.2008 10:50	3.1.2008 12:25	11 - technical failure	K21 - link of the belt change
3	2	3.1.2008 13:50	3.1.2008 14:00	19 - other cause	failure of backer
					...

There are data about number of line and work shift, data about start and end of downtime, failure mode and note in the current data collecting system. All data are entered manually (there is not uniform style in the data collecting system and nothing is automatically). Especially start and end of downtime can be distorted. These data are very hardly processible, because is impossible separate these data by individual items or cause of downtime. We can only get downtime divided into unit time (days, weeks, months or years), individual lines or work shift.

Therefore new operation reliability data collecting system is introduced in this company. Foundation of this system is automatic record of some information.

Automatically entered data:

- number of line,
- number of work shift,
- time and date of start and end of downtime,
- item or part of the production line,
- type of processed material.

Then worker has to fill in following data:

- failure mode,
- part of item, or cause of failure (depends on the indenture level),
- note,
- who did the repair (name of repairer or name of outsourcing provider).

#### Indicator of Downtime

Decide what is an indicator of downtime is sometimes difficult, because processing of material from start to end of the production line can take some hours. It means one part of production line is stopped and following part is still in process. There was chosen flow of main material (latex) as an indicator of downtime in this production line (it is possible see in the figure 1). Latex is supplied on the start of the

production line and flow is stopped if is failure on any item. Flow of latex is the best indicator of downtime in this production line.

#### Failure Modes

Other problem is failure mode does not often correspond to note and failure mode number 19 - *Other Cause* was chosen in 597 cases from 2938 written records in the year 2009. People who wrote the note have got insufficient knowledge of complicated items. It is necessary to more competent worker write the note and failure mode. There is not any different between preventive purification and corrective purification (blockage) in this system. Both purifications are included in the failure mode No. 14 - *Purification, Blockage*.

Old system of failure modes:

- 01 - *Overhauling*,
- 02 - *Purification, Change of Type*,
- 03 - *Planned Performance Reduction*,
- 04 - *Preventive Maintenance*,
- 05 - *Device in Reserve*,
- 10 - *Technological Downtime*,
- 11 - *Technical Failure*,
- 12 - *Electric Failure*,
- 13 - *Measuring and Regulation Failure*,
- 14 - *Purification, Blockage*,
- 15 - *Lack of Raw Materials*,
- 16 - *Power Failure*,
- 19 - *Other Cause*.

There is introduced new system of failure modes in this company. New failure modes are in the figure 4. This dividing is better for expression of downtime. If the maintenance manager wants to express a downtime cost it is suitable express downtime for failure mode 2 - Maintenance depend downtime. This expression of downtime is suitable for vindication of investment costs. If the manager wants to know which failure cause downtime he

selects failure mode number 21 - Corrective maintenance. There is not any failure mode *Other Failure* in this system. If worker does not

know case of failure he can use the higher level of failure mode.

Figure 4. Failure modes and their coding.

<b>1 – Maintenance Independent Downtime</b>	
<b>11 – Lack of Orders</b> 111 - Device in Reserve 112 - Performance Reduction	<b>12 – Lack of Material or Energy</b> 121 - Lack of raw materials 122 - Power failure
<b>2 – Maintenance Depend Downtime</b>	
<b>21 – Corrective Maintenance</b> 211 - Technological Downtime 212 - Technical Failure 213 - Measuring or Regulation Failure 214 - Electric Failure	<b>22 – Planning Maintenance</b> 221 - Overhauling 222 - Preventive Maintenance
<b>23 - Purification, Blockage</b> 231 - Purification - Blockage	232 - Purification – Preventive 233 - Purification – Change of Type

### Operation Reliability Data Processing

There is an example of processed data in the Figure 5. There is sum of downtime (only failure mode 21 – *Corrective Maintenance*) by items in this figure. Pareto principle determines the most important items. Maintenance manager can fixate on items which caused many hours of downtime. Every item in the Pareto principle can be divided by cause of failure. And it is possible express

downtime by months or availability by months. Everything is possible in MS Excel with using pivot tables.

Figure 5. Pareto principle – downtime by items 2009 (sum for same three lines by items) and selection of one group of items (sum for three same V9 – vibratory sieve) and their failure case and trends for one V9 on the first line.

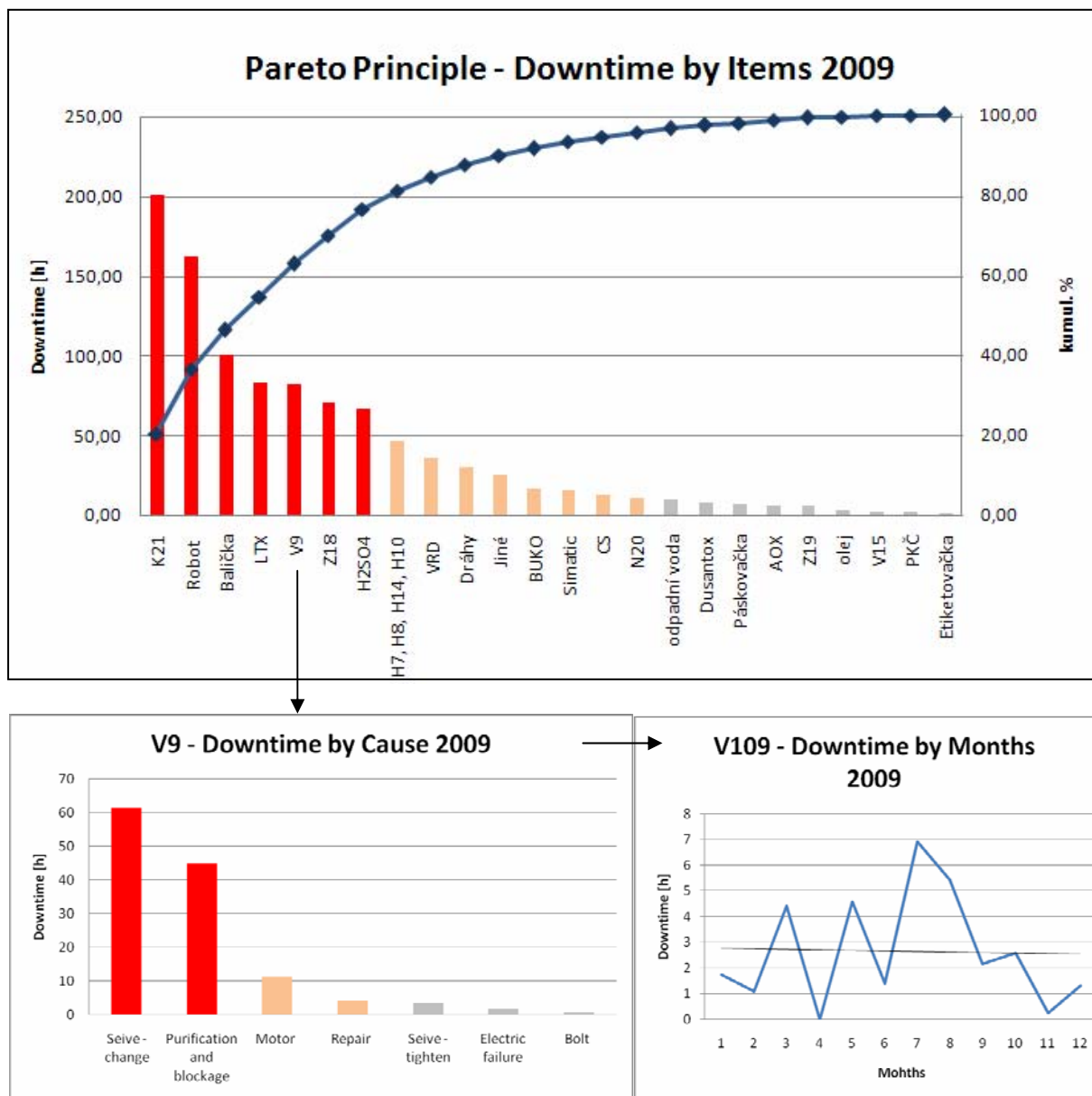


Figure 6. Production lines availability – downtime by failure mode 23.

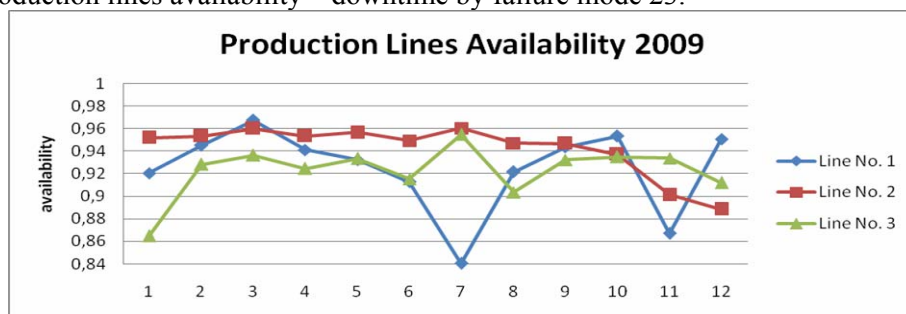


Figure 7. Availability by type of caoutchouc.

Type of caoutchouc	Availability		Availability only purification, blockage		Availability without purification, blockage	
	2008	2009	2008	2009	2008	2009
<b>Krallex SBR 1500</b>	0,9115	0,9224	0,9639	0,9747	0,9527	0,9533
<b>Krallex SBR 1502</b>	0,9336	0,9558	0,9658	0,9837	0,9728	0,9749
<b>Krallex SBR 17xx</b>	0,9443	0,9384	0,9770	0,9827	0,9708	0,9590

### Influence of Processed Material

If the one production line processes different material (material of different attribute) it is suitable monitor availability by processed type of caoutchouc. For expression of downtime worker has to eliminate determinate items and some failure modes. He has to calculate only with parts of production line whose reliability can influence processed material. It means eliminate conveyor belt and packing section in example in the figure 7.

### **Conclusion**

Data about operation reliability are very useful but they require high accuracy of entered data. Automatically collecting is especially very suitable for record of start and end of downtime. Flow of main material on the start of the line is the best indicator of downtime in this production line. Failure mode is indispensable for dividing downtime. But maintenance manager has to

know what he wants to express (purpose of information). Operation reliability by type of processed material monitoring is suitable, because there is different availability of type of caoutchouc in the figure 7. Every graphs in this article is possible to do in the MS Excel with using pivot tables.

### **Reference Example:**

- [1] BENBOW, D. W. – BROOME, H. W. *The Certified Reliability Engineer Handbook*. Milwaukee: American Society for Quality, Quality Press, 2009. 305 s. ISBN 987-0-87389-721-1.
- [2] ČSN EN 13306. *Maintenance terminology*. [s.l.] : Český normalizační institut, 2002. 42 s.
- [3] EBELING, Charles E. *An introduction to reliability and maintainability engineering*. Second Edition. Long Grove : Waveland Press, Inc., 2010. 544 s. ISBN 1-57766-625-9.

## OPTIMUM USE OF THE IRRIGATIONAL WATER IN A MAIZE (GRAIN) FIELD

GEORGI KOSTADINOV, MILENA MOTEVA\*

Research institute for Land Reclamation and Agricultural Engineering, 3 Shosse Bankya Str.,  
Sofia 1331, Phone: +359 886 919353, Fax: +359 2 8247842,  
E-mail: [milena\\_moteva@yahoo.com](mailto:milena_moteva@yahoo.com)

### Abstract

The contemporary climatic conditions and insufficient water resources in Bulgaria are the reason for applying regionally adapted and economically efficient water saving irrigational technologies. It is difficult to match high water use efficiency with low production costs. The highly efficient technologies require large scale investments. In this sense, gravitational irrigation method is the cheapest and most feasible one for field crops.

In this study the main irrigation scheduling parameters - application/irrigation depth and number of the applications and the space of irrigation were adopted as factors. The additional yield and water use efficiency were adopted as model's parameters. The complex impact of the irrigation scheduling parameters on the irrigation efficiency at certain irrigation water deficit was analyzed. Parameters of a maize (grain) irrigation scheduling under temporal and spatial water deficit conditions were obtained as a result of an optimization. Isolines that permit selection of an appropriate irrigation scheduling at certain water availability are suggested. Parameters of an irrigation scheduling permitting maximum water use efficiency under water deficit conditions are substantiated.

### Introduction

Water is considered a scarce and valuable resource. It requires rigorous management and extreme caution to prevent its depletion. A way for water waste restriction is by applying water saving and efficient irrigation technologies to increase irrigation water use efficiency (WUE). Deficit irrigation reasonably increases WUE. Farmers are open to adjust their water use with some degree of yield risk to gain some economic profits [1]. Deficit irrigation should be well managed in order to gain a moderate risk for crop yield and farmer's income.

The basic items for its planning and management are: 1) the efficiency of the irrigation technology applied and 2) the relation between the yield obtained and the water consumed/applied. The gravitational irrigation technologies perform possibilities for water saving at a certain wetting irregularity. One of the possible methods is wide-spaced irrigation. A substantial increase of the irrigation WUE can be achieved at wide-spaced irrigation. The magnitude in water savings can be 40-50% at acceptable 15-20% lower yields [2, 3, 4, 5]. Evapotranspiration losses can be reduced by 20 to 50% [6].

So far, the approaches in establishment the impact of different factors on yield and WUE

have been founded on single regression analyses. Their impact has been treated separately, but not in their complexity. The relationship yield-water, for example, studied by a great number of authors, takes into account only the given amount of water either seasonal or per stages. It does not consider the other parameters of the irrigation scheduling – the number of applications, the application depth, the pre-irrigation soil moisture, or the peculiarities of the irrigation technology, the wetting pattern and regularity. These features of the applied irrigation practice may have great impact on the final results of the production process – as on the yield so on the economic balance. We find it better that the farmers can make decisions about the elements of the irrigation process on a basic scheme that accounts for more than one yield factor.

The goal of the paper is to suggest, on the base of a multiple regression analysis and an optimization, facilitating tools for an appropriate choice for maize (grain) irrigation scheduling under wide-spaced irrigation. Our farmers need them, because Bulgaria has insufficient and uncertain water resources and deficit irrigation in the gravitational irrigation practice should be rationally planned and managed.

## Material and Methods

A multiple regression analysis of the complex impact of the irrigation depth, number of applications and space between the irrigated furrows on the yield and WUE was developed. By an optimization of the multiple regression models were established the conditions for obtaining maximum yield and maximum WUE. The numerical investigation used the results of a field experiment, conducted in Sofia region on Chromic Cambisols. The soils are moderate to heavy textured with high saturation conductivity in the 0-30-cm soil layer – 93 cm/day and low – down to 15 cm/day in the rest of the top 100-cm layer [7]. These soils are considered suitable for wide-spaced irrigation due to the clay-loamy part of the soil profile (40-100 cm from the surface) with good side infiltration, so that a relatively uniform moisturizing of the rooting zone is ensured and long time kept. Thanks to the high hydraulic conductivity, the 0-30 cm soil layer contributes for deep layers soil moisture preservation and for its efficient usage [8].

The variants of the experiment are presented in Tables 1 and 2 (columns 1, 2 and 3). The

optimum pre-irrigation soil moisture is accepted to be 80% of field capacity (FC) [9]. Two other variants of pre-irrigation soil moisture were tested – 75% and 70% of FC. The application depth at 80% of FC is 60 mm, at 75% of FC – 80 mm, and at 70% of FC – 100 mm. The applications have been spatially distributed in three variants of distance between the irrigated furrows – every furrow (EF), every other furrow (EOF) and every third furrow (ETF). The distance between the rows in the cultivar (between the furrows respectively) is 70 cm. The irrigated furrows in EOF lie 140 cm apart from one another, and in ETF – 210 cm respectively.

The field experiment was conducted in the periods 1987-1989 and 1996-1998. The years cover a great variety of meteorological conditions hence the results are considered representative. The number of given applications vary from 2 to 5, and the irrigation depths – from 60 to 320 mm (Table 1).

The results of the yields and WUE are given in Table 2.

**Table 1** Number of applications and irrigation depths

Irrigation schedule	Variants, Pre-irrig. Soil moisture, Application depth (m), mm	Irrig. Depth %	1987		1988		1989		1996		1997		1998	
			Appl nb	Irr. Dpth, mm	Appl nb	Irr. Dpth, mm	Appl nb	Irr. Dpth, mm	Appl nb	Irr. Dpth, mm	Appl nb	Irr. Dpth, mm	Appl nb	Irr. Dpth, mm
1	2	3	4	5	6	7	8	9	10	11	12	13	14	15
	Rain-fed													
Irrigated on the date of var. of 80% of FC	EF 80% of FC $m=60$	100	5	300	4	240	3	180	3	180	3	180	3	180
	EOF	100	-	-	-	-	-	-	3	180	3	180	3	180
	ETF	100	-	-	-	-	-	-	3	180	3	180	3	180
	EF	50	-	-	-	-	-	-	3	90	3	90	3	90
	EOF	50	5	150	4	120	3	90	3	90	3	90	3	90
	ETF	50	-	-	-	-	-	-	3	90	3	90	3	90
	EF	33	-	-	-	-	-	-	3	60	3	60	3	60
	EOF	33	-	-	-	-	-	-	3	60	3	60	3	60
Irrigated on the date of var. of 75% of FC	ETF	33	5	100	4	80	3	60	-	-	-	-	-	-
	EF 75% of FC $m=80$	100	4	320	3	240	2	160	-	-	-	-	-	-
	EOF	50	4	160	3	120	2	80	-	-	-	-	-	-
Irrigated on the date of var. of 70% of FC	ETF	33	4	104	3	78	2	52	-	-	-	-	-	-
	EF 70% of FC $m=100$	100	3	300	2	200	2	200	-	-	-	-	-	-
	EOF	50	3	150	2	100	2	100	-	-	-	-	-	-
	ETF	33	3	99	2	66	2	66	-	-	-	-	-	-



The irrigation depth, the number of irrigation applications and the distance between the irrigated furrows are taken as factors in the regression model, the additional yield and water use efficiency (WUE) - as estimated parameters.

In order to isolate the impact of the meteorological condition the assessed parameters are introduced as relative values (%) of the standards. The standard for the additional yield is taken the yield, obtained under rain-fed conditions, and for WUE - the WUE of the variant of maintaining the optimum pre-irrigation

soil moisture – 80% of FC. The standard for the irrigation depth is also the variant of 80% of FC.

The factors are coded as shown in Table 3. The minimum values are taken -1 and the maximum ones – 1.

Statistica, Mathcad and Excel software were use for data processing and illustration. Optimization is done for the full model without removing the insignificant coefficients, considering the fact that they also contain certain process information.

**Table 2** Yield results and water use efficiency (WUE)

	Variants, Pre-irrig. soil moisture, Application depth, mm	Irrig. depth %	Yield, Mg/ha						WUE, kg/m <sup>3</sup>					
			1987	1988	1989	1996	1997	1998	1987	1988	1989	1996	1997	1998
1	2	3	4	5	6	7	8	9	10	11	12	13	14	15
	Rain-fed		2,69	3,70	6,91	4,13	7,14	5,21	-	-	-	-	-	-
Irrigated on the date of var. of 80% of FC	EF 80% of FC appl.depth=60	100	12,24	14,34	9,34	9,79	8,53	12,57	3,21	4,59	1,35	2,54	0,81	4,09
	EOF	100	-	-	-	10,74	8,04	11,90	-	-	-	5,71	1,51	5,3
	ETF	100	-	-	-	9,15	8,19	12,58	-	-	-	6,28	2,65	7,61
	EF	50	-	-	-	7,52	7,95	85,5	-	-	-	3,05	0,47	3,72
	EOF	50	9,25	11,63	9,01	8,80	7,72	9,98	4,4	6,84	2,33	6,17	1,57	4,82
	ETF	50	-	-	-	7,85	7,56	9,68	-	-	-	5,73	1,72	7,44
	EF	33	-	-	-	6,02	7,69	6,78	-	-	-	1,45	0,77	4,09
	EOF	33	-	-	-	6,69	7,20	7,68	-	-	-	2,87	0,77	4,96
	ETF	33	5,91	8,80	8,30	-	-	-	3,24	8,0	2,32	-	-	-
Irrigated on the date of var. 75% of FC	EF 75% of FC appl.depth=80	100	10,21	12,26	9,09	-	-	-	2,37	3,64	1,37	-	-	-
	EOF	50	8,07	10,40	8,81	-	-	-	3,39	5,78	2,38	-	-	-
	ETF	33	5,59	7,67	8,12	-	-	-	2,71	5,21	2,28	-	-	-
Irrigated on the date of var. 70% of FC	EF 70% of FC appl.depth=100	100	9,88	12,03	9,28	-	-	-	2,42	4,31	1,19	-	-	-
	EOF	50	7,44	9,36	8,12	-	-	-	3,19	7,12	1,21	-	-	-
	ETF	33	4,66	7,26	7,90	-	-	-	1,99	8,3	1,47	-	-	-
<i>GD<sub>5%</sub></i>			1.08	1.11	0.51	0.78	0.59	1.01						
<i>GD<sub>1%</sub></i>			1.46	1.50	0.69	1.05	0.80	1.38						
<i>GD<sub>0,1%</sub></i>			1.94	1.99	0.92	1.41	1.07	1.85						

**Table 3.** Levels of variation of the independent factors

Factors	Coded value of the factor			Natural value of the factor		
	Lower level	Basic level	Upper level	Lower level	Basic level	Upper level
Spacing of irrigation, $X_1$	-1	0	1	EF	EOF	ETF
Number of applications, $X_2$	-1	-0,33   0,33	1	2	3   4	5
Irrigation depth, $X_3$	-1	0	1	30%	70%	110%

## Results

The results from the multiple regression analyses are presented in Table 4 and Table 5. Since the variables are turned into relative values, the developed models describe the estimated parameters adequately. The results in Table 4 show that:

- The significant factors for the additional yield are the number of the applications

and the irrigation depth, but not the distance between the irrigated furrows;

- The impact of the number of applications impact is stronger than that of the irrigation depth.

If  $Y_1$  is the additional yield, then:

$$Y_1 = 162,7 + 122,8X_2 + 72,5X_3, \quad r=0,75 \quad (1)$$

**Table 4.** Results from the multiple regression analysis for the additional Yield

Regression Summary for Dependent Variable: Y (Corn) R= ,74950097 R <sup>2</sup> = ,56175170 Adjusted R <sup>2</sup> = ,46555086 F(9,41)=5,8394 p<,00003 Std.Error of estimate: 64,861						
N=51	Beta	Std.Err. of Beta	B	Std.Err. of B	t(41)	p-level
Intercept			162,7116	24,12931	6,74332	0,000000
X1	0,023328	0,251294	2,5544	27,51729	0,09283	0,926491
X2	0,675701	0,147937	122,7906	26,88360	4,56749	0,000045
X3	0,567189	0,254510	72,5468	32,55338	2,22855	0,031388
X12	0,213835	0,374487	40,9107	71,64644	0,57101	0,571111
X13	-0,200245	0,121069	-31,2831	18,91381	-1,65398	0,105769
X23	0,501371	0,390696	109,0869	85,00664	1,28328	0,206602
X11	-0,077538	0,117108	-14,2536	21,52755	-0,66211	0,511606
X22	0,137507	0,113489	32,0292	26,43480	1,21163	0,232591
X33	-0,148772	0,117753	-51,4344	40,71020	-1,26343	0,213573

The results in Table 5 show that:

- The significant factors for WUE are the space of irrigation and the irrigation depth, but not the number of applications;
- .

- The space of irrigation between the furrows has a stronger impact than that of the irrigation depth.

**Table 5.** Results from the multiple regression analysis for WUE

Regression Summary for Dependent Variable: WUE (Corn norm) R= ,78050170 R <sup>2</sup> = ,60918291 Adjusted R <sup>2</sup> = ,52339379 F(9,41)=7,1009 p<,00000 Std.Error of estimate: 39,201						
N=51	Beta	Std.Err. of Beta	B	Std.Err. of B	t(41)	p-level
Intercept			166,5686	14,58347	11,42174	0,000000
X1	0,828214	0,237306	58,0438	16,63113	3,49007	0,001169
X2	-0,070477	0,139702	-8,1969	16,24813	-0,50448	0,616625
X3	0,507968	0,240343	41,5831	19,67488	2,11351	0,040687
X12	-0,014923	0,353641	-1,8272	43,30227	-0,04220	0,966547
X13	0,316586	0,114329	31,6540	11,43128	2,76907	0,008404
X23	0,115483	0,368949	16,0813	51,37702	0,31301	0,755863
X11	-0,051209	0,110589	-6,0248	13,01100	-0,46305	0,645774
X22	-0,008131	0,107172	-1,2121	15,97688	-0,07587	0,939893
X33	-0,133160	0,111198	-29,4642	24,60477	-1,19750	0,237989

If  $Y_2$  is WUE, then:

$$Y_2 = 166,6 + 58,0X_1 + 41,6X_3 + 31,7X_1X_3, \\ r=0,78 \quad (2)$$

The results from the multiple regressions analysis are:

- Reasonable.
- Show that except for the irrigation depth, there are some irrigation technological peculiarities that have competitive impact on the production process and its final results.

The distance between the irrigated furrows in this soil type is not the determinant factor for the yield increase, it is determinant for WUE. This is because the soil structure permits regular moisture distribution in the deep soil layers. No matter how the irrigation water is distributed over the irrigated surface EF, EOF or ETF, the essential amount infiltrates into the lower layers and is kept there. This is because the first layer dries quickly and its dusty texture embarrasses the evaporation through it from the lower layers to the atmosphere. The loamy fraction down the soil profile sets the pattern for good side infiltration, so that certain moisture regularity is achieved there and the water is productively used by the crop. In this case the significant factor for WUE is actually the seasonal water amount, given to the crop.

The frequency of water supply is more significant for the yield increase. The number of applications is determined by the pre-irrigation soil moisture. Consequently, pre-irrigation soil moisture is of greater importance for the yield formation than the irrigation depth. Actually, in conditions of one and the same irrigation depth at three levels of pre-irrigation soil moisture the highest yields - 9,34 to 14,34 Mg/ha (Table 2) are obtained at the highest pre-irrigation soil moisture - 80% of FC, which predetermines the distribution of the irrigation depth through the smallest portions (application depths) with the greater frequency during the vegetation season. The yield at the other two levels of pre-irrigation soil moisture is around 13% less. The similar yields, i.e. the similar yield reduction at these

two pre-irrigation soil moisture levels in comparison with the optimum one is also reasoned by the hydraulic properties of the soil. Breaking of the capillary contacts in this soil type occurs at 78% of FC. If soil is dried to lower % of FC, plant water supply is embarrassed [6]. Hence irrigation at a lower than 80% of FC pre-irrigation soil moisture is not expedient. This peculiarity has impact on the results of our numerical investigation which show the significance of the number of applications for the additional yield accumulation.

The distance between the irrigated furrows in this soil type is a determinant factor for WUE, because the physical evaporation from the deep soil layers is restricted by its texture. Hence soil water is exhausted mainly by transpiration. When the distance between the furrows increases, the contact surface of the irrigation water with the atmosphere decreases hence open water evaporation losses are restricted.

The space of irrigation has more significant impact on WUE for two more reasons. If the application depths are great (in the cases of delivering of 100% of the application depth in EOF and ETF) the gravitational power would surpass the side infiltration, so there would occur water losses out of the rooting zone. If the application depths are small (in the cases of 50% and 33% EOF and ETF) the capillary forces prevail over the gravitational ones as it is in the deficit irrigation in principle and the water is kept in the rooting zone. It is obvious that wide-spaced irrigation, when it is deficit irrigation, contributes for water preservation and for higher WUE.

It stems from this analysis that yield accumulation is related not only to the seasonal irrigation water amount given to the crop, i.e. the irrigation depth, but also to some other features of the irrigation practice - the irrigation schedule and the surface spacing of the irrigated furrows. Further economic analyses would show the optimum conditions for a profitable irrigation practice and would assist for the right choice of the farmer. A partial contribution to that choice is the optimization of our two regression models.

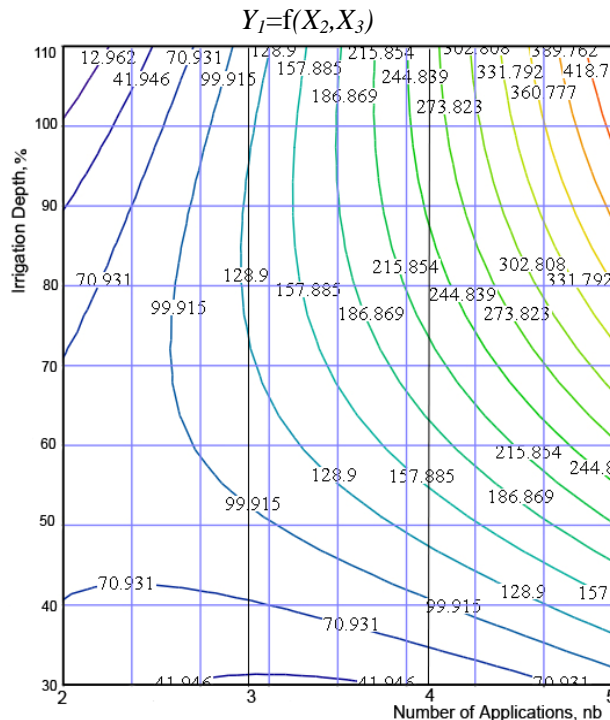


**Fig. 1** Lines of the identical response of the yield to the number of applications ( $X_2$ ) and the irrigation depth ( $X_3$ ) at EOF.

The optimization of the yield and WUE models shows that:

- Maximum additional yield (447,7%) is obtained at coded levels of the factors  $X_1=0$ ;  $X_2=1$  and  $X_3=1$ . Maximum additional yield is obtained when the maximum irrigation depth is delivered in EOF by the maximum number of applications. This result confirms the suitability of the soil type for wide-spaced irrigation.
- The maximum value of the parameter WUE (up to 280%) is obtained at maximum values of all factors –  $X_1=1$ ,  $X_2=1$ ,  $X_3=1$ . Maximum WUE is obtained when maximum irrigation depth is delivered in ETF by the maximum number of applications. This result confirms the efficiency of wide-spaced irrigation and its suitability in cases of water insufficiency

On Fig. 1 are drawn the lines of the identical response of the yield to the two most significant factors – the number of applications and the irrigation depth at EOF. On Fig. 2 are drawn the lines of the identical response of WUE to the space of irrigation and the irrigation depth when the latter is divided into 3 application depths – the most frequent case in Bulgarian conditions. These nomograms permit the farmers choose the

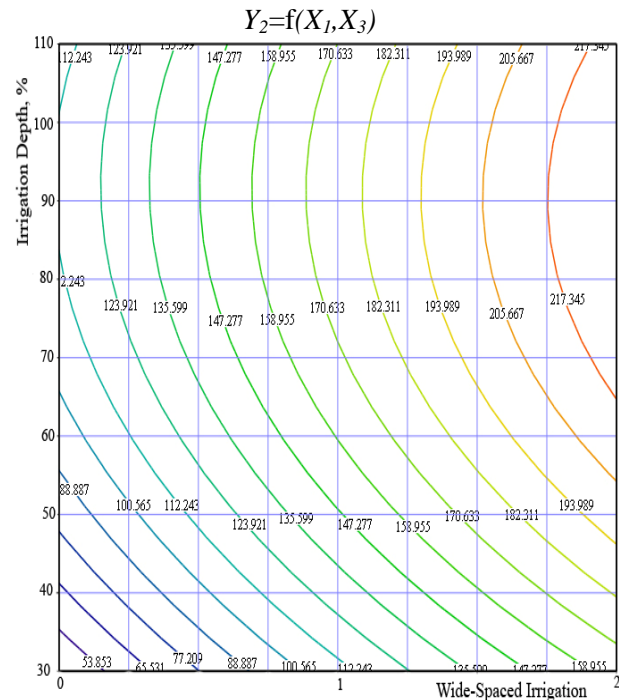


**Fig. 2** Lines of the identical response of the WUE to the space of irrigation ( $X_1$ ) and the irrigation depth ( $X_3$ ) at  $X_2=-0.3333$  ( three applications )

optimal combination of irrigation depth and the number of applications and distance between the irrigated furrows in order to obtain the desirable additional yield and WUE.

## Conclusions

1. Significant factors for yield accumulation are the number of the applications and the irrigation depth, but not the distance between the irrigated furrows. The impact of the application number is stronger than that of the irrigation depth. Water use efficiency is controlled by the number of applications and the distance between the irrigated furrows. The irrigation depth is not a significant factor.
2. Optimum additional yield (448%) is obtained when the maximum irrigation depth is given through 5 applications in every other furrow. Optimum WUE is obtained at ETF distribution of the maximum irrigation depth with maximum number of applications.
3. Nomograms for making proper decision about the irrigation depth, number of applications and distance between the irrigated furrows are suggested.

## Acknowledgements

The authors express their high appreciation to the Bulgarian National Science Fund for its financial support - Project DO 02-47/10.12.2008 "Regional Center for Sustainable Development and Application of the Agricultural and Transport Equipment".

## References

1. English, M.J.: The uncertainty of crop models in irrigation optimization. Transactions of the ASAE, 1981, 24, 917–921, 928
2. Crabtree, R.J.-Yassin, A.-Kargougou, A.I.-McNew, R.W.: Effects of alternate-furrow irrigation: Water conservation on the yields of two soybean cultivars, Agricultural Water Management, 1985, 10, 3, p.253-264
3. Moteva, M.: On the distance between the irrigated furrows at maize (grain). Agricultural Engineering, 2005, 6, p.32-37 (in Bulgarian)
4. Stoyanova, A.: Irrigation parameters of maize (grain) under the conditions of Second Agroclimatic Group, 2006, Thesis, S., p.163 (in Bulgarian)
5. Kang, Sh.-Liang, Z.-Pan, Y.-Shi, P.-Zhang, J.: Alternate furrow irrigation for maize production in an arid area, Agricultural Water Management, 2000, 45(3), p.267-274.
6. Stone, J.F.-Reeves, H.E.-Garton, J.E.: Irrigation water conservation by using wide-spaced furrows. Agricultural Water Management, 1982, 5(4), p.309-317
7. Varlev, I.-Popova, Z.: Water-Evapotranspiration-Yields. 1999, Sofia, p.144 (in Bulgarian)
8. Koleva, S.: An investigation of the water exchange within the system soil-plant-atmosphere. Thesis. (1974) Petersburg, p.153 (in Russian)
9. Boyanov, P.,-Tatarova-Krasteva, V.-Koleva, S.: An investigation of the admissible minimum soil moisture at irrigation conditions. Soil Science and Agrochemistry, 1970, 5(2), p.9-17 (in Bulgarian)



## EFFECT OF SOIL LOOSENING INTENSITY ON WATER RUNOFF RATE UNDER SIMULATED RAIN CONDITIONS

PAVEL KOVAŘÍČEK<sup>1\*</sup>, KAROLÍNA MAREŠOVÁ<sup>1</sup>, JOSEF HŮLA<sup>1,2</sup>,  
MILAN KROULÍK<sup>1,2</sup>, MARCELA VLÁŠKOVÁ<sup>1</sup>

<sup>1</sup> Research Institute of Agricultural Engineering, p.r.i., Prague  
tel: 233022236, fax: 233312507, e-mail: pavel.kovaricek@vuzt.cz  
<sup>2</sup> Czech University of Life Sciences Prague, Faculty of Engineering

### Abstract

Water runoff was evaluated under simulated rainfall a field with maize (*Zea mays* L.) in year 2008. Two variants of soil treatment were established with heavy loamy soil. The sloping for the measurement was between 3° and 4°. First field experiment was established with ridge tillage which was created by autumn and second variant was established with pre-sowing tillage by spring. Direction of ridge and soil tillage was oriented along slope.

The different technologies of a soil tillage lead to the changes of the water runoff. Water infiltration into soil was more favorable under variant with pre-sowing tillage in comparison with ridge tillage. At the simulated rainfalls intensity of 87.8 mm.h<sup>-1</sup> (1.463 mm.min<sup>-1</sup>) the water runoff under variant with ridge tillage increase four times and soil loss increased ten times in comparison with spring tillage treatment

**Keywords:** ridge tillage, pre-sowing preparation, water runoff, rainfall simulation

### Introduction

More than a half of arable land in the Czech Republic is at risk from water erosion. Farming on this land requires special treatments and conservation tillage technologies play important role with this respect. Conservation tillage is based on only shallow tillage and mixing the upper part of soil profile including crop residues. Especially plant remains particles incorporated in soil profile are very important factor for good water infiltration. These particles make so called preferential ways for water infiltration, significant mainly during intense rainfalls. After several years of conservation technologies utilization, particular changes of physical soil properties can be observed in fields. This fact together with a need for occasional deeper tillage, required especially for row crops and crops planted in ridges, was the reason for detailed evaluation of water runoff in different fields.

Deep tillage together with making ridges for particular plants is used nowadays for maize, soya, potatoes, sorghum, sunflower, cotton plant and in addition especially in Europe also carrot, asparagus and sugar beet (Liu et al. 2006; Schlinder et al. 2007; Krause et al. 2009). Plant growing in ridges is used with good effect as

prevention from wind and water erosion (Liu et al. 2006). This technology also helps with water management concerning water saving in soil profile (Bruneau, Twomlow 1999; Lamb et al. 1998; Hatfield et al. 1998, Tomer et al. 2006).

### Materials and methods

Agricultural farm HNG-CZECH s.r.o. is one from several companies in the Czech Republic which uses row crops sowing into ridges in large scale. The farm has 1950 hectares and as a main crop produced there belongs maize, winter wheat and oil seed rape. Conservation tillage technology is used for all fields on the farm which results in high performance and efficiency of machinery used in fields and also in cost reduction. Soil types in the farm are represented by heavy clayey soils which are hard to cultivate both under wet and under dry conditions.

Deeper tillage is usually done for all mentioned plants in order to achieve better soil moisture and temperature conditions. This kind of tillage is carried out after winter wheat planting, at optimum moisture level concretely for maize with chisel tiller (chisel distance 375 mm). This tiller is equipped with a tool for ridges making (ridges distance 750 mm). When the soil moisture conditions are not favorable,



only deep tillage is performed. The, fields treated in this way require spring pre-seeding tillage every time.

Hydro-physical properties of soil and water infiltration into soil profile were evaluated in June 2008 simultaneously at two places.

- maize stand sown in spring into ridges which had been made during autumn deep tillage
- maize stand sown by combined seeding machine with rotary harrows, with pre-seeding shallow tillage and consequently deep tillage (chisel plough).

Water runoff was measured by means of artificial raining simulator at the area of 0.5 m<sup>2</sup> and with the raining intensity of 87,8 mm.h<sup>-1</sup> (1,46 l.m<sup>-2</sup>.min<sup>-1</sup>) at constant spraying pressure 100kPa (Kováříček et al. 2008). Water runoff flowing down from the measuring area is lead into a box which is weighed by digital scales. Weight of the cumulative runoff in chosen time interval of 5 s was recorded into PC memory.

Water infiltration velocity is then determined from the constant rain intensity during one trial run and from the sum of runoff water from measuring area. Captured runoff water is further filtered, soil particles from filtration process are dried and this dry soil matter is unit soil loss - (kg.m<sup>-2</sup>.h<sup>-1</sup>) caused by water erosion. Also other derived variables recounted for 1 m<sup>2</sup> are calculated from the constant rain intensity during one trial run and from the sum of runoff water from measuring area – such as cumulative rainfall, cumulative surface runoff, and cumulative infiltration. These parameters are mutually comparable if measuring parameters and soil properties at measured places are similar – grain size distribution, soil moisture content, field slope, roughness, plant remains coverage etc.

Spatial distribution of soil particles was evaluated by means of undisturbed soil samples taken into Kopecky's rings (100 cm<sup>3</sup>) – bulk density reduced and instant soil moisture. The rings with soil samples are taken from layer in different depths up to 350 mm with the step of 50 mm. The plane going through the tops of ridges was taken as the starting surface layer. Thus, the first samples taken from the area between ridges were evaluated as taken from the depth of 100 – 150 mm (average height of ridges was 110 mm). The samples were processed in

the standard way and soil bulk density reduced and instant moisture content was determined.

Gravimetric method was used for determination of soil moisture content in disturbed soil samples. Water content in soil was observed in percent of total weight (drying at 105 °C). Soil samples are taken by U-shaped probe from desired depth.

Plant remains coverage (possibly also vegetation coverage) evaluation was evaluated by color image analysis method and software COREL 11 was used for this analysis. The outcome from plant coverage evaluation is the percentage representation of the area covered by plant remains, vegetation or by weed plants.

Soil surface roughness is one of the factors which influence soil erosion. This feature was determined by the Chain Method. Measuring chain with the specified length (i.e. L = 100 cm) is placed on field surface and the horizontal projection of its contracted length is measured, in reference to real field surface (L<sub>0</sub>). Roughness or curvature of the field surface is then determined from the following formula  $T = (L - L_0) / L_0$ , where L is real length of the profile (100 cm) and L<sub>0</sub> is the horizontal projection of this length. By using the empiric formula (Klik et al. 2002), written down, it is possible to calculate also the random roughness of the field surface.

$$R [\text{cm}] = -29,37 \cdot T^2 + 37,59 \cdot T + 0,75$$

## Results and discussion

Undisturbed soil samples (Kopecky's rings) were taken from the fields in the beginning of April, 2 month prior to rain simulation trials and water runoff measurements. The soil bulk density reduced, measured throughout the ridges up to depth of 150 mm showed significantly loose soil (Table 1). The variant with deep tillage showed loosened soil profile only up to depth of 100 mm. Soil moisture values does not show any important difference in spring time (Table 2). Concerning roughness of soil surface, field with spring shallow tillage presented twice as big values as ridges variant. The beginning time for water runoff, cumulative water runoff and erosive wash-off was three to four times smaller in the spring tillage variant than in the ridges variant (Table 3). In the repetition variant "ridges

+ tillage<sup>2</sup>”, water runoff and also soil wash-off was insignificant.

The course in time of the intensity of water runoff and infiltration into soil profile are charted in Picture 1 and Picture 2. Picture 3 shows comparison of cumulative water runoff of the variant with making autumn ridges plus direct

seeding into ridges in spring time and of the variant with autumn deep tillage plus combined spring shallow tillage with seeding.

Water runoff after 60 minutes of rain simulation reached 52.28 % in ridges field and 7.25 % in the field with pre-seeding shallow tillage.

**Tab. 1** Bulk density and gravimetric moisture of soil profile for autumn tillage. Term of measuring - April

Depth [mm]	Bulk density [g.cm <sup>-3</sup> ]			Moisture gravimetric [%]		
	Ridge	Between ridge	Deeper loosening	Ridge	Between ridge	Deeper loosening
50	1.01	-	1.06	19.3	-	21.3
100	1.20	-	1.40	24.6	-	25.4
150	1.42	1.23	1.41	24.5	30.1	22.7
200	1.70	1.67	1.64	17.3	18.7	18.3
250	1.73	1.79	1.64	17.5	16.5	18.0
300	1.68	1.80	1.69	17.5	15.0	15.9
350	1.74	1.76	1.74	14.7	15.7	15.5

**Tab. 2** Physical properties of soil profile and soil surface before runoff measuring

Variant	Rep.	Slope [°]	Roughness [mm]	Residues cover [%]	Moist. [% grav.] for profile layer [mm]			
					surface	0-100	100-200	200-300
Deep tillage + ridge	1	4,3	15,23	4,35	2,5	12,8	11,3	13,2
	2	3,2	15,26	2,17	3,8	13,5	11,7	12,7
Deep tillage + shallow tillage	1	2,8	30,32	1,42	2,8	18,9	19,9	20,1
	2	3,4	27,93	1,67	2,9	19,9	19,1	19,3

**Tab. 3** Runoff measuring results

Variant	Rep.	Runoff beginning tp [min]	Runoff [mm] after some time [min]				Erosive wash-off after 1 hour of rainfall [g.m <sup>-2</sup> .h <sup>-1</sup> ]
			30	40	50	60	
Deep tillage + ridge	1	8,9	8,657	19,375	31,347	43,542	50,9
	2	10,9	14,065	25,173	36,916	48,217	105,6
Deep tillage + shallow tillage	1	31,9	0	2,209	6,263	11,565	11,9
	2	40,6	0	0	0,591	1,168	0,6

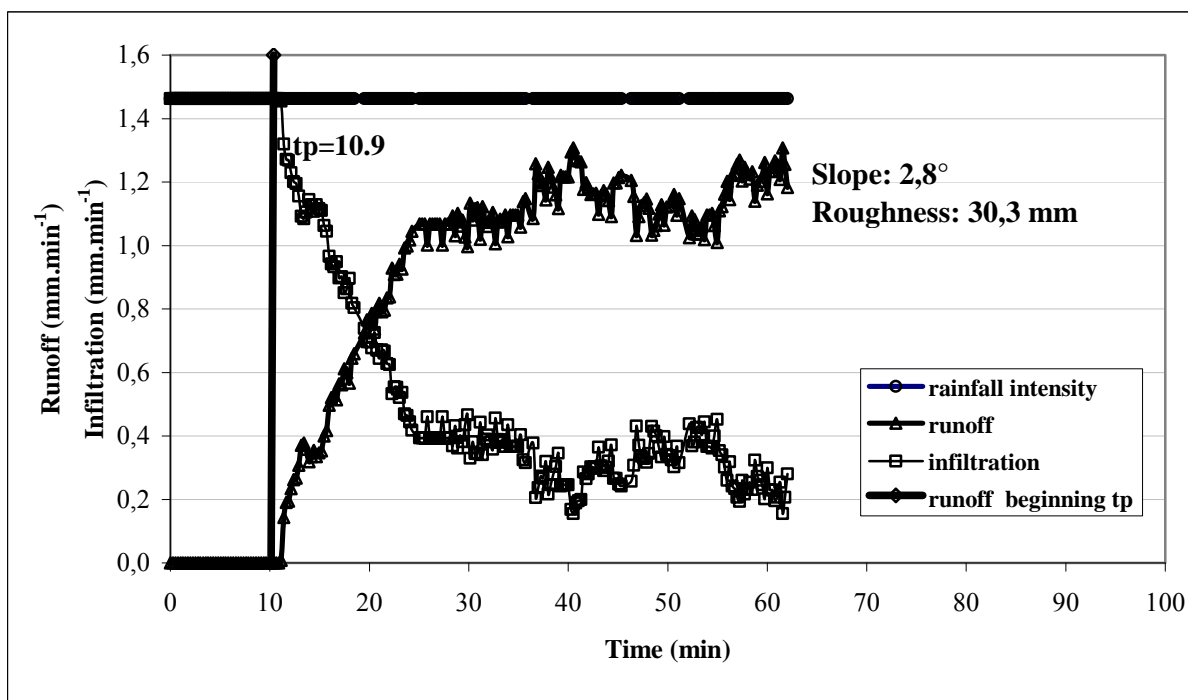


**Fig. 1** Runoff and water infiltration under 87,8 mm.h<sup>-1</sup> rainfall for deep tillage and ridge tillage variant

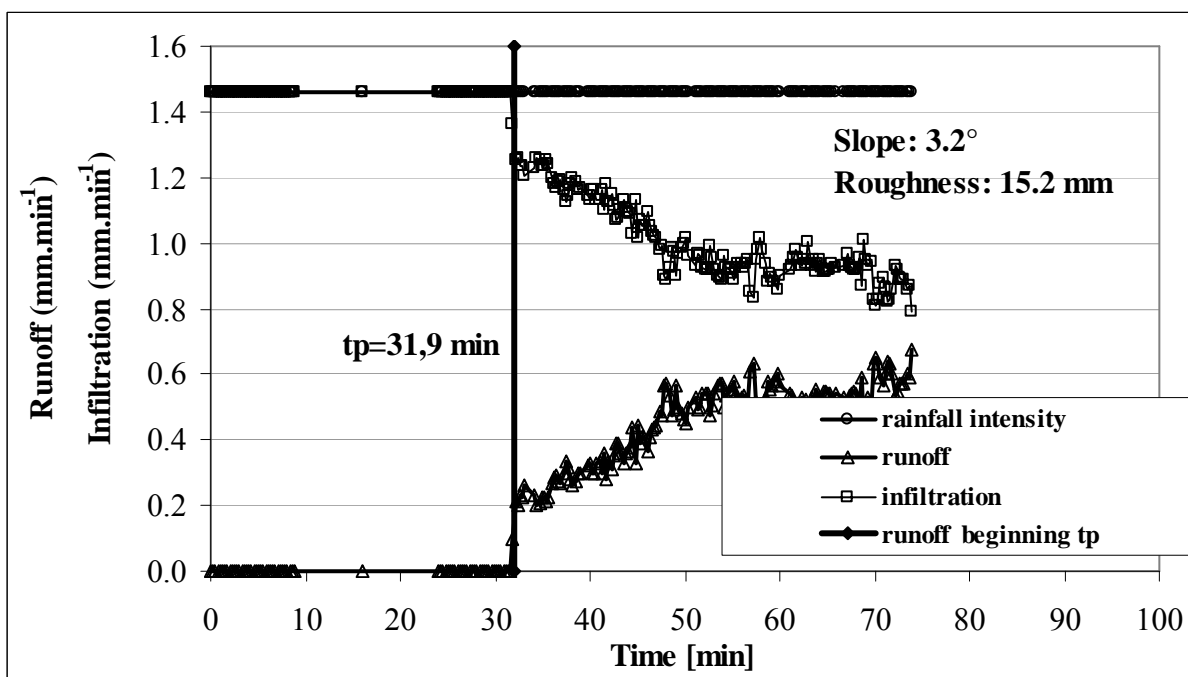


**Fig. 2** Runoff and water infiltration under 87,8 mm.h<sup>-1</sup> rainfall for deep tillage and shallow tillage variant

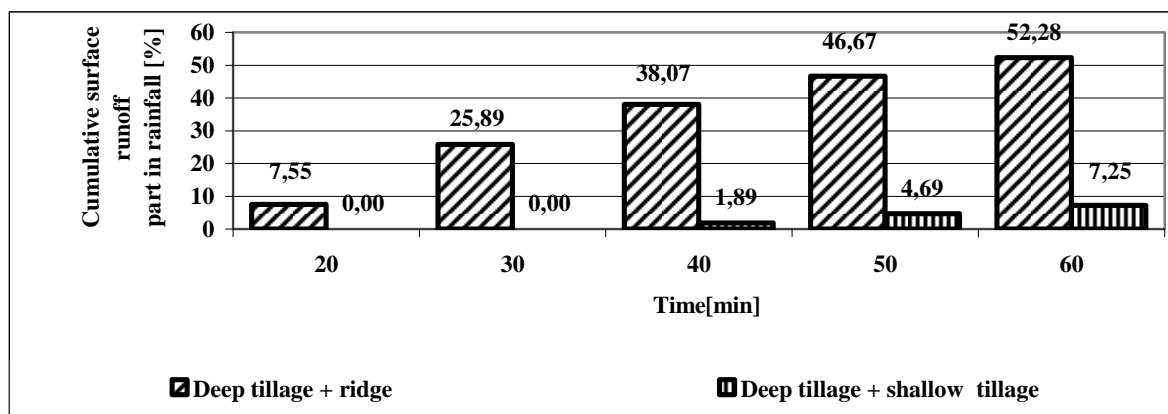


**Fig. 3** Comparison of cumulative surface runoff in two different tillage variants

### Conclusions

When observing the field with maize sown and planted in ridges on gentle slope (inclination of 4°), in the fall-line direction, under the raining rate of 87,8 mm.h<sup>-1</sup>, the greater intensity of soil loosening in ridges had no effect on water runoff decrease. Water erosion was evident on the sides of ridges with the inclination angle 8 - 11° after 3 minutes from the rain simulation start. When observing field with maize sown by the combined seeding machine (shallow tillage with rotary harrows and then seeding) with autumn deep tillage, the water runoff was up to ten times smaller.

The ridges in the fall-line direction combined with heavy clayey soil conditions in the field had not so significant influence on water erosion intensity as shallow pre-seeding tillage in spring. This shallow tillage reduced water runoff to ¼ and soil losses caused by water erosion was reduced ten times comparing with ridges.

### Acknowledgements:

This research and outcomes were supported by research project NAZV QH82191 and research project MZE0002703102.

### References

- [1] Bruneau, P.M.C.-Twomlow, S.J.: Hydrological and Physical Responses of a Semi-arid Sandy Soil to Tillage. *J. Agric. Engng. Res.* 72, 1999, p. 385-391.
- [2] Hatfield, J.L.-Allmaras, R.R.-Rehm, G.W.-Lowery, B.: Ridge Tillage for Corn and Soybean Production: Environmental Quality Impacts. *Soil & Tillage Research* 48, 1998, p. 145-154.
- [3] Klik, A.-Kaitana, R.-Badraoui, M.: Desertification hazard in a mountainous ecosystem in the High Atlas region, Morocco. In *Proc. 12<sup>th</sup> ISCO Conference*, Beijing, 2002, p. 636-644.
- [4] Kovaříček, P.-Šindelář, R.-Hůla, J.-Honzik, I.: Measurement of water infiltration in soil using the rain simulation method. *Research in Agricultural Engineering* 54, 2008, no. 3, p. 123-129.
- [5] Krause, U.-Koch, H.J.-Maerlaender, B.: Soil properties effecting yield formation in sugar beet under ridge and flat cultivation. *Europ. J. Agronomy* 31, 2009, p. 20-28.
- [6] Lamb, J.A.-Dowdy, R.H.-Anderson, J.L.-Allmaras, R.R.: Water quality in an irrigated sandy soil: ridge tillage in rotated corn and soybean compared with full-width tillage in continuous corn. *Soil & Tillage Research* 48, 1998, p. 167-177.
- [7] Liu, M.X.-Wang, J.A.-Yan, P.-Liu, L.Y.-Ge, Y.Q.-Li, X.Y.-Hu, X.-Song, Y.-Wang, L.: Wind tunnel simulation of ridge-tillage effects on soil erosion from cropland. *Soil & Tillage Research* 90, 2006, p. 242-249.
- [8] Schlinder, G.-Sander, G.-Decker, M.-Kremer-Schillings, W.-Burcky, K.-Koch, H.J.: Ridge cultivation of sugarbeet - recent experiences and experimental results from Germany. *Zuckerindustrie* 12, vol. 132, 2007, p. 920-924.
- [9] Tomer, M.D.-Cambardella, C.A.-James, D.E.-Moorman, T.B.: Surface-Soil Properties and Water Contents across Two Watersheds with Contrasting Tillage Histories. *Soil Sci. Soc. Am. J.*, vol. 70, March- april 2006, p. 620-630.

## SPATIAL DIFFERENTIATION OF THE INFRASTRUCTURAL EQUIPMENT OF RURAL AREAS IN POLAND

ANNA KRAKOWIAK-BAL

University of Agriculture in Krakow, ul. Balicka 116B, 30-149 Kraków, Poland,

Phone: +48 12 6624655, E-mail: anna.krakowiak-bal@ur.krakow.pl

### Abstract

The estimation of spatial diversification of the technical infrastructure development in rural areas in Poland is the main purpose of this paper. Furthermore there was analyzed efficiency of secured EU funding which was confronted with level of infrastructural equipment.

The researches have covered rural areas in 1620 communes (LAU2). As infrastructural equipment there were analyzed: sewerage network, water supply system, roads and the gas grid.

There were used chosen methods of multidimensional comparative analysis which enable clustering the multicriterial objects: the Perkal's method and Jenks Optimization. There were indicated rural regions with the most and the least balanced structures of infrastructural equipment as the main result of paper. The trends of regional infrastructure development in analyzed regions were indicated.

### Introduction

A major component of competitiveness in agricultural value chains is access to affordable physical infrastructure. This includes infrastructure that supports on-farm production (irrigation, energy, transportation, pre- and post-harvest storage), ensures efficient trading and exchange (telecommunications, covered markets), adds value to the domestic economy. A number of empirical studies have demonstrated the importance of public infrastructure in real economies (Anwar S., 2008). National public infrastructure investment has a positive effect on both the number of intermediate input producers and the return to the immobile factor in the home country (Egger H., Falkinger J., 2006). The relationships between infrastructural level and economic activity were also analyzed (Chandra A., Thompson E., 2000, Krakowiak-Bal, 2007). It can be concluded that the greatest impediment to growth of agribusinesses is insufficient access to infrastructure services (FAO, 2008). Also the principles of the European Union's Programme for developing rural areas aim at: increasing the productivity of agriculture, providing agricultural people with a proper standard and level of living, stabilizing agricultural and food product markets (Sochacka D., 2007). Achievement of those targets and goals is possible only thanks to appropriate infrastructural equipment.

### Material and Method

1620 rural Polish communes (LAU2) described with 4 variables relating to the infrastructural equipment and 2 variables presenting efficiency of secured EU funding are objects analyzed in this paper. Data base regards year 2009. In the Table 1 are specified all variables.

The Perkal's method and Jenks Optimization were used for objects' clustering.

Perkal's method of natural indicators allows the comparability of different metrics and receives a single synthetic indicator of the region's development level. It provides a convenient classification schemes for the regionalization, allowing the classification of the surveyed units in terms of derived indicators of the level of regional development.

Procedure of Perkal's method includes (Heffner, Gibas, 2007):

- definition of data matrix,
- grouping the variables,
- variables standardization,
- calculate the total volume ratio ( $W_i$ ), the residual coefficients values ( $C_i$ ) and the indicator of proportional development ( $D_i$ ).

Table 1. Basic characteristics of variables

Variable	Unit	Symbol	Average	Standard deviation	Coefficient of variation
Persons using the water supply system	%	I1	73,1	23,75	0,32
Persons using the sewerage network	%	I2	22,1	19,46	0,88
Persons using the sewerage network	%	I3	13,3	23,35	1,75
Road system	km·(100 km <sup>2</sup> ) <sup>-1</sup>	I4	66,63	62,63	0,94
Investment earnings from the EU budget	%	F1	22,08	36,79	1,67
Investment expenditure for the municipal economy and environmental protection	%	F2	78,98	39,91	0,51

Through  $W_i$  application there is obtained arrangement of spatial units depend on the characteristics of the whole set of variables. Analysis of the harmonious of spatial arrangement allows  $D_i$  calculation. The most balanced structure is representing by lowest  $D_i$  value. Each commune was described with  $D_i$  indicator. Then for objects clustering was used Jenks Optimization.

This method (also known as the Jenks Natural Breaks Classification method, the goodness of variance fit (GVF)) is a data classification method designed to determine the best arrangement of values into different classes. It seeks to reduce the variance within classes and maximize the variance between classes.

$$GVF = SDAM - SDCM / SDAM$$

where:

SDAM = sum of squared deviations from array mean

SDCM = sum of squared deviations from class means

Optimization is achieved when the quantity GVF is maximized. There are four steps that must be repeated (Jenks, 1967):

1. calculate the sum of squared deviations between classes (SDBC),
2. calculate the sum of squared deviations from the array mean (SDAM),
3. subtract the SDBC from the SDAM (SDAM-SDBC). This equals the sum of the squared deviations from the class means (SDCM),
4. after inspecting each of the SDBC, a decision is made to move one unit from the class with the largest SDBC toward the class with the lowest SDBC.

New class deviations are then calculated, and the process is repeated until the sum of the

within class deviations reaches a minimal value (SDCM) and therefore increase the GVF statistic. This process continues until the GVF value can no longer be increased.

## Results

On the basis of Perkal's method the  $D_i$  values were calculated. Among all 1620 analyzed rural communes, the most balanced structure of infrastructural equipment has Mszana in Slaskie Province. It was described with a minimum  $D_i$  value (0,91). However the most unbalanced structure presents Łodygowice in the same province ( $D_i$  is 16,55). Clearly visible are the advantages of the road system (I4) over the other infrastructural elements.

On the Fig.1,2. those structures are presented. The average  $D_i$  value is 3,7.

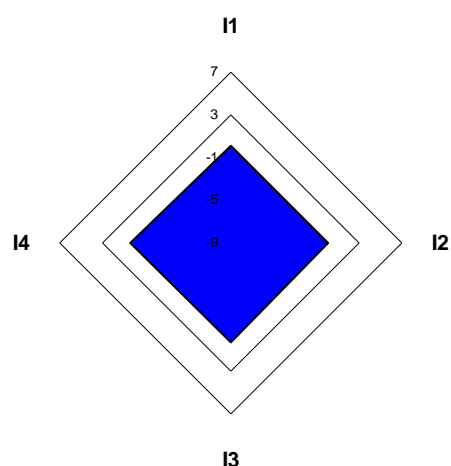


Fig.1. Balanced structure of infrastructural equipment according to residual coefficients values  $C_i$  (Muszyna commune)



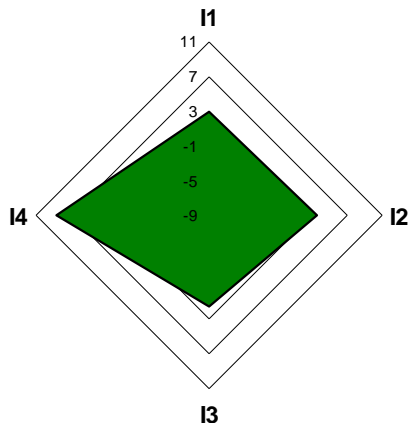


Fig.2. Unbalanced structure of infrastructural equipment according to residual coefficients values  $C_i$  (Łodygowice commune)

To extract groups of rural communes with similar infrastructural equipment there was used Jenks Natural Breaks Classification. The results are shown on the fig.3.

All objects have been divided into five groups. There can be seen a great disparity in  $D_i$  values.

The most numerous is the interval between 2,5 and 4,2. There are few communes with a highest  $D_i$  values.

The group I includes 424 communes (26%) with the most proportional infrastructural development. The most numerous is group II with 717 objects (45%). The indicator of proportional development ranges from 2,97 to 4,08. The weakest group represents only 7 objects (0,4%).

There can be concluded that the level of technical infrastructure on rural areas in Poland is very different. It should be emphasized that the harmonious structure does not represent the best infrastructural equipment. It illustrates the most balanced system without dominant infrastructural element. A common situation in the analyzed commune is on the one hand a well-developed road network or water supply and on the other hand the total absence of gas or sewerage networks.

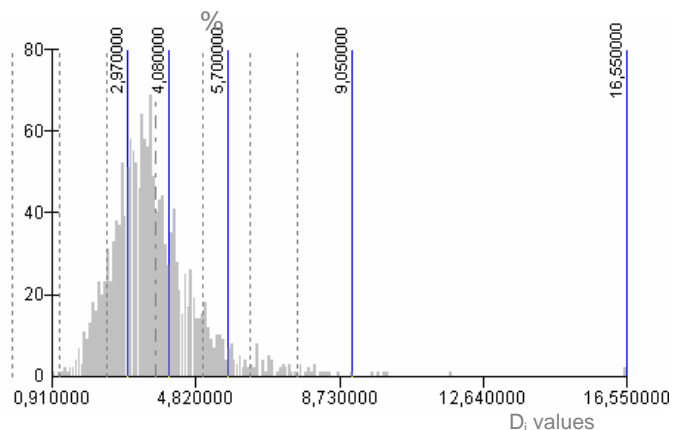


Fig.3. Classification results according Jenks Natural Breaks

The spatial arrangement of the determined groups is shown on the fig.4.

The analysis of the communes' financial management did not give satisfactory results. Among the analyzed rural communes nearly 80% have acquired funds from the EU, but only 34% received funds for investments.

There is no statistically significant correlation between the proportionality of the infrastructural development and the level of EU funds assigned for investment. This shows still a significant deficiency of infrastructure in rural areas in Poland. Regardless of the amount of resources spent on infrastructure, its level is unsatisfactory and uneven. In almost 80% of rural communes 100% of expenditure on environmental protection and utilities are appropriated for investment. Hence the need to increase EU funding for this purpose.

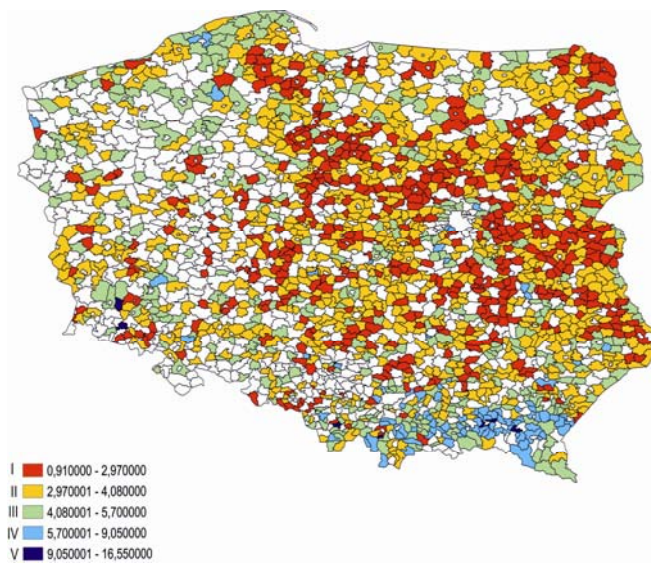


Fig.4. Spatial differentiation of rural areas in Poland in terms of technical infrastructure development

## Conclusions

1. The analysis of obtained results indicates significant differences in infrastructural development of rural areas in Poland. This applies to both the value and spatial distribution.
2. The most numerous rural communes represent an average balance of infrastructural development.
3. The majority of communes from the best group (group I), with the most proportional infrastructural development are located in central Poland, near Warsaw agglomeration.
4. The communes with most unbalance structure of infrastructural development are mountain areas on the South of Poland.
5. There were no significant correlation between the proportionality of the infrastructural development and the level of EU funds assigned for investment.
6. Methods of economic and spatial analysis used for evaluation of infrastructure development have produced satisfactory results.

## References

- [1] Anwar S.: Labour supply, foreign investment and welfare in the presence of public infrastructure. *Economic Modelling*, Volume 25, Issue 5, 2008, p.959-967
- [2] Chandra A., Thompson E.: Does public infrastructure affect economic activity? : Evidence from the rural interstate highway system. *Regional Science and Urban Economics*, Volume 30, Issue 4, 2000, p. 457-490
- [3] Egger H., Falkinger J.: The role of public infrastructure and subsidies for firm location and international outsourcing. *European Economic Review*, Volume 50, Issue 8, 2006, p. 1993-2015
- [4] Heffner K., Gibas P.: The economic and spatial analysis. *Economic University in Katowice*, 2007, p.87-98 (in polish)
- [5] Jenks G.F.: The Data Model Concept in Statistical Mapping, *International Yearbook of Cartography* 7, 1967, p.186-190.
- [6] Kanungo, T.; Mount, D. M.; Netanyahu, N. S.; Piatko, C. D.; Silverman, R.; Wu, A. Y.: An efficient k-means clustering algorithm: Analysis and implementation. *IEEE Trans. Pattern Analysis and Machine Intelligence* 24, 2009, p.881-892.
- [7] Krakowiak-Bal A.: Time delayed correlations between the enterprise level and the infrastructural equipment on the rural areas, *Infrastructure and Ecology of Rural Area*, 2/2007, p.173-180 (in polish)
- [8] Manthey B., Röglin H.: Improved Smoothed Analysis of the k-Means Method. *Proceedings of the Twentieth Annual ACM-SIAM Symposium on Discrete Algorithms*, 2009, n.461
- [9] Market-oriented agricultural infrastructure: appraisal of public-private partnerships. *FAO*, 2008, p.136
- [10] Sochacka D.: Programme guidelines on the pro-ecological policy of rural areas development, *Infrastructure and Ecology of Rural Areas*, 2007/ 1, p. 81-89 (in polish)

## INVESTIGATION OF COMMON REED CUTTING METHODS

ANDRIS KRONBERGS\*, ERIKS KRONBERGS, MAREKS SMITS AND ELGARS  
SIRAKS

Latvia University of Agriculture, Institute of Mechanics

J. Cakstes bulv. 5, Jelgava, LV-3001, Latvia.

Phone: +371 63080674, Fax: +371 63020762, E-mail: andrisk@llu.lv

### Abstract

Latvia has target in 2020 for renewable energy resources to be 40% in gross final consumption of energy. In 2005 EU biomass accounted for 66 % of renewable primary energy production. Herbaceous energy crops would be as the main basis for solid biofuel production in agricultural ecosystem in future. In Latvia approximately of 14.6% of unfarmed agricultural land can be used for herbaceous energy crop growing. Beside that there is possibility to utilize for bioenergy production natural biomass of common reeds (*Phragmites Australis*) overgrowing shorelines of Latvian more than 2000 lakes. Peat can be used as best additive for manufacturing of solid biofuel, because it improves density, durability of stalk material briquettes (pellets) and avoid corrosion of boilers. The main conditioning operation before preparation of herbaceous biomass compositions with peat is shredding. Experimentally stated common reed stalk material ultimate tensile strength is  $330 \pm 29 \text{ N mm}^{-2}$ . This value testifies that common reeds are the strongest material between other stalk materials, mentioned before, because experimentally stated value of wheat stalk (with moisture content  $\sim 10\%$ ) ultimate tensile strength is only  $118.7 \pm 8.6 \text{ N mm}^{-2}$ . Energy crop stalk material cutting properties were investigated in order to find minimum of energy consumption for shredding. The main hypothesis for cutter design is that cutting method has to be used with minimum of energy consumption, reducing frictional forces to a minimum. Cutting using different types of knives had been investigated. Flattened reed stalks were used for cutting experiments. It was stated that flattened reed test package thickness change from 0.4 to 3.8 mm rise specific cutting energy from 0.025 to  $0.078 \text{ J mm}^{-2}$ . Specific cutting energy per mass unit is growing considerably from  $2000 \text{ J kg}^{-1}$  to  $4000 \text{ J kg}^{-1}$  then shredding size is changed from 20 to 10 mm. If cutting energy per mass unit is advisable less than  $2000 \text{ J kg}^{-1}$  and homogeneity of composition with peat is preferable then shredding size 20 mm is recommended.

### Introduction

Target for share of energy from renewable sources [1] in gross final consumption of energy, 2020 in Latvia is 40%. In 2005 EU biomass accounted for 66 % [2] of renewable primary energy production. Biomass has relatively low costs, less dependence on short-term weather changes and it is possible alternative source of income for farmers. Herbaceous energy crops would be as the main basis for solid biofuel production in agricultural ecosystem in future. There is not problem in Latvia that if bioenergy crops are encouraged, then less land will be available for growing food. In 2005 year investigation was stated that 14.6% of agricultural land [3] of Latvia was unfarmed. Therefore herbaceous energy crop growing on these lands can provide sustainable farming practice. Beside that there is possibility to utilize

for bioenergy production natural biomass of common reeds (*Phragmites Australis*) overgrowing shorelines of Latvian more than 2000 lakes. Peat can be used as best additive for manufacturing of solid biofuel, because it improves density, durability of stalk material briquettes (pellets) and avoid corrosion of boilers. For these reason herbaceous energy crop biomass compositions with peat for solid biofuel production is recommended. The main conditioning operation before preparation of herbaceous biomass compositions with peat is shredding. There are different cutting methods of agricultural materials. According this stalk material cutting properties has to be investigated in order to find minimum of energy consumption for shredding.

## Materials and methods

Herbaceous biomass as cereal crop straw (mainly wheat straw), common reeds, rape straw and reed canary grass are the most prospective stalk materials for solid biofuel production in Latvia. For production of solid biofuel mainly herbaceous plant stalks are used. Experimentally stated common reed stalk ultimate tensile strength is  $330 \pm 29 \text{ N mm}^{-2}$ . This value testifies that common reeds are the strongest material between other stalk materials, mentioned before, because experimentally stated value of wheat stalk (with moisture content  $\sim 10\%$ ) ultimate tensile strength is only  $118.7 \pm 8.6 \text{ N mm}^{-2}$ . Experimentally obtained values of common reed cutting properties therefore would be more reliable for herbaceous energy crop shredder design in solid fuel production technologies. The main hypothesis for cutter design is that cutting method has to be used with minimum of energy consumption, reducing frictional forces also to a minimum. Flattened common reeds (*Phragmites Australis*), with moisture content  $\sim 10\%$ , were used for cutting experiments, because the previous research verify that reed flattening before cutting allows to save total shredding energy. Ultimate shear strength and energy consumption for reed stalk cutting has been investigated using the Zwick materials testing machine TC-FR2.5TN.D09 with force resolution 0,4% and displacement resolution  $0,1 \mu\text{m}$ , the maximal force for testing is 2,5 kN. For shear cutting parameter determination original cutting device has been designed. Cutting device was equipped with eighteen types of cutting knives (Fig. 1). For all knives were three different bevel angles and six different blade angles. All knives simulated cutting mechanisms (Fig. 2), which are used in industrial shredders. For any knife cutting experiment were used 15 flattened reed samples and test piece has been fixed on one side by pressure plate.

Knives with blade angle more than  $25^\circ$  were not used because nip angle for flattened reed stalk material is  $24^\circ \pm 1^\circ$ .

Specific cutting energy  $E_{scQ}$  was calculated:

$$E_{scQ} = \frac{E_C}{A}, \quad (1)$$

where:

$E_C$  - cutting energy, J;

$A$  - cutting area,  $\text{mm}^2$ .

		Blade angle					
		$\varphi=0^\circ$	$\varphi=5^\circ$	$\varphi=10^\circ$	$\varphi=15^\circ$	$\varphi=20^\circ$	$\varphi=25^\circ$
Bevel angle	$\beta=25^\circ$						
	$\beta=45^\circ$						
	$\beta=90^\circ$						

Fig. 1. Cutting knives with different blade and bevel angles

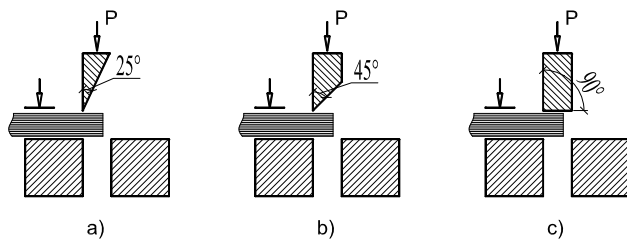


Fig. 2. Layout of cutting experiments

Displacement and stress data were collected and processed by using Zwick software program TestXpert V9.01. The energy consumption was obtained by integrating force – displacement diagram.

Straw cutter design theory, developed in previous century by academician V. Gorjackin [4] recommended sliding cutting method in order to reduce normal component of cutting force to the knife edge. For investigation of sliding cutting of flattened common reeds, equipment (Fig. 2.) to Zwick materials testing machine TC-FR2.5TN.D09 has been designed. The knife 1 is strengthened vertically in Zwick 2.5 clamping system. The specimen 3 is rigidly secured to the vertical support by the plates 4 on both sides. Normal force  $P$  to the knife cutting edge is applied to the specimen 3, but the force of knife vertical displacement is registered as function of displacement. During experiments the value of force  $P$  is adjusted and value of vertical displacement force is registered. Software of Zwick 2.5 let obtain graphs of force and cutting energy consumption for vertical displacement of knife. Vertical displacement of knife 0.1 m has been adjusted. After measurement of the depth of cut-in into specimen the energy consumption in force  $P$  direction can to be calculated and added

to energy consumption for vertical displacement of knife.

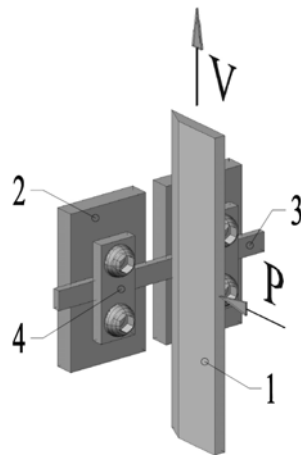


Fig. 3. Cutting device.

## Results and discussion

Results of flattened reed specific shear cutting energy determination are presented in Fig. 4. The thicknesses for all test pieces were  $0.38 \pm 0.06$  mm (slices of common reed stalks). There is no significant difference in specific cutting energy for knives with different bevel angle. Specific cutting energy for flattened reed is within  $0.012 - 0.016$  J m<sup>-2</sup>. If easy maintenance is preferred, then simple shape of cutter knife with bevel angle 90° has to be used for shredder design.

Results of flattened reed cutting force determination are presented in Fig. 5. In experiments were used knives with bevel angle 45°. By increasing knife blade angle from 0° to 20° it is possible to decrease maximal shear specific cutting force from 36 to 7 N·mm<sup>-2</sup>.

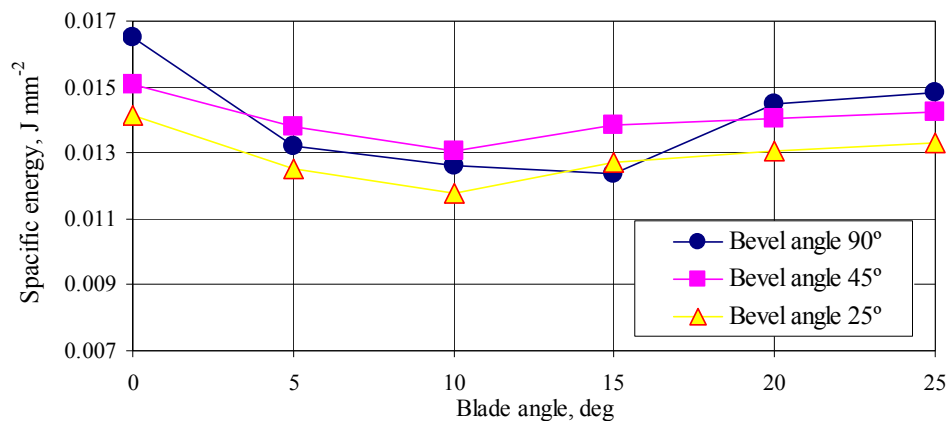


Fig. 4. Specific cutting energy in dependence on blade and bevel angle.

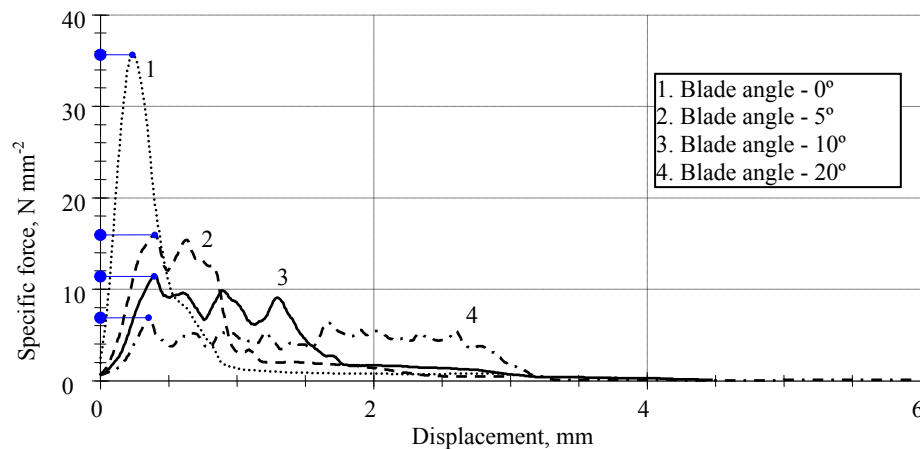


Fig. 5. Cutting force in dependence on blade angle.



Decreased maximal cutting force improves operation of cutting mechanism and increases the service life of shredder. Specific cutting force in cutting process depends on cutting material dimensions and knife blade angle.

Records obtained in common reeds sliding cutting experiments (Fig. 6.) show force for vertical displacement of knife. Numbering of curves done in accordance with the values of normal force  $P$  (Fig. 3.) pressing specimen against cutting edge of knife as follows: 1 - 5 N; 2 - 10 N; 3 - 15 N; 4 - 20 N; 5 - 25 N and 6 - 30 N. The knife vertical displacement force is sum of friction force from moving the blade in cut-in of specimen and force for cutting common reed material. It can be seen (Fig. 6.) that average vertical displacement force value for curves 3, 4 and 5 is the same as value of normally pressing force  $P$ . Considering that the main part of vertical displacement force is friction force  $F$ , it can be calculated:

$$F = f' \cdot P, \quad (2)$$

where:  $f'$  – generalized coefficient of friction;

$P$  – normally pressing force.

The generalized coefficient of friction  $f'$ :

$$f' = \frac{F}{P}. \quad (3)$$

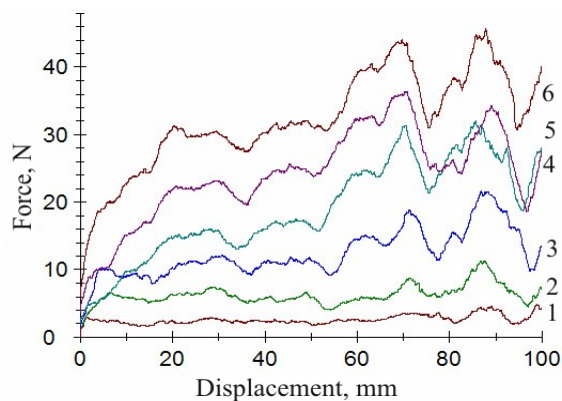


Fig. 6. Knife vertical displacement force

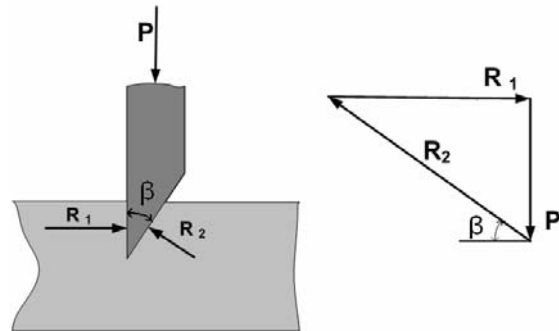


Fig. 7. Reactions for sliding of knife wedge

From sliding cutting experiments the generalized coefficient of friction  $f'$  has been investigated for three knives with bevel angles  $10^\circ$ ;  $20^\circ$  and  $30^\circ$ . Theoretically approximate value of coefficient of friction  $f'$  can be found considering longitudinal friction and disregarding transverse friction of knife. Then according Fig. 7 reactions can be found:

$$R_1 = \frac{P}{\tan \beta}, \quad R_2 = \frac{P}{\sin \beta} \quad (4)$$

Longitudinal friction force  $F$  considering (4) can be found:

$$F = f(R_1 + R_2) = f \left( \frac{1 + \cos \beta}{\sin \beta} \right) P. \quad (5)$$

Then

$$f' = f \frac{1 + \cos \beta}{\sin \beta} \quad (6)$$

Fig. 8. demonstrates generalized coefficient of friction  $f'$  for three knives with edge angles  $10^\circ$ ,  $20^\circ$  and  $30^\circ$ , obtained experimentally and theoretically, using  $f = 0.25$ .



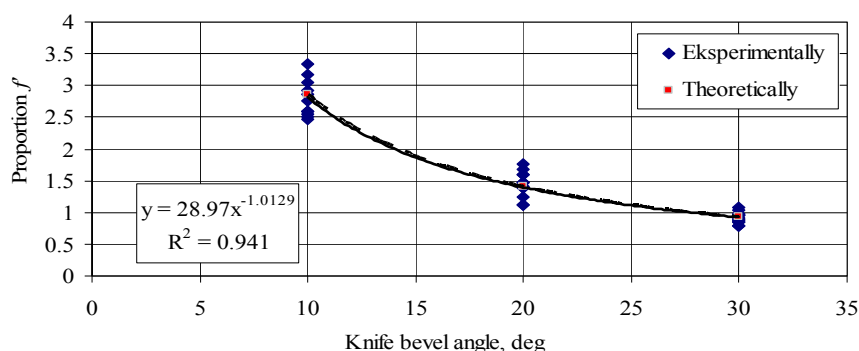


Fig. 8. Generalized coefficient of friction  $f$

Generalized coefficient of friction for knife sliding longitudinally in cut-in gap is approximately three times higher for 10° bevel angle knife comparing with 30° bevel angle knife.

Changing the knife normally pressing force into reeds specimen from 5 - 30 N, the specific energy consumption values for sliding cutting are calculated within 0.653 – 1.500 J mm<sup>-2</sup>. Thereby in sliding cutting is obtained the smallest value of knife normally pressing force into reeds specimen, but the highest value of specific energy consumption.

### Conclusion

1. Experimentally stated common reed stalk ultimate tensile strength is 330 ± 29 N mm<sup>-2</sup>.
2. Specific shear cutting energy for flattened reed is within 0.012 – 0.016 J m<sup>-2</sup>. There is no significant difference in specific cutting energy for knives with different bevel angle. If easy maintenance is preferred, then simple shape of cutter knife edge with angle 90° has to be used for shredder design.
3. By increasing knife blade angle from 0° to 20° it is possible to decrease maximal shear specific cutting force from 36 to 7 N mm<sup>-2</sup>. Decreased maximal cutting force improves operation of cutting mechanism and increases the service life of shredder.
4. Generalized coefficient of friction for knife sliding longitudinally in cut-in gap is approximately three times higher for 10° bevel angle knife comparing with 30° bevel angle knife.
5. The calculated specific energy consumption for common reed flattened stalk sliding cutting are within 0.653 – 1.500 J mm<sup>-2</sup>. The friction force of sliding cutting in cut – in

gap is reason of energy consumption greater than for shear cutting method.

### Acknowledgment

The authors are grateful for the financial support of this research from the European Structural Fund – Mobilization of human resources to renewable energy research – realized by Project department of Latvia University of Agriculture (project No 2009/0225/1DP/1.1.1.2.0/09/APIA/VIAA/129).

### References

1. Directive 2009/28/EC of the European Parliament and of the Council of 23 April 2009 on the promotion of the use of energy from renewable sources and amending and subsequently repealing Directives 2001/77/EC and 2003/30/EC (Text with EEA relevance). <http://eur-lex.europa.eu/LexUriServ/LexUriServ.do?uri=CELEX:32009L0028:EN:NOT>, (Accessed on 30.03.2010).
2. Alan Swinbank. EU Support for Biofuels and Bioenergy, Environmental Sustainability. Criteria and Trade Policy. <http://www.ictsd.org>, (Accessed on 30.03.2010).
3. Land politics statement for years 2008. – 2014. The Order of the Cabinet of Ministers of the Republic of Latvia Nr. 613 (in Latvian), <http://www.mk.gov.lv>, (Accessed on 30.03.2010).
4. Горячкин В. Теория соломорезки и силосорезки. В сборнике Теория конструкция и производство сельскохозяйственных машин. Т4. М. Сельхозгиз, 1936, 226 – 263.

## INFLUENCE OF SOIL TILLAGE TREATMENT AND COMPOST APPLICATION ON SOIL PROPERTIES AND WATER INFILTRATION

MILAN KROULÍK<sup>1\*</sup>, VÁCLAV BRANT<sup>1</sup>, JIŘÍ MAŠEK<sup>1</sup>, PAVEL KOVAŘÍČEK<sup>2</sup>

<sup>1</sup>Czech University of Life Sciences Prague, Kamycka 129, 16521 Prague 6 – Suchbát, Czech Republic, Phone: +420224383130, E-mail: [kroulik@tf.czu.cz](mailto:kroulik@tf.czu.cz)

<sup>2</sup>Research Institute of Agricultural Engineering Prague, Drnovská 507, 161 01 Prague, Czech Republic.

### Abstract

Composting is an important tool in waste management and its importance increases in connection with an effective disposal of biodegradable matter.

Compost application in a field also leads to soil organic matter increase. Organic matter influences positively soil fertility, improves soil aggregate stability and soil structure. On the basis of literature sources it is possible to expect a positive and long time influence on water infiltration into soil as well. Soil infiltration ability is one of the key factors of soil protection against unfavourable water erosion effects.

Soil physical properties, pH, distribution of soil organic carbon (C<sub>org</sub>) in the soil profile, soil aggregates stability and water infiltration into soil were evaluated under different soil tillage treatments and different amounts of compost applied.

Conventional tillage with ploughing (O) to the depth 0.20 m and conservation tillage with shovel tiller (M) to the same depth were used for soil treatment. Two different rates of compost were applied. Measured variables were compared with the results where no compost was applied and field was without plant cover.

The different technologies of soil tillage lead to soil properties changes and different soil infiltration ability within long-time period. The results proved differences in layering of soil organic matter depending on the soil tillage treatment. On the other hand, the layering of soil organic matter did not influence the values of pH and the soil aggregate stability.

According to values of water infiltration it is possible to observe that the water infiltration increases with the compost application rate.

### Introduction

Reduction of the surface water run-off on formed plots is one of basic objectives of landscape farming, because it represents significant factor influencing rainfall balance of sites and risk of water soil erosion (Janeček 2002). From agricultural aspect, environment protection and water management the fundamental importance has water motion speed in soil. Mainly soil erosion is a global problem of today with a high economical and environmental impact (Pimentel et al 1995). Human induced soil erosion is a problem because it occurs more rapidly than the process of soil formation. The soil water erosion is a significant problem mainly in the sector with higher rainfalls and plots slope rate. There exists a direct connection between the soil erosion and intensive agricultural production (Reicosky et al. 2005). According to

Franzluebbers (2002) organic matter is a key factor of soil preparation and water infiltration.

Application of organic fertilizer like compost or other bio-fertilizer plays very important role in connection with always higher popularity of organic farming.

It is benefit for soil and also solution of organic waste problems due to composting and recycling (Lalande et al 2000; Masciandaro et al 2000).

Fertilizing by composts increase organic matter content in the soil and due to increasing number of middle size pores to retentive ability of soil as well (Mayer 2004). But this has significant influence in long term horizon of compost application.

Positive influence of compost application on a 50 % improving retentive ability of soil in comparison with soil without compost application is describing by Gil et al. (2008).

Ahmad et al. 2008 mention that 43,1 % increasing of soil retentive ability compare with control plots variant without compost fertilizing. Mayer (2004) on a base of literary sources mention that positive and long term effect of composts application on water infiltration to the soil could be expecting after perennial and periodical application.

The main goal of research project is estimation of compost application influence and soil tillage systems influence on the physical properties of soil, organic matter Cox in soil, soil aggregates' stability (SAS) and water infiltration.

### Materials and methods.

Work started on a research field after harvest of previous crop in year 2008. The experiment is held like fields plot with 4 random repetitions, under soil condition clay-loamy Haplic Luvisol (WBR 2006). On field plots has been applied compost in dose of 1 (80 Mg/ha) and 2 (150 Mg/ha) of dry matter. As control variants are guided field plots without compost application (0) and field plots without application and crop residues (B). Soil on the filed was tilled by conventional tillage with ploughing (O) to the depth 0.20 m and conservation tillage with shovel tiller (M) to the same depth were used for soil treatment. Malting barley was growth during year 2009.

In years 2008, at the same time like the infiltration SAS – soil aggregate stability, pH and  $C_{org}$  was monitored. The equipment Wet Sieving Apparatus (produced by Eijkelkamp) and a method wet sieving was used for determination of the soil aggregate stability. The method recommended by the producer was used.

Soil acidity was determine as  $pH_{(KCl)}$ . Organic carbon ( $C_{org}$ , %) was determined oxidometrically by means of  $K_2Cr_2O_7$ . Titration to dead-point was used. The soil samples were taken from the soil layer 0 – 0.10 m and 0.10 – 0.20 m.

Near the points where the infiltration was measured the soil samples always were collected for soil physical properties determination. Kopecky rings were collected during spring period. The soil samples were taken each 0.05 m to depth 0.25m.

A double ring infiltrometer Eijkelkamp was used for determining water infiltration. The water layer fall was measured with a telemetric ultrasonic sensor (Figure 1). The output signal from the sensor was recorded by the measuring unit. The recording time interval of 10 s was chosen.



Fig. 1: Double rings infiltrometer Eijkelkamp with telemetric ultrasonic sensor

### Statistical evaluation

The Statistica Cz 7 statistics package using ANOVA was used. When significant differences appeared in the *F*-test, multiple comparisons according to Tukey were used to determine the individual significant differences.

### Results and discussion

In Table 1 are presented values of soil bulk density in the topsoil and in the subsoil profile after five year of the soil tillage application to different depth.

Tab. 1: Values of soil bulk density ( $Mg.m^{-3}$ ) for variants with ploughing O and loosening M, without vegetation B, compost dose 0 and 2

Depth (m)	Variants					
	OB	O0	O2	MB	M0	M2
0-0.05	1.21	1.29	1.13	1.15	1.06	1.10
0.05-0.10	1.51	1.49	1.40	1.30	1.32	1.27
0.10-0.15	1.46	1.48	1.38	1.39	1.32	1.45
0.15-0.20	1.52	1.49	1.34	1.39	1.31	1.55
0.20-0.25	1.53	1.45	1.35	1.41	1.32	1.46

Granulometric analyze shows that on a filed is majority of clay-loamy soil Haplic Luvisol. According to Lhotský (2000) is limiting value of bulk density  $1,4 \text{ Mg.m}^{-3}$ . Chart in the figure 2 shows graphic description bulk density values including limiting values for bulk density. In all cases weren't limiting values overlap in top soil level. Generally we can observe changes in bulk density values and porosity by different soil tillage technologies.

Lowest values of bulk density were mainly observed under tilled variants. Beside top layer of soil profile and variant M2, the values of bulk density are stable. Variant M2 records a differences between depths and bulk density increase with depth whereas variant O2 with same compost rate has opposite trend. It could relate with compost layering, which describe for example Franzluebbbers (2002).

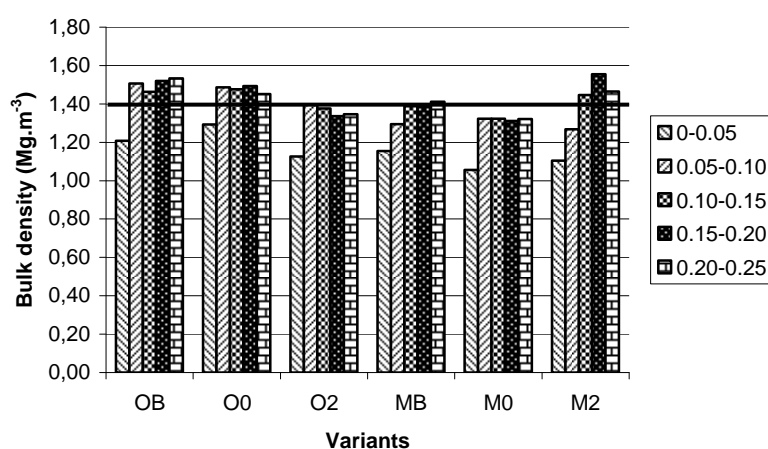


Fig. 2: Bulk density ( $\text{Mg.m}^{-3}$ ) for ploughed variants (O), tilled variants (M), without plant cower and compost ration 0 and 2. The line representing the value  $1.4 \text{ Mg.m}^{-3}$ , which is the limit value for clay-loamy soil

According to Franzluebbbers (2002) the organic matter is a key factor at soil cultivation and water infiltration into the soil. Layering of the compost is given by differential work technique of the plough or the tiller. Differences in a layering of organic matter could be indicated

like soil quality indicator, because the soil organic matter is main device for protection against the soil erosion. Organic matter influences mainly soil infiltration and nutrients retention. In the table 2 are presented the results from the soil organic matter  $C_{\text{org}}$ .

Tab. 2: Effects of the tillage systems and compost application on  $C_{\text{org}}$  (%) at different depths. Significant differences at  $\alpha = 0.05$  between variants are indicated by the different letters (a, b, c)

Variants	0 - 0.10 m $C_{\text{org}}$ %	0.10 - 0.20 m $C_{\text{org}}$ %	$C_{\text{org}}$ rate (upper layer/lower layer)
M 0	2.26 a,b	1.94 a,b	1.16
M 1	2.35 b	2.00 a,b	1.18
M 2	3.28 c	2.42 a	1.35
M B	1.87 a,b	2.03 a,b	0.92
O 0	1.83 a,b	1.86 b	0.98
O 1	2.20 a,b	2.33 a,b	0.95
O 2	1.76 a	2.21 a,b	0.79
O B	1.79 a	1.89 b	0.95

It is possible to see differences in  $C_{org}$  content between variants and between upper and lower soil layers. Soil tillage treatment causes this layering. It could be described by  $C_{org}$  rate. The covering of the manure, composts and plants residues into the deeper layers is typical for the ploughing. The tiller mixes it with the soil profile. According to some authors, mixing of the organic matter and higher content in upper layer means significantly influence on a soil protection.

Results and differences between  $C_{org}$  content under different soil tillage treatment are demonstrated in the graph (Figure 3).

In the table 3 are presented the results from the pH.

The layering of compost and its influence on pH is visible as well. The results are in accordance with literature sources, when pH values grew up with compost application (Gil et al 2008, Odlare et al 2008). Results and differences between pH under different soil tillage treatment are demonstrated in the graph (Figure 3).

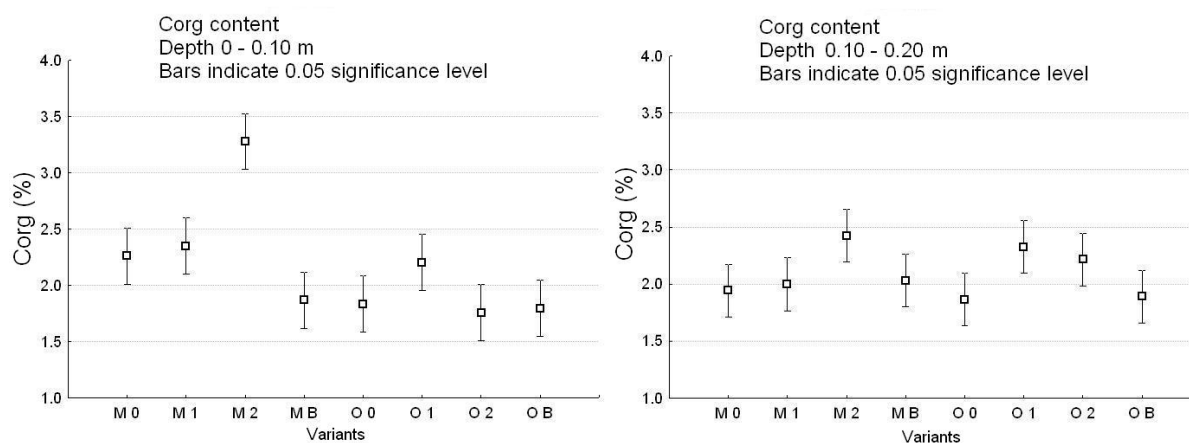


Fig. 3:  $C_{org}$  content under different variants of compost rate and soil tillage treatment

Tab. 3: Effects of the tillage systems and compost application on pH at different depths. Significant differences at  $\alpha = 0.05$  between variants are indicated by the different letters (a-e)

Variants	0 – 0.1 m	0.1 – 0.2 m
M 0	5.63 a,b	5.70 a
M 1	6.26 d	5.81 a,c
M 2	6.53 e	6.04 b,c
M B	5.50 a	5.56 a
O 0	5.60 a,b	5.71 a
O 1	5.93 c	6.29 b
O 2	5.76 b,c	6.10 b
O B	5.56 a,b	5.69 a

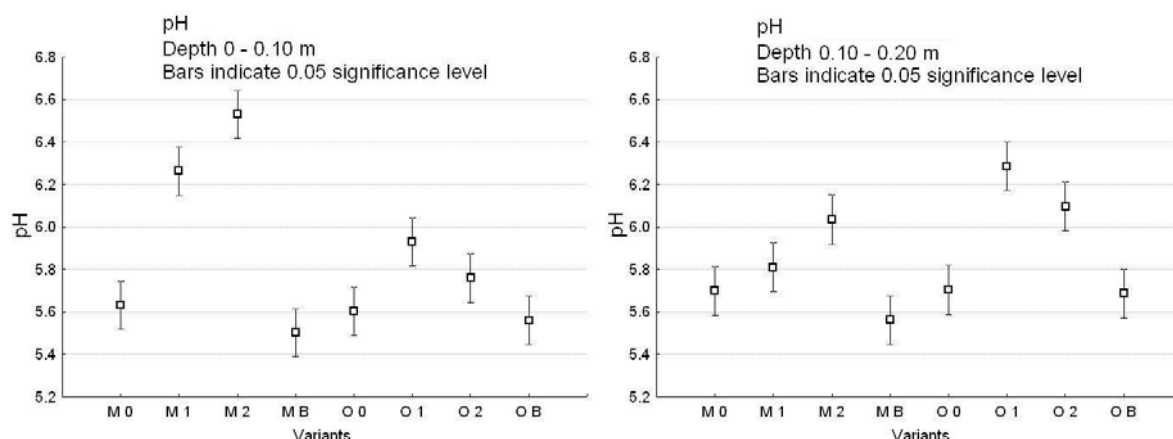


Fig. 3: pH under different variants of compost rate and soil tillage treatment

Soil aggregates stability (SAS) plays important role in protection in soil protection against unfavourable effect. According to Williams and Cooke (1961), Hassink and Whitmore (1997), Ahmad et al (2008) and Wortmann et al (2008), compost addition improves soil productivity and soil structure. In the table 4 and figure 4 are presented the results from the soil aggregate stability (SAS). Results also confirm influence of compost layering.

Tab. 4: Effects of the tillage systems and compost layering on soil aggregate stability (share of stable aggregate weight). Significant differences at  $\alpha = 0.05$  between variants are indicated by the different letters (a, b)

Variants	SAS	
	0 – 0.10 m	0.10 – 0.20 m
M 0	0.51 a,b	0.40 a
M 1	0.45 a,b	0.47 a
M 2	0.58 b	0.52 a
M B	0.39 a	0.39 a
O 0	0.42 a	0.45 a
O 1	0.42 a	0.49 a
O 2	0.36 a	0.43 a
O B	0.47 a,b	0.39 a

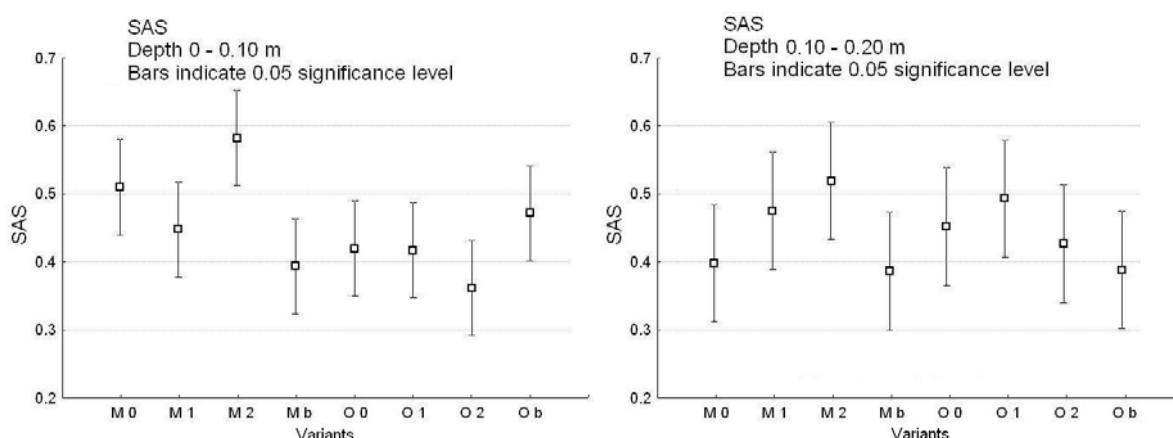


Fig. 4: SAS under different variants of compost rate and soil tillage treatment



According to some authors, compost addition also leads to increases of organic matter content in soil. On the basis of this infiltration capacity of soil increase as well. Graphics on the figures 5 and 6 bring infiltration trends for different tillage treatments and compost application. Infiltration intensity was described by logarithmic function.

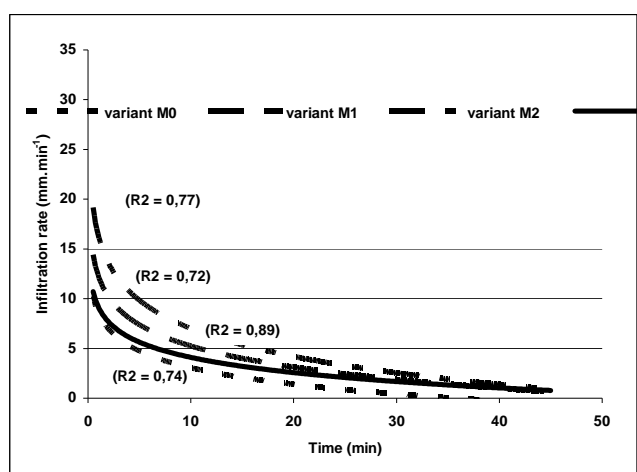


Fig. 5. Time course of the infiltration intensity at tilled site

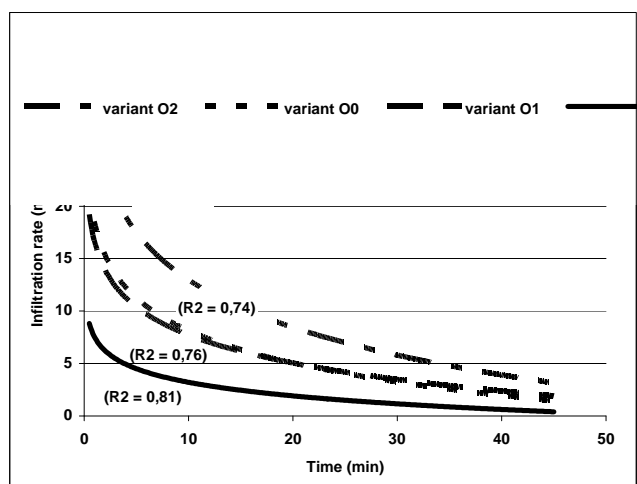


Fig. 6. Time course of the infiltration intensity at ploughed site

According to the results, it is possible to see that the infiltration intensity was influenced by the tillage variants and especially compost ration. Infiltration intensity increases especially with highest compost ration in both events of soil tillage treatment. These results confirm the influence of compost application on infiltration

intensity. On the other hand, the infiltration under tilled technology embodies lower values of infiltration in comparison with ploughed treatment.

## Conclusion

First year of measuring showed these conclusions. According to the results the application of compost and its layering influences soil physical properties,  $C_{org}$  content, pH and soil aggregate stability SAS. Rate of compost influences infiltration rate as well. The distribution and the layering of the organic matter were influenced by soil tillage treatment. On the other hand, the soil organic matter layering did not influence infiltration rate. Higher values of infiltration rate were observed for the ploughed area in comparison with the tilled area.

**Acknowledgement:** Supported by the Ministry of Agriculture of the Czech Republic, Projects No.QH 82191.

## References

- [1] Ahmad R., Khalid A., Arshad M., Zahir Z.A., Mahmood T. 2008. Effect of compost enriched with N and L-tryptophan on soil and maize. *Agronomy for Sustainable Development*, 28(2), 299-305.
- [2] Franzluebbers, A.J. 2002. Water infiltration and soil structure related to organic matter and its stratification with depth. *Soil & Tillage Research* [66], 197-205.
- [3] Gil, M. V., Carballo, M. T., Calvo, L. F. 2008. Fertilization of maize with compost from cattle manure supplemented with additional mineral nutrients. *Waste management*, 28 (8), 1432-1440.
- [4] Gil, M.V., Calvo, L.F., Blanco, D., Sanchez, M.E., 2008: Assessing the agronomic and environmental effects of the application of cattle manure compost on soil by multivariate methods. *Bioresource Technology* 99(13): 5763-5772.
- [5] Hassink, J., Whitmore, A. P., 1997: A model of the physical protection of organic matter in soil. *Soil Science Society of America Journal*, 61, 131-139.

- [6] Janeček, M., 2002. Protection of Agricultural Soil from Erosion. ISV Nakladatelství, Czech republic. 301 pp.
- [7] Lalonde, R., Gagnon, B., Simard, R.R., Co' te, D., 2000. Soil microbial biomass and enzyme activity following liquid hog manure in a long-term field trial. *Canadian Journal of Soil Science* 80, 263–269.
- [8] Lhotský, J. (2000): Zhutňování půdy a opatření proti němu. Praha, Studijní informace ÚZPI č. 7, ISBN 80-7271-067-2: 61 p.
- [9] Masciandaro, G., Ceccanti, B., Garcia, C., 2000. "In situ" vermicomposting of biological sludges and impacts on soil quality. *Soil Biology & Biochemistry* 32, 1015–1024.
- [10] Mayer, J., 2004: Einfluss der landwirtschaftlichen Kompostanwendung auf bodenphysikalische und bodenchemische Parameter. 43-58. In: Fuchs, J.G., Bieri, M., Chardonnens, M. (eds), 2004. Auswirkungen von Komposten und von Gärgut auf die Umwelt, die Bodenfruchtbarkeit sowie die Pflanzengesundheit. Zusammenfassende Übersicht der aktuellen Literatur. FiBL-Report. Forschungsinstitut für biologischen Landbau (FiBL), Frick, Schweiz.
- [11] Odlare M., Pell M., Svensson K. 2008, Changes in soil chemical and microbiological properties dutiny 4 years of application of various organic residuem. *Waste Management* 28, (7), 1246-1253.
- [12] Pimentel, D., C. Harvey, P. Resosudarmo, K. Sinclair, D. Kurz, M. McNair, S. Crist, L. Shpritz, L. Fitton, R. Saffouri e, R. Blair, 1995. Environmental and economic costs of soil erosion and conservation benefits. *Science* [267], 1117–1123.
- [13] Reicosky, D.C., M. J. Lindstrom, T. E. Schumacher, D. E. Lobb e D. D. Malo, 2005. Tillage-induced CO2 loss across an eroded landscape. *Soil & Tillage Research* [81], 183-194.
- [14] Williams, R. J. B., Cooke, G. W., 1961: Some effects of farmyard mature and of grass residues on soil structure. *Soil Science*, 92, 30–39.
- [15] Wortmann C. S., Shapiro C. A. 2008. The effects of manure application on soil aggregation. *Nutriet cycling in agroekosystems*, 80 (2) 173-180.

## GRANULOMETRIC STUDY FERTILIZERS SUPERPHOSPHATE

JOSEF KRUPÍČKA\*, BLAHOŠLAV HANOUSEK

Czech University of Life Sciences in Prague, Technical Faculty, 165 21 Prague 6, Czech  
Republik, Phone +420-2-24383127, Fax + 420-2-34381828, E-mail: krup@tf.czu.cz

### Abstract

Physical properties of commercial fertilizers play important role from precision application point of view. Granulometric evaluation is usually performed by sieve separation according ČSN 01 50 30 standard. The main subject of this work is the presentation of separation results when vertical airflow is used.

### Introduction

The effectiveness of mineral fertilizers in plant cultivation depends on the particle stability and speed of their transformation to solution state to be acceptable by plants. This process depends on the particles dimensions, so that the dimension of particles is one of the main parameters that influence the fertilizer effectiveness.

Application of solid commercial fertilizers play important role in precision farming technologies. The application quality is depended on chemical composition and physical properties of fertilizer. Important from physical properties point of view is the grading of aggregate evaluation that is still performed by standard ČSN 01 50 30. The dimension of particulars only is characterized by this way.

In this paper we continue in the previous research program, in which the granulometric study mineral fertilizers were studied. In contrary to the similar study of other authors seat and airflow sorting were combined.

This paper contains results obtained by this method is applied to two mineral fertilizers Superphosphate.

Experiments with particles can be designed differently. An elutriator was designed and constructed in which an airflow is supplied by a centrifugal fan (Csizmazia, 2000). Methods for measuring the coefficient of friction, the coefficient of restitution, the aerodynamic resistance coefficient, and the breaking force (particle strength) of fertilizers (Hofstee, 1992) were taken into account. The breaking force feature was skipped. The problem of particle destruction was overcome by fertilizer Superphosphate selection. The control of fertilizer discharge was studied for different designs of distributors and an experimental

accurate fertilizer distributor with a rotary vessel type feeder was developed (Kudoh, 1989) what shows that dissolution of fertilizer also makes some problems. Consequent logistical problems are the same difficult for both pumping liquids, and transportation of particles by the air.

The size of particles makes the fertilizer's shelf life and stability of particulars behavior in the airflow more stable in storage, and better acceptable by the plant. Therefore, experiments studying motion of particles through the air were accompanied by grading of particles.

This paper contains results obtained for two mineral fertilizers Superphosphate using the method developed previously.

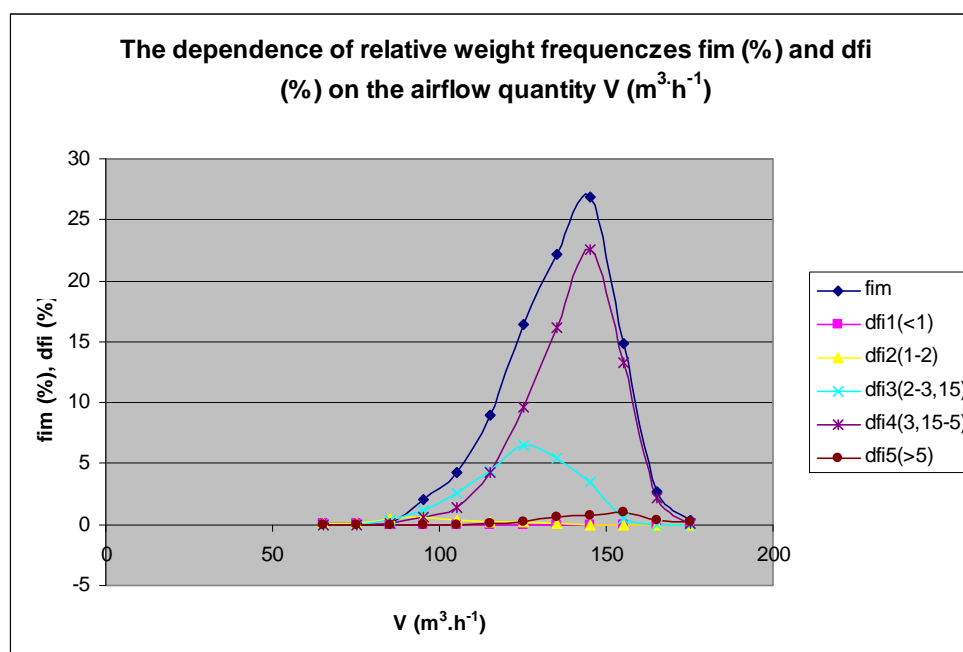
### Experimental arrangement

Experimental material was supplied by its producer Synthesia Pardubice. Total weight of the supplier sample was 25 kg. The sample was divided into 8 individual specimens of 0.5 kg weight that was measured repeatedly. The homogenization of the individual specimens was saved by previous mixing of the sample and then by stochastic composite sampling (ten parts per specimen). The specimens were separated at first in the vertical air flow stream with steeply increasing flow speed. The airflow speed was regulated by airflow volume between 65 to 175 m<sup>3</sup>.h<sup>-1</sup> for Superphosphate. The steps of airflow speeds are given in Table 1. The results of this separation were expressed by the mass classes  $f_{im}$  in percent of the specimen mass. Every class of the specimen was than sieved on the seats with holes 1mm, 2-3,15, 3,15-5mm, and 5 mm resulting four new subclasses characterized by the seat mesh dimension. They were marked as  $f_{id}$  expressed by percentage of the grain number in the total class particles.

Tab. 1 Averaged relative weight frequencies of Superphosphate fertilizer (n = 12)

V(m <sup>3</sup> .h <sup>-1</sup> )		65	75	85	95	105	115	125	135	145	155	165	175
v (m.s <sup>-1</sup> )		7,94	9,15	10,37	11,6	12,82	14,04	15,26	16,48	17,70	18,91	20,15	21,35
f <sub>im</sub> (%)		0,14	0,39	0,86	2,11	4,26	8,95	16,46	22,13	26,86	14,79	2,65	0,34
f <sub>id</sub> (%)	<1mm	0,05	0,05	0,01	0,00	0,00	0,00	0,00	0,00	0,00	0,00	0,00	0,00
f <sub>id</sub> (%)	1-2mm	0,09	0,32	0,53	0,59	0,39	0,24	0,16	0,07	0,00	0,00	0,00	0,00
f <sub>id</sub> (%)	2-3,15mm	0,00	0,00	0,30	1,17	2,54	4,35	6,45	5,48	3,53	0,45	0,00	0,00
f <sub>id</sub> (%)	3,15-5mm	0,00	0,00	0,04	0,67	1,34	4,31	9,64	16,17	22,58	13,29	2,23	0,15
f <sub>id</sub> (%)	>5mm	0,00	0,00	0,00	0,00	0,00	0,03	0,20	0,57	0,77	0,96	0,40	0,18

Figure 1



## Results

Mean values of the obtained data:  $f_{im}$  (%) (based on 0.5 kg specimen) are presented in Table 1. The averages were calculated from measurements repeated eight times. The results are graphically presented in Figures 1. It was achieved by statistical evaluation that relative frequencies are in agreement with N-distribution. It is clear from achieved values that in fertilizer samples there are in Superphosphate 94,4 of particles with dimension from 2 to 3.15 mm and from 3.15 to 5 mm. The method that was used for the critical airflow speeds for different dimensions and weights of particles groups. The method could be used in this form also for determination of the critical airflow speeds in case of other products in form of particles. In our

case the mean critical speed  $v_k = 13.12 \text{ m.s}^{-1}$  (coefficient of variation 22%) from dimension 2-3,15 mm and critical  $15,26 \text{ m.s}^{-1}$  (CV = 20 %). The mean critical speeds, standard deviations, and CVs were derived for significant groups of particles.

## Conclusion

Classical seat analysis was enriched by aerodynamic particle testing that can be used directly in evaluation of the aerodynamic spreading of the fertilizer in the field conditions. The data for two tested fertilizers are in agreement with demanded range.

### Acknowledgements

This project was funded by Ministry of Education, Youth and Sports of the Czech Republic, Research project number MSM 6046070905.

### References

- [1] V. Bartoš, W. Waradzin, K problematike hodnocenia granulovaných hnojív, *Agrochémia*, 21, 220 (in Slovak)
- [2] L. Jager, P. Hegner, *Kvalita tuhých průmyslových hnojiv*, SNTL, Praha (1987), 226 s. (in Czech)
- [3] Hofstee,-J-W (1992): Handling and spreading of fertilizers: part 2, physical properties of fertilizer, measuring methods and data. *Journal of Agricultural Engineering Research*,

Wageningen Agricultural University, pp. 141-162

- [4] Csizmazia,-Z (2000): Some physical properties of fertiliser particles. Department of Agricultural Engineering, Faculty of Agricultural Sciences, Debrecen University, Hungary. *Aspects-of-Applied-Biology*, pp. 219-226
- [5] Allan,-G-G; Freepons,-D-E; Crews,-G-M (1989): Fertilizer compositions, processes of making them, and processes of using them. United-States-Patent. Division of United States Patent 4 560 400.
- [6] Kudoh,-M (1989): Flowability of fertilizers and development of an accurate fertilizer distributor. Department of Forestry & Landscape, Hokkaido College, Senshu University, Japan. *Journal of Hokkaido College, Senshu University*, pp. 1-87

## EVALUATION OF TRANSPORT PROCESSES IN AGRICULTURE

KAREL KUBÍN<sup>1\*</sup>, MARTIN PEXA<sup>2</sup>

Czech University of Life Sciences Prague, Faculty of Engineering  
16521 Prague 6 – Suchbát, Czech Republic,

<sup>1</sup>Department of Mechanical Engineering

<sup>2</sup>Department for Quality and Dependability of Machines

Phone: +420 224 38 3174, E-mail: [kubin@tf.czu.cz](mailto:kubin@tf.czu.cz)

### Abstract

The agricultural transport forms a significant proportion of operations in the area of agriculture. Due to this fact the agricultural transport significantly participates on the energy intensity of agricultural production. It is also substantial that operations of transport machines negatively influence the environment, mainly through emissions of gaseous and solid pollutants. It is necessary to know the indicators of agricultural transport operations such as the transport output, the unit fuel consumption or unit emissions production for the efficient organization of transport processes on the farm. This paper deals with the analysis of the possibility of calculating these indicators using computer technology. The paper also describes a program running under MS Windows which was designed for calculating the above indicators. The measured data on the fuel consumption and the emissions production represent the main basic input data, together with the route description. The text also contains the results of model calculation for selected transport sets.

**Key words:** agricultural transport, fuel consumption, emission production, model of drive

### Introduction

#### *Transport Processes in Agriculture*

Material handling, which also includes transportation, forms an important part of all production processes in the area of agriculture. It connects the various phases of the production process and ensures circulation of goods. The agricultural transport transfers about 100 million tons of materials annually in the Czech Republic. Therefore agricultural transport takes a great share in production costs of an agricultural company. A substantial part of transportation costs are the costs for diesel fuel. Agricultural transport operations consume about 118 million litres of diesel annually in the Czech Republic. It is also significant that operation of transport machines negatively influences the environment, mainly through gaseous and solid pollutants, which are produced by diesel engine. This adverse influence of the agricultural machines operation cannot be fully eliminated; however, it can be reduced by means of suitable organization of the transport processes.

Although agricultural transportation has many common features with transport in other sectors of the economy, there are quite differences in many respects which are mainly

caused by the nature of agricultural production. Transport in the area of agriculture is mainly characterized by: shorter transport distances and one-way material flows, transportation of various materials (mostly voluminous), the movement of vehicles on paved roads or in the field, significant seasonality and dependence on climatic conditions (Sýrový et al., 2008).

#### *Indicators of Agricultural Transport Operations*

Due to the above mentioned reasons, it is evident that for each farm which wishes to operate successfully in the market, it is necessary to deal with the efficient organization of transport processes. The basic premise for the effective agricultural transportation is the knowledge of energetic, exploitation, economic and environmental indicators of transport operations (Tab. 1).

The productivity and transportation output are the most important indicators that evaluate the transport process mainly in terms of time demands. High productivity makes it possible to reduce labour costs and it also allows respecting the necessary agricultural deadlines. Energy indicators characterize the energy required for carrying out the operation. The consumption of diesel is almost exclusively used because the



energy means are driven by diesel engines. Economic indicators are represented by direct costs which are expended by the farm for the implementation of transport operations. These are primarily the costs for depreciations, energy, maintenance, repairs, salaries, etc. Environmental indicators evaluate mainly negative effects of agricultural transport on the environment. These are especially the emissions of gaseous pollutants such as carbon monoxide (CO), hydrocarbons (HC), nitric oxide (NO) and particulate matter (PM). Due to that the European Union aims to reduce greenhouse gas emissions, it is important also to monitor carbon dioxide (CO<sub>2</sub>) emissions from agricultural transport.

#### *Expert Systems for Transport Operations in Agriculture*

Computer expert systems can be used for decision support about the use of farm machinery. Results of these systems can also be used in determining energy consumption and emissions production of agricultural transport for whole country. Several authors were dealing with these problems. Sogaard and Sørensen (2004) have developed a simulation model for optimal machine selection from the point of view of the lowest costs in the framework of the farm machine system. Similar expert system was developed by Syrový and Podpěra (2009a). This system takes into consideration the specific natural and production conditions and the characteristics of the technical means when calculating the model. Today, the bulk of agricultural transport is provided by tractor transport sets, which consist of an agricultural tractor and trailer or semitrailer. Therefore, it is particularly important to correctly evaluate the fuel consumption of a tractor. Grisso et al. (2004) describe the possibility of determining the fuel consumption of a tractor on the basis of experimentally derived dependence of hourly fuel consumption at rated power and its utilization. A similar problem was also solved by Syrový et al. (2008), who describe the possibility of calculating the fuel consumption for different types of work.

In order to determine the fuel consumption during transport operations, various simulation programs have been proposed. Syrový and Podpěra (2009b) created a program in MS Access, which allows determining the energy,

the exploitation and the economic indicators of the selected tractor transport set. Programs in Visual Basic was also created by Kumar and Pandey (2009) or Sahu and Raheman (2007). All the above mentioned programs consider that the engine is working in steady state during calculation. It is due to the fact that simulation model does not include the effects of variability in some parameters of simulation, such as speed or slope angle. The operating mode of the engine is constantly changing due to the influence of external conditions in a real drive of a tractor with a trailer. This fact has a significant impact on fuel consumption and emissions production. Lindgren and Hansson (2002) proposed a simulation model for use in SIMULINK software. This simulation model allows consideration of the impact of variability of the driving conditions on the result of simulation. Fuel consumption and emissions production are computed by interpolating values of fuel consumption and emissions production measured on the tractor in eight points according to standard ISO 8178.

This paper describes a simulation program for calculating energy, exploitation and environmental indicators for a tractor transport set. The program was developed in Visual Basic.NET for computers running Windows XP and higher.

*Tab. 1: Agricultural transport indicators*

Indicator	Units
<b>Exploitation indicators</b>	
Productivity	t h <sup>-1</sup> , m <sup>3</sup> h <sup>-1</sup>
Transportation output	tkm·h <sup>-1</sup>
<b>Energetic indicators</b>	
Overall fuel consumption	l
Unit fuel consumption	l t <sup>-1</sup> , l tkm <sup>-1</sup>
<b>Economic indicators</b>	
Overall direct costs	CZK
Unit direct costs	CZK t <sup>-1</sup> , CZK tkm <sup>-1</sup>
<b>Environmental indicators</b>	
Overall emission production	g
Unit emission production	g t <sup>-1</sup> , g m <sup>-3</sup> , g tkm <sup>-1</sup>

## **Materials and Methods**

### *Basic information about the simulation model*

During the transportation, the fuel consumption and emissions are mainly influenced by technical parameters of means of transport, characteristic of transported material

and the route, and of course behaviour of the driver. Most parameters influencing investigated indicators change during the drive and so the engine works in transient conditions. Therefore, the suggested calculation model considers splitting of the route into elementary sections, where these parameters can be regarded as constant.

While we know engine speed at the beginning of the calculation of each route section, it is necessary to decide whether it is essential to change the speed gear. If it is necessary to change the speed gear, the acceleration of the set is determined with regard to the route resistance. If the shift is not necessary, the current speed of the set is compared with the required speed in the particular route section. The acceleration of the transport set is evaluated based on the speed comparison and the accessible engine power. Finally, with regard to the acceleration of the set and its motion resistance the operating point of the engine (engine speed and torque) is determined. Fuel consumption and emissions production in the route section are evaluated from the determined operating point and input data. The above mentioned calculation process is repeated for every single section of the route, until its end is reached. Subsequently, the investigated indicators for the whole route are calculated out of values from single sections.

#### *Evaluating the operation point of the engine*

Operating point of the engine is defined by engine speed and torque. Engine speed of the set going at speed  $v_s$  can be calculated by means of Eq. (1).

$$n_M = \frac{30 \times v_s \times i_c}{(1 - \delta) \times \pi \times r_d} \quad (1)$$

where:  $n_M$  is engine speed ( $\text{min}^{-1}$ ),  $v_s$  is actual speed of the transport set ( $\text{m s}^{-1}$ ),  $r_d$  is dynamic radius of drive wheels (m),  $i_c$  is total gear ratio between the engine and the drive wheels (-),  $\delta$  is the slippage of drive wheels of the tractor (-).

The slippage of drive wheels of the tractor depends on the ratio between the driving force and the wheel vertical load and then on the characteristic of the surface and the tyre. Slippage of the drive wheels in the particular route section can be calculated according the relevant literature (Grečenko, 1994).

The engine of the tractor has to provide necessary driving force to its wheels, which helps to overcome the motion resistance. The current engine torque can be calculated according to the following Eq. (2). (Bauer et al., 2006)

$$M_M = \frac{F_h \times r_d}{i_c \times \eta_m} = \frac{(F_f + F_v + F_s + F_a + F_t) \times r_d}{i_c \times \eta_m} \quad (2)$$

where:  $M_M$  is engine torque (Nm),  $F_h$  is driving force (N),  $\eta_m$  is transmissions efficiency between the engine and the driving wheels (-),  $F_f$  is rolling resistance (N),  $F_v$  is air resistance (N),  $F_s$  slope resistance (N),  $F_a$  is inertial force (N),  $F_t$  is pull force (N).

The driving force  $F_h$  can be calculated according the relevant literature e.g. Syrový et al. (2008) or Buaer et al. (2006).

#### *Fuel consumption and emission production*

With regard to the fact, that in each moment of the drive, the fuel consumption and the emissions production are determined by the current operation mode of the engine, it is necessary for the calculation to know the overall characteristic of the particular engine. The basic input data of the simulation model is the dependence of the fuel consumption and the investigated pollutants production on the engine speed and the torque, i.e. so called engine map. Twenty-five measuring points and four checkpoints (Fig. 1) were chosen to create the above maps.

Fuel consumption and emission production were measured using the following apparatuses in all measuring points. The engine was loaded using mobile dynamometer AW NEB 400 (Tab. 2) connected to the tractor by rear power take-off (PTO). For the measurement of fuel consumption was used fuel box, which consists of two flow indicators Macnaught MSeries FlowMeter M2ASP-1R (Tab. 3). Emissions were measured by combination of three apparatuses (Tab. 4), of which the most important one was analyzer Atal AT 505 ( $\text{CO}$ ,  $\text{CO}_2$ ,  $\text{HC}$ ,  $\text{O}_2$ , air temperature). Another apparatus was Atal AT 600, which measured smokiness and temperature of diesel. The last one was Asin FG34, which measured  $\text{NO}$ .

Measured points were interpolated with the software MathCad 2001 Professional using appropriate function. The dot matrixes with 41 rows and 41 columns were created for further

computer processing from measured data. The examples of engine fuel consumption map measured for the tractor Case IH JX90U is showed in Fig. 2.

#### The route description

The transportation route is defined by its length, elevation profile, characteristic of the surface and routing. The route can be described with the use of the sequence of points that are determined by means of geographic coordinates (latitude, longitude and altitude). The distance between single points should be of such a length that enables to consider the set driving resistance between these points as constant.

Tab. 2: AW NEB 400 parameters

Parameter	Value	Unit
Maximal PTO torque	2850	Nm
Maximal PTO speed	3200	min <sup>-1</sup>
Maximal braking power	343	kW
Braking power at PTO speed 540 min <sup>-1</sup>	172	kW
Braking power at PTO speed 1000 min <sup>-1</sup>	298	kW
Error in measurement	2	%

Tab. 3: Flow indicators parameters

Parameter	Value	Unit
Maximal flow rate	500	l·h <sup>-1</sup>
Resolution	400	pulses·l <sup>-1</sup>
Error in measurement	1	%

Tab. 4: Emission analyzers parameters

Component	Resolution	Accuracy
<b>Atal AT 505</b>		
CO	0,01 % vol	0,03 % vol
CO <sub>2</sub>	0,1 % vol	0,5 % vol
HC	1 ppm vol	10 ppm vol
O <sub>2</sub>	0,01 % vol	0,1 % vol
Temperature	1 °C	2 °C
<b>Atal AT 600</b>		
Opacity	0,1 %	2 %
Temperature	1 °C	2 °C
<b>Asin FG34</b>		
NO	1 ppm	1000 ppm (4000 ppm)

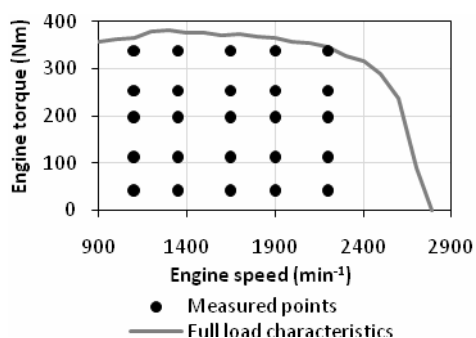


Fig. 1: Measured points

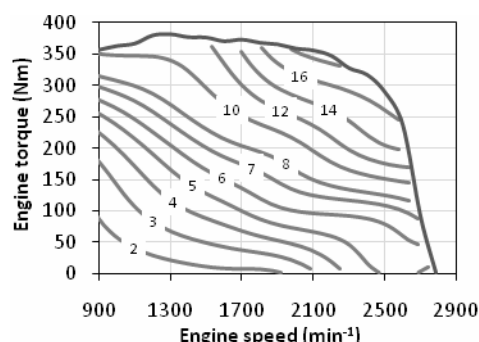


Fig. 2: Case IH JX90U fuel consumption map (kg·h<sup>-1</sup>)

## Results

### Program for Calculating the Indicators of Agricultural Transport

A program in Visual Basic.NET was created according to the above mentioned computational model. Input data for the program are stored in a database file; the calculated values are displayed on the output screen and can be exported to MS Excel for further processing. The program consists of the main screen, and few dialog screens, which can be used for setting the parameters of the simulation. The main screen contains a list of saved transport sets and a list saved transport routes. The parameters of selected transport set or route can be adjusted using the appropriate buttons. It is also possible to add a new transport set or route to in the database. The basic parameters of the tractor, which are needed for the calculation, are the weight of the tractor, its dimensions and the parameters of the engine and the gearbox. It is also needed to load the maps of fuel consumption and emission production into the database.

The calculation will start after pressing the button "Calculate Simulation" on the main screen. When it is finished, the output screen appears (see Fig. 3). Brief information about the input data of the simulation are given at the top of this screen. The bottom of the screen contains the calculated values of energy, exploitation and environmental indicators for the selected transport set.

### Results of the Calculation

The determination of the investigated indicators of the transport process according to the above mentioned method can be done for any agricultural transport set, which is provided with required input data. The transportation of the

forage in the mountains was chosen for the validation of the suggested calculation method.

The simulated transport set consists of the tractor Case IH JX90U and the silage trailer. The calculation was done for different capacity weight of the silage trailer, so that the dependence of the investigated indicators on the capacity weight of the silage trailer could be determined. The route, on which was simulated the set drive, represents real route in the mountainous area of Šumava (South Bohemia), where the transportation of the forage is commonly realized. Calculation results for the sets with the capacity weight from 3 t to 9 t are presented in Fig. 4.

The results show the expected tendency of the transport output of the set, which increased along with increasing of its weight capacity, and it was accompanied by decreasing of the unit fuel consumption. The transport set with the weight capacity 3 t performs the transportation output of 39.22 tkm h<sup>-1</sup> and the unit consumption of 0.28 l tkm<sup>-1</sup>. On the other hand, the set with the weight capacity of 7 t reaches the transport output of 69.46 tkm h<sup>-1</sup>, while the unit consumption is 0.18 l tkm<sup>-1</sup>. However, increasing the weight capacity of the attached vehicle has its limits, and that is especially because of the limited engine power. Transport set with very high weight capacity reaches a very low average speed, which leads into the increase in total transport costs.

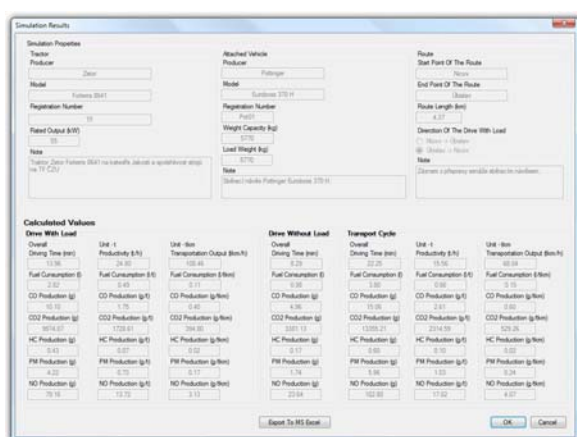


Fig. 3 – Program output screen

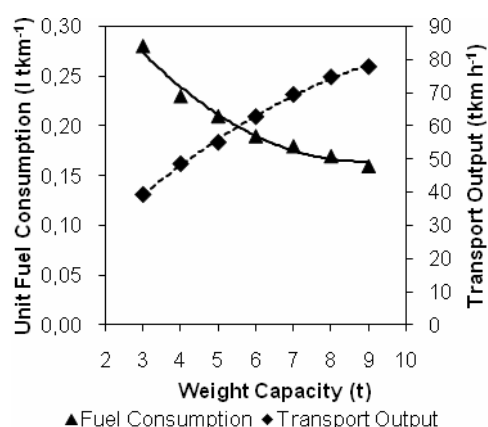


Fig. 4: Dependence of the transport output and fuel consumption on weight capacity

## Conclusions and Discussions

The above described program for calculating the energetic, exploitative and environmental indicators enables their calculation with regard to important parameters of the transport set and the route. The program allows storing a database of various parameters of tractors, trailers and transport routes. Then the model can be simply calculated on different combinations of tractors, trailers and routes. The example of the calculation was applied on the set, which consisted of Case IH JX90U tractor and the silage trailer. The results of calculation confirm the importance of correct choice of a trailer for the specific tractor. Transport set with the low weight capacity does not fully exploit the power of the engine which results in cost increases due to excessive fuel consumption.

The results of the calculation may serve either for the determination of suitable set for a particular transport operation, but mainly for the simulation of drive of the transport set in different conditions, which enables to determine the investigated indicators without the need to carry out difficult field-laboratory tests. The simulation calculations can be used e.g. for setting the amount of emissions produced during various transport operations. The results of simulation calculations can also be used as base in determining the energy consumption and emissions of the agricultural transport in the agricultural sector.

When the results of the calculation are evaluated, it should be taken into account that the fuel consumption and emissions production are calculated on the basis of the measured static



characteristics of the engine. Especially the productions of the emissions are different in unsteady engine state. Therefore it is necessary to pay more attention to the impact of unsteady engine regime for the production of emission in further research.

## References

- [1] Bauer, F. - Sedlák, P. - Šmerda, T. (2006): *Tractors* (in Czech). Praha: Profi Press, 2006. 192 p. ISBN 80-86726-15-0
- [2] Grečenko, A. (1994): *Properties of Terrain Vehicles* (in Czech). Praha: VŠZ, 1994. 118 p. ISBN 80-213-0190-2
- [3] Grisso, R. D. - Kocher, M. F. - Vaughan, D. H. (2004): Predicting tractor fuel consumption. *Applied Engineering in Agriculture* (2004), 20(5), p. 553-561. ISSN: 0883-8542.
- [4] Kumar, R. - Pandey, K. P. (2009): A program in Visual Basic for predicting haulage and field performance of 2WD tractors. *Computers and Electronics in Agriculture* (2009). 67, p. 18-26. ISSN 0168-1699.
- [5] Lindgren, M. - Hansson, P. A. (2002): Effects of Engine Control Strategies and Transmission Characteristics on the Exhaust Gas Emissions from an Agricultural Tractor. *Biosystems Engineering* (2002), 83(1), p. 55-65. ISSN 1537-5110.
- [6] Sahu, R. K. - Raheman, H. (2007): A decision support system on matching and field performance prediction of tractor-implement system. *Computers and Electronics in Agriculture* (2007), 60(1), p. 76-86. ISSN 0168-1699.
- [7] Sogaard, H. T. - Sørensen, C. G. (2004): A Model for Optimal Selection of Machinery Sizes within the Farm Machinery System. *Biosystems Engineering* (2004), 89(1), p. 13-28. ISSN 1537-5110.
- [8] Syrový, O. - Podpěra, V. (2009a): Simulation mathematical model of expert system for working processes management. *Research in Agricultural Engineering* (2009), 55(1), p. 1-9. ISSN 1212-9151.
- [9] Syrový, O. - Podpěra, V. (2009b): Programme for Evaluation of Transport Process in Agriculturalenterprise (in Czech). *Agritech Science* (2009). 3(2). ISSN 1802-8942.
- [10] Syrový, O. et al. (2008): *Agricultural transport* (in Czech). Praha: Profi Press, 2008. 248 p. ISBN 978-80-86726-30-4.

## Acknowledgement

This paper was created with the grant support by Czech University of Life Sciences Prague, Faculty of Engineering, Project No. CZU 31130/1312/3112 „Modeling of the Transport Processes in Agriculture“.

## THE SENSITIVITY OF CAPACITIVE THROUGHPUT SENSOR ON MEASURED MATERIAL MOISTURE CONTENT CHANGES

FRANTIŠEK KUMHÁLA\*, VÁCLAV PROŠEK

Czech University of Life Sciences in Prague, 16521 Prague 6 – Suchbátka, Czech Republic,

Phone: +420-2-24383135, Fax: +420-2-34381828, E-mail: kumhala@tf.czu.cz

### Abstract

The influence of material moisture content changes on capacitive throughput sensor measurement accuracy has been tested. Small laboratory capacitor was developed for that purpose. Stationary laboratory experiments were arranged with balsa blocks. For materials with relatively high moisture content (i.e. potatoes, sugar beets, carrots, tomatoes etc.) changes of about 5% of material moisture content have very little influence on capacitive throughput sensor measurement. However, for materials with lower material moisture content (less than about 65 %), the changes in material moisture content itself can influence the results of capacitive throughput measurement.

### Introduction

Precision agriculture makes use of information technologies in agriculture and will likely gain in importance when viable additional benefits, such as reduced environmental burdens and increased flow of information are recognised and evaluated (Auernhammer, 2001). Yield monitoring is an essential tool for gaining information about yield distribution. To measure instantaneous material throughput during the harvest is one of the ways how to collect this information.

Capacitance sensor techniques can be used for determining different properties of a range of plant materials. The function of capacitance sensors is based on the fact that the dielectric constant of an air/material mixture between two parallel plates increases with increasing material volume concentration.

Capacitance sensors have been widely used for plant material moisture content determination (Eubanks and Birrell 2001; Lawrence et al., 2001; Osman et al. 2002). Snell et al. (2002) used a radio-frequency application device for sensing dry matter content of various agricultural products.

According to many authors (e.g. Kim et al., 2003; Nelson, 2005; Wild and Haedicke, 2005; Jones et al., 2006) dielectric properties of many materials depend on frequency, moisture content, volume density, temperature, chemical composition, and permanent dipole moment association with water and other constituent molecules.

Savoie et al. (2002) used a capacitance controlled oscillator placed at the discharge end

of the forage harvester spout to measure changes induced by forage particles. This equipment showed a linear drop in the frequency of the oscillator as the wet mass flow increased. The frequency drop of the capacitance controlled oscillator correlated poorly with mass flow rate and correlated better with water flow rate.

Williams et al. (2000) used electrical capacitance tomography for particular solids flow rate measurement on a conveyor belt. This sophisticated method can be used to measure an image of the dielectric constant directly in a cross section of conveyor belt with transported solids and showed potential for on-line feed rate measurement.

In an earlier paper (Kumhála et al., 2007) a parallel plate capacitive sensor suitable for determining forage throughput was designed. Consequently, the arrangement of laboratory set-up was improved and capacitive sensor was tested for sugar beets and potatoes throughput measurements (Kumhála et al., 2009). It followed from theoretical considerations as well as from laboratory experiments that the way of filling of the sensor plays a very important role, which has to be respected during its calibration. Theoretical considerations also predicted that this type of sensor is less sensitive to material moisture content changes, because the capacities of two series-combined capacitors are measured in every case. The dimensions of the plates of both capacitors are the same and dielectric of first one is air and dielectric of second one is measured material.



Therefore, the main aim of our research was to determine the influence of material moisture content changes on measurement accuracy.

### Experimental arrangement

Stationary laboratory experiments were arranged with balsa blocks in order to determine the influence of material moisture content changes on obtained results. Another, small laboratory capacitor was made for that purpose (Fig. 1). The capacitor was integrated into an electronic circuit similar to the ones used for dynamic laboratory experiments with bigger capacitive throughput sensor (Kumhála et al., 2007, 2009). The dimensions of capacitor plates were 67 mm in length and 40 mm in width. The distance between the plates was 20 mm. Four balsa blocks with the dimensions 57 mm in length, 40 mm in width and 16 mm in height were used for those experiments. Dry matter of 1<sup>st</sup> balsa block was 4.79 g, of 2<sup>nd</sup> balsa block 4.83 g, of 3<sup>rd</sup> 3.71 g and of 4<sup>th</sup> balsa blocks 3.75 g.

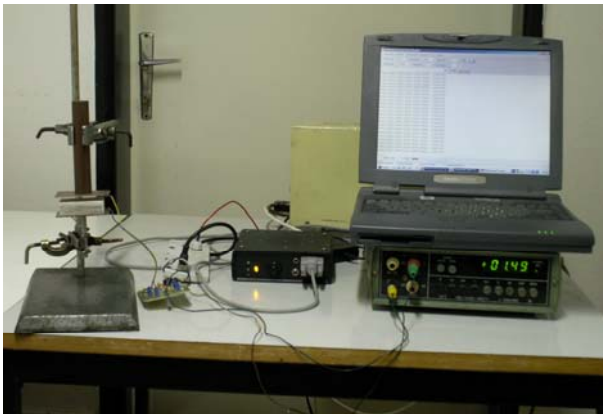


**Figure 1** - The arrangement of laboratory set-up for determining the influence of material moisture content changes on measuring circuit output voltage with small capacitive sensor integrated into similar electronic circuit as used for dynamic laboratory measurements with conveyor

At start of the experiments, balsa blocks were moistened to about 80% of moisture content and then slowly dried in our laboratory. After about 45 minutes of drying, balsa blocks were placed into plastic bags and sealed in order to homogenize moisture content distribution inside each of balsa blocks. After that, each balsa block was separately weighted and placed between smaller capacitor plates. The values of balsa blocks weight and measuring circuit output

voltage were logged and used for further calculations of balsa blocks moisture content and charting. This procedure was repeated until balsa blocks equilibrium moisture content was achieved. During the measurements the dimensions of balsa blocks were checked to make sure that they hadn't changed. Wooden blocks material moisture content was determined by modified ASABE Standard S358.2 (oven drying at 103<sup>0</sup>C up to constant weigh of the dry sample, wet basis).

### Results and discussion

Experiments with balsa blocks were conducted with the aim to understand better the influence of material moisture content changes to measured signal from capacitive throughput sensor in the case when material volume remains nearly constant. The results of those experiments can be seen in Fig. 2.

The dependence of measured output voltage on material moisture content can be divided into three sections. At start in the first section of the chart in Fig. 2, it means when material moisture content of balsa block 1 and 2 varied from about 75% to 65% and balsa blocks 3 and 4 from about 80% to 65%, a relatively very small decrease of measured output voltage was observed. The results of statistical analysis of this part of the chart were following. It was found by the analysis of variance that there was no difference between the data sets from 1<sup>st</sup> and 2<sup>nd</sup> balsa block measurements much like the data sets from 3<sup>rd</sup> and 4<sup>th</sup> balsa block. However, there was a difference between those two groups. It can be explained by the differences of dry matter weight (4.79 g and 4.83 g compared to 3.71 g and 3.75 g). When regression analysis, linear model was applied, the coefficients of determination were relatively low ( $R^2=0.702$  or  $0.825$ ) because of the dispersion of measured values and regression coefficient ranged from 0.0053 to 0.0039 which means that the decrease of measured values was relatively very slow.

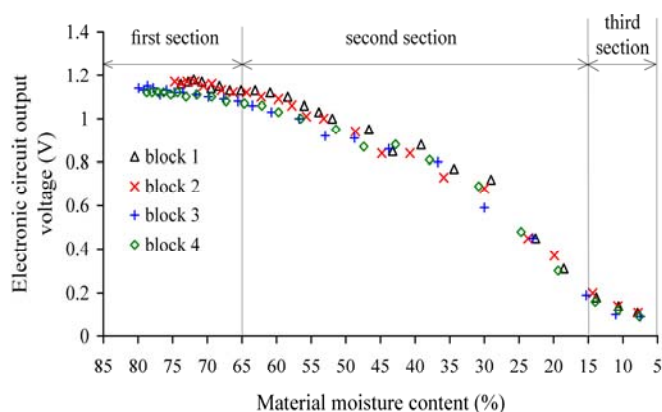


**Figure 2** - Dependence of measured capacitive sensor output voltage on balsa blocks moisture content (wet basis) changes. Dry matter content of 1<sup>st</sup> balsa block was 4.79 g, of 2<sup>nd</sup> balsa block 4.83 g, of 3<sup>rd</sup> 3.71 g and of 4<sup>th</sup> balsa block 3.75 g.

Very little observed changes in measured output voltage in the first section of the chart are also in good correspondence with our theory of capacitive throughput sensor (Kumhála et al., 2009) which predicts that this type of sensor is less sensitive to material moisture content changes. Since the permittivity of wood depends on many factors, as it is composed of fibres, rays, vessels, air, imbedded water, free water etc. (Daian et al., 2006), a closer study of processes inside the capacitor with balsa wood dielectric is just beyond the scope of this article. Nevertheless, wood dielectric permittivity strongly depends on the moisture content.

After that, in the second section of this chart (Fig. 2), when about 65% of material moisture content was obtained, measured output voltage decreased faster with the wooden blocks with diminishing moisture content up to app. 15% of material moisture content. According to the analysis of variance results for this section, there was no difference between the data sets from particular wooden blocks. It was difficult to determine the waveform describing the course of data obtained in this section of the chart because of wood dielectric permittivity changes. However, for the aim of this article linear model can be applied as well.

Coefficient of determination was  $R^2=0.937$  in that case and regression coefficient resulted 0.0175. It means that the decrease of measured voltage values with material moisture content decreasing in second section of the chart is more than three times faster than in the first section.

The results of Kruskal-Wallis test for the data sets from first and second section of the Fig. 2 also determined statistically significant differences between the data displayed in the first and second section of the chart.

In the third section of the chart the decrease of measured output voltage values with material moisture content decreasing is slower again. The reason is probably hidden in wood material structure. Nevertheless described capacitive throughput sensor was not designed to be used with plant materials with so small moisture content. That is why a detailed analysis of the third part of the chart is just also beyond the scope of this article.

It can be concluded that if materials with relatively high moisture content are measured (i.e. potatoes, sugar beets, carrots, tomatoes etc.), changes of about 5% of material moisture content have very little influence on capacitive throughput sensor measurement and which can therefore be neglected.

However, in the case when materials with lower material moisture content are measured (i.e. chopped maize or forages), the changes in material moisture content itself can influence the results of capacitive throughput measurement. This must be respected during the operation of capacitive throughput sensor. Independent measurement of material moisture content can be recommended for plant materials with material moisture content in the range from 65 to 15%.

Although changes in plant material moisture content involve mainly changes of material volume density and by means of this capacitive sensor output signal, in the case when plant materials with lower value of material moisture content are measured the changes in material moisture content itself have to be taken into account as well.

## Conclusion

Changes in material moisture content can play an important role which has to be respected during capacitive throughput sensor calibration, especially for the materials with material moisture content less than 65% (wet basis). Independent measurement of material moisture content for the materials as copped maize or forages seems to be necessary under practical conditions from that reason.

## Acknowledgements

This project was funded by Ministry of Education, Youth and Sports of the Czech Republic, Research project number MSM 6046070905

## References

- [1] ASABE Standards. *S358.2 Moisture measurement-Forages*. St. Joseph, Michigan. ASABE, USA, 2006.
- [2] Auernhammer, H. *Precision farming-the environmental challenge*. Comput. Electron. Agric. 30, 2001, p. 31-43, ISSN 0168-1699.
- [3] Daian, G., Taube, A., Birnboim, A., Daian, M., Shramkov, Y. *Modeling the dielectric properties of wood*. Wood Science and Technology 40(3), 2006, p. 237-246, ISSN 1432-5225.
- [4] Eubanks, J. C., Birrell, S. J. *Determining moisture content of hay and forages using multiple frequency parallel plate capacitors*. ASAE paper No. 011072, ASAE, St. Joseph, Michigan, USA, 2001.
- [5] Jones, C. L., Stone, M. L., Maness, N. O., Solie, J. B., Brusewitz, G. H. *Plant biomass estimation using dielectric properties*. ASABE paper No. 063092, ASABE, St. Joseph, Michigan, USA, 2006.
- [6] Kim, K. B., Lee, J. W., Lee, S. S., Noh, S. H., Kim, M. S. *On-line measurement of grain moisture content using RF impedance*. Transaction of ASAE, 46(3), 2003, p. 861-867, ISSN 0001-2351.
- [7] Kumhála, F., Kvíz, Z., Kmoch, J., Prošek, V. *Dynamic laboratory measurement with dielectric sensor for forage mass flow determination*. Research in Agricultural Engineering 53(4), 2007, p. 149-154, ISSN 1212-9151.
- [8] Kumhála, F., Prošek, V., Blahovec, J. *Capacitive throughput sensor for sugar beets and potatoes*. Biosystems Engineering 102, 2009, p. 36-43, ISSN 1537-5110.
- [9] Lawrence, K. C., Funk, D. B., Windham, W. R. *Dielectric moisture sensor for cereal grains and soybeans*. Transaction of ASAE, 44(6), 2001, p. 1691-1696, ISSN 0001-2351.
- [10] Nelson, S. O. *Dielectric properties measurement for agricultural applications*. ASABE paper No. 053134, ASABE, St. Joseph, Michigan, USA, 2005.
- [11] Osman, A. M., Savoie, P., Grenier, D., Thériault, R. *Parallel-plate capacitance moisture sensor for hay and forage*. ASAE paper No. 021055, ASAE, St. Joseph, Michigan, USA, 2002.
- [12] Savoie, P., Lemire, P., Thériault, R. *Evaluation of five sensors to estimate mass-flow rate and moisture of grass in a forage harvester*. Applied Engineering in Agriculture, 18(3), 2002, p. 389-397, ISSN 0883-8542.
- [13] Snell, H. G. J., Oberndorfer, C., Lücke, W., Van den Weghe, H. F. A. *Use of electromagnetic fields for the determination of the dry matter content of chopped maize*. Biosystems Engineering 82(3), 2002, p. 269-277, ISSN 1537-5110.
- [14] Wild, K., Haedicke, S. *Improving the accuracy of moisture sensors for forage crops*. In: Book of Abstracts 5 ECPA-2 ECPLF, JTI Sweden, 2005, pp. 326-328.
- [15] Williams, R. A., Luke, S. P., Ostrowski, K. L., Bennett, M. A. *Measurement of bulk particulates on belt conveyor using dielectric tomography*. Chemical Engineering Journal 77(1-2), 2000, p. 57-63, ISSN 1385-8947.

## SHAPE DETERMINATION OF TOMATO FRUITS (*Lycopersicon esculentum* Mill) BASED ON MOIRÉ METHODS

FERNANDO KUNINARI<sup>1</sup>, CELINA DE ALMEIDA<sup>1</sup>, INACIO MARIA DAL FABBRO<sup>2\*</sup>,  
ENRICO DI RAIMO<sup>1</sup>, ADILSON MACHADO ENES<sup>1</sup>

<sup>1</sup>Faculty of Agricultural Engineering, State University of Campinas, Campinas, SP, Brazil

<sup>2</sup>Faculty of Agricultural Engineering, State University of Campinas, Campinas, SP, Brazil,  
Phone: 55-19-35211059, Fax: 55-19-352110, E-mail: inacio@agr.unicamp.br

### Abstract

Tomato is considered a very important crop in Brazil, yielding 70 metric tons per hectare, spread through several states, showing irregular production as well as lack of quality control. A fast shape determination would be considered one of the basic requirements for quality control. The literature discloses several research works devoted to vegetable shape determination, including moiré methods, which are considered of low cost and reliable. This research reports the application of a phase shift moiré method supported by a conventional experimental setup including a digital camera, real tomato specimens and a multimedia projector. Applied software included RisingSun Moire and Image J. Four digital grids, out of phase one from each other by  $\pi/2$ , were projected onto a flat white opaque reference surface, having these image captured by the camera. Following, the grid was projected onto the testing object surface, i.e., the tomato, generating further images. Images subtraction generated a set of four images presented in gray gradient as well as with the moiré fringes. The image set was then filtrated by means of the ImageJ software which applies the Gaussian Blur method to eliminate the original grid, preventing, that way, undesirable interferences. Moiré fringes generated on tomato surfaces were captured and processed to obtain fruit surface topography. It is concluded that the method can give support for future technological development applied to fruit sorting and selection.

### Introduction

Tomato was the first produce to join the process defined as harvesting – classification – packing – commercialization, starting at the time when its production became important in the regional as well as in the national economy. Annual consumption *per capita* of tomato in Brazil reaches the figure of 18,5 Kg/inhabitant/year. With the introduction of mechanical harvesters, the industry started to require fruits of simultaneous maturation time because a unique and not scaled harvesting should be scheduled (Filgueira, 2002). The literature discloses several topics on tomato selection based on sphericity, size, shape, color and firmness. Instrumented tomato sorting is considered highly reliable if compared with hand process. A significant variety of optical methods have been developed to support technologies associated to fruit selection and sorting. *Moiré* methods have been reported by several authors, claiming simplicity, low cost as well as reliability (Dal Fabbro, I.M *et ali.*, 2005). The *moiré* phenomenon is observed when screens of certain mesh density are superposed, producing

wave like patterns or fringes, which move when its relative positions are displaced (Sciammarella, 1982). A new technique named “phase shifting” *moiré* is proposed, which can be viewed as a variation of the *moiré* methods. The objective of this research work is to carry *moiré* tests on tomato to copy fruit surface topography to generate a three dimensional geometrical description, giving, this way, scientific support to future selection and sorting techniques.

### Experimental arrangement

The experimental part of this research work was carried at the Laboratory of Optics at the Faculty of Agricultural Engineering at UNICAMP, Campinas, SP, Brazil, selecting a “phase shifting” *moiré* technique to generate the optical fringes. Experimental tests were carried by means of a conventional *moiré* setup as shown on Figure 01, which included a multimedia projector, a grid set, and an acquisition system coupled to a digital camera. Tomatoes were firstly painted with white opaque color to improve optical contrast.



## Results and discussion

Figure 02 shows the first processing step with a Ronchi grids projected onto a white background surface meanwhile Figure 03 shows the second processing step with the grid projected onto a tomato surface which was forwarded to the ImageJ and RisingSun software for processing. Figure 04 Shows the difference between the grid and the tomato surface. Figure 05 shows the images after grid elimination to

prevent undesirable interferences, showing also the *moiré* fringes generated on the fruit surface by the ImageJ software, meanwhile Figure 06 shows the mask to remove the area of no interest. Figure 07 shows *Moiré* fringes generated on the fruit surface after interferences removal. Figure 08 exhibits the final images of each sample to determine the surface topographic expressed in grayscale by means of the RisingSun Moire software.

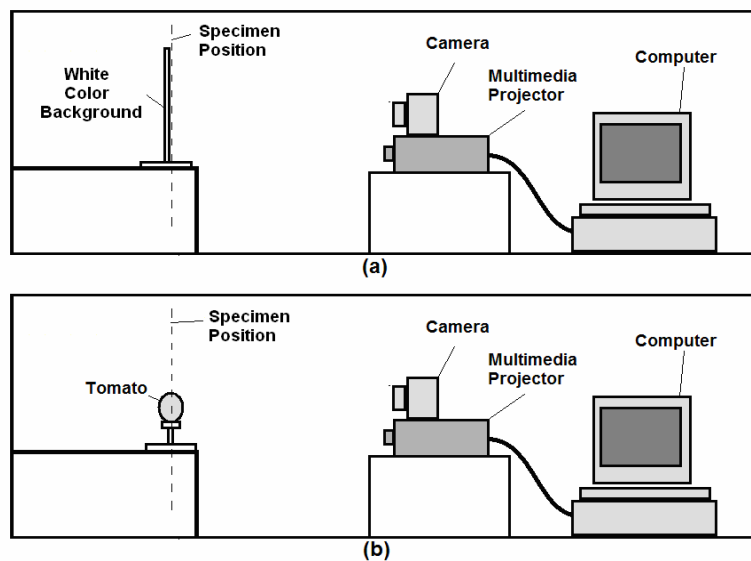


Figure 01. Details of the experimental setup to carry Phase Shift *moiré* tests on real tomato specimens

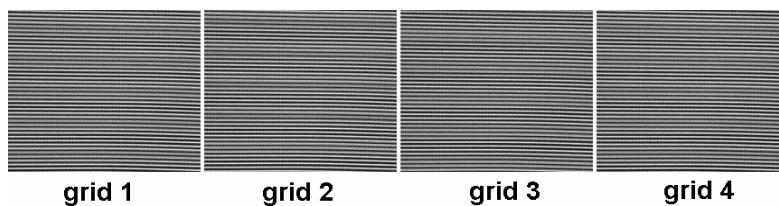


Figure 02. Ronchi grid projected onto a white background surface

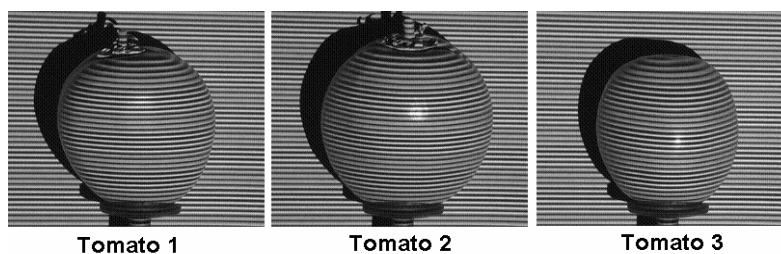


Figure 03. The same Ronchi grid projected onto the tomatoes surface

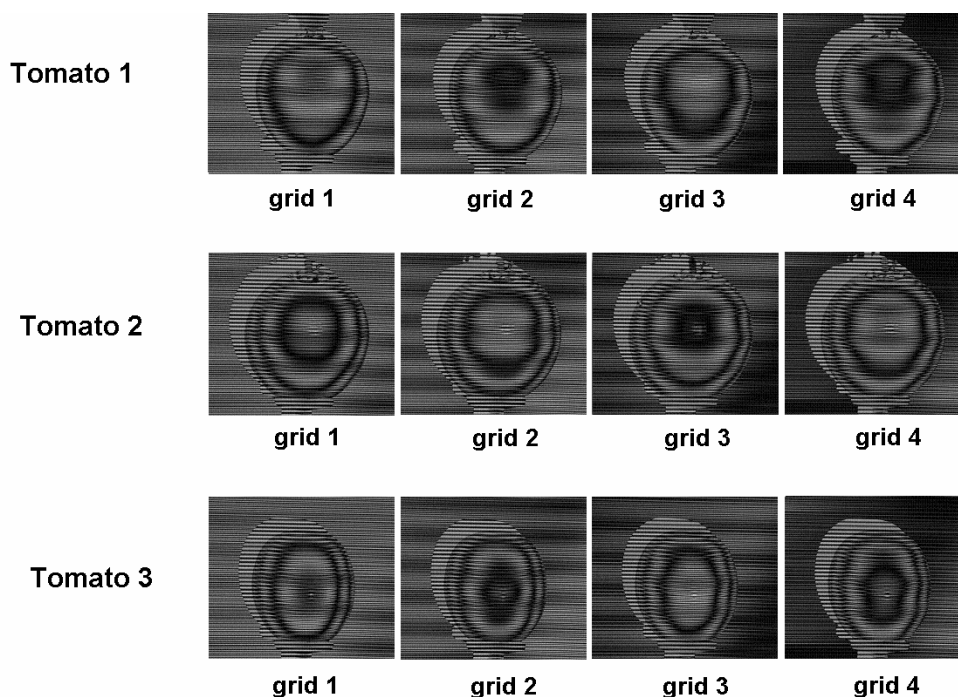


Figure 04. The difference of the Ronchi grid from the tomato surface

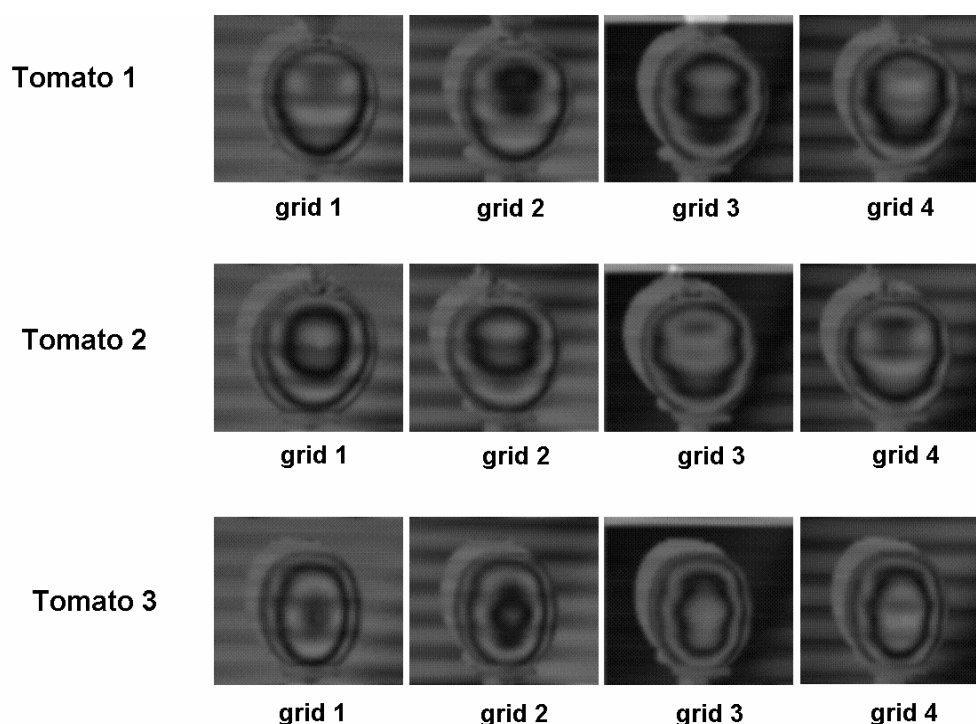


Figure 05. *Moiré* fringes generated on the fruit surface by the ImageJ software

The topographic variations on the fruit surface are displayed in gray scale as shown of Figure 08. The **Z** coordinate is normal to the

image surface and indicates the fruit surface height, reaching the maximum value at the central point.



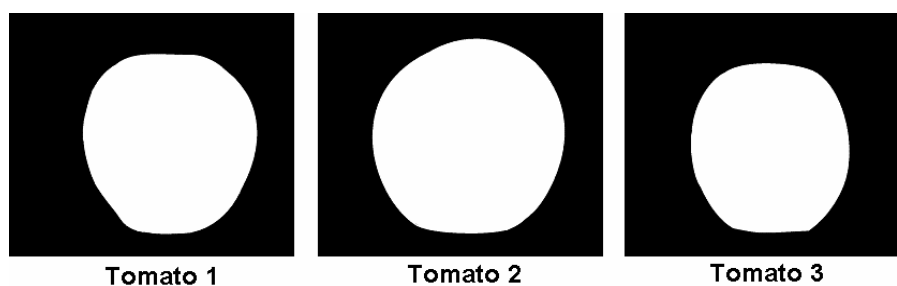


Figure 06. Masks generated by the ImageJ for interferences removal

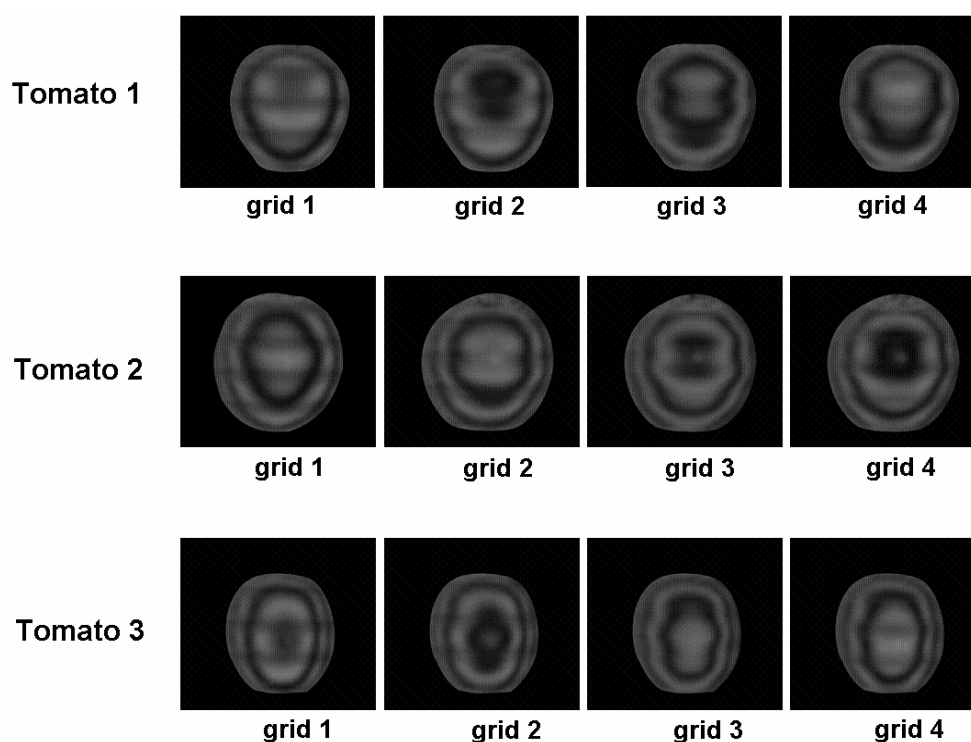


Figure 07. *Moiré* fringes generated on the fruit surface after interferences removal

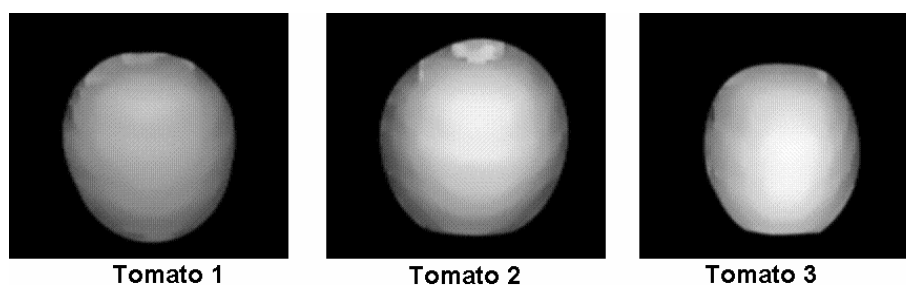


Figure 08. Topographic variation of the tomato surfaces expressed in gray gradient

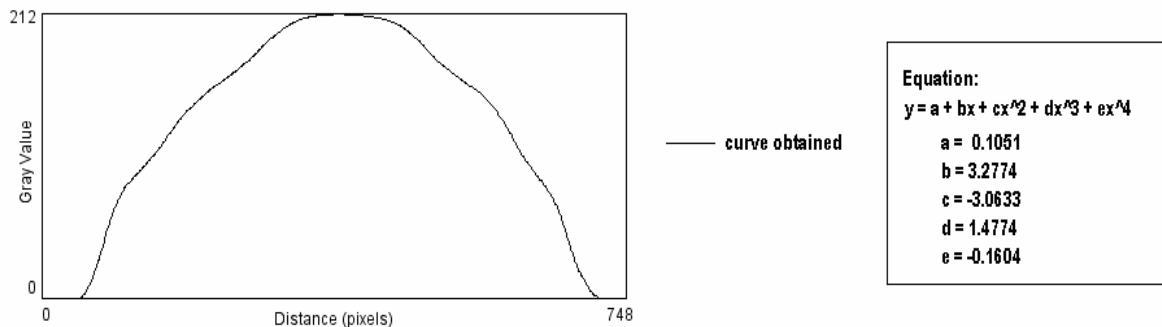


Figure 09. Curve drawn on the tomato surface

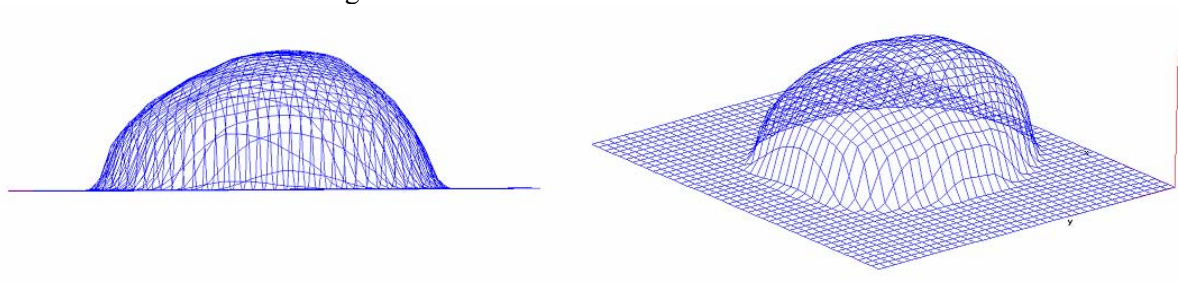


Figure 10. Three dimensional view of one tomato surface

## Conclusion

Based on what it has been exposed above it can be concluded that the proposed method is viable as well as reliable. The digital elevation model (DEM) can expose the region of interest and also the fruit sphericity. Despite the studied product was represented by the tomato fruit, other agricultural products can also be considered. The method requires low cost equipment and is of simple application.

## References

[1] Dal Fabbro, I.M., Rodrigues, S., Braga Jr., R.A.. Applications of the *Moiré* Optical Technique in Agricultural Engineering Problems. In: Proceedings of The 5<sup>th</sup> Conference of the European Federation for Information Technology in Agriculture, Food and Environment and The 3<sup>rd</sup> World Congress on Computers in Agriculture and Natural Resources. EFITA/WCCA 2005 Joint Conference. (ISBN 972-669-646-1).

Universidade de Trás-os-Montes e Alto Douro, Vila Real, Portugal, 25 - 28 July 2005.

[2] Filgueira, F. A. Manual de olericultura: agrotecnologia moderna na produção e comercialização de hortaliças. 1 ed. Viçosa: Universidade Federal de Viçosa, 2002. 401p.

[3] LINO, A, C, L. Técnica óptica de *moiré* visando a aplicação no estudo de superfícies irregulares. 2002. 86p. Dissertação (Mestrado) – Faculdade de Engenharia Agrícola, Universidade estadual de Campinas, Campinas, Brazil.

[4] Mazzeti Filho, V. Utilização da Interfilometria de Moiré no Estudo de Tensões Dinâmicas em Discos Flexíveis. 2004. 52p. Dissertação (Mestrado) – Faculdade de Engenharia Agrícola, Universidade estadual de Campinas, Campinas, Brazil.

[5] Kuninari, F. ; Fabbro, I. M. D ; Lino, A. C. L ; Almeida, C . Moiré Aided Soil-Tractor Tire Contact Area and Contact Volume Determination. Journal of Agricultural Machinery Science, v. 4, p. 39-43, 2008.

## MEASURING OF CONDUCTING POLYMER PROPERTIES

MARTIN KÜNZEL<sup>1</sup>, BŘETISLAV BENDA<sup>2</sup>, GUNNAR KÜNZEL<sup>3\*</sup>

<sup>1</sup>University of Pardubice, Faculty of Chemical Technology, Institute of Energetic Materials

<sup>2,3</sup>Czech University of Life Sciences Prague, 16521 Prague 6 – Suchbát, Czech Republic, E-mail: kunzel@tf.czu.cz

### Abstract:

Conducting polymers are quite new and attractive materials and great attention is paid to them in present. Although these polymers cannot replace usual metals because of lower conductivity, they can be widely used in semiconductor technology. The main advantages of conducting polymers over inorganic semiconductors are: good cost efficiency, more environmental-friendly nature and ease of properties variation. In contrast, the main disadvantage is limited operating life [2], [3]. This article deals with experimental determination of some electrical properties of conducting polymers. Cylinder shaped samples of polymers were prepared by hydraulic pressing using commercial polypyrrole and laboratory prepared polyaniline hydrochloride, synthesized according to [4]. Some additional samples were prepared from these polymers with 10 % and 20 % of graphite powder. Testing apparatus was then designed and constructed for measurement using four-probe method. At first, volt-ampere characteristics of polymer samples were determined and resistivity values were calculated. Resistivity dependence on temperature was then examined in the range from 23°C to 60°C. In addition, resistivity dependence on input frequency was measured in the range from 50 Hz to 400 Hz.

**Keywords:** Conducting Polymer, Resistivity, Four-Probe Method

### Introduction

Experimental determination of electrical properties of conducting polymers is not specified in any norm. The only available norm is ISO 3915 international standard from 1981 which was created in order to measure usual non-conducting polymers with carbon black addition. Easily obtainable cylinder shaped samples of conducting polymers can not be measured according to this norm because there are strict sample shape demands. Therefore, testing apparatus was designed and constructed for measurement using four probe method.

### Theory

The principle of the four-probe method is now described briefly. Stable current flows through the sample between two current electrodes while voltage drop is measured between two voltage electrodes by the help of electronic voltmeter. The resistance of the sample between voltage electrodes is given by equation

$$R = \frac{\Delta U}{I} [\Omega; V, A] \quad (1)$$

where  $\Delta U$  is the voltage drop between voltage electrodes and  $I$  is the current flows through measured sample. Specific resistivity can be then calculated using equation

$$\rho = \frac{R \cdot S}{d} [\Omega \cdot cm; \Omega, cm^2, cm] \quad (2)$$

where  $R$  is the resistance from equation (1),  $S$  is the cross section of the sample given in  $cm^2$  and  $d$  is the distance between voltage electrodes in cm.

### Experimental Measured samples

Polyaniline hydrochloride (PANI) and doped polypyrrole were chosen as good candidates for measurement in view of easy preparation of samples and low cost [3]. Fine graphite powder was used as an additive to enhance conductivity. It also simplifies pressing and extraction of samples out of the die. There is a list of measured samples composition:

1. 100% PANI
2. 90% PANI + 10% graphite
3. 80% PANI + 20% graphite
4. 100% PP

### 5. 90% PP + 10% graphite

Polyaniline hydrochloride was prepared according to modified method from [4]. The method was adapted to ten times larger scale, starting from 25.9 g (0.2 mol) aniline hydrochloride. Starting polymerization temperature was somewhat lowered to 13°C in order to preclude overheating. Powdery polymer was dried at 60°C and then mixed with graphite using mortar and pestle. Polypyrrole doped with organic sulfonic acid was obtained from Aldrich (product number 577030).

Powdery mixtures were then compacted to cylindrical pellets weighing approximately 1 g with the use of hydraulic press. Samples were 12.5 mm in diameter with cross section 1.2272 cm<sup>2</sup>. Its height reached 5 to 10 mm (Figure 1).



**Figure 1** - Cylinder shaped samples

### Measuring apparatus

Above stated samples were connected to measuring circuit with the help of measuring apparatus which consist of two parts:

#### a) Current electrodes

Electrodes were made of electrolytic copper having dimensions 20 x 30 x 1 mm. Isolation was done using ceramic plate with dimensions 15 x 20 x 6 mm and parts were bonded together using silicone glue. These electrodes also provide firm clamping of samples.

#### b) Voltage electrodes

Electrodes were made of electrolytic copper with dimensions 20 x 30 x 0.3 mm and relative distance 3 mm. Isolation was ensured by thermoplastic holder and parts were bonded together with the use of epoxy resin.

Copper wires connecting electrodes with measuring unit had cross section of 1.5 mm<sup>2</sup>. The measuring apparatus is depicted in Figure 2 while the measuring circuit scheme is shown in Figure 3. More complex description of the measuring methodology is discussed in 0.

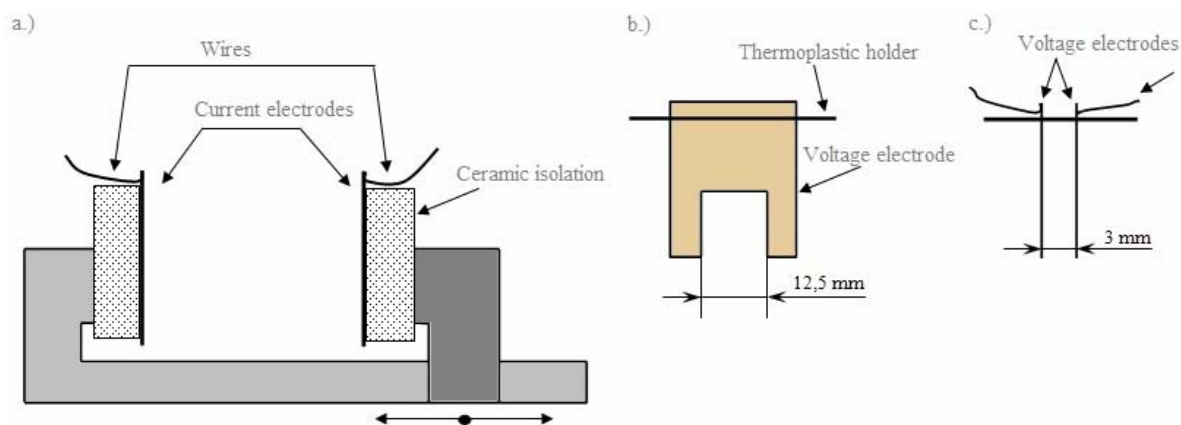


**Figure 2** - Side view of measuring apparatus (a) and voltage electrodes front view (b) and side view (c)

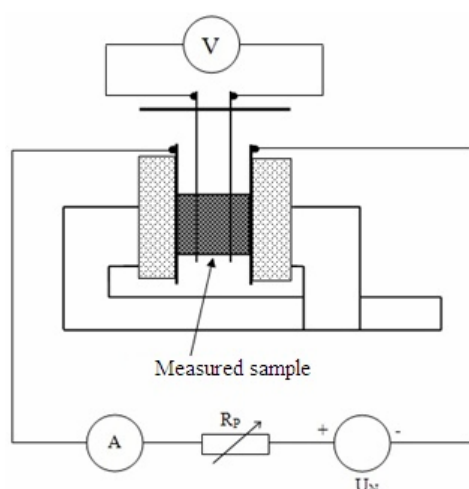


**Figure 3** - Scheme of measuring circuit

## Results and discussion

Five samples of each composition were prepared and measured. Results were very similar for all samples having the same

composition and differences were given by their making quality. Therefore, results are shown just for one of each sample set.

Measured volt-ampere characteristics of samples are shown in Figure 4. All dependencies are approximated linearly. Calculated resistivity and conductivity values are summarized in Table 1. Resistivity dependencies on temperature are shown in Figure 5. Resistance dependencies on input frequency are shown in Figure 6. These dependencies were approximated by parabolic curves described by quadratic equations. All data were compiled using common Microsoft Excel software and regression equations are shown as well as determination coefficients.

**Table 1** - Electrical properties of measured samples

Sample	Composition	Resistivity at 23°C [Ω.cm]	Conductivity at 23°C [S.cm <sup>-1</sup> ]
1	100% PANI	0.16882	5.92350
2	90% PANI + 10% graphite	0.07111	14.06320
3	80% PANI + 20% graphite	0.04819	20.75364
4	100% PP	0.28316	3.53170
5	90% PP + 10% graphite	0.30691	3.25849

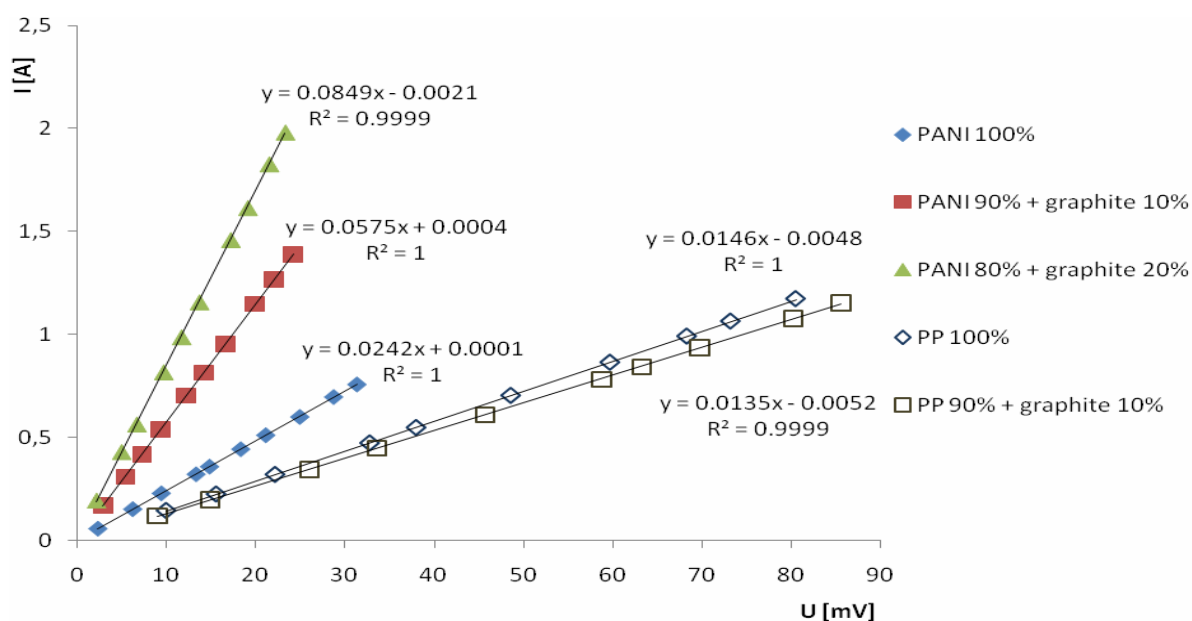


**Figure 4** - Volt-ampere characteristics of polymer samples

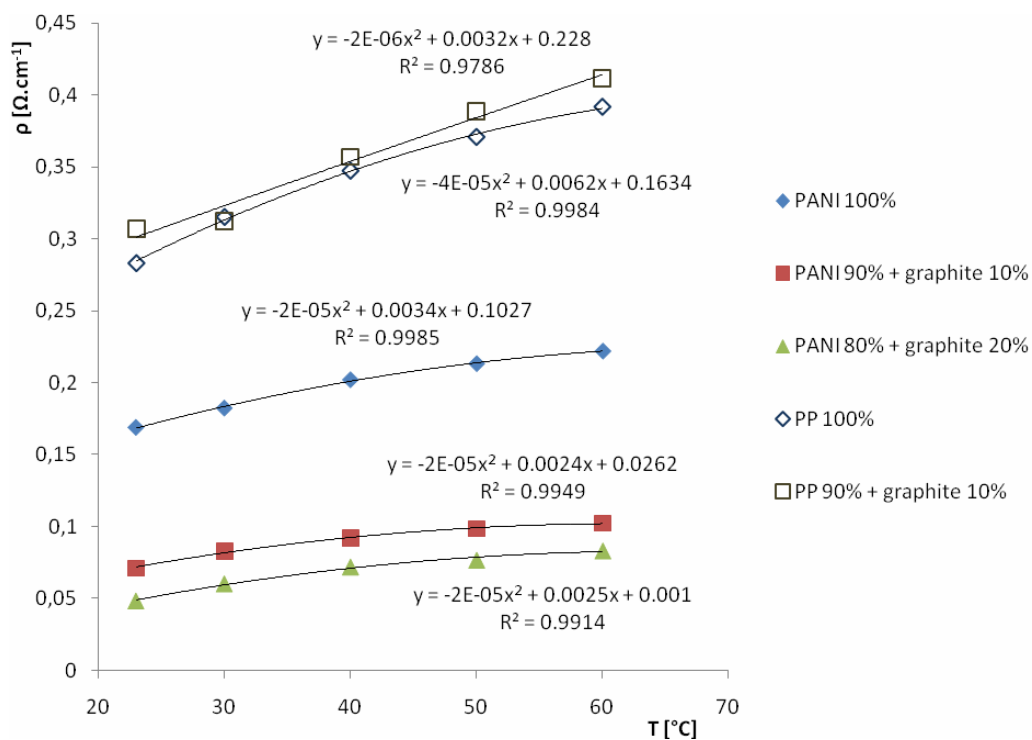


Figure 5 – Temperature-dependence of polymer samples specific resistivity

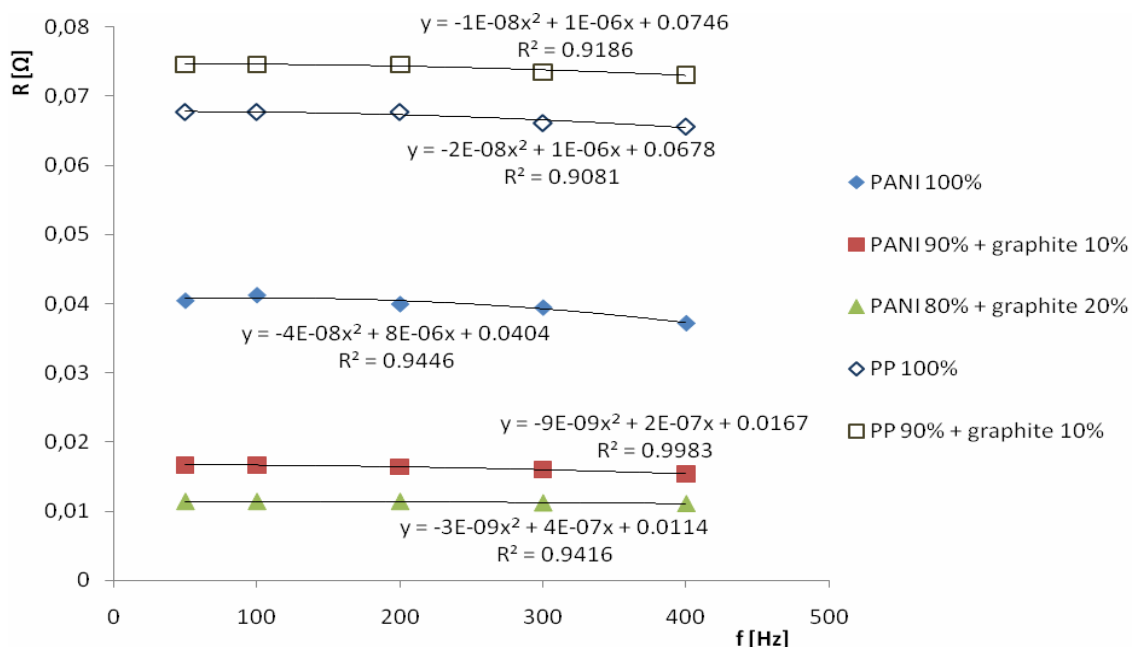


Figure 6 – Frequency-dependence of polymer samples resistance



## Conclusions

Measurement of basic electrical properties of samples made of laboratory prepared polyaniline hydrochloride and commercial doped polypyrrole was done with the help of designed measuring apparatus using four-probe method. All volt-ampere characteristics of conducting polymer samples were linear and can be described by linear equations, i.e. specific resistivities are not voltage-dependent. Temperature dependencies of resistivity were measured in temperature range 23 – 60°C. These dependencies are parabolic and can be described by quadratic equations. Resistance dependencies on input frequency are described by quite flat parabolic curves given by quadratic equations as well.

Designed method of resistance measurement is useful in order of laboratory measurement of conducting polymer properties.

## References:

- [1] Benda, B.: *Měření a hodnocení vlastností vodivých polymerů*. Diploma work, Technical Faculty of Czech Agricultural University, Prague, 2009. (in Czech)
- [2] Bouda, V.: Vodivé polymery – struktura, vlastnosti a použití. *Elektrotechnický obzor*, 1990, Vol. 79, Iss. 4, p. 213 – 218. (in Czech)
- [3] Prokeš, J.-Stejskal, J.-Omastková, M.: Polyanilin a polypyrrol – dva představitelé vodivých polymerů. *Chemické listy*, 2001, Vol. 95, p. 484 – 492. (in Czech)
- [4] Stejskal, J.: *Polyanilin: vodivý polymer* [online]. Published 30.8.2006 [quoted 19.6.2010]. Available at: <http://archiv.otevrenaveda.cz/users/Image/default/C1Kurzy/NH2006pdf/16.pdf> (in English)

## FERMENTATION OF CELLULOSE AND HEMICELLULOSE CARBOHYDRATES TO ETHANOL AND HYDROGEN BY ANAEROBIC SACCHAROLYTIC BACTERIA

KVESITADZE G., SADUNISHVILI T., \*DUDAURI T., METREVELI B.,  
PARTSKHALADZE G., UGREKHELIDZE V.

Durmishidze Institute of Biochemistry and Biotechnology, Tbilisi, Georgia  
David Agmashenebeli Kheivani 10<sup>th</sup> km, 0159 Tbilisi, Georgia; Phone :+( 995 32) 398 993;  
e-mail: tamaradudauri@hotmail.com

### Abstract

Although ethanol production from hexose sugars is a mature biotechnology, the high feedstock costs (about 50% of ethanol cost) pose one of the major barriers to the wide implementation of ethanol as the alternative transportation fuel. Lignocellulosic waste streams from agriculture, paper and wood industry are renewable and low cost raw materials that are plentiful and can be used for large-scale production of liquid and gaseous fuels. However, simultaneous fermentation of C6 and C5 sugars derived correspondingly from cellulosic and hemicellulosic fraction of lignocellulosic residues remains a bottleneck and the reveal of microorganisms with high tolerance to fermentation end products and ability to ferment both hexose and pentose sugars in a single-stage process is one of the main R&D points in fuel ethanol biotechnology. For these purposes anaerobic thermophilic saccharolytic bacteria in the genus *Clostridia* have been chosen for the following reasons: (i) the optimum growth temperature of thermophilic *Clostridia* is 55-60°C and therefore the problems of contamination are lessened; (ii) fermentation at high temperature facilitates the constant removal of ethanol by evaporation and distillation and thus has additional benefit of addressing economic problems (iii) thermophilic microorganisms in general are industrially relevant and robust microorganisms and (iv) *Clostridia* based fermentation by-products like hydrogen and volatile fatty acids are high valuable chemicals that also can be used for on-site energy production. With aim to reveal high effective micro organisms 65 strains of saccharolytic *Clostridia* have been isolated from different wetlands in Georgia. They were studied for morphological, biochemical and physiological specificities. Fermentation of glucose-xylose mix was done in thermophilic conditions (T=55°C and pH 7.1) under the oxygen free nitrogen environment. Fermentation duration was 96 hours. Liquid and gaseous products of fermentation were analyzed on the daily basis using Perkin Elmer gas chromatographs with flame ionization and thermal detectors. Residual xylose and glucose was determined by the standard methods. Eight of isolated strains indexed as GSX-2, GSX-4, GSX-5, GSX-6, GSX-8, GSX-9, GSX-14 and GSX-15 fermented xylose - glucose mix (1:1) with improved ethanol productivity and decreased acids production. Specifically maximum yield of ethanol was reached at 36 h of fermentation and varied between 2.9 – 3.2 g/l per 10 g of substrate. Acetic acid content in the fermentation broth didn't exceed 0.35 g/l. Other volatile fatty acids were detected in trace quantities. Hydrogen production started after 6 hours and was finished in 8 hours. Composition of hydrogen biogas was the following: H<sub>2</sub> – 52%; CO<sub>2</sub> – 48%.

**Key words:** cellulose, hemicellulose, carbohydrates, anaerobic bacteria, fermentation, fuel ethanol

### 1. Introduction

Dwindling fossil fuel resources make the search for renewable energy resources more urgent than ever. In the short term, ethanol has been trusted as an environmentally sound motor fuel alternative that can be used either in blend

with gasoline or alone. Although ethanol production from starch and sugar crops is a mature biotechnology, the high feedstock costs accounting for about 50% of the ethanol production costs, and the relatively limited contractibility of starch and sugars, pose major

barriers to a large-scale implementation of ethanol as the alternative transportation fuel [1]. Widely available and renewable lignocellulosic waste streams from agriculture, paper and wood industry as well as specially grown energy crops are recognized as the plentiful and low cost feedstock for fuel ethanol large-scale production. Such an approach is strengthened further by the fact that cellulosic ethanol exhibits a net energy content three times higher than corn ethanol, and emits a low, net level of greenhouse gases [2]. The primary impediment to widespread production of ethanol from recalcitrant lignocellulosic materials is the general absence of a low cost technology [3]. Plant biomass, mostly referred to a lignocellulose, is predominantly composed of three major polymers: cellulose (an insoluble linear unbranched homopolysaccharide consisting of glucose subunits linked via  $\beta$ - (1,4) glycosidic linkages), hemicellulose (polysaccharide mainly composed of xylan, mannans, glucans) and lignin (an intricate polyphenolic structure). It is built up as cellulose fibers that are partially arranged in a crystalline structure, integrated with hemicellulose and embedded in a matrix of lignin [4]. Both the cellulose and hemicellulose are the sources of fermentable - C6 and C5 - sugars. However effective fermentation of cellulose and hemicellulose carbohydrates is the issue that needs to be resolved.

The yeast *Saccharomyces cerevisiae* is used in ethanol industry for large scale production of ethanol from molasses and starch crops. These industrial yeasts are capable of effective fermentation of C6 sugars –glucose and fructose and can tolerate high ethanol concentration (up to 17 vol %) in the fermentation broth [5]. On the other hand this microorganism is not able to ferment C5 sugars. To overcome this drawback, R&D had been focused on genetic modification of *Saccharomyces cerevisiae* yeasts. The genes encoding xylose reductase and xylitol dehydrogenase were cloned into *S. cerevisiae*. The above enzymes are responsible for the conversion of xylose via xylitol to xylulose which is a C5 sugar that can be fermented by *S. Cerevisiae*. After transformation, *S. cerevisiae* was able to produce ethanol from xylose, but the productivity was low and xylitol was formed as

byproduct, diverting substrate from ethanol production [6]. Other yeasts like *Pichia stipitis*, *Candida shehatae* and *Panchysolen tannophilus* are able to ferment C5 sugars. However, when using above yeasts ethanol production rate with glucose as a substrate is at least five times lower than observed in *S. cerevisiae* [7]. Moreover, these yeasts require oxygen and their tolerance to ethanol is 2-4 times lower than *S. cerevisiae* [8].

Amongst the ethanol-producing bacteria, *Zymomonas mobilis* isolated from the fermented juice of agave seemed promising for industrial application. This bacterium converts hexoses and has a fairly high ethanol tolerance, allowing concentrations up to 100g/l. Furthermore, *Z. mobilis* has a higher optimal growth temperature than *S. cerevisiae* which reduces the cost for cooling during the fermentation. One drawback is that the substrate range of *Z. mobilis* is limited as only glucose, fructose and sucrose, which limits application of this bacterium at the industrial scale [9]. In this regard revealing of new strains of thermophilic bacteria in the genus *Clostridia* with high tolerance to fermentation end products and ability to ferment both hexose and pentose sugars in a single-stage process is considered one of the main R&D points in fuel ethanol biotechnology [10].

Anaerobic thermophilic saccharolytic bacteria in the genus *Clostridia* have been chosen for simultaneous fermentation of C6 and C5 sugars. These microorganisms are considered promising for application at the industrial scale for the following reasons: (i) the optimum growth temperature of thermophilic *Clostridia* is 55-60°C and therefore the problems of contamination are lessened; (ii) fermentation at high temperature facilitates the constant removal of ethanol by evaporation and distillation and thus has additional benefit of addressing economic problems, (iii) thermophilic microorganisms in general are industrially relevant and robust microorganisms and (iv) *Clostridia* based fermentation by-products like hydrogen and volatile fatty acids are high valuable chemicals that also can be used for on-site energy production.

## 2. Materials and methods

### 2.1 Microorganisms, media and cultivation

65 accumulating cultures of anaerobic thermophilic saccharolytic *Clostridia* were isolated from the soil samples taken at different wetlands in Georgia. Taking into account that in natural environment like wetland cellulolytic, saccharolytic and methane forming bacteria coexist, initially soil and water samples were heat-treated at 90°C for 3 -5 min to depress non-spore forming methanogens. Inoculum was prepared by mixing 5 g of each heat-treated soil sample with double-distilled water (1:2) and homogenized in a blender under the oxygen-free nitrogen atmosphere. The above samples were placed in 15 ml volume flasks and kept for 24 hours in the anaerostate where temperature was gradually increased from 20°C to 55°C.

For isolation of saccharolytic bacteria of *Clostridia* sp. two different composition liquid medium were used. Composition of medium #1 was the following: (g/l) NH<sub>4</sub>Cl – 2; K<sub>2</sub>HPO<sub>4</sub> 3H<sub>2</sub>O – 4; KH<sub>2</sub>PO<sub>4</sub> – 2; MgCl<sub>2</sub> 6H<sub>2</sub>O – 0, 42; CaCl<sub>2</sub> – 0, 05; yeast extract – 1. Content of micro elements' solution which was added to nutrient media was as follows (mg/l): CuSO<sub>4</sub> 5H<sub>2</sub>O – 6,4; FeSO<sub>4</sub> 7H<sub>2</sub>O – 1,1; MnSO<sub>4</sub> 4H<sub>2</sub>O – 7,9; ZnSO<sub>4</sub> 7H<sub>2</sub>O – 1,5 – 1 ml/l. Medium #2 contained (g/l) yeast extract-2,0; (NH<sub>4</sub>)<sub>2</sub>SO<sub>4</sub>-1,3; KH<sub>2</sub> PO<sub>4</sub> -1,5; K<sub>2</sub> H PO<sub>4</sub> – 2,9; MgCl<sub>2</sub> .6H<sub>2</sub>O- 1.0; CaCl<sub>2</sub> -0,15; 1 ml of 0,2% of resazurine, 0,025 of 5% solution of FeSO<sub>4</sub>, pH-7,0; 0,4 ml of 1,25% solution of cysteine hydrochloride monohydrate. pH was adjusted to 7,5. Glucose, xylose and their combination was used as the only source of carbon.

To obtain pure strains of saccharolytic bacteria the following composition liquid nutrient medium was used (g/l): NH<sub>4</sub>Cl- 2; K<sub>2</sub>HPO<sub>4</sub>.3H<sub>2</sub>O; - 4; KH<sub>2</sub>PO<sub>4</sub> – 2; MgCl<sub>2</sub>.6HCl - 0.42; CaCl<sub>2</sub>- 0.05; yeast extract – 1; glucose (used as the only source of carbon) – 10 g/l; solution of microelements 1ml/l. pH - 7.1.

### 2.2 Morphological and biochemical studies

Morphology studies were performed using dyed preparations, liquid cultures and cells grown on agar. Light microscope with resolutions 100/1, 25 was used. Considering that during the initial phase of sporulation variations

in length, form and diameter of rods for the most part of cellulolytic and saccharolytic *Clostridia* are common, along with microscopic examinations additional tests for precisely detection of bacteria species have been conducted. Formation of butyric acid and pH decrease to 5.8-5.3 in the course of stationary growth phase of the culture was chosen as the indicator for the presence of glycolytic anaerobes. The second criterion was protease activity in the culture supernatant. Biochemical and physiological studies of isolated microorganisms included determination of the following characteristics: growth rate, optimum growth temperature and pH, ability to ferment different substrates including monosaccharides and resistance to antibiotics like ampicillin, actinomycin, streptomycin sulfate and rifampin. To study optimum growth temperature and pH, in different experiments isolates were grown at T 45°C; 55°C and 65°C and pH – 6. 0 and 7. 1.

Bacteria strains able to simultaneously ferment glucose and xylose with high yield of ethanol and decreased acids production have been studied deeper. For these purposes 3 l volume fermenter with water jacket and equipped with on-line pH - and gas flow meters, temperature and pH controller was used. Experiments were run in batch conditions. Oxygen free nitrogen was used to maintain anaerobic conditions in the fermenter. Fermentation temperature and pH were 55°C and 7.1 correspondingly. pH was controlled by adding 0.1% sterile NaOH solution. To determine optimum growth conditions, in series of experiments content of nitrogen source and yeast extract in nutrient medium was varied in the range of 2-5 g/l and 1-3 g/l correspondingly.

### 2.3. Analytical methods

Protease activity in the late logarithmic growth phase was studied by using cell suspensions and azoalbumine and azocasein. The test was performed by Tomarelli method but with incubation temperature T= 55°C and total incubation time – 18 h. Analytical samples were taken at the start of incubation process and at 2.8 and 18 h.

Bacteria growth in liquid media was determined by the changes in optical density at

600 nm. Perkin Elmer UV-VIZ spectrophotometer -Lambda EZ- was used for these purposes.

Fermentation end-products like ethanol, volatile fatty acids and hydrogen were analyzed on a daily basis using gas chromatograph with flame ionization and thermal detectors.

Dinitrosalicylic acid (DNS) method was used for reducing sugars assay. Glucose was determined by glucose-peroxidase method.

Antibiotic resistance was tested by using liquid medium containing glucose and xylose as the sole source of carbon.

### 3. Results

Eight of isolated strains indexed as GSX-2, GSX-4, GSX-5, GSX-6, GSX-8, GSX-9, GSX-14 and GSX-15 showed ability to ferment xylose - glucose mix (1:1). Morphology studies showed that all strains listed above grow by making the medium equally muddy. Formations of granules were not observed. When grown in liquid medium containing glucose - xylose mix these saccharolytic *Clostridia* are of slight brown color. Growing on agar, most of them (GSX-2, GSX-4, GSX-5, GSX-6, GSX-8) exhibit light beige pigmentation. On glucose containing agar these isolates form translucent colonies which are of mucus consistence. Cells have a rod-like shape; their spores are round with terminal arrangement. During the spore formation the sporangium swells. The young cells are Gram-positive. Colonies of GSX-9, GSX-14 and GSX-15 grown on the agar are of R form, diameter – 1-2 mm. They are brown with coggled edges. Cells have straight-line or slightly curved rod-like shape. These rods join together and mostly

form short chains. Young cells are motile. At the end of the cells large size spores form.

None of above isolates grows on beef-extract broth. They don't coagulate milk and digest meat. They don't acidify meat broth. No peptidase or proteolytic activity was detectable in the cultures' supernatants. None of above anaerobic saccharolytic bacteria strains grows in the presence of antibiotics like ampicillin, actinomycin, streptomycin sulfate and rifampin in amount of 1 µg/l.

The best growth rate for GSX-2, GSX-4, GSX-5, GSX-6, GSX-8, GSX-9, GSX-14 and GSX-15 strains was achieved at T=55°C and pH-7.1. Optimum amount of NH<sub>4</sub>Cl and yeast extract was defined as 2.5 g/l and 0.8 g/l correspondingly. Growth characteristics of anaerobic, thermophilic saccharolytic bacteria strains reported here are given in table #1.

All strains given in table #1 exhibited hyperbolic growth on mixed carbohydrate substrates when grown in pH-controlled batch culture. Hyperbolic growth was observed with xylose in combination with glucose. Diauxic growth ways were observed when above strains were grown on a glucose plus cellobiose substrate mix. The major fermentation end-products under all substrate conditions were ethanol and acetate. Ethanol production varied depending on the substrate supplied and was always greatest on mixtures that included xylose (i.e. hyperbolic growth).

Ethanol yield and biogas composition during the batch fermentation (T=55 °C; pH 7.1) of glucose-xylose mix (1:1) by strains GSX-2, GSX-4, GSX-5, GSX-6, GSX-8, GSX-9, GSX-14; GSX-15 are given in table #2.

Table #1

Strain	Carbon source (10g/l)	*Optical density in the stationary growth phase	Strain	Carbon source (10g/l)	*Optical density in the stationary growth phase
GSX-2	glucose-xylose	1.88	GSX-8	glucose-xylose	1.83
GSX-4	glucose-xylose	1.54	GSX-9	glucose-xylose	1.87
GSX-5	glucose-xylose	1.71	GSX-14	glucose-xylose	1.69
GSX-6	glucose-xylose	1.49	GSX-15	glucose-xylose	1.63

\* Initial optical density was 0,01 – 0,03.



Table #2

Strain	Substrate (10 g/l)	Ethanol (g/l)	Acetic acid (g/l)	Residual glucose (g/l)	Residual xylose (g/l)	Gas composition (%)	
fermentation duration 48 h						H <sub>2</sub>	CO <sub>2</sub>
GSX-1	glucose-xylose	3.5	0.27	1.02	0.72	53	47
GSX-7	glucose-xylose	3.6	0.31	1.09	0.93	54	46
GSX-1	glucose-xylose	3.4	0.23	1.11	1.02	52	48
GSX-7	glucose-xylose	3.2	0.30	1.14	1.01	54	46
GSX-4	glucose-xylose	3.1	0.28	1.21	1.12	51	49
GSX-5	glucose-xylose	3.8	0.22	0.92	0.87	55	45
GSX-6	glucose-xylose	2.9	0.26	1.22	1.16	49	51
GSX-8	glucose-xylose	3.2	0.28	1.12	0.89	52	48
GSX-14	glucose-xylose	3.4	0.31	1.07	1.02	56	44
GSX-15	glucose-xylose	3.7	0.27	0.98	0.09	53	47

#### 4. Conclusions

Comparing results obtained for wild saccharolytic strains reported here with those described in recent publications, it can be concluded that GSX-7, GSX-5 and GSX-15 are the most active microorganisms fermenting glucose-xylose mix with highest yield of ethanol and decreased acids production. Substrate conversion rate makes 87-90%.

#### References

- [1]. Den Ridder, J. 2000. Presentation for the closing meeting of International Energy Agency: Biotechnology for the conversion of lignocellulosics to ethanol.
- [2]. Arnold L. Demain et al. Microbiology and Molecular Biology Reviews, March, 2005; p. 124-154, vol. 69, #1)
- [3]. Lynd RR; Germgross TU, Wyman CE: Biocommodity engineering. Biotechnol Prog 1999, 15:777-793
- [4]. Coombs J. Bioconversion assessment study. 1996; EC, DG XII, Science, Research and Development; Brussels.
- [5]. Laluece C et al. 1999, Biotechnology & Bioengineering, vol. 37: 528-536

- [6]. Hahn-Hagerdal et al. 1994, Enzyme Microbiol Technol 16:933-943; J.H. Reith et al. Co-production of bio-ethanol, electricity and heat from biomass wastes: potential and R&D issues
- [7]. Hann-Hagerdal et al. Biochemistry and physiology of xylose fermentation by yeasts. 1994, Enzyme Microbiol Technol 16:933-943.
- [8]. Hinam et al. 1989, Xylose fermentation: an economic analysis. Appl Biochem Biotech 20/21: 391-401.
- [9]. Lynd L. R. et al, Likely features and costs of mature biomass ethanol technology. 1996, Appl Biochem Biotech 57/58:741-761
- [10]. Zhang Y-HP et al. Cellulose utilization by *Clostridium thermocellum*: bioenergetics and hydrolysis product assimilation, Proc Natl Acad Sci USA, 2005, 102: 7321-7325

#### Acknowledgement

This work was supported financially by the International Science and Technology Center (ISTC), Moscow. Project # G – 1624. Financing parties - EU and Korea.



## POSSIBILITIES OF POTATO TUBERS YIELD MONITORING IN POTATO HARVESTING TECHNOLOGIES

ZDENĚK KVÍZ\*, ADOLF RYBKA, MARTIN TACHECÍ

<sup>1</sup>Czech University of Life Sciences Prague, 16521 Prague 6 – Suchbát, Czech Republic,  
Phone: +420224383131, Fax: +420224383122, E-mail: kviz@tf.czu.cz

### Abstract

The main aim of this research was to map possibilities for potato yield monitoring, describe sensors which could be capable of yield monitoring and find out the most suitable method for instantaneous material throughput rate measurement of potato tubers on potato harvesters under real field conditions. Firstly, several laboratory measurements were carried out with the strain gauge sensor placed on picking belt's support rollers. A model of a picking belt was used for the measurements. By means of this device and mentioned sensor, the picking belt with potato tubers was weighed and the instantaneous material throughput rate was determined. From the results of the measurements, it has been proved that the principle of potato tubers yield measurement by means of continuous material weight determination on a harvester's conveyor belt using a strain gauge (tension-metric) sensors placed on belt support rollers is suitable for real yield measurements on potato harvesters when low amount of additional mixtures is present (stone-removal technologies etc.). In the future, other possible methods and principles for mass throughput rate determination of potato tubers will be observed and tested in our laboratory.

**Keywords:** potatoes, harvesting, precision farming, throughput rate, yield maps.

### Introduction

In order to realize site specific agro-technical treatments it is necessary to determine and localize all differences in the field. Field diversity is a common feature in agriculture and therefore, there are variations in crop yields even within one field. Information about a particular part of a field and its condition could be obtained from yield maps, soil analysis maps, remote sensing of crop and field or from combinations of all mentioned alternatives. Those data are used as input data for further precise operation in the field. By applying of this procedure it is possible to reduce considerably production costs (saving of chemical agents, mineral fertilizers and fuel and also savings due to less machines utilization) and likewise it could contribute to protect the environment which would be therefore exposed only to lower chemical agents' and fertilizers' dosages.

#### *Systems for throughput rate measurement*

Systems for instantaneous throughput rate monitoring of potato tubers during harvest are possible to divide according to principles of measurement and used sensors into two groups: contact methods and non-contact methods.

Contact methods for throughput rate measurement are based on weighing a particular part of a harvester on which potato tubers passes through the machine, it means determination of mass flow rate of tubers. Or it is also possible to weigh a bunker and record increases in weight inside the bunker in real time or lastly to weigh a whole transport vehicle. All above mentioned methods use tension-metric sensors. However, it is not possible to distinguish between potato tubers and additional mixtures by using these methods.

Conveyor belt weighing – this method enables continuous measurement of weight passing on a conveyor belt. The principle lies in data reading of compression force, which is caused by potatoes passing on the belt. The magnitude of the force together with time data enables to count mass flow rate passing through the harvester. Force sensing is realized by means of specially designed support rollers for a conveyor belt which are equipped with tension-metric bridges or another possibility is a belt scale fitted into the whole conveyor belt. The weight is automatically recorded into electronic processing unit. This device could be mounted on a picking table conveyor belt or on a discharging belt of a harvester because there are

minimum additional mixtures there. The data are further led into central processing unit and it is possible to transfer them into portable PC.

Trailer weighing – it is necessary to have a trailer which is able to scan continuously its load. The principle is very simple but the practical application brings along some technical problems connected with disturbances of the device such as impacts when crossing inequalities on the ground etc. and their difficult elimination. To cope with this problem and to assure sufficient accuracy, the frame of a machine has to be insulated from the body of a bunker. From the obtained cumulative weight it is possible to determine instant weight in a particular place of a field (Wheeler et al., 1997).

Impact plate – there is one necessary condition for successful using of this method and it is constant speed difference of potato tubers flow rate. Then, there is a direct proportionality between overall force and mass flow of potatoes. The constant speed difference of potatoes tubers flow rate is possible to achieve when potatoes hit the plate in vertical or almost vertical direction in relation to discharging trajectory. Rubber coated plate equipped with a force sensor was mounted at different places in relation to the discharging trajectory. The results showed very clear dependence between mass flow and force (Ehlert, 2000). The real design is realized in the way that the rubber coated plate is placed as close as possible to discharging conveyor belt within the range of potatoes' trajectory.

Non-contact methods – by means of non-contact methods it is possible to detect indirectly potato tuber's volumetric flow which is further recalculated into potato tuber's mass flow. Instantaneous volume mass flow is possible to measure with the help of optical sensor, radiometric or ultrasonic sensor etc. There are currently also other methods under development and investigation such as measurement of power requirement of electric or hydraulic drivers (driving motors) for conveyor belts on harvesters in dependence of their load.

Optical sensors scan cross section surface of potato tubers and are able to determine not only instantaneous mass flow rate of potatoes through a harvester but also their quality features especially size of tubers.

Measurements with optical sensors are usually carried out in two ways which differs one from another in the different placement of the sensor for mass flow rate measurement. In the first case the sensor is mounted above a picking conveyor belt and scans its particular part - works as a camera and the second variant is a device with two sensors placed at the end of a conveyor belt. The first variant is a digital camera placed together with an artificial lightning on the steel framework which serves also as a shield protection of the scanning area from daylight. The yield determination is done by an instant scanned pictures evaluation. The picture is made up from separate pixels from which it is possible to determine limiting points (edges) of tubers and mixtures. Then it is possible to calculate their surface area. Together with the number of potato tubers (measured further in a machine) and statistically proved relations (for instance between dimensions and mean value of tubers' weight) it is possible to determine the yield (Gogineni, 2002). The second variant is a device with two sensors placed at the end and on both sides of a conveyor belt facing each other and potato tubers fall down between the two sensors. The sensors are photodiodes and detect the time when a particular number of light beams between the diodes are interrupted by tubers. The number of light beam interruptions is dependent on the size and number of tubers and the time of interruption is dependent on the size of a tuber and its speed. Thus, by means of an extrapolation it is possible to determine and count number and weight of potato tubers (Hara et al., 2000). Instead of photodiodes it is also possible to use a digital camera at that place and pictures from that camera could be used for further image analysis and further for the potato tubers size and shape determination. As a result we can count a cross section of tubers.

#### *Overall evaluation of methods for yield maps creation*

Potato harvest in itself is carried out usually under very heterogeneous conditions. Sensors which are used on harvesters are exposed to lots of adverse effects. It is mainly dusty environment and very changeable weather conditions as temperature and air humidity. Another influence on using electronic systems on harvesters is

indisputably their design. Unfortunately, there are just few places on potato harvesters where it is possible to mount a particular sensor because of vibrations and the presence of additional mixtures. Also the risks of sensor damage, potato bulbs damage by additionally mounted device have to be taken into account. Sensors must not complicate operators' work and reduce machine's capacity.

When it comes to advantages and disadvantages of all above mentioned principles for potato tubers mass flow rate determination the following has to be stated.

Non-contact optical methods for material throughput rate determination involves a source of inaccuracy resulting firstly from the indirect measurement of volumetric flow and further from the conversion of this data to mass flow rate. This inaccuracy is mainly caused by an unknown third dimension of a tuber and when having irregular shape of a tuber it is not possible to determine a precise weight just from scanning the area (from two dimensions). This device is also very fragile and susceptible to damage under real field conditions. It is possible to encounter the same problem when using an ultrasonic sensor. Sequential cumulative measurement of weight (contact method) is only possible when using a trailer driving along the harvester or more advantageous is weighing a bunker of the harvester. However, there are lots of problems related to this principle and there are certain limits for the usage of this method in real conditions. Another mentioned possibility for mass throughput rate determination is using an impact plate which also involves risk of plate damage by stones and for precise data record it is necessary to control and correlate speed, inclination angle of discharging belt and distance between the plate and belt.

The optimal method for potato yield maps creating, when taking into account all negative effects which are possible to encounter during real potato harvest, appears to be the usage of a belt scale. For the mass flow rate measurement on a harvester it is possible to use very similar device to that explained above. The conveyor belt on a harvester has to be chosen at the place where minimum additional mixtures (stones, clods of clay...) go on the belt. The support rollers of the upper belt way have to be fitted with tension-metric load sensors and the speed

sensor has to be mounted as well. The theoretical calculation and force analysis is necessary to be made after the device installation to find out and simulate how the whole frame with sensors will behave in dependence on vibrations and operational conditions. Finally, precise calibration procedure has to be done.

### Materials and methods

Measurement principle of potato yield determination by means of continuous material weight recording on a harvester's conveyor belt when using strain gauge (tension-metric) sensors placed on belt support rollers was used for the first laboratory measurements. These measurements were carried out under laboratory conditions on a real conveyor belt taken out from a potato harvester. Between the last two supporting rollers under the upper arm of the picking table conveyor, new rollers with the strain gauge sensors were mounted on both sides. A sensor for conveyor speed reading was placed on the conveyor drum's driving shaft. The outputs from the weight sensors and speed sensor are transmitted into the evaluation unit. The data gained from this measurement are further processed and statistically evaluated. The final outcome is a record of instantaneous throughput of potato tubers in time calibrated in  $\text{kg}\cdot\text{s}^{-1}$  and together with possible GPS receiver (position data) it is possible to create yield maps.

### Results and discussion

Before the instantaneous material throughput measurement was performed, it was necessary to conduct the measuring device calibration. This was carried out in the way that the upper part of the conveyer (above the measuring device) was gradually loaded with the exactly known weight. By doing this, signal values from the sensor were recorded and the device was calibrated. Subsequently, a simulation with crop was realized. The exact amount of potatoes was placed on the front end conveyor belt with the length of 4 m. Potatoes were falling from this conveyor to the picking conveyor of the testing rig. The measurements were realized with different speeds of picking conveyor belt. The lowest frequency of conveyor belt driving roller ( $30\text{ s}^{-1}$ ) corresponded with the surface speed of the conveyor  $0,267\text{ m}\cdot\text{s}^{-1}$  and the highest frequency of conveyor belt driving roller ( $90\text{ s}^{-1}$ )

corresponded with the surface speed  $0,801 \text{ m.s}^{-1}$ . The measurements were realized with potato samples with the weight of 5, 10, 15, 20, 25, a 30 kg. The combinations of those two variables resulted in the instantaneous throughput rate ranging between  $1.1 \text{ kg.s}^{-1}$  and  $20.3 \text{ kg.s}^{-1}$ . Each measurement was realized five times. Figure 1 shows an example of the data obtained during one measurement.

The values from the measuring apparatus were saved to a notebook as the text documents. Those data were converted into Microsoft Excel for further processing and evaluation. The results were tables with tension-metric sensor output data in Hz measured in the time interval of 0,5 s long. The next step was the calculation of potatoes throughput rate. The calculated throughput rate of each single measurement was compared with the real potatoes throughput rate that was fed onto the conveyor belt and the errors of the measurements were determined (Tab. 1).

The errors in the measurements ranged from 2.7 % to 5.6 %.

The average material throughput rate on the picking conveyor belt on a real two rows potato harvester during harvest is usually  $3 - 6 \text{ kg.s}^{-1}$  and the surface speed of the belt is  $0,4 \text{ m.s}^{-1} - 0,6 \text{ m.s}^{-1}$ . These values correspond with the frequency of conveyor belt driving roller within the range of  $50 - 70 \text{ s}^{-1}$  and this was exactly the point where the lowest values of the measurement errors of the throughput rate were measured. The highest values of the measurement errors were measured at very low or very high values of revolutions and also at extreme throughputs rates. However, it is necessary to say that presumably the measurement errors would be a little bit worse under real harvesting conditions. To cope with this fact, it would be necessary to use better and also more expensive sensors and to record data in shorter intervals then just each 0.5 s as it was measured during our research.

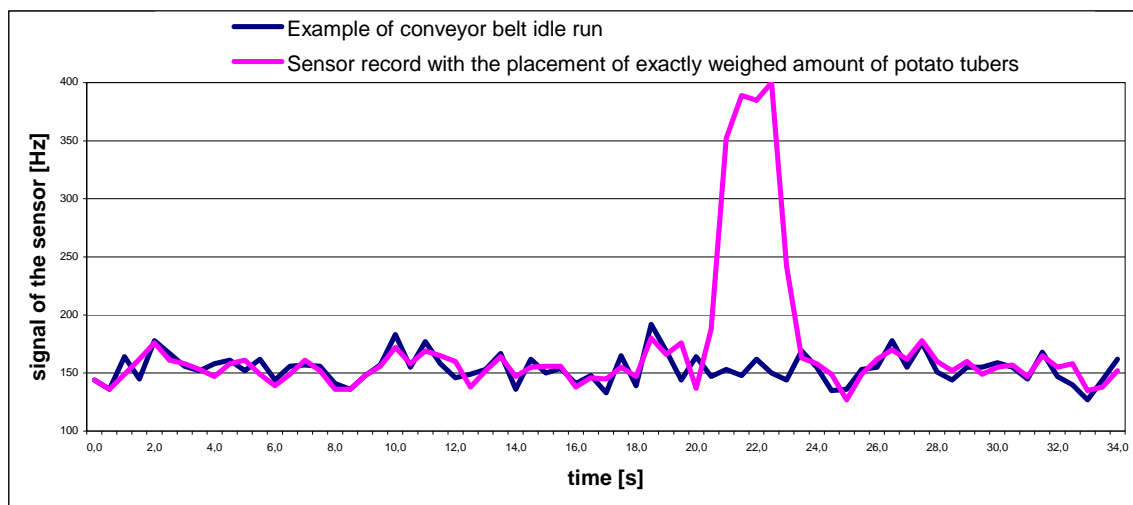


Figure 1: Example of data logging during the potato tuber's throughput rate measurement.

Table 1: Measurement errors during instantaneous throughput rate measurements [%]

Rotational frequency of conveyor belt driving roller [ $\text{s}^{-1}$ ]	Amount of potato tubers [kg]					
	5	10	15	20	25	30
30	4,3	4,3	4,1	4,3	3,4	3,4
40	4,7	4	4,4	3,5	4,3	3,1
50	3,8	4,1	3,3	3,5	3,7	3,3
60	2,9	3,8	3,1	3,3	2,7	3,7
70	3,1	4	3,4	3,6	3,3	4,2
80	5,1	4,2	4,9	4,9	3,6	4,9
90	5,2	5,5	5,6	5,2	4,6	5,1

## Conclusions

At present, the values and results obtained from our laboratory measurements are being further processed and more statistically evaluated. However, from the pilot measurements and results, it has been already proved that the principle of potato tubers yield measurement by means of continuous material weight determination on a harvester's conveyor belt using a strain gauge (tension-metric) sensors placed on belt support rollers is suitable for real yield measurements on potato harvesters when low amount of additional mixtures is present (stone-removal technologies etc.). It is mainly due to zero sensitivity of used sensors to additional mixtures in potatoes passing through a harvester. Therefore, other possible methods and principles for mass throughput rate determination of potato tubers, which are additional mixtures sensitive (are able to distinguish between potato tubers and mixtures), will be observed and tested in our laboratory in the future.

**Acknowledgements:** Supported by the Ministry of Education, Youth and Sports of the Czech Republic, Project No. MSM 604 6070905.

## References

- [1] BAGANZ K.,: Yield Estimation on Potato Harvesters. International Symposium on Locating Systems for Agricultural Machines, Gödöllő, 1991, p. 18.
- [2] DEHAAN K.R., VESSEY G.T., HOLMSTROM D.A., MACLEOD J.A., SANDERSON J.B., CARTER M.R.,: Relating potato yield to the level of soil degradation using a bulk yield monitor and differential global positioning systems. Computers and Electronics in Agriculture, **23**, 1999, p. 133 – 143.
- [3] EHLERT D.: Measuring Mass Throughput by Bounce Plate for Yield Mapping of Potatoes. In: Precision Farming., Springer Netherlands, 2000, p. 119-130.
- [4] EHLERT D., (1997): Measuring mass throughput of potatoes for yield mapping. In: Precision Agriculture. BIOS Scientific Publishers Ltd, p. 797 – 804.
- [5] GOGINENI S. (14.3.2006): The Design and Implementations of Yield Monitor for Sweet potatoes. Accessible from:  
<http://sun.library.msstate.edu/ETDdb/theses/available/etd-04082002-122320/unrestricted/thesis.pdf>.
- [6] WHEELER P. N. et al. (14.3.2006): Trailer Based Yield Mapping. Accessible from:  
<http://www.bios.co.uk/book.asp?isbn=185996236X>.



## IMPLEMENT TRANSPORT IMPACT ON HITCH-SYSTEM PRESSURE OSCILLATION

JANIS LACEKLIS-BERTMANIS\*, ERIKS KRONBERGS, EDGARS REPSA

Latvia University of Agriculture, Institute of Mechanics,

J. Cakstes bulv. 5., Jelgava LV3001 Latvia

Tel: +371 63080674; Fax.: +371 63020762; E-mail: Janis.Laceklis@llu.lv

### Abstract

The paper presents experimental investigation results of pressure oscillation in hydraulic hitch-system of tractor Claas Area ATX 557 with attached soil cultivation implement - disc harrow. During tractor moving over artificial roughness road at the different driving speed, tire pressure and hitch-system oscillation damping control (switch on/off) pressure oscillation were investigated. Tractor hydraulic hitch-system was equipped with pressure sensor Wika Transmitter and data processing software PicoLog. Results of experiments presents maximum pressure peak of 210 bar in tractor hydraulic system when hydraulic hitch-system oscillation damping system at driving speed  $7.8 \text{ km h}^{-1}$  is not used and system pressure peak reduces to value of 182 bar if hydraulic hitch-system oscillation damping is used. The paper presents also simulation results of tractor movement over the same artificial surface with attached disc harrow. Working Model software is used for simulation. Hitch-system hydro cylinder is replaced as coupler with spring and damper characteristic in model. Dynamic force on coupler is obtained as simulation result and depending on it hydraulic pressure in hitch-system cylinder had been calculated. Simulation results are evaluated on basis of experimental investigations. The maximum pressure oscillation amplitude is observed at the speed  $7.8 \text{ km h}^{-1}$ , and reaches 210 bar in simulation results. The differences between simulation and experimental investigation results vary within 0.4 - 9%. Working Model simulation for tractor hydraulic hitch-system can be recommended for investigation of possibility to reduce amplitude of pressure pulsations by changing parameters of hydraulic system.

**Key word:** tractor hitch system, pressure oscillation investigation

### Introduction

During tractor movement, with attached to hitch-system working equipment (plough, harrow), over rough road surfaces vertical oscillations of machine take place. These oscillations are a reason of pressure pulsations in hydraulic hitch-system and reduce the service life of hydraulic system components, especially the lifetime of hydraulic hoses. The pressure pulse in hydraulic hoses arises when tractor moves along rough terrain with mounted soil cultivation tools on hydraulic hitch-system.

Pressure pulse reduction in tractor hitch-system is important for increasing of system components lifetime. Pressure oscillations damping in the tractor hydraulic hitch-system can reduce overall system oscillations and improve the driving control.

Simulation of tractor hydraulic system oscillation enables determination of hydraulic system stiffness and damping parameters for

minimizing amplitude of pressure pulsations. Working Model software let to create dynamic model for tractor vertical oscillations and simulate movement with different speed and road roughness values.

The main task of simulation experiment is to reduce the tractor Claas Area 557 ATX hitch-system hydraulic pressure pulse values changing the hydro cylinder stiffness and damping parameters.

### Materials and methods

For evaluation of Working Model simulation results preliminary experiments on tractor movement over artificial roughness test road had been carried out. During experiments tractor Claas Area 557 ATX with engine power of 102 hp was used. LEMKEN short disk harrow and LEMKEN rubber rings roller was [1, 2]. attached to the tractor.



Using the Working Model software [3] is necessary to determinate the hydraulic system pressure in tractor (Class Ares 557 ATX) hydraulic hitch-system hydro cylinder depending on the attached equipment weight, road roughness and tractor speed.

Therefore, in experiment the tractor hydraulic hitch-system was equipped with pressure oscillation sensor Wika Transmitter ECO-1. The sensor was chosen such that its free oscillation frequency was 10 times higher than frequency of measured pressure changes [4]. For data acquisition and processing software of Pico Technology was used [5]. Using Wika Transmitter ECO-1 and universal data collection and processing device PicoLog the hydraulic

pressure oscillation in tractor hydraulic hitch-system was measured.

In order to study the dynamic oscillation of tractor hydraulic hitch-system experimental road with artificial roughness was used (see Fig.1). Road roughness was established according to rural conditions. Total road length is 24 meters which is divided into 12 equal parts by 2 meters each, respectively. Road roughness is constructed from wood planks with dimensions 150 x 50 x 1000 mm. Planks are connected with steel angle shaped bars 40 x 40 x 3 mm by screw-bolts M10 x 1.5. Roughness columns are placed in two parallel rows with 1.8 m distance on asphalt road surface.



Fig. 1. Tractor Claas Area ATX 557 movement over artificial roughness test road  
1 – Artificial roughness test road; 2 – Tractor Claas Ares ATX 557; 3 – LEMKEN short disk harrow; 4 – LEMKEN rubber rings roller.

Road roughness amplitude is constant value  $a = 0.05$  m. Frequency of forced oscillations depends on tractor driving speed and road roughness step  $s = 2$  m and can be found:

$$\omega_f = \frac{v \cdot 2\pi}{s}, \quad (1)$$

where  $v$  – tractor drive speed,  $\text{m} \cdot \text{s}^{-1}$ ;  
 $s$  – road roughness step, m.

By changing tractor hydraulic hitch-system oscillation damping position (switch on or off) and driving speed from 3 – 14  $\text{km h}^{-1}$  various hydraulic hitch-system oscillation characteristics were obtained, which resulted as pressure pulsations in hydraulic system. The maximum

pressure oscillation amplitude was observed at driving speed of 7.8  $\text{km h}^{-1}$  and reached 210 bar. For hydraulic hitch-system longer service life it would be necessary to reduce the hydraulic pressure oscillation amplitude and for this reason the Working Model simulation programme was used.

In Working Model software dynamic model with the same parameters of tractor and attached equipment [6] weight, road roughness and movement speed as in experimental investigation had been used. Oil volume stiffness for tractor hydraulic system was calculated [7]. Simulation model (see Fig.2) was used in the side-view. The parameters of hydraulic cylinder and tyres were entered two times larger in simulation model.

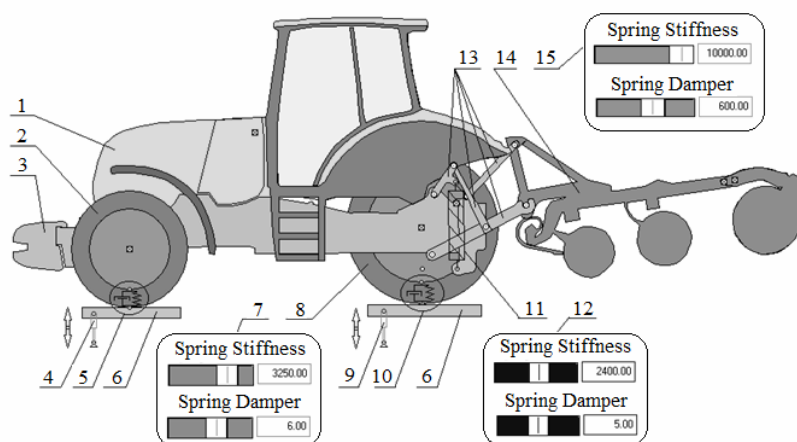


Fig. 2. Tractor model in Working Model software:

1 – tractor Class Ares 557 ATX, 2 – tractor front tyres (13.6R28), 3 – front weight, 4 – front actuator, 5 – front tyres (characterization by spring and damper), 6 – road roughness, 7 – front tyres control units, 8 – tractor rear tyres (16.9R38), 9 – rear actuator, 10 – rear tyres (characterization by spring and damper), 11 – hydraulic cylinder (characterization by spring and damper), 12 – rear tyres control units, 13 – tractor hitch-system, 14 – soil cultivator implements, 15 – hitch-system control units.

Tractor wheelbase is  $l_t = 2.564\text{m}$ . As it does not coincide with road roughness step, the time delay  $\Delta t$  between roughness impact on front wheels and rear wheels is calculated:

$$\Delta t = \frac{\Delta l}{v}, \quad (2)$$

where  $\Delta t$  – time delay, s;

$\Delta l$  – step difference between tractor wheelbase and road roughness, m.

$\Delta l$  is calculated:

$$\Delta l = l_t - s. \quad (3)$$

Function of road roughness surface in Working Model program was assured with actuators 4 and 9 (see Fig.2). Actuator functions of the front and rear wheels was given in

program by equation (4), where  $y_1$  was the function of front wheel oscillations, but  $y_2$  was for rear wheels.

$$\begin{aligned} y_1 &= b + \text{if}(a \cdot \sin(\omega_f \cdot (t + \Delta t)) < 0, 0, (a \cdot \sin(\omega_f \cdot (t + \Delta t)))) \\ y_2 &= b + \text{if}(a \cdot \sin(\omega_f \cdot t) < 0, 0, (a \cdot \sin(\omega_f \cdot t))) \end{aligned} \quad (4)$$

where  $b$  – initial length of actuator, m.

If the function  $y = a \cdot \sin(\omega_f \cdot t) < 0$ , then the function value was 0, but if  $y = a \cdot \sin(\omega_f \cdot t) > 0$ , then the function value was  $y = a \cdot \sin(\omega_f \cdot t)$ . Road roughness simulation was showed in Fig. 3.

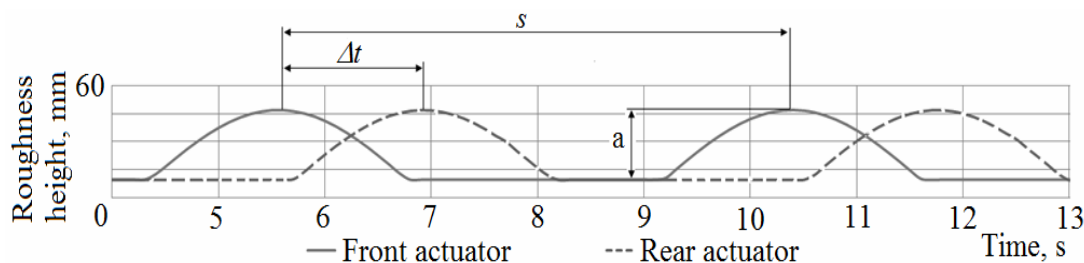


Fig.3. Road roughness:

$\Delta t$  – oscillation time delay,  $s$  – road roughness step,  $a$  – road roughness amplitude

In the model hitch-system hydraulic cylinder 11 (Fig.2) was created and described with spring and damper characteristic. The spring and damper was characterized by stiffness and damping coefficients. Tractor hitch-system hydraulic cylinder parameters were changed with control button 12 (Fig.2). Approximate spring stiffness coefficient can be calculated from formula (5).

$$k = \frac{F}{x}, \quad (5)$$

where  $k$  – spring stiffness coefficient, N m<sup>-1</sup>;

$F$  – force, N;

$x$  – displacement, m.

The force  $F$  value was obtained from experiment results ( $F = 328564$ N). Displacement  $x$  was equal to the hitch-system hydraulic cylinder displacement at pressure pulse. It can be calculated [8] from volume change  $\Delta V$  in hydraulic cylinder from equation:

$$\frac{1}{E} = \frac{\Delta V}{\Delta p \cdot V_0}, \quad (6)$$

where  $E$  – liquid modulus of elasticity, N m<sup>-2</sup>;

$\Delta V$  – volume change in the size of the pressure changes, m<sup>3</sup>;

$V_0$  – initial volume of liquid at atmospheric pressure, m<sup>3</sup>;

$\Delta p$  – pressure change, N m<sup>-2</sup>.

Values of pressure changes was determined from experimental tests  $\Delta p = 57 \cdot 10^5$  N m<sup>-2</sup>. Oil modulus of elasticity  $E = 729 \cdot 10^6$  N m<sup>-2</sup>. Initial fluid volume in hydraulic hitch-system cylinder at atmospheric pressure is calculated:

$$V_0 = \frac{\pi \cdot d^2 \cdot h}{4}, \quad (7)$$

where  $d$  – hydraulic cylinder diameter, m;  
 $h$  – hydraulic cylinder stroke, m.

From tractor Class Ares hydraulic hitch-system cylinder determinate sizes  $d = 0.075$ m and  $h = 0.23$ m. Displacement  $x$  is calculated from formula (8).

$$x = \frac{4\Delta V}{\pi \cdot d^2}. \quad (8)$$

The approximate stiffness coefficient can be calculated after the displacement  $x$  determination according formula (5). Force was measured when tractor model hydraulic hitch-system hydraulic cylinder oscillation was simulated with Working Model software.

Corresponding pressure was calculated:

$$p = \frac{F_u}{A}, \quad (9)$$

where  $p$  – pressure, Pa;

$F_u$  – hydraulic hitch-system hydro cylinder force, N;

$A$  – area of hydraulic cylinders, m<sup>2</sup>.

With constant spring stiffness coefficient, reducing the damping coefficient, the force of hydraulic hitch-system hydro cylinder decreases. Changing the damping coefficient values from  $(2.3-3.3)10^6$  N s m<sup>-1</sup> the pressure values similar to experimental values was obtained. Working Model tractor simulation model checking on the basis of experimental investigations let improve it coincidence with real machine aggregate.

## Results and discussion

Using the Working Model software and changing the tractor hydraulic hitch-system hydro cylinder (stiffness and damping) parameters and driving speed from 3 - 14 km h<sup>-1</sup> were obtained the different pressure values in linkage cylinder.

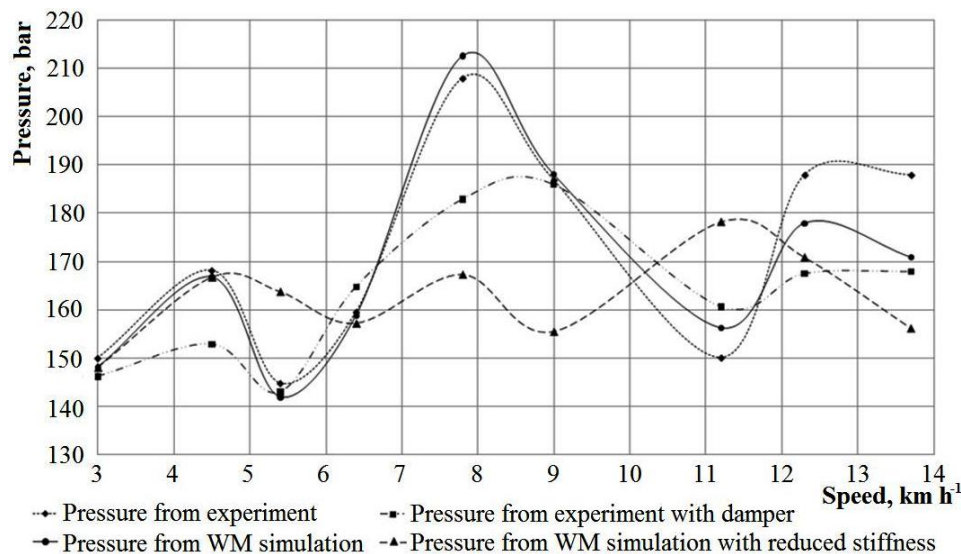


Fig. 4. Pressure in tractor hydraulic hitch-system of hydraulic cylinder

The experimentally obtained hydraulic hitch-system pressure values and the Working Model program simulation pressure values were shown in Fig.4. The maximum pressure oscillation amplitude was observed at the speed  $8 \text{ km h}^{-1}$ , and reaches 210 bar in experiments, but at the same speed reaches 212 bar in simulation results. These difference is caused with some inconsistency for stiffness of tyres in simulation model and can be eliminated. Reducing of hydraulic cylinder stiffness value let to reduce pressure value to 178 bar at driving speed  $11.5 \text{ km h}^{-1}$  during simulation. Therefore Working Model simulation for tractor hydraulic hitch-system can be recommended for investigation of possibility to reduce amplitude of pressure pulsations by changing stiffness and damping parameters of hydraulic system.

### Conclusion

1. Working Model software let to create dynamic model for tractor vertical oscillations and simulate movement with different driving speed over road roughness.
2. Working Model tractor simulation model checking on the basis of experimental investigations let improve it coincidence with real machine aggregate.
3. Oscillation of pressure can be reduced by exploitation of oscillation damper that can be established on instrument panel of tractor. If oscillation damper is not used, than at driving speed of  $8 \text{ km h}^{-1}$  pressure

oscillation in hydraulic system reaches 210 bar but, when oscillation damper is used, pressure in hydraulic system decreases to 170 bar.

4. Reducing of hydraulic cylinder stiffness value let to reduce maximum pressure value to 178 bar at driving speed  $11.5 \text{ km h}^{-1}$  during simulation.
5. Working Model simulation for tractor hydraulic hitch-system can be recommended for investigation of possibility to reduce amplitude of pressure pulsations by changing stiffness and damping parameters of hydraulic system.

### Acknowledgement

Paper is written by financial support of European Structural Fund – Support for Realization of Doctoral Studies in Latvia University of Agriculture - realized by Project Department of Latvia University of Agriculture (contract no. 2009/0180/1DP/1.1.2.1.2/09/IPIA/VIAA/017).

### References

- [1] LEMKEN GmbH & Co.KG [online]. Technical Data Compact Disc Harrow Heliodor, 2010 [cited March 25, 2010]. Available: [http://lemken.com/appc/content\\_manager/page.php?ID=200741&dbc=d41c7cade764dc9bb388a723591737a9](http://lemken.com/appc/content_manager/page.php?ID=200741&dbc=d41c7cade764dc9bb388a723591737a9)

- [2] LEMKEN GmbH & Co.KG [online]. Technical Data Rubber rings Rullers, 2010 [cited March 25, 2010]. Available: [http://lemken.com/appc/\\_upload/2009\\_27/Walzen\\_de.pdf](http://lemken.com/appc/_upload/2009_27/Walzen_de.pdf)
- [3] MSC.Software Corporation. Working Model 2D software, User's Manual (2000).
- [4] Kakitis A., Galins A., Lescevics P. (2008) Sensors and measuring systems *Jelgava*, pp. 380-390. (in Latvian)
- [5] Kakitis A. (2008) Non-electric parameter electrical measuring and sensors: Study aid. *Jelgava*, pp. 640-668. (in Latvian)
- [6] Company Claas KGaA mbH, Harsewinkel. Claas Areas 5543 Handbook (2007).
- [7] Basta T. M. Volume Pumps and Hydraulic Motors of Hydraulic System. Moscow: Engineering, 1974. 606 p. UDK 62-82(075.8) (in Russian)
- [8] Jacenko N. N. The Release Motion of Trucks. Moscow: Engineering, 1968. 218 p. (in Russian)

## ANALYSE OF UTILISED BEDDING MATERIALS IN CUBICLES

JANA LENDELOVÁ, ŠTEFAN MIHINA, ŠTEFAN POGRAN

Slovak University of Agriculture in Nitra, Tr. A Hlinku 2, 949 76 Nitra, Slovakia,

Phone: +421-37-6415777, Fax: +4212-37-7417003,

E-mail: jana.lendelova@uniag.sk, stefan.mihina@uniag.sk, stefan.pogran@uniag.sk.

### Abstract

Proper flooring management and free-stall design is critical for effective control of production parameters, cattle health, longevity and comfort. Thermo-technical properties of organic materials (straw, sawdust, separated slurry with thickness of 200 mm on concrete base) in comparison to rubber mats and rubber foam mattresses used for bedding of cubicles for dairy cows were evaluated. Thermal resistance and thermal effusivity were calculated according to official technical standards. Coefficient of thermal conductivity needed for these calculations were obtained in real conditions of experimental farms. Thermal resistance of straw varied from 0.966 to 2.914 m<sup>2</sup>.K.W<sup>-1</sup>, wooden sawdust from 0.688 to 1.781 m<sup>2</sup>.K.W<sup>-1</sup>, separated slurry from 0.908 to 1.274 m<sup>2</sup>.K.W<sup>-1</sup>, and rubber mattresses and mats from 0.76 to 1.47 m<sup>2</sup>.K.W<sup>-1</sup>. Thermal effusivity of straw ranged from 162.34 to 423.63 W.s.<sup>1/2</sup>m<sup>-2</sup>K<sup>-1</sup>, wooden sawdust from 333.5 to 773.52 W.s.<sup>1/2</sup>m<sup>-2</sup>K<sup>-1</sup>, separated slurry from 308.97 to 469.36 W.s.<sup>1/2</sup>m<sup>-2</sup>K<sup>-1</sup>. Data were collected in summer as well as in winter conditions and both with dry and wet organic materials.

### Introduction

Many studies have investigated the bedding preferences of dairy cows by comparing different types of floor structures [1, 2, 3]. Results of similar experiments indicate that cows prefer stalls with softer, elastic, dry and slip resistant floors. A variety of flooring surfaces are used on dairy farms, but not much is known about their impact on thermal comfort of cattle. Dairy cow free stalls have traditionally been bedded with different organic materials or synthetic products available locally. Bedding material has ranged from straw, wood chips, dolomite limestone and sawdust to separated manure solids. Organic bedding materials in dry conditions are characterized with a big absorbability and low thermal conductivity. However, most organic bedding materials support bacterial growth [4]. Control of bacterial growth means depriving bacteria of substrate for their growth: moisture, organic matter, and proper temperature and pH. Keeping litter in dry conditions and lower temperature results also in decreasing ammonia emissions from this source [5]. These properties also affect thermo-technical magnitudes [6]. Thermal comfort during lying is caused by a structure of bed characterised by thermal resistance and thermal effusivity. Thermo-technical condition in stable creates a non-stationary process caused by climatic conditions and farm management [7]. To avoid heat loss

from building in winter periods thermal resistance should be as high as possible. On the other hand, thermal effusivity should be as low as possible, to prevent heat conduction from animal body while lying. The aim of this work was to evaluate the thermo-technical properties of organic materials (straw, sawdust, separated slurry with thickness of 200 mm on concrete base) in comparison to rubber mats and rubber foam mattresses used for bedding in cubicles for dairy cows.

### Experimental arrangement

Thermo-technical properties of five different cubicle floors of bed structures were tested in Slovak farms. Three cubicles with deepened concrete stall base were covered by 200 mm layer of straw, sawdust and separated manure, respectively and two cubicles with elevated concrete stall base covered by rubber mats and rubber foam mattresses, respectively, were used.

Thermal resistance and thermal effusivity were calculated according to official technical standards (STN 73 0540-1,-2,-3,-4, STN EN ISO 10456). Data needed for the calculations were obtained in real conditions of experimental farms, both in summer and winter conditions and both with dry and wet organic materials.

Thermal effusivity of equivalent three-layer floor structure was computed from formula:



$$b = b_1(1 + K_{1,2,3}), \quad (1)$$

where

$$b_1 = \sqrt{\lambda_1 \cdot c_1 \cdot \rho_1} \quad (2)$$

and

$$K_{1,2,3} = f\left(\frac{b_{2,3}}{b_1}, \frac{d_1^2}{a_1 \cdot \tau}\right) \quad (3)$$

where

$$b_{2,3} = b_2(1 + K_{2,3}) \quad (4).$$

Then  $K_{2,3}$  is computed from function

$$K_{2,3} = f\left(\frac{b_3}{b_{21}}, \frac{d_2^2}{a_2 \cdot \tau}\right) \quad (5)$$

and

$$b_2 = \sqrt{\lambda_2 \cdot c_2 \cdot \rho_2}, \quad (6)$$

$$b_3 = \sqrt{\lambda_3 \cdot c_3 \cdot \rho_3} \quad (7)$$

More than three equivalent layers floor is not common in animal housing practise.

Calculation of quantity  $K_{1,2}$ ,  $K_{2,3}$  a  $K_{1,2,3}$  is analytics was done according to

$$K_{x,y} = 2 \cdot \sum_{n=1}^{\infty} \left( \frac{x-1}{x+1} \right)^n \cdot e^{(-n^2 \cdot y)} \quad (8)$$

where “x” – is first parameter; “y” – is second parameter in formula 6, 8

(Chmúrny, 2003)

Thermal resistance was calculated as follows:

$$R = \sum_{j=1}^n R_j = \sum_{j=1}^n \frac{d_j}{\lambda_j} = \frac{d_1}{\lambda_1} + \frac{d_2}{\lambda_2} + \dots + \frac{d_n}{\lambda_n}, \quad (9)$$

$\text{m}^2 \cdot \text{K} \cdot \text{W}^{-1}$

where  $R_j$  – thermal resistance of „j“ floor layer,  $\text{m}^2 \cdot \text{K} \cdot \text{W}^{-1}$

$d_j$  – thickness of „j“ layer, m

$\lambda_j$  – thermal conductivity coefficient „j“ layer,  $\text{W} \cdot \text{m}^{-1} \cdot \text{K}^{-1}$

## Results and discussion

Thermo-technical parameters varied according to climatic conditions and farm management (Tables 1 - 4). Very good results were obtained for all dry organic materials. They had very good absorption and cushioning. Average value of thermal resistance ( $R_{\text{dry}}$ ) varied

from  $1.274 \text{ m}^2 \cdot \text{K} \cdot \text{W}^{-1}$  (for separated slurry) to  $2.914 \text{ m}^2 \cdot \text{K} \cdot \text{W}^{-1}$  (for dry straw), and thermal conductivity coefficient ( $\lambda_{\text{dry}}$ ) from  $0.06$  to  $0.16 \text{ W} \cdot \text{m}^{-1} \cdot \text{K}^{-1}$ , respectively. The organic beddings tested in wet conditions recorded their thermal resistance ( $R_{\text{wet}}$ ) with in the range  $0.688$  to  $0.966 \text{ m}^2 \cdot \text{K} \cdot \text{W}^{-1}$ , and thermal conductivity coefficient ( $\lambda_{\text{wet}}$ ) from  $0.23$  to  $0.32 \text{ W} \cdot \text{m}^{-1} \cdot \text{K}^{-1}$ .

The rubber mats and mattresses had lower thermal resistance ( $0.76$  to  $1.469 \text{ m}^2 \cdot \text{K} \cdot \text{W}^{-1}$ ) than dry organic materials. However, it was much higher and better than concrete base without any bedding ( $0.12 \text{ m}^2 \cdot \text{K} \cdot \text{W}^{-1}$ ).

Results of thermal effusivity had similar tendency as thermal resistance data. Again, dry straw ( $162.34 \text{ W} \cdot \text{s}^{1/2} \cdot \text{m}^{-2} \cdot \text{K}^{-1}$ ) was the best among organic materials. The thermal effusivity of rubber foam mattresses was little bit better than dry straw ( $144.35 \text{ W} \cdot \text{s}^{1/2} \cdot \text{m}^{-2} \cdot \text{K}^{-1}$ ). All investigated materials had manifolds better thermal effusivity than concrete not covered by any bedding (from  $144.35$  to  $773.52 \text{ W} \cdot \text{s}^{1/2} \cdot \text{m}^{-2} \cdot \text{K}^{-1}$ , in comparison to  $1880 \text{ W} \cdot \text{s}^{1/2} \cdot \text{m}^{-2} \cdot \text{K}^{-1}$ ). Thermal comfort on synthetic materials (rubber mats and mattresses) could be improved by spreading of a small amount of organic material (Fig. 1).

Thermal resistance values increased with the increase in thickness of top layer (Tables 1 & 3). However, from the thermal comfort point of view values of thermal resistance are important only from higher thickness of layer (more than  $150 \text{ mm}$ ). Higher values of thermal resistance of beds for animals also positively influence entire the thermal balance of the housing building.

On the other hand, total value of thermal effusivity rapidly improved by addition of litter material (straw, sawdust or separated manure solids) only up to the so called boundary thickness value of top layer (Tables 2 & 4). Additional supplement of organic litter material had only slight almost no influence. A boundary equivalent thickness has a crucial role. It depends on type of material and thermal diffusivity factor (Table 5).

## Conclusion

All types of investigated bedding materials improved thermo-technical properties of cubicle bed both from their thermal resistance and thermal effusivity point of view. Better thermal comfort can be expected for organic materials,

straw first of all, however, only in drier weather conditions. Rubber foam mattresses have thermo-technical properties comparable to straw. Thermal comfort on synthetic materials (mats and mattresses) could be improved by spreading small amount of organic material. It can also absorb moisture and increase cleanliness and hygiene of cubicle bed. Cubicles with separated manure bed create good comfort for lying

animals comparable to straw and sawdust bedding. From a thermo-technical point of view, separated manure solids bedding is comparable to rubber foam, and also to straw, but only to a wet straw. The question is, whether the hygiene of “manure” bed is satisfactory. To reach an objective evaluation of the above mentioned problems a new project has been undertaken recently.

Table 1. Thermal resistance of different types of bedding in concrete cubicles

Thickness of bedding, m	$R_{dry}$ - Thermal resistance of lying concrete structure with different thickness of bedding in dry conditions, $m^2.K.W^{-1}$			$R_{wet}$ - Thermal resistance of lying concrete structure with different thickness of bedding in wet conditions, $m^2.K.W^{-1}$		
	Chopped straw	Wooden sawdust	Separated slurry	Chopped straw	Wooden sawdust	Separated slurry
0*	0.057	0.057	0.054	0.057	0.057	0.057
0.005	0.128	0.100	0.084	0.080	0.073	0.078
0.01	0.200	0.143	0.115	0.102	0.089	0.100
0.015	0.271	0.186	0.145	0.125	0.104	0.121
0.02	0.343	0.229	0.176	0.148	0.120	0.142
0.05	0.771	0.488	0.359	0.284	0.215	0.270
0.1	1.486	0.919	0.664	0.512	0.372	0.483
0.2	2.914	1.781	1.274	0.966	0.688	0.908

\*The values of Thermal resistance “R” in first row represent a concrete floor without bedding; R remains the same (in case of 100 mm concrete thickness above waterproof insulation). Thermal resistance of structure layers under waterproof insulation is unthinkable by Slovak technical standards.

Table 2. Thermal effusivity of different types of bedding in concrete cubicles

Thickness of bedding, m	$b_{dry}$ - Thermal effusivity of lying concrete structure with different thickness of bedding in dry conditions, $W.s^{1/2}.m^{-2}.K^{-1}$			$b_{wet}$ - Thermal effusivity of lying concrete structure with different thickness of bedding in wet conditions, $W.s^{1/2}.m^{-2}.K^{-1}$		
	Chopped straw	Wooden sawdust	Separated slurry	Chopped straw	Wooden sawdust	Separated slurry
0**	1882	1882	1882	1882	1882	1882
0.005	494.2	794.2	921	947	1247	968
0.010	306.4	606.4	576	679	979	697
0.015	208.8	508.8	387	518	819	524
0.020	162.3	333.5	308.9	423.6	773.5	499.4
0.050	162.3	333.5	308.9	423.6	773.5	499.4
0.100	162.3	333.5	308.9	423.6	773.5	499.4
0.200	162.3	333.5	308.9	423.6	773.5	499.4

\*\* The values of Thermal effusivity “b” in first row represent a concrete floor without bedding.

Table 3. Thermal resistance of different structure types in cubicles with rubber mats on high concrete floor and different bedding

Thickness of bedding, m	$R_{dry}$ - Thermal resistance of lying concrete structure with rubber insulated mats and different thickness of bedding in dry conditions,	$R_{wet}$ - Thermal resistance of lying concrete structure with rubber insulated mats and different thickness of bedding in wet conditions,

	$\text{m}^2 \cdot \text{K} \cdot \text{W}^{-1}$			$\text{m}^2 \cdot \text{K} \cdot \text{W}^{-1}$		
	Chopped straw	Wooden sawdust	Separated slurry	Chopped straw	Wooden sawdust	Separated slurry
0*	0.734	0.734	0.734	0.734	0.734	0.734
0.005	0.808	0.771	0.764	0.757	0.750	0.755
0.01	0.881	0.820	0.795	0.779	0.766	0.777
0.015	0.955	0.863	0.825	0.802	0.781	0.798
0.02	1.028	0.906	0.856	0.825	0.797	0.819
0.05	1.469	1.165	1.039	0.961	0.892	0.947
0.1	2.205	1.596	1.344	1.189	1.049	1.160

\* R remains the same as without bedding (calculated only for the structure of 100 mm concrete thickness above waterproof insulation, 35 mm of insulation and 15 mm of rubber covering). Thermal resistance of structure layers under waterproof insulation is unthinkable by Slovak technical standards.

Table 4. Thermal effusivity of different types of bedding in concrete cubicles

Thickness of bedding, m	$b_{\text{dry}}$ - Thermal effusivity of lying concrete structure with rubber insulated mats and different thickness of bedding in dry conditions, $\text{W} \cdot \text{s}^{1/2} \cdot \text{m}^{-2} \cdot \text{K}^{-1}$			$b_{\text{wet}}$ - Thermal effusivity of lying concrete structure with rubber insulated mats and different thickness of bedding in wet conditions, $\text{W} \cdot \text{s}^{1/2} \cdot \text{m}^{-2} \cdot \text{K}^{-1}$		
	Chopped straw	Wooden sawdust	Separated slurry	Chopped straw	Wooden sawdust	Separated slurry
0**	522.1	522.1	522.1	522.1	522.1	522.1
0.005	340.2	444.1	417.8	503.2	611.1	501.8
0.010	234.2	370.6	364.1	471.1	663.5	468.8
0.015	185.3	340.0	329.5	446.0	744.0	454.0
0.020	167.6	333.5	315.6	433.7	770.4	433.3
0.050	162.3	333.5	309.0	423.6	773.5	429.3
0.100	162.3	333.5	309.0	423.6	773.5	429.3

\*\* The values of thermal effusivity "b" in the first row represent a high concrete lying floor with insulated mats without bedding.

Table 5. Boundary thickness of different materials for cow lying area

Top layer material	Thermal diffusivity factor of top layer	Boundary thickness of single-layer equivalent floor structure
	$a_1 = \frac{\lambda_1}{c_1 \cdot \rho_1}, \text{m}^2 \cdot \text{s}^{-1}$	$d_{1b} = 42,4 \cdot \sqrt{a_1}, \text{m}$
Chopped straw - dry	$1.594 \cdot 10^{-7}$	0.0188
Chopped straw - wet	$2.697 \cdot 10^{-7}$	0.0220
Wooden sawdust - dry	$1.210 \cdot 10^{-7}$	0.0147
Wooden sawdust - wet	$1.679 \cdot 10^{-7}$	0.0174
Separated slurry - dry	$2.853 \cdot 10^{-7}$	0.0226
Separated slurry - wet	$2.216 \cdot 10^{-7}$	0.0199
Hard rubber	$0.940 \cdot 10^{-7}$	0.0130
Rubber-foam	$1.730 \cdot 10^{-7}$	0.0176
Wood	$0.931 \cdot 10^{-7}$	0.0129
Concrete	$8.652 \cdot 10^{-7}$	0.0305

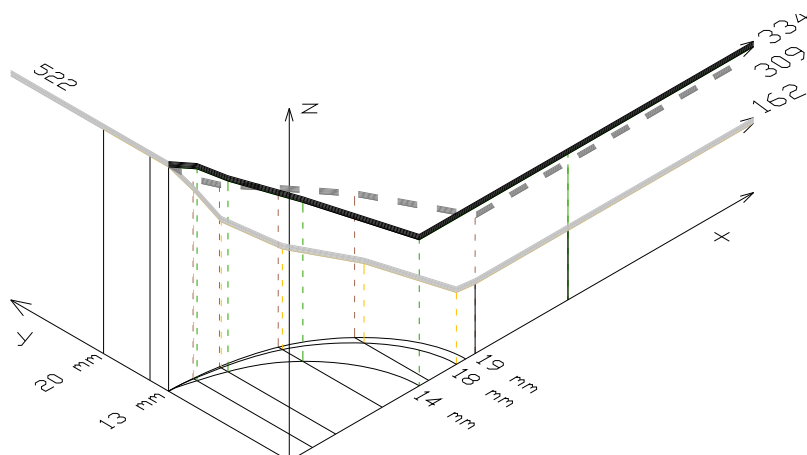


Figure 1. Changes in thermal effusivity by adding straw (light grey), sawdust (black), or separated slurry (dark grey) on rubber surface in dry conditions.

x – thickness of first layer floor structure with organic bedding

y – thickness of second layer structure from rubber

z – thermal effusivity,  $Ws^{1/2} m^{-2} K^{-1}$

## References

- [1] PALMER, R. W. – WAGNER-STORCH, A. M. 2003. Cow Preference for Different Freestall Bases in Pens with Different Stocking Rates. Proc. From the Fifth International Dairy Housing Conference. ASAE, St. Joseph, MI, pp. 155-164
- [2] WECHSLER B., SCHAUB J., FRIEDLI K., HAUSER R. 2000. Behaviour and leg injuries in dairy cows kept in cubicle systems with straw bedding or soft lying mats. In Applied Animal Behaviour Science, vol. 69, 2000, p. 189-197.
- [3] TUCKER, C. B., WEARY, D. M., FRASER, D. 2003. The Effects of Three Types of Free-Stall Usage by Dairy Cows. In: J. Dairy Sci., vol. 86, 2003, p. 521-529.
- [4] RUSSEL, B. F., J. K. RENAULT, FARNSWORTH, R. J. 2002. The role of bedding management in udder health. Proceedings of the 41st Annual Meeting of the National Mastitis Council, p. 45-55.
- [5] KNÍŽATOVÁ, M. – MIHINA, Š. – KARANDUŠOVSKÁ, I. – ORSÁG, J. – ŠOTTNÍK, J. 2007. Production of gaseous compounds in broiler chickens breeding and their dependence on litter conditions. In: Bioclimatology and natural hazards, Štřelcová, K., Škvarenina, J., Blaženec, M. (eds.), International Scientific Conference, Poľana nad Detvou, Slovakia, September 17 - 20, 2007, p. 100. ISBN 978-80-228-17-60-8.
- [6] CHMÚRNÝ, I. 2003. Tepelná ochrana budov. Bratislava : Jaga group, 2003. 214 p. ISBN 80-88905-27-3.
- [7] POGRAN, Š., LENDELOVÁ, J., VERNAREC, J. 2000B. Analysis of moisture of construction materials used in housing buildings (In Slovak language). In Construmat 2000. Nitra: SPU, 2000, p. 154-158.

**Acknowledgements.** This work was supported by project VEGA 1/0771/09.

## COMPARISON OF PV SYSTEMS WITH FIXED AND ADJUSTABLE INCLINATION OF PV PANELS

MARTIN LIBRA<sup>1</sup>, PETR SEDLÁČEK<sup>1</sup>, JAN MAREŠ<sup>1</sup>, VLADISLAV POULEK<sup>2</sup>

<sup>1</sup> Czech University of Life Sciences Prague, Faculty of Engineering, Kamycka 129,  
16521 Prague, Czech Republic, [libra@tf.czu.cz](mailto:libra@tf.czu.cz)

<sup>2</sup> Poulek Solar, Ltd., Velvarska 9, 1600 Prague, Czech Republic, [info@solar-trackers.com](mailto:info@solar-trackers.com)

### Introduction

In recent years in the Czech Republic as well as in a number of other states electric power produced in photovoltaic (PV) power plants is financially subsidized. This is why a high number of photovoltaic power plants have been built. In Germany the development of photovoltaics was even more marked and they adopted the policy of subsidies already several years earlier. In the years 2006-2008 several photovoltaic power plants with the peak output higher than 1 MW<sub>p</sub> have been put into operation in the Czech Republic. So far the biggest photovoltaic power plant with the peak output of 3.8 MW<sub>p</sub> is in Hrušovany, but these record numbers could change very rapidly. There exists already a project of a PV power plant of the peak output of 30 MW<sub>p</sub> near Milovice. Topical information on photovoltaics and new power plants in the Czech Republic could be found in the internet pages of Solar league (Solární liga) <http://www.solarniliga.cz>.

Information on the construction and testing of our PV systems has been already presented on the pages of the journal “Jemná mechanika a optika” (Fine mechanics and optics) [1,2]. In this paper we would like to present the results of a year-round monitoring and comparison of two small photovoltaic systems with a fixed stand installed in the years 2009-2010 in the Czech University of Life Sciences Prague (locality: Prague 6 – Suchbátka, 50° north latitude).

### Experimental arrangement

Photovoltaic systems with fixed stand have been built so that three PV panels of Chinese manufacturing with the rated output  $P_{\max} = 170$  W<sub>p</sub> and with the efficiency of the photovoltaic energy conversion  $\eta = 16$  % have been installed on a fixed stand oriented to the south. In the first case the stand had a fixed inclination of 35°, in the second one the stand had a adjustable inclination of 35° during the summer period and 45° during the winter period. The three panels were connected in series and connected to a German inverter of the brand Sunny Boy, type SB 700, installed in the laboratory. Via this inverter the PV systems were directly connected to the grid of standard AC voltage of 230 V. The data were simultaneously stored by a data logger on a memory card and, after login, the data were monitored in real time by a server. The connection was accomplished using cables and water-proof connectors of the company Tyco. The view of both PV systems in winter period is

presented in Fig. 1 (the lone PV panel on the left-hand side is not a part of this system). The block scheme of both PV systems is identical and it is presented in Fig. 2. Each of these systems had thus the peak output power of 0.51 kW<sub>p</sub> and the year-round monitoring of data started in March 2009.

### Results and discussion

Systematic measurement of the produced amount of electric energy in the above mentioned photovoltaic systems with fixed stands and rated output of 0.51 kW<sub>p</sub> in the year 2009-2010 is given in Fig. 3, a survey of the values is summarized in Table 1. From this survey it is evident that during the monitored period the highest amount of electric power was produced in April. This finding is in agreement with the findings of our partners in several other PV power plants in the Czech Republic. On the other hand, in June a local summer minimum was found due to the rainy weather and overcast.



Tab. 1 Comparison of the amount of produced electric power in PV system with fixed inclination of 35° and with adjusted inclination 35°/45° during one year

month	produced power fixed inclination (kWh)	recalculated power fixed inclination (kWh/kW <sub>p</sub> )	produced power adjusted inclination (kWh)	recalculated power adjusted inclination (kWh/kW <sub>p</sub> )
April 2009	64.10	125.69	64.11	125.71
May 2009	57.47	112.69	57.48	112.71
June 2009	53.73	105.35	52.84	103.61
July 2009	60.49	118.61	59.90	117.45
August 2009	61.70	120.98	62.82	123.18
September 2009	46.18	90.55	47.16	92.47
October 2009	24.01	47.08	24.18	47.41
November 2009	17.22	33.76	20.50	40.20
December 2009	10.07	19.75	13.08	25.65
January 2010	12.12	23.76	14.36	28.16
February 2010	21.64	42.43	22.66	44.43
March 2010	43.32	84.94	44.61	87.47
<b>Total</b>	<b>472.05</b>	<b>925.59</b>	<b>483.70</b>	<b>948.45</b>

During this annual monitoring period the amount of produced electric energy was  $W = 472.05$  kWh/year in the system with fixed inclination and  $W = 483.70$  kWh/year in the system with adjustable inclination. The recalculated value of annual production of electric energy per 1 kW<sub>p</sub> of installed PV panels is  $W_p = 925.59$  kWh/kW<sub>p</sub>.year in the PV system with fixed inclination and  $W_p = 948.45$  kWh/kW<sub>p</sub>.year in PV system with adjustable inclination. During the summer sunny days with the maximum values of the incident radiation intensity moderately exceeded the value of  $1000 \text{ W} \cdot \text{m}^{-2}$ .

These values correspond to the values expected in Prague at the 50° of north latitude. If the PV panel inclination is not adjusted during the year, the inclination of 35° is optimal for the maximum annual production of electric energy. This inclination corresponds to the operation in the summer period as thus maximum amount of electric power is produced. It is evident that the adjustment of a higher inclination in the winter period increased the total annual amount of produced electric energy by about 2.5 %. It is possible that with a more frequent adjustment of the inclination the amount of produced power could be a little higher but the difference would not be very important. Fig. 4 presents examples of the dependence of the instantaneous output power on the time during selected days of the monitored period with different inclination of panels. For comparison also the values of produced electric energy in the respective day

are presented, they are corresponding to the area under the graph.



Fig. 1 PV systems with fixed stand installed in CULS Prague

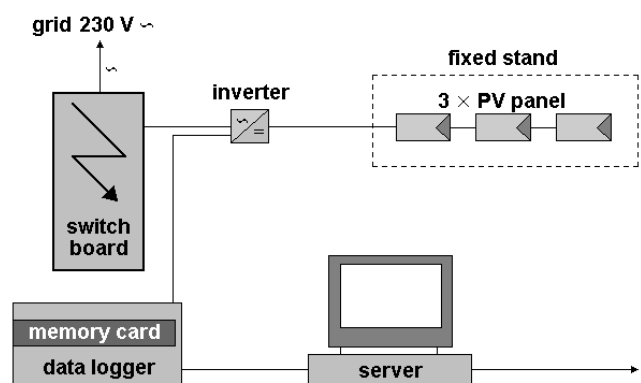


Fig. 2 Block scheme of the photovoltaic systems



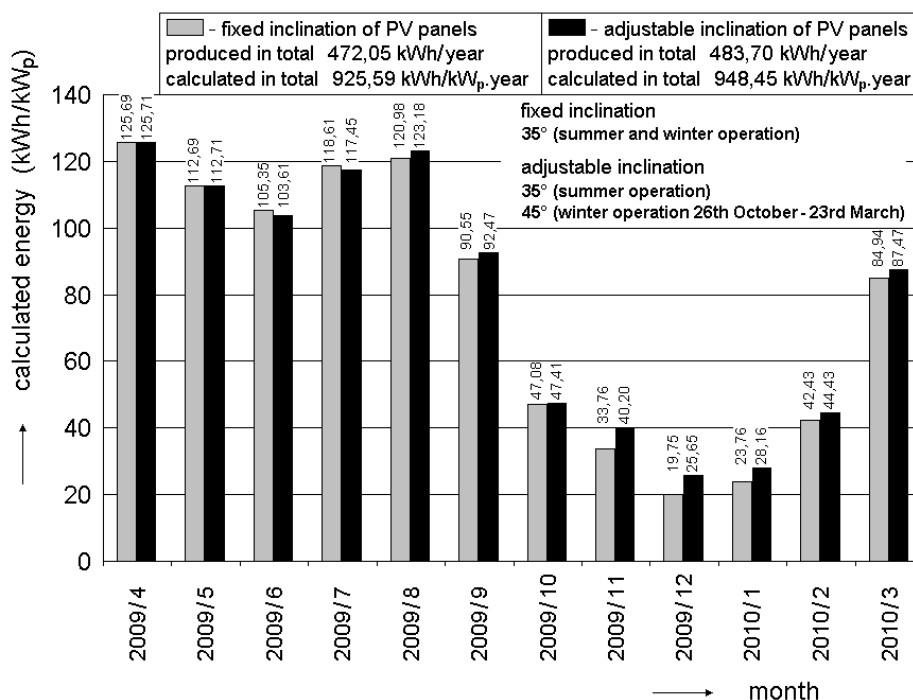


Fig. 3 Systematic measurements of the amount of produced electric power in the given photovoltaic system during one year

## Conclusion

Our endeavor was aimed to the construction and realization of photovoltaic systems with fixed stands and a comparison of the fixed and adjustable inclination of PV panels from the point of view of the amount of produced electric energy during one year. The photovoltaic systems were installed in the Czech University of Life Sciences Prague, the obtained values correspond to the assumption and they are also in relation with the values of larger PV power plants in the Czech Republic. From the measured and evaluated data it can be seen that the adjustment of the PV panel inclination during the year can enhance the amount of produced energy

maximum by several per cents. Therefore, it has some sense if the PV system is well accessible and the adjustment of the inclination makes no problems. If the adjustment would cause problems, it depends on the consideration of the operator whether the adjustment of the inclination during the year will pay off.

More information can be found, for instance, in our book [3] or on the internet pages <http://www.solar-trackers.com>.

This paper has been prepared within the framework of the research project MSM 6046070905.

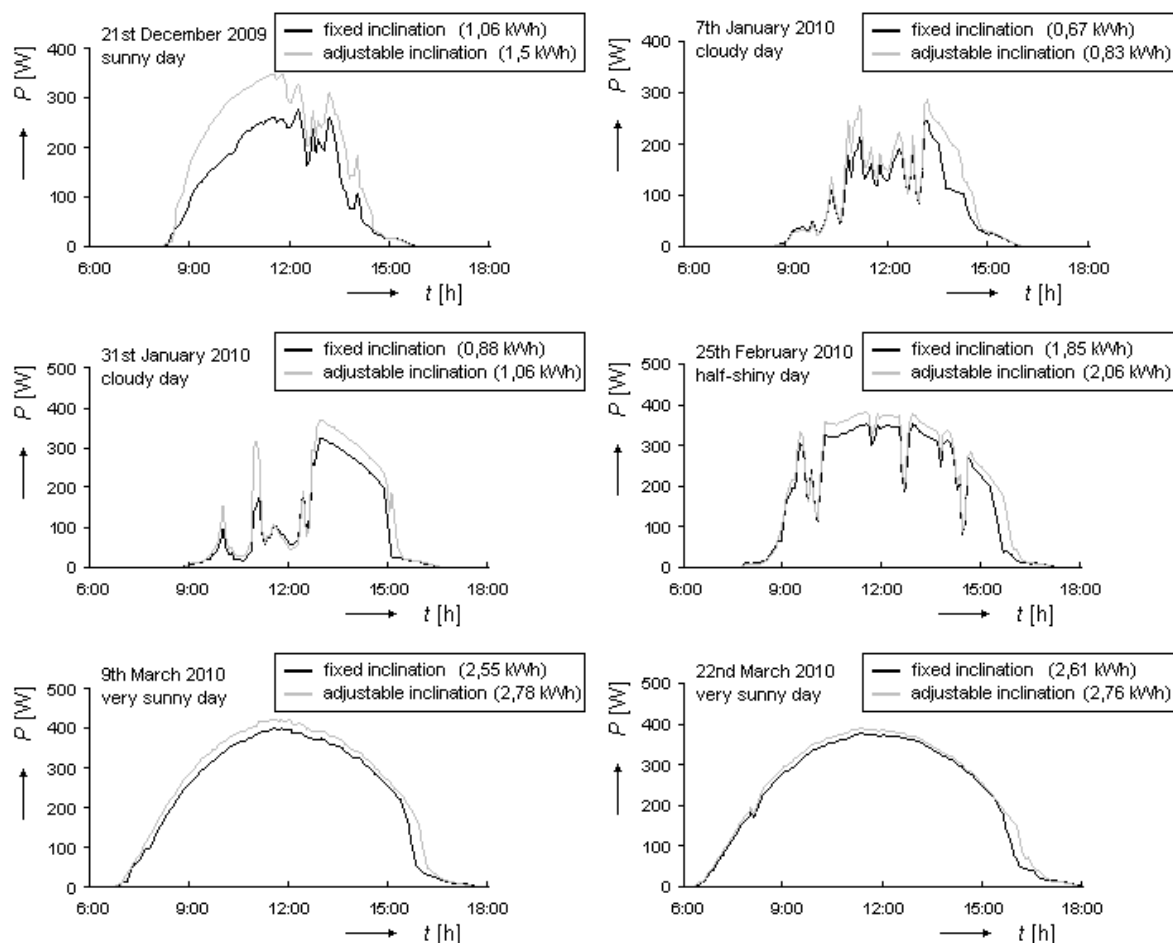


Fig. 4 Examples of the dependence of the instantaneous output power on the time during selected days

## References

- [1] Poulek, V., Bican, P., Mareš, J., Libra, M., *Nový fotovoltaický systém se zvýšenou efektivitou na ČZU v Praze (New photovoltaic system with enhanced efficiency in the Czech University of Life Sciences in Prague)*, *Jemná mechanika a optika*, 53, 2, (2008), pp.48-49, (in Czech)
- [2] Mareš, J., Libra, M., *Zařazení fotovoltaických systémů do struktury automatizace (Inclusion of photovoltaic systems into the structure of automation)*, *Jemná mechanika a optika*, 54, 2, (2009), pp.47-49, (in Czech)
- [3] Libra, M., Poulek, V., *Photovoltaics, theory and practice of the solar energy utilization*, book-monograph, ILSA, Prague, (2010), 169 pages, ISBN 978-80-904311-2-6

## DRYING PROCESS OF POULTRY MANURE AT VARIOUS TEMPERATURES

RADEK LISKA\*, PAVEL KIC

Czech University of Life Sciences Prague, Faculty of Engineering, Department of  
Technological Equipment of Buildings, 165 21 Prague 6 – Suchbátka, Czech Republic

Phone: + 420 224 383 141, E-mail: [liska.radek@gmail.com](mailto:liska.radek@gmail.com)

### Abstract

The main objective of this work was to investigate the evolution of the role of temperature during drying of poultry manure. The experiments were carried out in a laboratory of Czech University of Life Sciences, Prague. The samples were dried by different drying methods. During the drying process the temperatures were varied between 21.5 °C to 110 °C.

The lowest rate of 19.43 % of dryness of the manure matter was achieved. The lowest rate of dry matter as measured in an environment approximating working conditions was 33.65 %. These values were gained in two cases and whole drying procedure lasted 48 hours. The samples were compared taking into account the type of breeding system.

The measurement demonstrates that different design of drinking system significantly influenced the moisture content ( $p < 0.05$ ) of the manure. Spillage causes excessive manure moisture. It was observed that higher moisture content was measured for laying hens using nipple drinkers compared to those equipped with downspout accessories. Results from this study provide new data for updating standards that could be used in design and operation of laying hen houses.

### Introduction

The rapid growth of the poultry industry in recent years and the application of poultry waste to agricultural land has resulted in excessive Phosphorus content in the soil in many locations. The welfare of poultry and environmental protection can be increased by reduction of ammonia emissions from housing buildings [1].

The following treatment methods relevant for land application of poultry manure are currently being used: drying, composting, anaerobic digestion, combustion, pasteurization and palletizing [2].

Direct fertilizing using fresh excrement is strictly limited by its consistence which does not allow for uniform spreading. Another limitation is the seasonality of application – it can be used only in a specific time-frame and is limited by quantity. If straw was used as opposed to sawdust in deep litter production, fertilizing would be possible. The high rate of lignin in sawdust complicates composting which is more complicated compared to straw [3].

An application without treatment or non-appropriate disposal can become risky for environment and humans as such application might lead to the spread of diseases and may pollute soil and groundwater [2].

Composting is an effective and safe way for reduction of the manure's mass and volume,

destruction of pathogens, and stabilization of nutrients and the organic matter in it [4, 5]. Composting is one of the natural processes capable of stabilizing organic wastes [6].

Biogas technology is next option of treatment with manure. This is becoming more and more common nowadays. The process of biogas production appears to be a progressive, economically viable method of ultimate disposal and hygienic process [7].

A study was conducted to determine the effect of drying methods and temperature influence on drying characteristics of poultry manure. The results from this study provide useful information for developing cost-effective mitigating techniques.

### Material and methods

The experiments were done in the Faculty of Engineering of Czech University of Life Science Prague (CULS). For measurement purposes three different samples of poultry manure were used. First (Rak\_v1) and second (Rak\_v2) were produced on a farm using an intensive breeding system for laying hens. The third one sample was from the experimental facilities of CULS.

The first house was equipped with four-tier cages. Manure disposal was by a belt-clean system below each tier. Nipple drinkers were used without downspout accessories. The second

house was equipped with three-tier cages and nipple drinkers with downspout equipment. Ventilation of manure facilities in both systems was provided by fans mounted in the side walls drawing air through inlets in the ridge. The third house was designed as a simple battery of three cages with a manure belt. There was natural ventilation of manure facilities without special equipment, influenced only by forced ventilation of the room.

Temperature and humidity were measured by the Almemo 2590-9 with sensor FHA646-E1C device. The moisture content in the manure was identified by gravimetrics using an MEMERT UNB-200 air oven. Samples were weighted on a Kern 440-35N laboratory scale with a range from 0 to 400 g and accuracy to 0.01 g.

The three drying methods were measured by gravimetric methods during oven drying at 70 °C, oven drying at 110 °C, and drying at 21.5 °C. The weights of fresh samples were 5, 10, 15 and 20 g. A representative sample was weighed ( $M_S$ ) and put into a preheated oven at the required temperature ( $\pm 3$  °C). It was dried and continuously weighed till absolute dry state – dry matter ( $M_{DM}$ ). Measured values were used for relative (1) and specific (2) moisture content calculation.

$$w = \frac{M_{H_2O}}{M_S} \cdot 100 \quad [\%] \quad (1)$$

$$X = \frac{M_{H_2O}}{M_{DM}} \quad [g \cdot g^{-1}] \quad (2)$$

$$M_{H_2O} = M_S - M_{DM} \quad [g]$$

Where:

w ... relative moisture [%]

X ... specific moisture [ $g \cdot g^{-1}$ ]

$M_{H_2O}$  ... mass of water [ $g \cdot g^{-1}$  DM]

$M_S$  ... sample mass of manure being dry [g]

The obtained data were processed by statistical methods using a computer program. The results are accepted as reliable when  $P < 0.05$ .

## Results

The specific and relative humidity of all samples were compared. The average data of relative and specific humidity, their variability and standard deviations are in the table 1.

Generally, drying rates were highest during the first 1 h of drying, when the moisture content was greatest. The analyses of the temperature influence on drying of the poultry manure are shown in Table 2 and Figure 1. Moisture contents achieved levels of similar values during drying at the temperature 70 °C and 110 °C. It took 48 hours (see table 2) of drying in conditions similar to the ambient to reach about 35 % relative humidity.

Tab. 1 Statistical evaluation of manure samples

t [°C]	relative / specific MC	Agro			Rak_v1			Rak_v2		
		avr(x)	$\sigma$	$s_x^2$	avr(x)	$\sigma$	$s_x^2$	avr(x)	$\sigma$	$s_x^2$
110	w [%]	74.514	0.659	0.434	76.012	1.811	3.278	80.472	0.704	0.495
	u [ $g \cdot g^{-1}$ ]	2.891	0.155	0.024	3.020	0.589	0.347	4.127	0.192	0.037
70	w [%]	76.087	1.744	3.043	73.270	0.492	0.242	79.607	0.669	0.474
	u [ $g \cdot g^{-1}$ ]	3.197	0.319	0.102	2.740	0.070	0.005	3.907	0.168	0.028
21,5	w [%]	61.040	11.477	131.725	66.347	6.601	43.577	66.350	9.486	96.948
	u [ $g \cdot g^{-1}$ ]	1.727	0.821	0.674	2.043	0.549	0.302	2.187	1.100	1.210

Tab. 2. Comparison of values by different measurement methods.

Drying stage / Drying time	Sample	t [h]	$M_{MC}$ [%]	X [ $g \cdot g^{-1}$ ]
110 °C / 16 hr	Agro	16	25.73	2.89
	Rak_v1	16	23.99	3.19
	Rak_v2	16	19.43	4.13
70 °C / 16 hr	Agro	16	23.99	3.19
	Rak_v1	16	26.73	2.74
	Rak_v2	16	20.40	3.91
21.5 °C / 48 hr	Agro	48	38.94	1.73
	Rak_v1	48	33.65	2.04
	Rak_v2	48	33.65	2.18

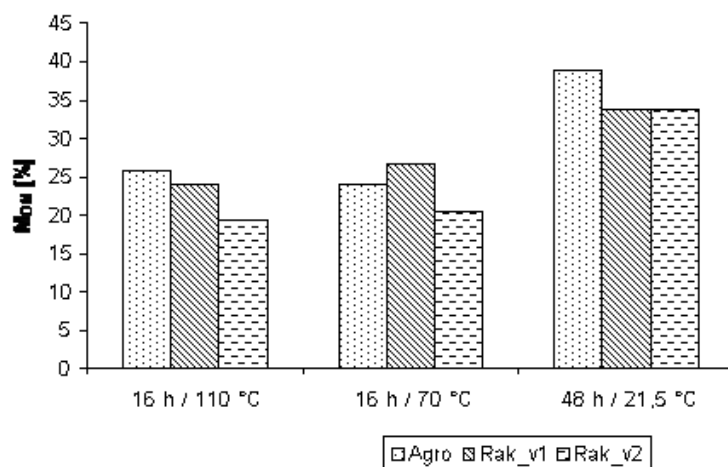


Fig. 1. Comparison of values by different measurement methods

Moisture content was significantly affected by different designs of drinking systems between samples Rak\_v1, Rak\_v2 and Agro ( $p < 0.05$ ). The difference between sample Rak\_v2 and other samples (Rak\_v1 and Agro) was statistically significant.

### Conclusion

The process keyed to drying effects should be taken into consideration in evaluation of manure utilization. In this way, the emission of ammonia from the poultry manure can be minimized. The effect of different drinker types on moisture contents was studied. Design of drinkers influences manure moisture content and the use of water. In two types of tested manure, the different moisture in dependence on drinker types was recognized as statically significant.

### References

- [1] Codling, E. E., R. L. Chaney, and J. Sherwell. 2002. Poultry litter ash as a potential phosphorus source for agricultural crops. *Journal of Environmental Quality*, 31:954-961.
- [2] Roeper, H., S. Khan, I. Koerner, and R. Stegmann, 2005. Low-tech options for chicken manure treatment and application possibilities in agriculture. Tenth International Waste Management and Landfill Symposium, 10.
- [3] Kosar, K., A. Matousek, J. Matejka, and I. Zakova. 1994. Pre-drying of poultry manure. (in Czech).
- [4] Michel, F. C. Jr, L. J. Forney, A. J. Huang, S. Drew, M. Czuprenski, J. D. Lindeneg, and C. A. Reddy. 1996. Effects of turning frequency, leaves to grass ratio and windrow vs pile configuration on composting of yard trimmings. *Compost Sci Util*, 4:26-43.
- [5] Tiquia, S. M., T. L. Richard, and M. S. Honeyman. 2000. Effects of windrow turning and seasonal temperatures on composting of hog manure from hoop structures. *Environ Technol*, 21:1037-1046.
- [6] Petric, I., and V. Selimbasic. 2008. Composting of poultry manure and wheat straw in a closed reactor: optimum mixture ratio and evolution of parameters. *Biodegradation*, 19:53-63.
- [7] Babicka, L., and L. Kourimska. 2007. Biogas Station as a Part of Ecological Farm. Proceeding of conference „Organic farming 2007“, 195-199. (in Czech)

### Acknowledgements

This work has been supported by the CIGA and IGA grants, “Optimal management of poultry manures.” Nr. 31170/1312/3106 and 31170/1313/3102.

## CHARACTERISTICS OF PARTICLES OF MILLED ENERGETIC PLANT MATERIAL

ALEKSANDER LISOWSKI\*, MAGDALENA DĄBROWSKA, MICHAŁ SYPUŁA  
Warsaw University of Life Sciences – SGGW, 02-787 Warsaw, Nowoursynowska 166, Poland,  
Phone: +4822-5934527, Fax: +4822-5934514, E-mail: aleksander\_lisowski@sggw.pl  
Department of Agricultural and Forest Engineering, Warsaw, Poland

### Abstract

The aim of this work was to determine and compare particle sizes and their critical speed of milled material of seven energetic plants species.

The testing material used was plants of willow, giant miscanthus, spartina, polygonaceous, rose, Virginia mallow and topinambour.

The polygonaceous mixture material was characterized by the highest critical speed of particles and Virginia mallow and spartina – the lowest; these formed a homogeneous group of speed. The values of particles critical speed of milled material of topinambour, giant miscanthus, rose and willow formed another intermediate homogeneous group.

For the homogeneous groups regression equations between the critical speed and geometric mean particles size were presented that can be used to predict the speed of the particles size at the investigated range.

The arithmetic mean value was greater than the geometric critical speed of particles and the dependence of this equation was described by a straight line.

Differences in characteristics of critical speed among energetic plants species are due to differences in their physical properties, because each plant has a different build of shoot or tissue, stem stiffness, hardness and material moisture content.

### Introduction

Energetic plants, rich in cellulose and lignin compounds, can be used to generate electricity or heat and to produce both liquid and gas fuels. Plant material may be burned in the form of chips or chaff, or after processing in the form of briquettes or pellets. Plants grown for energy purposes allow for the usage of low-productive or degraded agricultural land, which is important in our country, where the concentration of heavy metals in soil in more than 20% of the area used for agriculture exceeds acceptable norms.

The harvest of energetic plants in the broken-up form and the processing of material to solid fuels requires appropriate processes, which include loading, unloading, transportation and raw material drying. One of the best ways to implement these processes is pneumatic transport (Rautiainen et al., 1999). In order to properly select the parameters of machines and equipments used for such transport is necessary to know aerodynamic characteristics of the comminuted material. One of the most important features is the critical speed of particles (Klasek et al., 2006).

The aim of this work was to determine and compare the particle sizes and the critical speed of milled material of seven energetic plants species. The study was performed at the Department of Agricultural and Forest Engineering, Warsaw University of Life Sciences.

### Materials and methods

Chopped plant particles of: willow, Virginia mallow, topinambour, spartina, polygonaceous, rose and giant miscanthus were used in the study. These plants are cultivated on the plots of Experimental Station in Skierniewice belonging to the Faculty of Agriculture and Biology, Warsaw University of Life Sciences.

Harvesting of energetic plants was carried out directly from the field on 17-18 December 2007 with the use of a tractor trailed forage harvester Z374. The chopping unit of the forage harvester was equipped with 10 knives and straight thrower blades with a sharp tool rake and also with a smooth-surface bottom plate. Cutting disc rotational speed amounted to 1000 rpm. The set working parameters allowed to obtain cutting



frequency 167 Hz and theoretical length of chopped plant material particles 8.8 mm.

The plant moisture content during harvest varied from 22.6 to 52.2% (wet basis). The obtained chips and chaff of mean size from 9 to 11 mm were dried in natural conditions to moisture content within the narrow range from 5.6 to 7.3%. The dried plant material was milled in a beater mill equipped with a sieve with openings diameter of 10 mm.

Separation of the material mixture of seven energetic plants on a sieve separator with five sieves of square openings (their diagonals form the approximate geometric sequence) allowed to develop a histogram of particles lengths (Fig. 1.). Dimensions of the sieve opening diagonals (from top) are as follows: 26.90, 18.00, 8.98, 5.61, 1.65 mm (ANSI/ASAE S424.1). The results of particle sizes distributions of ground material is presented in the work of Dąbrowska and Lisowski (2008, 2009).

Critical speed of particles in the milled material was determined by means of a laboratory pneumatic classifier K-293 Petkus. Each sample weighed 50 g. On the basis of a preliminary test for each mixture of energetic plants a speed range was selected, which was then divided into 10 class intervals. Fractions of the intervals were weighed with an accuracy 0.01 g. The measurements were performed three times for each sieve fraction of the seven energetic plants species.

On the basis of the results of particles distribution on a pneumatic classifier critical particle speeds for each fraction and the average values for the mixture were estimated. Due to the uneven weight of the extracted fractions the weighted average was estimated and for comparison the arithmetic and geometric critical speeds were calculated. The values of critical speed of particles were compared with the values of their sizes, which were presented in the work of the authors cited.

Critical speed for each particle fraction was established on the basis of the regression function depending on the volume flow estimated on the basis of the standard graph (Laboratory ..., 2001):

$$v_{ki} = \frac{7}{60} V_{pi} + 1 \quad (1)$$

where:

$v_{ki}$  – critical speed for  $i$ th particle fraction,  $\text{m}\cdot\text{s}^{-1}$ .

$V_{pi}$  – volume flow for  $i$ th particle fraction,  $\text{m}^3\cdot\text{s}^{-1}$ .

To determine the weighted arithmetic average critical speed of particles, the procedure was as follows. Critical speed for the class intervals middle was calculated as the arithmetic mean:

$$v_{kai} = \frac{v_{ki} + v_{k(i+1)}}{2} \quad (2)$$

where:

$v_{kai}$  – the class intervals middle of the critical speed for  $i$ th and  $(i+1)$ th particle fractions,  $\text{m}\cdot\text{s}^{-1}$ ,

$v_{ki}$  – critical speed for  $i$ th particle fraction,  $\text{m}\cdot\text{s}^{-1}$ ,

$v_{k(i+1)}$  – critical speed for  $(i+1)$ th particle fraction,  $\text{m}\cdot\text{s}^{-1}$ .

The weighted arithmetic average of the critical particles speed was calculated from a mixture of class intervals middle of the critical speed and related non-negative values of weights from the formula:

$$v_{ka} = \frac{\sum_{i=1}^n m_i v_{kai}}{\sum_{i=1}^n m_i} \quad (3)$$

where:

$v_{ka}$  – weighted arithmetic average of the critical speed of the mixture particles,  $\text{m}\cdot\text{s}^{-1}$ ,

$m_i$  – weight (decimal), the  $i$ th particle fraction with critical speed  $v_{kai}$ , g.

When calculating the geometric mean of the critical speed, the procedure was as follows. Critical speed for the class intervals middle was calculated as the geometric mean:

$$v_{kgi} = \sqrt{v_{ki} v_{k(i+1)}} \quad (4)$$

where:

$v_{kgi}$  – geometric mean values of the class intervals critical speed for the  $i$ th and the  $(i+1)$ th particle fractions,  $\text{m}\cdot\text{s}^{-1}$ .

Geometric weighted average of the critical particles speed of the mixture was calculated from the geometric mean values of the class intervals critical speed and related non-negative values of weights from the formula:

$$v_{kg} = \ln^{-1} \left[ \frac{\sum (m_i \ln v_{kgi})}{\sum m_i} \right] \quad (5)$$

where:

$v_{kg}$  – weighted geometric average of the critical speed of the mixture particles,  $\text{m}\cdot\text{s}^{-1}$ .

The obtained results were statistically analyzed using the Statistics v.17 packet.

## Results and discussion

Statistical analysis showed that both the particles from different plant species and the sieve fraction statistically had significantly different critical speeds (Table 1). A unique

impact of these factors referred to the critical speed calculated from the two weighted averages, arithmetic and geometric. Basing on Duncan test it was found that the arithmetic mean value of particle critical speed for almost all mixtures obtained from the comminution of energy plants formed separate homogeneous groups (Table 2). Only the arithmetic mean of the particles critical speed of rose was not clearly differentiated, especially in comparison with the arithmetic mean of particles critical speed of the giant Miscanthus mixture as the differences between these averages were lower than the standard error.

Table 1. The results of variance analysis for the arithmetic and geometric mean of the critical particles speed for the plant species and the sieve fraction

Critical speed	Descriptive characteristics	Sum of squares	Degrees of freedom	Mean square	F <sub>emp</sub>	p-value
Arithmetic	plant species	15.5	6	2.6	265.51	<0.0001
	sieve fraction	70.1	5	14.0	10.25	<0.0001
Geometric	plant species	13.5	6	2.2	271.19	<0.0001
	sieve fraction	15.5	5	3.1	5.76	0.0001

A ranking of homogeneous groups close to the arithmetic average values of particle critical speed, in relation to plant species, was also formed by the geometric mean values of the particle critical speed. (Table 2).

The lowest value of the critical speed arithmetic mean of particles ( $1.87 \text{ m}\cdot\text{s}^{-1}$ ) characterized the smallest fraction remaining at the bottom of the sieve separator, with a theoretical particle size average of 0.82 mm, and the highest ( $4.24 \text{ m}\cdot\text{s}^{-1}$ ) - fraction of a theoretical particle size of 7.1 mm (Table 2). The fraction of the mixture with a particle mean size of 7.1 mm was characterized by a clearly separate homogeneous group of the arithmetic mean value of particle critical speed, and the remaining mixture fractions were characterized by not so clearly different aerodynamic properties. This

applies especially to the fraction with an average particle size of 22 mm, which belonged to three separate homogeneous groups, which means a large variety of these particles in terms of physical properties that determine their aerodynamic characteristics. Probably these particles were characterized by high variability of dimension, cross-section, specific density, porosity, outer surface roughness and weight related to plant material moisture content.

Geometric means of particle critical speed for the sieve fractions were even more uniform, especially in the area covering mixture fractions with particle mean size (Table 2).

The maximum difference between the arithmetic mean value of particle critical speed for fraction amounted to  $2.37 \text{ m}\cdot\text{s}^{-1}$ , and the geometric –  $1.09 \text{ m}\cdot\text{s}^{-1}$ .

Table 2. Results of a detailed statistical analysis of the average critical speed of particles mixtures divided into homogeneous groups according to the plant species and the sieve fraction

divided into homogeneous groups according to the plant species and the sieve fraction

Level Factor	Numbers	$v_{ka}$ , $m \cdot s^{-1}$	$s_{ka}$ , $m \cdot s^{-1}$	Homogeneous group						$v_{kg}$ , $m \cdot s^{-1}$	$s_{kg}$	Homogeneous group					
Plant species																	
Spartina	3	1.94	0.06	x						1.87	0.05	x					
Virginia mallow	3	2.41	0.06		x					2.25	0.05		x				
Topinambour	3	3.47	0.06			x				3.25	0.05			x			
Rose	3	3.63	0.06			x	x			3.51	0.05				x		
Giant miscanthus	3	3.66	0.06				x			3.51	0.05				x		
Willow	3	4.08	0.06					x		3.83	0.05					x	
Polygonaceous	3	4.62	0.06						x	4.31	0.05						x
Sieve fraction																	
0.82 mm	21	1.87	0.25	x						1.61	0.16	x					
3.04 mm	21	3.26	0.25	x	x					2.24	0.16	x	x				
7.1 mm	21	4.24	0.25	x	x	x				2.70	0.16		x	x			
12.7 mm	21	2.80	0.25			x	x			2.12	0.16				x		
22 mm	12	2.71	0.34				x			2.38	0.21				x	x	
36 mm	9	2.03	0.39					x		1.66	0.24						x

The average values of geometric critical speed of particles of fragmented energy plants were smaller than the corresponding average arithmetic values. This is due to the properties of the arithmetic mean, which is usually greater than the geometric mean and the larger the relative changes in the values of critical speed, the greater the differences. Both averages are equal to the normal distribution and the distribution of critical speed was similar to the log-normal distribution. The geometric mean increased at a lower rate and decreased at a higher rate, but the relationship between the geometric and the arithmetic mean of the critical speed of particles was made possible by the regression equation describing it a simple form:  $v_{ka} = 0.93v_{kg} + 0.06$  where the determination coefficient is 99.68%.

Based on the analysis and research of particle sizes of comminuted material (Dąbrowska and Lisowski, 2008, 2009) an attempt was made to look for a relationship between average critical speeds and particle sizes. Distinguishing a homogeneous groups of critical speed (Table 2) and graphical interpretation (Fig. 1) indicate the possibility to

separate three areas of critical speed, for which regressions should be sought. The group with the smallest of critical speeds, a similar trend (Fig. 1), included particles of Virginia mallow and spartina, another group - particles of topinambour, giant miscanthus, rose and willow, and the largest one - polygonaceous particles. The location of points on the Cartesian coordinates (Fig. 1) indicates that the search for equations can be narrowed down to the linear regression form. Results of regression analysis are summarized in Table 3 Regression ( $t_{emp}$ ) and determination ( $R^2$ ) coefficients for the regression and the Fisher- Snedecor test values ( $F_{emp}$ ) for the set of linear equations (Fig. 1) involving the arithmetic  $v_{ka}$  or geometric  $v_{kg}$  critical speed with particles size  $x_{gm}$  are sufficiently high to approve them and to propose them for prediction of critical speeds of particles of comminuted energetic plants.

Differences in the characteristics of the critical speed distributions between energetic plant species result from differences in their physical properties, because each plant has a different build of shoot or tissue, stem stiffness, hardness and material moisture content.

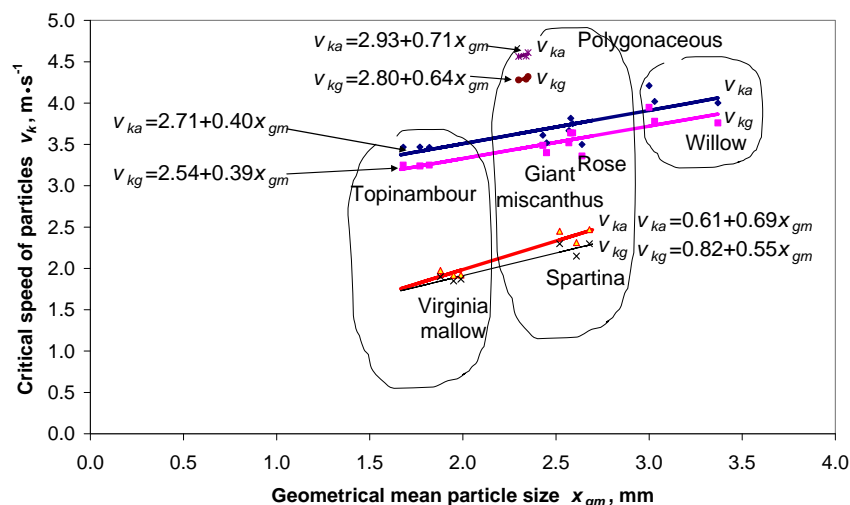


Figure 1. Dependence of arithmetic  $v_{ka}$  and geometric  $v_{kg}$  critical speed on the geometric mean particle sizes of comminuted energetic plants (points mark measuring results, and lines mark linear regressions)

## Conclusions

1. Mixtures of plant materials milled in a beater mill were characterized by different aerodynamic properties, because in almost all cases for the seven species plants separate homogeneous groups of particle critical speed, calculated as both arithmetic and geometric averages, were distinguished. Such uniqueness is not found for the giant miscanthus mixtures, which belonged to a homogeneous critical speed group of rose, and arithmetic mean of rose particle critical speed formed a homogeneous group with a topinambour.

The highest critical speed of particles characterized the polygonaceous mixture material and the lowest – Virginia mallow and spartina, which formed a homogeneous group of speed. The values of particles critical speed of milled material of topinambour, giant miscanthus, rose and willow formed another intermediate homogeneous group.

2. For the homogeneous groups regression equations between the critical speed and geometric mean particles size were presented that can be used to predict the speed of the particle sizes at the investigated range.

3. The arithmetic mean value was greater than the geometric critical speed of particles and the dependence of this equation was described by a straight line.

## References

- [1] Dąbrowska, M. Lisowski, A.: Investigation of the particles length distribution of energetic plants for briquettes. III International Students Scientific Conference on Problems of Agro and Forestry Engineering. Ed. SGGW, Warsaw 2008, p. 40-47 (in Polish).
- [2] Dąbrowska, M. Lisowski, A.: Investigation of the particles length distribution of energetic plants for briquettes. IV International Students Scientific Conference on Problems of Agro and Forestry Engineering. Ed. SGGW, Warsaw 2009, p. 55-60 (in Polish).
- [3] Dąbrowska, M. Lisowski, A.: Critical speed of particles of milled energetic plant material. XIX International Students Scientific Conference on Problems of Agro and Forestry Engineering. Ed. SGGW, Warsaw 2010, p. 78-87 (in Polish).
- [4] Klasek, S.E., Womac, A.R., Yoder, D.C., Hayes, D.G.: Terminal velocity determination for component separation of biomass. ASAE 2006, Paper No 066218, pp. 8.
- [5] Laboratory of agricultural machines. Collective work. Ed. SGGW, Warsaw 2001, 140 pp. (in Polish).
- [6] Rautiainen, A., G. Stewart, V. Poikolainen, and P. Sarkomaa.. An experimental study of vertical pneumatic conveying. Power Technology. 1999, 104, p. 139-150.

## DIAGNOSIS OF GEARBOX FAULTS IN AGRICULTURAL MACHINERY USING ENERGY OF TRANSIENT FEATURES

S. LOUTRIDIS<sup>1\*</sup>, I. GRAVALOS<sup>2</sup>, D. MOSHOU<sup>3</sup>, TH. GIALAMAS<sup>2</sup>,  
D. KATERIS<sup>3</sup>, P. XYRADAKIS<sup>2</sup>, Z. TSIROPOULOS<sup>2</sup>

<sup>1</sup>Technological Educational Institute of Larissa, School of Technological Applications,  
Department of Electrical Engineering, 41110 Larissa, Greece.

Phone: +302410-684550, Fax: +302410-613249, E-mail: loutridi@teilar.gr

<sup>2</sup>Technological Educational Institute of Larissa, School of Agricultural Technology,  
Department of Biosystems Engineering, 41110 Larissa, Greece.

<sup>3</sup>Aristotle University, School of Agriculture,  
Agricultural Engineering Laboratory, 54124 Thessaloniki, Greece.

### Abstract

Gear mechanisms are widely used in agricultural and other kind of machinery. For this reason, gear health monitoring has been the subject of intensive investigation and research. Among several other methods, vibration measurement and analysis is considered as a practical means for fault detection in gearboxes. In this work, a hypothesis is made that local faults appear as transient signals in the vibration time-series. The energy content of these transient features increases as the magnitude of damage increases. Data were collected from an experimental rig that consists of two electrical machines, a pair of spur gears, a power supply unit and the necessary speed control electronics. The vibration signal generated by the gearbox was picked up by an accelerometer bolted to the pinion body and the electrical signal was transferred to an external charge amplifier through slip rings and recorded by a PCMCIA acquisition card. The time-series was then analyzed with the newly proposed Empirical Mode Decomposition scheme [1], in which the signal is decomposed to a group of oscillatory functions called the intrinsic mode functions. The instantaneous energy is shown to obtain high values when defected teeth are engaged and therefore it can be directly related to damage magnitude. By using the results of these experiments, an online diagnostic system could be built resulting in improved reliability and reduced maintenance cost.

### Introduction

Gear mechanisms are an important element in a variety of mechanical systems. For this reason, early fault detection in gears has been the subject of intensive investigation and many methods based on vibration signal analysis have been developed. Conventional methods include kurtosis, power spectrum and cepstrum estimation and envelope detection, which have proved to be effective in fault diagnosis and are now well established [1], [2], [3]. Their main drawback, however, is that they are based on the assumption of stationarity and linearity of the vibration time-series under study.

To deal with non-stationary signals, new techniques such as time-frequency distributions and wavelets have received attention and gained acceptance [4], [5], [6]. The wavelet transform is by far the most popular technique. The time and frequency resolution however is a compromise, as a large scale wavelet is chosen for determining

general signal features and a small scale wavelet for extracting the signal details. Consequently, time localization is poor for low frequency signals and frequency resolution is poor for high frequency signals. Another shortcoming of the wavelet method is the fact that the analysis depends on the choice of the wavelet function and only signal features that correlate well with the shape of the wavelet function have a chance to lead to coefficients of high value.

In the quest of accurate time and frequency localization Huang et al. [7] proposed the Empirical Mode Decomposition (EMD) scheme which offers a different approach in time-series processing. In this work, the EMD algorithm is used for detection and prediction of gear faults. A hypothesis is made that local faults appear as transient signals in the vibration time-series. Their energy content increases as the magnitude of damage increases. A detection and prediction



is presented that is based on the energy content of transient features.

### Empirical mode decomposition

The EMD method decomposes a time-series into a finite set of oscillatory functions called the intrinsic mode functions (IMF). An IMF is a function that satisfies two conditions: (1) the number of extrema and the number of zero crossings must either equal or differ at most by one; (2) the running mean value of the envelope defined by the local maxima and the envelope defined by the local minima is zero. The procedure to decompose a signal into intrinsic mode functions is as follows. First, the local extrema of the signal  $x(t)$  are identified. The local maxima are connected together forming the upper envelope  $u(t)$  and the local minima are connected forming the lower envelope  $l(t)$ . This connection is implemented by a cubic spline interpolation scheme. The running mean is defined as

$$m_1(t) = \frac{l(t) + u(t)}{2} \quad (1)$$

Then  $m_1(t)$  is subtracted from the signal  $x(t)$ , resulting in the first component  $h_1(t)$ , i.e.:

$$h_1(t) = x(t) - m_1(t) \quad (2)$$

The component  $h_1(t)$  is now examined if it satisfies the conditions to be an IMF. If not, a process named by Huang as the *sifting process* should be followed until  $h_1(t)$  becomes an IMF. In the sifting process  $h_1(t)$  is treated as the new data. The first IMF  $C_1(t)$  is subsequently subtracted from the original signal  $x(t)$ , the difference called the first residue  $r_1(t)$ .

$$r_1(t) = x(t) - C_1(t) \quad (3)$$

The residue  $r_1(t)$  is taken as the new signal and the sifting process is applied from the beginning. As a result, the signal  $x(t)$  will be decomposed into a finite number of IMFs  $C_j(t)$ . The sifting process ends when the last residue  $r_N(t)$  is a constant or a monotonic function.

### Experimental set-up

The experimental rig consists of two electrical machines, a pair of spur gears, a power supply unit with the necessary speed control electronics and the data acquisition system. Referring to figure 1, a DC machine of 1.5 kW

rotates the pinion. The load is provided by an AC asynchronous machine, which is configured as a brake. The transmission ratio is  $35/19 = 1.842$ , which means that an increase in rotational speed is achieved. The vibration signal generated by the gearbox was picked up by an accelerometer bolted to the pinion body and the electrical signal was transferred to an external charge amplifier through slip rings. The sampling interval was  $\Delta t = 0.05$  ms corresponding to a sampling frequency  $f_s$  of 20 kHz. The signal was lowpass filtered at 5 kHz through a 4<sup>th</sup> order Bessel type filter. Data was stored for post processing to a portable PC. The acquisition system was flexible enough to be used in actual industrial conditions. A number of  $2^{15} = 32768$  samples have been acquired in all experiments corresponding to a time-history length of 1.638 s.

### Fault identification procedure

In all cases the rotational speed of the pinion axis was kept relatively constant at 300 rpm (5 Hz). This resulted in a meshing frequency of  $35 \times 5 = 175$  Hz. The load varied from 10 Nm to 18 Nm. The magnitudes of damage tested varied from a crack of 15% of tooth root up to a crack of 75% of the tooth root. The intermediate damage levels were 33% and 50%. The cases of a healthy gear and a gear with tooth loss have been also examined for completeness. For each single damage scenario 10 experimental runs were conducted and the vibration data were stored on the hard disk of a portable computer.

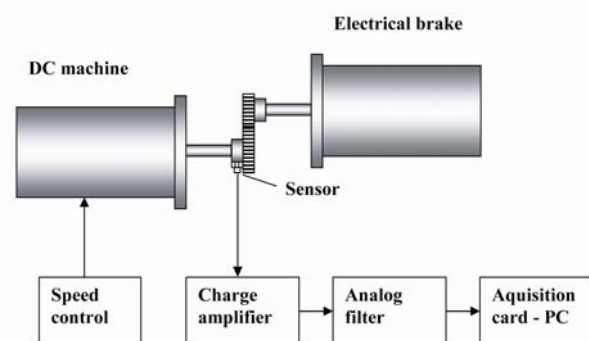


Figure 1: Experimental test rig

The vibration time-series of a gear pair with a 15% crack (load 10 Nm) is decomposed using the EMD algorithm. The IMFs are presented in figure 2. The first row represents three periods (600 ms) of the vibration signal for time reference. From a total of nine intrinsic mode



functions found, only the first four are depicted, because the energy of modes  $C_5$  to  $C_9$  is very low. Mode  $C_1$  contains the highest signal frequencies, mode  $C_2$  the next higher frequency band and so on. The transient caused by the crack is clearly captured in modes  $C_1$  and  $C_2$  and takes the form of periodic pulses with a period of 200 ms, which coincides with the period of shaft revolution.

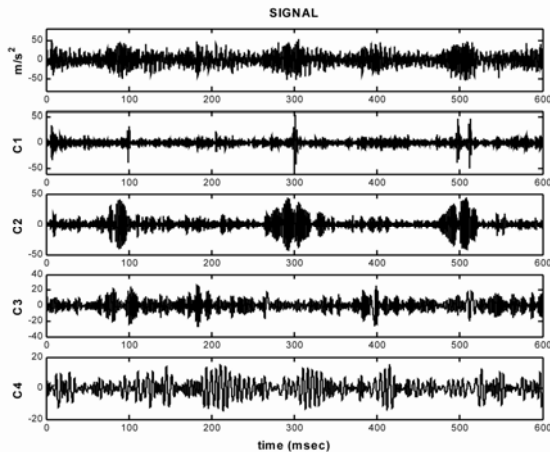


Figure 2: Decomposition of the vibration signal into intrinsic mode functions

It seems that mode  $C_2$  best represents the time scale of the transient caused by gear damage and for this reason it is selected as a suitable diagnostic feature for all subsequent experiments. In particular, the energy of mode  $C_2$  will be used defined as

$$E_2(t) = \frac{1}{2} A_2^2(t) \quad (4)$$

where  $A_2(t)$  is the mode envelope obtained from the Hilbert transform procedure. In figure 3 the calculated energies for the damaged gear pair with a relative crack magnitude ranging from 15% to 75% are presented. In addition, the case of a healthy pair and a pair that suffers from tooth loss have been added for completeness. The energy of mode  $C_2$  of the healthy pair is relatively low and lacks the periodic pulses associated with crack type damage. The peak energy of a gear pair with a 75% crack is more than three times that of a pair with a 15% crack. Tooth loss as expected is easily identified, because the energy is more than ten times greater than the worst crack scenario.

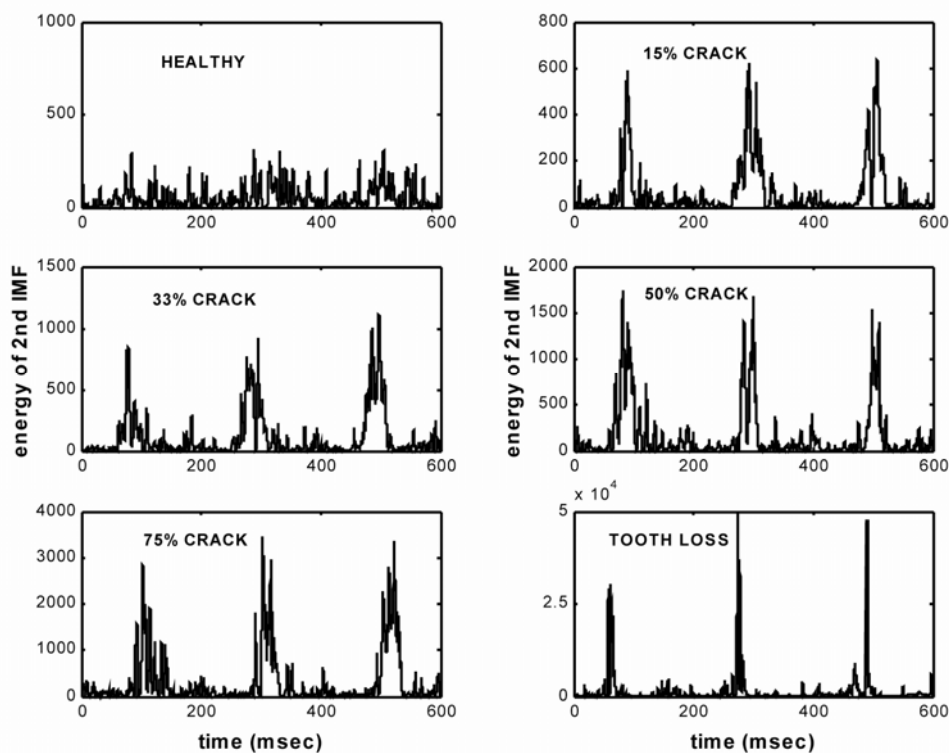


Figure 3: From top to bottom, energy of 2<sup>nd</sup> IMF for a healthy gear pair, a pair with 15%, 33%, 50%, 75% crack and tooth loss

To derive an empirical curve that relates the energy to the crack magnitude, first the peak energy values for a certain crack size from all 10 experimental runs are recorded. This means that for a specific crack magnitude there will be  $8 \times 10 = 80$  peak energy values available. Next, the extreme values are dropped out so that 90% of the total figures are kept. This is to make sure that the results have statistical meaning. The average value is finally computed. Figure 4 depicts the average energy versus crack magnitude.

## Conclusions

In this paper, a method for gear fault identification was presented based on the newly developed Empirical Mode Decomposition algorithm. The method is not based on the *a priori* selection of a kernel function, but instead it decomposes the signal into intrinsic oscillation modes derived from the succession of extrema. It has been shown that any defect in the form of a crack or tooth loss is manifested as an increase in the envelope amplitude of one or more of the intrinsic modes. The defect evolution can be monitored by computing the energy of the intrinsic mode that is most sensitive to damage.

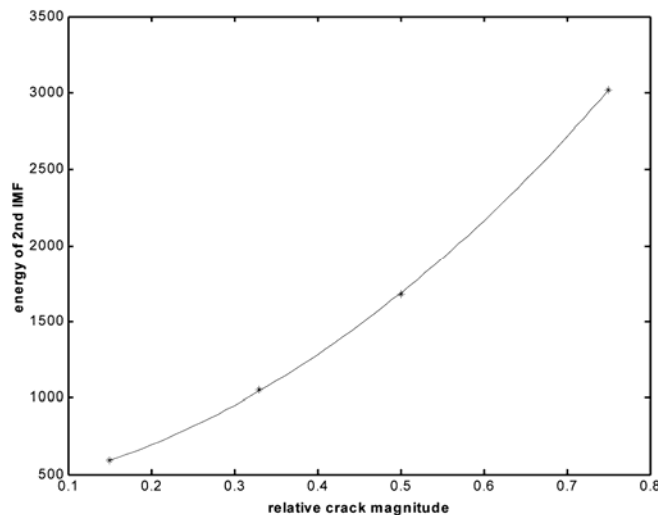


Figure 4: Energy of 2<sup>nd</sup> IMF as a function of relative crack magnitude

## References

- [1] Stewart, R. M.: Application of Time Series Analysis. Some useful data analysis techniques for gearbox diagnostics. Institute of Sound and Vibration Research, Southampton University, 19-22 September 1977.
- [2] Randall, RB.: Application of cepstrum analysis to gearbox diagnosis. Bruel & Kjaer, \ IMECHE 1980.
- [3] McFadden, PD and Smith, JD.: A signal processing technique for detecting local defects in a gear from the signal average of the vibration. Proceedings of the Institute of Mechanical Engineers, 1985, 199, p. 287-292.
- [4] Staszewski, W. and Tomlinson, G.: Application of the wavelet transform to fault detection of a spur gear. Mechanical Systems and Signal Processing, 1994, 8(3), p. 289 - 307.
- [5] Boulahbal, D., Golnaraghi, M. and Ismail, F.: Amplitude and phase wavelet maps for the detection of cracks in geared systems. Mechanical Systems and Signal Processing, 1999, 13(3), p. 423-436.
- [6] Sung, S., Tai, HM. and Chen, CW.: Locating defects of a gear system by the technique of wavelet transform. Mechanism & Machine Theory, 2000, 35, p. 1169-1182.
- [7] Huang, N. E., Shen, Z., Long, S. R., Wu, M. C., Shih, H. H., Zheng, Q., Yen, N., Tung, C. C., Liu, H. H.: The empirical mode decomposition and Hilbert spectrum for nonlinear and nonstationary time series analysis, Proceedings of Royal Society of London Series A454, 1998, p. 903-995.

## TRANSPORT LINKS IN THE EDUCATIONAL CENTRES

MARIAN LUKEŠ<sup>1</sup> - MICHAL KOSTELECKÝ<sup>2</sup>

<sup>1</sup>Czech University of Life Sciences Prague, Faculty of Engineering, 165 21 Prague 6  
– Suchbát, Czech Republic, Phone: +420224383112, Fax: +4202-20921361, E-mail:  
lukesm@tf.czu.cz

<sup>2</sup>Czech University of Life Sciences Prague, Faculty of Engineering, 165 21 Prague 6  
– Suchbát, Czech Republic, Phone: +420224383112, Fax: +4202-20921361, E-mail:  
kosteleckym@tf.czu.cz

### Abstract

The increase in passenger car transport affects not only the transport systems but public transport as well. It is often associated with new construction of roads and other transport facilities used primarily for passenger car traffic and its further growth. This fact limits other forms of transport development such as walking or cycling modes. Unfortunately it is preferred in areas of educational centres as well where walking and cycling should be mainly supported. The aim of this paper is to analyze the characteristics of educational institutions in relation to transport even including universities' surroundings on the example of Czech University of Life Sciences. At the same time to propose ways of enhancement of the attractiveness of public transport systems and the use of alternative transport modes.

### Introduction

Contemporary society has a very high dependence on cars. Trends in the car usage in university campuses comply with changes in society as a whole. In recent years, increasing emphasis is put on providing access and mobility without disturbing the specific required "calm mood" of campuses. The increasing frequency of traffic congestion, demanding air quality requirements, limited space for parking and high costs for the construction of parking buildings can cause efforts to reduce traffic on campus and mitigate impacts on the surrounding neighbourhood. Universities and training centres can focus on environmentally acceptable solutions to alleviate traffic congestion and improve safety for all users on campuses (Poinsatte and Toor, 2001). These solutions are usually based on the principle of transport demand management which include toll parking, enhanced transport accessibility of public transport, park and ride, rideshare programs (car-sharing, bike-sharing), promoting cycling and walking infrastructure and transport systems calming.

Although the number of publications concerning with sustainable transportation increases, most of them are focused on increasing

motorization and its impacts (Newman and Kenworthy, 1999; Vuchic, 1999), and the resulting increase in parking needs (Shoup, 1997). Research on non-motorized transport planning is still less widespread compared to other modes of transport, much less in a specific field which are campuses. It should include specifications that differ from the usual campus located in urban areas and regions. The increased traffic movement is bind with the end and beginning of teaching, an irregular schedule of teaching, and continuous movement throughout the day. Some research has focused on the relationship of public transport to the university campus (Farris and Radwan, 1989, Brown et al., 2001), except Tolley (1996), which was also included cycling on campus in the UK. Another parameter to be considered is the location of educational institution to the city or residential sprawl and to make use of the capacity of the transport system to ensure the transport requirements - in this context it is important whether is university provides accommodation in a campus or not.

The main task of this research is to assess the transportation facilities in educational centres. To take into account what it is most appropriate modal split and what methods can these training centres

use to encourage alternative modes of transport compared to individual passenger car transport. The main purpose is to strike a path for sustainable development of transport operation in the university campus and other campuses of educational centres to include bicycle and pedestrian traffic. Due to the nature of university campuses, acting as urban areas, it can be used as model situations. Since there are a number of students (young people) there, it is possible to build traffic behaviour patterns, which are then incorporated them into later working life. One problem is that the management and transport planning within the campus is often based on the dominance of car traffic and a change of belief is difficult (Poinsatte and Toor, 2001). Creating a cyclists and pedestrian friendly campus leads to expansion of the use of these modes outside the campus, which will increase pressure on the subsequent construction of pedestrian and cycling infrastructure. This document should be in order to address transportation, land planning and landscape architecture and the environment. It should help traffic in the campus implementation team with the application of alternative transport strategies. Outputs should also be relevant to other solutions campus environments such as shopping centres, hospitals, parks and office complexes. Traffic in the Campus is divided into two parts. The first part deals with transport within the campus (internal transport) and how to address the traffic may affect the campus. The second part deals with research and external traffic impacts on surrounding traffic.

## Materials and methods

### Campus - internal and external transport

University campuses are very specific locations. They create space where people with different backgrounds, with different incomes, lifestyles and attitudes live together, learn, work and spend free time. College campuses build social ties or links that are temporal or become permanent. Traditional campus observes the basic principles of a city because the focus of many functions within the reach of pedestrians (Dulken, 1992, Turner, 1995). Campuses can be seen as separate areas where all the elements of

(educational buildings, offices, student centres, exhibition halls, facilities, sports facilities, shops, community facilities etc.) are in close proximity, often easily accessible by pedestrian traffic. Campus has its own streets and open spaces where people can walk and move freely.

College campuses can be located in non-urban or urban areas. Their distribution varies in dependency on their location. Extra-urban campus has a tendency to large surface area (horizontal proliferation), while urban campus to meet with more vertical sprawl (multi-storey buildings, terraces). Extra-urban areas are generally more oriented to vehicular traffic, than in urban areas. In a number of sites is limited by the passage of vehicles, and vehicular traffic it is not eliminated. When solving transport links within the site appears to be the best walking and cycling.

College campuses are often areas with their own technical infrastructure, have their own energy facilities. In addition to energy, water and waste, college campuses are also major generators of traffic, which require large parking lots. By Tolley (1996) are the main effects of transport on the environment, habitat loss and green stereotypical environment (large parking areas), health effects on workers and students, and negative impacts on other transport (walking and cycling).

Universities also have an impact on neighbouring areas in several respects. Especially parking causes the increasing traffic impacts. It is important to minimize the effects of educational centre, so as not to disturb even the development neighbourhood. Parking students or staff moves into the vicinity campus, where parking is limited into residential area in the morning and afternoon. Conversely campus can be used for parking by residents from surroundings. Thus, both groups negatively affect each other. But the position is outstanding, parking restrictions on residents of surrounding neighbourhoods in the campus make quite simply, limited parking for students and staff around campus requires the use of sliding boundary stone or a more sophisticated method of paid parking.

Sustainable transport system is defined as the one that meet current needs of transport and



mobility, without compromising the ability of future generations to meet their own (Richardson, 1999). On campus can be understood as a sustainable transport planning initiatives for walking and cycling for transport and public transport systems.

## Results and discussion

Campus CULS Prague is located approximately 6 km north of the city centre of Prague (see Fig.1). CULS was founded in the first half of the 60s of the 20th century on the outskirts of the Prague and it means that is located in a suburban area type. It causes the generation of higher proportion of road transport. There are any access to university by a rail transport.

Campus of the Czech University of Life Sciences (CULS) Prague – internal transport links: The major problem is linked with cars' usage i.e. possibilities of their parking. Car parking space on campus is very demanding and with increasing motorization within the campus it calls for building

more and more new parking places. Campus is divided into a public free area (students, guests) and the area with permit accessible only (staff, post- doctoral students.). Parking areas are located unevenly due to the destination (most often near to individual faculty). This fact leads to the relocation of parked vehicles near campus CULS outside Prague, to hamper the movement of residents. This problem could be solved by the construction of a parking building or other common garages. Parking is not organised or control by some special directive. Capacity of public car parking places is filled up to their limit during the day. But it is not balanced, more attractive parking lots are filled quickly, parking on the others (remote ones) be filled later. However, the complex is achieved by full utilization of public parking lots after 9 hours (Fig.2), other vehicles illegally parked outside designated parking and traffic often prevent or restrict communication to a view of the pedestrian crossing. These results (Fig.2) were obtained traffic survey carried by authors of this paper.

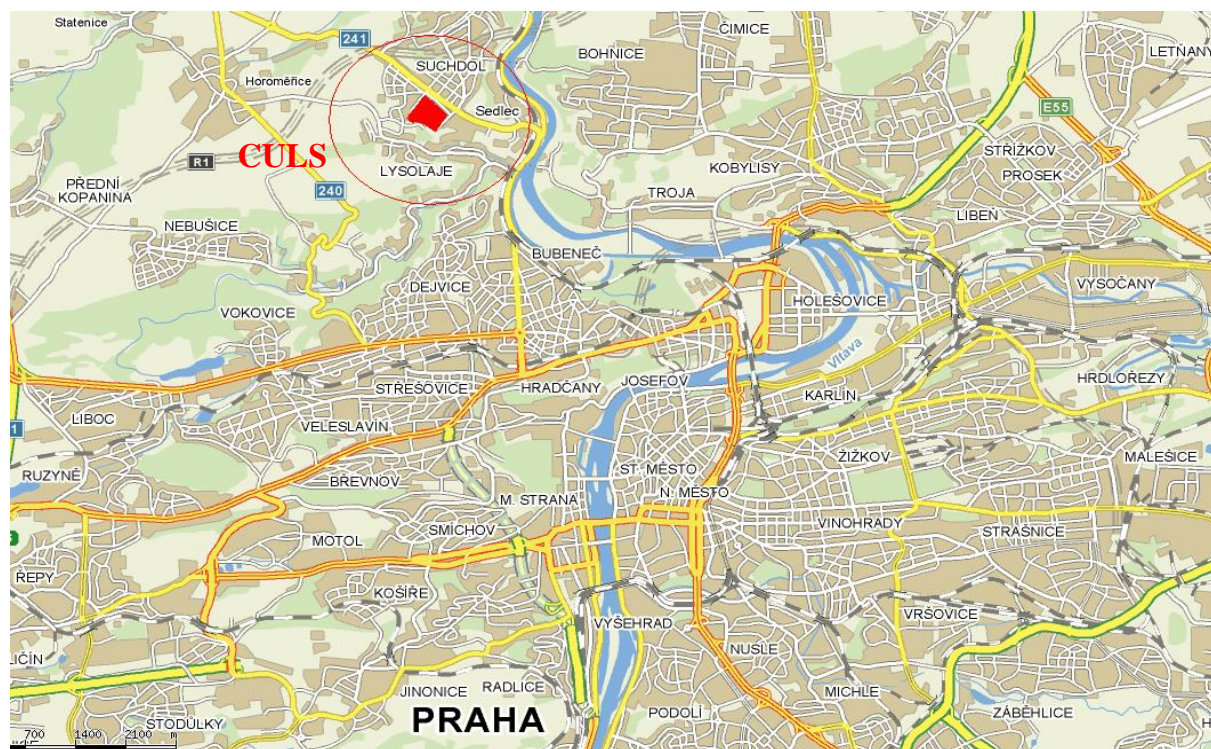


Fig.1 – Campus CULS Prague location

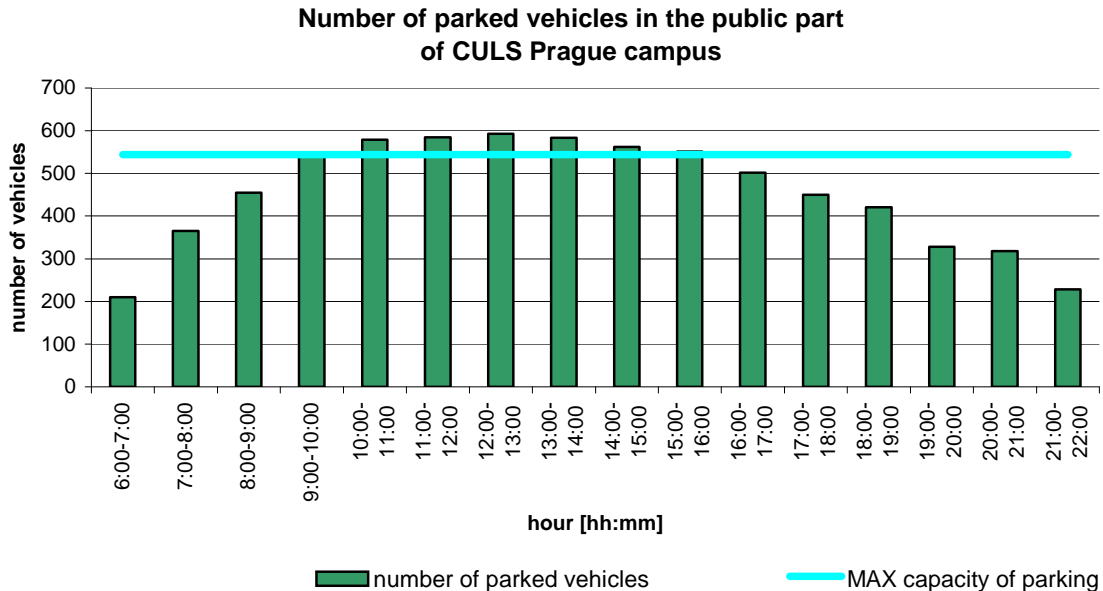


Fig.2. Number of parked vehicles in public part of CULS Prague campus (authors' survey)

The main result should be the proposal of parking design and vehicle movement in the CULS Prague campus, building facilities and organizational adjustments of traffic. The aim is to ensure the safe movement of pedestrians, cyclists and vehicles throughout the campus CULS Prague. At the same time on the basis of traffic surveys carried out to create the characteristic cross-traffic connections to assess the existing transport infrastructure and identify problematic places.

Campus CULS Prague - external transport links: As mentioned above, the resort is situated in a remote location from the city centre. A disadvantage of public transport is the missing mass public transport system (rail transport). Now the only public transport is realised by buses. Possibility of transferring to the subway is approx. 15 minutes away by bus. There is the possibility of transferring to the commuter rail (10 minutes by bus) but its potential is fully exploited by the carrier, especially in diametrically transport relations. So the last link on the way to campus

will stay bus service with its disadvantages as overcrowded vehicles i.e. traffic demand is always surge in the beginning or end of instruction. In contrast, outside these rush periods, demand is low. Availability of buses and varies from one extreme to another in case of high occupancy travel is inconvenient. It means that people deals with a travel to CULS Prague campus by passenger car transport. The number of cars is also visible surge in incoming traffic (Fig.3) i.e. in the morning. These results (Fig.3) were obtained from traffic survey carried by authors of this paper during the semester. Data for 24 hours are the average value of 10 days (normal workdays). Movement of vehicles on campus is high, so as to minimize pedestrian crossing streams (bus stop) with the arrival and departure routes of vehicles. Walking is often moving at a dose (collective output of the bus, the end of lectures, etc.), so it is necessary to ensure adequate pedestrian infrastructure.



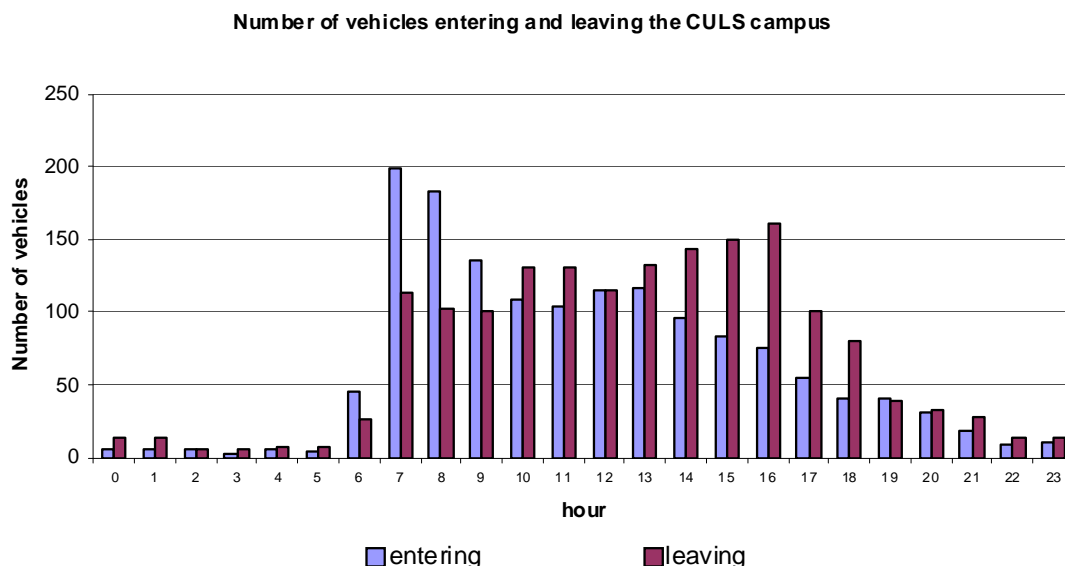


Fig.3 – Number of vehicles entering and leaving the CULS Prague campus (authors' survey)

## Conclusion

The solution of transport within the CULS Prague campus should be carried out with a strategic and coordinated approach. The proposal should be focused on more transport modes. The solution of transport should involve other possibilities as traffic calming, possibilities for disabled people etc. At the same time, it is important to improve external public transport to be competitive with a passenger car transport. Campus must become integral part of their neighbourhood in the way that people living around the campus would welcome its development.

## References:

- [1] Brown, J., Hess, D., Shoup, D., 2001. Unlimited access. *Transportation* 28,233–267.
- [2] Dulken, D., 1992. The very model of a suburban community, what we can learn from the university campus. *Planning* 58 (8), 24–25.
- [3] Farris, M., Radwan, A., 1989. A campus transportation alternative. *Transportation Quarterly* 43 (1), 89–99.
- [4] Newman, P., Kenworthy, J., 1999. *Sustainability and Cities—Overcoming Automobile Dependence*, Island Press, Washington, DC.
- [5] Poinsett, F., Toor, W., 2001. *Finding a New Way: Campus Transportation for the 21st Century*, 2nd ed, University of Colorado, Boulder.
- [6] Richardson, B., 1999. Towards a policy on a sustainable transportation system. *Transportation Research Record* 1670, 27–34.
- [7] Shoup, D., 1997. The high cost of free parking. *Journal of Planning Education and Research* 17 (1), 3–20.
- [8] Tolley, R., 1996. Green campuses: cutting the environmental cost of commuting. *Journal of Transport Geography* 4 (3), 213–217.
- [9] Turner, P., 1995. *Campus: An American Planning Tradition*, MIT Press, Cambridge.
- [10] Vuchic, V., 1999. *Transportation for Livable Cities*, CUPR, New Brunswick.

## PHOTO-OPTICAL IMAGE ANALYSIS AS AN ALTERNATIVE METHOD FOR DETECTION OF THE FERTILIZER PARTICLE SIZE DISTRIBUTION

MIROSLAV MACAK, LADISLAV NOZDROVICKY\*

Slovak University of Agriculture in Nitra, A. Hlinku 2, 949 76 Nitra, Slovakia,

Phone: +421 37 641 43 66, E-mail: [miroslav.macak@uniag.sk](mailto:miroslav.macak@uniag.sk);

[ladislav.nozdrovicky@uniag.sk](mailto:ladislav.nozdrovicky@uniag.sk)

### Abstract

In many branches of industrial production there is a need for a continual monitoring of the quality of manufactured product. Such requirements arise in the production of fertilizers, as the physical and mechanical properties of the fertilizers effect the quality of application provided by fertilizer spreaders. The aim of the presented paper was to compare suitability and applicability of the photo-optical image analysis with sieve analysis used for determination of the fertilizer particle size distribution. Photo-optical method was used by Grift a Hofstee, 1997 to study the fertilizer particle size distribution. These researchers have tried to measure the size and velocity of the flying particles in relation to the quality of the application of a centrifugal spreaders.

During our comparative experiments we have compared photo-optical method image analysis and sieve analysis. In experiments we have used the samples of granulated fertilizers NMgS produced by company DUSLO a.s. The sieve analysis was conducted according to national standard STN EN 1235 in laboratories of the Department of Machines and Production Systems at the Faculty of Engineering, Slovak University of Agriculture in Nitra.

### Introduction

Particle size distribution of the fertilizers belongs among the most important physical and mechanical property of fertilizers. It affects in high degree the quality of the work of centrifugal fertilizer spreaders. (Hofstee, 1993) In many case during fertilizers production process occur unwanted effects, that can negatively effect not only the chemical composition of the fertilizer particles but also the important physical and mechanical property of fertilizers. It is therefore necessary to find ways to best monitor the manufacturing process from the point of the quality of manufactured product.

The complete chemical characteristics of the fertilizer and its granulometric structure declared by manufacturer is given in Table. 1.

In order to study the particle size distribution of the fertilizers, as a basis physical and mechanical property of fertilizers we have used two methods. The first method was the sieve analysis, based on the national standard *STN EN 1235 – Solid fertilizers. Sieve analysis.* The seconf method was based on digital processing of the photo images of the fertilizer particles. Both methods have been implemented for the same sample of the fertilizers with weight 0,845 kg. The sampling of the solid fertilizers have been done according to the national standard *STN EN 1482 (Sampling of the solid fertilizers).*

### Material and Methods

For the laboratory experiments we have used the samples of the granulated fertilizer NMgS.

Table1 Basic characteristics of the NMgS fertilizer (Source: [www.duslo.sk](http://www.duslo.sk))

Fertilizer trade mark				Fertilizers type		Manufacturer			
NMgS 21-5-11				granulated		Duslo, a.s.			
Nutrition content				Particle size distribution					
Total nitrogen				21%		over 10 mm		0%	
Magnesium				5%		2 – 5 mm		min. 90 %	
Sulphur:				11%		under 1 mm		max. 1 %	

Procedure used for determination of the fertilizers particle size distribution by sieve analysis

1. Distribution of the basic sample of fertilizer into smaller parts. The weight of individual samples has been determined with regard to the national standard *STN EN 1235*, which determines the maximal load of the upper sieve during sieve analysis.
2. Sieve analysis by using of set of sieves and having a quadratic sieve mesh according to the standard *STN ISO 565* and sieving apparatus FRITSCH with the possibility of vertical and horizontal motion of the sieves. For the laboratory experiments there was selected seven experimental sieves within the range of basic sizes according to standard *STN ISO 565* to cover estimated particle size range. The sieves have been arranged in ascending order by the size of the mesh in direction from the top to the collector. The sample analysed was weighted with the accuracy of 0,01g. In the next step the sample has been put on the upper sieve and covered by the lid. The arranged sieves was then put on the sieving device. The duration of the sieving (10 minutes) was determined according to the above mentioned standard.
3. After the sieving the set of sieves was dismantled and the amount of the fertilizer captured on each sieve was weighed. Fertilizer particles captured in the mesh were added to the over-sieve portion of the given sieve. For the removing of the fertilizer particles from the mesh the soft brush was used not to damage any particles.
4. On the basis of the obtained data the over-sieve percentage share of individual fractions in given sample has been calculated. The final particle size distribution of each fraction was determined as an arithmetic mean value of individual over-sieve shares obtained from 10 replications.

Weight percentage of material that remains in the collector (bottom cup) and on each sieve ( $x_n$ ) after the sieving can be calculated by using the equation (1).

$$x_n = \frac{m_n}{m_t} \cdot 100 \quad (1)$$

where:  $m_n$  – weight of the fertilizer remained on the sieve  $n$ , g;

$m_t$  – total weight of fertilizer sample, g.

For the calculation of the total amount of the fertilizer under the sieve we have used the following equation:

$$c_n = \sum_{i=0}^{n-1} x_i \quad (2)$$

kde:  $c_n$  – total under-sieve share of share for the sieve  $n$  as a total weight percentage;

$x_i$  - weight percentage of the fertilizer remained on the sieve  $i$ .

For the determination of the fertilizer particle size distribution we have used also the photo-optic image analysis method. This method is based on the optical scanning of the fertilizer particles by using of digital camera and processing of the images by software Impor Basic 4.0, which is owned by Department of Machines and Production systems? Faculty of Engineering of the Slovak University of Agriculture in Nitra.

Procedure used for determination of the particle size distribution by using of photo-optic image analysis:

1. placing of the fertilizer samples on the platform,
2. shooting of individual samples (photo-camera, holder, over-head projector),
3. processing of the images (PC, software Impor BASIC 4.0),
4. recalculation of the data, obtained in pixels on the metric units (mm), (PC, software MS Office Excel 2003),
5. statistic processing of the data obtained (PC, software MS Office Excel 2003).

For the receiving of the digital images we have used a digital camera OLYMUS C-3000 ZOOM, which was mounted on the holder and during all experiments its setting (optical and digital zoom, etc) was constant. The fertilizer particles were placed on the white paper surface. In order to distinguish colour shades from the surface (white paper) we have paid attention to correct illumination of the paper surface. In first we have tested the lighting directed from the top in the direction perpendicular to the display area, but there occurred unwanted shadows. The lighting was not sufficient and the fertilizer particles could not be resolute from the display area by using of software. Better results we have

obtained when the over-head projector Meotar was used. As a display area we have used the projection surface of the over-head projector. The projection surface was covered by white paper and the bottom of the surface was transilluminated from the bottom

The fertilizer particles were placed on the display area in such a way that there were no contacts among fertilizer particles. If one particle has contact with other particle the software identifies such object as a one big particle and it means inaccuracy – unjustified increase of the share of higher fertilizer particles fractions.

After copying of the photos from the memory card to the PC the digital processing of images was done by using of software Impor Basic 4.0. Output data characterizing the dimensions of the fertilizer particles were

presented in the format of coordinates of Gaussian plane. The values of the  $x$  and  $y$  coordinates were calculated on the basis of simple difference between the maximal and minimal value.

The numerical values of these coordinates are given in pixels (pixels) and therefore it was necessary to make the conversion. The conversion coefficient was found using the calibration image, done by photographing of the metric measure (translucent ruler). By using of the software Impor Basic 4.0 at the beginning of the measurements the conversion coefficient was determined (see Fig. 1). Settings of the camera have been the same as they were used for photograph Camera settings were the same as when shooting granular fertilizer.

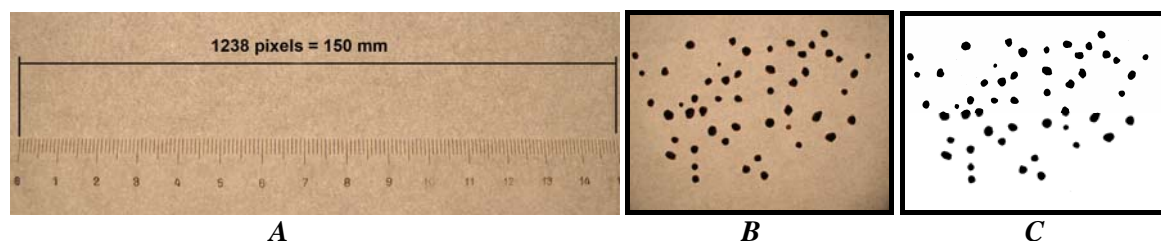


**Fig. 1** *A* Photo used to determine the conversion rate (conversion coefficient) for the recalculation of the metric units and the image pixels; *B* Photo of the fertilizer granules before the conversion; *C* Photo of the fertilizer granules in black-and-white shades after the conversion

The calculation of the coordinates (dimensions of the fertilizer particles) was done according to equation (4) and (5):

$$PK = \frac{1238}{150} = 8,3333 \Rightarrow 1 \text{ mm} = 8,3333 \text{ image pixels} \quad (3)$$

$$X = \frac{X_{\max} - X_{\min}}{PK}, \text{ mm} \quad (4)$$

$$Y = \frac{Y_{\max} - Y_{\min}}{PK}, \text{ mm} \quad (5)$$

where: PK – conversion coefficient,

$Y_{\max}$  – maximal value of the component of the  $y$  coordinate in image pixels,

$Y_{\min}$  – minimal of the component of the  $y$  coordinate in image pixels,,

$X_{\max}$  – maximal value of the component of the  $x$  coordinate in image pixels,

$X_{\min}$  – minimal of the component of the  $x$  coordinate in image pixels.

After the conversion of the data to the metric system we have obtained values of the coordinates  $X$  and  $Y$ , which presents the numerical data in metric units – dimensions of the fertilizer particles in millimetres. As each fertilizer particle was characterised by two values, it was necessary to determine the method of selection only one value from two values. The selected value will represent the given particle during evaluation of the fertilizer particle size distribution. Our aim was to compare the image analysis method with the sieve analysis method which is based on the sorting of the fertilizer particles according to their smallest dimensions. Therefore we have decided to prefer the smaller value when selecting from  $X$  or  $Y$  dimension. Such filtering of the data, as well as other calculations have been done in Microsoft's Excel™ spreadsheet programme.

## Results and Discussion

### Sieve analysis

The data obtained from all experiment replications of individual fertilizer fractions shares have been summarised and the results are presented in Table 2. Before the providing of the sieving analysis the weight of the fertilizer sample was determined (in Table 2 it is the value 844,73 g). The percentage difference between the weight of samples before and after the sieve analysis is 0.02%.. This value satisfies the requirement of the standard, which says that during the measurement may not be the weight loss of fertilizer more than 1%.

Standard STN 65 4804 presents the particle size distribution for the various types of fertilizers in order to declare the fertilizers quality. As it can be seen from the Table 5, our experiments have confirmed that fertilizers we

have used for measurements match the requirements given by respective standard.

### Photo-optic image analysis

On the Fig. 1 A,B there are presented examples of the images converting. This converting was important as our aim was to achieve the highest accuracy (high colour shades diversity between the background and fertilizer particles) in order to identify individual particles of the fertilizers during scanning of individual photos by software Impore Basic 4.0.

Output data from the software Impor Basic 4.0 were recorded to the formate \*.txt. In order to simplify the comparing of the results obtained, the borders of individual intervals for the group data sorting, was the same as they were used for sieve analysis.

Table 2 Results of the sieve analysis, fertilizer NMgS

Size interval, mm	Sieve, mm	Under-sieve share, %	Weight, g	Cumulative frequency, g	Over-sieve share, weight percentage, %	Cumulative weight percentage, %
<10 ; and more)	10	100,00	0	0	0,00	0,00
<8 ;10)	8	99,98	6,23	6,23	0,74	0,74
<5 ; 8)	5	94,87	64,18	70,41	7,60	8,34
<4 ; 5)	4	46,90	474,7	545,11	56,21	64,54
<3,15 ; 4)	3,15	6,34	257,74	802,85	30,52	95,06
<2 ; 3,15)	2	0,12	40,08	842,93	4,75	99,81
<1 ; 2)	1	0,04	1,25	844,18	0,15	99,95
(0 ; 1)	0	0	0,39	844,57	0,05	100,00
Total			844,57			

Table 3 Data sorted for the photo-optic analysis

Interval borders, mm		Absolute frequency	Relative frequency	Absolute cumulative frequency	Relative cumulative frequency
DH	HH	ni, pcs	fi, %	Ni, pcs	Fi, %
10	and more	0	0,00	0	0,00
8	10	3	0,03	3	0,03
5	8	1506	14,57	1509	14,60
4	5	4061	39,28	5570	53,88
3,15	4	3929	38,01	9499	91,88
2	3,15	809	7,83	10308	99,71
1	2	30	0,29	10338	100,00
0	1	0	0	0	0
Total		10338	100	—	—



### Comparison of the both methods

Table 4 Comparison of the measured and declared values of particle size distribution

Particle size distribution	Values declared by manufacturer	Standard STN 65 4804 requirements	Measured values	
			Sieve analysis	Photo-optic analysis
Less than 1 mm	max 3%	max 3%	0,15 %	0 %
2 – 5 mm	min 90%	min 90%	91,47 %	85,11 %
More than 10 mm	0%	0%	0 %	0 %

In the Table. 4 there are presented limit values, which are required both by standard and production process. It is necessary to note that respective standard, which determines the limit values of particle size distribution of the solid fertilizers, determines also the methods how to measure the particle size distribution – sieve analysis. It is possible to state, that the fertilizer used in tests matches requirements defined by standard and manufacturer correctly declares its quality.

When comparing sieve analysis and photo-optic analysis it is necessary to take into account that, final values of the fertilizer particle size distribution are in the case of sieve analysis expressed in weight percentage of the fertilizer distributed on the individual sieves during sieving. In the case of photo-optic analysis the obtained results represent the frequency of the fertilizer particles occurrence in respective granulometric fractions, which was determined

on the basis of statistical classification of the data into different size intervals

On the Fig. 2 there is presented the graphical comparison of the particle size distribution for the fertilizer NMgS. Bigger differences obtained by both methods can be observed in bigger size fractions (3,15 – 4; 4 – 5; 5 - 8). Such results can be explained by the fact that the position of fertilizer particles effects the final results as the digital image analysis based on the software Impor BASIC 4.0, which allows to scan the diameter of the particles only in two average particle only in two perpendicular axes (x and y). Bigger fertilizer particles had bigger shape non-uniformity and during the digital image scanning the software programme was not able always to record the smallest dimensions of the fertilizer particle. Smaller particles of fertilizer are more close to the ideal spherical shape, so the differences in these lower fractions were not so great. That uncertainty could be eliminated by measuring of particles in multiple axes.

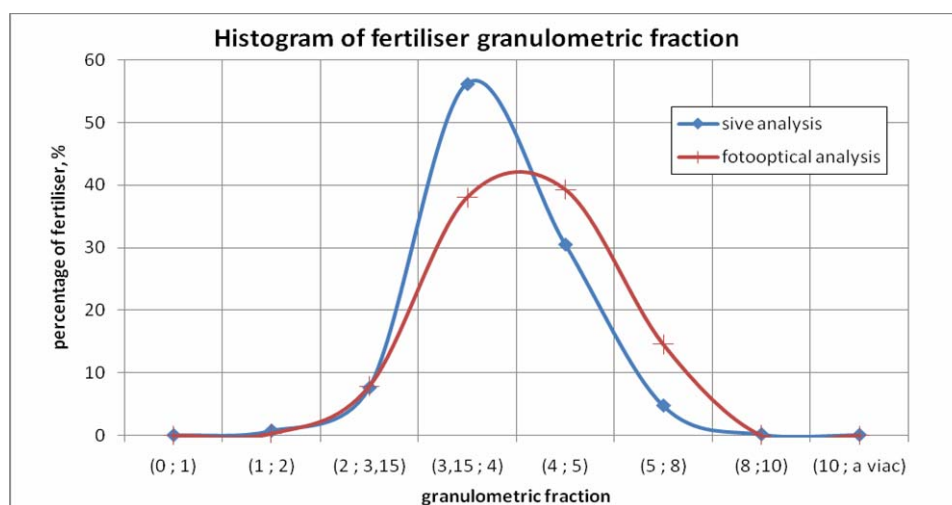


Fig. 2 Particle size distribution of the fertilizer NMgS by sieve analysis and photo-optical analysis



## Conclusion

Measuring and evaluation of the physical and mechanical properties belong among the basic activities related to the quality measurement in solid fertilizer production. Particle size distribution can be considered as a most important fertilizer property as it effects not only storage and handling operations but also the quality of the fertilizer application by means of centrifugal fertilizer spreaders. The results of the sieve analysis of the given sample of the granulated fertilizer confirm the quality declared both by fertilizer manufacturer and respective standard. The results presented in Table 4 show that in the case of sieve analysis the share of granulometric fraction 2 – 5 mm was 91,47 % (weight percentage), while in the case of photo-optic analysis it was only 85,11 % (percentage frequency). The final data obtained by photo-optic analysis can be considered as a challenge for new possibilities of monitoring and inspection of the fertilizer particle size distribution within the process of fertilizer production.

## Reference

- [1] Grift, T.E. - Hofstee, J.W. 1997. Measurement of velocity and diameter of individual fertilizer particles by an optical method. Transactions of the ASAE, VOL. 40(1):21-27.
- [2] Hofstee, J.W. 1993. Physical properties of fertilizer in relation to handling and spreading. 145 s. ISBN 90-5485-149-X
- [3] Impor Basic 4.0 Software – Digital Image Procesing. Kvant s.r.o. FMFI UK Mlynská dolina, 842 48 Bratislava, Slovakia, Europe
- [3] STN EN 1235 – Tuhé priemyselné hnojivá sitová skúška
- [4] STN EN 1235/A1 – Tuhé priemyselné hnojivá sitová skúška (Príloha A1)
- [5] STN ISO 3310-1 – Skúšobné sitá. Technické požiadavky a skúšanie. 1. časť: Skúšobné sitá z kovovej tkaniny
- [6] STN ISO 565 – Skúšobné sitá. Kovové tkaniny, dierovaný plech a elektroformované fólie. Menovité veľkosti otvorov
- [7] STN EN 1482 - Odber vzoriek tuhých priemyselných hnojív.
- [8] STN 65 4804 – Hnojivá, pestovateľské substráty, pôdne pomocné látky. Zoznam typov, požiadavky na označovanie a balenie.

## EVALUATION OF SMALL COMBUSTION EQUIPMENTS FOR SOLID BIOMASS

MALAŤÁK JAN<sup>1</sup>, PETR JEVIČ<sup>2</sup>, PETR VACULÍK<sup>1</sup>

<sup>1</sup>Czech University of Life Sciences Prague, Faculty of Engineering, Department of Technological Equipment of Buildings, Kamýcká 129, 165 21 Praha 6 - Suchbátka

<sup>2</sup>Research Institute of Agricultural Engineering – Drnovská 507, 161 01 Prague  
Czech Republic

### Abstract

Together with the foreseeable exhaustibility of fossil energy sources the importance of renewable energy sources is growing and becoming one of the main conditions of sustainable development not only of agriculture, but also of the whole society.

The submitted article addresses the urgent questions regarding the use of biomass as a fuel for combustion equipment of the heat output up to 25 kW. The article is based on the determined elemental analyses of four samples of fuel taken both from the wood mass and vegetal biomass. These samples underwent the stoichiometric analysis of fuels. After the stoichiometric analysis the heat-emission characteristics are determined on two combustion equipments.

The results of thermal-emission analyses show higher values of nitrogen oxides, sulphur and chlorine concentrations in the vegetal biomass compared to the analyzed wood mass. The emission concentrations of carbon monoxide for wood fuels and vegetal biomass also depend on the type of combustion equipment and setting of combustion air volume.

**Key words:** biomass, chemical analysis, stoichiometric analysis, calorific value, emission

### 1. Introduction

The economic growth in less developed parts of the world (China, India etc.) is attended by increasing consumption of energy materials and energy itself. Energetics is becoming one of the limiting factors of further development of the countries. The basic contemporary tasks are to reduce the strategic dependence on oil and natural gas supplies from danger regions and to arrange the reduction of CO<sub>2</sub> emissions worldwide even if the consumption of energy will grow (1).

In the long term perspective of a sustainable development it is very important to use the energy resources in the most efficient way. Of course also the use of financial "resources" should be optimized in order to reduce as much as possible the impacts on human health and the environment, while the created abundance is becoming more easily available to all parts of the world's population. In the medium-term perspective the climate changes are influenced by the emissions of greenhouse gases from human activities. These changes should be appropriately identified (2 and 3).

The fossil fuels can be partially replaced with the solid biofuels; thereby the volumes of

waste arising from fossil fuels extraction and processing are reduced, which means a contribution to an increased efficiency of resources. It can be expected that solid fuels based on biomass will reduce the emissions of fossil carbon into the atmosphere and similarly they will be reduced the emissions of greenhouse gasses from anthropogenic activities. Therefore the solid biofuels based on biomass constitute the source of storable solar energy (4, 5 and 6).

If it has to be decided whether the biomass is suitable for burning in a particular type of combustion equipment and to assess the quality of the biofuels from the phytomass in view of their use is necessary to know the properties of biofuels that characterize them sufficiently. From the energy perspective the elemental and stoichiometric analyses are the crucial in assessing. The fuel characteristics are supported by the stoichiometric calculations of the combustion processes and any thermal calculation is based on them. They are particularly important for solving many problems in the design practice as well as for controlling the work of existing combustion plants (4 and 7).

In the article there are defined other options and limit values of the utilization of solid biomass energy. Therefore it is based on the chemical composition of used fuels, ashes, stoichiometric calculations and the operational parameters of a given type of combustion equipment.

## 2. Methods

The article is mainly based on elemental and stoichiometric analysis. The resulting values of the stoichiometric analysis are inserted into the

equations for pollutant concentrations conversion and into the equations for determining the coefficient of excess air. From the stoichiometric analysis first of all the theoretical volume concentration of carbon dioxide in dry flue gas, the theoretical volume of dry flue gas and the theoretical volume of air for complete combustion of fuels are inserted into these relations.

The analyzed wood fuels and vegetal biomass according to the CEN / TS 15234 specification are listed in Table 1.

**Tab. 1** Analyzed wood fuels and vegetal biomass (specification according to CEN/TS 15234)

Wood fuels	Vegetal biomass
Forest wood chips (spruce) – pellets (Ø 10 mm)	Energy sorrel– pellets (Ø 11 mm)
Poplar – pellets (Ø 10 mm)	Knotweed – pellets (Ø 11 mm)

**Tab. 2** Chemical analysis of original samples of fuels taken from the wood and vegetal mass

Sample		Symbol	Forest wood chips (spruce) – pellets (Ø 10 mm)	Poplar – pellets (Ø 10 mm)	Energy sorrel– spruce pellets (Ø 11 mm)	Knotweed – pellets (Ø 11 mm)
Water content	(% wt.)	$W_t^r$	6,79	6,17	7,95	5,93
Ashes	(% wt.)	$A^r$	3,02	4,04	4,45	3,99
Combustible matter volatile	(% wt.)	$V^r$	75,55	75,43	70,07	72,03
Combustible matter non-volatile	(% wt.)	$(NV)^r$	14,64	14,36	17,53	18,05
Combustion heat	(MJ.kg <sup>-1</sup> )	$Q_s^d$	18,74	18,2	16,54	17,62
Calorific value	(MJ.kg <sup>-1</sup> )	$Q_i^r$	17,18	16,84	15,16	16,31
Carbon C	(% wt.)	$C_t^r$	47,37	46,16	42,7	45,87
Hydrogen H	(% wt.)	$H_t^r$	6,4	5,51	5,42	5,33
Nitrogen N	(% wt.)	$N_t^r$	0,19	0,52	1,65	0,29
Sulphur S	(% wt.)	$S_t^r$	0,01	0,03	0,11	0,03
Oxygen O	(% wt.)	$O_t^r$	36,2	32,54	37,61	38,49
Chlorine Cl	(% wt.)	$Cl_t^r$	0,04	0,03	0,11	0,07

The determination of the chemical properties is the first task of the solution of the assessed fuel samples as follows:

- The water content in the original sample  $W$  (% wt.) – the method of drying in an oven - the water content in the analytical test sample (CEN / TS 14774-3);
- The ashes content in the original sample  $A$  (% wt.) (CEN / TS 14775);
- Determination of combustion heat  $Q_s$  (MJ.kg<sup>-1</sup>) (CEN / TS 14918);

- The non-volatile and volatile combustible matter  $V^{daf}$  and  $NV^{daf}$  (% wt.);
- The content of carbon, hydrogen and nitrogen - instrumental methods (CEN / TS 15104);
- The content of oxygen, sulphur and chlorine (% wt.).

The elemental analyses are developed in the form of services provided by the accredited laboratory: Institute for research and use of fuels - Prague Běchovice and Chemical Technology College (VŠCHT) in Prague - Energy institute.

The resulting values of the elemental analysis for individual samples of fuel taken from wood and vegetal mass are given in Table 2.

The chemical properties are followed by the stoichiometric analysis of combustion processes that supports the characteristics of fuel and constitutes the basis for any thermal calculation. This analysis is particularly important for addressing a range of problems in the design practice or controlling the work of existing combustion equipments. This analysis will identify:

- The calorific value of the sample  $Q_i$  ( $\text{MJ.kg}^{-1}$ );

- The oxygen (air) volume required for complete combustion of the sample ( $\text{kg.kg}^{-1}$ ), ( $\text{m}^3\text{N.kg}^{-1}$ );

- The quantity and composition of flue gas ( $\text{kg.kg}^{-1}$ ), ( $\text{m}^3\text{N.kg}^{-1}$ );

- The specific weight of flue gas (% wt., % Ob.).

The stoichiometric analysis is converted to the standard conditions and reference oxygen content in the flue gas. Calorific value of fuel in the calculations is given by the calorific value of the original sample, i.e. when taken the sample in the original condition. The resulting values of the stoichiometric analysis are shown in Table 3.

**Tab. 3** The stoichiometric analysis of the original fuel samples under normal conditions and reference oxygen content in the flue gas  $O_r = 11\%$

	Volume combustion	Forest wood chips- spruce pellets (Ø 10 mm)	Poplar – pellets (Ø 10 mm)	Energy sorrel– pellets (Ø 11 mm)	Knotweed – pellets (Ø 11 mm)
$O_{\min}$	Theoretical volume of oxygen for a complete combustion ( $\text{m}^3\text{N.kg}^{-1}$ )	0,99	0,94	0,83	0.88
$L_{\text{actual}}$	The actual volume of air for complete combustion ( $\text{m}^3\text{N.kg}^{-1}$ )	9,85	9,39	8,35	8.82
$n$	Coefficient of excess air (-)	2,10	2,10	2,10	2.10
$v_{\text{sp}}^s$	Volume quantity of dry flue gas ( $\text{m}^3\text{N.kg}^{-1}$ )	9,75	9,31	8,32	8.79
$\text{CO}_{2\text{max}}$	Theoretical volume of carbon dioxide in dry flue gas (% vol.)	19,34	19,57	20,26	20.59
$\text{CO}_2$	Carbon dioxide (% vol.)	8,06	8,28	8,49	8.70
$\text{SO}_2$	Sulphur dioxide (% vol.)	0,00	0,00	0,01	0.00
$\text{H}_2\text{O}$	Water (% vol.)	10,88	10,26	11,07	10.39
$\text{N}_2$	Nitrogen (% vol.)	70,32	70,76	69,79	70.20
$\text{O}_2$	Oxygen (% vol.)	9,91	9,95	9,82	9.89

The setting of emission concentrations of individual flue gas components is an important task. The measurements must be carried out in accordance with ČSN 07 0240 "Hot water and low pressure steam boilers - basic provisions", with ČSN 124070 "Separating equipment - Methods of variables measurement", with ČSN 44 1310 "Identification of analytical indicators and formulas for analyses results conversion to different states of fuel" and with ČSN 38 5509 (the values of molecular weight and molar volume).

The device Madur GA-60 is used for the determination of emission concentrations of individual flue gas components developed during the combustion of used vegetal biomass and wood mass samples. This is a multi-purpose

analyzer of flue gas. Its principle is based on the use of electrochemical converters. The standard equipment includes the converters for analysis of following flue gas components: oxygen ( $\text{O}_2$ ), carbon monoxide (CO), nitric oxide (NO), nitrogen dioxide ( $\text{NO}_2$ ), sulphur dioxide ( $\text{SO}_2$ ) and hydrogen chloride (HCl).

All volumes and weights of the combustion air and flue gas are given under so-called normal conditions, i.e. at  $t = 0^\circ\text{C}$  and pressure  $p = 101,325\text{ kPa}$  and to the reference content of oxygen in the flue gas  $O_r = 11\%$ .

The resulting concentrations of flue gas in ppm from the analyzer Madur GA 60 are converted into normal conditions and into  $\text{mg.m}^{-3}$  and the reference volume of oxygen in the flue gas that is  $O_r = 11\%$  for the used

equipment according to the specified decree and directive. The average resulting concentrations are shown in Table 5 and are compared with the emission limits according to directive No. 13 - 2006 (this directive applies to appliances with the definition of the hot water boilers for combustion of biomass with manual or automatic supply of nominal output up to 300 kW according to ČSN 07 0240 and ČSN EN 303-5). These resulting average values are determined in the whole range of measurement of individual samples.

For the actual measurements there are selected two types of representative combustion equipments:

- The retort stoking (lower stoking) – the pellets are pushed by the screw feeder through the retort (knee) into the combustion chamber.
- The gravity stoking – the pellets are pushed by the screw feeder from the reservoir above the grate on which they then fall down.

This is automatic hot water combustion equipment with the heat output of 25kW for solid fuels in the form of pellets intended primarily for heating family houses, cottages, office buildings, small business premises, etc.

### 3. Results and discussion

The resulting values from the chemical analysis of the original samples taken from wood and vegetal mass are given in Table 2. The values selected from the stoichiometric analysis carried out with the original samples of fuel under normal conditions and at the reference oxygen content in flue gas  $O_r = 11\%$  are shown in Table 3. In Table 4 there are shown the average concentrations from the thermal-emission measurements of analyzed samples that were carried out on two different types of combustion equipment with heat output of 25kW. The graphic evaluation of carbon monoxide and carbon dioxide in dependence on the excess air coefficient for each sample is shown in Figure 3.

In the selected samples of fuels in terms of emission concentration the quantities of sulphur, nitrogen and chlorine are the most decisive. At the samples there is apparent an increase in nitrogen emissions since the energy plants have

higher values of nitrogen in the fuel (Table 3) compared to the fossil fuels. Especially by an increased content of this element the use of these fuels is restricted.

Sulphur during the combustion largely goes over into the gas phase as  $SO_2$  and  $SO_3$ . The sulphur emissions at heat installations for the use of the solid fuels from renewable resources in terms of limit values usually do not constitute any problem, which is confirmed by the selected samples see Table 3. The corrosive behaviour can constitute the decisive factor of sulphur concentration in the fuel. Other values of the elemental analysis meet the optimal parameters for the use of biofuels in the combustion equipment (2 and 5).

The contents of water and ashes are the most determining for the thermic use of fuels. The range of all water content in the samples is quite low, which has a positive contribution to the fuels calorific value. By the content of water and ashes the thermal properties of the examined samples are significantly influenced and subsequently both the selection and configuration of the combustion equipment are influenced.

The vegetal biomass compared to the wood mass contains more ashes as it is clear from the results (Table 2), which can cause an increased emphasis on the removal of solid residues after combustion and increase in the the quantity of solid emissions.

The values resulting from the stoichiometric analysis show very good thermal - emission parameters of examined samples. As it results from the stoichiometry of examined fuels the selection and design of the combustion equipment are influenced by the calorific value, water content and energy density. The concentrations of N (nitrogen), S (sulphur) and Cl (chlorine) in the samples are relatively very broad, which is confirmed by the carried out analyses of samples. The values resulting from the stoichiometric analysis serve for further necessary calculations of thermal efficiency and heat losses of the combustion equipments, but mainly they serve for control and optimization of the combustion equipment.

**Tab. 4** The average concentrations of the thermal-emission measurement ( $O_2=11\%$ )

		Flue gas temper ature	O <sub>2</sub>	CO <sub>2</sub>	n	CO	NO	SO <sub>2</sub>	HCl	NO <sub>x</sub>
		°C	%	%	-	mg.m <sup>-3</sup>	mg.m <sup>-3</sup>	mg.m <sup>-3</sup>	mg.m <sup>-3</sup>	mg.m <sup>-3</sup>
Forest wood chips (spruce) pellets (Ø 10 mm) – retort stoking	Average	280,89	8,80	11,11	1,75	916,00	140,93	31,98	1,73	172,86
	Directive no. 13 – 2006					2000		60		250
Forest wood chips (spruce) pellets (Ø 10 mm) – gravity stoking	Average	231,39	15,27	5,27	3,93	1006,1	415,13	-	412,04	509,39
	Directive no. 13 – 2006					2000		60		250
Poplar – pellets (Ø 10 mm) – retort stoking	Average	251,50	6,94	12,98	1,63	4600,8	116,18	3,87	116,29	143,71
	Directive no. 13 – 2006					2000		60		250
Poplar – pellets (Ø 10 mm) – gravity stoking	Average	290,58	13,96	6,48	3,05	1612,1	316,71	-	314,22	388,46
	Directive no. 13 – 2006					2000		60		250
Energy sorrel- pellets (Ø 11 mm) – retort stoking	Average	292,06	8,48	11,56	1,76	711,78	91,73	45,48	92,70	112,51
	Directive no. 13 – 2006					2000		60		250
Energy sorrel- pellets (Ø 11 mm) – gravity stoking	Average	282,67	12,66	7,68	2,66	656,21	106,87	53,18	106,3	131,08
	Directive no. 13 – 2006					2000		60		250
Knotweed – pellets (Ø 11 mm) – retort stoking	Average	238,67	11,84	8,43	2,35	1122,87	141,83	-	140,71	173,96
	Directive no. 13 – 2006					2000		60		250
Knotweed – pellets (Ø 11 mm) – gravity stoking	Average	279,49	13,89	6,54	3,18	928,94	242,15	-	240,24	297,00
	Directive no. 13 – 2006					2000		60		250

The resulting average emission concentrations of carbon monoxide on combustion equipment with lower stoking according to directive no. 13-2006 achieve several times higher emission concentrations at the poplar pellets. In case of other measurements the average emission concentrations of examined samples are optimal. The resulting average emission concentrations of carbon monoxide of individual samples of fuels at the combustion equipments are given in Table 4.

The coefficient of excess air is an important parameter influencing the combustion efficiency. The combustion equipment with lower fuel supply has an optimal average coefficient of excess air in contrast to the combustion

equipment with gravity stoking that at all examined samples of fuels has a high value of the coefficient of excess air. The resulting average values of the coefficient of excess air of individual fuel samples at the combustion equipments are given in Table 4.

On combustion equipments there are defined the dependencies of carbon dioxide – the product of perfect combustion- on the coefficient of excess air and these dependencies are similar in all cases. With increasing volume of air the concentration of carbon dioxide decreases from the maximum to the minimum concentration, which leads to cooling the flame and dilution of flue gas with the combustion air (Fig. 1).



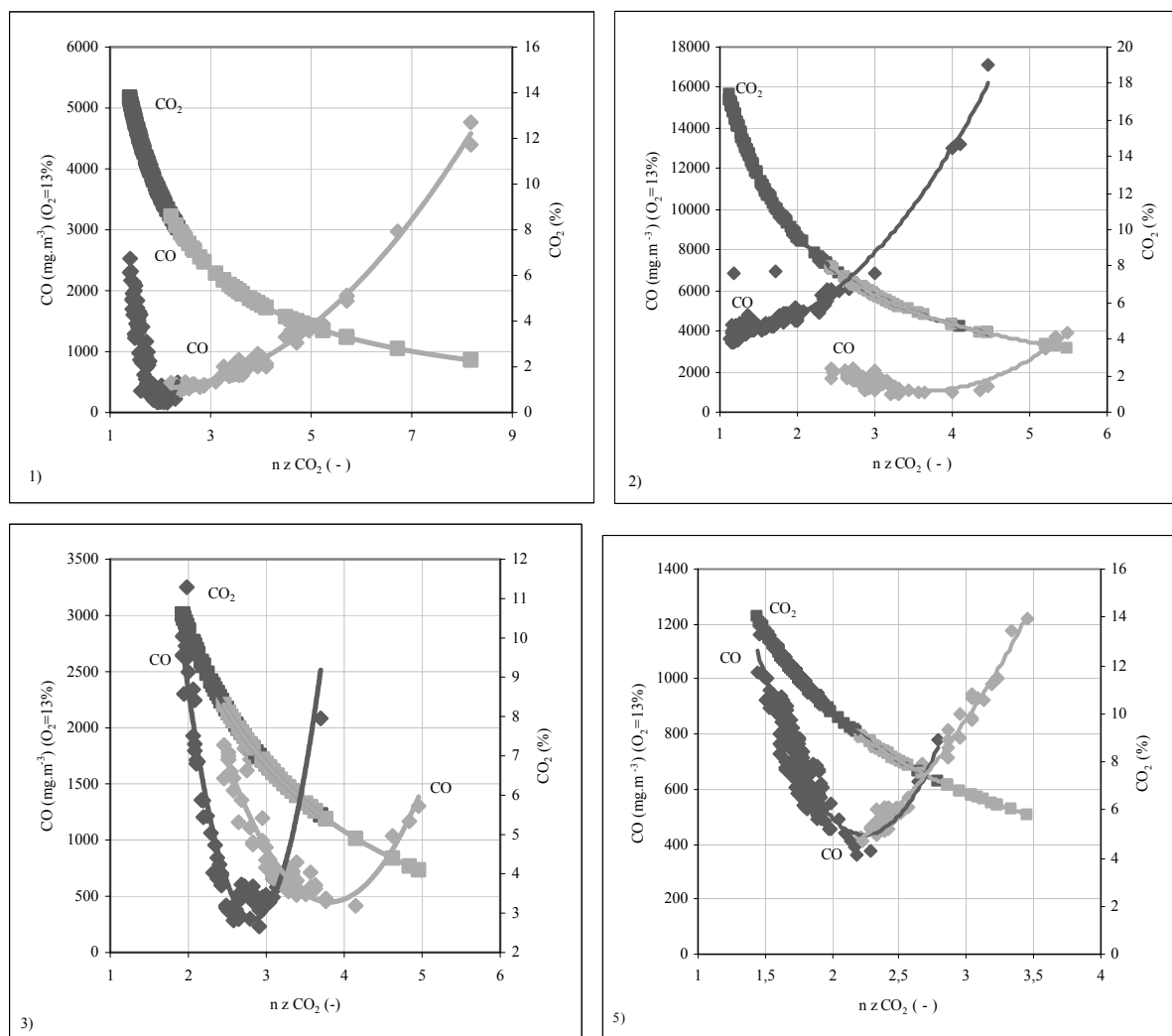


**Fig. 1** The measured emission concentrations of CO and CO<sub>2</sub> depending on the coefficient of excess air and combustion equipment

**Legend:** 1) Forest wood chips (spruce) pellets (Ø 10 mm); 2) Poplar – pellets (Ø 10 mm);  
4) Knotweed – pellets (Ø 11 mm); 5) Energy sorrel– pellets (Ø 11 mm);  
◆ lower stoking; ◆ gravity stoking.

Carbon monoxide (Fig. 1), the product of incomplete combustion, at every examined sample of fuel and the combustion equipment in the dependency on the coefficient of excess air at first in the area with a very low coefficient of excess air is decreasing down to the optimal values, but after the optimal values of the coefficient of excess air have been exceeded there occurs gradual increase of carbon monoxide up to the maximum concentration. This process can be observed at all fuels except for poplar pellets at the combustion equipment with lower fuel supply, when at these measurements from the beginning the carbon monoxide is gradually increasing. The reason

why there occurs a different process of combustion at the fuel samples can be attributed to multiple factors such as the calorific value, the proportion of volatile matter in the sample and the volume of combustion air brought into the combustion chamber. Also in the combustion equipment there can occur an insufficient mixing of volatile flammable substances with the combustion air thus an insufficient fire penetration on the refractory retorts.

At present there arises the question regarding the biomass utilization and generation of dioxins. Dioxin is the name for the two groups of compounds being close to each other regarding their structure and chemical behaviour. These

groups are polychlorinated dibenzo-p-dioxins (PCDD) and polychlorinated dibenzofurans (PCDF); the first group includes about seventy and the other about one hundred and thirty individual substances. Dioxins belong to the most toxic substances on the Earth and even at concentrations of one to a billion they are life-threatening (they are seventy times more toxic than potassium cyanide). Moreover they are the substances with carcinogenic and teratogenic affects (capable to harm unborn fetus) (12).

The cause of increased production of hydrogen chloride emissions at individual combustion equipments can be attributed especially to the volume of combustion air and the quantity of chlorine in the fuel itself. The greater is the volume of brought combustion air (excess air coefficient, see Table 4), the greater is the generation the hydrogen chloride emissions.

On the basis of analyses we also can draw a conclusion that during the combustion the boiler spaces should be maximally burdened with the vegetal biomass. But it is common that within the phytomass of herbs the city and municipal heating plants are heated with straw most frequently without taking into account that this heating might be inappropriate.

Washing (leaching) with water is one of the possibilities to reduce these high chlorine concentrations from the vegetal biomass in order to prevent the chlorine effect on the combustion equipment. As recommended by the author Khor, during the washing there is released an artificial fertilizer rich in chlorine (8 and 9).

Therefrom result the requirements for the quality of fuels from biomass. A high quality of pellets from biomass is mainly required for combustion in small combustion equipments. For larger combustion equipments that are equipped with gas cleaning and combustion controlled by process the fuel quality is not critical. It is therefore important to distinguish two types of pellet fuels it means those for industrial and for small domestic combustion equipments (13).

The use of already available sensors for monitoring the carbon oxide is another way to reduce emissions. The use of sensors for unburnt hydrocarbons especially for carbon monoxide in combination with a lambda probe can provide the combustion equipment with an optimal performance with respect to emissions and the efficiency of combustion

equipment regardless the changes in fuel quality and heat outputs.

*This paper was originated within the solution of IGA and CIGAs internal grants at the Czech Agricultural University in Prague.*

## References:

1. COM/2007/0723 final: Communication from the Commission to the Council, the European Parliament, the European Economic and Social Committee and the Committee of the Regions - A European strategic energy technology plan (SET-plan) - 'Towards a low carbon future'.
2. Hedberg, E.; et al.: Chemical and physical characterization of emissions from birch wood combustion in a wood stove. In: Atmospheric Environment 36 (2002), Published by Elsevier Ltd., pp. 4823–4837, ISSN: 1352-2310
3. Malat'ák, J.; Karanský, J.; Altman, V.; Jevič, P.; Gálik, R.: 2007. Alternative fuels – agricultural waste material utilization. In: Agriculture – journal for agricultural sciences, roč. 53, 2007, č. 1, pp. 38-48. ISSN 0551-3677
4. Jevič, P.; Hutla, P.; Malat'ák, J.; Šedivá, Z.: Efficiency and gases emissions with incineration of composite and one-component biofuel briquettes in room heater. In: Research in Agricultural Engineering, č. 3, roč. 53 (2007), Prague 2007, s. 94-102, ISSN 1212-9151
5. Malat'ák, J.; Vaculík, P: Biomasa pro výrobu energie. ČZU v Praze, Technická fakulta, tisk. Powerprint, Praha 2008, 206 s., ISBN: 978-80-213-1810-6
6. Fiedler, F.; Persson, T.: Carbon monoxide emissions of combined pellet and solar heating systems. In: Applied Energy, 86, 2009 Published by Elsevier Ltd., pp. 135–143, ISSN: 0306-2619
7. Jevič, P.; Malat'ák, J.; Šedivá, Z.: Tuhé alternativní palivo z pohledu rozdílu mezi jeho biologicky rozložitelnými a biogenními složkami. In: 4. Zemědělská technika a biomasa 2005. VZÚT Praha, VÚZT a MZČR 2005, s. 116-119 z 138, ISBN 80-8684-07-4
8. Van der Lans, R.P.; et al: Modelling and experiments of straw combustion in a grate furnace. In: Biomass and Bioenergy 19 (2000), Published by Elsevier Ltd., pp. 199–208, ISSN: 0961-9534
9. Khor, A.; et al.: Straw combustion in a fixed bed combustor. In: Fuel - The Science and Technology of Fuel and Energy 86, 2007

Published by Elsevier Ltd., pp. 152 - 160, ISSN: 0016-2361

**10.** Malat'ák, J.; Gurdil, G.A.; Jevič, P.; Pinar, Y.; Selvi, K.C.: Heat-emission Characteristics of Some Energy Plants. In: The Journal of Agricultural Faculty of Ondokuz Mayıs University, volume 22, 2007, issue 2, pp. 202-206, ISSN 1300-2988

**11.** Malat'ák, J.; Gurdil, G.A.; Pinar, Y.; Vaculík, P.; Selvi, K.C.: Solid recovered fuels from agricultural wastes. In: The Journal of Agricultural Faculty, OMU, 2008, 23(1), pp. 51-58, ISSN: 1300-2988

**12.** Nordin, A.: Chemical elemental characteristics of biomass fuels. In: Biomass Bioenergy 6 (1994), Published by Elsevier Ltd., pp. 339-347, ISSN: 0961-9534

**13.** Obernberger, I.; Theka, G.: Physical characterisation and chemical composition of densified biomass fuels with regard to their combustion behaviour. In: Biomass and Bioenergy 27 (2004) Published by Elsevier Ltd., pp. 653-669, ISSN: 0961-9534

## CONSERVATION SOIL TILLAGE TECHNOLOGIES

JIRÍ MAŠEK\*, MILAN KROULÍK, ZDENĚK KVÍZ, PAVEL PROCHÁZKA  
Czech University of Life Sciences Prague, 16521 Prague 6 – Suchbát, Czech Republic,  
Phone: +420224383137, E-mail: masekj@tf.czu.cz

### Abstract

Conservation agriculture is a concept for resource-saving agricultural crop production that strives to achieve acceptable profits together with high and sustained production levels while concurrently conserving the environment. Conservation agriculture (CA) is based on enhancing natural biological processes above and below the ground. Interventions such as mechanical soil tillage are reduced to an absolute minimum, and the use of external inputs such as agrochemicals and nutrients of mineral or organic origin are applied at an optimum level and in a way and quantity that does not interfere with, or disrupt, the biological processes. CA is characterized by two principles which are linked to each other. It is continuous minimum mechanical soil disturbance and permanent organic soil cover. Special kind of conservation tillage can be Controlled Traffic Farming system.

Conservation tillage (agriculture) technologies where ploughing by a moldboard plough is replaced by tillers and shallow soil loosening is increasingly used as a soil treatment. It is typical for shallow soil tillage that all plant residues are left on the soil surface, or in the tilled upper soil layer. The plant residues can play very important role by next plant cultivation. The shovel and disc tillers are possible to use to advantage in conventional soil tillage systems and also by using conservation soil tillage technologies where is ploughing replaced by shallow tillage. In the experimental section the aim of research was described which is possible to summarize briefly as follows – the evaluation of soil physical properties on tillers work quality (especially on size of clods after soil treatment on the top and in the soil profile), evaluation of sweep tillers and disc tillers work quality by stubble ploughing.

**Key words:** *conservation soil tillage, conservation agriculture, sweep tiller*

### Introduction

Conventional "arable" agriculture is normally based on soil tillage as the main operation. The most widely known tool for this operation is the plough, which has become a symbol of agriculture. Soil tillage has in the past been associated with increased fertility, which originated from the mineralization of soil nutrients as a consequence of soil tillage. This process leads in the long term to a reduction of soil organic matter. Soil organic matter not only provides nutrients for the crop, but it is also, above all else, a crucial element for the stabilization of soil structure. Therefore, most soils degrade under prolonged intensive arable agriculture. This structural degradation of the soils results in the formation of crusts and compaction and leads in the end to soil erosion. The process is dramatic under tropical climatic situations but can be noticed all over the world. Mechanization of soil tillage, allowing higher working depths and speeds and the use of certain implements like ploughs, disk harrows and rotary

cultivators have particularly detrimental effects on soil structure [1].

Soil erosion resulting from soil tillage has forced us to look for alternatives and to reverse the process of soil degradation. The logical approach to this has been to reduce tillage. This led finally to movements promoting conservation tillage, and especially zero-tillage, particularly in southern Brazil, North America, New Zealand and Australia. Over the last two decades the technologies have been improved and adapted for nearly all farm sizes; soils; crop types; and climatic zones [2].

Conservation agriculture systems utilize soils for the production of crops with the aim of reducing excessive mixing of the soil and maintaining crop residues on the soil surface in order to minimize damage to the environment. One of the conservation agriculture systems can be Controlled Traffic farming (CTF). CTF is all about managing soil compaction – confining it to narrow strips across the land and maximizing the remaining undamaged soil area for cropping. In

practice it means matching machinery tracks so they take up the least possible area. Although this is made simpler by satellite guidance, it can be achieved with conventional marking systems. Farm conversion to CTF in the first instance means adopting a CTF "mindset" – the belief that separating wheels and crops is a key method of reducing costs and increasing returns. From here on it is simply a matter of good planning and timely investment that ensures a minimum 15% return on capital, an increase in crop returns and a substantial reduction in costs [3].

The constant addition of crop residues leads to an increase in the organic matter content of the soil. In the beginning this is limited to the top

layer of the soil, but with time this will extend to deeper soil layers. Organic matter plays an important role in the soil: fertilizer use efficiency, water holding capacity, soil aggregation, rooting environment and nutrient retention, all depend on organic matter [4].

Residues on the soil surface reduce the splash-effect of the raindrops, and once the energy of the raindrops has dissipated the drops proceed to the soil without any harmful effect. This results in higher infiltration and reduced runoff, leading to less erosion. The residues also form a physical barrier that reduces the speed of water and wind over the surface. Reduction of wind speed reduces evaporation of soil moisture.

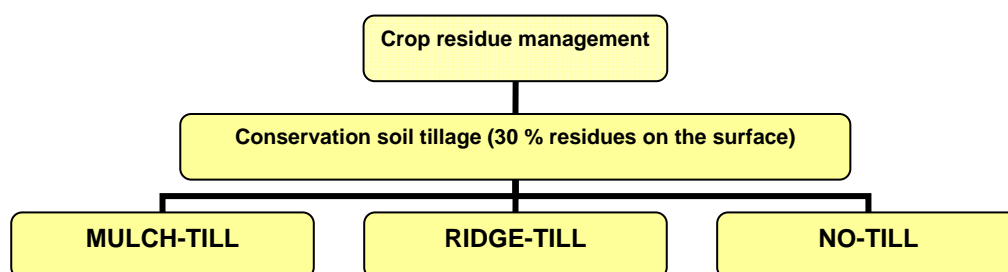


Fig. 1 - Soil tillage conservation technologies by different crop residue management [5].

Keeping the soil covered is a fundamental principle of conservation agriculture. Crop residues are left on the soil surface, but cover crops may be needed if the gap is too long between harvesting one crop and establishing the next. Cover crops improve the stability of the conservation agriculture system, not only on the improvement of soil properties but also for their capacity to promote an increased biodiversity in the agro-ecosystem [6,7].

### Material and Methods

Observation was dividing to two parts. First is soil tillage system evaluation and the second is evaluation of tramlines during one year on 1 ha field plot.

The experiment was prepared in real field conditions for different soil tillage technologies provided with different working tools. On first experimental field plot were evaluated difference between sweep and disc tillers work quality with accent on plant residues distribution and size of

clods after shallow ploughing. On the second experimental field was marked divers' variants according to different working speed and different working depth. Very important for observation is distribution plant residues after stubble ploughing in work-in-process level and rate of plant residues on the top of soil. For evaluation of surface covering by crop residues we used software Photoshop 7. There is very easy way to recognized grade of covering according to count white and black pixels in the picture of surface.

For influence of speed and working depth evaluation on a working quality, especially on a crop residue distribution in a working profile and surface we used sweep tiller Horsch Tiger. There were evaluated four working depth and four working speeds in a cross combination. It means 16 variants of soil tillage.

For tramline observation we needed equipment (fig. 2) for data collections of tramlines positions.



Fig. 2. Equipment for data collection, 1 – DGPS receiver, 2 - data storage unit, 3 - battery.

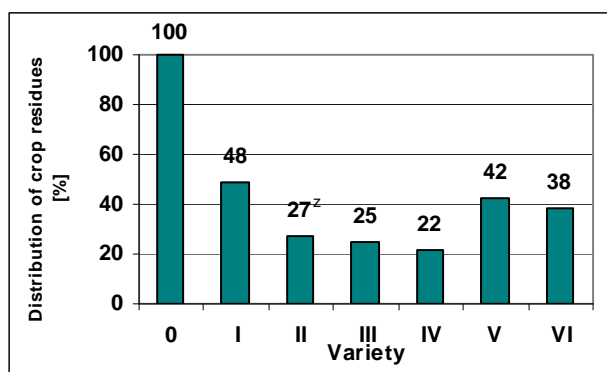


Fig. 3 – Distribution of crop residues by different variant of tillage

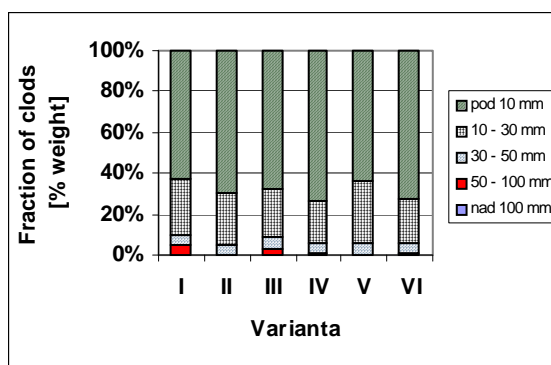


Fig. 4 – Clods fraction by different soil tillage.

## Results and Discussion

In the field experiment we had prepare 6 variants of tillage. I – 1x sweep tiller, II – 2x sweep tiller, III – 1x sweep tiller and 1x discs tiller, IV – 1x discs tiller, V – 2x discs tiller and VI 1x discs and 1x sweep tiller. Option 0 is without tillage.

The sweep tiller left more plant residues on the soil surface than disc tiller (fig. 3). By using disc tiller two times was observed that crop residues going up back on surface. Size of clods is smaller by sweep tiller cultivation (fig. 4). There was recognized significant statistical difference of plant residues distribution in different work depth. There is minimum clods fraction with size more than 50 mm. This value is very important because size of clods greater than 50 mm can make problem by secondary tillage and by seeding also.

In the measurement on the second field was evaluated sweep tiller work quality according to work speed and work depth (evaluation of sweep tiller by stubble ploughing after winter wheat harvest without straw collection). On the experiment field was marked divers' variants according to different working speed and different working depth. Very important for observation is distribution plant residues after stubble ploughing in work-in-process level and rate of plant residues on the top of soil. There was recognized significant important difference of plant residues distribution in different work depth (fig. 5). The working speed (fig. 6) had not statistically significant difference in the variants with different working speed by the same depth level.



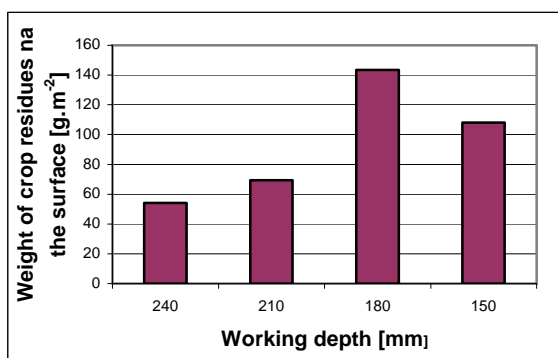


Fig. 5 – Weight of crop residues according to working depth.

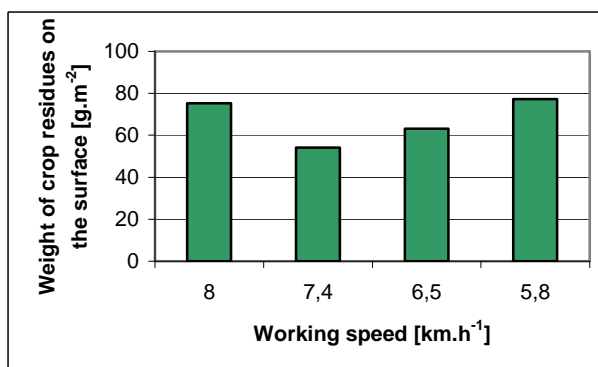


Fig. 6 – Weight of crop residues according to working speed.

Tab. 1 – Weight of crop residues in different working layers.

Working layer	Weight of crop residues [g.m <sup>-2</sup> ]				
	1	2	3	4	5
surface	94,00	156,00	104,00	240,80	122,00
depth 0 - 60 mm	894,80	402,80	320,40	520,40	212,80
depth 60 - 120 mm	58,80	61,60	62,40	32,00	160,00
depth 120 - 180 mm	0,00	0,00	0,00	0,00	0,00

Evaluation of crop residue distribution in a tilled soil profile give this results. The most of residues is covered by soil in depth from 0 to 60 mm and on the soil surface (tab. 1). In depth 60 to 120 mm is it smaller part of total quantum crop residues and in a lower layer is not any crop residues. By tillage by this kind of tiller by different working speed and different working depth the plants rest are covering up to maximum 120 mm depth. Between variants isn't significant statistically difference.

In the picture 7 is described different ratio of covering the soil surface. According to Johnson (1988) must be surface covered more than 30 %. This is the main signature of conservation soil tillage technologies. By measurement on experimental field was soil surface covered from 28 to 42 %. So this tiller is suitable for conservation soil tillage technologies.

By total tramlines observation of all working operation during year was discovered very important information. On the field is using conventional soil tillage system with ploughing as main working operation for soil tillage. The picture 8 shows tramlines on the surface of field in 1 ha segment. For better visibility we use trajectory of individual passages only. The total area covered/run-over by all machine's tyres were calculated with help of the software

ArcGIS 9. The results show considerable high number of tyre's contacts with soil. Total area covered by tyres passages calculated for conventional soil tillage is in average 96 % total area of field.

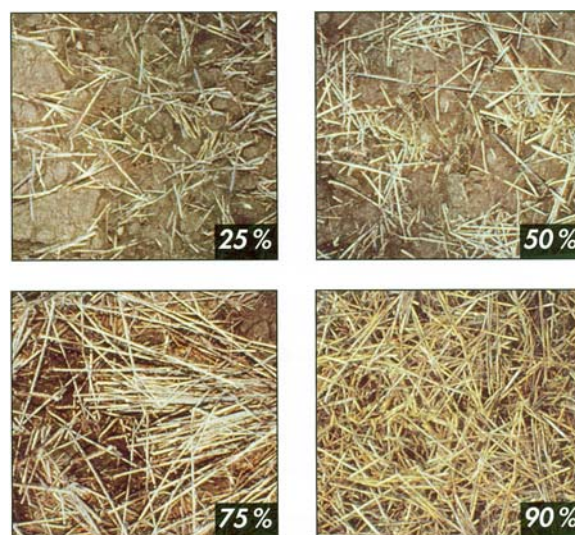


Fig. 7 – Soil surface covered by plant residues.

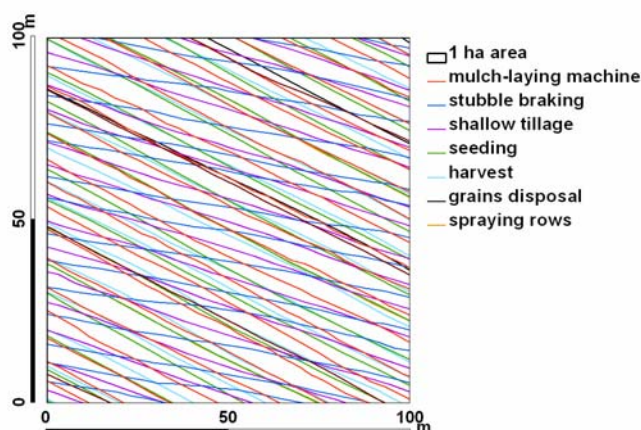


Fig. 8 - Working operation tramlines trajectory on a 1 ha field segment.

### Conclusion

Results of this work are important because conservation (minimal) soil tillage technologies play an important role in plant production. Especially conservation tillage systems with their modification are increasingly being introduced under an economic pressure on the field around the world. By evaluation working quality of sweep tiller and discs tiller we can say that sweep tiller put more residues on the surface than disc tiller. But by second tillage by discs tiller covered plant residues are going up on the surface and the number of plant rests is similar like by tillage by sweep tiller. It is interesting that by shallow tillage by sweep tiller are the crop residues put in to up layer and soil surface as well. In all scale of working depth crop residues contains the soil to the deep of 120 mm. Lower layer are only tilled but without crop residues which are normally in deep layer by classical ploughing. It means that soil tillage based on shallow tillage have a very good influence on a soil protection from water and wind erosion. The soil tillage working mechanism plays a crucial role in soil protection system. Different working tools take different quantity of plant residues on the soil surface.

In order to gain enter data for further Controlled Traffic Farming systems observation, several measurements concerning frequency and total area of machinery passages in a field were done. The results show considerable high number of tyre's contacts with soil in conventional soil tillage system and by using random traffic farming.

### Acknowledgement

This paper has been supported by the Ministry of Education, Youth and Sports of the Czech Republic as part of research plant MSM 6046070905.

### References

1. FAO, 2005. Conservation agriculture for soil moisture. Briefing notes: Production systems management, Rome. FAO. 4 p.
2. FAO, 2004. Conservation of natural resources for sustainable agriculture: training modules. FAO Land and Water Digital Media Series CD-ROM 27. FAO, Rome
3. Chamen, T., Alakukku, L., Pires, S., Sommer, C., Spoor, G., Tijink, F., Weisskopf, P. 2003. Prevention strategies for field traffic-induced subsoil compaction: a review Part 2. Equipment and field practices. Soil tillage research. 73. p. 161 – 174.
4. Hanna, H., et al. Tillage implement operational effects on residue cover. *Applied Engineering in Agriculture*, 1995, Vol. 11, s. 205-210.
5. Hůla, J., Procházková, B., et al. *Vliv minimalizačních a půdoochranných technologií na plodiny, půdní prostředí a ekonomiku*. Praha: ÚZPI, 2002. 104 s.
6. Johnson, R. R. Soil enganging effects on surface residue and roughnees with chisel-type implements. *Soil Science Am. Journal*, 1988, Vol. 52, s. 237-243.
7. Köller, K., Linke, Ch. *Erfolgreicher Ackerbau ohne Pflug (Wissenschaftliche Ergebnisse-praktische Erfahrungen)*. Frankfurt am Mein: DLG –Verl., 2001. 176 s.

## ECOLOGICAL BENEFIT OF FUEL E50

PETR MILER\*, JAN HROMÁDKO

Czech University of Agriculture in Prague, 16521 Prague 6 – Suchbátka, Czech Republic,

Phone: +420 22438 3105, E-mail: [miler@tf.czu.cz](mailto:miler@tf.czu.cz)

### Abstract

The article deals with ecological benefit analysis of fuel E-50 that consists of 50 % of petrol Natural 95 and 50 % of bioethanol. The virtual simulation of European homologation test NEDC was used for ecological benefit evaluation. The base of simulation forms the engine characteristics measured on a test bed. In the first step the emission characteristics and characteristic of fuel consumption were measured with the use of petrol Natural 95. In the second step the same characteristics are measured, using fuel E-50. By reason that the Skoda Felicia engine was used as a testing engine therefore it was needed to use a special adjustment of control section for the engine burning of E-50. The special programme was developed in the department of vehicles and ground transport at The Czech University of Life Sciences Prague. The programme is able to determine the specific production of individual emission components and fuel consumption related to one travelled kilometre (0.6214 mile) on the engine characteristics and course of speed in the driving cycle NEDC.

### Introduction

A part of global effort of European Union (EU) is to reach at least 20 % of greenhouse gas reduction by the end of the year 2020 compared with the year 1990. In order to discharge this resolve, the EU involved into the directive 2009/28/ES the promotion of the use of energy from renewable sources. According this directive there is a goal set 20 % of part from renewable sources done by an actual energy consumption and obligatory minimal goal 10 % for the part of bio-fuels used in transportation sector in every EU state. The aim has been stated by the end of the year 2020. [1, 2, 3]

There are three other main reasons for bio-fuels implementation in the Czech Republic beside above mentioned greenhouse gas reducing:

- Bio-fuels are renewable energy source;
- Use of bio-fuels decrease dependence on crude oil, which is mostly imported and its price is permanently imbalanced and therefore its price development is unpredictable,
- Bio-fuel generates consequences in agricultural practices and it becomes one of opportunity how to set up new working position in the agricultural and forestry resort.

Bio-ethanol is the one of the suitable bio-fuels manufactured in the Czech Republic. Production of bio-ethanol can be divided into three groups in accordance to input raw

materials. The first group is made up of biomass that contains simple sugar (obtained from sugar-beet or sugar cane). The second group is made up of biomass that contains starch (obtained from cereals or potatoes). The last group is made up of biomass that contains lignocellulose (obtained from wood, wooden sawdust or waste in cellulose and paper production). Bio-ethanol that is made up of lignocelluloses material is known like the biofuel of the second generation, because this fuel is produced from non-food products. [4, 5]

Bio-ethanol can be used for low-percentage mixture into the automobile petrols, which comply with law No. 180/2007 Sb. and high-percentage bio-ethanol blends, especially fuel E85 containing 85 % of bioethanol and 15 % of petrol natural 95. The low-percentage mixture of bio-ethanol up to 10 volume percent does not cause almost any problem during the burning in an engine and therefore is no need to adjust the engine. High-percentage blends are not possible to burn in common engine without adjustment owing to low ethanol efficiency.

According authors' experience with both of these possibilities of bio-ethanol use the fuel E50 was used and tested in the workplace with content of 50 % Natural 95 and 50 % bio-ethanol.



### Experimental arrangement

The benefit of fuel E50 burning was analysed via virtual simulation of European homologation driving cycle for the vehicles up to 3,5 t. Emission engine characteristics and characteristics of fuel consumption were measured on the test bed and they served as the base of the simulation. In the first step these characteristics were measured by using automobile petrol Natural 95 and, in the second step, by using fuel E50. By using a special algorithm, developed in the Mathcad software, the individual points of the emission characteristics and fuel consumption characteristics were transformed into the continuous characteristics of measured values (fuel consumption and individual emission components) which are dependent on the speed and the engine torque. All these parameters of the vehicle that could influence dynamic vehicle parameters (rolling resistance coefficient, cross-sectional area, aerodynamic resistance coefficient, individual gear ratio etc.) were involved into the transformation of speed of

cycle into rpm and torque. Through the interconnection both of these programmes, the possibility to determine the production of immediate and cumulated value of the individual emission components towards the speed course in the driving cycle was developed.

The driving cycle was applied to Skoda Felecia car equipped with engine 1,3 MPi. The basic parameters of the engine are shown in the

Tab. 1. Positioning of the engine on the test bed is shown in

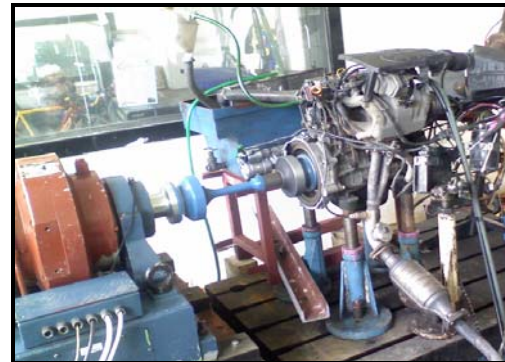


Fig. 1.

**Tab. 1** Engine parameters

Maximum engine output	50 kW
Maximum torque	106 Nm
Fuel	petrol
Cylinder number	4
Drilling	75,5 mm
Stroke	75,5 mm
Compression ratio	10:1
Nominal rpm	5000 min <sup>-1</sup>

### Results and discussion

In the first step, the measured values were filled up with zero values by sequential interpolation facing a torque and then facing speed. These values were transformed into the square matrix P, which is the base for the creation of continuous engine characteristics. Afterwards, the engine speed range and engine torque is necessary to be defined for the creation of continuous engine characteristics. This definition is executed through the matrix M. The final continuous characteristic is given by this quadratic (1).

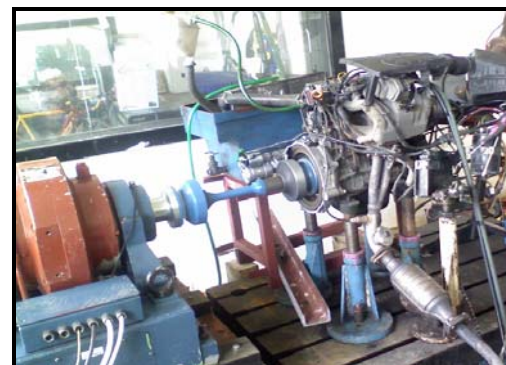


**Fig. 1** Engine positioning on the test bed

$$\text{fit}(x,y) := \text{interp} \left[ \text{cspline}(M,P), M, P, \begin{pmatrix} x \\ y \end{pmatrix} \right] \quad (1)$$

where:  $\text{fit}(x,y)$  is the continuous characteristic of an individual component, M is the matrix, which defines rpm range and motor torque, P is the interpolated value matrix of an individual emission component.

The final continuous characteristic was delimited by the maximum and lossy engine torque. The example of the final delimited characteristic of carbon monoxide production for the fuel E50 is shown in Fig. 2. The same way was used for determination of fuel

consumption characteristic and characteristics of individual emission component for both fuels.

In the second step, the engine speed and torque which had been defined in percentage were transformed into rpm and Nm. For this

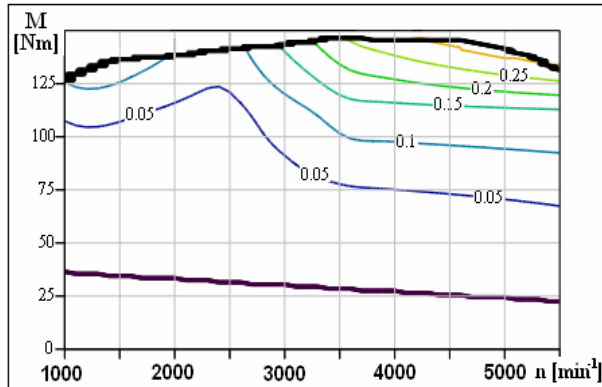


**Fig. 2** Production of carbon monoxide per hour for E50

In the last step continuous characteristics of fuel consumption and emission components production are connected through the course of engine rpm and torque in the driving cycle. By this connection we got a possibility to determine instantaneous and after it cumulated values of emissions production and fuel consumption. Cumulated values for the whole cycle can be converted, through the known distance driven of the cycle, into the specific value which is related to the one driving kilometre. The course of cumulated carbon monoxide production in the urban part of driving cycle NEDC for both fuels is shown in Fig. 4. Fuel consumption as well as individual emission component productions for both fuels can be diagrammed by the same way. Specific fuel consumption and specific emission productions which is related to the one driving kilometre for the individual part of driving cycle NEDC are digestedly shown in Tab. 2. In Tab. 2 there are also combined values of specific fuel

speed vehicle transformation is necessary to define the road resistance course, shifting model of individual speed gears, drive slip, etc. Resulting course of engine rpm and torque is shown in Fig. 3.

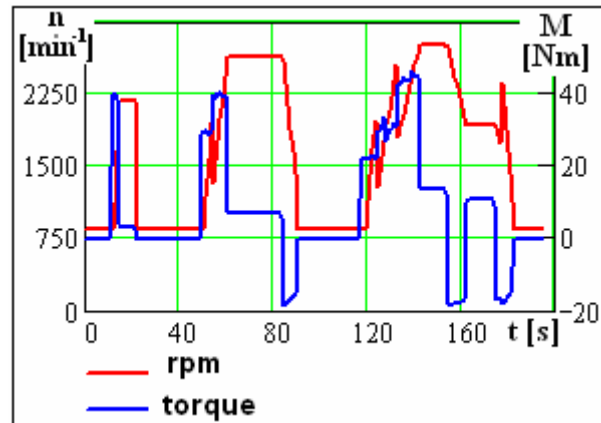


**Fig. 3** Course of rpm and torque in UDC

consumptions and specific emissions that are specified by the weight mean of specific production from urban and extra urban part of the cycle. Urban part is represented by 36,8 % and extra urban part by 63,2 %.

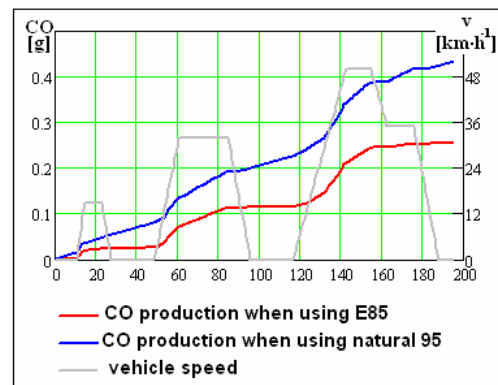


**Fig. 4** Cumulated production of CO in the urban driving cycle NEDC for the fuel E50 and Natural 95

**Tab. 2** Resulting fuel consumption and specific emission productions

Specific emission	Urban driving cycle	Extra urban driving cycle	Combined driving
Fuel consumption E50	77	43	55
Fuel consumption natural 95	64	36	46

Specific emission	Urban driving cycle	Extra urban driving cycle	Combined driving
CO <sub>2</sub> when using E50 [g·km <sup>-1</sup> ]	220	124	159
CO <sub>2</sub> when using natural 95 [g·km <sup>-1</sup> ]	226	127	163
CO when using E50 [g·km <sup>-1</sup> ]	0,25	0,26	0,25
CO when using natural 95 [g·km <sup>-1</sup> ]	0,43	0,33	0,37
HC when using E50 [mg·km <sup>-1</sup> ]	3,14	1,87	2,33
HC when using natural 95 [mg·km <sup>-1</sup> ]	3,2	1,86	2,35
NO <sub>x</sub> when using E50 [mg·km <sup>-1</sup> ]	21	21	21
NO <sub>x</sub> when using natural 95 [mg·km <sup>-1</sup> ]	24	25	25

## Conclusion

The results of the carried out experiments show the relatively high increase of fuel consumption caused by the use of E50. This increase is mainly caused by the low efficiency of ethanol. While using combined way of driving the weight fuel consumption increases in 19,5 %. The increase of fuel consumption can not be considered as a negative phenomenon but it has to be considered during fuel E50 price calculation. Recalculated price into energetic equivalent of standard petrol must be competitive. Direct fall in CO<sub>2</sub> is almost unsubstantial. This CO<sub>2</sub> fall is necessary to see in the way of ethanol production. In the Czech Republic cereals and sugar beet are the most suitable plants for obtaining of bio-ethanol. Sugar beet brings more reduction in CO<sub>2</sub> production (sugar beet approximately 40 – 45 %, cereals 30 – 35 %) in comparison with cereals. In term of reduction CO<sub>2</sub> production the biggest benefit is brought by the biofuels of the second generation that are produced from lignocelluloses. However this production of the second bio-fuel generation is technically demanding and currently technology is mainly topic of research works. Even the production of directly limiting pollutants, such as carbon monoxide, unburned hydrocarbon and nitrogen oxides has an expressive benefit. The production of carbon monoxide when using fuel E85 decreases about 30,6 %, production of unburned hydrocarbons decreases about 0,9 % and

production of nitrogen oxides decreases about 14,6 %, considering combined way of driving.

Above performed analysis of the experiments proves an expressive ecological potential of E50 fuel. This fuel would be suitable to use in adapted spark ignition engines that are able to burn high percentage bio-ethanol blends and currently have a problems with burning of fuel E85.

## References

- [1] Directive 2009/28/EC of the European Parliament and of the Council on the promotion of the use of energy from renewable sources, Brussels 8.5. 2009.
- [2] Proposal for a Directive of the European Parliament and of the Council on the promotion of the use of energy from renewable sources. COM(2008) 30 final, 23.1.2008.
- [3] Law Nb. 180/2007 Sb., which change the law Nb. 86/2002 Sb. about air protection.
- [4] Proposal for a Directive of the European Parliament and of the Council on the use of biofuels for transport and proposal for a Council Directive amending Directive 92/81/EEC with regard to the possibility of applying a reduced rate of excise duty on certain mineral oils containing biofuels and on biofuels. COM (2001) 547 final, Brussels, 7.11. 2001.
- [5] Directive 2003/96/EC of the European Parliament and of the Council on restructuring the Community framework for the taxation of energy products and electricity the, Brussels 27.10. 2003.



## THE EFFECT OF COMPOSTS APPLICATION ON SUGAR BEET

MIROSLAV MIMRA\*, VLASTIMIL ALTMANN

Czech University Life Sciences Prague, 16521 Prague 6 – Suchbát, Czech Republic,

Phone: Phone: +420224383144, E-mail: mimra@tf.czu.cz

### Abstract:

Sugar beet belongs among nutrient-intensive crops. To achieve good sugar beet yield, it is necessary to provide a sufficient amount of nutrients. Small experimental plots were established for three years to evaluate the effect of compost application in amounts of 0, 25, 50, and 100 tons per hectare upon yield and some other properties of sugar beet. The impact of compost application upon yield proved to be statistically significant. It was found out that the influence of compost application upon polarized sugar content was statistically insignificant. The best resulting yield was achieved when 50 tons of compost was applied per hectare. All alternatives of compost application provided better yields of bulbs compared with the control alternative, where compost was not used.

**Key words:** Sugar beet (*Beta vulgaris* L.), compost, crop yield, sugar content

### Introduction

Owing to decreasing livestock quantities and thus reduced production of manure, utilization of composts may become a suitable means for replenishing the soil with organic matter. Increasing number of cases have been reported recently that non-composted plant remains, composts and their extracts, or manure reduced the occurrence of pests and diseases of crops being grown, and cases, where these products added into the soil influenced positively the soil condition and allowed for proliferation of beneficial microorganisms. (2, 3) The mechanism of plant remains action against pests is as follows: some plant remains emanate substances, which are toxic to pests, such as phenols, tannins, azadirachtins, and ricinin. Others release substances, which are subsequently converted into toxic products, such as ammonia, nitrates, and hydrosulfides. (1)

The results of project, which focused on testing the compost utilization as an alternative of chemical products, confirm positive effects of compost obtained from bark and solid municipal waste against soil-borne diseases. Compost was used as a replacement of methylbromide used for soil disinfection and particularly for protection against *Fusarium oxysporum*, *Phytophthora* spp., *Verticillium* spp., and some other undesirable nematodes. Various amounts of additives added into composts were tested. pH of the medium was 6.5 and the compost was heated to 60 °C for six days to remove microflora. Thanks to higher pH and lower accessibility of microelements,

compost from the grapevine pulp showed better effects against diseases compared with, for example, cork compost. (4)

The effect of vermicompost application on the surface of the plot before and after sowing in the quantity of 60 tons per hectare upon yield and some properties of the sugar beet root was reported by (6). Vermicompost application increased the root yield as well as sugar content in the beet, if it was applied together with fertilizer containing microelements. Vermicompost applied before sowing improved the emergence rate of plants and reduced the amount of weeds.

Organic fertilization is a basis of the sugar beet fertilization system. Besides participation in nutrients supply, it is the most significant factor for keeping the soil fertility. For sugar beet, all types of organic fertilization may be applied. The most wide spread fertilizer is manure, which is currently used for about 90 % of the sugar beet plots. The amounts of manure differ according to the soil type. For medium-heavy and very heavy soils, preferable doses are 40 – 50 tons per hectare, while 30 – 35 tons per hectare will be sufficient for light soils with a good content of humus. Compost may also be used for fertilizing sugar beet. The advantage of using well-decomposed composts is a possibility of subsequent underplowing.

### Materials and methods

Small-plot experiments have been established with three repetitions and five alternatives. Experimental plot may be

characterized as flat with a loamy soil and pH of soil equal to 7.0; organic matter 1.12, reduced bulk density  $1.45 \text{ g.cm}^{-3}$ , electric conductivity of soil  $45 \text{ mS.m}^{-1}$  and compost  $137 \text{ mS.m}^{-1}$ . Compost and manure were applied onto the surface of the plot in fall with subsequent underplowing. In spring, soil preparation and seeding took place.

During vegetative period, identical agrotechnical principles were applied within the complete experimental plot. Besides application of compost and manure, no fertilizer was used in individual alternatives, both before seeding and during vegetative period. Identical variety of sugar beet, Impact, was used for all alternatives with the uniform seeding rate of 70 thousand plants per hectare. Twenty sugar beet plants were seeded on each plot with the area of  $3 \text{ m}^2$ . Seeds were sowed to the same depth of 30 mm in April. All alternatives were irrigated regularly after sowing. Summary of alternatives used during this experiment is given in Table 1. Alternative without fertilizer application was used as a control and for comparisons.

Biological yield of bulbs was recorded for all alternatives. Bulbs from each plot were harvested, cleaned, and counted. Tops were cut away from the bulbs, which were then weighted. Upon completing the harvesting of each alternative, sample was taken to determine the polarized sugar content.

Table 1: Summary of alternatives

Var.	Alternatives
1	control alternative, where compost was not used
2	compost application in amounts of $25 \text{ t.ha}^{-1}$
3	compost application in amounts of $50 \text{ t.ha}^{-1}$
4	compost application in amounts of $75 \text{ t.ha}^{-1}$
5	compost application in amounts of $100 \text{ t.ha}^{-1}$

## Results and discussion

Table 2 shows obtained results. The effect of compost application upon the yield of sugar beet bulbs and tops, as well as the contents of nitrogen, phosphorus, potassium, were statistically significant. The highest biological yield of

102.5 tons per hectare was achieved for alternative 3, where 50 tons of compost was applied per hectare. On the contrary, the lowest yield was obtained for alternative 1 without fertilization that provided biological yield of 74.3 tons per hectare.

The difference between the best and the worst alternative was 28.2 tons per hectare and the average biological yield for all alternatives was 94.47 tons per hectare. Yields for alternatives utilizing fertilization was 21.8 % up to 37.95 % higher than the control alternative without fertilization. Comparison of hectare yields was carried out using the one-sample t-test, which compares the sample mean and certain constant value. Yield value for alternative without fertilization was used as a control constant.

The difference in biological hectare yield values in comparison with the control alternative without fertilization was shown to be statistically significantly higher ( $t=4.265 > t_{0.1}=2.963$  upper-tailed test). Differences between alternatives using fertilization were not statistically significant. The difference between the best and the second alternative was only 0.27 %. Biological yield for sugar beet grew with increasing compost application amount. When increasing the fertilizer amount applied by 1 ton per hectare, biological yield of bulbs increased by 0.1308 tons per hectare and for tops the yield increased by 0.132 tons per hectare. Application of compost resulted in increased biological yield of sugar beet.

The difference between nitrogen, phosphorus, and potassium contents was also statistically significant. The content of polarized sugar and calcium was reported as statistically nonsignificant. Some authors describe the relation between phosphorus content and sugar content (3), but during this experiment, the relation could not be confirmed. Nitrogen, phosphorus, and potassium contents rose with increasing compost amount. Statistically significant difference of calcium contents in individual alternatives was not recorded.

Table 2: Analysis results

Variants	Beetroot yield	Leaves yield	Sugar yield	N	P	K	Ca
	(t.ha <sup>-1</sup> )	(t.ha <sup>-1</sup> )	(%)	(%)	(%)	(%)	(%)
1	52.0	22.3	19.8	0.454	0.57	4.40	5.73
2	61.1	29.4	20.3	0.521	0.69	5.31	5.81
3	67.3	35.2	20.5	0.592	0.76	5.29	5.64
4	65.4	34.8	20.7	0.671	0.79	5.52	5.77
5	66.2	36.1	20.3	0.698	0.82	5.49	5.75
Significance	*	*	N	*	*	*	N

Note: \* – statistically significant  $\alpha = 0.01$ , N – statistically nonsignificant

Various authors obtained differing results from their experiments. Some confirm significant effect of compost upon sugar beet yield, but others did not detect such significant influence. For example, during their experiments (7) reported the effect of compost and nitrogen upon yield and technological properties of sugar beet bulbs at compost dose of 0, 10, 20 and 4 tons per hectare and nitrogen in a quantity of 0, 90, and 150 kg per hectare, where achieved bulb yields ranged from 68.7 up to 91 tons per hectare.

The influence of compost and nitrogen fertilization was not proved in the first year, when experiments were established on light soils. On the contrary, it was proved for experiments established on heavy soils. The sugar content in bulbs was dependent upon the quantity of applied nitrogen, but the amount of compost applied did not have any influence upon the sugar content.

### Conclusion

Performed experiments compared the influence of applied compost upon biological yield of sugar beet. Yield rose with increased compost amount, which has also been confirmed by other authors. The best results were achieved when 50 tons of compost was applied per hectare. The Liebig's law of minimum fertilizer elements may play its role here, when the increase of additional yield slowed down due to the lack of certain element important for growth of plants. As stated by (8), compost may be applied successfully to vegetation, especially when it is complemented and mixed with mineral nitrogen. Based on their statement, this leads to increased yield and better utilization of soil nitrogen by plants. During experiments performed in Italy, (9) concluded that the sugar beet yield is influenced not only by the amount of compost used, but also period when it is

applied to sugar beet. He also states that compost application allows reducing the mineral nitrogen dose.

### Acknowledgement

This paper was processed within the framework of the Research Project of MŠMT č. MŠM 6046070905 "Studium zemědělského technologického systému s ohledem na jeho racionalizaci a šetrnou interakci s ekosystémy kulturní krajiny" financed by Ministry of education, youth and sports of Czech republic.

### Literature

1. LITTERICK, A. M., HARRIER, L., WALLACE, P., WATSON, C.A., WOOD, M.: The Role of Uncomposted Materials, Composts, Manures and Compost Extracts in Reducing Pest and Disease Incidence and Severity in Sustainable Temperate Agricultural and Horticultural Crop Production – A
2. FRIEND, D.: Using Compost To Reduce Irrigation Costs, BioCycle World, December 2004
3. CAYUELA, M. L., SÁNCHEZ-MONEDERO, M. A., MOLINA, J., ROIG, A.: Compost Production From Olive Oil Processing, BioCycle World, February 2005
4. KERNER, A.; ÁLVAREZ, J. M.: Broadening Compost Use In Southern Europe, BioCycle World, October 2004
5. MAREŠOVÁ, Karolina, KASPEROVÁ, Vanda, JANDOVÁ, Lenka, TOLLRIANOVÁ, Zuzana, ŠEVČÍKOVÁ, Ivana, KONVIČKOVÁ, Vendula: Utilization of compost and other organic preparation in agriculture. (in Czech language) Biom.cz [online]. 2006-08-24

- <<http://biom.cz/index.shtml?x=1918409>>.  
ISSN: 1801-2655.
6. Kopczynski,-J; Bury,-M; Denkwicz,-J: The influence of surface application of vermicompost and calcium on the yield and quality of sugarbeet roots. *Folia-Universitatis-Agriculturae-Stetinensis,-Agricultura*. 1999; ( 78): p. 49-54
  7. Gaj,R.; Gorski, D.: Influence of compost produced from municipal solid wastes and of nitrogen fertilization on yields and technological quality of sugarbeet. Part I. Yields of roots and technological quality of sugarbeet. *Biuletyn-Instytutu-Hodowli-i-Aklimatyzacji-Roslin*. 2004; (234): p. 145-154
  8. Montemurro, F.; Maiorana, M.; Convertini, G.; Ferri, D.: Effects of municipal solid waste compost on yield and nutritional status of the industrial crops. *Atti-del-XX-Convegno-Nazionale-della-Societa-Italiana-di-Chimica-Agraria*, Padova, Italy 24-27. Settembre 2002. 2002; p. 287-294
  9. Tugnoli, V.: Quality compost: effective help for sugar-beet. Rome, Italy: UNACOMA Service srl., Mondo-Macchina. 2002; volume 11,number 1: p. 26-29.

## CLIMATIC RISKS FOR RAPESEED (*BRASSICA NAPUS*, *L.*) PRODUCTION IN BULGARIA

TOTKA MITOVA<sup>1</sup>, MILENA MOTEVA<sup>2\*</sup>, VALENTIN KAZANDJIEV<sup>3</sup>,  
VESKA GEORGIEVA<sup>3</sup>, GALIN GANCHEV<sup>4</sup>

<sup>1</sup>“N. Pushkarov” Soil Science Institute, Sofia, Bulgaria

<sup>2</sup>Research institute for Land Reclamation and Agricultural Engineering, 3 Shosse Bankya Str.,  
Sofia 1331, Phone: +359 886 919353, Fax: +359 2 8247842,

E-mail: [milena\\_moteva@yahoo.com](mailto:milena_moteva@yahoo.com)

<sup>3</sup>National Institute of Meteorology and Hydrology, Sofia, Bulgaria

<sup>4</sup>Forestry University, Sofia, Bulgaria

### Abstract

The agroclimatic conditions of Bulgaria permit rapeseed growing. They are considered risky in some regions of the country, because of the drought conditions during the seeding and flowering periods and the extremely low air temperatures in winter and extremely high air temperatures in late spring. The goal of the paper is to assess the climate risks for rapeseed (*Brassica napus*, *L.*) growing in three representative for the agricultural production regions – around the towns of Lom and Ruse in Northern Bulgaria and Pazardjik in Southern Bulgaria. Thirty-year (1971-2000) meteorological data - minimum and maximum air temperatures, relative air humidity and rainfalls have been processed. The following parameters of the hydro-thermal conditions have been analyzed: long-term dynamics, probability and trends of the minimum and maximum air temperature, rainfalls and relative air humidity; duration and frequency of the rainless periods during flowering & seed filling; duration and frequency of the periods with minimum daily air temperature less than -10°C in the period of winter dormancy; duration and frequency of the periods with maximum daily air temperature above 27°C in the period of flowering & seed filling; the dynamics of the available soil water within a yearly production cycle. The future conditions for rapeseed production in our country have been assessed.

### Introduction

Despite of the plant breeding efforts, rapeseed yield and oil concentration still strongly depend on the meteorological conditions [1]. Seeding dates for winter forms should permit achievement of 6-8 true leaves and good rooting before the first frost in order the plants to be able to sustain 4-10 days of -15°C - -20°C minimum air temperature. Snowcover is a desirable and friendly factor [1]. Best growth in spring occurs when air temperature is at optimum of 21°C. Heat stress for *Brassica napus* *L.* occurs at critical temperatures from as low as 25 to 27°C to as high as 30 to 32°C [2]. Rapeseed plants drop or abort their flowers at  $T_{max} > 27^{\circ}\text{C}$  [3].

Rapeseed has low drought tolerance. The risks for yield reduction come from insufficiency of water supply in the periods of seeding-germination and flowering-maturing. Sufficient water and firm seedbed are needed to ensure good and uniform germination [4, 5]. Water stress during flowering has severe impact as on seed yield, so on oil concentration [6, 7].

Moisture stress, low relative air humidity inclusive, combined with high temperature from flowering to maturity would decrease the number of pods, number of seeds, seed weight, oil content and yield [2, 8].

Growing *Brassica napus*, *L.* in Bulgaria meets several problems – drought conditions during the seeding period, risks of extremely low January temperatures and extremely high May temperatures at some sites of the country, risk of soil and atmospheric drought during flowering. Furthermore, our country is subjected to negative climatic changes – increasing of the water deficit and the number of the extreme events – high and low air temperatures, intensive rainfalls. These phenomena will probably expand in future [9].

The goal of the paper is to assess the climate conditions and risks for rapeseed (*Brassica napus*, *L.*) production in three regions in Bulgaria – around the towns of Lom and Ruse in Northern Bulgaria and Pazardjik in Southern Bulgaria. The selected regions are representative for the climate

and soil variety and agricultural background for rapeseed production.

### Material and methods

Thirty year (1971-2000) meteorological data from three agrometeorological stations have been processed. The analysis is based on data of minimum and maximum air temperature, relative air humidity and rainfalls, taken from the National Institute of Meteorology and Hydrology database. Regression analysis was applied. The following parameters of the hydro-thermal phenomena and conditions have been analyzed: long-term dynamics, probability and trends; duration and frequency of the rainless periods during flowering & seed filling; duration and frequency of the periods with minimum daily air temperature less than  $-10^{\circ}\text{C}$  at winter dormancy; duration and frequency of the periods with maximum daily air temperature above  $27^{\circ}\text{C}$  at flowering & seed filling; the dynamics of the available soil water within a yearly production cycle.

### Results and discussion

#### Temperature risks

##### Winter dormancy

The risks for rapeseed surviving during winter are low. The lowest minimum air temperatures (climatic data) are observed in the second decade of January (Fig. 1). The regions of Ruse and Pazardjik have similar conditions with synchronic variation of the minimum

temperature. Winter conditions of Lom region are milder than those of the other two regions. Less than  $-10^{\circ}\text{C}$  should be expected in 4,6% of the cases at Lom, 7,6% at Pazardjik and 10,9% at Ruse (Fig. 2).

The average duration of the periods of 3 and more consecutive days with  $T_{\min} \leq -10^{\circ}\text{C}$  is shortest at Lom – 3,7 with variance coefficient  $c_v=26,7\%$ , and longest - at Ruse – 4,6 with  $c_v=49,0\%$  (Table 2). The distribution of the cold periods per month confirms that the conditions in the regions of Lom are mildest. All 15 periods are uniformly distributed in the three winter months. The essential part of these extremely cold periods at Ruse and Pazardjik are performed in January. Ruse and Lom January tendencies of minimum air temperature are negative. The tendency of Pazardjik is insignificant. Minimum air temperature tends to drop in the 30-year period with  $1,5^{\circ}\text{C}$  at Ruse and with  $2,5^{\circ}\text{C}$  at Lom. (Fig. 3).

Snowcover conditions are most favorable at Ruse and worst at Pazardjik [10]. Maximum depth of snow cover occurs in Ruse region - 35 cm, followed by Pazardjik and Lom – 29 and 25 cm respectively. Snowcover duration is longest at Ruse – 40 days - 43% of the snowcover formation period. At Lom it holds 38 days – 46% respectively. At Pazardjik this period is considerably shorter – 27 days – 34% respectively. The prevailing wind speed for the days with  $T_{\min} \leq -10^{\circ}\text{C}$  at Ruse is 1-4 m/s, while the same at Pazardjik and Lom is 0-2 m/s.

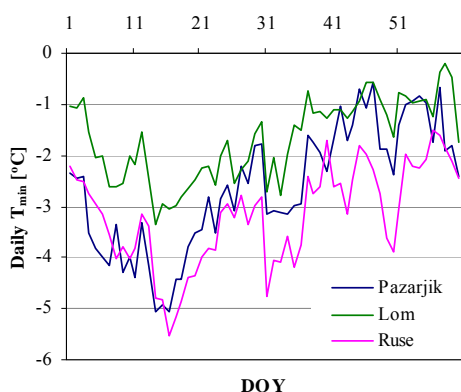


**Fig. 1** Dynamics of Jan–Feb minimum daily air temperature (climatic data, 1971-2000)

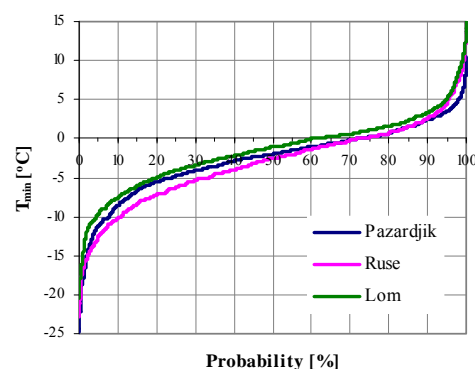


**Fig. 2** Probability of Jan minimum daily air temperature



**Table 2.** Number and duration of the periods of 3 and more consecutive days with  $T_{\min} \leq -10^{\circ}\text{C}$  per month

Month	Pazardjik		Lom		Ruse	
	Number of periods	Ave. dur. [days]	Number of periods	Ave. dur. [days]	Number of periods	Ave. dur. [days]
December	4	4	4	3,8	2	3,5
January	10	3,7	5	4,6	17	4,6
February	2	3	6	3,7	10	4,7
Sum	16		15		27	

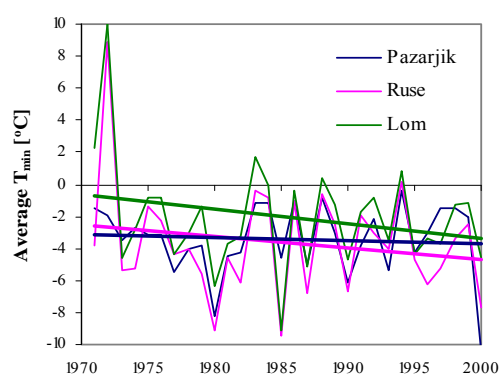


**Fig. 3.** Dynamics of January minimal daily air temperature

#### Flowering & seed filling

The temperature conditions in the regions of Pazardjik, Ruse and Lom are alike. Rapeseed reproductive stage does not fall in the climatically heat stress period, it is already completed at that time. The thirty-year average maximum air temperature reaches  $27^{\circ}\text{C}$  on 10 June (Fig. 4). The risk of reaching temperatures, higher than  $27^{\circ}\text{C}$ , is 23,7% for Pazardjik, 21,9% - for Lom and 18,1% - for Ruse (Fig. 5). The average duration of the periods of 3 and more consecutive days with  $T_{\max} \geq 27^{\circ}\text{C}$  are: 5,4 days with  $c_v=52,1\%$  for Pazardjik, 5,4 days with  $c_v=43,4\%$  for Lom and 4,6 days with  $c_v=57,5\%$  for Ruse. The great variance coefficients reveal the instability of the temperature factor and the related to that risk for rapeseed yield (Table 3). The tendencies of 15 April-15 June maximum air temperature are increasing with around  $2^{\circ}\text{C}$  for all stations (Fig. 6).

#### Drought risks

##### Seeding

The seeding period in Bulgaria - end of August-beginning of September - is traditionally dry. The thirty-year average rainfall sum of the

two months is 63,9 mm at Pazardjik, 77,9 mm at Lom and 110,6 mm at Ruse (Fig. 7 and Table 4). The variance coefficients of the three averages are quite high - 49,8% to 67,9%, hence there can be expected from very dry to very moist conditions. In 75% of the years the rainfall sum will be 31,8 mm and up for Pazardjik, 42,1 mm and up for Lom and 64,8 mm and up for Ruse. The driest decade in Southern Bulgaria is the first one of September with a rainfall sum around 7 mm. It is the same one for Northwestern Bulgaria and the second one of September for Northeastern Bulgaria. The tendencies of August rainfalls are decreasing with around 50 mm at Ruse, 20 mm at Pazardjik and 10 mm at Lom (Fig. 8).

#### Flowering & seed filling

Heat injury on crops is commonly associated with drought injury. The thirty-year average April-June rainfall sum is 149,3 mm at Pazardjik, 174,1 mm at Lom and 191,7 mm at Ruse. The region of Ruse is best water supplied. The rainfall sums at the three regions vary around 30% (Fig. 9 and Table 4). In 75% of the years are expected more than 100 mm rainfalls at Pazardjik, 150 mm at Lom and 160 mm at Ruse. These water amounts are far insufficient to meet the evapotranspiration demand of 300-400 mm for the spring period. Irrigation is certainly needed. The driest decades are the third one of April and the first one of May with rainfalls from 12 to 20 mm. The worst tendency of April-June rainfall sum is for Pazardjik with a decrease of around 90-100 mm, while for the other two regions it is around 30 mm. (Fig. 10). On average, there are 14 days in the period 15 April-15 June without rain (Table 5). The average duration of the drought period at Pazardjik is greatest - 15,4 days with the greatest  $c_v=34,3\%$ .

Air drought can also be killing for pollen. Relative air humidity (RH) of the three regions is low. The highest is observed established for Lom – 72% (Table 6). RH for Ruse and Pazardjik is 69% and 67% respectively.  $c_v$  are very low – around 3%, hence RH is a stable factor. In 75% of the years RH is expected to be

above 65% at Pazardjik, 67% at Lom, and 69% at Ruse. RH is unfavourable for rapeseed. The tolerance to it can be improved by optimization of soil water supply and the other managed crop growing factors. RH tendencies are negative and if keeping the same course in future, the drought conditions will get to the worse.

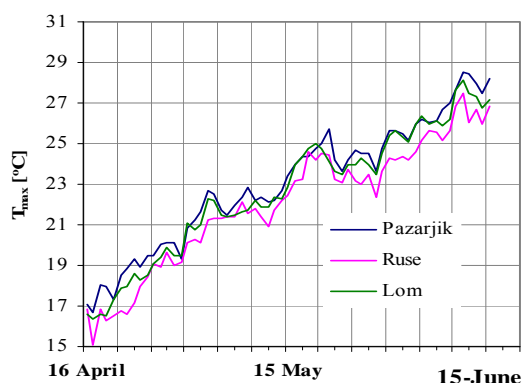


**Fig. 4.** Dynamics of 15 Apr-15 Jun maximum daily air temperature (climatic data, 1971-2000)

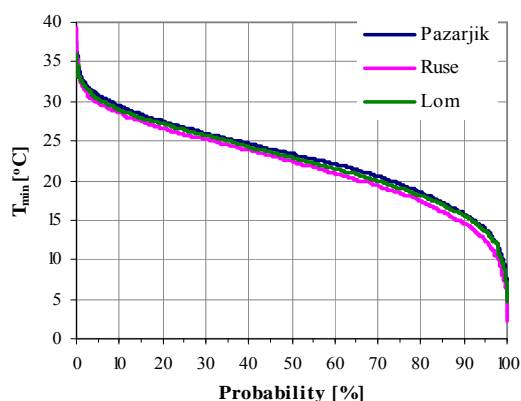


**Fig. 5.** Probability of 15 Apr-15 Jun maximum daily air temperature

**Table 3.** Number of cases and average duration of the periods of 3 and more consecutive days, with  $T_{\max} \geq 27^\circ\text{C}$ , 15 April-15 June, 1971-2000

Station	Total day nb	Days with $T_{\max} \geq 27^\circ\text{C}$	Ratio Col. 3 to Col. 2, [%]	Ave. dur. of the per., longer than 3 days, $T_{\max} \geq 27^\circ\text{C}$ , [days]	$c_v$ of the periods, longer than 3 days, with $T_{\max} \geq 27^\circ\text{C}$ , [%]
1	2	3	4	6	7
Pazardjik	1860	508	27,3	5,6	52,1
Ruse	1860	371	19,9	4,6	57,5
Lom	1860	448	24,1	5,4	43,4

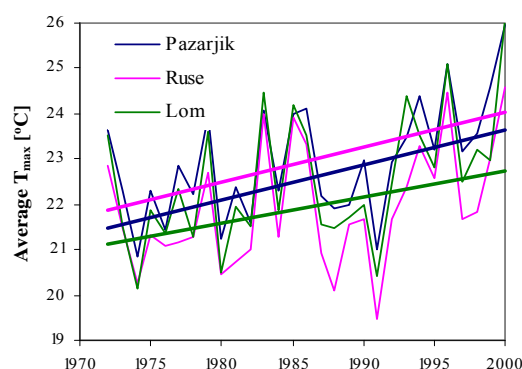


**Fig. 6** Tendency of 15 Apr-15 Jun maximum daily air temperature

### Soil water regime

The available water content (AWC) in the top 100 cm under winter wheat during the production year cycle varies a lot (Fig. 11). Since there are no soil moisture measurements under rapeseed in our country, we will get to know about it from the measurement under the winter wheat, which has analogous vegetation period and evapotranspiration. AWC does not complete field capacity at its highest level during winter and early spring in neither of the three soil types. It is around 90% of FC in March. At the time of sowing it is around 50% of FC and is the same at flowering & seed filling in May and June.

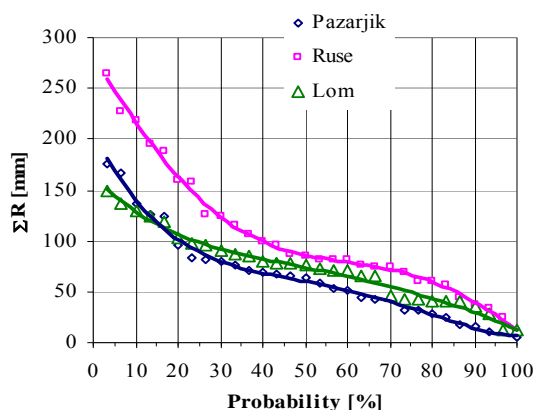


**Fig. 7** Probability of Aug-Sept rainfall sum

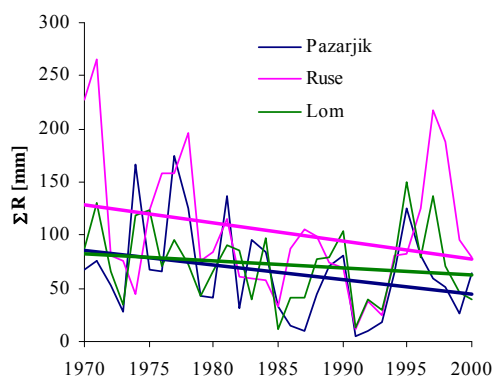


**Fig. 8** Tendency of Aug-Sept rainfall sum

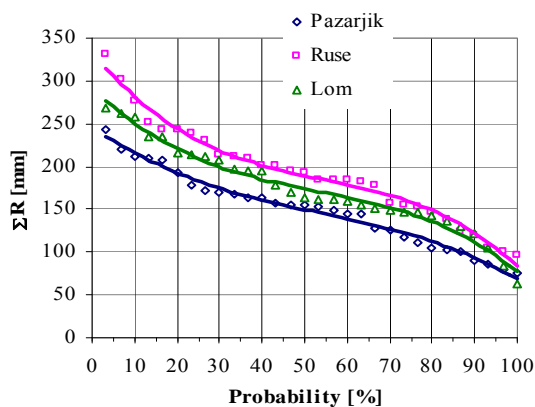


**Fig. 9.** Probability of Apr-Jun rainfall sum

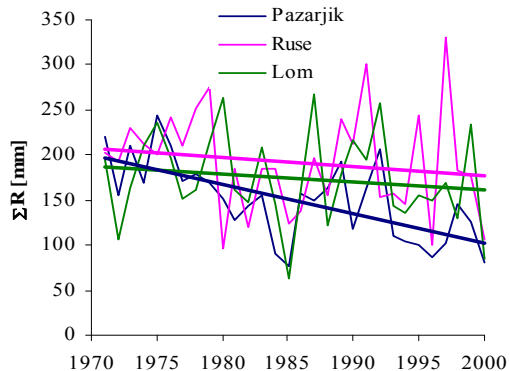


**Fig. 10.** Tendency of Apr-Jun rainfall sum

**Table 4** Statistical properties of the rows of August-September and April-June rainfall sums

Indices	August-September			April-June		
	Pazardjik	Lom	Ruse	Pazardjik	Lom	Ruse
Aver. [mm]	63,9	77,9	110,6	149,3	174,1	191,7
St.dev. [mm]	43,4	38,8	70,5	44,3	50,6	57,6
$c_v$ [%]	67,9	49,8	63,7	29,7	29,1	30,1

**Table 5.** Number and average duration of the periods, longer than 9 days, without rain

Station	Number of more than 9-day per. without rain	Average duration [days]	$c_v$ of period duration [%]
Pazardjik	30	15,4	34,3
Ruse	33	14,3	31,0
Lom	28	14,5	30,9

**Table 6.** Statistical properties of the row of 15 April-15 June relative air humidity

Indices	Pazardjik	Lom	Ruse
Aver. [%]	67	72	69
St.dev. [%]	1,8	1,9	2,3
$c_v$ [%]	2,7	2,7	3,4

binding agronomic practice for germination and emergence and the best solution for obtaining high and stable yields in drought years with low rainfalls, which may also guarantee the producer income.

Growing rapeseed as in Southern, so in Northern Bulgaria needs irrigation. It should be a

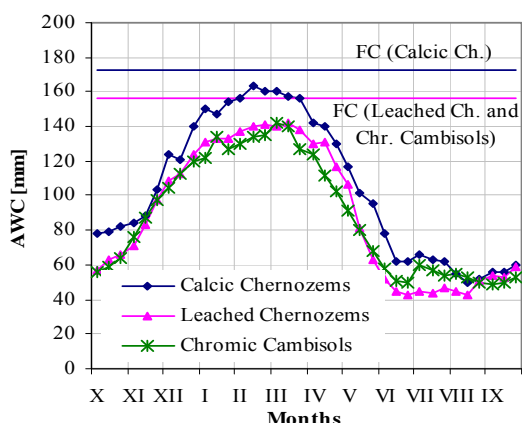


**Fig. 11** Dynamics of the available water content within a production year cycle under winter wheat (climatic data 1971-2000)

### Conclusions

1. The soil and climatic peculiarities of the regions of Lom (Northwestern Bulgaria), Ruse (Northeastern Bulgaria) and Pazardjik (South Central Bulgaria) permit rapeseed growing under certain agronomic practices.
2. The risks of killing minimum air temperatures in winter – less than  $-10^{\circ}\text{C}$  – is 4,6% at Lom, 7,6% at Pazardjik and 10,9% at Ruse. The risks of stressing high May-June temperatures – above  $27^{\circ}\text{C}$  – is 23,7% at Pazardjik, 21,9% at Lom and 18,1% at Ruse. The length of stress periods that can be endured by the hardened rapeseed are expected to be around 4 days in winter and 14 days in spring vegetation period, with around 50% variability. Relative humidity in spring is low – under 70% of FC.
3. Right timing of the sowing date will guarantee good winter surviving of the rapeseed cultivars. Irrigation should be a binding agronomic practice for ensuring germination and emergence and the best solution for obtaining high and stable yields in drought years with low rainfalls in spring.

### Acknowledgements

The authors express their high appreciation to the Bulgarian National Science Fund for its financial support - Project DO 02-8/03.02.2009 “Present and Future Climate change, mitigation and development of sustainable Agriculture in Bulgaria”.

### References

- [1]. Walton, G. H.-Si, P.-Bowden, B.: Environmental impact on rapeseed yield and oil. Proceedings 10<sup>th</sup> International Rapeseed Congress, Canberra, 1999, p.26-29.
- [2]. Rapeseed Growers Manual, Rapeseed Council of Canada. Internet: [https://rapeseed-council.merchantsecure.com/rapeseed\\_resources/product6.aspx](https://rapeseed-council.merchantsecure.com/rapeseed_resources/product6.aspx)
- [3]. Morrison, M.J.-Stewart, D.W.: Heat stress during flowering in summer Brassica. Crop Science, 2002, 42, p.797-803.
- [4]. Tesfamariam, E.H.: Modelling the soil-water balance of rapeseed *Brassica napus* L. (Hyola 60), University of Pretoria etd., 2004, Internet: <http://upetd.up.ac.za/thesis/available/etd-09212004-082030/unrestricted/00dissertation.pdf>
- [5]. Sinaki, J.M.-Heravan, E.M.-Rad, A.H.S.-Noormohammadi, G.-Zarei, G.: The effects of water deficit during growth stages of rapeseed (*Brassica napus* L.). American-Eurasian J. Agriculture and Environment Sciences, 2007, 2(4), p.417-422.
- [6]. Ahmadi, M.-Bahrani, M.J.: Yield and yield components of rapeseed as influenced by water stress at different growth stages and nitrogen levels. American-Eurasian J. Agric. and Environ. Science, 2009, 5(6), p.755-761.
- [7]. Faraji, A.-Latifi, N.-Soltani, A.-Rad, A.H.S.: Effect of high temperature stress and supplemental irrigation on flower and pot formation in two rapeseed (*Brassica napus* L.) cultivars at Mediterranean climate. Asian Journal of Plant Science, 2008, 7(4), p.343-351.
- [8]. Nuttall, W.P.-Molin, A.P.-Townley-Smith, L.J.: Yield response of rapeseed to nitrogen, phosphorus, precipitation, and temperature. Agronomy Journal, 1992, 84, p.765-768.
- [9]. Slavov, N.-Alexandrov, V.: Influence of global climatic change on agroclimatic resources in Bulgaria. Coptes rendus de L'Academie Bulgare des Sciences, 1997, 50, 2, p.31-34 (in Bulgarian).
- [10]. Petkova, N.-Alexandrov, V.-Koleva, E.: Snow Cover Variability in North Bulgaria. Bulgarian Journal of Meteorology and Hydrology, v.15 (1), 2010, p.9-20

## DETERMINATION OF FAULT TOPOLOGY IN MECHANICAL SUBSYSTEMS OF AGRICULTURAL MACHINERY BASED ON FEATURE FUSION AND NEURAL NETWORKS

DIMITRIOS MOSHOU<sup>1\*</sup>, DIMITRIOS KATERIS<sup>1</sup>, IOANNIS GRAVALOS<sup>2</sup>,  
SPYROS LOUTRIDIS<sup>3</sup>, NADER SAWALHI<sup>4</sup>, THEODOROS GIALAMAS<sup>2</sup>,  
PANAGIOTIS XYRADAKIS<sup>2</sup>, ZISIS TSIROPOULOS<sup>2</sup>

<sup>1</sup>Aristotle University, School of Agriculture, Agricultural Engineering Laboratory, 54124  
Thessaloniki, Greece, Phone: +302310992864, Fax: +302310998729,  
E-mail: dmoshou@auth.gr

<sup>2</sup>Technological Educational Institute of Larissa, School of Agricultural Technology,  
Department of Biosystems Engineering, 41110 Larissa, Greece.

<sup>3</sup>Technological Educational Institute of Larissa, School of Technological Applications,  
Department of Electrical Engineering, 41110 Larissa, Greece.

<sup>4</sup>School of Mechanical and Manufacturing Engineering, The University of New South  
Wales, Sydney 2052, Australia

### Abstract

Bearings form an essential part of the mechanical subsystems of agricultural machinery and their failure is one of the most common causes of machine breakdowns. Accordingly, in order to increase reliability and reduce loss of production, condition monitoring of bearings has become more and more important in recent years. The use of vibration signals is quite common in the field of condition monitoring and fault diagnosis of bearings. Vibration analysis is based on the use of acceleration measurements from bearings in order to assess their health status. Advanced signal processing is used to construct a number of informative features that are sensitive to specific bearing faults and fault locations. The fusion of specific statistical features and the introduction of new features enable the accurate discrimination of faults based on their location. The capability of neural networks to visualize high-dimensional data is well known. They map nonlinear statistical relationships among variables of high dimensional input data on a low dimensional network, in a topology preserving fashion. The presented work concerns a neural network based diagnostic system architecture for monitoring the topology of extended faults in bearings. A Self-Organizing Map (SOM) based approach has been used to map time series of feature data produced by acceleration sensors in order to capture the process dynamics. The evolution of system states following the bearing health trend has been shown to successfully identify different bearing faults according to their location.

### Introduction

Bearings are located at the heart of rotating machinery and play a very important role in industrial applications and are mainly used to support and fix the axle in rotating machinery. Their failure in practical operation can lead to the breakdown of the whole machine. Accordingly, to increase reliability and reduce loss of production condition monitoring of bearing gets more and more important in recent years. The use of vibration signals is quite common in the field of condition monitoring and fault diagnosis of bearings [1].

A machine vibration signal is composed of three parts, stationary vibration, random vibration, and noise. To inspect raw vibration signals, a wide variety of techniques have been introduced that may be categorized into two main groups: classic signal processing [2] and intelligent systems [3]. To make mention of a few, FFT, Wigner–Ville distribution [4], wavelets [5], blind source separation [6], statistical signal analysis [7], and their combinations [8] are classic signal processing methods. ANN-based, GA-based, FL-based, various similar classifiers [9], expert systems [10], and hybrid algorithms [11] can be classified



as intelligent systems. Currently, industrial applications of intelligent monitoring systems have increased due to the progress of intelligent systems.

### The SOM algorithm

The Self-Organizing Map also called SOM [12] is a neural network that maps signals from a high-dimensional space to a one- or two-dimensional discrete lattice of neuron units. Each neuron stores a weight. The map preserves topological relationships between inputs in a way that neighbouring inputs in the input space are mapped to neighbouring neurons in the map space. SOM mimics the clustering behaviour observed in biological neural networks by grouping units that respond to similar stimuli together.

The learning rule of the SOM consists of two distinct phases: first phase starts when an input  $\mathbf{x}$  is presented, search for the best matching unit or *bmu* through competition, and the second phase consists of the incremental update or learning of the codebook patterns of the *bmu* and its neighbours. In the basic SOM the activations of the units are inversely proportional to their Euclidean distances from the input pattern hence the *bmu* can therefore be defined as:

$$b(\mathbf{x}) = \arg \min_{i \in M} \|\mathbf{x} - \mathbf{m}_i\| \quad (1)$$

where  $b(\mathbf{x})$  is the index of the *bmu*,  $\mathbf{m}_i$  is the codebook vector of unit  $i$  and  $\mathbf{x}$  is the input pattern vector. The update part of the rule moves the *bmu* and its neighbours toward  $\mathbf{x}$  to slightly enforce maps response to the pattern. The update rule can be written as follows:

$$\Delta \mathbf{m}_i = \gamma \cdot h(b(\mathbf{x}), i) (\mathbf{x} - \mathbf{m}_i) \quad (2)$$

where  $\gamma$  is a learning rate parameter and  $h(b(\mathbf{x}), i)$  captures the neighbourhood interaction between the *bmu*  $b(\mathbf{x})$  and the unit  $i$  being updated.

### Diagnosis of faults in rotating machinery

Today's industry uses increasingly complex rotating machines, some with extremely demanding performance criteria. Attempting to

diagnose faults in these systems is often a difficult and daunting task for operators and plant maintainers. Machine failure can lead to economic loss and safety problems due to unexpected and sudden production stoppages. In rotating machinery, the root cause of faults is often faulty rolling element bearings. One way to increase operational reliability and thereby increase machine availability is to monitor incipient faults in these bearings.

The use of vibration signals is quite common in the field of condition monitoring of rotating machinery. By comparing the signals of a machine running in normal and faulty conditions, detection of faults like mass unbalance, rotor rub, shaft misalignment, gear failures and bearing defects is possible. These signals can also be used to detect the incipient failures of the machine components, through the on-line monitoring system, reducing the possibility of catastrophic damage and the down time.

The procedure of fault diagnosis starts with data acquisition, followed by feature extraction, fault detection and identification. Feature extraction is critical for the success of the diagnostic procedure. Rolling element bearings often fail due to spall and extended defects in the inner and outer races (see an example in Fig. 1), and the rolling elements.



**Fig. 1.** Example of a extended fault in the inner race.

A gearbox test rig has been used in order to collect signals from different types of bearing faults. A photograph of the rig showing the position of the accelerometers and the encoder at the output shaft is shown in Fig. 2 [13]. Two types of faults (inner race and outer race crack) were tested under a 50 Nm load, while setting the



output shaft speed to 10 Hz (600 rpm). Vibration signals were collected using two accelerometers positioned on the top of the gearbox casing above the defective bearing and sideways respectively. The 1.35 seconds (65536 samples)

signals were sampled at 48 kHz. A photo-reflective switch was placed near the output shaft to measure its speed by providing a once per rev tacho signal. The torque for each case was measured at the input shaft.

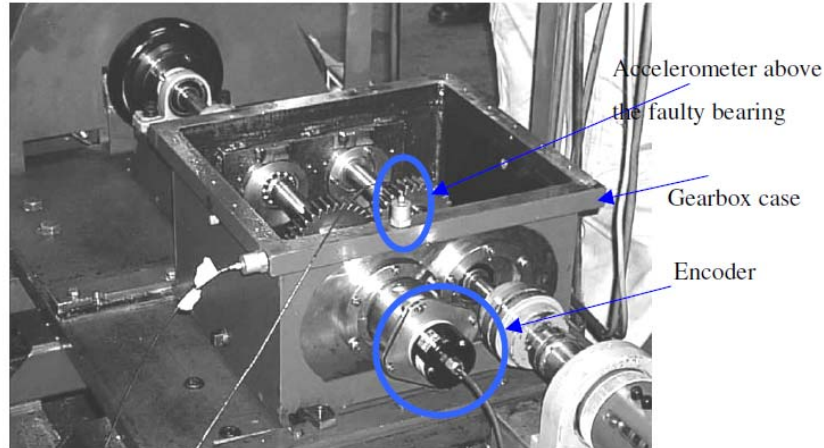


**Fig. 2.** The spur gear rig.

### SOM approach for monitoring fault topography

The algorithm of Kohonen for training the SOM is a nonlinear projection method. It maps different characteristic features into the clusters on the map, without performing an explicit modeling of the system. The feature selection stage is one of the most important factors in the success of modeling. Using Kohonen's algorithm the feature data get mapped onto different regions on a 2D topographic map. Once the SOM network is trained, it is exposed to actual data from the system (in the form of the same type of features used for the training set) representing a yet unknown state. The data points are mapped onto the network as they are sequentially fed to the map describing the current state of the system. The current state SOM based estimation can be retrieved based on already stored labels representing fault classes.

Feature extraction was performed using two features, Kurtosis and a newly proposed feature consisting of the line integral of the acceleration signal. Both provide statistical information about the nature of data, and were found to be reasonably good features for bearing fault detection. The Kurtosis is the fourth moment about the mean normalized with variance and for

a sliding window of N sampling points is given by Eq (3):

$$K = \frac{\sum_{i=1}^N (x_i - \mu_x)^4}{N\sigma_x^4} \quad (3)$$

The new line integral feature for a sliding window of N sampling points is given by Eq (4):

$$LI = \int_a^b ds \approx \sum_{i=1}^N \|\vec{r}(t_i + T_s) - \vec{r}(t_i)\| = \sum_{i=1}^N \sqrt{(x(t_i + T_s) - x(t_i))^2 + T_s^2} \approx \sum_{i=1}^N |x(t_i + T_s) - x(t_i)| \quad (4)$$

Where N is the number of sample points (equal to 500) in the window used to calculate Kurtosis and the newly proposed line integral feature and  $T_s$  is the sampling period. Given the high sampling rate of 48 kHz and the domination of the signal from high frequencies (especially due to the presence of faults), the final approximation contains only acceleration values. The feature vectors are then fed to the SOM for training. To test the effectiveness of SOM, the 75% have been used for training while the 25% have been used in order to test the generalization of the SOM. The implementation used the SOM Matlab Toolbox [14].

## Results and discussion

For the experiments a map size of 7x32 was used. Following a voting procedure for allocation of labels on the SOM in Fig. 3(a) shows clusters formed on the SOM with their fault classes.

For the case of the fusion vector of features, the component maps in Figs. 3(b) and 3(c) show the distribution of Kurtosis and the component maps in Figs. 3(d) and 3(e) show the distribution

of line integral values respectively for the units of the SOM. The fusion (by direct concatenation) of features from both the vertical and the horizontal accelerometer, due to their complementary nature, results in more accurate separation of classes regarding fault position as one can deduce from the results presented in Table 1 which indicates the superiority of the fusion based classification result.

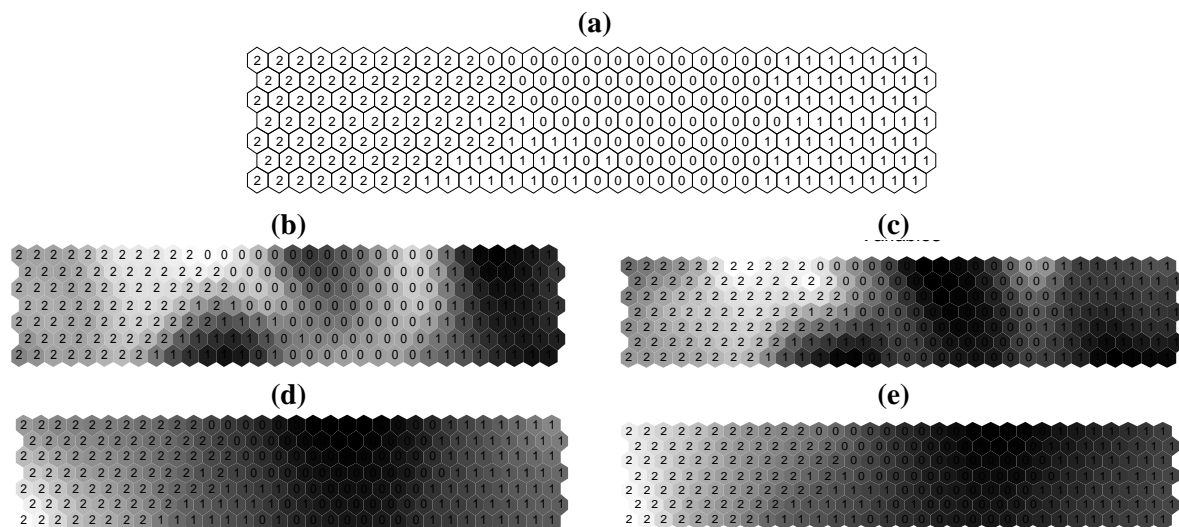


**Fig. 3.** Different manifestations of the features are shown for the fusion vector:

- (a) Labels correspond to extended fault types (0:intact, 1:inner race fault, 2:outer race fault).
- (b) Component map corresponding to Kurtosis (vertical accelerometer).
- (c) Component map corresponding to Kurtosis (horizontal accelerometer).
- (d) Component map corresponding to Line integral (vertical accelerometer).
- (e) Component map corresponding to Line integral (horizontal accelerometer).

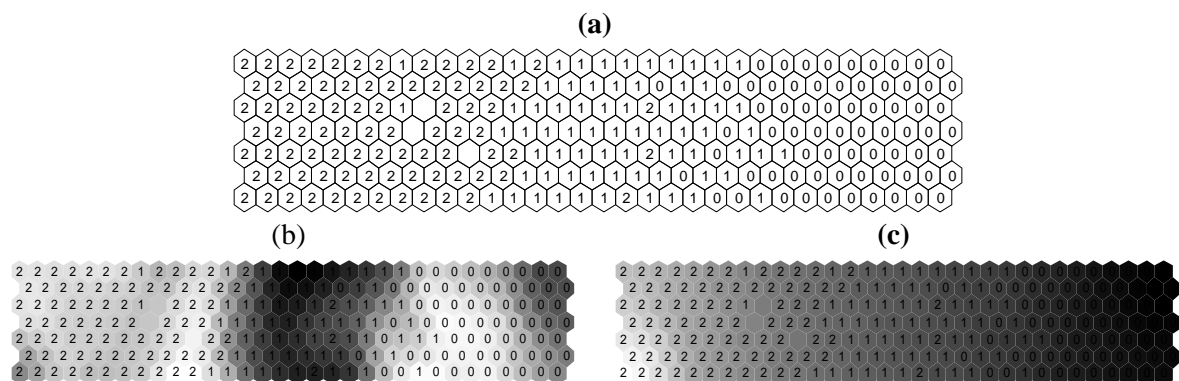


**Fig. 4.** Different manifestations of the features are shown for the vertical accelerometer:

- (a) Assigned labels corresponding to different extended faults (0: no fault, 1: inner race fault, 2: outer race fault).
- (b) Component map corresponding to Kurtosis (vertical accelerometer).
- (c) Component map corresponding to Line integral (vertical accelerometer).

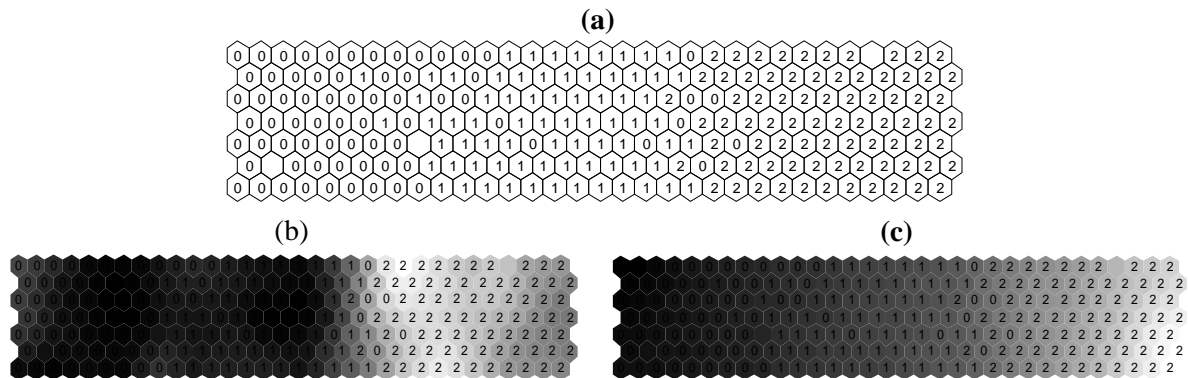


**Fig. 5.** Different manifestations of the features are shown for the horizontal accelerometer:  
(a) Assigned labels corresponding to different extended faults (0: no fault, 1: inner race fault, 2: outer race fault).  
(b) Component map corresponding to Kurtosis (horizontal accelerometer).  
(c) Component map corresponding to Line integral (horizontal accelerometer).

**Table 1.** Results of classification of faults depending on their position by using a vertical accelerometer, a horizontal accelerometer and the fusion features from both. The testing set has been used consisting of the 25% of the data

<i>Fusion (% correct class estimate for healthy-inner race fault-outer race fault)</i>			<i>Vertical (% correct class estimate similar to fusion)</i>			<i>Horizontal (% correct class estimate similar to fusion)</i>		
91.4504	7.1756	1.3740	91.4504	8.2443	0.3053	76.4885	20.4580	3.0534
6.2595	92.0611	1.6794	11.6031	75.8779	12.5191	17.0992	81.8321	1.0687
1.5267	3.5115	94.9618	1.3740	18.4733	80.1527	1.0687	5.4962	92.8244

## Conclusions

It has been shown that the SOM can be used to detect faults in roller bearings and discover the position of the faults, and can therefore prove to be a powerful tool for bearing health monitoring. Different bearing faults can be detected with high accuracy by using the collective response of several features and the fusion of different sensors, which may not be obvious by just looking at the data using other diagnostic techniques. The use of kurtosis and a newly introduced feature, the line integral of the acceleration signal has given promising results in detecting the position of bearing faults. The feature based fusion of the vertical and horizontal acceleration signals has increased the accuracy of fault detection to 92-95% for different fault types. This result represented a substantial increase in discrimination performance of at least 10% for certain types of fault. It is planned that this work be extended to include more real data, different features and

spall sizes for bearings in gearboxes or other machines.

## References

- [1] Xu, Z.-Xuan, J.-Shi, T.-Wu, B.-Hu, Y.: Application of a modified fuzzy ARTMAP with feature-weight learning for the fault diagnosis of bearing. *Expert Systems with Applications*. 36, 2009, p. 9961-9968.
- [2] McFadden, P. D. & Smith, J. D.: Vibration monitoring of rolling element bearings by the high-frequency resonance technique – A review. *Tribology International*, 17(1), 1984, p. 3–10.
- [3] Paya, B. A.-Esat, I. I.-Badi, M. N. M.: Artificial neural network based fault diagnostics of rotating machinery using wavelet transforms as a preprocessor. *Mechanical Systems and Signal Processing*. 11(5), 1997, p. 751–765.
- [4] Baydar, N.-Ball, A.: A comparative study of acoustic and vibration signals in detection of

- gear failures using Wigner–Ville distribution. *Mechanical Systems and Signal Processing*. 15(6), 2001, p. 1091–1107.
- [5] Wang, C.-Gao, R. X.: Wavelet transform with spectral post-processing for enhanced feature extraction. *IEEE Transactions on Instrumentation and Measurement*. 52(4), 2003, p. 1296–1301.
- [6] 13. Tse, P. W.-Yang, W. X.-Tam, H. Y.: Machine fault diagnosis through an effective exact wavelet analysis. *Journal of Sound and Vibration*. 277, 2004, p. 1005–1024.
- [7] Jardine, A. K. S.-Lin, D.-Banjevic, D.: A review on machinery diagnostics and prognostics implementing condition-based maintenance. *Mechanical Systems and Signal Processing*. 20(7), 2006, p. 1483–1510.
- [8] Fan, X.-Zuo, M. J.: Gearbox fault detection using Hilbert and wavelet packet transform. *Mechanical Systems and Signal Processing*. 20, 2006, p. 966–982.
- [9] Saravanan, N.- Kumar Siddabattuni, V. N. S.- Ramachandran, K. I.: A comparative study on classification of features by SVM and PSVM extracted using Morlet wavelet for fault diagnosis of spur bevel gearbox. *Expert Systems with Applications*, 35(3), 2008, p. 1351–1366.
- [10] Ebersbach, S.-Peng, Z.: Expert system development for vibration analysis in machine condition monitoring. *Expert Systems with Applications*. 34(1), 2008, p. 291–299.
- [11] Rafiee, J.-Tse, P. W.-Harifi, A.-Sadeghi, M. H.: A novel technique for selecting mother wavelet function using an intelligent fault diagnosis system. *Expert Systems with Applications*. 36, 2009, p. 4862–4875.
- [12] Kohonen, T.: *Self-organizing Maps*. Springer-Verlag, Berlin Heidelberg New York, 2001.
- [13] Sawalhi, Nader, *Diagnostics, Prognostics and Fault Simulation For Rolling Element Bearings*, PhD Thesis, University of New South Wales, 2007, Australia.
- [14] URL: SOM Toolbox  
<http://www.cis.hut.fi/projects/somtoolbox/>
- [15]

## MECHANICAL PROPERTIES OF POLYMERIC PARTICLE COMPOSITES

MIROSLAV MÜLLER \*, PETR VALÁŠEK, LUKÁŠ TOMEK

Czech University of Life Sciences, 165 21 Prague 6 – Suchbát, Czech Republic,

Phone: +420224383261, E-mail: muller@tf.czu.cz

### ABSTRACT

Polymeric particle composites make possible not only the further usable properties extension of adhesives application for jointing, but for renovation of worn-out parts, too. For economical profitability specification of machine parts renovation using polymeric particle composites their research is important. The research targets the knowledge of the dependence between the epoxy adhesives and the filler particles fraction of different concentration. As the connecting phase the two-component. Epoxy adhesive LEPOX UNIVERSAL P11 ECO was used. Epoxy resins are the versatile thermosets for structural use. They are of medium degradation processes resistance. The  $\text{Al}_2\text{O}_3$  particles were the discontinuous phase.

### INTRODUCTION

The knowledge of applied materials behaviour is the basic presumption of the optimal material choice. The plastic materials and materials developed on their basis are without question the dynamic developing materials group. In this group the polymeric particle composites can be included. They combine synergic the mechanical properties of the filler with the suitable properties of the matrix. Cementing is the primary determination of these material systems, where the static and dynamic stress can be supposed. For the mechanical properties specification at the present economic indicators consideration their behaviour and with it connected research is important.

The substantial change of mechanical properties can be reached by addition of optimal filler content in adhesive. In this way the polymeric particle composite of specific properties comes into being. The optimal usable properties of these composites are limited above all by the risk of the cohesion failure, which is caused by the filler unsuitable concentration and material.

All parameters, depending on the composite materials, are connected either with their structure or with the interphase relations. Single phases influence the material resulting properties partly by their own characteristics, partly by the mutual interaction of matrix and filler. Just thanks to interaction between single components it is possible to reach other good-quality materials [1]. Composite materials can include

fillers of various sizes. In engineering such micro-composite materials are of the greatest importance, whose maximum cross size usually does not exceed  $10\text{ }\mu\text{m}$  [2]. In the matrix the particles must be uniformly distributed, because otherwise the composite strength decreases related to the single matrix strength, namely at the relatively low portions of particles [3]. By the addition of the solid micro-size filler optimal portion in polymer its strength and wear resistance often increases [1, 4]. Concentration is generally considered to be one of substantial parameters influencing the whole composite properties [5]. Misek [6] presents the important criterion for the multiphase material system submission among composites, i.e. content of minimal 5% filler content. Other multi-component systems, which do not fulfil the mentioned criterion, cannot be considered to be composite materials [6]. The next important characteristic is homogeneity. The non-guaranteed homogeneity is posing a great risk of fractures formation and propagation [5, 7, 8, 9, 10]. In particle composites the fillers from hard and thermodynamic stable compounds are used. The silicon carbide (SiC) and the aluminium carbide ( $\text{Al}_2\text{O}_3$ ) are the most significant, both in form of irregular particles [11].

The main task of the matrix is to interconnect the discontinual filler phase. This task should be kept also after first failures. This demand is met above all by metal and polymer matrix [12]. The subject of carried out experiments was the polymeric particle



composite, whose continuous phase was in the form of two-component epoxy adhesive and discontinuous phase of corundum ( $\text{Al}_2\text{O}_3$ ). By experiments the tensile stress, rated relative elongation and impact strength related to the filler part by volume were determined. The research of the given problems proposes the deeper knowledge of the dependence between the two-component epoxy adhesive and the filler in form of  $\text{Al}_2\text{O}_3$ . The research target is to obtain such polymeric particle composite whose properties are optimal and stable with regard to competitive systems of similar base offered on the market.

## MATERIALS AND METHODS

The particle composite was made from two basic phases. The two-component epoxy adhesive LEPOX UNIVERSAL P11 ECO was the matrix, the abrasive corundum micro grains  $\text{Al}_2\text{O}_3$ , grit F 600 (grain size 9.3  $\mu\text{m}$ ), F 800 (grain size 6.5  $\mu\text{m}$ ) or F 1200 (grain size 3.0  $\mu\text{m}$ ) were the filler [13]. The determination of component parts concentration was expressed by means of volume percentage. Composites were prepared using from 5 to 25 volume percentage of filler (gradation 5%). The encompassment of injection/casting technology of prepared polymeric mixture in ready moulds was the substantial step. The form and size of moulds meets the corresponding standards. The moulds for casting were made from the material Lukapren N using models. The composite mixture injection in the moulds was carried out using syringe of 20 ml capacity.

In the first phase before the preparation technology encompassment the specimens were of low compactness and homogeneity. After the technology encompassment this status was eliminated. For elimination of test specimens of low compactness and for minimizing of results affected by this factor the X-ray analysis in the Physics department of CUA was carried out. By mixing of the specified matrix – filler phases ratio the composite was made, which was used for the preparation of test specimens according to the specified standards. The impact strength was measured according to the standard CSN EN ISO 179-1 (Plastics – Determination of Charpy impact properties – Part 1: Non-instrumented impact test) using the test specimens with the A type notch [14]. For experiments the 50 J Charpy

impact machine was used. At experiments smaller values than 2 J were reached. The scale division did not allow the more accurate readout of consumed energy. This fact led to the use of the Dynstat method. Its scale range (max. 2 J) and the scale division were fully satisfactory. The test specimen preparation and impact tests were carried out according to the standard CSN 64 0611 (Determination of the impact resistance of rigid plastics by means of Dynstat apparatus). By the destructive testing the impact strength  $a_n$  was determined according to the relation (1) [15].

$$a_n = \frac{A_n}{b \cdot h} \quad (1)$$

Where  $a_n$  – impact strength [MPa],  
 $A_n$  – energy consumed for the test specimen breakage [kJ],  
 $b$  – test specimen width [m]  
 $h$  – test specimen thickness [m].

The test specimens for the tensile properties determination according to the standard CSN EN ISO 527-1 (Plastics – Determination of tensile properties – Part 1: General principles) [16] were prepared according to the standard CSN EN ISO 3167 (Plastics – Multipurpose test specimens, Czech Standard Institution) [17]. By the destructive testing the tensile strength  $\sigma_M$  and the rated relative elongation  $\varepsilon_t$  were determined. The tensile strength  $\sigma_M$  was calculated using the relation (2) [12].

$$\sigma_M = \frac{F}{A} \quad (2)$$

Where:  $\sigma_M$  – tensile strength [MPa],  
 $F$  – measured force [N],  
 $A$  – initial cross-section of the test specimen (width x thickness) [ $\text{mm}^2$ ].  
The rated relative elongation  $\varepsilon_t$  was calculated using the relation (3)

$$\varepsilon_t = \frac{\Delta L}{L} \cdot 100 \quad (3)$$

Where:  $\varepsilon_t$  – rated relative elongation [%],  
 $\Delta L$  – distance increase between jaws [mm],  
 $L$  – initial distance between jaws [mm].

## RESULTS

The cast composite test specimens were of Ra 0.44  $\pm$  0.11  $\mu\text{m}$ , Rt 5.42  $\pm$  0.75  $\mu\text{m}$  surface roughness. The tensile test (CSN EN ISO 527-1)



is the most wide-spread static test. The result file showed that the one-phase mixture of the two-component epoxy adhesive without filler phase showed the maximal values of the tensile strength. But the  $\sigma_{CSN\ EN\ ISO\ 3167 - 0\%}$  value  $45.48 \pm 1.11$  MPa is not too high compared with the strength of particle composite with 5% filler phase of  $Al_2O_3$  F800 value of  $\sigma_{CSN\ EN\ ISO\ 3167 - 5\%} = 44.07 \pm 0.72$  MPa. From the 3D contour graph made from interlayered measured values using the least square method {Fig. 1) it is visible that with the increasing amount of filler and increasing filler grit (i.e. with the grain size decrease) the tensile strength decreases.

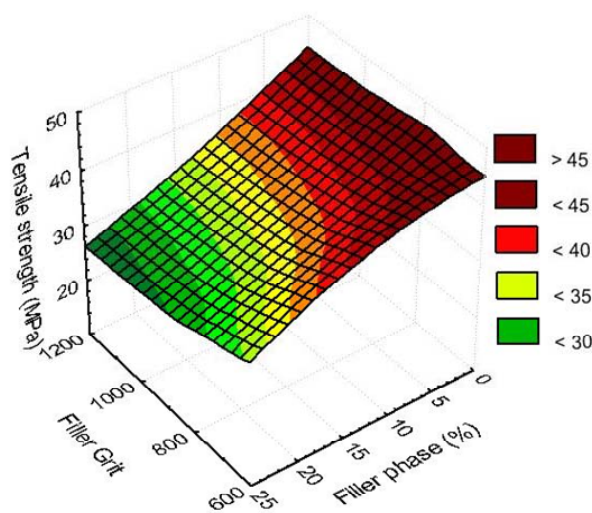


Fig. 1 Polymeric composite on the basis of epoxy resin and filler  $Al_2O_3$

The particle composite tensile strength showed the decreasing trend at the increasing amount of the filler phase. The tensile strength of the own adhesive and of the composite containing the filler phase in form of  $Al_2O_3$  of F600 grit from 5 to 15% showed the average decrease of 7.3%. The more expressive tensile strength decrease occurred at the F800 and F1200 grit, about 18%. The expressive tensile strength decrease occurred at all grits at 20% and 25% filler concentration, namely in the range from 20 to 44%.

From the 3D contour graph (Fig. 2) the behaviour of the dependence between the rated relative elongation  $\epsilon_{t\ CSN\ EN\ ISO\ 3167}$  and the filler percentage amount and the  $Al_2O_3$  grit is evident. From Fig. 2 it is evident the rated relative

elongation decrease with the increasing filler phase part and decreasing filler grit (i.e. grain specific size increase).

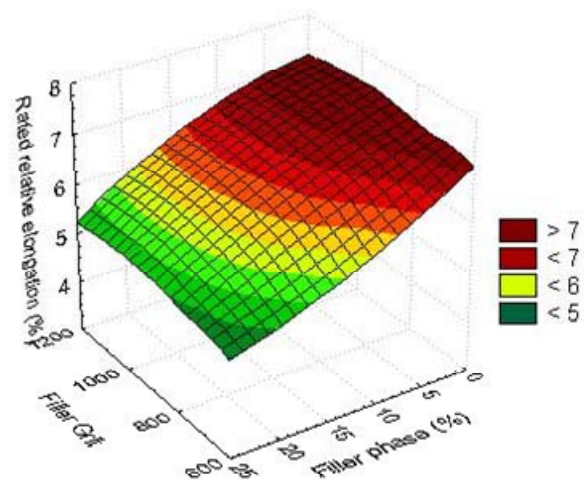


Fig. 2 Polymeric composite on the basis of epoxy resin and filler  $Al_2O_3$

The rated relative elongation decrease up to 33% was reached at the F600 grit (i.e. higher fraction size) and filler phase increasing amount.

The impact strength results  $a_n$  are visible in Fig. 3. The increasing filler volume percentage reappears itself negatively in the reached impact strength values  $a_n$ . From the results the trend of reached values culmination at the grit F800 compared with other grits of F600 and F1200 is visible.

The plane of break of broken specimens showed mild marks of “filler deposition” during the curing process in the test specimen’s bottom part. This fact was confirmed by the resulting hardness values. The hardness was measured using the Shore D method.

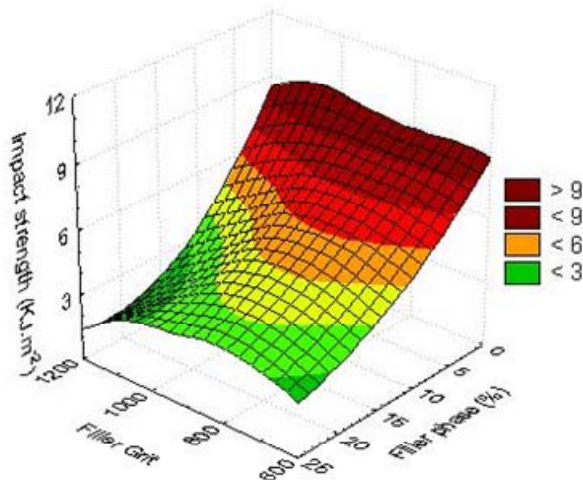


Fig. 3 Polymeric composite on the basis of epoxy resin and filler  $\text{Al}_2\text{O}_3$

## CONCLUSIONS

Composite materials represent the group which asserts oneself increasingly in many fields of human activity and knowledge. By the synergic effect these materials connect the properties of single phases and in this way they enable to reach better properties than it is given by their simple sum. On this effect the production philosophy and these materials use are based. Experimental measuring was intended to demonstrate the definite dependences between “particle” composites of different filler phase part by volume and their properties. The particle composite demonstrated the decreasing trend of the tensile strength at the filler phase part increase.

On the basis of laboratory results it is possible to agree to the statement of Jiao Weizhou et al. that epoxy adhesives are of low impact strength and that they are brittle [18]. Contrariwise the statement of authors Jiao Weizhou et al. [18] and Xue X. Wang [19] did not prove true who present that by the resin modification by filler on the basis of  $\text{Al}_2\text{O}_3$  and others the properties may be significantly improved.

The brittleness and decreasing strength with increasing filler content are the disadvantages of propounded composite materials. On the other side they offer considerable wear resistance,

when wear is the integral part of the practical use and implicated considerable material losses [20].

The economical evaluation of composite materials submitted to laboratory experiments was based on the costs calculation. The unit costs related to 1 g of prepared composite mixture (epoxy resin and filler) are on the average  $0.38 \text{ CZ.g}^{-1}$ . The average costs on the similar basis prepared cement are  $1.5 \text{ CZ.g}^{-1}$ . For the comparison of parameters, their evaluation and filler phase optimal part determination it is necessary to define the composites possible use. The materials put to the tests are suitable for the use as cements eventually as adhesives. The decision on use must be a trade-off between given indexes. For the concrete application it is possible to respect and point out properties, which are in concrete conditions important.

## Acknowledgement

*This paper has been done in the framework of the solution of the grant IGA TF, No. 31140/1312/3117 under the title “Interaction of adherend, adhesive and bonded joint”*

## REFERENCES

- [1] BYUNG CHUL KIM, SANG WOOK PARK, DAI GIL LEE: Fracture toughness of the nano-particle reinforced epoxy composite. *Composite Structures*, 86 (2008), Elsevier, 2008, p. 69 – 77
- [2] KOŘÍNEK, Z.: Composites [online], [cit. 2008-11-20]. Available: <http://www.volny.cz/zkorinek> (in Czech)
- [3] MACEK, K., ZUNA, P. et al. *Material science*. ČVUT, Prague 1996, 209 p. (in Czech)
- [4] DONG CHANG PARK, et al.: Wear characteristics of carbon-phenolic woven composites mixed with nano-parcicles. *Composite Structures*, 74 (2006), Elsevier, 2006, p. 89 – 98
- [5] LENERT, J.: *Mechanics of composite materials*. VŠB, TU Ostrava, 2002, 80 p. (in Czech)
- [6] MÍŠEK, B.: *Composites*. Technický dozorčí spolek, Brno, 2003, 81 p. (in Czech)
- [7] KULBAGOVÁ, J., RUŽBARSKÝ, J.: Duroplast materials used in compression moulding in production process. In: Scientific paper. Operation and diagnostics of machines and production systems

- operational states. Volume 2. Lüdenschied: RAM, Verlag, 2009, p. 122 - 127.
- [8] RAGAN, E., RUŽBARSKÝ, J., MAŇAS, M. et al.: *Vstrekovanie a spracovanie plastických hmôt*. Prešov: FVT Prešov, 2008, 548 p. (in Slovak)
- [9] KULBAGOVÁ, J., RUŽBARSKÝ, J.: Lisovanie výrobkov z duroplastov a ich kontrola kvality. In: *Nové trendy v prevádzke technických systémov 2009*. Prešov: FVT Prešov, 2009, p. 44 - 46. (in Slovak)
- [10] RAGAN, E., ŽARNOVSKÝ, J.: Testing of plasma and heat sprayed layers on dies and further parts with liquid metal at pressured die casting. *Manufacturing technology*, no. 9, 2009, p. 11 – 15.
- [11] Micromechanics, reference material for lectures [online]. [cit. 2008-9-4]. Available: <http://delta.fme.vutbr.cz/mikromechanika/kompozityA4.pdf> (in Czech)
- [12] MACEK, K., ZUNA, P. et al.: *Engineering materials*. ČVUT, Prague, 2003. 204 p. (in Czech)
- [13] Abrasive grain size: FEPA „F“ 42-D-86: [online]. 2009, [2009-01-20]. Available: <http://www.bestb.cz/velikost.php>. (in Czech)
- [14] CSN EN ISO 179-1 (2001): Plastics – Determination of Charpy impact properties – Part 1: Non-instrumented impact test, Czech Standard Institution, Prague, 2001. 19 p. (in Czech)
- [15] CSN 64 0611 (1968): Determination of the impact resistance of rigid plastics by means of Dynstat apparatus, Czech Standard Institution, Prague, 1968. 5 p. (in Czech)
- [16] CSN EN ISO 527-1 (1997): Plastics – Determination of tensile properties – Part 1: General principles, Czech Standard Institution, Prague, 1997. 15 p. (in Czech)
- [17] CSN EN ISO 3167 (2004): Plastics – Multipurpose test specimens, Czech Standard Institution, Prague, 2004. 11 p. (in Czech)
- [18] WEIZHOU JIAO, YOUZHILI LIU, GUIHENG QI: Studies on mechanical properties of epoxy composites filled with the grafted particles PGMA/Al<sub>2</sub>O<sub>3</sub>. *Composites Science and Technology*, 69 (2009), p. 391 – 395.
- [19] XUE QUNJI, WANG QIHUA: Wear mechanisms of polyetherketone composites filled with various kinds of SiC. *Wear*, 213 (1997), 54 – 58 p.
- [20] MÜLLER, M., VALÁŠEK, P.: Polymeric composites based on waste reinforcing particles coming from surface mechanical treatment process. *Strojírenská technologie*, special number (2010), p. 183 – 186. (in Czech)

## THE QUALITY OF CUT SURFACE WITHOUT COOLING

MIROSLAV MÜLLER <sup>1</sup>, JURAJ RUŽBARSKÝ <sup>2</sup>, JÁN PAŠKO <sup>2</sup>, JOZEF ŽARNOVSKÝ <sup>3</sup>,  
PETR HRABĚ <sup>1\*</sup>

<sup>1\*</sup> Czech University of Life Sciences, 165 21 Prague 6 – Suchbát, Czech Republic,

Phone: +420224383274, E-mail: hrabe@tf.czu.cz

<sup>2</sup> Faculty of Manufacturing Technologies of the Technical University of Košice with a seat in  
Prešov, Štúrova 31, 080 01 Prešov, Slovakia

<sup>3</sup> Technical faculty, Slovak University of Agriculture of Nitra, Slovakia

### Abstract

The paper deals with the evaluation of machining quality with a high ecological level when some machining parameters are changed. The criteria of the quality were the machined surface roughness as well as the temperature during machining.

A temperature measured during machining is possible to judge from the measured values that the temperatures increase intensely on the beginning of machining. During machining a next area the temperature was stabilized and rose smoothly only. The temperature measured at speed 140 m.min<sup>-1</sup> have an analogous course but with higher increase of temperatures during the whole machining. The roughness of the so machined surface was also ascertained at the material machining. An increase of the surface roughness in dependence on the machined area is obvious from the results. Deteriorating the surface roughness in dependence on the machined area at machining with the cutting speed 140 m.min<sup>-1</sup> is minimum only. The values of cutting tip wear after machining ascertained with microscope demonstrate that the smallest wear was reached at the lowest feed.

### INTRODUCTION

The development of products trends to pretentious constructions almost in all lines of economy. Therefore greater accuracy of dimensions, geometrical shapes and quality of their surface are demanded. Thus machining technology in spite of lower productivity as well will have an exercising. The machining has the exercising in lot and mass production mainly in finishing operations, where the manufacturing technologies are not sufficient to fulfill the demands of the dimensional and geometrical accuracy and the quality of surface. The new materials of the cutting tools, the sintered carbides, the cubic nitride of boron and the cutting ceramic tools with ten up to hundred times greater resistance to wear than the steel cutting tools are developed for the increase of the quality of finish and the geometrical dimensions. The advantage of these materials is that they secure the stability of cutting at high cutting speeds, as well. We reach lower cutting forces and more favorable thermal conditions at cutting with these materials. The present experiences refer on using possibilities of these materials at dry machining. At machining without cutting

liquids on their working and liquidation fall off simultaneously.

The assumption for economical utilizing of the modern full automatic and program controlled automatic machines is the optimum course of the cutting process i.e. the use of the optimum working conditions. The choice of the optimum working conditions supposes a perfect knowledge of regular ness of their influence on economical and qualitative results of machining. The knowledge of physical laws of the process of metals cutting always widens and deepens. It is impossible to say that the matter of theoretical rudiments of cutting process is already managed and solved up in all extend. The reason is a great complicatedness of physical and chemical processes that create the substance of the cutting process and a great number and extend of parameters influencing its course. Therefore it is impossible to use always successfully the laws of physics of rigid phase, theory of plasticity, mechanics of rigid phase and thermo mechanics. Their deriving is founded on the row of simplified assumptions.

It is possible to reach the improvement of the finish quality and the geometrical accuracy, as well by the new cutting materials. It is possible



to reach the lower energetic pretension at machining also the increase of environment protection at the use of these materials.

One of progressive possibilities how to lower the costs substantially and how to eliminate an unfavorable effect of cutting liquids on the environment ecologically is a use of machining without the cutting liquid so named dry machining. The arguments for the dry machining and the possibilities for the application of the dry machining at turning and milling grow.

The adjusted parameters of machining also the cutting material and its properties influence the quality of the machined part, the finish and total machining in a great extend. The temperature of cutting, the cutting resistance and the plastic deformation influence the measured qualitative parameters how the roughness of a surface, the strain hardness, the remainder stress and the tribological properties.

The aim of the work was to evaluate the quality of surfaces machined by turning without the use of the cutting liquids by technology of hard turning. The contribution deals with the increase of ecological level of production process with the possibility of the choice and optimalization of machining parameters.

## MATERIAL AND METHODS

The test specimens were produced from the cylindrical bar from the material 14 100 with the dimensions  $\varnothing 40 \times 350$ . This material was

hardened in whole cross section on the hardness 58 HRC. The surface was machined after hardening by roughing. After it the finish machining followed by the cutting blade from the material Cerment. The machining parameters were equal at all specimens. The cutting speed and the edge of the cutting blade simultaneously were changed only. Machining parameters:

Cutting speed:

- specimen No.1:  $v_{c1} = 95 \text{ m.min}^{-1}$
- specimen No.2:  $v_{c2} = 140 \text{ m.min}^{-1}$
- specimen No.3:  $v_{c3} = 185 \text{ m.min}^{-1}$

Feed:  $f = 0.098 \text{ mm}$

Depth of cutting:  $a_p = 0.1 \text{ mm}$

The cutting blade from the ceramic material with the designation DNGA 15 04 08T 01020 was used for machining at turning. For measurement the used appliances:

- The set for measurement of temperature during machining by direct thermocouple.
- The device for measurement of roughness SurfTest 301 Mitutoyo Kawasaki – for measurement of surface roughness.
- The microscope CARL ZEISS JENA 5763 – for measurement of a wear of cutting blades.
- The wear of the cutting blade characterized the measured dimensions " $KV_p$ ", " $VC$ ", " $s$ " of the wearied part of the tool point according fig. 1.

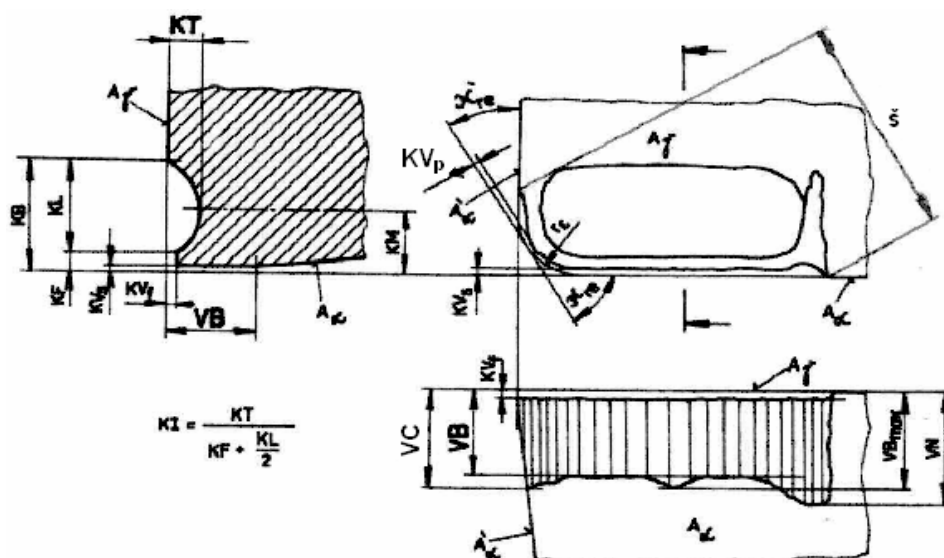


Fig. 1 Measured parameters of cutting blade wear

## RESULTS

The temperature during machining ( $\theta$ ), the mean arithmetic deviation of profile (Ra) and the cutting blade wear as the evaluating criteria were recorded. Figure 2 records the temperatures measured during machining. It is possible to judge from the measured values that the temperatures grow intensely in the beginning of machining. The temperature stabilized and grew temperately only during machining course of the following area.

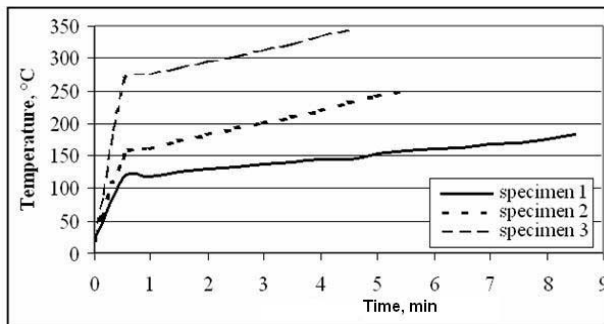


Fig. 2 Measured values of temperature during cutting operation

The values of the temperatures measured at the speed  $140 \text{ m} \cdot \text{min}^{-1}$  have the analogous course but with higher growth of the temperatures during whole machining. The temperature grows considerably in the short time at the cutting speed  $185 \text{ m} \cdot \text{min}^{-1}$  with regard to greater volume of cut material in equal time. The roughness of the so machined surface, as well was found out after material machining. The measured values of the roughness characterized by the mean arithmetic deviation (Ra) are in figure 3.

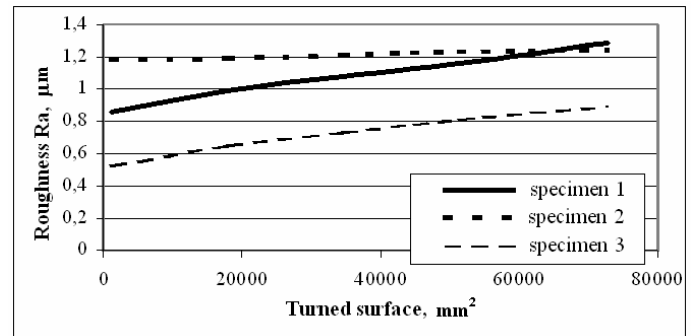


Fig. 3 Measured values of turned surface roughness in relation to turned surface

The growth of the surface roughness in dependence from the machined area is obvious from the results. The deterioration of the surface roughness in dependence on the machined area is minimum only at machining with the cutting speed  $140 \text{ m} \cdot \text{min}^{-1}$ . This growth is more evident at the other cutting speeds. The surface roughness in dependence from the cutting speed is lower visibly at its increase. It is necessary to choice the machining parameters rightly for reaching the lowest roughness at turning. It is possible to reach the roughness on the grinding level by right combination of the cutting speed, the feed, the cut depth, the tool point radius and further machining parameters.

The values of cutting blade wear after machining found out with help of microscope prove that the smallest wear was reached at the lowest feed. The wears of the individual cutting blade points after turning are recorded on figures 4, 5 and 6.

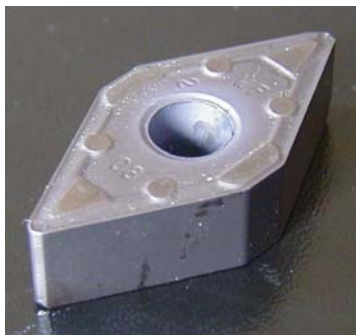


Fig. 4 Worn cutting blade after turning of the specimen No. 1



Fig. 5 Worn cutting blade after turning of the specimen No. 2



Fig. 6 Worn cutting blade after turning of the specimen No. 3



The values of the blade wear measured under microscope are:

- Specimen No. 1: No visible wear, a fine increase only was.
- Specimen No. 2:
  - The width of the point wear  $W_{PW} = 0,15$  mm
  - The point wears on back  $VC = 0,48$  mm
  - The point wears on front  $KV_P = 0,11$  mm
- Specimen No. 3:
  - The width of the point wear  $W_{PW} = 1,14$  mm
  - The point wears on back  $VC = 0,86$  mm
  - The point wears on front  $KV_P = 0,89$  mm

## CONCLUSIONS

Technology of dry machining contributes significantly to ecologization of manufacturing processes and to lowering costs for liquidation of damages of ecological accidents due to cutting liquids. Costs on working cutting liquids fall off from economic point of view. Tool life influence expressively on manufacturing economy therefore it is necessary to give greater attention to evaluating tool life. The advantage of changeable cutting blades is that they have more points.

By measurements and evaluating results it was come to conclusion that by increasing cutting speed also working temperature was increased. Temperature was increased equably and slowly at lower cutting speeds. The intense increase of temperature was at higher speeds. At higher cutting speed quality of machined surfaces is increased, manufacturing times are lowered but also life of cutting edge is lowered and working temperature is increased. With regard to this temperature it would be necessary to reconsider dimensional accuracy of work pieces. From the point of view of the described advantages and disadvantages it would be

convenient to judge choice of machining parameters from the point of view of manufacturing productivity a quality. It influences economic indicators.

## REFERENCES

- [1] BROŽEK, M.: Cutting Conditions Optimization when Turning Overlays. *Journal of Materials Processing Technology*. Volume 168, 2005, Issue 3, pp. 488 - 495.
- [2] BROŽEK, M.: The Turning of Overlays Using Sintered Carbide Tools. *International Journal of Advanced Manufacturing Technology*. Volume 40, 2009, Issue 5 - 6, pp. 438 - 446.
- [3] DREYER, K., HINTZE, W.: Schneidstoffe zur Trockenbearbeitung. In: *Werkstatt und Betrieb*. Hannover, 1997, no.6, p. 420 - 426.
- [4] HUMÁR, A.: *Slinuté karbidy a řezná keramika pro obrábění*. Brno:CCB s.r.o. 1995. 265 p.
- [5] KOCMAN, K., PROKOP, J.: Technologické aspekty soustružení kalených ocelí. In: *Nové směry vo výrobnom inžinierstve 2002*. Prešov: FVT, pp.190 - 193.
- [6] TOMÁŠ, J., KROČKO, V.: Smery vývoja technológie obrábania z hľadiska ekológie. In: *Zborník z medzinárodnej vedeckej konferencie*. Nitra: SPU, 1999, pp. 123 - 125.
- [7] TOMÁŠ, J., KROČKO, V., DRLIČKA, R.: Suché sústruženie ako ekologická technológia obrábania tvrdých materiálov. In: *Technológia '99*, Bratislava: STU, 1999, pp. 607 - 609.

## PHOTOVOLTAIC POWER SUPPLY FOR A DISTANT STANDPOINT

STANISLAVA PAPEZOVA<sup>1</sup>, VACLAV PAPEZ<sup>2</sup>

<sup>1</sup>Czech University of Life Science Prague, 165 21 Praha 6, Czech Republic,  
Phone: +420 224 383 206, E-mail: papezovas@tf.czu.cz

<sup>2</sup>Czech Technical University in Prague, 166 27 Praha 6, Czech Republic,  
Phone: +420 224 352 165, E-mail: papez@fel.cvut.cz

### Abstract

Contribution describes a small autonomic source of electrical power, which is used for continual power supply of a small radio relay terminal station. The station is placed on a hilltop in a distance about 1,5 km from the village. This source is realized as photovoltaic system, which consists of silicon solar cells, accumulators and control circuits. The parameters of the arrangement during one year of the operation are presented in conclusion of our paper.

### Introduction

It is hardly solvable problem to ensure a delivery of an object by electrical power from power network, which is placed out of any village and in the distance about 1 or more kilometres from existing mains. The construction of mains line is too expensive. The costs of a line length 1 kilometre are approximately 10 000 euro, but only in the case, if problems with placing of a lead at foreign parcels do not come into.

An independent electric power supply can be easier solution, especially at that time, if the power consumption is small, or if continuous power supply isn't being asked. For example an electro-central with combustion engine is such source in common use. At present it is possible to provide it from the smallest load about 0,5 kW at the cost of 150 euro up to load of order tens and hundreds of kW at the much higher cost.

Photovoltaic power supply is another advantage solution, especially at that time, if a low power consumption is anticipated (about of units kWh in a week). Use of this kind of photovoltaic power supply is described in our contributions.

This source is used for a power supply of a small relay station of an internet system for a data transmission. It permanent supplies the power supply of the relay station with the energy input about 5 W and occasional short-time power supply of the load up to 1 kW in the case of adjusting or repair work of the station. Source operates practically unattended, only with a random verification roughly once a week.

An arrangement of photovoltaic panels with monocrystalline photocells [1] with maximum power about 320W is primary power supply. This produced power is saved in electrochemical accumulator.

Generated energy is stored in electrochemical accumulator 33 V 280 Ah. The accumulator contains 9 kWh and it can, in the state of a full charge and without further power supply, supply the station approximately 50 days. On the other side, in sunny period, the photovoltaic source charges nearly discharged and at the same time loaded accumulator, in the course of charging affectivity 80 %, during 3 weeks.

System is completed with converter 230 V/50 Hz of maximal continuous output power 1 kW for occasional line voltage power supply of instruments and equipments.

Instantaneous state of the accumulator is monitored by an ampere-hour counter [2] that records the difference of the charge incoming into accumulator and the charge leaving the accumulator

### Construction of a photovoltaic source

Block diagram of the photovoltaic source is displayed in figure 1.

A system of photovoltaic panels is a source of electrical power. An accumulator is charged by produced power. The charging process is controlled by a simple regulator without using a DC/DC convertor, which obstruct accumulator overcharging. Voltage from the accumulator is stabilized by the regulator, which ensures approximately constant output voltage

independent on the state of discharging or accumulator charging, for loading of the relay station. Storage capacity of accumulator is registered by ampere-hour counter, which registers its discharging and also charging current. AC/DC convertor also allows supplying arrangement designed for common mains from the source for a short term.

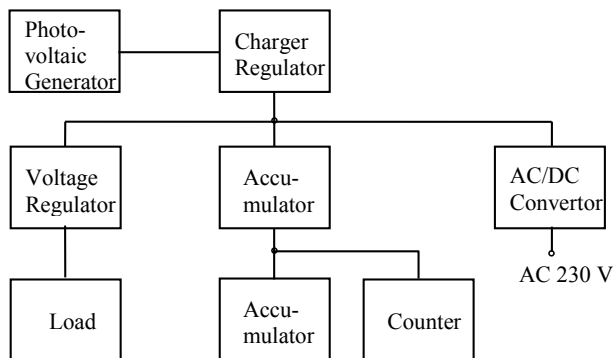


Fig. 1 Block diagram of the photovoltaic source

The construction of the photovoltaic generator goes out of an analysis of incident solar energy in the place of the generator. But for our purpose the design was optimized other way than any other commercial solar panels. There it has not been purpose to optimize an achievement of a maximal produced energy in a year, but to ensure the production at least such energy quantum, which is continuously consumed throughout the year and in each selected time of the year.

Supposed average values of produced energy in a month for photovoltaic generator with peak power 1 kW are displayed in figure 2 [3], [4]. This course is, from above-mentioned reasons, generated for expected optimal panels position with southwards orientation and 60 degree elevation. In figure 2 there are further displayed also reached actual average values in years 2003 till 2005 and minimal values for each month during this period. One month was also considered at the proposal as a suitable time, during which it should delivery the working of the arrangement out of accumulator.

Similar dependence is valid also for generator with the peak output current 1 A and its produced charge. If we next suppose, that the optimal voltage at the loading of photovoltaic generator is constant, which is also approximately fulfilled in practice, dependencies

are equivalent. Therefore the peak current estimation of the generator, which produce in a month required charge (scaling to 100 Ah), was set according to the power production displayed in figure 2. This estimation is displayed in figure 3.

A season of late autumn and winter, months November and December, are the critical season for function photovoltaic source. Especially in December the estimated, average and minimum power of the photovoltaic generator very varies owing to weather. The operation out of the power stored in the accumulator has to be anticipated in the month December for the provision of safe function of the source. The situation is already much better later in the winter after winter solstice, barring permanent coverage with snow panels. Therefore we considered on to operation without charge falling in accumulator or with its charging in all the others months.

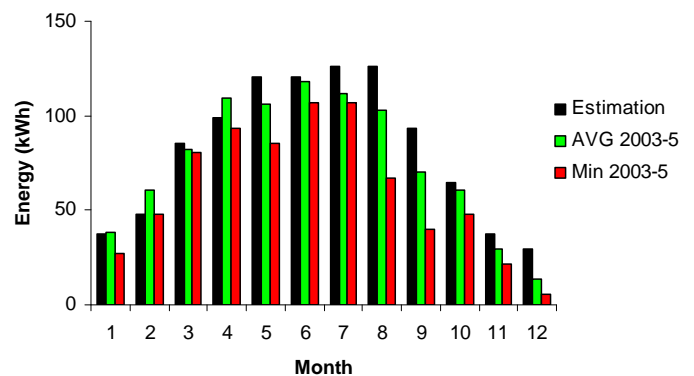


Fig. 2 Energy production of the photovoltaic system in particular months

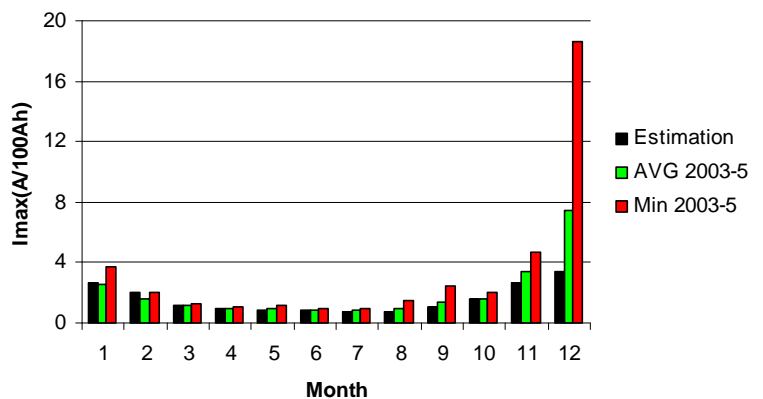


Fig. 3. The peak current estimation for production of charge 100 Ah

The parameter selection of the photovoltaic generator has been basically effected heuristic in final phase, because the final solution of the FV generator is not anyway identified with finding of his optimal parameter, but parameters of parts, which are available on market. So that the verification of the possibility functions on market available panels in generator according to above-mentioned working algorithm and calculation needed minimum capacity accumulator was further procedure. Therefore configuration photovoltaic generator with parallel sequencing panels shouldered with monocrystalline silicon cells, whose peak power is 53 W and optimal voltage 17,5 V at the current 3,03 A [5], was selected in the year 2006. At the operation of the photovoltaic generator according to minimum output power (see figures 2 and 3), the accumulator will be certainly charging in months since February till October. In November the discharge can reach about 40 Ah. A charge minimum probably occurs during January, when further charge fall reaches approximately 160 Ah.

Today we would probably select panels with peak power 125 up to 135 W and voltage approximately 18 V and current approximately 7A for the same parameters of the system. At the same time there is possible to use panels from polycrystalline silicium or from amorphous silicium, that are roughly about 40 % cheaper, but they have roughly about 50 % bigger surface for the same power [6], [7].

Mechanical arrangement photovoltaic generator has been solved with regard on optimal insolation of panels, which will not be affected by surrounding vegetation and at least medium prevention of panels against stealing and damage. That is why the panels were set up to pole up high, where man fails to reach without using tool. Further the panels were closed into a protection cover from wire-netting, which saves panels also before thrown rocks to a great extent. The view of generator system is presented in figure 4.



Fig. 4 Photovoltaic generator

Accumulator for photovoltaic source, as it has been realized, was set together out of alkaline NiCd cells with liquid electrolyte and pocket electrodes [8]. Alkaline accumulator, although its actual price is roughly 4x higher than at cheap lead accumulator, has 4x as much as 5x longer working life. So it has operation costs lower than lead accumulator from the point of view of long-time usage. Alkaline accumulator is able to work in wide temperature interval than lead accumulator, especially in the area of low temperatures. Further its running is less demanding on service. It is able to work with electric parameters, that are away of optimal values without a risk of damage of the accumulator. Gases and exhalation, which are developed at a running of the alkaline accumulator, effects on metallic constructions round far less belligerently, than at lead accumulator.

Accumulator capacity (5 hour capacity) of 280 Ah has been chosen. Accumulator is arranged from 27 battery cell. Under voltage is then, in case of discharge on 1 V per one cell, 27 V for the whole accumulator. It is sufficient for stabilization of the output source voltage 24 V with a small voltage margin. The charging voltage is 1,65 V per one cell for peak voltage, that is 46 V for the whole accumulator. It is



possible to guarantee at the voltage drop approximately 2 V at the regulator and with photovoltaic generator, which is arranged of 3 panels in series connection and with the optimal voltage for maximum power output 17,5 V. Regulator works in linear mode only as voltage peak limiter. Peak power losses on regulator are lower than 50 W at the end of the process charging.

Ampere-hour counter is a basic monitor instrument of the photovoltaic generator. Requirements posed onto the ampere-hour meter of the photovoltaic system are considerably high. Measuring instrument has to enable precise indication of the charge, taken away out of the accumulator at the load current since tenths A until approximately 100 A, with maximum inaccuracy of order units per cent. Next it must embody a good zero stability accordant with absolute measurement error in the area of small currents to the limit of several mA. It is necessary to respect the charging effectivity of the accumulator at the indication of the charge, which is fetched into the storage battery. The measuring instrument in itself must have minimal power losses.

Ampere-hour counter has been developed and realized as a unique apparatus according to the specific requirements of the photovoltaic source. A shunt resistance with resistance 1 milliohm was used for the current scan. It is inserted in the central connection of the accumulator. Instantaneous strength of the current is evaluated by the converter according to the voltage drop at the shunt by the voltage – frequency converter. The counter, which evaluates total sum of converter output impulse, determines the searched charge as an integral of the current in time. Indicated charge is displayed in LCD display of four digits with resolution 0,1 Ah. Amper - hour counter answers above-mentioned requirements from the standpoint of accuracy, stability and dynamic range in the range of the service temperature -10 to + 30 deg C. Its total electric input power is lower than 100

mW at its direct power supply out of positive and negative branches of the accumulator.

Accumulator together with ampere-hour counter is placed in the case from fire-resistant non-conducting material on concrete floor in heatless cubby. The space inside of the case is ventilated out of building. Positive branch of the accumulator and ampere-hour counter are displayed in photo (see figure 5).



Fig. 5 The part of the accumulator arrangement and ampere-hour counter

### Experiences from arrangement operating

Photovoltaic source has been operated since the year 2007. It continually provided service to the relay station. The control has been executed periodically once a week, in order to be always possible to prognoses the source capacity in a period into next check hazardless.

Valuables of the charge, which has been led in accumulator or led out of accumulator, as they were determined by the ampere-hour counter within a year, are displayed in figure 6 (green colour). Real state of the charge in accumulator is restricted of its capacity for full charge (280 ampere-hour) and it's displayed in figure 6 too (red colour). Minimal charge in accumulator was at the end of the 3rd week in January; the charge value 117 ampere-hour has been read, which presents the power reserve on next 3 weeks of the operation.

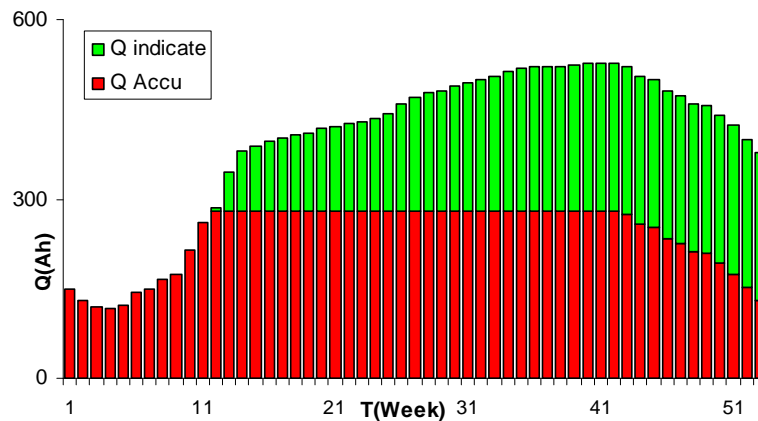


Fig. 6 Changes of the storage capacity of accumulator during of the year 2007

#### Reference

- [1] Goetberger, A., Knobloch, J. and Voss, B.: Crystalline Silicon Solar Cells. Chichester: J.Wiley & Sons. 1998
- [2] Wagemann, H.G., Eschrich, H.: Principles of photovoltaic energy transformations, Mnichov: Teubner Studienbucher. 1994 (German)
- [3] Henze, A. – Hillebrand, W.: Electric current from the sun. HEL Ostrava 2000 (Czech)
- [4] Benda, Macháček: Experiences from operation photovoltaic system FVS 2003A at the Faculty of electrical engineering, CTU in Prague (Czech)
- [5] [www.solartec.cz](http://www.solartec.cz)
- [6] [www.kyocerasolar.de](http://www.kyocerasolar.de)
- [7] [www.neosolar.cz](http://www.neosolar.cz)
- [8] FERAK Nickel-cadmium accumulators, Saft-Ferak a.s., Business office Prague 2004 (Czech)



## CALCULATIONS AND MEASUREMENTS OF ENERGY GAIN FROM SEMI-SPHERICAL SOLAR COLLECTOR

ILZE PELECE

Latvia University of Agriculture,  
Liela 2, Jelgava, Latvia, LV3000  
E-mail: ilze.pelece@llu.lv

### Abstract

In Latvia because of its geographical and climatic conditions are some features in use of the solar energy. There is a long path of the sun at summer, but frequently large nebulosity, which both enlarges necessity to receive the energy from all sides. Therefore conditional flat plate solar collectors are not efficient enough, but new constructions of solar collectors are required. One of such new constructions can be a semi-spherical solar collector, capable receive the solar energy from all sides.

Such semi-spherical solar collector with radius 0.56 m what corresponds to base area 1 m<sup>2</sup> has been made, and measurements of water heating have been carried out at summer 2009.

Theoretical calculations of the energy gain from such collector have been performed and verified by comparison of calculated daily energy sums with measured ones, and good coincidence has been obtained. Results obtained from these calculations shows, that the energy gain from the semi-spherical solar collector with base area 1 m<sup>2</sup> is similar to that of tracking to sun flat collector of 1 m<sup>2</sup> area. The tracking to sun solar collector is complicated, expensive and not durable, but the semi-spherical solar collector is simpler, durable against impact of wind and with good appearance.

Measurements shows, that the energy gain from such semi-spherical solar collector, made from simple materials, is similar to that from 1 m<sup>2</sup> of the industrially manufactured vacuum tubes solar collector.

The energy gain from the semi-spherical solar collector can be increased by using in its construction contemporary special materials and technologies, such as special absorbing colours and selective coatings.

### Introduction

Align with decrease of reserves of fossil fuel, as well as impact of use of fossil fuel on climate, in the world more attention has been paid to renewable sources of energy, including solar energy.

Also in Latvia the solar energy has been used, mostly in solar collectors for hot water production [2,9]. However in Latvia because of its geographical and climatic conditions there are some features in comparison with traditional solar energy using countries [3,4]. In Latvia at summer the length of day excides twelve and maximally reaches seventeen hours, accordingly is also long path of sun, but rather small height of sun (maximally 56 degrees above horizon) and therefore also small intensity of solar radiation. There is also frequently considerable nebulosity. At winter the height of sun is very small (10°) and

the length of day 7 h, therefore use of solar energy at winter in Latvia is not possible.

Because of mentioned above features traditional flat plate collector without tracking to sun is not appropriate enough for use in Latvia, but new collector constructions are required, that would be able to collect the energy from all sides as well as to use the diffused radiation more efficiently.

Such construction a semi-spherical solar collector [1] proposed in this article can be. Such collector has been made and measurements of heated water amount and temperature have been done. Obtained results have been compared with both calculated ones [3,4,6] and measured using vacuum pipes collector.

## Materials and methods

Calculations and measurements of the solar radiation as well as the received energy of the solar collector have been performed in this article.

Measurements of the global solar radiation have been performed using an ISO 1. class pyranometer from “Kipp&Zonen”. Measurements have been performed automatically, taking intensity of radiation after every 5 minutes and accumulating data in a logger. Thereafter from these data the daily energy density has been calculated. Measurements have been carried out from April 2008 till November 2009.

Data on the nebulosity from "Latvian Environment, Geology and Meteorology Centre" have been obtained. The nebulosity is evaluated visually in grades from 0 (clear sky) to 10 (entirely overcast) accordingly the World Meteorology Organization methodology after every 3 hours.

Measurements of the received energy of the solar collector have been performed using a new construction – solar collector with a semi-spherical absorber (Fig.1). The collector is made from a copper sheet shaped as semi-sphere and coloured black. Inside the dome is a copper tube shaped close to dome. Diameter of the tube is 10 mm, length 21 m. In this tube flows heat remover – water, transporting heat to the reservoir. The collector is covered with transparent polyethylene terephthalate (PET) dome. Radius of the collector is 0.56 m, what corresponds to 1 m<sup>2</sup> base area. In order to determine the received energy of collector temperatures of incoming and outgoing water have been measured after every 5 min. Water flow ensured a pump, which productivity was 30 l/h. Measurements with the semi-spherical solar collector have been carried out at 2009 from 1 August to 31 October.



**Figure 1.** Semi-spherical solar collector

In order to measure energy gain from semi-spherical solar collector water flow was measured as well as temperature of incoming and outgoing water. Measurements of temperatures have been done using thermocouples and “Pico” TC-8 termologer, ensuring measurements automatically after every 5 minutes. Then a daily energy gain of collector can be calculated from formula (1).

$$E = \sum C \cdot K \cdot (t_2 - t_1) \cdot \Delta t \cdot 10^{-6} \quad (1)$$

Where:  $E$  – daily energy sum, MJ;  
 $C$  – specific heat of water, J kg<sup>-1</sup> K<sup>-1</sup>;  
 $K$  – water pump productivity, l s<sup>-1</sup>;  
 $t_1$  – cold water (input) temperature, °C;  
 $t_2$  – hot water (output) temperature, °C.  
 $\Delta t$  – interval between measures, s.

The summarizing must include all positive (output water temperature higher than input temperature) values of the day.

At the same time measurements of water heating have been done also using factory-built vacuum tubes solar collector “Vitasol” and energy gain from both collectors has been compared.

For the theoretical calculation of the received energy of some surface [5] at first solar coordinates (declination and azimuth) must be calculated at every moment (we used interval 15 min). From solar coordinates and the orientation of the surface (normal of the surface) the angle of incidence of solar rays  $\beta$  can be calculated. Then the intensity of the radiation received of a surface element can be calculated as

$$I = SP^m \cos \beta + I_D \quad (2)$$

Where:  $I$  – intensity of radiation received by surface,  $\text{W m}^{-2}$ ;

$S$  – solar constant,  $\text{W m}^{-2}$ ;

$P$  – atmosphere lucidity;

$m$  – air mass;

$\beta$  – inclinity of receiving surface, degrees;

$I_D$  – intensity of diffused radiation,  $\text{W m}^{-2}$ .

Intensity of a diffused radiation has been assumed to be constant and equal to  $75 \text{ W/m}^2$ .

The air mass  $m$  accordingly to literature [6] can be calculated from such empirical expression

$$m = \frac{1.002432 \cos^2 z_t + 0.148386 \cos z_t + 0.0096467}{\cos^3 z_t + 0.149864 \cos^2 z_t + 0.0102963 \cos z_t + 0.000303978} \quad (3)$$

Where:  $m$  – air mass;

$z_t$  – true zenith angle, degrees.

In order to determine the daily energy sum received by some surface the intensity calculated from formula (2) have to be integrated (summed up) in time from sunrise to sunset as well as over all irradiated surface.

Impact of clouds can be taken into account using several empirical models [7] with experimentally evaluated numerical coefficients.

Comparison of calculated and measured values has been done using graphical method. The model can be evaluated from the scatter plot of calculated daily energy sums via measured ones. About correspondence of calculated values to measured ones indicate slope (must be close to one) and intercept (must be near to zero) of best-fit line, as well as coefficient of determination  $R^2$  (must be close to one).

## Results and discussion

For calculation of solar coordinates following expressions from astronomical considerations can be obtained via coordinate transformation. For height of the sun

$$\sin \delta = (\cos s \cos \lambda + \sin s \sin \lambda \cos \varepsilon) \cos \gamma + \sin \varepsilon \sin \gamma \quad (4)$$

Where:  $\delta$  – height of the sun, degrees;

$s$  – sidereal time, degrees;

$\lambda$  – ecliptical length of the sun, degrees;

$\varepsilon$  – slope of the earth axis, degrees;

$\gamma$  – latitude of the location.

And for azimuth

$$\sin A = \frac{\sin s \cos \lambda - \cos s \sin \lambda \cos \varepsilon}{\sqrt{1 - \sin^2 \delta}} \quad (5)$$

Where:  $A$  – azimuth of the sun, degrees;

$s$  – sidereal time, degrees;

$\lambda$  – ecliptical length of the sun, degrees;

$\varepsilon$  – slopness of the earth axis, degrees;

Using solar coordinates obtained from these expressions, the intensity of the solar radiation on the horizontal flat surface was calculated from formula (2). Then daily energy density (on  $1 \text{ m}^2$ ) has been calculated using integration of obtained values from sunrise to sunset.

For evaluating of impact of nebulosity following expression has been used

$$E = E_C \left( 1 - 0.76 \left( \frac{M}{10} \right)^{1.7} \right) \quad (6)$$

Where:  $E$  – energy received at cloudy conditions, MJ;

$E_C$  – energy received at clear-sky conditions, MJ;

$M$  – nebulosity, grades.

This expression is improved model from literature [6] with experimentally determined numerical coefficients.

Figure 2 shows calculated intensity received by  $1 \text{ m}^2$  horizontal flat surface via measured with pyranometer from 1 January to 31 October 2009. Good coincidence has been obtained: slope 0.95, intercept 1 and  $R^2$  0.88.

In order to calculate the energy received by any surface, inclination of solar rays on surface has to be calculated from solar coordinates and orientation and declivity of surface.

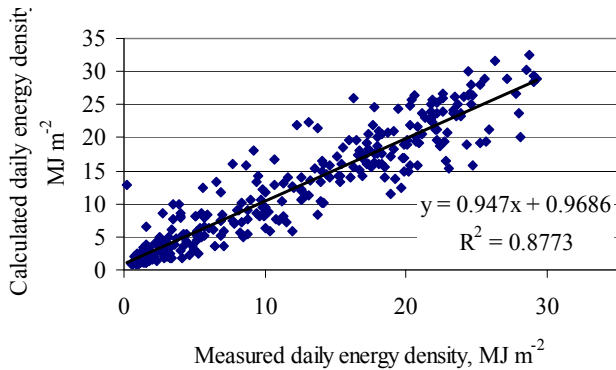


**Figure 2.** Calculated daily energy density on flat horizontal surface via measured with pyranometer, 1 January to 31 October 2009

Let's examine as example calculation of the received energy of a semi-spherical solar collector.

The cosine of angle  $\beta$  between surface normal and direction of ray's incidence (incidence angle) can be expressed as vector product of these two vectors

$$\cos \beta = \vec{n} \times \vec{l} = \sin \theta \cdot \cos(\delta - \varphi). \quad (7)$$

Then the intensity of the direct radiation received by a surface element accordingly formula (2) can be expressed as

$$dJ = I r^2 \sin^2 \theta \cdot \cos(\delta - \varphi) d\theta d\varphi, \quad (8)$$

Where:  $I$  is the radiation density calculated from formula (2).

In order to calculate the received energy of whole surface this expression has to be integrated over all irradiated surface, *i.e.*,  $\theta$  from 0 to  $\pi$  and  $\varphi$  from 0 to  $\pi/2 + \delta$

$$J = I \cdot r^2 \cdot \int_0^\pi d\theta \int_0^{\pi/2+\delta} \sin^2 \theta \cos(\delta - \varphi) d\varphi \quad (9)$$

After integrating we obtain

$$J = I \cdot r^2 \cdot \frac{\pi}{2} (1 + \sin \delta). \quad (10)$$

Then, similarly as previously in case of horizontal surface, obtained results have to be integrated numerically from sunrise to sunset for

calculating of daily energy sum, and impact of nebulosity has to be evaluated using formula (6). Results of these calculations have been compared with measured daily energy gain of hot water, calculated by formula (1). Plot of calculated daily energy sums via measured ones have been shown in Fig.3.

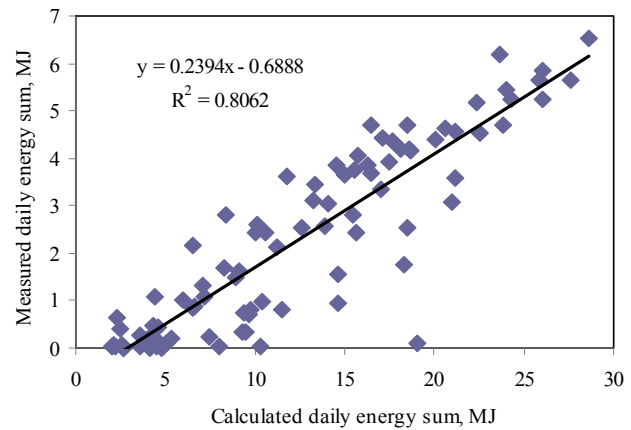


**Figure 3.** Calculated and measured daily energy sums received by semi-spherical solar collector (29 July to 31 October 2009)

Best-fit line obtained using method of smallest squares gives slope 0.24, which in this case characterizes less method of calculations, but efficiency of collector (heat loss), intercept -0.69 and coefficient of determination  $R^2 = 0.81$ .

Measured daily energy gain from semi-spherical solar collector was compared also with that of 1 m<sup>2</sup> of factorialy-made vacuum pipes solar collector. Plot of daily energy gain from both collectors via daily solar energy sum measured with pyranometer has been shown in Fig. 4.

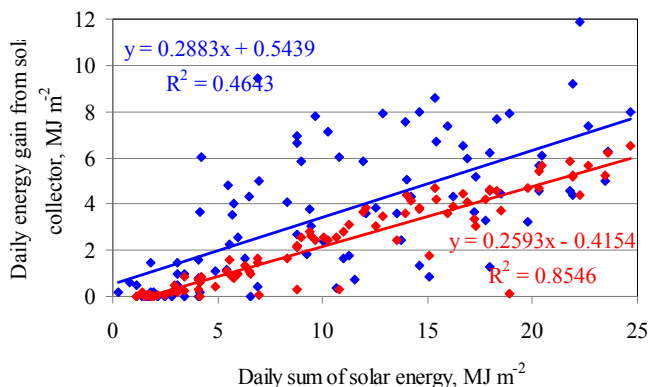


**Figure 4.** Daily energy gain from semispherical (red dots and line) and vacuum pipes (blue dots and line) solar collector via daily sum of solar energy, measured with pyranometer

It can be seen from this graph that daily energy gain from home-made semi-spherical solar collector is to that from factory-made vacuum pipes solar collector. It means that semi-spherical solar collector is appropriate for use of solar energy in Latvia. Additionally, it is more durable against wind impact and good-looking in comparison with other kinds of solar collectors.

It is interesting that coefficient of determination of best-fit line  $R^2$  is 0.85 for semi-spherical collector, but only 0.46 for vacuum pipes collector. It can suggest on smaller dependence of energy gain of semi-spherical solar collector on several meteorological conditions.

## Conclusions

1. Method of calculation of received energy by a solar collector taking into account shape and orientation of the absorber as well as nebulosity has been developed.

2. Results of these calculations for the semi-spherical solar collector are adequate to experimental results.

3. For utilization of the solar energy in Latvia a solar collector with the semi-spherical absorber can be used.

## References

1. Iljins U., Ziemelis I., Pelece I., Ziemelis E. Solar collector with spherical absorber and its applications (In Latvian). *Patent LV 13550 B*
2. Kancevica L., Navickas J., Ziemelis E., Ziemelis I. (2006). Increase of the Efficiency of Solar Collectors. *Proceedings of the Second International Scientific Conference "Biometrics and Information Technologies in Agriculture: Research and Development"*, pp. 89-92, Lithuanian University of Agriculture.
3. Pelece I. (2008). Influence of nebulosity on use of solar energy in Latvia. *Proceedings of the International Scientific Conference "Engineering for rural development 2008"*, pp. 28-33, Latvia University of Agriculture.
4. Pelece I., Iljins U., Ziemelis I. (2008). Theoretical calculation of energy received by semi-spherical solar collector. *Proceedings of the International Scientific Conference "Engineering of Agricultural Technologies 2008"*, Vol. 6. pp. 263-269, Lithuanian University of Agriculture.
5. Pelece I., Iljins U., Ziemelis I. Forecast of energy received by solar collectors. *Proceedings of the International Scientific Conference "Applied Information and Communication Technologies"*. - Jelgava: LLU, 2008. - lpp. 62-67. - ISBN 978-9984-784-68-7.
6. Young, A. T. (1994). Air mass and refraction. *Applied Optics*. 33, pp. 1108-1110.
7. Younes S., Muneer T. (2006). Improvements in solar radiation models based on cloud data. *Building Serv. Eng. Res. Technol.* 27,1 pp. 41-54.
8. Zagars J., Vilks I. Astronomy for high schools (In Latvian). LU 2005.
9. 2] Ziemelis I., Iljins U., Navickas J. (2004). Economical Comparison of Some Parameters of Flat-Plate Solar Collectors. *Proceedings of the International Research Conference "The Role of Chemistry and Physics in the Development of Agricultural Technologies"*, pp. 23 - 25, Lithuanian University of Agriculture.



## DEVICE FOR LONG-TERM DURABILITY TESTING OF TRANSMISSION OILS

BOHUSLAV PETERKA\*

Czech University of Life Sciences Prague, Faculty of Engineering  
Department for Quality and Dependability of Machines  
Kamycka 129, 165 21 Prague 6 – Suchbátov  
Phone: +420 224384334, E-mail: [peterka@tf.czu.cz](mailto:peterka@tf.czu.cz)

### Abstract

Many different transmission oils are available today. These oils are different both in chemical constitution and their purpose. This paper describes simple testing device for long-term durability testing of two different transmission oils. There is short overview of construction and the mode of operation of designed device. Designed and assembled device was operated under a load over 4000 hours. Unfortunately, initial testing had to be stopped due to fatal failure of one of used gearboxes. The final part of this paper briefly discusses the possible reason of this operational fault. In conclusion there are some results and recommendations which are related to operating experience.

### Introduction

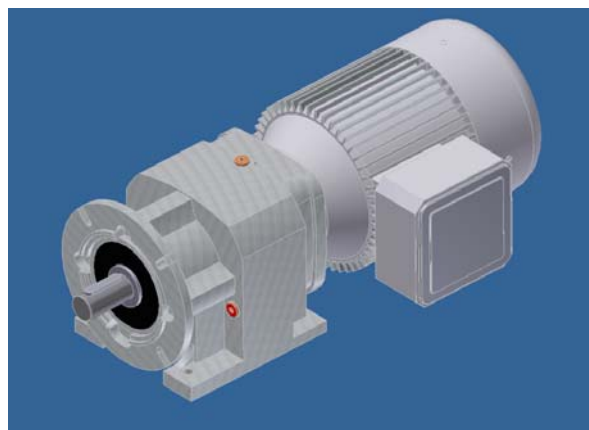
Presently there is wide spectrum of transmission oils on the market. These oils are different both chemical constitution and their purpose of usage. It is appropriate to make independent laboratorial tests to verify of their lubricant and anti-abrasion capabilities. In principle we talk about mechanical-dynamic testing which is simulating stressing of oil in different operational conditions. Based on results of these tests we can presume on ability of the tested oil to be sufficiently anti-wear protecting.

It is possible carry out the check of oils properties by confrontation of manufacturer's specifications of two oils with identical purpose, by making conventional laboratory tests or by using of empirically experience obtained while work load of the machinery. While operational time testing it is necessary to keep tabs on total operational time of the machine, tribological properties of tested oil and on the structural changes of the mechanical parts. The weak observation of frictional couples of gearbox wheels is very complicated (especially in case of robust and more complex machine units). Testing during the operational time of machinery seems to be difficult due to both organization planning and costingness.

In support of testing of couple of transmission oil fillings there has been designed and assembled the testing device for long-term stress testing and continuous analyzing of transmission oils in laboratory conditions.

### Experimental arrangement

Idea of realization of testing device is conceptually based on two gearboxes, which are exposed to approximately equal work load. For construction purposes there has been selected 2 gearmotors NORDBLOCK of nominal power 0.75kW (Picture 1).



**Picture 1** 3D model of NORDBLOCK gearmotor

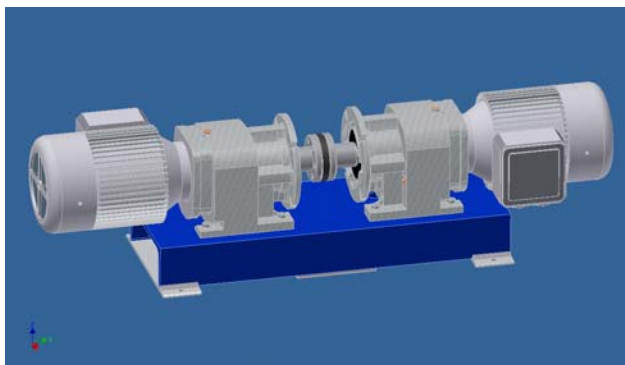
Design of testing device is based on few basic requirements:

- symmetrical design with possibility of observing of two different oil fillings
- adjustable work load
- small dimensions
- autonomous operation
- low power consumption
- user friendly

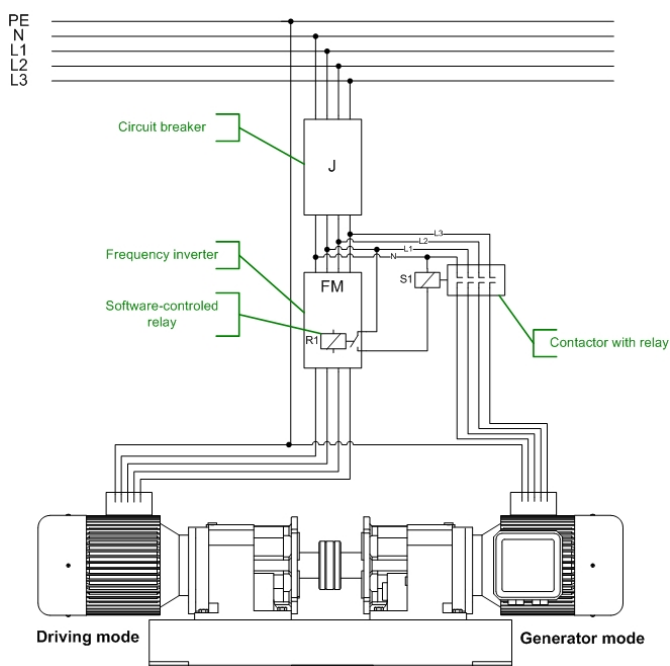


The couple of gearboxes are placed in opposite direction on one common frame. Machine set includes the flexible coupling, which provide transmission of power and partially reduces both parallel and angle axes misalignment (Picture 2).

One of two electromotor is controlled by frequency inverter, which keeps his speed in over synchronous level (driving mode). On this ground the second electromotor works as generator and supply retroactively the electrical network with AC current. To be guaranteed, that the second electromotor is working as AC generator, the second motor is connected to the electrical network programmatically after run up the first electromotor.



**Picture 2** 3D model of testing devices assembly



**Picture 3** Wiring diagram

Presented laboratory testing device provides stressing of pair of oil fillings. Stressing of oil can be both constant and time variable. Evaluation of observed oils can be made continuously while periodic taking of the oil samples or by a single samples taking at the end of each testing. In second case, there are no available trends of evaluated parameters which can be assumed as inconvenient.

### Results and discussion

There was designed and realized laboratory testing device for long-term durability testing of pair of transmission oils. Consequently, this device was equipped with measurement points which provide possibility both of mounting accelerometers and temperature reading. The testing device was plugged via personal computer into computer network. This concept allows remote control and setting up of operation parameters of frequency inverter.



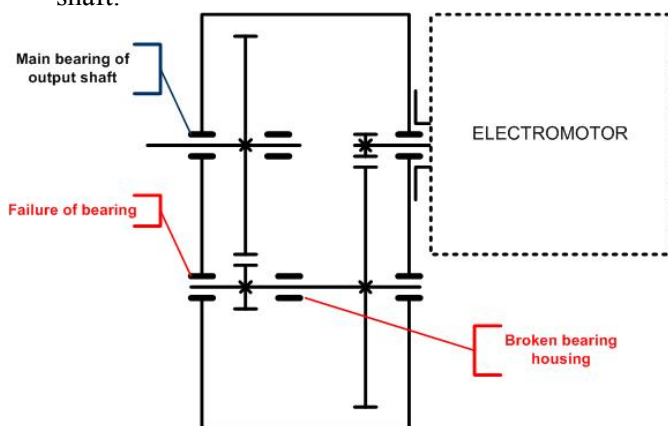
**Picture 4** Final assembly of testing device

Using of complete assembly of testing device was started the laboratory tribological test of pair of transmission oils - mineral oil and biological degradable one which meets the class ISO VG220. Analysis of oil samples were ensured using particle counter and shape classifier LaserNet Fines. During the whole test period the testing device worked under the constant load. The operational load was set at 80% of nominal power of used electromotor-generator (it means 1,8A of 2,2A of each phase current).

Unfortunately the test had to be stopped (after over 4000 operational hours) because of fatal failure of one of two gearboxes. After

disassembling the failed gearbox there was a lot of damaged parts. That includes part of gearbox case and two of ball bearing. It can be assumed that the reason of fatal failure was caused by fraction of gearbox case, which was probably caused by material defect. Consequently the ball bearing was stressed more by parasitic forces and damaged by fatigue wear.

There is important to say, that none of continuously obtained and evaluated diagnostic signals were not predictive the future failure. None of signal levels were over their alarm levels. Presumption, that unexpected failure was caused by material defect of gearbox case or bearing, was supported after inspecting of kinematic conditions of the gearbox (Picture 5). In the case when the failure could be caused by some kind of misalignment of both shafts, it can be supposed that growing failure had to be detected most likely on main bearing of input shaft.



**Picture 5** Schematics of gearbox

## Conclusions

The testing device for long-term durability testing of transmission oils can be used in variable load mode if convenient control software will be developed. Whole circuitry and used frequency inverter can be assumed as proven. The test philosophy is coming out of few simplifications. First one is fact that we assume the structural properties of both gearboxes are the same. In a second case we think the operational load (during overall elapsed-time) is equal for both of gearboxes. The presented device worked well over 4000 operational hour, after this period unexpected failure occurred. This failure can be assigned to material defect of bearing housing (part of gearbox case).

If there will be prepared a new test, there will be appropriate to replace both of gearboxes or make overhauling of them – this can lead to equal structural properties at the beginning of the test. In the future we want to replace both of gearmotors and begin a new set of tests. In order to fully utilize testing device, there will be appropriate to make wide spectrum of tribological analysis (acidity, water content, viscosity index etc.). Detailed results of tribological comparison of both oil filings mentioned above will be presented in another paper.

## References

1. ALEŠ, Zdeněk. *Tribological properties of transmission oils*. Praha, 2010. 134 p. Dissertation thesis. Czech University of Life Sciences Prague.
2. NORD-Drive systems – company publications

## MOMENT OF INERTIA OF ENGINE

MARTIN PEXA

Czech University of Life Sciences Prague, 16521 Prague 6 – Suchbát, Czech Republic

Department for Quality and Dependability of Machines

Phone: +420 224 383 278, E-mail: pexa@tf.czu.cz

### Abstract

The use of dynamic methods for measuring operational parameters of road vehicles begins to increase due to its low demands on time and investment funds. Dynamic measurement of engine performance parameters are generally based on knowledge of the rotating mass moment of inertia of engine and gearing mechanisms including driving wheels. However, it is difficult to obtain an indication of the correct moment of inertia. This paper describes a newly proposed possibility of measurement that is carried on roll test bed with loose rollers. The result of measurement is the moment of inertia, which can also be used in the measurement of performance parameters, brake performance, etc. Example measured data is introduced for vehicles of producer Hyundai, Peugeot and especially Škoda.

### Introduction

Wide development of the dynamic measurement of operating parameters of vehicles and internal combustion engines in recent years offers new possibilities in the diagnosis. One of many possible applications of dynamic acceleration measurement is the measurement of performance parameters (torque, power) of the combustion engine [4]. Measurements can be made only on the engine itself or on the roll test bed or on the test road [3]. In all cases it is necessary to include the correct value in the calculation of the engine moment of inertia, or the whole vehicle. Effect of moment of inertia is essential when measuring the engine itself.

This article focuses on the description of the possibility of measuring the moment of inertia of the engine by itself. Application for the whole vehicle is quite similar. There are several ways to obtain the moment of inertia of the engine:

- *Obtaining information from the manufacturer* - This is not usually a problem with modern engines, factory diagnostic devices offer the possibility of measuring the performance parameters through the acceleration method. Information about the moment of inertia of the engine should be in the diagnostic tools available. The problem is if there is no factory diagnostics, detailed information about the vehicle, or in the case of obsolete vehicles.
- *Calculation* - Moment of inertia can be determined and calculated from the dimensions and other information of various components. This option is very time consuming and requires precise knowledge of the mechanical design and dimensions of all components [9].
- *With makeweight* - Using makeweight of known moment of inertia can be performed two measurements. One measurement with makeweight and second without it. Then, by comparing the results of both measurements can be calculated moment of inertia of the engine. [8].
- *New engine* - If there is a new engine for which the manufacturer guarantees performance parameters, acceleration measurements can be carried out. Then it is possible to determine the value of moment of inertia of the engine by return in order to match the performance parameters with the table values.
- *Dynamometer* - Similarly, as a new engine dynamometer can be used [8]. Moment of inertia is assigned to the resulting values of the acceleration measurements in order to correspond to the values measured on the dynamometer.
- *Average* - Exactness of this method assume measurement of large number of vehicles with the same engine and a gradual refining of moment of inertia.

But sometimes it is impossible to get to the actual moment of inertia with any of described ways [10]. For example, because there is no dynamometer or a new vehicle or the manufacturer's information and it is not possible to mount the make-weight of known moment of inertia. In such cases, there are suitable several other ways, such as measuring of vehicle acceleration on the road or on roll test bed with loose rollers or on the roll test bed itself.

This paper describes the possibility of determining the moment of inertia using modified roll test bed. Authors of the paper invented this method and applied for its patent. It is possible to use proposed method in order to realize dynamic measurement of power parameters [2]. Based on behaviour of power parameters there can be determined technical state and potential faults of engine [7]. Such approach can contribute to better economy and primarily to ecology of vehicle utilization [1], [5].

### Material and methods

Structural adjustment of roll test bed, originally designed only to check the brakes, consisted in the removal of gearbox and connecting electric motors to frequency converters (this is not strictly necessary). Detail of the test bed adjustments is shown in the figure 1, frequency converters are shown in the figure 1B. Angular velocity and angular acceleration of the vehicle engine are calculated from the time recorded data of incremental rotating speed sensor. The sensor (Figure 1A) gives 1024 pulses per revolution (with time accuracy within 20 nanoseconds) at this described specific application.

The sensor is attached to the rollers of test bed. Required values of vehicle's engine are defined by reduction of measured values in the overall speed ratio between vehicle's engine and rollers of test bed.

Possibilities of utilization of roll test bed are extensive and include dynamic measurement of performance parameters of engines of vehicles, measurement of transmission ratios, measuring the dynamic braking forces, etc. Data collection is carried out with eight-channel collector, which ensures online data preprocessing and passes data to the operating computer type PC which is connected through the USB port.



Figure 1 Roll test bed: A - Incremental sensor of roller's revolution, B - Frequency converter

Procedure finding moment of inertia of the vehicle engine is implemented in three steps, which are logically connected and, if necessary, it is possible to print a protocol.

1. The first step is to measure gear ratio between the engine and rollers of test bed for each vehicle. Revolutions of roller test bed measured by an incremental sensor and revolutions of engine measured by the other external sensor are compared. To measure the revolutions of the vehicle engine, it is most suitable to use the diagnostic plug OBD. For instance, if a motor vehicle has 820 rpm, and rollers of test bed have 265 rpm, then the overall gear ratio is 3,094. (1)

$$i_c = \frac{n_m}{n_v} \quad (1)$$

$i_c$  total ratio (-)  
 $n_m$  engine rpm (1/min)  
 $n_v$  rollers rpm of test-room (1/min)

2. The second step is to measure all inertial mass, i.e. the mass of engine, transmission and wheels of the vehicle and rolls and other rotating masses of test bed, reduced to the circumference of rollers. Frequency converters controlled by electric motors are used to measure and it is possible for them to change the performance of approximately 15 to 30 kW (according overload set on converter). Given procedure, in view of the performance characteristics of electric motors roll test bed, is different for engines of vehicles with low inertia mass (lower stroke volume, approximately up to 1,4 dm<sup>3</sup>) and for vehicles with engines higher inertia mass (higher stroke volume more than 1,4 dm<sup>3</sup> and diesel engines).
  - a) Measurement of inertial mass of smaller engines is simpler. The vehicle's engine is running at idling speed revolution, there is geared up chosen gear speed

(recommended is the second). Rollers of test bed are driven by vehicle's wheels and these wheels are spinning with revolutions according idle revolution of engine. After that the electric motors of roller test bed are connected; the frequency converters are set higher speed revolutions than speed revolutions that correspond to idle revolutions of the vehicle. All rotating mass are accelerated by virtue of known power of electric motors. During the acceleration are measured values of the immediate velocity and acceleration, which is calculated from the mass inertia of the rotating mass, reduced with the circumference of rollers. (2)

$$m_{sm} = \frac{m_{v1} \cdot (a_{av1} - a_{dv1}) + m_{v2} \cdot (a_{av2} - a_{dv2})}{(a_{asm} - a_{dsm})} \quad (2)$$

$m_{sm}$	inertial mass of all rotating masses reduced on circumference of rollers inclusive inertial mass of engine (kg)
$a_{asm}$	rollers acceleration of test bed at electromotor acceleration with all inertial masses reduced on circumference rollers ( $m/s^2$ )
$a_{dsm}$	rollers acceleration of test bed at electromotor deceleration with all inertial masses reduced on circumference rollers ( $m/s^2$ )
$m_{v(1,2)}$	rollers inertial mass on left (1) or right (2) side of test - room reduced on their circumference (kg)
$a_{av(1,2)}$	rollers acceleration of test bed at electromotor acceleration on left (1) and right (2) side of test - room ( $m/s^2$ )
$a_{dv(1,2)}$	rollers acceleration of test bed at electromotor deceleration on left (1) and right (2) side of test - room ( $m/s^2$ )

- b) For vehicles' engines with larger inertial mass it is not enough electric power to accelerate the testing of all the rotating mass of the idling speed revolutions. At first the vehicle on the rollers is started by using its own engine to a speed of about 50 km/h and then electric motors are connected. Gas pedal is fully released and all the rotating mass starts to decelerate. The performance of the electric motors

which drives rollers of test bed slows down this deceleration. During deceleration, there are again measured values of instantaneous velocity and acceleration (i.e. deceleration) of them is again calculated inertial mass of the rotating mass, reduced with the circumference of rollers. (3)

$$m_{sm} = \frac{m_{v1} \cdot (a_{av1} - a_{dv1}) + m_{v2} \cdot (a_{av2} - a_{dv2})}{(a_{dsme} - a_{dsm})} \quad (3)$$

$m_{sm}$	inertial mass of all rotating masses reduced on circumference of rollers inclusive inertial mass of engine (kg)
$a_{dsme}$	rollers acceleration of test bed at electromotor deceleration (connected electromotor) with all inertial masses reduced on circumference rollers ( $m/s^2$ )
$a_{dsm}$	rollers acceleration of test bed at electromotor deceleration (unconnected electromotor) with all inertial masses reduced on circumference rollers ( $m/s^2$ )
$m_{v(1,2)}$	rollers inertial mass on left (1) or right (2) side of test - room reduced on their circumference (kg)
$a_{av(1,2)}$	rollers acceleration of test bed at electromotor acceleration on left (1) and right (2) side of test-room ( $m/s^2$ )
$a_{dv(1,2)}$	rollers acceleration of test bed at electromotor deceleration on left (1) and right (2) side of test-room ( $m/s^2$ )

3. In the third step is necessary to determine the inertial mass of all rotating parts except the engine and the relevant parts of the gearbox. The procedure is the same as in the second step, but is no gear shifted. (4)

$$m_{bm} = \frac{m_{v1} \cdot (a_{av1} - a_{dv1}) + m_{v2} \cdot (a_{av2} - a_{dv2})}{(a_{abm} - a_{dbm})} \quad (4)$$

$m_{bm}$	inertial mass of all rotating masses reduced on circumference of rollers without inertial mass of engine (kg)
$a_{abm}$	rollers acceleration of test bed at electromotor acceleration with all inertial masses reduced on circumference rollers, but without inertial mass of engine ( $m/s^2$ )



$a_{dbm}$  rollers acceleration of test bed at electromotor deceleration with all inertial masses reduced on circumference rollers, but without inertial mass of engine ( $m/s^2$ )

$m_{v(1,2)}$  rollers inertial mass on left (1) or right (2) side of test - room reduced on their circumference (kg)

$a_{av(1,2)}$  rollers acceleration of test bed at electromotor acceleration on left (1) and right (2) side of test - room ( $m/s^2$ )

$a_{dv(1,2)}$  rollers acceleration of test bed at electromotor deceleration on left (1) and right (2) side of test - room ( $m/s^2$ )

Result is measured and calculated inertial moment engine (equation number 5). Concrete result is measured moment of inertia at engaged idling position. Segment clutch and gear - box accrue any to the moment inertia engine. Performance engine specifications measured at engaged idling position are required as general result in principle, this measured moment of inertia engine is accurate value. (5)

$$I_m = \frac{(m_{sm} - m_{bm}) \cdot r_v^2}{i_c^2} \quad (5)$$

$I_m$  inertial mass of engine ( $kg \cdot m^2$ )

$m_{sm}$  inertial mass of all rotating masses reduced on circumference of rollers inclusive inertial mass of engine (kg)

$m_{bm}$  inertial mass of all rotating masses reduced on circumference of rollers without inertial mass of engine (kg)

$r_v$  rollers radius of test bed (m)

$i_c$  total ratio (-)

## Results

The method of measuring the moment of inertia the engine was applied to the vehicle Skoda Octavia II 2,0 TDI (103 kW). It is a vehicle that belongs to the category 2b - engines with higher mass of inertia. The resulting measured and calculated values are in the Table 1, where the columns listed in the overall gear ratio between motor vehicles and the roll test bed, the total inertial mass of the rotating mass of vehicle reduced the circumference of rollers, the rotating mass inertia weight without motor vehicles reduced the circumference of a roller the resulting moment of inertia of the rotating mass of the vehicle engine.

Table 1 Results of measurement of vehicle Skoda Octavia II 2,0 TDI

Measure ment	Gear ratio (-)	The total inertial mass of the vehicle (kg)	The inertia mass without engine of vehicle (kg)	Moment of inertia of engine ( $kg \cdot m^2$ )
1.	3,07	589,31	390,62	0,329
2.	3,07	573,12	388,32	0,306
3.	3,07	580,64	389,94	0,316
4.	3,07	576,84	387,36	0,314
5.	3,07	579,14	387,43	0,318
6.	3,07	572,89	385,61	0,310
7.	3,07	579,21	388,04	0,317
8.	3,07	572,22	386,48	0,308
9.	3,06	578,47	387,07	0,317
10.	3,06	576,78	386,55	0,315

The average value of moment of inertia of the vehicle engine Skoda Octavia II 2,0 TDI (103 kW) is  $0,3152 \text{ kg} \cdot m^2$ . A greater deviation from the average (4.5%) for the first measurement is probably due to the fact that the engine was before heated to operating temperature, but the transmission was cold. The differences are negligible in the individual measurements after

the temperature stabilization of the engine and gearbox.

Table 2 describes an example of measured moment of inertia of chosen vehicles. Besides moment of inertia there is also nominal power of engine (according producer), volume of engine, type of fuel, year of production, producer and vehicle model.



Table 2 List of vehicles – an example of measured moment of inertia

Producer	Vehicle model	Year of production	Fuel type	Engine volume (dm <sup>3</sup> )	Power (kW)	Moment of inertia of engine (kg·m <sup>2</sup> )
Hyundai	i20	2008	gasoline	1,2	57,2	0,0961
Peugeot	107	2008	gasoline	1,0	50	0,0741
Peugeot	308 SW	2008	diesel oil	1,6 HDI	80	0,2082
Škoda	Octavia II	2006	diesel oil	2,0 TDI	103	0,3152
Škoda	Octavia II	2004	gasoline	2,0 FSI	110	0,3293
Škoda	Favorit	1991	gasoline	1,3 carburetor.	46	0,1317
Škoda	Octavia	2005	gasoline	1,6 MPI	75	0,1882
Škoda	Roomster	2007	diesel oil	1,4 TDI	59	0,2619
Škoda	Felicia	1998	gasoline	1,3 MPI	50	0,1361
Škoda	Felicia	2000	gasoline	1,4 Sport	100	0,1556

### Discussion and conclusion

Moment of inertia is one of the necessary input data for diagnostic non-assembling acceleration measurement. The correct and accurate detection is usually the main problem of these measurements. There are several options for finding moment of inertia, however, there are not always easily feasible.

Moment of inertia of all parts (rotating with the engine in neutral) can be obtained by the procedure described above. This is not a moment of inertia of the engine by itself, but for the purposes of measuring the acceleration performance parameters is not misleading. These are precisely those masses which are accelerating during the acceleration measurement.

Method proposed by authors is suitable for cases where it is available roll test bed, even with low power. The method provides a specific value of moment of inertia of the rotating mass of the vehicle engine and immediately after provides its basic performance characteristics.

The method was experimentally verified on the vehicle Skoda Octavia II 2,0 TDI (103 kW) using a roll test bed with electric motor with mere output (7,5 kW) of one pair of rolls. The moment of inertia for the vehicle was set 0,3152 kg·m<sup>2</sup>. This value seems very likely correct. The first practical measurements of chosen vehicles were launched after an experimental validation of the method. An example of results is given in Table 2.

Known value of moment of inertia can be used for dynamic measurements of the engine of entire vehicle, both in measuring the performance parameters as well as the performance of automotive brakes.

There are still other methods applicable to the measurement of the roll test bed or the test section of the road, except that the proposed method of finding the moment of inertia of the engine of vehicle.

### Follow-up projects

*Paper was created with the grant support - CZU 31190 / 1312 / 313121 - Accuracy of measurement of performance parameters on the roll test bed.*

### Reference

- [1] Chlopek Z. Ecological aspects of usány bioethanol fuel to power combustion engines. *Eksplatacja i Niezawodnosc - Maintenance and Reliability* 2007; 3(35): 65-68.
- [2] Hromádko J, Hromádko J, Kadleček B. Problems of power parameters measurement of constantspeed engines with small cylinder volume by acceleration method. *Eksplatacja i Niezawodnosc - Maintenance and Reliability* 2007; 1(33): 19-22.
- [3] Hromádko J, Hönig V, Miler P. Applications of NRTC cycle to determine a different fuel combustion and harmful emissioins cause by changes of engine's technical conditions. *Eksplatacja i Niezawodnosc - Maintenance and Reliability* 2008; 4(40): 63-65.
- [4] Kadleček B, Pejša L, Pexa M. Virtual Vehicle - Driving Cycle Aplication for Measuring Emission and Fuel Consumption on HDVS. *Eksplatacja i*

- Niezawodnosc - Maintenance and Reliability 2002; 4(16): 40-42.
- [5] Kadleček B, Pejša L, Ružička M, Svítek M, Tvrzský T. The possibilities of electronic toll's utilization in relation to environment conservation and road safety. *Eksploracja i Niezawodnosc - Maintenance and Reliability* 2006; 3(31): 66-71.
  - [6] Pexa M, Červenka V. Dynamic performance parameters measuring on free rollers problems. *Reliability, Safety and Diagnostics of Transport Structures and Means*. Pardubice 2008: 255-258.
  - [7] Sawicki P, Zak J. Technical diagnostic of a fleet of vehicles using rough set theory *European Journal of Operational Research* 2009; 193 (3): 891-903.
  - [8] United States Patent. <[www.freepatentsonline.com](http://www.freepatentsonline.com)>, cit. [20090925]
  - [9] Zhang D, Hu X, Yuan L. Error analysis on measuring the moment of inertia of complex shaped components with trilinear pendulum. *Nongye Jixie Xuebao/Transactions of the Chinese Society of Agricultural Machinery* 2008; 39 (3): 37-40.
  - [10] Zhu M, Deng Z, Fang Z. Measuring methods for mass parameters of an engine. *Nongye Jixie Xuebao/Transactions of the Chinese Society of Agricultural Machinery* 2005; 36 (4): 34-38.

## INTRODUCING A PRACTICAL MODEL FOR TURBINES' DESIGNING IN SMALL HYDROPOWER PLANTS

MARTIN POLÁK<sup>1\*</sup>, VÁCLAV POLÁK<sup>2</sup>

<sup>1</sup> Czech University of Life Science, Technical Faculty Department of Mechanics and Engineering, 165 21 Praha 6 – Suchbát, Czech Republic, e-mail: [karel@tf.czu.cz](mailto:karel@tf.czu.cz)

<sup>2</sup> Institute of Geophysics, Czech Academy of Science, Prague, Czech Republic

### Abstract

Correctly designed turbine is a necessary condition for efficient usage of water energy as a renewable resource. In solving this issue, the Theory of Physical Similarity of Hydraulic Machines is a useful tool. Its application in calculation model allows in approachable way by means of so-called specific speed to gain information on type and size of turbine for proposed hydropower plant. It is apparent from comparison of model outcomes and already realized solution (in this case hydropower plant Slapy on river Vltava) that the calculated values do not differ from the real ones more than by 10 %.

### Introduction

Designing of water turbine is a complex process requiring many knowledge, computations and considerable experience. Technical profession uses with advantage for this purpose the Theory of Physical Similarity of Hydraulic Machines. Its principle stems from Euler's turbomachine equation, or from geometric similarity of velocity triangles. On the basis of this theory it is possible to realize complete proposal of suitable turbine for particular hydropower plant (HPP), if need be to choose turbine from already existing type, as every turbine can satisfy more orders. Besides it is possible to use the theory for construction of trial model turbine. With this turbine in laboratory conditions it is possible to measure and by means of recalculation to determine the performance characteristic (maximum usable flow, efficiency, output power, cavitation durability, etc.) of the real turbine designed by us. In case that the model does not fulfil some of the construction requirements, it is possible to adjust it, which would be very expensive if not impossible with completed, for supply intended turbine.

### Material and Method

*The Theory of Physical Similarity of Hydraulic Machines*

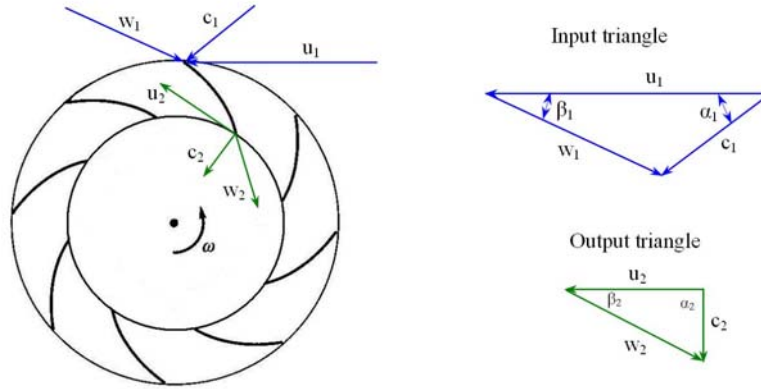
According to this theory, two turbines show hydraulic similarity, if their corresponding velocity triangles are similar – on input and output. To apply this presumption it is necessary to find criterion connecting velocity triangles with values needed for turbine construction. This criterion is so called specific speed. With its help we can determine above all suitable type of turbine for particular HPP, further its size, obtained by recalculation of model turbine. Specific speed can at the same time serve to evaluate some of the turbine's characteristics, e.g. velocity ratio, cavitation inclination, etc.

*Velocity triangles* – determine size and direction of three main vectors of speed during water flow in turbine runner:

$\vec{c}$  ... absolute velocity of water given from water head of HPP

$\vec{u}$  ... frame velocity given from turbine runner circumferential speed

$\vec{w}$  ... relative velocity of water relating to runner vane



Pic. 1.: Sketch of turbine runner with velocity triangles

For geometrical similarity of two triangles applies:

$$\left(\frac{u_1}{c_1}\right)_M = \left(\frac{u_1}{c_1}\right)_A \quad (1)$$

(Index „M“ indicates values connected with model, index „A“ real turbine)

$$\text{If } u_1 = \omega \cdot R = \frac{\pi \cdot N}{30} \cdot \frac{D}{2} \approx N \cdot D \quad (2)$$

and at the same time:

$$c_1 = \sqrt{2gh} \approx \sqrt{h} \quad (3)$$

than after substitution (2) and (3) in (1) it will apply:

$$\left(\frac{N \cdot D}{\sqrt{h}}\right)_M = \left(\frac{N \cdot D}{\sqrt{h}}\right)_A \quad (4)$$

i.e.

$$N_M = N_A \left(\frac{D_A}{D_M}\right) \cdot \left(\frac{h_M}{h_A}\right)^{\frac{1}{2}} \quad (5)$$

If we have water flow in turbine expressed by product of its speed and flow space:

$$\dot{V} \approx D^2 \cdot c_1 \approx D^2 \cdot \sqrt{h} \quad (6)$$

i.e.

$$D = \frac{\dot{V}^{\frac{1}{2}}}{h^{\frac{1}{4}}} \quad (7)$$

after substitution in (5):

$$N_M = N_A \cdot \left(\frac{\dot{V}_A^{\frac{1}{2}} \cdot h_M^{\frac{1}{4}}}{\dot{V}_M^{\frac{1}{2}} \cdot h_A^{\frac{1}{4}}}\right) \cdot \left(\frac{h_M}{h_A}\right)^{\frac{1}{2}} = N_A \cdot \left(\frac{\dot{V}_A}{\dot{V}_M}\right)^{\frac{1}{2}} \cdot \left(\frac{h_M}{h_A}\right)^{\frac{3}{4}} \quad (8)$$

More detailed information about theory is in [1, 3]

From presumption that model turbine performs at the water head of  $h_M = 1 \text{ m}$  and flowrate  $\dot{V}_M = 1 \text{ m}^3 \cdot \text{s}^{-1}$ , we derive its revolutions. We called them specific speed according to flow  $N_q$  ( $N_q = N_M$ ). Speed  $N_A$  is therefore speed of real turbine ( $N = N_A$ ).

*Specific speed according to flow* – it is defined as speed of turbine with geometrical similarity, that runs with flowrate  $1 \text{ m}^3 \cdot \text{s}^{-1}$  at the water head of 1 metre, and it is determined by relation:

$$N_q = N \cdot \frac{\dot{V}^{1/2}}{h^{3/4}} \quad (9)$$

Where:

$N$  ... rotation speed of real runner  
(= synchronous speed of connected generator)  
[ $\text{min}^{-1}$ ]

$\dot{V}$  ... turbine flowrate [ $\text{m}^3 \cdot \text{s}^{-1}$ ]

$h$  ... usable water head of HPP [m]

Model turbines are in detail processed by theory of similarity in nomograms, from which we by return, with the help of recalculations, determine main size parameters for real turbine. Further proportions are then determined by relation of fluid mechanics

All design of turbine would be therefore possible to transform quite easily into computing programme. But the difficulty is the very nomograms, from which it is necessary to „manually“ subtract at every calculation, or its correction. If we would found equations of individual curves in nomograms (they are again functions of specific speed), it would be possible to remove this difficulty. The functions were already found for below described calculation model and are already included in the programme. In many cases it was polynomic function which apparent to be the most suitable from the point of view of correlation coefficient. For example: the curve representing turbine efficiency was determined as:

$$\eta_T = -0,0000055 \cdot n_q^2 + 0,0014 \cdot n_q + 0,84 \quad (10)$$

Value of correlation coefficient is in this case  $R^2 = 0,999$ .

Other necessary curves were described by the similar way. The programme elaborates them in computer environment MS Excel.

### Computing programme

The computing programme described in this article is an instrument for construction design of turbine and stems out of basic parameters HPP, i.e. its water head and flowrate. Those are at disposal as input variables. Further necessary input parameter is rotation speed of generator, which will be connected to the turbine. In the programme the values are submitted into the green-grounded cells. Those are the variables we can adjust if necessary. From the input values the programme will calculate specific speed according to (9), which together with submitted water head of HPP determines suitable type of turbine – Pelton, Francis, Kaplan or Bánki. The optimising is done

in a way to reach the highest efficiency  $\eta$  (see nomogram on Pic. 2 and 3).

According to type of turbine we process further in calculating by stating main proportions of turbine runner. They are stated again from nomogram (Pic. 2) for given type of turbine.

From the nomogram on the basis of specific speed derives following:

The flowrate of etalon turbine  $Q'$  (Etalon turbine is such a turbine which operates at the water head of  $h_M = 1m$  and diameter of its runner is  $D_M = 1m$ ;  $Q' = \dot{V}_M$ ).

Outer diameter of turbine runner  $D_I$  is determined by using the theory of similarity. With reaction turbine we use the relation (6) and the flowrate of real and etalon turbine is stated ( $\dot{V}_A / \dot{V}_M$ ):

$$\frac{\dot{V}_A}{\dot{V}_M} = \left( \frac{D_A}{D_M} \right)^2 \cdot \left( \frac{h_M}{h_A} \right)^{\frac{1}{2}} \quad (11)$$

From here we separate  $D_A$ :

$$D_A = D_M \cdot \left( \frac{\dot{V}_A}{\dot{V}_M} \right)^{\frac{1}{2}} \cdot \left( \frac{h_M}{h_A} \right)^{\frac{1}{4}} \quad (12)$$

If we input  $D_A = D_I$ ;  $D_M = 1$ ;  $\dot{V}_A = \dot{V}$ ;  $\dot{V}_M = Q'$ ;  $h_M = 1m$  and  $h_A = h$ , then we get relation for  $D_I$ :

$$D_I = \left( \frac{\dot{V}}{Q'} \right)^{\frac{1}{2}} \cdot \left( \frac{1}{h} \right)^{\frac{1}{4}}, \quad (13)$$

where:

$D_I$  ... outer diameter of real turbine runner [m]

$\dot{V}$  ... flowrate in designed turbine [ $m^3 \cdot s^{-1}$ ]

$Q'$  ... flowrate in etalon turbine (see nomogram on Pic. 2) [ $m^3 \cdot s^{-1}$ ]

$h$  ... usable water head of HPP [m]

From the nomogram it is further determined (Pic. 2): diameter of hub  $D_N$  – from curve  $D_N/D_I$ ; width of inlet canal – from curve  $B_o/D_I$ . The efficiency of turbine is given by curve  $\eta$ ; the zone  $\sigma$  is given by Thoma cavitation coefficient and the line  $\delta$  determines the best angle of opening of the suction pipe. Detected proportions are presented in layout on Pic. 2.

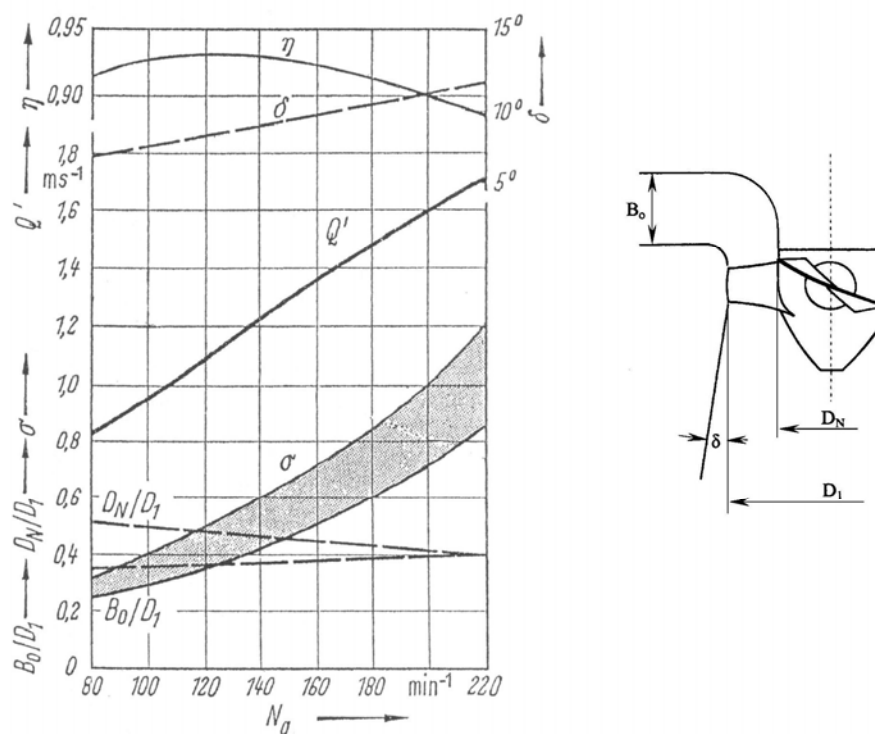
As stated before, individual curves of nomogram were described by equations and were included into the programme. Values “subtracted” from nomograms are presented in yellow-grounded cells.

Further required proportions of turbine are determined by means of relations of fluid mechanics, empirical formulas and velocity triangles. From triangles we determine above all geometry of runner blade. The angle  $\beta_1$ , let us say  $\beta_2$ , made by vectors of frame and relative velocity, corresponds to setting angle of blade on inlet edge, let us say setting angle of blade on output edge. In the case of Kaplan turbine the geometry of a blade is calculated on three cross sections – on outer, middle and inner diameter. Calculated values are included in general table (Pic. 3) and marked in attached draft of turbine runner. There are also outlined velocity triangles on a scale at the inlet and outlet of turbine runner. At the close of the

calculation the power output of turbine is determined with regard to its efficiency. Appearance of cavitation is controlled with reaction turbine.

### Discussion and Results

In the calculation here stated as an example of turbine's design following input variables were chosen: usable water head of HPP  $h = 56m$ , flowrate  $\dot{V} = 100m^3 \cdot s^{-1}$  and rotation speed of generator  $N = 230,8min^{-1}$  (it corresponds to synchronous speed of generator with 13 pairs of pole). Those values correspond to parameters of HPP Slapy on river Vltava, which will at the same time serve us for comparison of calculation model outcome and real turbine. On the basis of available information on turbine following comparison is summarized in Tab. 1.



Pic. 2.: Nomogram for stating main parameters of Kaplan turbine; outline of subtracted parameters.



Tab. 1.: Comparison of calculated values and reality

Parameter	calculation model	reality	comparison
Turbine type	Kaplan	Kaplan	correspond
Number of blades of runner	8	8	correspond
Outside runner diameter ( $D_1$ )	3 562 mm	3 700 mm	- 3,7 %
Hub diameter ( $D_N$ )	1 725 mm	1 900 mm *	- 9,2 %
Channel width ( $B_0$ )	1 291 mm	1 200 mm *	+ 7,6 %
Setting angles of blade ( $\beta_1 - \beta_2$ )	6,5°	6° *	+ 8,3 %
Power output	51,021 MW	50,3 MW	+ 1,4 %
Suction height ( $h_s$ )	-12,01 m	- 13,2 m	- 9 %

Notice: Values marked \* are measured from technical documentation

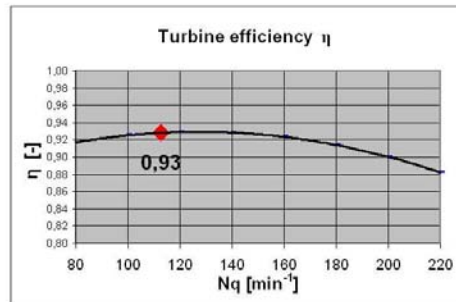
It is apparent from comparison of calculated and real values that the deviation between programme outcomes and installed turbine do not exceed in any parameter 10 %. Furthermore higher values are noticed at parameters, where there were not available exact numeric data and values are measured out from technical documentation. Besides in case of suction height it is probably not a real deviation but a reserve for case of water level elevation on HPP. The calculation programme is therefore, on the basis of this comparison, possible to consider as successful and well exercisable for wider use. Identical procedures for Pelton, Francis and Banki turbines design are also included in above described calculation model.

## References

- [1] ULRYCH, E.: Aplikované hydromechanika I (základy hydroenergetiky). Praha 2007, Technická fakulta ČZU v Praze, 126 stran, ISBN 978-80-213-1609-6.
- [2] NECHLEBA, M.: Vodní turbíny, konstrukce a příslušenství. Praha 1962, SNTL, 673 stran.
- [3] BRADA, K.; BLÁHA, J.: Metoda experimentů a modelování. Praha 1995, ČVUT v Praze, 103 stran, ISBN 80-01-01236-0.
- [4] MUNSON, B. R.; ZOUNY, D. F.; OKIISHI, T., H.: Fundamentals of fluid mechanics – fifth edition, 2006, John Wiley & Sons, Inc., USA, 770 p.
- [5] MELICHAR, J.; BLÁHA, J.; BRADA, K.: Hydraulické stroje – konstrukce a provoz. Praha 2002, ČVUT v Praze, 378 stran, ISBN 80-01-02657-4.
- [6] HUTAREW, G.: Einführung in die Technische Hydraulik, Springer-Verlag Heidelberg New York 1973., USA, 205 s., ISBN 3-540-05979-2.

## Kaplan turbine

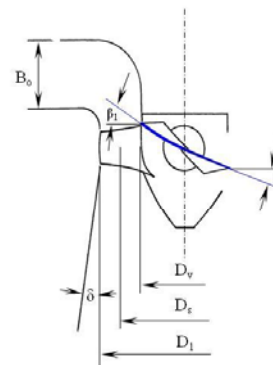
<b>Input parameters</b>	
Water head	$h = 56$ m
Flowrate	$Q = 100$ m <sup>3</sup> .s <sup>-1</sup>
Pairs of pole of generator	$p = 13$ -
<b>Runner design</b>	
Turbine speed	$N = 230,8$ min <sup>-1</sup>
Specific speed	$N_q = 112,7$ min <sup>-1</sup>
Etalon flowrate	$Q' = 1,053$ m <sup>3</sup> .s <sup>-1</sup>
Outside runner diameter	$D_1 = 3,562$ m
Channel width ratio	$B_o/D_1 = 0,36$ -
Channel width	$B_o = 1,291$ m
Hub diameter ratio	$D_N/D_1 = 0,48$ -
Hub diameter	$D_N = 1,725$ m
Angle of suction pipe	$\delta = 7,8^\circ$
Computed number of blades	$z' = 7,9$ -
Number of blades	$z = 8$ pcs
Blade spacing	$T = 1,399$ m
Relative spacing	$T/L = 0,8$ $0,62 - 0,87$
Blade lenght	$L = 1,749$ m
Clear opening	$S = 7,630$ m <sup>2</sup>
Meridian velocity	$c_m = 13,1$ m.s <sup>-1</sup>
Wheel angular speed	$\omega = 24,17$ s <sup>-1</sup>
Blade speed on $D_1$	$u_1 = 43,0$ m.s <sup>-1</sup>
Specific head energy	$Y_t = 549,4$ J.kg <sup>-1</sup>
Projection of $c_t$ to $u_t$	$C_{u1} = 12,8$ m.s <sup>-1</sup>
Inlet angle of streamline	$\alpha_1 = 45,76^\circ$
Outlet angle of streamline	$\alpha_2 = 90^\circ$
Inlet blade angle	$\beta_1 = 23,40^\circ$
Outlet blade angle	$\beta_2 = 16,93^\circ$
Middle diameter of runner	$D_s = 2,644$ m
Blade-hub clearance	$r_v = 3$ mm
Inside runner diameter	$D_v = 1,731$ m
Turbine efficiency	$\eta = 0,93$ -
Real power output	$P = 51021$ kW
<b>Cavitation check</b>	
Barometric pressure	$p_a = 100$ kPa
Pressure of saturated water	$p_s = 4$ kPa
Thoma cavitation coefficient	$\sigma = 0,39$ -
Max. suction height	$h_s = -12,01$ m



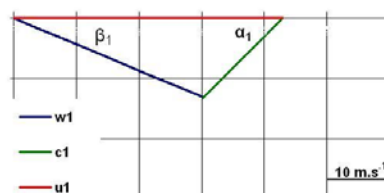
View of computed data - blade geometry

cut	D [m]	$u_1$ [m.s <sup>-1</sup> ]	$c_{u1}$ [m.s <sup>-1</sup> ]	$\alpha_1^\circ$	$\alpha_2^\circ$	$\beta_1^\circ$	$\beta_2^\circ$
$D_1$	3,562	43,0	12,8	45,8	90	23,4	16,9
$D_s$	2,644	31,9	17,2	37,3	90	41,6	22,3
$D_v$	1,731	20,9	26,3	26,5	90	67,8	32,1

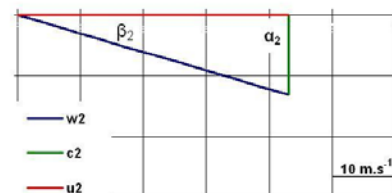
Sketch of turbine runner



Velocity triangle ( $D_1$ ) - input



Velocity triangle ( $D_1$ ) - output



Pic. 3.: Calculation protocol of turbine's design for HPP Slapy

## EXTERNAL PURIFICATION OF HYDRAULIC AND MACHINE OILS

JOSEF POŠTA

Czech University of Life Sciences Prague, Faculty of Engineering  
165 21 Prague 6 – Suchbátka, Czech Republic  
E-mail: posta@tf.czu.cz

### Abstract

The primary cause of problems with the hydraulic pressure fluids and machine oils is their pollution and aging of these fluids, which in effect leads to wear of the precise components. Operational options of care for hydraulic machinery and hydraulic oils are also dependent on their specific operating conditions. One option is the external purification. This paper is focused on comparing methods of external removing particle contamination from the pressure hydraulic fluids and machine oils.

### Introduction

The basic function of hydraulic pressure fluids is the pressure transmission there are other important and required properties as lubricating ability, the ability to remove heat, steady viscosity, the ability to separate air and water, long-term oxidation stability. The same demands are imposed on machine oils, with the priority feature is its lubricating ability. Operating care of hydraulic pressure fluid and engine oil is largely the same.

The primary cause of problems with the hydraulic pressure fluids and machine oils (further in text only “operational fluids”) is their pollution and aging of these fluids, which in effect leads to wear of the precise components. Therefore, in these systems are normally integrated operational filters. These filters are not able to remove all particles from the system and solve problems of these systems only partially, [1]. Furthermore, it is possible to use different methods of external purification, which give different results depending on the specific operating conditions. In order to choose the best system of care for the working fluid is therefore a complicated task, for which the correct solution is also required knowledge of the technical possibilities of purification methods.

Substances contaminating the operational fluids are the hard pollution, soft pollution, water, and air.

Hard pollution is formed of metal, ceramic and other particles that cause wear on functional surfaces of the mechanical systems. Metal particles are usually generated from the worn surfaces. Ceramic particles are mostly remnants

of the abrasive used during manufacturing of machine parts and dust particles from penetrating from the surrounding environment. Other particles are often corrosion products, formed in the system.

Soft pollution consists of particles that are products of oxidation of the operational fluids and products of chemical reactions of additives which create sticky deposits. The creation of soft pollution supports many operating factors, the most important are the effects of temperature, the presence of catalysts, the presence of moisture, the presence of oxygen (air). Catalysts are often very fine abrasive particles of hard metal pollution. Formed oxidation products generally polymerise and form large molecules, which adhere very firmly to the surface of all elements of the system.

Water contamination usually arises by condensation of atmospheric moisture within the system, in places where the temperature falls below the dew point. In open systems water contamination can still grow. Water contamination may also occur by direct impact of improper operation or maintenance. Water causes internal corrosion of metal surfaces and contributes to the creation of oxidation products.

Air pollution usually arises due to improper operation or in an inappropriate design configuration of the system, if in consequence of foam of the operational fluid. Air disrupts the proper functioning of the system change in volume compressibility of the operational fluid. It also supports the oxidation of the operational fluid, raising its temperature during pressure

changes and deteriorating of additives, all these aspects contribute to creation of soft pollution.

The effort to maintain the hydraulic pressure fluid or engine oil clean leads designers and constructors to assign operational filters integrated to the system as full flow or bypass. The higher the purity requirements of liquid that is used for smaller porosity of filters. The current standards are filters with porosity 5  $\mu\text{m}$  but there are used also finer filters. But experience and recent findings show that in this way can not be achieved consistently satisfactory condition in technical or economic terms. The solution may

be external purification carried out either continuously or periodically.

### Materials and methods

When examining the general pollution of the working fluid is usually separated from a sample as individual components and they are analyzed separately. How to determine the overall content and character of particulate pollution is schematically illustrated in Figure 1. Particle size distribution of different types of impurities in the working fluid is shown in Table 1. Separation efficiency of various processes and examples of the size of the particulate pollutants are shown in Figure 2.

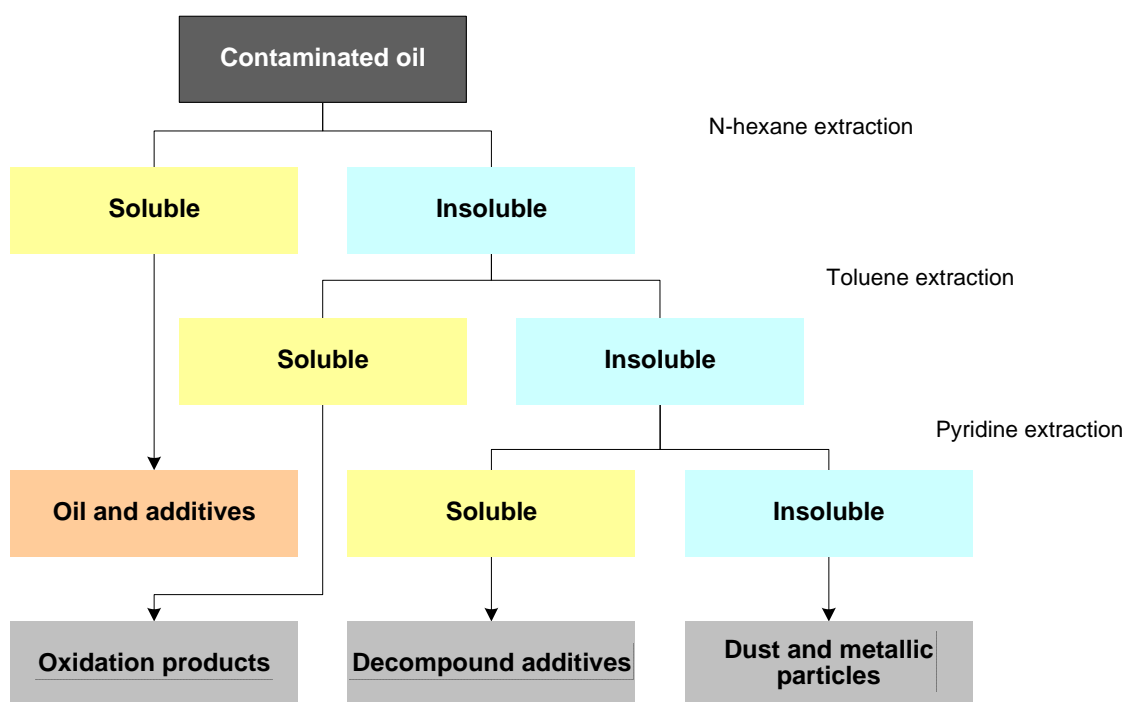


Fig. 1 Scheme of separation of individual components of the hydraulic pressure fluid contamination

Table 1 Typical size distribution of operational fluid pollution, [1]

Size	$\mu\text{m}$	> 25	20 – 25	15 – 20	10 – 15	5 – 10	1 – 5	< 1
Content	%	0,4	0,6	1,0	2	6	20	70

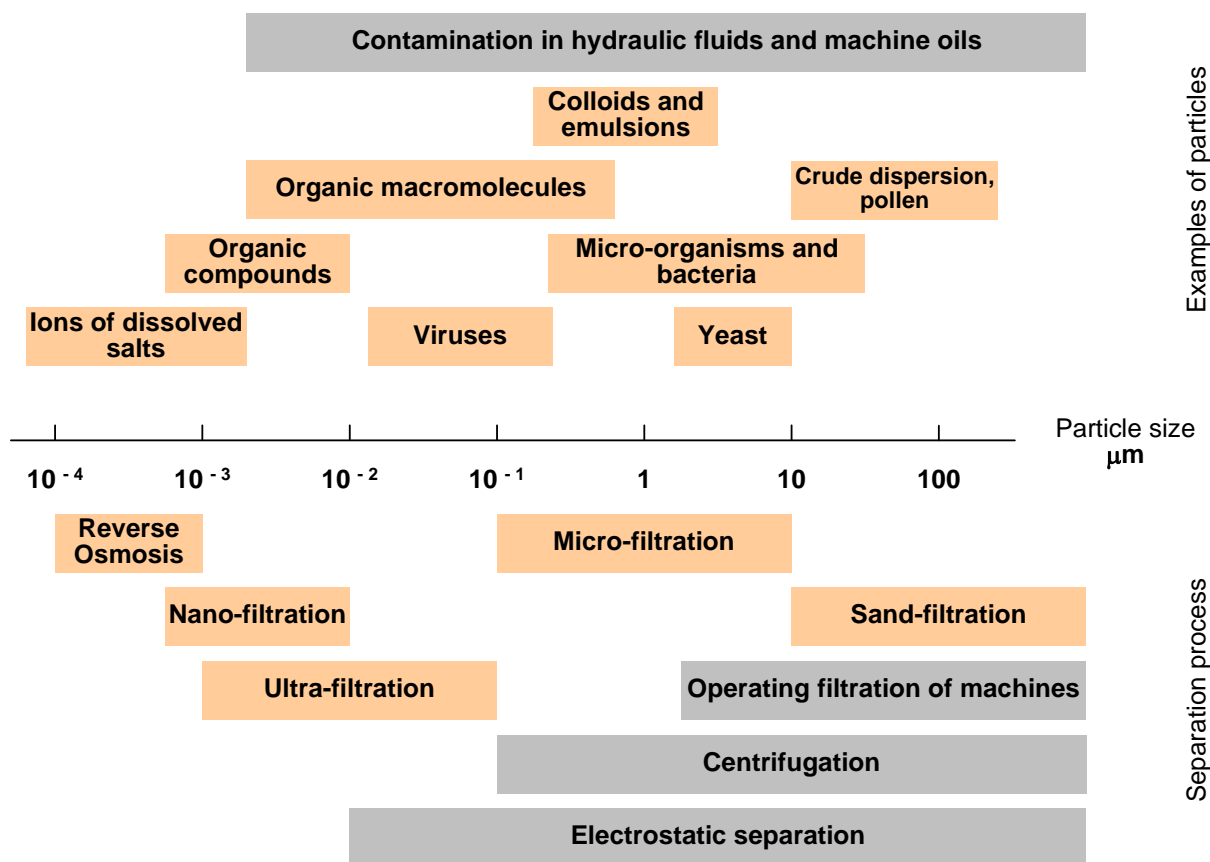


Fig. 2 Typical sizes of pollution particles and the separation ability of various processes

Cleanliness requirements of hydraulic fluid and machine oil provide a number of standards the most commonly used are ISO 4406-1999 and NAS 1638. Both these standards provide the so-called cleanliness code, which expresses the content (number) of particles of a certain size in a 100 ml sample of oil. Cleanliness codes are usually recommended by different types of machines [3, 4] an example is shown in Table 2.

Cleanliness code according to ISO 4406-1999 contains three numbers which determine the limits of (number) of particles of a certain size in a unit volume of the sample. The first number of the code indicates the permitted number of particles larger than 4  $\mu\text{m}$ , the second

number indicates the permitted number of particles larger than 6  $\mu\text{m}$ , which is a subset of the first group, third number indicates the permitted number of particles larger than 14  $\mu\text{m}$ , which is a subset of the second groups.

Cleanliness code according to NAS 1638 is a single number, which is determined by the number of particles in different size intervals in the 100 ml sample. According to the table that is part of the standard, for each size interval the number (code) is assigned according the number of particles. The resulting cleanliness code according to this standard is then assigned to the largest of the numbers.

Table 2 Example of recommended cleanliness codes for hydraulic and machine oils, [4]

Type of machine	ISO 4406-1999		NAS 1638	
Mobile machines with hydraulic systems	20/18/15	in a sample of 100 ml of oil may be 500.000 to 1000.000 particles larger than 4 $\mu\text{m}$ of which may be 130.000 to 250.000 particles larger than 6 $\mu\text{m}$ of which may be 16.000 to 32.000 particles larger than 14 $\mu\text{m}$	9	in a sample of 100 ml of oil may be than maximally 128.000 particle size of 5-15 $\mu\text{m}$ , maximally 22.800 particles in size 15-25 $\mu\text{m}$ , maximally 4.050 particles in size of 25-50 $\mu\text{m}$ , maximally 720 particles in size of 50-100 $\mu\text{m}$ , maximally 128 particles in size of over 100 $\mu\text{m}$
Industrial machines	19/17/14	in a sample of 100 ml of oil may be 250.000 to 500.000 particles larger than 4 $\mu\text{m}$ of which may be 64.000 to 130.000 particles larger than 6 $\mu\text{m}$ of which may be 8.000 to 16.000 particles larger than 14 $\mu\text{m}$	8	in a sample of 100 ml of oil may be than maximally 164.000 particle size of 5-15 $\mu\text{m}$ , maximally 11.400 particles in size 15-25 $\mu\text{m}$ , maximally 2.025 particles in size of 25-50 $\mu\text{m}$ , maximally 360 particles in size of 50-100 $\mu\text{m}$ , maximally 64 particles in size of over 100 $\mu\text{m}$
Hydrostatic transmiss	18/16/13	in a sample of 100 ml of oil may be 130.000 to 250.000 particles larger than 4 $\mu\text{m}$ of which may be 32.000 to 64.000 particles larger than 6 $\mu\text{m}$ of which may be 4.000 to 8.000 particles larger than 14 $\mu\text{m}$	7	in a sample of 100 ml of oil may be than maximally 32.000 particle size of 5-15 $\mu\text{m}$ , maximally 5.700 particles in size 15-25 $\mu\text{m}$ , maximally 1.012 particles in size of 25-50 $\mu\text{m}$ , maximally 180 particles in size of 50-100 $\mu\text{m}$ , maximally 32 particles in size of over 100 $\mu\text{m}$
Robots, precision systems	17/15/12	in a sample of 100 ml of oil may be 640.000 to 130.000 particles larger than 4 $\mu\text{m}$ of which may be 16.000 to 32.000 particles larger than 6 $\mu\text{m}$ of which may be 2.000 to 4.000 particles larger than 14 $\mu\text{m}$	6	in a sample of 100 ml of oil may be than maximally 16.000 particle size of 5-15 $\mu\text{m}$ , maximally 2.850 particles in size 15-25 $\mu\text{m}$ , maximally 506 particles in size of 25-50 $\mu\text{m}$ , maximally 90 particles in size of 50-100 $\mu\text{m}$ , maximally 16 particles in size of over 100 $\mu\text{m}$

## Results and Discussion

Stated requirements and knowledge are summarized and illustrated in Figure 3, which is plotted on the vertical axis of particle size on the horizontal axis the percentage average, [2]. The figure also shows the lower limits of particle size, which is practically achievable by the various separation methods.



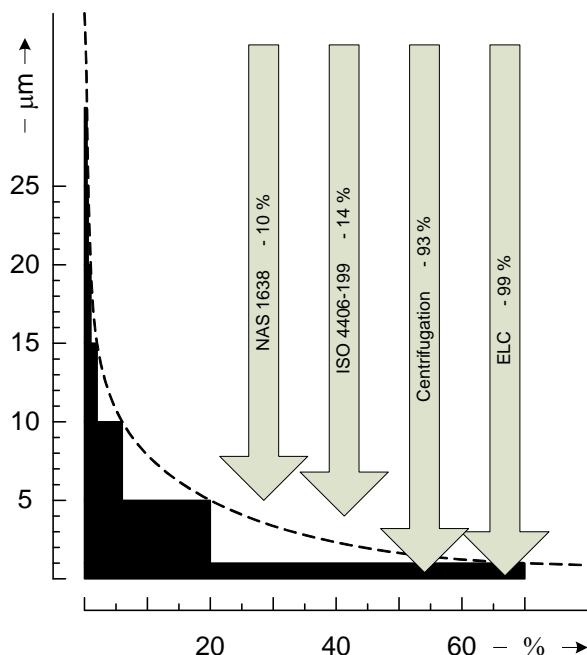


Fig. 3 Distribution of polluting particles and comparing of different cleaning processes

It is clear from Table 2 that the operational standard for cleanliness pressure hydraulic fluids and machine oils, which is usually ISO 4406-1999 and NAS 1638, means the requirement for removal of pollution particles in size 4 µm and larger. To meet this requirement operational filters are integrated into the systems as full flow or bypass. Porosity of these filters is usually 5 µm, less often 3 µm.

Assuming that the operation is usually not satisfied that the filter captures any particles of given size and larger, may be operating such filters remove only a small proportion of total particle pollution. Table 1 and Figure 3 shows that a proportion of 10 to 14% of the total pollution. Operating filtration can not fully solve the cleanliness of hydraulic pressure fluids and machine oils.

Figure 2 shows that the operational filtration can remove only a minor proportion of particulate contamination of hydraulic pressure fluids and machine oils. It can not remove all organic macromolecules, which are polymerized

oil oxidation products, so-called soft pollution. It appears that the soft pollution is the primary cause of major pollution problems of hydraulic pressure fluids and machine oils. It is therefore clear that in addition to operational filtration, which can effectively remove rough contamination, is effective for long-term and reliable operation of systems operating with pressure hydraulic fluids and machinery oils, further treatment of these fluids is needed. Centrifugation and electrostatic cleaning appears as real methods for external cleaning of operational fluids.

### Conclusions

There are a number of problems caused by their pollution by particulate substances, nature, water and gases in the operation of hydraulic systems operating with pressure fluids and machine oils. Particle pollution can not be sufficiently effective to remove operational filtration. As an important measure appears external purification in addition to the operating filtration. Among possible methods of cleaning is currently realistic centrifugation and electrostatic cleaning. Both of these methods have higher order in terms of separation ability in comparison to the capability of operational filtration.

### References

- 1 Sasaki, A.: The Overlooked Root Cause of Varnish Problems of Gas Turbines. In: Proceedings of Gas Turbine Symposium, Česká strojnická společnost, Praha, 2007
- 2 Chvalina, V.: Údržba hydraulických zařízení a péče o hydraulické kapaliny. In: Sborník referátů konference „Tribotechnika a spolehlivost v provozu“, Česká strojnická společnost, Praha, 2004
- 3 <http://www.precisionfiltration.com/products/iso-cleanliness-code.asp> (2.6.2010)
- 4 <http://www.ufihyd.com/> (2.6.2010)

## THE SIMULATION OF THE ENERGY INTENSITY BY USING THE TWO SECTIONAL SELF-PROPELLED MIXER FEEDER

RADEK PRAŽAN<sup>1\*</sup>, VÁCLAV PODPĚRA<sup>2</sup>

<sup>1</sup> Research Institute of Agricultural Engineering, p.r.i Prague, Drnovská 507, Prague 6, 161 01  
Phone: +420739057413, E-mail: radek.prazan@vuzt.cz

<sup>2</sup> Czech University of Life Sciences Prague, 16521 Prague 6 – Suchbát, Czech Republic

### Abstract

The article deals with the measurement and calculation of the energy intensity and exploitative indicators during feeding total mixed ration (TMR) by the means of self-propelled mixer feeder in concrete conditions on the farm. The self-propelled mixer feeder is substituted by the two-sectional self-propelled mixer feeder, and the energetic intensity of both feeders is compared and calculated by means of the model calculation of the exploitative indicators.

### Introduction

Mixer feeders are relatively new machines and their technical development is rather fast. Their constructional solution is very distinguished. This article deals with the possibility of changing the construction of the mixer feeders (MF) and the influence of such change on the energetic and exploitative parameters. The variation is based on the fact that two separated mixing hoppers with the mixing augers are installed in MF, instead of one. This mixer feeder is further described as the two sectional mixer feeder (TSMF). The suggestion of this particular technical solution is the result of laboratory measurements and longtime observation of MF in operation.

### Materials and methods

The target of the laboratory measurements of MF in operation, was to determine the exploitative and energetic parameters of the operation process of feeding, with the help of mobile feeding systems on the farm ZD Želiv. The measurements lasted throughout one feeding day. We did not interfere in the operation process of feeding. The measurement was done with the self-propelled mixer feeder Faresin with the engine power 128 kW, one vertical mixing auger (capacity 12 m<sup>3</sup>), and self-loading equipment (the rotary cutter). Distribution of TMR was provided by the dosing gate valve.

To calculate the energetic intensity of this feeding unit, it was necessary to monitor the contents, weight (taken from the MF display showing current overall weight) and the loading sequence of individual components of the feed

mixture. To monitor the energetic and exploitative parameters of the whole feeding unit (time, path of the motion, motor oil consumption), several equipments were installed on MF: the flow meter EDM 1404, GPS with the integrated antenna in a protective case (GPS - LPHVS35), and the data logger PC/104. The data logger recorded with the frequency 0,5 s the immediate consumption of the motor oil and the coordinates of the machine movement, the average speed and real time. The detailed time recording, i.e. operation processes of this working unit was provided – i.e. loading, mixing, transport, distribution.

Calculation processes for determination of the exploitative and energetic parameters.

The relation for calculating the duration of the operation cycle of MF:

$$T_{MKV} = T_{d1} + T_{VP1} + T_{d2} + T_{VP2} + \dots T_{dn} + T_{VPn} \dots + T_{dz} + T_{z1} \quad [h] \quad (1)$$

The relation for calculating the duration of the cycle of TSMF:

$$T_{DMKV} = T_{d1} + T_{VP1} + T_{d2} + T_{VP2} + \dots T_{dn} + T_{VPn} \dots + T_{dz} + T_{z1} + T_{dz2} + T_{z2} \quad [h] \quad (2)$$

where:

$T_{MKV}$  .... duration of the feeding cycle of MF [h]

$T_{DMKV}$  .... duration of the feeding cycle of TSMF (loading, mixing, transport and distribution of two TMR) [h]

$T_{d1}$  ... time of transport of MF (TSMF) to the place of the first loading [h]

$T_{VP1}$  .... loading time of 1 component of the TMR (duration of component feeding to both load compartments of TSMF – sum of periods) [h]

- $T_{d2}$  ... time of transport of MF (TSMF) to the place of the second loading [h]  
 $T_{VP2}$  .... loading time of 2 components of the feeding mixture in determined order (duration of components feeding to both mixing hoppers of TSMF – sum of periods) [h]  
 $T_{dn}$  ... time of transport of MF (TSMF) to the place of  $n^{\text{th}}$  loading [h]  
 $T_{VPn}$  .... loading time of  $n^{\text{th}}$  component of feeding mixture (duration of component feeding to both mixing hoppers of MF) [h]  
 $T_{dz}$  ... time of transport of MF (TSMF) to the first place of distribution, while mixing [h]  
 $T_{z1}$  ... duration of distribution of the first feeding mixture into the mixing hoppers [h]  
 $T_{dz2}$  ... time of transport from the first distribution to the place of the second feeding distribution [h]  
 $T_{z2}$  ... duration of the distribution of the second feeding mixture into the mixing hoppers [h]

Calculation of the MF performance for two operation cycles:

$$W_{MKV} = (m_1 + m_2) / (t_1 + t_2) \quad [t/h] \quad (3)$$

where:

$W_{MKV}$  ... MF performance (t/h)

$m_1, m_2$  ... ultimate weight of the individual feeding mixtures in the particular operation cycle [t]

$t_1, t_2$  ... duration of one operation cycle of MF [h]

Calculation of TSMF performance for two operation cycles (1 model operation cycle):

$$V_{DMKV} = (m_1 + m_2) / t_{DMKV} \quad [t/h] \quad (4)$$

where:

$V_{DMKV}$  ... performance TSMF [t/h]

### Measurement results

Cattle feeding was done twice a day. 34,6 t of the feeding mixture divided into 21 operation cycles were prepared for various cattle categories. 8 mixer feeders were prepared and loaded for the morning feeding and 13 for the afternoon. The individual components of the TMR and their weight is shown in the figure 1.

The component loading, feeding mixture mixing and distribution of TMR was done in the farm. The storehouses with individual components were less than 100 m far from each other, and the housing of farm animals was not further than 200 m.

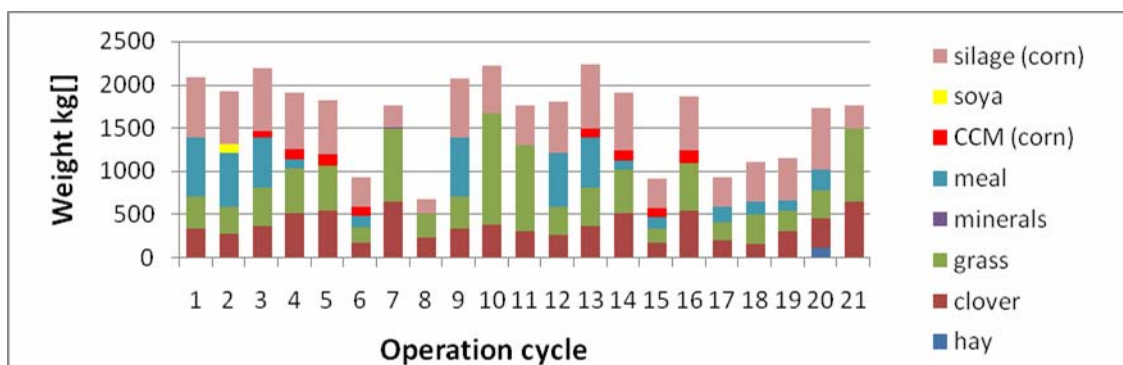
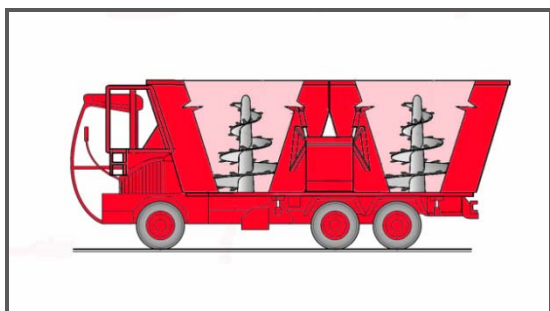


Figure 1 Weight and number of individual components of TMR for individual operation cycles

Out of large number of prepared TMR with different composition and number of components for the particular group of animals, the following technical solution for TSMF was suggested, which is based on measurements done on MF. The chassis of TSMF was provided with two separate mixing hoppers. This solution brings a modification of operation cycles of MF, while the number and amount of feeding mixtures for

the individual groups of animals is maintained. It is also supposed, that this solution will increase the productivity of labour and reduce the unit consumption of motor oil.



**Figure 2** Two sectional mixer feeder (TSMF)

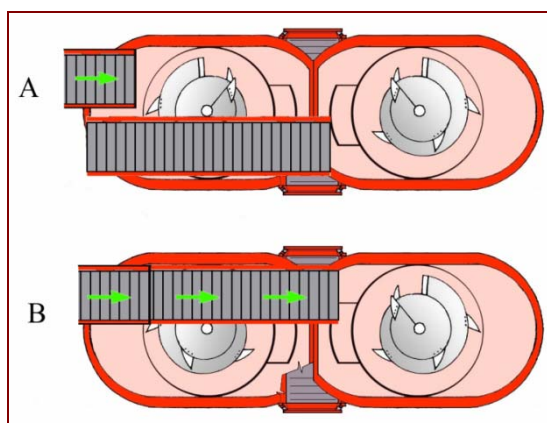


**Figure 3** Top view of TSMF, A – self-loading of the 1st mixing hopper, B – self-loading of the 2nd mixing hopper

### Principles of the technical solution for TSMF

The technical solution of TSMF with the vertical mixing mechanism is simply innovated already established construction of self-propelled vertical mixing feeders. The newly suggested technical solution of MF increases utility parameters (performance, productivity of labour, economic returnability), and reduces the energetic intensity of cattle feeding.

This is achieved by the fact, that during one operation cycle, it is possible to load, mix and distribute two different TMR for various cattle categories.

The TSMF consists of two mixing hoppers (Figure. 2). Each mixing hopper of TSMF is provided with one vertical mixing auger. The mixing hoppers are connected to the chassis of the feeder by means of weighing rods. Drive of the vertical mixing augers is provided by the energy means. Each mixing auger can be driven independently.

### Loading – technical solution

Loading of individual components, which are present in the feeding mixture, is provided by self loading equipment. Loading of individual components of the feeding mixture can be done during mixing switched on or off. At the first place, one component of the feeding mixture is loaded into the first load mixing hopper of TSMF (in the driving direction), until the required amount is reached (Figure 3A). Then, in case of need, this component of the feeding mixture is loaded into the second mixing hopper of TSMF, until the the required amount is reached (Figure 3B). That is how all components of the feeding mixture – total mixed ration (TMR) are loaded.

The weight of the feeding mixture in the mixing hopper is continually monitored by the weighing rods.

### Distribution of feeding – technical solution

Distribution is provided by the dosing gate valve in the mixing hopper of MF and the discharge belt. The discharge belt is placed in the middle of the trailer, between the mixing hoppers. By means of the discharge belt, it is possible to distribute TMR to both sides, left or right. Otherwise, the distribution may be realised independently for each mixing hopper – as it is done in case of classical MFs.

### Modeling of the energy intensity of TSMF

When considering the substitution of MF (capacity 12 m<sup>3</sup>) by TSMF (capacity 2 x 12 m<sup>3</sup>), the number of feeding cycles reduces to half (reduction from 21 to 11 cycles). The model calculation of duration of individual operations and the motor oil consumption in case of TSMF, considers the connection of 2 adjacent feeding cycles into one. The loading sequence of individual components of a particular feeding mixture would be maintained for both feeding mixtures.

We suppose, that one feeding component is loaded to the first mixing hopper and then to the second mixing hopper, if the component is part of a particular feeding mixture.

As the Figure 4A shows, with the usual utilization of MF, the number of operation steps (loading, transport, mixing and distribution) is 22 within two feeding cycles. In case of TSMF, the number of operation steps is reduced to 14,



mainly because there is no need of transport among storehouses (Figure 4B). These operation

steps are presented as the model operation cycle of TSMF.

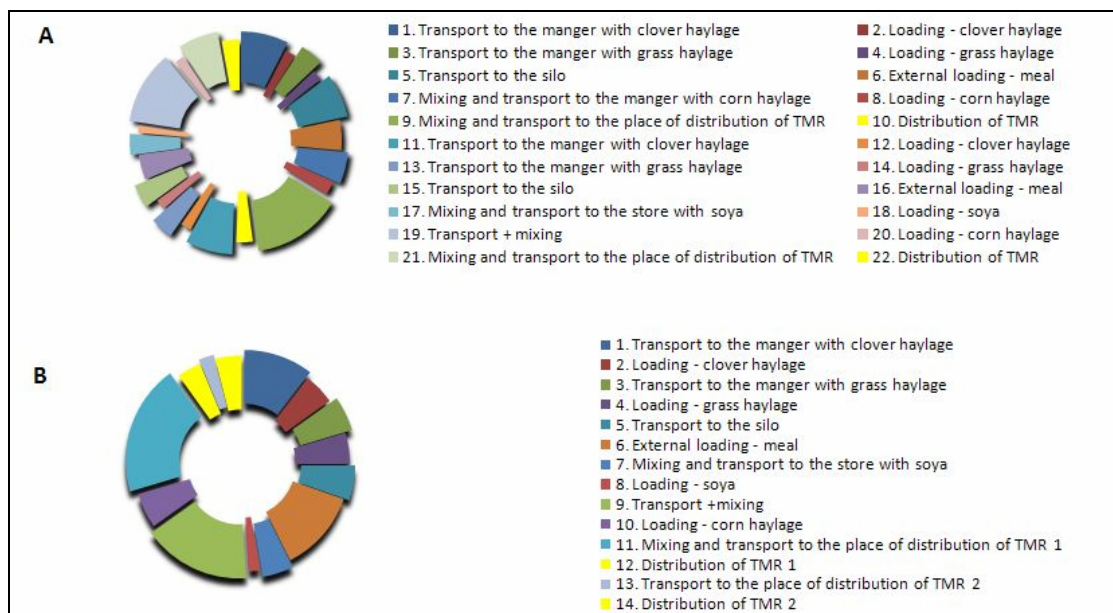


**Figure 4** First two operation cycles of MF (A) and TSMF (B)

The input data for the model calculation of exploitative and energetic parameters of the two sectional mixer feeder, were based on the measured and calculated data for MF (i.e. time intensity and motor oil consumption per one operation step).

Based on the knowledge of the operation cycle of MF (Figure 4A), as the individual components of the feeding mixture are loaded into mixing hoppers, the operation cycle for TSMF was developed (Figure. 4B).

It was discovered from the time recording, that the time needed for the preparation and distribution of 2 feeding mixtures within first two operation cycles is 26 minutes in case of MF. The model calculation according to the Eq. (2) shows, that in case of TSMF, necessary time is 28% shorter, i.e. 18 minutes.

Based on the calculation of time needed for the preparation and distribution of feeding for two

feeding cycles, the efficiency of both feeding mixtures was calculated. According to the Eq. (3), the average efficiency of MF during first 2 operation cycles is 9 t/h. According to Eq. (4), the efficiency of TSMF raised by 39%, i.e. to 13 t/h.

32,84 l of motor oil was consumed during one feeding day. Approximately half of the consumption was needed for the operating step „transportation“ (transport among the storehouses, mixing and transport to the place of distribution). The unit consumption for MF and TSMF was calculated out of the overall consumption of the motor oil and processed material per one feeding day. The unit consumption of MF motor oil is 0,95 l/t, while in case of TSMF, the consumption dropped to 0,75 l/t.

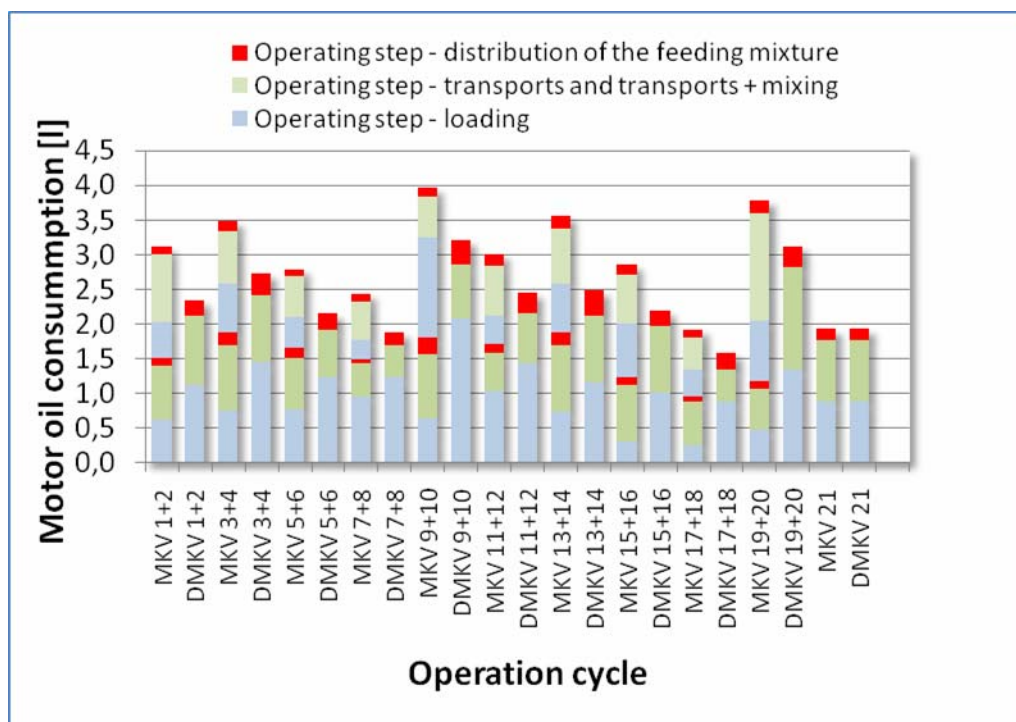


**Figure 5** Motor fuel consumption per individual operation cycles for MF and TSMF

### Discussion and conclusion

The technical solution of the two sectional self-propelled mixer feeder brings a new solution to mobile feeding systems. It is possible to load, mix and distribute two different TMR for various kinds of cattle within one operation cycle. High standards of quality of feeding are met, while it is possible to reduce the energetic intensity of the whole feeding unit at the same time. This solution may be used in cases when more than two various feeding mixtures are distributed.

The number of transports of TSMF can be reduced when the individual components of the feeding mixture are not deployed within the farm, and when one component of the total mixed ration is loaded into two load mixing compartments simultaneously. Then the unit consumption of the feeding unit is reduced as well as the operation time.

During the operating step „loading“, the performance is the same as in case of MF, or higher. It is caused by the fact, that the preparatory operations for setting and turning-on the equipment for loading of TSMF, join for both feeding mixtures. At the first time, the front mixing hopper is loaded. After reaching the required amount of the feeding component, the back mixing hopper is loaded by means of

movable belt conveyor (Figure 4), which provides the transport of components into the second mixing hopper.

The time needed for the next operating step “mixing“ is the same. Because two total mixed rations are mixed simultaneously within one operating cycle, it is supposed that the unit consumption is reduced and the performance of TSMF increases.

Long time measurements processed and described in my dissertation thesis, concern the trailed MF aggregated with the front loader. The results show, that the energetic parameters of TSMF would be even more distinct compared to MF. Mainly because of the large number of prepared feeding mixtures for various kinds of cattle and minimal utilization of the load compartment of MF.

### Reference:

- [1] BARTALI, E.H., WHEATON, F.W.: SINGH S.; Animal Production and Aquacultural Engineering; The International Commission of Agricultural Engineering (CIGR); 1999; ISBN: 0-929355-98-9



- [2] JAUSNEGG, E.: Annual report BOKU 2005; Universität für Bodenkultur Wien; 2005; ISBN: 20-030021-99-6.
- [3] PRAŽAN, R.: Porovnání pracovních ústrojí pro vlastní plnění a míchání u míchacích krmných vozů z hlediska energetických parametrů; Mechanizace zemědělství; 2009; č. 6; ISSN 0373-6776; str. 51-52.
- [4] SYROVÝ, O. a kol.: Doprava v zemědělství; 1. Vyd; Praha - Profi Press; ISBN 978-80-86726-30-4 (QF3145); 2008; 248 s.
- [5] VEGRICHT, J., MILÁČEK, P.: Homogenita komplexní krmné dávky - důležitá vlastnost MKV; Mechanizace zemědělství; 2008; č. 12.
- [6] VEGRICHT, J., MILÁČEK, P., MACHÁLEK, A., AMBROŽ, A.: Parametric analysis of the properties of selected mixing feeding wagons; Research in Agricultural Engineering; 2007; vol.53; no. 3; s. 85-93

## ASSESSMENT OF SOIL COMPACTION RISK BY AGRICULTURAL TYRES

PATRIK PRIKNER\*, ZDENĚK ALEŠ

Faculty of Engineering, Czech University of Life Sciences Prague, 165 21 Prague 6 Suchbát, Czech Republic, \*Phone: +420 224 383 316, Fax: +420 234 381 828, E-mail:

[prikner@tf.czu.cz](mailto:prikner@tf.czu.cz)

### Abstract

The compaction capacity rating of tyres (further CC rating) is a numerical index expressing the risk of soft soil compaction by loaded wheels with tyres and reflecting tyre dimensions, load and inflation pressure. The compaction is defined by soil dry density. The CC rating is based on processed laboratory measurements of soil compaction by pressure plates and thus avoids dealing with complicated stress field in the ground. The compaction profile under an evaluated tyre is computed using a databank of compaction functions measured under round flat pressure plates in a laboratory testing bin filled with Suchbát loam. A tyre itself is represented by a substituting plate of the same footprint area and mean contact pressure. The tyre footprint area on firm ground can be established either by measurement on a stand or using a convenient formula as will be the case in this paper. CC rating compares the average soil compaction by evaluated tyre in the depths between 20 and 50 cm under the ground surface with critical soil compaction after Lhotský [1]. The paper applies the CC rating to several practical cases.

**Keywords:** agricultural tyres, soil compaction, compaction capacity tyre rating

### 1. Introduction

Tyre – ground interaction has two principal aspects, namely the traction and the soil compaction, which became a weighty research subject since the tyre became a standard. Both these aspects undergo a steady development. Particularly, the compaction can be expected to receive a deserved attention because of necessity to keep food production and comply with ecological trends. The existing methods of evaluating soil compaction are mostly indirect, through intermediary of stresses (e.g. pressure bulbs).

The CC tyre rating is apparently the only existing direct assessment of soil compaction risk, which means that it evaluates directly the compaction of a central soil column under the tyre contact area. This rating reflects tyre design parameters, inflation pressure and loading. The CC rating can with advantage be applied to complete vehicles or machines; the product with

lower total rating can in general be more expensive, however, may raise the production and economy of operation. The CC rating has the character of trademark meaning that it refers to a defined soil type, soil status and evaluation procedure [2]. The actual paper demonstrates the practical use of this approach by comparing the CC rating of typical groups of agricultural tyres.

### 2. CC rating computer program

The team of researchers under supervision of prof. Grečenko developed a tyre CC rating computerized evaluation. The CC rating program is implemented in an Excel file (Fig. 1). It contains several macros that are written in Visual Basic. As an option, the user assesses the CC rating as the change of soil compaction state directly (without dealing with the stresses in the ground). The results of CC rating are derived from this program for all compared tyres.

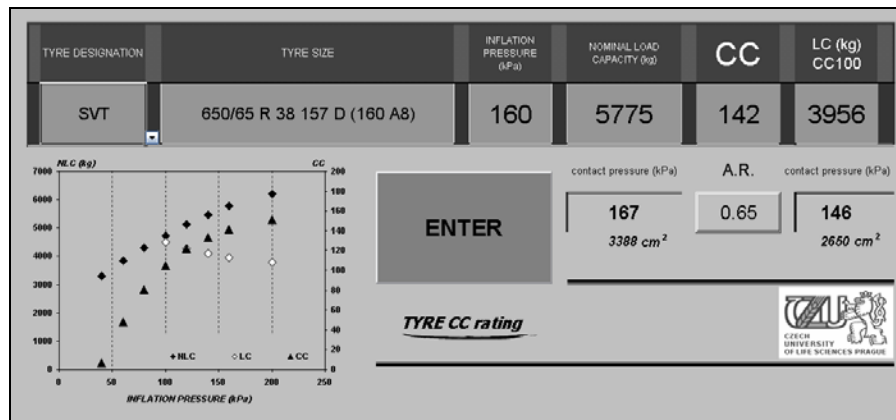


Fig. 1. Design of tyre CC rating computer program, (demo version 2010).

### 3. Comparative chart of selected radial tyres

In the mild climatic conditions and on loam soil, the compaction risk can be qualified as follows (CC rating/risk): 0/no (tyre soil – friendly); 50/small; 100/considerable; 150/great; 200/very great; above 200/extreme. The CC rating = 100 (CC100) means that the average soil dry density in the mentioned range of depths is

10 % above the critical dry density. This may present a conventional upper limit for ecological field operation of a tyre. The list of selected three radial tyre sizes shown in Fig. 2 includes correct tyre catalogue conversions to the same rim and CC rating for *operating* inflation pressure (IP) 100 and 120 kPa at *Nominal Load Capacity* (NLC) after manufacture's catalogue.

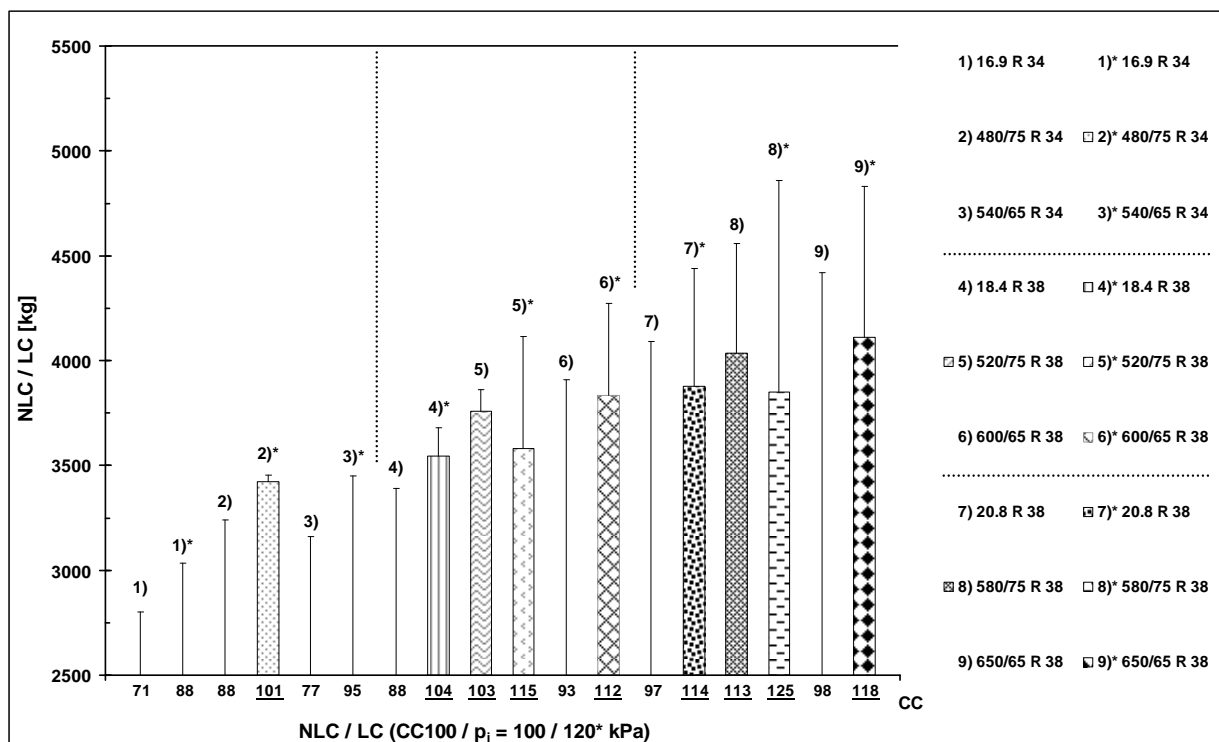


Fig. 2. CC rating of selected radial tyres and hypothetically required NLC reduction (LC) to reach to CC rating 100.

*Load Capacity (LC)* as a load reduction in relation to the level *CC100* indicates hypothetically recommended load limit. In comparison, only two standard radial tyres (aspect ratio *AR* 85) and five low-profile tyres (*AR* 75 and 65) for inflation pressure 120 kPa exceed the *CC* rating = 100. Unsuitable catalogue load can be reason of a *CC* rating increase above 100 as well; see two tyres (*AR* 75) at inflation pressure 100 kPa.

#### 4. Effect of load on large sized tyre *CC* rating

Large tyres are considered as soil friendly at the lowest permitted inflation pressure and corresponding reduced *LC*. Apparently, the performance of large tyres would be inadequate and their substitution by smaller tyres advantageous. Reduction of existing *CC* ratings of most presented large sized tyres namely *Super Volume Tyres* to the acceptable value *CC100* at the same inflation pressure 100 kPa could be reached by a considerable reduction of their loads (Fig. 3).

The tyre sizes 580/70 R 38 (drive traction tyre) and 650/75 R 32 (large harvester tyre) were previously compared by Way et al. [4, 5]. Stresses in the soil were determined and rut depths were measured, net traction and tractive efficiency were compared in dependence on soil bulk density and cone index at two dynamic loads. The authors state that in summary no fundamental differences were found that would clearly indicate that one tyre was better than the other.

The evaluation by *CC* rating essentially seconds this conclusion, however, discloses that the tyre 650/75 R 32 with greater *NLC* extends the *CC* rating to higher values than the tyre 580/70 R 38 and thus can be ecologically more risky (see Fig. 4). Reduction of existing *CC* ratings of most presented large sized tyres to the acceptable value *CC100* at the same *IP* could be reached by a considerable reduction of their loads. The load reduction, indeed, is accompanied by a change of footprint area and mean contact pressure [3, coefficient  $\alpha_N$ ].

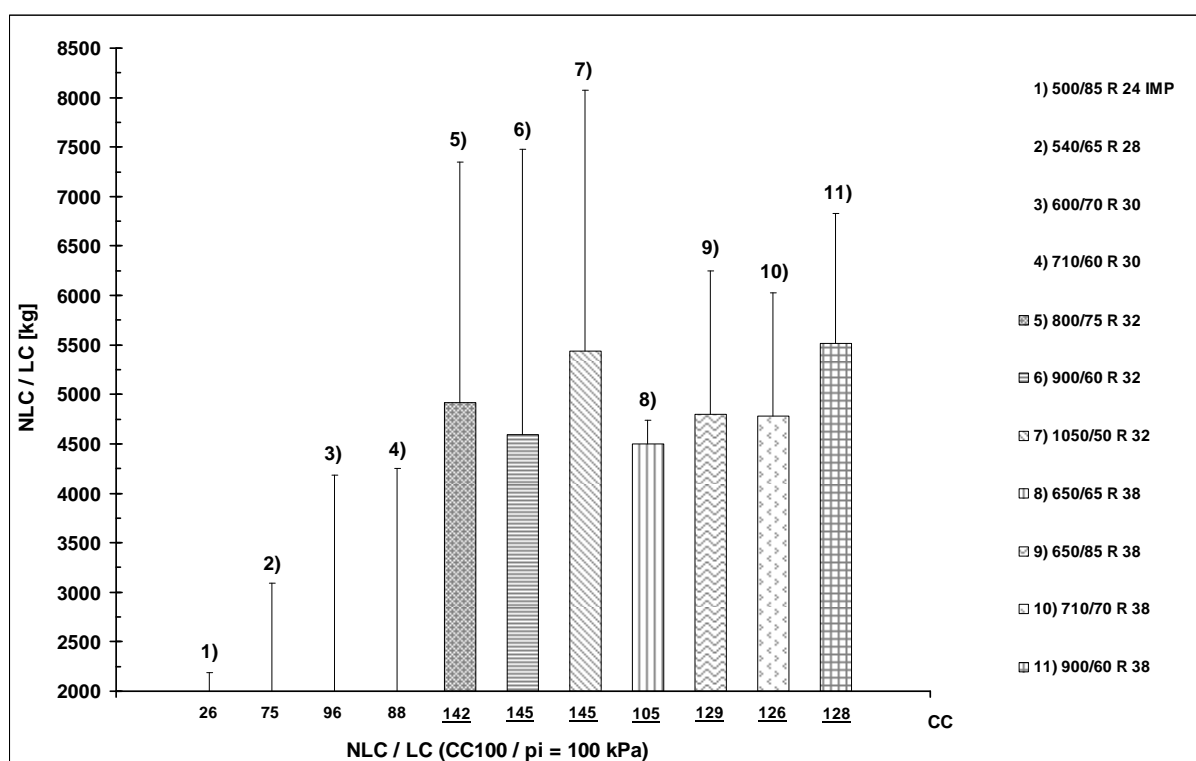


**Fig. 3.** *CC* rating of super volume tyres and hypothetically required *NLC* reduction (*LC*) to reach to *CC* rating 100.

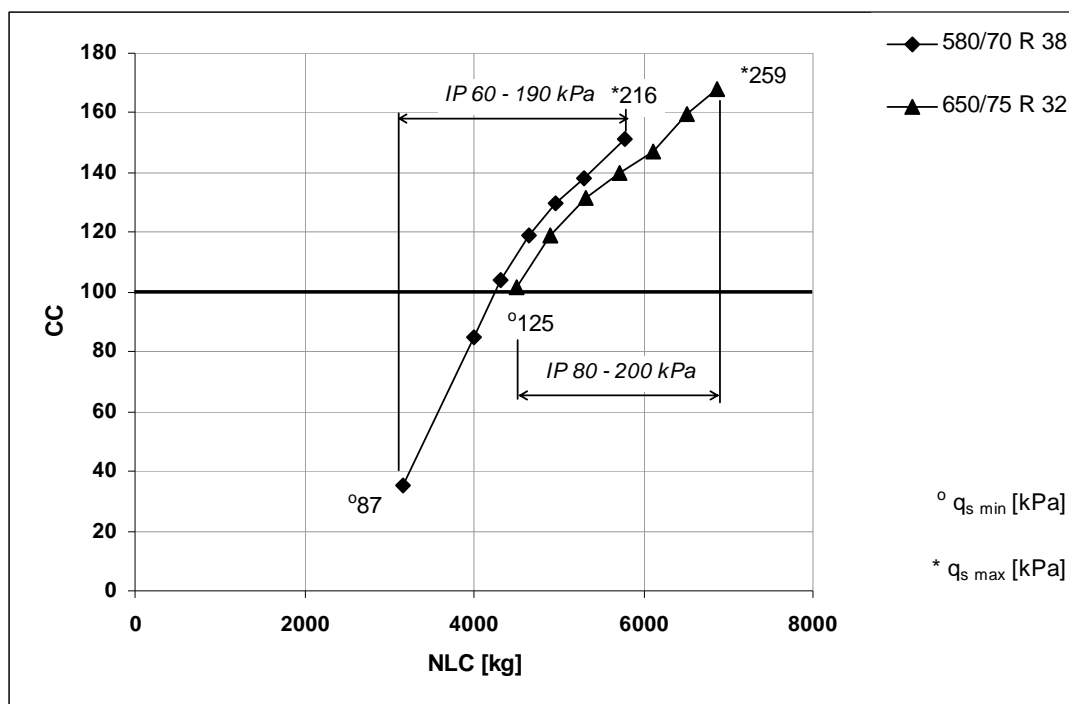


**Fig. 4.** Shape of tyre CC ratings for tyres 580/70 R 38 and 650/75 R 32 in the *NLC* range.

On example of compared tyres [4, 5] with 32" and 38" rim diameters (*AR* 0.70, 0.75), Fig. 5 documents that decisive for CC rating is the tyre load; under this unloaded conditions, tested tyres 580/70 R 38 and 650/75 R 32 have almost the same contact areas  $S_T$  (similar tyre dimensions)

and thus both tyre types are able to reach the *CC100* at identical *LC*. Generally, the results confirm that tyre aspect ratio (at unloaded tyre state) has no significant effect on soil compaction.

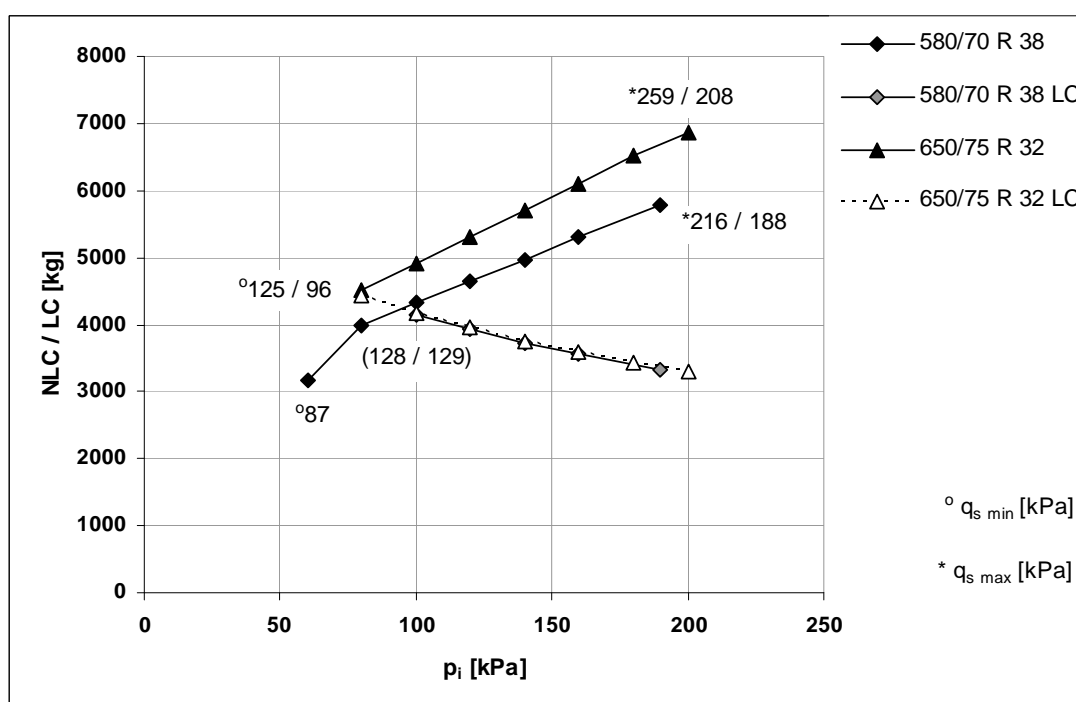


**Fig. 5.** Shape of *NLC / LC* for tyres 580/70 R 38 and 650/75 R 32 in the *IP* range.

## 5. Tyre construction and design affects the CC rating

Tables 1-4 document that standard radial tyres (AR 85) regularly exhibit higher CC ratings than cross-ply tyres due to their higher *NLC*. The tyres 520/75 R 38 and 600/65 R 38 are regularly

low-profile supplements of the standard radial tyre 18.4 R 38. Representative combinations, *NLC* (*LC*),  $S_T$  ( $S_{T\ red}$ ) and  $q_s$  ( $q_{s\ red}$ ) (full, dashed and dotted lines), support credibility of CC rating evaluation including *LC* assessment in relation to the level *CC100*.

**Tab. 1.** Computed data for cross-ply tyre 18.4-38.

$p_i$ [kPa]	CC	NLC [kg]	$S_T$ [cm <sup>2</sup> ]	LC $_{CC100}$ [kg]	$S_{T\ red}$ [cm <sup>2</sup> ]	$q_s$ [kPa]	$q_{s\ red}$ [kPa]
80	63	2575	2011	0	0	126	0
100	83	2905	1925	0	0	148	0
120	99	3230	1842	0	0	172	0
140	110	3540	1763	3208	1621	197	194

**Tab. 2.** Computed data for standard radial tyre 18.4 R 38.

$p_i$ [kPa]	CC	NLC [kg]	$S_T$ [cm <sup>2</sup> ]	LC $_{CC100}$ [kg]	$S_{T\ red}$ [cm <sup>2</sup> ]	$q_s$ [kPa]	$q_{s\ red}$ [kPa]
60	43	2745	2748	0	0	98	0
80	68	3080	2630	0	0	115	0
100	88	3390	2517	0	0	132	0
120	104	3680	2408	3543	2332	150	149
140	116	3945	2304	3340	2000	168	164
160	125	4225	2205	3151	1719	188	180
200	146	4875	2019	2790	1257	237	218

**Tab. 3.** Computed data for low-profile tyre 520/75 R 38.

$p_i$ [kPa]	CC	NLC [kg]	$S_T$ [cm <sup>2</sup> ]	LC $_{CC100}$ [kg]	$S_{T\ red}$ [cm <sup>2</sup> ]	$q_s$ [kPa]	$q_{s\ red}$ [kPa]
60	63	3200	2844	0	0	110	0
80	86	3555	2721	0	0	128	0
100	103	3860	2604	3758	2552	145	144
120	115	4115	2492	3582	2246	162	156
140	127	4545	2385	3325	1886	187	173
160	138	4970	2282	3109	1605	214	190
200	153	5325	2090	2952	1343	250	216

**Tab. 4.** Computed data for low-profile tyre 600/65 R 38.

$p_i$ [kPa]	CC	NLC [kg]	$S_T$ [cm <sup>2</sup> ]	LC $_{CC100}$ [kg]	$S_{T\ red}$ [cm <sup>2</sup> ]	$q_s$ [kPa]	$q_{s\ red}$ [kPa]
40	4	2655	3560	0	0	89	0
60	38	3100	3407	0	0	105	0
80	68	3520	3260	0	0	120	0
100	93	3910	3120	0	0	136	0
120	112	4275	2985	3833	2766	151	136
140	126	4695	2857	3590	2367	167	149
160	136	5110	2734	3383	2048	196	162
200	156	5995	2503	3025	1551	196	191



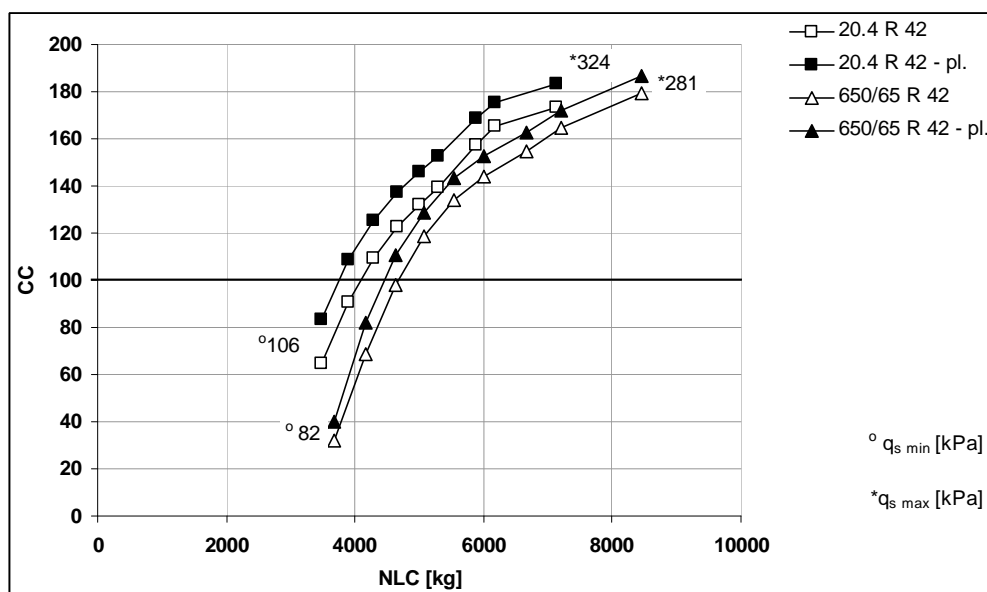


**Fig. 6.** Shape of CC rating for tyres 20.8 R 42 and 650/65 R 42 in the *NLC* range at traffic and ploughing.

## 6. Tyres operating in a furrow

Tractors when ploughing often go with wheels on one side in the furrow. This situation consequently increases the soil compaction of previous run. The CC rating technique can cope with this matter. Figure 6 shows CC rating evaluation of two different tyre types under two alternatives: field traffic conditions for speed 10 km/h and when both tyres run in a furrow 20 cm deep.

## 7. Conclusions

Following conclusions may be drawn from the preceding text: (1) CC rating provides simple and concrete soil compaction risk assessment in terms of soil dry density unattained other known methods; (2) lower *IP* must be combined with lower loading to reduce soil compaction; (3) the mass of heavy vehicles should be distributed among more than two axles with smaller tyres; (4) radial ply tyres loaded to their nominal capacity have higher CC rating than equivalent cross ply tyres because of their greater nominal load capacity; (5) CC rating technique enables to evaluate the increased soil compaction risk for tyres operating in a furrow.

## Acknowledgement

This project has been financed by the Ministry of Education of the Czech Republic (grant N°. MSM 6046070905).

## Reference:

- [1] Lhotský, J.: Soil compaction and measures against it [in Czech, abstract in English]. Study Inf Plant Product No. 7, Prague: IAEI; 2000.
- [2] Grečenko, A. – Prikner, P.: Progress in tire rating based on soil compaction potential. *J Terramech* 46(5),2009,p.211-216.
- [3] Grečenko, A.: Tire footprint area on hard ground computed from catalogue values. *J Terramech* 32(6),1995,p.326-33.
- [4] Way, T.R. – Kishimoto, T. – Burt, E.C. – Bailey, A.C.: Tractor tire aspect ratio effects on soil stresses and rut depths. *Trans ASAE* 40(4),1997,p.871-81.
- [5] Way, T.R. – Kishimoto, T. – Torbert, H.A. – Burt, E.C. – Bailey, A.C.: Tractor tire aspect ratio effects on soil bulk density and cone index. *J Terramech* 46(1),2009,p.27-34.

## THE POSSIBILITIES OF REDUCTION OF MILKING ENERGY COMSUMPTION

MIROSLAV PRIKRYL, JOSEF MALOUN, JIRI KLIMA<sup>†</sup>

Czech University of Life Science Prague, 165 21 Prague 6 – Suchdol, Czech Republic

### Abstract

Power consumption required to drive a vacuum pump largely depends, among others, on the assignment of a proper electric motor. The selection of electric drives for vacuum pumps used with milking machines in agriculture, encounters a problem of fluctuating load, depending on the level of the operation vacuum in the system. The power of the drive unit is frequently selected to comply with its need of the maximum vacuum attainable by the vacuum pump. It follows, that with the nominal level of the vacuum, the electric motor does not operate at the optimum power rating. From the results of the measurements a conclusion has been drawn, that it is both advantageous and possible to assign an electric motor for the vacuum pumps to comply with the power required to attain the nominal vacuum in the system and to safeguard the machine set against overload by means of a safety valve integrated in the body of the vacuum pump or by the thermal circuit breaking protection of the motor.

### Introduction

Continued search for ways of decreasing power consumption per unit of useful production is an inevitable exigency if we want to reduce the load on the environment, resulting nowadays frequently from the ever increasing demand for the supply of power.

Vacuum pumps, as a mechanical equipment for the exhausting of gases have mostly the task to create a space with a required level of evacuation for the subsequent technical utilization. The requirements of the vacuum level will, of course, considerably differ with respect to the purpose and application.

### Experimental arrangement

Power requirements of the vacuum pumps are generally influenced by several principal factors. The first of them is the actual design of a vacuum pump with regard to the thermodynamics.

With a sliding-vane rotary vacuum pump, it is, besides a suitable choice of dimensions of the main parts of the design, for example the determination of the angle under which the uncovering of the discharge duct is to occur. The air compression in the vacuum pump is to reach approximately the value of the outlet, i.e. atmospheric pressure. From the operating parameters, the power consumption is notably influenced by the required performance and level of the nominal vacuum, which the vacuum pump maintains in the evacuated system, i.e. in the milking machine.

Another factor, apart from the power consumption, influencing the rational utilisation, is the decision on the assignment of an adequate electric motor. The reason is, that it is useful to take into consideration the relation between the power of the electric motor and the requirement of the vacuum pump, continually operating at a nominal vacuum, with a known requirement of the power take-off. In the designing of the electrodrive for the vacuum pump of the milking machines, the power of the assigned drive unit is usually chosen near to the maximum needed power, which would come into consideration with the attainment of the maximum vacuum of the given vacuum pump. As these two power requirements may considerably differ, it can be deduced, that with a nominal vacuum the electric motor so assigned does not operate within a mode of adequate power.

In order to examine a feasible improvement in accuracy of the assigning of the electrodrive, some measurements were conducted with the vacuum pumps DLV and ALFA-LAVAL of the Czech and foreign manufacture respectively. A dynamometric testing stand DS 546/4V of the Czech manufacture, substituting the driving unit, was used for the purpose, which enabled to determine accurately the power taken off to drive the vacuum pump, from the values of the torque  $/\text{N.m}/$  and of the revolutions  $/\text{l.min}^{-1}/$ . Simultaneously were established the input and output temperatures and pressures of the air flowing through the vacuum pump and by means of a flow indicator the volume of the rate of flow  $/\text{m}^3.\text{s}^{-1}/$  was measured.

By a conventional method of a thermodynamic calculation for a polytropic change of state, from the relations

$$p_1 \cdot v_1 = R \cdot T_1, \quad p_2 \cdot v_2 = R \cdot T_2$$

where  $R = 287 \text{ J} \cdot \text{kg}^{-1} \cdot \text{K}^{-1}$ ,  
were determined specific volumes  $v_1$  and  $v_2$   
 $/\text{m}^3 \cdot \text{kg}^{-1}/$

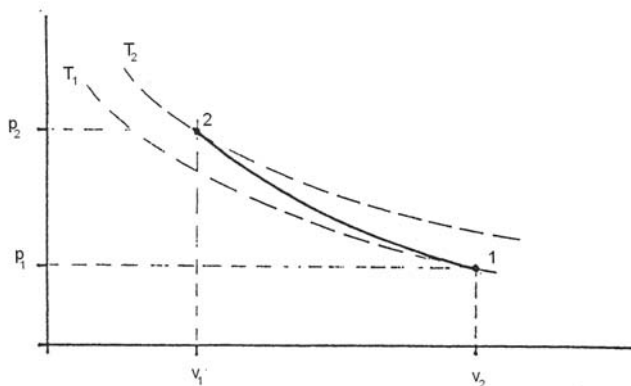


Fig. 1 Polytropic compression with heat removal

Sliding vane rotary vacuum pumps belong to a group of vacuum pumps called vacuum pumps with an integrated compression ratio. This compression ratio is given by a relation of pressures at the inlet and outlet side of the vacuum pump. The next part of the calculation determines the mean polytropic exponents for the operation with the nominal vacuum for a 50.7 kPa milking machine :

$$n = \frac{\log p_1 - \log p_2}{\log v_2 - \log v_1}$$

The knowledge of the mean polytropic exponent ( $n$ ) further enabled to determine first the absolute work, by a relation :

$$L_{1,2} = \frac{p_1 \cdot v_1}{n-1} \left[ 1 - \left( \frac{p_2}{p_1} \right)^{\frac{n-1}{n}} \right] \quad [\text{J} \cdot \text{kg}^{-1}]$$

from which, by means of the expression :  
 $L_{1,2} = L_{1,2} \cdot n \quad / \text{J} \cdot \text{kg}^{-1}/$  was expressed the technical work.

From the values of the known barometric pressure ( $p_b$ ) and the input air temperature ( $t_1$ ) the corresponding air density  $\rho_{\text{AIR}}$  was

established from the tables. From the measured volume of the rate of flow  $Q \text{ /m}^3 \cdot \text{s}^{-1}/$  was subsequently calculated the mass of the rate of flow

$$Q_m = Q_v \cdot \rho_{\text{AIR}} \quad / \text{kg} \cdot \text{s}^{-1}/$$

which was then used for the calculation of the theoretical requirement of the power for the drive of the vacuum pump for the operation with the nominal vacuum

$$P_t = L_{1,2} \cdot Q_m \quad / \text{W}/$$

By a comparison of the actually required power established from the data of the dynamometric testing stand, serving for drive :

$P_R = M_K \cdot \omega \quad / \text{W}/$ , could be also determined the total efficiency of the vacuum pumps

$$\eta_c = \frac{P_t}{P_R}$$

The effected thermodynamic calculations, which can not be given here for exigency of space, confirm the tenor of our recommendation concerning the selection of electrodrive for sliding vane vacuum pumps.

For the DLV vacuum pump, used for the milking machines of the Czech production, the following values were calculated for the operation with the nominal vacuum 50,7 kPa and the volume of the rate of flow  $1 \text{ 220 l} \cdot \text{min}^{-1}$  :

$$P_t = 1 \text{ 630 W}, \quad P_R = 1 \text{ 951 W (from the dynamometric measurement), } \eta_c = 0,835$$

An asynchronous motor with a squirrel-cage armature has been assigned, of

$$P = 3 \text{ kW}, \quad \cos \varphi = 0,84, \quad 6,7/11,6 \text{ A}, \\ n = 1 \text{ 430 min}^{-1}$$

Repeated measurements furthermore confirmed the linear dependence of the power required for the drive of the vacuum pump, at the level of the vacuum in the system. The measurements were effected within the range of the values of the vacuum from 35 kPa to the accessible maximum for the given vacuum pumps, i.e. 88,9 kPa and 91,3 kPa with the DVL and the Alfa- Laval vacuum pumps respectively. It has been established, that the effect of the size of the vacuum on the necessary size of the drive from the relation of the regression gradients of

lines of the function  $P = f(p)$  is about 2,7 times larger for the DVL vacuum pump than with the Alfa-Laval, when the latter featured less sensitivity to the increase of the vacuum level from the view of the taken-off power.

The course of the power-vacuum dependence in the system (Fig.2) reveals, that the power required to reach the nominal vacuum, e.g. 50 kPa with our milking machines is considerably lower than the power required for the maximum attainable vacuum (88,9 and 91,3 kPa respectively). A rational electric power utilization of machines with asynchronous

motors is characterized by efficiency and power factor.

The former case concerns the assessment of the active power, which is transformed to the required mechanical work on the shaft of the motor. The power factor is characterized by the share of the reactive energy required to generate and maintain the magnetic field and inductance of the motor. Consequently, there is the aim to reach the highest possible values of the efficiency and of the power factor within the whole range of the motor.

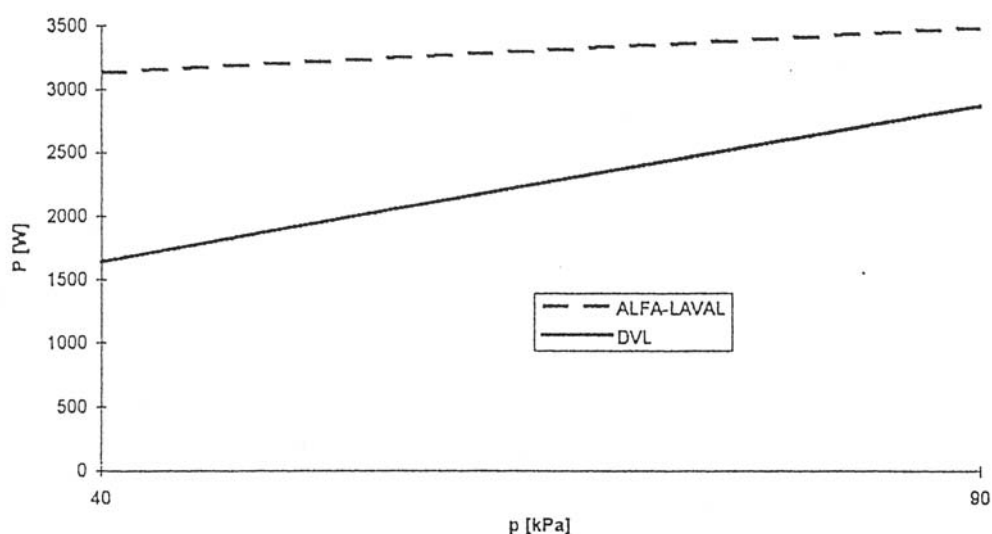


Fig. 2 Dependence of vacuum pump drive power and the vacuum rate

Fig. 3 presents a substitution diagram of an asynchronous motor with a squirrel-cage armature, in which is valid for the individual impedances as follows :

$$\bar{Z}_{11}' = R_1 + iX_1\sigma : \bar{Z}_0 = jX_0 : \bar{Z}_{22} = \frac{R_2}{s} + iX_2\sigma$$

$R_1, R_2$  - stator, rotor winding resistance,  
 $X_{1\sigma}, X_{2\sigma}$  - leakage reactance of the stator, rotor  
 $X_0$  - magnetization reactance,  $s$  - motor slip

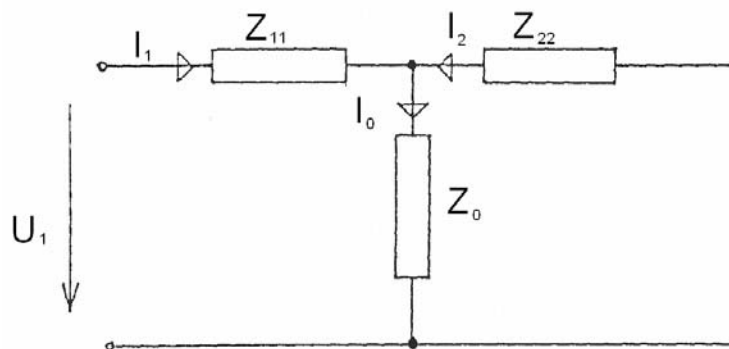


Fig. 3 Substitution diagram of an asynchronous motor with a squirrel-cage armature

For total losses of the motor holds true :

$$\Delta P_c = \Delta P_{j1} + \Delta P_{Fe} + \Delta P_{j2} + \Delta P_m + \Delta P_d$$

$\Delta P_{j1}, \Delta P_{j2}$  - stator, rotor winding losses,  $\Delta P_{Fe}$  -

losses in iron,  $\Delta P_m$  - mechanical losses

$\Delta P_d$  - additional losses

In view of the substitution diagram according to Fig.3 are hereafter considered only the losses

$\Delta P_j = \Delta P_{j1} + \Delta P_{j2}$ , These losses are respected in the diagram by resistances  $R_1, R_2$ .

Efficiency  $\eta' = \frac{P}{P + \Delta P_j}$ ,  $P$  is the power of the

motor. For the efficiency so established, it can be derived :

$$\eta' = \frac{R_2 X_o^2 (1-s)}{s R_1 X_2^2 + \frac{R_1 R_2^2}{s} + R_2 X_o^2}$$

$$\sigma = 1 - \frac{x_o^2}{x_1 x_2}$$

From the condition for the extreme of efficiency origination there follows

$$\frac{d\eta'}{ds} = 0 \Rightarrow s_\eta = \frac{R_2}{x_2} \sqrt{\frac{1}{1 + \left( (1-\sigma) \frac{R_2}{R_1} \cdot \frac{x_1}{x_2} \right)}}$$

For the motor driving the vacuum pump  $P = 3$  kW, the extreme values are  $s_\eta = 0,0163$  and  $\eta_{\max} = 0,937$  (with the DVL vacuum pump)

Fig. 4 presents the dependence  $\cos \varphi$  and  $\Delta P_c$  as a function of load given by relation

$I_m = \frac{M}{M_N}$ , The motor operates with a load of

$$m = \frac{1950}{3000} = 0,65 \text{ to which correspond values}$$

$$\cos \varphi = 0,74 : \Delta P_c = 550 \text{ W} : \eta = 0,79$$

As evident, the motor operates at this load with low values of  $\cos \varphi$  and  $\eta$  far from the optimum values.

If a motor of  $P = 2,2$  kW power is used, the power efficiency of the motor is increased and, consequently, the utilization of electric power is more rational.

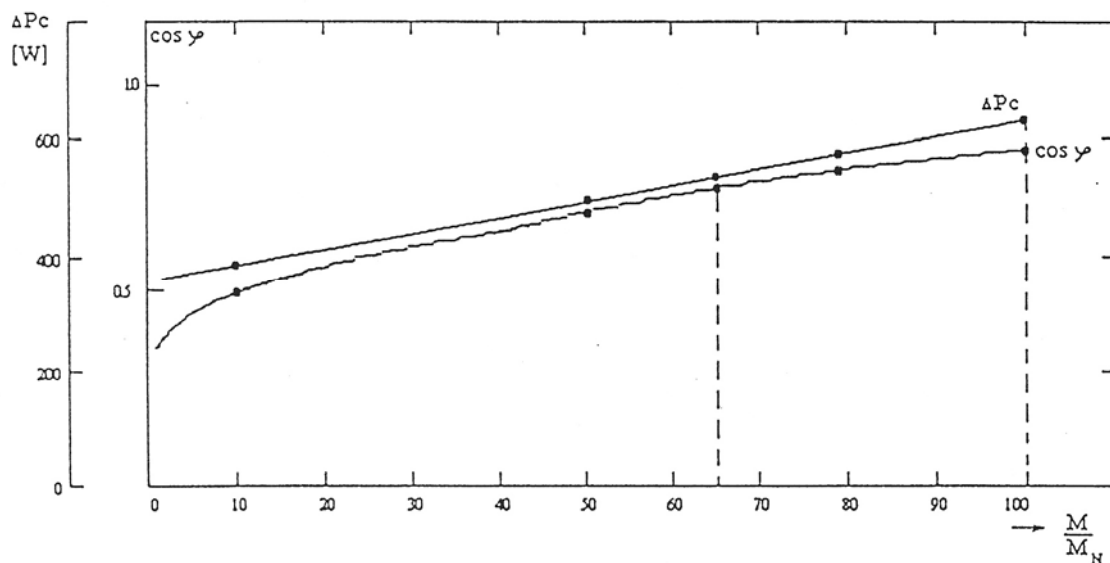


Fig. 4 Dependence of losses and power factor of the motor on the load

## Conclusions

Consequently, our investigations lead to a conclusion, that it is possible and advantageous to assign an electric motor (or other means of drive) for the vacuum pumps to comply with the power required to attain the nominal vacuum in the system and to safeguard the machine set against overload by means of a safety valve integrated in the body of the vacuum pump or by the thermal circuit breaking protection of the motor. The valve should restrict the vacuum level attainable to a value near the operating value and thus to secure the drive against overload caused by an undesired increase of the vacuum and the resulting higher power required for the drive. The application of the proposed

approach reveals savings of both the active and idle energy, including an improved power factor of the network and the savings accomplished by the application of an electric motor of less power.

## References

- 1) Chlumský, V.: Rotační kompresory a vývěvy (Rotary Compressors and Vacuum Pumps) SNTL, Prague Czech Republic, 1985, 277 p.
- 2) Kalčík, J.: Technická termodynamika (Technical Thermodynamics) SNTL, Prague Czech Republic, 1989, 514 p.



## FIELD AERIAL PHOTOGRAPHS TAKING FROM AN AIRCRAFT MODEL

PAVEL PROCHAZKA<sup>1\*</sup>, KROULIK MILAN<sup>1</sup>, JIRI MASEK<sup>1</sup>, HULA JOSEF<sup>1</sup>,  
PROSEK VACLAV<sup>2</sup>

<sup>1</sup>Czech University of Life Sciences Prague, Faculty of Engineering, Department of  
Agricultural Machines, Kamýcká 129, 165 21 in Prague, Czech Republic,

Phone: +420224383133, E-mail: prochazkap@tf.czu.cz

<sup>2</sup>Czech University of Life Sciences Prague, Faculty of Engineering, Department of Utilization  
of Machines, Kamýcká 129, 165 21 in Prague, Czech Republic

### Abstract

Nowadays, the precision agriculture is one of the widely spread technologies of plant production management. As a one source of information about soil and produced plants it is possible to use remote sensing, which is based on aerial and satellite photographs. This article describes the utilisation of radio control operated aircraft model equipped with digital camera for the monitoring of the fields and taking aerial photographs.

The aerial photographs from which is possible to recognize the parts of the field with higher and smaller crop density were taken. Obtained information can be used for differential fertilization of this field. Another part of this observing is focused on using aerial photographs to soil erosion survey.

### Introduction

In the precision farming system applied in practice, it is necessary to have as much information as possible, which is essential and is the basis for site specific crops treatments. This information is possible to gain in different ways, for instance from yield sensor on combine harvester, from soil sampling etc. In addition to these possibilities of obtaining data from on-ground measurement and observation, it is also possible to acquire data about a particular field covered with crop from remote sensing.

Aerial and satellite photographs provide high density measurement. According to current literature sources, the remote sensing are widely used for prediction of Nitrogen needs in cereals, for yields, soil moisture and in-soil organic matter estimation. Further, it can be used for weeds detection, for number of insect pests estimation and according to this the application rate of chemical agents determination, insect damage on crop assessment and also for sampling grid optimisation.

A relatively new method is the multispectral photography, which provides information in visible light continuous spectrum and in NIR and MIR wave scale. This information is usable for yields estimation, for distinguishing between crop plant and weeds between residues and mineral salts. It can be also used for quantitative measurement of water content in plants and for

the LAI (Zhang et al., 2002). Techniques of spectral reflectance describe (Scotford et Miller, 2005).

For small heights and short distances the remote controlled airplanes could be used for the purpose of a crop and a soil conditions monitoring. Vegetation monitoring with using Remote sensing technology from unmanned helicopter were deal with Sugiura et al.(2005). Pudělko et al, (2007) were taken aerial photographs by digital camera, fixed to the UAV - paraglider construction similar to moto-paraglider.

The shape and contours scanning of plants and soil top surface became a very efficient means for gaining information about a field, for the crop growth rate and soil state observation and also for better plant protection (Thomson, et al. 1999, Cox, 2002, Häusler, et al. 2002). Vellidis et al. (2004) were predicting yield maps from aerial photographs.

### Experimental arrangement

Through the use of Remote Control (RC) aircraft model on 14. 6. 2005 observed piece of land „Kuchař“ with spring barley growth. On this field was placed points, theirs position was survey by the GPS apparatus, before taking of photographs. The placement scheme of individual points is on figure 1.

For the aerial photographs taking, a glider model powered with an electromotor was chosen. This model has 3100 mm in wing span and the wing surface is 84.1 dm<sup>2</sup>. The model length is 1455 mm. The model is powered with the driving motor „Mega ACn 22/20/2 “ with embodied gearbox „Mega Gear Planeta“. The total airplane weight with a camera with attachment is 3980g. The five-channel Remote Control (RC) set is used for the operation control and the on-plane part is supplied with power from an accumulator consists of 4 NiMh cells with the capacity of 2100 mAh. The driving accumulator consists of 8 NiMh cells with the capacity of 3300 mAh. The engine is controlled by the regulator Jes 40 – P Opto. It is possible to control and regulate engine rpm, rudder, elevator and control unit of camera release. The aerial photography is provided by digital camera Olympus C-50 zoom. This camera is placed underneath one wing in a case. The control unit of camera release which is placed in aircraft model allows the periodic photograph taking. This function allows recording of the photographs with partial covering which make easier their following processing.

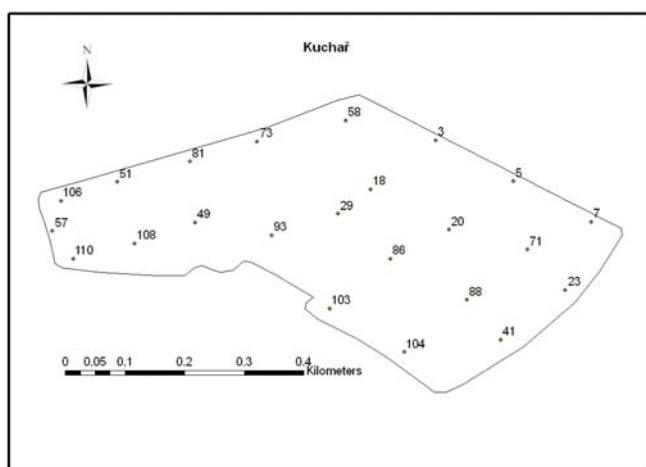


Figure 1. The placement scheme of individual on piece of land „Kuchař“.

### Results and discussion

For remote sensing was chosen fields „Kuchař“, with area 16.4 ha on ŠZP Lány. The photographs take hold of spring barley growth (strain Jersey, seeding amount 200 kg.ha<sup>-1</sup>), in 14.6.2005. The seeding was made by seeding machine Accord with swath 4m in first half of April 2005. The distance of tracking is 24 m.

To pull the trigger of camera was used an equipment, with periodic pull the trigger of camera function. With thanks this function was takes the photos with partial overlapping, which is necessary for connecting constituent photos and consecutive processing.

The picture of whole observes field was assembled from individual photos by Adobe Photoshop program tools. This way created picture was supported by application Image Analysis program ArcGis 9. The figure 2 represents compound picture of observed field inset to coordinate system.

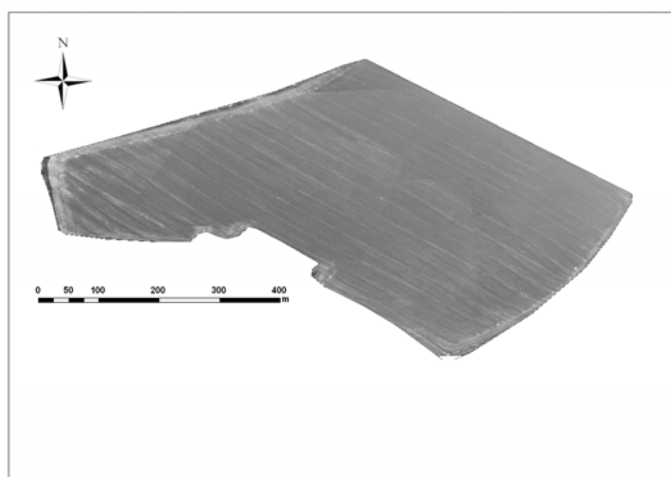


Figure 2. Compound picture of observed field inset to coordinate system.

On this picture was make image analysis one colour was assign to soil without growth and second colour assign to growth. Image analysis is on figure 3. Furthermore was calculating covering soil by growth – the covering value was 82.64 %. The soil without vegetation ranked 17.36 % from whole area of observed field, which are 16.4 ha. The areas, where is soil surface without vegetation covering, are occurred particularly in border parts of field. The aerial photographs from which is possible to recognize the parts of the field with higher and smaller crop density were taken. Obtained information can be used for differential fertilization of this field.

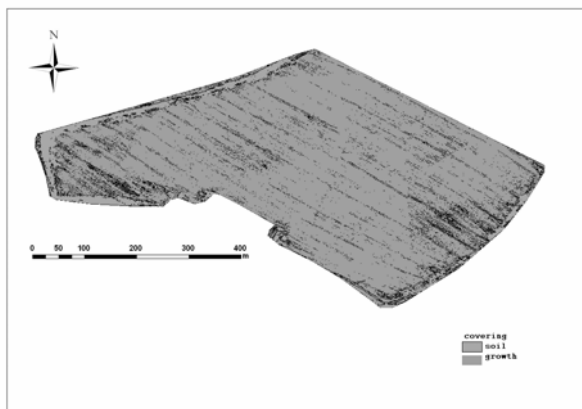


Figure 3. Image analysis of picture, represent the covering soil by growth.

The figure 4 represents area with corn growth. In upper part of picture are perceptible consequences of water erosion. The direction of erosion is signifying arrow direct on the picture from the left to the right. On the left side is lesser damage and the direction to right part of picture are consequences water erosion striking. The most is impacted headland, were the ultimate growth damage.

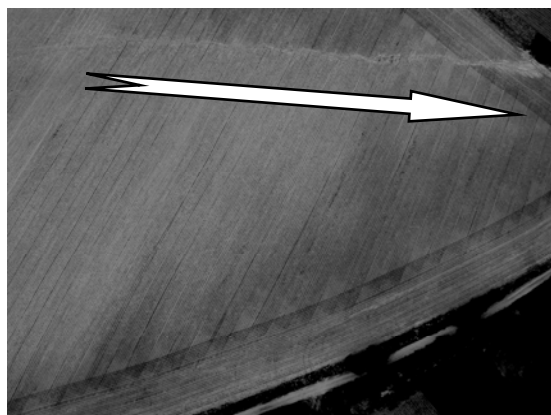


Figure 4. Picture of plot with corn growths (arrow highlight area impacted water soil erosion)

## Conclusion

The using of RC operated aircraft model for remote sensing and following processing for another working operations is very easy, quick and cheap method with opposite of satellite photos. Their most advantage is in speed of data processing and using outcome of analysis in a few ours after taking the photos. It is meaning that for example creation application map for nitrogen additional fertilizing is determine on actual growth stage. The problems by the using that acquired photos present correct assembling

individual photos and their inset to coordinate system. If these manage problems, acquire agronomist important element for decision of agriculturalist operations on given field. One of the another using the RC operated aircraft model is finding of soil erosion consequences.

## References:

- [1] Cox, S. 2002. Information technology: the global key to precision agriculture and sustainability, *Computers and Electronics in Agriculture*, N. 36, p. 93-111.
- [2] Häusler, A., Nordmeyer, H. 2003. Using aerial photography to detect weed for site-specific weed control – perspectives and limitations. *Proceedings of the 4th European Conference on Precision Agriculture*, 2003, p. 271-278.
- [3] Pudelko, R., Igras, J., Kozyra J., Evaluation of a field's spatial variability using an UAV. In: *6th European Conference on Precision Agriculture*[CD-ROM]. Skiathos, Řecko, 2007.5 s.
- [4] Sugiura, R., Noguchi, N., Ishii, K., 2005. Remote-sensing Technology for Vegetation Monitoring using an Unmanned Helicopter, *Biosystems Engineering*, 90(4), p. 369 – 379.
- [5] Scotford, I. M., Miller, P. C. H. 2005. Applications of Spectral Reflectance Techniques in Northern European Cereal Production: A Review. *Biosystems Engineering*, 2005, 90, 3, p. 235 – 250.
- [6] Thomson, S. J., Hanks. J. E. 1999. Remote sensing system for agricultural spray planes - preliminary field observations. *An ASAE Meeting Presentation*, Paper No. 99-1137.
- [7] Vellidis, G., Tucker, M. A., Perry, C. D., Thomas, D. L., Wells, N., Kvien, C. K. 2004. Predicting Cotton Lint Yield Maps from Aerial Photographs. In: *Precision Agriculture – An International Journal on Advances in Precision Agriculture*, 2004, volume 5, Number 6, December 2004, p. 547 – 564.
- [8] Zhang, N., Wang, M., Wang, N. 2002. Precision agriculture – a worldwide overview. *Computers and Electronics in Agriculture*, 2002, N. 36, p. 113 – 132.

This particular research has been supported by the Ministry of Education, Youth and Sports of the Czech Republic as part of research plant MSM 6046070905

## THE MASS FLOW SENSORS - CURRENT STATE

DENIS PRONITSYN, FRANTISEK KUMHALA

Czech University of Life Science in Prague, 16521 Prague 6 – Suchbát, Czech Republic, Phone:  
+420 775 178 684, E-mail: pronidenis@gmail.com, kumhala@tf.czu.cz

### Abstract

During the harvesting yield monitoring is an integral part in the purpose of creating yield maps. It is an essential technique for grain growers, which helps them to make appropriate decisions in cropping activities.

This kind of system is available for grain combines, but still have some shortcomings. For other harvester machines, this equipment remains at a developing level. This field has been investigated by a number of scientists and a large amount of different techniques have been created.

In reference to this work, which a problematic review was conducted in the current state and the literature review of articles with the subsequent analysis of existing devices and the methods were applied to the formulated problem.

Through analysis of the literature review articles it becomes clear that developed devices still have some disadvantages, such as relatively high errors, difficulties in real field application and high costs in manufacturing. Correspondingly, with popularity growth of precision agriculture the current problem is topical, and it is assumed further development will take place with the aim of designing a device that could be up to the requirements.

### Introduction

It is necessary to acquire information about the exact amount of agricultural crop, which is in the bunker of the harvester. This information is vital for the direct transportation to the consumer once a crop has just been harvested. It will essentially reduce expenses for transportation and storage of a product for a producer. Thus both the supplier and the customer possess the information about transported product and have the ability to supervise it on any site from a place of harvesting to a place of transportation.

The information for construction of maps of productivity is also an important factor in which creation of a similar device together with a navigation system, can become an irreplaceable assistant. These maps give possibility to define the low-yielding sectors, demanding additional research for finding-out of the reasons.

To solve the problems previously mentioned above of an amount of agricultural crop in a harvest-time it is necessary to have a device, capable to help with the decision of the given problem and to combine an exact accuracy, reliability and simplicity in use.

The purpose of this work is problematic

consideration in a current state and literary review of articles with the subsequent analysis of existing devices and the methods applied to the decision of a task in view. As part of the study and analysis of existing information a large number of publications related to this topic was found. The precursors have researched and developed large number of different types of devices aimed at achievement of an objective.

### Materials

Stafford et al. (1996) described the principle of a capacitive sensor, which he used to develop a grain mass flow system to create yield maps of cereal crops. The disadvantages of the capacitive sensor, the authors consider its sensitivity to moisture content of the crop and to the material distribution within the sensing volume. The authors suggested compensating the effect of moisture content by measuring the capacitance at two widely spaced frequencies. Thus has been developed a sensor that works on two frequencies, one section at 10kHz and the other at 2MHz. This sensor was installed at the discharge point of the auger of the harvester. The resulting signal at the output is digitized and sent to a computer located



in the cab. The output signal was linearly proportional to the value of mass flow at a value of moisture content of 15% for barley. Analysis of information by using cultures of different moisture content has been conducted. He has showed that the output value of sensor is less dependent on moisture content than expected. According to the authors, for correct operation of the sensor must be provided with two conditions. It should present minimal impedance to the flow of crop and it should be insusceptible to appeared mechanical vibration.

DeHaan et al. (1999) used a bulk monitoring equipment, installed on the potato harvester. By calibration it was obtained that the bulk recorded weights had been within 5% of actual weights. Gogineni et al. (2002) describe the image-based system for monitoring the yield of sweet potato based on multiple-linear regression. On the basis of laboratory studies, they had got good results ( $R^2 = 0.96$ , where  $R^2$  is coefficient of determination). But the results were slightly worse ( $R^2 = 0.91$ ) when installed on a harvester's conveyor belt. Hofstee and Molema (2002) applied machine vision method for mass estimation of potatoes. This method is based on 2D information from a line scan camera, installed on the conveyor belt. Faced with the problem of cluster forming (clusters defined as one piece of potatoes) they had improved the method. Using the software they were able to identify and separate the clusters into individual pieces of potatoes. The average error of this method was 0.27%. In the following publication Hofstee and Molema (2003) describe the use of the same method for the determination of volume of potatoes, partially covered with soil. In this work, they had received an average error of 1%. Nevertheless, the authors aim at further improving of this method.

In articles published by Kumhala et al., (2007, 2008, 2009), describes the principle of the sensor for throughput determination of plant material, developed at the Technical Faculty of Czech University of Life Sciences. The results obtained in laboratory studies using this sensor have been presented also.

One of the main objectives of this study was to ascertain whether there is a relationship between

throughput of plant material passing through a sensor and its output level.

For this purpose a capacitive throughput sensor has been developed. A testing installation consists of a conveyor belt, carrying a measured quantity of material into sensor, equipped with an electronic measurement device. Operating principle of the sensor is based on the fact that the dielectric constant of an air/material mixture between two parallel plates increases with increasing of volume concentration of the measured substance. Laboratory tests were conducted using various types of plant material, such as potatoes, sugar beets, chopped corn and etc. The studies have found that the way of loading the material in the sensor plays significant part. According Kumhala et al. (2009) it is possible to divide the loading method into two groups:

1. LF (Layer filling) - fills layers of fine plant material;

2. FSP (Filing by simple particles) partial filling (tuberous material, as sugar beet).

For each method of loading a graphical description of material throughput, and output signal was derived. For the LF regime it is a hyperbolic plot, and for the regime FSP - linear. Also it was found that the measurements are influenced by such parameters as the variation in material permittivity, volume density, material moisture content and particle shape. According to the authors, the results are evaluated with sufficient experience to start tests in real conditions.

Ehlert D. (2002) proposes to improve the principle of measuring the width of the gap between the feed rolls of a forage harvester. By way of taking into consideration the material behavior of selected typical forage crops (forage rye, pasture grass, spring barley, silo maize) he obtained better results.

The possibility of practical application of two mass flow sensors, installed on the clean grain elevator explores Chaplin et al., (2004) in his articles. First of them is impact plate mass flow sensor and the second one is torque-based sensor.

The analysis has showed that the first sensor has an error of up to 25% at small flow rate while the second sensor showed better results, and its

error is about 5%. According to the author's work an improvement of the sensors will be in the future.

Veal et al., (2004) describes a new technique for measuring mass flow. He offers a device that is installed on the harvesters in addition to the existing classical mass flow sensor in the clean grain elevator.

This device measures the voltage of the feed conveyor drive chain, because it's assumed that the voltage on this circuit is connected with the flow of plant material through the feeder housing. Based on the studies it is established that coupled with classic sensor, designed device shows good results, but needs further improvement and calibration.

Of the five sensors presented in the paper Savoie et al., (2002), the most successful was an instance, measuring crop impact force, which error was 0.7 kg/s within the range from 1 to 15 kg/s. A feed-roll displacement transducer has showed slightly worse results – 1.2 kg/s. Torque transducer also has showed good results, but had a better attitude to the dry mass-flow rate, than to the wet mass-flow rate. The frequency drop of the capacitance-controlled oscillator was well correlated with humidity, but has showed poor results in relation to the mass-flow rate.

Fuchs and Zangl (2007) suggest using a capacitive sensor to determine the mass flow in screw conveyor. The sensor consists of a ring of transmitter electrodes, which is divided into segments and a continuous receiver ring, mounted on a nonconducting pipe section. The electrodes of transmitter are provided with a signal in a few MHz, either the electric potential or the charge at the receiver electrode is evaluated to determine the inter-electrode capacitance between active transmitter segment and the receiver ring. Experiments have shown that the capacitance variations of the device are suitable to estimate the material fill level. Simulation results had showed that field-draining effects due to metal parts in the device have to be considered.

Zandonadi et al., (2010) developed and tested mass flow sensor for the beans, mounted on the grain bucket elevator. The range of mass flow during the experiments ranged from 0 to 3.4 kg/s and the maximum error was  $\pm 4.2\%$  with the flow

of 3.3 kg/s. The average mass error was 3.1%. The advantages of this device are its low cost, simplicity and ease of installation on the harvesting machine, but a significant percentage of error requires further improvement of the sensor.

During the literature review a large number of articles, devoted to the devices for determination of plant material moisture content, such as Lawrence et al (2001), Osman et al. (2002), Benning et al (2004), Casada and Armstrong (2009) have been found. The basis for these devices is usually a capacitive sensor. According to the authors, the capacitive technique, is one of the promising in use of throughput sensors development, in this article, these kind of devices will not be considered, cause this publication aims to review the mass flow techniques.

## Conclusions

From this review it becomes apparent the fact that have researched and developed a number of devices for mass flow determination, which are based on different techniques, but these techniques are not irreproachable and devices themselves have several disadvantages. The presence of errors in measurements, the influence of multiple environmental factors on the measurement results suggest that further research is needed in this area.

According to authors for the mass flow determination of various types of crops the best technical solution could be a device, built on the basis of a capacitive sensor, because this type of sensor is simple from the technical side and does not cost much. Also, according to the literature review, constructed on its base unit, shows good results, confirmed by laboratory and field tests.

## Acknowledgements

This project was funded by Ministry of Education, Youth and Sports of the Czech Republic, Research project number MSM 6046070905.

## References

- **Benning R., Birrell S., Geiger D., (2004).** Development of a multi-frequency dielectric sensing system for real-time forage moisture measurement. ASAE Paper No: 041100, an



- ASAE meeting presentation 16 p.
- **Chaplin J., Hemming N., Hetchler B.,** (2004). Comparison of impact plate and torque-based grain mass flow sensor. Transactions of the ASAE vol. 47(4), 1337-1345.
  - **Casada M.E., Armstrong P.R.,** (2009). Wheat Moisture Measurement with a Fringing Field Capacitive Sensor. Transactions of the ASABE Vol. 52(5): 1785-1791.
  - **DeHaan K.R., Vessey G.T., Holmstrom D.A., MacLeod J.A., Sanderson J.B., Carter M.R.,** (1999). Relating potato yield to the level of soil degradation using a bulk yield monitor and differential global positioning systems. Computers and Electronics in Agriculture, 23(2), 133–143.
  - **Ehlert D.,** (2002). Advanced throughput measurement in forage harvesters. Biosystems Engineering, 83 (1), 47–53.
  - **Fuchs A., Zangl H.,** (2007). Analysis of a capacitive mass flow sensor for a screw conveyor. Excerpt from the proceedings of the COMSOL Users Conference 2007 Grenoble
  - **Gogineni S., Thomasson J.A., Wooten J.R., White J.G., Thompson P.G., Shankle M.** (2002). Image-based sweetpotato yield and grade monitor. ASAE Paper No.021169, 16 p.
  - **Hostfee J.W., Molema G.J.** (2002). Machine vision based yield mapping of potatoes. ASAE Paper No. 021200, 10 p.
  - **Hostfee J.W., Molema G.J.** (2003). Volume estimation of potatoes partly covered with dirt tare. ASAE Paper No. 031001, 12 p.
  - **Kumhala F., Prosek V., Blahovec J.,** (2009). Capacitive throughput sensor for sugar beets and potatoes. Biosystems engineering 102 (2009) 36 – 43
  - **Kumhala F., Kviz Z., Kmoch J., Prosek V.,** (2007). Dynamic laboratory measurement with dielectric sensor for forage mass flow determination. Research in Agricultural Engineering 53 (4), 149–154.
  - **Kumhala F., Kroulik M., Kviz Z., Masek J., Prosek V.,** (2008). Sugar beets and potatoes throughput measurement by capacitive sensor. In: Proceedings of Conference Agricultural Engineering 2008. Stuttgart-Hohenheim, VDI Verlag GmbH, Germany, pp. 199–204.
  - **Kumhala F., Prosek V., Blahovec J.,** (2009). Capacitive throughput sensor for sugar beets and potatoes. Biosystems Engineering 102, 36–43.
  - **Lawrence K.C., Funk D.B., Windham W.R.,** (2001). Dielectric Moisture Sensor for Cereal Grains and Soybeans. Transactions of the ASAE Vol. 44(6): 1691-1696.
  - **Osman A.M., Savoie P., Grenier D., Thériault R.,** (2002). Parallel-Plate Capacitance Moisture Sensor for Hay and Forage. ASAE Paper No: 021055, an ASAE meeting presentation 12 p.
  - **Savoie P., Lemire P., Theriault R.,** (2002). Evaluation of five sensors to estimate mass-flow rate and moisture of grass in a forage harvester. ASAE vol.18(4), 389-397
  - **Stafford J.V., Ambler B., Lark R.M., Catt J.** (1996). Mapping and interpreting the yield variation in cereal crops. Computers and Electronics in Agriculture, 14(2-3), 101-119.
  - **Veal M.W., Shearer S.A., Fulton J.P.,** (2004). Improved mass flow sensing for yield monitoring in grain combines. ASAE, Paper No 041101
  - **Zandonadi R.S., Stombaugh T.S., Shearer S.A., Queiroz D.M., Sama M.P.,** (2010). Laboratory performance of a mass flow sensor for dry edible bean harvesters. ASABE, vol.26 (1), 11-20

## QUANTITATIVE AND QUALITATIVE SIMULATION OF GROUNDWATER BY MATHEMATICAL MODELS IN AN ARID REGION USING MODFLOW & MT3DMS

RAHNAMA MOHAMMAD BAGHER<sup>1\*</sup> & ZAMZAM ABBAS<sup>2</sup>

<sup>1</sup>Assistant Professor, 22 Bahman Blv., Shahid Bahonar University, Water Engineering Department, Kerman, Iran, e-mail: [mbr@mail.uk.ac.ir](mailto:mbr@mail.uk.ac.ir), phone: +989131404423

<sup>2</sup>Graduate Student, Shahid Bahonar University, Kerman, Iran

### Abstract:

Agriculture sector by using 80 percent of fresh water is the greatest water consumer in Iran. Excessive use of agricultural fertilizers in last decade, caused accumulation of enormous amounts of salts and subsequence declined the physical properties of soil. In desert and dry regions such as Rafsanjan plain, use of the groundwater resources is more than the surface water resources. Therefore, information about the quality of these resources remains a necessary task for optimum management, protection of water resources and stopping the future damages. In this study the groundwater quantity and quality of Rafsanjan plain was investigated by MODFLOW and MT3DMS. The presented qualitative model for this aquifer was compared by observed data and calibrated. Then sensitivity analysis was preformed and this model was used to predict the next 2 and 5 years. Results show that water level decrease in coming years dramatically and most quantity parameters will increases in plain, too. Electrical conductivity will increase more than other parameters. Therefore, discharge should be decrease and recharge increase in this plain.

**Keywords:** Groundwater, Rafsanjan plain, Qualitative and quantitative models, MODFLOW and MT3DMS

### Introduction

Water has an important role in comprehensive development of rural and urban areas. Life is not possible without water and agricultural and industrial activities will stop. Groundwater resources are the largest freshwater storages. In areas where surface water resources are limited and are not easily accessible, to supply water for agricultural and industrial activities, groundwater resources distributed widely everywhere can be exploited. Iran is almost a dry country and has 250 mm average annual rainfall that is about one third of the average annual rainfalls of the world. Groundwater in Iran with a dry climate is important. Rapid population growth in last years, urban and Agricultural developments, limited surface water resources and extra exploitation of groundwater resources, have caused irreparable damages to groundwater resources, and will continue to do so in oncoming years.

Therefore, appropriate management and careful studies of groundwater in these areas are necessary. In this context, in recent decades the use of computer based models for modeling of

groundwater as an effective and rapid method for studying the evaluation of the water balance, water movement and utilization management of groundwater resources has attracted great attention.

Simulation of groundwater flow by mathematical models is an indirect method of study that is very cheaper than direct methods like sand tank models and this method can eliminate practical problems in direct methods. The goal of mathematical model is simulation of real conditions of aquifer by using a series of mathematical equations. If a mathematical model is carefully used, it can predict the future status of water resources and also clarify the effect of conditions imposed on an aquifer, and can be used to apply proper management. One of this models that has many capabilities in the study of groundwater is McDonald and Harbaugh model, it is known as PMWIN which was presented in 1998 and widely was used by many researchers in the world.

### Study site

Rafsanjan study area is a sub basin of Kerman

plain that located in southeast of Iran (Fig.1). This plain include 3 sub basin; Rafsanjan, Nogh and Anar plains. This region has warm summers and cold and dry winters. Rafsanjan aquifer is used for domestic, agricultural and industrial purposes. The water table is high, annual precipitation ranges between 60 mm in

the lowland to about 120 mm in the upland. Recharge to the aquifer is largely due to the infiltration of precipitation and irrigation. Evaporation is highest during June- to-August period and annual average is 3m. Table one show general characteristics of Rafsanjan plain.

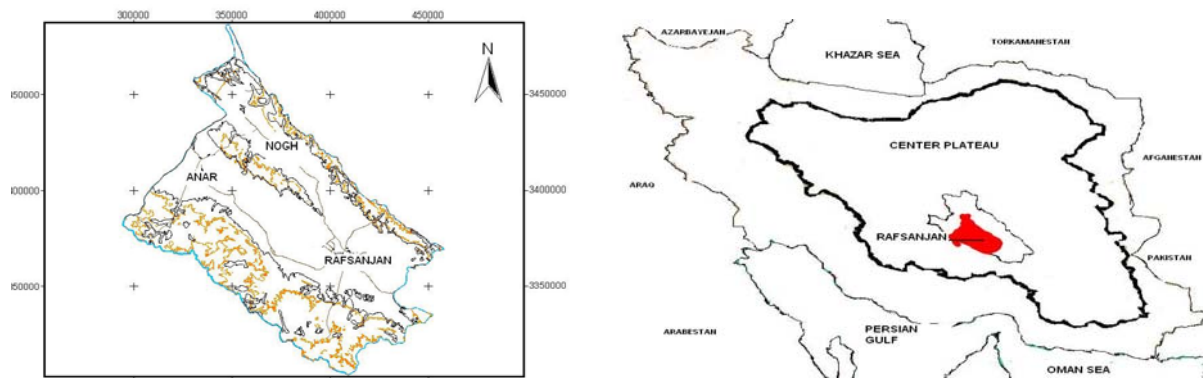


Figure 1 - Location of Rafsanjan Plain

Table1- General Characteristics of Rafsanjan plain

Area	12421km <sup>2</sup>
Annual precipitation	90mm
Evaporation	3m
Longitude	54'52 to 56'34
Latitude	29'51 to 31'31
Height	1400-3434m

### Model of groundwater flow and transport solution

Among the programs simulated the movement of groundwater; PMWIN and MT3D were used. Most groundwater numerical models based on solving two partial differential equations, which are include groundwater motion three-dimensional equation and the equation of transport solution. Movement equation of three-dimensional groundwater (constant density) in porous medium is expressed as follows (Schwartz and Zhang, 2003):

$$\frac{\partial}{\partial x} \left( K_{xx} \frac{\partial h}{\partial x} \right) + \frac{\partial}{\partial y} \left( K_{yy} \frac{\partial h}{\partial y} \right) + \frac{\partial}{\partial z} \left( K_{zz} \frac{\partial h}{\partial z} \right) - W = S_s \frac{\partial h}{\partial t} \quad (1)$$

Where  $K_{xx}$ ,  $K_{yy}$  and  $K_{zz}$  are values of hydraulic conductivity along x, y and z coordinate axes, h is the hydraulic head, W is a flux term that account for pumping, recharge, or other sources and sinks;  $S_s$  is the specific storage and t is time.

The partial differential equation that governs the three-dimensional transport of a single chemical constituent in groundwater, considering advection, dispersion, fluid sinks/sources, equilibrium-controlled, and first-order irreversible rate reaction is described in the following (Zheng and Bennett, 1995):

$$R \frac{\partial(\theta C)}{\partial t} = \frac{\partial}{\partial x_i} \left( D_{ij} \frac{\partial C}{\partial x_j} \right) - \frac{\partial}{\partial x_i} (v_i C) + \frac{q_s}{\theta} C_s - \lambda \left( C + \frac{\rho_b}{\theta} \bar{C} \right) \quad (2)$$

Where C is the dissolved concentration;  $\bar{C}$  is the adsorbed concentration; t is time;  $D_{ij}$  is the hydrodynamic dispersion coefficient tensor;  $V_i$  is the pore water velocity;  $q_s$  is the volumetric flow rate per unit volume of aquifer and represents fluid source or sinks;  $C_s$  is the concentration of fluid source or sinks flux;  $\lambda$  is the reaction rate constant; R is the retardation factor;  $\rho_b$  is the bulk density of the porous

medium; and  $\theta$  is the porosity.

## Methods

In this study, at first quantitative model for groundwater flow prepared by MODFLOW, and then model was calibrated and verification was performed. In next stage, this model was used for prediction of water level in coming years. Then the qualitative model was used to prepare

qualitative model. In this research, qualitative model was prepared by MT3DMS. Various qualitative parameters such as calcium (Ca), magnesium (Mg), chloride (Cl) and other ions and electrical conductivity were evaluated and modeled. Data that were used for supplying quantitative and qualitative models are presented in table 2.

Table2- Data that used for supply models

Model	Used data	Number of wells	Boundary conditions	Initial conditions
quantitative	Level water	72 monitoring wells	Topography, geology and level water maps	October 2001
qualitative	Value of Cl, Mg, Ca, EC, ...	65 agriculture wells	Quantitative boundary conditions and iso chlorine map	November 2001

## Results and discussion

### Quantitative model

#### Calibration

For Calibration of the model, difference between the measured and calculated values should be minimized. In this study, water levels from October 1999 to October 2006 were used for model calibration. Figure 2 shows a comparison between measured and calculated values in the well No. 16. As shown in this figure, calculated values fit the measured values very well.

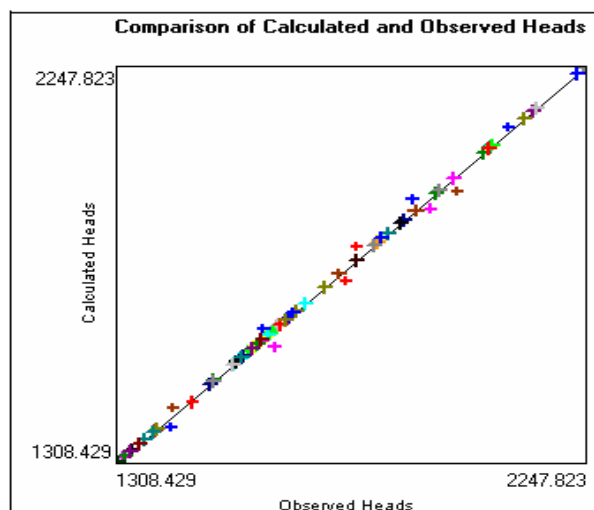


Figure 2- Comparison between calculated and measured values for model calibration in well No. 16

### Verification

To ensure the accuracy of the model, it should be able to calculate the values of verification period with a good agreement with measured values of this period.

To ensure the accuracy of the prepared model, we used a 6 months period (Sep 2006 to April 2007) by assuming that the trend of the system is like the previous years. To evaluate the precision of the model, errors of the model for calculated and measured values are determined. Figure 3 shows the calculated and measured values of water levels.

As shown in these figures calculated and measured values of water levels in the verification period are in good agreement. Therefore, this model can be used for prediction of water levels in oncoming years.

### Prediction

The calibrated and verified model was used to predict the future conditions of aquifer. The system behavior for 1 and 5 years periods was predicted. (Figure 4)

In table 3 water level values in 3 different monitoring wells in various times are presented.

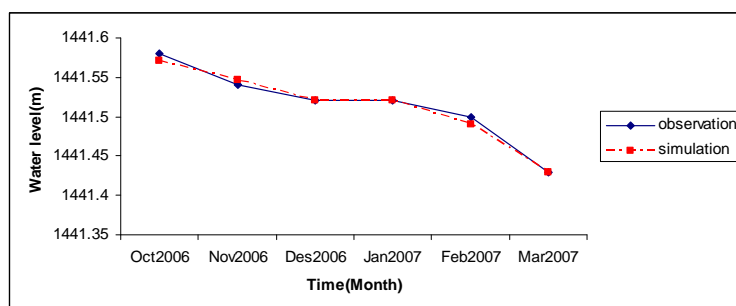


Figure 3- Comparison calculation and observation hydrographs at the end of verification period for well No.23

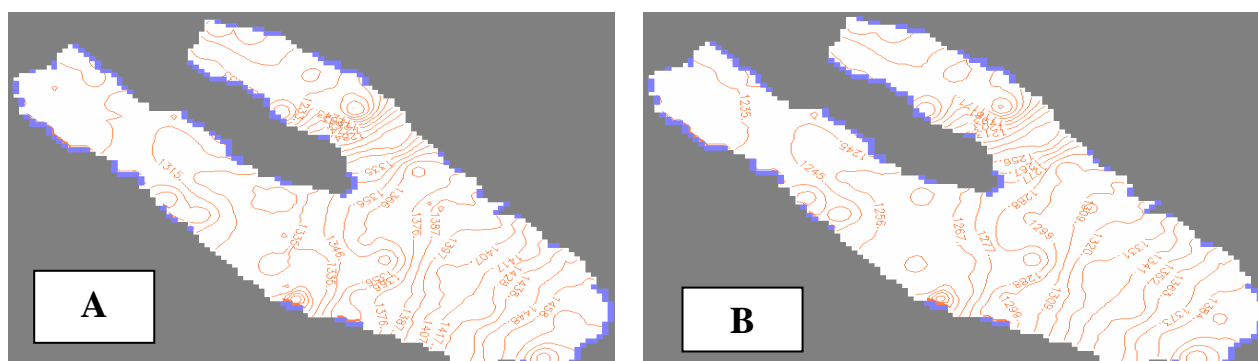


Figure 4- Prediction of water level in Rafsanjan plain: A-For 1 year,B-For 5 years

Table 3- water level for 3 monitoring wells in various times

Time	Water level in well No. 7(m)	Water level in well No. 33(m)	Water level in well No.49(m)
Pervious 5 years	1499	1294	1385
Pervious 1 year	1491	1290	1379
Now	1490	1288	1378
next 1 year	1489	1286	1377
next 5 years	1483	1282	1371

Table above shows that water level will decrease in Rafsanjan plain for future years. Also, for the next 1 year the decrease in water level is lower than 5 next years. Results show that average water level decrease in each monitoring well is about 15m during 10 years.

### Qualitative model

The prepared quantitative model data was used for preparing the qualitative model. In this research several quality parameters existing in groundwater were modeled for Rafsanjan plain. But only calculated values for chloride are represented completely and final values of other

parameters are shown in table 5 at the end of the results section.

### Calibration

In the qualitative Aquifer modeling, only those parameters that are effective on the dispersion process should be calibrated. These parameters are: absorption coefficient (AC), horizontal dispersion ratio to dispersion length (HDRL), vertical dispersion ratio to length of dispersion (VDRL) and length of dispersion (LD). Table 4 shows the calibrated parameters in this model.

Table 4- values of calibrated parameters in qualitative model

parameter	HDRL	VDRL	AC	LD
value	0.1	0.1	0.0001	35

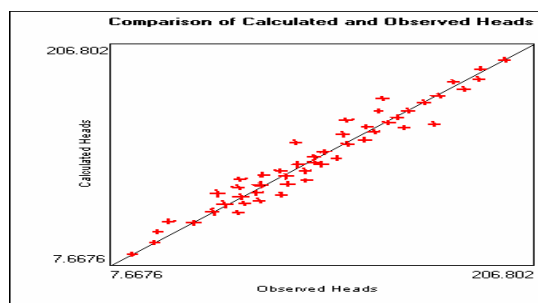


Figure 5- comparison of measured and calculated values for chloride concentration in calibration step

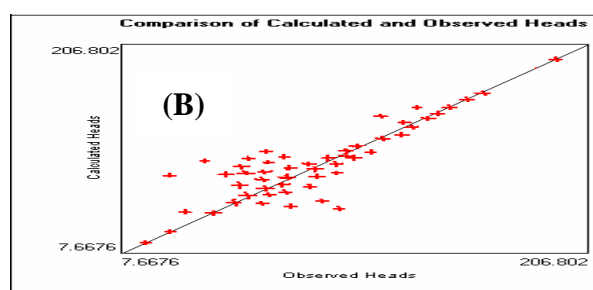
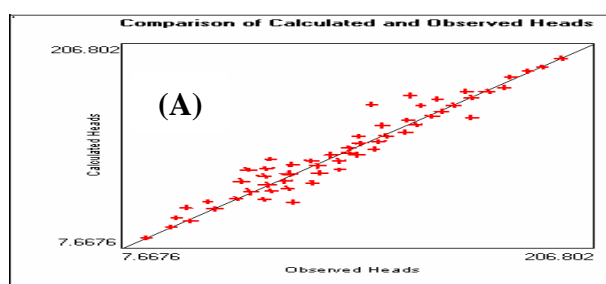


Figure 6 - comparison of measured and calculated chloride concentration in verification step: A- for next 2 years B- for next 5 years

In figure 5 a comparison between measured and calculated values for chloride is represented. This curve shows that this model is well calibrated.

### Verification

For verification and determination of the accuracy of the model, it was run for different periods. In this research verification of model was performed for 6 months periods and calculated data was compared with the observed data. According to the model results, as longer the verification time is, the prediction error is greater. This trend is seen clearly for periods of 2 and 5 years in Figure 6. This suggests not using of this model for predictions for more than five years.

### Prediction

In this section, the model was used to predict chloride concentration for next 2 and 5 year periods. But this increase is seen around the city of Rafsanjan (agricultural well No.60) and Nogh

(agricultural well No.10) less than Anar (agricultural well No.33). In evaluation of the other parameters it was observed that all the parameters increase in this plain too. This increase is observed more in agricultural well No.33. pH parameter does not change in next 5 years. Amounts of Cl and Na were high in the previous years and these amounts will increase to a dangerous level in the next years. EC has reached to a dangerous level in most parts of the plain so groundwater resources will become inappropriate for agricultural uses in the future years. Some of the parameters such as: Ca, SO<sub>4</sub> and Mg are almost in a good range.

### Conclusion

This study showed that PMWIN is a suitable option for simulation of water quality and quantity of groundwater for the unconfined layers especially Rafsanjan aquifer. The results showed that the prepared model with sufficient accuracy is able to simulate the real conditions in this aquifer. The results showed that the water level in all parts of the plain is decreasing now.



The results also showed that if the recharge and discharging is like previous years, increasing of water level in most of the wells will continue in the future.

In evaluation of quality parameters existing in groundwater it was observed that some parameters such as Cl, EC and Na have a trend to increase during pervious and next years. Amounts of these parameters in groundwater are dangerous for agricultural and drinking consumptions. The results showed that PH of groundwater is almost constant and suitable for groundwater resources in this plain. Other

parameters such as Ca, Mg and SO<sub>4</sub> are normal and are not minatory for groundwater resources.

For increasing of water level, decreasing of EC and ions and for protecting groundwater resources, we suggest that exploitation of water from these resources should be reduced and discharge from some of agricultural wells stop, also we suggested that recharge to groundwater resources should be increased and agricultural activities should be limited.

Table 5 showed that the amount of chloride in groundwater increases in whole of the plain.

Table 5- Previous and future values for all quality parameters existing in groundwater for Rafsanjan plain

parameter	Well number	No.10	No.33	No.60
Ca(maq/lit)	Previous 5 years	7.3	39.7	6.1
	Previous 1 years	9.3	40.2	6.2
	Now	12.1	40.3	6.3
	Next2 years	13.6	40.3	6.3
	next 5 years	16.3	41.2	6.4
Mg(maq/lit)	Previous 5 years	24.4	52	7.4
	Previous 1 years	28.3	58	8.6
	Now	29	60.4	9
	Next2 years	30.6	63.2	9.2
	next 5 years	34.2	67.5	9.6
Na(maq/lit)	Previous 5 years	40	73	24.3
	Previous 1 years	46.5	105	24.4
	Now	47	120	26
	Next2 years	49	134.9	26.3
	next 5 years	63	166	27.1
pH	Previous 5 years	6.9	6.9	7.3
	Previous 1 years	7	7.1	7.4
	Now	7.1	7.1	7.4
	Next2 years	7.1	7.1	7.4
	next 5 years	7.2	7.3	7.3
EC(mic.mho)*10 <sup>6</sup>	Previous 5 years	10053	12150	3805
	Previous 1 years	10149	13137	3824
	Now	10202	13639	3835
	Next2 years	10253	14346	3846
	next 5 years	10430	15400	3870
SO <sub>4</sub> (maq/lit)	Previous 5 years	10.6	24.3	7.6
	Previous 1 years	12.1	30.7	11.1
	Now	12.8	32.4	11.4
	Next2 years	13.9	32.5	11.9
	next 5 years	15.4	35	12.9
Cl(maq/lit)	Previous 5 years	84	147	39
	Previous 1 years	88	147	42.4
	Now	89	147	44
	Next2 years	92	159	46
	next 5 years	97	196	53

## References

- 1- Schwartz, F., Zhang, H.: Fundamentals of groundwater, John Wiley and sons, 2003.
- 2- Xu, M., Eckstein, Y.: Use of weighted least-squares method in evaluation of the relationship between dispersivity and field scale. Groundwater 33(6), 1995, 905-908.
- 3- Zheng, C., Bennett, and G.D.: Applied contaminant transport modeling, Theory and Practice. Van Nostrand Reinhold, New York, 1995, 440p.

## ELECTRO HYDRAULIC CONTROL OF AN AGRICULTURAL TRACTOR STEERING SYSTEM ALONG WITH THE SIDE SHIFT CONTROL OF THE ATTACHED ROW CROP CULTIVATOR

JAVAD ROBATI<sup>1\*</sup>, MEHDI REZAEI<sup>2</sup>, HOSSEIN NAVID<sup>3</sup>

<sup>1</sup> Ph.D. student, Agricultural Machinery Department, Tabriz University, Tabriz, I.R. Iran & Maragheh University, Maragheh, I.R. Iran, Phone: +98-411-332-0458,

Fax: +98-21-228-00109, E-mail: [javad\\_rebati2000@yahoo.com](mailto:javad_rebati2000@yahoo.com)

<sup>2</sup> Mahdi Rezaei, Mechanical Engineering Department, Sahand University of technology, Tabriz, I.R. Iran, E-mail: [m.rezaei@sut.ac.ir](mailto:m.rezaei@sut.ac.ir)

<sup>3</sup> Hossein Navid, Assistant Professor, Agricultural Machinery Department, Tabriz University, Tabriz, I.R. Iran, E-mail: [navid@tabrizu.ac.ir](mailto:navid@tabrizu.ac.ir)

### Abstract

Mechanical control of weed is still utilized by a significant number of farmers. Accurate guidance of the tractor and cultivator is one of the precision farming challenges in mechanical weed controlling. This paper presents the control of an agricultural tractor steering system and the side motions of the attached row crop cultivator using electro-hydraulic actuators. The bicycle model was adopted to simulate the dynamic behaviour of the tractor with an implement hitched to it. It is assumed that steering angle sensor, IMU and DGPS technologies are used for measurement of the steering angle, yaw rate and the lateral position of the tractor, respectively. The lateral position data are disturbed with the DGPS and FOG noises and used to both the position control of the tractor and the side shift control of the cultivator. The cultivator control system can move its sub frame laterally and guide the blades near the crop rows without any crop damages. The kinematics model was used for the implement and the position was calculated through the geometric relations between the tractor and the implement. Calculation of the applying forces on the steering system of the tractor and cultivator side-shift mechanism showed that these forces are in the same range. Therefore, the MOOG servo valve series 72 and the Shore-Western servo cylinder series 910 were adopted as the hydraulic actuator for both systems. The simulations were carried out separately for each system using MATLAB. Then, these two systems were combined and the performance of the whole mechanism was evaluated through the simulation results.

**Key words:** servo valve, servo cylinder, cascade controller, yaw rate, row crop cultivator

### Introduction

Tractor operating is known as a difficult, tiresome and in some conditions hazardous task and precision control of a tractor requires the unremitting attention of the operator. Tractor driver dedicates 80 % of its time to driving mission and less time remain to check the quality of the field operations [6,8].

Several attempts have been done to automate the tractor guidance task for covering the following objectives [8]:

- Reducing the difficulty of tractor guidance task
- Allow the operator to dedicate more time to check the quality of the field operations
- Reducing operation costs and increasing positioning accuracy all over the field

Farm tractors are utilized along with different implements on the various soil conditions. These factors affect the path tracking performance of a tractor. Because of the probable crop damages or uneven performance of the tractor, design and utilization of a reliable positioning controller with a suitable dynamic response, is inevitable in agricultural applications [9].

Before developments of GPS positioning systems, control of the agricultural tractors was done using computer vision techniques [11].

Using multiple sensors of GPS and machine vision improved the positioning accuracy [12].

Sub centimetre accuracy in vehicle position and 0.1 degree accuracy in attitude determination

will be obtainable by using carrier phase DGPS measurements [13,14].

Kinematics model is usually adopted for low speed vehicles where the effects of the lateral forces can be neglected [17].

Majority of researches have been done on non holonomic systems (with no side slip) but these assumptions are not adaptable for tractor-implement systems [10].

O'Conner proposed a bicycle model in which the hitch forces are modelled as an extra wheel behind the rear axle. Tractor models and controllers with sub inch tractor position accuracy using Carrier-phase DGPS has been developed at Stanford [2]. This work has been done by using bicycle model and completed by adding implement forces. In this model lateral forces are functions of the tires slip angles. In the linearized model, lateral forces are proportional to the slip angles by the coefficients  $C_{af}$ ,  $C_{ar}$  and  $C_{ah}$  [1,9]

Some researchers have used system identification method for controller design by developing relationship between steering angle and yaw rate through tractor dynamics [15,16].

Since the implement lateral forces have significant effects in yaw rate dynamics, "3-wheeled" bicycle model is known the best model to predict yaw dynamics of a tractor with an implement. It was indicated that this model is valid for implements attached to the three-point hitch of a tractor [19].

PID controller has been used for tractor guidance for grain harvesting and calculation of the actuator command signal was carried out by PID controller [18].

This research has been built upon previous work in design of a control system for centimetre

precision guidance of a row crop cultivator [20]. In this study an agricultural tractor with an attached row crop cultivator modelled through "3-wheeled" bicycle model and cascade controllers designed to control the steering angle, yaw rate, heading angle and lateral position of the tractor as well as the lateral position of the cultivator. For this purpose the constant forward speed of  $2 \text{ ms}^{-1}$  was assumed for the tractor. Subsequently the side shift mechanism was assumed to move the attached implement laterally and an electro hydraulic controller was designed and simulated to set the cultivator blades in the middle of the rows independent of the tractor side motions.

### Experimental arrangement

John Deere 3140 tractor was selected in this study because that is the common medium power range tractor with hydrostatic steering mechanism that is utilized in Iran. Modelling and simulations were carried out by assuming the constant speed of  $2 \text{ ms}^{-1}$ . The "3-wheeled" bicycle model that has presented better results for the combination of the tractor and hitch forces was used to modelling the yaw dynamics. In the bicycle model of a four wheeled vehicle the outer and inner tires are unified. This model neglects the weight transfer.

Fig. 1. shows the schematic of bicycle model with attachment lateral forces.

Some of the tractor parameters that are useful in modelling of the tractor steering and designing of the control system were measured and some of them were obtained from the manufacturer catalogue. These parameters have been presented at table 1.

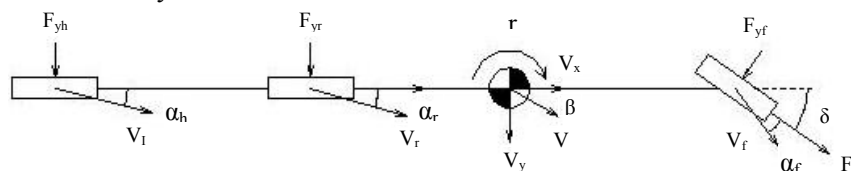


**Fig. 1.** Schematic of bicycle model with attachment lateral forces

**Table 1.** Parameters used for the analytical model

Tires			Tractor	
Parameter	Front	Rear	Parameter	Value
Tire	7.5-18, 6 ply	18.4-34, 8 ply	$a$	1.60 m
Air Pressure	28 psi	20 psi	$b$	1.00 m
Tire Radius	0.384 m	0.754 m	$L$	2.60 m
$C_a$	1800 N/deg	3500 N/deg	$m$	3991 kg

Previous Research has indicated that  $C_{ah}$  can range between 0 N/deg and 4000 N/deg [21]. In this study  $C_{ah}$  is assumed to be 3000 N/deg. Maximum steering angle was measured 40 degrees. The vehicle's yaw inertia can be calculated using the following approximation [7]:

$$I_{zz} \approx m \times a \times b \quad (1)$$

According to the values of the parameters at table 1, the yaw inertia estimated 6700 kg.m<sup>2</sup>.

The steering torque was calculated by [22]:

$$T = W \cdot \mu \cdot \sqrt{\frac{B^2}{8} + e^2} \quad (2)$$

Where, B is the tire section width and e indicates the king pin offset of the steering wheels. King pin offset is 5.7 cm and front tire width is 19.05 cm for the front tires of the selected tractor. For  $\frac{e}{B} = 0.3$ , friction coefficient ( $\mu$ ) will be 0.4 using the following diagrams [22].

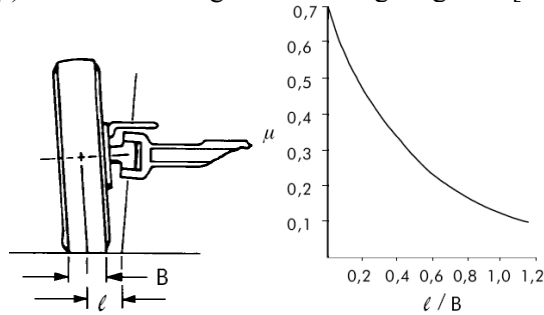


**Fig.2.** Schematic of front wheel configuration (left) and diagram of  $\mu$  via  $\frac{e}{B}$  (right)

By assuming the front wheels weight of 1535 kg, the steering torque was calculated 532 N.m using equation (2) and the steering force was calculated 3925 N. By applying the overload factor of about 2 the lateral force will be around 7850 N.

Calculation of the applying forces on the steering system of the tractor and cultivator side-shift mechanism showed that these forces are in

the same range. Therefore, the MOOG servo valve series 72 and the Shore-Western servo cylinder series 910 were adopted as the hydraulic actuators for both systems. This type of servo cylinder is equipped with LVTD sensor originally [3,4,5].

To make the controller design less complicated, a set of cascade controllers were used for tractor lateral position control. Four feedback loops were assumed using the measurements from GPS receiver ( $y$ ), IMU with fiber optic gyroscope (FOG) ( $r$ ), GPS receiver ( $\psi$ ) and LVTD ( $\delta$ ). It should be mentioned that LVTD measures the displacement of the hydraulic cylinder rod and by assuming the rigid connection between the cylinder rod and the steering linkage of the front wheels; this measurement is attributed to the steering angle of the front wheels. The block diagram of these controllers is given in Fig. 3.

The second order linear bicycle yaw model which was used in this study, is [8,9 ]:

$$G_{Pr} = \frac{R(s)}{\delta(s)} = \frac{n_1 \cdot s + n_0}{d_2 \cdot s^2 + d_1 \cdot s + d_0} \quad (3)$$

$$d_0 = \frac{C_2 C_3 - C_1^2}{m V_x^2} + C_1$$

$$d_1 = \frac{C_2 I_{zz}}{m V_x} + \frac{C_3}{V_x}$$

$$n_0 = \frac{C_1 C_{af} - a C_{af} C_2}{m V_x}$$

$$n_1 = a C_{af}$$

$$C_1 = ((a+b) \cdot C_{ah} + b \cdot C_{ar} - a \cdot C_{af})$$

$$C_2 = (C_{af} + C_{ar} + C_{ah})$$

$$C_3 = ((b+c)^2 \cdot C_{ah} + b^2 C_{ar} + a^2 C_{af})$$

The second order lateral position model which is linear bicycle model has been shown by [9]:

$$G_{Py} = \frac{Y(s)}{R(s)} = \frac{V}{s^2} \quad (4)$$

The steering plant consists of second order and third order transfer functions for the servo valve and servo cylinder, respectively [20]. Fig. 4. shows the block diagram of the steering plant with the designed steering controller.

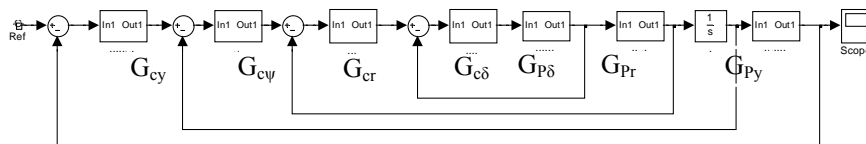


**Fig. 3.** Cascade control block diagram

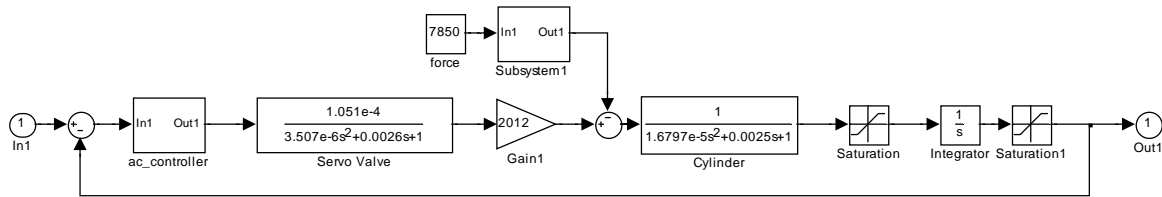


Fig. 4.  $G_{p\delta}$  block diagram

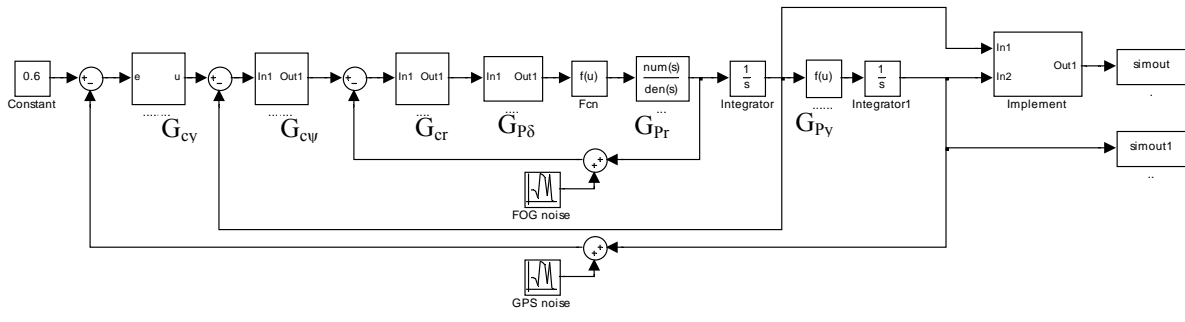


Fig. 5. Tractor and implement control block diagram

After controlling the lateral position of the tractor, the Implement model which had been designed previously, was added to this model [20]. For this purpose the kinematics relationships between the tractor and implement was utilized. Tuning the parameters of the controllers was performed by running the simulation program without applying any noises. Then the noises of GPS and FOG sensors that had been measured by previous researchers [16], were added to the simulated model and by modifying the parameters of the controllers using the response optimization toolbox and control laws, the appropriate results were achieved.

## Results and discussion

In this study four cascade controllers were designed and simulated which consists of P, PI, PID and PI controllers for  $G_{cy}$ ,  $G_{c\psi}$ ,  $G_{cr}$  and  $G_{p\delta}$ , respectively. Other PI and PID controllers also were designed as the Implement side shift controller and hydraulic actuator internal controller, respectively. During the evaluation, step commands of 0.2, 0.4, 0.6, 0.8 and 1 m were

applied to the system that indicates the magnitude of the deviation from the desired path, and the system responses (tractor and implement paths) were evaluated. At first, the noise of GPS and FOG sensors was neglected and system was run. Fig 6 shows the results of simulation by applying 0.2 m step command. According to the Fig 6, tractor reaches around the desired path after less than 10 seconds. It should be mentioned that in this situation maximum overshoot of about 2 centimetres would be dispensable. Because of the high forward speed of the tractor and limitation in maximum values of  $\delta$  and  $\delta'$ , tractor controller response is slower than that of the implement. It is also clear from this figure that the measurements noises didn't have any significant effects on the system performance. Fig 7. shows the system response to the 0.4, 0.6, 0.8 and 1 m step commands. Although the system has optimal response for the 0.4 m step, but because of the dispensable deviations for the other commands, this controller can be utilized for this range of step commands without any modifications.



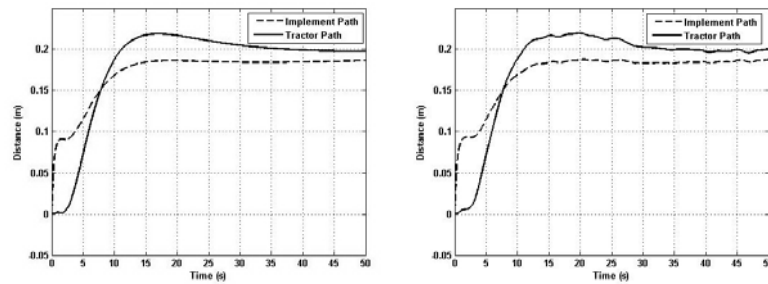


**Fig.6.** Tractor and Implement path by applying 0.2 step command without applying any noise (left) and in presence of sensors noise (right)

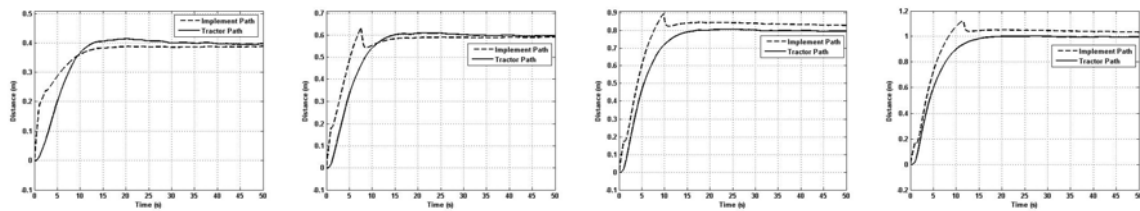


**Fig.7.** Tractor and Implement path by applying 0.4, 0.6, 0.8 and 1 m step commands in presence of sensors noise

## Conclusion

In this study, system displayed proper responses to the wide range of step commands without any needs to design complicated control system such as adaptive controllers. Also by assuming that the crop row distance is about 50 cm, system would be operated around its optimal response area. In future research, system behaviour can be optimized by applying Kalman filter in presence of process noises. Furthermore,

other controlling mechanisms such as optimal or adaptive controllers can be adopted with this model. Since row crop cultivator blades operate within a given row distance, the exact position of the tractor and attached implement blades related to the crop rows should be imputed as a feedback signal to the controllers. Then the controllers should guide the tractor and its implement to their nearest proper positions with minimum crop damages and steering attempts.

**Table 2.** Nomenclature of variables used in paper

Variable	Definition	Variable	Definition
$V$	Tractor Velocity	$r$	Heading Angle Rate or Yaw Rate
$V_x$	Tractor Longitudinal Velocity	$y$	Lateral Position
$V_y$	Tractor Lateral Velocity	$n_i, d_i, c_i$	Yaw Rate Model Coefficients
$F_f$	Lateral Force at Front Axle	$G_{p\delta}$	Steering Actuator Plant
$F_r$	Lateral Force at Rear Axle	$G_{pr}$	Yaw Rate Plant
$F_h$	Lateral Force at Hitch	$G_{py}$	Lateral Position Plant
$C_{af}$	Cornering stiffness of Front Axle	$G_{cv}$	Heading Angle Controller
$C_{ar}$	Cornering stiffness of Rear Axle	$G_{c\delta}$	Steering Actuator Controller
$C_{ah}$	Cornering stiffness of the Hitch	$G_{cr}$	Yaw Rate Controller
$a$	Distance From CG to Front Axle	$G_{cy}$	Lateral Position Controller
$b$	Distance From CG to Rear Axle	$\omega_n$	Steering Actuator natural Frequency
$c$	Distance From Rear Axle to Hitch	$\xi$	Steering Actuator Damping Ratio
$L$	Tractor Wheel Base	$\beta$	Slip Angle at CG
$m$	Tractor Mass	$\alpha_f$	Slip Angle at Front Axle
$I_{zz}$	Mass Moment of Inertia About the CG	$\alpha_r$	Slip Angle at Rear Axle
$\delta$	Tractor Steering Angle	$\alpha_h$	Slip Angle at Hitch
$\dot{\delta}$	Tractor Steering Angle Rate	$B$	Tire Section Width
$\psi$	Heading Angle	$\mu$	Friction Coefficient Between Tire and soil

## References

- [1] Gillespie, T. D.: Fundamentals of vehicle dynamics. Society of Automotive Engineers, Warrendale, PA, 1992.
- [2] O'Conner, M.: Carrier-phase GPS for automatic control of land vehicles . Ph.D. dissertation, Department of aeronautics and astronautics, Stanford University, 1997.
- [3] Thayer, W. J.: Transfer functions for MOOG servo valves. 1958.
- [4] <http://www.moog.com/Industrial>.
- [5] <http://www.shorewestern.com>
- [6] Cariou, C.-Cordesses, L.-Thouilot, B.: CP-DGPS farm tractor control along curved path. In proceedings of the 3rd European Conference on Precision Agriculture, ECPA'01, Montpellier, France, pp. 1-6, June 2001.
- [7] Garrott, W. R.-Monk, M. W.-Chrstos, J. P.: Vehicle inertial parameters-Measured values and approximations. SAE passenger car meeting and exposition, Detroit, MI, SAE paper No. 881767, 1988.
- [8] Bevly, D. M.-Gerdas, C. Parkinson, B. W.: A new dynamic model for improved high speed control of a farm tractor. Journal of dynamic systems, measurement and control. Vol. 124, 2002.
- [9] Derrick, B.-Bevly, D.-Rekow, A.: Model-reference adaptive steering control of a farm tractor with varying hitch forced. In American Control Conference, p. 3677-3682, 2008.
- [10] Murry, R. M.-Li, Z.-Sastry, S.: A mathematical introduction to robotic manipulation. CRC Press, Boca Raton, 1994.
- [11] Reid, J. F.-Searcy, S.: Vision- based guidance of an agricultural tractor. IEEE control system journal, Vol. 7, pp. 39-43, 1987
- [12] Zhang, Q.-Reid, J.-Noguchi, N.: Agricultural vehicle navigation using multiple guidance sensors. Proceedings of the international conference on field and service robotics, 1999.
- [13] Cohen, C. P.-Parkinson, B. W.McNully, B. D.: Flight tests of attitude determination using GPS compared against an inertia navigation unit. Navigation, Vol. 41, No. 1, pp. 159-174, 1994
- [14] Cohen, C. P.: autolandig a 737 using GPS integrity beacons. Navigation, Vol. 41, No. 3, pp. 83-97, 1995
- [15] Stombaugh, T. S.-Benson, E. R.-Hummel, J. W.: Automatic guidance of agricultural vehicles at high field speeds. In proceedings of ASAE annual meeting, Orlando, FL. Paper No. 983110, 1998.
- [16] Bevly, D. M.: High speed , dead reckoning and towed implement control for automatically steered farm tractors using GPS. Ph.D. dissertation, Stanford University. 2001.
- [17] Cordesses, L.-Cariou, C.-Martinet, P.-Thibaud, C.: CP-DGPS based combine harvester control without orientation sensor. In proceedings of the 12<sup>th</sup> international technical meeting of the satellite division of the institute of navigation, ION GPS99, Nashville, Tennessee, USA, pp. 2041-2046. 1999.
- [18] Benson, E. R.-Reid, J. F.-Zhang, Q.: Machine vision-based guidance system for an agricultural small-grain harvester. Transactions of the ASAE. Vol. 46(4): 1255–1264, 2003.
- [19] Pearson, P. J.: Modelling and validation of hitch loading effects on tractor yaw dynamics. M.Sc. dissertation, Auburn University, 2007.
- [20] Robati, J.-Navid, H.-Hassanzadeh, I.-Rezaei, M: Electro-hydraulic control system for centimeter precision guidance of a row crop cultivator. In proceedings of the international conferecnce on energy efficiency and agricultural engineering. Rousse, Bulgaria, pp. 739-748, 2009.
- [21] Pearson, P.-Bevly, D.: Comparison of analytical and empirical models to capture variations in off road vehicle dynamics. In Proceedings of the IMECE Conference, Orlando, FL, 2005
- [22] <http://www.hydrocap.net/pdf/ms/hsu.pdf>

## TRANSPORT ENERGY USED IN THE SUBURBAN SPACE

MIROSLAV RŮŽIČKA<sup>1</sup> - MARTIN KOTEK<sup>2</sup>

<sup>1</sup>Czech University of Life Sciences Prague, Faculty of Engineering, 165 21 Prague 6  
– Suchbátka, Czech Republic, Phone: +420224383106, Fax: +4202-20921361, E-mail:  
ruzicka@tf.czu.cz

<sup>2</sup>Czech University of Life Sciences Prague, Faculty of Engineering, 165 21 Prague 6  
– Suchbátka, Czech Republic, Phone: +420224383681, Fax: +4202-20921361, E-mail:  
kotekm@oikt.czu.cz

### Abstract

Traffic volumes and energy consumption from the transport sector continue to rise, yet the potential role of urban planning in contributing to reduced transport energy consumption continues to be largely underplayed. The growth of suburban areas tends to increase traffic volumes by dispersing activities and hence facilitates private car travel. Public transport orientated development as an evolving practice tends to be focused very much on urban areas. This paper draws on research in suburban Prague to suggest that urban planning can be applied more fully, at the strategic and local levels, to reduce energy consumption in car use. The main aim of this paper is to map fuel consumption and emission production under real traffic conditions on selected radial roads from Prague's suburb areas with different urban densities.

### Introduction

The role of urban structure, at the strategic and local scales, would appear, intuitively, to be critically important in facilitating travel. Urban structure provides the framework for the location of housing, employment and other developments, such as health, education and leisure facilities. Urban structure thus provides the physical rationale for travel alongside socio-economic and cultural factors. It might be expected that different urban forms (say low density sprawl and high density, public transport orientated development) to be clearly associated with different travel behaviours on the ground. (Hickman-Banister, 2007). Some authors contend that certain land use variables, for example density, are strongly associated with energy consumption in travel (e.g. Newman and Kenworthy, 1989 and 1999). Some are more cautious and suggest that land use factors are, at most, only a small part of the picture, and that other factors, such as income, are more important in influencing the variation in travel (e.g. Gordon et al, 1997). Others add a further dimension in contending that the suburbanisation of the labour force has actually led to reduced trip lengths, with both residences and jobs being located in the suburbs (Gordon and Richardson, 1989). Finally there are issues raised around the acceptability of various policy stances,

particularly the public acceptability of compaction (Breheny, 1992); it is argued here that suburbanisation has been stimulated by lifestyle choice and that attempts towards urban compaction are futile.

Ewing (1997) analyzed costs according to urban sprawl as follows. Firstly, from a vehicle miles travelled (VMT) aspect, there are many positive studies, which demonstrate that if density goes up, the travel distances are shortened then the use of public transportation and the walking increases and the use of automobiles reduces. The second aspect is that of energy consumption and air pollutant emitters. Concentrated development patterns reduce energy consumption more than low density diffused developments because of the short travel distances. Thirdly, there are many studies, which demonstrate that the infrastructure construction costs and public service supply costs go down as density goes up because of the scale of economies. Fourthly, there is the consideration of the squandering of land resources. Development of scattered urban form consumes much more land than high-density developments. Fifthly, central cities and downtown still remain the centre of culture, law, high-level functions, and many other industries such as finance, law service, and advertisement because face-to-face contact continues to be important. Sixthly, there

are mental and social costs. In suburbs, people who cannot drive have difficulties in gaining access to services, community facilities, and work, which penalizes youngsters, the elderly, and the poor. Above all, he insists that the problems associated with disordered sprawl can be solved through “the plan,” and growth management of America and that there are many possible ways to solve these problems.

The determination of fuel consumption per km can be affected through changes in the technological efficiency of cars or changes in driving habits. Urban density could have countervailing effects on fuel consumption per km see next (Karathodorou et al, 2009).

Congestions could also affect both car ownership and the distances travelled, as well as fuel consumption per km. Karathodorou et al, 2009, proposed model to estimate fuel consumption with the use of data providing an “average network speed” measure, which is “the average speed of vehicles (7 day/24 hour average) on all classes of road in the metropolitan area”. Including this variable in the model they found it to be insignificant and it did not greatly affect the remaining results, although the elasticity of fuel consumption with respect to density was somewhat lower. They concluded that this is largely unsurprising because congestions are both time and place are specific, and as such, average network speed provides a rather crude proxy. Consequently, Karathodorou et al, 2009 did not include this variable in the final model. This decision might influence results from the fuel consumption per kilometre component of this model. It has been hypothesized that urban density can have competing effects on fuel consumption per km. On one hand, parking issues in denser cities can lead to smaller, more fuel efficient cars. On the other hand, traffic conditions in denser cities can encourage ‘stop and go’ driving, which results in increased emissions. However was found that urban density not to have significant effects on the fuel consumption per km, perhaps because density can affect fuel efficiency both ways.

According to the above cited references it is evident that this topic is very complicated and is influenced by many local aspects and questions e.g. is actually more non-work trips than those of work-related travel; do the most trips occur from suburb to suburb; is a decentralized

concentration of cities very sustainable form etc. The main aim of this paper is to determine fuel consumption and emission production under real traffic conditions on radial roads from Prague’s suburb areas with different urban densities.

### Experimental arrangement

Suburban roads leading from areas with different urban densities were selected on the base of study (Proudy 2001 in Ouředníček – Urbánková, 2006). There are two red lines that mean origins and destinations from suburban areas. These routes are marked as the route SE (south/east) and the route NW (north/west). Both routes were selected on the same class of roads (according to the Czech classification – 2<sup>nd</sup> category road). The measurement was carried out during the morning peak of rush hours from the April to June 2010 on working days. Both routes start at suburban village and their destination is on the nearest parking place at metro station. NW’s origin is in Holubice village and its destination is on parking place near to metro station Dejvická – distance 17 (km). SE’s origin is in Psáry village and its destination is on a parking place near to metro station Budějovická – distance 16 (km). Details of measurement see Table 1. NW route consists of two junctions with traffic lights and one roundabout junction. SE route consists of three junctions with traffic lights and three roundabouts. Both routes were in specific distance from the main radial road NW 2,3 (km) and SE 3 (km); these partial routes were with low intensities of traffic (see Fig. 2.)

Route	Day	Start Time from the Origin	Duration of drive (min)
NW	Wednesday	7:18	26
NW	Thursday	7:25	25
NW	Thursday	7:20	27
NW	Wednesday	7:30	22
NW	Tuesday	7:51	21
SE	Wednesday	6:57	36
SE	Wednesday	8:02	40
SE	Wednesday	7:04	39
SE	Wednesday	8:13	44
SE	Tuesday	7:16	45

Table 1. Measurent layout



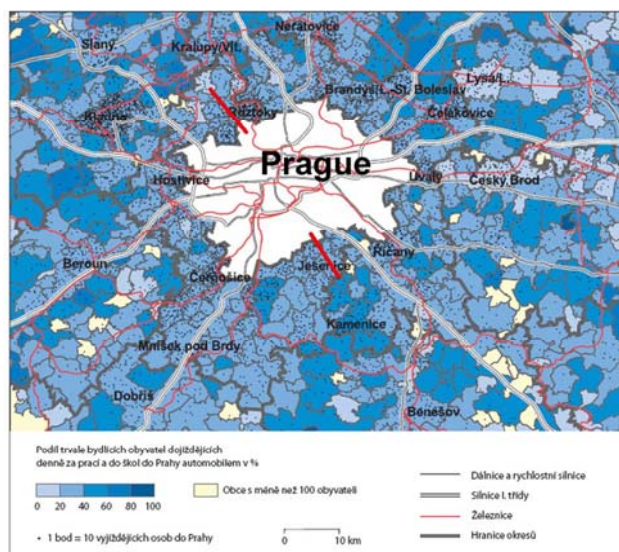


Fig. 1 Map (Proudy 2001 in Ouředníček – Urbánková, 2006)

The measurement was carried out with the aim to obtain the wide range of variables that are influenced by instantaneous traffic conditions. The laboratory car (Škoda-Octavia, diesel engine, 2 litres, manual gear shifting) was equipped with GPS device, mobile equipment enabling to analyse emission production (exhaust gases) and other variables (speed, fuel consumption and other engine's quantities) were obtained from car's onboard computer. All data were saved into the portable computer. The instantaneous speed in  $\text{km}\cdot\text{hour}^{-1}$  was measured in time intervals 0,2813 (s) as well as the fuel consumption in  $\text{litres}\cdot\text{hour}^{-1}$ . The preciseness of speed measurement was checked and compared with speed obtained from GPS data. Preciseness of the measurement of fuel consumption was checked and compared by manual filling of a car's petrol tank after the every drive. Other measured quantities are not the topic of this paper and that is why they are not specified in detail. Results of these two routes' measurements are values of instantaneous speed and fuel consumption in time intervals 0,2813 (s). NW routes consists of 26074 records, SE route consists of 39703 records.



Fig. 2. Routes of measurement

## Results and discussion

The first very simple result was the time duration of drives (see Table 1). NW [17 (km)] route takes in average 24,2 (min), SE [16 (km)] route 40,8 (min). The average speed on NW route was  $42 \text{ km}\cdot\text{h}^{-1}$  and on the SE route was  $25 \text{ km}\cdot\text{h}^{-1}$ . It means that average speed decreased to value 0,59. Explanation of the speed decrease is the occurrence of congestions on SE route in front of roundabouts and junctions with traffic lights in comparing with NW routes. On NW route congestions were as well but rarely.

Time spent during different speed intervals was compared in these two routes. Results of comparison proved an expectation see Fig. 3. NW route has 19,1% of time spent at speed intervals from 0 to  $20 \text{ km}\cdot\text{h}^{-1}$ , SE route has 54,4% of time spent at speed intervals from 0 to  $20 \text{ km}\cdot\text{h}^{-1}$ . It means in practice that more then half of time on route SE is spent by braking and acceleration in congestions. This way of transport leads to consequences of specific engine modes usage with higher fuel consumption and emission production.

The comparison of fuel consumption of the two routes is shown on Fig. 4. Results of measurements proved the expectation again. When these two measured routes are compared from the point of speed intervals the main difference is that SE route consumed 36% of fuel at speed 0 to  $20 \text{ km}\cdot\text{h}^{-1}$ , NW consumed 11% of fuel during the same intervals. It is evident that the increase of fuel consumption on SE route was caused by low speeds of car.

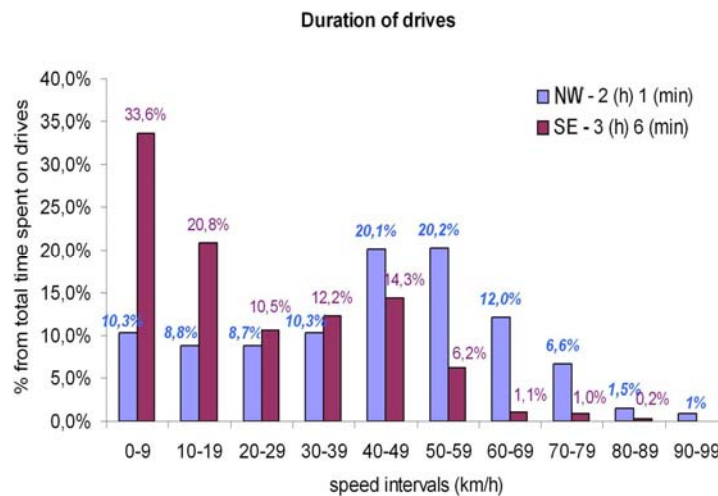


Fig. 3. Percentage of time spent during drives with different speed

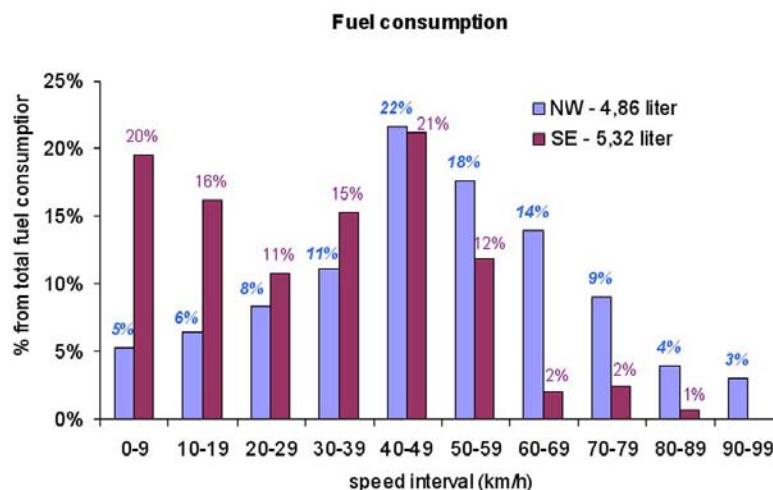


Fig. 4 Percentage of fuel consumption during drives with different speed

During drives occurring in the area (SE) with higher percentage of people commuting every working day to a downtown the consumption of fuel is higher about 16% (results of data processing determined NW route's fuel consumption 5,72 liter/100 km, SE 6,65 liter/100 km). This increase involves app. 15-20 thousands vehicles on SE route per day (according to traffic survey carried out in the year 2005). It would be possible to determine the total increase of fuel consumption caused by this situation according to structure of traffic flow but why?

### Conclusions

The open question stays the relevance between the number of people commuting to work (schools) or population density in suburban

areas and number of generated drives. Results of survey are shown in Fig. 1. but they are more ten years old. The real situation might be slightly different now but it was expected that processes of suburbanisation went on in both areas. Nevertheless obtained results indicate the expected increase of fuel consumption for every day commuting by passenger cars in selected areas with higher suburbanisation. The increase is caused mainly by congestions i.e. non-adequate (insufficient capacity) road infrastructure. The solution to build new, better or higher capacity infrastructure is the simplest but not the best. It will bring similar known problems caused by a traffic induction. The ad-hoc "pepperpotting" of new housing development around the edge of or in urban



centres, or in rural areas, no longer remains an option. It is needed a strategic and coordinated approach to new housing location, together with the consideration of location of public services and facilities, jobs and public transport. Development like this can bring reduced transport energy consumption (in the journey to work at least) and transport sustainability could be achieved in these locations of new development.

## References

- [1] Breheny, M.: The Contradictions of the Compact City: A Review, in Breheny, M. (Ed) Sustainable Development and Urban Form. 1992, London: Pion, pp. 138-159.
- [2] Ewing R: Is Los Angeles style sprawl desirable? 1997, J Am Plan Assoc 63(1):107–126
- [3] Gordon, I., - Breheny, M., - Archer, S.: Urban Compaction Versus Higher Gas Prices: The Feasibility and Effectiveness of Alternative Approached to Securing Sustainable Levels of Urban Travel. Paper presented to Association of American Geographers, Fort Worth, 1997 Texas.
- [4] Gordon, P. - Richardson, H. W.: Gasoline Consumption and Cities: A Reply, Journal of American Planning Association, 1989, Vol. 55, pp. 342-345.
- [5] Hickman, R. - Banister, D.: Transport and reduced energy consumption: what role can urban planning play?, 2007, Transport Studies Unit Oxford University Centre for the Environment, Working paper No 1026 (dostupné 12.1.2010) <http://www.tsu.ox.ac.uk/pubs/1026-hickman-banister.pdf>
- [6] Karathodorou, N., - Graham, D J., - Noland, R. B.: Estimating the Effect of Urban Density on Fuel Demand. <http://www.feem-web.it/ess/files/karathodorou.doc.pdf>, dostupné 7. 5. 2010 <http://www.feem-web.it/ess/files/karathodorou.doc.pdf>
- [7] Newman, P.W.G.-Kenworthy, J.R.: Cities and Automobile Dependence. An International Sourcebook. 1989, Aldershot: Gower.
- [8] Newman. P.W.G. - Kenworthy. J.R.: Sustainability and Cities: Overcoming Automobile Dependence. California: 1999 Island Press.
- [9] Shim, G., - Rhee, S., -Ahn, K. -Chung, S.: The Relationship Between the Characteristics of Transportation Energy Consumption and Urban Form, Annals of Regional Science, 2006, 40 (2), 351-367.
- [10] Ouředníček, M. -Urbánková, J.: Urbanizační procesy v Pražském městském regionu Kapitola 5. Vliv suburbanizace na dopravu v Pražském městském regionu. 2006, vystaveno 1.1.2008. [cit. 2009-12-11]. Dostupné z: <http://www.natur.cuni.cz/~slamak/gacr/kniha/>

## ANALYSIS OF TENSILE STRENGTH OF HOP STRINGS AND THEIR ATTACHMENTS TO HOPFIELD SUPPORTING STRUCTURE

ADOLF RYBKA, PETR HEŘMÁNEK, IVO HONZÍK, KAREL BERNÁŠEK

Czech University of Agriculture in Prague, 165 21 Prague 6 – Suchbát, Czech Republic,

Phone: +4202-24383121, Fax: +4202-24383122, E-mail: [rybka@tf.czu.cz](mailto:rybka@tf.czu.cz)

### Abstract

It has been proven that making of hop strings and the way they are attached to hopfield supporting structure has a subsequent influence on the quality of the final hop product. On the basis of laboratory experiments with different materials, and measurements of tensile strength, there have been analysed some alternative solutions with the aim of improving the quality of the whole technology of growing and post-harvest hop processing.

**Keywords:** hop string, hop-string attachment, hop

### Introduction

Besides brewing parameters, present hops purchasers lay more and more stress on perfect purity of the final product. One of the places that are most at risk if we consider the whole hop growing technology and the post-harvest hop processing is the way how hop strings are hung on the hopfield supporting structure (Šnobl et al., 2004).

The current way of hop-string attachment (being wires of different diameter) to a supporting structure by means of polypropylene twines bears the risk of hop product contamination by these attachment residues (Rybáček et al., 1980), (Srivastava et al., 1993).

There are a number of requirements for hop strings and their attachments. A hop string (presently a steel wire) must enable its easy hanging on supporting structure with the use of suitable attachments, sticking of the other ending in the ground, and an easy spiral hopvine distribution. A guide wire must be, from the point of view of strength, proportioned for the gradually increasing weight of growing hop bushes, for the risk of weather impact (wind gusts, persistent rains, etc.), and for the corrosive effects resulting from frequent application of agrochemicals. Hop-string attachments must enable the pulling machinery an easy and fluent hopvine pull-down, and the hop-string attachment residues on the supporting structure must not make the hanging in the following years impossible. Last but not least, the operation makes heavy demands on both manual and machine work as well as on total financial inputs.

The present conception, which is used by practically all growers, does not present an ideal strength proportions between hop strings and their attachments. When the hopvines are pulled down (during the harvest), the hopstrings are mostly broken and the attachments are left on the hopfield trellis. In the following years these attachments, mainly by the influence of applied chemicals, loosen of themselves and are one of the causes for penetration of impurities into another stage of technological process where they are separated only with difficulty (Vent et al., 1970).

Thus with technology of hop growing, it would be suitable for mechanized pull-down of harvested hops to pull down the guide wire together with hopvines and their attachments in a way so that all of the attachment stayed connected with wire and there would be no attachment residues left on the hop trellis (Ciniburk et al., 2009). After hop cones would be picked off, both hopvine bines and hop strings (ideally including attachments) would be left at the stationary hop picker. These would then be cut up into little pieces by a cutting machine and taken to be composed, possibly to be ploughed in. Wire and attachment residues will decompose in short time in the ground.

On the basis of laboratory and subsequent field experiments there should be devised such a technological procedure in the hopfield which would substitute the current state and optimise the realization of hop strings as well as the way they are attached.

## Material and Methods

The first step in dealing with the presented issues are laboratory measurements of tensile strength at guide wires used as hop strings, and at polypropylene twines determined to be their attachments to hopfield supporting structure.

Measuring equipment:

Shredder Amsler-200 (Figure 1) – speed of shredding mechanism shift -  $100 \text{ mm} \cdot \text{min}^{-1}$ , shift controlled by electric motor, distance of shredder jaws (wire or twine length before testing) – 85 mm, present record of shredding power and elongation of both measured wire and twine.

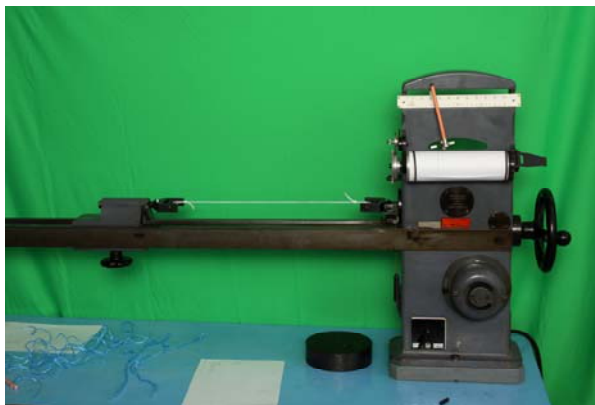


Fig. 1 Shredder Amsler-200

Theoretical analysis of tensile strength:

Measurements result in a permanent deformation of the material. A material of a length of  $l \text{ [mm]}$  is attached to the fixed jaw at its one end and to the movable jaw at the other end, where the force  $F \text{ [N]}$  takes a tensile effect horizontally. By the effect of this force the material breaks. When taking the difference of material length after breaking and at the beginning of the test, we can determine the elongation  $\Delta l \text{ [mm]}$ . Division of elongation  $\Delta l$  and original length  $l$  results in *relative elongation*  $\varepsilon$ :

$$\varepsilon = \frac{\Delta l}{l}; \quad \varepsilon \text{ is a non-dimensional number.}$$

Division of the force  $F$  which takes an effect in the direction of the normal to material cross-section  $S \text{ [mm}^2\text{]}$  is *direct stress*  $\sigma$ :

$$\sigma = \frac{F}{S}; \quad \sigma \text{ has a dimension of } \text{[N} \cdot \text{mm}^{-2}\text{]}.$$

Wire or twine *strength* is a stress under which a material breaks.

Measured material:

- wire – black annealed; 0.90, 1.00, 1.04, 1.06, 1.12, 1.20, 1.30, and 1.40 mm in diameter,
- polypropylene twine (producer JUTA Inc.): 10 000, 12 500, 14 000, 17 000, and 20 000 (according to producer designation).

Methodology of measurement:

Measuring equipment was set up for required parameters (see measuring equipment description), 10 sample pieces of each kind of material were available for repeated measurements, and the recorded items were measurement number, measured sample diameter -  $d \text{ [mm]}$ , horizontally (axially)-acting force needed for breakage -  $F \text{ [N]}$ , and corresponding elongation length at guide wire -  $\Delta l \text{ [mm]}$ . For all of 10 repeats the calculation assessed *relative elongation*  $\varepsilon$ , *direct stress*  $\sigma \text{ [N} \cdot \text{mm}^{-2}\text{]}$  and their average values  $[\bar{\varepsilon}, \bar{\sigma}]$ . The variability of ten repeats was assessed by a standard deviation and variation coefficient.

## Results of Measurements

The measurements were carried out in the laboratory of the Department of Agricultural Machines, the Faculty of Engineering, CULS in Prague, at the air temperature of  $24^\circ\text{C}$  and the air humidity of 22%. Each measurement was repeated ten times for each diameter of the wire and each kind of the twine. Tables 1 and 2 then present the average measurement values and statistic data characterizing the sets shown.

Graphic dependence of measured or calculated values on the diameter of wire sample is not carried out due to a different level of heat treatment of samples with different diameter. The different quality of individual guide wires is i.a. apparent from the data about wire strength ( $\sigma$ ), which should be approximately the same

for all wire diameters, which however mutually differs in a substantial way (Table 1). At samples of individual polypropylene twines after their breakage a substantial fraying occurs, thus it is impossible to measure the twine length after breakage. That is the reason why the elongation measurement of twines was abandoned and neither it is presented in the result table.

Figure 2 represents a block diagram for a guide wire with a diameter of 1.06 mm which is currently used by app. 90% of hop growers for the variety of Žatec Semi-early Red, and a block diagram for a guide wire with a diameter of 1.12 mm which is used for hybrid varieties (Sládek, Premiant, Agnus, etc.). From the diagram a process of breakage force ( $F$ ) is apparent, depending on guide-wire elongation ( $\Delta l$ ).

Tab.1 Average values resulting from measurements of 10 samples of guide wire

Wire diameter according to producer	d – measured wire diameter	S – wire cross section	F – breakage force	s – standard deviation of breakage force	v – variation coefficient of breakage force	$\Delta l$ – elongation	$\varepsilon$ – relative elongation	$\sigma$ – wire strength
mm	mm	mm <sup>2</sup>	N		%	mm	%	N.mm <sup>-2</sup>
0,90	0,900	0,64	215	12,2	5,7	20,3	24	338
1,00	1,056	0,88	313	12,0	3,8	22,7	27	358
1,04	1,050	0,87	333	1,0	0,3	27,4	32	384
1,06	1,063	0,89	344	23,5	6,8	19,3	23	388
1,12	1,131	1,00	392	4,5	1,1	22,5	26	390
1,20	1,200	1,13	467	6,8	1,5	24,9	29	413
1,30	1,330	1,39	539	3,2	0,6	23,3	27	388
1,40	1,400	1,54	584	5,4	0,9	25,3	30	379

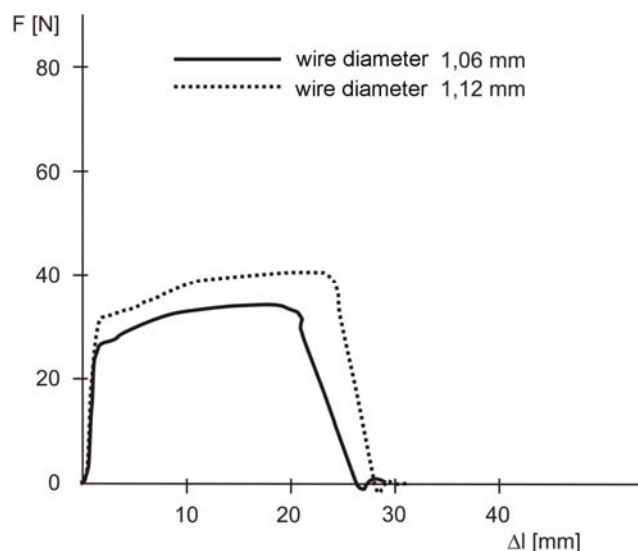


Fig. 2 Block diagram for a guide wire with diameter of 1.06 mm and 1.12 mm

Tab. 2 Average values resulting from measurements of 10 samples of JUTA twine

Twine designation	F – breakage force	s – standard deviation of breakage force	v – variation coefficient of breakage force
	N		%
10000	268	21,2	7,9
12500	538	37,6	7,0
14000	556	14,9	2,7
17000	652	54,5	8,4
20000	862	27,9	3,2

Figure 3 presents block diagrams for polypropylene twine 17 000, which is the most widespread, and twine 14 000, which is the second most used.

For hanging of guide wires a part of growers uses twines with single hanging, however, some other use twines with double hanging. A rough measurement of the double twine on the shredder logically confirmed the need of double breakage force compared to the measurement of the single twine.

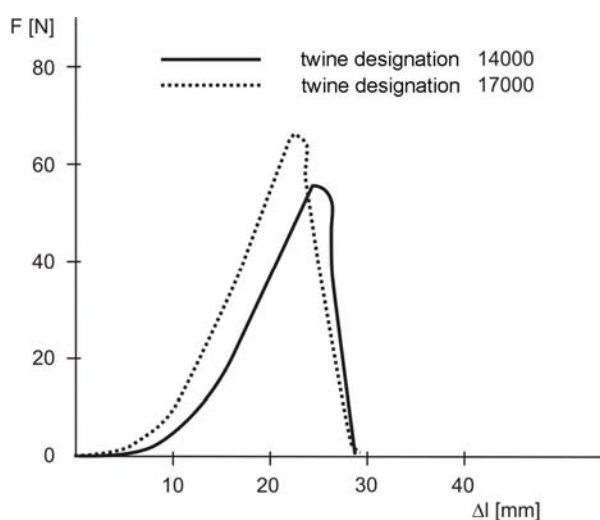


Fig. 3 Block diagram for a twine with the designation of 14000 and 17000

## Discussion

The aim of the laboratory measurement of tensile strength was to find out the qualitative

features of currently used materials in the function of hop strings and their attachments to hopfield supporting structure just before their use for hop growing.

By comparison of the data found in tables 1 and 2, the force necessary for material breakage ( $F$ ) logically rises with the diameter of given material ( $d$ ). There is an interesting evidence that the force necessary for material breakage is bigger with the most frequently used twines (14000 and 17000) than with the most frequently used wires (1.06 and 1.12 mm). The given measurements clearly show that any combination of these wires and twines is used, the wire being pulled down is accidentally broken, whether just in the place of attachment or at a different height of wire, while the attachments stay on the supporting structure. The wire parts together with the hopvines are then taken away to the stationary hop picker. Definitive conclusions to given issues, however, can be drawn only after measuring the pull-down force during the harvest, as the measurement results will be, in comparison to the affordmentioned measurement, substantially influenced by the corrosive and abrasive impact of a hopfield microclimate in the course of app. half a year of cultivation season.

Table 1 clearly shows the highest variability of the measured force at the breakage of the most frequently used guide wire with a diameter of 1.06 mm which is characterized by standard deviation and variation coefficient. This is indicative of very changeable qualitative characteristics of this wire. Similar conclusion to the variability of the measured force at the breakage may be drawn also for the most frequently used twine with the producer designation of 17000.

## Conclusion

From the experimental measurements that have been carried out we may come to the conclusion that the combination of the most frequently used materials for hop strings and their attachments, from the point of view of measured forces at their breakage, does not meet the requirements necessary so that during the harvest when the hops are pulled down, the guide wire is pulled down together with hopvines and their attachments in a way that the hopfield trellis stays clean without any attachments. From the

measurements also results a diverse quality of used materials for hop strings and their attachments, and mainly a substantial variability of quality regarding the most frequently used materials.

However, to get a detailed analysis of the values it will be necessary to gain some comparable data about strength and lifetime of the materials used during the harvest when an important negative role is played by the increasing weight of hopvines, calamitous weather conditions, and corrosion caused by the impact of used chemicals.

From the field and laboratory experiments must result a concept combining suitable materials used for hop strings and their attachments to minimize the amount of impurities contained in the harvested hops which gets into further parts of technological line proceeding to completion of the final product. The proposed solution variations must be compared and assessed on the basis of need for

human labour and its intensity, energy and material costs.

*This article was written with the contribution of the Ministry of Agriculture of the Czech Republic as a part of solutions of NAZV QI101B071 research project.*

## References

- [1] Ciniburk,V. et al.: Navrhování lanových chmelnicových konstrukcí. Metodika pro praxi 02/09, Chmelařský institut s.r.o., 2009, 23 p., ISBN 978-80-87357-01-9
- [2] Rybáček,V. et al.: Chmelařství. SZN Praha, 1980, 426 p., ISBN 07-068-80
- [3] Srivastava,A.K. et al.: Engineering Principles of Agricultural Machines. ASAE, Michigan, USA, 1993, 601 p. ISBN 0-929355-33-4
- [4] Šnobl,J. et al.: Rostlinná výroba IV. ČZU v Praze, 2004, 119 p. ISBN 80-213-1153-3
- [5] Vent,L. et al.: Mechanizované linky ve chmelařství. VÚCH Žatec, 1970, 141 p.



## THIN LAYER CONVECTIVE DRYING AND MATHEMATICAL MODELING OF EINKORN

KAMIL SACILIK<sup>1\*</sup>, Y. BENAL YURTLU<sup>2</sup>, H. GURAN UNAL<sup>3</sup>

<sup>1</sup>Department of Agricultural Machinery, Faculty of Agriculture, Ankara University, 06130, Aydinlikevler, Ankara, Turkey, Phone: +90 312 5961592, Fax: +90 312 3183888, E-mail: sacilik@agri.ankara.edu.tr

<sup>2</sup>Department of Agricultural Machinery, Faculty of Agriculture, Ondokuz Mayıs University, Samsun, Turkey

<sup>3</sup>Program of Mechanical, Kastamonu Vocational School, Kastamonu University, Kastamonu, Turkey

### Abstract

Einkorn (*Triticum monococcum*) was one of the first wheat to be domesticated some 10 000 years ago in the Near East. It originated in the mountainous areas of Turkey and its wild progenitor. However, it is now rarely grown in western Turkey, the Balkan countries, Germany, Switzerland, Spain. This study was undertaken to investigate the thin layer drying characteristics of the einkorn in a convective hot-air dryer. The drying characteristics of einkorn were examined at air temperature range of 40-70°C. During the dehydration experiments, air velocity was held stable at 0.8 m/s. Moisture transfer from the test samples was described by applying the Fick's diffusion model and the effective diffusivity was calculated. Temperature dependence of the effective diffusivity was described by the Arrhenius-type relationship. The experimental drying data of einkorn obtained were fitted to the well-known semi-theoretical drying models. Drying rate constants and coefficients of models tested were determined by non-linear regression analysis. The accuracies of the models were measured using the coefficient of determination, mean relative percent deviation, root mean square error and reduced mean square of the deviation. All models are acceptable for describing drying characteristics of einkorn.

**Keywords:** Einkorn; Convective air drying; Moisture ratio; Effective diffusivity.

### Introduction

Einkorn (*Triticum monococcum*) was one of the first wheat to be domesticated some 10 000 years ago in the Near East. It originated in the mountainous areas of Turkey and its wild progenitor. However, it is now rarely grown in western Turkey, the Balkan countries, Germany, Switzerland, Spain (Nesbitt & Samuel, 1996) and Italy (Troccoli & Codianni, 2005).

Historically, einkorn was cultivated in cool environments on marginal agricultural land through the mid-east and south-western Europe, whilst in Italy it is still cultivated in harsh environments and poor soil (Perrino & Hammer, 1984). Under adverse Italian growing conditions, einkorn selections produced protein with a yield equal to or higher than barley and durum wheat (Vallega, 1979). In contrast, under intensive Italian cropping management, the yields of 15 einkorn accessions were significantly lower than those of modern wheats (Vallega, 1992). Other

works reported einkorn to have a lower grain yield when compared to durum wheat grown in northern and southern Italy (Codianni et al., 1996) also emmer and spelt (Troccoli & Codianni, 2005). Compared to common wheat, einkorn is generally more resistant to diseases and has the ability to withstand drought (Vallega, 1979).

Einkorn is of significance due to including high level of protein, carotenoids, phosphorus and antioxidant (Abdel-Aal et al., 1995; Brandolini et al., 2007; Matuz et al., 2000). Several studies concluded that einkorn is a promising in terms of developing new or special food such as bakery products, baby food or products with high content of dietary fibre, carotenoids and tocopherols (Borghi et al., 1996; Corbellini et al., 1999; Hidalgo et al., 2006; Løje et al., 2003). Einkorn flour is often considered to have poor dough and baking properties (Abdel-Aal et al., 1997; D'Egidio et al., 1993; D'Egidio

& Vallega, 1994). Its dough was weak, sticky, difficult to handle and had a low mixing tolerance. In Turkey (the birthplace of einkorn) einkorn is often used for bulgur making. Bulgur can be defined as dry and wet cleaned, cooked, dried, peeled then grinded and classified wheat product. In Turkey, approximately 1 million ton of bulgur is produced annually (250 000 tones in America). This production is 2.5 times greater than macaroni (pasta), with an average consumption 12 kg per person (Bayram, 2000; Bayram & Oner, 2002). Furthermore, it is an important wheat product due to its high dietary fibre content, having 18.3 g dietary fibre per 100 g. Its dietary fibre content is 3.5, 6.8, 1.1, 1.8, 7.0, 15.3, 9.2, 2.3, 1.3 and 4.3 times higher than rice, wheat flour, barley, oat meal, spinach, tomato, turnip, whole wheat bread, soybean and pasta, respectively (Dreher, 2001). Einkorn especially cultivates for bulgur making in western Black Sea Region of Turkey.

Drying is the most important process in bulgur production from einkorn wheat. Einkorn for producing bulgur is traditionally sun-dried in open air. Commercially, hot-air drying is used. However, einkorn wheat has different characteristic properties because of its husky structure. Knowledge of the drying characteristics of biological materials is essential to the design, optimization and control of the drying processes. Data on the drying characteristics of einkorn wheat, however, are not available for engineering design of drying systems. This study was undertaken to investigate the thin layer drying characteristics of the einkorn in a convective hot-air dryer, to calculate the effective diffusivity and activation energy of samples and to fit the experimental drying data obtained to drying models widely used to describe thin-layer drying of agricultural products.

## Materials and Methods

### *Sample preparation*

Einkorn grains of Kaplica variety were used in this study. Samples were randomly selected in Seydiler district of Kastamonu province (1100 m) in Western Black Sea Region of Turkey. Kaplica einkorn has one kernel kernels (Figure

1). The grains were cleaned manually and foreign matter such as stones, straw and dirt were removed. About 1500 g of einkorn wheat was cooked at boiling water at 70°C temperature for 50 min (Bayram & Oner, 2005). Moisture content was determined through an oven method at 105°C  $\pm$  3 °C during 24 h (Gupta & Das, 1997). Initial moisture content of samples was found to be about 151% d.b. The samples were then packed in self-sealed polythene bags for preventing surface moisture dehydration until the drying experiments.

### *Drying equipment*

Drying experiments were performed in a laboratory scale convective air dryer shown in Figure 2. The drying system consists of a fan, an electrical heater and a weighing system. The dryer has a height of 57 cm, a width of 68 cm and a depth of 57 cm. The air velocity in the drying chamber was measured using a hot-wire anemometer in the measurement range of 0-5 m/s. Samples were dried in a drying basket of 576 cm<sup>2</sup> by 12 cm high. During the drying process, weight loss in the drying basket was measured by means of load cell and continuously recorded at 1 min intervals throughout runs by specially designed software connected to a PC.

### *Drying Experiments*

About 100 g of einkorn wheat sample was used in each drying run. Prior to starting the experiment, the dryer was run idle for about half an hour to reach thermal stabilisation. With the fan off, the samples were uniformly spread within the basket as a single layer and dried there. Drying experiments were conducted at 40, 50, 60 and 70°C air temperatures. The air velocity was kept constant at 0.8 m s<sup>-1</sup> in all drying experiments. Experiments were continued until no further changes in their mass were observed (about 12% d.b.).

### *Analysis of drying data*

The experimental drying data obtained were fitted to the five well-known drying models given in Table 1.



Figure 1. Einkorn grains and kernels



Figure 2. Drying system used in experiments

Table 1. Thin-layer drying models used for drying curves

Model name	Model	References
Page	$M_R = \exp(-kt^m)$	Agrawal and Singh (1977)
Logarithmic	$M_R = a \exp(-kt) + c$	Yagcioglu, Degirmencioglu, and Cagatay (1999)
Two-term	$M_R = a \exp(-kt) + b \exp(-k_0t)$	Henderson (1974)
Approximation of diffusion	$M_R = a \exp(-kt) + (1 - a) \exp(-kbt)$	Yaldiz and Ertekin (2001)
Midilli <i>et al.</i>	$MR = a \exp(-kt^m) + bt$	Midilli, Kucuk, and Yapar (2002)

The moisture ratio is given as follows:

$$M_R = \frac{M - M_e}{M_0 - M_e} \quad (1)$$

Where:

- $M_R$  is the dimensionless moisture ratio,  $M$ ,  $M_e$  and  $M_0$  are the moisture content at any time, the equilibrium moisture content and the initial moisture content in % w.b., respectively.

However,  $M_R$  is simplified to  $M/M_0$  instead of Eq. (1) due to the continuous fluctuation of the relative humidity of the drying air during their drying processes (Diamante &

Munro, 1993). The drying rate constants and coefficients of models were estimated using a non-linear regression procedure. The estimation method was Levenberg-Marguardt and the statistical validity of models was evaluated and compared by means of the coefficient of determination  $R^2$ , mean relative percent deviation  $E_{MD}$ , root mean square error  $E_{RMS}$  and reduced chi-square  $\chi^2$ . These comparison criteria methods can be calculated as follows:

$$E_{MD} = \frac{100}{N} \sum_{i=1}^N \frac{|M_{R,ex,i} - M_{R,pre,i}|}{M_{R,ex,i}} \quad (2)$$

$$E_{RMS} = \left[ \frac{1}{N} \sum_{i=1}^N (M_{R,ex,i} - M_{R,pre,i})^2 \right]^{1/2} \quad (3)$$

$$\chi^2 = \frac{\sum_{i=1}^N (M_{R,ex,i} - M_{R,pre,i})^2}{N - z} \quad (4)$$

where:

- $M_{R,ex,i}$  is the  $i$ th experimental dimensionless moisture ratio;  $M_{R,pre,i}$  is the  $i$ th predicted dimensionless moisture ratio;  $N$  is the number of observations; and  $z$  is the number of constants.
- $R^2$  was used as the primary comparison criteria for selecting the best model to fit the four models to the experimental data. Also, the lower values of the mean relative percent deviation  $E_{MD}$ , the root mean square error  $E_{RMS}$  and the reduced chi-square  $\chi^2$  were chosen as the comparison criteria for the goodness of fit of the experimental data obtained.

## Results and Discussion

### *Drying characteristics*

Figure 3 shows the moisture content versus drying time curves for the hot-air drying of einkorn wheat samples as influenced by various air temperatures. Initially, the moisture content decreased rapidly, and then the decrease in moisture content slowed down considerably as expected. The samples of initial moisture content of around 150% d.b. were dried to the final moisture content which changed between 10 and 13% d.b. It is clearly evident from these curves that the moisture content decreases continuously with the drying time. The air temperature water

had a significant effect on the moisture content of samples. The drying time required to reduce the moisture from the initial moisture content to a desired moisture content for einkorn wheat samples was 600, 700, 810 and 960 min at air temperatures of 40, 50, 60 and 70 °C, respectively. The decrease in the drying time with an increase in the air temperature have been observed by Ozdemir & Devres (1996) for hazelnut and Mohapatra & Rao (2005) for parboiled wheat.

The effect of air temperature on the drying rate of einkorn wheat at 40, 50, 60 and 70°C air temperatures is indicated in Figure 4. It can be seen that the drying rate decreased continuously with a decrease in the moisture content or with an increase in the drying time at a given air temperature. There is no constant-rate drying period in these curves and all the drying processes have been occurred in the falling rate drying period. During the falling rate drying period, the drying rate of einkorn wheat was found to be greatly dependent on the air temperature. In other words, the drying rate increased with an increase in the air temperature. It was observed that the main factor influencing the dehydration rate is the air temperature, as reported in earlier researches by Ozdemir and Devres (1999) for hazelnut, Akpinar et al., (2003) for red pepper, Mohapatra & Rao (2005) for parboiled wheat. Therefore, a higher air temperature produced a higher drying rate and consequently the drying time decreased. This is due to the increase of heat transfer between the air and the einkorn wheat samples, and the acceleration of water migration inside them.

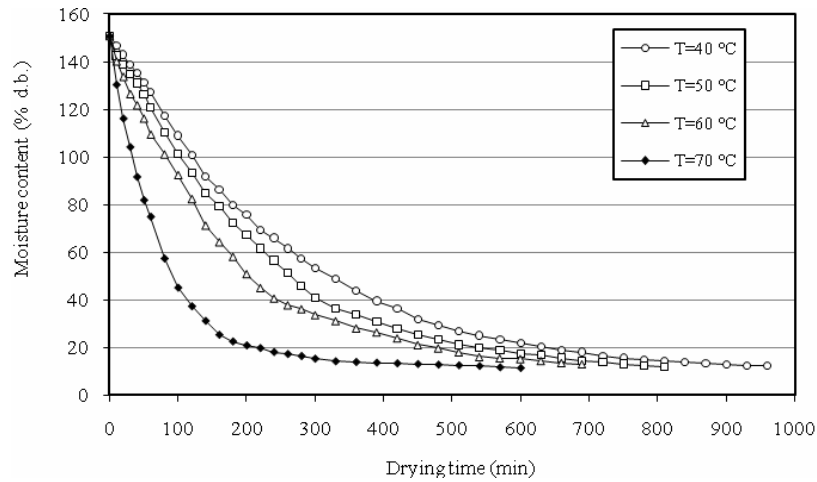


Figure 3. Hot-air drying curves for einkorn wheat samples at indicated air temperatures

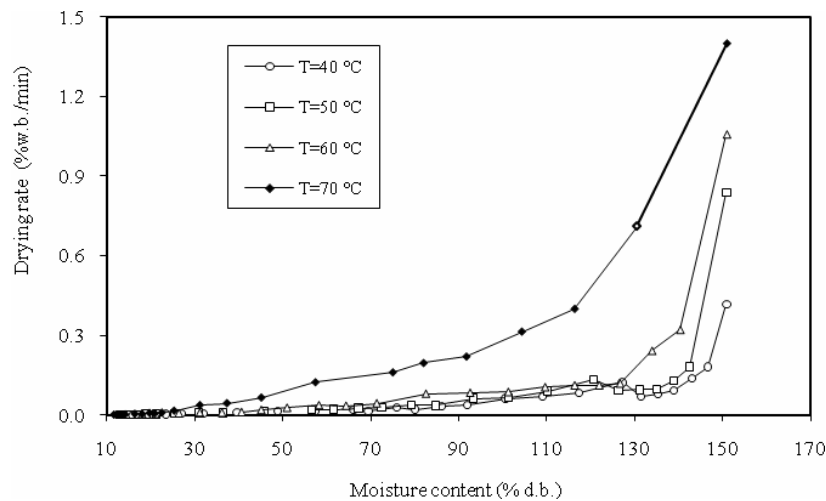


Figure 4. Drying rate curves of einkorn wheat at indicated air temperatures

#### Determination of effective diffusivity and activation energy

As previously mentioned, the drying of apple slices occurred in the falling rate drying period only and liquid diffusion controls process. Accordingly, Fick's second law can be used to describe the drying behaviour. The solution of Fick's second law in slab geometry, with the assumptions of moisture migration being by diffusion, negligible shrinkage, constant diffusion coefficients and temperature was as follows (Crank, 1975):

$$M_R = \frac{M - M_e}{M_0 - M_e} = \frac{6}{\pi^2} \sum_{n=1}^{\infty} \frac{1}{n^2} \exp\left(-\frac{n^2 \pi^2 D_{eff} t}{R_e^2}\right) \quad (5)$$

For long drying periods, Eq. (5) can be further simplified to only the first term of the series and the moisture ratio  $M_R$  was reduced to  $M/M_0$  because  $M_e$  was relatively small compared to  $M$  and  $M_0$ . Then, Eq. (5) can be written in logarithmic form:

$$\ln \frac{M}{M_0} = \ln \left( \frac{6}{\pi^2} \right) - \left( \frac{\pi^2 D_{eff} t}{R_e^2} \right) \quad (6)$$

where  $R_e$  is the equivalent radius of the einkorn wheat being dried in m,  $n$  is a positive integer and  $D_{eff}$  is the effective diffusivity in  $m^2/s$ .



The effective diffusivity was determined using the method of slopes. The effective diffusivity is typically calculated by plotting experimental drying data in terms of  $\ln(M_R)$  versus drying time. From Eq. (6), a plot of  $\ln(M_R)$  versus the drying time gives a straight line with a slope of:

$$\text{Slope} = \frac{\pi^2 D_{eff}}{R_e^2} \quad (7)$$

The values of effective diffusivity at 40, 50, 60 and 70°C air temperatures were found to be 1.19, 1.40, 1.56 and  $1.74 \times 10^{-10}$  m<sup>2</sup>/s, respectively. These values were close to those of  $1.2181\text{--}2.8611 \times 10^{-10}$  m<sup>2</sup>/s in the air temperature range of 40–60°C (Mohapatra & Rao 2005) for parboiled wheat. The effective diffusivity was greatly influenced by the air temperatures. However,  $D_{eff}$  values found in this study are within the general range  $10^{-9}\text{--}10^{-11}$  m<sup>2</sup>/s for drying of food materials. The small differences among values could be due to the differences in varieties, drying equipment and other uncontrolled parameters.

The effect of the temperature on the effective diffusivity is often expressed using the Arrhenius-type relationship:

$$D_{eff} = D_0 \exp\left(-\frac{E_a}{RT_a}\right) \quad (8)$$

where  $D_0$  is the pre-exponential factor of the Arrhenius equation in m<sup>2</sup>/s,  $E_a$  is the activation energy in kJ/mol,  $R$  is the universal gas constant in kJ/mol K and  $T_a$  is the absolute air temperature in K.

The activation energy was calculated by plotting the natural logarithm of  $D_{eff}$  versus reciprocal of the absolute temperature as presented in Figure 5. The plot was found to be a straight line in the range of air temperatures studied, indicating Arrhenius dependence. The activation energy for diffusion calculated from the slopes of straight lines of Figure 5 was found to be 11.15 kJ/mol with a value for  $R^2$  of 0.9998 for einkorn wheat.

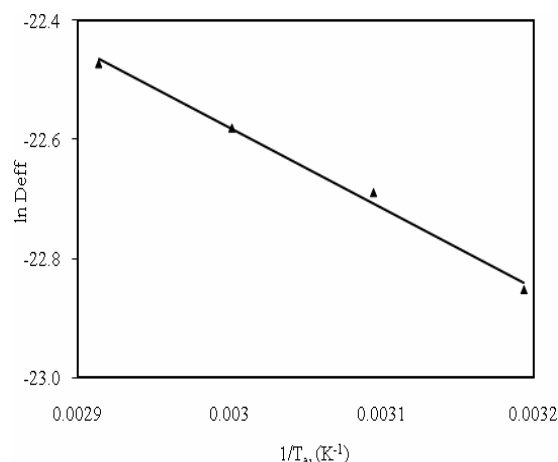


Figure 5. Arrhenius-type relationship between the effective diffusivity and absolute temperature

#### Fitting of the drying curves

Table 2 presents the results of nonlinear regression analysis of fitting the five mathematical drying models to the experimental data and comparison criteria used to evaluate goodness of fit namely,  $R^2$ ,  $E_{MD}$ ,  $E_{RMS}$  and  $\chi^2$  for einkorn wheat samples at 60 °C air temperature. All the five models other than the Page model provided an excellent fit to the experimental data with a value for  $R^2$  of greater than 0.9939, indicating a good fit. The values of  $E_{MD}$  for obtained from the logarithmic, two-term, approximation of diffusion and Midilli models were less than 10%, which is in the acceptable range. Of all the models tested, the logarithmic model offered the highest value for  $R^2$ , followed by the two-term, approximation of diffusion and Midilli models. The values for  $E_{RMS}$  and  $\chi^2$  obtained from the logarithmic model were less than those attained from other models. Hence, the logarithmic model was considered the best model in present study to represent the hot-air drying behavior of einkorn wheat samples within the experimental range of study. Figure 6 suggest the experimental moisture ratios fitted with the logarithmic model at various air temperatures for einkorn wheat samples. It can be seen from these there was a good conformity between experimental and predicted moisture ratios.



Table 2. Parameter estimation,  $R^2$ ,  $E_{MD}$ ,  $E_{RMS}$  and  $\chi^2$  of the four drying models for the hot air drying of einkorn wheat at an air temperature of 60 °C.

Model	Estimated values		$R^2$	$E_{MD}$ , (%)	$E_{RMS}$	$\chi^2$
Page	$k$	0.0091	0.9939	10.27	0.02325	0.00057
	$m$	0.8855				
Logarithmic	$a$	0.9273	0.9982	2.85	0.01244	0.00016
	$k$	0.0059				
	$c$	0.0735				
Two-term	$a$	0.0444	0.9983	3.26	0.01265	0.00017
	$k$	-0.0007				
	$b$	0.9542				
	$k_0$	0.0057				
Approximation of dif.	$a$	0.9547	0.9984	3.26	0.01245	0.00016
	$k$	0.0057				
	$b$	-0.1283				
Midilli <i>et al.</i>	$a$	0.9907	0.985	3.94	0.01263	0.00018
	$k$	0.0048				
	$b$	1.0244				
	$m$	0.0001				

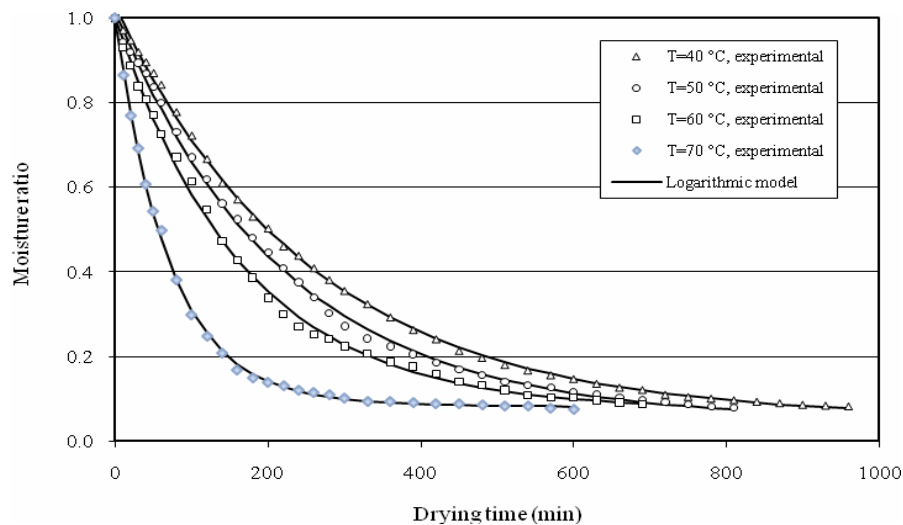


Figure 6. Comparison of the experimental and predicted moisture ratio obtained using the logarithmic model for einkorn wheat samples dried at indicated air temperatures

## Conclusion

The results from this study showed that drying curves were greatly affected by the air temperatures. The drying time required to reduce the moisture from the initial moisture content to a desired moisture content for einkorn wheat samples was 600, 700, 810 and 960 min at air temperatures of 40, 50, 60 and 70 °C, respectively. The effective diffusivity increased with increasing the air temperature and varied

from  $1.19$  to  $1.74 \times 10^{-10} \text{ m}^2/\text{s}$  in the air temperature range of 40-70 °C. The activation energy was found to be 11.15 kJ/mol. Of all the five models tested, the logarithmic model gave an excellent fit to the experimental data obtained with a value for  $R^2$  of greater than 0.9982 within the experimental range of study.

## References

- Abdel-Aal,E-S.M.-Hucl,P.-Sosulski,F.W.:  
Compositional and nutritional characteristics of  
spring einkorn and spelt wheats. *Cereal  
Chem.*,72,1995,p.621-624.
- Abdel-Aal,E-S.M.-Hucl,P.-Sosulski,F.W.-  
Bhirud,P.R.: Kernel, milling and baking  
properties of spring-type spelt and einkorn  
wheats. *J. Cereal Science*,26,1997,p.363-370.
- Agrawal,Y.C-Singh,R.D.: Thin layer drying  
studies on short grain rice. ASAE Paper No:  
3531,1977,ASAE, St. Joseph, MI.
- Akpinar,E.K-Bicer,Y-Yildiz,C.: Thin layer  
drying of red pepper. *Journal of Food  
Engineering*, 59(1),2003,p.99-104.
- Bayram,M: Bulgur around the world. *Cereal  
Foods World*,45,2000,p.80-82.
- Bayram,M.-Oner,M.D.: The new old wheat:  
convenience and nutrition driving demand for  
bulgur. *World Grain* (November),2002,p.51-53.
- Bayram,M.-Oner,M.D.: Stone, disc and hammer  
milling of bulgur. *J. Cereal Science*.  
41,2005,p.291-296.
- Borghi,B.-Castagna,R.-Corbellini,M.-Heun,M.-  
Salamini,F.: Breadmaking quality of einkorn  
wheat (*Triticum monococcum* ssp.  
*monococcum*). *Cereal Chem.*,73,1996,p.208-  
214.
- Brandolini,A.-Hidalgo,A.-Moscaritolo,S.:  
Chemical composition and pasting properties of  
einkorn (*Triticum monococcum* L. Subsp.  
*monococcum*) whole meal flour. *J. Cereal  
Science*,2007,doi:10.1016/j.jcs.2007.07.005
- Codianni,P.-Ronga,G.-Di Fonzo,N.-Troccoli,A.:  
Performance of selected strains of “farro”  
(*Triticum monococcum* L., *Triticum dicoccum*  
Schübler, *Triticum spelta* L.) and durum wheat  
(*Triticum durum* Desf cv. Trinakria) in the  
difficult flat environment of southern Italy. *J.  
Agron. Crop Sci.*,176,1996,p.15-21.
- Corbellini,M.-Empilli,S.-Vaccino,P.-  
Brandolini,A.-Borghi,B.-Heun,M.-Salamini,F. :  
Einkorn characterization for bread and cookie  
production in relation to protein subunit  
composition. *Cereal Chem.*,76,1999,p.727-733.
- Crank,J.: *Mathematics of Diffusions*. 2nd ed.  
Oxford University Press,1975,London.
- D’Egidio,M.G.-Nardi,S.-Vallega,V.: Grain, flour  
and dough characteristics of selected strains of  
diploid wheat, *Triticum monococcum* L. *Cereal  
Chem.*,70,1993,p.298-303.
- D’Egidio,M.G.-Vallega,V.: Bread baking and  
dough mixing quality of diploid wheat,  
*Triticum monococcum* L. *Italian Food and  
Beverage Technology IV*,20,1994,p.6-8.
- Diamante,L.M.-Munro,P.A.: Mathematical  
modelling of the thin layer solar drying of  
sweet potato slices. *Solar  
Energy*,51(4),1993,p.271-276.
- Dreher,M.L.: Dietary fiber overview. In S.  
Sungsoo (Ed.), *Handbook of dietary fiber*,2001  
p. 21-36,New York,USA: Marcel Dekker Inc.
- Gupta,R.K.-Das,S.K.: Physical Properties of  
Sunflower Seeds. *J. Agr. Eng. Res.*  
66,1997,p.1 -8.
- Henderson,S.M.: Progress in developing the thin-  
layer drying equation. *Transactions of the  
ASAE*,17,1974,p.1167-1168/1172.
- Hidalgo,A.-Brandolini,A.-Pompei,C.-  
Piscozzi,R.: Carotenoids and tocopherols of einkorn  
wheat (*Triticum monococcum* ssp *monococcum*  
L.). *J. Cereal Science*,44,2006,p.182-193.
- Løje,H.-Møller,B.-Laustsen,A.M.-Hansen,Å.:  
Chemical composition, functional properties  
and sensory profiling of einkorn (*Triticum  
monococcum* L.). *J. Cereal  
Science*,37,2003,p.231-240.
- Matuz,J.-Bartok,T.-Morocz-Salamon,K.-  
Bona,L.: Structure and potential allergenic  
character of cereal proteins. I. Protein content  
and amino acid composition. *Cereal Res.  
Commun.*, 28,2000,p.263-270.
- Midilli,A.-Kucuk,H.-Yapar,Z.: A new model for  
single-layer drying. *Drying Technology*,  
20(7),2002,p.1503-1513.
- Mohapatra,D.-Rao,P.S.: A thin layer drying  
model of parboiled wheat. *Journal of Food  
Engineering*,66,2005,p.513-518.
- Nesbitt,M.-Samuel,D.: From staple crop to  
extinction? The archaeology and history of the  
hulled wheats. In: Padulosi, S., Hammer, K.,  
Heller, J. (Eds.), *Hulled Wheats. Proceedings of  
the First International Workshop on Hulled  
Wheats*. Castelveccchio Pascoli, Tuscany,  
Italy,1996,p.41-100.
- Ozdemir,M.-Devres,Y.O.: The thin layer drying  
characteristics of hazelnuts during roasting.  
*Journal of Food Engineering*,42(4),1999,p.225-  
233.
- Perrino,P.-Hammer,K.: The Farro: further  
information on its cultivation in Italy,  
utilization, and conservation. *Genetica  
Agraria*,38,1984,p.303-311.

- Trocchi, A.-Codianni, P.: Appropriate seeding rate for einkorn, emmer, and spelt grown under rainfed condition in southern Italy. *Europ. J. Agronomy*, 22, 2005, p. 293-300.
- Yagcioglu, A.-Degirmencioglu, A.-Cagatay, F.: Drying characteristics of laurel leaves under different drying conditions. In *Proceedings of the 7th International Congress on Agricultural Mechanization and Energy*, 1999, p. 565-569, 26-27 May, Adana, Turkey.
- Yaldiz, O.-Ertekin, C.: Thin layer solar drying some different vegetables. *Drying Technology*, 19(3), 2001, p. 583-596.
- Vallega, V.: Field performance of varieties of *Triticum monococcum*, *T. durum* and *Hordeum vulgare* grown at two locations. *Genetic Agriculture*, 33, 1979, p. 363-370.
- Vallega, V.: Agronomic performance and breeding value of selected strains of diploid wheat, *Triticum monococcum*. *Euphytica*, 61, 1992, p. 13-23.

## YIELDS AND HARVEST LOSSES OF SUGAR-BEET VARIETIES IN THE YEARS 2008 AND 2009

PETR ŠAŘEC\*, ONDŘEJ ŠAŘEC

Czech University of Life Sciences Prague, 165 21 Prague 6– Suchbátka, Czech Republic

Phone: +4202-24383147, Fax: +4202-24383155, E-mail: psarec@tf.czu.cz

### Abstract

For several years already, field trials on harvest losses of various sugar-beet varieties have taken place in Agro Slatiny. Each year with approximately 35 sugar-beet varieties, the following items have been measured and calculated: biological yield, plant number per 1 m<sup>2</sup>, sugar content of beets, real yield harvested by HOLMER Terra Dos, polarization sugar yield, losses connected with not dug up beets and with beets left in the field and total losses. This paper discusses the results from the years 2008 and 2009. The weather in the year 2008 was remarkable by substantially warm and dry spring, further weather development was favorable in terms of sugar beet growing and harvest. The year 2009 displayed high temperatures in April. Afterwards, the weather varied frequently. The end of June and of July was abundant in precipitations. In 2008, total harvest losses ranged in general from 0.68 (Imperial) to 4.10 % (Noricum) and exceptionally reached on top 5.06 % (Caruso). The harvest losses in 2009 were slightly higher, with their top value 7.55 % (Katka) and second highest 5.47 % (Vedeta). The other varieties' harvest losses ranged around 2 %. The variety Noricum attained the highest biological yield (171.8 t.ha<sup>-1</sup>) in 2008. The highest yield at 16% sugar reached by mechanized harvest was produced by the variety Esperanza (121.50 t.ha<sup>-1</sup>). In the year 2009, the highest yield at 16% sugar was attained by the variety SR-141 (Golem) (137,11 t.ha<sup>-1</sup>), and again the variety Esperanza (134,13 t.ha<sup>-1</sup>). The variety Canyon demonstrated the highest biological yield (120.6 t.ha<sup>-1</sup>).

**Key words:** sugar beet, variety, harvest losses, soil moisture, biological yield, plant number per m<sup>2</sup>

### Introduction

The field trials focused on harvest losses of various sugar beet varieties have been established at Agro Slatiny in the Czech Republic each year since 1994. Generally, more than 30 varieties are tested each year. Composition of the varieties changes from year to year considerably due to a high number of newly introduced ones. Mechanized harvest has been always done employing a six-row harvester by Holmer. In the year 2005, a new type of harvester, i.e. Holmer Terra Dos, was used for the first time. The field speed of the harvester thus increased to up to 9 to 10 km.hour<sup>-1</sup> according to soil moisture and sugar beet yield. For all the varieties, the following variables are measured or calculated: biological yield, plant number per 1 m<sup>2</sup>, sugar content of beets, real yield harvested by HOLMER Terra Dos, polarization sugar yield, losses connected with not dug up beets and with beets left on the surface of the field and total losses. Harvester bunker is emptied into tractor trailers during harvester's turns at both headlands. The trailers commute between a field and a disposal site

where they are weighed prior emptying. During harvest in a field, harvest losses due to not-dug-up beets and due to beets left on the surface of a field are measured. The sum of the both of them returns total harvest losses. Further on, assessment of beets harvested mechanically is done with respect to quality of cutting, degree of beet damage and gross to net weight ratio.

### Material and Methods

All the varieties are sown, fertilized, sprayed and harvested in the same manner. A twelve-row drilling machine BECKER is used for sowing, a six-row sugar beet harvester Holmer Terra Dos is used for mechanized harvest. One variety takes most often a plot of 24-row width depending on the field size and shape. Individual plots are located side by side in the same field and growing technology is invariable for all the varieties within a year.

When evaluating harvest, biological yield of beets is measured first. In the same time, number of plants per 1 m<sup>2</sup> is measured as well. A rectangle of 10 m<sup>2</sup> is demarked. If there is a row spacing of 0.45 m, the rectangle takes six rows of

3.7 m length. Beets are dug up manually, then cleaned and counted, and beet leaves are cut off. Harvested beets and leaves are then weighed separately.

Evaluation of harvest losses, i.e. losses due to not-dug-up beets and due to beets left on the surface of a field, is carried out straight after the mechanized harvest. A rectangle of 10 m<sup>2</sup> is demarked again. Firstly, all beet material from the surface is collected, and then all beet remains are dug up from topsoil to the depth of 0.25 m. Both fractions are weighed and total losses enumerated as their sum. Measurements are repeated five times. Beet yield of mechanized harvest is determined by weighing the tractor trailers. Values found are converted to weight units per one hectare. Additionally, measurements of soil moisture and soil penetration resistance are done.

When evaluating sugar beet variety results, it is important to take into account not only beet yields (BY), but as well sugar content (SC). Beet yield at 16% sugar (CBY, see Eq. (1)) covers both above mentioned outputs and thus gives better possibility for comparing varieties. Moreover, higher sugar content requires less material handling relatively to sugar gained.

$$CBY = \frac{BY \cdot (SC - 3)}{13} [t \cdot ha^{-1}] \quad (1)$$

## Results and Discussion

### *Harvest Conditions in the Years 2008 and 2009*

Harvest conditions, e.g. soil moisture, soil compaction, belongs to the key factors influencing the extent of harvest losses. Therefore, the above mentioned variables are measured each year and Table 1 shows their values. During harvest in both years in question, soil moisture reached rather high values. The field speed of the harvester Holmer Terra Dos reached from 9 to up to 10 km.hour<sup>-1</sup> in both years in question.

### *Harvest Yields in the years 2008 and 2009*

Table 2 shows that the best results of the year 2008 in terms of mechanized harvest yield combined with sugar content were reached by the varieties Esperanza and Scorpion. From the same point of view, i.e. from the point of view of beet yield at 16% sugar, the varieties Modex and Mondial proved the worst. In general, sugar content was in the year 2008, and some varieties surpassed even 20 %.

Table 1 – Soil moisture and soil penetration resistance during the sugar-beet harvest in the years 2008 and 2009

Measurement Depth [m]	Soil Specific Moisture [%]						Penetration Resistance [MPa]		
	Beet Row		Harvester Track		Headlands		Beet Row	Harvester Track	Headlands
	2008	2009	2008	2009	2008	2009			
< 0.01	24.4	25.8	24.3	25.9	26.9	27.3	0.42-1.92	0.60-1.74	0.84-2.10
0.01 – 0.02	24.6	25.9	24.9	25.1	26.4	27.5	3.42-4.86	2.42-3.88	3.08-4.76
0.02 – 0.03	25.1	25.3	25.3	24.5	25.8	25.2	5.54-7.18	4.44-6.94	5.76-8.36

Table 2 – Yields and other indicators of sugar beet variety trials of manual and mechanized harvest in the year 2008

Variety	Plant Number [10 <sup>3</sup> .ha <sup>-1</sup> ]	Manual Harvest		Mechanized Harvest				Rating According to Yield at 16% Sugar
		Beet Yield [t.ha <sup>-1</sup> ]	Beet Leave Yield [t.ha <sup>-1</sup> ]	Beet Yield [t.ha <sup>-1</sup> ]	Sugar Content [%]	Polarized Sugar Yield [t.ha <sup>-1</sup> ]	Beet Yield at 16% Sugar [t.ha <sup>-1</sup> ]	
Antilla	105	135.2	69.0	87.57	20.00	17.51	114.51	7
Bellini	95	98.6	43.0	88.26	19.80	17.48	114.06	9
Britannia	112	131.0	126.0	87.18	19.43	16.94	110.18	16
Canyon	114	112.4	80.0	88.52	19.41	17.18	111.74	12
Caruso	109	127.6	82.0	89.73	19.59	17.58	114.51	8
DEL 636	97	114.6	66.6	80.44	20.71	16.66	109.58	19
Esperanza	110	130.0	85.2	95.44	19.55	18.66	121.50	1
Felicita	112	120.0	82.0	81.39	20.08	16.34	106.93	23
Festina	109	140.0	94.0	95.54	18.74	17.90	115.68	5
HI 0337 (Helita)	102	124.0	65.0	84.87	19.88	16.87	110.20	15
Imperial	93	62.0	35.6	85.91	19.72	16.94	110.49	14
Julietta	106	117.2	56.0	87.14	19.20	16.73	108.59	21
Lucata	103	95.6	68.8	88.97	18.45	16.41	105.74	25
Marietta	94	133.2	73.8	88.07	19.26	16.96	110.16	17
Merak	103	128.4	88.0	82.20	19.75	16.23	105.91	24
Modex	95	145.6	120.0	77.91	19.46	15.16	98.65	29
Mondial	95	70.0	42.0	81.81	19.10	15.63	101.32	28
Monza	109	140.6	62.0	88.28	19.16	16.91	109.74	18
Nancy	102	94.4	52.0	85.91	19.31	16.59	107.78	22
Noricum	115	171.8	112.0	90.71	18.94	17.18	111.22	13
Pohoda	103	130.0	82.2	89.04	19.57	17.43	113.49	10
Python	98	107.6	5.7	94.33	19.21	18.12	117.62	4
Scorpion	98	100.4	65.4	95.45	19.19	18.32	118.87	2
SD13606	114	163.2	110.0	87.12	20.24	17.63	115.53	6
Silvetta	99	104.4	60.8	86.12	20.10	17.31	113.28	11
SR-73 (Integral)	101	87.2	43.2	88.44	20.37	18.02	118.17	3
SR-74 (Predator)	105	108.0	42.0	77.41	20.02	15.50	101.35	27
Taifun	114	138.0	98.0	78.82	19.80	15.61	101.86	26
Victor	114	158.0	108.0	83.09	20.08	16.68	109.17	20
<b>Average</b>	<b>104.3</b>	<b>120.3</b>	<b>73.0</b>	<b>86.75</b>	<b>19.59</b>	<b>16.98</b>	<b>110.62</b>	

The relative differences between manual and mechanized harvest yields varied considerably, and was also high, i.e. 24.1 % in average. Generally, the bigger the difference between manual and mechanized harvest, the less suitable a variety is for mechanized harvest by a beet harvester. In the year 2008 in Agro Slatiny, the average sugar content reached the highest value, i.e. 19.59 %, since the beginning of trials at 1994. Sugar content of some of the varieties surpassed even 20 %.

In the following year 2009 (Table 3) in terms of beet yield at 16% sugar, SR-141 (Golem) and again Esperanza varieties attained the best results. Though Canyon variety

produced the highest beet yield harvested by Holmer harvester, due to its low sugar content it ended merely seventh. On the other hand, Taifun and Katka varieties showed the lowest results in this respect.

The relative differences in beet yields between manual and mechanized harvest ended low that year, i.e. 5.8 % in average. Generally, the differences between manual and mechanized harvest yields of successful varieties ranged below or around the average one, whereas varieties having showed worst results demonstrated as well higher than average differences. The sugar content demonstrated again good values with an average of 18.7 %.

Table 3 – Yields and other indicators of sugar beet variety trials of manual and mechanized harvest



in the year 2009

Variety	Plant Number [10 <sup>3</sup> .ha <sup>-1</sup> ]	Manual Harvest		Mechanized Harvest				Rating According to Yield at 16% Sugar
		Beet Yield [t.ha <sup>-1</sup> ]	Beet Leave Yield [t.ha <sup>-1</sup> ]	Beet Yield [t.ha <sup>-1</sup> ]	Sugar Content [%]	Polarized Sugar Yield [t.ha <sup>-1</sup> ]	Beet Yield at 16% Sugar [t.ha <sup>-1</sup> ]	
Antilla	93.0	113.4	38.0	96.90	18.81	18.23	117.85	19
Bellini	98.5	107.6	38.0	102.30	18.27	18.69	120.16	16
Britannia	95.0	104.0	40.4	98.50	18.59	18.31	118.12	18
Canyon	88.5	120.6	53.0	114.00	17.62	20.09	128.21	7
DS 4172	88.0	108.0	23.2	100.80	17.89	18.03	115.45	21
DS 8040	99.0	109.0	37.2	94.90	18.41	17.47	112.49	25
Esperanza	81.0	116.0	35.0	112.50	18.50	20.81	134.13	2
Halina	94.3	97.6	39.2	89.50	19.10	17.09	110.84	28
HI 0337 (Helita)	102.0	108.0	54.0	101.80	18.82	19.16	123.88	12
Imperial	86.0	112.0	34.0	103.40	19.69	20.36	132.75	5
Julietta	61.0	103.4	29.8	97.70	18.14	17.72	113.78	22
Katka	78.5	112.6	53.2	89.40	18.74	16.75	108.24	31
Kiringa	95.0	114.0	48.6	106.00	18.84	19.97	129.16	6
Laska	84.5	104.0	35.6	100.00	18.96	18.96	122.77	13
Limonica	78.0	108.0	59.4	93.70	18.58	17.41	112.30	26
Lucata	64.0	105.0	58.6	110.90	17.98	19.94	127.79	8
Marietta	90.5	99.2	3.5	104.40	18.70	19.52	126.08	10
Merak	83.5	106.4	32.8	95.10	18.88	17.95	116.17	20
MK 3702 (Debut)	66.9	109.4	33.2	97.10	18.14	17.61	113.08	24
MK 3804	92.0	102.0	40.0	98.80	17.52	17.31	110.35	29
Mondial	101.0	103.2	3.6	92.70	18.72	17.35	112.10	27
Monza	72.0	102.6	45.0	100.60	17.67	17.78	113.52	23
Nancy	83.0	109.2	37.0	100.70	17.09	17.21	109.14	30
Pavla	95.0	109.0	40.0	102.30	19.00	19.44	125.91	11
Pohoda	91.0	117.6	45.2	113.90	18.30	20.84	134.05	3
Python	84.5	116.0	2.4	113.40	18.34	20.80	133.81	4
SD12837	84.0	101.2	41.4	99.40	18.62	18.51	119.43	17
Severa	88.0	105.8	26.0	101.80	19.16	19.50	126.55	9
SR-141 (Golem)	85.5	107.0	40.6	107.70	19.55	21.06	137.11	1
Taifun	92.5	98.2	30.0	91.90	18.30	16.82	108.16	32
Vedeta	91.5	94.2	21.2	95.90	19.32	18.53	120.39	15
Victor	94.0	105.0	38.0	100.00	18.88	18.88	122.15	14
<b>Average</b>	<b>86.9</b>	<b>107.2</b>	<b>36.2</b>	<b>100.88</b>	<b>18.54</b>	<b>18.69</b>	<b>120.50</b>	

#### Harvest Losses in the years 2008 and 2009

Table 4 shows harvest losses in the years 2008 and 2009. For all the varieties, particularly in the year 2008, the harvest losses were favourable compared to previous years of trials (Šařec, P., Šařec, O., Dobek, T., 2008). Higher soil moisture in the year 2009 did not enable to show again the good result of the previous year. Average total harvest losses, i.e. sum of losses incurred due to not-dug-up beets and beets left

on the surface of the field, were 2.15 % in the year 2008 and 2.71 % in the year 2009. In the year 2008, Imperial (0.68 %) and Esperanza (0.94 %) attained the lowest total losses, whereas Caruso (5.06 %) and Noricum (4.10) demonstrated the highest ones. In the year 2009, Imperial's (0.85 %) and Halina's (1.19 %) total losses were the lowest ones, and on the opposite Katka's (7.55 %) and Vedeta's (5.47 %) the highest ones.

Table 4 – Harvest losses of sugar beet variety trials in the years 2008 and 2009

Year 2008					Year 2009				
Variety	Harvest Losses [%]			Rating by Total Losses	Variety	Harvest Losses [%]			Rating by Total Losses
	Not Dug up Beets	Beets Left on Surface	Total			Not Dug up Beets	Beets Left on Surface	Total	
Antilla	0.80	0.32	1.12	5	Antilla	0.85	0.46	1.31	4
Bellini	0.36	0.60	0.96	3-4	Bellini	2.34	0.43	2.77	23
Britannia	0.80	0.54	1.34	7	Britannia	3.46	1.19	4.65	29
Canyon	0.65	2.00	2.65	22	Canyon	2.26	2.16	4.42	28
Caruso	3.24	1.82	5.06	29	DS 4172	0.89	0.91	1.80	11
DEL 636	0.66	1.04	1.70	10-11	DS 8040	3.85	1.38	5.23	30
Esperanza	0.12	0.82	0.94	2	Esperanza	0.70	0.71	1.41	5
Felicita	0.84	0.76	1.60	8	Halina	0.55	0.64	1.19	2
Festina	1.52	0.98	2.50	21	HI 0337 (Helita)	0.89	1.35	2.24	16
HI 0337 (Helita)	0.96	0.98	1.94	15	Imperial	0.64	0.21	0.85	1
Imperial	0.20	0.48	0.68	1	Julietta	2.03	1.39	3.42	24
Julietta	1.16	1.24	2.40	20	Katka	5.06	2.49	7.55	32
Lucata	0.60	1.32	1.92	14	Kiringa	0.79	0.70	1.49	6
Marietta	0.96	0.92	1.88	13	Laska	1.15	1.38	2.53	21
Merak	2.04	0.92	2.96	25	Limonica	1.67	0.59	2.26	17
Modex	0.86	2.70	3.56	27	Lucata	2.02	0.42	2.44	19
Mondial	0.90	1.80	2.70	23	Marietta	1.35	2.78	4.13	27
Monza	1.26	0.42	1.68	9	Merak	1.80	0.26	2.06	13
Nancy	2.90	0.60	3.50	26	MK 3702 (Debut)	0.66	1.41	2.07	14
Noricum	0.96	3.14	4.10	28	MK 3804	1.65	0.39	2.04	12
Pohoda	1.08	1.05	2.13	16	Mondial	1.32	1.34	2.66	22
Python	1.34	0.90	2.24	19	Monza	2.05	1.66	3.71	25
Scorpion	0.24	0.92	1.16	6	Nancy	0.62	0.58	1.20	3
SD13606	1.56	0.60	2.16	17	Pavla	1.10	1.23	2.33	18
Silveta	0.35	1.48	1.83	12	Pohoda	0.87	0.78	1.65	8
SR-73 (Integral)	0.74	0.96	1.70	10-11	Python	0.83	0.76	1.59	7
SR-74 (Predator)	1.86	0.96	2.82	24	SD12837	1.82	0.36	2.18	15
Taifun	0.66	1.54	2.20	18	Severa	0.87	0.81	1.68	9
Victor	0.06	0.90	0.96	3-4	SR-141 (Golem)	0.73	0.99	1.72	10
					Taifun	1.85	0.65	2.50	20
					Vedeta	3.80	1.67	5.47	31
					Victor	3.00	1.05	4.05	26
<b>Average</b>	<b>1.02</b>	<b>1.13</b>	<b>2.15</b>			<b>1.67</b>	<b>1.04</b>	<b>2.71</b>	

## Conclusions

The year 2008 was exceptionally favorable for sugar beet growing in terms of moisture and temperature. The highest yield gained by manual harvest was reached by the variety Noricum (171.8 t.ha<sup>-1</sup>). The highest polarized sugar yield and yield at 16% sugar were demonstrated by the varieties Esperanza and Scorpion. On the other hand the varieties Modex and Mondial showed the lowest yields. The highest relative differences between manual and mechanized harvest yields were demonstrated by the varieties Victor, Noricum and SD13606. Number of plants per 1 m<sup>2</sup> may be one of the factors influencing

the extent of the difference, since longer distance between plants in a row may have adverse impact on the work of cutting and lifting mechanisms.

The year 2009 was also favorable for sugar beet growing in terms of moisture and temperature. The highest yield gained by manual harvest was reached by the variety Canyon (120.6 t.ha<sup>-1</sup>). The highest polarized sugar yield and yield at 16% sugar were demonstrated by the varieties SR-141 (Golem), Esperanza and Pohoda. On the other hand the varieties Taifun and Katka showed the lowest yields. The highest

relative differences between manual and mechanized harvest yields were demonstrated by the varieties Katka, Antilla and Limonica.

There were 19 varieties each year that were tested repeatedly in both years in question (Fig. 1). Esperanza and Python varieties proved best results in terms of yield and sugar content in

both years in question, i.e. attained beet yield at 16% sugar 127.82 t.ha<sup>-1</sup>, respectively 125.72 t.ha<sup>-1</sup>. Average beet yields at 16% sugar of Taifun (105.01 t.ha<sup>-1</sup>), Mondial (106.71 t.ha<sup>-1</sup>) or Nancy (108.46 t.ha<sup>-1</sup>) varieties were on the other hand the lowest.

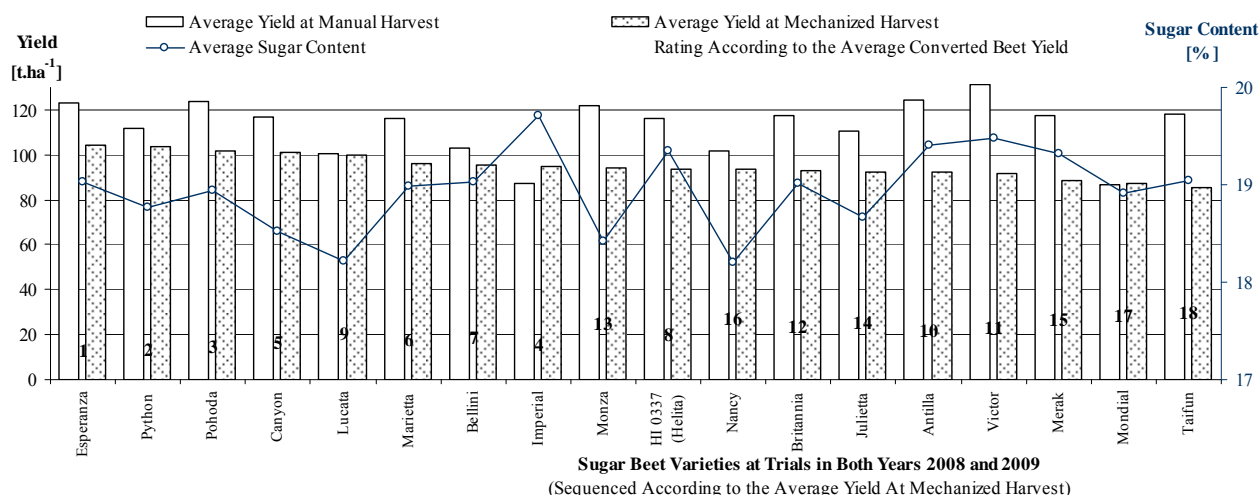


Fig. 1 – Graph of sugar beet yields at manual and mechanized harvest, and sugar content for the varieties having occurred in both years 2008 and 2009

In 2008, varieties Imperial (0.68 %) and Esperanza (0.94 %) attained the lowest total harvest losses, whereas varieties Caruso (5.06 %) and Noricum (4.10) demonstrated the highest ones. The variety Imperial (0.85 %) reached the lowest harvest losses as well in 2009, followed by Halina (1.19 %). Katka (7.55 %) and Vedeta (5.47 %) on the opposite showed the highest harvest losses. The outcomes imply that using suitable and good quality harvest equipment results in relatively low harvest losses even at higher soil moisture

*This work was supported by Research Project of the Ministry of Education of the CR no. MSM 6046070905, and by the project NAZV QH72257.*

## References

- [1] Šařec, P. – Šařec, O. – Przybyl, J. – Srb, K.: Yields and Harvest losses of sugar-beet varieties in the years 2005 and 2006. In Trends in Agricultural Engineering 2007, Praha: Czech University of Life Sciences Prague. Faculty of Engineering, 2007. s. 422-427. ISBN 978-80-213-1668-3.
- [2] Šařec, P. – Šařec, O. – Dobek, T.: Straty plonu podczas zbioru różnych odmian buraka cukrowego. Inżynieria Rolnicza, 2008, vol. 100, no. 2, s. 239-245. ISSN 1429-7264.
- [3] Šařec, P. – Šařec, O. – Przybyl, J. – Srb, K.: Porovnání sklizečů cukrovky. Listy cukrovarnické a řepářské, 2009, vol. 125, no. 7/8, s. 212-216. ISSN 1210-3306.
- [4] Šařec, P. – Šařec, O. – Srb, K. – Dobek, T. K.: Ocena plonów i strat przy zbiorze korzeni buraka cukrowego w latach 2005-2007. Inżynieria Rolnicza, 2009, vol. 110, no. 1, s. 281-288. ISSN 1429-7264.
- [5] Srb, K. – Šařec, P. – Šařec, O. – Dobek, T.: Výnosy a sklizňové ztráty odrůd cukrové řepy v roce 2008. In New trends in Design and Utilisation of Machines in Agriculture, Landscape Maintenance and Environment Protection, Prague, 5 – 7 May 2009, Praha: Česká zemědělská univerzita v Praze, 2009. s. 249-254. ISBN 978-80-213-1897-7.

## VARIETY TRIALS OF MAIZE FOR GRAIN IN THE YEARS 2008 AND 2009

PETR ŠAŘEC<sup>1\*</sup>, ONDŘEJ ŠAŘEC<sup>1</sup>, MAREK RYNKIEWICZ<sup>2</sup>

<sup>1</sup>Czech University of Life Sciences Prague, 165 21 Prague 6– Suchbátka, Czech Republic

Phone: +4202-24383147, Fax: +4202-24383155, E-mail: psarec@tf.czu.cz

<sup>2</sup>West Pomeranian University of Technology, Szczecin, Poland

### Abstract

In the years 2008 and 2009, field trials focused on maize varieties for grain took place at two agricultural businesses, i.e. at ZD Senice na Hané and at Agro Saltiny a.s. When comparing yields at 14% moisture, varieties Kaifus, KWS 2376 and Kladdus ended among the firsts repeatedly. Concerning the varieties with lower FAO, the same can be stated about varieties Zidane, Podium and Ronaldinio. Aggregate yield averages between both agricultural businesses differed statistically significantly in all the cases. This suggests that the maize is well capable of taking advantage of good climatic conditions of a lower situated region where ZD Senice na Hané is located.

**Key words:** grain maize, variety, field trials, yield, FAO

### Introduction

In the Czech Republic, maize is grown in all of its production areas, at all soil types, and using various soil cultivation technologies. Maize is a crop that ensures maximum nutrient production per area unit for prevalent production conditions of the Czech Republic. Hereat, it is still possible to increase its yield potential, as can be seen from the use of new hybrids intended chiefly for biogas stations. Furthermore, the yield potential can be improved by growing GMO maize. This increase in yield potential means also to adhere to a precise cultivation technology with the use of corresponding hybrids. While in the case of selection of a hybrid and of a cultivation technology, nutrient formation is decided upon, then the way of harvest and conservation are decisive in terms of reduction of energetic component losses. Energy in maize silage is generated mainly by starch, next by the content of soluble and digestible components of structural polysaccharides presentable and chemically specifiable as the content of hemicelluloses. The content of pentose is more marginal as well as the content of N-substances.

From the point of view of maize *stand establishment*, it is clear that ploughing is still widely used. Long-time experience shows that no technology of soil cultivation should be left out or prioritized, because each has its pros and cons. The most important is always the way of implementation of a chosen technology. Especially farmers producing in prone fields

must give an increased attention to agronomical practices, because there is a higher erosion danger with nutrient downwash related to it than on the flat.

*Soil preparation* influences water and air in soil to a great extent. That is why in arid areas, there is a rule to move the soil as little as possible, and to sow at earlier dates and with appropriately set sowing depth. In humid areas and on heavier soils, the limiting factor for maize is the content of air in soil. Soil compaction is another adverse factor, primarily at headlands and at entries to fields.

*Sowing date* depends mostly on maturity and temperature of soil that should be at least 8 °C at the sowing depth. But whether to quicken or postpone the sowing at existing conditions rests upon the farmer, and his feeling. The use of precision seeders is an important prerequisite for quality crop stand establishment. In majority of cases, optimum sowing depth ranges from 4 to 6 cm. In very dry and warm spring, the sowing depth could be increased to up to 10 cm.

*Optimum plant density* presents a significant measure leading to better exploitation of yield potential of a given hybrid, and to stabilization of yield. Sedláček (2008) observed influence of sowing density on yield reached of selected hybrids with FAO 200-250. Experiments took place at 200 to 420 m above sea level, and were harvested and evaluated both for silage and for grain. All of the hybrids tested for silage demonstrated higher dry mass yield

when the sowing density increased from 88,900 to 102,600 plants per hectare while quality parameters of silage remained unchanged. The same hybrids harvested for grain showed in the same way increase in grain yield by 0.15 (Salgado) to 2.52 t.ha<sup>-1</sup> (Zidane). When evaluating the experiments of higher plant density of maize harvested for grain as well as for silage, it can be concluded that for good standpoints and standard climatic conditions, higher yields of dry mass as well as of grain are reached while quality parameters remain unaffected. In many cases of harvest for grain, stands with higher density demonstrated also decrease of grain moisture (often by 1.5 to 2 %).

Concerning *plant nutrition and fertilization*, maize draws off 380 to 450 kg of pure nutrients from one hectare when cultivated intensively (Prokeš, 2008). Those should be returned to soil. The beginning of maize vegetation is characteristic by its very slow growth and low nutrient take-off. During the period prior to milk ripeness, maize needs high quantity of nitrogen, later on of phosphorus, and mainly of potash.

Regarding *protection against weeds and pests*, pre-emergence application of herbicides with water quantity ranging from 300 to 400 l.ha<sup>-1</sup> should be perceived as a basic maize protection against weeds. Company KWS SAAT signals time of insecticide application against European corn borer to its customers. It stems from aggregate temperatures which a corn borer needs to its development, and from invasion monitoring straight in maize stands (egg monitoring).

When *harvesting maize for silage*, optimum silage ripeness could be characterized as such development stage that ensures the highest feeding value. The development stage is strongly influenced by the hybrid type. Optimum feeding value is reached when the following conditions are fulfilled:

- starch deposition into grain is finished;
- the rest of the mass is in good health and attains 22 to 24 % of dry matter.

Harvest is carried out by a forage harvester equipped with a maize header.

When *harvesting maize for grain*, harvest time is often delayed for the sake of grain moisture reduction and of the related production profitability enhancement. The postponement stems from sometime vain expectation that the

grain gets drier. Big difference between the grains harvested on time and behind time remains in extent of mould in corn cob, and in subsequent content of mykotoxins. Timely sowing, eventually emergence positively influences grain moisture. Harvest of corn for grain is carried out by a combine harvester equipped by a corn header.

## Material and Methods

The trials are the common variety field trials of maize hybrids for grain carried out at two agricultural businesses, i.e. at ZD Senice na Hané and at Agro Slatiny a.s. All of the varieties in question were sown and harvested by the same machinery at both farms. Sowing was accomplished by a six row precision seeder Kinze, and harvest was done by a combine harvester Claas Lexion 540 equipped with a corn header. Within each year, the tested varieties were sown in one field on twelve-row wide trial plots, i.e. plots wide as two passes of the seeder and the harvester. In majority of fields, sowing of one selected variety was carried out repeatedly for the sake of yield control. The same cultivation technology was applied for all of the varieties grown in one field. During vegetation period, number of plants of individual varieties was measured five times. Yields during harvest were measured using a tensometric scale with accuracy below 1 kg. Grain moisture measurement was done at the same time.

## Results and Discussion

Yield control by sowing one control variety on several places of a field proved that the influence of trial plot location on yield was negligible. In all of the cases, there were only minimum differences in yields of a control variety (see Figure 1 and 2). Control yields varied the most at ZD Senice na Hané in 2009, nevertheless not more than by 4 % around the average.

Table 1 shows results of variety trials from ZD Senice na Hané in the years 2008 and 2009. In the first year, harvest took place in the 14<sup>th</sup> October 2008. Concerning early varieties with low FAO, Zidane and Podium reached high yields. Regarding the varieties with longer vegetation period, Kaifus and Kladdus varieties demonstrated excellent results (see Figure 1).

In the year 2009, harvest took place in the



13<sup>th</sup> October 2009. Concerning early varieties with low FAO, Podium, Ronaldinio and Zidane reached high yields. Regarding the varieties with longer vegetation period, KXA 6671 and KWS 2376 varieties demonstrated excellent results (see Figure 1).

Table 2 shows results of variety trials from Agro Slatiny a.s. in the years 2008 and 2009. In

the year 2008, harvest took place in the 3<sup>rd</sup> November. Concerning early varieties with low FAO, Zidane and Amoros reached high yields. Regarding the varieties with longer vegetation period, KXA 6372 Kamelias and KWS 2376 varieties demonstrated excellent results (see Figure 2).

Table 1 – Results of harvest of maize for grain from ZD Senice na Hané in the years 2008 and 2009

Hybrid	FAO	Moist Grain Yield [t.ha <sup>-1</sup> ]		Harvest moisture [%]		Yield at 14% moisture [t.ha <sup>-1</sup> ]		Sowing rate [10 <sup>3</sup> grains.ha <sup>-1</sup> ]	
		2008	2009	2008	2009	2008	2009	2008	2009
Ambrosini	220/230	–	16.75	–	30.6	–	13.51	–	95
Amoroso	240/250	16.91	16.69	28.1	28.9	14.13	13.80	90	95
Graneros	270/260	15.33	–	30.6	–	12.37	–	90	-
Havane	330/330	17.55	–	29.1	–	14.47	–	88	-
Chambord-average	300/300	15.29	–	30.5	–	12.36	–	89	-
Kaifus	320/320	18.99	18.72	29.9	32.3	15.48	14.74	88	77
Kipous-average	280/290	–	14.99	–	30.9	–	12.04	–	89
Kladdus	310/300	18.35	18.19	29.3	31.4	15.08	14.51	90	77
Kuratus	270/280	16.40	15.99	31.6	31.0	13.04	12.75	88	89
Kvalitas YG	260/270	18.45	16.48	31.6	30.2	14.68	13.38	88	89
KWS 2376	340/340	18.40	18.99	30.9	30.0	14.78	15.45	88	77
KWS 5133 Eco	250/250	15.09	17.81	30.7	31.6	12.16	14.17	90	89
Podium	210/210	17.92	16.80	28.1	28.6	14.98	13.95	90	95
Ronaldinio	240/250	18.00	17.60	31.1	32.1	14.42	13.90	90	95
Salgado	200/210	16.85	14.56	29.2	29.7	13.87	11.90	90	95
Severo	260/270	–	17.04	–	31.0	–	13.67	–	89
Symbol	300/310	–	17.12	–	31.1	–	13.72	–	77
Zidane	240/240	18.37	17.23	29.1	30.8	15.15	13.86	89	95
Amadeo	220/230	17.81	16.61	31.1	29.1	14.27	13.70	90	95
Beatus	280/280	16.96	17.49	31.2	31.7	13.57	13.89	90	89
Bellevue	240/240	14.72	–	30.1	–	11.96	–	90	-
Karas YG	430/430	18.03	–	31.3	–	14.40	–	88	-
Kipous	280/290	16.53	–	31.5	–	13.17	–	90	-
Kosinus	240/240	16.24	–	29.0	–	13.41	–	90	-
Krabas	290/290	–	18.56	–	30.6	–	14.98	–	77
KXA 6471	330/320	–	19.09	–	30.2	–	15.50	–	77
<b>Total Average</b>		<b>17.07</b>	<b>17.20</b>	<b>30.1</b>	<b>30.6</b>	<b>13.68</b>	<b>13.69</b>	<b>89</b>	<b>87</b>



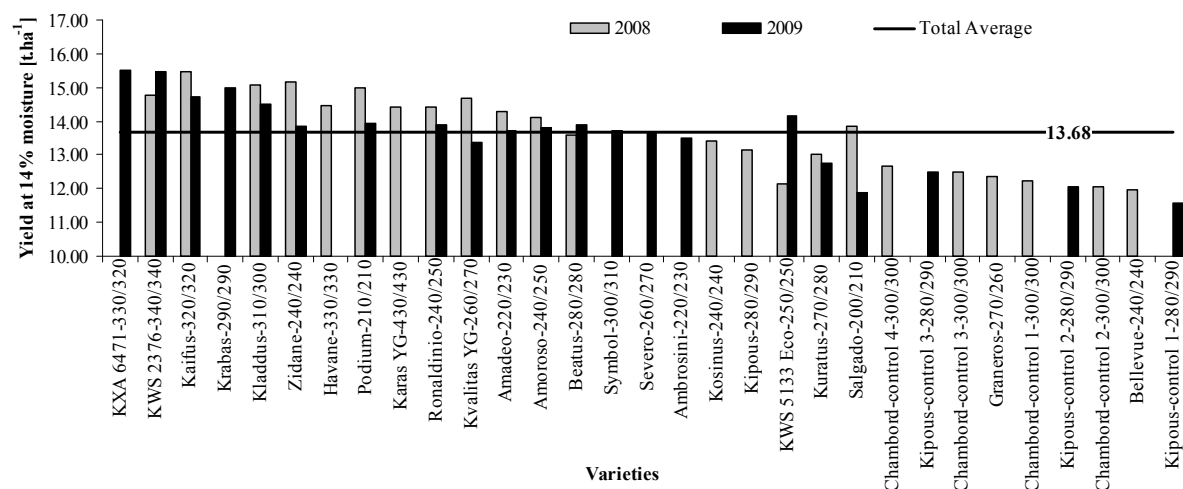


Fig. 1 – Graph of maize-for-grain yields at 14% moisture sequenced in descending order, and average yield of all the varieties at ZD Senice na Hané in the years 2008 and 2009

Table 2 – Results of harvest of maize for grain from Agro Slatiny a.s. in the years 2008 and 2009

Hybrid	FAO	Moist Grain Yield [t.ha <sup>-1</sup> ]		Harvest moisture [%]		Yield at 14% moisture [t.ha <sup>-1</sup> ]		Sowing rate [10 <sup>3</sup> grains.ha <sup>-1</sup> ]	
		2008	2009	2008	2009	2008	2009	2008	2009
Ambrosini	220/230	–	15.29	–	28.4	–	12.73	–	89
Amoroso	240/250	11.91	14.13	28.0	28.0	9.97	11.83	86	86
Atletico	290/300	–	13.08	–	31.8	–	10.37	–	80
Graneros	270/260	11.60	–	30.0	–	9.44	–	86	–
Havane	330/330	11.98	–	30.9	–	9.63	–	74	–
Chambord-average	300/300	11.05	–	28.9	–	10.12	–	90	–
Kaifus	320/320	–	15.13	–	30.3	–	12.26	–	76
Kipous-average	280/290	–	11.49	–	28.2	–	10.57	–	89
Kladdus	310/300	–	15.85	–	31.2	–	12.68	–	76
Koherens	260/250	–	13.42	–	29.0	–	11.08	–	86
Kuratus	270/280	11.72	–	32.0	–	9.27	–	86	–
Kvalitas YG	260/270	11.53	13.35	30.0	31.0	9.38	10.71	86	86
KWS 2376	340/340	13.99	–	31.2	–	11.19	–	74	–
KWS 5133 Eco	250/250	–	14.49	–	29.2	–	11.93	–	86
KXA 6336	260/Zea	11.94	–	29.5	–	9.79	–	86	–
KXA 6338 Symbol	300/310	12.78	–	31.0	–	10.25	–	86	–
KXA 6372 Kamelias	350/Z ml	14.93	–	32.7	–	11.68	–	74	–
Lacta	240/240	11.34	12.36	27.7	29.0	9.53	10.20	89	89
Podium	210/210	11.34	14.04	28.2	28.0	9.63	11.73	89	89
Ronaldinio	240/250	11.72	15.34	31.0	28.7	9.40	12.75	86	89
Salgado	200/210	–	12.89	–	27.5	–	10.87	–	89
Severo	260/270	–	13.82	–	30.7	–	11.14	–	86
Symbol	300/310	–	13.04	–	30.5	–	10.62	–	76
Touran	260/260	–	13.20	–	27.5	–	11.13	–	86
Zidane	240/240	12.44	14.42	29.0	28.8	10.27	11.94	86	89
<b>Total Average</b>		<b>12.16</b>	<b>13.84</b>	<b>30.0</b>	<b>29.3</b>	<b>9.98</b>	<b>11.40</b>	<b>84</b>	<b>85</b>

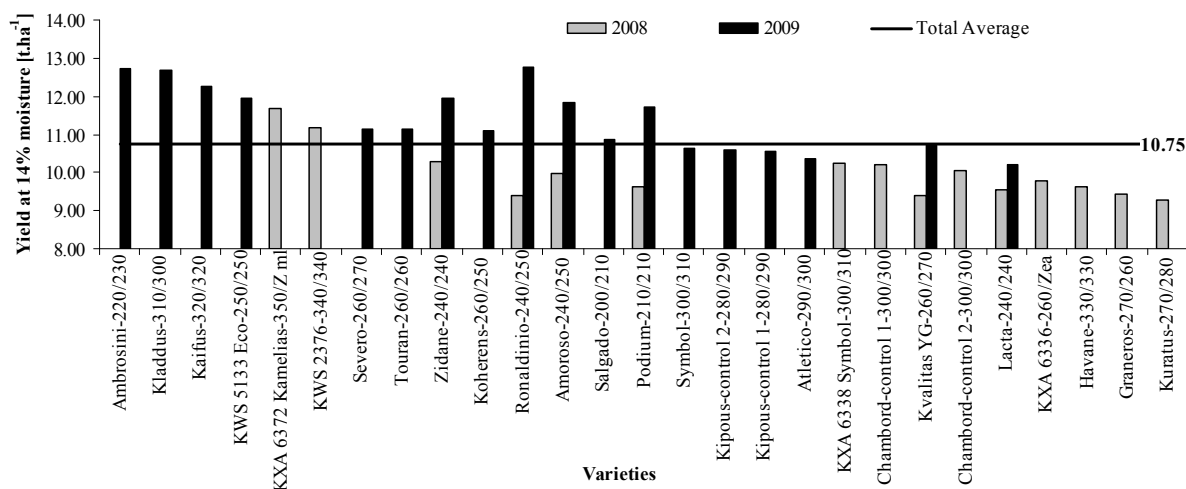


Fig. 2 – Graph of maize-for-grain yields at 14% moisture sequenced in descending order, and average yield of all the varieties at Agro Slatiny a.s. in the years 2008 and 2009

In the year 2009, harvest took place in the 29<sup>th</sup> October. Concerning early varieties with low FAO, Ronaldinio and Ambrosini reached high yields. Regarding the varieties with longer vegetation period, Kladdus and Kaifus varieties demonstrated excellent results (see Figure 2).

According to the Table 3, the varieties Kaifus, KWS 2376 and Kladdus repeatedly reached good results in the terms of yield at 14% moisture. Regarding the varieties with lower FAO, Zidane, Podium and Ronaldinio ended frequently among the firsts.

Table 3 – Rating of maize-for-grain varieties, which were sown repeatedly during the trials, according to the placement of their yields at 14% moisture within individual trial fields and years

Hybrid	FAO	Počet	Average placement
Kaifus	320/320	3	3.0
KWS 2376	340/340	3	3.0
Kladdus	310/300	3	3.7
Zidane	240/240	4	5.0
Podium	210/210	4	7.0
Ronaldinio	240/250	4	7.3
Havane	330/330	2	7.5
Ambrosini	220/230	2	8.5
Amoroso	240/250	4	8.8
KWS 5133 Eco	250/250	3	10.7
Beatus	280/280	2	11.0
Amadeo	220/230	2	11.5
Severo	260/270	2	11.5
Chambord	300/300	2	12.0
Kvalitas YG	260/270	4	12.0
Symbol	300/310	2	13.0
Salgado	200/210	3	14.3
Graneros	270/260	2	14.5
Kosinus	240/240	2	14.5
Lacta	240/240	2	14.5
Kuratus	270/280	3	16.0
Kipous	280/290	3	16.3

Table 4 – Results of Analysis of Variance with grouping criteria “Year” and “Agricultural Business”

regarding maize-for-grain average yields at 14% moisture

Grouping Criterion	F	p
Year	10.18	0.002083
Agricultural Business	178.32	0.000000
Year * Agricultural Business	9.76	0.002553

Table 5 – Results of Scheffé's tests of maize-for-grain average yields at 14% moisture with "Year" and "Agricultural Business" as grouping factors

Year	Agricultural Business	Group Average [t.ha <sup>-1</sup> ]	p		
			2008 ZD Senice na Hané	2008 Agro Slatiny a.s.	2009 ZD Senice na Hané
2008	ZD Senice na Hané	13.68	—	0.000000	0.999963
2008	Agro Slatiny a.s.	9.98	0.000000	—	0.000000
2009	ZD Senice na Hané	13.69	0.999963	0.000000	—
2009	Agro Slatiny a.s.	11.40	0.000000	0.001366	0.000000

Analysis of variance was employed in order to assess the differences among the average yields at 14% moisture. Trial year and agricultural business were the two grouping criteria.

Table 4 shows statistically significant differences in average yields at 14% moisture between both agricultural businesses, between both trial years, and finally also differences among the combinations of the both above mentioned groupings. Subsequent detailed analysis was carried out using Scheffé's method (see Table 5). There were statistically significant differences concerning average yields in all of the cases between both agricultural businesses, and also within Agro Slatiny a.s. between both trial years.

## Conclusions

The presented varietal field trials imply that the maize for grain can be grown practically everywhere in the climatic conditions of the Czech Republic. It is necessary to choose a suitable hybrid for given climatic conditions. The selection of an appropriate sowing rate is another matter, where increasing to some extent sowing rate boosts grain or silage material yield. Especially farmers producing in prone fields must give an increased attention to agronomical practices, because there is a higher erosion danger with nutrient downwash related to it than on the flat. On steeper slopes, it is advisable to sow the maize into freezing-out catch crop or

into some winter crop mixture. Beyond some minor exceptions, it is possible to state that maize returns higher yield in better climatic conditions, i.e. is able to take advantage of them (see Table 5). Within the field trials in question, the varieties Kaifus, KWS 2376 and Kladdus repeatedly reached good results in the terms of yield at 14% moisture. Regarding the varieties with lower FAO, Zidane, Podium and Ronaldinio ended frequently among the firsts. Application of organic fertilizers is convenient for maize nutrition.

*This work was supported by Research Project of the Ministry of Education of the CR no. MSM 6046070905, and by the project NAZV QH72257.*

## References

- [1] Prokeš, K.: Výživa kukuřice v podmínkách bramborářské výrobní oblasti. Disertační práce, MZLU Brno, 2008, 170 s.
- [2] Prokeš, K., Hlušek, J., Richter, R., Lošák, T.: Výživa kukuřice (*Zea mays*, L) v podmínkách bramborářské výrobní oblasti. Úroda, 2008
- [3] Sedláček, M.: KWS OSIVA s.r.o. Pod Hradbami 2004/5 Velké Meziříčí, ČR, 2004
- [4] Škarda, M.: Hospodaření s organickými hnojivy. SZN Praha, 1982, 324 s.

## TECHNOLOGICAL AND ECONOMIC PARAMETERS OF WINTER WHEAT PRODUCTION USING DIFFERENT SOIL CULTIVATION METHODS

PETR ŠAŘEC\*, ONDŘEJ ŠAŘEC, MILOŠ MALÝ

Czech University of Life Sciences Prague, 165 21 Prague 6– Suchbát, Czech Republic

Phone: +4202-24383147, Fax: +4202-24383155, E-mail: psarec@tf.czu.cz

### Abstract

Several years already, field monitoring and measurements focused on technological and economic comparison of conventional and reduced-tillage technologies of soil cultivation and drilling of winter wheat have been carried out in around 40 farm businesses located in all of the districts of the Czech Republic. The paper presents three-year results starting from the year 2006/07, where 119 fields were monitored. The collected data can be divided into two groups, i.e. the data measured that characterize plant and soil properties in each field and the data coming from observations and calculations that describe the field in question, all the operations carried, a pre-crop and its residue management, fertilizer and chemicals applications etc. The results were influenced by an uneven location of trial fields into the individual production areas. In general, reduced-tillage technologies prevailed. Conventional technology was more frequent only in potato production region. In each of the years in question, average wheat yield produced by the reduced-tillage technology slightly surpassed the yield of the conventional technology. Three-year average difference in yields amounted then to 4 %, i.e. to 0.28 t.ha<sup>-1</sup>. Over the three years, the highest yields were reached in beet production area, the lowest on the other hand in forage production area.

**Key words:** winter wheat, conventional technology, reduced tillage, costs, profit, fuel consumption, labor consumption

### Introduction

Long term field trials as well as farming experience in the Czech Republic show that cereals in general respond favourably to reduction of depth and intensity of tillage. For winter wheat production, reduced-tillage technology of soil cultivation and stand establishment are frequently employed. When choosing tillage technology, it is necessary to respect agricultural and ecological conditions. At large, the most suitable conditions for tillage depth and intensity reduction are on medium-textured soils with higher natural fertility in drier conditions of maize and beet production regions (Procházková, Dovrtěl, 2000; Procházková et al., 2000; Procházková et al., 2006; Horák L. et al., 2007).

Lately, the reduced-tillage technology is used also in the areas with poorer soil and climatic conditions. The results of long-term field trials and farming experience demonstrate the possibility to exploit this technology in potato production area (Humpolec), where the influence of various tillage intensities on yields of winter wheat grown after potatoes and red clovers was tested.

Reduced-tillage technology of soil cultivation

and winter wheat stand establishment are often applied to heavy-textured soils, where soil environment frequently impedes quality stand establishment using conventional soil cultivation technology including ploughing. In such case, reduced-tillage technology is practically the only way of stand establishment. Replacing ploughing with a shallow soil loosening followed by winter wheat sowing using no-till drills is a suitable alternative (Hůla, Procházková, et al., 2008).

### Material and Methods

During three production years from 2006/07 to 2008/09 at 42 farm businesses in all of the districts of the Czech Republic, field monitoring and measurements focused on different winter wheat production technologies from the viewpoint of conventional and reduced-tillage technologies were carried out. The total number amounted to 119 monitored fields.

The key aim of the work is to verify which technologies of winter wheat stand establishment are profitable.

The following items were monitored or measured:

- characteristics of individual fields (acreage, cadastre, preceding crop, plant residue treatment, year of last manure application ...),
- soil characteristics (bulk density, penetration resistance ...) - not analysed in this paper,
- crop stand characteristics - not analysed in this paper,
- data on every field operation performed (date, machinery used, its workrate, fuel consumption, age and purchasing price, material used, its application rate and price, and other supplementary information)

The latter enabled to calculate machinery and material costs. Subsequently, total costs of a field operation are the sum of the two above mentioned. The total costs could be as well increased due to possible manure application two or three years prior to the winter wheat. Accordingly, for the operations of manure and lime treatment of the winter wheat, only 40 % of the machinery and material costs are calculated in the first year. The total costs do not include costs of lease or ownership of land, and overhead costs.

## Results and Discussion

During three production years starting in 2006/07, trials were set up in 119 fields located in all of the districts of the Czech Republic. Reduced-tillage technology of winter wheat growing was employed in 81 cases, conventional in 38 cases, i.e. approximately two times less frequently. In each production year, the total average winter wheat yield gained from the trial fields exceeded the average of the Czech Republic by 27 to up to 37 %.

Prior to winter wheat sowing, manure was applied only in 2 out of 119 trial fields, i.e. in one field managed by reduced tillage and in one managed by conventional technology. Winter rape preceded winter wheat in more than 50 % of the trial fields. Concerning the quality types of winter wheat varieties, those of higher quality suitable for baking, i.e. class E and A, prevailed within both

technologies in question.

The most frequent tillage procedures within the reduced-tillage technology consisted of:

- twice stubble cultivation
- twice stubble cultivation + seedbed preparation

Within the conventional technology, the most frequent tillage procedures consisted of:

- stubble cultivation + ploughing + once or twice seedbed preparation
- ploughing + seedbed preparation
- stubble cultivation + ploughing

Disc cultivators prevailed within conventional technologies, whereas within the reduced-tillage technologies, where two stubble cultivations were common, tine cultivators were more frequent, particularly for the second cultivation.

Over the period of three production years, the average wheat yield of all 119 fields was 7.11 t.ha<sup>-1</sup>. Tab. 1 shows average wheat yields according to several criteria. Reduced-tillage technology reached yields exceeding slightly those attained by conventional technology in all of the production years in question. Concerning regionalization, the highest average yield demonstrated beet production area, followed by maize production area where only reduced-tillage technology was used. Forage production area, where reduced-tillage technology prevailed again, showed the less favourable. On the other hand, conventional technology prevailed in potato production area. Concerning organic fertilisers, if those were applied, which was the minority of cases (15 % only) generally within conventional technology, the average yield attained by 4.2 % lower value. With fertilizer application during winter wheat sowing, which was generally the case of reduced-tillage technology, the average yield exceeded the yield produced when no fertilizers were applied while sowing by 3.4 %. Relatively small frequencies and uneven distribution of cases in individual categories may have influenced the results.

Table 1 – Average winter wheat seed yields and frequencies of cases according to the tillage technology and other criteria over the whole monitored period

	Tillage Technology				Aggregate	
	Reduced		Conventional		Yield [t.ha <sup>-1</sup> ]	Frequency
	Yield [t.ha <sup>-1</sup> ]	Frequency	Yield [t.ha <sup>-1</sup> ]	Frequency		
Production Year						
2006/07	6.96	25	6.72	13	6.88	38
2007/08	7.63	28	7.18	13	7.49	41
2008/09	7.00	28	6.82	12	6.94	40
Production Area						
Forage	6.61	8	5.92	1	6.54	9
Potatoe	6.80	1	6.79	14	6.79	15
Cereal	6.89	24	6.20	6	6.75	30
Beet	7.54	43	7.32	17	7.48	60
Maize	6.87	5	—	—	6.87	5
Organic Fertilisers						
No	7.20	76	7.01	25	7.16	101
Yes	7.22	5	6.71	13	6.85	18
Fertilizers at Sowing						
No	7.17	51	6.88	37	7.05	88
Yes	7.26	30	8.21	1	7.29	31
Variety Quality						
A (Good Quality)	7.51	30	7.48	13	7.51	43
B (Bread Quality)	7.44	9	5.96	4	6.99	13
C (Unfit for Baking)	7.22	10	6.92	6	7.11	16
E (Elite-Top Quality)	6.84	32	6.66	15	6.79	47
Aggregate	7.20	81	6.91	38	7.11	119

Among technological and economic indicators, the following were monitored or calculated (see Tab. 2): fuel consumption, labour consumption of stand establishment (up to and including sowing), overall labour consumption, machinery costs, material costs, total costs, and unit costs per ton of production.

With respect to the tillage technologies, the average fuel consumption of the reduced-tillage technology was by 24.2 % lower than the one of the conventional technology, the labour consumption of stand establishment was lower by 43.5 %, and the overall labour consumption again lower by 25.0 %. The same can be stated about the machinery costs that were also lower with the reduced-tillage technology, namely by 16.0 %. The material costs were on the opposite by 6.0 % lower in case of conventional technology. The average total costs of the reduced-tillage technology were demonstrated by 4.2 % lower

value than those of the conventional technology. Together with the higher wheat yield, the reduced-tillage technology costs per ton of production were by 168 CZK.t<sup>-1</sup>, i.e. by 7.8 %, lower than using conventional technology. The cereal production area demonstrated the lowest unit costs per ton of production thanks to its lowest average total costs. Evaluation of the results according to the other criteria, such as organic fertilizer application etc., is only informative due to small frequencies and uneven distribution of cases in individual categories.

The fuel and labour consumption as well as the value of individual cost components were influenced by organic fertilizer application. Also due to the lower average yield, the unit cost per ton of production exceeded by 18.7 % the average of the cases where no organic fertilisers were applied.



Table 2 – Average fuel and labour consumption, average machinery, material and total costs, and average costs per ton of winter wheat production according to the tillage technology and other criteria over the whole monitored period

	Fuel Consum- ption [l.ha <sup>-1</sup> ]	Labour Consumption [hrs.ha <sup>-1</sup> ]		Average Costs			
		Stand Establish.	Overall	Machinery [CZK.ha <sup>-1</sup> ]	Material [CZK.ha <sup>-1</sup> ]	Total [CZK.ha <sup>-1</sup> ]	Unit [CZK.t <sup>-1</sup> ]
Tillage Technology							
Reduced	58.8	1.03	2.75	5 151.01	8 792.76	13 970.94	1 994.78
Conventional	77.6	1.82	3.67	6 129.95	8 297.81	14 585.65	2 162.61
Production Area							
Forage	62.5	1.44	3.53	5 712.78	7 967.48	13 680.26	2 120.17
Potatoe	75.6	1.37	3.62	5 791.20	8 281.26	14 379.13	2 149.46
Cereal	62.6	1.32	2.90	5 180.50	7 908.99	13 102.82	2 006.32
Beet	63.4	1.22	2.88	5 473.20	9 223.00	14 749.53	2 024.61
Maize	66.8	1.34	3.19	5 616.00	8 190.95	13 806.95	2 153.29
Organic Fertilisers							
No	61.5	1.10	2.82	5 253.05	8 546.40	13 866.78	1 991.91
Yes	83.4	2.29	4.32	6 645.11	9 130.22	15 853.11	2 365.17
Fertilizers at Sowing							
No	67.1	1.34	3.08	5 551.27	8 592.18	14 236.63	2 079.42
Yes	58.4	1.13	2.95	5 214.77	8 755.45	13 970.22	1 960.25
Variety Quality							
A (Good Quality)	64.8	1.26	2.98	5 494.70	9 296.61	14 865.73	2 024.20
B (Bread Quality)	62.1	1.20	2.77	5 409.00	6 809.24	12 218.24	1 788.22
C (Unfit for Baking)	61.9	1.23	3.08	5 436.69	8 063.94	13 588.12	1 955.81
E (Elite-Top Quality)	66.5	1.34	3.16	5 459.45	8 728.37	14 264.41	2 173.95
Aggregate	64.8	1.28	3.04	5 463.61	8 634.71	14 167.23	2 048.37

Fig. 1 shows combined influence of tillage technology and of organic fertilizer application on the individual cost component averages as well as on the unit cost averages. The lowest costs were attained using the reduced-tillage technology without organic fertilizer application. The reduced-tillage technology with organic fertilizer

application demonstrated, on the contrary, the highest total as well as unit costs.

The cases of fertilizers applied at sowing showed by 5.7 % lower value of unit costs compared to common sowing due to higher yields and slightly lower total costs.

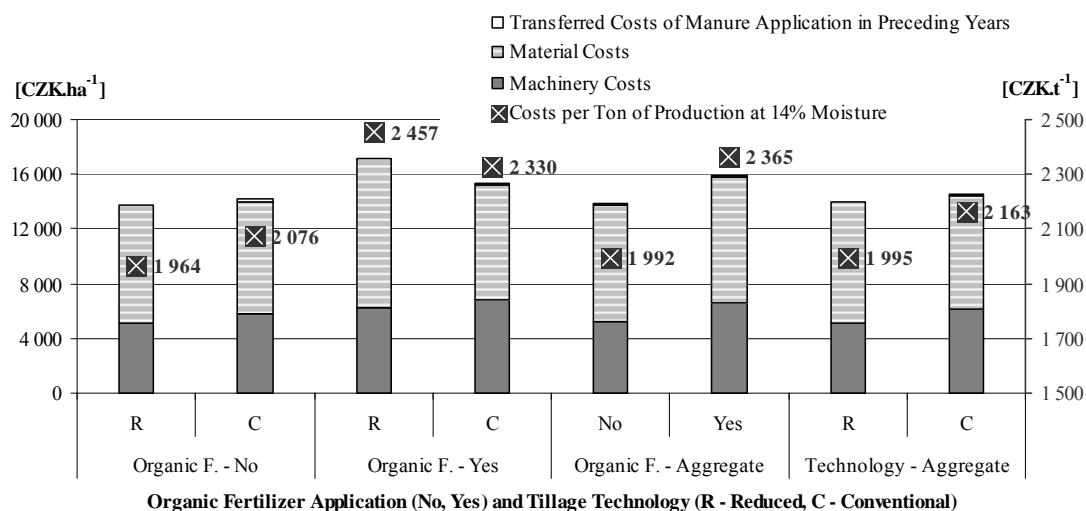


Fig. 1 – Graph of averages of individual cost components, and of average costs per ton of production according to tillage technology and according to organic fertilizer application over the whole monitored period

Fig. 2 shows in detail average values of individual components of material costs. Costs of pesticides amounted to 33.8 % of the total material costs, of that fungicides accounted for 19.2 %, herbicides for as much as 13.7 %, and insecticides a mere 1.0 %. Costs of fertilizers amounted to 39.8 % of the total material costs, of that mineral fertilizers accounted for 37.0 %, and organic fertilizers for mere 2.8 % (only 40 % of manure costs were calculated for the first year after the application). The remaining 23.3 % of the material

costs were the costs of seed, of other pesticides (molluscicides), stimulators, antitranspirants, additives etc. With regard to the tillage technology, the total material costs differed only by 6.0 % in favour of the conventional technology, particularly due to mineral fertilizer costs lower by 23.2 %, and also due to lower herbicide costs by 21.0 %. The costs of seed and the remaining material proved higher as well in the case of the reduced-tillage technology, namely by 4.1 %.

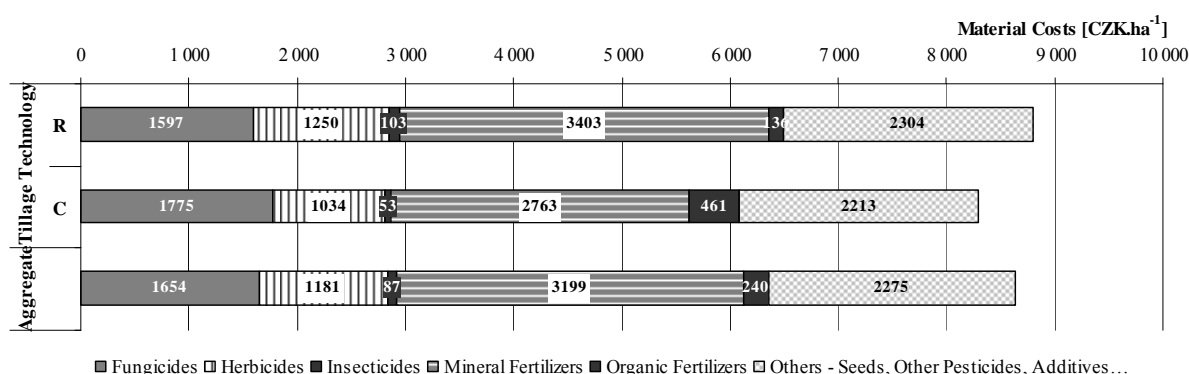


Fig. 2 – Graph of average individual components of material costs according to the winter wheat tillage technology (R – reduced, C – conventional) over the whole monitored period

From the point of view of economics as well as of labour and fuel consumption, the reduced-tillage technology proved to be an adequate alternative to the conventional technology. At some of the farm businesses, winter wheat acreages account for thousands of hectares. It would require a substantial increase in the number of workers, if the reduced-tillage technology was not employed.

### Conclusions

- Average total costs of the reduced-tillage technology amounted to 13 970.94 CZK.ha<sup>-1</sup>, those of the conventional technology to 14 585.65 CZK.ha<sup>-1</sup>. Hereat, machinery costs demonstrated 16% difference in favor of the reduced-tillage technology.
- The average fuel consumption of the reduced-tillage technology was by 24.2% lower than that of the conventional technology, the labour consumption of stand establishment was lower by 43.5 %, and the overall labour consumption again lower by 25.0 %.
- Average yield of the reduced-tillage technology reached 7.20 t.ha<sup>-1</sup> compared to 6.91 t.ha<sup>-1</sup> attained using the conventional technology.
- The reduced-tillage technology demonstrated unit costs per ton of production at the level of 1 995 CZK.t<sup>-1</sup>, the conventional technology at the level of 2 163 CZK.t<sup>-1</sup>, i.e. the difference was 7.8 %.

- From the point of view of economics as well as of labour and fuel consumption, the reduced-tillage technology proved to be an adequate alternative to the conventional technology.

*This work was supported by Research Project of the Ministry of Education of the CR no. MSM 6046070905, and by the project NAZV QH72257.*

### References

- [1] Horák, L. – Šařec, P. – Vozka P.: Porovnání klasického a půdoochranného způsobu založení porostu pšenice ozimé. Agromanuál, 2007, roč. 2, č 8, s. 56-59 ISSN 1801-7673.
- [2] Hůla, J. – Procházková, B.: Minimalizace zpracování půdy et al. Praha: Profi Press, 2008
- [3] Procházková, B. – Dovrtěl, J. (2000): Vliv různého zpracování půdy na výnosy ozimé pšenice. Rostlinná výroba, 2000, 10/46, s. 437 – 442
- [4] Procházková, B. – Hrubý, J. – Kňákal, Z.: Zjednodušené technologie zpracování půdy pro ozimou pšenici. Úroda, 2000, 7/46, s. 10 – 11
- [5] Procházková, B. – Hrubý, J. – Hartman, I.: Minimalizační technologie zpracování půdy u ozimé pšenice. Úroda, 2006, 9/52, s. 14

## TECHNOLOGICAL AND ECONOMIC PARAMETERS OF GRAIN MAIZE PRODUCTION USING DIFFERENT SOIL CULTIVATION METHODS

PETR ŠAŘEC\*, ONDŘEJ ŠAŘEC, MARTIN KLAIN

Czech University of Life Sciences Prague, 165 21 Prague 6– Suchbát, Czech Republic

Phone: +4202-24383147, Fax: +4202-24383155, E-mail: psarec@tf.czu.cz

### Abstract

Several years already, field monitoring and measurements focused on technological and economic comparison of conventional and reduced-tillage technologies of soil cultivation and drilling of maize have been carried out in 13 farm businesses located in beet and maize production areas of the Czech Republic. The paper presents four-year results starting from the year 2005/06, where around 40 fields were monitored. The collected data can be divided into two groups, i.e. the data measured that characterize plant and soil properties in each field and the data coming from observations and calculations that describe the field in question, all the operations carried, a pre-crop and its residue management, fertilizer and chemicals applications etc. In general, reduced-tillage technologies prevailed. The results were influenced by an uneven application of organic fertilizers into trial fields. In each of the years in question except the year 2007/08, average grain yield produced by the reduced-tillage technology slightly surpassed the yield of the conventional technology. Four-year average difference in yields amounted then to 7 %, i.e. to 0.70 t.ha<sup>-1</sup>.

**Key words:** winter wheat, conventional technology, reduced tillage, costs, profit, fuel consumption, labor consumption

### Introduction

History of maize (*Zea mays*) extends nine thousand years backward, particularly in South America. Obviously, it had a significant influence on development of South-American culture. In spite of its tropical origin, maize is a crop that is grown nowadays in various climatic conditions. This practice has been enabled by evolvement of breeding, which resulted in the fact that solely hybrid seed is applied at the present time. Maize growers are thus wholly dependent on specialized seed improvers. Maize grown for grain plays an important role in alimentation of population, but as well in livestock feeding where it ranks among the most important feeding crops.

In the Czech Republic, maize cultivation area increases yearly, e.g. from around 40 thousand hectares in the year 2000 to 113,8 thousand hectares in 2009.

Choice of a suitable variety depends mainly on nature and weather conditions of a grower. In the Czech Republic, varieties appropriate for various production areas are tested regularly. The key feature of a hybrid seed is the length of vegetative period that is indicated using the FAO scale as a number in proportion to a standard.

The number therefore doesn't represent any absolute length of vegetative period in days. In the conditions of the Czech Republic, a range of varieties starting with very early hybrids with 200 FAO, i.e. 120 days of vegetative period, to late hybrids with 600 FAO, i.e. 142 to 148 days of vegetative period, is used. Moth-resistant Bt maize is one of the few genetically modified crops allowed for growing in the Czech Republic at the moment. Its acreage increases gradually. In the year 2008, it was already 8 380 ha.

From the point of view of maize stand establishment, it is clear that ploughing is still widely used. Long-time experience shows that no technology of soil cultivation should be left out or prioritized, because each has its pros and cons. The most important is always the way of implementation of a chosen technology. Especially farmers producing in prone fields must give an increased attention to agronomical practices, because there is a higher erosion danger with nutrient downwash related to it than on the flat.

Soil preparation influences water and air in soil to a great extent. That is why in arid areas, there is a rule to move the soil as little as possible, and to sow at earlier dates and with

appropriately set sowing depth. In humid areas and on heavier soils, the limiting factor for maize is the content of air in soil. Soil compaction is another adverse factor, primarily at headlands and at entries to fields.

### Material and Methods

During four production years from 2005/06 to 2008/09 at eleven farm businesses located in the beet production region and two located in the maize production region of the Czech Republic, field monitoring and measurements focused on different maize for grain production technologies from the viewpoint of conventional and reduced-tillage technologies were carried out. The total number amounted to 37 monitored fields.

The key aim of the work is to verify which technologies of maize for grain stand establishment are profitable.

The following items were monitored or measured:

- characteristics of individual fields (acreage, cadastre, preceding crop, plant residue treatment, year of last manure application ...),
- soil characteristics (bulk density, penetration resistance ...) - not analysed in this paper,
- crop stand characteristics (number of plants per square meter ...) - not analysed in this paper,
- data on every field operation performed (date, machinery used, its workrate, fuel consumption, age and purchasing price, material used, its application rate and price, and other supplementary information)

The latter enabled to calculate machinery and material costs. Subsequently, total costs of a field operation are the sum of the two above mentioned. The total costs could be as well increased due to possible manure application two or three years prior to the maize. Accordingly, for the operations

of manure and lime treatment of the maize, only 40 % of the machinery and material costs are calculated in the first year. The total costs do not include costs of lease or ownership of land, and overhead costs.

### Results and Discussion

During four production years starting in 2005, trials were set up in 37 fields of the beet and maize production regions. Reduced-tillage technology of maize for grain growing was employed in 24 cases, conventional in 13 cases. In each production year, the total average yield gained from the trial fields exceeded the average of the Czech Republic by 21 to up to 56 %.

Prior to maize sowing, manure was applied in more than 30 % of trial fields managed by conventional technology and in mere 13 % of trial fields within reduced-tillage technology. Winter wheat preceded maize in almost 70 % of the trial fields. Concerning the types of maize varieties, those of lower FAO, i.e. maturing very early or early, prevailed. Within conventional technology in fact, these varieties were the only ones sown.

The most frequent tillage procedures within the reduced-tillage technology consisted of:

- twice stubble cultivation + once or twice seedbed preparation

Deeper soil loosening to more than 0.15 meters was performed in only 8,3 % of the cases.

Within the conventional technology, the most frequent tillage procedures consisted of:

- stubble cultivation + ploughing + once or twice seedbed preparation

Disc cultivators prevailed within conventional technologies, whereas within the reduced-tillage technologies, where two stubble cultivations were common, tine cultivators were more frequent, particularly for the second cultivation.

Table 1 – Average maize for grain yields at 14% moisture and frequencies of cases according to the tillage technology and other criteria over the whole monitored period

	Tillage Technology				Aggregate	
	Reduced		Conventional		Yield* [t.ha <sup>-1</sup> ]	Frequency
	Yield* [t.ha <sup>-1</sup> ]	Frequency	Yield* [t.ha <sup>-1</sup> ]	Frequency		
Production Year						
2005/06	8.78	5	8.53	2	8.71	7
2006/07	11.00	5	9.73	3	10.52	8
2007/08	9.56	6	9.97	4	9.72	10
2008/09	11.45	8	9.75	4	10.88	12
Production Area						
Beet	10.23	19	9.63	13	9.99	32
Maize	10.67	5	—	—	10.67	5
Organic Fertilisers						
No	10.69	11	—	—	10.69	11
Yes	10.01	13	9.63	13	9.82	26
Fertilizers at Sowing						
No	10.36	4	9.81	9	9.98	13
Yes	10.32	20	9.21	4	10.13	24
Catch Crop						
No	10.15	21	9.57	11	9.95	32
Yes	11.52	3	9.91	2	10.88	5
Hybrid Maturity**						
S-E/G-VE	11.29	2	8.66	5	9.41	7
S-E/G-E	—	—	9.65	1	9.65	1
G-E	11.24	2	—	—	11.24	2
S-ME/G-E	9.92	8	10.18	6	10.03	14
S-ME	8.45	2	—	—	8.45	2
S-ML/G-E	13.80	1	—	—	13.80	1
S-ML/G-ME	11.63	2	—	—	11.63	2
G-ME	9.30	1	—	—	9.30	1
S-ML/G-ML	10.36	5	—	—	10.36	5
S-ML	8.29	1	—	—	8.29	1
Mixture	—	—	11.07	1	11.07	1
Aggregate	10.32	24	9.63	13	10.08	37

Note: \* grain yield at 14% moisture

\*\* S- Hybrid for Silage; G- Hybrid for Grain; VE- Very Early; E- Early; ME- Medium Early; ML- Medium Late

Over the period of four production years, the average grain yield of all 37 fields was 10.08 t.ha<sup>-1</sup>. Tab. 1 shows average maize grain yields at 14% moisture according to several criteria. Reduced-tillage technology reached yields exceeding those of conventional technology in all of the monitored production years except the year 2007/08. The overall difference between the average yields of the technologies in question amounted to 7.3 %, i.e. 0.70 t.ha<sup>-1</sup>. Concerning regionalization, solely reduced-tillage technology was employed in the more arid conditions of maize production area, where the average yield surpassed the one given

by beet production area by 6.8 %. Concerning organic fertilisers, if those were applied, which was 70 % of all the cases and 100 % of the conventional technology cases, the average yield attained by 8.2 % lower value. With fertilizer application during maize sowing, which was generally the case of reduced-tillage technology, the average yield at 14% moisture slightly exceeded the yield produced when no fertilizers were applied while sowing, i.e. by 1.5 %. Concerning the catch crop, the average yield at 14% moisture differed by 9.3 % in favour of catch crops sown prior to maize. Small frequencies and



uneven distribution of cases in individual categories may have influenced the results and have impeded to draw conclusions.

Among technological and economic indicators, the following were monitored or

calculated (see Tab. 2): fuel consumption, labour consumption of stand establishment (up to and including sowing), overall labour consumption, machinery costs, material costs, total costs, and unit costs per ton of production at 14% moisture.

Table 2 – Average fuel and labour consumption, average machinery, material and total costs, and average costs per ton of maize grain production at 14% moisture according to the tillage technology and other criteria over the whole monitored period

	Fuel Consum- ption [l.ha <sup>-1</sup> ]	Labour Consumption [hrs.ha <sup>-1</sup> ]		Average Costs			
		Stand Establish.	Overall	Machinery [CZK.ha <sup>-1</sup> ]	Material [CZK.ha <sup>-1</sup> ]	Total [CZK.ha <sup>-1</sup> ]	Unit [CZK.t <sup>-1</sup> ]
Tillage Technology							
Reduced	65.1	1.71	3.15	6295.00	10508.82	16820.48	1654.50
Conventional	109.9	3.84	6.67	8361.26	12968.77	21360.81	2251.29
Production Area							
Beet	84.8	2.67	4.69	7120.79	11592.92	18738.71	1914.77
Maize	55.1	1.11	2.44	6382.20	9966.47	16348.67	1540.43
Organic Fertilisers							
No	50.5	1.07	2.24	5883.64	9991.83	15911.83	1503.08
Yes	93.7	3.04	5.30	7502.17	11957.52	19475.08	2016.96
Fertilizers at Sowing							
No	89.8	2.77	5.67	7826.46	12173.22	20030.45	2043.93
Yes	76.0	2.29	3.70	6584.68	10939.74	17541.09	1766.82
Catch Crop							
No	80.7	2.46	4.25	6882.79	11398.02	18305.82	1869.40
Yes	81.5	2.45	5.29	7905.40	11213.80	19119.20	1830.78
Hybrid Maturity*							
S-E/G-VE	80.7	2.04	4.72	7557.57	11922.94	19537.66	2145.52
S-E/G-E	122.3	5.02	8.91	8870.00	16066.75	24936.75	2584.12
G-E	62.6	1.98	3.87	6722.00	12750.20	19672.20	1718.44
S-ME/G-E	89.6	3.03	4.75	6939.31	10658.63	17597.95	1802.37
S-ME	108.7	3.18	4.74	6602.00	10368.65	16970.65	2014.07
S-ML/G-E	67.8	2.58	4.21	7654.00	21472.75	29126.75	2110.63
S-ML/G-ME	57.5	1.18	2.65	6625.50	9935.68	16561.18	1426.43
G-ME	70.1	2.07	3.83	5876.00	8479.25	14355.25	1543.58
S-ML/G-ML	54.1	1.09	2.36	6270.80	10805.76	17076.56	1649.71
S-ML	67.6	2.12	3.44	6570.00	9347.00	15917.00	1920.02
Mixture	115.8	4.22	8.11	9500.00	12620.65	22120.65	1998.25
Aggregate	80.8	2.46	4.39	7020.98	11373.13	18415.73	1864.18

Note: \* S- Hybrid for Silage; G- Hybrid for Grain; VE- Very Early; E- Early; ME- Medium Early; ML- Medium Late

With respect to the tillage technologies, the average fuel consumption of the reduced-tillage technology was by 40.8 % lower than the one of the conventional technology, the labour consumption of stand establishment was lower by 55.5 %, and the overall labour consumption again lower by 52.8%. The same can be stated about the machinery costs that were also lower with the

reduced-tillage technology, namely by 24.7%. The material costs differed also in favour of reduced-tillage, this time by 19.0 %. The average total costs of the reduced-tillage technology were then demonstrated by 21.3% lower value than those of the conventional technology. Together with the higher grain yield at 14% moisture, the reduced-tillage technology costs per ton of production at

14% moisture were by  $597 \text{ CZK.t}^{-1}$ , i.e. by 26.5 %, lower than using conventional technology. The results rendered by the conventional technology may have been adversely influenced by uneven distribution of application of organic fertilisers, which is cost and time consuming. Also evaluation of the results according to the other criteria, such as application fertilizers at sowing etc., is only informative due to small frequencies and uneven distribution of cases in individual categories. The fuel and labour consumption as well as the value of individual cost components were influenced by organic fertilizer application. Also due to the lower average yield, the unit cost per ton of production exceeded by 34.2 % the average of the cases where no organic fertilisers were applied. The cases of fertilizers applied at

sowing showed lower value of unit costs compared to common sowing due to slightly higher grain yields and lower total costs by 12.4 %. In the case of a catch crop preceding maize, the grain yields were also higher, but due to a higher value of the total costs, the unit costs were lower by mere 2.1 % compared to the average of the cases when no catch crop preceded.

Fig. 1 shows combined influence of tillage technology and of organic fertilizer application on the individual cost component averages as well as on the unit cost averages. The lowest costs were attained using the reduced-tillage technology without organic fertilizer application. The conventional technology with organic fertilizer application demonstrated, on the contrary, the highest total and unit costs.

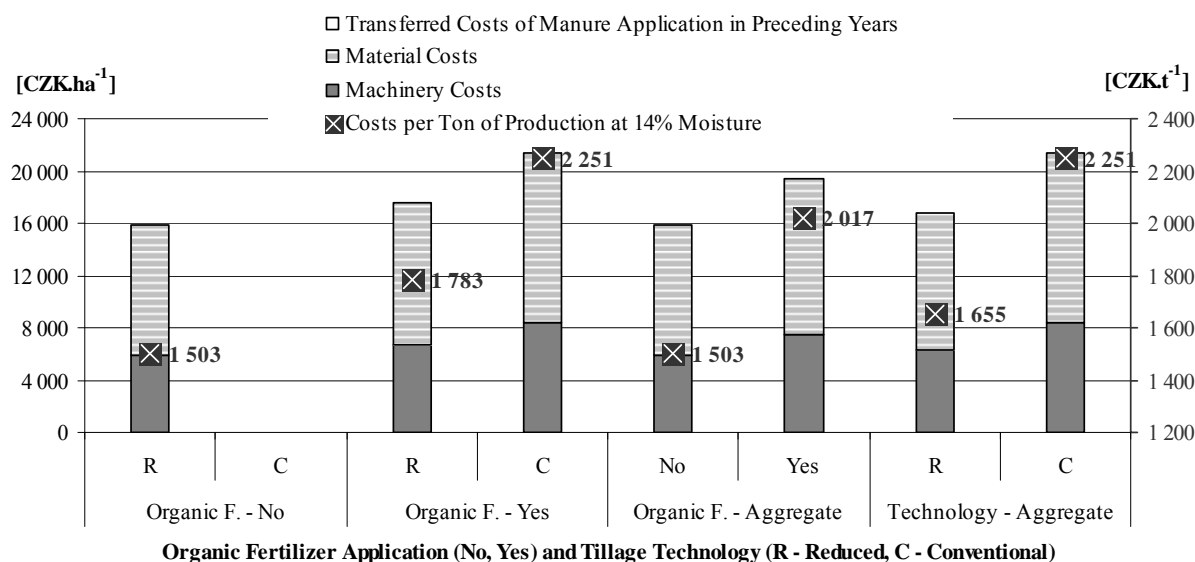


Fig. 1 – Graph of averages of individual cost components, and of average costs per ton of maize grain production at 14% moisture according to tillage technology and according to organic fertilizer application over the whole monitored period

Fig. 2 shows in detail average values of individual components of material costs. Costs of pesticides amounted to 22.0 % of the total material costs, of that herbicides accounted for as much as 17.9 %, insecticides a mere 4.1 %, and fungicides were not used altogether. Costs of fertilizers amounted to 45.6 % of the total material costs, of that mineral fertilizers accounted for 23.9 %, and organic fertilizers for 21.8 % (only 40 % of manure costs were calculated for the first year after the application). The remaining 32.3 % of the material costs were the costs of seed, of other

pesticides (molluscicides), stimulators, antitranspirants, additives etc. With regard to the tillage technology, the total material costs differed only by 19.0% in favour of the reduced-tillage technology, particularly due to organic fertilizer costs lower by 76.2 %. Mineral fertilizer costs and pesticide costs were on the opposite higher by 77.5 %, respectively by 17.3 %. The difference in costs of herbicides was 13.4 %, and in costs of insecticides 36.6 %. The costs of seed and the remaining material proved lower in the case of the reduced-tillage technology, namely by 13.0 %.

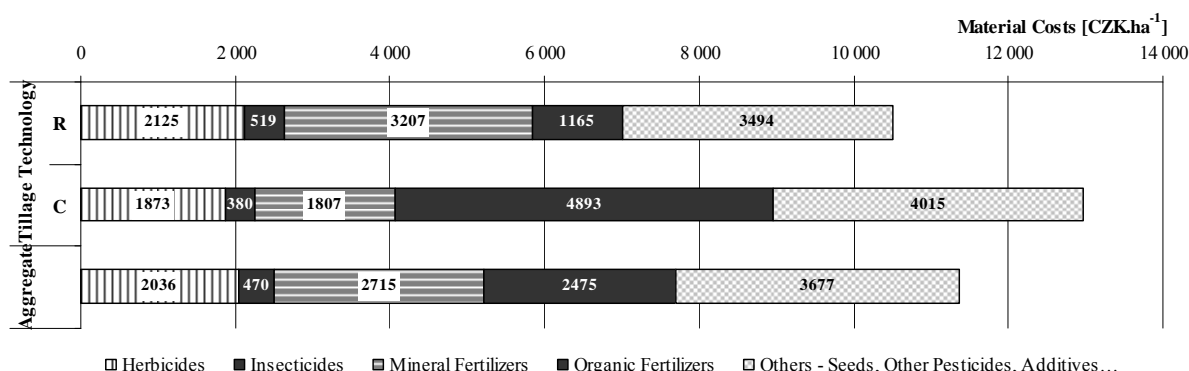


Fig. 2 – Graph of average individual components of material costs according to the maize for grain tillage technology (R – reduced, C – conventional) over the whole monitored period

From the point of view of economics as well as of labour and fuel consumption, the reduced-tillage technology proved to be more than an adequate alternative to the conventional technology.

### Conclusions

- Average total costs of the reduced-tillage technology amounted to 16 820.48 CZK.ha<sup>-1</sup>, those of the conventional technology to 21 360.81 CZK.ha<sup>-1</sup>, the difference made 4 540.32 CZK.ha<sup>-1</sup>.
- The average fuel consumption of the reduced-tillage technology was by 40.8 % lower than that of the conventional technology, the labour consumption of stand establishment was lower by 55.5 %, and the overall labour consumption again lower by 52.8%.
- Average grain yield at 14% moisture of the reduced-tillage technology reached 10.32 t.ha<sup>-1</sup> compared to 9.63 t.ha<sup>-1</sup> attained using the conventional technology.
- The reduced-tillage technology demonstrated unit costs per ton of production at the level of 1 654 CZK.t<sup>-1</sup>, the conventional technology at the level of 2 251 CZK.t<sup>-1</sup>, which made a difference of 26.5 %.
- From the point of view of economics as well as of labour and fuel consumption, the reduced-tillage technology proved to be more

than an adequate alternative to the conventional technology.

*This work was supported by Research Project of the Ministry of Education of the CR no. MSM 6046070905, and by the project NAZV QH72257.*

### References

- [1] Petr, J., Húska, J. 1997. Speciální produkce rostlinná– I. Praha: Agronomická fakulta ČZU v Praze, 1997, ISBN 80-213-0152-X
- [2] Prokeš, K.: Výživa kukuřice v podmínkách bramborářské výrobní oblasti. Disertační práce, MZLU Brno, 2008, 170 s.
- [3] Prokeš, K., Hlušek, J., Richter, R., Lošák, T.: Výživa kukuřice (Zea mays, L) v podmínkách bramborářské výrobní oblasti. Úroda, 2008
- [4] Sedláček, M.: KWS OSIVA s.r.o. Pod Hradbami 2004/5 Velké Meziříčí, ČR, 2004
- [5] Šařec, P. – Šařec, O. – Gil, K.: Field trials on grain maize cultivation technologies in 2004, 2005 and 2006. Annales UMCS, Sec. E-Agricultura, 2008, vol. 63, no. 2, s. 21-27. ISSN 0365-1118.
- [6] Škarda, M.: Hospodaření s organickými hnojivy. SZN Praha, 1982, 324 s.
- [7] Vrzal, J., Novák, D. et al. 1995. Základy pěstování kukuřice a jednoletých píceň. Praha: Institut výchovy a vzdělávání MZe ČR, 1995, str. 32

## TECHNOLOGICAL PROCESSES OF PRODUCTION OF MAJOR FARM CROPS RELATED TO SOIL CONDITIONS IN INDIVIDUAL PRODUCTION AREAS OF CR

PETR ŠAŘEC<sup>1\*</sup>, VÁCLAV VOLTR<sup>2</sup>, ONDŘEJ ŠAŘEC<sup>1</sup>

<sup>1</sup>Czech University of Life Sciences Prague, 165 21 Prague 6– Suchbát, Czech Republic

Phone: +4202-24383147, Fax: +4202-24383155, E-mail: psarec@tf.czu.cz

<sup>2</sup>Institute of Agricultural Economics and Information, Prague, Czech Republic

### Abstract

The paper evaluates most advantageous technological processes of production of major farm crops with relation to soil environment that is expressed using main soil units and climatic factors. Source materials are based on monitoring of selected agricultural businesses during the years 2002-2010. The evaluation makes use of crop yields reached, material inputs with price parameters, and field operation costs. Main soil units are described by average measured soil physical characteristics that enable to assess the influence of development of weather conditions on soil moisture. The results of winter wheat, oilseed rape and maize for grain growing suggest that reduced-tillage technology brings the highest advantage on heavier soils in drier and warmer climatic regions.

**Key words:** technological process, soil cultivation, soil unit, climate, farm-crop yield, costs

### Introduction

In the conditions of the Czech Republic, tillage belongs to one of the very important, and all at once energy demanding measures that are employed within farm crop production. Development of the new tillage technologies is distinctive by economic pressure towards reduction of costs, of energy consumption and by ecological demand for soil deterioration holdback. Reduced-tillage technologies, where intensity and depth of soil cultivation decreases, and furthermore tillage operations can be combined, are aimed mainly at cereals, i.e. also at maize for grain, but could be applied as well for other crops.

From the results of field trials carried out in the Czech Republic as well as abroad stems that many aspects should be taken into account when applying reduced-tillage technology, i.e. plant residues left on the soil surface, crop rotation, sowing methods, soil fertility, crop protection, microbiological aspects, physical soil properties and many others. Generally, reduced-tillage technologies and stand establishment depends chiefly on weather, climatic, and on soil conditions (mainly on topsoil depth and on humus content), and likewise on the quantity of persistent weeds.

The paper evaluates technological processes of production of winter wheat, winter oilseed rape and maize for grain with relation to soil environment that is expressed via main soil units

by soil texture, and to climatic factors represented by climate regions. Source materials are based on monitoring of selected agricultural businesses during the years 2002-2010. The evaluation makes use of crop yields reached, material inputs with price parameters, and field operation costs.

For winter wheat production, reduced-tillage technology of soil cultivation and stand establishment are frequently employed. At large, the most suitable conditions for tillage depth and intensity reduction are on medium-textured soils with higher natural fertility in drier conditions of maize and beet production regions. Lately, the reduced-tillage technology is used also in the areas with poorer soil and climatic conditions. The results of long-term field trials and farming experience demonstrate the possibility to exploit this technology in potato production area. Reduced-tillage technology of winter oilseed rape production also propagates. The major concern here is treatment of pre-crop residues that can cause problems to small rape seeds.

From the point of view of maize stand establishment, it is clear that ploughing is still widely used. Long-time experience shows that no technology of soil cultivation should be left out or prioritized, because each has its pros and cons. Especially farmers producing in prone fields must give an increased attention to agronomical

practices, because there is a higher erosion danger with nutrient downwash related to it than on the flat.

Reduced-tillage technology of soil cultivation and stand establishment are often applied to heavy-textured soils, where soil environment frequently impede quality stand establishment using conventional soil cultivation technology including ploughing. In such case, reduced-tillage technology is practically the only way of stand establishment.

### Material and Methods

Since the production year 2001/02 at more than 40 farm businesses in all of the districts of the Czech Republic, field monitoring and measurements focused on production technologies of major farm crops, in the case of this paper those are winter wheat, oilseed rape and maize for grain, from the viewpoint of conventional and reduced-tillage technologies have been carried out. The key aim of the work is to verify which technologies of their stand establishment and growing are profitable.

The following items have been monitored or measured:

- characteristics of individual fields (acreage, cadastre, preceding crop, plant residue treatment, year of last manure application, main soil unit, climatic region ...),
- soil characteristics (bulk density, penetration resistance, soil texture ...),
- crop stand characteristics - not analysed in this paper,
- data on every field operation performed (date, machinery used, its workrate, fuel consumption, age and purchasing price, material used, its application rate and price, and other supplementary information)

The latter enabled to calculate machinery and material costs. Subsequently, total costs of a field operation are the sum of the two above mentioned. The total costs could be as well increased due to possible manure application two or three years prior to the winter wheat. Accordingly, for the operations of manure and lime treatment of the winter wheat, only 40 % of the machinery and material costs are calculated in the first year. The total costs do not include costs of lease or ownership of land, and overhead costs.

For the purpose of this paper, the technologies, mainly stand establishment technology, are

evaluated with regard to soil texture and climate. Soil texture of the monitored fields is configured according to main soil unit into three groups:

- lighter: light and light to medium-textured soils,
- medium: medium-textured soils,
- heavier: medium to heavy and heavy-textured soils.

The grouping was forced by the frequency of individual cases of the monitored fields. For the same sake, the climate is also characterised by only two groups:

- drier and warmer climatic region (D, W): grouping of climatic regions no. 0 to 4,
- moister and colder climatic region (M, C): grouping of climatic regions no. 5 to 9.

### Results and Discussion

Since the production year 2001/02 at more than 40 farm businesses in all of the districts of the Czech Republic, field monitoring and measurements focused on production technologies of major farm crops, in the case of this paper those are winter wheat, oilseed rape and maize for grain, have been carried out. The production technologies are evaluated with regard to soil texture and climate. From the viewpoint of climate and production areas, the majority of fields, i.e. over 91 %, belonging to drier and warmer climatic region were located in beet and maize production area. The same can be said about moister and colder climatic region, where 92 % of fields were located in either forage, potato or cereal production areas. Concerning soil texture and production areas, heavier soils were monitored mainly in beet production area (78 %). 80 % of the fields with medium-textured soil were located in maize, beet or cereal production areas. Fields with soil of lighter texture were evenly spread among beet, cereal, potato and forage production areas (91 %).

Field monitoring has taken place mainly at large farm businesses (acreages over 1 000 ha) managed by well educated and experienced farmers that employ production technologies suitable for their conditions. Thus in drier and warmer climatic region, reduced-tillage technology prevailed over conventional technology. The same can be stated about heavier textured soils, where reduced-tillage technology was with few exceptions the only one employed. This fact on the other hand adversely influenced



the distribution of monitored fields into particular groups and left some categories unoccupied.

On lighter soils, the most frequent tillage procedures within the reduced-tillage technology consisted of:

- twice stubble cultivation 45 %
- twice stubble cultivation + seedbed preparation 30 %

Within the conventional technology, the most frequent tillage procedures consisted of:

- ploughing + once or twice seedbed preparation 63 %

On medium-textured soils, the most frequent tillage procedures within the reduced-tillage technology consisted of:

- twice stubble cultivation 48 %
- twice stubble cultivation + seedbed preparation 16 %

Deeper soil loosening to more than 0.15 meters was performed in 22 % of the cases.

Within the conventional technology, the most frequent tillage procedures consisted of:

- stubble cultivation + ploughing + once or twice seedbed preparation 50 %
- ploughing + once or twice seedbed preparation 34 %
- stubble cultivation + ploughing 15 %

On heavier soils, the most frequent tillage procedures within the reduced-tillage technology consisted of:

- twice stubble cultivation + seedbed preparation 50 %
- twice stubble cultivation 19 %

Within the conventional technology, the two tillage procedures used consisted of:

- ploughing + twice seedbed preparation 50 %
- stubble cultivation + ploughing + seedbed preparation 50 %

Tables 1 to 3 display for the three crops in question, i.e. for winter wheat, oilseed rape and for maize for grain, their yields, individual cost components, total and unit costs according to soil texture, climatic region and tillage technology.

In the case of winter wheat (see Table 1), average seed yields produced using reduced-tillage technology surpassed the yields of conventional technology except the instance of lighter soil and moister and colder climatic region. The difference was the highest, i.e. exceeding 13 %, in the case of a heavier soil. Surprisingly on lighter soils managed by conventional tillage, much higher pesticide and mineral fertiliser costs occurred. On medium-textured soils, the situation was opposite, but the differences were not that high. Due to that fact, reduced-tillage technology achieved lower unit costs per ton of production in all of the cases.

Table 1 – Average winter wheat yields, individual cost components, total costs and unit costs according to soil texture, climatic region and tillage technology

Soil Texture:		Lighter <sup>1</sup>			Medium <sup>2</sup>			Heavier <sup>3</sup>		
Climatic Region:		D, W <sup>4</sup>	M, C <sup>5</sup>	Total	D, W <sup>4</sup>	M, C <sup>5</sup>	Total	D, W <sup>4</sup>	M, C <sup>5</sup>	Total
Yield [t.ha <sup>-1</sup> ]	R <sup>6</sup>	5.28	6.25	6.00	8.25	6.93	7.71	6.83	6.70	6.81
	C <sup>7</sup>	5.02	6.41	5.72	7.60	6.75	6.92	—	5.92	5.92
Material Costs [CZK.ha <sup>-1</sup> ]	R <sup>6</sup>	8 866	7 694	7 987	9 669	8 756	9 299	10 262	6 518	9 638
	C <sup>7</sup>	10 219	11 818	11 019	9 035	8 284	8 434	—	6 773	6 773
Pesticides [CZK.ha <sup>-1</sup> ]	R <sup>6</sup>	1 838	2 659	2 454	2 988	3 357	3 138	3 365	1 674	3 083
	C <sup>7</sup>	4 220	6 288	5 254	2 860	3 085	3 040	—	2 649	2 649
Mineral Fertilizers [CZK.ha <sup>-1</sup> ]	R <sup>6</sup>	2 978	2 408	2 550	3 925	3 214	3 637	4 338	2 899	4 098
	C <sup>7</sup>	3 925	3 837	3 881	3 329	2 221	2 443	—	1 975	1 975
Organic Fertilizers [CZK.ha <sup>-1</sup> ]	R <sup>6</sup>	1 755	0	439	341	0	203	0	0	0
	C <sup>7</sup>	0	0	0	333	718	641	—	0	0
Machinery Costs [CZK.ha <sup>-1</sup> ]	R <sup>6</sup>	5 775	5 676	5 701	5 369	4 996	5 218	5 234	4 870	5 173
	C <sup>7</sup>	4 706	6 375	5 541	6 617	5 984	6 110	—	6 252	6 252
Total Costs [CZK.ha <sup>-1</sup> ]	R <sup>6</sup>	14 641	13 370	13 688	15 037	13 753	14 517	15 496	11 388	14 811
	C <sup>7</sup>	16 325	18 193	17 259	15 652	14 651	14 851	—	13 025	13 025
Unit Costs [CZK.t <sup>-1</sup> ]	R <sup>6</sup>	2 837	2 181	2 345	1 837	2 029	1 915	2 368	1 700	2 256
	C <sup>7</sup>	3 252	2 838	3 045	2 096	2 225	2 199	—	2 200	2 200

Note: <sup>1</sup>light and light to medium-textured soils; <sup>2</sup>medium-textured soils; <sup>3</sup>medium to heavy and heavy-textured soils; <sup>4</sup>drier and warmer climatic regions; <sup>5</sup>moister and colder climatic regions; <sup>6</sup>reduced-tillage technology; <sup>7</sup>conventional technology



Table 2 – Average oilseed rape yields, individual cost components, total costs and unit costs according to soil texture, climatic region and tillage technology

Soil Texture:		Lighter <sup>1</sup>			Medium <sup>2</sup>			Heavier <sup>3</sup>		
Climatic Region:		D, W <sup>4</sup>	M, C <sup>5</sup>	Total	D, W <sup>4</sup>	M, C <sup>5</sup>	Total	D, W <sup>4</sup>	M, C <sup>5</sup>	Total
Yield [t.ha <sup>-1</sup> ]	R <sup>6</sup>	3.66	3.59	3.61	3.99	3.63	3.79	4.14	3.84	4.05
	C <sup>7</sup>	3.35	3.43	3.40	3.81	3.44	3.57	3.13	—	3.13
Material Costs [CZK.ha <sup>-1</sup> ]	R <sup>6</sup>	12 291	10 006	10 837	12 389	10 290	11 238	11 033	9 277	10 531
	C <sup>7</sup>	10 367	11 689	11 160	11 909	9 874	10 601	15 273	—	15 273
Pesticides [CZK.ha <sup>-1</sup> ]	R <sup>6</sup>	5 605	4 544	4 930	6 010	5 353	5 650	6 903	4 537	6 227
	C <sup>7</sup>	2 985	6 303	4 976	5 445	4 310	4 715	4 542	—	4 542
Mineral Fertilizers [CZK.ha <sup>-1</sup> ]	R <sup>6</sup>	4 270	3 049	3 493	3 815	4 009	3 921	3 270	4 248	3 550
	C <sup>7</sup>	4 258	2 957	3 477	4 423	3 338	3 726	5 726	—	5 726
Organic Fertilizers [CZK.ha <sup>-1</sup> ]	R <sup>6</sup>	1 000	1 226	1 144	1 053	69	513	0	0	0
	C <sup>7</sup>	2 340	1 500	1 836	746	936	868	4 680	—	4 680
Machinery Costs [CZK.ha <sup>-1</sup> ]	R <sup>6</sup>	6 284	5 727	5 930	5 972	5 303	5 605	5 888	5 720	5 840
	C <sup>7</sup>	6 662	6 871	6 787	6 780	6 272	6 453	8 000	—	8 000
Total Costs [CZK.ha <sup>-1</sup> ]	R <sup>6</sup>	18 924	15 733	16 894	18 390	15 746	16 940	17 281	15 197	16 686
	C <sup>7</sup>	17 029	19 026	18 228	18 870	16 213	17 162	23 273	—	23 273
Unit Costs [CZK.t <sup>-1</sup> ]	R <sup>6</sup>	5 348	4 637	4 896	4 848	4 509	4 662	4 176	3 962	4 115
	C <sup>7</sup>	5 175	5 568	5 411	5 070	5 022	5 039	7 438	—	7 438

Note: <sup>1</sup>light and light to medium-textured soils; <sup>2</sup>medium-textured soils; <sup>3</sup>medium to heavy and heavy-textured soils; <sup>4</sup>drier and warmer climatic regions; <sup>5</sup>moister and colder climatic regions; <sup>6</sup>reduced-tillage technology; <sup>7</sup>conventional technology

Concerning yields of oilseed rape (see Table 2), reduced tillage technology generally demonstrated better results. The difference was again the highest, i.e. reaching almost 30 %, in the case of a heavier soil. Unit costs per ton of production showed therefore for reduced-tillage technology lower with one exception, i.e. lighter soil in drier and warmer climatic region. In the latter case, the costs of pesticides of reduced-tillage technology exceeded by 88 % those of conventional technology.

With regard to the yields of maize for grain (see Table 3), reduced tillage technology again demonstrated better results. Maize was generally sown in drier and warmer conditions. Costs of pesticides were higher in the case of reduced-tillage technology, costs of organic fertilisers on the other hand in the case of conventional technology. Organic fertiliser application was expensive, therefore the unit costs per ton of production showed unanimously lower for reduced-tillage technology.

Table 3 – Average maize for grain yields, individual cost components, total costs and unit costs according to soil texture, climatic region and tillage technology

Soil Texture:		Lighter <sup>1</sup>			Medium <sup>2</sup>			Heavier <sup>3</sup>		
Climatic Region:		D, W <sup>4</sup>	M, C <sup>5</sup>	Total	D, W <sup>4</sup>	M, C <sup>5</sup>	Total	D, W <sup>4</sup>	M, C <sup>5</sup>	Total
Frequency	R <sup>6</sup>	1	—	1	5	—	5	3	—	3
	C <sup>7</sup>	1	—	1	3	1	4	—	—	—
Yield [t.ha <sup>-1</sup> ]	R <sup>6</sup>	9.40	—	9.40	12.40	—	12.40	8.88	—	8.88
	C <sup>7</sup>	7.82	—	7.82	11.24	10.30	11.01	—	—	—
Material Costs [CZK.ha <sup>-1</sup> ]	R <sup>6</sup>	8 085	—	8 085	12 046	—	12 046	9 261	—	9 261
	C <sup>7</sup>	12 282	—	12 282	12 952	11 918	12 694	—	—	—
Pesticides [CZK.ha <sup>-1</sup> ]	R <sup>6</sup>	2 389	—	2 389	3 228	—	3 228	2 349	—	2 349
	C <sup>7</sup>	2 002	—	2 002	2 476	1 676	2 276	—	—	—
Mineral Fertilizers [CZK.ha <sup>-1</sup> ]	R <sup>6</sup>	3 341	—	3 341	4 003	—	4 003	2 558	—	2 558
	C <sup>7</sup>	0	—	0	1 493	1 741	1 555	—	—	—
Organic Fertilizers [CZK.ha <sup>-1</sup> ]	R <sup>6</sup>	0	—	0	1 140	—	1 140	1 040	—	1 040
	C <sup>7</sup>	6 000	—	6 000	5 333	3 440	4 860	—	—	—
Machinery Costs [CZK.ha <sup>-1</sup> ]	R <sup>6</sup>	4 770	—	4 770	6 786	—	6 786	5 765	—	5 765
	C <sup>7</sup>	7 874	—	7 874	8 737	7 850	8 515	—	—	—

Soil Texture:		Lighter <sup>1</sup>			Medium <sup>2</sup>			Heavier <sup>3</sup>		
Climatic Region:		D, W <sup>4</sup>	M, C <sup>5</sup>	Total	D, W <sup>4</sup>	M, C <sup>5</sup>	Total	D, W <sup>4</sup>	M, C <sup>5</sup>	Total
Total Costs [CZK.ha <sup>-1</sup> ]	R <sup>6</sup>	12 855	—	12 855	18 832	—	18 832	15 159	—	15 159
	C <sup>7</sup>	20 156	—	20 156	21 823	19 768	21 309	—	—	—
Unit Costs [CZK.t <sup>-1</sup> ]	R <sup>6</sup>	1 368	—	1 368	1 524	—	1 524	1 761	—	1 761
	C <sup>7</sup>	2 577	—	2 577	1 932	1 919	1 929	—	—	—

Note: <sup>1</sup>light and light to medium-textured soils; <sup>2</sup>medium-textured soils; <sup>3</sup>medium to heavy and heavy-textured soils; <sup>4</sup>drier and warmer climatic regions; <sup>5</sup>moister and colder climatic regions; <sup>6</sup>reduced-tillage technology; <sup>7</sup>conventional technology

## Conclusions

- Reduced-tillage technology compared to conventional technology attained good results within winter wheat, oilseed rape and maize for grain cultivation concerning yields as well as unit costs over the whole spectrum of soil texture and climatic regions.
- The highest differences in favor of reduced-tillage technology were demonstrated on heavier soils. In the case of winter wheat, the differences were 5.05 % on lighter soils, 11.49 % on medium-textured soils, and 15.06 % on heavier soils. In the case of oilseed rape, the differences attained 6.30 % on lighter soils, 6.19 % on medium-textured soils, and 29.57 % on heavier soils.
- The results suggest that drier and warmer climatic regions are more suitable for application of reduced-tillage technology. In these regions, the differences in yields in favour of reduced tillage were for winter wheat 12.13 % and for oilseed rape 7.68 %. In the moister and colder regions, these differences attained only 1.01 % and 5.62 % respectively.

*This work was supported by the project NAZV QH72257.*

## References

- [1] Hébing, H.: Quelques pistes pour adapter la densité de peuplement, Oleoscope, n 64, 2001, s. 21-22
- [2] Horák, L. – Šařec, P. – Vozka P.: Porovnání klasického a půdoochranného způsobu založení porostu pšenice ozimé. Agromanuál, 2007, roč. 2, č 8, s. 56-59 ISSN 1801-7673.
- [3] Hůla, J. – Procházková, B.: Minimalizace zpracování půdy et al. Praha: Profi Press, 2008
- [4] Palteau, J.-P.: Après une céréale, agir rapidement pour bien planter son colza, Oleoscope, n 64, 2001, s. 10-11
- [5] Procházková, B. – Hrubý, J. – Hartman, I.: Minimalizační technologie zpracování půdy u ozimé pšenice. Úroda, 2006, 9/52, s. 14
- [6] Prokeš, K., Hlušek, J., Richter, R., Lošák, T.: Výživa kukuřice (Zea mays, L) v podmínkách bramborářské výrobní oblasti. Úroda, 2008
- [7] Sauzet, Gilles 2001: Un déchaumage adapté: la clé de la réussite du colza en TCS, Oleoscope, n 64, 2001, s. 12-16

## PHYSICAL DESCRIPTION OF COFFEE COOLING IN A POT – PRINCIPLE OF DRINKS COOLING

JAN SEDLACEK<sup>1\*</sup>, JIRI DOLEJSI<sup>2</sup>

<sup>1</sup>Czech University of Agriculture in Prague, 16521 Prague 6 – Suchbát, Czech Republic,  
Phone: +420-224383286, Fax: +420-234381850, E-mail: sedlacek@tf.czu.cz,

<sup>2</sup>Charles University in Prague, Faculty of Mathematics and Physics, Inst. of Particle and  
Nuclear Physics, V Holesovickách 2, 180 00 Prague 8, Czech Republic

### Abstract

One everyday phenomenon – coffee getting cold in a pot – is studied as an example of a typical method used in physics. We meet this topic in many articles in which authors usually limit themselves on using of Newton's law of cooling (see references [1], [2], [3], [4], [5], [6]). Our effort is aimed at the non-professional audience, we suppose only elementary knowledge of the subject and our approach should be obvious in the common sense. The obvious beginning is to focus attention to the phenomenon and to collect some experience. The second step is the experiment in controlled conditions and with different variants of studied objects. The third step is an attempt to understand the results of the experiment and the nature of the phenomenon. To reach that in the case of cooling coffee, we try to follow the pathway of heat in the studied system within a model realised as a spreadsheet in Excel. We can guess that some heat is used for evaporation, some heat is radiated to surroundings and other amount of heat accepted from surroundings and we must not forget transport of heat between liquid and pot, through the pot and finally between pot and surroundings. We do not measure the individual heat flows, but we put them into the model and from comparison of the model prediction for the time-dependent temperature with the data we deduce the role of different mechanisms and the parameters which enter the model. We can extend the whole experiment to range of other drinks.

### Introduction

A standard situation from the everyday life is a pot of coffee slowly getting cold when we forget about it (see fig. 1). Does it matter what kind of the pot we use? What are the physics processes which play some role in this ordinary occurrence? Which are more important, which less? Can we influence the evolution in the direction we need, like cool faster to drink in a hurry or cool slower during our busy activity?

Let us turn to experiments. At first we measure the time-dependent temperature of the cooling coffee in a china pot on a table. The measurement should be done in reasonable intervals, e.g. in every five minutes, either with a usual mercury thermometer (our case) or with some more sophisticated equipment. The estimated error of our measurement is about 0.3°C.

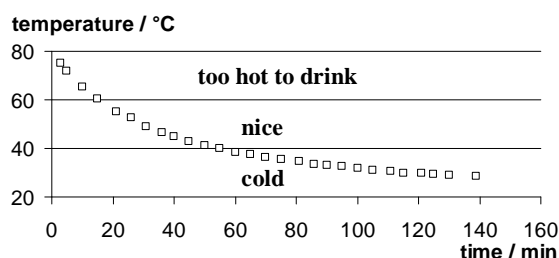


**Fig.1** The measured cooling of coffee. The personal views of the optimal drinking temperature could be different, of course.

We would like to concentrate to the detailed understanding of the measured dependence and to identifying the relevant physics phenomena contributing to the process. We will try to achieve this goal by constructing a suitable simulation model and by refining it to fit the data.

### The first model

We will start with a simple assumption that the heat transferred from the hot coffee to the colder surroundings per unit time is dependent

only on the temperature difference and that the dependence is linear:  $\frac{\Delta Q}{\Delta \tau} = k(t_c - t_s)$ , where  $k$  is the coefficient of the heat exchange between coffee and surroundings,  $t_c$  is the changing temperature of the coffee,  $t_s$  is the constant temperature of surroundings. We assume that the temperature of coffee is uniform. Then we can write the equation relating the heat loss with the change of the coffee temperature either in the form  $\frac{m c \Delta t}{\Delta \tau} = \frac{\Delta Q}{\Delta \tau} = k(t_c - t_s)$ , where  $m$  is the mass of coffee and  $c$  is the specific heat

capacity of it. This relates to Newton's law of cooling.

This equation we approximately and naively solve in the simplest possible manner doing small steps in time with the help of Excel (ignoring all the knowledge on solution of differential equations), we only check that the time step is sufficiently small not to influence the results. We fitted the coefficient  $k$  to meet the data (using solver from Excel).

As we may conclude from fig. 2, the first model systematically underestimates the heat loss at the early moments and overestimates it later.

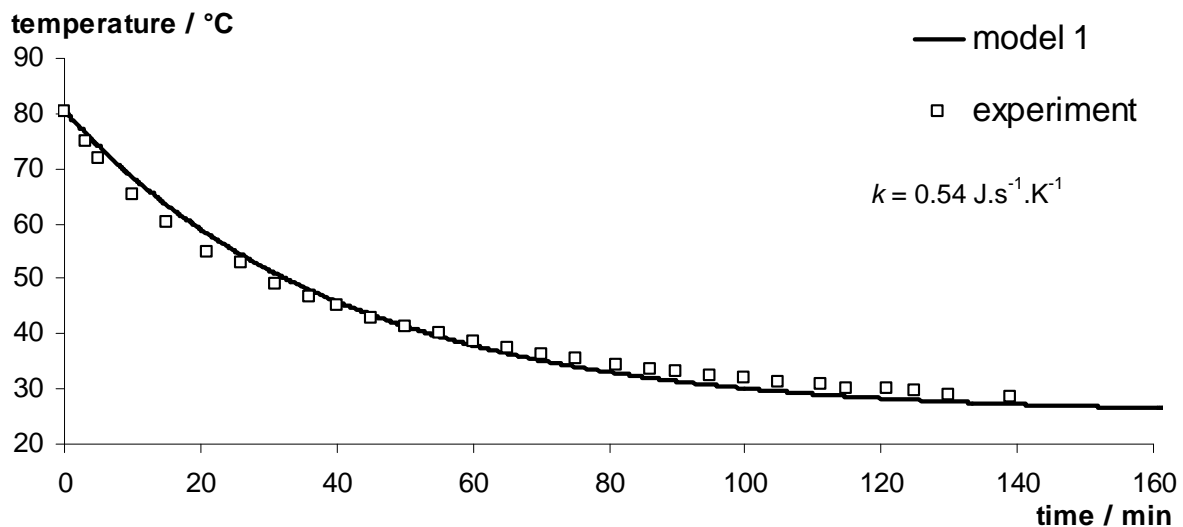


Fig.2 The time-dependent temperature of the experiment and the first model.

### The second model

To improve the agreement of the model and data we will try to use the “brute force method” – we introduce the arbitrary exponent  $x$  into the heat transfer:  $\frac{\Delta Q}{\Delta \tau} = k(t_c - t_s)^x$ . The introduction of this exponent is clearly a substitute for better and more detailed description of the process. Both parameters  $k$  and  $x$  are fitted with Excel. The fig. 3 shows better accuracy of the second model. The quality of the fit we judge from the value of residual sum of squares divided by the number of degrees of

freedom – “ $\chi^2/\text{NDF}$ ”, see any textbook on statistical methods, e.g. [2]. Values much larger than 1 signalize the poor fit.

What are the effects which are mimicked by the power in the heat transfer? We may expect heat losses by evaporation and related loss of coffee mass. Heat could be radiated to surroundings and accepted from it. The pot is heated first and then it cools, it may have the temperature different from coffee. Heat is transferred through all the surfaces. Maybe there are other effects still missing in our list ...

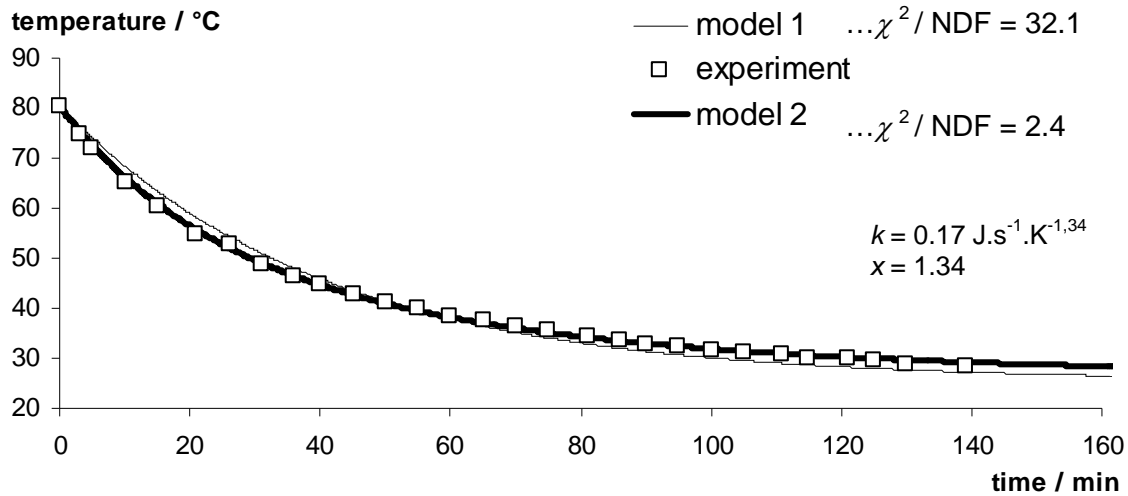


**Fig.3** The time-dependent temperature of the experiment and the both models.

### The third model

We will try to introduce all the abovementioned effects:

- transfer of heat from coffee to the pot:

$$\frac{\Delta Q_1}{\Delta \tau} = k_1 (t_c - t_p)$$

- coffee evaporation to surroundings:

$$\frac{\Delta Q_2}{\Delta \tau} = \nu l_v t_c P$$

where  $\nu$  is the speed of evaporation,  $l_v$  is specific heat of vaporisation,  $P$  open surface

- radiation from coffee to surroundings:

$$\frac{\Delta Q_3}{\Delta \tau} = \alpha \sigma T_c^4 P$$

where  $\sigma$  is the Stefan-Boltzmann constant,  $\alpha$  is the absorptivity of coffee

- radiation from surroundings to coffee:

$$\frac{\Delta Q_4}{\Delta \tau} = \alpha \sigma T_s^4 P$$

- transfer of heat from pot to surroundings:

$$\frac{\Delta Q_5}{\Delta \tau} = k_2 (t_p - t_s)$$

- radiation from pot to surroundings:

$$\frac{\Delta Q_6}{\Delta \tau} = \beta \sigma T_p^4 S$$

where  $S$  is the emitting surface of the cup,  $\beta$  is the absorptivity of its material

- radiation from surroundings to pot:

$$\frac{\Delta Q_7}{\Delta \tau} = \beta \sigma T_s^4 S$$

Our model 3 (see fig. 4) is not yet ideal – the pot is still thin (i. e. it has only one temperature). But that model is more “physical” than the former – at least coffee evaporates. We are lacking any insight into the details of evaporation, so we employed the linear dependence on  $t_c$ . We are not much successful with this model – the residual sum  $\chi^2/\text{NDF} = 81.3$  compared to  $\chi^2/\text{NDF} = 32.1$  for the first model. Before turning to the next model we include one more experimental datum – the change of coffee weight = the weight of evaporated liquid. With this datum included we have  $\chi^2/\text{NDF} = 81.6$ .

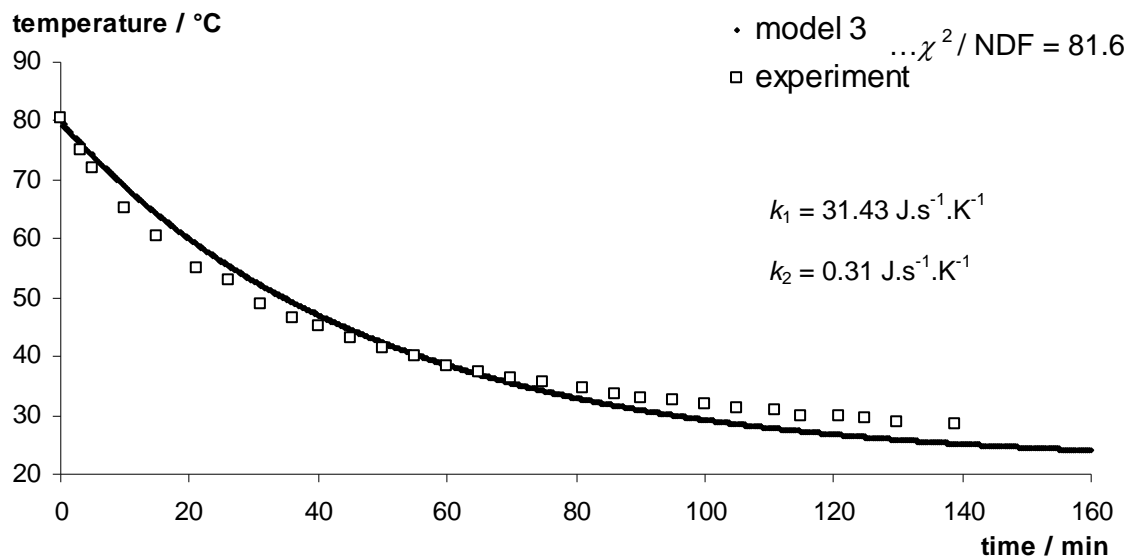


**Fig.4** The time-dependent temperature of the experiment and the third model.

The lack of faster cooling at the beginning persists in the model. Maybe the evaporation speed linear in temperature is unrealistic?

#### The fourth model

Although we do not have any detailed knowledge on the dependence of evaporation speed on temperature and other conditions, we can try to put a free power  $z$  in the “vaporising” term:  $\Delta Q_2 / \Delta \tau = \nu l_v t_c^z P$ . The fit results in  $z =$

**3.73!** Then the agreement of the model and data is remarkable (see fig. 5) –  $\chi^2 / \text{NDF} = 1.0$ .

But the natural question appears: Is the funny value **3.73** reasonable? We made a simple dedicated experiment for measuring of evaporation speed, see fig. 6. The result of the experiment, power  $z = 3.73$ , really agrees with the above value.

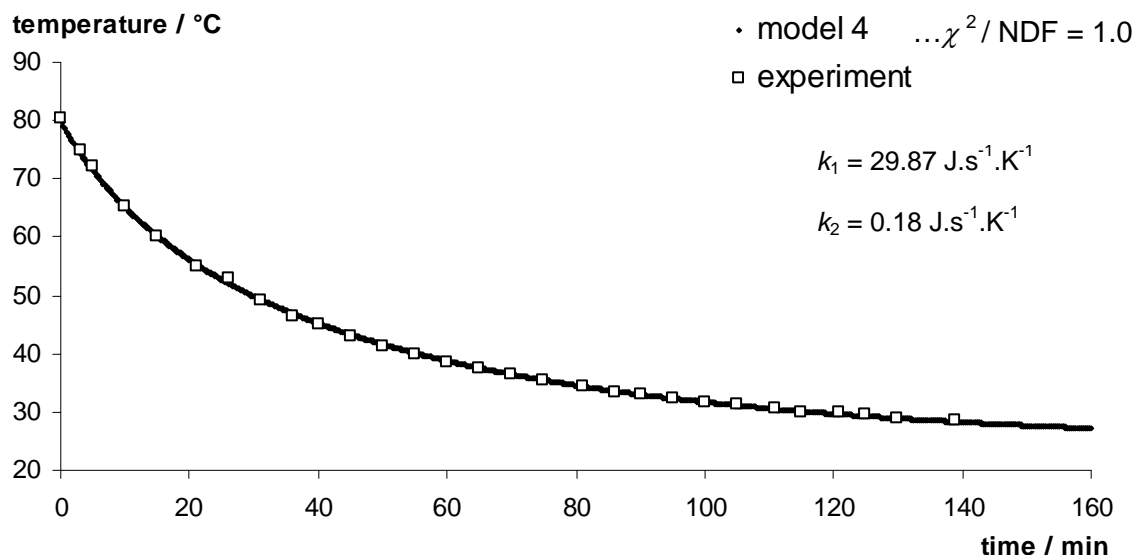


**Fig.5** The time-dependent temperature of the experiment and the fourth model.





**Fig.6** The experiment for measuring of evaporation speed

### The fifth model

In the next model we suppose the pot with nonzero thickness to treat different pots. It means we assume there are an external and an internal temperature of the pot. Then we need adapt above mentioned two terms in the following way:

$$\frac{\Delta Q_1}{\Delta \tau} = k_1 (t_c - t_{pi}) \text{ and}$$

$$\frac{\Delta Q_5}{\Delta \tau} = k_2 (t_{pe} - t_s), \text{ where } t_{pi}, t_{pe} \text{ are the}$$

internal and the external temperature of the pot. Also we introduce another term in our model – heat transfer through the pot:

$$\frac{\Delta Q_8}{\Delta \tau} = k_3 (t_{pi} - t_{pe}).$$



**Fig.7** Three various experimental pots

### The comparison of the influence of different parameters

By introduction of the parameters in the sequence of our models and by fitting them to meet best the data we get sets of parameters, which describe the experiment comparatively well. Clearly we need further experiments with exactly directed setup for specification of different parameters. To check the importance of the evaporation we put some fat on the liquid surface. We use various pots with various specific heat capacities and the heat conductivities, see fig. 7. Comparison of dark coffee and clear water shows us the role of the absorptivity of the liquid surface.

We performed a set of experiments with different conditions: At first we discovered the results doesn't depend on surface tension what is important for the comparison of coffee and water. The next step was measurement for:

- three pots (china, ordinary metal sheet pot and vacuum-pot, it means the pot with double wall)
- three liquids (coffee, water and water with fat on its surface)

By determination and matching of all coefficients we have justified following facts:

- coffee surface (dark) radiates and absorbs heat better than water surface
- shining stainless pot radiates and absorbs heat worse than the dim one
- fat on the liquid surface prevents evaporation
- heat transfers through china pot a little worse than through thin metal pot and much better than through vacuum-pot

**Tab. 1:** The quantitative comparisons show relatively good quality our model

*	coffee- china	Water- china	fat- china	coffee- metal	water- metal	fat- metal	coffee- vac.pot	water- vac.pot	Fat- vac.pot
$\alpha$	0.990	0.005	0.005	0.990	0.005	0.005	0.990	0.005	0.005
$\beta$	0.192	0.192	0.192	0.178	0.178	0.178	0.050	0.050	0.050
$\nu \cdot 10^{11}$ (kg/s/°C/m <sup>2</sup> )	15.8	15.8	1.94	15.8	15.8	1.94	15.8	15.8	1.94
$k_1$ (J/s/K)	2.90	2.90	2.90	2.90	2.90	2.90	2.90	2.90	2.90
$k_2$ (J/s/K)	0.360	0.360	0.360	0.360	0.360	0.360	0.360	0.360	0.360
$k_3$ (J/s/K)	2.04	2.04	2.04	2.42	2.42	2.42	0.187	0.187	0.187

## Conclusion

This contribution shows the beginning of a story originating from one phenomenon of our everyday life. We formulated few models to describe the cooling down of a cup of coffee with good result. The sequence of approximations shows how we are pushed towards more detailed description and which processes are important and which not. We were forced to introduce some nonlinearity; we tried to do it by introducing power into evaporation speed. We verified the power dependence on temperature in an independent experiment. The whole story shows by simple means the path from observation to the description on some level and may continue in further studies and extension of experiment to range of other drinks.

## References:

- [1] Karls, M. A. - Scherschel, J. E.: Modeling heat flow in a thermos, Am. J. of Physics 71, 2003, p. 678-683
- [2] Brandt, S.: Statistical and computational methods in data analysis, North Holland/ American Elsevier Publishing Company, 1970
- [3] Greenwald, Sarah J. - Bauldry, William C.: Coffee cooling on a TI-CBL unit and in maple, <http://www.mathsci.appstate.edu/~sjg/papers/CoffeeCooling.pdf>, (on the date 2010-1-13)
- [4] Cooling a Cup of Coffee, <http://hyperphysics.phy-astr.gsu.edu/hbase/thermo/coocof2.html> (on the date 2010-1-13)
- [5] The Coffee problem, <http://www.rogerfrost.com/cof.htm> (on the date 2010-1-13)
- [6] Yanik, E.: Coffee, tea or not?, <http://archives.math.utk.edu/ICTCM/EP-7/SA14/pdf/paper.pdf> (on the date 2010-1-13)

## DESTRUCTIVE AND NON-DESTRUCTIVE EVALUATION OF PEACH FIRMNESS

LIBOR SEVERA<sup>1\*</sup>, JAN TRNKA<sup>2</sup>, ŠÁRKA NEDOMOVÁ<sup>1</sup>, PAVLA STOKLASOVÁ<sup>2</sup>,  
JAROSLAV BUCHAR<sup>1</sup>

<sup>1</sup>Mendel University in Brno, Zemedelska 1, 613 00 Brno, Czech Republic

Phone: +420545132093, e-mail: severa@mendelu.cz

<sup>2</sup>Institute of Thermomechanics, Dolejskova 5, 182 00 Praha 8, Czech Republic

### Abstract

The firmness of peach fruit („Red haven“) was monitored during 5 weeks within its harvesting period. Non-destructive impulse response and destructive Magness-Taylor puncture tests were used. Non-destructive impact was realized by the free falling bar. After impacting, the peach response was measured in terms of the surface displacement and/or surface velocity. The peach response was evaluated both in time and frequency domain. The correlation between response frequency and physical parameters of the peaches was analyzed. The dominant frequency, stiffness coefficient and elasticity coefficient as a function of time can be expressed as a decreasing, nearly linear function. The impulse response is more sensitive to firmness changes than the Magness – Taylor firmness test. When determining fruit fitness, the non-destructive impulse response test could replace conventional destructive tests.

### Introduction

Firmness has been as a criterion for sorting fresh fruits and vegetables for many years. The methods used include squeezing between the fingers or hands, pushing a thumb into the flesh, biting and chewing, and the penetrometer method, generally referred to as a Magness–Taylor (M–T) or Effe-gi test. Because of the destructive nature of these tests and an increasing emphasis on quality, non-destructive methods have been sought to quickly measure individual fruit for sorting by firmness to obtain a more uniform pack of consistent high-quality fruit and facilitate timely marketing investigated.

Some promising non-destructive methods for fruit quality evaluation are based on measurement of fruit response to forced vibration. For example, Affeldt and Abbott [1], Van Woensel, Verdonck, and De Baerdermaecker [2], and others found good correlation between the resonant frequencies derived from vibration tests and the mechanical properties of fruits. Armstrong, Zapp, and Brown [3] caused mechanical impulse by striking an apple with a ball of wax. Young's modulus which was calculated from the acoustic response, had good correlation with the measurement in compression tests of specimens taken from the same fruit. Poor correlation was found with the results of a

standard M-T test. Chen and De Baerdemacker [4] tested apples and concluded that the acoustic impulse response method appeared to be more efficient and accurate than random vibration methods.

The specific objectives of the research presented in the given paper were to :

- (1) analyze the response time signals and their frequency representation of peaches
- (2) establish relationship between the dominant frequency and the time of the peaches harvesting.

### Results and discussion.

Peaches (*Red Heaven*) were hand-harvested from the experimental orchard in the Department of Horticulture, Mendel University. Fruit were picked at the different days during July 2007. Fruit was transported immediately to the laboratory, and upon arrival, For size determination, three measurements (mm) at right angles were taken per fruit. Firmness was measured based on the resistance of the fruit flesh to deformation by the puncture probe. The Magness-Taylor technique measured the maximum force to pierce the pear to a puncturing depth. Typical dependence force – depth of the penetration is shown in the Fig.1

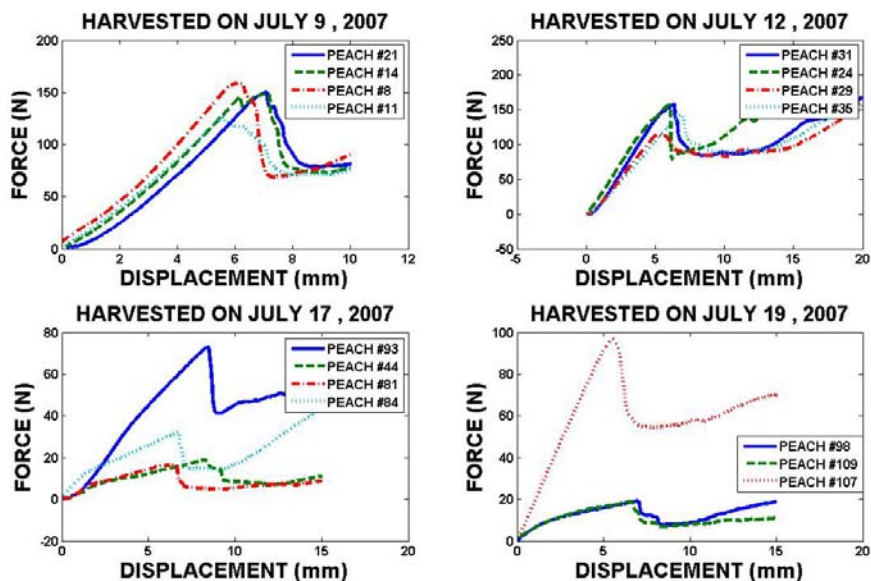


**Fig.1** Example of the firmness measurement. The diameter of the penetrator was 11 mm.

The maximum force which is denoted as the firmness depends on the data of the harvesting as shown in the Fig.2.

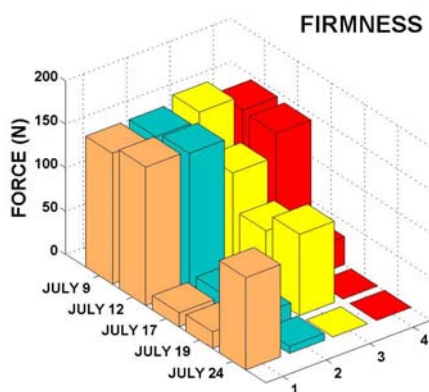


**Fig.2.** The firmness at the different days of the peach harvesting.

Generally the firmness decreases with the peach maturity as it is shown in the Fig.3.

The acoustic response has been measured using of an experimental setup which was developed and built to evaluate the resonance signal and analyze the frequency domain for peach fruit. The experimental setup consisted of a peach-bed, a mechanical impulse excitation device (a ball falling on the peach from a definite height), signal amplifiers and a personal computer and software to control the experimental setup and to analyze its results. The peach response has been measured in terms of

the surface displacement and/or surface velocity as well. The laser interferometer has been used. The response of the peach has been measured in two points A and B. The point A is located 10 mm from the point of ball impact. The point B is 30 mm far from the point A - see Fig. 4 .

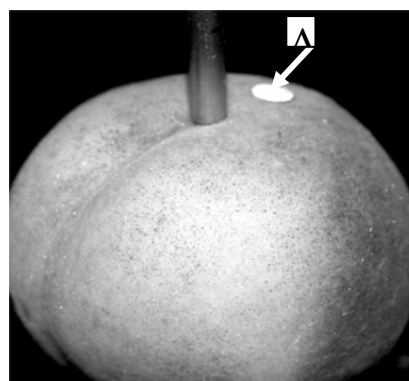


**Fig.3.** Detail of the peach loading.

The signals were sampled at a rate of 200,000 samples/s per second for a period of 50 ms. The MATLAB computer program transformed the response from time to frequency domain (Fig. 3) by means of Fast Fourier Transform (FFT). A search algorithm was used to identify the dominant frequency (the peak frequency, where the response magnitude is the greatest) of the pear. A typical result is shown in Fig. 5.

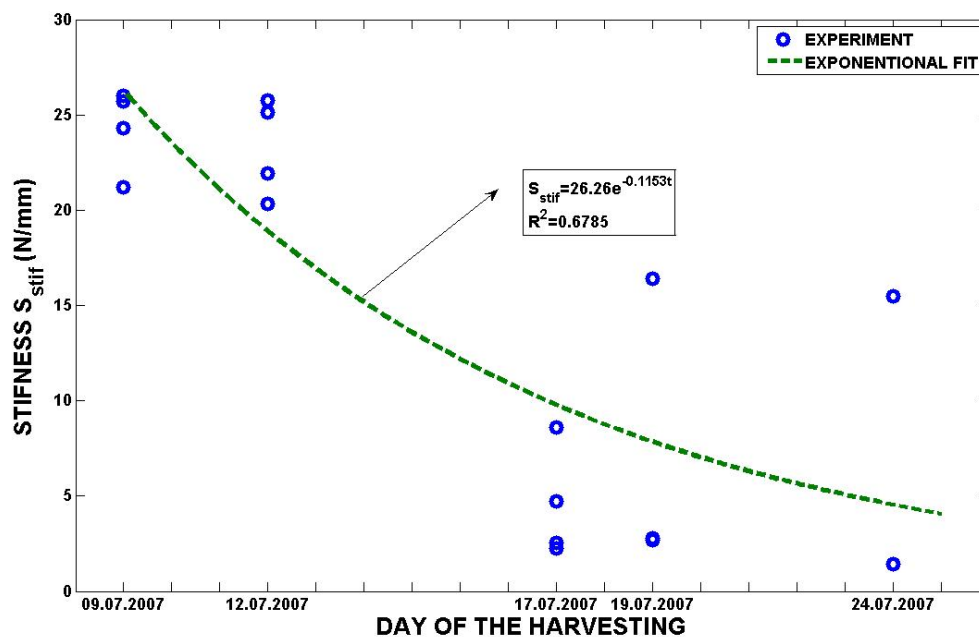


Fig.3. The decrease in the peach stiffness with the time of its harvesting.

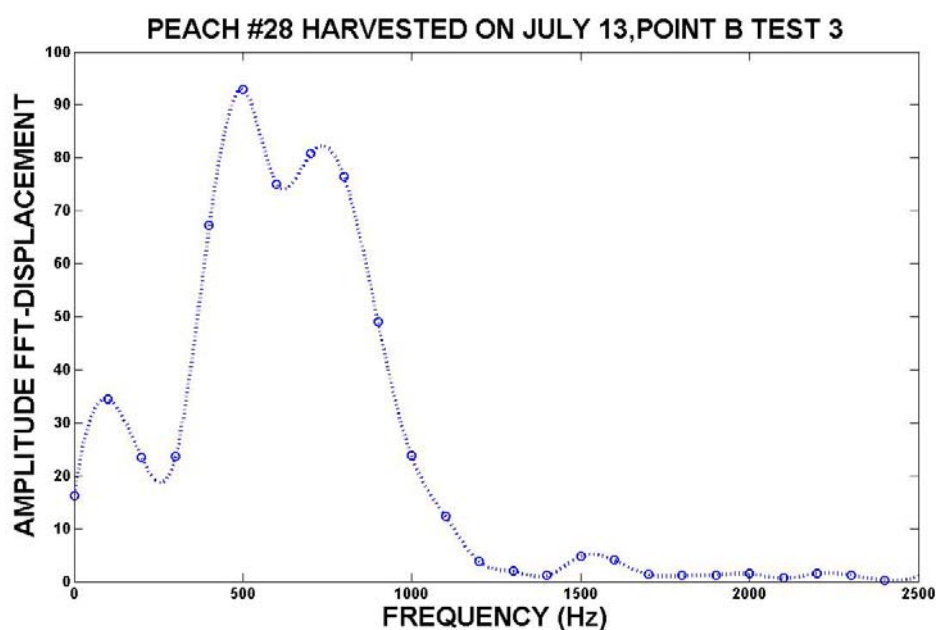


Fig.4. Example of the amplitude spectrum of the FFT displacement.

The frequency at which the maximum of the amplitude has been observed has been denoted as a resonance frequency and/or dominant frequency, respectively. This dominant

frequency decreases with peach maturity – see Fig.5. It means this quantity behaves like the firmness.



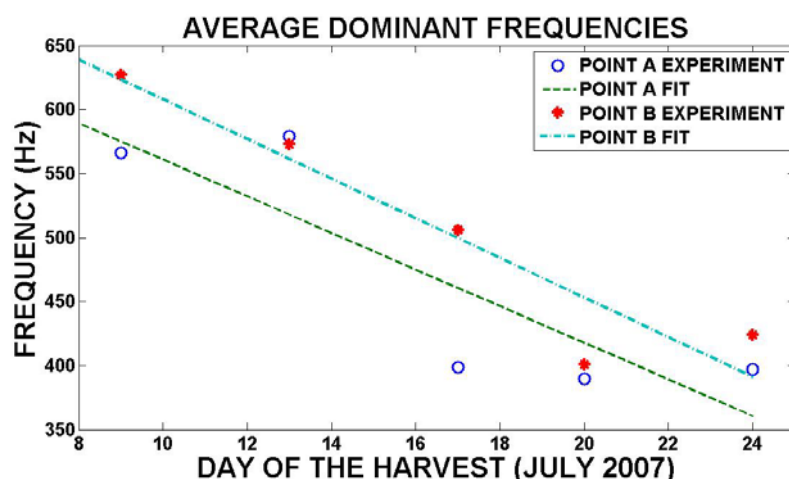


Fig.5. The dependence of the dominant frequency on the time of the harvesting.

The dependence of the dominant frequency  $f_d$  (Hz) on the time of the peach harvesting  $t$  (days) can be fitted by the functions :

$$\text{POINT A} \quad f_d = 703.7 - 14.3t \quad R^2 = 0.7428$$

$$\text{POINT B} \quad f_d = 763.3 - 15.4t \quad R^2 = 0.8921$$

If we assume that the peaches exhibit a nearly spherical shape the firmness can be expressed using of a stiffness coefficient (first introduced by [5] Abbott et al., 1968, modified by [6] Cooke and Rand, 1973) which can be calculated as:

$$S = f^2 m^{\frac{2}{3}}$$

where  $S$  is the stiffness coefficient,  $f$  the dominant frequency where response magnitude is the greatest (Hz) and  $m$  the fruit mass (g).

## Conclusions

The presented results suggest that the acoustic response of the peach to some dynamic excitation (ball impact) can be used for the peach maturity evaluation. Namely the frequency response seems be very promising. Dominant frequency increased with peach firmness increasing, and dominant frequency decreased with increasing of peach mass. The better relationship was obtained between dominant frequency and peach firmness or peach mass, and stiffness coefficient regressed on Magness–Taylor firmness had a good relationship also. The peach firmness could be considered to detect by using the dynamic resonance frequency analysis

## ACKNOWLEDGEMENTS

The research has been supported by the Grant Agency of the Czech Academy of Sciences under Contract No. IAA201990701

## REFERENCES

- [1] Abbott, J.A., Bachman, G.S., Childers, N.F., Fitzgerald, J.V., Matusik, F.J., Sonic techniques for measuring texture of fruit and vegetables. *Food Technol.* 1968, 22, 635–645.
- [2] VanWoenselt, G., Verdonck, E., De Baerdemaeker, J., Measuring the mechanical properties of apple tissue using modal analysis. *J. Food Proc. Eng.* 1988, 10, 151–163.
- [3] Armstrong, P.H., Zapp, R., Brown, G.P., Impulse excitation of acoustic vibrations in apples for firmness determination. *Trans. ASAE* 1990, 33, 1353–1359.
- [4] Chen, H., De Baerdemaeker, J., 1993. Effect of apple shape on acoustic measurements of firmness. *J. Agr. Eng. Res.* 56, 253–266.
- [5] Abbott, J.A., Bachman, G.S., Childers, N.F., Fitzgerald, J.V., Matusik, F.J., 1968. Sonic techniques for measuring texture of fruit and vegetables. *Food Technol.* 22, 635–645.
- [6] Cooke, J.R., Rand, R.H., 1973. A mathematical study of resonance in intact fruit and vegetables using a three media elastic sphere model. *J. Agric. Eng. Res.* 18, 141–157.



## PERSONAL REMOTE SENSING SYSTEM FOR PRECISION FARMING

HIROSHI SHIMADA<sup>1\*</sup>, EIKICHI SHIMA<sup>2</sup>, KATSUYUKI TANAKA<sup>2</sup>, TAKESHI  
NAGAYOSHI<sup>1</sup>, MITSUHIKO KATAHIRA<sup>3</sup>

<sup>1</sup>Akita Prefectural University, 2-2 Minami, Ogata-mura, Minami-Akita-gun, Akita, 010-0444,  
Japan, Phone: +81-185-45-3945, Fax: +81-185-45-2377, E-mail: hiro@akita-pu.ac.jp

<sup>2</sup>Kitasato University, Towada, Aomori, Japan,

<sup>3</sup>Yamagata University, Tsuruoka, Yamagata, Japan

### Abstract

We developed the personal remote sensing system which consisted with the following element for the extremely small area like a Japanese paddy field (100 \* 100m) : radio controlled helicopter, two digital still cameras, network camera board, wireless LAN, notebook computer for the ground station and image processing software of the own work.

And, as for this system, one of two digital still cameras was remodeled to have the sensitivity of the near-infrared stage to 1100nm mostly. The image data of 4 band (NIR, R, G, B) can be acquired by these two digital still cameras. Furthermore, image processing software of its own work can do the composition of the false and natural color image, and can do the computation of the NDVI, G/R ratio and HSV. Therefore, the acquisition of the adjacent image due to handheld photography image and aerial one to the absolute altitude circa 200m by the helicopter system can be acquired and real-time remote sensing in the field become possible. It tries the identification of the crown rust in the pasture and the survey of the coverage in the field, and availability to precision farming is discussed in this paper.

### Introduction

Recently, remote sensing by the artificial satellite and aircraft is used even for the agriculture field actively. The acquisition cost of the image data by the satellite and the aircraft for the remote sensing is very expensive. And, it may not be able to get a required image by conditions of weather. Particularly, satellite image data is lengthy in case of remote sensing of the extremely narrow area like a paddy field (100 \* 100m) in Japan. It grappled with the development of the simple personal remote sensing system to solve these problems.

This system consists from the 4 band camera system which used two digital still camera on the market, a small-scale radio control helicopter, the wireless LAN device and image processing software of the own work. R, G, B and near infrared (NIR) data are acquired with 4 band camera, and this system does image processing corresponding to the necessity, and it can calculate Normalized Difference Vegetation Index (NDVI), G/R ratio and HSV (Shimada at

et.,2006; Shimada at et., 2003; Shimada at et., 2006;).

Furthermore, the system which used unmanned industrial helicopter as the career base was made, too. The purpose of this new system is the realization of the efficient aerial photography at the field of the 5ha scale. Therefore, the acquisition of the adjacent image due to handheld photography image and aerial one to the absolute altitude circa 200m by the helicopter system can be acquired. (Shimada at et.,2008;).

The availability examination of this system was done at the soybean in the early stages of growth and at the pasture. Then, it got a handheld photography image and the aerial one. In this paper, it is reported about characteristics of NDVI and G/R ratio by personal remote sensing system. And, it tries the identification of the crown rust in the pasture and the survey of the coverage in the field, and availability to precision farming is discussed.

### Overview of Personal remote sensing system

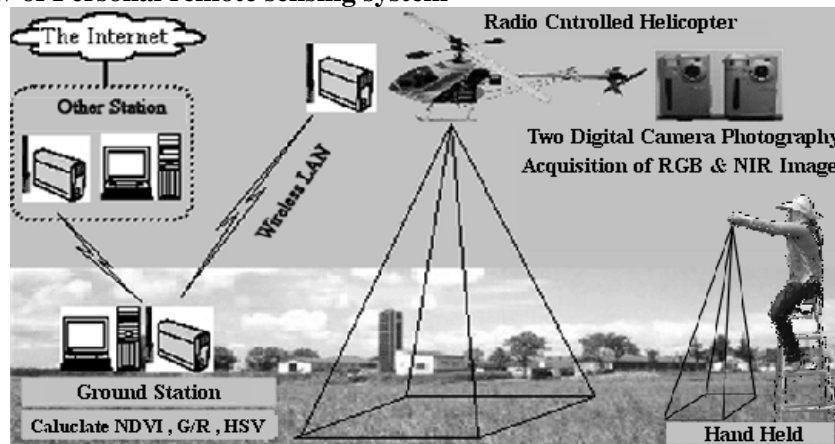


Figure 1. Schematic diagram of personal remote sensing system

The schematic diagram of personal remote sensing system is shown in Figure 1. A developed personal remote sensing system is consisting with the radio controlled small-scale helicopter or industrial, the photography device and the personal computer for the ground station. A ground station PC does the monitoring of the finder movie and image processing. A photography device is composed of the two digital still cameras, a board computer for the network camera server and relay switch, on the network camera server board, to control shutter.

And, near-infrared (NIR) cutoff filter is removed from one digital still camera, and a NIR pass filter is attached to get a clear NIR image. Therefore, 4 band data (R, G, B, NIR) can be acquired by taking pictures with two RGB • NIR cameras of the same model. The photography with confirming a finder movie, the confirmation of the RGB • NIR image which acquired it and image processing can be done by these immediately at the investigation applicable field.

### Overview of Aerial photography system



Figure 2. Aerial photography system with the hobby-use radio controlled helicopter

An aerial photography system by the radio controlled small-scale helicopter for the hobby-use is shown in the figure 2. Because weight of aerial photography system is 19.6N mostly, it

can fly as to the payload capacity of the hobby use helicopter beyond 50 classes (Engine displacement : about 8.19cc output : 1.3kW).

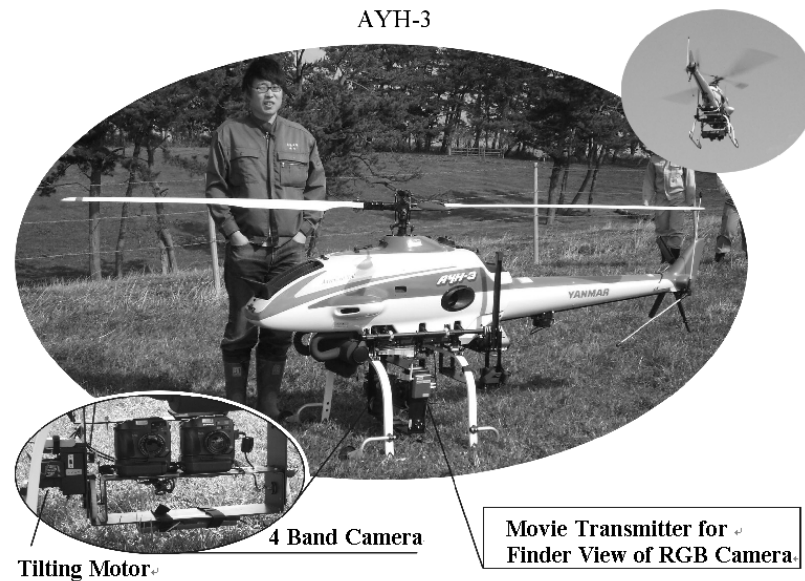


Figure 3. Aerial photography system with the industrial-use unmanned helicopter

And an aerial photography system by the industrial-use unmanned helicopter is shown in the figure 3. Used helicopter is AYH-3 (Yammer Ltd). Its entire length is 3.63m, weight is 568.8N, engine output is 15.4kW, rotor diameter is 3.12m and payload is 274.6N. These aerial photography system are operated with two man people.

#### Overview of software for personal remote sensing system

The screen shot of developed software is shown in the figure 4. The following is processed with this software. 1) The sRGB Value is convert into the linear RGB, because pixel value output

from digital still camera is non-linear sRGB. 2) When RGB and a NIR image are composed, four tie points are chosen in each image, and geometry compensation is given. 3) When a ratio calculation between the RGB and NIR value such as NDVI is done, the proportional correction of the pixel value is done due to the exposure value of the RGB and NIR camera in the photography. 4) The false and natural color image are composed. 5) And, the NDVI, G/R ratio and Hue-Saturation-Value (HSV) are calculated. 6) Furthermore, the various visualization images of the index are made if necessary, and an identification or survey by the threshold is done.

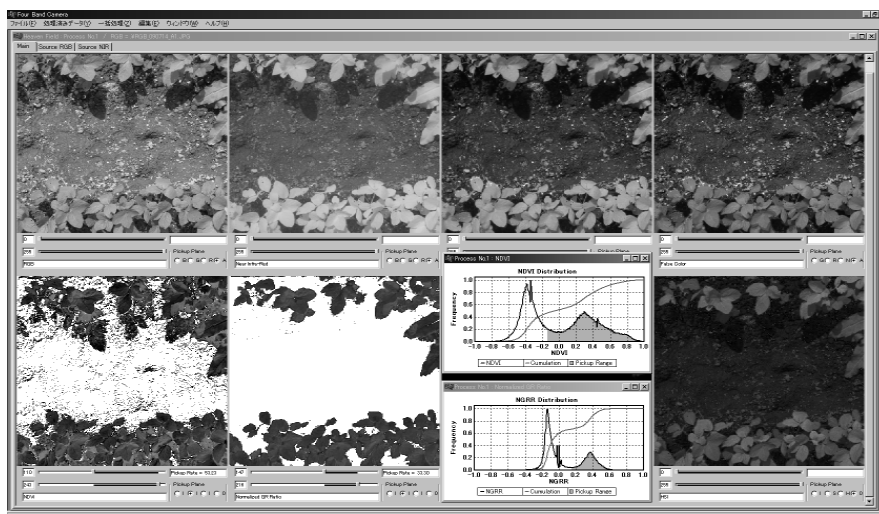


Figure 4. Developed software for personal remote sensing

And, the value range of the G/R ratio is infinity from 0, and hard to use as an index. So, a G/R ratio is normalized with the following expression, and it uses for the various verification by this paper.

$$\text{NGRR} = (G - R) / (G + R)$$

NGRR : Normalized G/R Ratio ( -1  
≤ NGRR ≤ +1 )

G : Linear G value    B : Linear R value

### Material and Method

The hand held photography system was used for soybean field. The person who had a camera took pictures of the soybean inside the one meter quadrat from the top of the stepladder. At this time, photography height was circa 2.6m. And, the photography period of the soybean is circa 100 days in about every 1 week on the 2nd after the budding.

The unmanned industrial helicopter system was used for the aerial photography of the pasture. The pasture's photography was done after the first cutting on about the 45th. And, perennial ryegrass occupies most of the pasture of which it took pictures.

After the compensation of the lens distortion is given, as for 4 band data acquired by this two photography, NDVI and NGRR are calculated by the developed software. Furthermore, the various visualization images of the index are made if

necessary, and an identification or survey by the threshold is done.

### Result and Discussion

It tried the extraction of the vegetation area by NDVI with an image of the soybean field. This image was acquired by the hand-held photography. The result of extraction is shown in the figure 5. This RGB image is consisted. This image consists in the leaf, the shadow of the leaf and the surface of the soil. It is understood that NDVI of the vegetation area where direct sunlight shines is on the same level as the leaf shadow (Figure 5. B). Furthermore, it tried the distinction of the vegetation area by the threshold of NDVI. But, it was extracted as a vegetation, and a leaf shadow area couldn't get correct coverage (Figure 5. C). It can think as this reason as follows. The transmitted G and NIR intensity of light rates increase relatively because R and B light are absorbed by photosynthesis more abundantly, and NDVI grows large as that result. Furthermore, it confirms that a high NDVI problem occurs in case as a shade area like furrow that direct sunlight doesn't shine as well with a dent corn field image.

Therefore, the high NDVI problem of this leaf shadow and shade area doesn't occur in a remote sensing like an artificial satellite, and guesses to be the problem which is unique to proximity remote sensing like a this system.

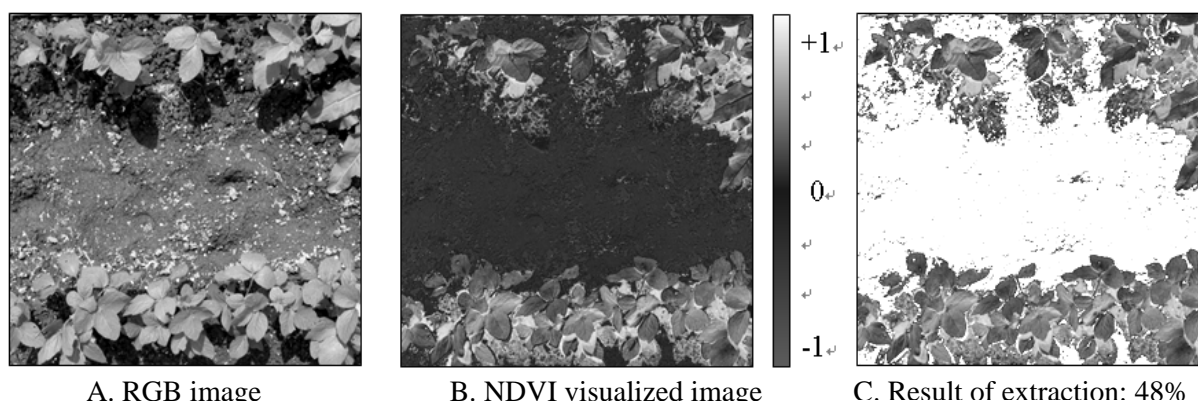


Figure 5. A extraction of the vegetation area by NDVI in the soybean image



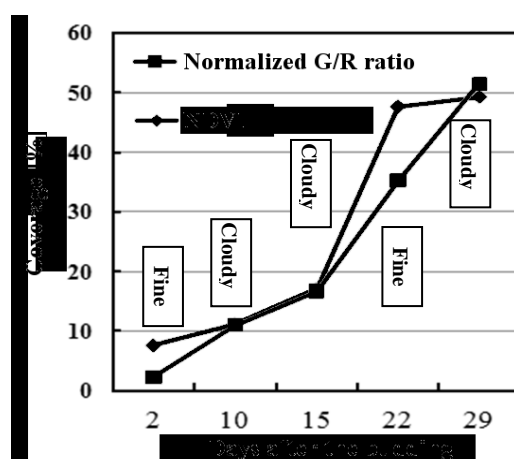


Figure 7. Relations between the coverage based on NDVI • NGRR and the weather

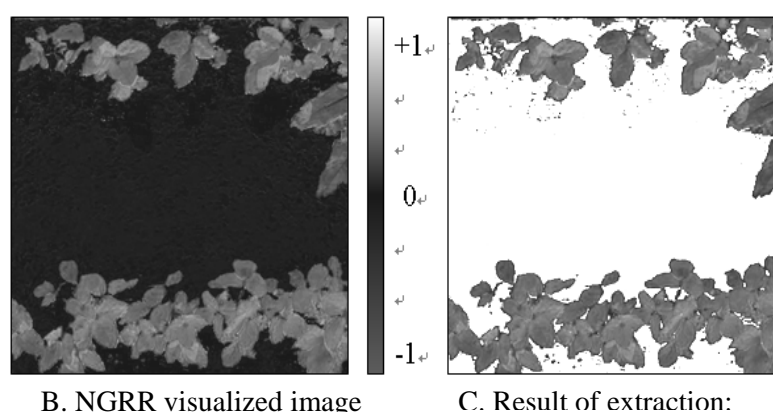


Figure 6. A extraction of the vegetation area by NGRR in the soybean image

The result that it tried a vegetation distinction with NGRR which it got from the RGB image of the figure 5 is shown in the figure 6.

It is understood that vegetation is distinguished clearly when a figure 6.B and C are seen. Relations between the coverage and the weather are shown in the figure 7. In case of a vegetation distinction by NDVI, though it is accurate as well as NGRR with fine sky image, a leaf shadow becomes a large error cause with cloudy sky image.

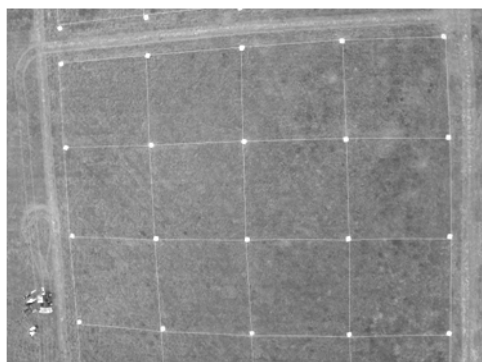
Therefore, if the weather doesn't have an influence and wants to survey more securely, vegetation should have coverage distinguished with not NDVI but NGRR. NGRR can be thought to use like NDVI in the remote sensing because it is an observed value based on the leaf color, too.

The identification of 'Crown rust' in the pasture by Normalized G/R ratio is shown as an application example of personal remote sensing

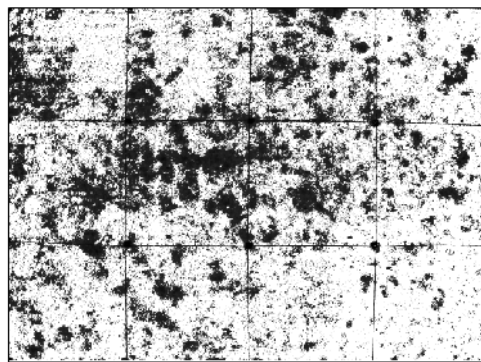
system in the figure 8. The object of the distinction is the region corrected by the ground control point on the pasture geometrically. In this case, a contraction area was distinguished by NGRR. Furthermore, it confirms that a good result can get even a distinction by the hue, too. These distinction corresponded to a result of observation in the actual pasture favorably.

## Conclusion

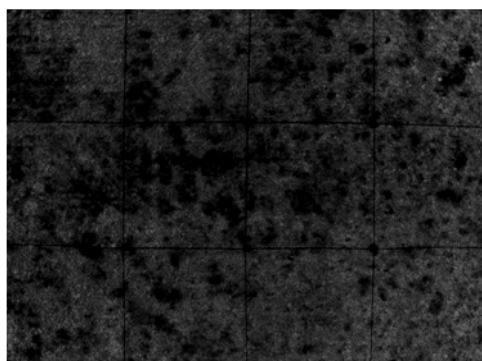
It found that it could get coverage and plant activation more precisely by NGRR as a result of the verification of the neighboring image. Furthermore, it was shown that the identification of the crown rust was possible by NGRR and the hue. It is judged that it can be applied to rice blast as well with a similar process. And, it can think that the preventive observation of the occurrence of crown rust and rice blast is possible by making use of the mobility of this system because remote sensing can be done thickly when it is necessary.



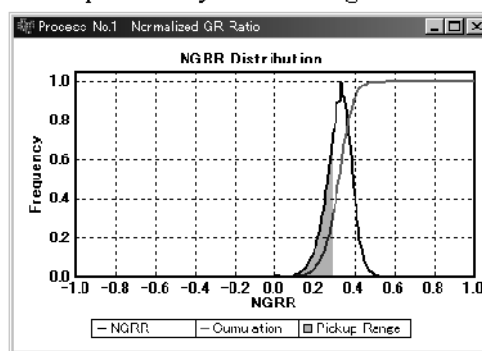
RGB image



Pickup Pixels by thresholding of NGRR



Visualized image of Normalized G/R ratio



NGRR distribution and thresholding

Figure 8. Identification of 'Crown rust' in the pasture by Normalized G/R ratio  
(Result: 32.99% / Photography advanced: about 50m )

From now on, it will improve availability by linking with GIS as a personal remote sensing system for the precision farming.

#### Reference:

- [1] Hiroshi Shimada, Eikichi Shima, Takeshi Nagayoshi, Katsuyuki Tanaka: Development of Personal Remote Sensing System for an Extremely Narrow Area. ASABE Technical library (On-line), 2006, Paper number 061169.
- [2] Hiroshi Shimada, Eikichi Shima, Takeshi Nagayoshi, Katsuyuki Tanaka: Use of Personal Remote Sensing System in Grazing Land. ASABE Technical library (On-line), 2008, Paper number 084473.

- [3] Shimada Hiroshi: Development of Simple 4 Band Camera System with Stereo Photography. Tohoku Branch Report of JSAM. 50, 2003, p.25-28, (in Japanese)
- [4] Shimada Hiroshi, Shima Eikichi, Tanaka Katsuyuki, Nagayoshi Takeshi, Yoshino Kunihiro, Hattori Toshihiro, Kato Wataru, Watanabe Kazuya: Monitoring for Investigation of Field by Simple 4Band Camera System with Stereo Photography. Journal of the Japanese Society of Irrigation, Drainage and Reclamation Engineering 74(11), 2006, p.969-972., (in Japanese)



## CLIMATIC CONDITIONS FOR DESIGNING HEATING/COOLING SYSTEM

VLADIMÍR ŠLEGER\*, PAVEL NEUBERGER, MARTIN POLÁK

Czech University of Life Sciences in Prague, 16521 Prague 6 – Suchbát, Czech Republic,

E-mail: sleger@tf.czu.cz

### Abstract

In this paper the climatic conditions are assessed based on daily data collected from 30 weather stations in the Czech Republic throughout the period from 1 January 1961 to 31 December 2000.

A method for estimating the number of hours during which air temperature is lower than preselected limiting level in situations where only the minimum, average, and maximum daily temperature data are available has been suggested and tested. If the limiting temperature ( $\theta_{lim}$ ) lies between the minimum ( $\theta_{min}$ ) and average ( $\theta_{avg}$ ) temperatures, the number of hours ( $\tau_d$ ) with temperatures lower than the limiting level during one day is calculated by using the equation

$$\tau_d = \frac{24}{\pi} \cdot \arcsin \left( \frac{\theta_{lim} - \theta_{avg}}{\theta_{avg} - \theta_{min}} \right) + 12 \quad (\text{all temperatures in degrees Centigrade}).$$

If the limiting temperature lies between the average and maximum ( $\theta_{max}$ ) daily temperatures, the relationship

$$\tau_d = \frac{24}{\pi} \cdot \arcsin \left( \frac{\theta_{lim} - \theta_{avg}}{\theta_{max} - \theta_{avg}} \right) + 12 \quad (\text{temperatures in degrees Centigrade})$$

is applied. Statistical analysis revealed that a significant interdependence exists between the average number of hours in a year with temperatures below the limiting level and the average annual temperature at an area.

The results can be used when calculating the power demands of heating/cooling facilities in agricultural and other buildings at sites with average annual temperatures between 2.8°C and 9°C.

### Introduction

Climatic conditions at a site are among important input parameters when assessing the efficiency and effectiveness of an agricultural building heating/cooling facility at that site. It is necessary to know the total time of occurrence of a given temperature during a year.

The data from a site can only be assessed based on long-term meteorological information. In fact, data used by current national standards to describe climatic conditions in the Czech Republic are from the years 1901 to 1950.

Information on climatic conditions in the Czech Republic can be found for example in the ASHRAE – Fundamentals handbook (2005), summarizing data collected from 4422 stations especially in the US and Canada, as well as from other countries worldwide. However, the data have been compared based on old or short measuring series and do not match each other enough from the time and/or space aspects.

The new standard, ČSN EN 12831:2005, uses old data (1901 – 1950) to describe the

climatic conditions in the various areas of the country. There have been published more recent meteorological data measured and observed in the Czech Republic over the period from 1961 to 1990 or 2000 (Křiváncová and Vavruška, 1997), (Květoň, 2001), (Tolasz et al., 2007). The data, however, are not detailed enough to enable the estimation of effectiveness of air-conditioning facilities to be assessed.

Although not impossible, collecting new and, at the same time, long-run and detailed data from the Czech Hydrometeorological Institute would be a very expensive project, requiring processing of a large volume of data, which are often difficult to obtain.

The aim of the present paper is to calculate, based on current meteorological data the average number of hours during a year during which the temperature at a given site is below a specific limiting level, in dependence on the average annual temperature at the area.

## Material and methods

Climatic conditions at specific areas were assessed based on daily meteorological data over the period from 1 January 1961 to 31 December 2000, obtained from the NGO “National Climate Programme for the Czech Republic” (NKP). The maximum, minimum, and average daily temperatures collected from 30 weather stations are available in the electronic format. The maximum and minimum daily air temperature was determined by using extreme thermometers. The average daily temperature was calculated from data measured in predetermined time points (at 7 am, at 2 pm, and at 9 pm).

Weather stations performing continuous measurements at fixed sites (as far as possible)

were selected. All of them in the Czech Republic lie between 48.8° and 50.8° north latitude at altitudes from 158 m to 1324 m.

The average annual temperature served as a parameter describing the site for the purpose of comparison and generalization of the climatic conditions in the various areas. It is necessary to take into account, that this parameter is time variable. A comparison of long-term average temperature at various altitudes over the 1991 – 2000 period and the 1961 – 1990 period (Šleger et al., 2009) is shown in Fig. 1. The plot demonstrates that the average temperature during the 1991 – 2000 period was nearly 0.6 K higher than during the 1961 – 1990 period, irrespective of the altitude.

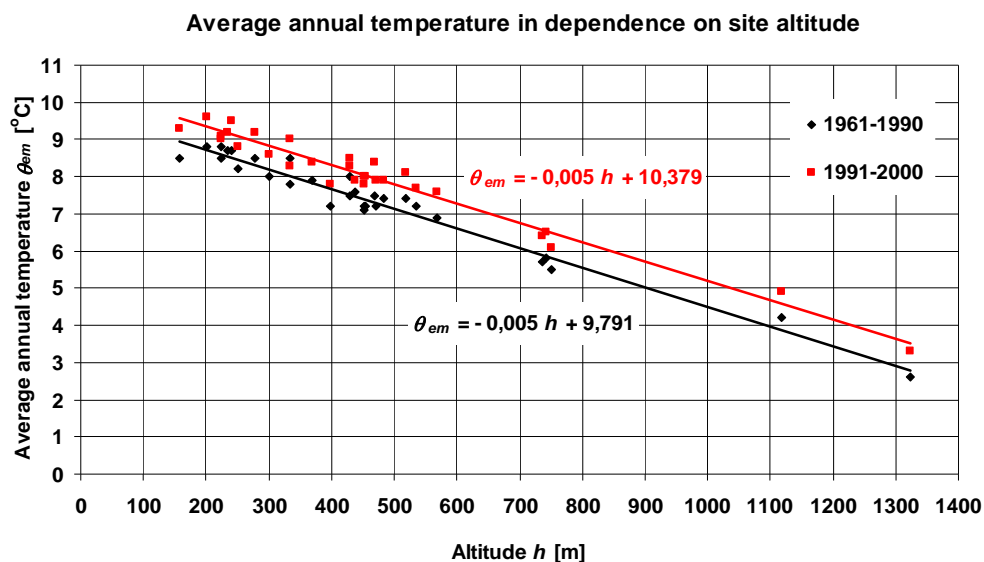


Fig. 1. Average annual temperature at different sites over two different periods of time

Considering a typical temperature development during the day, the number of hours during which air temperature is lower than the predetermined limiting level can be estimated. Now, if the limiting temperature is higher than the maximum daily temperature, air temperature is lower than the limiting level for 24 hours of the day, whereas if the limiting temperature is lower than the minimum daily temperature, air temperature is never lower than the limiting level that day.

A problem only occurs if the limiting level lies between the maximum and minimum daily temperatures. It is suggested that the actual interdependence between the number of hours

with lower temperatures during the day  $\tau_d$  (hours) and the limiting temperature  $\theta_{lim}$  (degrees Centigrade) lying within this range can be fitted with function defined in Table 1.

The function was tested on data from the year 2005, a year for which hourly air temperature data collected by the weather station at the Czech University of Life Sciences in Praha-Suchdol are available (<http://meteostanice.agrobiologie.cz>).

The function was then used to calculate the number of hours with temperatures lower than 55 selected limiting levels (from -21°C to 33°C) over the entire 40-year period at all of the 30 weather stations. The least squares method

was applied to fit the large volume of resulting data with a quadratic regression dependence of the number of hours on the average annual temperature of the specific site. Only such

regression functions whose coefficient of determination (correlation coefficient squared) was higher than 0.9 were considered significant.

Tab. 1. Definition of the function suggested

Relationship validity range	
$\theta_{min} \leq \theta_{lim} \leq \theta_{avg}$	$\theta_{avg} < \theta_{lim} \leq \theta_{max}$
$\tau_d = \frac{24}{\pi} \cdot \arcsin\left(\frac{\theta_{lim} - \theta_{avg}}{\theta_{avg} - \theta_{min}}\right) + 12$	$\tau_d = \frac{24}{\pi} \cdot \arcsin\left(\frac{\theta_{lim} - \theta_{avg}}{\theta_{max} - \theta_{avg}}\right) + 12$

## Results and discussion

The true measured values are good fitted by the arc sine function defined in Table 1 passing through the minimum, average, and maximum daily temperature levels. The average absolute difference between the estimate and the true value is lower than 14 hours for this function. The calculated estimates in comparison with

actual data measured by the Praha-Suchbát weather station in 2005 are shown in Figure 2.

Statistical analysis revealed that a significant interdependence, given in Table 2, exists between the average number of hours ( $\tau$ ) in a year with temperatures below the limiting level (from  $-9^{\circ}\text{C}$  to  $29^{\circ}\text{C}$ ) and the average annual temperature ( $\theta_{yr}$ ).

Tab. 2. Interdependence between the annual number of hours with temperatures lower than the limiting level and the average annual temperature

limiting temperature (°C)	quadratic regression function $\tau$ (hr), $\theta_{yr}$ (°C)	coefficient of determination	limiting temperature (°C)	quadratic regression function $\tau$ (hr), $\theta_{yr}$ (°C)	coefficient of determination
29	$\tau = -3.420 \cdot \theta_{yr}^2 + 28.29 \cdot \theta_{yr} + 8711$	0.901	9	$\tau = 6.123 \cdot \theta_{yr}^2 - 411.47 \cdot \theta_{yr} + 7593$	0.988
28	$\tau = -4.700 \cdot \theta_{yr}^2 + 36.68 \cdot \theta_{yr} + 8697$	0.919	8	$\tau = 8.580 \cdot \theta_{yr}^2 - 435.43 \cdot \theta_{yr} + 7302$	0.989
27	$\tau = -6.282 \cdot \theta_{yr}^2 + 46.35 \cdot \theta_{yr} + 8682$	0.932	7	$\tau = 9.584 \cdot \theta_{yr}^2 - 439.38 \cdot \theta_{yr} + 6952$	0.989
26	$\tau = -7.970 \cdot \theta_{yr}^2 + 54.53 \cdot \theta_{yr} + 8670$	0.941	6	$\tau = 8.502 \cdot \theta_{yr}^2 - 417.02 \cdot \theta_{yr} + 6528$	0.988
25	$\tau = -9.686 \cdot \theta_{yr}^2 + 60.30 \cdot \theta_{yr} + 8664$	0.951	5	$\tau = 7.308 \cdot \theta_{yr}^2 - 396.32 \cdot \theta_{yr} + 6122$	0.985
24	$\tau = -11.030 \cdot \theta_{yr}^2 + 59.29 \cdot \theta_{yr} + 8671$	0.958	4	$\tau = 5.391 \cdot \theta_{yr}^2 - 369.77 \cdot \theta_{yr} + 5710$	0.982
23	$\tau = -11.838 \cdot \theta_{yr}^2 + 50.33 \cdot \theta_{yr} + 8690$	0.965	3	$\tau = 3.615 \cdot \theta_{yr}^2 - 348.77 \cdot \theta_{yr} + 5322$	0.978
22	$\tau = -12.386 \cdot \theta_{yr}^2 + 37.18 \cdot \theta_{yr} + 8707$	0.970	2	$\tau = 2.654 \cdot \theta_{yr}^2 - 342.51 \cdot \theta_{yr} + 4983$	0.975
21	$\tau = -12.596 \cdot \theta_{yr}^2 + 19.10 \cdot \theta_{yr} + 8724$	0.975	1	$\tau = 3.013 \cdot \theta_{yr}^2 - 354.60 \cdot \theta_{yr} + 4685$	0.972
20	$\tau = -12.865 \cdot \theta_{yr}^2 + 0.85 \cdot \theta_{yr} + 8726$	0.979	0	$\tau = 6.207 \cdot \theta_{yr}^2 - 395.75 \cdot \theta_{yr} + 4427$	0.968
19	$\tau = -13.094 \cdot \theta_{yr}^2 - 18.11 \cdot \theta_{yr} + 8709$	0.982	-1	$\tau = 11.623 \cdot \theta_{yr}^2 - 445.73 \cdot \theta_{yr} + 4143$	0.968
18	$\tau = -13.718 \cdot \theta_{yr}^2 - 33.81 \cdot \theta_{yr} + 8666$	0.984	-2	$\tau = 17.222 \cdot \theta_{yr}^2 - 488.92 \cdot \theta_{yr} + 3852$	0.969
17	$\tau = -14.176 \cdot \theta_{yr}^2 - 52.43 \cdot \theta_{yr} + 8607$	0.985	-3	$\tau = 20.253 \cdot \theta_{yr}^2 - 491.77 \cdot \theta_{yr} + 3461$	0.972
16	$\tau = -14.184 \cdot \theta_{yr}^2 - 77.60 \cdot \theta_{yr} + 8542$	0.986	-4	$\tau = 21.285 \cdot \theta_{yr}^2 - 467.54 \cdot \theta_{yr} + 3027$	0.971
15	$\tau = -12.992 \cdot \theta_{yr}^2 - 116.60 \cdot \theta_{yr} + 8483$	0.986	-5	$\tau = 20.118 \cdot \theta_{yr}^2 - 416.35 \cdot \theta_{yr} + 2555$	0.970
14	$\tau = -10.913 \cdot \theta_{yr}^2 - 164.25 \cdot \theta_{yr} + 8413$	0.986	-6	$\tau = 17.745 \cdot \theta_{yr}^2 - 351.85 \cdot \theta_{yr} + 2084$	0.967
13	$\tau = -7.808 \cdot \theta_{yr}^2 - 220.96 \cdot \theta_{yr} + 8333$	0.986	-7	$\tau = 14.440 \cdot \theta_{yr}^2 - 281.17 \cdot \theta_{yr} + 1646$	0.959
12	$\tau = -4.138 \cdot \theta_{yr}^2 - 279.42 \cdot \theta_{yr} + 8221$	0.986	-8	$\tau = 11.164 \cdot \theta_{yr}^2 - 215.16 \cdot \theta_{yr} + 1261$	0.942
11	$\tau = -0.215 \cdot \theta_{yr}^2 - 335.10 \cdot \theta_{yr} + 8069$	0.987	-9	$\tau = 8.668 \cdot \theta_{yr}^2 - 164.80 \cdot \theta_{yr} + 964$	0.911
10	$\tau = 3.431 \cdot \theta_{yr}^2 - 381.61 \cdot \theta_{yr} + 7862$	0.988			

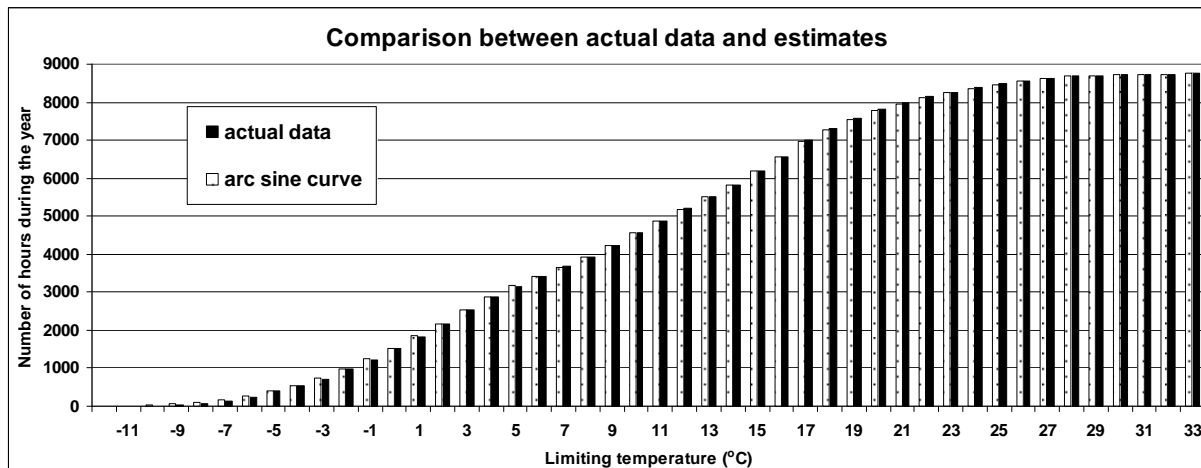


Fig. 2. Number of hours in 2005 during which air temperature at the Praha-Suchdol weather station was lower than the limiting level

## Conclusion

The method presented in this contribution allows to calculate, based on daily meteorological data the numbers of hours in a year during which air temperature at a site with a specific average temperature is lower than a chosen limiting level. It has been applied at 30 weather stations in the Czech Republic at different altitudes and with different average temperatures, using weather data from the 1961 – 2000 period. Statistical analysis revealed that a significant interdependence exists between the annual number of hours with temperatures lower than the limiting level and the average annual temperature.

The results can be used when calculating the power demands of heating/cooling facilities in agricultural and other buildings at sites with average annual temperatures between 2.8°C and 9°C.

## Reference:

- [1] ASHRAE Handbook – Fundamentals (Include CD). American Society of Heating, Refrigerating and Air-Conditioning Engineers, 2005. ISBN 1931862702.
- [2] ČSN EN 12831: Heating systems in buildings – Method for calculation of the design heat load. Czech Office for Standards, Metrology and Testing, 2005. (in Czech)
- [3] Krivancová, S. - Vavruška, F.: Basic meteorological elements in different weather situations in the Czech Republic over the 1961 – 1990 period. Czech Hydrometeorological Institute, Prague, 1997, 114 p. ISBN 80-85813-52-1. (in Czech)
- [4] Květoň, V.: Air temperature normals in the Czech Republic in 1961 – 1990 and selected temperature parameters over the 1961 – 2000 period. Czech Hydrometeorological Institute, Prague, 2001, 217 p. ISBN 80-85813-91-2. (in Czech)
- [5] Šleger, V. – Neuberger, P. – Polák, M.: Feasibility of using heat-recovery exchangers in livestock buildings at a site at a specific altitude with a specific average outdoor air temperature. Infrastructure and ecology of rural areas, 7, 2009, p. 47 – 56. ISSN 1732-5587.
- [6] Tolasz et al.: Climate Atlas of Czechia. Czech Hydrometeorological Institute, Prague, 2007, 255 p. ISBN 978-80-86690-26-1. (in Czech)

## THE OPTIMUM MANAGEMENT IN THE AGRARIAN PRODUCTION AND NATURE-USE ON THE SELF-ORGANIZATIONAL BASE

STREBKOV D.S., SVENTICKIY I.I., ZHMAKIN I.K., KOROLEV V.A., MUDRIK V.A.

All-Russian Research Institute for Electrification of Agriculture,

2, 1st Veshnyakovsky pr., 109456. Moscow, Russia

Phone: +7-499-171-19-20, Fax: +7-499-170-51-01, E-mail: viesh@dol.ru

### Abstract

In this paper are considered the ideal characteristics of the self-organizing evolving natural systems - their spontaneous aspiration in development to economy: energy, material and information. With complication of the system its progressive evolution speeds up. These characteristics of the self-organization it is necessary to take into account in having a special purpose functions of optimum management in agrarian industrial complex (AIC) and nature use.

### Introduction

The agrarian production, either as row other productions, uses the natural resources, created by self-organizing nature in process of its evolution. Creation of machine technologies production of agricultural product on base of the systems "exact" (differentiated) of the husbandry and stock-breeding is recognized by general direction of agrarian engineering studies in XXI century [1]. Management by highly efficient agrarian technologies must be ecological compatible and provide minimization of negative influences of technologies on nature and on used by them resources.

The studies on decision of the problem of the energy saving in AIC is grounded the law of the survival (LS), the essence of which is opposite essence second element of thermodynamics (SET). LS and SET logically conceptual, in the shape of mirror dynamical symmetry, form the principles of energy extremeness self-organization and progressive evolution (PEES and PE). All problems of the classical thermodynamics managed to allow on base LS, SET, PEES and PE that has allowed to solve the main problem biophysicists – to unite the physics and biology [2,3]. On modern presentations evolutionists and researchers of the adjacent branches of the knowledges all stages to progressive evolution (physico-chemical, biological, social) have a general energy economical directivity. The SY#STEM studies called on with use the law of the survival, principle energy extreme self-organization and progressive evolution, have exposed the ideal general directivity to progressive evolution of the nature.

The development (individual, evolutionary) of the systems of the self-organizing nature has a spontaneous directivity to increasing of energy efficiency (the energy economy) of the processes and structures, reduction their material capacity, economical use to information. On measure of the complication of the structures and processes of the developing system its evolutionary process speeds up.

### Initial positions of the new approach

Agroecological and ecological natural systems are a complex dynamic systems, reliable analysis them and management them is in principal hampered. For overcome this difficulty use idealizational of like systems, for instance, idealization of complex electric energy systems [4]. Under idealization is understood separation defining and casting-out secondary characteristics (in condition of the solved problem) that or other phenomenas, process or device. Like idealized systems often name as the mathematical models. Modeling of the agrozenoses, agroecosystems and ecosystems is denoted enormous amount of the studies [3, 5]. In most cases in these studies use the simulation models, for which is typical very low accuracy. Only ecological model "predator - victim" Volitera-Lotki, in which is used not formalized idealization on base of the trophic (bioenergy) relationships, provides required accuracy of the reflection of the real interaction in nature two components of part of ecosystem – "predator – victim".

The analysis of the ecobiological models has allowed to reach a conclusion that for reliable modeling of agrzenoses and



agroecological systems it is necessary to use biotechnoenergy idealization. Practicability of such approach results from theoretical presentations B.I. Kudrin about technical zenoses [6], as well as from principle "engineering resemblance", grounded by ecologists and successfully used in functional ecology [7]. To such conclusion brings and revealed need of the joint analysis as transformations of technical energy in agrarian and ecological systems, so and biological conversion to natural energy of organisms used in agrarian production [3, 8]. In connection with transition with 80-h years XX centuries in industrial energy from the entropy analysis of the transformations energy to exergy analysis in model of technobioenergy idealization it is necessary to use exergy analysis. As is well known, entropy analysis biological conversion energy of organisms in principal is impossible. By us successfully is designed and used method exergy analysis of the transformations to energy of the optical radiation by plants in process of the photosynthesis [3, 8].

### **Analytical model of the agrarian systems**

The Notion "zenos" before recent time was considered purely by biological term. In the last ten years due to opening in technique of the phenomenal scientific direction - an theknetic [6], under which is understood history development technology and technique, in this branch of the knowledges began to use the notion "technical zenos. The generalization of experimental date is installed [6] that history development technologies and technique have such undeliberate (unconscious) energy efficient general evolutiational history directivity, either as evolution of the alive nature. In spite of this distribution of different technical products in shops, factories and more large formations of technical products, in particular electro technical, in such either as destribution of different types of organisms in biological zenoses.

Scientifically grounded need of directed high energy efficient (energy economical) of the development technologies and technique, as is well known, appeared only at the beginning 70-h years XX centuries, but such not deliberate by person development this spheres to activity was realized on length of the whole its histories.

This is indicative of self-organizing general essence of the development technologies and technique, which corresponds to the law of the survival and naturally scientifically is explicable by this law. Uncomplicated foresee, coming from law of the survival, principle of the energy extremness self-organization and progressive evolution that the most further development high-effective plant growing must bring to shaping scientific foundations to optimization of the systems biological technical zenoses. The important role in creation these foundations must execute the studies on development of the theory of optimum management in agroindustrial complex (AIC).

Below we consider the general initial positions and the main forming this theory. The main process of agrarian production is an energy process of the transformation of energy of the solar radiation in chemical energy of the agricultural product - initial product of provisions and organic raw. The main energy entry in system AIC - an energy of the solar radiation (97 - 98 %) and technegen energy (2 - 3 %). The main process of the transformation of energy in plant growing and husbandries - a photosynthesis of the plants and technological processes natural forming agrarian technologies. The main part agrarian technologies - a natural self-organizing processes of the plants, on increasing of efficiency which are directed natural forming technologies, requiring expenses technical and muscular energy.

Initial forming theory of optimum management AIC, coming from considered above, must be a biotechnoenergy model. Such model is designed on base of the principle of the subservience synergy [3]. Essence of this principle is in this what for convenience of analysis of the complex system with many parameters and variables, in the chooses as "variable order" that from variable, which most quickly changes and most powerfully influences upon the main process of the system. Hereinafter analysis only variable order use as variable, but rest consider as parameter of management. In models AIC as variable order is accepted value of the influx to plants of that part to energy of the solar radiation, which potentially suitable to photosynthesis of the plants and shaping them of harvests - exergy solar energy for plant growing [3, 8].



In the opinion of leading researchers on modeling of ecological and biological objects this model without alternative in considered area. Important its advantage is a possibility of the unlimited expansion of amount taken into account factor (the parameters, variables) without change of the same model and reliability of modeling [3, 8]. On base of this model for the first time is realized quantitative (analytical) mutually coordinated determination of the key agrarian ecological values: agrarian climatic (bioclimatic) reclamative potential arable land, their fertilities, as well as productivity of the plants in given ecological conditions. All these values denominated in alike units of the free energy - exergy solar energy for plant growing. Such determination of the agrarian ecological values has provided the possibility of the development of the computer systems of ecological compatible, resources and energy saving to optimization production of product plant growing.

Exergy of solar energy is used as initial value for quantitative determination of the agrarian ecological values. Its role in husbandry, plant growing and ecology is analogous analogous to roll of the velocities of the light in theoretical physics [3]. Importance exergy of solar energy limits maximum importance both fertilities please lands, and potential productivity of the plants (the type, sort, hybrid) in given ecological condition. The Determination of this value is specified branch standards [3, 9, 10]. The estimation of the optical radiation by method to similar determination exergy, is provided German national rates DIN [3]. Instrument is designed In GNU VIESH for direct measurement of the value exergy radiations. With VNII optometrist-physical measurements Gosstandarta RF (VNIIOFI) is designed primary metrology of the measurement of the value exergy radiations. VNIIOFI gave the GNU VIESH certificate on instrument as on facility of the measurement and kit device for check of the instrument.

### **The management by processes in agrarian systems**

Important forming theory management are a main having a special purpose functions of management. In computer system of the optimization to energy and resource ecological

compatible production separate type to product plant growing, designed in GNU VIESH, the main having a special purpose functions are accepted: minimization to technical energy capacity and material expenses on reception of the product, as well as maximization of the use exergy radiations and other ecological conditions of arable land. The realization of these functions in system is realized by choice of the optimum combination elements from three groups ensemble alternative to reception required product: ecological conditions of arable land; the ecological physiological features type (the sort, hybrid) of the plants; zonal high-quality agrarian technologies with facilities of their realization.

For the general systems of optimum management in AIC and nature-use considered having a special purpose functions, obviously, it is not enough. The having a special purpose functions of these systems of optimum management in AIC must also reflect mentionned above ideal characteristics to progressive evolution of the self-organizing nature. They deserve more detailed consideration. Due to spontaneous energy economical directivity of the development of the natural ecological systems, their components and biological sphere as a whole, were formed that natural resource, which consume AIC and the other nature-users. In this connection we shall pay attention to forecast scientific work S. A. Podolinsky "Labour of the person and its attitude to distribute the energy" [3, 11], in which is elaborated the understanding of the labour in K. Marks' determination. The labour in [11] is understood as "such physical and psychic work, which enlarges the contents to free energy" on surfaces of the land. This same is paid attention to need of the account not only labour of the person, but also "labour" of nature, created in process its progressive evolution. The second history example of attention to account in production activity of energetics of the nature is an offer V.I. Vernadsky "to value all productive forces of the country in energy units" [12].

This position agree with the law of the survival, principle energy extremeness and with need of the use in theory of optimum management AIC joint exergy analysis of the transformations of

technogen energy and biological conversion of natural energy by organisms.

The material economy of the biological systems is known broadly in theoretical biology as notion about their "optimum design" [13]. The material economical structure appearing on determined stage to evolutions then goes in structures of following stage self-organizing systems, as this is shown in [13]. The multiple examples of the resemblance of the structures of the self-organizing systems of different hierarchical levels (physico-chemical, biological, social), provided in [13], are evidence not only of their energy and material economy, but as well as about information one.

The Information economy of the self-organizing systems most was brightly shown in structure of the gold proportion, which is discovered in sharing the energy at interaction of the elementary particles [14]. Then she has altered into crystals, afterwards in biological molecules, organisms and social-cultural phenomenas (the architecture, music, economy) [16]. The gold proportion, as well as fractional of the structure, being kept in self-organizing objects, possess the beauty [16,17]. The favourable aesthetic perception of self-organizing objects of nature - their harmony and beauty it is necessary to rank to ideal characteristic of the progressive evolution. In real metabolic processes of organisms and their community ideal characteristic to economy of energy, material and information indissoluble are united in so named "triad to lifes".

By the amazing ideal characteristic of progressive evolution is a speed-up of the process of evolution on measure of the complication evolutioning system. This characteristic was discovered by collation of results calculation to velocity to evolution on positions of the Darwin's theory (the casual mutations, their natural selection) with real velocity of the evolution [18]. The velocity of evolution turned out to be on much orders above. The empirical results on determination genomes organisms, for instance person and mouse, have confirmed this characteristic evolution. In genomes mouse approximately only 1% structures differs from structures genom person, but structures genom person approximately on 10 % differ from genom mouse. This allows to conclude that since time

of the separation genetic branch of person from branch of the general ancestor with mouse the evolution genom person; speeded up approximately tenfold in contrast with development genom mouse for this period [3].

Considered ideal characteristics to progressive evolution of the nature can be shown not plausible, but the their reality confirm as theoretical, so and experimental results of the studies. The account them in motivation having a special perpose functions of optimum management in AIC and other sphere nature-use introduces inevitable.

The well-known mathematical theory of optimum management, which has developed L.S.Pontryagin, coming from variational calculus [18]. Making the variational calculus was commenced by L. Eyler on base of the principle of the extremel action, motivated by him development of the principle of the least action in the form Mopertyui [3]. As it is shown in [3], on the law of the survival allows to explain essence of the phenomenal principle of the least action and logically to unite it with other phenomenal physico-chemical principle (Farm, Le Shatelie). The principle energy exstremness of self-organisation and progressive evolution on the general analytical essence identical to Eyler's principle extremal action of [3]. This relationship of general principle nature is evidence of possibility of the use to mathematical theory of optimum management when making the theory of optimum management in AIC and natural-use.

## References

- [1] Hovel YU. F. Exact husbandry and stock-breeding - a general direction of the development agricultural production in 21 century. //Machine technologies production to product in system of the exact husbandry and stock-breeding, M., GNU VIM, 2005. s. 8-11.
- [2] Strebkov D. S. and others "Oborachivanie method" in energy and phisics.. //Science: from methodology to ontologies. M., 2009, s. 98 - 122.
- [3] Sventickiy I.I. Energoseberezheniya in APK and energy extremum self-organizing M., GNU VIESH, 2007, 366 s.
- [4] Kartverishvilli N.A., Galaktionov YU.I. Ideal complex dynamic systems. The Science, M., 1976, 272 s.

- [5] Sventickiy I.I., Tkachenko I. I. Categorization of the models of the biological block global systems and their biological energy aspects. //Studies of the geosystems in purpose of the monitoring. M., AN USSR, 1981, s. 46-56.
- [6] Kudrin B.I. The Classics technical zenoses. Cenologicheskie studies. The Issue 31, M., 2006, 220 s.
- [7] Kerzhencev A.S. The Functional ecology. M., Science, 258 s.
- [8] SHEveluha V.S.(under ред.). Agricultural technology. M., High school, 2008, 610 s.
- [9] EAST 60.689 27-74 Minelektrotehproma USSR Photosinteticheskyy efficient radiators. 1974.
- [10] EAST 46.140-83 Minselihoza USSR Radiation optical. The Estimation photosynthesis to efficiency. The Terms and determinations. M., MSH USSR, 1983.
- [11] Podolinskiy S.A. The Labour of the person and his(its) attitude to distribution energy. - a Word. 1880, t. IV-V, s. 135-211.
- [12] Vernadskiy V.I. About problem in organizations of the applied scientific work AN USSR. L. Izd. AN USSR 1928.
- [13] Rashevskiy N. Models and mathematical principles in biology. // Theoretical and mathematical biology. M., the World, 1968, s. 48-66.
- [14] LIMA-de-Faria A. Evolution without selection. Avtoevolution forms and functions. M., the World, 1991.
- [15] Savruhin A.P. The Nature of the elementary particles and gilded section. M.; Izd. Mosk. institute of wood, 2004.
- [16] Flower V.D. The System organization of activity heart mammals. Puschino: PNC WOUNDS, 1993..
- [17] Paytgen H.O., Rihter P.H. The Beauty fractals. The Images of the complex dynamic systems. M.: the World, 1993, 176 s.
- [18] Tarasov E. To.. The Physical aspects of the problem of biological evolution. M., Izd. teor. and eksper. physics, 1979.
- [19] Pontryagin L.S., Boltyanskiy R.V., Gamkrelidze E.F. and others Theory of motion management. I., 1968.

## APPLICATION OF THE METHOD OF DYNAMIC MODEL IDENTIFICATION FOR GRAIN WATER CONTENT ESTIMATION

DARIUSZ TOMKIEWICZ

Koszalin University of Technology (Politechnika Koszalińska), Division of Control  
Engineering, 15 Raclawicka Street, 75-640 Koszalin, Poland, Phone: +48 94 3478272,  
e-mail: [dariusz.tomkiewicz@tu.koszalin.pl](mailto:dariusz.tomkiewicz@tu.koszalin.pl)

### Abstract

The information about changes of water content in the dried material is an essential issue during the drying and storing process. The present-day water content sensors are not suited for the hot, dirty and corrosive atmosphere inside the dryers. In the paper a method based on the relationship between the input variable voltage signal passing through grain layer and output signals is presented. The relationship was described by the dynamic ARX type model. Coefficients of the model were applied to estimate grain water content. The correlation between coefficients of the model and grain water content was checked.

### Introduction

Water content of cereal grains is one of the most important parameters determining their suitability for long-term storage. When dealing with grain drying automatic control systems or the process of monitoring the grain quality during storage it is necessary to use measurement methods that would make possible the observation this value on-line continuously in time.

System for continuous measurement of water content of grain supporting feedback control system should provide: a sufficiently small measurement error, should be resistant to a prolonged stay in an atmosphere with wide temperature fluctuations, dust, humidity and vibration. The system should work faultlessly for many months without maintenance by the operator, allowing the data transmission describing the water content of dried material to the other sections of the control system. An important requirement is to ensure that measurement system would be working in real-time and the cost of the water content sensor will be affordable for the user [3].

Water content measurement is especially difficult in the case of such materials as cereal grains. This is due to the diversity of the water bonds in this material, the diversity of the mechanisms of water movement and the complex internal caryopsis structure. In particular, different factors impede the measurement of water content in the grain and they can be identified as the structure and chemical

composition of the measured material, mechanical condition, content of electrolytes, temperature of material, colour, presence of dust scattering light rays, surface texture, and the distribution of water in the material.

In the materials of such a structure, water is in a wide variety of states. Moreover during drying or moistening the water is passing through the successive layers of caryopsis changing its physical properties.

There are many methods of water content measurement in solids materials. A review of many commercially available water content measurement techniques is presented in [1]. This summary emphasising the fact that there is a common lack of the reliable on-line water content measurement techniques, and more research effort should be necessary to find a suitable solution of that problem.

In industrial environment the most commonly used methods of water content measurement are the techniques measuring electrical resistance or capacitance of the moist sample. The principle of electrical methods relies on measurement of material properties affecting the interaction of an electric wave with the material at a single frequency and identifying correlations between these parameters and water content. Traditionally in electrical methods only static parameters are measured such as dielectric constant, capacitance, resistance etc [4].

Unfortunately those properties are described by a non-linear function of the water content and also by other factors such as temperature, sample

size and other chemical or physical properties of the dried material. The advantages of these methods may include immunity to environmental conditions. Moreover, the cost of the measuring system is relatively low. Electrical water content methods, however, are characterized by high uncertainty.

The next type of currently used methods in rapid water content assessment is the radiometric method. They rely on measuring the attenuation of the selected band or bands of the electromagnetic wave passing through or reflected from the sample of measuring material. Wavelengths in the near infrared (NIR) and microwave region are playing the most important role for water content estimation. Unfortunately, radiometric methods are difficult to apply in industrial environments where there is considerable amount of dust. Moreover, their price is relatively high.

### Research objectives

During the research, a new method of water content estimation was tested. The grain sample was excited by a variable electrical signal. The electric signal was recorded after passing through the grain sample. The relationship between the input and output signals was described by the mathematical model. To estimate the coefficients of the model, the methods of dynamic model identification were applied. The correlation between coefficients of the model and grain water content was checked. The sensor principle relies on the measurement of electric signal parameters affected by the relationship between an alternating electric voltage moving through the wet material and water content of the material.

The aim of the research was to test the hypothesis that a grain layer can be treated as electric filter whose parameters are strongly correlated with grain water content and the parameters of the filter could be estimated by the methods of dynamic model identification.

### Methodology

Experiments were carried out on wheat grain. During the experiments the grain samples came from the same batch of material. Before the experiments the grain was moistened. After moistening the grain has been stored for two days to homogenize moisture content in grain bulk. Grain was moistened to  $0.272 \text{ kg}_{\text{H}_2\text{O}} \cdot \text{kg}_{\text{db}}^{-1}$ ;  $0.250 \text{ kg}_{\text{H}_2\text{O}} \cdot \text{kg}_{\text{db}}^{-1}$ ;  $0.235 \text{ kg}_{\text{H}_2\text{O}} \cdot \text{kg}_{\text{db}}^{-1}$ ;  $0.197 \text{ kg}_{\text{H}_2\text{O}} \cdot \text{kg}_{\text{db}}^{-1}$ ;  $0.183 \text{ kg}_{\text{H}_2\text{O}} \cdot \text{kg}_{\text{db}}^{-1}$ ;  $0.170 \text{ kg}_{\text{H}_2\text{O}} \cdot \text{kg}_{\text{db}}^{-1}$  of dry base water content. In addition, in order to check the influence of temperature, the grain samples were heated to four different temperatures. Grain samples temperature was in the range of  $17^\circ\text{C}$  to  $44^\circ\text{C}$ .

Voltage of the electric signal, which excited the grain layer, was in a shape of a rectangular wave with a frequency of 10 kHz. This signal can be described mathematically by equation (1).

$$x(t) = \frac{A}{2} + \frac{2A}{\pi} \sum_{k=0}^{+\infty} \frac{1}{2k+1} \sin[(2k+1)2\pi f t] \quad (1)$$

where:  $A$  - amplitude,  
 $f$  - base frequency,  
 $t$  - time.

The square signal consists of the infinite series of sinus function of the frequencies started from the base frequency of 10 kHz with infinity number of odd multipliers of base frequency.

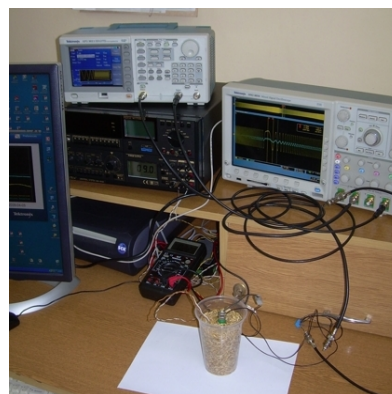
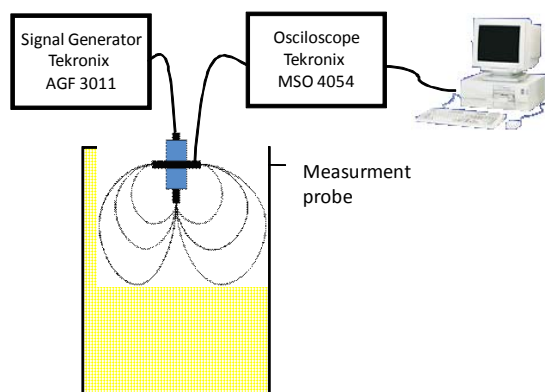


Fig. 1. Laboratory set-up for water content measurement.



The measurement system consists of a container with a grain and measurement probe, which was placed inside the grain bulk. Probe was constructed of two metal electrodes placed at a distance of 10 cm from each other (figure 1). The temperature of the sample was checked at the beginning of experiment and on the end by PT100 sensor. Signal was generated by Tektronix AGF 3011 Arbitrary Signal Generator and recorded with Tektronix MSO4054 Digital Oscilloscope.

Arbitrary Signal Generator has generated a square voltage signal, which passed through a grain layer. Signals from the input and output electrodes were recorded by digital oscilloscope (figure 2).

The generator and oscilloscope communicated with the computer via USB interface. The temperature sensor was connected to the transducer and then to the data acquisition card Advantech PCL-818HG. Measurement data from oscilloscope and data acquisition card were downloaded to the computer and were processed in Matlab environment.

### Estimation of grain moisture

During the tests, it was assumed that the value of the output voltage is a function of:

- signal voltage excitation,
- frequency,
- grain moisture,
- grain temperature.

The voltage signal was kept constant during the tests. Its peak to peak value was equal to 2.0 V and the average voltage was equal 0.0 V. Also, the value of the input signal frequency is maintained at a constant level.

Frequency components of the electrical signal passing through the grain layer were attenuated. Grain layer acts as an electric filter. It was assumed that the filter could be described by the linear ARX type equation (2) [2].

$$A(q, \Theta)y(n) = q^{-k}B(q, \Theta)u(n) + e(n) \quad (2)$$

$$A(q, \Theta) = [1 \quad a_1 q^{-1} \quad \dots \quad a_{la} q^{-la}]$$

$$B(q, \Theta) = [b_0 q^{-k} \quad \dots \quad b_{lb-1} q^{-(k+lb)}]$$

where:

$a_k$  - output signal parameter,

$b_k$  - input signal parameter,

$e(n)$  - white noise signal in n-th time moment,

$u(n)$  - input signal in n-th time moment,

$y(n)$  - output signal in n-th time moment,

$q^{-k}$  - time shift operator.

Equation (2) can be estimated by equation

(3):

$$\hat{y}(n) = \varphi^T \Theta \quad (3)$$

$$\varphi(n)^T = [u(n-k) \quad \dots \quad u(n-k-lb) \quad -y(n-1) \quad \dots \quad -y(n-la)]$$

$$\Theta = [b_0 \quad \dots \quad b_{lb} \quad a_1 \quad \dots \quad a_{la}]^T$$

where:

$\varphi(n)$  - estimated model input vector,

$\Theta$  - estimated parameters vector.

After the experiments the most suitable ARX structure was chosen and it consisted of three elements: input vector with two input signals elements and one output signal element. It is presented as equation (4).

$$y(n)(1 + a_1 q^{-1}) = u(n)(b_1 q^{-1} + b_2 q^{-2}) + \varepsilon(n) \quad (4)$$

Three parameters  $[b_1 \quad b_2 \quad a_1]$  of equation (4) were estimated by Recursive Least Square Method.

Discrete time equation describing the grain layer is presented in a form of equation (5)

$$y(n) = \frac{b_1 q + b_2}{q + a_1} u(n). \quad (5)$$

The equation (5) is then transformed to continuous time form with Backward Time Euler Approximation - equation (6).

$$q \approx \frac{1}{1 - \Delta T s} \quad (6)$$

where:

$\Delta T$  - sampling time step,

$s$  - complex variable.

After the substitution (6) to the equation (5) we obtain the transmittance function (7).

$$G(s) = \frac{y(s)}{u(s)} = \frac{-\left(\frac{b_2 \Delta T}{1 + a_1}\right)s + \left(\frac{b_1 + b_2}{1 + a_1}\right)}{-\left(\frac{a_1 \Delta T}{1 + a_1}\right)s + 1} \quad (7)$$



Parameters of equation (7) can be presented in a simpler form when we substitute

$$A_1 = \left( \frac{a_1 \Delta T}{1 + a_1} \right), B_1 = \left( \frac{b_2 \Delta T}{1 + a_1} \right), B_2 = \left( \frac{b_1 + b_2}{1 + a_1} \right).$$

In the next step, the relationship between parameters of equation (7) and grain moisture content were examined. The relation between  $A_1$  parameter and water content presented on figure 3, parameter  $B_1$  in figure 4a and parameter  $B_2$  in figure 4b.

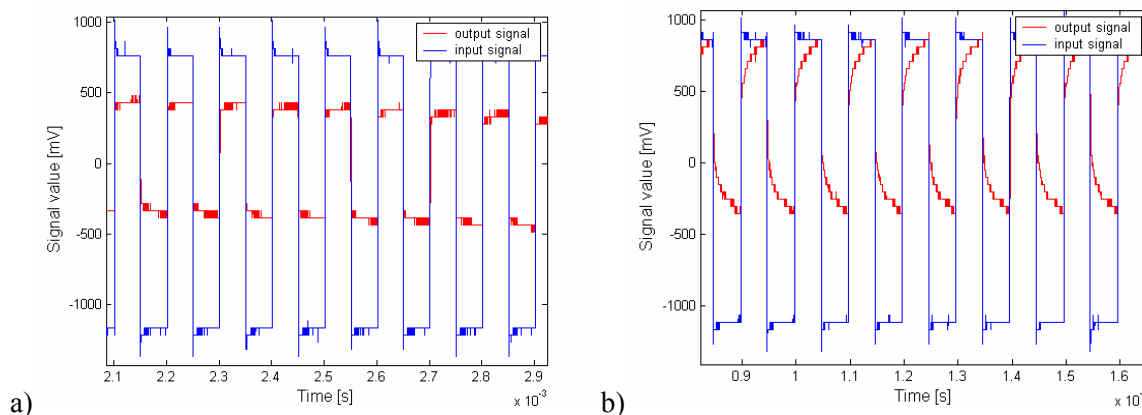


Fig 2. Value of input and output voltage signals a) grain water content  $0.170 \text{ kg}_{\text{H}_2\text{O}} \cdot \text{kg}_{\text{db}}^{-1}$  b) grain moisture content  $0.272 \text{ kg}_{\text{H}_2\text{O}} \cdot \text{kg}_{\text{db}}^{-1}$

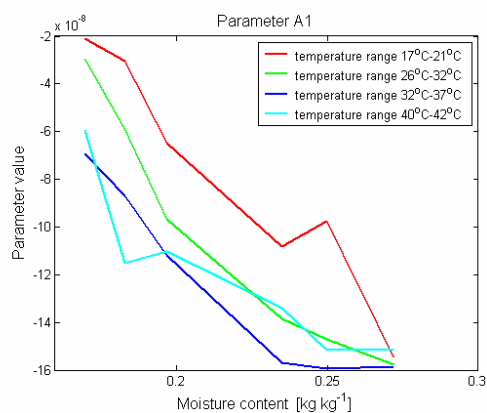


Fig 3. Relationship between  $A_1$  parameter (model (7)) and water content

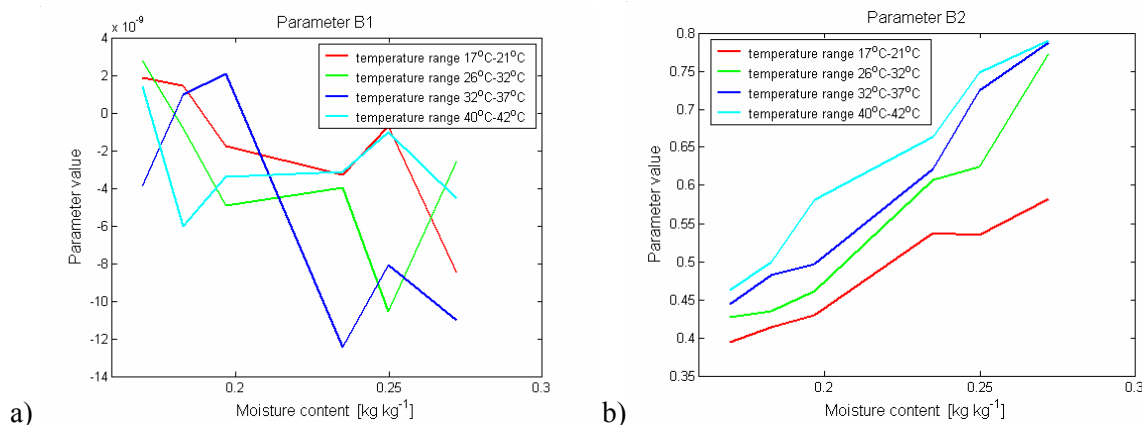


Fig 4. Relationship between  $B_1$  (a) and  $B_2$  (b) parameters (model (7)) and water content

To describe the relationship between the water content and the equation (7) parameters a regression model (8) has been utilized.

$$M = a_1 A_1 + a_2 B_1 + a_3 B_2 + a_4 T + a_5 \quad (8)$$

where:

$a_k$  - regression model parameters

$M$  - water content,

$T$  - averaged grain sample temperature.

Model parameters were estimated by the least square method and results are presented in figure 5. Estimated water content and measured values were combined together.

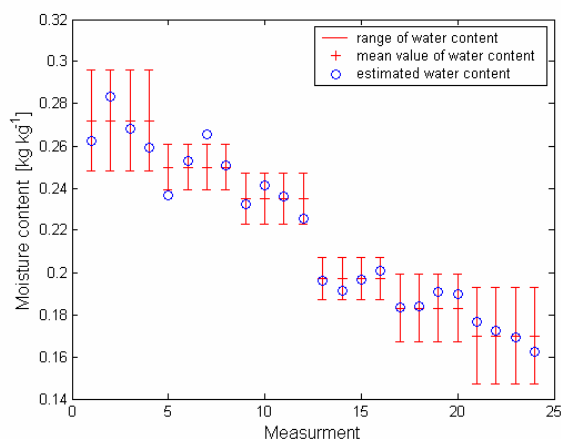


Fig 5. Estimation of water content based on the equation (8)

The maximal error of estimation is equal  $0.015 \text{ kg}_{\text{H}_2\text{O}} \cdot \text{kg}_{\text{db}}^{-1}$  and correlation coefficient between estimated data and measured during experiment water content data is equal 0.981.

## Conclusions

The grain water content estimation method presented in the paper is very robust and can be applied in industrial environment. The correlation between estimated and measured values of grain water content is high. The estimation error is small and it can be reduced even more by replacing the averaged temperature applied in the model (8) by the actual temperature of the grain from the measurements. Additionally the multiple repetitions of measurements are able to improve the accuracy of grain water content estimation.

## Acknowledgements

Author thank the Polish Ministry of Science and Higher Education for funding of this study (project No N N313 211337), and company Tespol for the kind loan measuring apparatus.

## References

- [1] Cancilla P.A., Barrette P., Rosenblum F., On-line moisture determination of ore concentrates a review of traditional methods and introduction of a novel solution, *Minerals Engineering* 16 (2003) 151–163 2003
- [2] Ljung L., *System Identification. Theory for the User*, Prince Hall PTR, 1987
- [3] Tomkiewicz D., *The Measurement System for Estimation of The Water Content in Grain Based on Dynamic Drying Process Model*, *Metrology and Measurement Systems Vol IX*, No 4 (2002) p. 403-412, Polish Scientific Publishers Warsaw 2002.
- [4] Zoerb G. C., Moore G. A., Burrow R. P.; *Continuous Measurement of Grain Moisture Content During Harvest*; *Transactions of the ASABE*. 36(1): 5-9. 1993

## OPTICAL COHERENT METHODS FOR ANALYSING TRANSIENT RESPONSES IN AGRICULTURE PRODUCTS

TRNKA JAN\*, STOKLASOVÁ PAVLA

Institute of Thermomechanics AS CR, v.v.i., Dolejškova 1402/5, 182 00 Prague 8, Czech Republic, Phone: +420 266 053 763, Fax: +420 286 584 695, E-mail: [trnka@it.cas.cz](mailto:trnka@it.cas.cz)

### Abstract

The paper deals with an application of point-wise and full-field interferometry methods as double-channel laser vibrometry and double-pulsed holographic interferometry to analyse transient phenomena in eggs, coconuts, peaches and cheeses. Transient state is generated by different ways e.g. by an element with exploding wire, by a small steel sphere, by a slender bar or by a focused ruby laser beam. History of the generated impact forces are recorded by semiconductor strain gauges in time domain and analysed by Fast Fourier Transform in frequency domain.

The knowledge of transient responses of agriculture products to dynamic loading is important from several points of view such as transport condition, testing of ripeness or storage interval.

### Introduction

Bruise, cuts and abrasions damage of agricultural products are a type of mechanical injury that results from rough handling procedures and occurs on the way from plant to consumer when these products drop, roll, and collide with each other, containing material or handling equipment. Besides the obvious loss of quality mechanical damages are possible entry sites for pathogens and fungi. Very similar problems are typical of eggs as well. The development of new appropriate damage prevention methods is therefore important. The above mentioned reasons inspired us to apply experimental methods used in stress wave propagation in solids in a little uncommon branch of experimental mechanics. We hope that use of these methods contributes to the analysis of the dynamic responses of agricultural products undergoing impact loading.

Impact loading initiates a transient state associated with the stress wave propagation. One of the most significant things in the experimental research of the transient phenomena is generation of well-defined impact. For the mentioned experiments, the direction of the acting impact force and its point of application, as well as time history, are known and very important not only for the experimental realization but also for comparison of the experimental results with the numerical or analytical results, respectively [1].

Impacts in experimental mechanics are generated through mechanical or electromechanical loading. The mechanical impact can be realized by different types of

impactors, for example, by the ballistic pendulum, drop cylindrical or spherical hammer, or shooting different projectiles. The electromechanical loading is often carried out via exploding wire method. In some special cases, it is possible to generate the stress waves by focusing either a pulse laser beam [2,3] or an electromagnetic impulse generator [4].

In presented experiments the waves were generated by either a sample with exploding wire, an impactor i.e. a slender aluminium rod, by shooting a small glass sphere or a focused ruby laser beam. Use of a focused ruby laser beam to generate the guided waves is common in experimental mechanics of solids; however, exact analysis of the interaction between the generated waves and biological structures under investigation is complicated.

Detection and analyse of transient phenomena in the products was carried out both by full field and point wise non-contact or contact methods.

### Experimental procedures

Shooting of small glass spheres by an air gun at an egg tested its impact resistance. Figure 1a shows a part of the testing equipment setup and the results of the experiments. The displacement waveforms -see Fig.1b- was measured at the point I by the Polytec Laser Vibrometer CLV 2000. The measurement by laser vibrometer is non-contact, so there is no need to attach any measuring devices, which would negatively influence experimental results.

The amplitude of a surface point displacement is measured at a point where the laser beam of laser vibrometer strikes the investigated structure. Figure 1c presents a circular failure of an eggshell due to an impact of the glass sphere (5mm in diameter). The macro-

photo shows both the eggshell layers and the pellicle of the egg. The dynamic threshold value was evaluated as the kinetic energy and it was 0.02 Joule in this case. The air gun chase velocity of the sphere was 20 m/s

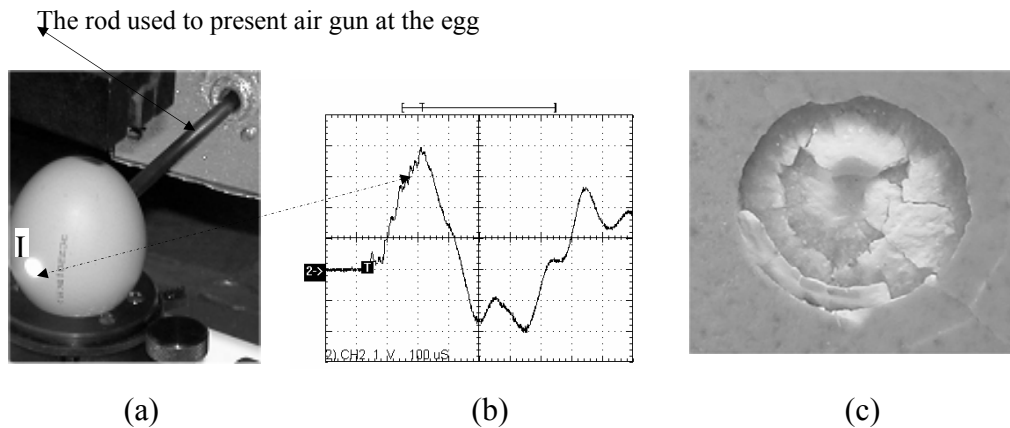


Fig.1 Raw henn egg shot by the glass sphere (a), waveform of displacement at the point I (b), detail of the interface the sphere – the egg after impact

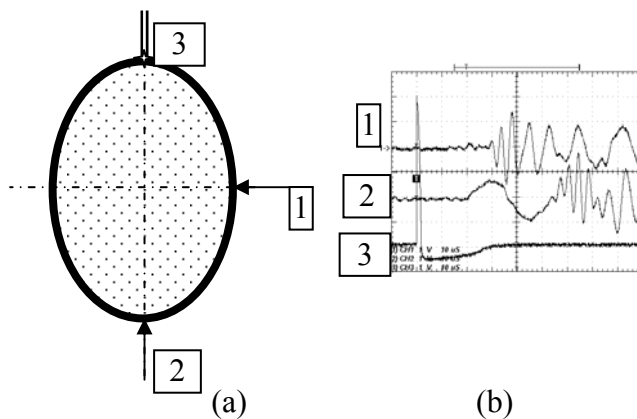


Fig.2 Hard boiled henn egg loaded by the focused ruby laser beam (a), waveform of the displacement detected at the points 1 and 2 (b).

Focusing of a ruby laser beam on an egg surface generates an extremely short impact with time duration about  $1\mu\text{s}$ . The schema used in the experiments is shown in Fig.2. The investigated egg was laid on the soft foam plastic, and was dynamically loaded by the focused ruby laser beam acting at point 3, see Fig.2a. The time histories of displacement at points 1 and 2 are shown in Fig. 2b. The laser pulse serves as the loading and simultaneously as the triggering signal. Its history is shown as channel 3. Not

only did the focused laser beam not damage the egg shell but also it left no visible mark on the surface. If the same energy level is used as the pulse for the stress wave generation in a metal material, its surface is slightly damage.

The same technique, i.e. focusing of the ruby laser beam on the subject surface and detection of the responses by laser vibrometer, was used in analysis of stress wave propagation in a biscuit and a chocolate bar. Results are shown in Fig. 3a, b, c.

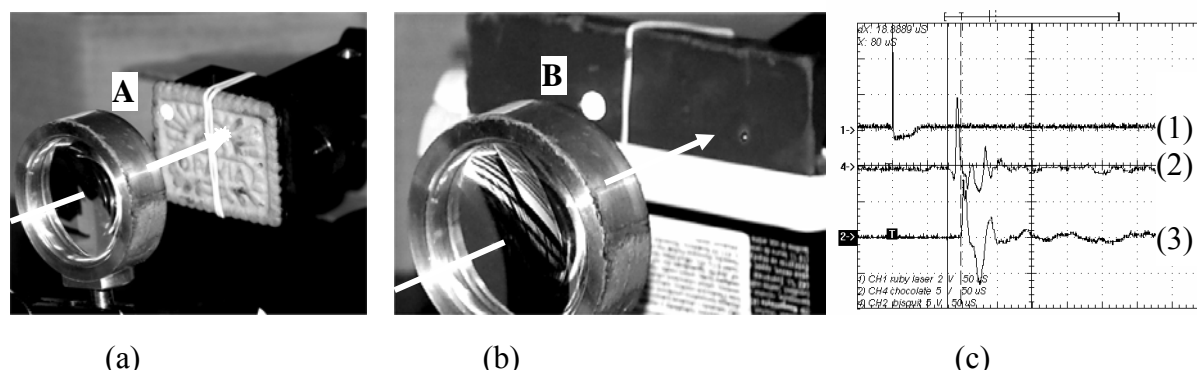


Fig.3 Biscuit and chocolate bar loaded by the focused ruby laser beam (a) and (b) respectively. Waveforms of the velocity detected at the points A (2) and B (3) respectively are in (c). Waveform (1) represents history of loading pulse.

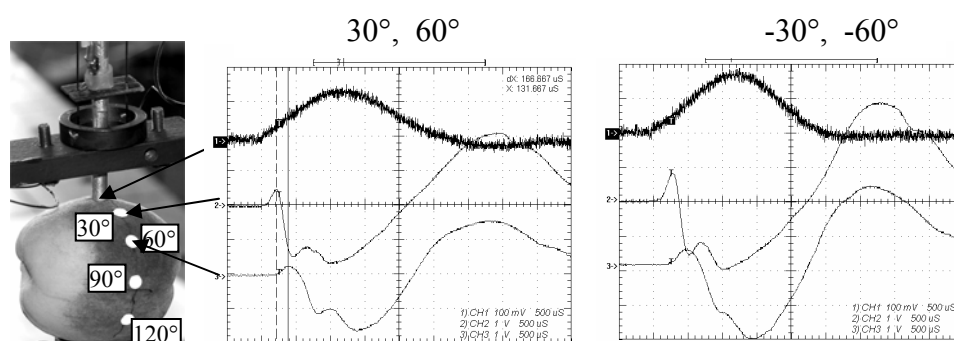


Fig. 4 Peach impacted by impactor in the point 1, (a), waveforms of loading force -wl, waveforms of displacement at point +30° and +60° from point 1 on the meridian of peach and -30°, -60° respectively.

Fig.3c shows that the stress wave velocity is 500 m/s in chocolate bar and 400 m/s in biscuit. While the ruby laser beam did not visibly damage the biscuit, the part of chocolate ablated.

The experimental scheme used for measuring of a relation between ripeness and dynamic responses of peaches is shown in Fig.4a. The impactor, a thin aluminium rod with miniature semiconductor strain gauges, was dropped from a point 70mm above peach surface.

Figs. 4b,c show the waveforms of loading force (1) and displacements at two different places ( $\pm 30^\circ$  and  $\pm 60^\circ$ ). History of the displacements was detected by the double channel vibrometer. Analysis of recorded waveforms unable us to get the material properties of the flesh of the peaches and their

changes caused by ripeness. These diagnostic methods are promising to analyse local mechanical properties as well.

Aforementioned laser vibrometer measurement offers point wise and contact less measurement. Another widely used method of coherent optics is holographic interferometry. It gives us full-field measurement of an object under investigation. The holographic interferometry (HI) has been recently a conventional method for measuring displacement fields of elements undergoing static or dynamic loading. The double pulse holographic interferometry (DPHI) - one of known HI methods - allows us to record and analyse transient phenomena, e.g. to visualize the stress wave propagation in solids. The sensitivity of the

HI is usually  $\lambda/4$  where  $\lambda$  is the wavelength of laser light used for image recording.

The deformations smaller than  $\lambda/4$  are not visible. Generally speaking, the holointerferograms - the results of HI- seem to be, at first glance, a perfect way to depict object deformations. However, their conversion into numerical data is not an easy task [5].

One of our research aims was to combine the full-field holography information with the point-wise quantitative measurements by the miniature accelerometers in study of transient state in a coconut [6]. The coconut under investigation was impacted by an element with exploding wire - see Fig.3a.

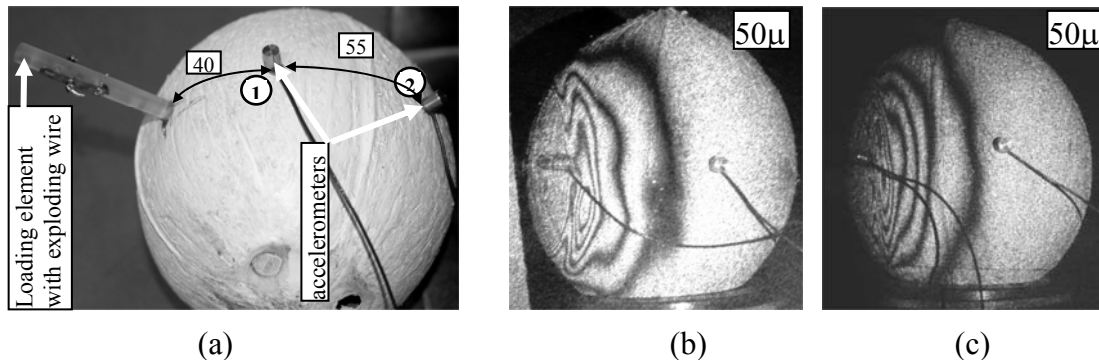


Fig.3 Coconut with loading element and with pair of accelerometers (a), Holointerferogram of stress wave propagation in coconut with its nutty white (b), Holointerferogram of stress wave propagation in empty coconut (c).

The holointerferograms of “frozen” stress waves propagating in the full and empty coconut respectively at 50μs after laser pulse triggering are shown in Fig. 3b and in Fig. 3c respectively. The conversion of interference patterns into numerical data is not a trivial problem. Counting the fringes on recorded holointerferograms, for example, in Fig. 3c for the time 50 μs, we can evaluate that the amplitudes of displacements are about up to 2μm.

The drawbacks of DPHI are the reason why we combined the full-field holographic information with the point-wise measurements by means of miniature accelerometer (Brüel & Kjær type 4374). The waveforms of acceleration in Figs. 4(a) and 5(b) are recorded in time

domain. It is convenient to apply frequency analysis instead of the time domain analysis to analyze effect of the nutty white in the coconut. Comparing fast Fourier transform (FFT) of these signals, we can quantitatively evaluate the effects of damping and filtration of the coconut arising by fullness of the coconut on the measured signal.

The power spektra (PS) of history of acceleration at point 1 are results of the FFT analyses of recorded waveforms. They are shown in Fig. 4b for the full coconut and in Fig. 5b for the empty coconut. The PS maximum of acceleration at the point 1 of the full coconut has approximately the magnitude 1250, while in the case of the empty coconut its magnitude is almost 3000.



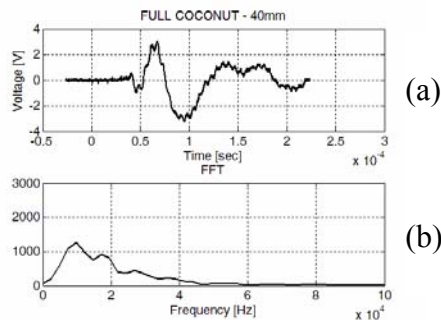


Fig.4 History of acceleration measured at the point 1, (a), Power Spectrum of history of acceleration at the points 1 of the full coconut.

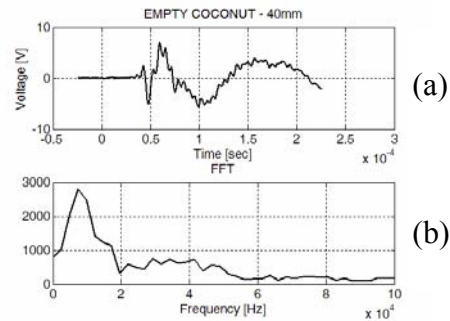


Fig. 5 History of acceleration measured at the point 1, (a), Power Spectrum of history of acceleration at the points 1 of the empty coconut.

## Conclusion

The main aim of this contribution was to show how to use optical methods of experimental mechanics, which are frequently used in analysis of the stress wave propagation in solids, for determination of mechanical properties of the agriculture products. The attention was focused both on stress wave generation and on the detection of transient responses. The waves were generated by the sample with an exploding wire, steel impactor, or by focused ruby laser beam. The histories of the transient responses were recorded by laser vibrometer and by the miniature accelerometers respectively. The waveforms were recorded in the time domain and transformed by FFT into the frequency domain. Double Pulse Holointerferometry visualized the full-field view of the stress wave propagation.

The employment of the impact methods with the frequency analysis of acceleration and displacement waveforms is promising in evaluation of material properties of agricultural products. The combination of a small-energy impact loading with point-wise measurement by noncontact laser interferometric method allows to evaluate a stage of fruit ripeness objectively, to analyze mechanical properties of their parts or to investigate fractures of eggshells. Determination of the impact elasticity is also important for evaluation of quality of fruits and vegetables [7], [8].

## Acknowledgements

The authors would like to acknowledge the support of the Grant Agency of the Czech Academy of Sciences through the project “Behaviour of selected agriculture products at impact loading” (IAA 201990701).

## References

- [1] Trnka, J., Landa, M., Dvořáková, P.: Dynamic Responses of Plate and Shell Structures Studied by Nondestructive Testing Methods. 40. International Conference Experimental Stress Analysis, Prague, Czech Republic, pp. 3–6 VI (2002).
- [2] Fallstrom, K.-E., Olofsson, K., Saradi, I., Wahlin, A.: Generating and Recording Transient Bending Waves in Plates by Pulsed Lasers. *Experimental Techniques* 20(1):15–19 (1996).
- [3] Trnka, J., and Landa, M.: Double Pulse Holointerferometry and Ultrasonic Techniques used in Study of Guided Waves Propagating in a Thin Cylindrical Shell. *Acta Technica CSAV* 47(1):87–97 (2002).
- [4] Vesely, E., and Trnka, J.: Transient Loading of Thin-Walled Structures by Electromagnetic Impulse Generator,” Colloquium “Dynamics of Machines”, Prague, Czech Republic, pp. 225–228 (February 11–12, 2003).
- [5] Stetson KA. The Problems of Holographic Interferometry. *Experimental Mechanics* 1999; 39(4):249-255.
- [6] Trnka, J., Dvořáková, P.: Transient Stress Waves in Study of Coconut Physical

- Properties. Experimental Techniques. Vol. 34, č.1 (2010) p. 19-25. ISSN 0732-8818.
- [7] Dvořáková, P., Nedomová, Š., Severa, L., Trnka, J., and Buchar, J., “The Impulse Response Method for Measuring the Overall Firmness of Fruit,” Book of Contributions of 46th International Scientific Conference “EXPERIMENTAL STRESS ANALYSIS 2008,” VŠB–Technical University of Ostrava, Ostrava, Czech Republic, pp. 43–47 (2008).
- [8] Nedomová, Š., Trnka, J., Dvořáková, P., Severa, L., and Buchar, J.: “Fracture of the Eggshell Under Impact,” Fuxa, J. (ed.), Book of Contributions of 46th International Scientific Conference “EXPERIMENTAL STRESS ANALYSIS 2008,” VŠB–Technical University of Ostrava, Ostrava, Czech Republic, pp. 171–175 (2008).

## VALUE ADDED CHAIN ASSESSMENT OF FOREST INDUSTRY IN LATVIA

SIGITA TUNKELE<sup>1\*</sup>, JĀNIS MĀRCIŅŠ<sup>2</sup>

<sup>1</sup>Latvia university of Agriculture in Latvia, Lielaiela 2, Jelgava, LV-3001, Latvia,  
Phone: +371 63010605, Fax: +371 63010609, E-mail: sigita.tunkele@e-koks.lv

<sup>2</sup>Latvia university of Agriculture, Jelgava, Latvia

### Abstract

European forest industry contributes a complex value added chain, including forestry, processing sector of timber industry and further development sector of timber. Each sector is being collected, processed and stored the specific data, which is necessary to collect in the single data system for all forest industry. This data system would allow to understand and to analyze the economic contribution of each sector.

European Union (EU) member states is should seek to harmonize the forest industry data system, it is, to establish a single economic value of forests and consistently linked the forest balance with wooden land, timber, forestry economic activities in the cash flow accounts and wood supply / use in the natural and monetary values. In EU is the data system of forest industry, but each European country is necessary assess its suitability and to adapted to situation which is in the country.

Latvian various institutions and organizations deal with the data collection of forest industry and with publicly available data interpretation and additional calculation in Latvia. In Latvia is not been complete a complex forest industry analysis, is not been complete its data suitability and conformity assessment according to the situation in Latvia, and the analysis of other European countries of experience.

Is necessary to introduce and develop harmonized the forest industry data system in Latvia then is necessary make the current situation evaluation, including a stored information analysis of forest industry, identify all institutions and organizations which deal with forest industry data collection, processing and analysis. Additional is necessary to analyze a regulatory environment which to assess this data suitability and compliance in the forest industry as well the key problems and failures.

### Introduction

According with European framework for integrated environmental and forest economic accounting for forests (abbreviation – IEEAF) – European Commission, Eurostat, EU member states should strive on harmonize forest resource accounting system, through a single forests economic value determination on the national accounts system. IEEAF objective is to consistently to link a forest balance with wooden land, wood resources, forestry economic activities of cash flow accounts and wood supply / use of economy the physical and monetary values in the framework [1].

At the moment various Latvian institutions and organizations engaged in the collection of data on the forest sector, where the one of the most important is the Ministry of Agriculture (abbreviation - MA) and the Central Statistical Bureau (abbreviation - CSB). At the same time is the other institutions dealing with various data collection, what can attributable to the forest sector in accordance with institutions responsible

of delegation, as also after their initiative, mostly non-governmental in case. In parallel, many institutions deal with the publicly available of MA or CSB data interpretation, as also deal with in addition calculation to conducting.

#### *Forest industry description*

The forest industry composed of forestry, timber industry and wood thermal and chemical processing industry. The forest sector combines forest resources and based on the very diverse productions, trades and consumption in the single system whose elements are interrelated.

The forest products includes the key raw materials (a round wood, pulpwood, wood chips and wood technology) and the primary processing of wood products (a sawn wood, wood based panels and energy products (a pellets and briquettes), as also the further development of timber products (a carpentry and joinery products and furniture) [2].

Forestry supplied in the forest obtained goods and services directly to the consumption market or raw materials for further processing.

The forest products may be of material (wood as raw material, mushrooms, berries, etc.), non-material (forest biodiversity, recreation facilities and other services) and the cumulative value (carbon attraction) [2].

The forest industry development driving forces and influencing factors are located outside of forest industry. Socio-economic trends (population incomes, technology changes, a human and public choice) determines the demand in the industry. Environmental factors - the trees growth pace, climate changes and the natural events (disasters) mainly influence not only wood resources, but also a product and service offerings [2].

The wood resource extraction has been divided in roughly two equal parts between the state and private forest owners. After forest statistical inventory data (April 1, 2009) 47% of the total forest areas is the state forest and 53% - the others forests including the private forests [3]. The last 70 years, the forest area in Latvia has more or less doubled, while the volume of wood has increased to 630 million m<sup>3</sup> after forest inventory statistical data (Figure 1) [3].

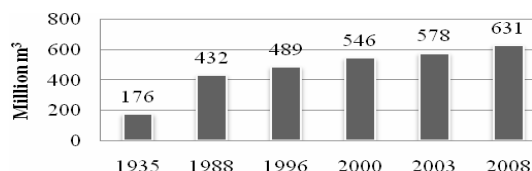


Fig.1. Total wood resource extraction, million m<sup>3</sup>

The economic activity of state forest happens according to sustainable with forest management principles, namely, respect for both the economic and environmental requirements, as well social requirements. The wood resources extraction happen a systematic and regularly from the state forest, as a result the planning and forecasting process about wood resource availability is easier (Forest sector in Latvia, 2008). The private forest to do it is much more difficult, because the economic activity is not regularly.

The wood resource volumes in Latvian forests each year remains quite stable position – between 10 and 11 million m<sup>3</sup> of wood each year. In 2009, according to State Forest Service data, the felling output was 10.73 million m<sup>3</sup>. 7.73 million m<sup>3</sup> of wood was obtained from state

forests, and 3.00 million m<sup>3</sup> – from other forests, including from private forests (Figure 2) [4].

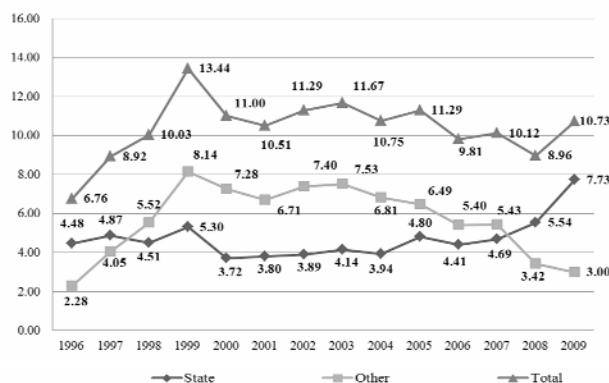


Fig. 2 Wood resource extraction dynamics, million m<sup>3</sup>

### Forestry industry

In 2008, the forestry contribution to economic in value added was 187 million lats and its share of GDP was 1.2%. Compared with 2007 in the sub-sectors decreased the goods and services value added almost by 10%. This is related with the timber cutting volumes, what decreased almost by 12% (Figure 3) [5].

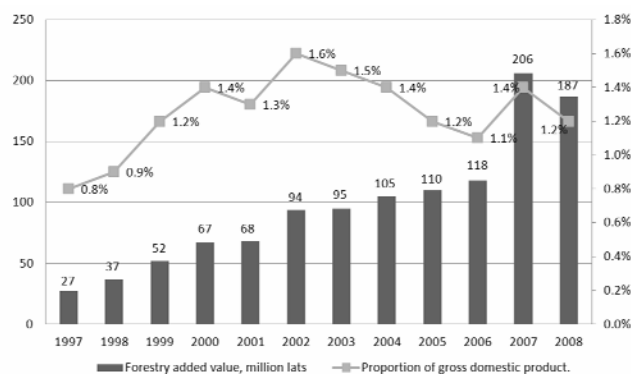


Fig. 3 The forestry value added dynamics and its proportion of gross domestic product

### Timber industry

The timber industry is one of the most important Latvian industries. In 2008, the sub-sector - the woodworking, paper and furniture industry to the total contribution in value-added was almost 410 million lats, which make up a more than 2% of gross domestic product.

Compared sub-sectors, an one of highest proportion is in the woodworking sector (76%), then the furniture industry with 19% or 65 million lats. The timber industry value-added

recession trend is also in 2009, where in the first quarter the industry's added value decreased by 30% compared with 2008 first quarter (Figure 4) [5]. The timber industry output decreased not only because of the low domestic demand and demand recession in trade countries, but also because of the decreased price and the lower value-added products increase in the share of exports.

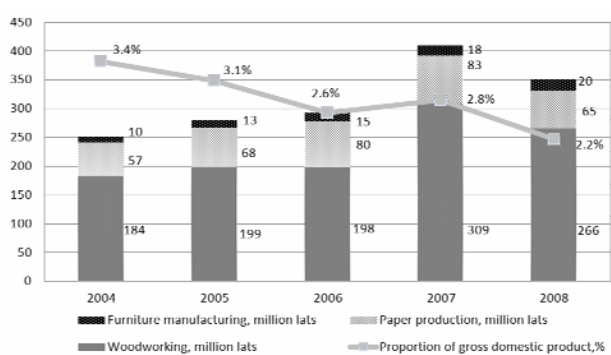


Fig.4 The timber industry value added dynamics and its proportion of gross domestic product  
*The products realization dynamics*

Reasons why the forest industry trade was decreasing from 1.5 billion lats (in 2007) to 0.8 billion lats (in 2009) attributable to the direct price drop, the product cart structure changes and the decreased production (Figure 5) [6].

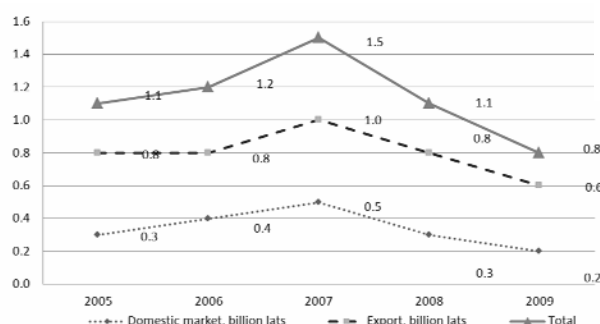


Fig.5 Forest industry of the marketed output changes

Over the past four years, the forest industry growth increased by 27%, where most rapidly evolved forestry sub-sector - an increase was 41% (Figure 6) [5].

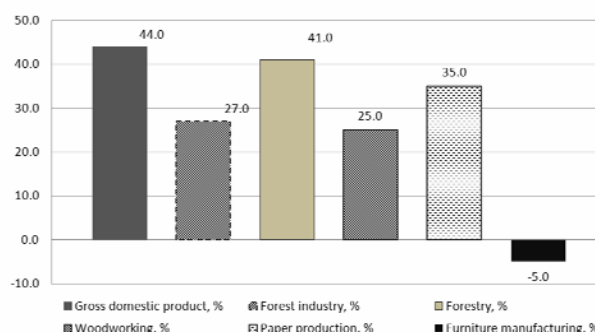


Fig.6 The economy and forest industry growth rates

### Forest industry information flow

The forest industry is complex, what incorporating not only a wide range of production activities and a range of services, institutions and administrative bodies, but also in other sector activities aspects and an influence to forest industry. The forest industry linkage with other industries is referred to as forest industry cluster (Figure 7) [7].

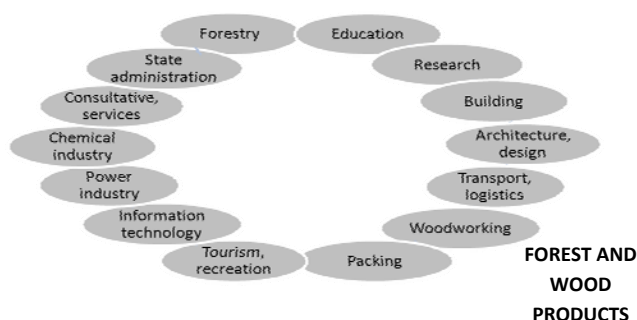
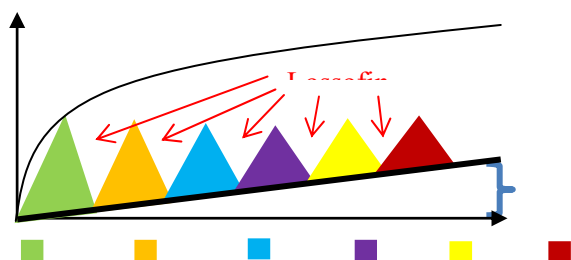


Fig.7 Forest industry cluster

Since the forest sector has a different processes and activities complex, which complicates the information tracking in the single system. World practice shows that where there are several sectors or actors then are often set up in the large variety data processing and storage methods and systems that make harder traced the common material flow. In the forest industry material flow, starting from the forestry and logging to finished product trades, is the risk not enumerated the all information in one system - for example, the industry with high added value, because less information about it (Figure 8) [8].



Analyzing information not only on forest information sources, their beneficiaries, but also about the related transactions, is created an information exchange scheme for the forest sector. With green arrows denotes the forestry information flow, with red - the timber industry information flow, with blue - the transport information flow, but with black - the internal information flow (Figure 9) [7].

Fig. 8 Information accumulated with traceability

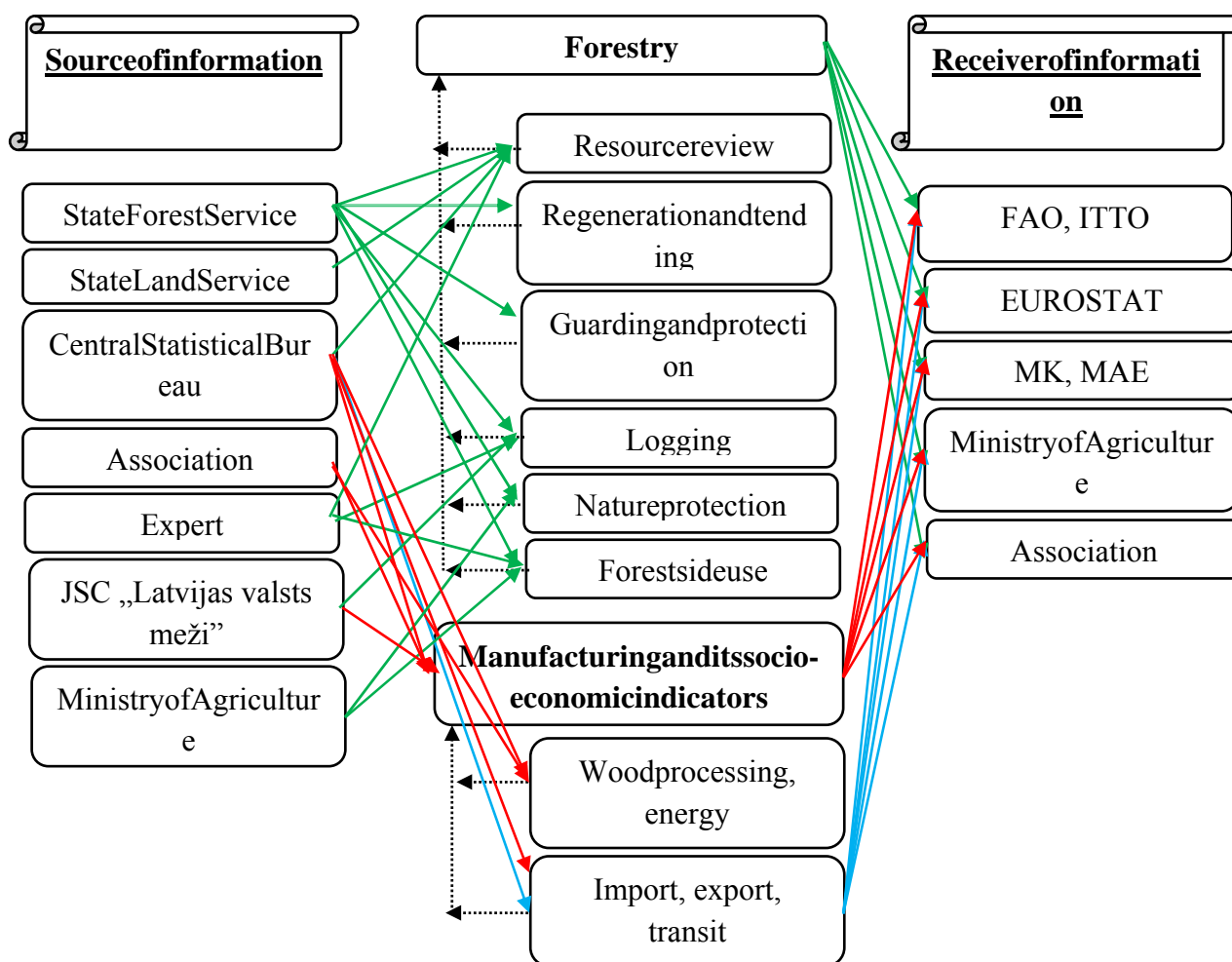


Fig.9 Forest industry information exchange scheme

## Conclusion

1. At the moment various Latvian institutions and organizations engaged in the collection of data on the forest sector, where the one of the most important is the Ministry of Agriculture (abbreviation - MA) and the Central Statistical Bureau (abbreviation - CSB), but there are other institution that deal with it in accordance with

institutions responsible of delegation. In parallel, many institutions deal with the publicly available of MA or CSB data interpretation, as also deal with in addition calculation to conducting

2. Latvian forest sector includes two significant sub-sectors - forestry (industry, what dealing with forest husbandry, conservation, orderly utilization and restoration) and timber industry



(which include woodworking, paper and articles of manufacture, as well a furniture manufacturing). Both these sub-sectors play a crucial role in the Latvian economy.

3. The wood resource volumes in Latvian forests each year remains quite stable position – between 10 and 11 million m<sup>3</sup> of wood each year. In 2009, according to State Forest Service data, the felling output was 10.73 million m<sup>3</sup>.

4. Given the current economic downturn trend in the world, Latvian gross domestic product has decreased in 2008 and a similar situation is also observed in the forest industry, including in the forestry and timber sector, where has decreased their contribution to the value added formation.

5. Since the forest sector has a different processes and activities complex, which complicates the information tracking in the single system. In the forest industry information flow, starting from the forestry and logging to finished product trades, is the risk not enumerated the all information in one system - for example, the industry with high added value, because less information about it.

6. Latvian forest industry information flow scheme is complex, therefore should be necessary a single information system for forest sector data storage and a full accounting by subsectors.

## References

- [1] European Commission: The European Framework for Integrated Environmental and Economic Accounting for Forests – IEEAF, 2002, p. 7.
- [2] Ministry of Agriculture: 1.pielikums “Meža un saistīto nozaru attīstības pamatnostādņu informatīvā daļai” (Annex No. 1 “Forest and based industries development of guidelines for the informative part”), Available at:

[http://www.zm.gov.lv/doc\\_upl/Pielikums\\_1.pdf](http://www.zm.gov.lv/doc_upl/Pielikums_1.pdf), 1 Juli, (in Latvian).

[3] Ministry of Agriculture: Mežaplatības (Forest area), 2009, Available at:

[http://www.zm.gov.lv/doc\\_upl/Meza\\_nozare\\_katalogs\\_LV.pdf](http://www.zm.gov.lv/doc_upl/Meza_nozare_katalogs_LV.pdf), 16 March, (in Latvian).

[4]

Forest and Wood Product Research and Development Institute: projekts

„Mežanozare ekonomiskās situācijas monitorings” (project “Forest sector economic situation monitoring”), 2009, Available at:

<http://www.llu.lv/?mi=81&op=true>, 2 March, (in Latvian).

[5] Ministry of Agriculture: buklets “Mežanozare Latvijā, 2009” (booklet “Forest sector in Latvia, 2009”), 2009, p. 3-4, Available at:

[http://www.zm.gov.lv/doc\\_upl/Pielikums\\_1.pdf](http://www.zm.gov.lv/doc_upl/Pielikums_1.pdf), 5 Juli, (in Latvian).

[6] Latvia Forest Industry federation: prezentācija “Latvijas Kokrūpniecības federācijas politika, mērķi un atbildības jautājumi” (presentation “The Latvia Forest Industry Federation of policy, purpose and responsibility for sustainable forest management promoting”), 2010, Available at:

[http://priede.bf.lu.lv/konf/citi/mezhi2010/Kokrupn\\_feder\\_ilgtspejibai\\_KKlauss\\_2010\\_02\\_16.pdf](http://priede.bf.lu.lv/konf/citi/mezhi2010/Kokrupn_feder_ilgtspejibai_KKlauss_2010_02_16.pdf), 5 Juli, (in Latvian).

[7] Forest and Wood Product Research and Development Institute: projekts “Latvijas kontumodelis un tā pamatojums”, 1. ziņojums (project “The developed Latvian economic Forest Accounts model”, 1<sup>st</sup> report), 2010, p. 30 – 32, (in Latvian).

[8] G. Niblaeus: presentation “Industrial breakthrough of new methods and technologies in the wood industry”, 2009.

## RECENT TRENDS IN THE PROCESSING OF CONSTRUCTION AND DEMOLITION WASTE

PETR VACULÍK, JAN MALAŤÁK, LADISLAV CHLÁDEK

Czech University of Life Sciences Prague,  
Faculty of Engineering, Department of Technological Equipment of Buildings  
Kamýcká 129, Praha 6 – Suchbát, 165 21, Czech Republic

### Abstract

The recycling of construction and demolition waste is relatively simple, whenever possible, individual structural elements (pre-fabricated parts, steel and wooden structures, plastics, etc.) are re-used in building industry. When not possible, construction and demolition waste (especially steel parts) is ground, sorted and impurities removed to achieve characteristics similar to gravel and aggregate. If the amount of harmful substances in water extract exceeds the relevant standards, the waste is deemed unrecyclable and harmful and deposited in hazardous waste dumps. The utilization of construction and demolition waste depends on the purity of waste, collection logistics, and content of organic and inorganic additives and heavy metals (such as Zn, Pb, Cd). Many toxic additives can be eliminated during recycling (e.g. some polystyrene-based plastics can be recycled when they are dissolved in special solvents, resulting in very pure material without toxic contamination).

**Key words:** construction waste, demolition waste, recycling, technological equipment, environment

### 1 Introduction

#### Types of construction and demolition waste

Concrete or reinforced concrete - due to concrete sturdiness, waste concrete recycling methods required special crushers and even special grinding lines. The output fractions are sorted in accordance with the expected utilization. Recycled concrete or reinforced concrete is mainly used for landfills (for backfilling operations) as or as an aggregate in bituminous mixtures, in exceptional cases it can also replace natural aggregate. Ferromagnetic contamination (steel parts) can be removed by magnetic separator installed in the crusher.

Aggregates and excavation soil - this type of recycling requires the sorting of the soil and aggregates into individual grains and decontamination when contaminated by i.e. plastics, wood, petroleum products. The increasing price of natural construction materials (natural aggregates) used for backfilling and the growing environmental concerns have led to an effort to replace those materials recycled materials derived from with aggregates and excavation soil.

Building ceramics and bricks and masonry - brick recycling works is relatively simple: bricks sorted from construction and demolition waste are ground and used for landfill, as red clay or as filling for monolithic structures of new houses,

while gross fractions are used as an aggregate for light concretes. The same recycling technology applies to building ceramics, which is then used for pathways and bike tracks, tennis courts or as a filling material.

Wood waste and construction wood - this type of waste is usually incinerated or brought to municipal dumps. It is necessary to distinguish between contaminated and uncontaminated wood construction and demolition waste. Uncontaminated construction and demolition wood waste (splinters, sawdust, wood shavings and chips) is used for the production agglomerated and cement wood boards and profiled bricks. Contaminated construction and demolition wood waste (i.e. impregnated products) is recycled in correspondence to the amount of contamination. Contamination by water-soluble substances containing toxic inorganic salts or oils containing organic working substances and solvents turns this type of waste into hazardous waste which can be recycled into timber sleepers, burn or stored in municipal dumps.

Metals - large metal (ferrous metals) fragments (particularly of steel reinforcement in concrete) are sorted manually from construction and demolition waste; undesirable metal scraps can be sorted out by magnetic separator installed in the crushers or screeners. Sorted metal is

subsequently processed by specialized companies.

Asphalt - in the Central and Eastern Europe, only petroleum asphalt is used in the building industry manufactured by means of vacuum distillation of petroleum, which can be recycled and used in bituminous concrete (unless the asphalt contains tar, in which case it must be disposed as a hazardous waste).

Asbestos - construction and demolition waste containing asbestos or asbestos-cement is treated as hazardous waste (tiny splinters with 25  $\mu\text{m}$  diameter and up to 8 mm length break away from asbestos during handling, and when inhaled, they are highly carcinogenic). This is why asbestos recycling is stabilization; soft asbestos insulation is usually deposited in dumps.

Glass - recycling technology depends on the type of glass (colored, clear, glued, wire glass etc). Glass manufactures buy glass waste from waste collection companies and use it in their normal production, because e.g. glass shards and fragments represent up to 25percents of the material used in the manufacture of new glass products.

Gypsum and plaster-based building materials - gypsum and plaster from construction and demolition waste is added to cement in cement factories. However, impure plaster materials such as plasterboards go to municipal dumps.

### **Technological equipment used for the recycling of construction and demolition waste**

The construction and demolition waste recycling usually proceeds in mobile or semi-mobile recycling lines.

Stationary units need regular and sufficient supply of material for best economy, although high transportation costs make those units less profitable than their fully mobile counterparts, therefore mainly used in quarries.

The capacity of mobile recycling units is limited by the fact that the units must be transportable via normal roads, which is why they process to more than 200 tons/hour. Mobile units (loaders, crushers, screeners atc.) can be used directly on-site and allow for a fast and easy separation of the recycling line into crushers and screeners, which can than be used separately. Mobile recycling unit work independently on power grind and boast a high profitability. Semi-

mobile recycling units have their own caterpillar undercarriage or wheeled chassis (towed trailer is used for longer distances) or container frame, and their capacity ranges to more than 300 tons/hour.

The technological lines for recycling of construction and demolition waste are composed from many technological types of equipment.

The most important part of the recycling line, which due to its wear at the same time swallows a significant part of operational cost, is a crusher (impact or dynamic and jawed). Impact crushers can be used for the crushing of slightly sticky fragments with up to 400 MPa resistances. Material is crushed by fast-rotating ledges, from which it rebounds to armored plates, thus producing larger proportion of cubic grains. Crushing is also affected by the change of the speed of rotor revolutions and by the amount and position of rebound plates. High grinding ratio (1 to 50) and possibility to grind large fragments are also advantageous. Jawed crushers are used for the crushing of non-clogging materials with resistance to crushing not exceeding 400 MPa. They are relatively quiet and they are particularly recommended for the processing of large fragments. Their grinding ratio is low (4 to 10) and they get clogged easily when grinding sticky materials such as bituminous (asphalts) material in summer.

The second most important part of the recycling line for recycling of construction and demolition waste after a crusher is a screener (recycling separator). Screeners are installed after the crusher, where it sorts out the ground material (concrete, reinforced concrete, aggregates, excavation soil, building ceramics, bricks, masonry, construction wood, metals, asphalt etc.) into individual fractions. The material is sorted by screen platforms or sieves of different construction depending on the sorting technology (for fine fraction of up to 63 mm or for coarse fraction of 63 to 250 mm). Screens are usually woven from steel wires or made of rubber. The most commonly used separators contain vibrating screens with sieves arranged in parallel (capacity 150 to 200 tons/hours), drum separators operate on the principle of rotating sieves (capacity 200 tons/hour).

## 2 Methods and results

### Determination of granularity of recycled construction and demolition waste

The characteristics of the recycled material predetermine its further utilization. The ideal granularity of the construction and demolition waste fraction has been calculated and set to be in the range of 0 to 32 mm. The measurement aims to set the grain-size accumulation curve for recycled construction and demolition waste 0 to 32 mm fractions. Pursuant to the terminology of ČSN EN 933-1 “Testing of geometrical characteristics of aggregate” – Part 1: Determination of granularity – Sieve analysis”, grain-size accumulation curve  $Z = f(x)$  is a graphic representation of granularity, where  $Z$  is the percentage of siftings with the  $(x)$  size holes.

The comparison of the curves of the recycled material with standard ČSN 721512 “Solid aggregate for construction purposes – Technical specifications” for coarse gravel will show whether the recycled material can be used in the road construction – uncemented layers (ČSN 736126) with respect to its granularity.

The method and equipment required for the calculation of the grain-size accumulation curve is set by standard ČSN EN 933-1. The measurements are transformed into a curve of the granularity of the measured sample (with size of holes in the net on the “x” axis and percentage of material which fell through the sieve ( $Z$ ) is recorded in the “y” axis). The set of sieves and the limit curves (weight percentage of siftings) pursuant to ČSN 721512, for 0 to 32 mm fraction aggregate are described in fig. 1 to 3.

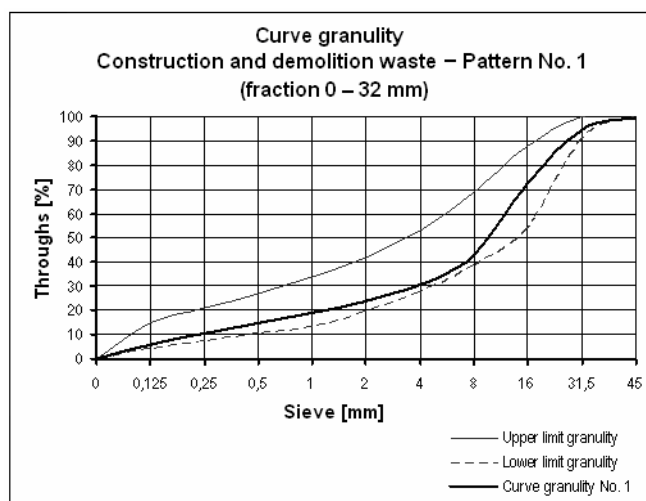


Fig. 1 Curve granularity – Construction and demolition waste – Pattern No. 1 (fraction 0 – 32 mm)

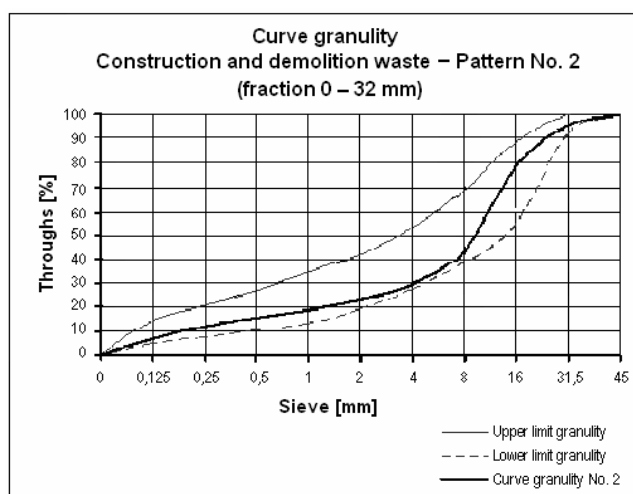


Fig. 2 Curve granularity – Construction and demolition waste – Pattern No. 2 (fraction 0 – 32 mm)

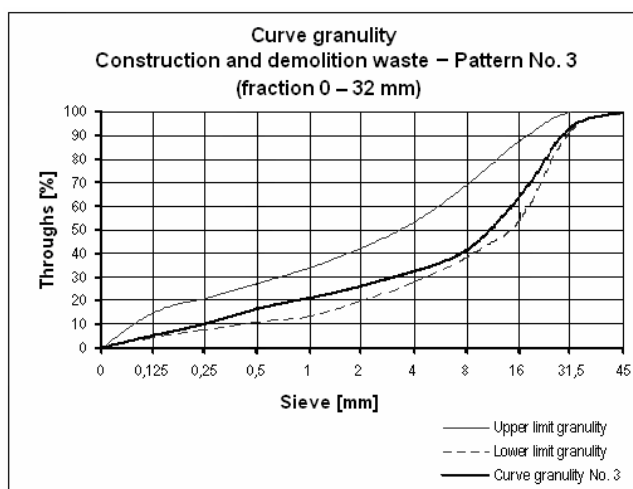


Fig. 3 Curve granularity – Construction and demolition waste – Pattern No. 3 (fraction 0 – 32 mm)

The overall granularity of the recycled material was calculated from average weight of sieve residues ( $\bar{\phi}_R$ ), which means that the granularity curve depicts the relationship between the size of sieve hole and percentage of siftings. The weight of siftings is calculated from the average weight of sieve residues.

### 3 Conclusion

The assessment of a series of measurements of the recycled 0 to 32 mm fraction resulted in the drawing of the granularity curves (Fig. 1 to 3), which proves that the tested recycled material complies with granularity requirement for class A solid aggregate for building purposes pursuant to ČSN 721512 “Solid aggregate for construction purposes – Technical specifications”. The recycled material has therefore been proved to be suitable for the construction of uncemented layers of roads with respect to its granularity. Measurements were taken on recycled material manufactured over the period of several months.

Other test of recycled materials made from construction and demolition waste focus on the chemical composition of the material, its strength, absorbability, volume stability etc. The determination of curve granularity (grain-size accumulation curve) of recycled materials made from construction and demolition waste and the comparison with the corresponding curves set by the relevant standard represent only one of the many tests and specifications that the recycled material must meet to pass as a quality substitute of the primary raw material.

### 4 Literatures

- ŠKOPÁN et al. Recycling 2009 – Možnosti a perspektivy recyklace stavebních odpadů jako zdroje plnohodnotných surovin. *Proceedings*. FSI VUT v Brně, Brno: 2009, ARSM – Asociace pro rozvoj recyklace stavebních materiálů v ČR. 151 pages. ISBN 978-80-214-3842-2
- ŠKOPÁN et al. Recycling 2007 – Možnosti a perspektivy recyklace stavebních odpadů jako zdroje plnohodnotných surovin. *Proceedings*. FSI VUT v Brně, Brno: 2007, ARSM – Asociace pro rozvoj recyklace stavebních materiálů v ČR. 220 pages, ISBN 978-80-214-3381-6
- ŠKOPÁN et al. Recycling 2006 – Možnosti a perspektivy recyklace stavebních odpadů jako zdroje plnohodnotných surovin. *Proceedings*. FSI VUT v Brně, Brno: 2006, ARSM – Asociace pro rozvoj recyklace stavebních materiálů v ČR. 191 pages, ISBN 80-214-3142-3



## STATISTICAL COMPARISON OF THE HARDNESS OF POLYMERIC PARTICLE COMPOSITES WITH A FILLER ON THE BASIS OF WASTE FROM MECHANICAL SURFACE TREATMENT, CAUSED BY GRAVITATION INDUCED SEDIMENTATION

PETR VALASEK\*, MIROSLAV MÜLLER

Department of Material Science and Manufacturing Technology, Faculty of Engineering,  
Czech University of Life Sciences, 165 21 Prague 6 – Suchbátka, Czech Republic

Phone: +420224383262, E-mail: valasekp@tf.czu.cz

### Abstract

Polymeric particle composites are materials synergically combining characteristics of both parts – matrix and filler. Because of their resulting characteristics, these composites can be used in various branches of different fields of industry. The properties of these composites are defined by the matrix and an adequate amount of filler. The matrix (connecting phase) usually comprises the epoxy resin, as filler metal particles can be used. If we replace the primary raw material by a secondary one, materials on waste based filler are created. The use of the waste as filler contributes to the improvement of some mechanical properties of the composite. It also presents an interesting possibility of the recycled material use. The most prominent characteristic of these materials is their enhanced hardness. During the polymeric particle composite curing process some sedimentation of filler particles occurs, induced by the gravitational force. As a result of this occurrence, the hardness of the composite can be different in different parts of the composite body. This makes different mechanical properties in the composite. The hardness of polymeric particle composites created in this way was then measured in their different parts. The aim of the experiment was to gain comprehensive data on the hardness of the composites. Afterwards, statistical analysis of the data was carried out, resulting in figures concerning the diversification of hardness in individual parts of the composite depending on the kind and amount of the used filler on the basis of waste from mechanical surface treatment.

**Keywords:** Polymeric particle composites, mechanical treated surface waste, hardness

### Introduction:

Particle composites are materials whose reinforcement is formed by non fibrous particles. Particle size is in all directions approximately equal. Particles are of spherical, cubical, quadrilateral lamellar or similar form [2]. The properties of polymeric particle composites are defined by the synergic sum of the matrix properties (continuous phase) and filler properties. Matrix can be made from a two-component epoxy adhesive. In the matter of polymeric particle composites in this continuous phase the filler in form of particles is dispersed. The particle reinforcements are used above all for the hardness and wear resistance increase [1]. The polymeric particle composite, whose filler was the waste from mechanical treatment processes and the matrix was the two-component epoxy adhesive, was the subject of carried out experiments. With regard to the waste classification in Czech Republic the abrading

agent from shot-blasting processes was used. The waste was neither of dangerous properties mentioned in addendum No 2 nor containing components mentioned in addendum No 5 of the Collection law 185/2001 of waste [3]. The substitution of the primary raw material by the secondary one (i.e. waste) offers the possibility of the waste thrifty recycling. This possibility should be preferred. Such filler can effectively substitute the primary raw material, but it is necessary to remember that its properties can vary from the properties of the primary raw material, e.g. by various particles size [4]. Just the mentioned property can cause variations of new composites properties. As mentioned, particle reinforcements are used among others for the resulting hardness increase. The aim of carried out experiments was the evaluation of the filler content influence over the resulting composite hardness in different test specimen points. From carried out experiments the



statistical sets (hardness values) were drawn up and consequently statistically analyzed.

### Experimental arrangement

The waste from mechanical surface treatment, coming by the waste catalogue under the identification 12 01 17, i.e. abrasion agent from shot-blasting [3], performed the function of the composite filler. Concretely the fractions F80 and F240 were used. The two-component epoxy adhesive LEPOX UNIVERSAL ECO P11 performed the function of the matrix. Epoxy resins are the very high-quality adhesives, suitable above all for bonding of metals, glass and ceramics. One of epoxy adhesives characters is the possibility of their filling by organic fillers [7, 8]. They are characterized by a high adhesion to metals and at a right choice of anorganic fillers they make possible to influence on a large scale the mechanical properties of the resulting material [6, 9]. The polymeric particle composites were prepared using 25, 50, 75, 100 and 125 filler volume percentage. The use of volume percentage prevents the influence of the filler and matrix different density. Single groups of test specimens were cast so that more specimens of the same fraction (F80, F240) and of the same filler volume percentage were prepared. Using these specimens in the form of the cube of the 25 mm side length the hardness Shore D according to the standard CSN EN ISO 868 (Plastics and ebonite – Determination of indentation hardness by means of a Durometer-Shore hardness) was determined [5].

At mixing of exactly determined filler volume with epoxy resin (matrix) the emphasis on the resulting mixture homogeneity was accentuated. Therefore at the specimen preparation the ultrasound was used, which was the cause of better immixture and the number of air bubbles decreased. The presence of air bubbles after curing would be negatively responsible for the specimen properties. The prepared mixture was moulded. Moulds were made from the two-component silicon rubber LUKOPREN N. Before the mixture casting the moulds were degreased and disinfected in order to prevent the material properties affecting. The cast specimens were cured according to the technological instructions for used adhesive.

The measured data sets were statistically analyzed. These basic statistical quantities were

used: arithmetic mean, standard deviation and variation coefficient. For determination of data sets abnormality the statistical abnormality testing was carried out. For comparison of monitored parameter values (Shore D hardness) between two data sets the Fischer's test of equality of two basic data sets variance according to the equation (1) was used. In this equation  $s_1^2$  and  $s_2^2$  are the variances impartial estimations calculated from the values listed in two independent sets of ranges m and n. This test evaluates the relation between two independent sets.

$$F = \frac{s_1^2}{s_2^2} \quad (1)$$

Next the T-test was used, i.e. the two-leapfrog test of the mean values equality of two basic sets. From the variances impartial estimations  $s_1^2$  and  $s_2^2$  the total impartial variances estimation was calculated.

$$s = \sqrt{\frac{1}{m+n-2} \cdot [(m-1)s_1^2 + (n-1)s_2^2]} \quad (2)$$

If we introduce the relation (2) in the relation (3), we calculate the T-test criterion. This test is based on the assumption that basic sets are of normal distribution of equal variances. This was verified by the foregoing F-test. Consequently the test criterions were evaluated by comparison with tabular values. In some cases the F-test proved the different data sets variances. In this case the two-leapfrog T-test of variances inequality was used.

$$t = \frac{\bar{x}_1 - \bar{x}_2}{s \cdot \sqrt{\frac{1}{m} + \frac{1}{n}}} \quad (3)$$

### Results and discussion

The specimen hardness measuring of single fractions was realized always on several specimens of the same filler volume percentage. In that way the independent data collection took place in order that the possible hardness variability of one specimen did not affect adversely the whole statistical set. The hardness measuring proceeded in two layers. The first layer – with sediments – was situated in the

bottom part of the specimen, the second one – non sediment – was situated in the top part of the specimen, see Fig. 1, where  $F_g$  means the gravitation affecting the specimen.

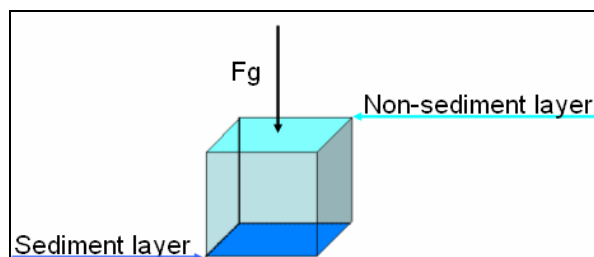


Fig. 1 Diagram of the hardness measurement

In the first case the relation between the sediment and the non-sediment layers at the concrete filler volume in the matrix were tested. The results are presented in Tab. 1. In the table top part we see the results of the relation between the sediment and non-sediment layers at the fraction F80, where  $F$  means the calculated F-test value according to the above mentioned equation and  $F_\alpha$  the table value of the critical value of the Student's distribution for the significance level  $\alpha = 0.05$ . Symbol “yes” (✓) in the line  $F < F_\alpha$  acknowledges the validity of this argument, i.e. it is no difference between the variances. Symbol “no” (x) excludes this hypothesis with the probability at the significance level  $\alpha=0.05$ ,  $T$  means the criterion of the T-test, which was compared with the critical value for the corresponding degree of freedom for  $\alpha=0.05$ . Corresponding “yes” in the line  $t < t_\alpha$  acknowledges the zero hypothesis, i.e. the averages of chosen sets are equal. If it be to the contrary this hypothesis is disallowed (symbol “x”).

Tab. 1 Statistical analysis results

statistical set	F80: sediment x non-sediment				
% of the filler	25	50	75	100	125
$F < F_\alpha$	x	✓	✓	✓	✓
$t < t_\alpha$	x	x	x	x	x
statistical set	F240: sediment x non-sediment				
% of the filler	25	50	75	100	125
$F < F_\alpha$	x	✓	✓	✓	✓
$t < t_\alpha$	x	x	x	x	x

Next the relation between the sediment layer and the non-sediment layer for the fractions F80 and F240 was tested, namely for the concrete filler volume. The results are presented in

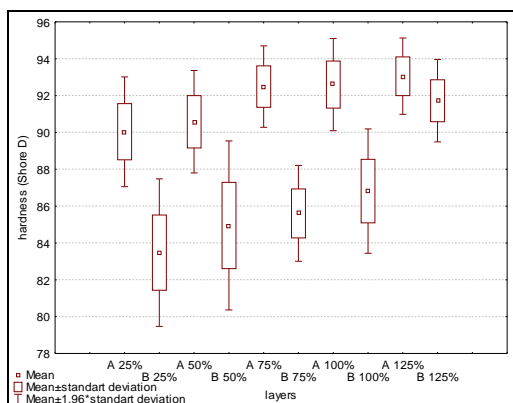
Tab. 2. The evaluation principle is the same as at the previous table.

Tab. 2 Statistical analysis results

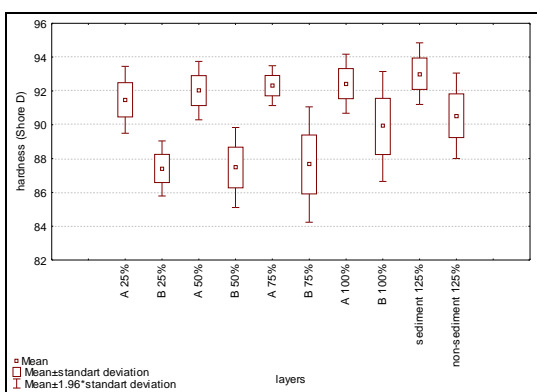
statistical set	Sediment layer: F80 x F240				
% of the filler	25	50	75	100	125
$F < F_\alpha$	✓	x	✓	✓	✓
$t < t_\alpha$	x	x	✓	✓	✓
statistical set	Non-sediment layer: F80 x F240				
% of the filler	25	50	75	100	125
$F < F_\alpha$	x	x	✓	✓	✓
$t < t_\alpha$	x	x	x	x	x

From the above presented tables it follows that if we compare the hardness data sets of the specimens containing the same filler volume in the matrix between the sediment and non-sediment layer, these data are incomparable, i.e. statistically different. The similar situation occurs at the hardness data sets of the non-sediment layers between both fractions (F80, F240) always at the concrete filler volume, see the bottom part of the Tab. 2. The different situation was in the case of the data set comparison for the sediment layer, where over the 75% filler volume these data sets were comparable, i.e. statistically identical.

The concrete hardness values of single fractions are presented in graphs. 1 and 2, where the sediment layer is lettered as “A”, the non-sediment layer as “B”. The recorded hardness of the sediment layer is of higher value than of the non-sediment layer. The highest value reached using the Shore D method was noted at the sediment layer of 125% filler volume in the matrix. At the F80 fraction this value was of  $93.05 \pm 1.02$ , at the fraction F240 of  $93.02 \pm 0.90$ . At the specimens containing the filler F80 the maximal hardness value was reached of  $93.05 \pm 1.02$ , at the fraction F240 of  $93.02 \pm 0.90$ . At specimens containing the filler F80 the maximal hardness value was reached of  $93.5 \pm 1.9$  at the sediment layer and of  $91.7 \pm 1.1$  at the non-sediment layer. At the specimens with the F240 filler the maximal hardness value was reached of  $93.0 \pm 0.9$  at the sediment layer and of  $90.5 \pm 1.3$  at the non-sediment layer. The lowest recorded hardness was determined in the non-sediment layer. At the fraction F80 this value was of  $83.48 \pm 1.98$  and at the fraction F240 of  $87.41 \pm 0.80$ . The resin hardness (etalon) was of  $83.1 \pm 3.2$  on the whole surface.



Graph 1. Hardness Shore D (F80)



Graph 2. Hardness Shore D (F240)

## Conclusions

From carried out experiments it is perceptible that the presence of the particle filler on the basis of waste from mechanical surface treatment enhanced the composite hardness for up to 20% (composites containing 125 % filler volume in the matrix) compared with the hardness of the resin without filler (etalon). By experiments it was confirmed the presumption of Vocel and Dufek [1] that particle fillers improve the composites resulting hardness. It is interesting to observe the gravistatic influence on the particles, which are at first homogeneous dispersed in the matrix (it is related to the mixture before filling in moulds) and afterwards in the course of curing they settle. It is possible to say that at the higher filler volume percentage in the matrix the resulting hardness between fractions did not differ, then the hardness data sets were statistically equal (sediment layer of more than 75% filler volume). At the non-sediment layer data sets comparison this trend was not observed. At the same time it is possible for a certainty to say that the hardness of the

sediment as well as non-sediment layers of the concrete fraction (F80, F240) and the same filler volume percentage in the matrix is not comparable, i.e. it is statistically different. By the substitution of the primary filler by the secondary filler (in case of carried out experiments by the filler on the basis of waste from mechanical surface treatment) the hardness improvement occurs. At the same time it is possibility to dispose economically of this waste. It is sensitive to environment and should be preferred.

## Acknowledgement

This paper has been done when solving the grant of the title "Possibilities of use of mechanical surface treatment waste in form of polymeric particle composite fillers" nr. 31140/1312/3118.

## References

- [1] VOCEL M., DUFEK V.: Friction and wear of machine. SNTL, Prague, 1976, 374 p. (In Czech)
- [2] MACHEK, V. - SODOMKA, J.: Polymers and composites with polymeric matrix. Prague: ČVUT, 2008. 86 p. (In Czech)
- [3] Law nr. 185/2001 (Zákon č. 185/2001 SB., o odpadech a o změně některých dalších zákonů)[online],[27.9.2009.] Available at <[http://portal.gov.cz/wps/portal/\\_s.155/701/.cmd/ad/.c/313/.ce/10821/.p/8411?PC\\_8411\\_l=185/2001&PC\\_8411\\_ps=10](http://portal.gov.cz/wps/portal/_s.155/701/.cmd/ad/.c/313/.ce/10821/.p/8411?PC_8411_l=185/2001&PC_8411_ps=10)> (In Czech)
- [4] MÜLLER, M., VALÁŠEK, P.: Polymeric composites based on waste reinforcing particles coming from surface mechanical treatment process. Strojírenská technologie, volume 14, 2010. pp. 183-186. (In Czech)
- [5] CSN EN ISO 868: Plastics and ebonite - Determination of indentation hardness by means of a durometer-Shore hardness. Prague: Czech standard institution, Prague, 2003. 12 p. (In Czech)
- [6] JANOVEC, J. – CEJP, J. – STEIDL, J.: Promising material. Prague: ČVUT, 2008. 143 p. (In Czech)

## LEAN REVERSE LOGISTICS IN BEVERAGES

VERONIKA VITKOVA<sup>1</sup>, VLADIMIR JURCA<sup>1</sup>, PETR TULACH<sup>2</sup>

<sup>1</sup>Czech University of Life Sciences Prague, 16521 Prague – Suchbátka, Czech Republic, Phone:  
+420 224 383 322, E-mail: jurca@tf.czu.cz

<sup>2</sup>Institute of Chemical Technology, 166 28 Prague 6, Czech Republic  
Phone: +420 724 337 592

### Abstract

Current Reverse Logistics is not generally managed in accordance with effective and lean logistics principles therefore there is an expected improvement and saving potential. It draws attention to the detailed investigation of the saving potential range in order to adapt to the present economic crisis and to introduce a new method in business practices. The paper presents a method of determining cost saving potential of reverse logistics flows. The research was carried out in the beverages sector where a substantial saving range in comparison to other sectors is expected due to extensive reverse logistics flows. Distribution simulation in order to identify sufficient number of outsourced centers and its optimized locations in the Czech Republic was used to obtain results. Furthermore, the total production and consumption volumes were simulated in accordance with competitive insourcing and outsourcing distribution reverse flows costs. The simulation outputs were the expected saving potential of reverse logistics achieved by outsourcing. Further the estimated saving potential of distribution reverse logistics costs were calculated, which generally causes a decrease in total logistics costs. The proposed method represents one of the lean logistics procedures which is recommended to be put into business practice.

### Introduction

Reverse logistics in beverages represents a significant aspect of all logistics flows. The current situation of reverse flows is not comparable to forward logistics flows in terms of processing, monitoring or controlling. In the majority of warehouse operations does not exist expenses documentation of reverse flows. Hence is expected to have the substantial potential to optimize costs. In today's competitive global, business environment, management is continually challenged to decrease expenses and increase customer service levels. In order to specify the range of saving potential, one must begin with definition of the investigation. The investigation was split into three single stages, which were conducted in the following order:

- 1. Quantitative research** – the objective of this stage was to investigate several opinions and perception of reverse flows in the whole logistics chain. The present description of reverse logistics on a macro level is known as a supporting service to the sales or production department. An established group of respondents was given several questions for the purpose of hypothesis (non-) confirmation.
- 2. Segments determination which create expense loadings** – in many cases logistics

management is not capable to separate reverse logistics cost out of total logistics cost or even specify the segments generating reverse logistics cost. A systematic approach was required to develop particular segments that create expense loading of reverse logistics.

**3. Synergic effect (saving potential) performance** between insourcing and outsourcing. In accordance with results of second stage is required to evaluate the range of potential in the area of transportation. The saving potential was proved and evaluated on the basis of collected and analyzed data acquired from simulated programs (Roadnet Transport Suite, Simul8).

### Experimental arrangement

The first stage is based on quantitative responding methods. For the research needs were chosen 150 respondents from Transport and logistics industry according to the Czech Status Ranking Industry (in Czech OKEČ - Odvětvová klasifikace ekonomických činností). By using Pareto analysis companies were selected in a group which is generating 80 % of market share according to the financial turnover in the selected industry - beverages. The established group was addressed and 46 respondents were participating

in the final research, performed by on-line interviewed methods (email, web pages) in the first half-year of 2009. The questioned group of respondents was created mainly from logistics managers (32 %), top managers (29 %), and purchase managers (12 %). From a different point of view the respondents were mainly set of sales companies (37 %) and production companies (34 %). The aim of this stage was to set up credibility composition of respondents group within the meaning of strategic and complex management because of the fact that reverse logistics is now playing one of the strategic roles across the whole supply chain management (Pernica, 2005)

The target of the second stage is to provide areas with predictable saving potential caused by reverse logistics operations. This part might summarize the scope of all logistics activities concerned with reverse flows. On behalf of comparison it is shown a Figure 1, which is illustrating insourced and outsourced reverse logistics flows. The principle of outsourcing is to provide precise amount of packaging just in time to the producer or seller based on customer demand planning. The objective is to create sufficiently dense network of outsourced centers in order to collect packaging from customer locations on the shortest possible distances (Frazzele, 2004).

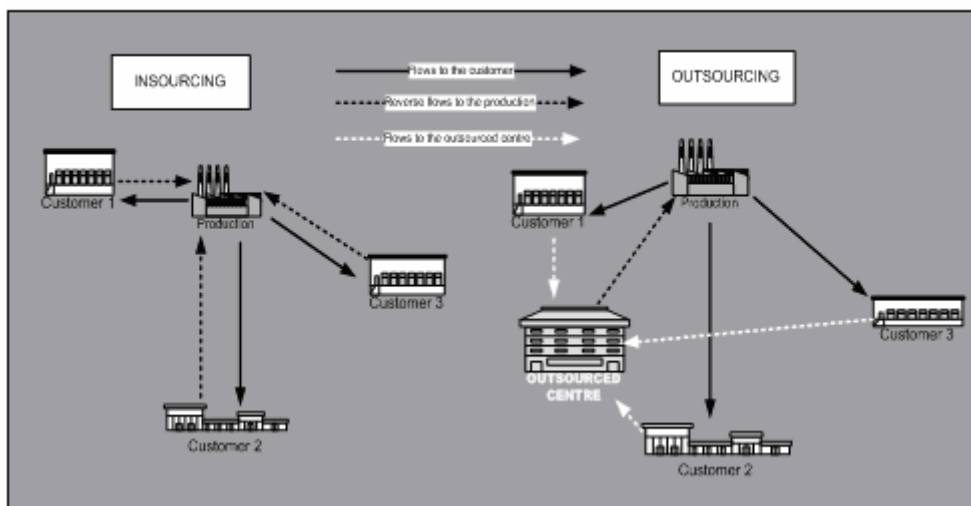


Figure 1: Logistics flows realized insourced versus outsourced

One solution to above mentioned issues is to identify all feasible areas which produce costs regarding to reverse logistics. Once the areas are developed, it becomes a requirement to assess the range of saving potential in particular areas. The third stage is based on data resources of five dominant companies acting in beverage industry (non-alcoholic) and presenting approx. 80 percent of the whole trade share in the Czech Republic. On the ground of beverages generally represent large-volume distribution flows, the research was focused on transport saving potential.

#### Solution procedure:

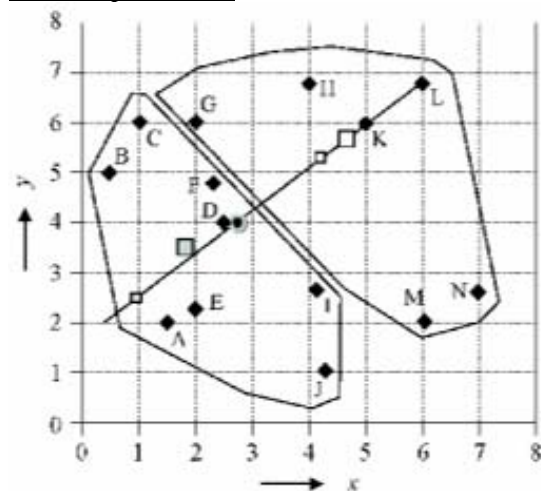


Figure 2: Example of two centers location model (Gros, 2009)



**a. Distribution flows modeling** – the model was generated by using RTS (Roadnet Transport Suite) and imported data regarding the locations with appropriate volumes of production and consumption. The result of a distribution model was a determination of an optimal amount of outsourced centers and its exact locations. The obtained results were based on the model which is one of the multi-location tasks without knowledge of the amount of centers. In practice the model is segmenting the whole area in particular segments as it is illustrated on the Figure 2. In all segments is creating unique optimal center. In the next step is a number of locations algorithmised in order to derive an optimal number of centers in the complex model.

**b. Potential saving determination** – bulk logistics flows were simulated statically as compared current state (insourcing) with proposed state (outsourcing). In dependence on bulk production and consumption was rated a balance of distribution flows within Czech regions. In the next steps were balanced kilometers converted into the financial statements beside insourcing and outsourcing.

### Results and discussion

Once the methods of research identification are known, the obtained results are described in the equivalent order. An **estimated saving potential considered by the questioned group was determined in appraised value of 11-20 % in majority** of respondents (see Tab. 1). This fact has confirmed the fundamental prerequisite of saving potential in reverse logistics realized by outsourcing.

*Table 1: Estimated range of savings in reverse logistics by outsourcing*

Question	Answers rating	
	Number of answers	Percentage rate
Estimated range of saving in reverse logistics by outsourcing		
1-5 %	6	15%
6-10 %	10	24%
<b>11 - 20 %</b>	<b>13</b>	<b>32%</b>
over 21 %	2	5%
don 't know	10	24%
<b>TOTAL RATING</b>	41	100%
	5 skipped question	

In regard of management perspective was created a matrix of arguments which represents the key optimization indicators in reverse logistics (see Tab. 2) . The indicators were separated in the group of indicators representing principles of Lean Logistics – indicators 1, 2, 3, 5, 6 and in the group represent Value added Logistics principles – indicators 4, 7. The highest values (4, 5) at the most frequent rate (9, 10) have acquired following indicators:

- operational cost savings
- customer service improvement
- raising hands “release” (focusing on core-business)
- supplier relationships improvement

Apart from the above mentioned indicators, there are other significant indicators such as the locked-up capital release and physical storage ground release. In reference to the fact that, none of the indicators is statistically insignificant, it is proved that indicators were correctly selected. In business practice it is predictable that companies give a priority to the indicators according to the chosen strategy in the particular time period. Aside from the evaluated indicators was listed an absence of sufficient packaging evidence and process monitoring in two mentioned cases.



Table 2: Optimization significance of particular indicators

Question	Rating scale (how much the indicator affect the optimization) 1 = make no account of it, 5= make a significant account of it					Answers rating	
	1	2	3	4	5	Weighted average	Number of answers
1 - Operational cost savings	16,7 % (6)	5,6 % (2)	25,0 % (9)	27,8 % (10)	25,0 % (9)	3,39	36
2 - Release of locked-up capital in packaging	16,7 % (6)	16,7 % (6)	19,4 % (7)	25,0 % (9)	22,2 % (8)	3,19	36
3 - Seasonal influence reduction (different demand of packaging within a year)	17,6 % (6)	20,6 % (7)	26,5 % (9)	17,6 % (6)	17,6 % (6)	2,97	34
4 - Packaging availability and reliability increase	19,4 % (7)	16,7 % (6)	36,1 % (6)	2,8 % (1)	25,0 % (9)	2,97	36
5 - Physical storage ground release	6,3 % (2)	9,4 % (3)	37,5 % (12)	25,0 % (8)	21,9 % (7)	3,47	32
6 - Raising hands "release" (focusing on core business)	2,9 % (1)	28,6 % (10)	28,6 % (10)	28,6 % (10)	11,4 % (4)	3,17	35
7 - Supplier relationships improvement	17,1 % (6)	17,1 % (6)	14,3 % (5)	28,6 % (10)	22,9 % (8)	3,23	35
TOTAL RATING						36	
						10 skipped question	

In order to summarize a quantitative research it might be appointed that the group of respondents was highly interested in reverse logistics issues. The main interest was drifted towards the possibility of outsourcing in order to enhance the core business activities.

The majority of respondents have perceived reverse logistics as:

- a strategic instrument to regulate and optimize SCM (Supply Chain Management)
- one of the objectives of lean and value added logistics principles
- a complex service realizable by third party (outsourcing)

From the saving potential perspective, it has been continued to identify a complete range of expense savings with the objective of making precise instantiation of saving potential in particular loadings segment. In this issue were identified seven segments of saving potential:

### 1) Ownership of packaging

*Data requirement relative to the determined time period: number of self-owned and rental packaging, count of purchased packaging, production increase, number of worn packaging, number of sold packaging*

### 2) Products transport and reverse flow of packaging

*Data requirement relative to the determined time period: self-realized transport (number of kilometers, number of drivers), outsourced transport (cost and transport conditions)*

### 3) Packaging selection and reparation

*Data requirement relative to the determined time period: working hours demand and*

*related height of salary, costs of used spare part*

### 4) Physical storage of packaging

*Data requirement relative to the determined time period: storage areas (internal, external) used for warehousing packaging in average*

### 5) Packaging handling

*Data requirement relative to the determined time period: number of handling equipment used for packaging handling (with specification of maintenance and service cost, purchase value), number of operators with related height of salary*

### 6) Ecological liquidation of packaging

*Data requirement relative to the determined time period: self-realized liquidation (number of operators with related height of salary), outsourced transport (cost and conditions)*

### 7) Damages due to the low-quality packaging

*Data requirement relative to the determined time period: number of damaged goods and its financial value.*

All above listed segments of saving potential introduce very attractive saving possibility in operational cost except the first segment, which represents mainly investment costs. Each of chosen saving segments will play a significant saving role in a different business sector. Beverage industry presents high-volume flow of packaging in the low value of goods. Seeing that the beverages have such a specified property, this industry has been prioritized for the further research in the saving segment number 2: Product transport and the reserve flow of packaging.

Based on provided data from beverage companies was created a transportation model of product flows from the production locations to the determined customers locations. The main object was to develop a number of outsourced centers and its location accordingly to the region's customer networks. On the RTS model basis were set four centers in Rakovník, Kolin, Jihlava, Prerov which will assure effective and optimized logistics flows.

In the second step was necessary to establish static models of packaging flows managed by insourcing principles and in comparison the model managed by outsourcing principles. The balanced value of packaging flows from the production location to the consumption location was converted in to the financial cost matrix by the same settling criteria in both principles (see Tab. 3a, 3b).

Table 3a,3b: Comparisons of packaging transportation realized by insourcing and outsourcing in CZK

TRANSPORTATION COST MATRIX	Prague region	Central Bohemia region	Liberec region	Ústí nad Labem region	Karlovy Vary region	Pízen region	South Bohemia region
Capital Prague region	27 300	29 900	29 172	36 400	54 600	37 050	31 980
Central Bohemia region	5 720	42 900	4 004	6 240	4 914	3 718	10 920
Liberec region	0	0	0	0	0	0	0
Ústí nad Labem region	0	0	0	0	0	0	0
Karlovy Vary region	84 500	239 980	48 204	18 720	6 084	28 054	60 840
Pízen region	0	0	0	0	0	0	0
South Bohemia region	35 360	106 080	19 188	19 188	19 500	17 472	6 864
Vysočina region	0	0	0	0	0	0	0
Hradec Králové region	0	0	0	0	0	0	0
Pardubice region	0	0	0	0	0	0	0
Moravia-Silesia region	312 312	264 264	14 612	32 916	21 996	29 406	31 512
Olomoucký kraj	0	0	0	0	0	0	0
South Moravia region	0	0	0	0	0	0	0
Zlín region	0	0	0	0	0	0	0
<b>Total cost in insourcing form (CZK)</b>	<b>465 192</b>	<b>683 124</b>	<b>115 180</b>	<b>113 464</b>	<b>107 094</b>	<b>115 700</b>	<b>142 116</b>
<b>IN TOTAL (CZK)</b>	<b>1 741 870</b>						
Outsourced centre Jihlava	0	0	0	0	0	0	235 248
Outsourced centre Rakovník	53 924	199 368	0	32 500	397 800	48 256	0
Outsourced centre Kolin	313 040	62 244	50 232	0	0	0	0
Outsourced centre Prerov	0	0	0	0	0	0	0
<b>Total cost in outsourcing form (CZK)</b>	<b>366 964</b>	<b>261 612</b>	<b>50 232</b>	<b>32 500</b>	<b>397 800</b>	<b>48 256</b>	<b>235 248</b>
<b>IN TOTAL (CZK)</b>	<b>1 392 612</b>						

TRANSPORTATION COST MATRIX	Vysočina region	Hradec Králové region	Pardubice region	Moravia-Silesia region	Olomouc region	South Moravia region	Zlín region
Capital Prague region	0	43 264	0	113 256	54 756	126 672	0
Central Bohemia region	5 200	7 280	6 760	41 964	13 494	22 360	19 266
Liberec region	0	0	0	0	0	0	0
Ústí nad Labem region	0	0	0	0	0	0	0
Karlovy Vary region	39 156	71 500	67 496	265 512	99 528	138 112	76 804
Pízen region	0	0	0	0	0	0	0
South Bohemia region	5 408	22 880	18 200	67 808	25 792	23 010	14 040
Vysočina region	0	0	0	0	0	0	0
Hradec Králové region	0	0	0	0	0	0	0
Pardubice region	0	0	0	0	0	0	0
Moravia-Silesia region	26 910	24 310	13 728	30 316	29 640	48 360	19 344
Olomoucký kraj	0	0	0	0	0	0	0
South Moravia region	0	0	0	0	0	0	0
Zlín region	0	0	0	0	0	0	0
<b>Total cost in insourcing form (CZK)</b>	<b>76 674</b>	<b>169 234</b>	<b>106 184</b>	<b>518 856</b>	<b>223 210</b>	<b>358 514</b>	<b>129 454</b>
<b>IN TOTAL (CZK)</b>	<b>1 582 126</b>						
Outsourced centre Jihlava	15 600	0	0	0	0	54 912	0
Outsourced centre Rakovník	0	0	0	0	0	0	0
Outsourced centre Kolin	0	140 244	22 100	42 588	0	0	0
Outsourced centre Prerov	0	0	0	426 218	34 320	53 300	14 196
<b>Total cost in outsourcing form (CZK)</b>	<b>15 600</b>	<b>140 244</b>	<b>22 100</b>	<b>468 806</b>	<b>34 320</b>	<b>108 212</b>	<b>14 196</b>
<b>IN TOTAL (CZK)</b>	<b>803 478</b>						
<b>Insourcing cost (CZK)</b>	<b>3 323 996</b>						
<b>Outsourcing cost</b>	<b>2 196 090</b>						
<b>SAVINGS (CZK)</b>	<b>1 127 906</b>						
<b>SAVINGS (%)</b>	<b>34%</b>						

It has been found that the transportation realized in the insourcing form has reached the amount of 3,3 Mio. CZK by the 70 % of transport vehicle utilization. In the outsourcing form of reverse logistics realization has reached the amount of 2,2 Mio. CZK by the 90 % of transport vehicle utilization. Based on these values it was identified a saving potential of 34 % in beverage sector.

## Conclusion

There are several reasons why cost demands of reverse logistics are lower by outsourcing form of realization. The first are transportation costs, which have proved the existence of 34% saving potential. Recognition of existing saving potential in these segments incites to further investigation in order to identify the whole range of potential. Furthermore the questionnaire

illustrated how the current situation is unaffected by methods serving the purpose of effectiveness enhancement of reverse flows. At the present time while facing a economic crash, there is an indisputable lack of knowledge in this issue. As the results proved, there is an extensive interest and saving potential across the whole supply chain management. In several cases, there usually does not exist one optimization method that would dominate in all business sectors. Accordingly to the saving achievement in each segment separately, there must be realized an integrated combination of optimization across all segments.

## References

1. FRAZELLE, Edward. World-class warehousing and material handling. New York: McGraw-Hill/Irwin, 2002. 242 s. ISBN 0-07-137600-3.
2. GRAY, CLIFFORD F., LARSON, Erik W. Project Management: the managerial process. New York: McGraw-Hill/Irwin, 2008. 589 s. ISBN 978-0-07-128751-7.
3. GROS Ivan: Matematické modely pro manažerské rozhodování (in Czech: Mathematical models for manager decision making) [online]. Version 1.0. Praha : VŠCHT Praha, 2009 [cit. 2009-11-02]. P. 123. Available from [http://vydavatelstvi.vscht.cz/knihy/uid\\_isbn-978-80-7080-709-5/pages-img/123.html](http://vydavatelstvi.vscht.cz/knihy/uid_isbn-978-80-7080-709-5/pages-img/123.html).
4. PERNICA, Petr. Logistika Supply chain management pro 21. století 1.díl. (in Czech: Logistics Supply Chain management in 21. Century 1. part). Praha: Radix, 2005. 570 s. ISBN 80-86031-59-4.
5. SVOBODA, Vladimír. Doprava jako součást logistických system (in Czech: Transport as a part of Logistics system). Praha: Radix, 2006. 152 s. ISBN 80-86031-68-3.

## PROCESSING OF TACTILE INFORMATION BY USING OF HELMHOLTZ EQUATION

JAROMIR VOLF<sup>1\*</sup>, MIROSLAV DVORAK<sup>2</sup>, JOSEF VLCEK<sup>3</sup>

<sup>1</sup>Czech University of Life Sciences in Prague, Faculty of Engineering, 165 21 Prague 6, CZ  
Phone: +420224383203, Fax: +4202-20921361, E-mail: volf@tf.czu.cz

<sup>2</sup>CTU in Prague, Faculty of Mechanical Engineering, Czech Republic

<sup>3</sup>CTU in Prague, Faculty of Mechanical Engineering, Czech Republic

### Abstract

This paper describes new and original methods of tactile pattern recognition in general position applying the solution of Helmholtz's equation for a tactile transducer. Three groups of methods have been formed, based on: (a) calculation of the A matrix eigen value, with the matrix being formed either from the whole pattern, or from the limit points; (b) the scalar characteristic distribution of the components of the pattern's A matrix; (c) the geometrical properties of the A matrix of the pattern. The patterns have been classified into five groups.

**Keywords:** pattern recognition, Helmholtz's equation, tactile image, tactile information

### Introduction

The ability to make the right decision and the orientation of intelligent robot in given surroundings are connected directly to the efficiency of the sensor system and the ability to process the information obtained. Here the processing of the tactile information is of major importance.

Several processing methods may be used. This paper deals with the processing of two-dimensional tactile patterns by solving Helmholtz's equation to create the tactile image that is in general position.

### Solution of the Helmholtz's equation

If we consider the part of the tactile sensor that comes into contact with the object as a diaphragm deformed by pressure, where a definite function determines the pressure distribution on the diaphragm, the methods for computing elastic diaphragms may be analogously used for determining the tactile pattern. The use of Helmholtz's equation, a special type of general partial differential equation, seems to be especially advantageous. Let us identify the pattern limit by the border C and the internal pattern zone by R. There Helmholtz's equation may be written in the form:

$$\Delta\Phi + \lambda\Phi = 0 \quad \text{in} \quad R$$

$$\Phi = 0 \quad \text{on} \quad C$$

where

$\lambda$  eigen value of continuous pattern  
 $\Phi$  pressure function on transducer area  
that  $\Phi \neq 0$

If the pattern is discretized by the sensor or transducers, Helmholtz's equation has to be solved in differential form. The continuous Laplace's operator is transformed into the five-point one or the nine-point one where

$h$  - the separation of the sensor centers

$I, J$  - the coordinates of the sensor centers

The matrix  $A$  characterizing the tactile pattern and is formed from the appropriate differential Laplace's operator. The Helmholtz equation changes into the form:

$$\left[ -\frac{1}{h^2} A + \lambda_h E \right] \vec{\Phi} = 0$$

which is solved in form:

$$\det(\Lambda E - A) = 0$$

where

$h$  distance between sensors centre

$\lambda_h$  eigen value of discretized pattern

$\Lambda$  minimum eigen value of matrix

$A$

$A$  pattern matrix type  $N \times N$

$\vec{\Phi}$  vector of dimension  $N$

representing value of function  $\Phi$

Three groups of methods are formed, based upon:

1. the computation of the eigen value of the matrix **A**:
  - the matrix **A** was formed for the whole pattern;
  - the matrix **A** was produced from the ground points after the internal points are filtered by use of the five-or nine-point Laplace's operator;
2. the scalar characteristic distribution of the components of matrix **A** of the tactile pattern;
3. the geometric properties of the matrix **A**.

For all cases five pattern groups were selected: circles, rectangles, squares, rectangle triangles and isosceles triangles.

#### Methods using the eigen value of the matrix **A**

The plane is considered to be the pattern space. Therefore two features are necessary to indicate the tactile pattern. The first is the minimum eigen value  $\lambda$  of the matrix **A**; the other must be carefully selected.

If we take into consideration that the eigen values depend upon the pattern area, the latter may be that area whose unit is  $h^2$ . The dependence of  $\lambda_5$  (the minimum eigen value for the matrix **A** made by the five-point Laplace's operator) upon the pattern area is the same for all patterns. Another feature may be the number  $N$  of activated sensors 'inside' the discretized pattern. Feature  $\lambda_5$  or  $\lambda_9$  (the minimum eigen value for the matrix **A** formed by the nine-point Laplace's operator) may be chosen. In both cases the basic pattern groups are distinguishable.

Kharkevich [4] has proved that the edges of the pattern bring more information than its area. This has also been proved in [5]. With this knowledge, the number of activated sensors  $P_0$  at the border  $C_{hr5}$  of the area  $R_{hr}$  is chosen as the second feature. This border is computed from the matrix **A** formed by the five-point Laplace's operator.

#### Method using the scalar characteristic distribution of the components of matrix **A**

If we start from the knowledge that the vertices and edges are the points containing the most information and that the inside pattern points bring less information, another method can be formulated.

The information measure in the pattern is expressed by

$$\tilde{I}_k = \frac{1}{N} \sum_{i=1}^N \left( \sum_{j=1}^N a(i, j) \right)^2$$

where

$k$  the Laplace operator used for forming the matrix **A**

$\tilde{I}_k$  the norm coefficient of patternability

$a(i, j)$  elements of matrix **A**

$N$  pattern sensor numbers (order of matrix **A**)

#### Methods using the geometric properties of the matrix **A**

The operator being the representation that in our case transforms the matrix of activated sensors to the matrix **A**, the geometric properties of this matrix may be investigated.

The matrix **A** is always square and order to get comparable results for different matrices, let us introduce normalization, after which the matrix area will have unity dimension. If we suppose the elements of matrix **A** are the points in a plane, then after normalization the element with the coordinates  $(i, j)$  is transformed to  $(ii, jj)$ . The normalization is given by the relations

$$ii = \frac{i-1}{N-1} ; \quad jj = \frac{j-1}{N-1}$$

Considering that the matrix **A** is symmetrical, which is a disadvantage in this case, because its centrum of gravity will always lie at the main diagonal, its lower triangular part will be used. The centrum of gravity coordinates may be expressed in two ways: in rectangular Cartesian coordinates  $T(x, y)$  or in polar coordinates  $T(V, \alpha)$ , where  $V$  is the distance from the origin of coordinates  $(ii, jj)$  and  $\alpha$  is the angle between the axis  $jj$  and the connecting line between the origin and the centrum of gravity  $T$  (see Fig. 1).



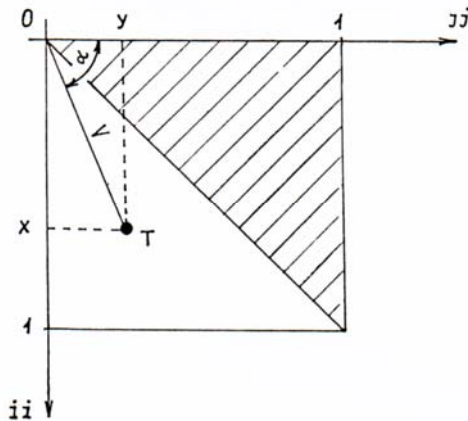


Fig. 1 The centrum of gravity of the normalized matrix  $A$

The elements of matrix  $A$  act as weighting coefficients during the computation. The centrum of gravity coordinates in the Cartesian system is determined according to the relations:

$$x = \frac{1}{N_o} \sum_{i=1}^N \sum_{j=1}^{i-1} \frac{i-1}{N_o-1} a(i, j)$$

$$y = \frac{1}{N_o} \sum_{i=1}^N \sum_{j=1}^{i-1} \frac{j-1}{N_o-1} a(i, j)$$

$$N_o = \sum_{i=1}^N \sum_{j=1}^{i-1} a(i, j)$$

where

$N$  the activated sensor number in the pattern area  $R_{hr}$  ( $\dim A = N$ )  
 $N_o$  elements number of down triangle normalized matrix  $A$

For polar coordinates we get

$$V = \sqrt{x^2 + y^2} \quad \alpha = \arctg \frac{x}{y}$$

By analogy with the foregoing cases, the matrix  $A$  may also be formed from the five- or nine-point Laplace's operator, for either all the activated sensors or for the reduced matrix. The individual Cartesian coordinates of the polar centrum of gravity  $T$  in combination with a number  $P_{05}$  of activated sensors may be selected for marks.

### Way of making rotation patterns

Experimentally has been chosen pattern rotation about  $4^\circ$  in interval  $180^\circ$ . Self pattern rotation is executed by next rules:

### Determine pattern centrum of gravity:

$$T_x = \frac{\sum_{i=1}^N L_{xi}}{N} ; \quad T_y = \frac{\sum_{i=1}^N L_{yi}}{N}$$

where

$L_{xi}$  distance  $i$  – point from axis  $y$  thorough coordinate basic origin  
 $L_{yi}$  distance  $i$  – point from axis  $x$  thorough coordinate basic origin  
 $N$  activation sensors number

### Pattern completion by fictive points

By computing and the pattern discretization, the various abnormality and teeth rise on patterns border. Then we insert other fictive points between original points that present active tactile sensors. By this way we increase texture and increase expressively rotate pattern quality.

### Sequential rotation of all pattern points

In last step cycles is executed, in which all pattern points are rotated (real and fictive) around its centrum of gravity step by step about  $0, 4, 8, \dots, 180^\circ$ . We calculate features in each from these angles. E. q. for each feature we obtain  $(180^\circ/4^\circ) + 1 = 46$  values. From these values we used only minimal, maximal or difference between maximal and minimal feature value.

After rotation calculation we decrease texture for next processing (calculation features). For next calculation we keep only points, where fulfill condition:

$$x \bmod 5 = 0 \quad \text{together} \quad y \bmod 5 = 0$$

where

$x, y$  are points coordinates (real and fictive) in are tactile sensor  
 $\bmod$  residue after division (e.g.  $6 \bmod 5 = 1$ )

From pattern with decrease texture we calculate all features and then we make next rotation about  $4^\circ$ .

Analogously as irregularities and teeth rise on the pattern border by the pattern rotation from computer calculation, than holes rise inside of pattern from the same reason. Than we have to make three rules for correction turning pattern.



rule – if in axis y of tactile sensor area rises situation sensor - space – sensor than we insert sensor instead the space

rule - if in axis x of tactile sensor area rises situation sensor - space - sensor than we insert sensor instead the space

rule - if in diagonal of tactile sensor area rises situation sensor - space - sensor than we insert sensor instead the space

Using of these rules shows Fig. 2.

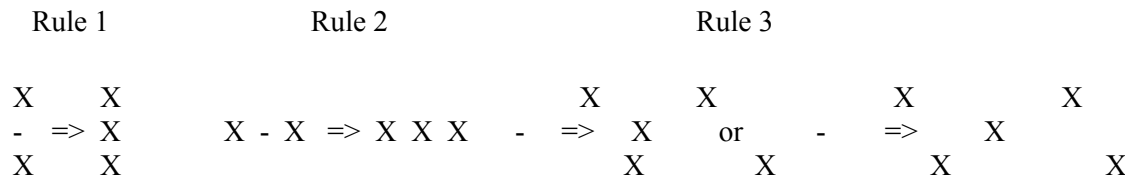


Fig. 2 Rules for holes correction in pattern

### Classification and the used features

For classification we used net features. All were defined up.

$\alpha_9$  polar coordinate of centrum of gravity of normalize matrix  $A$

$N$  number of activate sensors in area  $R_{hr}$

$I_{t5}$  scalar characteristic distribution of the components of matrix  $A$

$P_{o5}$  number of active sensors on border  $R_{hr}$ , border is created by 5 point Laplace's operator

In front of these features we will write symbol min, max, dif. Min or max present minimal or maximal features value through its turn. Dif presents difference between maximal and minimal value.

In first step, by classification was used features dependence  $\text{dif } \alpha_9 = f(N)$ . This dependence shows Fig. 3.

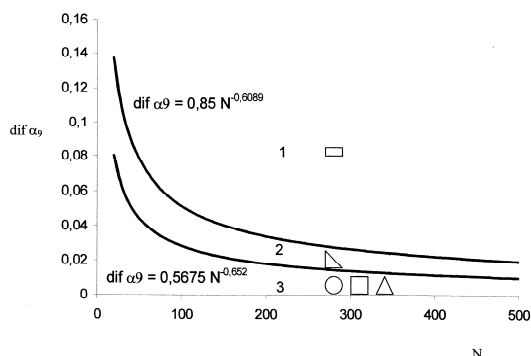


Fig. 3 Features dependence  $\text{dif } \alpha_9 = f(N)$

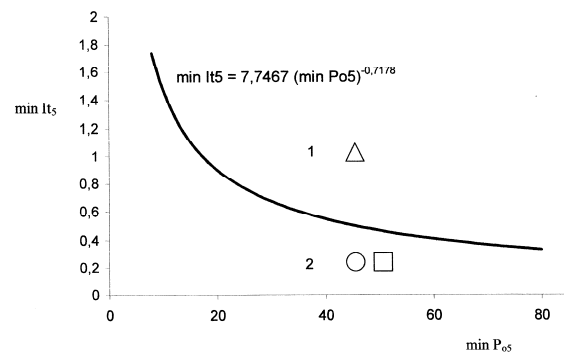


Fig. 4 Features dependence  $\text{min } I_{t5} = f(\text{min } P_{o5})$

By two curves we select the graph to three parts. To area 1 the rectangle pattern class belongs, to area 2 rectangle triangles pattern class belongs and to area 3 remaining patterns classes (circles, squares, equilateral triangles).

For selecting of equilateral triangles from circles and squares the dependence  $\text{min } I_{t5} = f(\text{min } P_{o5})$ . This dependence shows Fig 4. The pattern classes of circles and squares are in area under curve and the pattern classes of triangles are up curve.

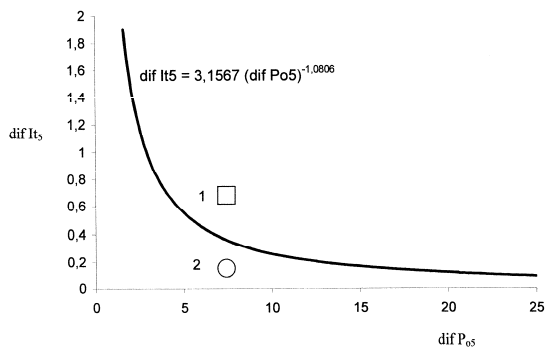


Fig. 5 Features dependence  $\text{dif } I_{t5} = f(\text{dif } P_{o5})$

By combination of up procedures we can select four pattern classes: rectangle triangles, equilateral triangles, rectangles and last group create squares and circles. For differentiation of circles from squares we used dependence  $\text{dif } I_{t5} = f(\text{dif } P_{o5})$ , see Fig. 5.

By three features dependences (Fig. 3 to Fig.5) we can right classify five pattern classes by probability dependent from inside sensors  $N$ . For inside sensors number  $N \geq 35$  is right pattern recognition more as 90 %, for  $N \geq 100$  is right pattern recognition about 99,9 %. Minimal size of pattern is  $N=20$ . In this case is right pattern recognition about 70%.

## Conclusion

This paper has dealt with the new and original methods for processing tactile information and distinguishing tactile patterns. These methods are based on the solution of Helmholtz's differential equation in discrete form.

## References

- [1] Dyga, R. - Chart, P.: Raspoznavanije obrazov i analiz scen. Mir, Moskva 1976.
- [2] Forsythe, G.E. - Wasow, W.R.: Finite Difference Methods for Partial Differences Equations, Wiley, New York, 1967
- [3] Pugh, A.: Robot Sensors, Vol. 2, Tactile and Nonvision Sensors, Springer, Berlin, 1986.
- [4] Kharkevich, A.A.: O cennosti informacii, Problemy Kibernetiky, 4(1960) 53-57.
- [5] Kanajev, E.M. and Shnejder, A.J.: Principy postrojenija osjazatelných racpoznajuscich ustrojstv, Mechanika Masin, Nauka, Moskow, 1974, pp. 29-32.
- [6] Volf, J.: Methods of Processing Tactile Information based on the Solution of Helmholtz's Equation. Sensors and Actuators A. Physical, Vol 41, No. 1-3. ELSEVIER SEQUOIA S.A., Lausanne. Switzerland. 1994. SSDI 0924-4247(93)00648-N. pp. 174-179

## SOIL RESISTANCE IN THE RELATION TO THE USED TECHNOLOGY OF THE SOIL CULTIVATION

V. VOLTR<sup>1\*</sup>, Z. HOFMAN<sup>1</sup>, P. ŠAŘEC<sup>2</sup>

<sup>1</sup>Institute of Agricultural Economics and Information, Prague, Czech Republic, Slezská 7, Post Code: 120 56, Tel.: +420222000390, Fax: 222725450 E-mail: [voltr.vaclav@uzei.cz](mailto:voltr.vaclav@uzei.cz)

<sup>2</sup>Czech University of Life Sciences Prague, 165 21 Prague 6 – Suchbátka, Czech Republic

### Annotation

The soil compaction is assessed by the penetrometric resistances and is compared with the yields of winter wheat on the 360 homogenous land pieces of typical soil-climatic conditions of the Czech Republic according to the type of soil cultivation. Penetrometric resistances are measured for each level of soil depth up to 18 cm, 19–38 cm and until the 72 cm. The correlation coefficients for the achieved excess soil compaction, excluding the texture impact confirm the correctness of the achieved result connections of penetrometric resistances and winter wheat yields. The lowest levels of penetrometric resistances were achieved in case of stubble plowing with tillage and in case of double stubble plowing. The maximum yield of winter wheat was achieved by stubble plowing with tillage, but with a large number of chemical treatments.

**Key words:** Penetrometric resistance, soil compaction, yields of winter wheat, soil compaction limit, soil texture, soil cultivation

### Introduction

The cultivation of soil and soil fertility is based on many factors, especially soil depth, texture, soil type, sorption complex, pH, humus content, and soil structure. The increased intensification of production in excess of tolerable limits may cause a temporary increase in soil productivity, but with a subsequent negative impact on its value. The soil compaction is, nevertheless, a complex factor linked to the soil structure, the input of organic matter, the soil load by means of mechanization, and with the impact on the reduced soil fertility and erosion formation [2]. It thus creates a major interaction between the intensification of the agricultural production and the environmental protection. For the interpretation of penetrometric resistances a comprehensive assessment of factors, particularly in relation to soil texture, is necessary.

The assessment of yields within the QH72257 project of the National Agency for Agricultural Research, "The evaluation of agricultural land resources with respect to the environmental protection", is based on an operational monitoring, under the main soil-climatic conditions, which consist of about 500 homogeneous lands with the total area of 9,200 hectares, including 127 most represented bonited soil-ecological units and 65 major soil

units covering three quarters of total arable land in the Czech Republic. For these lands the production data were determined for the years 2002 to 2009. The monitoring is carried out on homogeneous lands with the majority representation of the major soil unit from 80% of the land area with the total area of over 5 hectares [6].

The full-area data processing requires an objective assessment of the individual factors affecting the yield, which need to be subsequently standardized in terms of yields and costs required to be able to compare the soil-climatic units. For this statistical analysis and expert evaluation of the achieved yields will be used. The general assumption is the contribution of the identified connections for the theoretical understanding of the problem and for the agricultural practice.

The effect of soil compaction on yields is often quoted in literature - for example, [2], [4], [5], but a systematic evaluation of the major factors affecting the yields and the costs in a broader perspective is lacking.

### Methodology

In choosing the method for monitoring the state of land the hand penetrometric method of static testing was proposed with continuous pushing down of a standard cone into the soil in relation

to the allocation of the lands, which allows a sufficiently fast manner of quantifying the compaction in the individual soil layers. In measuring the P 70 penetrometer produced by ČZU Prague (Czech University of Life Sciences) was used.

The main principles of penetrometric measurement are given in Lhotský's work (1984) [3]. For the project's purpose the methodology was adapted, so that one sampling site was approximately 5 hectares. On a land with an area of up to 10 hectares there are three sampling sites selected, and on the other lands there is always one site chosen for each 5 hectares; however, the sufficient number of sampling sites is 10. The locations of these sites are chosen, so that they are evenly spread throughout the whole land and not interfering in the headland. During each measurement a continuous injection rate was maintained and in case of an impact of the needle into a stone the measured value on the penetrometer was reset. From each land samples of soil are taken to determine its moisture from the softened ground, thus maximally into the depth of tillage and from the subsoil layer [7].

Another part of this report is the evaluation of the relation between the soil fertility and the penetrometric resistances on lands in 2008 and 2009 in producing winter wheat, which makes a substantial portion of the vegetation observed on the lands within the project.

For each land the data from the registration of land blocks, from the penetrometric

monitoring and the data from agricultural plants were analyzed. The analysis gives an overview of the values achieved, of the possible evaluations and the connections of yield formation, which will be supplemented by additional data and measurements over the duration of the project.

**Crop yields** are taken from agricultural plants and the effects of crop damage are excluded. In the evaluation of the achieved **penetrometric resistances** the standardized procedures for evaluation of compacted soils, as cited by Lhotský [3.] in Table no. 1, were used. The penetrometric resistance shows a significant dependence of value on soil moisture. For example, Busscher [1] was investigating this connection and he proved a mutual slightly nonlinear relation. For the purposes of this monitoring, however, there is an assumption of a sufficient precision of the linear evaluation taken from the work of Lhotský [3]. According to this work, when the moisture lies out of the interval given in Table 1, for each material percentage of moisture 0.25 Mpa is either added to the stated value of critical resistance in case of lower moisture, or in case of high moisture 0.25 MPa is subtracted from the critical resistance value.

The number of doses of mineral nitrogen, organic fertilizers and chemical treatment is taken from the survey results at agricultural plants.

**Table 1.** Limit values for the critical properties of compacted soils

Property	Soil					
	Clay	Clay-Loamy	Loamy	Sandy-Loamy	Loamy-Sandy	Sandy
Porosity	<48	<47	<45	<42	<40	<38
Penetration Resistance [MPa]	2,8 – 3,2	3,3-3,7	3,8-4,2	4,5-5,0	5,5	6,0
Moisture [weight%]	28-24	24-20	18-16	15-13	12	10

Source: Lhotský 1984 [3].

The reached values of **penetrometric resistances**, which are available from the recorder each 4 cm, were expressed in the form of the average resistance of three layers: 0–18 cm, 19–38 cm and 39–72 cm. The bottom layer up to 72 cm is only indicative for the monitoring,

due to the fact that for this depth the soil moisture is not monitored.

The **soil texture** is indicated in categories according to the belonging of the main soil unit basic characteristics to the basic soil types. The texture will be validated during the project based on the actual status of texture on the site.

## Results

The comparison of the basic connections of the relation of the monitored factors to the yields was carried out using the partial and bivariate

correlation method. Table 2 shows the values for *winter wheat* in 43 cases. The texture was excluded because of the interdependence of the penetrometric resistance and texture.

**Table 2.** Correlation coefficients of the connection between the winter wheat yield and the selected factors

Year	2008				2009			
	Bivariate		Partial (Soil texture)		Bivariate		Partial (Soil texture)	
	Correlation	Significance (2-tailed)	Correlation	Significance (2-tailed)	Correlation	Significance (2-tailed)	Correlation	Significance (2-tailed)
Winter wheat yield [t/ha]	1		1		1		1	
Resistance averages 0-18 cm [MPa]	-0,263	0,006	-0,219	0,033	0,492	0,008	0,455	0,038
Resistance averages 18-38 cm [MPa]	-0,496	0,000	-0,464	0,000	0,520	0,005	0,419	0,059
Resistance averages 38-72 cm [MPa]	-0,392	0,000	-0,398	0,000	0,065	0,774	0,066	0,777
Equivalent resistance 0-18 cm [MPa]	-0,136	0,157	-0,020	0,846	0,474	0,011	0,519	0,016
Equivalent resistance 18 - 38 cm [MPa]	-0,429	0,000	-0,386	0,000	0,472	0,011	0,469	0,032
Excess compaction [MPa]	-0,394	0,000	-0,392	0,000	0,438	0,020	0,471	0,031

Table 2 indicates that the greatest correlation with soil fertility of the monitored indicators in 2008 is shown in the greatest significance of subsoil compaction in the 18–38 cm depth, in 2009 the soil compaction in the 0–18 cm depth. The compaction of soil in the depth of 38–72 cm achieves a very variable link to the wheat yield also in connection with the accuracy of the measurement, which is worse in the lower layers due to soil skeleton. Through converting the identified resistances to soil moisture in 2008 the correlation coefficient decreased in relation to the yield particularly in the topsoil layer, in 2009 the correlation coefficient increased through the conversion. This statistical survey has not shown a fundamental need for conversion of penetrometric resistances to soil moisture in

order to identify the links to the winter wheat yield.

The high correlation of the soil depth according to the evaluated penetrometric resistances applies even with the exclusion of the soil texture impact, and there is a presumption of continued use of this indicator to evaluate the impact of soil and of the achieved yields.

The increased correlation coefficients for the achieved excess soil compaction, excluding the texture impact (including the data with a negative sign in absolute value) confirm the correctness of the achieved result connections of penetrometric resistances and winter wheat yields.

The comparison of penetrometric resistances and soil texture in correlation to the wheat yield is shown in Table 3.

**Table 3.** The comparison of the significance of soil texture and penetrometric resistances in relation to the winter wheat yields in 2008 and 2009

Description	Equivalent yield for standard soil moisture [t/ha]	Resistance average in topsoil	Resistance average in subsoil 18 - 38 cm	Resistance average in subsoil 38 - 72 cm	Excess compaction	Percentage of clay particles up to 0,01 mm	Percentage of particles from 0,01 to 0,05 mm	Percentage of particles from 0,25 to 2 mm	Texture category according to USDA	Texture category according to Novák in a 6-digit scale	Texture category according to Novák in a 7-digit scale
Pearson Correlation	1	-,263**	-,496**	-,392**	-,394**	0,079	,373**	-,278**	,315**	-0,131	0,186
Sig. (2-tailed)		0,006	0,000	0,000	0,000	0,367	0,000	0,002	0,009	0,134	0,111
N	133	110	110	96	110	133	127	127	68	133	75

\*\* . Correlation is significant at the 0.01 level (2-tailed).

\* . Correlation is significant at the 0.05 level (2-tailed).

The penetrometric resistances show greater correlation coefficients in relation to the yield, than the soil texture itself. In the case of soil categorization according to texture the USDA category shows a correlation to the yield, but lower than the penetrometric resistances. The categories of texture according to Novák and according to the assignment to the main soil units

do not show any direct link to the winter wheat yield.

The relation of soil compaction and the basic technological processes of winter wheat production performed in 2008 and 2009 is listed in Table 4. The yields are given for all lands with winter wheat growing in these years, the penetrometric resistances are stated only on the lands with the measured resistance values.

**Table 4.** The relation between the achieved penetrometric values and the selected technological processes in 2008 and 2009

Tillage Stubble Plowing_Name	Statistical Indicator	Standardized winter wheat yield for single dry matter [t/ha]	Equivalent soil resistance 0-18 cm [MPa]	Equivalent subsoil resistance 18-38 cm [MPa]	Excess compaction [MPa]	Average of resistances in Topsoil [MPa]	Average of resistances in subsoil [MPa]
One stubble plowing without tillage	N	34	27	27	27	27	27
	Mean	6,59	3,43	6,90	3,01	2,51	5,83
Two stubble plowings without tillage	N	74	53	53	53	53	53
	Mean	6,61	1,87	4,91	0,96	1,61	4,77
Multiple stubble plowing	N	41	17	17	17	17	17
	Mean	5,84	2,61	5,93	1,88	2,23	5,62
Tillage without stubble plowing	N	41	17	17	17	17	17
	Mean	6,57	1,72	4,78	0,67	1,38	4,31
Tillage with stubble plowing	N	65	37	37	37	37	37
	Mean	6,70	2,34	5,21	1,04	1,81	4,57

The table shows that the lowest values of penetrometric resistances in topsoil were achieved in all cases with the tillage without stubble plowing technology, achieving medium yields of 6.57 t/ ha. In terms of production economy the highest yields of winter wheat in a

given sample are achieved through a conventional tillage with stubble plowing.

The evaluation of the connection between the yield formation, the penetrometric resistances and other factors of production are shown in Table 5.



**Table 5.** The quantification of factors of production in the years 2002–2009 and of penetrometric resistances of the soil in 2008 and 2009

Technology	Average of resistances in topsoil [MPa]	Average of resistances in subsoil [MPa]	Excess compaction[MPa]	Doses of farm fertilizers [kg N/ha]	Doses of mineral fertilizers[kg N/ha]	Number of chemical treatments inputs	Standardized winter wheat yield for single dry matter [t/ha]
One stubble plowing without tillage	2,51	5,83	3,01	39	134	3,743	6,287
Two stubble plowings without tillage	1,61	4,77	0,96	48	133	5,686	6,062
Multiple stubble plowing	2,23	5,62	1,88	49	131	5,000	5,706
Tillage without stubble plowing	1,38	4,31	0,67	48	125	3,900	5,951
Tillage with stubble plowing	1,81	4,57	1,04	46	143	5,800	6,700

## Conclusion

To evaluate the soil compaction the method of static measurements of penetrometric resistance was chosen. Based on the evaluation of the achieved resistances and other texture factors, doses of organic and mineral fertilizers and the number of chemical treatments, a link has been established from the observed plots during the years 2008 and 2009 between the yield and the soil compaction in case of winter wheat also in the framework of the individual technological methods of soil tillage.

The lowest levels of penetrometric resistances were achieved in case of stubble plowing with tillage and in case of double stubble plowing. The maximum yield of winter wheat was achieved by stubble plowing with tillage, but with a large number of chemical treatments.

This statistical survey has not shown a fundamental need for conversion of penetrometric resistances to soil moisture in order to identify the links to the winter wheat yield.

The penetrometric resistance is an important item in modeling the connection of yield formation and represents a closer link to the yield than simply defining the yield according to the soil texture. The impact of compaction is a complex application towards other impacts measured here, such as soil erosion, nutrient management and water retention in the landscape.

*This report originated based on the support of the QH72257 project, “The evaluation of*

*agricultural land resources with respect to the environmental protection”*

## Literature

- 1 Busscher, W.J; Bauer, P.J; Camp, C.R.; Sojka, R.E: Correction of cone index of soil water content differences in a coastal plain soil. *Soil & Tillage Research* 43 (1997) 205–217
- 2 Lhotský, J.: Zhutňování půd a opatření proti němu. *Studijní informace ÚZPI*, 7/2000, 61 s.
- 3 Lhotský, J. a kol: Zhutňování půd a opatření proti němu. Soustava opatření ke zúrodnění zemědělských půd. *Metodika pro praxi č. 14*, ÚVTIZ Praha, 1984, 39 s.
- 4 Riedel, W, Pikul, J., Osborne, S, Schumacher, T.: Soil penetrometer resistance and corn yield under tilled and no-till soil management. *South Dakota State University Soil/Water Research Report, Soil PR 04-40*. 2005
- 5 Brtnický, M., Vlček V., Pokorný, E., Denešová, O.: Míra pedokompakce půdního typu kambiem na vybraných pozemcích. In: *Hodnocení zemědělského půdního fondu v podmínkách ochrany životního prostředí*. Seminář ÚZEI Praha, 20.11.2008, 144-153, ISBN 978-80-86671-56-7
6. Voltr, V.: Metodika hodnocení zemědělského půdního fondu se zohledněním ochrany životního prostředí. *Economics of Agriculture*, VIII.,2008, No 4., p. 82–89, ISSN 1335–6186
7. Voltr, V., Fronek, P.: Sledování utužení půdy jako faktoru stavu úrodnosti půdy a jeho dopadu na životní prostředí. In: *Hodnocení zemědělského půdního fondu v podmínkách ochrany životního prostředí*.Seminář ÚZEI Praha, 20.11.2008, 154-162, ISBN 978-80-86671-56-7

## USING OF INVESTMENT SIMULATIONS FOR PLANNING OF MAINTENANCE

JIRI VONDRICKA, ZDENEK ALES, MARTIN PEXA, VLADIMIR JURCA

Czech University of Life Sciences Prague, Faculty of Engineering

Department for Quality and Dependability of Machines

Kamycka 129, 165 21 Prague 6 – Suchbát

Phone: +420 224 383 322, E-mail: Jirka.Vondricka@centrum.cz

### Abstract

Wide range of requirements must be considered and wide range of different product parameters has to be evaluated when purchasing new production equipment. Methodology of integrated product quality assessment was developed for product evaluation. All the parameters which are affecting the product costs or revenues are processed separately within financial simulations in this method. This concerns especially processing of risk variables. The outputs of the financial simulations are the expected net product value and the risk of the product purchasing in form of standard deviation of the simulation results.

Primary technical considered aspects as product maintenance and risk of failure are compared within the financial simulations as well. All the planned maintenance operations are represented and calculated as costs per produced unit. The failures are simulated as well as cost depending on failure size and susceptibility of failure.

The results of simulations showed that enhancing of preventive maintenance i.e. maintenance costs directly reduce the expected net product value. On the other hand, the reduction of the susceptibility of the failure was detected as enhancement of the net product value and reduction of the risk of product purchasing. Finally, different maintenance alternatives can be simulated and compared based on the expected risk of failure using the financial simulations.

### Introduction

The process of product evaluation becomes on importance in case of purchasing of big investments like production equipment. Than wide range of requirements of different interests groups within a company must be considered and wide range of different product parameters has to be evaluated. Therefore a methodology of integrated product quality assessment was developed. In this method, all the product parameters are divided into different groups and evaluated separately. Finally, the results are put together to one product quality index, based on the importance of each parameter. Newly all the financial parameters are processed separately within financial simulations in this method. This enables especially processing of risk variables. The outputs of the financial simulations are the expected net product value and the risk of the product purchasing in form of standard deviation of the simulation results. Because the technical aspects as maintenance and risk of failure affect the incomes and expenditures too, they can be compared within the financial simulations as well.

There are two basic economical theories of optimal investment decision known as static and dynamic methods for investment evaluation. The static methods [1, 3] evaluate investment according to average values as average costs or revenues, based on some average period of the product life. On the other hand, the dynamic methods concern the whole product life [1, 3, 4, 5, 7, 8] and discount e.g. the incomes of whole product life time to its certain value. The most known is the Net Product Value (NPV) describing today's product value. Another type of dynamic method is the internal income method; however Halberstock and Dellmann [4] demonstrated that this method can be confusing under specific conditions.

### Materials and methods

The method of economical evaluation is considering the product incomes and revenues to estimate the economical profit of the product. To calculate the profit, the cash flow, i.e. all the incomes and payments caused by the product, has to be calculated. The product cash flow is defined as follows:

$$cf = (c_t - m_t - mat_t) \cdot x_t - o_t \quad (1)$$

Where the cash flow  $cf$  is calculated as the product income per product (i.e. product price  $c_t$  in a time period  $t$  reduced by personal  $m_t$  and material costs  $mat_t$ ) is multiplied by the amount of sold products  $x_t$  and reduced by other non-specified costs  $o_t$ .

To simplify the financial calculations, one interest tariff  $i$  for credit and deposit is used. Than, based on the Fischer separation [2] the economic goals of the company (maximising of incomes or maximising of residual value) can be considered as equivalent. Finally, to compare expected company profit, net product value (NPV) is calculated. For the non-linear interest tariff, the NPV can be calculated as follows:

$$NPV = \sum_{t=0}^T cf_t \prod_{\tau=0}^t (1 + i_{\tau-1,\tau})^{-1} \quad (2)$$

The accuracy of this calculation depends on the input variables. The NPV is calculated based on the future i.e. unsafe parameters. To reduce the risk of the calculation, the method of risk management is used. So, the expected distribution of NPV is calculated using computational simulations [6]. In this method, for each unsafe variable a range of values is generated from estimated values of this variable and its distribution. Than, based on the random values generated before, the NPV distribution is simulated. The mean value of this distribution defines the expected value of NPV and the mean deviation of the distribution defines the risk of the investment. Finally, the NPV calculation becomes:

$$NPV_R = \sum_{t=0}^T E(\tilde{P})_t \prod_{\tau=0}^t (1 + i_{\tau-1,\tau})^{-1} \quad (3)$$

Where  $NPV_R$  is the expected net product value.

### Reliability

Reliability reflects the probability of a product's failing within a specified period of time. Among the most common measures of reliability are the mean time to first failure (MTFF), the mean time between failures (MTBF), and the failure rate per time unit. Because these measures require a product being

used for some time, they are more relevant to durable goods than they are to products and services that are consumed instantly. Other possibility to measure the product reliability is the comparison within the financial simulations. This idea is based on the fact, that all product failures are affecting costs. Therefore, the estimated failures can be defined as costs and simulated within the cash flow calculation. For more accuracy, the failures have been subdivided in three groups on (a) small, (b) middle and (c) big failures, where big failures occur sporadic and they are distinguish by very high costs caused by requirement of external service and expensive spare parts. On the other side the small failures occur often and they are mostly removed directly by the staff. In the methodology, reliability is evaluated as a risk costs within the financial calculations.

### Serviceability

The speed, courtesy, and competence of repair are called serviceability. Customer concern not only about product breaking down, but also about the elapsed time before service is restored. The timelines with which service appointments are kept, the nature of their dealings with service personnel, and the frequency with which service calls or repairs fail to resolve outstanding problems can be partially measured quite objectively, others reflect differing personal standard of what constitutes acceptable service. Serviceability of the product is given by three aspects: the product design, the preventive maintenance system and the maintenance after failure. Product features as diagnostics or availability of lubrication places are given in the design stage. So they can be evaluated as features alias measurable or non-measurable parameters. The preventive maintenance can be planed and affect first of all the costs. Therefore the impact of preventive maintenance is evaluated within the financial simulations. Finally the maintenance after failure has two dimensions; one meets the costs and was discussed within reliability, second dimension is the communication with the service department of the producer and has to be evaluated as a non-measurable product parameter.

### Implementation of costs for product failure and maintenance costs

Preventive maintenance costs can be divided into costs depending on time, i.e. preventive maintenance applied independent on the workload and costs depending on the product workload. Time dependent preventive maintenance costs can be summarised and added to other costs  $o$ . Workload dependent preventive maintenance costs are calculated for each product and reduce the product income as defined in Equation 1.

Furthermore, the financial simulation is extended with the repair costs  $RC_T$ . These are defined as follows:

$$RC_T = ARC \cdot z_D \quad (4)$$

Where  $ARC$  are average repair cost in a given time  $t$  and  $z_D$  is the expected amount of failures in a given time  $t$ . Varying of these inputs allows to simulate different alternatives. As described above, to simulate the repair costs precisely, the failures were divided into three groups: (1) small, (2) middle and (3) big, depending on the failure costs. Small failures are characteristic by low costs and short repair time and are occurring relatively often, on the other hand big failures occur sporadically, but are much cost intensive. In the simulation, following definition is used:

$$RC_T = z_{DS} \cdot ARC_s + z_{DM} \cdot ARC_M + z_{DB} \cdot ARC_B \quad (5)$$

Where the total repair cost  $RC_T$  is a sum of small, middle and big repair cost (index  $s, m, b$ ). These are defined as a multiple of average costs of given type of failure  $ARC$  and its expected amount  $z$ .

When the maintenance costs  $mt_t$  and the failure costs  $RC_T$  are integrated, the cash flow equation (1) becomes:

$$cf = (c_t - m_t - mat_t - mt_t)x_t - RC_{Tt} - o_t \quad (6)$$

Based on this equation, the net product value was simulated.

It is expected, that the preventive maintenance cost and the maintenance costs after failure are not independent. Thus, enhancing of the preventive maintenance cost should primary reduce the maintenance costs after failure and secondary reduce the risk of evaluated product.

Six different alternatives were simulated and compared. For comparison one given simulation with preventive maintenance cost of 0,12 € per product and defined amount of failures was used (AA1). Than using the same settings the amount of failures  $z_{DS}$ ,  $z_{DM}$  and  $z_{DB}$  (Equation 2) were halved (AA2) and finally set to zero (AA3). Similar to these alternatives, the alternatives AB1, AB2, AB3 were simulated with preventive maintenance costs extended to 0,13 € per product. In all simulations, stable average repair costs  $ARC$  were used. All the alternatives are listed in following table.

Table 1 Simulation alternatives with different preventive maintenance costs and amount of failures (the 100% of failure is mentioned the original parameters of alternative AA1)

Alternative	AA1	AA2	AA3	AB1	AB2	AB3
Preventive maintenance, €/product	0,12	0,12	0,12	0,13	0,13	0,13
Failures $z$ (%)	100	50	0	100	50	0

Table 2 Simulation results of given alternatives

Alternative	AA1	AA2	AA3	AB1	AB2	AB3
Min. Value	-938,1	-954,1	-929,5	-1082,4	-943,7	-874,7
Max. Value	3559,1	3416,3	3449,0	3370,1	3516,8	3488,2
NPV <sub>R</sub>	1236,6	1238,8	1243,9	1223,2	1227,0	1226,9
$\sigma$	538,8	537,1	535,4	538,9	536,0	535,5
$\sigma / NPV_R$	0,436	0,434	0,430	0,441	0,437	0,436

## Results and discussion

The results of the simulations are presented in Table 2. The expected net product value representing the value of the alternative and the mean deviation representing the risk are further presented in Figure 1 and respectively in Figure 2.

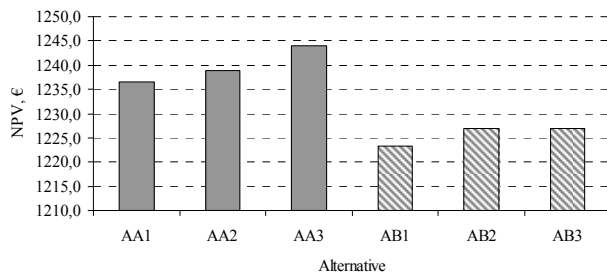


Figure 1 Net Product Value simulated for six given alternatives

As it could be seen in Figure 1, enhancing of the preventive maintenance costs from 0,12 € per product (Alternatives AA1-3) to 0,13€ per product (Alternatives AB1-3) can be directly recognised as Net Product Value reduction. However reducing of the expected amount of the failures  $z$  enhances directly the  $NPV_R$  and reduce the risk of the product as could be seen as the mean deviation reduction presented in Figure 2.

Based on presented simulations can be stated, that enhancing the preventive maintenance cost from 0,12 € to 0,13 € per product (~8,3 %) is not compensated by savings resulting from reduced failure occurrence by halve (AA1 vs. AB2) or even to zero (AA1 vs. AB3). However, it reduces the risk of the product by 0,5 % and 0,6 % respectively.

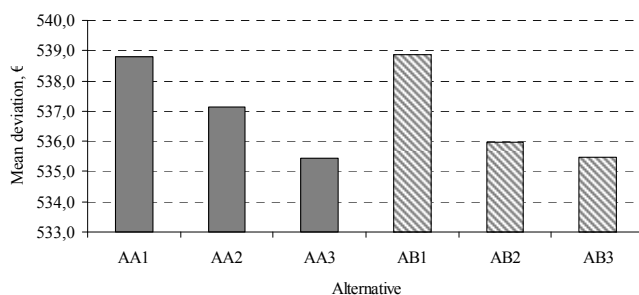


Figure 2 Product risk as mean deviation of six simulated alternatives

## Conclusion

The outputs of the financial simulations are the expected product value and risk of the investment. It was demonstrated, that the simulation can provide a very good summary concerning all the incomes and expenditures of company compared to one product i.e. production facility. Implementing the preventive maintenance costs and maintenance costs after failure into the financial simulation of net product value is helpful for simulation of different alternatives of maintenance strategy. The user can simulate the impact of enhancing or reducing the preventive maintenance represented by costs to state, which impact has the alternative on his income or on the risk of the product. In the presented example, each enhancing of the preventive maintenance costs causes significant reducing of the net product value and small, but recognisable, reducing of the product risk. Depending on the company goals, the impact of the different maintenance strategies can be investigated and tested to vote the optimal one, before introducing a new maintenance strategy. Therefore, this method is an alternative to the known commonly used measures for product maintenance and failures.

## References:

- [1] BLOHM, Hans; LÜDER, Klaus; SCHAEFER, Christina. *Investment: Area weak point analysis and capital budgeting*. Auflage 9. München : Vahlen, 2006. p. 357, ISBN 3800631687, ISBN 978-3800631681. (In German)
- [2] FISCHER, Irwing.: *The Theory of Interest, as determined by Impatience to Spend Income and Opportunity to Invest it*. New York : Macmillan, 1930. p. 347, Available at WWW: <<http://oll.libertyfund.org/title/1416>>.
- [3] GÖTZE, Uwe.: *Capital budgeting: Models and analysis for investment evaluation*. 6. Auflage. Heidelberg : Springer-Verlag, 2008. 506 s. ISBN 978-3-540-78872-0, e-ISBN 978-3-540-77873-7. (in German)
- [4] HABERSTOCK, L.; DELLMANN, K.: *Capital value and internal interests as a measure of investment profitability*, Kostenrechnungspraxis. 1971, 5, s. 195-206. (in German)



- [5] HAX, Herbert.: *Theory of investment*.  
5.bearb. Aufl., korrig. Nachdr. Würzburg :  
Physica-Verlag, 1993. 212 s. ISBN  
3790803235, ISBN 9783790803235. (in  
German)
- [6] HERZ, David B.: *Risk Analysis in Capital  
Investment*. Harward Business Review.  
1964, January/February, s. 95-106.
- [7] KERN, Werner.: *Capital budgeting*.  
Stuttgart : Poeschel, 1974. 393 s. ISBN  
3791001612, ISBN 978-3791001616. (in  
German)
- [8] SCHNEIDER, Dieter. *Investment, financing  
and taxation*. 7., vollst. überarb. u. erw. A.  
Wiesbaden : Dr. Th. Gabler Verlag, 1992.  
814 s. ISBN 3409690239, ISBN 978-  
3409690232. (in German)



## CALCULATIONS OF A HEATED FLOOR PANEL FOR PIGLETS RESTING PLACES

VIKTORIJA ZAGORSKA, ULDIS ILJINS, IMANTS ZIEMELIS

<sup>1</sup>Latvia University of agriculture, Liela Street 2, Jelgava, Latvia, Phone: +37129740492, E-mail: vzagorska@gmail.com

### Abstract:

The article deals with problem solving of mathematical physics using the method of separation of variables optimizing heating element – heating with electricity wire coil or hot water tube layout in housing of concrete heating panel. If an electro-heated cable in the panels body is placed, than amount of heat conducted from the cable is the same along all the length of the cable. If hot water circulating through tube is used, than amount of heat energy taken off the heater decreases along its length. Distribution of temperature over the working surface of the panel at different position  $x$  and  $y$  coordinates of heating elements, different heat transfer coefficients and variable heating element intensity was calculated using MS Excel software and obtained temperature distribution solution over the cross-section of the panel.

**Key words:** mathematical model, panel, temperature, heater, coordinates.

### Introduction

New born piglets together with the sow are kept. The optimal surrounding air temperature for a sow is about 16...20°C, but for new born piglet during the first days of their life the temperature in its lairs has to be within the limits of 32...36°C. Gradually the lair's temperature must be decreased until 22...24°C when piglets are two months of age and weaned (Priekulis et al., 1992). That means that comfortable surrounding temperature for sows and piglets is different despite the fact that during first days they are kept together. Therefore in cold winter countries like Latvia piglets resting place local warming ought to be used.

For ensuring piglets comfort, concrete floor panels heated by electric current or hot water are used. If an electro-heated cable in the panels body is placed, than amount of heat conducted from the cable is the same along all the length of the cable. If hot water circulating through tube is used, than amount of heat energy taken off the heater decreases along its length. The aim of the research is to create the mathematical model of a panel, which evaluates variable: heating element intensity and heat transfer coefficients of the surfaces. Making the analysis of previous solution of Laplace equation of heat transfer for heating panel using the method of separation of

variables at definite boundary conditions (Iljins U. et al., 1999) it was made a conclusion about necessity of modification of boundary conditions. Firstly, it is necessary to take into account variable intensity of a heating element. Secondly, there should be a possibility to make the simulation of use of heating panel, when heat transfer coefficients from both side surfaces are different. Thirdly, the model should take into consideration the under panel insulation influence on the temperature distribution over the cross-section of the panel.

The obtained solution should allow to calculate the temperature at every point of the cross-section of a panel including its surface, depending on the coordinates of heating element coils.

### Materials and methods

It is being solved the problem of mathematical physics to calculate the temperature in every point of panel cross-section. To solve this problem it is not enough to use the Laplace equation of heat transfer

$$\nabla^2 T = 0, \quad (1)$$

boundary conditions have to be determined as well:

$$\lambda \frac{\partial T}{\partial x} \Big|_{x=0} = \alpha_{s_1} (T|_{x=0} - T_0) \quad (2)$$

$$-\lambda \frac{\partial T}{\partial x} \Big|_{x=d} = \alpha_{s_2} (T|_{x=d} - T_0) \quad (3)$$

$$-\lambda \frac{\partial T}{\partial y} \Big|_{y=H} = \alpha_{s_3} (T|_{y=H} - T_0) \quad (4)$$

$$\lambda \frac{\partial T}{\partial x} \Big|_{y=0} = q(x), \quad (5)$$

$$T_i|_{y=y_{i+1}} = T_{i+1}|_{y=y_{i+1}}, \quad (6)$$

$$-\lambda \frac{\partial T_i}{\partial y} \Big|_{y=y_{i+1}} + \lambda \frac{\partial T_{i+1}}{\partial y} \Big|_{y=y_{i+1}} = q \sum_{j=1}^{m_i} \delta(x - x_{0ij}), \quad (7)$$

where  $m_i$  - number of coils into  $i$  group;  
 $\delta(x - x_{0ij})$  - delta function;  
 $\alpha_{s_1}, \alpha_{s_2}, \alpha_{s_3}$  - the surface heat transfer coefficients from upper and side surfaces,  $\text{W m}^{-2} \text{K}^{-1}$ ;

$q(x)$  - function which determines the heat loss through lower surface,  $\text{W m}^{-2}$ ;  
 $T_0$  - air temperature in the piggery,  $^{\circ}\text{C}$ ;  
 $\lambda$  - the heat transfer coefficient of concrete,  $\text{W m}^{-2} \text{K}^{-1}$ .

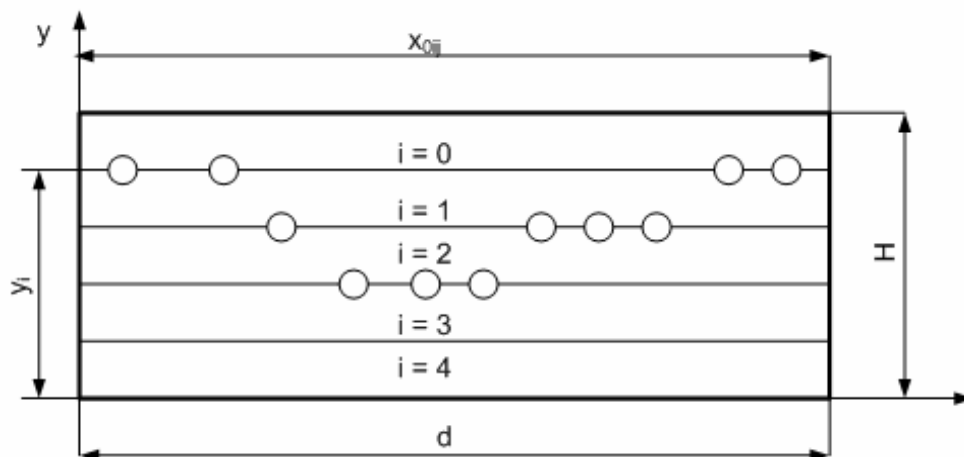


Fig. 1. Scheme of calculation:  $i$  - index of the region where the point is located which temperature is calculated;  $x_{0ij}, y_i$  - coordinates of the heater coils

Boundary conditions (2), (3), (4) formulate the third kind boundary problem, and boundary condition (5) formulate second kind boundary problem. In mathematics, the Neumann (or second-type) boundary condition is a type of boundary condition when imposed on an ordinary or a partial differential equation, it specifies the values that the derivative of a solution is to take on the boundary of the domain. Third type boundary condition is a type

of boundary condition, when imposed on an ordinary or a partial differential equation, it is a specification of a linear combination of the values of a function and the values of its derivative on the boundary of the domain. In  $x, y$  coordinate system the general solution of the equation (1) is expressed by series of trigonometric and hyperbolic functions (Riekstins, 1969):

$$T_i = T_e + \sum_{k=1}^{\infty} \sin(\xi_k x + \varphi_k) \cdot [A_{k_i} \cdot \text{sh} \xi_k (y_i - y) + B_{k_i} \cdot \text{ch} \xi_k (y_i - y)] \quad (8)$$

where  $x, y$  - coordinates of the point where the temperature is calculated, m;  
 $A_{k_i}, B_{k_i}$  - free chosen constants;

$\xi_k$  – particular value,  $m^{-1}$ ;

$\varphi_k$  – free chosen constant.

Equation (8) is inserted into boundary conditions (2) and (3) in consecutive order, wherefrom

$$\varphi_k = \arctg b_1 \xi_k d, \quad (9)$$

and  $\xi_k d$  is found solving the transcendental equation:

$$\tan \xi_k d = \frac{(b_1 + b_2) \xi_k d}{b_1 b_2 (\xi_k d)^2 - 1}, \quad (10)$$

where  $k = 1, 2, \dots, \infty$ ;

$$b_1 = \frac{\lambda}{\alpha_{k_1} d};$$

$$b_2 = \frac{\lambda}{\alpha_{k_2} d}.$$

In order to establish values of the constants  $A_{k_i}$  and  $B_{k_i}$  equation (8) is inserted into the boundary conditions (4). Then solution (13) is tied up at the boundary between two zones with

different indexes  $i$  by using conditions (6) and (7).

Inserting the expression (8) into the boundary conditions (4) results in:

$$\lambda \xi_k [A_{k_n} \operatorname{ch} \xi_k (y_0 - y|_{y=y_n=H}) + B_{k_n} \operatorname{sh} \xi_k (y_0 - y|_{y=y_n=H})] = \alpha_u [A_{k_n} \operatorname{sh} \xi_k (y_0 - y|_{y=y_n=H}) + B_{k_n} \operatorname{ch} \xi_k (y_0 - y|_{y=y_n=H})], \quad (11)$$

from which

$$\lambda \xi_k A_{k_n} = \alpha_u B_{k_n}. \quad (12)$$

As the number of zones  $i_{\max} = n$  can change, it is necessary to look for the expression to calculate the temperature in a way, which does

not change when we are going from zone number  $i$  to zone number  $i+1$ . Such will be the expression:

$$T_i = T_e + \sum_{k=1}^{\infty} \sin(\xi_k x + \varphi_k) \left\{ \frac{A_{k_i} [a_{k_i} \operatorname{sh} \xi_k (y_i - y) + b_{k_i} \operatorname{ch} \xi_k (y_i - y)] + c_{k_i} \operatorname{sh} \xi_k (y_i - y) + d_{k_i} \operatorname{ch} \xi_k (y_i - y)}{c_{k_i} \operatorname{sh} \xi_k (y_i - y) + d_{k_i} \operatorname{ch} \xi_k (y_i - y)} \right\}, \quad (13)$$

where  $a_{k_i}, b_{k_i}, c_{k_i}, d_{k_i}$  – free chosen constants which are unchangeable when going to zone  $i+1$ .

After inserting the expression (13) into condition (6) it follows:

$$\begin{aligned} b_{k_{i+1}} &= a_{k_i} \operatorname{sh} \xi_k (y_i - y_{i+1}) + b_{k_i} \operatorname{ch} \xi_k (y_i - y_{i+1}); \\ d_{k_{i+1}} &= c_{k_i} \operatorname{sh} \xi_k (y_i - y_{i+1}) + d_{k_i} \operatorname{ch} \xi_k (y_i - y_{i+1}). \end{aligned} \quad (14)$$

In the same way inserting the expression (13) into condition (7), multiplying both sides by

$\sin(\xi_k x + \varphi_k)$  and integrating in the limits from 0 to  $d$  the following is obtained:

$$\begin{aligned} a_{k_{i+1}} &= a_{k_i} \operatorname{ch} \xi_k (y_i - y_{i+1}) + b_{k_i} \operatorname{sh} \xi_k (y_i - y_{i+1}); \\ c_{k_{i+1}} &= c_{k_i} \operatorname{ch} \xi_k (y_i - y_{i+1}) + d_{k_i} \operatorname{sh} \xi_k (y_i - y_{i+1}) - \frac{\sum_{j=1}^m q_j \sin(\xi_k x_0(j) + \varphi_k)}{N_k}; \\ N_k &= \frac{\lambda \xi_k d}{2} \left[ 1 + \frac{\cos 2(\xi_k d + \varphi_k) - \cos 2\varphi_k}{2 \xi_k d} \right]. \end{aligned} \quad (15)$$

It is seen that expression (13) with the new constants  $a_{k_{i+1}}, b_{k_{i+1}}, c_{k_{i+1}}, d_{k_{i+1}}$  is invariant.

Inserting the formulas (12) and (14) into expression (15) the following is obtained:

$$\begin{aligned} a_{k_2} &= 1; \quad b_{k_2} = \frac{\lambda \xi_k}{\alpha_u}; \quad c_{k_2} = 0; \quad d_{k_2} = 0; \\ a_{k_3} &= \operatorname{ch} \xi_k (H - y_1) + \frac{\lambda \xi_k}{\alpha_u} \operatorname{sh} \xi_k (H - y_1); \\ b_{k_3} &= \operatorname{sh} \xi_k (H - y_1) + \frac{\lambda \xi_k}{\alpha_u} \operatorname{ch} \xi_k (H - y_1); \end{aligned} \quad (16)$$

$$c_{k_i} = - \frac{\sum_{j=1}^m q_j \sin(\xi_k x_{0ij} + \varphi_k)}{N_k};$$

$$d_{k_i} = 0$$

and so on until  $i_{\max} = n$ .

At certain fixed  $i = p$  after a row of algebraically changes the formula (16) is as follows:

$$\begin{aligned} a_{kp} &= \text{ch } \xi_k (H - y_p) + \frac{\lambda \xi_k}{\alpha_u} \text{sh } \xi_k (H - y_p); \\ b_{kp} &= \text{sh } \xi_k (H - y_p) + \frac{\lambda \xi_k}{\alpha_u} \text{ch } \xi_k (H - y_p); \\ c_{kp} &= - \frac{2 \sum_{j=1}^p \sum_{i=1}^{m_p} q_j \sin(\xi_k x_{0ij} + \varphi_k) \text{ch } \xi_k (y_i - y_p)}{\lambda \xi_k d \left[ 1 + \frac{\cos 2(\xi_k d + \varphi_k) - \cos 2\varphi_k}{2 \xi_k d} \right]}; \\ d_{kp} &= - \frac{2 \sum_{j=1}^p \sum_{i=1}^{m_p} q_j \sin(\xi_k x_{0ij} + \varphi_k) \text{sh } \xi_k (y_i - y_p)}{\lambda \xi_k d \left[ 1 + \frac{\cos 2(\xi_k d + \varphi_k) - \cos 2\varphi_k}{2 \xi_k d} \right]}. \end{aligned} \quad (17)$$

Inserting the formulas (17) into equation (13) boundary condition (5), the following formula is at  $p=n$ , and also expression (13) into the obtained:

$$A_k = \frac{2 \sum_{i=1}^n \sum_{j=1}^{m_n} q_j \sin(\xi_k x_{0ij} + \varphi_k) \text{ch } \xi_k y_i - b_k}{\lambda \xi_k d \left[ 1 + \frac{\cos 2(\xi_k d + \varphi_k) - \cos 2\varphi_k}{2 \xi_k d} \right] [\text{ch } \xi_k H + b_1 \xi_k d \text{sh } \xi_k H]}, \quad (18)$$

where  $b_2 = \frac{\lambda}{\alpha_u d}$ ;

$$I_k = \int_0^d q(x) \sin(\xi_k x_{0ij} + \varphi_k) dx. \quad (19)$$

The function  $q(x)$  is connected with coils depth and is conversely proportional to the

where  $\Delta x_i$  is the width of the operation zone (m), the following is gotten:

thermal resistance. Using  $q(x) = \frac{q_i}{\Delta x_i} \frac{\frac{H-y_{i-1}}{2} + \frac{a_u}{\lambda}}{\frac{H-y_i}{2} + \frac{a_u}{\lambda} + \frac{d_{iz}}{\lambda_{iz}}}$ ,

$$I_k = \sum_{ij} q_j \frac{\frac{H-y_{i-1}}{2} + \frac{a_u}{\lambda}}{\frac{H-y_i}{2} + \frac{a_u}{\lambda} + \frac{d_{iz}}{\lambda_{iz}}} \sin(\xi_k x_{0ij} + \varphi_k). \quad (20)$$

Taking into consideration the formulas (13)...(15) and carrying out a row of algebraically changes the following is obtained:

$$\begin{aligned} T_p &= \sum_{i=1}^n \sum_{j=1}^{m_p} \frac{q_j}{\xi_k d \left[ 1 + \frac{\cos 2(\xi_k d + \varphi_k) - \cos 2\varphi_k}{2 \xi_k d} \right]} T_0 + \frac{2}{\lambda} \times \\ &\left[ \frac{\text{sh } \xi_k (H - y) + b_1 \xi_k d \text{ch } \xi_k (H - y)}{\text{ch } \xi_k H + b_1 \xi_k d \text{sh } \xi_k H} \times \left( \sum_{i=1}^n \text{ch } \xi_k y_i \sum_{j=1}^{m_i} \sin(\xi_k x_{0ij} + \varphi_k) - I_k \right) \right. \\ &\quad \left. - \sum_{i=1}^p \text{sh } \xi_k (y_i - y) \sum_{j=1}^{m_i} \sin(\xi_k x_{0ij} + \varphi_k) \right] \sin(\xi_k x_{0ij} + \varphi_k) \end{aligned} \quad (21)$$

By changing coordinates of the discrete heater coils, it is possible to obtain desirable distribution of the temperature along the working surface. Using the formula 21 temperature on the surface was calculated.

## Results

Using the general solution (8) of Laplace differential equation (1) at given boundary conditions (2)...(7) the formula (21) was used. It had been done by a computer.

Assuming that concrete heat transfer coefficient  $\lambda = 1 \text{ W (m} \cdot \text{K)}^{-1}$ , panel width  $d = 1 \text{ m}$ , heat transfer coefficient through working surface  $\alpha_u = 10 \text{ W (m} \cdot \text{K)}^{-1}$ , pigsty air temperature  $20^\circ\text{C}$ , panel thickness  $H = 0.1 \text{ m}$ , bottom side insulation thickness  $0.1 \text{ m}$ , insulation heat transfer coefficient  $\lambda = 0.04 \text{ W (m} \cdot \text{K)}^{-1}$  using the Ms Excel software temperature on the working surface was calculated.

As it is seen in the Table 1 and Figure 2, where four cases of simulation are represented the necessary temperature on the upper surface of a panel can be reached not only by placing all the coils at the same depth ( $y = \text{const}$ ), but using smaller steps among outer twines and making minimal decrease of step in the  $x_{0ij} = 0.405$  to compensate the minimal decrease of the heating element intensity. If we do not take into account area of 5 cm from the side surfaces, than temperature variation accounts  $0.68^\circ\text{C}$ . For example, in the case when panel from the left side is enclosed to the 0.1 m wide wooden lath, than the temperature variation only of  $0.63^\circ\text{C}$  is achieved. To land it is necessary to use smaller step among outer twine at the right side surface, and little variation of steps over the panel is required as well (to compensate the variety of heating element intensity). It is important to add that heat source flows from the right side, where

heat transfer coefficient is higher. Speaking about third case when equal steps are used than temperature variation of  $4.6^\circ\text{C}$  appears.

In order to get maximum equability of temperature over the upper surface the outer twines have to be not only packed but placed at smaller depth too. In Figure 2 it is seen as the case 4, when temperature variation accounts  $0.53^\circ\text{C}$ . As it is seen from Figure 2 the lines 1 and 4 are the similar. Line 1 depicts the situation, when only the steps are variable. It is allowable to have the variation of temperature over the panel by  $2^\circ\text{C}$  that means that in the case, when heated floor for piglets is simulated, there is no need to make variable depth, because of more complicated construction and non significant changes in the temperature variations over the panel.

**Table 1** Variation of parameters to get evenness of the temperature distribution over the panel

Number of twines	Variable step $\alpha_{t1} = \alpha_{t2} = 10 \text{ W m}^{-2}\text{K}^{-1}$ $y = 0.06, \text{ m}$			Variable step $\alpha_{t1} = 1.26 \text{ W m}^{-2}\text{K}^{-1}$ $\alpha_{t2} = 10 \text{ W m}^{-2}\text{K}^{-1}$ $y = 0.06, \text{ m}$			Equal step $\alpha_{t1} = \alpha_{t2} = 10 \text{ W m}^{-2}\text{K}^{-1}$ $y = 0.06, \text{ m}$			Variable step $\alpha_{t1} = \alpha_{t2} = 10 \text{ W m}^{-2}\text{K}^{-1}$ $y_1 = y_{10} = 0.065, \text{ m}$ $y_2 \dots y_9 = 0.055, \text{ m}$		
	m	m	$\text{W} \cdot \text{m}^{-2}$	m	m	$\text{W} \cdot \text{m}^{-2}$	m	m	$\text{W} \cdot \text{m}^{-2}$	m	m	$\text{W} \cdot \text{m}^{-2}$
	$x_{0ij}$	$\Delta x$	$q_i$	$x_{0ij}$	$\Delta x$	$q_i$	$x_{0ij}$	$\Delta x$	$q_i$	$x_{0ij}$	$\Delta x$	$q_i$
1	0.025		12	0.025		12	0.025		12	0.025		12
2	0.08	0.055	11.9	0.12	0.095	11.9	0.12	0.095	11.9	0.08	0.055	11.9
3	0.180	0.115	11.8	0.215	0.095	11.8	0.215	0.095	11.8	0.180	0.115	11.8
4	0.295	0.115	11.7	0.31	0.095	11.7	0.31	0.095	11.7	0.295	0.115	11.7
5	0.405	0.110	11.6	0.405	0.095	11.6	0.405	0.095	11.6	0.405	0.110	11.6
6	0.515	0.110	11.5	0.5	0.095	11.5	0.5	0.095	11.5	0.515	0.110	11.5
7	0.625	0.110	11.4	0.595	0.095	11.4	0.595	0.095	11.4	0.625	0.110	11.4
8	0.735	0.110	11.3	0.69	0.095	11.3	0.69	0.095	11.3	0.735	0.110	11.3
9	0.835	0.100	11.2	0.785	0.095	11.2	0.785	0.095	11.2	0.835	0.100	11.2
10	0.935	0.100	11.1	0.9175	0.0975	11.9	0.88	0.095	11.1	0.935	0.100	11.1
11	0.975	0.040	11	0.975	0.057	12	0.975	0.095	11	0.975	0.040	11

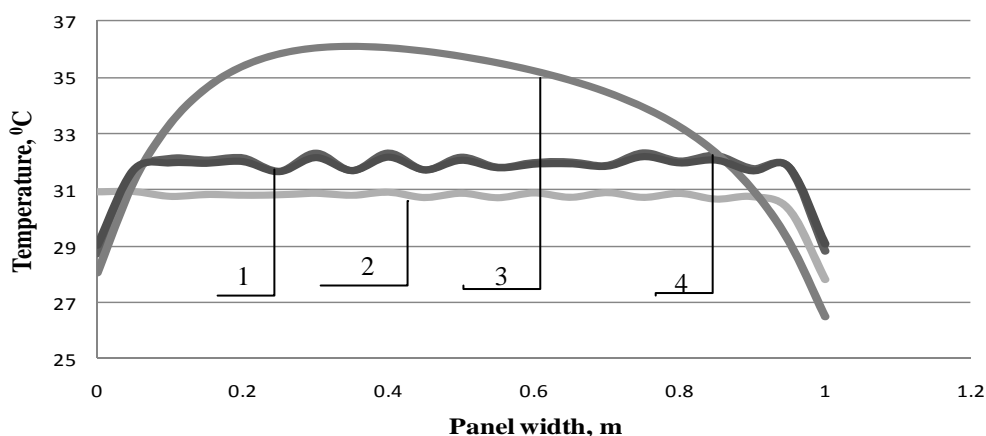


Fig. 2. The temperature on the upper surface of the panel: 1- variable steps, 2- variable steps and side heat transfer coefficients, 3 - unchangeable steps, 4 – variable steps and depth

### Conclusions

1. Method of separation of variables solving the problem about optimization of displacement of variable heating elements has been presented.
2. The formula 21 enables to calculate the temperature of the upper surface of a panel and every point of the cross-section of a panel at certain values of the parameters included into the formulas.
3. By placing the outer twines in the less depth it is possible to maintain the necessary evenness of the temperature along the entire working surface within the limits  $\pm 0.53^{\circ}\text{C}$ .
4. At the same heat source intensity and different position of coordinates of a heating element different mean temperature value over the upper surface is achieved.

5. It is necessary to continue modeling of the heating panel to simulate the heat flow from the side, upper and lower surfaces to calculate the necessary thickness of the insulation.

### Reference

1. Priekulis J.-Tilaks S.-Ziemelis I.: Mechanization of livestock farming. Zvaigzne, 1992, 379pp. (in Latvian)
2. Iljins, U. - Ziemelis, I.- Navickas, J.: Providing the equal temperature on the working surface of a heated floor panel. .International Conference: Hydraulic Engineering and Land Management. Kaunas, Lithuania, 1999. 60 - 67 pp.
3. Riekstins, E.: Methods of mathematical physics. Trans. Zvaigzne. 1969, p. 623. (in Latvian)



## MATHEMATICAL MODEL OF FLAT-PLATE SOLAR COLLECTOR

JESKO ZANIS<sup>1\*</sup>, ILJINS ULDIS<sup>2</sup>, ZIEMELIS IMANTS<sup>3</sup>

<sup>1</sup>Latvia University of Agriculture, Faculty of Engineering, PhD. student

J.Čakstes boulv.6, Jelgava, Latvia, LV-3001

Phone: +371-63080697, Fax: +371-63020762, E-mail: [Zanis.Jesko@llu.lv](mailto:Zanis.Jesko@llu.lv)

<sup>2</sup>Latvia University of Agriculture, Faculty of Information Technologies,  
Department of Physics

<sup>3</sup>Latvia University of Agriculture, Faculty of Engineering, Institute of Mechanics

### Abstract

In practice several types of solar collector constructions with efficiency 30 - 75 % exist. The amount of sunshine hours in Latvia (57' northerly altitude for Riga) is ~ 1800 hours yearly in average. In spite of that solar collectors for water heating in Latvia are used, mostly flat-plate, whose price is lower than for other collector types but efficiency often is not sufficient and water has to be additionally warmed-up. Too poor yearly sunshine hours, little efficiency of flat-plate collector and preeminent expenses of other collector types stimulate to look for possibilities to increase efficiency of flat-plate collector without radical, labour-consuming, time-consuming and materially investments. In order to investigate the possibility to increase efficiency of a flat-plate collector mathematical model of collector has been worked out. By solving Laplace heat transfer equation at the boundary conditions according to construction of real collector, obtained equations give possibility to simulate construction of flat-plate collector depending on physical and thermal values of materials used for construction of collector. In order to verify accuracy of mathematical model specific model of flat-plate collector and experimental equipment for temperature measuring in definite points of collector have been made. Theoretically calculated results and experimentally obtained ones shows good correlation and give evidence to use theoretical formulas for optimization of flat-plate collector.

### Introduction

Most important and most expensive single component of an active solar energy system is collector field, which may be performed in a several versions as from constructions of collectors as of collector configuration. Solar collector is a mechanical device which captures radiant solar energy and converts it to useful thermal energy [5]. In spite of Latvia's northern situation solar heating systems successfully are used as for hay and grain drying as for water and space heating. Cold and rainy Latvian climate with comparatively short summers and little annual solar irradiation requires for an efficient solar heating systems. As known with increase of systems efficiency increases its costs and that means that expenses of heat energy unit will be increase. Therefore in order to create solar heating system working with efficiency as high as possible it is necessary to know all relationships among constructive, thermal and economical parameters affecting operation of system. The aim of investigation is to create

mathematical model of flat-plate collector, which could be used for solar collector designing.

### Materials and Methods

For simulation of operation of solar collector and determination of optimum thermal and constructive parameters, mathematical model of collector by theory of mathematical physics was created. With mathematical model it becomes possible after known constructive and thermal parameters of collector to calculate temperature in several surfaces and structural materials of collector. On other hand, in order to verify accuracy of mathematical model the specific model of flat-plate collector and experimental equipment of 50 thermo-couples for temperature measuring at definite points of collector has been developed. Main parts of flat-plate collector are box made from wood, plastic or other material in which layer of heat insulation is placed in, and absorber – metal sheet with soldered, welded or glued metal tube true witch heat career runs, and transparent cover mostly made of glass. In line

with real construction, mathematical model also consist of these layers -  $\delta_1$ ,  $\delta_2$ ,  $\delta_3$  and  $\delta_4$  (Fig.1.).

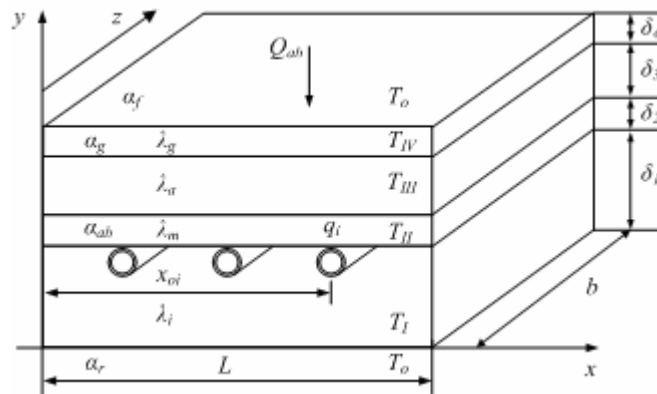


Fig.1. Scheme of mathematical model:

$x$ ,  $y$ ,  $z$  – co-ordinates;  $Q_{ab}$  – specific heat of absorbed energy,  $W \cdot m^{-2}$ ;  $\delta_1$ ,  $\delta_2$ ,  $\delta_3$ ,  $\delta_4$  thickness of insulation layer, absorber sheet, air layer and glass cover, m;  $\alpha_r$ ,  $\alpha_{ab}$ ,  $\alpha_g$ ,  $\alpha_f$  – contact heat transfer coefficients from rear side of collector, absorber, glass cover and front side of collector,  $W \cdot m^{-2} \cdot K^{-1}$ ;  $\lambda_i$ ,  $\lambda_m$ ,  $\lambda_a$ ,  $\lambda_g$  – heat transfer coefficient of heat insulation material, absorber sheet, air layer and glass cover,  $W \cdot m^{-1} \cdot K^{-1}$ ;  $T_0$ ,  $T_I$ ,  $T_{II}$ ,  $T_{III}$ ,  $T_{IV}$  – temperatures on front and rear surfaces, in insulation layer, absorber sheet, air layer and glass cover,  $^{\circ}C$ ;  $q_i$  – intensity of heat absorbed by circulating heat carrier,  $W \cdot m^{-1}$ ;  $x_{oi}$  – co-ordinate of heat transfer tube, m;  $L$ ,  $b$  – dimensions of model, m.

In stationary regime of heat flow temperature distribution in collector can be described by Laplace equation or differential equation of thermal conductivity [1, 2, 7, 8]

$$\frac{\partial^2 T}{\partial x^2} + \frac{\partial^2 T}{\partial y^2} = \Delta T = 0, \quad (1)$$

where  $T$  – temperature in point with co-ordinates  $x$  and  $y$ ,  $^{\circ}C$ .

For solving equation (1) boundary conditions of the solution have to be formulated. As the thickness of the absorber plate ( $\delta_2 = 0.8$  mm) in comparison with its width  $b$  and length  $L$  is considerably small, therefore it is possible to assume, that through the side surfaces at  $x = 0$  and  $x = L$  heat flow is equal to zero. Considering that following boundary conditions can be written

$$\left. \frac{\partial T}{\partial x} \right|_{x=0} = \left. \frac{\partial T}{\partial x} \right|_{x=L} = 0. \quad (2)$$

where  $\lambda_a$  – equivalent heat transfer coefficient of air layer,  $W \cdot m^{-1} \cdot K^{-1}$ ;

In compliance with the task of the investigation the temperature distribution in the following three layers have to be computed:

$T_I$  – temperature in heat insulation layer,  $^{\circ}C$ ;

$T_{II}$  – absorber plate temperature,  $^{\circ}C$ ;

$T_{III}$  – air temperature in space between glass cover and absorber,  $^{\circ}C$ .

On rear side of collector where  $y = 0$  heat convection occurs, therefore heat flow can be expressed as

$$\lambda_i \frac{\partial T_I}{\partial y} \Big|_{y=0} = \alpha_r (T_I|_{y=0} - T_0), \quad (3)$$

where  $\lambda_i$  – heat transfer coefficient of heat insulation material,  $W \cdot m^{-1} \cdot K^{-1}$ ;

$\alpha_r$  – contact heat transfer coefficient from rear side surface of collector,  $W \cdot m^{-2} \cdot K^{-1}$ ;

$T_0$  – temperatures on front and rear surfaces of collector,  $^{\circ}C$ .

Heat convection takes place also from front surface of collector and corresponding boundary condition for this surface is

$$-\lambda_a \frac{\partial T_{III}}{\partial y} \Big|_{y=\delta_1+\delta_2+\delta_3} = \alpha_f (T_{III}|_{y=\delta_1+\delta_2+\delta_3} - T_0), \quad (4)$$

$\alpha_f$  – contact heat transfer coefficient from front side surface of collector,  $W \cdot m^{-2} \cdot K^{-1}$

On border between heat insulation layer and metal sheet temperature and heat flows are equal and can be expressed as (5) and (6). For

calculations thickness of glass cover is assumed as  $\delta_4 = 0$ .

$$T_I|_{y=\delta_1} = T_{II}|_{y=\delta_1} \quad (5)$$

and

$$\lambda_m \frac{\partial T_{II}}{\partial y} \Big|_{y=\delta_1} - \lambda_i \frac{\partial T_I}{\partial y} \Big|_{y=\delta_1} = \sum_{i=1}^n q_i \delta(x - x_{oi}), \quad (6)$$

where  $\lambda_m$  – heat transfer coefficient of absorber sheet,  $\text{W} \cdot \text{m}^{-1} \cdot \text{K}^{-1}$ ;  
 $q_i$  – intensity of heat absorbed by circulating liquid,  $\text{W} \cdot \text{m}^{-1}$ ;  
 $n$  – number of heat absorbing tubes;  
 $x_{oi}$  – co-ordinates of tubes, m;  
 $\delta(x - x_{oi})$  – Dirake delta function for point-shape absorber,  $\text{m}^{-1}$ .

On boundary at  $y = \delta_1 + \delta_2$  heat flows are equal

$$\lambda_m \frac{\partial T_{II}}{\partial y} \Big|_{y=\delta_1+\delta_2} + \alpha_{ab} (T_{II} - T_{III}) \Big|_{y=\delta_1+\delta_2} = Q_{ab}, \quad (7)$$

where  $\alpha_{ab}$  – contact heat transfer coefficient between absorber and air,  $\text{W} \cdot \text{m}^{-2} \cdot \text{K}^{-1}$ ;

$Q_{ab}$  – specific power of absorbed solar energy,  $\text{W} \cdot \text{m}^{-2}$

and

$$\alpha_m (T_{II}|_{y=\delta_1+\delta_2} - T_{III}|_{y=\delta_1+\delta_2}) = -\lambda_a \frac{\partial T_{III}}{\partial y} \Big|_{y=\delta_1+\delta_2}. \quad (8)$$

## Results and Discussion

Broached problem of mathematical physics (1-8) can be solved by method of separating of variables at stated boundary conditions (2-8) [3,

4, 6]. For determination of temperature in separated points of each layer -  $\delta_1$ ,  $\delta_2$  and  $\delta_3$  – following expressions were achieved:

$$T_I(x, y) = T_0 + A^I + B^I y + \sum_k A_k^I (\exp(\mu_k y) + \varphi_k^I \exp(-\mu_k y)) \cos \mu_k x; \quad (9)$$

$$T_{II}(x, y) = T_0 + A^{II} + B^{II} (y - \delta_1) + \sum_k A_k^{II} (\exp(\mu_k (y - \delta_1)) + B_k^{II} \exp(-\mu_k (y - \delta_1))) \cos \mu_k x; \quad (10)$$

$$T_{III}(x, y) = T_0 + A^{III} + B^{III} (y - \delta_1 - \delta_2) + \sum_k B_k^{III} (\varphi_k^{III} \exp(\mu_k (y - \delta_1 - \delta_2)) + \exp(-\mu_k (y - \delta_1 - \delta_2))) \cos \mu_k x, \quad (11)$$

where coefficients  $A^I, A^{II}, A^{III}, B^I, B^{II}, B^{III}$  can be obtained by solving a system of 6 linear equations

$$\begin{cases} \lambda_i B^I = \alpha_r A^I \\ -\lambda_a B^{III} = \alpha_f (A^{III} + B^{III} \delta_3) \\ A^I + B^I \delta_1 = A^{II} \\ \lambda_m B^{II} - \lambda_i B^I = \frac{1}{L} \sum_{i=1}^n q_i \\ \lambda_m B^{II} + \alpha_{ab} (A^{II} + B^{II} \delta_2 - A^{III}) = Q_{ab} \\ \alpha_{ab} (A^{II} + B^{II} \delta_2 - A^{III}) = -\lambda_{ab} B^{III} \end{cases}. \quad (12)$$

Coefficient  $A_k^I$  can be defined as

$$A_k^I = \frac{e_k(a_k - b_k)}{c_k(b_k - a_k) - a_k(\exp(\mu_k \delta_1) + \varphi_k^I \exp(-\mu_k \delta_1))} \quad (13)$$

by equations:

$$\varphi_k^I = \frac{\frac{\lambda_i \mu_k}{\alpha_r - 1}}{\frac{\lambda_i \mu_k}{\alpha_r + 1}}; \quad (14)$$

$$a_k = \exp(\mu_k \delta_2) \left( \left( 1 + \frac{\lambda_m \mu_k}{\alpha_a} \right) \left( 1 - \frac{\lambda_a \mu_k}{\alpha_a} \frac{(\varphi^{III} - 1)}{(\varphi^{III} + 1)} \right) - 1 \right); \quad (15)$$

$$b_k = \exp(-\mu_k \delta_2) \left( \left( 1 - \frac{\lambda_m \mu_k}{\alpha_a} \right) \left( 1 - \frac{\lambda_a \mu_k}{\alpha_a} \frac{(\varphi^{III} - 1)}{(\varphi^{III} + 1)} \right) - 1 \right); \quad (16)$$

$$c_k = \frac{1}{2} \left( \exp(\mu_k \delta_1) \left( \frac{\lambda_i}{\lambda_m} - 1 \right) - \varphi_k^I \exp(-\mu_k \delta_1) \left( \frac{\lambda_i}{\lambda_m} + 1 \right) \right); \quad (17)$$

$$e_k = \frac{1}{\lambda_m \mu_k L} \sum_{i=1}^n q_i \cos \mu_k x_{oi}, \quad (18)$$

where  $\mu_k$  – eigenvalue, at which given task has solution:

$$\mu_k = \frac{\pi \cdot k}{L}, \quad (19)$$

where  $\pi$  – mathematical constant,  $\pi \approx 3.14159$ ;

$k$  – integer number,  $k = 1, 2, 3 \dots$ ;

$L$  – distance in direction  $x$ , m.

Coefficients  $A_k^{II}$  and  $B_k^{II}$  can be expressed from following equations:

$$-B_k^{II} - A_k^I \cdot c_k = e_k, \quad (20)$$

$$A_k^{II} = \frac{b_k}{a_k} (A_k^I \cdot c_k + e_k) \quad (21)$$

and coefficient  $B_k^{III}$  can be expressed as

$$B_k^{III} = \frac{1}{\varphi^{III} + 1} \left( A_k^{II} \left( 1 + \frac{\lambda_m \mu_k}{\alpha_a} \right) \exp(\mu_k \delta_2) + B_k^{II} \left( 1 - \frac{\lambda_m \mu_k}{\alpha_a} \right) \exp(-\mu_k \delta_2) \right) \quad (22)$$

by equation

$$\varphi_k^{III} = \frac{\frac{\lambda_a \mu_k}{\alpha_r - 1}}{\frac{\lambda_a \mu_k}{\alpha_r + 1}} \cdot \exp(-2\mu_k \delta_3). \quad (23)$$

Equations of created mathematical model (9)-(23) in MS Office Excel program were inputted. By known constructive and thermal parameters of experimental collector with area 0.2025 m<sup>2</sup> theoretical temperatures with mathematical model were calculated in points, where it was determinate experimentally. Surface of collector was irradiated with 1000 W glow-lamp. Collectors' absorber is made from sheet with thickness  $\delta_2 = 0.0008$  m and is black colored. On the rear side of absorber sheet

copper tubes are fixed with inner diameter 9 mm. As heat carrier water were used. Specific power of heater was 600 – 625 W·m<sup>-2</sup> and capacity of circulation pump of 21 l·h<sup>-1</sup> was adjusted. Temperature in 50 points on absorber sheet, heat carrier tubes and other surfaces with thermocouples were measured. Comparison of results for some performances of collector in Fig.2. and Fig.3. are shown.

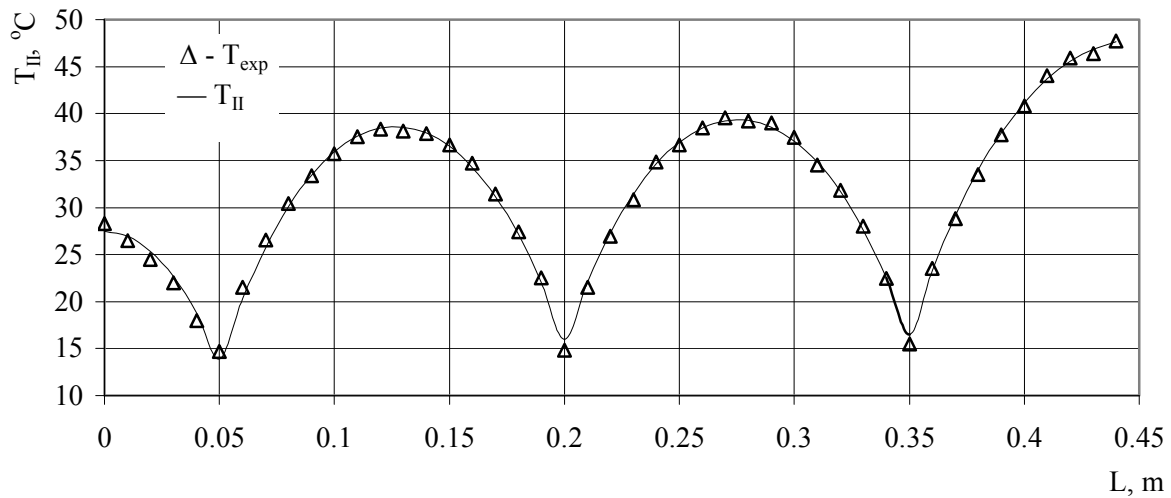


**Fig.2.** Calculated  $T_{II}$  and experimentally obtained  $T_{exp}$  temperatures on absorber surface for collector with three tubes, when  $\delta_2 = 0.0008$  m

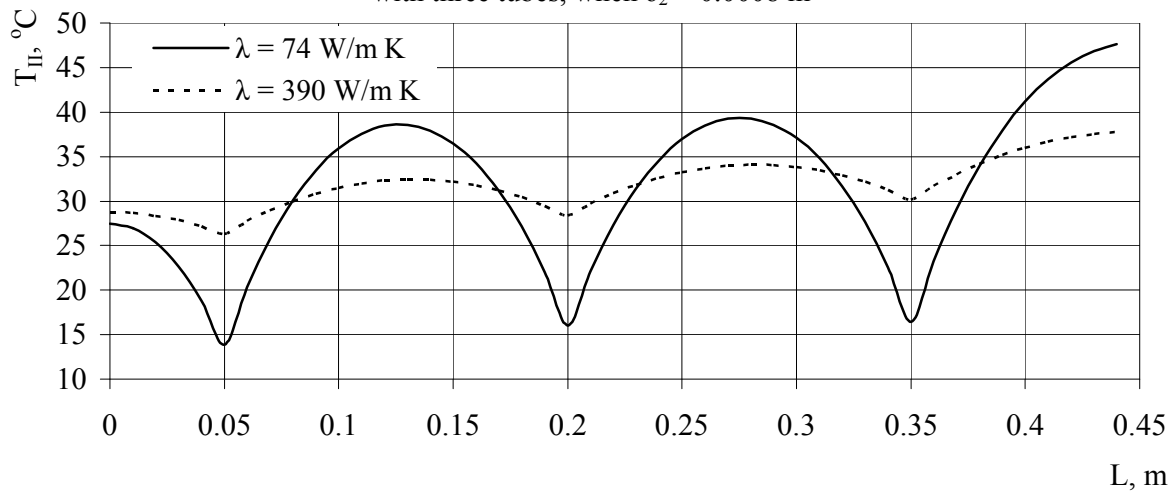


**Fig.3.** Theoretically calculated temperatures on absorber surface  $T_{II}$  with different heat transfer coefficients for collector with three tubes, when  $\delta_2 = 0.0008$  m

Analyzing theoretical and experimental data, empirical equation which describes temperature on absorber sheet surface were obtained

$$T_{II} = T_o m \cdot (1 - e^{-xm}), \quad (24)$$

where  $x$  – distance from tube, m;  
 $m$  – coefficient, can be expressed as

$$m = \frac{1}{\left(\frac{2\alpha_{ab}}{\delta_2 \lambda_m}\right)^2}. \quad (25)$$

In order to discuss about coincidence between experimental and theoretical data, it is useful to determine correlation coefficient between these data. By function CORREL in MS Office Excel program, whose mathematical expression in (26) is given [9], correlation between these two ranges is acquired as 0.99 that indicate about very high accuracy of

mathematical model. Have to remark, that MS Office Excel calculate square of correlation coefficient.

$$r^2(a, b) = \frac{\sum (a - \bar{a}) \cdot (b - \bar{b})}{\sqrt{\sum (a - \bar{a})^2 \cdot \sum (b - \bar{b})^2}}, \quad (26)$$

where  $a$  and  $b$  – theoretical and experimental values;

$\bar{a}$  and  $\bar{b}$  – average values from theoretical and experimental value ranges.

## Conclusions

By solving Laplace equation of thermal conductivity at definite boundary conditions mathematical model was created. To verify this model in practice, experimental model of flat-plate collector with area of 0.2025 m<sup>2</sup> was made. Comparing both theoretical and experimental data, correlation between them was acquired as 0.99. In order to verify model more accurately and feasible at other geometrical and thermal parameters of solar collector, it have to be more experimental study made.

## References

- [1] Buikis A. *Equations of Mathematical Physics*. Riga: University of Latvia, 2003. 57 p. (in Latvian). ISBN 9984-725-87-1.
- [2] Buikis M., Silina B. *Mathematics. Definitions, formulas, algorithms of calculations*. Riga: Zvaigzne ABC, 1997. 209 p. (in Latvian). ISBN 9984-04-398-3.
- [3] Iljins U., Ziemelis I. *The optimization of Some Parameters of a Flat Plate Solar Collector*. Proceedings of the Latvia University of Agriculture. No.12 (307), 2004. p. 64-75. ISSN 1407-4427.
- [4] Iljins U., Ziemelis I., Putans H., Skele A., Navickas J. Optimization of the Parameters of Solar Water Heating System. In: *Environment. Technology*. Resources: Proceedings of the 4<sup>th</sup> International Scientific and Practical Conference. Rezekne: Rezekne Higher Education Institution, Faculty of Engineering, 2003. p. 353-358. (in Latvian). ISBN 9984-585-68-9.
- [5] Jesko Z. Classification of Solar Collectors. In: *Engineering for Rural Development: Proceedings of 7<sup>th</sup> International Scientific Conference*. Jelgava: Latvia University of Agriculture, 2008. p. 22-27. ISSN 1691-3043.
- [6] Riekstins E. *Methods of Mathematical Physics*. Riga: Zvaigzne, 1969. 629 p. (in Latvian).
- [7] Nagla J., Saveljevs P., Cars A. *Calculations of Thermal Engineering in Examples*. Riga: Zvaigzne, 1982. 310 lpp. (in Latvian).
- [8] Nagla J., Saveljevs P., Turlajs D. *Theoretical Basics of Thermal Energetics*. Riga: Riga Technical University, Faculty of Transport and Mechanical Engineering, Institute of Mechanical Engineering Technologies, 2008. 194 lpp. (in Latvian).
- [9] Arhipova I., Balina S. *Statistics with Microsoft Excel 97 for everyone*. 2.part: teaching aid. – Riga: Datorzinibu centrs, 2000.-136 lpp. (in Latvian).





## EVALUATION OF PACKAGING BIODEGRADATION BY COMPOSTING TECHNOLOGY

ALTMANN VLASTIMIL<sup>1\*</sup>, MIMRA MIROSLAV<sup>1</sup>, SALCMAN MILOŠ<sup>2</sup>

<sup>1</sup>Czech University of Agriculture in Prague, 16521 Prague 6 – Suchbátka, Czech Republic,  
Phone: +420224383144, E-mail: altv@tf.czu.cz

<sup>2</sup>Centrum pro informace a mechanické testování obalů – CIMTO, s.p., U Michelského lesa  
366, 146 23 Praha 4, Czech Republic

### Abstract

The article deals with evaluation of disintegration of packaging materials using aerobic composting pilot test under defined conditions. Packaging materials are mixed with biological waste. Spontaneous process composting is 12 weeks. At the end of the process of the disintegration of packaging materials by sieving the compost and calculate the mass balance. Effect of sample quality compost can be monitored by chemical analysis and ecotoxicity tests. The method can also be used to assess visual and photographic documentation of the disintegration of packaging materials and also to evaluate the influence of additives on the process of composting.

### Introduction

Evaluation of disintegration of packaging materials using a pilot tests of aerobic composting under defined conditions is a process which is defined by the European Standard BS EN 140 45th. The importance of this process is given by the number of discarded packaging of any products that most people leave to be eliminated by land filling or incineration. Confirmation of the biodegradability of the packaging indicates that for this package you can search and find the process of material recovery in the form of conversion to compost instead of a simpler, but not always of value merely removing the cover.

### Materials and methods

Packaging materials are mixed with biological waste. Spontaneous process of composting takes 12 weeks. At the end of the process the disintegration of packaging materials is determined by sieving the compost and the mass balance is calculated. Sample influence on compost quality can be monitored by chemical analysis and ecotoxicity tests. The method can also be used to visual assessment and for photographic documentation of the disintegration of packaging materials and to measure the effect of additives on the process.

The essence of the test is standardized pilot composting process, which takes place at specified conditions. The test material is mixed

in exact proportion by weight of fresh biowaste and transferred to a designated composting environment where spontaneous process of composting begins. Present microbial populations initiate this process which increases the temperature. Composted material is regularly turned, mixed and aerated. Temperature, pH, moisture content and composition of gases (oxygen) are regularly recorded. These values are needed for proper microbial activity. Composting process continues till the stabilization of the compost (after 12 weeks). At the end of the process the mixture is sieved through a sieve with an aperture of 2 mm and 10 mm. After siftings the disintegration of packaging material is evaluated.

### Used test equipments:

- Composters K 330 – capacity 350 l
- Bimetallic stabbing thermometer – calibrated
- Soil pH meter – digital
- Oxymeter – digital
- Sieves with an aperture of 2mm and 10 mm
- Almemo – digital device for temperature and humidity measuring

### Preparation and composition of biological waste:

Poultry dropping (wet) – 12 kg	
Mature compost	9 kg
Vegetable waste	12 kg
Leaves	30 kg

Total 63 kg

During the test was necessary to complete the lied down mass with the fresh grass in the amount of 15 kg per 1 Composter (April 27, May 21 and June 3, 2009).

### Preparing samples 2 types:

A) paper sandwich (sulfate paper, waste office paper, sulfate paper)

B) sandwich JUTA (sulfate paper, waste office paper, jute)

### Sample adjustment:

Sample A – was crushed by garden shredder to pieces with size 5 x 5 cm

Sample B – was cut to pieces with size about 10 cm x 10 cm – because of the impossibility of crushing

### Validity of test:

- 1) Temperature is in all containers less than + 75 °C
- 2) In all containers temperature is higher above + 60 °C for 1 week
- 3) In each container temperature is higher than + 40 °C for at least consecutive weeks
- 4) pH at the end of the test is higher than 7.0, but during the process must not fall below 5.0.
- 5) The compost is mature after 12 weeks

A sample A was placed in composter 1A and 4A; sample B was placed in composter 2B and 4B, composters No.3 and No.6. were controls.

### Results and discussion

On April 14, 2009 composters were filled with prepared waste and tested sample. Everything was thoroughly mixed. Temperature measurement was carried out daily at determinate locations in composters (4 places). Results of temperature measurement are shown in Figure 1. Measurement of atmospheric oxygen was performed daily for a month, and then measured once a week. Also pH was monitored once a week. The disintegration of individual samples was visually controlled during converting.

At the beginning of the composting process temperature immediately increased over 50°C. Temperature rose slightly for about 3 weeks and then started to fall slightly. At this time the quantity of matter in composters began to diminish, so 15 kg of fresh grass to the

composter was added on April 27, 2009. The effect was already evident in the second day when the temperature raised again to a value around 60°C and started to slowly decline after one week. On 21 May 2009 15 kg of fresh grass were mixed in further for completing the composting materials.

To increase the efficiency of aeration containers were placed to an open place during work time, during the night time they were placed in a roofed-over room. The last addition of fresh grass was on June 6, 2009. It has shown only a slightly increase in temperature and affects only a part of amount of the composting mass. Since 06/22/2009 temperatures stabilized between 20 to 25 °C.

During regular controls of the sample, the gradual degradation without mould and rot was observed. Because a total collapse of the mass was not apparent yet, the mass started to be mixed more often, 2–3 times a week. The disintegration of mass was intensive, but without much effect on samples. Frequent mixing may be applied to the stage of compost maturation otherwise the temperature would be much reduced. After 12 weeks, it was stated, that the mass which showed the characteristics of compost was created, but the sample didn't yield to a sufficient decay, only a partial was observed.

On a closer examination it was apparent that the outer layers of the sample are damaged, but thanks to the glue used on the package, it still held together. In new samples no changes were detected (A sample can be bend, but cannot be torn up with hands, sample B can not be torn up and is flexible). After the experiment the samples were disturbed, they could be torn up apart and a new property of the samples was noted, they are flexible. The glue underwent chemical changes and became flexible. Although it can be separated, which can not be accomplished with the new sample, the sandwich is held together and need longer time for a total breakdown. The period of 12 weeks for these types of packaging is inadequate. Therefore it was not possible to accomplish ecotoxicity, because negligible amount of the sample completely disintegrated.

**The test was terminated on July 14, 2009 with the following result:**

**The test is valid, because it met all the points.**

### Temperature in composters

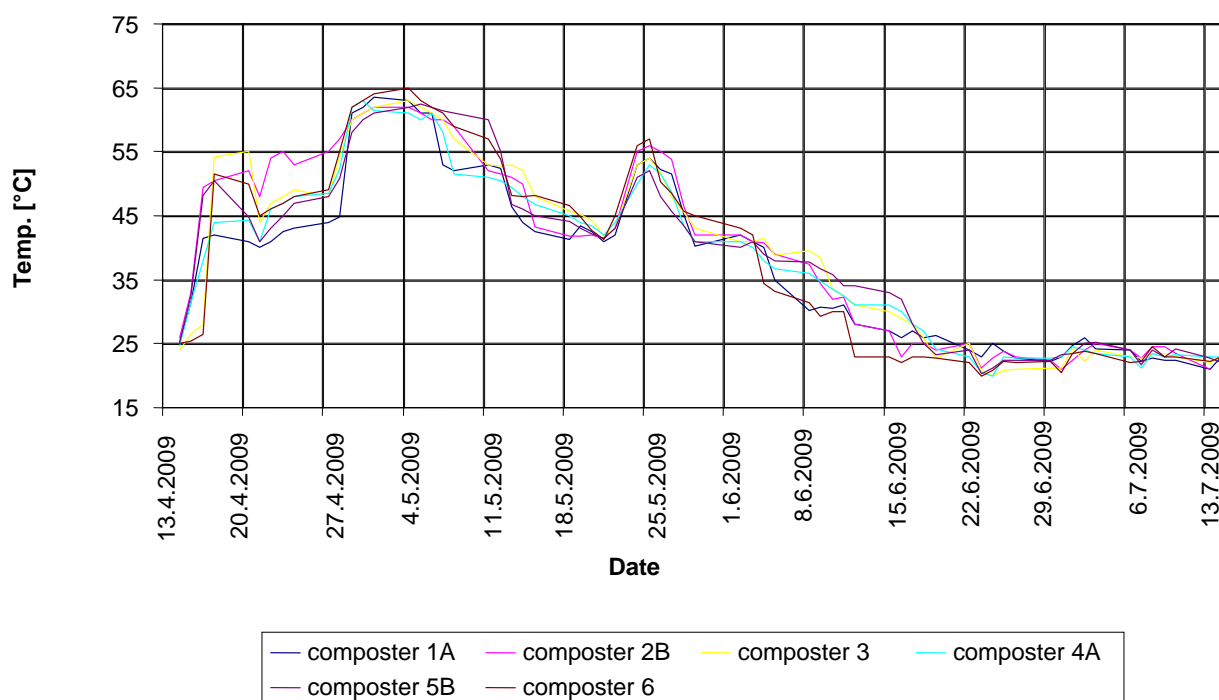


Figure.1: Record of temperatures during the test

### Conclusion

Although the samples could not be fully evaluated, this process allows evaluating the biodegradability of packages placed on the market and determining subsequent handling with them. The test results may also undermine a not always correctly set parameters for the preparation of standard samples for testing (mainly their size), because it is known that small pieces of material (waste, packaging, etc.) yield to degradation induced by composting technology much better.

The authors are trying to suggest possible modification in the objective standard for other tests that are currently being implemented.

### Acknowledgement

This paper was processed within the framework of the Research Project of MŠMT č. MŠM 6046070905 "Studium zemědělského technologického systému s ohledem na jeho racionalizaci a šetrnou interakci s ekosystémy kulturní krajiny".

## ASSESSMENT OF ECONOMIC IMPACT OF THE SIZE AREA ON PRODUCED COMPOST PRICE

ALTMANN VLASTIMIL\*, MIMRA MIROSLAV, KULHÁNKOVÁ ANNA  
Czech University of Agriculture in Prague, 16521 Prague 6 – Suchbát, Czech Republic,  
Phone: +420224383144, E-mail: altv@tf.czu.cz

### Abstract

The article describes the creation of the logistic model BW of new composting. Offers instantiation number and size of containers and calculate the amount BW suitable for processing. Important result is to answer the question of optimal radius collecting vehicles within a radius of composting sites. The solution is made for the radii of 10, 15 and 20 km from composting.

### Introduction

Handling the biodegradable waste (BW) is currently one of the most contemporary areas of waste management field. That is primarily due to the increasing volume of this component part of waste in general, also because of a pressure on the rigorous processing, but also because of continuous tightening up of legislation. On the one hand there is a significant impact on increasing the production of biodegradable waste due to the change of lifestyle, but also the influence of shifting away from the cultivation of vegetables and fruits on ones own land. That is why biodegradable waste currently makes up to 40 % of municipal waste, while the method of collecting and subsequent processing can both positively and negatively affect the various components of the environment.

### Materials and methods

The article comes with hypothetical model for collecting transport of biodegradable waste to a composting center in provincial built-up region near Prague. The object was to determine the objective amount of biodegradable waste in a monitored area, and an optimal method of collection and transport. An area with a radius of 10 km, which has been gradually increasing up to radius of 15 and 20 km, was proposed to determinate capacity of composting center. An optimal design for collecting and transport was developed for the area, including technological equipment. In the area of interest are 76 municipalities.

The analysis of the area includes:

1) An analysis of municipalities in the area within of 10 km from the composting plant,

while the radius was subsequently extended to 15 and 20 km. The analysis includes findings on:

- the number of municipalities in the locality,
- the number of inhabitants in each municipality,
- overall approach of the population to problematic of biodegradable municipal waste by using a questionnaire.

2) Determining the final amount of BW:

Determination of specific production of BW from maintenance of public green areas.

In order to evaluate the collected BW from the village of Pavlov, we used methodology based on relationship (1) where there is a total, real collected production featured in kg per capita per year [2]. The values of specific quantities calculated this way, better represent the production of biological waste in the assessed region.

$$q_{specific} = \frac{q_{total}}{1000 \cdot n} \quad [\text{kg.citizen}^{-1} \cdot \text{year}^{-1}] \quad (1)$$

Where:

$q_{specific}$  ... year specific production per capita  $[\text{kg.citizen}^{-1} \cdot \text{year}^{-1}]$

$q_{total}$  ... total year production in the area  $[\text{t} \cdot \text{year}^{-1}]$

$n$  ... number of citizens in the area [number]

Specific production of BW from public green area maintenance is expressed as the total annual mass relative to the surface using the following formula (2).



$$q_{BW\ green} = \frac{m_{BW\ green}}{S_{green}} \quad [t \cdot ha^{-1} \cdot year^{-1}] \quad (2)$$

Where:

qBWgreen ... specific year production of BW per ha of pub. green area [t.ha<sup>-1</sup>.year<sup>-1</sup>]

mBWgreen ... total year production of BW from pub. Green area [t.year<sup>-1</sup>]

Sgreen ... surface of public green area [ha]

Determine the number of collecting containers and bulk container (BC) based on production quantities.

Creating of a concept of transporting BW to the newly formed composting centers.

## Results and discussion

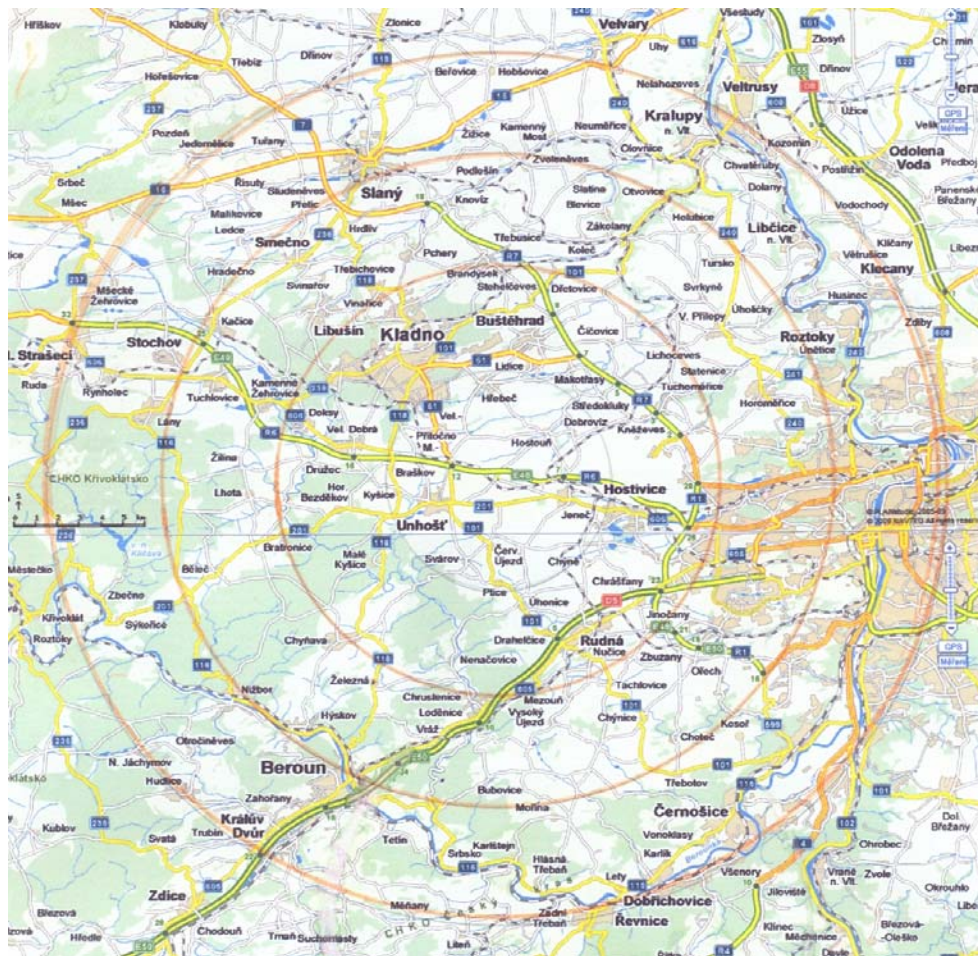
On fig. 1 there is a sample of an area map with specified radius distances that document increasing size of the catchment's area for the proposed composting center.

## Analysis of BW production

Based on the input parameters it was necessary to identify potential production biodegradable municipal waste (BMW) in a defined territory. The data for the resulting value BMW min. and BMW max in Tab. 1 were obtained accordance with projects in the CR and the values from the publications, which dealt with amount of biodegradable waste in each municipality.

Table 2 lists the amount of BW from public green areas in observed municipalities.

Concept of technological equipment for the municipalities is given in Table 3.



Pic. 1: Map of areas for collection of biodegradable waste



*Tab. 1: Amount of BMW from citizens*

Municipality	Number of citizens	gardens [ha]	Gardens product [t.year <sup>-1</sup> ]	BMW - min. [t.year <sup>-1</sup> ]	BMW - max. [t.year <sup>-1</sup> ]
Pavlov	105	8	120	10,5	21
Hostouň	959	32	480	95,9	191,8
...					
...					
...					
Malé Kyšice	349	20	300	34,9	69,8
Drahelčice	420	8	120	42	84
<b>total</b>	<b>39 228</b>	<b>756</b>	<b>11 340</b>	<b>3 922,8</b>	<b>7 845,6</b>

*Tab. 2: Total production of BW in community*

Municipality	BMW from citizens Ø value [t.year <sup>-1</sup> ]	BMW total from citizens [t.year <sup>-1</sup> ]	Fruit grove + public green + permanent grass grove [ha]	Fruit grove + public green + permanent grass grove production [t.year <sup>-1</sup> ]	BW in community total [t.year <sup>-1</sup> ]
Pavlov	15.8	135.8	1.5	22.5	158.3
Hostouň	143.9	623.9	43	645	1268.9
...					
...					
...					
Malé Kyšice	52.35	352.4	8	120	472.4
Drahelčice	63	183	17	255	438
<b>total</b>	<b>5 943.45</b>	<b>17 283.5</b>	<b>899.5</b>	<b>13 492.5</b>	<b>30 776.0</b>

*Tab. 3: Concept of technological equipment*

Municipaliti	Containers (240 l)	BC stabile	BC on call
Pavlov			YES
Hostouň	YES		
...	YES *	YES /1x14d. 6piec/*	*
...	*	*	YES *
...	YES *	*	*
Malé Kyšice			YES
Drahelčice			YES
<b>Total</b>	<b>17 municipalities</b>	<b>26 pieces</b>	<b>21 municipalities</b>

- the cells are only examples of the practical solutions without specification of community

### The proposed variants:

1) Containers (240 l) should be freely accessible, distributed according to individual municipalities demands in attendance distance about 50 m. They should be placed especially by residential buildings. They can be supplied with freely accessible BC which could provide the possibility of collecting larger bio-waste or large

amounts of biological waste (leaves, grass). BC number depends on the area of public green spaces.

2) Containers may be placed in each family house and tenement house, and its possible to supply them by BC again for defined waste. With the family house it could be considered a

container for 120 l and for tenement house 240 l in case of appropriate distribution of BC.

3) Municipalities with a low incidence of BW may be served by so-called “on call” (collecting to provided BC), which are taken away when needed.

### Conclusion

When evaluating the logistics of collection transport we calculated the total mileage and its increase depending on the increase in radius (10, 15 and 20 km). For a radius of 15 km from the composting center the increase was 248.7 km, an increase of 26 % and with 20 km radius from composting center the increase was 982.5 km, an increase of 103 %. Total mileage for the variant of 10 km radius was 951 km for 15 km it was 1 199.7 km and for 20 km radius, the number of kilometers was 1933.5. The increase in surface area is also interesting. It affects the production of BW, depending on the increase in area radius away distance from composting center. Area of gardens, orchards, public gardens, and permanent grassland was in a radius of 10 km 1 655.6 hectares, in 15 km area increased by 599 ha, an increase of 30%, and in the 20 km radius about 2087 hectares, an increase of 126%. From the above results we can evaluate the percentage increase in the mileage and hence the increase in the area with increase in radius from the composting of 5 and 10 km is similar and it can therefore be taken as a basis for general practice.

It is possible to state that there cannot be found any generally valid way to determine the

optimal distance of the collecting from composting center. Because it is clear that the increase in radius from the point of composting centers will increase the mileage, but at the same time there will be transported larger quantities of BW. Altogether the calculation with the increase in mileage it leads to results that transport costs for one ton of BW in these cases are comparable (13 to 16 CZK). Lower value is in the area of larger circle. But it needs to be stated that the production of BW highly varies in time and place and the resulting value may be reversed in some other areas.

With regard to the increased income for the transported hence charged BW, composting center's economy may be better, but it is necessary to anticipate some increased costs of processing the BW in compost production which may be covered by higher income. Final conclusion therefore is that the larger circle (the increase of intake area) will not come out as reduction or increase in transportation costs and possibly even the in the cost of processing of BW.

### Acknowledgement

This paper was processed within the framework of the Research Project of MŠMT č. MŠM 6046070905 "Studium zemědělského technologického systému s ohledem na jeho racionalizaci a šetrnou interakci s ekosystémy kulturní krajiny".

## MONITORING SYSTEM FOR PHOTOVOLTAIC POWER PLANTS

VÁCLAV BERÁNEK<sup>1,2</sup>, MARTIN LIBRA<sup>2</sup>

<sup>1</sup> Solar Systems, Ltd.

<sup>2</sup> Czech University of Life Sciences Prague, 16521 Prague 6 – Suchbátka, Czech Republic, Phone: +420 224383284, Fax: +420 234381850, E-mail: libra@tf.czu.cz

### Introduction

In recent years, in the Czech Republic were installed a series of photovoltaic (PV) power plants. At the beginning of 2009 there has been installed in total approximately 60 MWp of photovoltaic power plants and systems, but a year later in early 2010 it was up to 460 MWp. Thanks to the subsidies for energy from photovoltaic power plants in our country the building is supported since the 2006, but because of the decrease of prices of PV panels during the years 2007 and 2008, the overall price of the power plant decreased and the return on investment accelerated. The boom came in years of 2008 and 2009 and it is still continuing. Operators of the power plants obviously need to have a good monitoring of given parameters. This article is about the unique monitoring system developed specifically for this purpose.

### Description of monitoring system SOLARMON

SOLARMON unique monitoring system is aimed at gathering, diagnosis and treatment of data. It communicates with the converters, electrometers, weather stations and external elements of the photovoltaic plant. The whole system is based on proprietary technology for data collection. At the power plant is installed BBbox. Similar items are used by manufacturers of inverters SMA, Fronius and Schueco (webbox, sunyanalyzer, datalogger, etc). Solar power plants and photovoltaic parks are usually situated on a large area, therefore it is necessary to use communication technology capable of communicating over a long distance. Communication is designed for RS485. RS485 is the most ideal and cheapest solution for data collection. BBbox is able to communicate with many devices in solar power (see diagram in Fig. 1) with a speed of 1 ÷ 3 with up to a maximum distance of 1200 m. It is connected to the meter on the LV and HV converters of any kind, another part of the security station is intrusion detection, fire and motion sensors, weather stations, including thermometers, thermocouples, sensors measuring wind speed and the meter counting incident energy per square meter. It is also possible to connect the main switchboard transformer including protection NPR

/ NPU, and thus we are able to operate the plant as a whole. Output frequency, voltage and current supplies.

Data downloaded from the BBbox converters, transformers or other equipment are generally processed, stored and labeled. Subsequently, they are send over SSL encrypted channel to a database SOLARMON. Program evaluation, data and formulas are located on a central server in Prague. The database is able to receive and process data from other types of buses (see Fig. 1). BBbox can communicate with another BBboxem. This feature is mainly used in power plants with nominal power above 5MWp and a large area. Communication is mostly done trough an optical fiber.

SOLARMON adopts the basic flow of data from converters and transformer station according to their importance and it puts them into the assigned smaller databases. Individual triggers respectively sophisticated patterns put the data for individual diagnostic tests. The system uses the tests to calculate the errors, to compare the converters, to control the voltage in individual branches, to calculate the effect on detection of loss of individual facilities and forecasts, performance, etc. The processed output data is displayed in two interfaces - Service / Users.

Detailed service interface is designed for service technicians, who require more supervision

over the plant. Service section identifies and defines the causes of defects. It also allows a description of each error, and the events occurring in the meanwhile. Service interface allows to specify parameters of the power plant, which are an essential part of the formula (see Fig. 2)

It defines the responsibility for maintenance service of the plant, specifies e-mails and phone numbers for sending error reports and downtimes. It defines here a technical description of the plant, the type of panels, inverters and transformer stations. It can define the limits, temperature coefficients and input data for the prediction of performance (see Fig. 3). Based on these values, the performance of PV panels is predicted (see Fig. 4). Graph of the predicted performance is derived from the actual values sensed from the weather station (temperature + sensor illumination on the panel), user-defined values of the active panel area (area of silicon wafers), the performance of the panel, the tolerance of the panel, the performance characteristics of given type of panel, the temperature coefficient, the number of panels on the string, the number of strings on inverter and the number of inverters.

**USER INTERFACE.** Was developed specifically for investors, bankers, insurance companies and manufacturers of panels. The detailed performance is shown for the owners of the power plant in here, especially the current performance of converters. It also shows the daily supply and energy consumption, which is an important base for billing; there is also a monthly invoice template, reports of individual converters, the calculation of earnings and emission allowances. There is a tab called failure that indicates and sends reports of serious errors in the power plant. Table of values from weather stations is shown in Fig. 5.

Database system SOLARMON enables to track the current status of the individual inverters, including the possibility of a description of the error related to project number. Weather station monitoring provides information on wind and temperature, which is an essential base for insurance companies (for example if the value exceeds the hurricane it means lose of the

guarantee on the type of construction for investors). Most of the constructions are designed to withstand hurricane. The same is related to temperature - for example, panels CEEG have operating temperatures from -40 to +90 ° C. Whenever these values are exceeded it may cause that permanent damage occurs, thereby automatically voiding the warranty. Each part has its limits of power, including inverters. See Fig. 7

SOLARMON has the functions to control bad converters. This is a comparison of average values to actual performance. See Fig. 8. Furthermore, it monitors current string voltage and compares it with the limit values. The resulting values are reported and also re-trackable. Reports of serious failures are recorded and sent via SMS and e-mail to the responsible person or investor.

### Description and definitions of power loss

Loss of power can be defined in several respects. The most important and most complicated is the definition of losses on the DC side of inverter, see Fig. 9. This is a complicated formula that defines the current performance of the panels. Input parameters are derived from the temperature of a thermocouple placed on the panels, and the current value of the weather station, which is set at the same angle with the construction. To improve the accuracy of important information it is important to know about the type of module. Power temperature coefficient predicts the panel behavior under certain temperature conditions. This value is based on the detection conditions of the manufacturer (most often indicating 25 ° C exposure 1000W/m<sup>2</sup>  $t = 1s$ . But it's not the rule, often with the temperature set at 300K which is 27 ° C). Another base is the definition of active area of the panel. This is the number of articles on the panel (36/72). The number of parallel branches (3x12, 3x24), the size of the article (rounded corners) and communications outlets. Finally, it is important to minimize performance variations panels (manufacturer declares performance of the panel at a range of mostly + -3%). Deviation can be eliminated by grading panels into groups according to the Imp(aiming to achieve maximum power in

serial parallel involvement). Modules are classified into 4 groups AD (A = highest Imp). Sorting panels are linked to the implementation project and then set the Solarmon individual drives in commissioning the plant. So there is a map of each group of panels connected with the project. The most complicated part is the defining point of MPP panels in strings. Volt-Ampere characteristic of each panel is different and therefore can not be precisely defined. This is the place for further refinement and subsequent calculation of prediction performance (depending on the temperature and incident energy) of one particular type of panel. To determine the loss on DC cables involving drive should be calculated based on a project - A section of Fig. 5. That means the number of panels on the string and the number of strings on the panel. (Eg, SMC 7000TL has 3 strings with 13 modules CEEG 185). Point B is the input power measured on the drive. By comparing the actual performance of concrete power A and concrete drives B ( $B / A$ ) is counted lost on the DC line. Point C is given by the Pac (W) from the converter. It is therefore a current output. When comparing the actual inverter output power unto the input we get the efficiency drive. From the data we can declare that, at 90% load of the converter efficiency correspond to an accuracy of  $+ -1\%$ . There is a rule saying that the reduction of load converters increases the inaccuracy of measurement. Measurement of input in the transformer with the stamped meter point is given by D. By comparing point D and C Sumy gets lost in the AC side. The last part of the meter measuring output via an opto-element (E)

comparing the values of  $E / D$  we get the efficiency of the transformer. Electricity connection is important also in terms of billing. Finally, the overall efficiency of power plant can be determined by comparing the sum of  $E / A$ . The overall efficiency of the power plant is the most important base for the banks as lenders.

### Data Archive

An integral part of the system is back up and reviewing of the data. SOLARMON is able to maintain the database and create a preview of these files. It is a statement of values under the specified time. Data archive has four subfolders Converters / Weather station / Transformer / EZS. Viewing of the data is divided into daily / Monthly / Yearly. It is possible to extract data on specific drivers and summarized overall data. Data from individual drives are very much needed to allocate the occurring fault. All categories of time (daily / monthly / annual) are further divided into seconds, hours, and summarized. Files are saved in xls file therefore is also possible to download it. See Fig. 6 and 10.

### Conclusion

SOLARMON monitoring system was successfully tested on 5 of photovoltaic power plants with a total capacity 4.7 MWp. Successful testing has helped identify and eliminate installation errors and contributed to the smooth operation of PV power. It also provided an impetus for future development, which will appear in the next version SOLARMON.

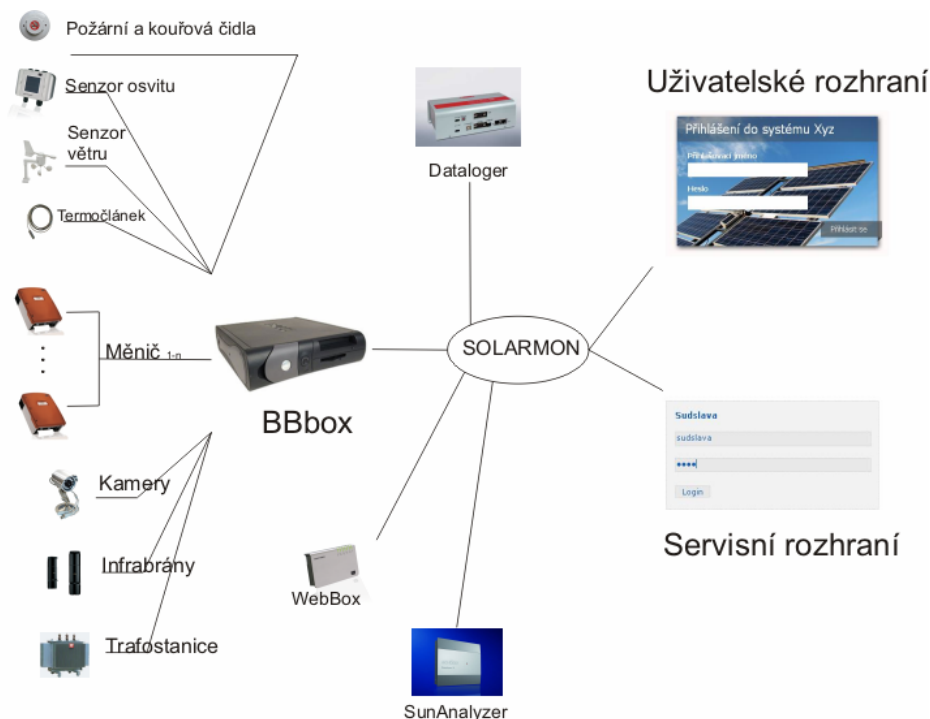


Fig. 1 Description of communication SOLARMON

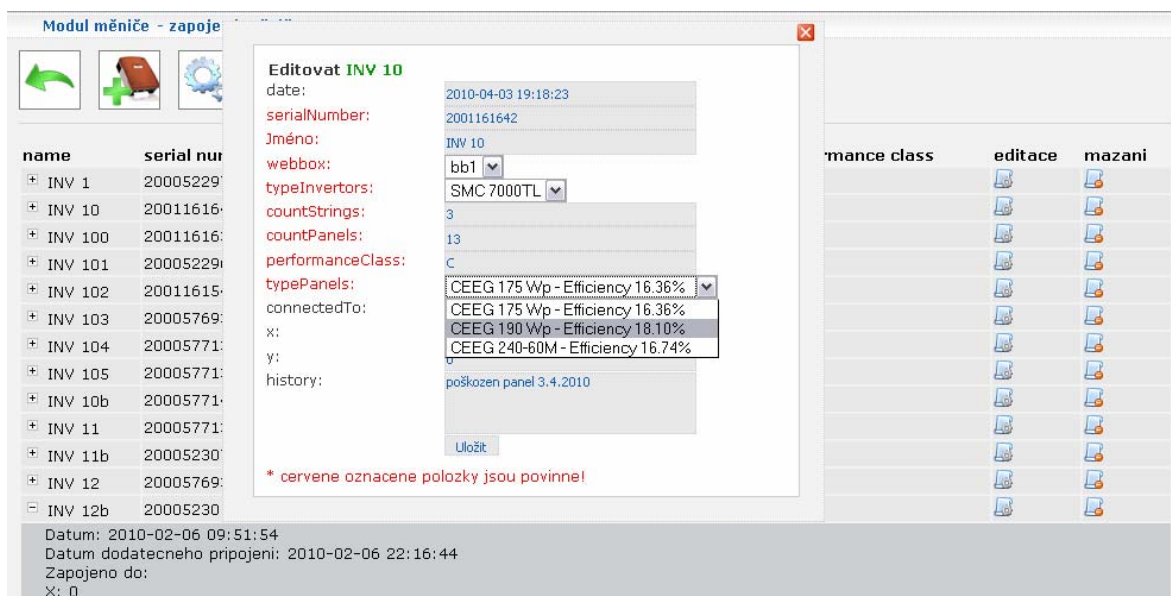


Fig. 2 Service interface – list of editation invertas



**Monitoring - Nastavení**

**Základní nastavení Rozšířené nastavení**

**Rozšířené nastavení**

Název elektrárny:

Instalovaný výkon:  kWp

Výkon panelu:  Wp

Účinnost panelu:  %

Teplotní výkonový koeficient:  %/K

Rozsah mezních teplot:   °C

Garance výkonu: +- %

Panel testován při:

Množství dopadajícího energie:  1000 W

Testovací teplota:  25 °C

Počet křemíkových destiček:  ks

Velikost křemíkových destiček:  mm

Počet druhů měničů:  ks

Počet stringů v jednotlivých měničích:  string

Počet panelů ve stringu:  ks

Fig. 3 Service interface – security setting

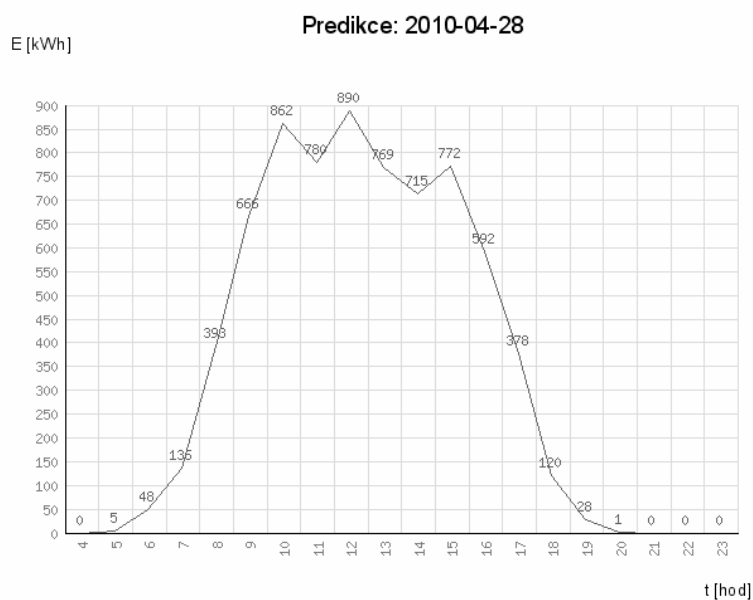


Fig. 4 Power prediction, 2010.04.28

Vypis dat z meteostanice




od   do  

Datum	Seriowe cislo	Dopadajici energie	Teplota okoli	Teplota panelu	Vitr
2010-04-29 10:44:33	6937	709	21.13 °C	34.73 °C	1.5 m/s
2010-04-29 10:44:35	6937	709	21.13 °C	34.73 °C	0.9 m/s
2010-04-29 10:44:38	6937	710	21.03 °C	34.73 °C	0.6 m/s
2010-04-29 10:44:41	6937	711	21.03 °C	34.73 °C	0 m/s
2010-04-29 10:44:43	6937	711	21.03 °C	34.73 °C	0.7 m/s
2010-04-29 10:44:46	6937	712	21.03 °C	34.73 °C	1.5 m/s
2010-04-29 10:44:49	6937	712	21.03 °C	34.73 °C	1.8 m/s
2010-04-29 10:44:52	6937	713	20.93 °C	34.83 °C	1.2 m/s
2010-04-29 10:44:54	6937	714	20.83 °C	34.83 °C	2.5 m/s
2010-04-29 10:44:57	6937	716	20.83 °C	34.83 °C	2 m/s
2010-04-29 10:45:00	6937	721	20.83 °C	34.83 °C	1.6 m/s
2010-04-29 10:45:02	6937	723	20.83 °C	34.83 °C	3.5 m/s
2010-04-29 10:45:05	6937	728	20.73 °C	34.83 °C	3 m/s
2010-04-29 10:45:08	6937	732	20.73 °C	34.83 °C	5.6 m/s
2010-04-29 10:45:11	6937	736	20.73 °C	34.83 °C	2 m/s
2010-04-29 10:45:13	6937	739	20.73 °C	34.83 °C	1.3 m/s
2010-04-29 10:45:16	6937	739	20.63 °C	34.83 °C	1.4 m/s
2010-04-29 10:45:19	6937	741	20.63 °C	34.83 °C	3.3 m/s

Fig. 5 Form of data select by meteostation

## Poruchy

Nastaveni vypisu poruch

Zkontrolovano 113 menicu z celkového počtu 114

Name	E total	Vykon menice	str. h.	Stav
INV 21	1326.55200	41.17798	0.974431391891	ok
INV 14	1338.65503	41.021	0.970716633666	ok
INV 100	1367.18506	42.12805	0.996913748542	ok
INV 43	756.24603	42.99603	1.01745353606	ok
INV 35	1450.66101	45.52893	1.07739181551	ok
INV 10	1360.06104	41.99598	0.993788457939	ok
INV 45	750.81006	42.68201	1.01002259977	ok
INV 70	741.60907	42.29901	1.00095932802	ok
INV 20	1345.19202	41.76697	0.988369189363	ok
INV 36	1397.91809	43.30603	1.02478934348	ok

Fig. 6 Test of error

Monitoring - Ztráty

**Ztráty**

Ztráty P na FV panelech vlivem teploty:	(+37,88% až -36,81%)
Ztráty netříděním FV panelů:	3%
Ztráty na kabelech DC:	0,55%
Ztráty na MX skříních:	0,5%
Ztráty na měniči:	2,7%
Ztráty na NN kabelech:	0,5%
Ztráty na RM rozvaděčích:	0,3%
Ztráty na traťu:	2,5%
<b>Celkový součet ztrát:</b>	<b>7,05%</b>

Fig. 7 Powerplant losses

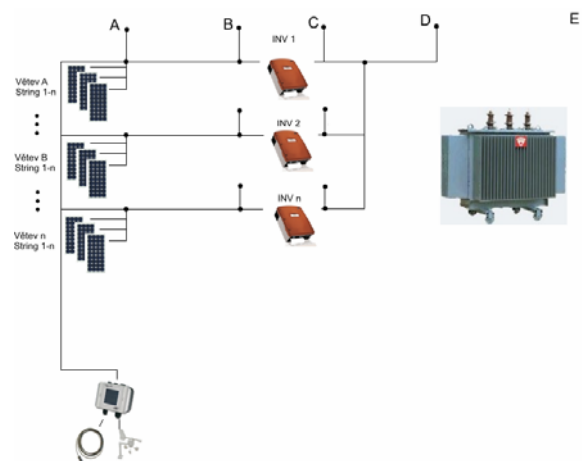


Fig. 8 Solar power plant diagram

**Ztráty**

Menic	Cidlo osvitu [W/m <sup>2</sup> ]	Ea	Ztráty na DC vedení [%]	Eb	Ztráty na menici [%]	Ec
138 - INV 1	761.16129032258	4165.78835783	4.60595187169	3973.91415099	2.53839634673	3872.63768116
137 - INV 2	761.16129032258	4165.78835783	7.13241146228	3868.6671915	1.29325101446	3818.31386861
137 - INV 3	761.16129032258	4165.78835783	5.38864620099	3941.30876174	2.00324115129	3862.10218978
114 - INV 10	761.16129032258	7220.69982024	1.59705974884	7105.38092982	2.68098457994	6914.35964912
115 - INV 11	761.16129032258	7220.69982024	1.89156919249	7084.11528696	2.71771368914	6891.07826087
115 - INV 12	761.16129032258	9025.8747753	2.35891066987	8812.96245217	3.03471491581	8544.99130435
121 - INV 4	761.16129032258	9025.8747753	1.82169195668	8861.4511405	3.03693439638	8591.89256198
119 - INV 5	761.16129032258	9025.8747753	0.8412440271	8949.94514286	3.06507393271	8675.1092437
121 - INV 6	761.16129032258	9025.8747753	2.62108627995	8789.29880992	3.01589696073	8523.73553719
119 - INV 7	761.16129032258	9025.8747753	0.496566804911	8981.05527731	3.06124583853	8705.62184874
121 - INV 8	761.16129032258	9025.8747753	2.80635107711	8772.57704132	3.02416773292	8506.79338843
118 - INV 9	761.16129032258	9025.8747753	1.22227445522	8915.55381356	3.03848459927	8644.07627119

Fig. 9 Losses

Základní přehled

Diagnóza

Archiv Dat

Měníče

Meteorostanice

Trafostanice

EZS

Měníče

Meteorostanice

Trafostanice

EZS

### Archiv dat z měničů

Archiv dat z měnicu  
 - denní data - INV 1 04 2010 zobrazit

Datum	Denní dodávka energie	Všechna data	Hodinová data	Sumarizovaná data
2010-04-01	10.56298 kWh			
2010-04-02	28.68991 kWh			
2010-04-03	17.28795 kWh			
2010-04-04	15.52508 kWh			
2010-04-05	9.59814 kWh			
2010-04-06	29.19394 kWh			
2010-04-07	35.10501 kWh			
2010-04-08	33.58893 kWh			
2010-04-09	28.01378 kWh			
2010-04-10	6.70010 kWh			
2010-04-11	4.24902 kWh			
2010-04-12	8.99700 kWh			

**Otevírání 2010-04-07\_00\_00-2010-04-07\_23\_59\_5...**

Zvolili jste otevřít:

**2010-04-07\_00\_00-2010-04-07\_23\_59\_59.xls**  
 což je: List aplikace Microsoft Office Excel 97-2003  
 z: http://louny.solarmon.eu

Co má aplikace Firefox udělat s tímto souborem?

☒ Otevřít pomocí Microsoft Office Excel (výchozí)  
☐ Uložit soubor  
☐ Provádět od teď automaticky s podobnými soubory.

OK Zrušit

Fig. 10 Data archive

## MEASUREMENT OF AGRICULTURAL ENERGY DEVICE POWER PARAMETERS USING GPS

MARTIN CINDR<sup>1\*</sup>, MARTIN PEXA<sup>1</sup>, KAREL KUBÍN<sup>1</sup>

<sup>1</sup>Czech University of Agriculture in Prague, 16521 Prague 6 – Suchbát, Czech Republic, E-mail: cindrm@tf.czu.cz

### Abstract

An understanding of the power parameters of an agricultural energy device (tractor) is very important in relation to the final outcome. It is necessary to achieve high performance with optimum fuel consumption (economic and ecological point of view). Monitoring the progress of power parameters (torque and engine power) is possible by several methods. The authors of this paper describe the possibility of using GPS to determine the torque and from that derive the backup torque. Improvement of this method is practically demonstrated on Case tractor. Possibility of application on passenger vehicle is mentioned too, and are assessed conveniences and limitations related with the construction of modern vehicles. The data thus collected will contribute to the timely detection of defects, and thus prevent the emergence of economic and ecological consequences that are related to the engine.

### Introduction

The power of the combustion engine is an important diagnostic sign, especially useful in detecting the conditions of the piston group, engine timing mechanism, fuel system and for petrol engine's spark-ignition system, as well. But, power alone is not sufficient to establish the condition. In a measurement of power output it is necessary to determine the efficiency and secondary effects which have been used to achieve this power. For example, if the power of a diesel engine is within the tolerance of the nominal value, but smoke emissions are above normal, this may be an indication of the engine's poor technical condition.

Unlike the measurement of power parameters, in terms of engine production or extensive engine repair, significantly simpler diagnostic methods are ordinarily used. It is possible to use accurate dynamometric stands for the measurement of the dismantled engines, or tractors, measuring power parameters directly to power take off, but it is not economically feasible for ordinary service. The same applies to the rolling test room for measuring power parameters, but it is not as accurate a measurement of dismantled engines. While it also offers the use of modern acceleration methods, which are sufficiently accurate and low-cost, the measurement still has some complications particularly for engines equipped with turbochargers and other special electronical controls.

The authors of this paper have focused on the acceleration method of measuring the power parameters of road vehicle and applied to the measurement of the tractor while driving on a road.

The power parameters were measured by GPS devices with frequencies of 20 Hz. Experiences with other devices with different frequencies are described in this paper too.

### Methodology and assumptions of measurement

The methodology consists of measuring the acceleration of a vehicle, usually at the higher gear on solid pavement from idle speed to normal running speed. During this time, the vehicle's position is tracked by the GPS sensor. The Škoda Octavia as a passenger car and tractor Fendt Farmer 412 Vario were selected for the tests.

In terms of evaluation, results should be expressed in terms of certain assumptions important for their treatment. Since the acceleration proceeded on the pavement, the following resistances are overcome the combination during the drive:

- *Air resistance* - Air resistance depends on the square of the speed and given the maximum speed of the tractor (40 km/h) is calculated only by tens of Newtons and therefore can be neglected. Speed of passenger vehicle is much higher and air resistance must be included. When measuring, it is necessary to select, if possible, windless conditions. If the headwind was blowing the same speed as the vehicle speed, magnitude of air resistance increases 4 times.

- *Rolling resistance* - the rolling resistance, as with air resistance, depends on the speed of the vehicle (besides the state of the tire and road), but as this dependence is very mild, so in practice, as in this paper are viewed as constant.

- *Gradient resistance* - was an attempt to select a communication, where the slope approaches zero. The altitude of the selected communication was measured with a GPS receiver equipped with a barometric altimeter. The force resulting from the gradient resistance, in addition to rising slope (change of altitude) also depends on the weight of the vehicle. The rising resistance can be neglected in calculation, because it was measured on a slope below 2% (size of force are hundreds of Newtons). While the communication is more inclined, but the slope is constant, then the gradient resistance is also constant and does not affect the final course of acceleration.

- *Mechanical resistance* - mechanical resistance is dependent on the loss of power between the engine and the driving wheels. The value of these losses depends primarily on the number and type of gear sets. Analysis shows that these losses depend on the speed (engine speed), but this dependence can be ignored (low dependence).

- *Resistance of inertia* - During acceleration it is necessary to overcome the inertia mass of all moving parts of the engine, gears, shafts and the wheels themselves. This can be expressed as the single number reduced to a wheel circumference. Value of the resistance, in addition to inertia moment, depends on the angular acceleration (in the case of reduction to the wheel circumference is it the angular acceleration of the wheel) and the radius of the wheel.

- *Acceleration resistance* - acceleration resistance depends on the weight of the vehicle and the longitudinal acceleration of the vehicle. The course of longitudinal acceleration is fully in line with the course of engine torque, which is the main prerequisite for the authors.

The conclusion of all assumptions is that either the individual resistors can be eliminated (the

resistance gradient), ignored with regard to speed (for tractor air resistance) or can be rated as constant (mechanical resistance, rolling resistance). Only the acceleration resistance and resistance of inertia, which expresses the course of the power parameters by the course of acceleration, remain.

From above mentioned ensue the resultant resistance force for tractor (or other low speed vehicle):

$$F_{rz} = F_a + F_I \quad (1)$$

$F_r$  (N) Resultant resistance force.

$F_a$  (N) Acceleration resistance.

$F_I$  (N) Resistance of inertia.

$$F_a = m \cdot a \quad (2)$$

$m$  (kg) Weight of the vehicle.

$a$  (m.s<sup>-2</sup>) Acceleration of the vehicle.

$$F_I = I_k \cdot \frac{\varepsilon}{r} \quad (3)$$

$I_k$  (kg.m<sup>2</sup>) Moment of inertia of the moving mass of the vehicle reduced on the wheel circuit.

$\varepsilon$  (rad.s<sup>-2</sup>) Angular acceleration of the vehicle.

$r$  (m) Vehicle wheel radius.

If we want to measure a passenger vehicle, is necessary to include air resistance do to higher speed. It means, that resultant resistance force is:

$$F_{rz} = F_a + F_I + F_v \quad (4)$$

$F_v$  (N) Air resistance

$$F_v = c_x \cdot S \cdot \rho \cdot \frac{v^2}{2} \quad (5)$$

$c_x$  (-) coefficient of air resistance

$S$  (m<sup>2</sup>) frontal area of the vehicle

$\rho$  (kg.m<sup>-3</sup>) density of air

$v$  (ms<sup>-1</sup>) vehicle speed

Basic parameters of the used GPS device (Fig. 1) are:

**Producer:** Dewetron  
**Model:** VGPS - 200C  
**Scanning frequency:** 20 Hz  
**Accuracy - Speed:** 0,028 m/s  
**Accuracy - Position:** < 0,4 m



Fig. 1 GPS device Dewetron VGPS 200C source: [www.dewetron.com](http://www.dewetron.com)



## Results

By GPS device Dewetron was logged actual speed of vehicle during acceleration with frequency 20 Hz. For example we used measured data of

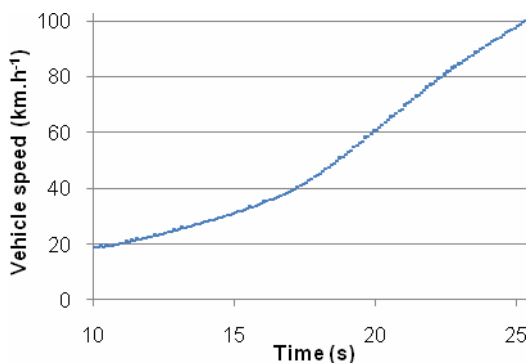


Fig. 2 Course of vehicle speed during acceleration.

vehicle Škoda Octavia. Figure 2 and Figure 3 shows measured data, Figure 4 shows the progress of power parameters (torque and engine power) measured by producer of this vehicle.

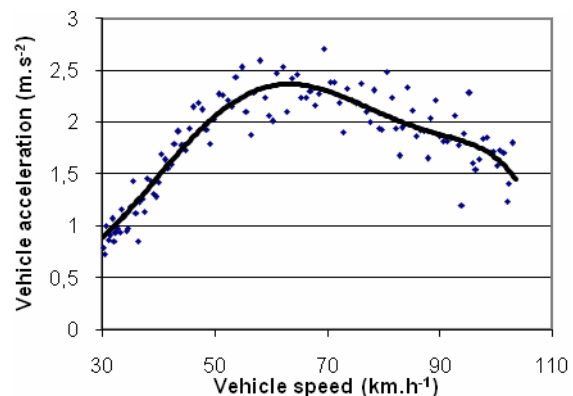


Fig. 3 Course of acceleration in dependence on vehicle speed.

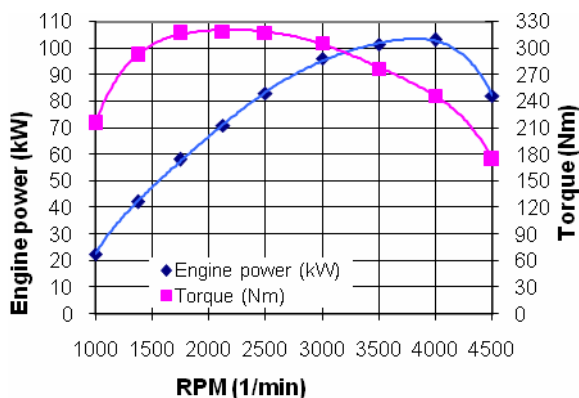


Fig. 4 Parameters of engine indicated by vehicle producer

From figure 3 and figure 4 is evidently similarity of course of torque and curves of acceleration in dependence on vehicle speed. This means, that measured data from GPS device can be converted to course of engine's torque. Divergence in higher speed is caused by increasing of air resistance and more energy is consumption for overcoming this resistance and acceleration is slowly. On the contrary in low RPM is course delayed because of reaction time of turbocharger.

The problem in assessing the log from the GPS device is displacement, which is dependent on the quality of this device, and which may complicate the correct deduction of the backup torque. The authors therefore recommend measuring the vehicle with a set GPS sensor on a particular track and

under specific conditions, which can be easily repeated and set as standard. Standards can be easily converted directly to the torque by using tabulated values and the observed rate. Courses can be compared for any other measurements in similar conditions. Any changes to the value of torque (acceleration) from the standard and the extrapolated changes to the backup torque, which mainly results from changes the technical conditions of the engine, can also be compared.

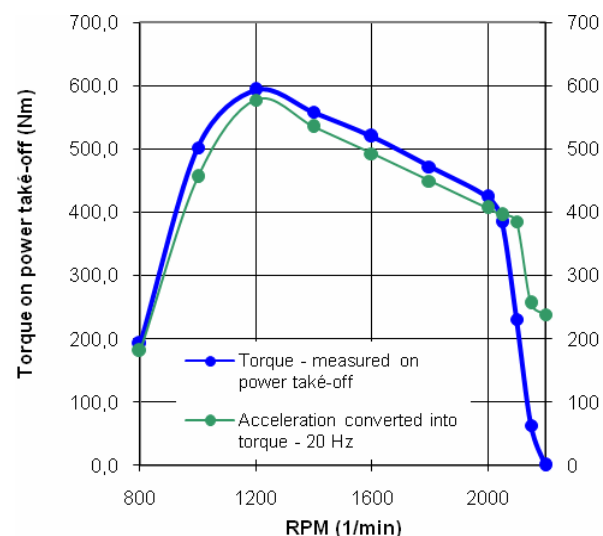


Fig. 5 Torque of tractor Fendt measured on PTO and converted from acceleration.

The backup torque for the Fendt tractor was found by measuring the power take-off with a dynamometer: **54,4 %**. Observed results for backup torque from 20 Hz GPS sensors is **49,9 %**. The results are consequently comparable. Course torque is shown on Fig. 5.

#### 4. Discussion and conclusion

Power parameters are a good diagnostic sign for assessing the technical condition of the combustion engine, but in practice they are difficult to detect. As a rule, the dynamometer is not available for detecting them directly. From the mathematical point of view, the torque and engine power are directly proportional to acceleration. It is possible to measure acceleration, and in turn, to derive course of the power parameters and the backup torque.

In the paper the acceleration is measured by the use of GPS devices with scanning frequencies 20 Hz. The authors tested GPS devices with different frequencies. 1 Hz GPS is for this measurements inconveniently. By contrast, 5 and 20 Hz GPS sensors showed accurate outcomes.

Fendt tractor was measured by the dynamometer torque backup 54,43 %, using GPS at 5 Hz 54,34%, and 20 Hz 49,94%. The problem may be that it is necessary for each individual GPS search points for calculate the backup torque and the measured points fit right continuous functions.

We tried to measur the two different vehicle – tractor and passanger vehicle. This method is optimal to use for tractor, do to speed of vehicle and course of acceleration. If the higher gear is choose for measurement, is possible to logged course of acceleration by GPS with frequency from under 5 Hz. For measurement of passenger car is necessary to include course of air resistance force which is indispensable from speed higher than about 50 km.h<sup>-1</sup>.

The authors of this paper believe that if the acceleration is measured by any GPS sensor when the tractor is new, you can create a standard that can be quite accurate by a coefficient to the measured value of torque. Assuming the same rate, the same track and similar climatic and technical (tire pressure, etc.) conditions, data from a GPS device may be directly converted to torque and the backup torque infered from the torque data. It can thus contribute to increasing economic and ecological running of tractor.

## MONITORING PAPAYA (*CARICA PAPAYA*) RIPENING THROUGH BIOSPECKLE TECHNIQUES

JULIANA APARECIDA FRACAROLLI<sup>1</sup>, ADILSON MACHADO ENES<sup>2</sup>, INACIO MARIA DAL FABBRO<sup>3</sup>, SILVESTRE RODRIGUES<sup>4</sup>

<sup>1</sup> MS candidate, Faculty of Agricultural Engineering, State University of Campinas, Campinas, SP, Brazil. E-mail: Juliana.fracarolli@gmail.com

<sup>2</sup> PhD candidate, Faculty of Agricultural Engineering, State University of Campinas, Campinas, SP, Brazil.

<sup>3</sup> Professor, Faculty of Agricultural Engineering, State University of Campinas, Campinas, SP, Brazil.

<sup>4</sup> Professor, Faculty of Agricultural Engineering, Federal University of Sergipe, Sergipe, SE, Brazil

### Abstract

Papaya is recognized as a fruit of outstanding nutritional qualities, exhibiting high vitamin A content, calcium and carbohydrates. A maturation phenomenon is close associated to biochemical activities and metabolic reorganizations, following an irreversible process. Climacteric characteristics of the papaya fruit include maturation and metabolic acceleration after harvesting. The optimum ripening level for harvesting is very important because a premature fruit collection would interfere on the maturation process and, by other side an over ripe fruit would exhibit a short shelf life which will generate substantial losses. Quality evaluation is normally carried by means of conventional methods as skin color, total soluble solids, mechanical firmness and pH determinations. Low fruit firmness value will not support transport, handling and storage. Elastic constants determinations are generally carried by means of destructive tests, turning the fruit impossible for further consumption. Based on these considerations, this research work proposed the determination of papaya maturation level by means of biospeckle laser technique associated to total soluble solids content. Biospeckle or dynamic speckle methods are based on optical interference which has shown outstanding results on several agricultural research areas as seed viability analysis, tissue biological activity, etc. The quantification of the biospeckle phenomenon is supported by the definition of the Moment of Inertia (MI) due to similarity with its mechanical counterpart. A number of ten samples of papaya tissue at two different maturation levels were submitted to total soluble solids determination and biospeckle determinations. It was concluded that the optical setup did not provide data to distinguish ripe from unripe papaya.

**Keywords:** papaya fruit, biospeckle, fruit maturation.

### Introduction

Papaya tree (*Carica papaya L.*) is one of the most fruit crop cultivated in tropical climate regions, to which Brazil contributes with 1.9 millions of tons a year, occupying 36,750 hectares, representing 20.8% of the world production (FAO, 2008). Based on data of world production reported by the FAO from 1990 to 1999, Manica & Oliveira Júnior (2000) concluded that papaya production had an expansion in that decade, indicating also an increase of 133,19%, from 55,883 to 127.866 tons in 1998, generating US\$ 105,280.

In despite crop production expansion and

demand for technology, papaya commercialization, transportation and handling are still associated to fruit quality losses. Automatic fruit quality inspection would greatly contribute to the production and handling efficiency.

The maintenance of papaya fruit overall qualities, strongly depends on an optimum maturation point to set the harvesting period. Post harvesting fruit quality and shelf life also depend on the adequate ripening point observation. Complete ripe harvesting will drastically reduce shelf life, complicating handling due to low fruit physical resistance

which accelerates loss process (Chitarra & Chitarra, 1990).

Papaya classification by maturity level is associated to skin color, total soluble solids, mechanical firmness and pH determinations. Skin color is a very diffused method in despite its subjectiveness. Though classification based on total soluble solids, pH and firmness are based on destructive tests, impeding further fruit sample uses. The considerations presented above gives strong support to the development of non destructive tests for fruit quality as well as to the selection and sorting process automation.

Rabelo (2000) reported correlations between post harvest period and biospeckle test results. As reported by Enes (2006) the biospeckle laser method is based on the investigations of physical- chemical parameters associated to tissue biological activities which generates changes in the interference patterns observed during laser incidence. The pertinent literature reports different methods of biospeckle quantification based on the first and second statistical order, including the Time History of Speckle Pattern (THSP). Figure 01 shows respectively the THSP image obtained from a high activity biological sample and a low activity biological sample.

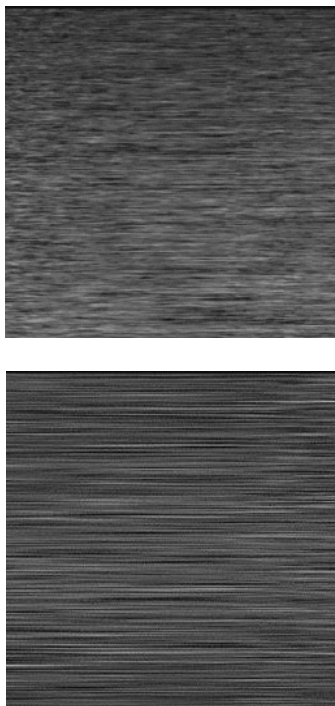


Figure 01. THSP obtained of a high activity and a low activity biological sample

The sequence of biochemical events and metabolic reorganizations turns irreversible the maturation process. Since papaya is a climacteric fruit, i.e., the maturation process continues to develop after harvesting, metabolic activities also increase during that period. The MI (moment of inertia) is an index defined to express, or to quantify the biospeckle phenomenon. Rabelo (2000) described the details of the MI calculation. Equation 01 provides the mathematical support for MI calculation.

$$MI = \sum_{i,j} MOC(i,j) \cdot (i - \bar{i})^2 + (j - \bar{j})^2$$

1

Where:

MI = moment of inertia;

MOC = Matrix of Occurrences;

i,j = indices relative to the position of pixels in the image.

The MOC is obtained through the modification of THSP matrix and the algorithm to generate such modification has been shown by Rabelo (2000).

Based on what it has been exposed above, the objective of this research work was to propose an experimental setup to obtain the MI level in order to differentiate ripe from unripe papaya fruits.

## Material and methods

Experimental tests were carried in the Laboratory of Optics, Faculty of Agricultural Engineering at the UNICAMP, Campinas, SP, Brazil. The selected experimental setup included an optical refractometer for total soluble solids determinations, a 60f/s digital camera, a PC, a conventional monochromatic light source, 632 nm and 10mW laser diode, a lens for beam dispersion and the softwares ImageJ v. 1.41 and Matlab v. 7 for image processing. Ten sample were obtained from ripe papaya and also ten sample were obtained from unripe papaya. Ripe and unripe papaya fruits are displayed on Figure 02.



Figure 02. Ripe and unripe papaya fruit used in the experimental tests

Samples were forwarded to biospeckle tests and further to total soluble solids determinations.

### Results and discussions

Table 01 displays the Brix values (percentage of total soluble solids) and MI level for tested samples.

**Table 01.** Total soluble solids (Brix) and MI values for ripe and unripe papaya samples.

replication	Ripe papaya samples		Unripe papaya samples	
	Brix	MI	Brix	MI
1	13,2	5,86	12,4	13,52
2	14,5	5,07	11,8	5,91
3	13,8	7,63	12,2	5,27
4	14,2	6,18	11,2	5,38
5	13,2	6,05	11,2	5,20
6	13,2	5,07	11,4	6,29
7	13,2	5,37	11,2	5,78
8	12,2	4,98	11,0	4,95
9	13,2	6,49	13,5	5,97
10	12,2	5,46	12,0	8,01
mean	13,29	5,82	11,79	6,63
Standard deviation	0,74	0,82	0,77	2,57

As it is shown on Table 01, Brix values were higher for ripe papaya samples, indicating higher total soluble solids, as it was expected. For unripe papaya samples the average Brix value was lower, due to low total soluble solids concentration, being possible the fruit classification through that criteria.

MI presented lower values for unripe papaya samples, however the standard deviation was quite high which did not permit an adequate maturity evaluation. The above mentioned high standard deviation for MI values is probably associated to unripe fruit lack of uniformity, indicating a necessary study on sampling procedure. Tested ripe papaya probably has shown a more uniform maturity throughout the fruit flesh.

The statistical significance of the treatments

are displayed on Table 02 by means of an analysis of variance, setting as (1) for ripe papaya and (2) for unripe papaya.

As it can be observed, MI values at 5% of probability did not present statistical difference between treatments, indicating that MI index did serve for adequate papaya fruit maturity evaluation. However well distributed sampling throughout the fruit flesh should be considered. Tukey test as presented on Table 03 is in close agreement with the analysis of variance results.

### Conclusions

Based on what it has been discussed above, it can be concluded the MI index did not differentiate papaya maturity levels. Unripe papaya fruit sample standards should better understood and proposed latter on.



**Table 02.** Analysis of variance for MI values for treatment (1) and treatment (2).

Source	DF	Sum of square	Mean square	F	Sigm.
treatment	1	3,3	3,3	0,87	0,38
replication	9	31,44	3,49	0,92	0,55
error	9	34,08	3,79		
Corrected total	19	68,82			
Variation	19				
Coefficient (%)					
Geral mean	6,22	Sample number	20		

**Table 03.** Tukey test for treatment.

Treatment	Median	Results
1	5,82	a1
2	6,63	a2

Minimal significative difference: 1,97

Standard Error: 0,62

## References

1. AFRÂNIO A. T. MONTENEGRO, FRANCISCO M. L. BEZERRA, RAIMUNDO N. de LIMA. EVAPOTRANSPIRAÇÃO E COEFICIENTES DE CULTURA DO MAMOEIRO PARA A REGIÃO LITORÂNEA DO CEARÁ. *Eng. Agríc., Jaboticabal*, 2004;24(2):9.
2. ARIZAGA, R.; TRIVI, M. R.; RABAL, H. J. *speckle* time evolution characterization by co-occurrence matrix analysis. *Optics & Laser Technology*, Oxford, v. 31, n. 2, p. 163-169, Mar. 1999.
3. BERGKVIST, A. Biospeckle-based study of the line profile of light scattered in strawberries. 1997. 60 p. Dissertação (Mestrado) - Faculty of technology at Lund University, Suécia.
4. BRAGA JR, R. A.; RABELO, G. F.; GRANATO, L. R.; SANTOS, E. F.; MACHADO, J. C.; ARIZAGA, R.; RABAL, H. J.; TRIVI, M. Detection of Fungi in Beans by the Laser Biospeckle Technique. *Biosystems Engineering*, San Diego, v. 91, n. 4, p. 465-469, Ago. 2005.
5. BRAGA Jr., R. A. "Bio-Speckle" : uma contribuição para o desenvolvimento de uma tecnologia aplicada à análise de sementes. 2000. 117 p. Tese (Doutorado em Engenharia Agrícola) – Universidade Estadual de Campinas, Campinas.
6. ENES, A. M. Análise do comportamento de tecidos vivos e tecidos mortos em sementes de feijão ( *Phaseolus Vulgaris* L.) pela ótica do *biospeckle* laser. 2005. 32 p. Trabalho de Conclusão de Curso (Graduação em Engenharia Agrícola) - Universidade Federal de Lavras, Lavras, MG.
7. ENES, A. M.; RABELO, G. F.; BRAGA JÚNIOR, R. A.; RODRIGUES, S. Utilização do Laser aplicado na diferenciação de tecidos vivos de tecidos mortos em sementes. In: CONGRESSO BRASILEIRO DE ENGENHARIA AGRÍCOLA, 33., 2004, São Pedro. Anais... Campinas: Unicamp/Embrapa, 2004.
8. ENES, Adilson Machado. Análise de resposta em frequência do biospeckle laser. 2006. 48 p. Dissertação (Mestrado em Engenharia Agrícola) – Universidade Federal de Lavras, Lavras, MG.
9. FAO (Roma, Itália). FAO statistical databases: agricultural production: crops primary: Brazil: bananas. Disponível em: <<http://faostat.fao.org/site/567/DesktopDefault.aspx?PageID=567#ancor>>. Acesso em: 08 jun. 2010.
10. MOREIRA, M. F. B.; BRAGA JÚNIOR, R. A.; BOREM, F. M.; RABAL, H. J.; RABELO, G. F.; FABBRO, I. M. Dal;



- TRIVI, M. R.; ARIZAGA, R. Caracterização da Transmissão da Luz Laser em semente de feijão ( *Phaseolus vulgaris* L.) . Revista Brasileira de Produtos Agroindustriais, Campina Grande, v. 4, n. 2, p. 119-126, 2002.
11. OULAMARA, A.; TRIBILLON, G.; DUVERNOY, J. Biological activity measurement on botanical specimen surface using temporal decorrelation effect of laser *speckle*, Journal of Modern Optics, London, v. 36, n. 2, p. 165-179, Feb. 1989.
  12. RABAL, H. J.; BRAGA Jr., R. A.; TRIVI, M. R.; DAL FABBRO, I. M. O Uso do Laser na Agricultura. In: CONGRESSO BRASILEIRO DE ENGENHARIA AGRÍCOLA, 27., 1998, Poços de Caldas. Anais... Poços de Caldas: Sociedade Brasileira de Engenharia, 1998. 1CD-ROM.
  13. RABELO, G. F. Avaliação da Aplicação do speckle Dinâmico no Monitoramento da Qualidade da Laranja. 2000. 149 p. Tese (Doutorado em Engenharia Agrícola) - Universidade Estadual de Campinas, Campinas.
  14. RABELO, G. F.; BRAGA JUNIOR, R. A.; FABBRO, I. M. D. . Laser speckle techniques in quality evaluation of orange fruits. Revista Brasileira de Engenharia Agrícola e Ambiental, Campina Grande, v. 9, n. 4, 2005. Available from: <[http://www.scielo.br/scielo.php?script=sci\\_arttext&pid=S1415-43662005000400021&lng=en&nrm=iso](http://www.scielo.br/scielo.php?script=sci_arttext&pid=S1415-43662005000400021&lng=en&nrm=iso)>. Acesso em: 25 Set. 2006.
  15. RODRIGUES, S.; BRAGA JUNIOR, R. A.; RABELO, G. F.; ENES, A. M.; BATISTA, C. A. M.; Dal FABBRO, I. M.; RESENDE, O. Efeito da umidade na determinação da atividade biológica de sementes de feijão. (*Phaseolus vulgaris* L.), utilizando imagens de speckle dinâmico. Revista Brasileira de Armazenamento, Viçosa - MG, v. 30, n. 2, p. 135-139, 2005.
  16. ROMERO, G. G. Estudio y caracterizacion de patrones de speckle que varian en el tiempo. 1999. 133 p. Tese (Doutorado em Física) - Universidad Nacional de Salta, Argentina.
  17. XU, Z. J.; JOENATHAN, C.; KHORANA, B. M. Temporal and spatial properties of the time-varying speckles of botanical specimens. Optical Engineering, Bellingham, v. 34, n. 5, p. 1487-1502, May 1995

## EXPECTED TRENDS IN DEPENDABILITY MANAGEMENT WITHIN AGRICULTURAL ENGINEERING AND MANUFACTURING

VACLAV LEGAT, ZDENEK ALES

Czech University of Life Sciences Prague, Faculty of Engineering,

Department for Quality and Dependability of Machines

Kamycka 129, 165 21 Prague 6 – Suchbát

Phone: +420 224 383 268, E-mail [legat@tf.czu.cz](mailto:legat@tf.czu.cz), [ales@tf.czu.cz](mailto:ales@tf.czu.cz)

### Abstract

Authors in this paper popularize and familiarize general standardized requirements on dependability management system, dependability elements and tasks and on life cycle costing for readers. Can be expected a new trend that progressive dependability method and tools will be penetrating to farm machinery industry and into agricultural engineering. This is a challenge for agricultural machinery designers.

### Introduction

**Dependability** is a key decision factor in today's global business environment in the field of machinery production generally and in the agricultural engineering and manufacturing particularly. Dependability affects product costs and processes. It is an inherent product design property influencing product performance. A dependable product is achieved through the implementation of dependability disciplines in the early concept and design phases of the product life cycle to provide cost-effective product operations.

Dependability is the collective term describing the availability performance of any simple to complex product [1]. The **factors influencing the availability performance** of a product are the reliability and maintainability design characteristics and the maintenance support performance.

Dependability reflects **user confidence in fitness for use** by attaining satisfaction in farm machinery performance capability, delivering service availability upon demand, and minimizing the costs associated with the acquisition and ownership throughout the life cycle.

Dependability properties and characteristics of farm machinery are really better than some years ago, but **agricultural customer requirements on dependability go up** and it will be necessary to introduce into agricultural

engineering standardized dependability management system to fulfil new higher dependability desires.

**Authors are aiming** to show basic standardized methods and tools for attaching dependability needs and requirements on farm machinery in order to deliver much more high-value products to farmers in near future.

#### **Dependability management system**

**Quality Management Systems (QMS)** structure facilitates incorporation of dependability activities in the overall management system. Dependability activities complement QMS processes to achieve the desired levels of reliability, maintainability, and maintenance support performance of farm machinery [2].

**Dependability management system (DMS)** identifies the generic processes in dependability for planning, resource allocation, control, and tailoring necessary to meet dependability objectives within agricultural engineering. DMS deals with the dependability performance issues in the farm machinery life-cycle phases concerning planning, design, measurements, analysis and improvement.

DMS is **managed according to standard IEC 60300-1 Dependability management Part 1: Dependability management systems are structured** as can see in the Figure 1 (the numbering is harmonized according to the standard).

<p><b>4 Dependability management system</b> - management system to direct and control an organization with regard to dependability.</p> <p>4.1 <b>Application</b> - the objective is to ensure achievement of the dependability of the product under consideration by addressing the essential dependability management processes.</p> <p>4.2 <b>General recommendations</b> - the organization should establish and maintain a dependability management system to direct and control the dependability activities. The dependability management system of an organization should be an integral part of its overall management system.</p> <p>4.3 <b>Documentation recommendations</b> – it should be documented – a statement of dependability policy and objectives, dependability plans, dependability methods relevant to the organization's project or business, dependability records.</p>	
<p><b>5 Management responsibility</b></p> <p>5.1 Management function and commitment on dependability</p> <p>5.2 Customer focus on dependability</p> <p>5.3 Dependability policy</p> <p>5.4 Dependability planning</p> <p>5.5 Responsibility, authority and communication</p> <p>5.6 Management review</p>	<p><b>6 Resource management</b></p> <p>6.1 Provision of resources</p> <p>6.2 Human resources</p> <p>6.3 Infrastructure</p> <p>6.4 Work environment</p>
<p><b>7 Product realization</b></p> <p>7.1 Planning of product realization</p> <p>7.2 Customer-related processes</p> <p>7.3 Design and development</p> <p>7.4 Purchasing and subcontracting</p> <p>7.5 Production and service provision</p> <p>7.6 Control of monitoring and measuring devices</p>	<p><b>8 Measurement, analysis and improvement</b></p> <p>8.1 General</p> <p>8.2 Monitoring and measurement</p> <p>8.3 Control of nonconforming product</p> <p>8.4 Analysis of data</p> <p>8.5 Improvement</p>

Figure 1 Structure of dependability management system

For dependability managers it is very important to know basic terms regarding to dependability management system:

**Dependability** is a collective term used to describe the availability performance and its influencing factors: reliability performance, maintainability performance and maintenance support performance.

**Availability performance** is the ability of an item to be in a state to perform a required function under given conditions at a given instant of time or over a given time interval, assuming that the required external resources are provided [see IEV 191-02-05].

**Reliability performance** is the ability of an item to perform a required function under given

conditions for a given time interval [see IEV 191-02-06].

**Maintainability performance** is the ability of an item under given conditions of use, to be retained in, or restored to a state in which it can perform a required function, when maintenance is performed under given conditions and using stated procedures and resources [see IEV 191-02-07].

**Maintenance support performance** is the ability of a maintenance organization, under given conditions, to provide upon demand, the resources required to maintain an item, under a given maintenance policy [see IEV 191-02-08].

Relationship among dependability characteristics is very simply shown on Figure 2.

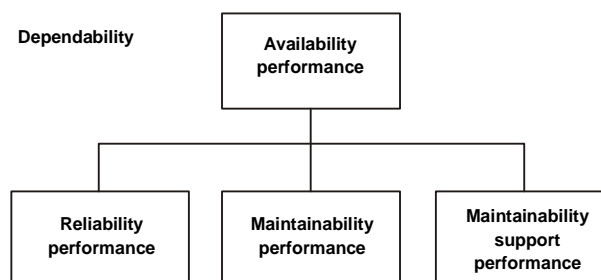


Figure 2 Dependability relationships

The process steps for managing dependability consist of a **sequence of activities** that could be applied to any phase of a product life cycle. A product life cycle consists of the following phases:

- concept and definition,
- design and development,
- manufacturing,

- installation,
- operation and maintenance,
- disposal.

The feedback loop to the various process steps **permits continual improvement** where appropriate – see Figure 3.

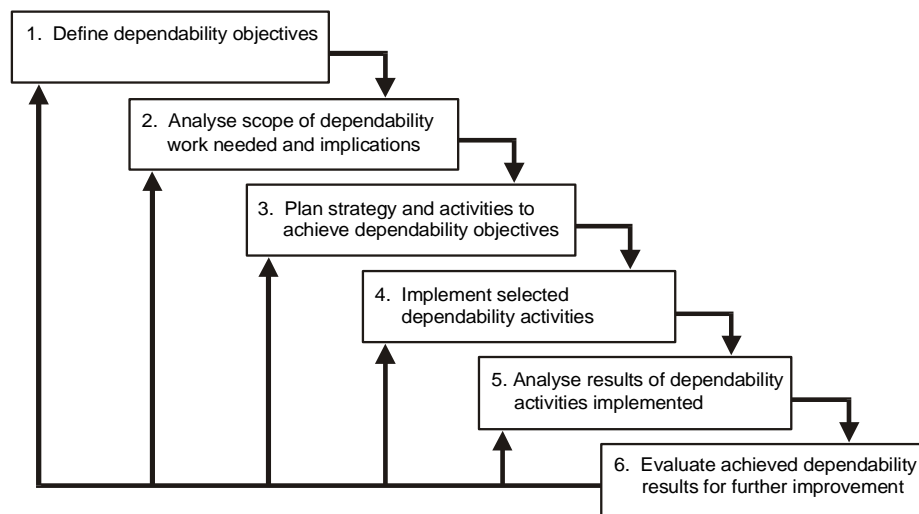


Figure 3 Sequence of dependability promotion and implementing activities

#### Dependability system elements and tasks

If we want to design a dependability management system, it is necessary to know an **association of product life cycle phases** with the applicable dependability elements and tasks –

see Figure 4, where C&D - Concept and definition, D&D - Design and development, MFG - Manufacturing, INS - Installation, O&M - Operation and maintenance, DIS - Disposal [3].

Dependability elements and tasks	Life cycle phases					
	C&D	D&D	MFG	INS	O&M	DIS
<b>Element 1: Management</b>						
Task 1: Dependability plan	xxx	xxx	xxx	xxx	xxx	xxx
Task 2: Dependability specifications		xxx	xxx	xxx		
Task 3: Control of processes		xxx	xxx	xxx	xxx	
Task 4: Design control		xxx	xxx	xxx		
Task 5: Monitoring and review		xxx	xxx	xxx	xxx	xxx
Task 6: Supply-chain management			xxx	xxx	xxx	xxx
Task 7: Product introduction				xxx	xxx	
<b>Element 2: Dependability disciplines</b>						
Task 8: Reliability engineering	xxx	xxx	xxx			
Task 9: Maintainability engineering	xxx	xxx	xxx			
Task 10: Maintenance support engineering		xxx	xxx	xxx	xxx	
Task 11: Standardization		xxx	xxx	xxx	xxx	
Task 12: Human factors	xxx	xxx	xxx	xxx	xxx	xxx
<b>Element 3: Analysis, evaluation and assessment</b>						
Task 13: Analysis of use environment	xxx	xxx	xxx			
Task 14: Reliability modelling and simulation	xxx	xxx	xxx			

Dependability elements and tasks	Life cycle phases					
	C&D	D&D	MFG	INS	O&M	DIS
Task 15: Parts evaluation and control		xxx	xxx			
Task 16: Design analysis and product evaluation		xxx	xxx			
Task 17: Cause-effect impact and risk analysis		xxx	xxx	xxx	xxx	xxx
Task 18: Prediction	xxx	xxx	xxx			
Task 19: Trade-off analysis	xxx	xxx	xxx			xxx
Task 20: Life cycle costing	xxx	xxx	xxx	xxx	xxx	xxx
Task 21: Reliability growth				xxx	xxx	
<b>Element 4: Verification and validation</b>						
Task 22: Verification and validation strategy		xxx	xxx	xxx		
Task 23: Dependability demonstration				xxx	xxx	
Task 24: Reliability stress screening			xxx			
<b>Element 5: Knowledge base</b>						
Task 25: Knowledge base establishment		xxx	xxx	xxx	xxx	xxx
Task 26: Data analysis		xxx	xxx	xxx	xxx	xxx
Task 27: Data collection and dissemination		xxx	xxx	xxx	xxx	xxx
Task 28: Dependability records		xxx	xxx	xxx	xxx	xxx
<b>Element 6: Improvement</b>						
Task 29: Preventive and corrective actions		xxx	xxx	xxx	xxx	
Task 30: Upgrade and modification				xxx	xxx	
Task 31: Competence development and enhancement	xxx	xxx	xxx	xxx	xxx	
Task 32: Management system improvement	xxx	xxx	xxx	xxx	xxx	

Figure 4 Association of product life cycle phases with the applicable dependability elements and tasks

### Dependability management needs a life cycle costing

Life cycle costing is *the process of economic analysis to assess the total cost of acquisition, ownership and disposal of a product*. This analysis provides important inputs in the decision-making process in the product design, development, use and disposal. Product suppliers can **optimize their designs** by evaluation of alternatives and by performing trade-off studies. They can evaluate various operating, maintenance and disposal strategies (to assist product users) to optimize life cycle cost (LCC). Life cycle costing can also be effectively applied to **evaluate the costs** associated with a specific activity, for example, the effects of different maintenance concepts/approaches, to cover a specific part of a product, or to cover only

selected phase or phases of a product's life cycle [4].

The **primary objective** of life cycle costing is to provide input to decision making in any or all phases of a product's life cycle. An important objective in the preparation of LCC models is to identify costs that may have a major impact on the LCC or may be of special interest for that specific application including dependability.

**Costs associated with dependability** elements may include the following, as appropriate:

- system recovery cost including corrective maintenance cost,
- preventive maintenance cost,
- consequential cost.

Figure 5 highlights some dependability elements translated into operation and maintenance costs.

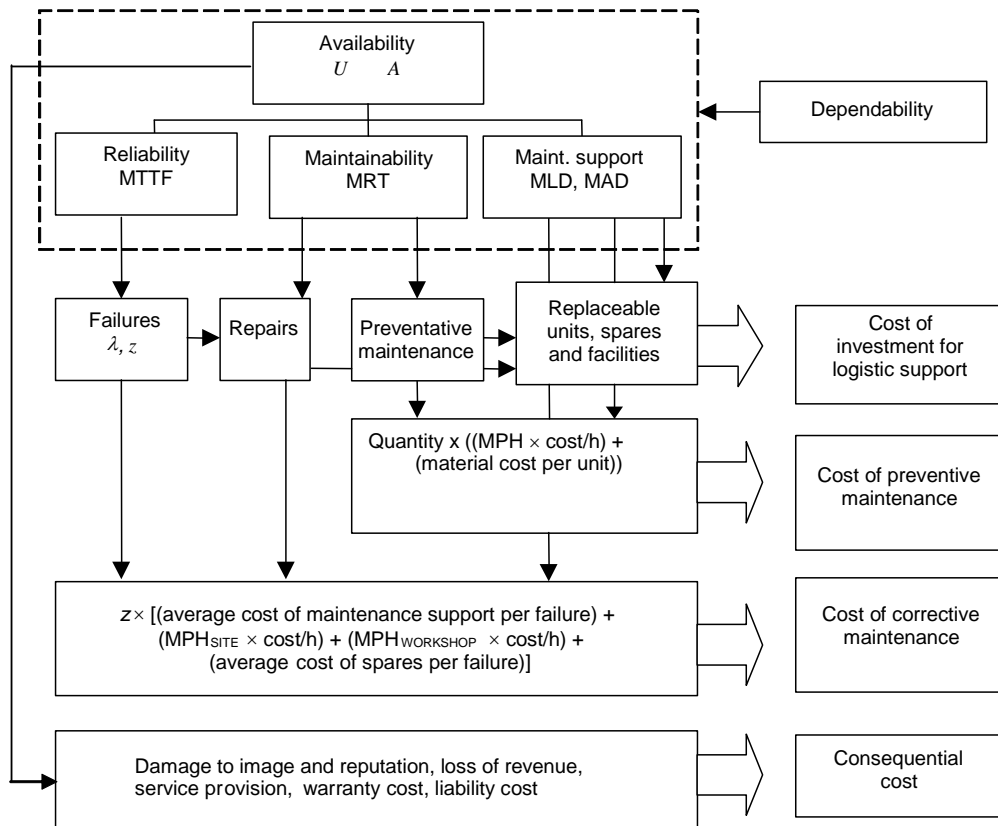


Figure 5 Typical relation between dependability and LCC for the operation and maintenance phase

One approach often used to identify the required cost elements involves the breakdown of the product to lower indenture levels, cost categories and life cycle phases.

This approach can best be illustrated by the use of a **three-dimensional matrix** shown in Figure 6.

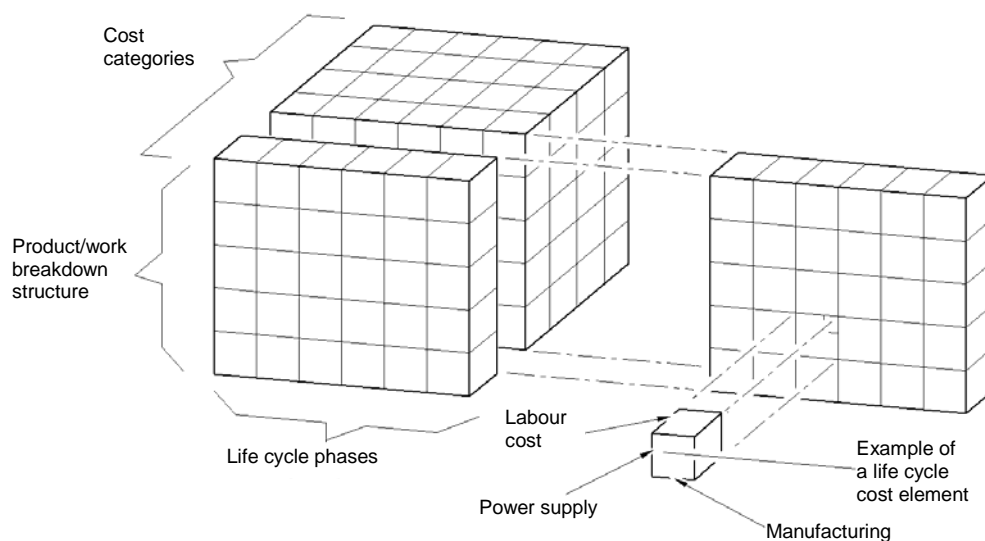


Figure 6 Concept of cost element



## Conclusion

At present time and mainly **in the future we can expect a trend** of many requirements not only on better quality but also on dependability increasing. Therefore a modern agricultural design, engineering and manufacturing need implementation of new and proper methods and tools for agriculture machines dependability improvement.

Authors in this paper **popularize and familiarize general standardized requirements** on dependability management system, dependability elements and tasks and on life cycle costing for readers. These are methods using within high technology industry (astronautics, aeronautics, nuclear energetic, automotive industry etc.). Nevertheless farmers also need very dependable (available, reliable, maintainable and perfect maintenance supported) machinery and equipment.

Producers of high technologies over the world clearly show that using and applying these modern dependability methods and tools bring very good reliability, maintainability and maintenance support resulting high availability of repairable machines and equipment. Very important **benefit** of this application is **increasing** overall machines and equipment **effectiveness** and **decreasing life cycle costs**.

## Reference

- [1] IEC 60050-191:1990, International Electrotechnical Vocabulary (IEV) – Chapter 191: Dependability and quality of service.
- [2] IEC 60300-1:2003, Dependability management – Part 1: Dependability management systems.
- [3] IEC 60300-2:2004, Dependability management – Part 2: Guidelines for dependability management.
- [4] IEC 60300-3-3:2004, Dependability management – Part 3-3: Application guide – Life cycle costing.

## COMMUNICATION SKILLS OF ENGINEERING STUDENTS

<sup>1\*</sup> LARISA MAĻINOVSKA, <sup>2</sup> ANETE MEŽOTE

<sup>1</sup> Latvia University of Agriculture, Lielā iela 2, Jelgava, LV-3001, Latvia,  
Phone: +371 29378511, E-mail: larisama@apollo.lv

<sup>2</sup> Latvia University of Agriculture, Jelgava, Latvia

### Abstract

The present article describes the major aspects of communication skills, as well as the results of a research in engineering student communication skills and in their motivation of acquiring and improving communication skills within the study process especially as regards learning foreign languages performed by the authors.

The first stage of the research was aimed at identifying communication skills of engineering students and analysing of opinions of the students on the opportunities to use communication skills in their professional activity at the beginning of the foreign language study course.

The second stage of the research was aimed at studying reasons for the lack of communication skills and of motivation of acquiring and improving communication skills, at relating the aforementioned reasons to the professional activity of the students, as well as at analysing of opinions of the students as regards communication skills at the middle of the foreign language study course in order to prove the necessity of communication skills in future professional life of engineering students.

**Keywords:** engineering students, professional activity, communication skills, motivation, foreign languages

### Introduction

To achieve positive results in the process of studies and in the professional life of engineering students, communication skills are of crucial importance, as the nowadays work environment is multinational, which involves communication in foreign languages, and as the labour market, the economic situation in Latvia and in the world and the professional development and career preconditions in any professional field including the engineering sector demand specialists that are able to communicate well in general in order to ensure appropriate personal professional development, oral and written business correspondence to partners and successful corporate cooperation in any aspect of business relations.

Professional skills alone cannot ensure promotion in work. The future specialists should be ready to understand their peers and react accordingly in compliance with the given situation. They should also be able to form external relationships that help firms strengthen and extend their traditional competences while responding to the demands of globalization, mass customization, enhanced quality and rapid

technological change (Mascarenhas, Baveja, Jamil, 1998).

To ensure strong relationships and successful cooperation among the future engineering specialists, not only language skills play a vital role. Similarly communication skills as such can help ensure the necessary results.

Theories within each of the seven "traditions" of communication theory that R.Craig suggests tend to reinforce one another, and retain the same ground epistemological and axiological assumptions. The aforementioned traditions include:

- rhetorical - practical art of discourse;
- semiotic – intersubjective mediation through signs in order to mediate between different perspectives;
- phenomenological - experience of otherness, dialogue;
- cybernetic - information processing and explains how all kinds of complex systems, whether living or nonliving, macro or micro, are able to function, and why they often malfunction;
- sociopsychological - expression, interaction and influence;
- critical - discursive reflection;

- sociocultural - reproduction of social order;

R.T.Craig finds each of these clearly defined against the others, and remaining cohesive approaches to describing communicative behaviour. As a taxonomic aid, these labels help to organize theory by its assumptions, and help researchers to understand why some theories may seem incommensurable.

For engineering specialists, it is necessary to develop all of the traditions as competences that would help them communicate in their future professions.

Communication encompasses a great deal of human activity. Reading, writing, listening, speaking, viewing images, and creating images are all acts of communication. There are as well many more subtle communication activities that may be conscious or unconscious, such as expression, gesture, "body language" and nonverbal sounds. The process of communication has been the subject of study for thousands of years, during which time the process has come to be appreciated with increasing complexity (Craig, 2007).

For students, it is necessary to simultaneously assess and improve skills in all of the aspects mentioned, as all of them might be required and used within the professional activity working in any company or institution nowadays in Latvia and abroad to deal with issues connected with agricultural engineering or any other aspect of business.

The process of communication can be reflected within a model (see Fig.1) indicating all of the parts of the communication process and the result.

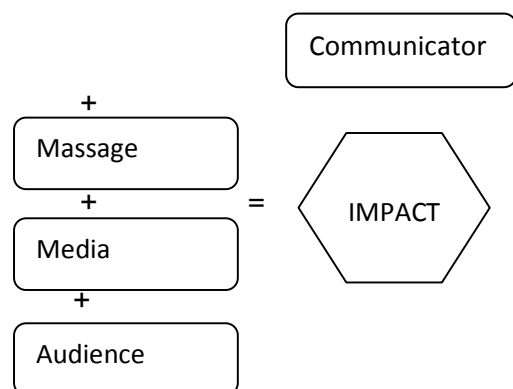


Fig.1 Laswell's Model of Communication

Communication is ensured, if a communicator interacts with the audience in order to convey a message using a medium and/or media, resulting in a particular impact which is considered the result of the communication process. To ensure successful communication, the communicator has to possess certain abilities known as communication skills, as well as has to have a certain aim as regards conveying the message. The way how the audience perceives the communicator depends on the communicator's skills, as well as the appropriate or inappropriate choice of particular media.

Interpersonal communications is usually defined by scholars in several ways, mainly describing participants who depend upon one another. Communication channels, the conceptualization of media that carry messages from sender to receiver, take two distinct forms: direct and indirect. Direct channels are obvious and easily recognized by the receiver. Both verbal and non-verbal information is completely controlled by the sender. Verbal channels rely on words, as in written or spoken communication. Non-verbal channels encompass facial expressions, controlled body movements (police present hand gestures to control traffic), colour (red signals 'stop', green signals 'go'), and sound (warning sirens). Indirect channels are usually recognized subconsciously by the receiver, and are not always under direct control of the sender. Body language comprising most of the indirect channel, may inadvertently reveal one's true emotions, and thereby either unintentionally taint or bolster the believability of any intended verbal message. Subconscious reception and interpretation of these signals is often described with arbitrary terms like gut-feeling, hunch, or premonition (Wertheim, 2010).

For engineering students, verbal communication skills are the ones to be developed more professionally by means of foreign language teaching, but simultaneously non-verbal communication skills are of importance, as they help ensure and maintain strong relationships with business partners and colleagues.

Usually people in organizations typically spend over 75% of their time in an interpersonal situation; thus it is no surprise to find that at the

root of a large number of organizational problems is poor communications. Effective communication is an essential component of organizational success whether it is at the interpersonal, intergroup, intragroup, organizational, or external levels (Wertheim, 2010).

Due to the described reason, if engineering specialists lack communication skills, lots of problems might arise as regards corporate culture and business relationships in the particular business sector.

Skill in communication involves a number of specific strengths. The most important skills in this respect are listening skills provided that the language skills have been taught sufficiently enough and the students are able to speak well. The following aspects of listening are crucial when communicating at work:

- Listen openly and with empathy to the other person
- Judge the content, not the messenger or delivery; comprehend before judgement
- Use multiple techniques to fully comprehend (ask, repeat, rephrase, etc.)
- Ask the other person for as much detail as he/she can provide; paraphrase what the other is saying to make sure that the content is understood
- Respond in an interested way that shows that the problem and the concern is understood
- Attend to non-verbal cues, body language, not just words; listen between the lines
- Ask the other for his/her views or suggestions
- State own position openly; be specific, not global
- Communicate feelings but don't act them out (e.g., tell a person that his/her behaviour is really upsetting; don't get angry)
- Be descriptive, not evaluative-describe objectively reactions, consequences
- Be validating, not invalidating; acknowledge other's uniqueness, importance
- Be conjunctive, not disjunctive
- Don't totally control conversation; acknowledge what was said
- Don't react to emotional words, but interpret their purpose

- Decide on specific follow-up actions and specific follow up dates (Wertheim, 2010).

To ensure successful problem solution and effective communication, the mentioned skills are considered to be utmost necessary for engineering students and therefore are promoted within the foreign language course (which promotes overall speaking skills) after which the results are analysed.

### Experimental methods

To justify the necessity of the research and to elaborate methods for performing the foreign language study course for engineering students, within communication skills are to be promoted, the methods of theoretical description and assessment of communication theories have been used. To obtain data, the methods of quantitative research have been used, by assessing the data of the surveys carried out at the beginning of the foreign language study course and in the middle of the foreign language study course, thus revealing how opinions of engineering students change as regards the possession and use of communication skills in their professional activity. The methods of practical analysis have been used to assess the survey results, indication to the importance and use of communication skills for engineering students, and provide conclusions regarding how to teach communication skills for engineering students within the foreign language study course.

### Results and discussion

During the first stage of the research communication skills of engineering students were identified at the beginning of the foreign language study course by means of a survey revealing the presence of the mentioned skills, as well as the opportunities for engineering students to use such skills in their professional activity. The results showed that more than half of the engineering students lacked communication skills (see Fig.2) at the beginning of the foreign language course.

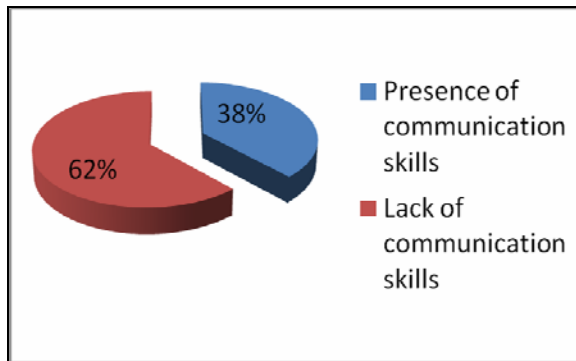


Fig.2 Communication skills of engineering students at the beginning of the foreign language study course

The results are interpreted to be indicating that 62% of the surveyed engineering students lack communication skills as they have had no opportunity to use them (see Fig.3) and as they do not exactly perceive their abilities to achieve good communication results as their communication skills, namely they do not acknowledge the possession of communication skills. Besides, communication skills of the surveyed engineering students have not yet been developed, as the foreign language course has just started, therefore a remarkable development of communication skills is predicted in future as regards the engineering specialists attending the foreign language study course during which certain communication and language skills are to be promoted.

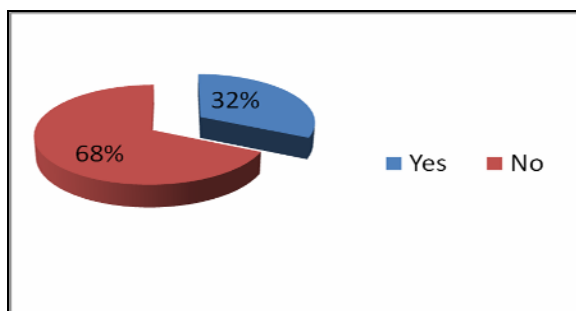


Fig.3 Opportunities of engineering students to use communication skills at the beginning of the foreign language study course

Similarly the results of the first stage of the research reveal that 68% of the surveyed engineering students have had no opportunity and consider that they will have no opportunity in future either to use communication skills in their professional activity, which means that they

do not understand the importance of the possession of such skills. A comparatively larger part of the surveyed students (38%) consider communication skills to be useful in their everyday life apart from their professional activity.

During the second stage of the research the student's opinions were analysed and discussions were organized within the foreign language course, as well as the communication skills were promoted within the foreign language studies in order to repeat the survey in the middle of the foreign language course with prospects of the communication skills to have been improved. The results revealed that indeed communication skill of the engineering students have improved (see Fig.4) showing that 66% of the engineering students acknowledge the possession of communication skills and only 34% of the students consider that they lack particular communication skills which might be of use in their everyday of professional life.

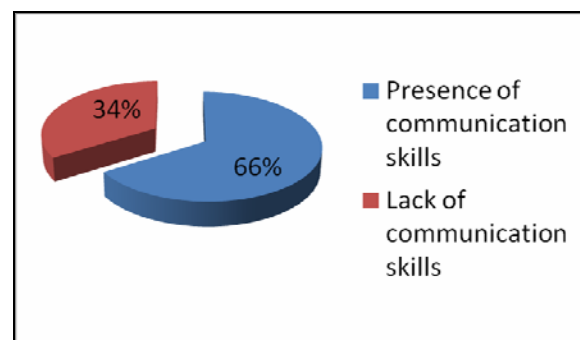


Fig.4 Communication skills of engineering students in the middle of the foreign language study course

In the middle of the foreign language study course, the majority of engineering students (64%) consider that they might use the obtained communication skills in their future professional activity thus ensuring successful business correspondence and cooperation to business partners. Only 36% of the surveyed engineering students still consider that communication skills are of no use in their profession in general and in their future professional activity, which means that their motivation to obtain communication skills has not increased.

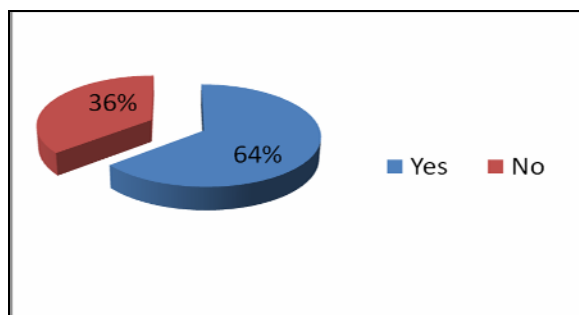


Fig.5 Opportunities of engineering students to use communication skills in the middle of the foreign language study course

To find out if the unmotivated part of the students would acknowledge the use of communication skills in their professional activity in future, it is necessary to repeat the survey at the end of the foreign language study course and/or at the moment when the particular students would have started work in the particular engineering professions, thus finding out if the reason for the lack of motivation is the lack of communication skills and non-acknowledgement of the possession of communication skills or the lack of necessity to possess communication skills in work in particular sectors of engineering.

### Conclusions

At the beginning of foreign language study course, the majority of engineering students lack communication skills and the surveyed students do not consider communication skills to be of use in their professional activity. At the middle of the foreign language study course, the surveyed students motivation to obtain communication skills has increased, as the majority of the students acknowledge the possession of communication skills and thus understand the possible ways of using the obtained skills, therefore the authors conclude that communication skills can be successfully taught to engineering students by means of foreign language course and that communication skills might be useful for the majority of the future engineering specialists. The authors have similarly found out the most successful methods of teaching communication skills within a foreign language course ("Content and Language Integrated Learning", communication practices, usage of communications skills in their

professional practices), as well as ways of motivating engineering students to acquire foreign language and communication skills within the study process such as indicating to the importance of communication skills within the today's business environment and necessity of communication skills for being competitive within the labour market.

### References:

- [1] Craig, R.T.: *Theorizing Communication: Readings Across Traditions*, Sage Publications, 2007, 544 pp.
- [2] Lasswell, H.: *The Structure and Function of Communication in Society*. In Lyman Bryson (ed.): *The Communication of Ideas*. Harper and Row, 1948, 434 pp.
- [3] Mascarenhas, B.-Baveja, A.-Jamil, M.: *Dynamics of Core Competencies in Leading Multinational Companies*, *California Management Review*, Vol 40, no. 4, 1998, pp. 117-132.
- [4] Wertheim, E.G.: *The Importance of Effective Communication*. Retrieved 05/02/10 from <http://windward.hawaii.edu/facstaff/dagrossa-p/ssci193v/articles/EffectiveCommunication.pdf>.



## SAFER AGRICULTURE FOR EMPLOYEES IN RURAL

Y. BENAL YURTLU<sup>1\*</sup>, KERIM EKMEKCI<sup>2</sup>, ELCIN YESILOGLU<sup>1</sup>,  
BAHADIR DEMIREL<sup>1</sup>, HUSEYIN SAUK<sup>1</sup>

<sup>1</sup>Department of Agricultural Machinery, Faculty of Agriculture, Ondokuz Mayıs University, 55139, Kurupelit, Samsun, Turkey, Phone: +90 362 3121919/1256, Fax: +90 362 4576034, e-mail: yurtlu@omu.edu.tr

<sup>2</sup> Directorate General for Agricultural Production and Development, Ministry of Agriculture and Rural Affairs, Ankara, Turkey

### Abstract

Education/training activities in agriculture forming permanent vocational safety culture is getting gradual importance in our country under the influence of increase in human centered policies executed in the world, harmonization of regulations of EU to our country, raise several projects to creating awareness in this area and pressure to human consciousness generated by accidents. Many works/studies are being conducted in developed and EU countries under the base of safer works in agriculture. With in these studies, two focal points are manufacturing of safe machinery and training of users. In this paper, works related to SAFER project- Safer Agriculture For Employees in Rural- that is conducted by OMU and supported by EU Life Long Learning Leonardo da Vinci Program Transfer of Innovation has been summarized.

**Keywords:** safety; agricultural machinery.

### Introduction

Agriculture is one of the most hazardous sectors in many countries. According to ILO, each year, approximately 170 000 agricultural workers die and a high number of world's 1.3 billion agricultural workers suffer from serious injuries or occupational diseases. Exposure to pesticides and other chemicals and farm machinery accidents are two important factors of these fatalities, injuries and diseases. The essential reasons of the insufficient level of occupational health and safety of the agricultural workers are almost similar in undeveloped and developing countries. Among the similarities, deprivation of collective voice because of inadequate organizations of workers, insufficiency of education levels, too many women workers, high level of translocation rate of seasonal farm workers within all agricultural employees are distinctive features (Roskam, 2001).

According to European Statistics Office (EUROSTAT), agriculture is the second most hazardous sector after construction works in the region. In England, agriculture has one of the worst fatal accident and occupational ill health records of any major employment sector. In France, mechanization is the main cause of

injury accounting for 25 % of all cases. In Spain and other European countries at a similar level of development, some 40 % of accidents are machinery related and half of them involve tractors alone (Dupre, 2005; Anonymus, 2000).

As a rule, the safety employees and experts attach high value on two points for the purpose of safety. The first one is safe design of product/material/manufacture and the second one is safety education/training. Thus, all products, machinery, systems that will be used in agriculture should be manufactured accepted safety standards. In this regard, it is very much crucial to put into force of 2006/42/EC Machinery Directive in the proper sense. Furthermore, market inspections which are conducted by the Ministry of Industry and Trade are also valuable works to provide safe and standard products to the agricultural employees in Turkey. But, the stated inspections are valid for manufacturers who apply to Ministries for certain purposes. Therefore, the products/machinery manufactured in small shop locally and in accordance with domestic demand have not been safety standards and out of certain inspection circumstances. This situation creates an important problem for safe works in agriculture. In this regard, to create awareness it

is necessary to perform multipurpose education/training for the people who manufactured these types of machineries been mostly in rural. The self employed people (needs education much more than others), professional farmers, farmers' families especially women, seasonal farm workers, agricultural machinery and equipment manufacturers and dealers should be in the context of safety education/training in agriculture.

### Project Description

“Safer Agriculture For Employees in Rural-SAFER” (Anonymous, 2010) is conducted by coordinator Ondokuz Mayıs University supported by EU Life Long Learning Leonardo da Vinci Programme Transfer of Innovation Project. Project is carried out by partnership with Agro-alimentary Federation of CCOO (CCOO)-Spain, Asesoria Declerq SI European Studies-Spain, Italian National Body for Agricultural Mechanization (ENAMA)-Italy, Ministry of Agriculture and Rural Affairs International Agricultural Training Centre (UTEM)-Turkey, Ankara University-Turkey, The Turkish Association of Agricultural Machinery and Equipment Manufacturers (TARMAKIBIR)-Turkey, The Union of Turkish Chambers of Agriculture (TZOB)-Turkey and Ministry of Agriculture and Rural Affairs Directorate General for Agricultural Production and Development-Turkey. SAFER project has been carrying out since December 2008. Total project period is 24 months.

The main aim of SAFER project is to transfer of innovative training materials from successfully completed projects and adapt them to the national and sectoral requirements and improving innovative training modules for safer working conditions of employees in agricultural sector. The project is based on transferring the pilot project “Training for the Correct Use of Farm Machinery–FORMAAGRI (<http://80.38.213.111/formaagri>)”. The prime aim of the FORMAAGRI project is to put together innovative training materials tailored to the needs of the specific target audience which is made up of small and medium-sized enterprises (SMEs) and self-employed workers in the agricultural sector from the standpoint of its productive structure and, given its employment structure, young people. Within this category,

special emphasis is placed on young apprentices and immigrants who represent an alternative for employment levels to be maintained in agriculture and for the sector itself. The training materials are devised to foster the correct use of tractors and other farm machinery in order to achieve several aims: improve safety and, therefore, reduce the excessively high number of accidents that occur in the workplace in this sector; ensure proper maintenance of farm machinery in the European Union and maximise its performance as a result.

Target groups in SAFER project are composed of two main sections: agricultural machinery manufacturers and end users that are self employed people, professional farmers, farmers' family member especially women, seasonal farm workers. Project partnership has been initially collected, compiled and analysed the training needs of stakeholders in the sector. Secondly, SAFER project partners have developed training modules and tools according to analysis result and previous experiences. Pilot training activities have organised in last step. In order to make good use of communication technology with computer, a website has developed and thus continuity in education has been provided. These types of websites are very common most of developed countries. Furthermore, some audio visual materials and leaflets produced to support safety training activities. To prepare these documents and tools, previous project's outputs used after adapting to national requirements by studying with experienced project partners. In this way transferred outputs tested on target groups with pilot studies. While the SAFER project is going on and after finished, it is expected that level of safety knowledge, awareness and consciousness of target group will be improving. In this way it is aimed that safer working conditions will catch in agricultural areas, in rural for employees. For increasing of the impact on target group, in the SAFER project, pilot areas will be created selected employees will be educated. In the long term qualified employees will share/transfer his/her knowledge with ordinary agricultural employee and other people who work in rural. Same method will be used for the agricultural machinery manufacturers. Web page and TV programmes will support the cascade effect of SAFER project.

## Results

The project is dedicated mainly to the elaboration of 17 training modules (in Turkish) (Table 1). Various dissemination activities has been carried out such as: participation to fairs, presentation of posters and papers at national and international events, distribution of leaflets, printing of articles in specific reviews and newsletters, TV broadcasting, creation of web pages and a CD presenting the project and including the full text of the training modules and materials. Also, Safety in Agriculture Workshop has done at the end of first year in Ankara-Turkey. Safety in Agriculture Conference will be organized at the end of the SAFER project. The deliverables of the project included: training modules and materials (practical sheets) in Turkish, animations, videos, CDs, web pages (<http://safer-omu.net>), various questionnaires, posters and papers, published articles and leaflets.

Table 1. SAFER project training modules.

• Plant protection machinery	• Silage machinery
• Pedestrian controlled tractors with mounted rotary cultivators, motor hoes, motor hoes with drive wheels	• Self-propelled agricultural machinery
• Soil working machines with powered tools	• Miller and mixers
• Rotary mowers and flail mowers	• Grinders
• Mixer feeders	• Drive shafts
• Harvesting machinery	• Trailers
• Balers	• Threshing machinery
	• Elevator and handling machinery
	• Agricultural tractors
	• Personal protective equipment

## Conclusions

The activities developed within SAFER project are a solid background for the future safety operations in agriculture. Important effort needs to be made to support training initiatives for safety in agriculture especially in Turkey as well as in the other developing countries. Furthermore, there is a need to increase information and dissemination, as well as to foster cross-information activities. Proactive initiatives are therefore necessary. As a result, safety issues should be included into the education system from the initial learning cycles to high educations, especially agricultural engineer's level.

## Acknowledgements

Special thanks to financial support received for the development of the SAFER project from European Commission Directorate General Education and Culture, Leonardo da Vinci Program. We also wish to extend our thanks to Turkish National Agency for their enthusiastic assistance.

## References

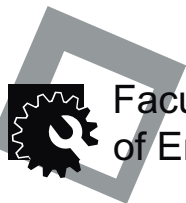
- [1] Anonymous: ILO Safety and Health in Agriculture. 88th Session, 2000, Report VI (1), p.100.
- [2] Anonymous: SAFER Project Interim Report. Leonardo da Vinci Transfer of Innovation, 2010, p.55.
- [3] Dupre, D: Work Related Accidents in the EU, 1998-1999. OSHA Magazine, Issue 4, 2005, p.5-8.
- [4] Rosskam, E: Tarımsal Çalışma Yasamının İyileştirilmesi İçin Eğitim İhtiyacı (in Turkish, Translated by Dursun Gülec). Turkish Doctors Occupational Health and Safety Journal, July, 2001, p.42-47.
- [5] <http://80.38.213.111/formaagri>
- [6] <http://safer-omu.net>











**Title:** Trends in Agricultural Engineering 2010

**Editor:** © 2010 Czech University of Life Sciences Prague;  
Faculty of Engineering ([www.tf.czu.cz](http://www.tf.czu.cz))

The conference is organised in cooperation with CIGR  
([www.cigr.org](http://www.cigr.org))

**Type publication:** Conference Proceedings

**Approved:** Deanship of Faculty of Engineering;  
Czech University of Life Sciences Prague

**Edition:** First

**Circulation:** 150

**Imprint date:** 2010

The articles in the publication are reviewed

The Conference Proceedings designed by Jan Malat'ák and Martin Libra

**ISBN: 978-80-213-2088-8**

---

**Note:** Objective correctness and language guaranteed by authors